Numerical Techniques in Electromagnetics

Second Edition

Numerical Techniques in Electromagnetics

Second Edition

Matthew N. O. Sadiku, Ph.D.

CRC Press
Boca Raton London New York Washington, D.C.

Library of Congress Cataloging-in-Publication Data

Sadiku, Matthew N. O.
Numerical techniques in electromagnetics / Matthew N.O. Sadiku.—[2nd ed.].
p. cm.
Includes bibliographical references and index.
ISBN 0-8493-1395-3 (alk. paper)
1. Electromagnetism. 2. Numerical analysis. I. Title.
QC760 .S24 2000
537′.01′515—dc21 00-026823
CIP

International Standard Book Number 0-8493-1395-3
Library of Congress Card Number 00-026823
Printed in the United States of America 1 2 3 4 5 6 7 8 9 0
Printed on acid-free paper

Preface

The art of computation of electromagnetic (EM) problems has grown exponentially for three decades due to the availability of powerful computer resources. In spite of this, the EM community has suffered without a suitable text on computational techniques commonly used in solving EM-related problems. Although there have been monographs on one particular technique or the other, the monographs are written for the experts rather than students. Only a few texts cover the major techniques and do that in a manner suitable for classroom use. It seems experts in this area are familiar with one or few techniques and not many experts seem to be familiar with all the common techniques. This text attempts to fill the gap.

The text is intended for seniors or graduate students and may be used for a one-semester or two-semester course. The main requirements for students taking a course based on this text are introductory EM courses and a knowledge of a high-level computer language, preferably FORTRAN or C. Software packages such as Matlab and Mathcad may be helpful tools. Although familiarity with linear algebra and numerical analysis is useful, it is not required.

In writing this book, three major objectives were borne in mind. First, the book is intended to teach students how to pose, numerically analyze, and solve EM problems. Second, it is designed to give them the ability to expand their problem solving skills using a variety of available numerical methods. Third, it is meant to prepare graduate students for research in EM. The aim throughout has been simplicity of presentation so that the text can be useful for both teaching and self-study. In striving after simplicity, however, the reader is referred to the references for more information. Toward the end of each chapter, the techniques covered in the chapter are applied to real life problems. Since the application of the technique is as vast as EM and author's experience is limited, the choice of application is selective.

Chapter 1 covers some fundamental concepts in EM. Chapter 2 is intended to put numerical methods in a proper perspective. Analytical methods such as separation of variables and series expansion are covered. Chapter 3 discusses the finite difference methods and begins with the derivation of difference equation from a partial differential equation (PDE) using forward, backward, and central differences. The finite-difference time-domain (FDTD) technique involving Yee's algorithm is pre-

sented and applied to scattering problems. Numerical integration is covered using trapezoidal, Simpson's, Newton-Cotes rules, and Gaussian quadratures.

Chapter 4 on variational methods serves as a preparatory ground for the next two major topics: moment methods and finite element methods. Basic concepts such as inner product, self-adjoint operator, functionals, and Euler equation are covered. Chapter 5 on moment methods focuses on the solution of integral equations. Chapter 6 on finite element method covers the basic steps involved in using the finite element method. Solutions of Laplace's, Poisson's, and wave equations using the finite element method are covered.

Chapter 7 is devoted to transmission-line matrix or modeling (TLM). The method is applied to diffusion and scattering problems. Chapter 8 is on Monte Carlo methods, while Chapter 9 is on the method of lines.

Since the publication of the first edition, there has been an increased awareness and utilization of numerical techniques. Many graduate curricula now include courses in numerical analysis of EM problems. However, not much has changed in computational electromagnetics. A major noticeable change is in the FDTD method. The method seems to have attracted much attention and many improvements are being made to the standard algorithm. This edition adds the noticeable change in incorporating absorbing boundary conditions in FDTD, FEM, and TLM. Chapter 9 is a new chapter on the method of lines.

Acknowledgements

I am greatly indebted to Temple University for granting me a sabbatical in Fall 1998 during which I was able to do most of the revision. I specifically would like to thank my dean, Dr. Keya Sadeghipour, and my chairman, Dr. John Helferty, for their support. Special thanks are due to Raymond Garcia of Georgia Tech for writing Appendices C and D in C++. I am deeply grateful to Dr. Arthur D. Snider of the University of South Florida and Mohammad R. Zunoubi of Mississippi State University for taking the time to send me the list of errors in the first edition. I thank Dr. Reinhold Pregla for helping in clarifying concepts in Chapter 9 on the method of lines. I express my deepest gratitude to my wife, Chris, and our daughters, Ann and Joyce, for their patience, sacrifices, and prayers.

A Note to Students

Before you embark on writing your own computer program or using the ones in this text, you should try to understand all relevant theoretical backgrounds. A computer

is no more than a tool used in the analysis of a program. For this reason, you should be as clear as possible what the machine is really being asked to do before setting it off on several hours of expensive computations.

It has been well said by A.C. Doyle that "It is a capital mistake to theorize before you have all the evidence. It biases the judgment." Therefore, you should never trust the results of a numerical computation unless they are validated, at least in part. You validate the results by comparing them with those obtained by previous investigators or with similar results obtained using a different approach which may be analytical or numerical. For this reason, it is advisable that you become familiar with as many numerical techniques as possible.

The references provided at the end of each chapter are by no means exhaustive but are meant to serve as the starting point for further reading.

Contents

To my teacher

Carl A. Ventrice

and my parents

Ayisat and Solomon Sadiku

Chapter 1

Fundamental Concepts

"Science knows no country because knowledge belongs to humanity and is the torch which illuminates the world. Science is the highest personification of the nation because that nation will remain the first which carries the furthest the works of thoughts and intelligence." Louis Pasteur

1.1 Introduction

Scientists and engineers use several techniques in solving continuum or field problems. Loosely speaking, these techniques can be classified as experimental, analytical, or numerical. Experiments are expensive, time consuming, sometimes hazardous, and usually do not allow much flexibility in parameter variation. However, every numerical method, as we shall see, involves an analytic simplification to the point where it is easy to apply the numerical method. Notwithstanding this fact, the following methods are among the most commonly used in electromagnetics (EM).

A. Analytical methods (exact solutions)

   (1) separation of variables
   (2) series expansion
   (3) conformal mapping
   (4) integral solutions, e.g., Laplace and Fourier transforms
   (5) perturbation methods

B. Numerical methods (approximate solutions)

   (1) finite difference method
   (2) method of weighted residuals
   (3) moment method
   (4) finite element method

(5) transmission-line modeling

(6) Monte Carlo method

(7) method of lines

Application of these methods is not limited to EM-related problems; they find applications in other continuum problems such as in fluid, heat transfer, and acoustics [1].

As we shall see, some of the numerical methods are related and they all generally give approximate solutions of sufficient accuracy for engineering purposes. Since our objective is to study these methods in detail in the subsequent chapters, it may be premature to say more than this at this point.

The need for numerical solution of electromagnetic problems is best expressed in the words of Paris and Hurd: "Most problems that can be solved formally (analytically) have been solved."[1] Until the 1940s, most EM problems were solved using the classical methods of separation of variables and integral equation solutions. Besides the fact that a high degree of ingenuity, experience, and effort were required to apply those methods, only a narrow range of practical problems could be investigated due to the complex geometries defining the problems.

Numerical solution of EM problems started in the mid-1960s with the availability of modern high-speed digital computers. Since then, considerable effort has been expended on solving practical, complex EM-related problems for which closed form analytical solutions are either intractable or do not exist. The numerical approach has the advantage of allowing the actual work to be carried out by operators without a knowledge of higher mathematics or physics, with a resulting economy of labor on the part of the highly trained personnel.

Before we set out to study the various techniques used in analyzing EM problems, it is expedient to remind ourselves of the physical laws governing EM phenomena in general. This will be done in Section 1.2. In Section 1.3, we shall be acquainted with different ways EM problems are categorized. The principle of superposition and uniqueness theorem will be covered in Section 1.4.

1.2 Review of Electromagnetic Theory

The whole subject of EM unfolds as a logical deduction from eight postulated equations, namely, Maxwell's four field equations and four medium-dependent equations [2]–[4]. Before we briefly review these equations, it may be helpful to state two important theorems commonly used in EM. These are the divergence (or Gauss's)

[1] *Basic Electromagnetic Theory,* D.T. Paris and F.K. Hurd, McGraw-Hill, New York, 1969, p. 166.

theorem,

$$\oint_S \mathbf{F} \cdot d\mathbf{S} = \int_v \nabla \cdot \mathbf{F}\, dv \tag{1.1}$$

and Stokes's theorem

$$\oint_L \mathbf{F} \cdot d\mathbf{l} = \int_S \nabla \times \mathbf{F} \cdot d\mathbf{S} \tag{1.2}$$

Perhaps the best way to review EM theory is by using the fundamental concept of electric charge. EM theory can be regarded as the study of fields produced by electric charges at rest and in motion. Electrostatic fields are usually produced by static electric charges, whereas magnetostatic fields are due to motion of electric charges with uniform velocity (direct current). Dynamic or time-varying fields are usually due to accelerated charges or time-varying currents.

1.2.1 Electrostatic Fields

The two fundamental laws governing these electrostatic fields are Gauss's law,

$$\oint \mathbf{D} \cdot d\mathbf{S} = \int \rho_v\, dv \tag{1.3}$$

which is a direct consequence of Coulomb's force law, and the law describing electrostatic fields as conservative,

$$\oint \mathbf{E} \cdot d\mathbf{l} = 0 \tag{1.4}$$

In Eqs. (1.3) and (1.4), $\mathbf{D}$ is the electric flux density (in coulombs/meter^2), ρ_v is the volume charge density (in coulombs/meter^3), and $\mathbf{E}$ is the electric field intensity (in volts/meter). The integral form of the laws in Eqs. (1.3) and (1.4) can be expressed in the differential form by applying Eq. (1.1) to Eq. (1.3) and Eq. (1.2) to Eq. (1.4). We obtain

$$\nabla \cdot \mathbf{D} = \rho_v \tag{1.5}$$

and

$$\nabla \times \mathbf{E} = 0 \tag{1.6}$$

The vector fields $\mathbf{D}$ and $\mathbf{E}$ are related as

$$\mathbf{D} = \epsilon \mathbf{E} \tag{1.7}$$

where ϵ is the dielectric permittivity (in farads/meter) of the medium. In terms of the electric potential V (in volts), $\mathbf{E}$ is expressed as

$$\mathbf{E} = -\nabla V \tag{1.8}$$

or

$$V = -\int \mathbf{E} \cdot d\mathbf{l} \tag{1.9}$$

Combining Eqs. (1.5), (1.7), and (1.8) gives Poisson's equation:

$$\nabla \cdot \epsilon \nabla V = -\rho_v \tag{1.10a}$$

or, if ϵ is constant,

$$\boxed{\nabla^2 V = -\frac{\rho_v}{\epsilon}} \tag{1.10b}$$

When $\rho_v = 0$, Eq. (1.10) becomes Laplace's equation:

$$\nabla \cdot \epsilon \nabla V = 0 \tag{1.11a}$$

or for constant ϵ

$$\boxed{\nabla^2 V = 0} \tag{1.11b}$$

1.2.2 Magnetostatic Fields

The basic laws of magnetostatic fields are Ampere's law

$$\oint_L \mathbf{H} \cdot d\mathbf{l} = \int_S \mathbf{J} \cdot d\mathbf{S} \tag{1.12}$$

which is related to Biot-Savart law, and the law of conservation of magnetic flux (also called Gauss's law for magnetostatics)

$$\oint \mathbf{B} \cdot d\mathbf{S} = 0 \tag{1.13}$$

where $\mathbf{H}$ is the magnetic field intensity (in amperes/meter), $\mathbf{J}_e$ is the electric current density (in amperes/meter^2), and $\mathbf{B}$ is the magnetic flux density (in tesla or webers/meter^2). Applying Eq. (1.2) to Eq. (1.12) and Eq. (1.1) to Eq. (1.13) yields their differential form as

$$\nabla \times \mathbf{H} = \mathbf{J}_e \tag{1.14}$$

and

$$\nabla \cdot \mathbf{B} = 0 \tag{1.15}$$

The vector fields $\mathbf{B}$ and $\mathbf{H}$ are related through the permeability μ (in henries/meter) of the medium as

$$\mathbf{B} = \mu \mathbf{H} \tag{1.16}$$

Also, $\mathbf{J}$ is related to $\mathbf{E}$ through the conductivity σ (in mhos/meter) of the medium as

$$\mathbf{J} = \sigma \mathbf{E} \tag{1.17}$$

This is usually referred to as point form of Ohm's law. In terms of the magnetic vector potential $\mathbf{A}$ (in Wb/meter)

$$\mathbf{B} = \nabla \times \mathbf{A} \tag{1.18}$$

Applying the vector identity

$$\nabla \times (\nabla \times \mathbf{F}) = \nabla(\nabla \cdot \mathbf{F}) - \nabla^2 \mathbf{F} \tag{1.19}$$

to Eqs. (1.14) and (1.18) and assuming Coulomb gauge condition ($\nabla \cdot \mathbf{A} = 0$) leads to Poisson's equation for magnetostatic fields:

$$\boxed{\nabla^2 \mathbf{A} = -\mu \mathbf{J}} \tag{1.20}$$

When $\mathbf{J} = 0$, Eq. (1.20) becomes Laplace's equation

$$\boxed{\nabla^2 \mathbf{A} = 0} \tag{1.21}$$

1.2.3 Time-varying Fields

In this case, electric and magnetic fields exist simultaneously. Equations (1.5) and (1.15) remain the same whereas Eqs. (1.6) and (1.14) require some modification for dynamic fields. Modification of Eq. (1.6) is necessary to incorporate Faraday's law of induction, and that of Eq. (1.14) is warranted to allow for displacement current. The time-varying EM fields are governed by physical laws expressed mathematically as

$$\boxed{\begin{aligned} \nabla \cdot \mathbf{D} &= \rho_v && \text{(1.22a)} \\ \nabla \cdot \mathbf{B} &= 0 && \text{(1.22b)} \\ \nabla \times \mathbf{E} &= -\frac{\partial \mathbf{B}}{\partial t} - \mathbf{J}_m && \text{(1.22c)} \\ \nabla \times \mathbf{H} &= \mathbf{J}_e + \frac{\partial \mathbf{D}}{\partial t} && \text{(1.22d)} \end{aligned}}$$

where $\mathbf{J}_m = \sigma^* \mathbf{H}$ is the magnetic conductive current density (in volts/square meter) and σ^* is the magnetic resistivity (in ohms/meter).

These equations are referred to as Maxwell's equations in the generalized form. They are first-order linear coupled differential equations relating the vector field quan-

tities to each other. The equivalent integral form of Eq. (1.22) is

$$\oint_S \mathbf{D} \cdot d\mathbf{S} = \int_v \rho_v dv \tag{1.23a}$$

$$\oint_S \mathbf{B} \cdot d\mathbf{S} = 0 \tag{1.23b}$$

$$\oint_L \mathbf{E} \cdot d\mathbf{l} = -\int_S \left(\frac{\partial \mathbf{B}}{\partial t} + \mathbf{J}_m \right) \cdot d\mathbf{S} \tag{1.23c}$$

$$\oint_L \mathbf{H} \cdot d\mathbf{l} = \int_S \left(\mathbf{J}_e + \frac{\partial \mathbf{D}}{\partial t} \right) \cdot d\mathbf{S} \tag{1.23d}$$

In addition to these four Maxwell's equations, there are four medium-dependent equations:

$$\boxed{\mathbf{D} = \epsilon \mathbf{E}} \tag{1.24a}$$

$$\mathbf{B} = \mu \mathbf{H} \tag{1.24b}$$

$$\mathbf{J}_e = \sigma \mathbf{E} \tag{1.24c}$$

$$\mathbf{J}_m = \sigma^* \mathbf{M} \tag{1.24d}$$

These are called *constitutive relations* for the medium in which the fields exist. Equations (1.22) and (1.24) form the eight postulated equations on which EM theory unfolds itself. We must note that in the region where Maxwellian fields exist, the fields are assumed to be:

(1) single valued,

(2) bounded, and

(3) continuous functions of space and time with continuous derivatives.

It is worthwhile to mention two other fundamental equations that go hand-in-hand with Maxwell's equations. One is the Lorentz force equation

$$\mathbf{F} = Q(\mathbf{E} + \mathbf{u} \times \mathbf{B}) \tag{1.25}$$

where $\mathbf{F}$ is the force experienced by a particle with charge Q moving at velocity $\mathbf{u}$ in an EM field; the Lorentz force equation constitutes a link between EM and mechanics. The other is the continuity equation

$$\boxed{\nabla \cdot \mathbf{J} = -\frac{\partial \rho_v}{\partial t}} \tag{1.26}$$

which expresses the conservation (or indestructibility) of electric charge. The continuity equation is implicit in Maxwell's equations (see Example 1.2). Equation (1.26) is not peculiar to EM. In fluid mechanics, where $\mathbf{J}$ corresponds with velocity and ρ_v with mass, Eq. (1.26) expresses the law of conservation of mass.

1.2.4 Boundary Conditions

The material medium in which an EM field exists is usually characterized by its constitutive parameters σ, ϵ, and μ. The medium is said to be *linear* if σ, ϵ, and μ are independent of **E** and **H** or nonlinear otherwise. It is *homogeneous* if σ, ϵ, and μ are not functions of space variables or inhomogeneous otherwise. It is *isotropic* if σ, ϵ, and μ are independent of direction (scalars) or anisotropic otherwise.

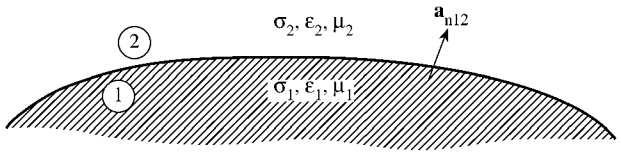

Figure 1.1
Interface between two media.

The boundary conditions at the interface separating two different media 1 and 2, with parameters $(\sigma_1, \epsilon_1, \mu_1)$ and $(\sigma_2, \epsilon_2, \mu_2)$ as shown in Fig. 1.1, are easily derived from the integral form of Maxwell's equations. They are

$$E_{1t} = E_{2t} \text{ or } (\mathbf{E}_1 - \mathbf{E}_2) \times \mathbf{a}_{n12} = 0 \tag{1.27a}$$

$$H_{1t} - H_{21} = K \text{ or } (\mathbf{H}_1 - \mathbf{H}_2) \times \mathbf{a}_{n12} = \mathbf{K} \tag{1.27b}$$

$$D_{1n} - D_{2n} = \rho_S \text{ or } (\mathbf{D}_1 - \mathbf{D}_2) \cdot \mathbf{a}_{n12} = \rho_S \tag{1.27c}$$

$$B_{1n} - B_{2n} = 0 \text{ or } (\mathbf{B}_2 - \mathbf{B}_1) \cdot \mathbf{a}_{n12} = 0 \tag{1.27d}$$

where $\mathbf{a}_{n12}$ is a unit normal vector directed from medium 1 to medium 2, subscripts 1 and 2 denote fields in regions 1 and 2, and subscripts t and n, respectively, denote tangent and normal components of the fields. Equations (1.27a) and (1.27d) state that the tangential components of **E** and the normal components of **B** are continuous across the boundary. Equation (1.27b) states that the tangential component of **H** is discontinuous by the surface current density **K** on the boundary. Equation (1.27c) states that the discontinuity in the normal component of **D** is the same as the surface charge density ρ_s on the boundary.

In practice, only two of Maxwell's equations are used (Eqs. (1.22c) and (1.22d)) when a medium is source-free ($\mathbf{J} = 0$, $\rho_v = 0$), since the other two are implied (see Problem 1.3). Also, in practice, it is sufficient to make the tangential components of the fields satisfy the necessary boundary conditions since the normal components implicitly satisfy their corresponding boundary conditions.

1.2.5 Wave Equations

As mentioned earlier, Maxwell's equations are coupled first-order differential equations which are difficult to apply when solving boundary-value problems. The difficulty is overcome by decoupling the first-order equations, thereby obtaining the wave equation, a second-order differential equation which is useful for solving problems.

To obtain the wave equation for a linear, isotropic, homogeneous, source-free medium ($\rho_v = 0, \mathbf{J} = 0$) from Eq. (1.22), we take the curl of both sides of Eq. (1.22c). This gives

$$\nabla \times \nabla \times \mathbf{E} = -\mu \frac{\partial}{\partial t}(\nabla \times \mathbf{H}) \tag{1.28}$$

From (1.22d),

$$\nabla \times \mathbf{H} = \epsilon \frac{\partial \mathbf{E}}{\partial t}$$

since $\mathbf{J} = 0$, so that Eq. (1.28) becomes

$$\nabla \times \nabla \times \mathbf{E} = -\mu\epsilon \frac{\partial^2 \mathbf{E}}{\partial t^2} \tag{1.29}$$

Applying the vector identity

$$\nabla \times \nabla \times \mathbf{F} = \nabla(\nabla \cdot \mathbf{F}) - \nabla^2 \mathbf{F} \tag{1.30}$$

in Eq. (1.29),

$$\nabla(\nabla \cdot \mathbf{E}) - \nabla^2 \mathbf{E} = -\mu\epsilon \frac{\partial^2 \mathbf{E}}{\partial t^2}$$

Since $\rho_v = 0$, $\nabla \cdot \mathbf{E} = 0$ from Eq. (1.22a), and hence we obtain

$$\boxed{\nabla^2 \mathbf{E} - \mu\epsilon \frac{\partial^2 \mathbf{E}}{\partial t^2} = 0} \tag{1.31}$$

which is the time-dependent vector Helmholtz equation or simply wave equation. If we had started the derivation with Eq. (1.22d), we would obtain the wave equation for $\mathbf{H}$ as

$$\boxed{\nabla^2 \mathbf{H} - \mu\epsilon \frac{\partial^2 \mathbf{H}}{\partial t^2} = 0} \tag{1.32}$$

Equations (1.31) and (1.32) are the equations of motion of EM waves in the medium under consideration. The velocity (in m/s) of wave propagation is

$$u = \frac{1}{\sqrt{\mu\epsilon}} \tag{1.33}$$

where $u = c \approx 3 \times 10^8$ m/s in free space. It should be noted that each of the vector equations in (1.31) and (1.32) has three scalar components, so that altogether we have six scalar equations for E_x, E_y, E_z, H_x, H_y, and H_z. Thus each component of the wave equations has the form

$$\nabla^2 \Psi - \frac{1}{u^2} \frac{\partial^2 \Psi}{\partial t^2} = 0 \tag{1.34}$$

which is the scalar wave equation.

1.2.6 Time-varying Potentials

Although we are often interested in electric and magnetic field intensities (**E** and **H**), which are physically measurable quantities, it is often convenient to use auxiliary functions in analyzing an EM field. These auxiliary functions are the scalar electric potential V and vector magnetic potential **A**. Although these potential functions are arbitrary, they are required to satisfy Maxwell's equations. Their derivation is based on two fundamental vector identities (see Prob. 1.1),

$$\nabla \times \nabla \Phi = 0 \tag{1.35}$$

and

$$\nabla \cdot \nabla \times \mathbf{F} = 0 \tag{1.36}$$

which an arbitrary scalar field Φ and vector field **F** must satisfy. Maxwell's equation (1.22b) along with Eq. (1.36) is satisfied if we define **A** such that

$$\boxed{\mathbf{B} = \nabla \times \mathbf{A}} \tag{1.37}$$

Substituting this into Eq. (1.22c) gives

$$-\nabla \times \left(\mathbf{E} + \frac{\partial \mathbf{A}}{\partial t} \right) = 0$$

Since this equation has to be compatible with Eq. (1.35), we can choose the scalar field V such that

$$\mathbf{E} + \frac{\partial \mathbf{A}}{\partial t} = -\nabla V$$

or

$$\boxed{\mathbf{E} = -\nabla V - \frac{\partial \mathbf{A}}{\partial t}} \tag{1.38}$$

Thus, if we knew the potential functions V and **A**, the fields **E** and **B** could be obtained from Eqs. (1.37) and (1.38). However, we still need to find the solution for the potential functions. Substituting Eqs. (1.37) and (1.38) into Eq. (1.22d) and assuming a linear, homogeneous medium,

$$\nabla \times \nabla \times \mathbf{A} = \mu \mathbf{J} + \epsilon \mu \frac{\partial}{\partial t} \left(-\nabla V - \frac{\partial \mathbf{A}}{\partial t} \right)$$

Applying the vector identity in Eq. (1.30) leads to

$$\nabla^2 \mathbf{A} - \nabla(\nabla \cdot \mathbf{A}) = -\mu \mathbf{J} + \mu \epsilon \nabla \frac{\partial^2 \mathbf{A}}{\partial t^2} + \mu \epsilon \nabla \frac{\partial V}{\partial t} \tag{1.39}$$

Substituting Eq. (1.38) into Eq. (1.22a) gives

$$\nabla \cdot \mathbf{E} = \frac{\rho}{\epsilon} = -\nabla^2 V - \frac{\partial (\nabla \cdot \mathbf{A})}{\partial t}$$

or

$$\nabla^2 V + \frac{\partial}{\partial t}\nabla \cdot \mathbf{A} = -\frac{\rho_v}{\epsilon} \tag{1.40}$$

According to the Helmholtz theorem of vector analysis, a vector is uniquely defined if and only if both its curl and divergence are specified. We have only specified the curl of **A** in Eq. (1.37); we may choose the divergence of **A** so that the differential equations (1.39) and (1.40) have the simplest forms possible. We achieve this in the so-called *Lorentz condition:*

$$\nabla \cdot \mathbf{A} = -\mu\epsilon\frac{\partial V}{\partial t} \tag{1.41}$$

Incorporating this condition into Eqs. (1.39) and (1.40) results in

$$\boxed{\nabla^2 \mathbf{A} - \mu\epsilon\frac{\partial^2 \mathbf{A}}{\partial t^2} = -\mu\mathbf{J}} \tag{1.42}$$

and

$$\boxed{\nabla^2 V - \mu\epsilon\frac{\partial^2 V}{\partial t^2} = -\frac{\rho_v}{\epsilon}} \tag{1.43}$$

which are inhomogeneous wave equations. Thus Maxwell's equations in terms of the potentials V and **A** reduce to the three equations (1.41) to (1.43). In other words, the three equations are equivalent to the ordinary form of Maxwell's equations in that potentials satisfying these equations always lead to a solution of Maxwell's equations for **E** and **B** when used with Eqs. (1.37) and (1.38). Integral solutions to Eqs. (1.42) and (1.43) are the so-called *retarded* potentials

$$\mathbf{A} = \int \frac{\mu[\mathbf{J}]\, dv}{4\pi R} \tag{1.44}$$

and

$$V = \int \frac{[\rho_v]\, dv}{4\pi\epsilon R} \tag{1.45}$$

where R is the distance from the source point to the field point, and the square brackets denote ρ_v and **J** are specified at a time $R(\mu\epsilon)^{1/2}$ earlier than for which **A** or V is being determined.

1.2.7 Time-harmonic Fields

Up to this point, we have considered the general case of arbitrary time variation of EM fields. In many practical situations, especially at low frequencies, it is sufficient to deal with only the steady-state (or equilibrium) solution of EM fields when produced

by sinusoidal currents. Such fields are said to be sinusoidal time-varying or time-harmonic, that is, they vary at a sinusoidal frequency ω. An arbitrary time-dependent field $\mathbf{F}(x, y, z, t)$ or $\mathbf{F}(\mathbf{r}, t)$ can be expressed as

$$\boxed{\mathbf{F}(\mathbf{r}, t) = \text{Re}\left[\mathbf{F}_s(\mathbf{r})e^{j\omega t}\right]} \tag{1.46}$$

where $\mathbf{F}_s(\mathbf{r}) = \mathbf{F}_s(x, y, z)$ is the phasor form of $\mathbf{F}(\mathbf{r}, t)$ and is in general complex, Re[] indicates "taking the real part of" quantity in brackets, and ω is the angular frequency (in rad/s) of the sinusoidal excitation. The EM field quantities can be represented in phasor notation as

$$\begin{bmatrix} \mathbf{E}(\mathbf{r}, t) \\ \mathbf{D}(\mathbf{r}, t) \\ \mathbf{H}(\mathbf{r}, t) \\ \mathbf{B}(\mathbf{r}, t) \end{bmatrix} = \begin{bmatrix} \mathbf{E}_s(\mathbf{r}) \\ \mathbf{D}_s(\mathbf{r}) \\ \mathbf{H}_s(\mathbf{r}) \\ \mathbf{B}_s(\mathbf{r}) \end{bmatrix} e^{j\omega t} \tag{1.47}$$

Using the phasor representation allows us to replace the time derivations $\partial/\partial t$ by $j\omega$ since

$$\frac{\partial e^{j\omega t}}{\partial t} = j\omega e^{j\omega t}$$

Thus Maxwell's equations, in sinusoidal steady state, become

$$\boxed{\begin{aligned} \nabla \cdot \mathbf{D}_s &= \rho_{vs} && \text{(1.48a)} \\ \nabla \cdot \mathbf{B}_s &= 0 && \text{(1.48b)} \\ \nabla \times \mathbf{E}_s &= -j\omega \mathbf{B}_s - \mathbf{J}_{ms} && \text{(1.48c)} \\ \nabla \times \mathbf{H}_s &= \mathbf{J}_{es} + j\omega \mathbf{D}_s && \text{(1.48d)} \end{aligned}}$$

We should observe that the effect of the time-harmonic assumption is to eliminate the time dependence from Maxwell's equations, thereby reducing the time-space dependence to space dependence only. This simplification does not exclude more general time-varying fields if we consider ω to be one element of an entire frequency spectrum, with all the Fourier components superposed. In other words, a nonsinusoidal field can be represented as

$$\mathbf{F}(\mathbf{r}, t) = \text{Re}\left[\int_{-\infty}^{\infty} \mathbf{F}_s(\mathbf{r}, \omega)e^{j\omega t} d\omega\right] \tag{1.49}$$

Thus the solutions to Maxwell's equations for a nonsinusoidal field can be obtained by summing all the Fourier components $\mathbf{F}_s(\mathbf{r}, \omega)$ over ω. Henceforth, we drop the subscript s denoting phasor quantity when no confusion results.

Replacing the time derivative in Eq. (1.34) by $(j\omega)^2$ yields the scalar wave equation in phasor representation as

$$\nabla^2 \Psi + k^2 \Psi = 0 \tag{1.50}$$

where k is the propagation constant (in *rad/m*), given by

$$k = \frac{\omega}{u} = \frac{2\pi f}{u} = \frac{2\pi}{\lambda} \tag{1.51}$$

We recall that Eqs. (1.31) to (1.34) were obtained assuming that $\rho_v = 0 = \mathbf{J}$. If $\rho_v \neq 0 \neq \mathbf{J}$, Eq. (1.50) will have the general form (see Prob. 1.4)

$$\boxed{\nabla^2\Psi + k^2\Psi = g} \tag{1.52}$$

We notice that this Helmholtz equation reduces to:

(1) Poisson's equation

$$\nabla^2\Psi = g \tag{1.53}$$

when $k = 0$ (i.e., $\omega = 0$ for static case).

(2) Laplace's equation

$$\nabla^2\Psi = 0 \tag{1.54}$$

when $k = 0 = g$.

Thus Poisson's and Laplace's equations are special cases of the Helmholtz equation. Note that function Ψ is said to be *harmonic* if it satisfies Laplace's equation.

Example 1.1

From the divergence theorem, derive Green's theorem

$$\int_v \left(U\nabla^2 V - V\nabla^2 U\right) dv = \oint_S \left(U\frac{\partial V}{\partial n} - V\frac{\partial U}{\partial n}\right) \cdot d\mathbf{S}$$

where $\frac{\partial \Phi}{\partial n} = \nabla\Phi \cdot \mathbf{a}_n$ is the directional derivation of Φ along the outward normal to S. □

Solution

In Eq. (1.1), let $\mathbf{F} = U\nabla V$, then

$$\int_v \nabla \cdot (U\nabla V)\, dv = \oint_S U\nabla V \cdot d\mathbf{S} \tag{1.55}$$

But

$$\begin{aligned} \nabla \cdot (U\nabla V) &= U\nabla \cdot \nabla V + \nabla V \cdot \nabla U \\ &= U\nabla^2 V + \nabla U \cdot \nabla V \end{aligned}$$

Substituting this into Eq. (1.55) gives *Green's first identity:*

$$\int_v \left(U\nabla^2 V + \nabla U \cdot \nabla V\right) dv = \oint_S U\nabla V \cdot d\mathbf{S} \tag{1.56}$$

By interchanging U and V in Eq. (1.56), we obtain

$$\int_v \left(V\nabla^2 U + \nabla V \cdot \nabla U\right) dv = \oint_S V\nabla U \cdot d\mathbf{S} \tag{1.57}$$

Subtracting Eq. (1.57) from Eq. (1.56) leads to *Green's second identity* or Green's theorem:

$$\int_v \left(U\nabla^2 V - V\nabla^2 U\right) dv = \oint_S (U\nabla V - V\nabla U) \cdot d\mathbf{S} \quad \blacksquare$$

Example 1.2

Show that the continuity equation is implicit (or incorporated) in Maxwell's equations. □

Solution

According to Eq. (1.36), the divergence of the curl of any vector field is zero. Hence, taking the divergence of Eq. (1.22d) gives

$$0 = \nabla \cdot \nabla \times \mathbf{H} = \nabla \cdot \mathbf{J} + \frac{\partial}{\partial t} \nabla \cdot \mathbf{D}$$

But $\nabla \cdot \mathbf{D} = \rho_v$ from Eq. (1.22a). Thus,

$$0 = \nabla \cdot \mathbf{J} + \frac{\partial \rho_v}{\partial t}$$

which is the continuity equation. ■

Example 1.3

Express:

(a) $\mathbf{E} = 10\sin(\omega t - kz)\mathbf{a}_x + 20\cos(\omega t - kz)\mathbf{a}_y$ in phasor form.

(b) $\mathbf{H}_s = (4 - j3)\sin x\mathbf{a}_x + \frac{e^{j10^\circ}}{x}\mathbf{a}_z$ in instantaneous form. □

Solution

(a) We can express $\sin\theta$ as $\cos(\theta - \pi/2)$. Hence,

$$\begin{aligned}
\mathbf{E} &= 10\cos(\omega t - kz - \pi/2)\mathbf{a}_x + 20\cos(\omega t - kz)\mathbf{a}_y \\
&= \text{Re}\left[\left(10e^{-jkz}e^{-j\pi/2}\mathbf{a}_x + 20e^{-jkz}\mathbf{a}_y\right)e^{j\omega t}\right] \\
&= \text{Re}\left[\mathbf{E}_s e^{j\omega t}\right]
\end{aligned}$$

Thus,

$$\begin{aligned}\mathbf{E}_s &= 10e^{-jkz}e^{-j\pi/2}\mathbf{a}_x + 20e^{-jkz}\mathbf{a}_y \\ &= \left(-j10\mathbf{a}_x + 20\mathbf{a}_y\right)e^{-jkz}\end{aligned}$$

(b) Since

$$\begin{aligned}\mathbf{H} &= \text{Re}\left[\mathbf{H}_s e^{j\omega t}\right] \\ &= \text{Re}\left[5\sin x e^{j(\omega t - 36.87^\circ)}\mathbf{a}_x + \frac{1}{x}e^{j(\omega t + 10^\circ)}\mathbf{a}_z\right] \\ &= \left[5\sin x\cos(\omega t - 36.87^\circ)\mathbf{a}_x + \frac{1}{x}\cos(\omega t + 10^\circ)\mathbf{a}_z\right] \quad \blacksquare\end{aligned}$$

1.3 Classification of EM Problems

Classifying EM problems will help us later to answer the question of what method is best for solving a given problem. Continuum problems are categorized differently depending on the particular item of interest, which could be one of these:

(1) the solution region of the problem,

(2) the nature of the equation describing the problem, or

(3) the associated boundary conditions.

(In fact, the above three items define a problem uniquely.) It will soon become evident that these classifications are sometimes not independent of each other.

1.3.1 Classification of Solution Regions

In terms of the solution region or problem domain, the problem could be an interior problem, also variably called an inner, closed, or bounded problem, or an exterior problem, also variably called an outer, open, or unbounded problem.

Consider the solution region R with boundary S, as shown in Fig. 1.2. If part or all of S is at infinity, R is exterior/open, otherwise R is interior/closed. For example, wave propagation in a waveguide is an interior problem, whereas while wave propagation in free space — scattering of EM waves by raindrops, and radiation from a dipole antenna — are exterior problems.

A problem can also be classified in terms of the electrical, constitutive properties (σ, ϵ, μ) of the solution region. As mentioned in Section 1.2.4, the solution region could be linear (or nonlinear), homogeneous (or inhomogeneous), and isotropic (or anisotropic). We shall be concerned, for the most part, with linear, homogeneous, isotropic media in this text.

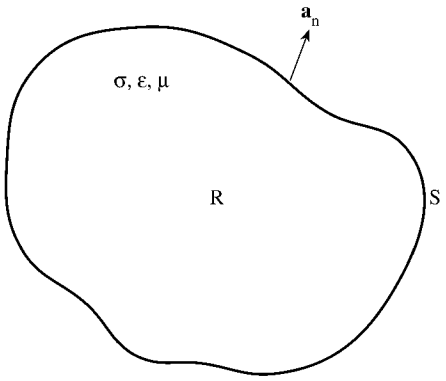

Figure 1.2
Solution region R with boundary S.

1.3.2 Classification of Differential Equations

EM problems are classified in terms of the equations describing them. The equations could be differential or integral or both. Most EM problems can be stated in terms of an operator equation

$$\boxed{L\Phi = g} \tag{1.58}$$

where L is an operator (differential, integral, or integro-differential), g is the known excitation or source, and Φ is the unknown function to be determined. A typical example is the electrostatic problem involving Poisson's equation. In differential form, Eq. (1.58) becomes

$$-\nabla^2 V = \frac{\rho_v}{\epsilon} \tag{1.59}$$

so that $L = -\nabla^2$ is the Laplacian operator, $g = \rho_v/\epsilon$ is the source term, and $\Phi = V$ is the electric potential. In integral form, Poisson's equation is of the form

$$V = \int \frac{\rho_v dv}{4\pi\epsilon r^2} \tag{1.60}$$

so that

$$L = \int \frac{dv}{4\pi r^2}, \quad g = V, \quad \text{and} \quad \Phi = \rho_v/\epsilon$$

In this section, we shall limit our discussion to differential equations; integral equations will be considered in detail in Chapter 5.

As observed in Eqs. (1.52) to (1.54), EM problems involve linear, second-order differential equations. In general, a second-order partial differential equation (PDE) is given by

$$a\frac{\partial^2\Phi}{\partial x^2} + b\frac{\partial^2\Phi}{\partial x\partial y} + c\frac{\partial^2\Phi}{\partial y^2} + d\frac{\partial\Phi}{\partial x} + e\frac{\partial\Phi}{\partial y} + f\Phi = g$$

or simply

$$\boxed{a\Phi_{xx} + b\Phi_{xy} + c\Phi_{yy} + d\Phi_x + e\Phi_y + f\Phi = g} \tag{1.61}$$

The coefficients, a, b and c in general are functions of x and y; they may also depend on Φ itself, in which case the PDE is said to be *nonlinear*. A PDE in which $g(x, y)$ in Eq. (1.61) equals zero is termed *homogeneous;* it is *inhomogeneous* if $g(x, y) \neq 0$. Notice that Eq. (1.61) has the same form as Eq. (1.58), where L is now a differential operator given by

$$L = a\frac{\partial^2}{\partial x^2} + b\frac{\partial^2}{\partial x \partial y} + c\frac{\partial^2}{\partial y^2} + d\frac{\partial}{\partial x} + e\frac{\partial}{\partial y} + f \tag{1.62}$$

A PDE in general can have both boundary values and initial values. PDEs whose boundary conditions are specified are called *steady-state equations*. If only initial values are specified, they are called *transient equations*.

Any linear second-order PDE can be classified as elliptic, hyperbolic, or parabolic depending on the coefficients a, b, and c. Equation (1.61) is said to be:

$$\boxed{\begin{aligned} \text{elliptic if} \quad & b^2 - 4ac < 0 \\ \text{hyperbolic if} \quad & b^2 - 4ac > 0 \\ \text{parabolic if} \quad & b^2 - 4ac = 0 \end{aligned}} \tag{1.63}$$

The terms *hyperbolic, parabolic,* and *elliptic* are derived from the fact that the quadratic equation

$$ax^2 + bxy + cy^2 + dx + ey + f = 0$$

represents a hyperbola, parabola, or ellipse if $b^2 - 4ac$ is positive, zero, or negative, respectively. In each of these categories, there are PDEs that model certain physical phenomena. Such phenomena are not limited to EM but extend to almost all areas of science and engineering. Thus the mathematical model specified in Eq. (1.61) arises in problems involving heat transfer, boundary-layer flow, vibrations, elasticity, electrostatic, wave propagation, and so on.

Elliptic PDEs are associated with steady-state phenomena, i.e., boundary-value problems. Typical examples of this type of PDE include Laplace's equation

$$\frac{\partial^2 \Phi}{\partial x^2} + \frac{\partial^2 \Phi}{\partial y^2} = 0 \tag{1.64}$$

and Poisson's equation

$$\frac{\partial^2 \Phi}{\partial x^2} + \frac{\partial^2 \Phi}{\partial y^2} = g(x, y) \tag{1.65}$$

where in both cases $a = c = 1, b = 0$. An elliptic PDE usually models an interior problem, and hence the solution region is usually closed or bounded as in Fig. 1.3 (a).

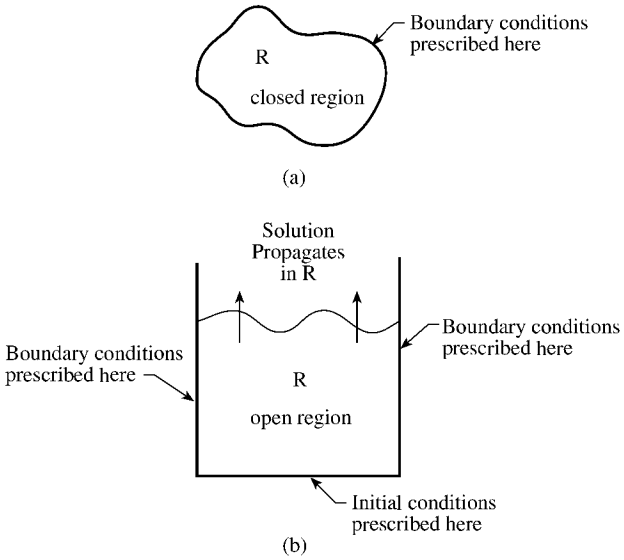

Figure 1.3
(a) Elliptic, (b) parabolic, or hyperbolic problem.

Hyperbolic PDEs arise in propagation problems. The solution region is usually open so that a solution advances outward indefinitely from initial conditions while always satisfying specified boundary conditions. A typical example of hyperbolic PDE is the wave equation in one dimension

$$\frac{\partial^2 \Phi}{\partial x^2} = \frac{1}{u^2} \frac{\partial^2 \Phi}{\partial t^2} \tag{1.66}$$

where $a = u^2, b = 0, c = -1$. Notice that the wave equation in (1.50) is not hyperbolic but elliptic, since the time-dependence has been suppressed and the equation is merely the steady-state solution of Eq. (1.34).

Parabolic PDEs are generally associated with problems in which the quantity of interest varies slowly in comparison with the random motions which produce the variations. The most common parabolic PDE is the diffusion (or heat) equation in one dimension

$$\frac{\partial^2 \Phi}{\partial x^2} = k \frac{\partial \Phi}{\partial t} \tag{1.67}$$

where $a = 1, b = 0 = c$. Like hyperbolic PDE, the solution region for parabolic PDE is usually open, as in Fig. 1.3 (b). The initial and boundary conditions typically associated with parabolic equations resemble those for hyperbolic problems except that only one initial condition at $t = 0$ is necessary since Eq. (1.67) is only first order in time. Also, parabolic and hyperbolic equations are solved using similar techniques, whereas elliptic equations are usually more difficult and require different techniques.

Note that: (1) since the coefficients a, b, and c are in general functions of x and y, the classification of Eq. (1.61) may change from point to point in the solution region, and (2) PDEs with more than two independent variables ($x, y, z, t, \ldots$) may not fit as neatly into the classification above. A summary of our discussion so far in this section is shown in Table 1.1.

Table 1.1 Classification of Partial Differential Equations

Type	Sign of $b^2 - 4ac$	Example	Solution region
Elliptic	$-$	Laplace's equation: $\Phi_{xx} + \Phi_{yy} = 0$	Closed
Hyperbolic	$+$	Wave equation: $u^2\Phi_{xx} = \Phi_{tt}$	Open
Parabolic	0	Diffusion equation: $\Phi_{xx} = k\Phi_t$	Open

The type of problem represented by Eq. (1.58) is said to be *deterministic*, since the quantity of interest can be determined directly. Another type of problem where the quantity is found indirectly is called *nondeterministic* or *eigenvalue*. The *standard eigenproblem* is of the form

$$L\Phi = \lambda\Phi \tag{1.68}$$

where the source term in Eq. (1.58) has been replaced by $\lambda\Phi$. A more general version is the *generalized eigenproblem* having the form

$$\boxed{L\Phi = \lambda M\Phi} \tag{1.69}$$

where M, like L, is a linear operator for EM problems. In Eqs. (1.68) and (1.69), only some particular values of λ called *eigenvalues* are permissible; associated with these values are the corresponding solutions Φ called *eigenfunctions*. Eigenproblems are usually encountered in vibration and waveguide problems where the eigenvalues λ correspond to physical quantities such as resonance and cutoff frequencies, respectively.

1.3.3 Classification of Boundary Conditions

Our problem consists of finding the unknown function Φ of a partial differential equation. In addition to the fact that Φ satisfies Eq. (1.58) within a prescribed solution region R, Φ must satisfy certain conditions on S, the boundary of R. Usually these boundary conditions are of the Dirichlet and Neumann types. Where a boundary has both, a mixed boundary condition is said to exist.

(1) Dirichlet boundary condition:

$$\Phi(\mathbf{r}) = 0, \qquad \mathbf{r} \quad \text{on S} \tag{1.70}$$

(2) Neumann boundary condition:

$$\frac{\partial \Phi(\mathbf{r})}{\partial n} = 0, \qquad \mathbf{r} \quad \text{on S}, \tag{1.71}$$

i.e., the normal derivative of Φ vanishes on S.

(3) Mixed boundary condition:

$$\frac{\partial \Phi(\mathbf{r})}{\partial n} + h(\mathbf{r})\Phi(\mathbf{r}) = 0, \qquad \mathbf{r} \quad \text{on S}, \tag{1.72}$$

where $h(\mathbf{r})$ is a known function and $\frac{\partial \Phi}{\partial n}$ is the directional derivative of Φ along the outward normal to the boundary S, i.e.,

$$\frac{\partial \Phi}{\partial n} = \nabla \Phi \cdot \mathbf{a}_n \tag{1.73}$$

where $\mathbf{a}_n$ is a unit normal directed out of R, as shown in Fig. 1.2. Note that the Neumann boundary condition is a special case of the mixed condition with $h(\mathbf{r}) = 0$.

The conditions in Eq. (1.70) to (1.72) are called *homogeneous boundary conditions*. The more general ones are the inhomogeneous:

Dirichlet:

$$\Phi(\mathbf{r}) = p(\mathbf{r}), \qquad \mathbf{r} \quad \text{on S} \tag{1.74}$$

Neumann:

$$\frac{\partial \Phi(\mathbf{r})}{\partial n} = q(\mathbf{r}), \quad \mathbf{r} \text{ on } \mathbf{S} \tag{1.75}$$

Mixed:

$$\frac{\partial \Phi(\mathbf{r})}{\partial n} + h(\mathbf{r})\Phi(\mathbf{r}) = w(\mathbf{r}), \quad \mathbf{r} \text{ on } \mathbf{S} \tag{1.76}$$

where $p(\mathbf{r})$, $q(\mathbf{r})$, and $w(\mathbf{r})$ are explicitly known functions on the boundary S. For example, $\Phi(0) = 1$ is an inhomogeneous Dirichlet boundary condition, and the associated homogeneous counterpart is $\Phi(0) = 0$. Also $\Phi'(1) = 2$ and $\Phi'(1) = 0$ are, respectively, inhomogeneous and homogeneous Neumann boundary conditions. In electrostatics, for example, if the value of electric potential is specified on S, we have Dirichlet boundary condition, whereas if the surface charge ($\rho_s = D_n = \epsilon \frac{\partial V}{\partial n}$) is specified, the boundary condition is Neumann. The problem of finding a function Φ that is harmonic in a region is called *Dirichlet problem* (or *Neumann problem*) if Φ (or $\frac{\partial \Phi}{\partial n}$) is prescribed on the boundary of the region.

It is worth observing that the term "homogeneous" has been used to mean different things. The solution region could be homogeneous meaning that σ, ϵ, and μ are constant within R; the PDE could be homogeneous if $g = 0$ so that $L\Phi = 0$; and the boundary conditions are homogeneous when $p(\mathbf{r}) = q(\mathbf{r}) = w(\mathbf{r}) = 0$.

Example 1.4

Classify these equations as elliptic, hyperbolic, or parabolic:

(a) $4\Phi_{xx} + 2\Phi_x + \Phi_y + x + y = 0$

(b) $e^x \dfrac{\partial^2 V}{\partial x^2} + \cos y \dfrac{\partial^2 V}{\partial x \partial y} - \dfrac{\partial^2 V}{\partial y^2} = 0$.

State whether the equations are homogeneous or inhomogeneous. □

Solution

(a) In this PDE, $a = 4, b = 0 = c$. Hence

$$b^2 - 4ac = 0 ,$$

i.e., the PDE is parabolic. Since $g = -x - y$, the PDE is inhomogeneous.

(b) For this PDE, $a = e^x, b = \cos y, c = -1$. Hence

$$b^2 - 4ac = \cos^2 y + 4e^x > 0$$

and the PDE is hyperbolic. Since $g = 0$, the PDE is homogeneous. ■

1.4 Some Important Theorems

Two theorems are of fundamental importance in solving EM problems. These are the principle of superposition and the uniqueness theorem.

1.4.1 Superposition Principle

The principle of superposition is applied in several ways. We shall consider two of these.

If each member of a set of functions $\Phi_n, n = 1, 2, \ldots, N$, is a solution to the PDE $L\Phi = 0$ with some prescribed boundary conditions, then a linear combination

$$\Phi_N = \Phi_0 + \sum_{n=1}^{N} a_n \Phi_n \tag{1.77}$$

also satisfies $L\Phi = g$.

Given a problem described by the PDE

$$L\Phi = g \tag{1.78}$$

subject to the boundary conditions

$$\begin{aligned} M_1(s) &= h_1 \\ M_2(s) &= h_2 \\ &\vdots \\ M_N(s) &= h_N \ , \end{aligned} \tag{1.79}$$

as long as L is linear, we may divide the problem into a series of problems as follows:

$$\begin{array}{lll} L\Phi_0 = g & L\Phi_1 = 0 & \cdots \quad L\Phi_N = 0 \\ M_1(s) = 0 & M_1(s) = h_1 & \cdots \quad M_1(s) = 0 \\ M_2(s) = 0 & M_2(s) = 0 & \cdots \quad M_2(s) = 0 \\ \vdots & \vdots & \qquad \vdots \\ M_N(s) = 0 & M_N(s) = 0 & \cdots \quad M_N(s) = h_N \end{array} \tag{1.80}$$

where $\Phi_0, \Phi_1, \ldots, \Phi_N$ are the solutions to the reduced problems, which are easier to solve than the original problem. The solution to the original problem is given by

$$\Phi = \sum_{n=0}^{N} \Phi_n \tag{1.81}$$

1.4.2 Uniqueness Theorem

This theorem guarantees that the solution obtained for a PDE with some prescribed boundary conditions is the only one possible. For EM problems, the theorem may be stated as follows: If in any way a set of fields $(\mathbf{E}, \mathbf{H})$ is found which satisfies simultaneously Maxwell's equations and the prescribed boundary conditions, this set is unique. Therefore, a field is uniquely specified by the sources $(\rho_v, \mathbf{J})$ within the medium plus the tangential components of $\mathbf{E}$ or $\mathbf{H}$ over the boundary.

To prove the uniqueness theorem, suppose there exist two solutions (with subscripts 1 and 2) that satisfy Maxwell's equations

$$\nabla \cdot \epsilon \mathbf{E}_{1,2} = \rho_v \tag{1.82a}$$

$$\nabla \cdot \mathbf{H}_{1,2} = 0 \tag{1.82b}$$

$$\nabla \times \mathbf{E}_{1,2} = -\mu \frac{\partial \mathbf{H}_{1,2}}{\partial t} \tag{1.82c}$$

$$\nabla \times \mathbf{H}_{1,2} = \mathbf{J} + \sigma \mathbf{E}_{1,2} + \epsilon \frac{\partial \mathbf{E}_{1,2}}{\partial t} \tag{1.82d}$$

If we denote the difference of the two fields as $\Delta\mathbf{E} = \mathbf{E}_2 - \mathbf{E}_1$ and $\Delta\mathbf{H} = \mathbf{H}_2 - \mathbf{H}_1$,

$\Delta\mathbf{E}$ and $\Delta\mathbf{H}$ must satisfy the source-free Maxwell's equations, i.e.,

$$\nabla \cdot \epsilon \Delta\mathbf{E} = 0 \tag{1.83a}$$

$$\nabla \cdot \Delta\mathbf{H} = 0 \tag{1.83b}$$

$$\nabla \times \Delta\mathbf{E} = -\mu \frac{\partial \Delta\mathbf{H}}{\partial t} \tag{1.83c}$$

$$\nabla \times \Delta\mathbf{H} = \sigma \Delta\mathbf{E} + \epsilon \frac{\partial \Delta\mathbf{E}}{\partial t} \tag{1.83d}$$

Dotting both sides of Eq. (1.83d) with $\Delta\mathbf{E}$ gives

$$\Delta\mathbf{E} \cdot \nabla \times \Delta\mathbf{H} = \sigma |\Delta\mathbf{E}|^2 + \epsilon \nabla\mathbf{E} \cdot \frac{\partial \Delta\mathbf{E}}{\partial t} \tag{1.84}$$

Using the vector identity

$$\mathbf{A} \cdot (\nabla \times \mathbf{B}) = \mathbf{B} \cdot (\nabla \times \mathbf{A}) - \nabla \cdot (\mathbf{A} \times \mathbf{B})$$

and Eq. (1.83c), Eq. (1.84) becomes

$$\nabla \cdot (\Delta\mathbf{E} \times \Delta\mathbf{H}) = -\frac{1}{2}\frac{\partial}{\partial t}\left(\mu |\Delta\mathbf{H}|^2 + \epsilon |\Delta\mathbf{E}|^2\right) - \sigma |\Delta\mathbf{E}|^2$$

Integrating over volume v bounded by surface $\mathbf{S}$ and applying divergence theorem to the left-hand side, we obtain

$$\oint_S (\Delta\mathbf{E} \times \Delta\mathbf{H}) \cdot d\mathbf{S} = -\frac{\partial}{\partial t}\int_v \left[\frac{1}{2}\epsilon |\Delta\mathbf{E}|^2 + \frac{1}{2}\mu |\Delta\mathbf{H}|^2\right] dv - \int_v \sigma |\Delta\mathbf{E}|\, dv \tag{1.85}$$

showing that $\Delta\mathbf{E}$ and $\Delta\mathbf{H}$ satisfy the Poynting theorem just as $\mathbf{E}_{1,2}$ and $\mathbf{H}_{1,2}$. Only the tangential components of $\Delta\mathbf{E}$ and $\Delta\mathbf{H}$ contribute to the surface integral on the left side of Eq. (1.85). Therefore, if the tangential components of $\mathbf{E}_1$ and $\mathbf{E}_2$ or $\mathbf{H}_1$ and $\mathbf{H}_2$ are equal over $\mathbf{S}$ (thereby satisfying Eq. (1.27)), the tangential components of $\Delta\mathbf{E}$ and $\Delta\mathbf{H}$ vanish on $\mathbf{S}$. Consequently, the surface integral in Eq. (1.85) is identically zero, and hence the right side of the equation must vanish also. It follows that $\Delta\mathbf{E} = 0$ due to the second integral on the right side and hence also $\Delta\mathbf{H} = 0$ throughout the volume. Thus $\mathbf{E}_1 = \mathbf{E}_2$ and $\mathbf{H}_1 = \mathbf{H}_2$, confirming that the solution is unique.

The theorem just proved for time-varying fields also holds for static fields as a special case. In terms of electrostatic potential V, the uniqueness theorem may be stated as follows: A solution to $\nabla^2 V = 0$ is uniquely determined by specifying either the value of V or the normal component of ∇V at each point on the boundary surface. For a magnetostatic field, the theorem becomes: A solution of $\nabla^2 \mathbf{A} = 0$ (and $\nabla \cdot \mathbf{A} = 0$) is uniquely determined by specifying the value of $\mathbf{A}$ or the tangential component of $\mathbf{B} = (\nabla \times \mathbf{A})$ at each point on the boundary surface.

References

[1] K.H. Huebner and E.A. Thornton, *The Finite Element Method for Engineers*. New York: John Wiley and Sons, 1982, Chap. 3, pp. 62–107.

[2] J.A. Kong, *Electromagnetic Wave Theory*. New York: John Wiley and Sons, 1986, Chap. 1, pp. 1–41.

[3] R.E. Collins, *Foundations of Microwave Engineering*. New York: McGraw-Hill, 1966, Chap. 2, pp. 11–63.

[4] M.N.O. Sadiku, *Elements of Electromagnetics*. New York: Oxford Univ. Press, 1994, Chap. 9, pp. 409–452.

Problems

1.1 In a coordinate system of your choice, prove that:

(a) $\nabla \times \nabla \Phi = 0$,

(b) $\nabla \cdot \nabla \times \mathbf{F} = 0$,

(c) $\nabla \times \nabla \times \mathbf{F} = \nabla(\nabla \cdot \mathbf{F}) - \nabla^2 \mathbf{F}$,

where Φ and $\mathbf{F}$ are scalar and vector fields, respectively.

1.2 If U and V are scalar fields, show that

$$\oint_L U \nabla V \cdot d\mathbf{l} = -\oint_L V \nabla U \cdot d\mathbf{l}$$

1.3 Show that in a source-free region ($\mathbf{J} = 0$, $\rho_v = 0$), Maxwell's equations can be reduced to the two curl equations.

1.4 In deriving the wave equations (1.31) and (1.32), we assumed a source-free medium ($\mathbf{J} = 0$, $\rho_v = 0$). Show that if $\rho_v \neq 0$, $\mathbf{J} \neq 0$, the equations become

$$\nabla^2 \mathbf{E} - \frac{1}{c^2} \frac{\partial^2 \mathbf{E}}{\partial t^2} = \nabla(\rho_v/\epsilon) + \mu \frac{\partial \mathbf{J}}{\partial t},$$

$$\nabla^2 \mathbf{H} - \frac{1}{c^2} \frac{\partial^2 \mathbf{H}}{\partial t^2} = -\nabla \times \mathbf{J}$$

What assumptions have you made to arrive at these expressions?

1.5 Determine whether the fields

$$\mathbf{E} = 20\sin(\omega t - kz)\mathbf{a}_x - 10\cos(\omega t + kz)\mathbf{a}_y$$
$$\mathbf{H} = \frac{k}{\omega\mu_o}\left[-10\cos(\omega t + kz)\mathbf{a}_x + 20\sin(\omega t - kz)\mathbf{a}_y\right] ,$$

where $k = \omega\sqrt{\mu_o\epsilon_o}$, satisfy Maxwell's equations.

1.6 In free space, the electric flux density is given by

$$\mathbf{D} = D_0\cos(\omega t + \beta z)\mathbf{a}_x$$

Use Maxwell's equation to find $\mathbf{H}$.

1.7 In free space, a source radiates the magnetic field

$$\mathbf{H}_s = H_0\frac{e^{-j\beta\rho}}{\sqrt{\rho}}\mathbf{a}_\phi$$

where $\beta = \omega\sqrt{\mu_0\epsilon_0}$. Determine $\mathbf{E}_s$.

1.8 An electric dipole of length L in free space has a radical field given in spherical system (r, θ, ϕ) as

$$\mathbf{H}_s = \frac{IL}{4\pi r}\sin\theta\left(\frac{1}{r} + j\beta\right)e^{-j\beta r}\mathbf{a}_\phi$$

Find $\mathbf{E}_s$ using Maxwell's equations.

1.9 Show that the electric field

$$\mathbf{E}_s = 20\sin(k_x x)\cos(k_y y)\mathbf{a}_z ,$$

where $k_x^2 + k_y^2 = \omega^2\mu_0\epsilon_0$, can be represented as the superposition of four propagating plane waves. Find the corresponding $\mathbf{H}_s$ field.

1.10 (a) Express $I_s = e^{-jz}\sin\pi x\cos\pi y$ in instantaneous form.

(b) Determine the phasor form of $V = 20\sin(\omega t - 2x) - 10\cos(\omega t - 4x)$

1.11 For each of the following phasors, determine the corresponding instantaneous form:

(a) $\mathbf{A}_s = (\mathbf{a}_x + j\mathbf{a}_y)e^{-2jz}$

(b) $\mathbf{B}_s = j10\sin x\mathbf{a}_x + 5e^{-j12z-\pi/4}\mathbf{a}_z$

(c) $\mathbf{C}_s = \frac{2}{j}e^{-j3x}\cos 2x + e^{3x-j4x}$

1.12 Show that a time-harmonic EM field in a conducting medium ($\sigma >> \omega\epsilon$) satisfies the diffusion equation

$$\nabla^2\mathbf{E}_s - j\omega\mu\sigma\mathbf{E}_s = 0$$

1.13 Show that in an inhomogeneous medium, the wave equations become

$$\nabla \times \left(\frac{1}{j\omega\mu}\nabla \times \mathbf{E}_s\right) + j\omega\epsilon\mathbf{E}_s = 0\,,$$
$$\nabla \times \left(\frac{1}{j\omega\epsilon}\nabla \times \mathbf{H}_s\right) + j\omega\mu\mathbf{H}_s = 0$$

1.14 Show that the time-harmonic potential function V_s and $\mathbf{A}_s$ satisfy the following inhomogeneous wave equation

$$\nabla^2 V_s + k^2 V_s = -\frac{\rho_{vs}}{\epsilon}$$
$$\nabla^2 \mathbf{A}_s + k^2 \mathbf{A}_s = -\mu\mathbf{J}_s$$

where $k^2 = \omega^2\mu\epsilon$.

1.15 Classify the following PDEs as elliptic, parabolic, or hyperbolic.

(a) $\Phi_{xx} + 2\Phi_{xy} + 5\Phi_{yy} = 0$

(b) $(y^2+1)\Phi_{xx} + (x^2+1)\Phi_{yy} = 0$

(c) $\Phi_{xx} - 2\cos x\Phi_{xy} - (3+\sin^2 x)\Phi_{yy} - y\Phi_y = 0$

(d) $x^2\Phi_{xx} - 2xy\Phi_{xy} + y^2\Phi_{yy} + x\Phi_x + y\Phi_y = 0$

1.16 Repeat Prob. 1.15 for the following PDEs:

(a) $\alpha\dfrac{\partial^2\Phi}{\partial x^2} = \beta\dfrac{\partial\Phi}{\partial x} + \dfrac{\partial\Phi}{\partial t}$ (α, β = constant)
which is called convective heat equation.

(b) $\nabla^2\phi + \lambda\Phi = 0$
which is the Helmholtz equation.

(c) $\nabla^2\Phi + [\lambda - \rho(x)]\Phi = 0$
which is the time-independent Schrodinger equation.

Chapter 2

Analytical Methods

"I've learned that about 90 percent of the things that happen to me are good and only about 10 percent are bad. To be happy, I just have to focus on the 90 percent."
Anonymous

2.1 Introduction

The most satisfactory solution of a field problem is an exact mathematical one. Although in many practical cases such an analytical solution cannot be obtained and we must resort to numerical approximate solution, analytical solution is useful in checking solutions obtained from numerical methods. Also, one would hardly appreciate the need for numerical methods without first seeing the limitations of the classical analytical methods. Hence our objective in this chapter is to briefly examine the common analytical methods and thereby put numerical methods in proper perspective.

The most commonly used analytical methods in solving EM-related problems include:

(1) separation of variables

(2) series expansion

(3) conformal mapping

(4) integral methods

Perhaps the most powerful analytical method is the separation of variables; it is the method that will be emphasized in this chapter. Since the application of conformal mapping is restricted to certain EM problems, it will not be discussed here. The interested reader is referred to Gibbs [1]. The integral methods will be covered in Chapter 5, and fully discussed in [2].

2.2 Separation of Variables

The method of separation of variables (sometimes called the method of Fourier) is a convenient method for solving a partial differential equation (PDE). Basically, it entails seeking a solution which breaks up into a product of functions, each of which involves only one of the variables. For example, if we are seeking a solution $\Phi(x, y, z, t)$ to some PDE, we require that it has the product form

$$\Phi(x, y, z, t) = X(x)Y(y)Z(z)T(t) \tag{2.1}$$

A solution of the form in Eq. (2.1) is said to be separable in x, y, z, and t. For example, consider the functions

(1) $x^2yz \sin 10t$,
(2) $xy^2 + \frac{2}{t}$,
(3) $(2x + y^2)z \cos 10t$.

(1) is completely separable, (2) is not separable, while (3) is separable only in z and t.

To determine whether the method of independent separation of variables can be applied to a given physical problem, we must consider the PDE describing the problem, the shape of the solution region, and the boundary conditions — the three elements that uniquely define a problem. For example, to apply the method to a problem involving two variables x and y (or ρ and ϕ, etc.), three things must be considered [3]:

(i) The differential operator L must be separable, i.e., it must be a function of $\Phi(x, y)$ such that

$$\frac{L\{X(x)Y(y)\}}{\Phi(x, y)X(x)Y(y)}$$

is a sum of a function of x only and a function of y only.

(ii) All initial and boundary conditions must be on constant-coordinate surfaces, i.e., $x =$ constant, $y =$ constant.

(iii) The linear operators defining the boundary conditions at $x =$ constant (or $y =$ constant) must involve no partial derivatives of Φ with respect to y (or x), and their coefficient must be independent of y (or x).

For example, the operator equation

$$L\Phi = \frac{\partial^2\Phi}{\partial x^2} + \frac{\partial^2\Phi}{\partial x\partial y} + \frac{\partial^2\Phi}{\partial y^2}$$

violates (i). If the solution region R is not a rectangle with sides parallel to the x and y axes, (ii) is violated. With a boundary condition $\Phi = 0$ on a part of $x = 0$ and $\partial\Phi/\partial x = 0$ on another part, (iii) is violated.

With this preliminary discussion, we will now apply the method of separation of variables to PDEs in rectangular, circular cylindrical, and spherical coordinate systems. In each of these applications, we shall always take these three major steps:

(1) separate the (independent) variables

(2) find particular solutions of the separated equations, which satisfy some of the boundary conditions

(3) combine these solutions to satisfy the remaining boundary conditions

We begin the application of separation of variables by finding the product solution of the homogeneous scalar wave equation

$$\nabla^2\Phi - \frac{1}{c^2}\frac{\partial^2\Phi}{\partial t^2} = 0 \tag{2.2}$$

Solution to Laplace's equation can be derived as a special case of the wave equation. Diffusion and heat equation can be handled in the same manner as we will treat wave equation. To solve Eq. (2.2), it is expedient that we first separate the time dependence. We let

$$\Phi(\mathbf{r}, t) = U(\mathbf{r})T(t) \tag{2.3}$$

Substituting this in Eq. (2.2),

$$T\nabla^2 U - \frac{1}{c^2}UT'' = 0$$

Dividing by UT gives

$$\frac{\nabla^2 U}{U} = \frac{T''}{c^2 T} \tag{2.4}$$

The left side is independent of t, while the right side is independent of $\mathbf{r}$; the equality can be true only if each side is independent of both variables. If we let an arbitrary constant $-k^2$ be the common value of the two sides, Eq. (2.4) reduces to

$$T'' + c^2k^2T = 0\,, \tag{2.5a}$$

$$\nabla^2 U + k^2 U = 0 \tag{2.5b}$$

Thus we have been able to separate the space variable $\mathbf{r}$ from the time variable t. The arbitrary constant $-k^2$ introduced in the course of the separation of variables is called the *separation constant*. We shall see that in general the total number of independent separation constants in a given problem is one less than the number of independent variables involved.

Equation (2.5a) is an ordinary differential equation with solution

$$T(t) = a_1 e^{jckt} + a_2 e^{-jckt} \tag{2.6a}$$

or

$$T(t) = b_1 \cos(ckt) + b_2 \sin(ckt) \tag{2.6b}$$

Since the time dependence does not change with a coordinate system, the time dependence expressed in Eq. (2.6) is the same for all coordinate systems. Therefore, we shall henceforth restrict our effort to seeking solution to Eq. (2.5b). Notice that if $k = 0$, the time dependence disappears and Eq. (2.5b) becomes Laplace's equation.

2.3 Separation of Variables in Rectangular Coordinates

In order not to complicate things, we shall first consider Laplace's equation in two dimensions and later extend the idea to wave equations in three dimensions.

2.3.1 Laplace's Equations

Consider the Dirichlet problem of an infinitely long rectangular conducting trough whose cross section is shown in Fig. 2.1. For simplicity, let three of its sides be

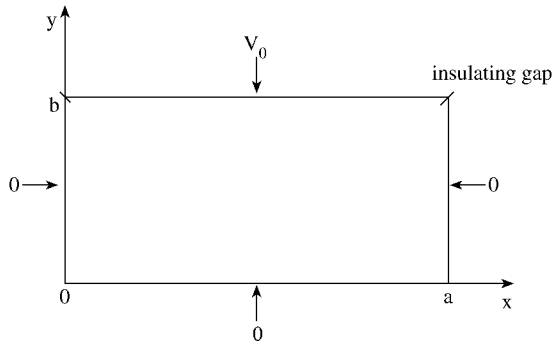

Figure 2.1
Cross section of the rectangular conducting trough.

maintained at zero potential while the fourth side is at a fixed potential V_o. This is a boundary value problem. The PDE to be solved is

$$\frac{\partial^2 V}{\partial x^2} + \frac{\partial^2 V}{\partial y^2} = 0 \tag{2.7}$$

subject to (Dirichlet) boundary conditions

$$V(0, y) = 0 \tag{2.8a}$$
$$V(a, y) = 0 \tag{2.8b}$$
$$V(x, 0) = 0 \tag{2.8c}$$
$$V(x, b) = V_o \tag{2.8d}$$

We let

$$V(x, y) = X(x)Y(y) \tag{2.9}$$

Substitute this into Eq. (2.7) and divide by XY. This leads to

$$\frac{X''}{X} + \frac{Y''}{Y} = 0$$

or

$$\frac{X''}{X} = -\frac{Y''}{Y} = \lambda \tag{2.10}$$

where λ is the separation constant. Thus the separated equations are

$$X'' - \lambda X = 0 \tag{2.11}$$

$$Y'' + \lambda Y = 0 \tag{2.12}$$

To solve the ordinary differential equations (2.11) and (2.12), we must impose the boundary conditions in Eq. (2.8). However, these boundary conditions must be transformed so that they can be applied directly to the separated equations. Since $V = XY$,

$$V(0, y) = 0 \quad \rightarrow \quad X(0) = 0 \tag{2.13a}$$

$$V(a, y) = 0 \quad \rightarrow \quad X(a) = 0 \tag{2.13b}$$

$$V(x, 0) = 0 \quad \rightarrow \quad Y(0) = 0 \tag{2.13c}$$

$$V(x, b) = V_o \quad \rightarrow \quad X(x)Y(b) = V_o \tag{2.13d}$$

Notice that only the homogeneous conditions are separable. To solve Eq. (2.11), we distinguish the three possible cases: $\lambda = 0$, $\lambda > 0$, and $\lambda < 0$.

Case 1: If $\lambda = 0$, Eq. (2.11) reduces to

$$X'' = 0 \quad \text{or} \quad \frac{d^2X}{dx^2} = 0 \tag{2.14}$$

which has the solution

$$X(x) = a_1 x + a_2 \tag{2.15}$$

where a_1 and a_2 are constants. Imposing the conditions in Eq. (2.13a) and Eq. (2.13b),

$$X(0) = 0 \quad \rightarrow \quad a_2 = 0$$

$$X(a) = 0 \quad \rightarrow \quad a_1 = 0$$

Hence $X(x) = 0$, a trivial solution. This renders case $\lambda = 0$ as unacceptable.

Case 2: If $\lambda > 0$, say $\lambda = \alpha^2$, Eq. (2.11) becomes

$$X'' - \alpha^2 X = 0 \tag{2.16}$$

with the corresponding auxiliary equations $m^2 - \alpha^2 = 0$ or $m = \pm\alpha$. Hence the general solution is

$$X = b_1 e^{-\alpha x} + b_2 e^{\alpha x} \tag{2.17}$$

or

$$X = b_3 \sinh \alpha x + b_4 \cosh \alpha x \tag{2.18}$$

The boundary conditions are applied to determine b_3 and b_4.

$$\begin{aligned} X(0) = 0 \quad &\rightarrow \quad b_4 = 0 \\ X(a) = 0 \quad &\rightarrow \quad b_3 = 0 \end{aligned}$$

since $\sinh \alpha x$ is never zero for $\alpha > 0$. Hence $X(x) = 0$, a trivial solution, and we conclude that case $\lambda > 0$ is not valid.

Case 3: If $\lambda < 0$, say $\lambda = -\beta^2$,

$$X'' + \beta^2 X = 0 \tag{2.19}$$

with the auxiliary equation $m^2 + \beta^2 = 0$ or $m = \pm j\beta$. The solution to Eq. (2.19) is

$$X = A_1 e^{j\beta x} + A_2 e^{j\beta x} \tag{2.20a}$$

or

$$X = B_1 \sin \beta x + B_2 \cos \beta x \tag{2.20b}$$

Again,

$$\begin{aligned} X(0) = 0 \quad &\rightarrow \quad B_2 = 0 \\ X(a) = 0 \quad &\rightarrow \quad \sin \beta a = 0 = \sin n\pi \end{aligned}$$

or

$$\beta = \frac{n\pi}{a}, \qquad n = 1, 2, 3, \ldots \tag{2.21}$$

since B_1 cannot vanish for nontrivial solutions, whereas $\sin \beta a$ can vanish without its argument being zero. Thus we have found an infinite set of discrete values of λ for which Eq. (2.11) has nontrivial solutions, i.e.,

$$\lambda = -\beta^2 = \frac{-n^2\pi^2}{a^2}, \qquad n = 1, 2, 3, \ldots \tag{2.22}$$

These are the eigenvalues of the problem and the corresponding eigenfunctions are

$$X_n(x) = \sin \beta x = \sin \frac{n\pi x}{a} \tag{2.23}$$

From Eq. (2.22) note that it is not necessary to include negative values of n since they lead to the same set of eigenvalues. Also we exclude $n = 0$ since it yields the trivial

solution $X = 0$ as shown under Case 1 when $\lambda = 0$. Having determined λ, we can solve Eq. (2.12) to find $Y_n(y)$ corresponding to $X_n(x)$. That is, we solve

$$Y'' - \beta^2 Y = 0\,, \tag{2.24}$$

which is similar to Eq. (2.16), whose solution is in Eq. (2.18). Hence the solution to Eq. (2.24) has the form

$$Y_n(y) = a_n \sinh \frac{n\pi y}{a} + b_n \cosh \frac{n\pi y}{a} \tag{2.25}$$

Imposing the boundary condition in Eq. (2.13c),

$$Y(0) = 0 \qquad \rightarrow \qquad b_n = 0$$

so that

$$Y_n(y) = a_n \sinh \frac{n\pi y}{a} \tag{2.26}$$

Substituting Eqs. (2.23) and (2.26) into Eq. (2.9), we obtain

$$V_n(x, y) = X_n(x) Y_n(y) = a_n \sin \frac{n\pi x}{a} \sinh \frac{n\pi y}{a}\,, \tag{2.27}$$

which satisfies Eq. (2.7) and the three homogeneous boundary conditions in Eqs. (2.8a), (2.8b), and (2.8c). By the superposition principle, a linear combination of the solutions V_n, each with different values of n and arbitrary coefficient a_n, is also a solution of Eq. (2.7). Thus we may represent the solution V of Eq. (2.7) as an infinite series in the function V_n, i,e.,

$$V(x, y) = \sum_{n=1}^{\infty} a_n \sin \frac{n\pi x}{a} \sinh \frac{n\pi y}{a} \tag{2.28}$$

We now determine the coefficient a_n by imposing the inhomogeneous boundary condition in Eq. (2.8d) on Eq. (2.28). We get

$$V(x, b) = V_o = \sum_{n=1}^{\infty} a_n \sin \frac{n\pi x}{a} \sinh \frac{n\pi b}{a}\,, \tag{2.29}$$

which is Fourier sine expansion of V_o. Hence,

$$a_n \sinh \frac{n\pi b}{a} = \frac{2}{b} \int_0^b V_o \sin \frac{n\pi x}{a}\, dx = \frac{2V_o}{n\pi}(1 - \cos n\pi)$$

or

$$a_n = \begin{cases} \dfrac{4V_o}{n\pi} \dfrac{1}{\sinh \frac{n\pi b}{a}}, & n = \text{odd}\,, \\ 0, & n = \text{even} \end{cases} \tag{2.30}$$

Substitution of Eq. (2.30) into Eq. (2.28) gives the complete solution as

$$V(x, y) = \frac{4V_o}{\pi} \sum_{n=\text{odd}}^{\infty} \frac{\sin \frac{n\pi x}{a} \sinh \frac{n\pi y}{a}}{n \sinh \frac{n\pi b}{a}} \tag{2.31a}$$

By replacing n by $2k - 1$, Eq. (2.31a) may be written as

$$\boxed{V(x, y) = \frac{4V_o}{\pi} \sum_{k=1}^{\infty} \frac{\sin \frac{n\pi x}{a} \sinh \frac{n\pi y}{a}}{n \sinh \frac{n\pi b}{a}}, \qquad n = 2k - 1} \tag{2.31b}$$

2.3.2 Wave Equation

The time dependence has been taken care of in Section 2.2. We are left with solving the Helmholtz equation

$$\nabla^2 U + k^2 U = 0 \tag{2.5b}$$

In rectangular coordinates, Eq. (2.5b) becomes

$$\frac{\partial^2 U}{\partial x^2} + \frac{\partial^2 U}{\partial y^2} + \frac{\partial^2 U}{\partial z^2} + k^2 U = 0 \tag{2.32}$$

We let

$$U(x, y, z) = X(x)Y(y)Z(z) \tag{2.33}$$

Substituting Eq. (2.33) into Eq. (2.32) and dividing by XYZ, we obtain

$$\frac{X''}{X} + \frac{Y''}{Y} + \frac{Z''}{Z} + k^2 = 0 \tag{2.34}$$

Each term must be equal to a constant since each term depends only on the corresponding variable; X on x, etc. We conclude that

$$\frac{X''}{X} = -k_x^2, \qquad \frac{Y''}{Y} = -k_y^2, \qquad \frac{Z''}{Z} = -k_z^2 \tag{2.35}$$

so that Eq. (2.34) reduces to

$$k_x^2 + k_y^2 + k_z^2 = k^2 \tag{2.36}$$

Notice that there are four separation constants k, k_x, k_y, and k_z since we have four variables t, x, y, and z. But from Eq. (2.36), one is related to the other three so that only three separation constants are independent. As mentioned earlier, the number of independent separation constants is generally one less than the number of independent variables involved. The ordinary differential equations in Eq. (2.35) have solutions

$$X = A_1 e^{jk_x x} + A_2 e^{-jk_x x} \tag{2.37a}$$

(2.37b)

$$+ A_4 e^{jk_y y} \tag{2.37c}$$

or

$$Y = B_3 \sin k_y y + B_4 \cos k_y y \,, \tag{2.37d}$$

$$Z = A_5 e^{jk_z z} + A_6 e^{-jk_z z} \tag{2.37e}$$

or

$$Z = B_5 \sin k_z z + B_6 \cos k_z z \,, \tag{2.37f}$$

Various combinations of X, Y, and Z will satisfy Eq. (2.5b). Suppose we choose

$$X = A_1 e^{jk_x x}, \qquad Y = A_3 e^{jk_y y}, \qquad Z = A_5 e^{jk_z z} \,, \tag{2.38}$$

then

$$U(x, y, z) = A e^{j(k_x x + k_y y + k_z z)} \tag{2.39}$$

or

$$U(\mathbf{r}) = A e^{j\mathbf{k}\cdot\mathbf{r}} \tag{2.40}$$

Introducing the time dependence of Eq. (2.6a) gives

$$\boxed{\Phi(x, y, z, t) = A e^{j(\mathbf{k}\cdot\mathbf{r} + \omega t)}} \tag{2.41}$$

where $\omega = kc$ is the angular frequency of the wave and k is given by Eq. (2.36). The solution in Eq. (2.41) represents a plane wave of amplitude A propagating in the direction of the wave vector $\mathbf{k} = k_x \mathbf{a}_x + k_y \mathbf{a}_y + k_z \mathbf{a}_z$ with velocity c.

Example 2.1

In this example, we would like to show that the method of separation of variables is not limited to a problem with only one inhomogeneous boundary condition as presented in Section 2.3.1. We reconsider the problem of Fig. 2.1, but with four inhomogeneous boundary conditions as in Fig. 2.2(a). □

Solution

The problem can be stated as solving Laplace's equation

$$\frac{\partial^2 V}{\partial x^2} + \frac{\partial^2 V}{\partial y^2} = 0 \tag{2.42}$$

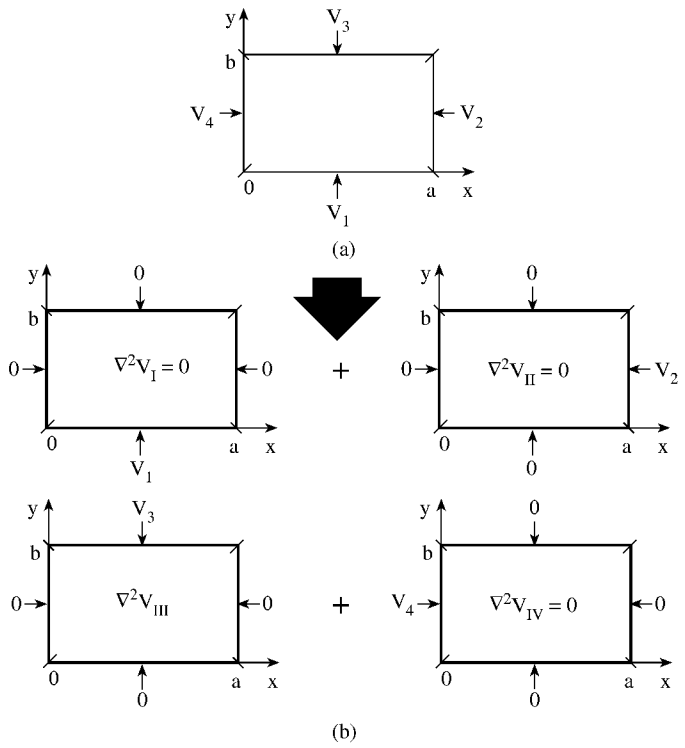

Figure 2.2
Applying the principle of superposition reduces the problem in (a) to those in (b).

subject to the following inhomogeneous Dirichlet conditions:

$$\begin{aligned} V(x, 0) &= V_1 \\ V(x, b) &= V_3 \\ V(0, y) &= V_4 \\ V(a, y) &= V_2 \end{aligned} \tag{2.43}$$

Since Laplace's equation is a linear homogeneous equation, the problem can be simplified by applying the superposition principle. If we let

$$V = V_I + V_{II} + V_{III} + V_{IV} \ , \tag{2.44}$$

we may reduce the problem to four simpler problems, each of which is associated with one of the inhomogeneous conditions. The reduced, simpler problems are illustrated in Fig. 2.2 (b) and stated as follows:

$$\frac{\partial^2 V_I}{\partial x^2} + \frac{\partial^2 V_I}{\partial y^2} = 0 \tag{2.45}$$

subject to

$$\begin{aligned} V_I(x, 0) &= V_1 \\ V_I(x, b) &= 0 \\ V_I(0, y) &= 0 \\ V_I(a, y) &= 0 \,; \end{aligned} \tag{2.46}$$

$$\frac{\partial^2 V_{II}}{\partial x^2} + \frac{\partial^2 V_{II}}{\partial y^2} = 0 \tag{2.47}$$

subject to

$$\begin{aligned} V_{II}(x, 0) &= 0 \\ V_{II}(x, b) &= 0 \\ V_{II}(0, y) &= 0 \\ V_{II}(a, y) &= V_2 \,; \end{aligned} \tag{2.48}$$

$$\frac{\partial^2 V_{III}}{\partial x^2} + \frac{\partial^2 V_{III}}{\partial y^2} = 0 \tag{2.49}$$

subject to

$$\begin{aligned} V_{III}(x, 0) &= 0 \\ V_{III}(x, b) &= V_3 \\ V_{III}(0, y) &= 0 \\ V_{III}(a, y) &= 0 \,; \end{aligned} \tag{2.50}$$

and

$$\frac{\partial^2 V_{IV}}{\partial x^2} + \frac{\partial^2 V_{IV}}{\partial y^2} = 0 \tag{2.51}$$

subject to

$$\begin{aligned} V_{IV}(x, 0) &= 0 \\ V_{IV}(x, b) &= 0 \\ V_{IV}(0, y) &= V_4 \\ V_{IV}(a, y) &= 0 \end{aligned} \tag{2.52}$$

It is obvious that the reduced problem in Eqs. (2.49) and (2.50) with solution V_{III} is the same as that in Fig. 2.1. The other three reduced problems are quite similar. Hence the solutions V_I, V_{II}, and V_{IV} can be obtained by taking the same steps as in

Section 2.3.1 or by a proper exchange of variables in Eq. (2.31). Thus

$$V_I = \frac{4V_1}{\pi} \sum_{n=\text{odd}}^{\infty} \frac{\sin \frac{n\pi x}{a} \sinh \frac{n\pi(b-y)}{a}}{n \sinh \frac{n\pi b}{a}}, \tag{2.53}$$

$$V_{II} = \frac{4V_2}{\pi} \sum_{n=\text{odd}}^{\infty} \frac{\sin \frac{n\pi x}{b} \sinh \frac{n\pi y}{b}}{n \sinh \frac{n\pi a}{b}}, \tag{2.54}$$

$$V_{III} = \frac{4V_3}{\pi} \sum_{n=\text{odd}}^{\infty} \frac{\sin \frac{n\pi x}{a} \sinh \frac{n\pi y}{a}}{n \sinh \frac{n\pi b}{a}}, \tag{2.55}$$

$$V_{IV} = \frac{4V_4}{\pi} \sum_{n=\text{odd}}^{\infty} \frac{\sin \frac{n\pi(a-x)}{b} \sinh \frac{n\pi y}{b}}{n \sinh \frac{n\pi a}{b}} \tag{2.56}$$

We obtain the complete solution by substituting Eqs. (2.53) to (2.56) in Eq. (2.44). ∎

Example 2.2

Find the product solution of the diffusion equation

$$\Phi_t = k\Phi_{xx}, \qquad 0 < x < 1, \quad t > 0 \tag{2.57}$$

subject to the boundary conditions

$$\Phi(0, t) = 0 = \Phi(1, t), \qquad t > 0 \tag{2.58}$$

and initial condition

$$\Phi(x, 0) = 5 \sin 2\pi x, \qquad 0 < x < 1 \tag{2.59}$$

□

Solution

Let

$$\Phi(x, t) = X(x)T(t) \tag{2.60}$$

Substitute this into Eq. (2.57) and divide by kXT to obtain

$$\frac{T'}{kT} = \frac{X''}{X} = \lambda$$

where λ is the separation constant. Thus

$$X'' - \lambda X = 0 \tag{2.61}$$

$$T' - \lambda kT = 0 \tag{2.62}$$

As usual, in order for the solution of Eq. (2.61) to satisfy Eq. (2.58), we must choose $\lambda = -\beta^2 = -n^2\pi^2$ so that $n = 1, 2, 3, \ldots$ and

$$X_n(x) = \sin n\pi x \tag{2.63}$$

Equation (2.62) becomes

$$T' + kn^2\pi^2 T = 0\,,$$

which has solution

$$T_n(t) = e^{-kn^2\pi^2 t} \tag{2.64}$$

Substituting Eqs. (2.63) and (2.64) into Eq. (2.60),

$$\Phi_n(x,t) = a_n \sin n\pi x \exp(-kn^2\pi^2 t)$$

where the coefficients a_n are to be determined from the initial condition in Eq. (2.59). The complete solution is a linear combination of Φ_n, i.e.,

$$\Phi(x,t) = \sum_{n=1}^{\infty} a_n \sin n\pi x \exp(-kn^2\pi^2 t)$$

This satisfies Eq. (2.59) if

$$\Phi(x,0) = \sum_{n=1}^{\infty} a_n \sin n\pi x = 5\sin 2\pi x \tag{2.65}$$

The coefficients a_n are determined as ($T = 1$)

$$a_n = \frac{2}{T}\int_0^1 5\sin 2\pi x \sin n\pi x\, dx = \begin{cases} 5, & n = 2 \\ 0, & n \neq 0 \end{cases}$$

Alternatively, by comparing the middle term in Eq. (2.65) with the last term, the two are equal only when $n = 2, a_n = 5$, otherwise $a_n = 0$. Hence the solution of the diffusion problem becomes

$$\Phi(x,t) = 5\sin 2\pi t \exp(-4k\pi^2 t) \quad \blacksquare$$

2.4 Separation of Variables in Cylindrical Coordinates

Coordinate geometries other than rectangular Cartesian are used to describe many EM problems whenever it is necessary and convenient. For example, a problem having cylindrical symmetry is best solved in cylindrical system where the coordinate variables (ρ, ϕ, z) are related as shown in Fig. 2.3 and $0 \le \rho \le \infty, 0 \le \phi < 2\pi, -\infty \le z \le \infty$. In this system, the wave equation (2.5b) becomes

$$\nabla^2 U + k^2 U = \frac{1}{\rho}\frac{\partial}{\partial \rho}\left(\rho \frac{\partial U}{\partial \rho}\right) + \frac{1}{\rho^2}\frac{\partial^2 U}{\partial \phi^2} + \frac{\partial^2 U}{\partial z^2} + k^2 U = 0 \tag{2.66}$$

As we did in the previous section, we shall first solve Laplace's equation ($k = 0$) in two dimensions before we solve the wave equation.

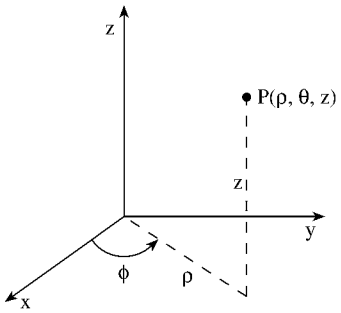

Figure 2.3
Coordinate relations in a cylindrical system.

2.4.1 Laplace's Equation

Consider an infinitely long conducting cylinder of radius a with the cross section shown in Fig. 2.4. Assume that the upper half of the cylinder is maintained at potential V_o while the lower half is maintained at potential $-V_o$. This is a Laplacian problem in two dimensions. Hence we need to solve for $V(\rho, \phi)$ in Laplace's equation

$$\nabla^2 V = \frac{1}{\rho}\frac{\partial}{\partial \rho}\left(\rho \frac{\partial V}{\partial \rho}\right) + \frac{1}{\rho^2}\frac{\partial^2 V}{\partial \phi^2} = 0 \tag{2.67}$$

subject to the inhomogeneous Dirichlet boundary condition

$$V(a, \phi) = \begin{cases} V_o, & 0 < \phi < \pi \\ -V_o, & \pi < \phi < 2\pi \end{cases} \tag{2.68}$$

We let

$$V(\rho, \phi) = R(\rho)F(\phi) \tag{2.69}$$

Substituting Eq. (2.69) into Eq. (2.67) and dividing through by RF/ρ^2 result in

$$\frac{\rho}{R}\frac{d}{d\rho}\left(\rho \frac{dR}{d\rho}\right) + \frac{1}{F}\frac{d^2 F}{d\phi^2} = 0$$

or

$$\frac{\rho^2}{R}\frac{d^2 R}{d\rho^2} + \frac{\rho}{R}\frac{dR}{d\rho} = -\frac{1}{F}\frac{d^2 F}{d\phi^2} = \lambda^2 \tag{2.70}$$

where λ is the separation constant. Thus the separated equations are:

$$F'' + \lambda^2 F = 0 \tag{2.71a}$$

$$\rho^2 R'' + \rho R' - \lambda^2 R = 0 \tag{2.71b}$$

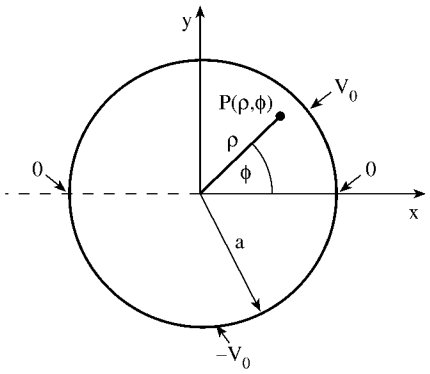

Figure 2.4
A two-dimensional Laplacian problem in cylindrical coordinates.

It is evident that Eq. (2.71a) has the general solution of the form

$$F(\phi) = c_1 \cos(\lambda\phi) + c_2 \sin(\lambda\phi) \tag{2.72}$$

From the boundary conditions of Eq. (2.68), we observe that $F(\phi)$ must be a periodic, odd function. Thus $c_1 = 0, \lambda = n$, a real integer, and hence Eq. (2.72) becomes

$$F_n(\phi) = c_2 \sin n\phi \tag{2.73}$$

Equation (2.71b), known as the *Cauchy-Euler equation,* can be solved by making a substitution $\rho = e^u$ and reducing it to an equation with constant coefficients. This leads to

$$R_n(\rho) = c_3\rho^n + c_4\rho^{-n}, \qquad n = 1, 2, \ldots \tag{2.74}$$

Note that case $n = 0$ is excluded; if $n = 0$, we obtain $R(\rho) = \ln\rho +$ constant, which is not finite at $\rho = 0$. For the problem of a coaxial cable, $a < \rho < b, \rho \neq 0$ so that case $n = 0$ is the only solution. However, for the problem at hand, $n = 0$ is not acceptable.

Substitution of Eqs. (2.73) and (2.74) into Eq. (2.69) yields

$$V_n(\rho, \phi) = \sin n\phi (A_n\rho^n + B_n\rho^{-n}) \tag{2.75}$$

where A_n and B_n are constants to be determined. As usual, it is possible by the superposition principle to form a complete series solution

$$V(\rho, \phi) = \sum_{n=1}^{\infty} (A_n\rho^n + B_n\rho^{-n}) \sin n\phi \tag{2.76}$$

For $\rho < a$, inside the cylinder, V must be finite as $\rho \to 0$ so that $B_n = 0$. At $\rho = a$,

$$V(a, \phi) = \sum_{n=1}^{\infty} A_n a^n \sin n\phi = \begin{cases} V_o, & 0 < \phi < \pi \\ -V_o, & \pi < \phi < 2\pi \end{cases} \tag{2.77}$$

Multiplying both sides by $\sin m\phi$ and integrating over $0 < \phi < 2\pi$, we get

$$\int_0^{\pi} V_o \sin m\phi \, d\phi - \int_{\pi}^{2\pi} V_o \sin m\phi \, d\phi = \sum_{n=1}^{\infty} A_n a^n \int_0^{2\pi} \sin n\phi \sin m\phi \, d\phi$$

All terms in the right-hand side vanish except when $m = n$. Hence

$$\frac{2V_o}{n}(1 - \cos n\pi) = A_n a^n \int_0^{2\pi} \sin^2 \phi \, d\phi = \pi A_n a^n$$

or

$$A_n = \begin{cases} \dfrac{4V_o}{nna^n}, & n = \text{odd} \\ 0, & n = \text{even} \end{cases} \tag{2.78}$$

Thus,

$$V(\rho, \phi) = \frac{4V_o}{\pi} \sum_{n=\text{odd}}^{\infty} \frac{\rho^n \sin n\phi}{na^n}, \quad \rho < a \tag{2.79}$$

For $\rho > a$, outside the cylinder, V must be finite as $\rho \to \infty$ so that $A_n = 0$ in Eq. (2.76) for this case. By imposing the boundary condition in Eq. (2.68) and following the same steps as for case $\rho < a$, we obtain

$$B_n = \begin{cases} \dfrac{4V_o a^n}{n\pi}, & n = \text{odd} \\ 0, & n = \text{even} \end{cases} \tag{2.80}$$

Hence,

$$V(\rho, \phi) = \frac{4V_o}{\pi} \sum_{n=\text{odd}}^{\infty} \frac{a^n \sin n\phi}{n\rho^n}, \quad \rho > a \tag{2.81}$$

2.4.2 Wave Equation

Having taken care of the time-dependence in Section 2.2, we now solve Helmholtz's equation (2.66), i.e.,

$$\frac{1}{\rho}\frac{\partial}{\partial \rho}\left(\rho \frac{\partial U}{\partial \rho}\right) + \frac{1}{\rho^2}\frac{\partial^2 U}{\partial \phi^2} + \frac{\partial^2 U}{\partial z^2} + k^2 U = 0 \tag{2.66}$$

Let

$$U(\rho, \phi, z) = R(\rho)F(\phi)Z(z) \tag{2.82}$$

Substituting Eq. (2.82) into Eq. (2.66) and dividing by RFZ/ρ^2 yields

$$\frac{\rho}{R}\frac{d}{d\rho}\left(\rho\frac{dR}{d\rho}\right)+\frac{\rho^2}{Z}\frac{d^2Z}{dz^2}+k^2\rho^2=-\frac{1}{F}\frac{d^2F}{d\phi^2}=n^2$$

where $n=0,1,2,\ldots$ and n^2 is the separation constant. Thus

$$F''+n^2F=0 \tag{2.83}$$

and

$$\frac{\rho}{R}\frac{d}{d\rho}\left(\rho\frac{dR}{d\rho}\right)+\frac{\rho^2}{Z}\frac{d^2Z}{dz^2}+k^2\rho^2=n^2 \tag{2.84}$$

Dividing both sides of Eq. (2.84) by ρ^2 leads to

$$\frac{1}{\rho R}\frac{d}{d\rho}\left(\rho\frac{dR}{d\rho}\right)+\left(k^2-\frac{n^2}{\rho^2}\right)=-\frac{1}{Z}\frac{d^2Z}{dz^2}=\mu^2$$

where μ^2 is another separation constant. Hence

$$-\frac{1}{Z}\frac{d^2Z}{dz^2}=\mu^2 \tag{2.85}$$

and

$$\frac{1}{\rho R}\frac{d}{d\rho}\left(\rho\frac{dR}{d\rho}\right)+\left(k^2-\mu^2-\frac{n^2}{\rho^2}\right)=0 \tag{2.86}$$

If we let

$$\lambda^2=k^2-\mu^2\,, \tag{2.87}$$

the three separated equations (2.83), (2.85), and (2.86) become

$$F''+n^2F=0\,, \tag{2.88}$$

$$Z''+\mu^2Z=0\,, \tag{2.89}$$

$$\rho^2R''+\rho R+\left(\lambda^2\rho^2-n^2\right)R=0 \tag{2.90}$$

The solution to Eq. (2.88) is given by

$$F(\phi)=c_1e^{jn\phi}+c_2e^{-jn\phi} \tag{2.91a}$$

or

$$F(\phi)=c_3\sin n\phi+c_4\cos n\phi \tag{2.91b}$$

Similarly, Eq. (2.89) has the solution

$$Z(z) = c_5 e^{jn\mu} + c_6 e^{-jn\mu} \tag{2.92a}$$

or

$$Z(z) = c_7 \sin n\mu + c_8 \cos n\mu \tag{2.92b}$$

To solve Eq. (2.90), we let $x = \lambda\rho$ and replace R by y; the equation becomes

$$x^2 y'' + xy' + (x^2 - n^2)y = 0 \tag{2.93}$$

This is called *Bessel's equation.* It has a general solution of the form

$$y(x) = b_1 J_n(x) + b_2 Y_n(x) \tag{2.94}$$

where $J_n(x)$ and $Y_n(x)$ are, respectively, *Bessel functions* of the first and second kinds of order n and real argument x. Y_n is also called the *Neumann function.* If x in Eq. (2.93) is imaginary so that we may replace x by jx, the equation becomes

$$x^2 y'' + xy' - (x^2 + n^2)y = 0 \tag{2.95}$$

which is called *modified Bessel's equation.* This equation has a solution of the form

$$y(x) = b_3 I_n(x) + b_4 K_n(x) \tag{2.96}$$

where $I_n(x)$ and $K_n(x)$ are respectively *modified Bessel functions* of the first and second kind of order n. For small values of x, Fig. 2.5 shows the sketch of some typical Bessel functions (or cylindrical functions) $J_n(x)$, $Y_n(x)$, $I_n(x)$, and $K_n(x)$.

To obtain the Bessel functions from Eqs (2.93) and (2.95), the method of Frobenius is applied. A detailed discussion is found in Kersten [4] and Myint-U [5]. For the Bessel function of the first kind,

$$\boxed{y = J_n(x) = \sum_{m=0}^{\infty} \frac{(-1)^m (x/2)^{n+2m}}{m!\Gamma(n+m+1)}} \tag{2.97}$$

where $\Gamma(k+1) = k!$ is the Gamma function. This is the most useful of all Bessel functions. Some of its important properties and identities are listed in Table 2.1. For the modified Bessel function of the second kind

$$I_n(x) = j^{-n} J_n(jx) = \sum_{m=U}^{\infty} \frac{(x/2)^{n+2m}}{m!\Gamma(n+m+1)} \tag{2.98}$$

For the Neumann function, when $n > 0$

$$Y_n(x) = \frac{2}{\pi} J_n(x) \ln \frac{\gamma x}{2} - \frac{1}{\pi} \sum_{m=0}^{n-1} \frac{(n-m-1)!(x/2)^{2m-n}}{m!} - \frac{1}{\pi} \sum_{m=0}^{\infty} \frac{(-1)^m (x/2)^{n+2m}}{m!\Gamma(n+m+1)} [p(m) + p(n+m)] \tag{2.99}$$

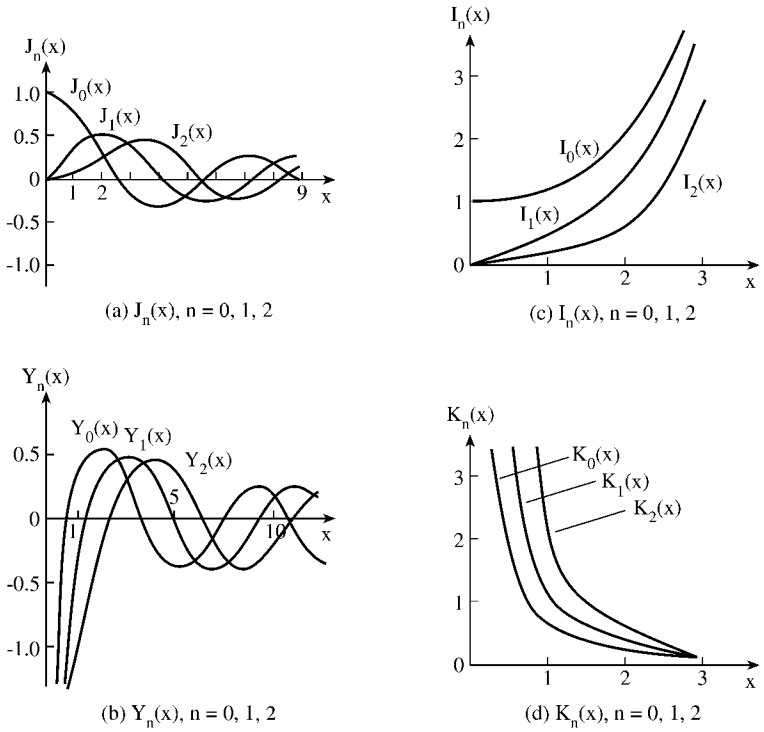

Figure 2.5
Bessel functions.

where $\gamma = 1.781$ is Euler's constant and

$$p(m) = \sum_{k=1}^{m} \frac{1}{k}, \quad p(0) = 0 \tag{2.100}$$

If $n = 0$,

$$Y_0(x) = \frac{2}{\pi} J_0(x) \ln \frac{\gamma x}{2} + \frac{2}{\pi} \sum_{m=0}^{\infty} \frac{(-1)^{m+1} (x/2)^{2m}}{(m!)^2} p(m) \tag{2.101}$$

For the modified Bessel function of the second kind,

$$K_n(x) = \frac{\pi}{2} j^{n+1} [J_n(jx) + jY_n(jx)] \tag{2.102}$$

Table 2.1 Properties and Identities of Bessel Functions[1] $J_n(x)$

(a) $J_{-n}(x) = (-1)^n J_n(x)$

(b) $J_n(-x) = (-1)^n J_n(x)$

(c) $J_{n+1}(x) = \frac{2n}{x} J_n(x) - J_{n-1}(x)$ (recurrence formula)

(d) $\frac{d}{dx} J_n(x) = \frac{1}{2}[J_{n-1}(x) - J_{n+1}(x)]$

(e) $\frac{d}{dx}[x^n J_n(x)] = x^n J_{n-1}(x)$

(f) $\frac{d}{dx}[x^{-n} J_n(x)] = -x^{-n} J_{n+1}(x)$

(g) $J_n(x) = \frac{1}{\pi} \int_0^{\pi} \cos(n\theta - x \sin\theta)\, d\theta, \quad n \geq 0$

(h) Fourier-Bessel expansion of $f(x)$:

$$f(x) = \sum_{k=1}^{\infty} A_k J_n(\lambda_k x), \quad n \geq 0$$

$$A_k = \frac{2}{[a J_{n+1}(\lambda_i a)]^2} \int_0^a x f(x) J_n(\lambda_k x)\, dx, \quad 0 < x < a$$

where λ_k are the positive roots in ascending order of magnitude of $J_n(\lambda_i a) = 0$.

(i) $\int_0^a \rho J_n(\lambda_i \rho) J_n(\lambda_j \rho)\, d\rho = \frac{a^2}{2}[J_{n+1}(\lambda_i a)]^2 \delta_{ij}$

where λ_i and λ_j are the positive roots of $J_n(\lambda a) = 0$.

1. Properties (a) to (f) also hold for $Y_n(x)$.

If $n > 0$,

$$K_n(x) = \frac{1}{2} \sum_{m=0}^{n-1} \frac{(-1)^m (n-m-1)!(x/2)^{2m-n}}{m!} + (-1)^n \frac{1}{2} \sum_{m=0}^{\infty} \frac{(x/2)^{n+2m}}{m!(n+m)!} \left[p(m) + p(n+m) - 2 \ln \frac{\gamma x}{2} \right] \tag{2.103}$$

and if $n = 0$,

$$K_0(x) = -I_0(x) \ln \frac{\gamma x}{2} + \sum_{m=0}^{\infty} \frac{(x/2)^{2m}}{(m!)^2} p(m) \tag{2.104}$$

Other functions closely related to Bessel functions are *Hankel functions* of the first and second kinds, defined respectively by

$$H_n^{(1)}(x) = J_n(x) + jY_n(x) \tag{2.105a}$$

$$H_n^{(2)}(x) = J_n(x) - jY_n(x) \tag{2.105b}$$

Hankel functions are analogous to functions $\exp(\pm jx)$ just as J_n and Y_n are analogous

to cosine and sine functions. This is evident from asymptotic expressions

$$J_n(x) \xrightarrow{x \to \infty} \sqrt{\frac{2}{\pi x}} \cos(x - n\pi/2 - \pi/4) , \tag{2.106a}$$

$$Y_n(x) \xrightarrow{x \to \infty} \sqrt{\frac{2}{\pi x}} \sin(x - n\pi/2 - \pi/4) , \tag{2.106b}$$

$$H_n^{(1)}(x) \xrightarrow{x \to \infty} \sqrt{\frac{2}{\pi x}} \exp[j(x - n\pi/2 - \pi/4)] , \tag{2.106c}$$

$$H_n^{(2)}(x) \xrightarrow{x \to \infty} \sqrt{\frac{2}{\pi x}} \exp[-j(x - n\pi/2 - \pi/4)] , \tag{2.106d}$$

$$I_n(x) \xrightarrow{x \to \infty} \frac{1}{\sqrt{2\pi x}} e^x , \tag{2.106e}$$

$$K_n(x) \xrightarrow{x \to \infty} \frac{1}{\sqrt{2\pi x}} e^{-x} \tag{2.106f}$$

With the time factor $e^{j\omega t}$, $H_n^{(1)}(x)$ and $H_n^{(2)}(x)$ represent inward and outward traveling waves, respectively, while $J_n(x)$ or $Y_n(x)$ represents a standing wave. With the time factor $e^{-j\omega t}$, the roles of $H_n^{(1)}(x)$ and $H_n^{(2)}(x)$ are reversed. For further treatment of Bessel and related functions, refer to the works of Watson [6] and Bell [7].

Any of the Bessel functions or related functions can be a solution to Eq. (2.90) depending on the problem. If we choose $R(\rho) = J_n(x) = J_n(\lambda\rho)$ with Eqs. (2.91) and (2.92) and apply the superposition theorem, the solution to Eq. (2.66) is

$$U(\rho, \phi, z) = \sum_n \sum_\mu A_{n\mu} J_n(\lambda\rho) \exp(\pm jn\phi \pm j\mu z) \tag{2.107}$$

Introducing the time dependence of Eq. (2.6a), we finally get

$$\Phi(\rho, \phi, z, t) = \sum_m \sum_n \sum_\mu A_{mn\mu} J_n(\lambda\rho) \exp(\pm jn\phi \pm j\mu z \pm \omega t) , \tag{2.108}$$

where $\omega = kc$.

Example 2.3

Consider the skin effect on a solid cylindrical conductor. The current density distribution within a good conducting wire ($\sigma/\omega\epsilon >> 1$) obeys the diffusion equation

$$\nabla^2 J = \mu\sigma \frac{\partial J}{\partial t}$$

We want to solve this equation for a long conducting wire of radius a. □

Solution

We may derive the diffusion equation directly from Maxwell's equation. We recall that

$$\nabla \times \mathbf{H} = \mathbf{J} + \mathbf{J}_d$$

where $\mathbf{J} = \sigma \mathbf{E}$ is the conduction current density and $\mathbf{J}_d = \frac{\partial \mathbf{D}}{\partial t}$ is the displacement current density. For $\sigma \omega \epsilon >> 1$, $\mathbf{J}_d$ is negligibly small compared with $\mathbf{J}$. Hence

$$\nabla \times \mathbf{H} \simeq \mathbf{J} \tag{2.109}$$

Also,

$$\nabla \times \mathbf{E} = -\mu \frac{\partial \mathbf{H}}{\partial t}$$

$$\nabla \times \nabla \times \mathbf{E} = \nabla \nabla \cdot \mathbf{E} - \nabla^2 \mathbf{E} = -\mu \frac{\partial}{\partial t} \nabla \times \mathbf{H}$$

Since $\nabla \cdot \mathbf{E} = 0$, introducing Eq. (2.109), we obtain

$$\nabla^2 \mathbf{E} = \mu \frac{\partial \mathbf{J}}{\partial t} \tag{2.110}$$

Replacing $\mathbf{E}$ with $\mathbf{J}/\sigma$, Eq. (2.110) becomes

$$\nabla^2 \mathbf{J} = \mu \sigma \frac{\partial \mathbf{J}}{\partial t}\,, \tag{2.111}$$

which is the diffusion equation.

Assuming harmonic field with time factor $e^{j\omega t}$,

$$\nabla^2 \mathbf{J} = j\omega\mu\sigma \mathbf{J} \tag{2.112}$$

For infinitely long wire, Eq. (2.112) reduces to a one-dimensional problem in cylindrical coordinates:

$$\frac{1}{\rho} \frac{\partial}{\partial \rho} \left(\rho \frac{\partial J_z}{\partial \rho} \right) = j\omega\mu\sigma J_z$$

or

$$\rho^2 J_z'' + \rho J_z' - j\omega\mu\sigma\rho^2 J_z = 0 \tag{2.113}$$

Comparing this with Eq. (2.95) shows that Eq. (2.113) is the modified Bessel equation of zero order. Hence the solution to Eq. (2.113) is

$$J_z(\rho) = c_1 I_0(\lambda\rho) + c_2 K_0(\lambda\rho) \tag{2.114}$$

where c_1 and c_2 are constants and

$$\lambda = \sqrt{j\omega\mu\sigma} = j^{1/2} \frac{\sqrt{2}}{\delta} \tag{2.115}$$

and $\delta = \sqrt{\frac{2}{\sigma\mu\omega}}$ is the skin depth. Constant c_2 must vanish if J_z is to be finite at $\rho = 0$. At $\rho = a$,

$$J_z(a) = c_1 I_0(\lambda a) \rightarrow c_1 = J_z(a)/I_0(\lambda a)$$

Thus

$$J_z(\rho) = J_z(a)\frac{I_0(\lambda\rho)}{I_0(\lambda a)} \tag{2.116}$$

If we let $\lambda\rho = j^{1/2}\frac{\sqrt{2}}{\delta}\rho = j^{1/2}x$, it is convenient to replace

$$\begin{aligned} I_0(\lambda\rho) &= I_0(j^{1/2}x) = J_0(xe^{j3\pi/4}) \\ &= ber_0(x) + jbei_0(x) \end{aligned} \tag{2.117}$$

where ber_0 and bei_0 are *ber* and *bei* functions of zero order. Ber and ber functions are also known as *Kelvin functions*. For zero order, they are given by

$$ber_0(x) = \sum_{m=0}^{\infty} \frac{\cos(m\pi/2)(x/2)^{2m}}{(m!)^2}, \tag{2.118}$$

$$bei_0(x) = \sum_{m=0}^{\infty} \frac{\sin(m\pi/2)(x/2)^{2m}}{(m!)^2} \tag{2.119}$$

Using ber and bei functions, Eq. (2.116) may be written as

$$J_z(\rho) = J_z(a)\frac{ber_0(x) + jbei_0(x)}{ber_0(y) + jbei_0(y)} \tag{2.120}$$

where $x = \sqrt{2}\rho/\delta,\ y = \sqrt{2}a/\delta$. ∎

Example 2.4

A semi-infinitely long cylinder ($z \geq 0$) of radius a has its end at $z = 0$ maintained at $V_o(a^2 - \rho^2),\ 0 \leq \rho \leq a$. Find the potential distribution within the cylinder. □

Solution

The problem is that of finding a function $V(\rho, z)$ satisfying the PDE

$$\nabla^2 V = \frac{\partial^2 V}{\partial\rho^2} + \frac{1}{\rho}\frac{\partial V}{\partial\rho} + \frac{\partial^2 V}{\partial z^2} = 0 \tag{2.121}$$

subject to the boundary conditions:

(i) $V = V_o(a^2 - \rho^2),\ z = 0,\ 0 \leq \rho \leq a$,

(ii) $V \rightarrow 0$ as $z \rightarrow \infty$, i.e., V is bounded,

(iii) $V = 0$ on $\rho = a$,

(iv) V is finite on $\rho = 0$.

Let $V = R(\rho)Z(z)$ and obtain the separated equations

$$Z'' - \lambda Z = 0 \tag{2.122a}$$

and

$$\rho^2 R'' + \rho R' + \lambda^2 \rho^2 R = 0 \tag{2.122b}$$

where λ is the separated constant. The solution to Eq. (2.122a) is

$$Z_1 = c_1 e^{-\lambda z} + c_2 e^{\lambda z} \tag{2.123}$$

Comparing Eq. (2.122b) with Eq. (2.93) shows that $n = 0$ so that Eq. (2.122b) is Bessel's equation with solution

$$R = c_3 J_0(\lambda\rho) + c_4 Y_0(\lambda\rho) \tag{2.124}$$

Condition (ii) forces $c_2 = 0$, while condition (iv) implies $c_4 = 0$, since $Y_0(\lambda\rho)$ blows up when $\rho = 0$. Hence the solution to Eq. (2.121) is

$$V(\rho, z) = \sum_{n=0}^{\infty} A_n e^{-\lambda_n z} J_0(\lambda_n \rho) \tag{2.125}$$

where A_n and λ_n are constants to be determined using conditions (i) and (iii). Imposing condition (iii) on Eq. (2.125) yields the transcendent equation

$$J_0(\lambda_n a) = 0 \tag{2.126}$$

Thus λ_n are the positive roots of $J_0(\lambda_n a)$. If we take λ_1 as the first root, λ_2 as the second root, etc., n must start from 1 in Eq. (2.125). Imposing condition (i) on Eq. (2.125), we obtain

$$V(\rho, 0) = V_o\left(a^2 - \rho^2\right) = \sum_{n=1}^{\infty} A_n J_0(\lambda_n \rho)$$

which is simply the Fourier-Bessel expansion of $V_o(a^2 - \rho^2)$. From Table 2.1, property (h),

$$A_n = \frac{2}{a^2[J_1(\lambda_n a)]^2} \int_0^a \rho V_o \left(a^2 - \rho^2\right) J_0(\lambda_n \rho)\, d\rho \tag{2.127}$$

To evaluate the integral, we utilize property (e) in Table 2.1:

$$\int_0^a x^n J_{n-1}(x)\, dx = x^n J_n(x)\Big|_0^a = a^n J_n(a), \qquad n > 0$$

By changing variables, $x = \lambda\rho$,

$$\int_0^a \rho^n J_{n-1}(\lambda\rho)\, d\rho = \frac{a^n}{\lambda} J_n(\lambda a) \tag{2.128}$$

If $n = 1$,

$$\int_0^a \rho J_0(\lambda\rho)\, d\rho = \frac{a}{\lambda} J_1(\lambda a) \tag{2.129}$$

Similarly, using property (e) in Table 2.1, we may write

$$\int_0^a \rho^3 J_0(\lambda\rho)\, d\rho = \int_0^a \frac{\rho^2}{\lambda} \frac{\partial}{\partial\rho}[\rho J_1(\lambda\rho)]\, d\rho$$

Integrating the right-hand side by parts and applying Eq. (2.128),

$$\begin{aligned}\int_0^a \rho^3 J_0(\lambda\rho)\, d\rho &= \frac{a^3}{\lambda} J_1(\lambda a) - \frac{2}{\lambda}\int_0^a \rho^2 J_1(\lambda\rho)\, d\rho \\ &= \frac{a^3}{\lambda} J_1(\lambda a) - \frac{2a^2}{\lambda^2} J_2(\lambda a)\end{aligned}$$

$J_2(x)$ can be expressed in terms of $J_0(x)$ and $J_1(x)$ using the recurrence relations, i.e., property (c) in Table 2.1:

$$J_2(x) = \frac{2}{x} J_1(x) - J_0(x)$$

Hence

$$\int_0^a \rho^3 J_0(\lambda_n\rho)\, d\rho = \frac{2a^2}{\lambda_n^2}\left[J_0(\lambda_n a) + \left(\frac{a\lambda_n}{2} - \frac{2}{a\lambda_n}\right) J_1(\lambda_n a)\right] \tag{2.130}$$

Substitution of Eqs. (2.129) and (2.130) into Eq. (2.127) gives

$$\begin{aligned}A_n &= \frac{2V_o}{a^2[J_1(\lambda_n a)]^2}\left[\frac{4a}{\lambda_n^3} J_1(\lambda_n a) - \frac{2a^2}{\lambda_n^2} J_0(\lambda_n a)\right] \\ &= \frac{8V_o}{a\lambda_n^3 J_1(\lambda_n a)}\end{aligned}$$

since $J_0(\lambda_n a) = 0$ from Eq. (2.126). Thus the potential distribution is given by

$$V(\rho, z) = \frac{8V_o}{a} \sum_{n=1}^{\infty} \frac{e^{-\lambda_n z} J_0(\lambda_n\rho)}{\lambda_n^3 J_1(\lambda_n a)} \qquad \blacksquare$$

Example 2.5

A plane wave $\mathbf{E} = E_o e^{j(\omega t - kx)}\mathbf{a}_z$ is incident on an infinitely long conducting cylinder of radius a. Determine the scattered field. □

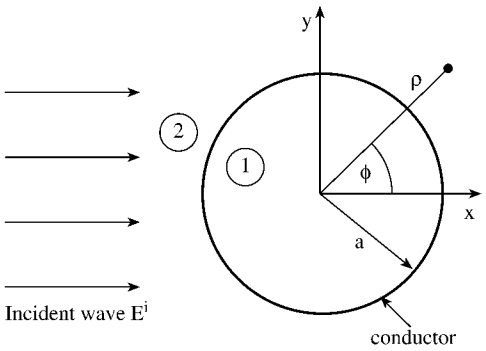

Figure 2.6
Scattering by a conducting cylinder.

Solution
Since the cylinder is infinitely long, the problem is two-dimensional as shown in Fig. 2.6. We shall suppress the time factor $e^{j\omega t}$ throughout the analysis. For the sake of convenience, we need to express the plane wave in terms of cylindrical waves. We let

$$e^{-jx} = e^{-j\rho\cos\phi} = \sum_{n=-\infty}^{\infty} a_n J_n(\rho) e^{jn\phi} \tag{2.131}$$

where a_n are expansion coefficients to be determined. Since $e^{jn\phi}$ are orthogonal functions, multiplying both sides of Eq. (2.131) by $e^{jm\phi}$ and integrating over $0 \le \phi \le 2\pi$ gives

$$\int_0^{2\pi} e^{-j\rho\cos\phi} e^{jm\phi} = 2\pi a_m J_m(\rho)$$

Taking the mth derivative of both sides with respect to ρ and evaluating at $\rho = 0$ leads to

$$2\pi \frac{j^{-m}}{2^m} = 2\pi a_m \frac{1}{2^m} \rightarrow a_m = j^{-m}$$

Substituting this into Eq. (2.131), we obtain

$$e^{-jx} = \sum_{n=-\infty}^{\infty} j^{-n} J_n(\rho) e^{jn\phi}$$

(An alternative, easier way of obtaining this is using the generating function for $J_n(x)$ in Table 2.7.) Thus the incident wave may be written as

$$E_z^i = E_o e^{-jkx} = E_o \sum_{n=-\infty}^{\infty} (-j)^n J_n(k\rho) e^{jn\phi} \tag{2.132}$$

Since the scattered field E_z^s must consist of outgoing waves that vanish at infinity, it contains

$$J_n(k\rho) - jY_n(k\rho) = H_n^{(2)}(k\rho)$$

Hence

$$E_z^s = \sum_{n=-\infty}^{\infty} A_n H_n^{(2)}(k\rho) e^{jn\phi} \tag{2.133}$$

The total field in medium 2 is

$$E_2 = E_z^i + E_z^s$$

while the total field in medium 1 is $E_1 = 0$ since medium 1 is conducting. At $\rho = a$, the boundary condition requires that the tangential components of E_1 and E_2 be equal. Hence

$$E_z^i(\rho = a) + E_z^s(\rho = a) = 0 \tag{2.134}$$

Substituting Eqs. (2.132) and (2.133) into Eq. (2.134),

$$\sum_{n=-\infty}^{\infty} \left[E_o(-j)^n J_n(ka) + A_n H_n^{(2)}(ka) \right] e^{jn\phi} = 0$$

From this, we obtain

$$A_n = -\frac{E_o(-j)^n J_n(ka)}{H_n^{(2)}(ka)}$$

Finally, substituting A_n into Eq. (2.133) and introducing the time factor leads to the scattered wave as

$$\mathbf{E}_z^s = -E_o e^{j\omega t} \mathbf{a}_z \sum_{n=-\infty}^{\infty} (-j)^n \frac{J_n(ka) H_n^{(2)}(k\rho) e^{jn\phi}}{H_n^{(2)}(ka)} \quad \blacksquare$$

2.5 Separation of Variables in Spherical Coordinates

Spherical coordinates (r, θ, ϕ) may be defined as in Fig. 2.7, where $0 \le r \le \infty$, $0 \le \theta \le \pi$, $0 \le \phi < 2\pi$. In this system, the wave equation (2.5b) becomes

$$\nabla^2 U + k^2 U = \frac{1}{r^2}\frac{\partial}{\partial r}\left(r^2 \frac{\partial U}{\partial r}\right) + \frac{1}{r^2 \sin\theta}\frac{\partial}{\partial \theta}\left(\sin\theta \frac{\partial U}{\partial \theta}\right) + \frac{1}{r^2 \sin^2\theta}\frac{\partial^2 U}{\partial \phi^2} + k^2 U = 0 \tag{2.135}$$

As usual, we shall first solve Laplace's equation in two dimensions and later solve the wave equation in three dimensions.

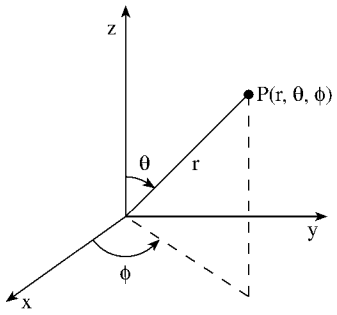

Figure 2.7
Coordinate relation in a spherical system.

2.5.1 Laplace's Equation

Consider the problem of finding the potential distribution due to an uncharged conducting sphere of radius a located in an external uniform electric field as in Fig. 2.8.

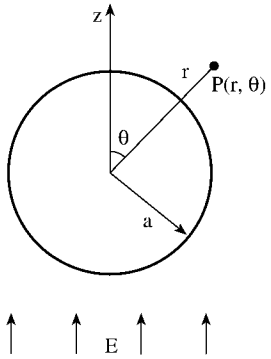

Figure 2.8
An uncharged conducting sphere in a uniform external electric field.

The external electric field can be described as

$$\mathbf{E} = E_o \mathbf{a}_z \tag{2.136}$$

while the corresponding electric potential can be described as

$$V = -\int \mathbf{E} \cdot d\mathbf{l} = -E_o z$$

or

$$V = -E_o r \cos\theta \tag{2.137}$$

where $V(\theta = \pi/2) = 0$ has been assumed. From Eq. (2.137), it is evident that V is independent of ϕ, and hence our problem is solving Laplace's equation in two dimensions, namely,

$$\nabla^2 V = \frac{1}{r^2}\frac{\partial}{\partial r}\left(r^2\frac{\partial V}{\partial r}\right) + \frac{1}{r^2\sin\theta}\frac{\partial}{\partial\theta}\left(\sin\theta\frac{\partial V}{\partial\theta}\right) = 0 \tag{2.138}$$

subject to the conditions

$$V(r,\theta) = -E_o r\cos\theta \quad \text{as} \quad r\to\infty\,, \tag{2.139a}$$

$$V(a,\theta) = 0 \tag{2.139b}$$

We let

$$V(r,\theta) = R(r)H(\theta) \tag{2.140}$$

so that Eq. (2.138) becomes

$$\frac{1}{R}\frac{d}{dr}(r^2R') = -\frac{1}{H\sin\theta}\frac{d}{d\theta}(\sin\theta H') = \lambda \tag{2.141}$$

where λ is the separation constant. Thus the separated equations are

$$r^2R'' + 2rR' - \lambda R = 0 \tag{2.142}$$

and

$$\frac{d}{d\theta}(\sin\theta H') + \lambda\sin\theta H = 0 \tag{2.143}$$

Equation (2.142) is the *Cauchy-Euler equation.* It can be solved by making the substitution $R = r^k$. This leads to the solution

$$R_n(r) = A_n r^n + B_n r^{-(n+1)}, \quad n = 0, 1, 2, \ldots \tag{2.144}$$

with $\lambda = n(n+1)$. To solve Eq. (2.143), we may replace H by y and $\cos\theta$ by x so that

$$\frac{d}{d\theta} = \frac{dx}{d\theta}\frac{d}{dx} = -\sin\theta\frac{d}{dx}$$

$$\begin{aligned}\frac{d}{d\theta}\left(\sin\theta\frac{dH}{d\theta}\right) &= -\sin\theta\frac{d}{dx}\left(\sin\theta\frac{dx}{d\theta}\frac{dH}{dx}\right)\\ &= \sin\theta\frac{d}{dx}\left(\sin^2\theta\frac{dy}{dx}\right)\\ &= \sqrt{1-x^2}\frac{d}{dx}\left[(1-x^2)\frac{dy}{dx}\right]\end{aligned}$$

Making these substitutions in Eq. (2.143) yields

$$\frac{d}{dx}\left[(1-x^2)\frac{dy}{dx}\right] + n(n+1)y = 0$$

or

$$(1-x^2)y'' - 2xy' + n(n+1)y = 0 \tag{2.145}$$

which is the *Legendre differential equation*. Its solution is obtained by the method of Frobenius [5] as

$$y = c_n P_n(x) + d_n Q_n(x) \tag{2.146}$$

where $P_n(x)$ and $Q_n(x)$ are Legendre functions of the first and second kind, respectively.

$$\boxed{P_n(x) = \sum_{k=0}^{N} \frac{(-1)^k (2n-2k)! x^{n-2k}}{2^n k!(n-k)!(n-2k)!}} \tag{2.147}$$

where $N = n/2$ if n is even and $N = (n-1)/2$ if n is odd. For example,

$$\begin{aligned}
P_0(x) &= 1 \\
P_1(x) &= x = \cos\theta \\
P_2(x) &= \frac{1}{2}(3x^2 - 1) = \frac{1}{4}(3\cos 2\theta + 1) \\
P_3(x) &= \frac{1}{2}(5x^3 - 3x) = \frac{1}{8}(5\cos 3\theta + 3\cos\theta) \\
P_4(x) &= \frac{1}{8}(35x^4 - 30x^2 + 3) = \frac{1}{64}(35\cos 4\theta + 20\cos 2\theta + 9) \\
P_5(x) &= \frac{1}{8}(63x^5 - 70x^3 + 15x) = \frac{1}{128}(30\cos\theta + 35\cos 3\theta + 63\cos 5\theta)
\end{aligned}$$

Some useful identities and properties [5] of Legendre functions are listed in Table 2.2. The Legendre functions of the second kind are given by

$$\begin{aligned}
Q_n(x) = P_n(x)\left[\frac{1}{2}\ln\frac{1+x}{1-x} - p(n)\right] \\
+ \sum_{k=1}^{n} \frac{(-1)^k (n+k)!}{(k!)^2 (n-k)!} p(k)\left[\frac{1-x}{2}\right]^k
\end{aligned} \tag{2.148}$$

where $p(k)$ is as defined in Eq. (2.100). Typical graphs of $P_n(x)$ and $Q_n(x)$ are shown in Fig. 2.9. Q_n are not as useful as P_n since they are singular at $x = \pm 1$ (or $\theta = 0, \pi$) due to the logarithmic term in Eq. (2.148). We use Q_n only when $x \neq \pm 1$ (or $\theta \neq 0, \pi$), e.g., in problems having conical boundaries that exclude the axis from the solution region. For the problem at hand, $\theta = 0, \pi$ is included so that the solution to Eq. (2.143) is

$$H_n(\theta) = P_n(\cos\theta) \tag{2.149}$$

Table 2.2 Properties and Identities of Legendre Functions[1]

(a) For $n \geq 1$, $P_n(1) = 1$, $P_n(-1) = (-1)^n$,

$$P_{2n+1} = 0, \; P_{2n}(0) = (-1)^n \frac{(2n)!}{2^{2n}(n!)^2}$$

(b) $P_n(-x) = (-1)^n P_n(x)$

(c) $P_n(x) = \frac{1}{2^n n!} \frac{d^n}{dx^n}(x^2 - 1)^n, \qquad n \geq 0$

(Rodriguez formula)

(d) $(n+1)P_{n+1}(x) = (2n+1)xP_n(x) - nP_{n-1}(x), \qquad n \geq 1$

(recurrence relation)

(e) $P_n'(x) = xP_{n-1}'(x) + nP_{n-1}(x), \qquad n \geq 1$

(f) $P_n(x) = xP_{n-1}(x) + \frac{x^2-1}{n} P_{n-1}'(x), \qquad n \geq 1$

(g) $P_{n+1}'(x) - P_{n-1}'(x) = (2n+1)P_n(x), \qquad n \geq 1$

or $\int Pn(x)\,dx = \frac{P_{n+1} - P_{n-1}}{2n+1}$

(h) Legendre series expansion of $f(x)$:

$$f(x) = \sum_{n=0}^{\infty} A_n P_n(x), \qquad -1 \leq x \leq 1$$

where

$$A_n = \frac{2n+1}{2} \int_{-1}^{1} f(x) P_n(x)\,dx, \qquad n \geq 0$$

If $f(x)$ is odd,

$$A_n = (2n+1) \int_0^1 f(x) Pn(x)\,dx, \qquad n = 0, 2, 4 \ldots$$

and if $f(x)$ is even,

$$A_n = (2n+1) \int_0^1 f(x) Pn(x)\,dx, \qquad n = 1, 3, 5 \ldots$$

(i) Orthogonality property

$$\int_{-1}^{1} Pn(x) P_m(x)\,dx = \begin{cases} 0, & n \neq m \\ \frac{2}{2n+1}, & n = m \end{cases}$$

1. Properties (d) to (g) are also valid for $Q_n(x)$.

Substituting Eqs. (2.144) and (2.149) into Eq. (2.140) gives

$$V_n(r, \theta) = \left[A_n r^n + B_n r^{-(n+1)} \right] P_n(\cos\theta) \tag{2.150}$$

To determine A_n and B_n we apply the boundary conditions in Eq. (2.139). Since as

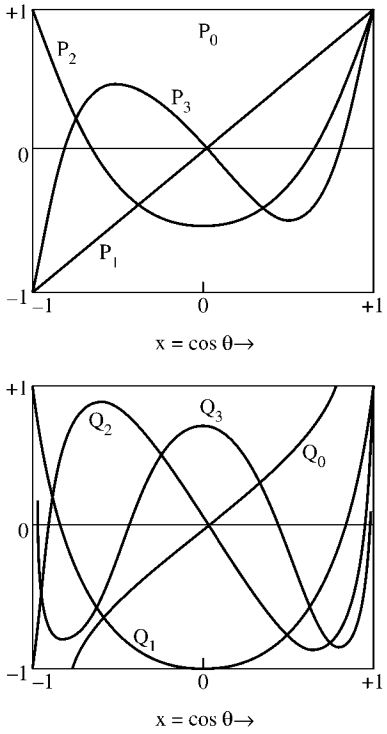

Figure 2.9
Typical Legendre functions of the first and second kinds.

$r \to \infty,\ V = -E_o r\cos\theta$, it follows that $n = 1$ and $A_1 = -E_o$, i.e.,

$$V(r,\theta) = \left(-E_o r + \frac{B_1}{r^2}\right)\cos\theta$$

Also since $V = 0$ when $r = a,\ B_1 = E_o a^3$. Hence the complete solution is

$$V(r,\theta) = -E_o\left(r - \frac{a^3}{r^2}\right)\cos\theta \tag{2.151}$$

The electric field intensity is given by

$$\begin{aligned}\mathbf{E} = -\nabla V &= -\frac{\partial V}{\partial r}\mathbf{a}_r - \frac{1}{r}\frac{\partial V}{\partial \theta}\mathbf{a}_\theta \\ &= E_o\left[1 + \frac{2a^3}{r^3}\right]\cos\theta\,\mathbf{a}_r + E_o\left[1 - \frac{a^3}{r^3}\right]\sin\theta\,\mathbf{a}_\theta\end{aligned} \tag{2.152}$$

2.5.2 Wave Equation

To solve the wave equation (2.135), we substitute

$$U(r,\theta,\phi) = R(r)H(\theta)F(\phi) \tag{2.153}$$

into the equation. Multiplying the result by $r^2\sin^2\theta/RHF$ gives

$$\frac{\sin^2\theta}{R}\frac{d}{dr}\left(r^2\frac{dR}{dr}\right) + \frac{\sin\theta}{H}\frac{d}{d\theta}\left(\sin\theta\frac{dH}{d\theta}\right) + k^2r^2\sin^2\theta = -\frac{1}{F}\frac{d^2F}{d\phi^2} \tag{2.154}$$

Since the left-hand side of this equation is independent of ϕ, we let

$$-\frac{1}{F}\frac{d^2F}{d\phi^2} = m^2, \qquad m = 0, 1, 2, \ldots$$

where m, the first separation constant, is chosen to be nonnegative integer such that U is periodic in ϕ. This requirement is necessary for physical reasons that will be evident later. Thus Eq. (2.154) reduces to

$$\frac{1}{R}\frac{d}{dr}\left(r^2\frac{dR}{dr}\right) + k^2r^2 = -\frac{1}{H\sin\theta}\frac{d}{d\theta}\left(\sin\theta\frac{dH}{d\theta}\right) + \frac{m^2}{\sin^2\theta} = \lambda$$

where λ is the second separation constant. As in Eqs. (2.141) to (2.144), $\lambda = n(n+1)$ so that the separated equations are now

$$F'' + m^2F = 0, \tag{2.155}$$

$$R'' + \frac{2}{r}R' + \left[k^2 - \frac{n(n+1)}{r^2}\right]R = 0\,, \tag{2.156}$$

and

$$\frac{1}{\sin\theta}\frac{d}{d\theta}(\sin\theta H') + \left[n(n+1) - \frac{m^2}{\sin^2\theta}\right]H = 0 \tag{2.157}$$

As usual, the solution to Eq. (2.155) is

$$F(\phi) = c_1e^{jm\phi} + c_2e^{-jm\phi} \tag{2.158a}$$

or

$$F(\phi) = c_3\sin m\phi + c_4\cos m\phi \tag{2.158b}$$

If we let $R(r) = r^{-1/2}\widetilde{R}(r)$, Eq. (2.156) becomes

$$\widetilde{R}'' + \frac{1}{r}\widetilde{R}' + \left[k^2 - \frac{(n+1/2)^2}{r^2}\right]\widetilde{R} = 0\,,$$

which has the solution

$$\widetilde{R} = Ar^{1/2} z_n(kr) = BZ_{n+1/2}(kr) \tag{2.159}$$

Functions $z_n(x)$ are *spherical Bessel functions* and are related to ordinary Bessel functions $Z_{n+1/2}$ according to

$$z_n(x) = \sqrt{\frac{\pi}{2x}} Z_{n+1/2}(x) \tag{2.160}$$

In Eq. (2.160), $Z_{n+1/2}(x)$ may be any of the ordinary Bessel functions of half-integer order, $J_{n+1/2}(x)$, $Y_{n+1/2}(x)$, $I_{n+1/2}(x)$, $K_{n+1/2}(x)$, $H^{(1)}_{n+1/2}(x)$, and $H^{(2)}_{n+1/2}(x)$, while $z_n(x)$ may be any of the corresponding spherical Bessel functions $j_n(x)$, $y_n(x)$, $i_n(x)$, $k_n(x)$, $h^{(1)}_n(x)$, and $h^{(2)}_n(x)$. Bessel functions of fractional order are, in general, given by

$$J_\nu(x) = \sum_{k=0}^{\infty} \frac{(-1)^k x^{2k+\nu}}{2^{2k+\nu} k! \Gamma(\nu + k + 1)} \tag{2.161}$$

$$Y_\nu(x) = \frac{J_\nu(x)\cos(\nu\pi) - J_{-\nu}}{\sin(\nu\pi)} \tag{2.162}$$

$$I_\nu(x) = (-j)^\nu J_\nu(jx) \tag{2.163}$$

$$K_\nu(x) = \frac{\pi}{2}\left[\frac{I_{-\nu} - I_\nu}{\sin(\nu\pi)}\right] \tag{2.164}$$

where $J_{-\nu}$ and $I_{-\nu}$ are, respectively, obtained from Eqs. (2.161) and (2.163) by replacing ν with $-\nu$. Although ν in Eqs. (2.161) to (2.164) can assume any fractional value, in our specific problem, $\nu = n + 1/2$. Since Gamma function of half-integer order is needed in Eq. (2.161), it is necessary to add that

$$\Gamma(n + 1/2) = \begin{cases} \dfrac{(2n)!}{2^{2n} n!}\sqrt{\pi}\,, & n \geq 0 \\ \dfrac{(-1)^n 2^{2n} n!}{(2n)!}\sqrt{\pi}\,, & n < 0 \end{cases} \tag{2.165}$$

Thus the lower order spherical Bessel functions are as follows:

$$j_0(x) = \frac{\sin x}{x}\,, \qquad y_0(x) = -\frac{\cos x}{x}\,,$$

$$h^{(1)}_0(x) = \frac{e^{jx}}{jx}\,, \qquad h^{(2)}_0(x) = \frac{e^{-jx}}{-jx}\,,$$

$$i_0(x) = \frac{\sinh x}{x}\,, \qquad k_0(x) = \frac{e^{-x}}{x}\,,$$

$$j_1(x) = \frac{\sin x}{x^2} - \frac{\cos x}{x}\,, \qquad y_1(x) = -\frac{\cos x}{x^2} - \frac{\sin x}{x}\,,$$

$$h^{(1)}_1 = -\frac{(x + j)}{x^2} e^{jx}\,, \qquad h^{(2)}_1(x) = -\frac{(x - j)}{x^2} e^{-jx}$$

Other $z_n(x)$ can be obtained from the series expansion in Eqs. (2.161) and (2.162) or the recurrence relations and properties of $z_n(x)$ presented in Table 2.3.

Table 2.3 Properties and Identities of Spherical Bessel Functions

(a) $z_{n+1} = \frac{(2n+1)}{x} z_n(x) - z_{n-1}(x)$ (recurrence relation)
(b) $\frac{d}{dx} z_n(x) = \frac{1}{2n+1}[n z_{n-1} - (n+1) z_{n+1}(x)]$
(c) $\frac{d}{dx}[x z_n(x)] = -n z_n(x) + x z_{n-1}(x)$
(d) $\frac{d}{dx}[x^{n+1} z_n(x)] = -x^{n+1} z_{n-1}(x)$
(e) $\frac{d}{dx}[x^{-n} z_n(x)] = -x^{-n} z_{n+1}(x)$
(f) $\int x^{n+2} z_n(x)\, dx = x^{n+2} z_{n+1}(x)$
(g) $\int x^{1-n} z_n(x)\, dx = -x^{1-n} z_{n-1}(x)$
(h) $\int x^2 [z_n(x)]^2\, dx = \frac{1}{2} x^3 [z_n(x) - z_{n-1}(x) z_{n+1}(x)]$

By replacing H in Eq. (2.157) with y, $\cos\theta$ by x, and making other substitutions as we did for Eq. (2.143), we obtain

$$\left(1 - x^2\right) y'' - 2xy' + \left[n(n+1) - \frac{m^2}{1 - x^2}\right] y = 0\,, \tag{2.166}$$

which is Legendre's associated differential equation. Its general solution is of the form

$$y(x) = a_{mn} P_n^m(x) + d_{mn} Q_n^m(x) \tag{2.167}$$

where $P_n^m(x)$ and $Q_n^m(x)$ are called associated Legendre functions of the first and second kind, respectively. Equation (2.146) is a special case of Eq. (2.167) when $m = 0$. $P_n^m(x)$ and $Q_n^m(x)$ can be obtained from ordinary Legendre functions $P_n(x)$ and $Q_n(x)$ using

$$P_n^m(x) = \left[1 - x^2\right]^{m/2} \frac{d^m}{dx^m} P_n(x) \tag{2.168}$$

and

$$Q_n^m(x) = \left[1 - x^2\right]^{m/2} \frac{d^m}{dx^m} Q_n(x) \tag{2.169}$$

where $-1 < x < 1$. We note that

$$\begin{aligned} P_n^0(x) &= P_n(x)\,, \\ Q_n^0(x) &= Q_n(x)\,, \\ P_n^m(x) &= 0 \quad \text{for} \quad m > n \end{aligned} \tag{2.170}$$

Typical associated Legendre functions are:

$$P_1^1(x) = (1-x^2)^{1/2} = \sin\theta\ ,$$
$$P_2^1(x) = 3x(1-x^2)^{1/2} = 3\cos\theta\sin\theta\ ,$$
$$P_2^2(x) = 3(1-x^2) = 3\sin^2\theta\ ,$$
$$P_3^1(x) = \frac{3}{2}(1-x^2)^{1/2}(5x-1) = \frac{3}{2}\sin\theta(5\cos\theta - 1)\ ,$$

$$Q_1^1(x) = (1-x^2)^{1/2}\left[\frac{1}{2}\ln\frac{1+x}{1-x} + \frac{x}{1-x^2}\right]\ ,$$
$$Q_2^1 = (1-x^2)^{1/2}\left[\frac{3x}{2}\ln\frac{1+x}{1-x} + \frac{3x^2-2}{1-x^2}\right]\ ,$$
$$Q_2^2 = (1-x^2)^{1/2}\left[\frac{3}{2}\ln\frac{1+x}{1-x} + \frac{5x^2-3x^2}{[1-x^2]^2}\right]$$

Higher-order associated Legendre functions can be obtained using Eqs. (2.168) and (2.169) along with the properties in Table 2.4. As mentioned earlier, $Q_n^m(x)$ is unbounded at $x = \pm 1$, and hence it is only used when $x = \pm 1$ is excluded. Substituting Eqs. (2.158), (2.159), and (2.167) into Eq. (2.153) and applying superposition theorem, we obtain

$$U(r,\theta,\phi,t) = \sum_{n=0}^{\infty}\sum_{m=0}^{n}\sum_{\ell=0}^{\infty} A_{mn\ell} z_n(k_{m\ell}r) P_n^m(\cos\theta)\exp(\pm jm\phi \pm j\omega t) \qquad (2.171)$$

Note that the products $H(\theta)F(\phi)$ are known as spherical harmonics.

Example 2.6

A thin ring of radius a carries charge of density ρ. Find the potential at: (a) point $P(0, 0, z)$ on the axis of the ring, (b) point $P(r, \theta, \phi)$ in space. □

Solution

Consider the thin ring as in Fig. 2.10.

(a) From elementary electrostatics, at $P(0, 0, z)$

$$V = \int \frac{\rho dl}{4\pi\epsilon R}$$

where $dl = ad\phi$, $\quad R = \sqrt{a^2+z^2}$. Hence

$$V = \int_0^{2\pi} \frac{\rho a d\phi}{4\pi\epsilon[a^2+z^2]^{1/2}} = \frac{a\rho}{2\epsilon[a^2+z^2]^{1/2}} \qquad (2.172)$$

Table 2.4 Properties and Identities of Associated Legendre Functions[1]

(a) $P_m(x) = 0, \quad m > n$

(b) $P_n^m(x) = \frac{(2n-1)xP_{n-1}^m(x) - (n+m-1)P_{n-2}^m(x)}{n-m}$

(recurrence relations for fixed m)

(c) $P_n^m(x) = \frac{2(m-1)x}{(1-x^2)^{1/2}} P_n^{m-1}(x) - (n-m+2)(n+m-1)P_n^{m-2}$

(recurrence relations for fixed n)

(d) $P_n^m(x) = \frac{[1-x^2]^{m/2}}{2^n} \sum_{k=0}^{\left[\frac{m-n}{2}\right]} \frac{(-1)^k(2n-2k)!x^{n-2k-m}}{k!(n-k)!(n-2k-m)!}$

where $[t]$ is the bracket or greatest integer function, e.g., $[3.54] = 3$.

(e) $\frac{d}{dx}P_n^m(x) = \frac{(n+m)P_{n-1}^m(x) - nxP_n^m(x)}{1-x^2}$

(f) $\frac{d}{d\theta}P_n^m(x) = \frac{1}{2}[(n-m+1)(n+m)P_n^{m-1}(x) - P_n^{m+1}(x)]$

(g) $\frac{d}{dx}P_n^m(x) = -\frac{mxP_n^m(x)}{1-x^2} + \frac{(1-x^2)^{m/2}}{2^n} \sum_{k=0}^{\left[\frac{m-n}{2}\right]} \frac{(-1)^k(2n-2k)!x^{n-2k-m-1}}{k!(n-k)!(n-2k-m)!}$

(h) $\frac{d}{d\theta}P_n^m(x) = -(1-x^2)^{1/2}\frac{d}{dx}P_n^m(x)$

(i) The series expansion of $f(x)$:

$$f(x) = \sum_{n=0}^{\infty} A_n P_n^m(x),$$

where $A_n = \frac{(2n+1)(n-m)!}{2(n+m)!} \int_{-1}^{1} f(x)P_n^m(x)\,dx$

(j) $\left.\frac{d^m}{dx^m}P_n(x)\right|_{x=1} = \frac{(n+m)!}{2^m m!(n-m)!}$

$\left.\frac{d^m}{dx^m}P_n(x)\right|_{x=-1} = \frac{(-1)^{n+m}(n+m)!}{2^m m!(n-m)!}$

(k) $P_n^{-m}(x) = (-1)^m \frac{(n-m)!}{(n+m)!}P_n^m(x), \quad m = 0, 1, \ldots, n$

(l) $\int_{-1}^{1} P_n^m(x)P_n^m(x)\,dx = \frac{2}{2n+1}\frac{(n-m)!}{(n+m)!}\delta_{nk},$

where δ_{nk} is the kronecker delta defined by $\delta_{nk} = \begin{cases} 0, & n \neq k \\ 1, & n = k \end{cases}$

1. Properties (b) and (c) are also valid for $Q_n^m(x)$.

(b) To find the potential at $P(r, \theta, \phi)$, we may evaluate the integral for the potential as we did in part (a). However, it turns out that the boundary-value solution is simpler. So we solve Laplace's equation $\nabla^2 V = 0$ where $V(0, 0, z)$ must conform with the result in part (a). From Fig. 2.10, it is evident that V is invariant with ϕ. Hence the solution to Laplace's equation is

$$V = \sum_{n=0}^{\infty} \left[A_n r^n + \frac{B_n}{r^{n+1}} \right] \left[A'_n P_n(u) + B'_n Q_n(u) \right]$$

where $u = \cos\theta$. Since Q_n is singular at $\theta = 0, \pi$, $B'_n = 0$. Thus

$$V = \sum_{n=0}^{\infty} \left[C'_n r^n + \frac{D'_n}{r^{n+1}} \right] P_n(u) \tag{2.173}$$

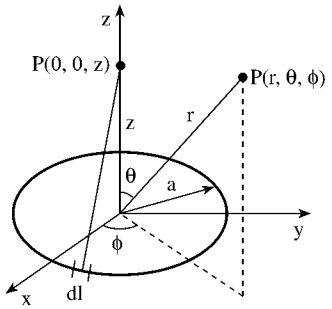

Figure 2.10
Charged ring of Example 2.6.

For $0 \leq r \leq a$, $D'_n = 0$ since V must be finite at $r = 0$.

$$V = \sum_{n=0}^{\infty} C'_n r^n P_n(u) \tag{2.174}$$

To determine the coefficients C'_n, we set $\theta = 0$ and equate V to the result in part (a). But when $\theta = 0$, $u = 1$, $P_n(1) = 1$, and $r = z$. Hence

$$V(0, 0, z) = \frac{a\rho}{2\epsilon[a^2 + z^2]^{1/2}} = \frac{a\rho}{2\epsilon} \sum_{n=0}^{\infty} C_n z^n \tag{2.175}$$

Using the binomial expansion, the term $[a^2 + z^2]^{1/2}$ can be written as

$$\frac{1}{a}\left[1 + \frac{z^2}{a^2}\right]^{-1/2} = \frac{1}{a}\left[1 - \frac{1}{2}(z/a)^2 + \frac{1 \cdot 3}{2 \cdot 4}(z/a)^4 - \frac{1 \cdot 3 \cdot 5}{2 \cdot 4 \cdot 6}(z/a)^6 + \ldots\right]$$

Comparing this with the last term in Eq. (2.175), we obtain

$$C_0 = 1, \quad C_1 = 0, \quad C_2 = -\frac{1}{2a^2}, \quad C_3 = 0\,,$$
$$C_4 = \frac{1\cdot 3}{2\cdot 4}\frac{1}{a^4}, \quad C_5 = 0, \quad C_6 = -\frac{1\cdot 3\cdot 5}{2\cdot 4\cdot 6}\frac{1}{a^6}\,, \ldots$$

or in general,

$$C_{2n} = (-1)^n \frac{(2n)!}{[n!2^n]^2 a^{2n}}$$

Substituting these into Eq. (2.174) gives

$$V = \frac{a\rho}{2\epsilon}\sum_{n=0}^{\infty}\frac{(-1)^n(2n)!}{[n!2^n]^2}(r/a)^{2n}P_{2n}(\cos\theta), \qquad 0 \le r \le a \tag{2.176}$$

For $r \ge a$, $C_n' = 0$ since V must be finite as $r \to \infty$, and

$$V = \sum_{n=0}^{\infty}\frac{D_n'}{r^{n+1}}P_n(u) \tag{2.177}$$

Again, when $\theta = 0$, $u = 1$, $P_n(1) = 1$, $r = z$,

$$V(0,0,z) = \frac{a\rho}{2\epsilon[a^2+z^2]^{1/2}} = \frac{a\rho}{2\epsilon}\sum_{n=0}^{\infty}D_n z^{-(n+1)} \tag{2.178}$$

Using the binomial expansion, the middle term $[a^2+z^2]^{-1/2}$ can be written as

$$\frac{1}{z}\left[1+\frac{a^2}{z^2}\right]^{-1/2} = \frac{1}{z}\left[1-\frac{1}{2}(a/z)^2+\frac{1\cdot 3}{2\cdot 4}(a/z)^4-\frac{1\cdot 3\cdot 5}{2\cdot 4\cdot 6}(a/z)^6+\cdots\right]$$

Comparing this with the last term in Eq. (2.178), we obtain

$$D_0 = 1, \qquad D_1 = 0, \qquad D_2 = -\frac{a^2}{2}, \qquad D_3 = 0\,,$$
$$D_4 = \frac{1\cdot 3}{2\cdot 4}a^4, \qquad D_5 = 0, \qquad D_6 = -\frac{1\cdot 3\cdot 5}{2\cdot 4\cdot 6}a^6, \ldots$$

or in general,

$$D_{2n} = (-1)^n\frac{(2n)!}{[n!2^n]^2}a^{2n}$$

Substituting these into Eq. (2.177) gives

$$V = \frac{a\rho}{2\epsilon r}\sum_{n=0}^{\infty}\frac{(-1)^n(2n)!}{[n!2^n]^2}(a/r)^{2n}P_{2n}(\cos\theta), \qquad r \ge a \tag{2.179}$$

We may combine Eqs. (2.176) and (2.179) to get

$$V = \begin{cases} a\sum_{n=0}^{\infty} g_n (r/a)^{2n} P_{2n}(\cos\theta), & 0 \le r \le a \\ \sum_{n=0}^{\infty} g_n (a/r)^{2n+1} P_{2n}(\cos\theta), & r \ge a \end{cases}$$

where

$$g_n = (-1)^n \frac{\rho}{2\epsilon} \frac{2n!}{[n!2^n]^2} \qquad \blacksquare$$

Example 2.7

A conducting spherical shell of radius a is maintained at potential $V_o \cos 2\phi$; determine the potential at any point inside the sphere. □

Solution

The solution to this problem is somewhat similar to that of the previous problem except that V is a function of ϕ. Hence the solution to Laplace's equation for $0 \le r \le a$ is of the form

$$V = \sum_{n=0}^{\infty}\sum_{m=0}^{\infty} (a_{mn}\cos m\phi + b_{mn}\sin m\phi)\,(r/a)^n P_n^m(\cos\theta)$$

Since $\cos m\phi$ and $\sin m\phi$ are orthogonal functions, $a_{mn} = 0 = b_{mn}$ except that $a_{n2} \neq 0$. Hence at $r = a$

$$V_o \cos 2\phi = \cos 2\phi \sum_{n=2}^{\infty} a_{n2} P_n^2(\cos\theta)$$

or

$$V_o = \sum_{n=2}^{\infty} a_{n2} P_n^2(x), \qquad x = \cos\theta$$

which is the Legendre expansion of V_o. Multiplying both sides by $P_m^2(x)$ gives

$$\frac{2}{2n+1}\frac{(n+2)!}{(n-2)!}a_{n2} = V_o \int_{-1}^{1} P_n^2(x)\,dx = V_o \int_{-1}^{1} \left(1-x^2\right)\frac{d^2}{dx^2}P_n(x)\,dx$$

Integrating by parts twice yields

$$a_{n2} = V_o \frac{2n+1}{2}\frac{(n-2)!}{(n+2)!}\left(2P_n(1) - 2P_n(-1) - 2\int_{-1}^{1} P_n(x)\,dx\right)$$

Using the generating functions for $P_n(x)$ (see Table 2.7 and Example 2.10) it is readily shown that

$$P_n(1) = 1, \qquad P_n(-1) = (-1)^n$$

Also

$$\int_{-1}^{1} P_n(x)\,dx = \int_{-1}^{1} P_0(x)P_n(x)\,dx = 0$$

by the orthogonality property of $P_n(x)$. Hence

$$a_{n2} = V_o(2n+1)\frac{(n-2)!}{(n+2)!}\left[1-(-1)^n\right]$$

and

$$V = V_o\cos 2\phi\sum_{n=2}^{\infty}(2n+1)\frac{(n-2)!}{(n+2)!}\left[1-(-1)^n\right](r/a)^n P_n^2(\cos\theta) \qquad \blacksquare$$

Example 2.8

Express: (a) the plane wave e^{jz} and (b) the cylindrical wave $J_0(\rho)$ in terms of spherical wave functions. □

Solution

(a) Since $e^{jz} = e^{jr\cos\theta}$ is independent of ϕ and finite at the origin, we let

$$e^{jz} = e^{jr\cos\theta} = \sum_{n=0}^{\infty} a_n j_n(r) P_n(\cos\theta) \tag{2.180}$$

where a_n are the expansion coefficients. To determine a_n, we multiply both sides of Eq. (2.180) by $P_m(\cos\theta)\sin\theta$ and integrate over $0 < \theta < \pi$:

$$\int_0^{\pi} e^{jr\cos\theta} P_m(\cos\theta)\sin\theta d\theta = \sum_{n=0}^{\infty} a_n j_n(r)\int_{-1}^{1} P_n(x)P_m(x)\,dx$$

$$= \begin{cases} 0, & n \neq m \\ \frac{2}{2n+1}a_n j_n(r), & n = m \end{cases}$$

where the orthogonality property (i) of Table 2.2 has been utilized. Taking the nth derivative of both sides and evaluating at $r = 0$ gives

$$j^n\int_0^{\pi}\cos^n\theta P_n(\cos\theta)\sin\theta d\theta = \frac{2}{2n+1}a_n\frac{d^n}{dr^n}j_n(r)\bigg|_{r=0} \tag{2.181}$$

The left-hand side of Eq. (2.181) yields

$$j^n\int_{-1}^{1} x^n P_n(x)\,dx = \frac{2^{n+1}(n!)^2}{(2n+1)!}j^n \tag{2.182}$$

To evaluate the right-hand side of Eq. (2.181), we recall that

$$j_n(r) = \sqrt{\frac{\pi}{2x}}J_{n+1/2}(r) = \sqrt{\frac{\pi}{2}}\sum_{m=0}^{\infty}\frac{(-1)^m r^{2m+n}}{m!\Gamma(m+n+3/2)2^{2m+n+1/2}}$$

Hence

$$\left.\frac{d^n}{dr^n} j_n(r)\right|_{r=0} = \sqrt{\frac{\pi}{2}} \frac{n!}{\Gamma(n+3/2)2^{n+1/2}} = \frac{2^n (n!)^2}{(2n+1)!} \tag{2.183}$$

Substituting Eqs. (2.182) and (2.183) into Eq. (2.181) gives

$$a_n = j^n (2n+1)$$

Thus

$$e^{jz} = e^{jr\cos\theta} = \sum_{n=0}^{\infty} j^n (2n+1) j_n(r) P_n(\cos\theta) \tag{2.184}$$

(b) Since $J_0(\rho) = J_0(r\sin\theta)$ is even, independent of ϕ, and finite at the origin,

$$J_0(\rho) = J_0(r\sin\theta) = \sum_{n=0}^{\infty} b_n j_{2n}(r) P_{2n}(\cos\theta) \tag{2.185}$$

To determine the coefficients of expansion b_n, we multiply both sides by $P_m(\cos\theta)\sin\theta$ and integrate over $0 < \theta < \pi$. We obtain

$$\int_0^{\pi} J_0(r\sin\theta) P_m(\cos\theta)\sin\theta\, d\theta = \begin{cases} 0, & m \neq 2n \\ \dfrac{2b_n}{4n+1} j_{2n}(r), & m = 2n \end{cases}$$

Differentiating both sides $2n$ times with respect to r and setting $r = 0$ gives

$$b_n = \frac{(-1)^n (4n+1)(2n-1)!}{2^{2n-1} n!(n-1)!}$$

Hence

$$J_0(\rho) = \sum_{n=0}^{\infty} \frac{(-1)^n (4n+1)(2n-1)!}{2^{2n-1} n!(n-1)!} j_{2n}(r) P_{2n}(\cos\theta) \qquad \blacksquare$$

2.6 Some Useful Orthogonal Functions

Orthogonal functions are of great importance in mathematical physics and engineering. A system of real functions $\Phi_n (n = 0, 1, 2, \ldots)$ is said to be *orthogonal with weight* $w(x)$ on the interval (a, b) if

$$\int_a^b w(x)\Phi_m(x)\Phi_n(x)\, dx = 0 \tag{2.186}$$

for every $m \neq n$. For example, the system of functions $\cos(nx)$ is orthogonal with weight 1 on the interval $(0, \pi)$ since

$$\int_0^{\pi} \cos mx \cos nx \, dx = 0 , \quad m \neq n$$

Orthogonal functions usually arise in the solution of partial differential equations governing the behavior of certain physical phenomena. These include Bessel, Legendre, Hermite, Laguerre, and Chebyshev functions. In addition to the orthogonality properties in Eq. (2.186), these functions have many other general properties, which will be discussed briefly in this section. They are very useful in series expansion of functions belonging to very general classes, e.g., Fourier-Bessel series, Legendre series, etc. Although Hermite, Laguerre, and Chebyshev functions are of less importance in EM problems than Bessel and Legendre functions, they are sometimes useful and therefore deserve some attention.

An arbitrary function $f(x)$, defined over interval (a, b), can be expressed in terms of any complete, orthogonal set of functions:

$$f(x) = \sum_{n=0}^{\infty} A_n \Phi_n(x) \tag{2.187}$$

where the expansion coefficients are given by

$$A_n = \frac{1}{N_n} \int_a^b w(x) f(x) \Phi_n(x) \, dx \tag{2.188}$$

and the (weighted) norm N_n is defined as

$$N_n = \int_a^b w(x) \Phi_n^2(x) \, dx \tag{2.189}$$

Simple orthogonality results when $w(x) = 1$ in Eqs. (2.186) to (2.189).

Perhaps the best way to briefly describe the orthogonal functions is in table form. This is done in Tables 2.5 to 2.7. The differential equations giving rise to each function are provided in Table 2.5. The orthogonality relations in Table 2.6 are necessary for expanding a given arbitrary function $f(x)$ in terms of the orthogonal functions as in Eqs. (2.187) to (2.189). Most of the properties of the orthogonal functions can be proved using the generating functions of Table 2.7. To the properties in Tables 2.5 to 2.7 we may add the recurrence relations and series expansion formulas for calculating the functions for specific argument x and order n. These have been provided for $J_n(x)$ and $Y_n(x)$ in Table 2.1 and Eqs. (2.97) and (2.99), for $P_n(x)$ and $Q_n(x)$ in Table 2.2 and Eqs. (2.147) and (2.148), for $j_n(x)$ and $y_n(x)$ in Table 2.3 and Eq. (2.160), and for $P_n^m(x)$ and $Q_n^m(x)$ in Table 2.4 and Eqs. (2.168) and (2.169). For Hermite polynomials, the series expansion formula is

$$H_n(x) = \sum_{k=0}^{[n/2]} \frac{(-1)^k n! (2x)^{n-2k}}{k!(n-2k)!} \tag{2.190}$$

Table 2.5 Differential Equations with Solutions

Equations	Solutions	
$x^2y'' + xy' + (x^2 - n^2)y = 0$	$J_n(x)$	Bessel functions of the first kind
	$Y_n(x)$	Bessel functions of the second kind
	$H_n^{(1)}(x)$	Hankel functions of the first kind
	$H_n^{(2)}(x)$	Hankel functions of the second kind
$x^2y'' + xy' - (x^2 + n^2)y = 0$	$I_n(x)$	Modified Bessel functions of the first kind
	$K_n(x)$	Modified Bessel functions of the second kind
$x^2y'' + 2xy' + [x^2 - n(n+1)]y = 0$	$j_n(x)$	Spherical Bessel functions of the first kind
	$y_n(x)$	Spherical Bessel functions of the second kind
$(1 - x^2)y'' - 2xy + n(n+1)y = 0$	$P_n(x)$	Legendre polynomials
	$Q_n(x)$	Legendre functions of the second kind
$(1 - x^2)y'' - 2xy' + \left[n(n+1) - \frac{m^2}{1-x^2}\right] y = 0$	$P_n^m(x)$	Associated Legendre polynomials
	$Q_n^m(x)$	Associated Legendre functions of the second kind
$y'' - 2xy' + 2ny = 0$	$H_n(x)$	Hermite polynomials
$xy'' + (1 - x)y' + ny = 0$	$L_n(x)$	Laguerre polynomials
$xy'' + (m + 1 - x)y' + ny = 0$	$L_n^m(x)$	Associated Laguerre polynomials
$(1 - x^2)y'' - xy' + n^2y = 0$	$T_n(x)$	Chebyshev polynomials of the first kind
	$U_n(x)$	Chebyshev polynomials of the second kind

where $[n/2] = N$ is the largest even integer $\leq n$ or simply the greatest integer function. Thus,

$$H_0(x) = 1, \quad H_1(x) = 2x, \quad H_2(x) = 4x^2 - 2\,, \quad \text{etc.}$$

The recurrence relations are

$$H_{n+1}(x) = 2xH_n(x) - 2nH_{n-1}(x) \tag{2.191a}$$

Table 2.6 Orthogonality Relations

Functions	Relations
Bessel functions	$\int_0^a x J_n(\lambda_i x) J_n(\lambda_j x)\, dx = \frac{a^2}{2}[J_{n+1}(\lambda_i a)]^2 \delta_{ij}$ where λ_i and λ_j are the roots of $J_n(\lambda a) = 0$
Spherical Bessel functions	$\int_{-\infty}^{\infty} j_n(x) j_m(x)\, dx = \frac{\pi}{2n+1}\delta_{mn}$
Legendre polynomials	$\int_{-1}^{1} P_n(x) P_m(x)\, dx = \frac{2}{2n+1}\delta_{mn}$
Associated Legendre polynomials	$\int_{-1}^{1} P_n^k(x) P_m^k(x)\, dx = \frac{2(n+k)!}{(2n+1)(n-k)}\delta_{mn}$ $\int_{-1}^{1} \frac{P_n^m(x) P_n^k(x)}{1-x^2}\, dx = \frac{(n+m)!}{m(n-m)!}\delta_{mk}$
Hermite polynomials	$\int_{-\infty}^{\infty} e^{-x^2} H_n(x) H_m(x)\, dx = 2^n n!(\sqrt{\pi})\delta_{mn}$
Laguerre polynomials	$\int_0^{\infty} e^{-x} L_n(x) L_m(x)\, dx = \delta_{mn}$
Associated Laguerre polynomials	$\int_0^{\infty} e^{-x} x^k L_n^k(x) L_m^k(x)\, dx = \frac{(n+k)!}{n!}\delta_{mn}$
Chebyshev polynomials	$\int_{-1}^{1} \frac{T_n(x) T_m(x)}{(1-x^2)^{1/2}}\, dx = \begin{cases} 0, & m \neq n \\ \pi/2, & m = n \neq 0 \\ \pi, & m = n = 0 \end{cases}$ $\int_{-1}^{1} \frac{U_n(x) U_m(x)}{(1-x^2)^{1/2}}\, dx = \begin{cases} 0, & m \neq n \\ \pi/2, & m = n \neq 0 \\ \pi, & m = n = 0 \end{cases}$

and

$$H_n'(x) = 2n H_{n-1}(x) \tag{2.191b}$$

For Laguerre polynomials,

$$L_n(x) = \sum_{k=0}^{n} \frac{n!(-x)^k}{(k!)^2(n-k)!} \tag{2.192}$$

so that

$$L_0(x) = 1, \quad L_1(x) = -x + 1, \quad L_2(x) = \frac{1}{2!}(x^2 - 4x + 2)\,, \quad \text{etc.}$$

The recurrence relations are

$$L_{n+1}(x) = (2n + 1 - x)L_n(x) - n^2 L_{n-1}(x) \tag{2.193a}$$

Table 2.7 Generating Functions

Functions	Generating function
	$R = [1 - 2xt + t^2]^{1/2}$
Bessel function	$\exp\left[\frac{x}{2}\left(t - \frac{1}{t}\right)\right] = \sum_{n=-\infty}^{\infty} t^n J_n(x)$
Legendre polynomial	$\frac{1}{R} = \sum_{n=0}^{\infty} t^n P_n(x)$
Associated Legendre polynomial	$\frac{(2m)!(1-x^2)^{m/2}}{2^m m! R^{m+1}} = \sum_{n=0}^{\infty} t^n P_{n+m}^m(x)$
Hermite polynomial	$\exp(2tx - t^2) = \sum_{n=0}^{\infty} \frac{t^n}{n!} H_n(x)$
Laguerre polynomial	$\frac{\exp[-xt/(1-t)]}{1-t} = \sum_{n=0}^{\infty} t^n L_n(x)$
Associated Laguerre polynomial	$\frac{\exp[-xt/(1-t)]}{(1-t)^{m+1}} = \sum_{n=0}^{\infty} t^n L_n^m(x)$
Chebyshev polynomial	$\frac{1-t^2}{R^2} = T_0(x) + 2\sum_{n=1}^{\infty} t^n T_n(x)$
	$\frac{\sqrt{1-x^2}}{R^2} = \sum_{n=0}^{\infty} t^n U_{n+1}(x)$

and

$$\frac{d}{dx} L_n(x) = \frac{1}{x}\left[n L_n(x) - n^2 L_{n+1}(x)\right] \tag{2.193b}$$

For the associated Laguerre polynomials,

$$L_n^m(x) = (-1)^m \frac{d^m}{dx^m} L_{n+m}(x) = \sum_{k=0}^{n} \frac{(m+n)!(-x)^k}{k!(n-k)!(m+k)!} \tag{2.194}$$

so that

$$L_1^1(x) = -x + 2, \quad L_2^2(x) = \frac{x^2}{2} - 3x + 3, \quad L_2^2(x) = \frac{x^2}{2} - 4x + 6 \text{ , etc.}$$

Note that $L_n^m(x) = 0, \quad m > n$. The recurrence relations are

$$L_{n+1}^m(x) = \frac{1}{n+1}\left[(2n + m + 1 - x) L_n^m(x) - (n+m) L_{n-1}^m(x)\right] \tag{2.195}$$

For Chebyshev polynomials of the first kind,

$$T_n(x) = \sum_{k=0}^{[n/2]} \frac{(-1)^k n! x^{n-2k}(1-x^2)^k}{(2k)!(n-2k)!}, \quad -1 \le x \le 1 \tag{2.196}$$

so that

$$T_0(x) = 1, \quad T_1(x) = x, \quad T_2(x) = 2x^2 - 1, \text{ etc.}$$

The recurrence relation is

$$T_{n+1}(x) = 2xT_n(x) - T_{n-1}(x) \tag{2.197}$$

For Chebyshev polynomials of the second kind,

$$U_n(x) = \sum_{k=0}^{N} \frac{(-1)^{k-1}(n+1)!\, x^{n-2k+2}(1-x^2)^{k-1}}{(2k+1)!(n-2k+2)!}, \qquad -1 \le x \le 1 \tag{2.198}$$

where $N = \left[\frac{n+1}{2}\right]$ so that

$$U_0(x) = 1, \qquad U_1(x) = 2x, \qquad U_2(x) = 4x^2 - 1, \quad \text{etc.}$$

The recurrence relation is the same as that in Eq. (2.197).

For example, if a function $f(x)$ is to be expanded on the interval $(0, \infty)$, Laguerre functions can be used as the orthogonal functions with an exponential weighting function, i.e., $w(x) = e^{-x}$. If $f(x)$ is to be expanded on the interval $(-\infty, \infty)$, we may use Hermite functions with $w(x) = e^{-x^2}$. As we have noticed earlier, if $f(x)$ is defined on the interval $(-1, 1)$, we may choose Legendre functions with $w(x) = 1$. For more detailed treatment of these functions, see Bell [7] or Johnson and Johnson [8].

Example 2.9

Expand the function

$$f(x) = |x|, \qquad -1 \le x \le 1$$

in a series of Chebyshev polynomials. □

Solution

The given function can be written as

$$f(x) = \begin{cases} -x, & -1 \le x < 0 \\ x, & 0 < x \le 1 \end{cases}$$

Let

$$f(x) = \sum_{n=0}^{\infty} A_n T_n(x)$$

where A_n are expansion coefficients to be determined. Since $f(x)$ is an even function, the odd terms in the expansion vanish. Hence

$$f(x) = A_0 + \sum_{n=1}^{\infty} A_{2n} T_{2n}(x)$$

If we multiply both sides by $w(x) = \dfrac{T_{2m}}{\sqrt{1-x^2}}$ and integrate over $-1 \le x \le 1$, all terms in the summation vanish except when $m = n$. That is, from Table 2.6, the orthogonality property of $T_n(x)$ requires that

$$\int_{-1}^{1} \frac{T_m(x) T_n(x)}{(1-x^2)^{1/2}}\, dx = \begin{cases} 0, & m \neq n \\ \pi/2, & m = n \neq 0 \\ \pi, & m = n = 0 \end{cases}$$

Hence

$$A_0 = \frac{1}{\pi} \int_{-1}^{1} \frac{f(x) T_0(x)}{(1-x^2)^{1/2}}\, dx = \frac{2}{\pi} \int_{0}^{1} \frac{x}{(1-x^2)^{1/2}}\, dx = \frac{2}{\pi},$$

$$A_{2n} = \frac{2}{\pi} \int_{-1}^{1} \frac{f(x) T_{2n}(x)}{(1-x^2)^{1/2}}\, dx = \frac{4}{\pi} \int_{0}^{1} \frac{x T_{2n}}{(1-x^2)^{1/2}}\, dx$$

Since $T_n(x) = \cos(n \cos^{-1} x)$, it is convenient to let $x = \cos\theta$ so that

$$A_{2n} = \frac{4}{\pi} \int_{\pi/2}^{0} \frac{\cos\theta \cos 2n\theta}{\sin\theta} (-\sin\theta\, d\theta) = \frac{4}{\pi} \int_{0}^{\pi/2} \cos\theta \cos 2n\theta\, d\theta$$

$$= \frac{4}{\pi} \int_{0}^{\pi/2} \frac{1}{2} [\cos(2n+1)\theta + \cos(2n-1)\theta]\, d\theta = \frac{4}{\pi} \frac{(-1)^{n+1}}{4n^2 - 1}$$

Hence

$$f(x) = \frac{2}{\pi} + \frac{4}{\pi} \sum_{n=1}^{\infty} \frac{(-1)^{n+1}}{4n^2 - 1} T_{2n}(x) \quad \blacksquare$$

Example 2.10

Evaluate $\dfrac{P_n^1(x)}{\sin\theta}$ at $x = 1$ and $x = -1$. □

Solution

This example serves to illustrate how the generating functions are useful in deriving some properties of the corresponding orthogonal functions. Since

$$\frac{P_n^1(x)}{\sin\theta} = \frac{P_n^1(x)}{\sqrt{1-x^2}},$$

direct substitution of $x = 1$ or $x = -1$ gives 0/0, which is indeterminate. But $P_n^1(x) = (1-x^2)^{1/2}\frac{d}{dx}P_n$ by definition. Hence

$$\frac{P_n^1(x)}{\sin\theta} = \frac{d}{dx}P_n\ ,$$

i.e., the problem is reduced to evaluating dP_n/dx at $x = \pm 1$. We use the generating function for P_n, namely,

$$\left(1 - 2xt + t^2\right)^{-1/2} = \sum_{n=0}^{\infty} t^n P_n(x)$$

Differentiating both sides with respect to x,

$$\frac{t}{\left(1 - 2xt + t^2\right)^{3/2}} = \sum_{n=0}^{\infty} t^n \frac{d}{dx}P_n \tag{2.199}$$

When $x = 1$,

$$\frac{1}{(1-t)^3} = \sum_{n=0}^{\infty} t^{n-1}\frac{d}{dx}P_n\bigg|_{x=1} \tag{2.200}$$

But

$$(1-t)^{-3} = 1 + 3t + 6t^2 + 10t^3 + 15t^4 + \cdots = \sum_{n=1}^{\infty}\frac{n}{2}(n+1)t^{n-1} \tag{2.201}$$

Comparing this with Eq. (2.200) clearly shows that

$$\frac{d}{dx}P_n\bigg|_{x=1} = n(n+1)/2$$

Similarly, when $x = -1$, Eq. (2.199) becomes

$$\frac{1}{(1+t)^3} = \sum_{n=0}^{\infty} t^{n-1}\frac{d}{dx}P_n\bigg|_{x=-1} \tag{2.202}$$

But

$$(1+t)^{-3} = 1 - 3t + 6t^2 - 10t^3 + 15t^4 - \cdots = \sum_{n=1}^{\infty}(-1)^{n+1}\frac{n}{2}(n+1)t^{n-1}$$

Hence

$$\frac{d}{dx}P_n\bigg|_{x=-1} = (-1)^{n+1}n(n+1)/2 \quad \blacksquare$$

Example 2.11

Write a program to generate Hermite functions $H_n(x)$ for any argument x and order n. Use the series expansion and recurrence formulas and compare your results. Take $x = 0.5, 0 \leq n \leq 15$. □

Solution

The program is shown in Fig. 2.11. Equation (2.190) is used for the series expansion method, while Eq. (2.191a) with $H_0(x) = 1$ and $H_1(x) = 2x$ is used for the recurrence formula. Note that in the program, we have replaced n by $n - 1$ in Eq. (2.191) so that

$$H_n(x) = 2xH_{n-1}(x) - 2(n-1)H_{n-2}(x)$$

The result of the computation is in Table 2.8. In this case, the two methods give identical results. In general, the series expansion method gives results of greater accuracy since error in one computation is not propagated to the next as is the case when using recurrence relations.

Table 2.8 Results of the Program in Fig. 2.11

Values of $H_n(x)$ for $x = 0.5, \quad 0 \leq n \leq 15$			
N	Series Expansion	Recurrence	Difference
0	1.00	1.00	0.00
1	1.00	1.00	0.00
2	−1.00	−1.00	0.00
3	−5.00	−5.00	0.00
4	1.00	1.00	0.00
5	11.00	1.00	0.00
6	31.00	31.00	0.00
7	−461.00	−461.00	0.00
8	−895.00	−895.00	0.00
9	6181.00	6181.00	0.00
10	22591.00	22591.00	0.00
11	−107029.00	−107029.00	0.00
12	−604031.00	−604031.00	0.00
13	1964665.00	1964665.00	0.00
14	17669472.00	17669472.00	0.00
15	−37341152.00	−37341148.00	−4.00

Generating functions such as this is sometimes needed in numerical computations. This example has served to illustrate how this can be done in two ways. Special techniques may be required for very large or very small values of x or n. ■

```
0001          ******************************************************
0002          THIS PROGRAM GENERATES HERMITE'S FUNCTIONS HN(X) IN
0003          TWO WAYS USING:   1) SERIES EXPANSION
0004                            2) RECURRENCE RELATION
0005    C     THE TWO METHODS ARE COMPARED
0006    C     X = ARGUMENT (FIXED IN THIS PROGRAM)
0007    C     N = ORDER OF THE FUNCTION  ( 0 < N < 15 IN THIS PROGRAM)
0008    C     ******************************************************
0009
0010          DIMENSION    HS(0:50), HR(0:50)
0011
0012          X = 0.5
0013          NMAX = 15
0014          WRITE(6,1)
0015    1     FORMAT(2X,68('-'),/)
0016          WRITE(6,2)
0017    2     FORMAT(3X,'N',14X,'SERIES HS(N)',7X,'RECURRENCE HR(N)',
0018         2      7X,'DIFFERENCE',/)
0019          WRITE(6,1)
0020          DO 60 N=0,NMAX
0021
0022    C     METHOD 1:  SERIES EXPANSION FORMULA
0023
0024          SUM = 0.0
0025          CALL FACTORIAL(N,FN)
0026          CALL GREATEST(N,I)
0027          DO 10 K=0,I
0028          M = N - 2*K
0029          CALL FACTORIAL(M,FM)
0030          CALL FACTORIAL(K,FK)
0031          A = ( ((-1.)**K)*FN*((2.*X)**M) )/( FK*FM )
0032    C     FK*FM MAY BE TOO LARGE IF N IS LARGE
0033          SUM = SUM + A
0034    10    CONTINUE
0035          HS(N) = SUM
0036
0037    C     METHOD 2:  RECURRENCE FORMULA
0038
0039          HR(0) = 1.0
0040          HR(1) = 2.*X
0041          IF(N-1) 40,40,20
0042    20    DO 30 I=2,N
0043          HR(I) = 2.0*X*HR(I-1) - 2.*FLOAT(I-1)*HR(I-2)
0044    30    CONTINUE
0045    40    CONTINUE
0046          DIFFERENCE = HS(N) - HR(N)
0047          WRITE(6,50) N,HS(N),HR(N),DIFFERENCE
0048          PRINT *,N,HS(N),HR(N),DIFFERENCE
0049    50    FORMAT(2X,I2,9X,F12.2,9X,F12.2,9X,F10.2,/)
0050    60    CONTINUE
0051          WRITE(6,1)
0052          STOP
0053          END
```

Figure 2.11
Program for Hermite function $H_n(x)$ *(Continued).*

```
0001    C*****************************************************************
0002    C
0003    C       SUBROUTINE FOR CALCULATING  N!
0004            SUBROUTINE FACTORIAL(N,FN)
0005
0006            FN = 1.0
0007            IF(N.EQ.0) GO TO 20
0008            DO 10 I=1,N
0009            FN = FN*FLOAT(I)
0010    10      CONTINUE
0011    20      RETURN
0012            END
```

```
0001    C*****************************************************************
0002    C       SUBROUTINE FOR CALCULATING THE GREATEST INTEGER FUNCTION
0003    C       M = [X]  WHERE X = N/2 IN THIS PARTICULAR CASE
0004            SUBROUTINE GREATEST(MAX,M)
0005
0006            A = MAX/2
0007            M = IFIX(A)
0008            IF(M) 10,20,20
0009    10      M = M - 1
0010    20      RETURN
0011            END
```

Figure 2.11
(Cont.) **Program for Hermite function $H_n(x)$.**

2.7 Series Expansion

As we have noticed in earlier sections, partial differential equations can be solved with the aid of infinite series and, more generally, with the aid of series of orthogonal functions. In this section we apply the idea of infinite series expansion to those PDEs in which the independent variables are not separable or, if they are separable, the boundary conditions are not satisfied by the particular solutions. We will illustrate the technique in the following three examples.

2.7.1 Poisson's Equation in a Cube

Consider the problem

$$\nabla^2 V = \frac{\partial^2 V}{\partial x^2} + \frac{\partial^2 V}{\partial y^2} + \frac{\partial^2 V}{\partial z^2} = -f(x, y, z) \tag{2.203}$$

subject to the boundary conditions

$$\begin{aligned} V(0, y, z) &= V(a, y, z) = V(x, 0, z) = 0 \\ V(x, b, z) &= V(x, y, 0) = V(x, y, c) = 0 \end{aligned} \tag{2.204}$$

where $f(x, y, z)$, the source term, is given. We should note that the independent variables in Eq. (2.203) are not separable. However, in Laplace's equation,

$f(x, y, z) = 0$, and the variables are separable. Although the problem defined by Eqs. (2.203) and (2.204) can be solved in several ways, we stress the use of series expansion in this section.

Let the solution be of the form

$$V(x, y, z) = \sum_{m=1}^{\infty} \sum_{n=1}^{\infty} \sum_{p=1}^{\infty} A_{mnp} \sin \frac{m\pi x}{a} \sin \frac{n\pi y}{b} \sin \frac{p\pi z}{c} \tag{2.205}$$

where the triple sine series is chosen so that the individual terms and the entire series would satisfy the boundary conditions of Eq. (2.204). However, the individual terms do not satisfy either Poisson's or Laplace's equation. Since the expansion coefficients A_{mnp} are arbitrary, they can be chosen such that Eq. (2.205) satisfies Eq. (2.203). We achieve this by substituting Eq. (2.205) into Eq. (2.203). We obtain

$$\begin{aligned}
&-\sum\sum\sum A_{mnp}(m\pi/a)^2 \sin \frac{m\pi x}{a} \sin \frac{n\pi y}{b} \sin \frac{p\pi z}{c} \\
&-\sum\sum\sum A_{mnp}(n\pi/b)^2 \sin \frac{m\pi x}{a} \sin \frac{n\pi y}{b} \sin \frac{p\pi z}{c} \\
&-\sum\sum\sum A_{mnp}(p\pi/c)^2 \sin \frac{m\pi x}{a} \sin \frac{n\pi y}{b} \sin \frac{p\pi z}{c} = -f(x, y, z)
\end{aligned}$$

Multiplying both sides by $\sin(i\pi x/a) \sin(j\pi y/b) \sin(k\pi z/c)$ and integrating over $0 < x < a, 0 < y < b, 0 < z < c$ gives

$$\begin{aligned}
&\sum\sum\sum A_{mnp} \left[(m\pi/a)^2 + (n\pi/b)^2 + (p\pi/c)^2\right] \cdot \\
&\int_0^a \sin \frac{m\pi x}{a} \sin \frac{i\pi x}{a}\, dx \int_0^b \sin \frac{n\pi y}{b} \sin \frac{j\pi y}{b}\, dy \int_0^c \sin \frac{p\pi z}{c} \sin \frac{k\pi z}{c}\, dz \\
&\quad = \int_0^a \int_0^b \int_0^c f(x, y, z) \sin \frac{i\pi x}{a} \sin \frac{j\pi y}{b} \sin \frac{k\pi z}{c}\, dx\, dy\, dz
\end{aligned}$$

Each of the integrals on the left-hand side vanishes except when $m = i, n = j$, and $p = k$. Hence

$$\begin{aligned}
&A_{mnp} \left[(m\pi/a)^2 + (n\pi/b)^2 + (p\pi/c)^2\right] \frac{a}{2} \cdot \frac{b}{2} \cdot \frac{c}{2} \\
&\quad = \int_0^a \int_0^b \int_0^c f(x, y, z) \sin \frac{i\pi x}{a} \sin \frac{j\pi y}{b} \sin \frac{k\pi z}{c}\, dx\, dy\, dz
\end{aligned}$$

or

$$\begin{aligned}
A_{mnp} = &\frac{8}{abc} \left[(m\pi/a)^2 + (n\pi/b)^2 + (p\pi/c)^2\right]^{-1} \cdot \\
&\int_0^a \int_0^b \int_0^c f(x, y, z) \sin \frac{i\pi x}{a} \sin \frac{j\pi y}{b} \sin \frac{k\pi z}{c}\, dx\, dy\, dz
\end{aligned} \tag{2.206}$$

Thus the series expansion solution to the problem is in Eq. (2.205) with A_{mnp} given by Eq. (2.206).

2.7.2 Poisson's Equation in a Cylinder

The problem to be solved is shown in Fig. 2.12, which illustrates a cylindrical metal tank partially filled with charged liquid [9]. To find the potential distribution V in the tank, we let V_ℓ and V_g be the potential in the liquid and gas portions, respectively, i.e.,

$$V = \begin{cases} V_\ell, & 0 < z < b \qquad \text{(liquid)} \\ V_g, & b < z < b + c \qquad \text{(gas)} \end{cases}$$

Thus we need to solve a two-dimensional problem:

$$\frac{1}{\rho}\frac{\partial}{\partial \rho}\left(\rho \frac{\partial V_\ell}{\partial \rho}\right) + \frac{\partial^2 V_\ell}{\partial z^2} = -\frac{\rho_v}{\epsilon}, \qquad \text{for liquid space} \tag{2.207a}$$

$$\frac{1}{\rho}\frac{\partial}{\partial \rho}\left(\rho \frac{\partial V_g}{\partial \rho}\right) + \frac{\partial^2 V_g}{\partial z^2} = 0, \qquad \text{for gas space} \tag{2.207b}$$

subject to

$$V = 0, \rho = a \qquad \text{(at the wall)}$$

$$V_g = V_\ell, z = b \qquad \text{(at the gas-liquid interface)}$$

$$\frac{\partial V_g}{\partial z} = \epsilon_r \frac{\partial V_\ell}{\partial z}, z = b \qquad \text{(at the gas-liquid interface)}$$

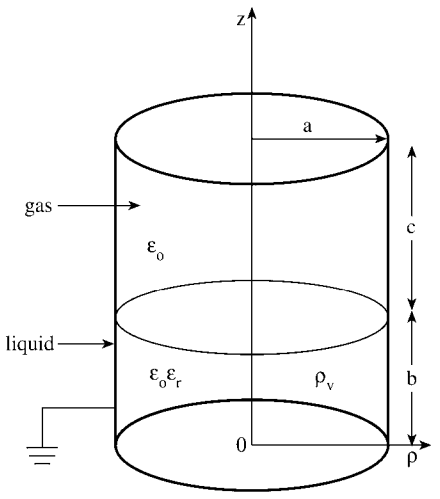

Figure 2.12
A cylindrical metal tank partially filled with charged liquid.

Applying the series expansion techniques, we let

$$V_\ell = \sum_{n=1}^{\infty} J_0(\lambda_n \rho) F_n(z) \tag{2.208a}$$

$$V_g = \sum_{n=1}^{\infty} J_0(\lambda_n \rho) \left[A_n \sinh[\lambda_n (b + c - z)] + B_n \cosh\left[\lambda_n (b + c - z)\right]\right] \tag{2.208b}$$

where $F_n(z)$, A_n, and B_n are to be determined.

At $z = b + c$, $V_g = 0$, which implies that $B_n = 0$. Hence, Eq. (2.208b) becomes

$$V_g = \sum_{n=1}^{\infty} A_n J_0\left(\lambda_n \rho\right) \sinh\left[\lambda_n (b + c - z)\right] \tag{2.209}$$

Substituting Eq. (2.208a) into (2.207b) yields

$$\sum_{n=1}^{\infty} J_0\left(\lambda_n \rho\right) \left[F_n'' - \lambda_n^2 F_n\right] = -\frac{\rho_v}{\epsilon}$$

If we let $F_n'' - \lambda_n^2 F_n = G_n$, then

$$\sum_{n=1}^{\infty} G_n J_0\left(\lambda_n \rho\right) = -\frac{\rho_v}{\epsilon} \tag{2.210}$$

At $\rho = a$, $V_g = V_\ell = 0$, which makes

$$J_0\left(\lambda_n a\right) = 0$$

indicating that λ_n are the roots of J_0 divided by a. Multiplying Eq. (2.210) by $\rho J_0(\lambda_m \rho)$ and integrating over the interval $0 < \rho < a$ gives

$$\sum_{n=1}^{\infty} G_n \int_0^a \rho J_0\left(\lambda_m \rho\right) J_0\left(\lambda_n \rho\right)\, d\rho = -\frac{\rho_v}{\epsilon} \int_0^a \rho J_0\left(\lambda_m \rho\right)\, d\rho$$

The left-hand side is zero except when $m = n$.

$$\int_0^a \rho J_0^2\left(\lambda_m \rho\right)\, d\rho = \frac{1}{2} a^2 \left[J_0^2\left(\lambda_n a\right) + J_1^2\left(\lambda_n a\right)\right] = \frac{a^2}{2} J_1^2\left(\lambda_n a\right)$$

since $J_0(\lambda_n a) = 0$. Also,

$$\int_0^a \rho J_0\left(\lambda_m \rho\right)\, d\rho = \frac{a}{\lambda_n} J_1\left(\lambda_n a\right)$$

Hence

$$G_n \frac{a^2}{2} J_1^2\left(\lambda_n a\right) = -\frac{\rho_v}{\epsilon} \frac{a}{\lambda_n} J_1\left(\lambda_n a\right)$$

or

$$G_n = -\frac{2\rho_v}{\epsilon a \lambda_n J_1(\lambda_n a)}$$

showing that G_n is a constant. Thus

$$F_n'' - \lambda_n^2 F_n = G_n$$

which is an inhomogeneous ordinary differential equation. Its solution is

$$F_n(z) = C_n \sinh(\lambda_n z) + D_n \cosh(\lambda_n z) - \frac{G_n}{\lambda_n^2}$$

But

$$F_n(0) = 0 \qquad \longrightarrow \qquad D_n = \frac{G_n}{\lambda_n^2}$$

Thus

$$V_\ell = \sum_{n=1}^{\infty} J_0(\lambda_n \rho) \left[C_n \sinh(\lambda_n z) + \frac{G_n}{\lambda_n^2} [\cosh(\lambda_n z) - 1] \right] \tag{2.211}$$

Imposing the conditions at $z = b$, i.e.,

$$V_\ell(\rho, b) = V_g(\rho, b)$$

we obtain

$$A_n \sinh(\lambda_n c) = C_n \sinh(\lambda_n b) + \frac{G_n}{\lambda_n^2} [\cosh(\lambda_n b) - 1] \tag{2.212}$$

Also,

$$\left.\frac{\partial V_g}{\partial z}\right|_{z=b} = \epsilon_r \left.\frac{\partial V_\ell}{\partial z}\right|_{z=b}$$

gives

$$\lambda_n A_n \cosh(\lambda_n c) = -\epsilon_r \lambda_n C_n \cosh(\lambda_n b) - \frac{\epsilon_r G_n}{\lambda_n} \sinh(\lambda_n b) \tag{2.213}$$

Solving Eqs. (2.212) and (2.213), we get

$$A_n = \frac{2\rho_v}{R_n K_n} [\cosh(\lambda_n b) - 1]$$

$$C_n = \frac{2\rho_v}{R_n \epsilon_r} [\cosh(\lambda_n b) \cosh(\lambda_n c) + \epsilon_r \sinh(\lambda_n b) \sinh(\lambda_n c) - \cosh(\lambda_n c)]$$

where

$$K_n = \sinh(\lambda_n b) \cosh(\lambda_n c) + \epsilon_r \cosh(\lambda_n b) \sinh(\lambda_n c)$$

$$R_n = \epsilon_o a \lambda_n^3 J_1(\lambda_n a)$$

Substituting A_n and C_n in Eqs. (2.209) and (2.211), we obtain the complete solution as

$$V_\ell = \sum_{n=1}^{\infty} \frac{2\rho_v}{R_n \epsilon_r} J_0(\lambda_n \rho) \left[\frac{\sinh(\lambda_n z)}{K_n} [\cosh(\lambda_n b) \cosh(\lambda_n c) + \epsilon_r \sinh(\lambda_n b) \sinh(\lambda_n c) - \cosh(\lambda_n c)] - \cosh(\lambda_n z) + 1 \right] \quad (2.214a)$$

$$V_g = \sum_{n=1}^{\infty} \frac{2\rho_v}{R_n K_n} J_0(\lambda_n \rho) [\cosh(\lambda_n b) - 1] \sinh[\lambda_n (b + c - z)] \quad (2.214b)$$

2.7.3 Strip Transmission Line

Consider a strip conductor enclosed in a shielded box containing homogeneous medium as shown in Fig. 2.13(a). If TEM mode of propagation is assumed, our problem is reduced to finding V satisfying Laplace's equation $\nabla^2 V = 0$. Due to symmetry, we need only consider one quarter-section of the line as in Fig. 2.13(b). This quadrant can be subdivided into regions 1 and 2, where region 1 is under the center conductor and region 2 is not. We now seek solutions V_1 and V_2 for regions 1 and 2, respectively.

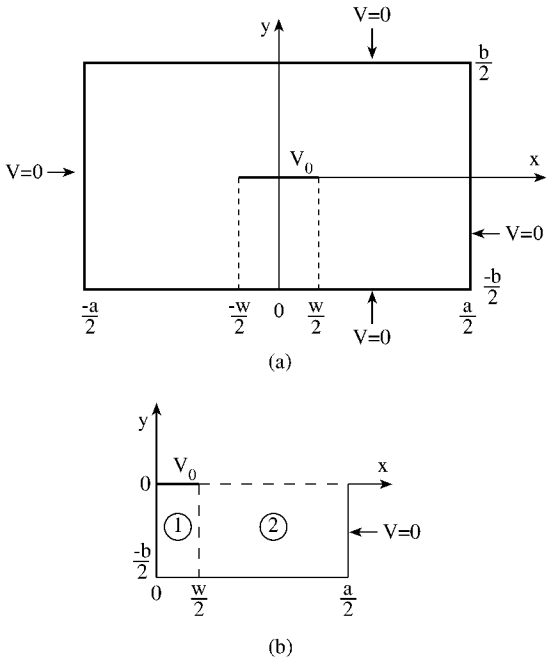

Figure 2.13
Strip line example.

If $w >> b$, region 1 is similar to parallel-plate problem. Thus, we have a one-dimensional problem similar to Eq. (2.14) with solution

$$V_1 = a_1 y + a_2$$

Since $V_1(y = 0) = 0$ and $V_2(y = -b/2) = V_o$, $a_2 = 0$, $a_1 = -2V_o/b$. Hence

$$V_1(x, y) = \frac{-2V_o}{b} y \tag{2.215}$$

For region 2, the series expansion solution is of the form

$$V_2(x, y) = \sum_{n=1,3,5}^{\infty} A_n \sin \frac{n\pi y}{b} \sinh \frac{n\pi}{b}(a/2 - x) , \tag{2.216}$$

which satisfies Laplace's equation and the boundary condition along the box. Notice that the even-numbered terms could not be included because they do not satisfy the boundary condition requirements about line $y = 0$, i.e., $E_y(y = 0) = -\partial V_2/\partial y\big|_{y=0} \neq 0$. To determine the expansion coefficients A_n in Eq. (2.216), we utilize the fact that V must be continuous at the interface $x = w/2$ between regions 1 and 2, i.e.,

$$V_1(x = w/2, y) = V_2(x = w/2, y)$$

or

$$-\frac{2V_o y}{b} = \sum_{n=\text{odd}}^{\infty} A_n \sin \frac{n\pi y}{b} \sinh \frac{n\pi}{2b}(a - w) ,$$

which is Fourier series. Thus,

$$A_n \sinh \frac{n\pi}{2b}(a - w) = -\frac{2}{b} \int_{-b/2}^{b/2} \frac{2V_o y}{b} \sin \frac{n\pi y}{b} dy = -\frac{8V_o \sin \frac{n\pi}{2}}{n^2\pi^2}$$

Hence

$$A_n = -\frac{8V_o \sin \frac{n\pi}{2}}{n^2\pi^2 \sinh \frac{n\pi}{2b}(a - w)} \tag{2.217}$$

It is instructive to find the capacitance per unit length C of the strip line using the fact that the energy stored per length is related to C according to

$$W = \frac{1}{2} C V_o^2 \tag{2.218}$$

where

$$W = \frac{1}{2} \int \mathbf{D} \cdot \mathbf{E}\, dv = \frac{1}{2} \epsilon \int |\mathbf{E}|^2\, dv \tag{2.219}$$

For region 1,

$$\mathbf{E} = -\nabla V = -\frac{\partial V}{\partial x}\mathbf{a}_x - \frac{\partial V}{\partial y}\mathbf{a}_y = \frac{2V_o}{b}\mathbf{a}_y$$

Hence

$$W_1 = \frac{1}{2}\epsilon \int_{x=0}^{w/2} \int_{y=-b/2}^{0} \frac{4V_o^2}{b^2}\, dy\, dx = \frac{\epsilon V_o^2 w}{2b} \tag{2.220}$$

For region 2,

$$E_x = -\frac{\partial V}{\partial x} = \sum \frac{n\pi}{b} A_n \cosh \frac{n\pi}{b}(a/2 - x) \sin \frac{n\pi y}{b}$$
$$E_y = -\frac{\partial V}{\partial y} = -\sum \frac{n\pi}{b} A_n \sinh \frac{n\pi}{b}(a/2 - x) \cos \frac{n\pi y}{b}$$

and

$$\begin{aligned} W_2 &= \frac{1}{2}\epsilon \iint \left(E_x^2 + E_y^2\right) dx\, dy \\ &= \frac{1}{2}\epsilon \int_{y=-b/2}^{0} \int_{x=w/2}^{a/2} \sum_n \sum_m \frac{mn\pi^2}{b^2} A_n A_m \cdot \\ &\quad \left[\sinh^2 \frac{m\pi}{b}(a/2 - x) \sinh^2 \frac{n\pi}{b}(a/2 - x) \cos \frac{m\pi y}{b} \cos \frac{n\pi y}{b}\right. \\ &\quad \left. + \cosh^2 \frac{m\pi}{b}(a/2 - x) \cosh^2 \frac{n\pi}{b}(a/2 - x) \sin \frac{m\pi y}{b} \sin \frac{n\pi y}{b}\right] dx\, dy \end{aligned}$$

where the double summation is used to show that we are multiplying two series which may have different indices m and n. Due to the orthogonality properties of sine and cosine functions, all terms vanish except when $m = n$. Thus

$$\begin{aligned} W_2 &= \frac{1}{2}\epsilon \sum_{n=\text{odd}}^{\infty} \frac{n^2\pi^2 A_n^2}{b^2} \cdot \frac{b/2}{2} \int_{w/2}^{a/2} \left[\sinh^2 \frac{n\pi}{b}(a/2 - x)\right. \\ &\quad \left. + \cosh^2 \frac{n\pi}{b}(a/2 - x)\right] dx \\ &= \frac{1}{2}\epsilon \sum_{n=\text{odd}}^{\infty} \frac{n^2\pi^2 A_n^2}{4b} \frac{b}{n\pi} \cosh \frac{n\pi}{2b}(a - w) \sinh \frac{n\pi}{2b}(a - w) \end{aligned}$$

Substituting for A_n gives

$$W_2 = \sum_{n=1,3,5}^{\infty} \frac{8\epsilon V_o^2}{n^3\pi^3} \coth \frac{n\pi}{2b}(a - w) \tag{2.221}$$

The total energy in the four quadrants is

$$W = 4(W_1 + W_2)$$

Thus

$$C = \frac{2W}{V_o^2} = \frac{8}{V_o^2}(W_1 + W_2)$$
$$= \epsilon \left[\frac{4w}{b} + \frac{64}{\pi^3} \sum_{n=1,3,5}^{\infty} \frac{1}{n^3} \coth \frac{n\pi}{2b}(a-w) \right] \tag{2.222}$$

The characteristic impedance of the lossless line is given by

$$Z_o = \frac{\sqrt{\mu\epsilon}}{C} = \frac{\sqrt{\mu_r \epsilon_r}}{cC} = \sqrt{\frac{\mu}{\epsilon}} \frac{1}{C/\epsilon}$$

or

$$Z_o = \frac{120\pi}{\sqrt{\epsilon_r} \left[\frac{4w}{b} + \frac{64}{\pi^3} \sum_{n=1,3,5}^{\infty} \frac{1}{n^3} \coth \frac{n\pi}{2b}(a-w) \right]} \tag{2.223}$$

where $c = 3 \times 10^8$ m/s, the speed of light in vacuum, and $\mu_r = 1$ is assumed.

Example 2.12

Solve the two-dimensional problem

$$\nabla^2 V = -\frac{\rho_s}{\epsilon_o}$$

where

$$\rho_s = x(y-1) \text{ nC/m}^2$$

subject to

$$V(x,0) = 0, \qquad V(x,b) = V_o, \qquad V(0,y) = 0 = V(a,y) \qquad \square$$

Solution

If we let

$$\nabla^2 V_1 = 0\,, \tag{2.224a}$$

subject to

$$V_1(x,0) = 0, \qquad V_1(x,b) = V_o, \qquad V_1(0,y) = 0 = V(a,y) \tag{2.224b}$$

and

$$\nabla^2 V_2 = -\frac{\rho_s}{\epsilon_o}\,, \tag{2.225a}$$

subject to

$$V_2(x, 0) = 0, \qquad V_2(x, b) = 0, \qquad V_2(0, y) = 0 = V(a, y) \tag{2.225b}$$

By the superposition principle, the solution to the given problem is

$$V = V_1 + V_2 \tag{2.226}$$

The solution to Eq. (2.224) is already found in Section 2.3.1, i.e.,

$$V_1(x, y) = \frac{4V_o}{\pi} \sum_{n=1,3,5}^{\infty} \frac{\sin \frac{n\pi x}{a} \sinh \frac{n\pi y}{a}}{n \sinh \frac{n\pi b}{a}} \tag{2.227}$$

The solution to Eq. (2.225) is a special case of that of Eq. (2.205). The only difference between this problem and that of Eqs. (2.203) and (2.204) is that this problem is two-dimensional while that of Eqs. (2.203) and (2.204) is three-dimensional. Hence

$$V_2(x, y) = \sum_{m=1}^{\infty} \sum_{n=1}^{\infty} A_{mn} \sin \frac{n\pi x}{a} \sin \frac{n\pi y}{b} \tag{2.228}$$

where, according to Eq. (2.206), A_{mn} is given by

$$A_{mn} = \frac{4}{ab} \left[(m\pi/a)^2 + (n\pi/b)^2 \right]^{-1} \cdot \int_0^b \int_0^a f(x, y) \sin \frac{n\pi x}{a} \sin \frac{n\pi y}{b} \, dx \, dy \tag{2.229}$$

But $f(x, y) = x(y - 1)/\epsilon_0$ nC/m^2,

$$\begin{aligned} &\int_0^b \int_0^a f(x, y) \sin \frac{n\pi x}{a} \sin \frac{n\pi y}{a} \, dx \, dy \\ &= \frac{10^{-9}}{\epsilon_o} \int_0^a x \sin \frac{n\pi x}{a} \, dx \int_0^b (y - 1) \sin \frac{n\pi y}{b} \, dy \\ &= \frac{10^{-9}}{10^{-9}/36\pi} \left(-\frac{a^2 \cos m\pi}{m\pi} \right) \left(-\frac{b^2 \cos n\pi}{n\pi} + \frac{b}{n\pi} [\cos n\pi - 1] \right) \\ &= \frac{36\pi(-1)^{m+n} a^2 b^2}{mn\pi^2} \left(1 - \frac{1}{b} [1 - (-1)^n] \right) \end{aligned} \tag{2.230}$$

since $\cos n\pi = (-1)^n$. Substitution of Eq. (2.230) into Eq. (2.229) leads to

$$A_{mn} = \left[(m\pi/a)^2 + (n\pi/b)^2 \right]^{-1} \frac{(-1)^{m+n} 144ab}{mn\pi} \left(1 - \frac{1}{b} \left[1 - (-1)^n \right] \right) \tag{2.231}$$

Substituting Eqs. (2.227) and (2.228) into Eq. (2.226) gives the complete solution as

$$V(x, y) = \frac{4V_o}{\pi} \sum_{n=1,3,5}^{\infty} \frac{\sin \frac{n\pi x}{a} \sinh \frac{n\pi y}{a}}{n \sinh \frac{n\pi b}{a}} + \sum_{m=1}^{\infty} \sum_{n=1}^{\infty} A_{mn} \sin \frac{n\pi x}{a} \sin \frac{n\pi y}{b} \tag{2.232}$$

where A_{mn} is in Eq. (2.231). ∎

2.8 Practical Applications

The scattering of EM waves by a dielectric sphere, known as the Mie scattering problem due to its first investigator in 1908, is an important problem whose analytic solution is usually referred to in assessing some numerical computations. Though the analysis of the problem is more rigorous, the procedure is similar to that of Example 2.5, where scattering due to a conducting cylinder was treated. Our treatment here will be brief; for an in-depth treatment, consult Stratton [10].

2.8.1 Scattering by Dielectric Sphere

Consider a dielectric sphere illuminated by a plane wave propagating in the z direction and $\mathbf{E}$ polarized in the x direction as shown in Fig. 2.14. The incident wave

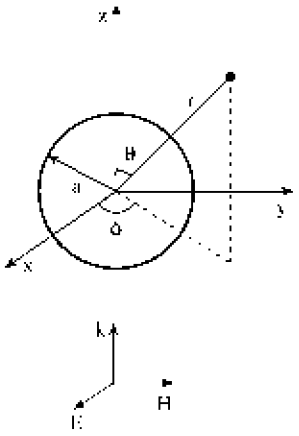

Figure 2.14
Incident EM plane wave on a dielectric sphere.

is described by

$$\mathbf{E}^i = E_o e^{j(\omega t - kz)} \mathbf{a}_x \tag{2.233a}$$

$$\mathbf{H}^i = \frac{E_o}{\eta} e^{j(\omega t - kz)} \mathbf{a}_y \tag{2.233b}$$

The first step is to express this incident wave in terms of spherical wave functions as in Example 2.8. Since

$$\mathbf{a}_x = \sin\theta\cos\phi\,\mathbf{a}_r + \cos\theta\cos\phi\,\mathbf{a}_\theta - \sin\phi\,\mathbf{a}_\phi \ ,$$

the r-component of $\mathbf{E}^i$, for example, is

$$E_r^i = \cos\phi\sin\theta E_x^i = E_o e^{j\omega t} \frac{\cos\phi}{jkr} \frac{\partial}{\partial\theta} \left(e^{-jkr\cos\theta} \right)$$

Introducing Eq. (2.184),

$$E_r^i = E_o e^{j\omega t} \frac{\cos\phi}{jkr} \sum_{n=0}^{\infty} (-j)^n (2n+1) j_n(kr) \frac{\partial}{\partial\theta} P_n(\cos\theta)$$

But

$$\frac{\partial P_n}{\partial\theta} = P_n^1$$

hence

$$E_r^i = E_o e^{j\omega t} \frac{\cos\phi}{jkr} \sum_{n=1}^{\infty} (-j)^n (2n+1) j_n(kr) P_n^1(\cos\theta) \tag{2.234}$$

where the $n = 0$ term has been dropped since $P_0^1 = 0$. The same steps can be taken to express E_θ^i and E_ϕ^i in terms of the spherical wave functions. The result is

$$\begin{aligned} \mathbf{E}^i &= \mathbf{a}_x E_o e^{j(\omega t - kz)} \\ &= E_o e^{j\omega t} \sum_{n=1}^{\infty} (-j)^n \frac{2n+1}{n(n+1)} \left[\mathbf{M}_n^{(1)}(k) + j\mathbf{N}_n^{(1)}(k) \right] \end{aligned} \tag{2.235a}$$

$$\begin{aligned} \mathbf{H}^i &= \mathbf{a}_y H_o e^{j(\omega t - kz)} \\ &= -\frac{kE_o}{\mu\omega} e^{j\omega t} \sum_{n=1}^{\infty} (-j)^n \frac{2n+1}{n(n+1)} \left[\mathbf{M}_n^{(1)}(k) - j\mathbf{N}_n^{(1)}(k) \right] \end{aligned} \tag{2.235b}$$

where

$$\begin{aligned} \mathbf{M}_n(k) = {} & \frac{1}{\sin\theta} z_n(kr) P_n^1(\cos\theta) \cos\phi \mathbf{a}_\theta \\ & - z_n(kr) \frac{\partial P_n^1(\cos\theta)}{\partial\theta} \sin\phi \mathbf{a}_\phi \end{aligned} \tag{2.236}$$

$$\begin{aligned} \mathbf{N}_n(k) = {} & \frac{n(n+1)}{kr} z_n(kr) P_n^1(\cos\theta) \cos\phi \mathbf{a}_r \\ & + \frac{1}{kr} \frac{\partial}{\partial r} [z_n(kr)] \frac{\partial P_n^1(\cos\theta)}{\partial\theta} \cos\phi \mathbf{a}_\theta \\ & + \frac{1}{kr\sin\theta} \frac{\partial}{\partial r} [z_n(kr)] P_n^1(\cos\theta) \sin\phi \mathbf{a}_\phi \end{aligned} \tag{2.237}$$

The superscript (1) on the spherical vector functions **M** and **N** in Eq. (2.235) indicates that these functions are constructed with spherical Bessel function of the first kind; i.e., $z_n(kr)$ in Eqs. (2.236) and (2.237) is replaced by $j_n(kr)$ when **M** and **N** are substituted in Eq. (2.235).

The induced secondary field consists of two parts. One part applies to the interior of the sphere and is referred to as the transmitted field, while the other applies to the

exterior of the sphere and is called the scattered field. Thus the total field outside the sphere is the sum of the incident and scattered fields. We now construct these fields in a fashion similar to that of the incident field. For the scattered field, we let

$$\mathbf{E}^s = E_o e^{j\omega t} \sum_{n=1}^{\infty} (-j)^n \frac{2n+1}{n(n+1)} \left[a_n \mathbf{M}_n^{(4)}(k) + j b_n \mathbf{N}_n^{(4)}(k) \right] \tag{2.238a}$$

$$\mathbf{H}^s = -\frac{kE_o}{\mu\omega} e^{j\omega t} \sum_{n=1}^{\infty} (-j)^n \frac{2n+1}{n(n+1)} \left[a_n \mathbf{M}_n^{(4)}(k) - j b_n \mathbf{N}_n^{(4)}(k) \right] \tag{2.238b}$$

where a_n and b_n are expansion coefficients and the superscript (4) on $\mathbf{M}$ and $\mathbf{N}$ shows that these functions are constructed with spherical Bessel function of the fourth kind (or Hankel function of the second kind); i.e., $z_n(kr)$ in Eqs. (2.236) and (2.237) is replaced by $h_n^{(2)}(kr)$ when $\mathbf{M}$ and $\mathbf{N}$ are substituted in Eq. (2.238). The spherical Hankel function has been chosen to satisfy the radiation condition. In other words, the asymptotic behavior of $h_n^{(2)}(kr)$, namely,

$$h_n^{(2)}(kr) \quad \sim \quad j^{n+1} \frac{e^{-kr}}{kr}, \tag{2.239}$$

when combined with the time factor $e^{j\omega t}$, represents an outgoing spherical wave (see Eq. (2.106d)). Similarly, the transmitted field inside the sphere can be constructed as

$$\mathbf{E}^t = E_o e^{j\omega t} \sum_{n=1}^{\infty} (-j)^n \frac{2n+1}{n(n+1)} \left[c_n \mathbf{M}_n^{(1)}(k_1) + j d_n \mathbf{N}_n^{(1)}(k_1) \right] \tag{2.240a}$$

$$\mathbf{H}^t = -\frac{kE_o}{\mu\omega} e^{j\omega t} \sum_{n=1}^{\infty} (-j)^n \frac{2n+1}{n(n+1)} \left[c_n \mathbf{M}_n^{(1)}(k_1) - j d_n \mathbf{N}_n^{(1)}(k_1) \right] \tag{2.240b}$$

where c_n and d_n are expansion coefficients, k_1 is the propagation constant in the sphere. The functions $M_n^{(1)}$ and $N_n^{(1)}$ in Eq. (2.240) are obtained by replacing $z_n(kr)$ in Eq. (2.237) by $j_n(k_1 r)$; j_n is the only solution in this case since the field must be finite at the origin, the center of the sphere.

The unknown expansion coefficients a_n, b_n, c_n, and d_n are determined by letting the fields satisfy the boundary conditions, namely, the continuity of the tangential components of the total electric and magnetic fields at the surface of the sphere. Thus at $r = a$,

$$\mathbf{a}_r \times \left(\mathbf{E}^i + \mathbf{E}^s - \mathbf{E}^t \right) = 0 \tag{2.241a}$$

$$\mathbf{a}_r \times \left(\mathbf{H}^i + \mathbf{H}^s - \mathbf{H}^t \right) = 0 \tag{2.241b}$$

This is equivalent to

$$E_\theta^i + E_\theta^s = E_\theta^t, \qquad r = a \tag{2.242a}$$

$$E_\phi^i + E_\phi^s = E_\phi^t, \qquad r = a \tag{2.242b}$$

$$H_\theta^i + H_\theta^s = H_\theta^t, \qquad r = a \tag{2.242c}$$

$$H_\phi^i + H_\phi^s = H_\phi^t, \qquad r = a \tag{2.242d}$$

Substituting Eqs. (2.235), (2.238), and (2.240) into Eq. (2.242), multiplying the resulting equations by $\cos\phi$ or $\sin\phi$ and integrating over $0 \le \phi < 2\pi$, and then multiplying by $\dfrac{dP_m^1}{d\theta}$ or $\dfrac{dP_m^1}{sin\theta}$ and integrating over $0 \le \theta \le \pi$, we obtain

$$j_n(ka) + a_n h_n^{(2)}(ka) = c_n j_n(k_1 a) \tag{2.243a}$$

$$\mu_1 [k a j_n(ka)]' + a_n \mu_1 \left[k a h_n^{(2)}(ka)\right]' = c_n \mu [k_1 a j_n(k_1 a)]' \tag{2.243b}$$

$$\mu_1 j_n(ka) + b_n \mu_1 h_n^{(2)}(ka) = d_n \mu j_n(k_1 a) \tag{2.243c}$$

$$k [k a j_n(ka)]' + b_n k \left[k a h_n^{(2)}(ka)\right]' = d_n k_1 [k_1 a j_n(k_1 a)]' \tag{2.243d}$$

Solving Eqs. (2.243a) and (2.243b) gives a_n and c_n, while solving Eqs. (2.243c) and (2.243d) gives b_n and d_n. Thus, for $\mu = \mu_o = \mu_1$,

$$a_n = \frac{j_n(m\alpha)[\alpha j_n(\alpha)]' - j_n(\alpha)[m\alpha j_n(m\alpha)]'}{j_n(m\alpha)[\alpha h_n^{(2)}(\alpha)]' - h_n^{(2)}(\alpha)[m\alpha j_n(m\alpha)]'} \tag{2.244a}$$

$$b_n = \frac{j_n(\alpha)[m\alpha j_n(m\alpha)]' - m^2 j_n(m\alpha)[\alpha j_n(\alpha)]'}{h_n^{(2)}(\alpha)[m\alpha j_n(m\alpha)]' - m^2 j_n(m\alpha)[\alpha h_n^{(2)}(\alpha)]'} \tag{2.244b}$$

$$c_n = \frac{j/\alpha}{h_n^{(2)}(\alpha)[m\alpha j_n(m\alpha)]' - j_n(m\alpha)[\alpha h_n^{(2)}(\alpha)]'} \tag{2.244c}$$

$$d_n = \frac{j/\alpha}{h_n^{(2)}(\alpha)[m\alpha j_n(m\alpha)]' - m^2 j_n(m\alpha)[\alpha h_n^{(2)}(\alpha)]'} \tag{2.244d}$$

where $\alpha = ka = 2\pi a/\lambda$ and $m = k_1/k$ is the refractive index of the dielectric, which may be real or complex depending on whether the dielectric is lossless or lossy. The primes at the square brackets indicate differentiation with respect to the argument of the Bessel function inside the brackets, i.e., $[x z_n(x)]' = \frac{\partial}{\partial x}[x z_n(x)]$. To obtain Eqs. (2.244c) and (2.244d), we have made use of the Wronskian relationship

$$j_n(x)\left[x h_n^{(2)}(x)\right]' - h_n^{(2)}(x)[x j_n(x)]' = -j/x \tag{2.245}$$

If the dielectric is lossy and its surrounding medium is free space,

$$k_1^2 = \omega\mu_o(\omega\epsilon_1 - j\sigma), \qquad k^2 = \omega^2\mu_o\epsilon_o \tag{2.246}$$

so that the (complex) refractive index m becomes

$$m = \frac{k_1}{k} = \sqrt{\epsilon_c} = \sqrt{\epsilon_{r1} - j\frac{\sigma_1}{\omega\epsilon_o}} = m' - jm'' \tag{2.247}$$

The problem of scattering by a conducting sphere can be obtained as a special case of the problem considered above. Since the EM fields must vanish inside the conducting sphere, the right-hand sides of Eqs. (2.242a), (2.242b), (2.243a), and (2.243d) must be equal to zero so that ($c_n = 0 = d_n$)

$$a_n = -\frac{j_n(\alpha)}{h_n^{(2)}(\alpha)} \tag{2.248a}$$

$$b_n = -\frac{[\alpha j_n(\alpha)]'}{[\alpha h_n^{(2)}(\alpha)]'} \tag{2.248b}$$

Thus we have completed the Mie solution; the field at any point inside or outside the sphere can now be determined. We will now apply the solution to problems of practical interest.

2.8.2 Scattering Cross Sections

Often scattered radiation is most conveniently measured by the scattering cross section Q_{sca} (in meter^2) which may be defined as the ratio of the total energy scattered per second W_s to the energy density P of the incident wave, i.e.,

$$Q_{\text{sca}} = \frac{W_s}{P} \tag{2.249}$$

The energy density of the incident wave is given by

$$P = \frac{E_o^2}{2\eta} = \frac{1}{2}E_o^2\sqrt{\frac{\epsilon}{\mu}} \tag{2.250}$$

The scattered energy from the sphere is

$$W_s = \frac{1}{2}\text{Re}\int_0^{2\pi}\int_0^{\pi}\left[E_\theta H_\phi^* - E_\phi H_\theta^*\right] r^2 \sin\theta\, d\theta\, d\phi$$

where the star sign denotes complex conjugation and field components are evaluated at far field ($r >> a$). By using the asymptotic expressions for spherical Bessel functions, we can write the resulting field components as

$$E_\theta^s = \eta H_\phi^s = -\frac{j}{kr}E_o e^{j(\omega t - kr)}\cos\phi S_2(\theta) \tag{2.251a}$$

$$-E_\phi^s = \eta H_\theta^s = -\frac{j}{kr}E_o e^{j(\omega t - kr)}\sin\phi S_1(\theta) \tag{2.251b}$$

where the amplitude functions $S_1(\theta)$ and $S_2(\theta)$ are given by [11]

$$S_1(\theta) = \sum_{n=1}^{\infty} \frac{2n+1}{n(n+1)} \left(\frac{a_n}{\sin\theta} P_n^1(\cos\theta) + b_n \frac{dP_n^1(\cos\theta)}{d\theta} \right) \tag{2.252a}$$

$$S_2(\theta) = \sum_{n=1}^{\infty} \frac{2n+1}{n(n+1)} \left(\frac{b_n}{\sin\theta} P_n^1(\cos\theta) + a_n \frac{dP_n^1(\cos\theta)}{d\theta} \right) \tag{2.252b}$$

Thus,

$$W_s = \frac{\pi E_o^2}{2k^2\eta} \operatorname{Re} \int_0^{\pi} \left(|S_1(\theta)|^2 + |S_2(\theta)|^2 \right) \sin\theta \, d\theta$$

This is evaluated with the help of the identities [10]

$$\int_0^{\pi} \left(\frac{dP_n^1}{d\theta} \frac{dP_m^1}{d\theta} + \frac{1}{\sin^2\theta} P_n^1 P_m^1 \right) \sin\theta \, d\theta = \begin{cases} 0, & n \neq m \\ \dfrac{2}{2n+1} \dfrac{(n+1)!}{(n-1)!} n(n+1), & n = m \end{cases}$$

and

$$\int_0^{\pi} \left(\frac{dP_m^1}{\sin\theta} \frac{dP_n^1}{d\theta} + \frac{P_n^1}{\sin\theta} \frac{P_m^1}{d\theta} \right) \sin\theta \, d\theta = 0$$

We obtain

$$W_s = \frac{\pi E_o^2}{k^2\eta} \sum_{n=1}^{\infty} (2n+1) \left(|a_n|^2 + |b_n|^2 \right) \tag{2.253}$$

Substituting Eqs. (2.250) and (2.253) into Eq. (2.249), the scattering cross section is found to be

$$Q_{\text{sca}} = \frac{2\pi}{k^2} \sum_{n=1}^{\infty} (2n+1) \left(|a_n|^2 + |b_n|^2 \right) \tag{2.254}$$

Similarly, the *cross section for extinction* Q_{ext} (in meter^2) is obtained [11] from the amplitude functions for $\theta = 0$, i.e.,

$$Q_{\text{ext}} = \frac{4\pi}{k^2} \operatorname{Re} S(0)$$

or

$$Q_{\text{ext}} = \frac{2\pi}{k^2} \operatorname{Re} \sum_{n=1}^{\infty} (2n+1) \, (a_n + b_n) \tag{2.255}$$

where

$$S(0) = S_1(0^o) = S_2(0^o) = \frac{1}{2}\sum_{n=1}^{\infty}(2n+1)\,(a_n + b_n) \tag{2.256}$$

In obtaining Eq. (2.256), we have made use of

$$\left.\frac{P_n^1}{\sin\theta}\right|_{\theta=0} = \left.\frac{dP_n^1}{d\theta}\right|_{\theta=0} = n(n+1)/2$$

If the sphere is absorbing, the *absorption cross section* Q_{abs} (in meter^2) is obtained from

$$Q_{\text{abs}} = Q_{\text{ext}} - Q_{\text{sca}} \tag{2.257}$$

since the energy removed is partly scattered and partly absorbed.

A useful, measurable quantity in radar communications is the *radar cross section* or *back-scattering cross section* σ_b of a scattering obstacle. It is a lump measure of the efficiency of the obstacle in scattering radiation back to the source ($\theta = 180°$). It is defined in terms of the far zone scattered field as

$$\sigma_b = 4\pi r^2 \frac{|\mathbf{E}^s|^2}{E_o^2}, \qquad \theta = \pi \tag{2.258}$$

From Eq. (2.251),

$$\sigma_b = \frac{2\pi}{k^2}\left[|S_1(\pi)|^2 + |S_2(\pi)|^2\right]$$

But

$$-S_1(\pi) = S_2(\pi) = \frac{1}{2}\sum_{n=1}^{\infty}(-1)^n(2n+1)\,(a_n - b_n)$$

where we have used

$$-\left.\frac{P_n^1}{\sin\theta}\right|_{\theta=\pi} = \left.\frac{dP_n^1}{d\theta}\right|_{\theta=\pi} = (-1)^n n(n+1)/2$$

Thus

$$\sigma_b = \frac{\pi}{k^2}\left|\sum_{n=1}^{\infty}(-1)^n(2n+1)\,(a_n - b_n)\right|^2 \tag{2.259}$$

Similarly, we may determine the *forward-scattering cross section* ($\theta = 0^o$) as

$$\sigma_f = \frac{2\pi}{k^2}\left[|S_1(0)|^2 + |S_2(0)|^2\right]$$

Substituting Eq. (2.256) into this yields

$$\sigma_f = \frac{\pi}{k^2}\left|\sum_{n=1}^{\infty}(2n+1)\,(a_n + b_n)\right|^2 \tag{2.260}$$

2.9 Attenuation Due to Raindrops

The rapid growth in demand for additional communication capacity has put pressure on engineers to develop microwave systems operating at higher frequencies. It turns out, however, that at frequencies above 10 GHz attenuation caused by atmospheric particles can reduce the reliability and performance of radar and space communication links. Such particles include oxygen, ice crystals, rain, fog, and snow. Prediction of the effect of these precipitates on the performance of a system becomes important. In this final subsection, we will examine attenuation and phase shift of an EM wave propagating through rain drops. We will assume that raindrops are spherical so that Mie rigorous solution can be applied. This assumption is valid if the rate intensity is low. For high rain intensity, an oblate spheroidal model would be more realistic [12].

The magnitude of an EM wave traveling through a homogeneous medium (with N identical spherical particles per unit volume) in a distance ℓ is given by $e^{-\gamma\ell}$, where γ is the attenuation coefficient given by [11]

$$\gamma = NQ_{\text{ext}}$$

or

$$\gamma = \frac{N\lambda^2}{\pi}\,\text{Re}\,S(0) \tag{2.261}$$

Thus the wave is attenuated by

$$A = 10\log_{10}\frac{1}{e^{-\gamma\ell}} = \gamma\ell 10\log_{10} e$$

or

$$A = 4.343\gamma\ell \qquad \text{(in dB)}$$

The attenuation per length (in dB/m) is

$$A = 4.343\gamma$$

or

$$A = 4.343\frac{\lambda^2 N}{\pi}\,\text{Re}\,S(0) \tag{2.262}$$

Similarly, it can be shown [11] that the phase shift of the EM wave caused by the medium is

$$\Phi = -\frac{\lambda^2 N}{2\pi}\,\text{Im}\,S(0) \qquad \text{(in radians/unit length)}$$

or

$$\Phi = -\frac{\lambda^2 N}{2\pi}\,\text{Im}\,S(0)\frac{180}{\pi} \qquad \text{(in deg/m)} \tag{2.263}$$

Table 2.9 Laws and Parsons Drop-size Distributions for Various Rain Rates

	Rain Rate (mm/hour)								
Drop diameter (cm)	0.25	1.25	2.5	5	12.5	25	50	100	150
	Percent of total volume								
0.05	28.0	10.9	7.3	4.7	2.6	1.7	1.2	1.0	1.0
0.1	50.1	37.1	27.8	20.3	11.5	7.6	5.4	4.6	4.1
0.15	18.2	31.3	32.8	31.0	24.5	18.4	12.5	8.8	7.6
0.2	3.0	13.5	19.0	22.2	25.4	23.9	19.9	13.9	11.7
0.25	0.7	4.9	7.9	11.8	17.3	19.9	20.9	17.1	13.9
0.3		1.5	3.3	5.7	10.1	12.8	15.6	18.4	17.7
0.35		0.6	1.1	2.5	4.3	8.2	10.9	15.0	16.1
0.4		0.2	0.6	1.0	2.3	3.5	6.7	9.0	11.9
0.45			0.2	0.5	1.2	2.1	3.3	5.8	7.7
0.5				0.3	0.6	1.1	1.8	3.0	3.6
0.55					0.2	0.5	1.1	1.7	2.2
0.6						0.3	0.5	1.0	1.2
0.65							0.2	0.7	1.0
0.7									0.3

To relate attenuation and phase shift to a realistic rainfall rather than identical drops assumed so far, it is necessary to know the drop-size distribution for a given rate intensity. Representative distributions were obtained by Laws and Parsons [13] as shown in Table 2.9. To evaluate the effect of the drop-size distribution, suppose for a particular rain rate R, p is the percent of the total volume of water reaching the ground (as in Table 2.9), which consists of drops whose diameters fall in the interval centered in D cm ($D = 2a$), the number of drops in that interval is given by

$$N_c = pN(D) \tag{2.264}$$

The total attenuation and phase shift over the entire volume become

$$A = 0.4343\frac{\lambda^2}{\pi} \cdot 10^6 \sum pN(D)\,\mathrm{Re}\,S(0) \qquad \text{(dB/km)} \tag{2.265}$$

$$\Phi = -\frac{9\lambda^2}{\pi^2} \cdot 10^6 \sum pN(D)\,\mathrm{Im}\,S(0) \qquad \text{(deg/km)} \tag{2.266}$$

where λ is the wavelength in cm and $N(D)$ is the number of raindrops with equivolumic diameter D per cm^3. The summations are taken over all drop sizes. In order to relate the attenuation and phase shift to the rain intensity measured in rain rate R (in mm/hour), it is necessary to have a relationship between N and R. The relationship obtained by Best [13], shown in Table 2.10, involves the terminal velocity u (in m/s)

of the rain drops, i.e.,

$$R = u \cdot N \cdot \quad \text{(volume of a drop)}$$
$$= uN\frac{4\pi a^3}{3} \quad \text{(in m/s)}$$

or

$$R = 6\pi NuD^3 \cdot 10^5 \quad \text{(mm/hr)}$$

Thus

$$N(D) = \frac{R}{6\pi uD^3}10^{-5} \tag{2.267}$$

Substituting this into Eqs. (2.265) and (2.266) leads to

$$A = 4.343\frac{\lambda^2}{\pi^2}R\sum\frac{p}{6uD^3}\,\text{Re}\,S(0) \quad \text{(dB/km)} \tag{2.268}$$

$$\Phi = -90\frac{\lambda^2}{\pi^3}R\sum\frac{p}{6uD^3}\,\text{Im}\,S(0) \quad \text{(deg/km)}\,, \tag{2.269}$$

where $N(D)$ is in per cm^3, D and λ are in cm, u is in m/s, p is in percent, and $S(0)$ is the complex forward-scattering amplitude defined in Eq. (2.256). The complex refractive index of raindrops [14] at 20°C required in calculating attenuation and phase shift is shown in Table 2.11.

Table 2.10 Raindrop Terminal Velocity

Radius (cm)	Velocity (m/s)
0.025	2.1
0.05	3.9
0.075	5.3
0.10	6.4
0.125	7.3
0.15	7.9
0.175	8.35
0.20	8.7
0.225	9.0
0.25	9.2
0.275	9.35
0.30	9.5
0.325	9.6

Example 2.13

For ice spheres, plot the normalized back-scattering cross section, $\sigma_b/\pi a^2$, as a function of the normalized circumference, $\alpha = 2\pi a/\lambda$. Assume that the refractive

Table 2.11 Refractive Index of Water at 20°C

Frequency (GHz)	Refractive index ($m = m' - jm''$)
0.6	$8.960 - j0.1713$
0.8	$8.956 - j0.2172$
1.0	$8.952 - j0.2648$
1.6	$8.933 - j0.4105$
2.0	$8.915 - j0.5078$
3.0	$8.858 - j0.7471$
4.0	$8.780 - j0.9771$
6.0	$8.574 - j1.399$
11	$7.884 - j2.184$
16	$7.148 - j2.614$
20	$6.614 - j2.780$
30	$5.581 - j2.848$
40	$4.886 - j2.725$
60	$4.052 - j2.393$
80	$3.581 - j2.100$
100	$3.282 - j1.864$
160	$2.820 - j1.382$
200	$2.668 - j1.174$
300	$2.481 - j0.8466$

index of ice is independent of wavelength, making the normalized cross section for ice applicable over the entire microwave region. Take $m = 1.78 - j2.4 \times 10^{-3}$ at 0°C. □

Solution
From Eq. (2.259),

$$\sigma_b = \frac{\pi}{k^2}\left|\sum_{n=1}^{\infty}(-1)^n(2n+1)\,(a_n - b_n)\right|^2$$

Since $\alpha = ka$, the normalized back-scattering cross section is

$$\frac{\sigma_b}{\pi a^2} = \frac{1}{\alpha^2}\left|\sum_{n=1}^{\infty}(-1)^n(2n+1)\,(a_n - b_n)\right|^2 \tag{2.270}$$

Using this expression in conjunction with Eq. (2.244), the subroutine SCATTERING in the FORTRAN code of Fig. 2.16 was used as the main program to determine $\sigma_b/\pi a^2$ for $0.2 < \alpha < 4$. Details on the program will be explained in the next example. It suffices to mention that the maximum number of terms of the infinite series in Eq. (2.270) was 10. It has been found that truncating the series at $n = 2\alpha$ provides sufficient accuracy. The plot of the normalized radar cross section versus α

is shown in Fig. 2.15. From the plot, we note that back-scattering oscillates between very large and small values. If α is increased further, the normalized radar cross section increases rapidly. The unexpectedly large cross sections have been attributed to a lens effect; the ice sphere acts like a lens which focuses the incoming wave on the back side from which it is reflected backwards in a concentrated beam. This is recognized as a crude description, but it at least permits visualization of a physical process which may have some reality. ∎

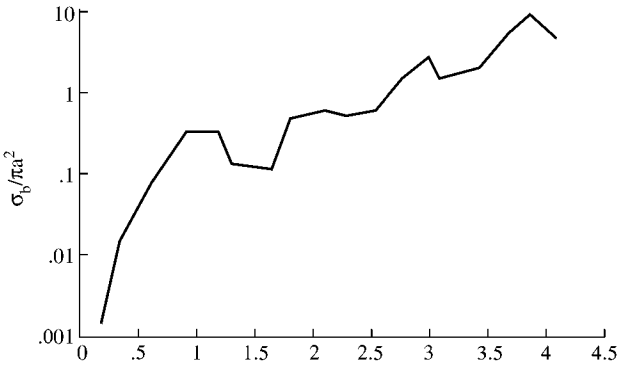

Figure 2.15
Normalized back-scattering (radar) cross sections $\alpha = 2\pi a/\lambda$ for ice at 0°C.

Example 2.14
Assuming the Laws and Parsons' rain drop-size distribution, calculate the attenuation in dB/km for rain rates of 0.25, 1.25, 2.5, 5.0, 12.5, 50.0, 100.0, and 150.0 mm/hr. Consider the incident microwave frequencies of 6, 11, and 30 GHz. □

Solution
The FORTRAN code developed for calculating attenuation and phase shift of microwaves due to rain is shown in Fig. 2.16. The main program calculates attenuation and phase shift for given values of frequency and rain rate by employing Eqs. (2.268) and (2.269). For each frequency, the corresponding value of the refractive index of water at 20°C is taken from Table 2.11. The data in Tables 2.9 and 2.10 on the drop-size distributions and terminal velocity are incorporated in the main program.

Seven subroutines are involved. The subroutine SCATTERING calculates the expansion coefficients a_n, b_n, c_n and d_n using Eq. (2.244) and also the forward-scattering amplitude $S(0)$ using Eq. (2.256). The same subroutine was used as the main program in the previous example to calculate the radar cross section of ice spheres. Enough comments are inserted to make the program self-explanatory. Subroutine BESSEL and BESSELCMPLX are exactly the same except that the former is for real argument, while the latter is for complex argument. They both employ Eq. (2.160) to

```
0001    C ***********************************************************
0002    C  MAIN PROGRAM
0003    C
0004    C  FOR SPHERICAL RAIN DROPS,
0005    C  THIS PROGRAM CALCULATES ATTENUATION IN dB/KM AND
0006    C  PHASE SHIFT IN DEG/KM FOR A GIVEN RAIN RATE
0007    C
0008    C  R = RAIN RATE IN MM/HR
0009    C  D = DROP DIAMETER IN CM
0010    C  F = FREQUENCY IN GHZ
0011    C  AT = ATTENUATION IN dB/KM
0012    C  PH = PHASE SHIFT IN DEG/KM
0013    C  V = TERMINAL VELOCITY OF RAIN DROPS
0014    C  P = PERCENT OF TOTAL VOLUME AS MEASURED
0015    C  BY LAWS AND PARSONS
0016    C  M = COMPLEX REFRACTIVE INDEX OF WATER AT T = 20 C
0017    C  X = ALPHA = K*A
0018
0019          DIMENSION R(9),P(14,9),V(14)
0020          REAL*8 LAM,MR,MI
0021          COMPLEX*8 M,S0,S00(15)
0022          DATA V/2.1,3.9,5.3,6.4,7.3,7.9,8.35,8.7,9.0,9.2,
0023         1       9.35,9.5,9.6,9.6/
0024          DATA R/0.25,1.25,2.5,5.0,12.5,25.0,50.0,100.0,150.0/
0025          DATA (( P(I,J),I=1,14),J=1,9) /28.0,50.1,16.2,3.0,0.7,
0026         1       9*0.0,  10.9,37.1,31.3,13.5,4.9,1.5,0.6,0.2,6*0.0,
0027         1       7.3,27.8,32.8,19.0,7.9,3.3,1.1,0.6,0.2,5*0.0,
0028         2       4.7,20.3,31.0,22.2,11.8,5.7,2.5,1.0,0.5,0.3,4*0.0,
0029         3       2.6,11.5,24.5,25.4,17.3,10.1,4.3,2.3,1.2,0.6,
0030         4       0.2,3*0.0,  1.7,7.6,18.4,23.9,19.9,12.8,8.2,3.5,2.1,
0031         5       1.1,0.5,0.3,2*0.0,  1.2,5.4,12.5,19.9,20.9,15.6,
0032         6       10.9,6.7,3.3,1.8,1.1,0.5,0.2,0.0,  1.0,4.6,8.8,
0033         7       13.9,17.1,18.4,15.0,9.0,5.8,3.0,1.7,1.0,0.7,0.0,
0034         8       1.0,4.1,7.6,11.7,13.9,17.7,16.1,11.9,7.7,3.6,2.2,
0035         9       1.2,1.0,0.3 /
0036
0037           F = 30.0
0038           LAM = 30.0/F       ! WAVELENGTH IN CM
0039           MR = 5.581
0040           MI = 2.848
0041           M = CMPLX(MR,-MI)
0042           PIE = 3.141592654
0043           DO  10  I = 1,14
0044           D = 0.05*DFLOAT(I)
0045           X = PIE*D/LAM
0046           CALL SCATTERING(X,M,S0,SB)
0047           S00(I) = S0
0048    10     CONTINUE
0049           DO 50 N = 1,9
0050           SUMAT = 0.0
0051           SUMPH = 0.0
0052           WRITE(6,20) R(N),F
0053    20      FORMAT(5X,'RAIN RATE =',F8.4,1X,'MM/HR',4X
0054         1              'FREQUENCY =',F10.5,1X,'GHZ',/)
0055          DO 30 K=1,14
0056          D = 0.05*DFLOAT(K)
0057          X = PIE*D/LAM
0058          S0 = S00(K)
0059    C
```

Figure 2.16
FORTRAN program for Examples 2.13 and 2.14 ***(Continued).***

```
0060    C       CALCULATE ATTENUATION AND PHASE SHIFT
0061    C
0062            ACO = REAL(SO)/(6.0*X*X)
0063            PCO =  AIMAG(SO)/(12.0*X*X)
0064            ATO = ACO*( P(K,N)/100.0 )/ (V(K)*D )
0065            SUMAT = SUMAT + ATO
0066            PHO = PCO*( P(K,N)/100.0 )/ (V(K)*D )
0067            SUMPH = SUMPH + PHO
0068    30      CONTINUE
0069            AT = 4.343*R(N)*SUMAT
0070            PH = 180.0*R(N)*SUMPH/PIE
0071            PRINT *,R(N),AT,PH
0072            WRITE(6,40) AT,PH
0073    40      FORMAT(3X,'ATTENUATION =',F12.6,1X,'dB/KM',3X,
0074           1          'PHASE SHIFT =',F12.6,1X,'DEG/KM',/)
0075    50     CONTINUE
0076    60       FORMAT(I5,F15.8,F15.8)
0077             STOP
0078             END

0001
0002    C ***********************************************************
0003    C       USING MIE'S SOLUTION,
0004    C       THIS SUBROUTINE CALCULATES THE SCATTERING COEFFIENTS
0005    C       AND THE FORWARD SCATTERING FUNCTION
0006    C
0007            SUBROUTINE SCATTERING(X,M,SO,SB)
0008
0009            IMPLICIT COMPLEX*8 (A-D)
0010            COMPLEX*8 M,SO,Y,JC,SUM,SUMB
0011            COMPLEX*8 JM(0:20),JMD(0:20),H(0:20),HD(0:20)
0012            REAL*8  J(0:20),JD(0:20)
0013            DIMENSION A(20),B(20),C(20),D(20)
0014
0015            Y = M*X
0016            JC=(0.0,1.0)
0017            SUM = (0.0,0.0)
0018            SUMB = (0.0,0.0)
0019            NMAX = 10
0020    C
0021    C       FIRST, CALCULATE THE SCATTERING COEFFICIENTS an and bn
0022    C
0023            DO 10 N=1,NMAX
0024            CALL BESSEL(X,N,J,JD)
0025            CALL BESSELCMPLX(Y,N,JM,JMD)
0026            CALL HANKEL(X,N,H,HD)
0027            A1 = JM(N)*JD(N) - J(N)*JMD(N)
0028            A2 = JM(N)*HD(N) - H(N)*JMD(N)
0029            A(N) =  A1/A2
0030            B1 = J(N)*JMD(N) - (M**2)*JM(N)*JD(N)
0031            B2 = H(N)*JMD(N) - (M**2)*JM(N)*HD(N)
0032            B(N) =  B1/B2
0033            C(N) = JC/(X*A2)
0034            D(N) = - JC*M/(X*B2)
0035    C
0036    C       CALCULATE THE FORWARD SCATTERING AMPLITUDE FUNCTION S(0)
0037    C
0038            F = 2.0*FLOAT(N) + 1.0
0039            SUM = SUM + F*( A(N) + B(N) )
0040            SUMB = SUMB + F*((-1.)**N)*( A(N) - B(N) )
0041    10      CONTINUE
```

Figure 2.16
(Cont.)* FORTRAN program for Examples 2.13 and 2.14 *(Continued).

```
0042          SO = SUM/2.0       ! FORWARD SCATTERING AMPLITUDE FUNCTION
0043          SB=(CABS( SUMB )/X)**2  ! NORMALIZED RADAR CROSS-SECTION
0044          RETURN
0045          END


0001    C ***********************************************************
0002    C       SUBROUTINE FOR SPHERICAL HANKEL FUNCTIONS H AND HD
0003    C       OF REAL ARGUMENT (SERIES EXPANSION METHOD)
0004
0005          SUBROUTINE HANKEL(X,N,H,HD)
0006          IMPLICIT REAL*8(A-G,J,O-Z),COMPLEX*8(H)
0007          DIMENSION J(0:20),JD(0:20),Y(0:20),YD(0:20)
0008          DIMENSION JN(0:20),JND(0:20),H(0:20),HD(0:20)
0009
0010          PIE = 3.141592654
0011          CALL BESSEL(X,N,J,JD)
0012          CALL BESSELN(X,N,JN,JND)
0013          V = DFLOAT(N) + 0.5
0014          Y(N) = ( DCOS(V*PIE)*J(N) - JN(N) )/DSIN(V*PIE)
0015          H(N) = CMPLX( J(N), - Y(N) )      ! HANKEL OF 2ND KIND
0016          YD(N) = ( DCOS(V*PIE)*JD(N) - JND(N) )/DSIN(V*PIE)
0017          HD(N) = CMPLX( JD(N), - YD(N) )
0018          RETURN
0019          END

0001    C ***********************************************************
0002    C       SUBROUTINE FOR SPHERICAL BESSEL FUNCTION J AND JD
0003    C       OF REAL ARGUMENT (SERIES EXPANSION METHOD)
0004    C
0005          SUBROUTINE BESSEL(X,N,J,JD)
0006          IMPLICIT REAL*8(A-H,J,O-Z)
0007          DIMENSION J(0:20),JD(0:20)
0008
0009          TOL = 0.00000001          ! TOLERANCE
0010          PIE = 3.141592654
0011          V = DFLOAT(N) + 0.5
0012          K = 0
0013          SUM1 = 0.0
0014          SUM2 = 0.0
0015    10    PN = V + DFLOAT(K) + 1.0
0016          CALL GAMMA(PN,GN)
0017          CALL FACTORIAL(K,FK)
0018          A = ((-1.)**K)*((.5)**(V+2*K))*(X**(V+2*K-.5))/(GN*FK)
0019          SUM1 = SUM1 + A
0020          B = A*(V + FLOAT(2*K) + 0.5)
0021          SUM2 = SUM2 + B
0022          K = K + 1
0023          IF(ABS(A).GE.TOL) GO TO 10
0024          CONTINUE
0025          Q = DSQRT(PIE/2.0)
0026          J(N) = Q*SUM1
0027          JD(N) = Q*SUM2
0028          RETURN
0029          END


0001    C ***********************************************************
0002    C       SUBROUTINE FOR SPHERICAL BESSEL FUNCTIONS JN AND JND
0003    C       OF REAL ARGUMENT BUT NEGATIVE ORDER (SERIES EXPANSION)
0004    C
```

Figure 2.16
(Cont.) **FORTRAN program for Examples 2.13 and 2.14** ***(Continued).***

```
0005          SUBROUTINE BESSELN(X,N,JN,JND)
0006          IMPLICIT REAL*8(A-H,J,O-Z)
0007          DIMENSION JN(0:20),JND(0:20)
0008
0009          TOL = 0.00000001          ! TOLERANCE
0010          PIE = 3.141592654
0011          V = DFLOAT(N) + 0.5
0012          K = 0
0013          SUM1 = 0.0
0014          SUM2 = 0.0
0015    10    PN = -V + DFLOAT(K) + 1.0
0016          CALL GAMMA(PN,GN)
0017          CALL FACTORIAL(K,FK)
0018          A = ((-1.)**K)*((.5)**(-V+2*K))*(X**(-V+2*K-.5))/(GN*FK)
0019          SUM1 = SUM1 + A
0020          B = A*(-V + FLOAT(2*K) + 0.5)
0021          SUM2 = SUM2 + B
0022          K = K + 1
0023          IF(ABS(A).GE.TOL) GO TO 10
0024          CONTINUE
0025          Q = DSQRT(PIE/2.0)
0026          JN(N) = Q*SUM1
0027          JND(N) = Q*SUM2
0028          RETURN
0029          END
```

```
0001    C ***********************************************************
0002    C       SUBROUTINE FOR SPHERICAL BESSEL FUNCTIONS JN AND JND
0003    C       OF COMPLEX ARGUMENT  (SERIES EXPANSION)
0004    C
0005          SUBROUTINE BESSELCMPLX(Z,N,JN,JND)
0006          IMPLICIT COMPLEX*8(A-D,J,S,Z),REAL*8(G,P-R,V)
0007          DIMENSION JN(0:20),JND(0:20)
0008
0009          TOL = 0.001          ! TOLERANCE
0010          PIE = 3.141592654
0011          V = DFLOAT(N) + 0.5
0012          K = 0
0013          SUM1 = (0.0,0.0)
0014          SUM2 = (0.0,0.0)
0015    10    PN = V + DFLOAT(K) + 1.0
0016          CALL GAMMA(PN,GN)
0017          CALL FACTORIAL(K,FK)
0018          A = ((-1.)**K)*((.5)**(V+2*K))*(Z**(V+2*K-.5))/(GN*FK)
0019          SUM1 = SUM1 + A
0020          B = A*(V + FLOAT(2*K) + 0.5)
0021          SUM2 = SUM2 + B
0022          K = K + 1
0023          IF( CABS(A).GE.TOL) GO TO 10
0024          CONTINUE
0025          Q = DSQRT(PIE/2.0)
0026          JN(N) = Q*SUM1
0027          JND(N) = Q*SUM2
0028          RETURN
0029          END
```

```
0001    C ***********************************************************
0002    C     SUBROUTINE FOR GAMMA FUNCTION
0003    C
```

Figure 2.16
***(Cont.)* FORTRAN program for Examples 2.13 and 2.14 *(Continued)*.**

```
0004          SUBROUTINE GAMMA(V,G)
0005          IMPLICIT REAL*8(A-H,O-Z)
0006
0007          PIE = 3.1415927
0008          IF(V-0.5) 10,20,20
0009     10   N = -V + 0.5
0010          N2 = 2*N
0011          CALL FACTORIAL(N,FN)
0012          CALL FACTORIAL(N2,FN2)
0013          G = ((-4.)**N)*DSQRT(PIE)*FN/FN2
0014          RETURN
0015     20   N = V - 0.5
0016          N2 = 2*N
0017          CALL FACTORIAL(N,FN)
0018          CALL FACTORIAL(N2,FN2)
0019          G = FN2*DSQRT(PIE)/(FN*(2.**N2))
0020          RETURN
0021          END


0001     C ********************************************************
0002     C     SUBROUTINE FOR FACTORIAL OF N, i.e. N!
0003     C
0004          SUBROUTINE FACTORIAL(N,F)
0005          REAL*8 F
0006
0007          F = 1.0
0008          IF(N.EQ.0) GO TO 20
0009          DO 10 I=1,N
0010     10   F = F*DFLOAT(I)
0011     20   RETURN
0012          END
```

Figure 2.16
***(Cont.)* FORTRAN program for Examples 2.13 and 2.14.**

find $j_n(x)$. Subroutine HANKEL employs Eq. (2.162) to find $y_n(x)$, which involves calling subroutine BESSELN to calculate $j_{-n}(x)$. The derivative of Bessel-Riccati function $[xz_n(x)]$ is obtained from (see Prob. 2.14)

$$[xz_n(x)]' = -nz_n(x) + xz_{n-1}(x)$$

where z_n is j_n, j_{-n}, y_n or $h_n(x)$. Subroutine GAMMA calculates $\Gamma(n + 1/2)$ using Eq. (2.165), while subroutine FACTORIAL determines $n!$. All computations were done in double precision arithmetic, although it was observed that using single precision would only alter results slightly.

Typical results for 11 GHz are tabulated in Table 2.12. A graph of attenuation vs. rain rate is portrayed in Fig. 2.17. The plot shows that attenuation increases with rain rate and conforms with the common rule of thumb. We must note that the underlying assumption of spherical raindrops renders the result as only a first order approximation of the practical rainfall situation. ▮

Table 2.12 Attenuation and Phase Shift at 11 GHz

Rain rate (mm/hr)	Attenuation (dB/km)	Phase shift (deg/km)
0.25	2.56×10^{-3}	0.4119
1.25	1.702×10^{-3}	1.655
2.5	4.072×10^{-3}	3.040
5.0	9.878×10^{-3}	5.601
12.5	0.3155	12.58
25	0.7513	23.19
50	1.740	42.74
100	3.947	78.59
150	6.189	112.16

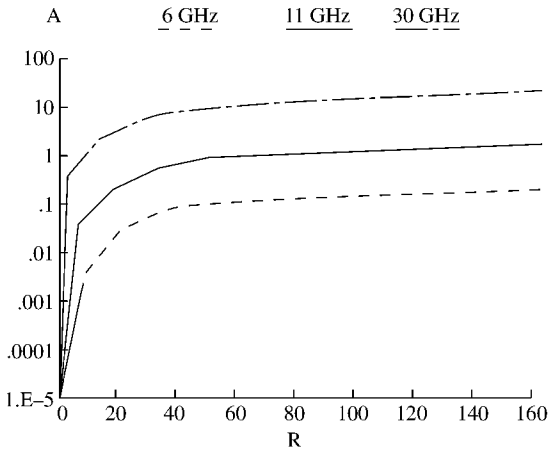

Figure 2.17
Attenuation vs. rain rate.

2.10 Concluding Remarks

We have reviewed analytic methods for solving partial differential equations. Analytic solutions are of major interest as test models for comparison with numerical techniques. The emphasis has been on the method of separation of variables, the most powerful analytic method. For an excellent, more in-depth exposition of this method, consult Myint-U [5]. In the course of applying the method of separation of variables, we have encountered some mathematical functions such as Bessel functions and Legendre polynomials. For a thorough treatment of these functions and their properties, Bell [7] and Johnson and Johnson [8] are recommended. The mathematical handbook by Abramowitz and Stegun [15] provides tabulated values of these functions

for specific orders and arguments. A few useful texts on the topics covered in this chapter are also listed in the references.

As an example of real life problems, we have applied the analytical techniques developed in this chapter to the problem of attenuation of microwaves due to spherical raindrops. Spherical models have also been used to assess the absorption characteristics of the human skull exposed to EM plane waves [16]–[20] (see Probs. 2.46 to 2.49).

We conclude this chapter by remarking that the most satisfactory solution of a field problem is an exact analytical one. In many practical situations, no solution can be obtained by the analytical methods now available, and one must therefore resort to numerical approximation, graphical or experimental solutions. (Experimental solutions are usually very expensive, while graphical solutions are not so accurate). The remainder of this book will be devoted to a study of the numerical methods commonly used in EM.

References

[1] W.J. Gibbs, *Conformal Transformation in Electrical Engineering.* London: Chapman & Hall, 1958.

[2] N. Morita et al., *Integral Equation Methods for Electromagnetics.* Boston, MA: Artech House, 1990.

[3] H.F. Weinberger, *A First Course in Partial Differential Equations.* New York: John Wiley, 1965, Chap. IV, pp. 63–116.

[4] R.D. Kersten, *Engineering Differential Systems.* New York: McGraw-Hill, 1969, Chap. 5, pp. 66–106.

[5] T. Myint-U, *Partial Differential Equations of Mathematical Physics.* New York: North-Holland, 1980.

[6] G.N. Watson, *Theory of Bessel Functions.* London: Cambridge University Press, 1966.

[7] W.W. Bell, *Special Functions for Scientists and Engineers.* London: D. Van Nostrand, 1968.

[8] D.E. Johnson and J.R. Johnson, *Mathematical Methods in Engineering and Physics.* Englewood Cliffs, NJ: Prentice-Hall, 1982.

[9] K. Asano, "Electrostatic potential and field in a cylindrical tank containing charged liquid," *Proc. IEEE,* vol. 124, no. 12, Dec. 1977, pp. 1277–1281.

[10] J.A. Stratton, *Electromagnetic Theory.* New York: McGraw-Hill, 1941, pp. 394–421, 563–573.

[11] H.C. Van de Hulst, *Light Scattering of Small Particles.* New York: John Wiley, 1957, pp. 28–37, 114–136, 284.

[12] J. Morrison and M.J. Cross, "Scattering of a plane electromagnetic wave by axisymmetric raindrops," *Bell Syst. Tech. J.,* vol. 53, no. 6, July-Aug. 1974, pp. 955–1019.

[13] D.E. Setzer, "Computed transmission through rain at microwave and visible frequencies," *Bell Syst. Tech. J.,* vol. 49, no. 8, Oct. 1970, pp. 1873–1892.

[14] M.N.O. Sadiku, "Refractive index of snow at microwave frequencies," *Appl. Optics,* vol. 24, no. 4, Feb. 1985, pp. 572–575.

[15] M. Abramowitz and I.A. Stegun, *Handbook of Mathematical Functions.* New York: Dover, 1965.

[16] C.H. Durney, "Electromagnetic dosimetry for models of humans and animals: a review of theoretical and numerical techniques," *Proc. IEEE.,* vol. 68, no. 1, Jan. 1980, pp. 33–40.

[17] M.A. Morgan, "Finite element calculation of microwave absorption by the cranial structure," *IEEE Trans. Bio. Engr.,* vol. BME-28, no. 10, Oct. 1981, pp. 687–695.

[18] J.W. Hand, "Microwave heating patterns in simple tissue models," *Phys. Med. Biol.,* vol. 22, no. 5, 1977, pp. 981–987.

[19] W.T. Joines and R.J. Spiegel, "Resonance absorption of microwaves by the human skull," *IEEE Trans. Bio. Engr.,* vol. BME-21, Jan. 1974, pp. 46–48.

[20] C.M. Weil, "Absorption characteristics of multilayered sphere models exposed to UHF/microwave radiation," *IEEE Trans. Bio. Engr.,* vol. BME-22, no. 6, Nov. 1975, pp. 468–476.

Problems

2.1 Consider the PDE

$$a\Phi_{xx} + b\Phi_{xy} + c\Phi_{yy} + d\Phi_x + e\Phi_y + f\Phi = 0$$

where the coefficients a, b, c, d, e, and f are in general functions of x and y. Under what conditions is the PDE separable?

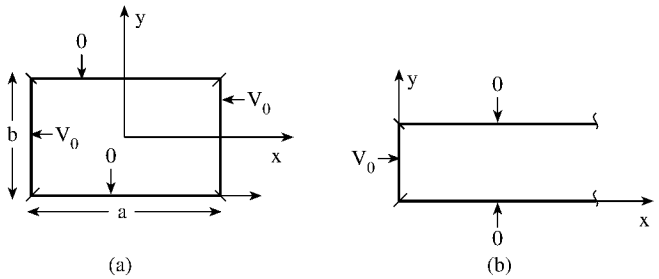

Figure 2.18
For problem 2.2.

2.2 Determine the distribution of electrostatic potential inside the conducting rectangular boxes with cross sections shown in Fig. 2.18.

2.3 The cross-sections of the cylindrical systems that extend to infinity in the z-direction are shown in Fig. 2.19. The potentials on the boundaries are as shown. For each system, find the potential distribution.

2.4 Find the solution U of:

(a) Laplace equation

$$\begin{aligned} \nabla^2 U &= 0, \qquad 0 < x, y < \pi \\ U_x(0, y) &= 0 = U_x(x, y), \qquad U(x, 0) = 0\,, \\ U(x, \pi) &= x, \qquad 0 < x < \pi \end{aligned}$$

(b) Heat equation

$$\begin{aligned} kU_{xx} &= U_t, \qquad 0 \le x \le 1,\ t > 0 \\ U(0, t) &= 0,\ t > 0, \qquad U(1, t) = 1,\ t > 0 \\ U(x, 0) &= 0, \qquad 0 \le x \le 1 \end{aligned}$$

(c) Wave equation

$$\begin{aligned} a^2 U_{xx} &= U_{tt}, \qquad 0 \le x \le 1,\ t > 0 \\ U(0, t) &= 0 = U(1, t),\ t > 0 \\ U(x, 0) &= 0, \qquad U_t(x, 0) = x \end{aligned}$$

2.5 Find the solution Φ of:

(a) Laplace equation

$$\begin{aligned} \nabla^2 \Phi &= 0, \qquad \rho \ge 1,\ 0 < \phi < \pi \\ \Phi(1, \phi) &= \sin\phi, \qquad \Phi(\rho, 0) = \Phi(\rho, \pi) = 0 \end{aligned}$$

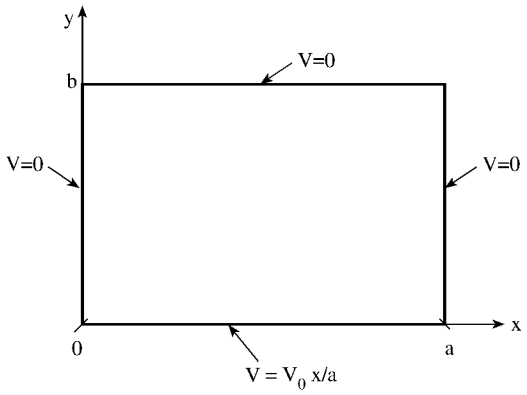

(a)

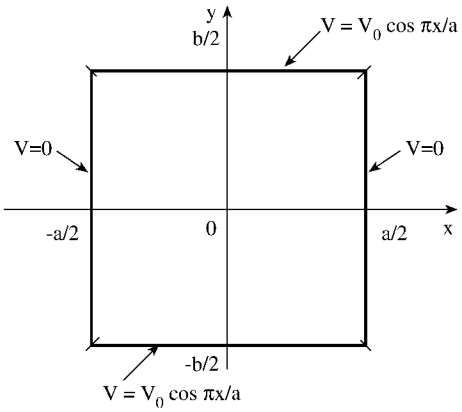

(b)

Figure 2.19
For problem 2.3.

(b) Laplace equation

$$\nabla^2\Phi = 0, \qquad 0 < \rho < 1,\ 0 < z < L$$
$$\Phi(\rho, \phi, 0) = 0 = \Phi(\rho, \phi, L),\ \Phi(a, \phi, z) = 1$$

(c) Heat equation

$$\Phi_t = k\nabla^2\Phi, \qquad 0 \le \rho \le 1, -\infty < z < \infty,\ t > 0$$
$$\Phi(a, \phi, t) = 0,\ t > 0, \qquad \Phi(\rho, \phi, 0) = \rho^2 \cos 2\phi, 0 \le \phi < 2\pi$$

2.6 Solve the PDE

$$4\frac{\partial^4\Phi}{\partial x^4} + \frac{\partial^2\Phi}{\partial t^2} = 0, \qquad 0 < x < 1,\ t > 0$$

subject to the boundary conditions

$$\Phi(0,t) = 0 = \Phi(1,t) = \Phi_{xx}(0,t) = \Phi_{xx}(1,t)$$

and initial conditions

$$\Phi_t(x,0) = 0, \qquad \Phi(x,0) = x$$

2.7 A cylinder similar to the one in Fig. 2.20 has its ends $z = 0$ and $z = L$ held at zero potential. If

$$V(a,z) = \begin{cases} V_o z/L, & 0 < z < L/2 \\ V_o(1 - z/L), & L/2 < z < L \end{cases}$$

find $V(\rho, z)$. Calculate the potential at $(\rho, z) = (0.8a, 0.3L)$.

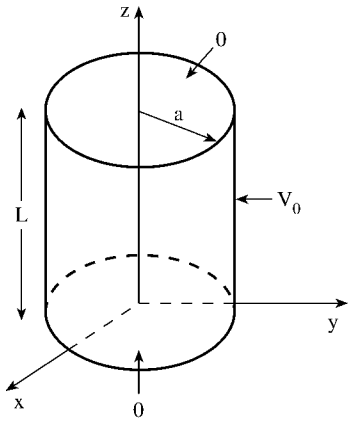

Figure 2.20
For problem 2.7.

2.8 Determine the potential distribution in a hollow cylinder of radius a and length L with ends held at zero potential while the lateral surface is held at potential V_o as in Fig. 2.20. Calculate the potential along the axis of the cylinder when $L = 2a$.

2.9 The conductor whose cross section is shown in Fig. 2.21 is maintained at $V = 0$ everywhere except on the curved electrode where it is held at $V = V_o$. Find the potential distribution $V(\rho, \phi)$.

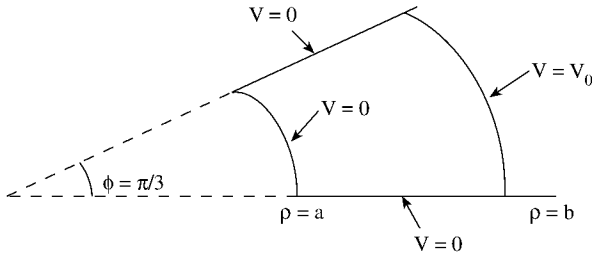

Figure 2.21
For problem 2.9.

2.10 Solve the PDE

$$\frac{\partial^2 \Phi}{\partial \rho^2} + \frac{1}{\rho}\frac{\partial \Phi}{\partial \rho} = \frac{\partial^2 \Phi}{\partial t^2}, \qquad 0 \le \rho \le a,\ t \ge 0$$

under the conditions

$$\Phi(0, t) \quad \text{is bounded}, \qquad \Phi(a, t) = 0,\ t \ge 0\,,$$
$$\Phi(\rho, 0) = \left(1 - \rho^2/a^2\right), \qquad \left.\frac{\partial \Phi}{\partial t}\right|_{t=0} = 0,\ 0 \le \rho \le a$$

2.11 The generating function for Bessel function is given by

$$G(x, t) = \exp\left[\frac{x}{2}\left(t - \frac{1}{t}\right)\right] = \sum_{n=-\infty}^{\infty} t^n J_n(x)$$

(a) By taking the derivatives of both sides with respect to x, show that

$$\frac{d}{dx} J_n(x) = \frac{1}{2}\left[J_{n-1}(x) - J_{n+1}(x)\right]$$

(b) By taking the derivatives of both sides with respect to t, show that

$$J_{n+1}(x) = \frac{x}{2(n+1)}\left[J_n(x) + J_{n+2}(x)\right]$$

2.12 (a) Prove that

$$e^{\pm j\rho \sin\phi} = \sum_{n=-\infty}^{\infty} (\pm 1)^n J_n(\rho) e^{jn\phi}$$

(b) Derive the *Bessel's integral formula*

$$J_n(\rho) = \frac{1}{\pi}\int_0^{\pi} \cos(n\theta - \rho \sin\theta)\, d\theta$$

2.13 Show that

$$\cos x = J_o(x) + 2\sum_{n=1}^{\infty}(-1)^n J_{2n}(x)$$

and

$$\sin x = 2\sum_{n=1}^{\infty}(-1)^{n+1} J_{2n+1}(x)$$

which demonstrate the close tie between Bessel function and trigonometric functions.

2.14 Prove that:

(a) $J_{1/2}(x) = \sqrt{\frac{2}{\pi x}}\sin x$,

(b) $J_{-1/2}(x) = \sqrt{\frac{2}{\pi x}}\cos x$,

(c) $\frac{d}{dx}[x^{-n}J_n(x)] = -x^n J_{n+1}(x)$.

(d) $\frac{d^n}{dx^n}J_n(x)\Big|_{x=0} = \frac{1}{2^n}$,

(e) $\frac{d}{dx}[xz_n(x)] = -nz_n(x) + xz_{n-1}(x) = (n+1)z_n(x) + xz_{n+1}(x)$

2.15 Given that

$$I_o = \int_0^{\infty} e^{-\lambda a} J_o(\lambda\rho)\, d\lambda = \frac{1}{(\rho^2 + a^2)^{1/2}}$$

find

$$I_1 = \int_0^{\infty} e^{-\lambda a}\lambda J_o(\lambda\rho)\, d\lambda$$

and

$$I_2 = \int_0^{\infty} e^{-\lambda a}\lambda^2 J_o(\lambda\rho)\, d\lambda$$

2.16 Write a computer program that will evaluate the first five roots λ_{nm} of Bessel function $J_n(x)$ for $n = 1, 2, \ldots, 5$, i.e., $J_n(\lambda_{nm}) = 0$.

2.17 Evaluate:

(a)

$$\int_{-1}^{1} P_1(x)P_2(x)\, dx\ ,$$

(b)

$$\int_{-1}^{1} [P_4(x)]^2\ dx\ ,$$

(c)

$$\int_0^{1} x^2 P_3(x)\, dx$$

2.18 In Legendre series of the form $\sum_{n=0}^{\infty} A_n P_n(x)$, expand:

(a) $f(x) = \begin{cases} 0, & -1 < x < 0, \\ 1, & 0 < x < 1 \end{cases}$

(b) $f(x) = x^3, \qquad -1 < x < 1,$

(c) $f(x) = \begin{cases} 0, & -1 < x < 0, \\ x, & 0 < x < 1 \end{cases}$

(d) $f(x) = \begin{cases} 1 + x, & -1 < x < 0, \\ 1 - x, & 0 < x < 1 \end{cases}$

2.19 Solve Laplace's equation:

(a) $\nabla^2 U = 0, \qquad 0 \le r \le a, \qquad U(a, \theta) = \begin{cases} 1, & 0 < \theta < \pi/2, \\ 0, & \text{otherwise} \end{cases}$

(b) $\nabla^2 U = 0, \qquad r > a, \qquad \left.\dfrac{\partial U}{\partial r}\right|_{r=a} = \cos\theta + 3\cos^3\theta, \quad 0 < \theta < \pi,$

(c) $\nabla^2 U = 0, \qquad r < a, \quad 0 < \theta < \pi, \quad 0 < \phi < 2\pi,$
$U(a, \theta, \phi) = \sin^2\theta$

2.20 A hollow conducting sphere of radius a has its upper half charged to potential V_o while its lower half is grounded. Find the potential distribution inside and outside the sphere.

2.21 A circular disk of radius a carries charge of surface charge density ρ_o. Show that the potential at point $(0, 0, z)$ on its axis $\theta = 0$ is

$$V = \frac{\rho_o}{2\epsilon}\left[\left(z^2 + a^2\right)^{1/2} - z\right]$$

From this deduce the potential at any point (r, θ, ϕ).

2.22 (a) Verify the three-term recurrence relation

$$(2n + 1)x P_n(x) = (n + 1)P_{n+1}(x) + n P_{n-1}(x)$$

(b) Use the recurrence relation to find $P_6(x)$ and $P_1(x)$.

2.23 Verify the following identities:

(a) $\int_{-1}^{1} P_n(x) P_m(x)\, dx = \dfrac{2}{2n + 1}\delta_{nm},$

(b) $\int_{-1}^{1} P_n^m(x) P_k^m(x)\, dx = \dfrac{2}{2n + 1}\dfrac{(n + m)!}{(n - m)!}\delta_{nk}$

2.24 Rework the problem in Fig. 2.8 if the boundary conditions are now

$$V(r = a) = V_o, \qquad V(r \to \infty) = E_o r \cos\theta + V_o$$

Find V and $\mathbf{E}$ everywhere. Determine the maximum value of the field strength.

2.25 In a sphere of radius a, obtain the solution $V(r, \theta)$ of Laplace's equation

$$\nabla^2 V(r, \theta) = 0, \qquad r \leq a$$

subject to

$$V(a, \theta) = 3\cos^2\theta + 3\cos\theta + 1$$

2.26 Determine the solution to Laplace's equation

$$\nabla^2 V = 0$$

outside a sphere $r > a$ subject to the boundary condition

$$\frac{\partial}{\partial r} V(a, \theta) = \cos\theta + 3\cos^3\theta$$

2.27 Find the potential distribution inside and outside a dielectric sphere of radius a placed in a uniform electric field E_o.

Hint: The problem to be solved is $\nabla^2 V = 0$ subject to

$$\epsilon_r \frac{\partial V_1}{\partial r} = \frac{\partial V_2}{\partial r} \qquad \text{on } r = a, \;\; V_1 = V_2 \text{ on } r = a\,,$$
$$V_2 = -E_o r\cos\theta \qquad \text{as } r \to \infty$$

2.28 (a) Derive the recurrence relation of the associated Legendre polynomials

$$P_n^{m+1}(x) = \frac{2mx}{(1 - x^2)^{1/2}} P_n^m(x) - [n(n+1) - m(m-1)] P_n^{m-1}(x)$$

(b) Using the recurrence relation on the formula for P_n^m, find P_3^2, P_3^3, P_4^1, and P_4^2.

2.29 Expand $V = \cos 2\phi \sin^2\phi$ in terms of the spherical harmonics $P_n^m(\cos\theta)$ $\sin m\phi$ and $P_n^m(\cos\theta)\cos m\phi$.

2.30 In the prolate spheroidal coordinates (ξ, η, ϕ), the equation

$$\nabla^2\Phi + k^2\Phi = 0$$

assumes the form

$$\frac{\partial}{\partial\xi}\left[\left(\xi^2 - 1\right)\frac{\partial\Phi}{\partial\xi}\right] + \frac{\partial}{\partial\eta}\left[\left(1 - \eta^2\right)\frac{\partial\Phi}{\partial\eta}\right] + \left[\frac{1}{\xi^2 - 1} + \frac{1}{1 - \eta^2}\right]\frac{\partial^2\Phi}{\partial\phi^2} + k^2 d^2\left(\xi^2 - \eta^2\right)\Phi = 0$$

Show that the separated equations are

$$\frac{d}{d\xi}\left[\left(\xi^2+1\right)\frac{d\Psi_1}{d\xi}\right]+\left[k^2d^2\xi^2-\frac{m^2}{\xi^2-1}-c\right]\Psi_1=0$$

$$\frac{d}{d\eta}\left[\left(1-\eta^2\right)\frac{d\Psi_2}{d\eta}\right]-\left[k^2d^2\eta^2+\frac{m^2}{1-\eta^2}-c\right]\Psi_2=0$$

$$\frac{d^2\Psi_3}{d\phi^2}+m^2\Psi_3=0$$

where m and c are separation constants.

2.31 Solve Eq. (2.203) if $a=b=c=\pi$ and:
(a) $f(x,y,z)=e^{-x}$, (b) $f(x,y,z)=\sin^2 x$.

2.32 Solve the inhomogeneous PDE

$$\frac{\partial^2\Phi}{\partial\rho^2}+\frac{1}{\rho}\frac{\partial\Phi}{\partial\rho}-\frac{\partial^2\Phi}{\partial t^2}=-\Phi_o\sin\omega t,\qquad 0\le\rho\le a,\ t\ge 0$$

subject to the conditions $\Phi(a,t)=0$, $\Phi(\rho,0)=0$, $\Phi_t(\rho,0)=0$, Φ is finite for all $0\le\rho\le a$. Take Φ_o as a constant and $a\omega$ not being a zero of $J_0(x)$.

2.33 Infinitely long metal box has a rectangular cross section shown in Fig. 2.22. If the box is filled with charge $\rho_v=\rho_o x/a$, find V inside the box.

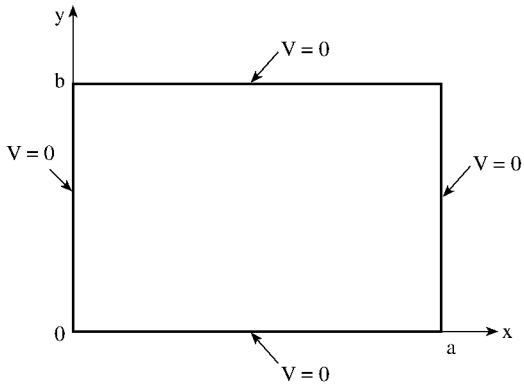

Figure 2.22
For problem 2.33.

2.34 In Section 2.7.2, find $\mathbf{E}_g$ and $\mathbf{E}_\ell$, the electric field intensities in gas and liquid, respectively.

2.35 Consider the potential problem shown in Fig. 2.23. The potentials at $x=0$, $x=a$, and $y=0$ sides are zero while the potential at $y=b$ side is V_o. Using the series expansion technique similar to that used in Section 2.7.2, find the potential distribution in the solution region.

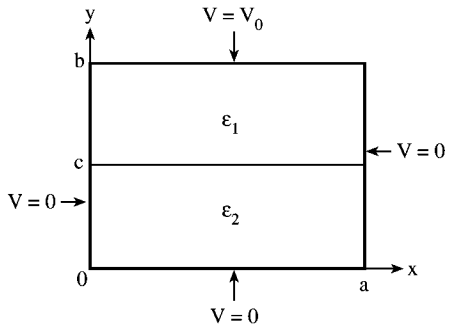

Figure 2.23
Potential system for problem 2.35.

2.36 Consider a grounded rectangular pipe with the cross section shown in Fig. 2.24. Assuming that the pipe is partially filled with hydrocarbons with charge density ρ_o, apply the same series expansion technique used in Section 2.7.2 to find the potential distribution in the pipe.

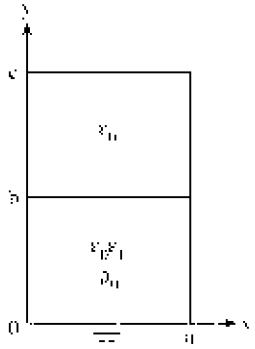

Figure 2.24
Earthed rectangular pipe partially filled with charged liquid—for problem 2.36.

2.37 Write a program to generate associated Legendre polynomial, with $x = \cos\theta = 0.5$. You may use either series expansion or recurrence relations. Take $0 \leq n \leq 15, 0 \leq m \leq n$. Compare your results with those tabulated in standard tables.

2.38 The FORTRAN program of Fig. 2.16 uses the series expansion method to generate $j_n(x)$. Write a subroutine for generating $j_n(x)$ using recurrence relations. For $x = 2.0$ and $0 \leq n \leq 10$, compare your result with that obtained using the subroutine BESSEL of Fig. 2.16 and the values in standard tables. Which result do you consider to be more accurate? Explain.

2.39 Use the product generating function

$$G(x+y,t) = G(x,t)G(y,t)$$

to derive the *addition theorem*

$$J_n(x+y) = \sum_{m=-\infty}^{\infty} J_m(x) J_{n-m}(y)$$

Recall that

$$G(x,t) = \exp\left[\frac{x}{2}\left(t - \frac{1}{t}\right)\right] = \sum_{n=-\infty}^{\infty} t^n J_n(x)$$

2.40 Use the generating function to prove that:

$$\frac{1}{R} = \frac{1}{r_o}\sum_{n=0}^{\infty}(r/r_o)^n P_n(\cos\theta), \qquad r < r_o\ ,$$

$\frac{1}{R} = \frac{1}{r}\sum_{n=0}^{\infty}(r_o/r)^n P_n(\cos\theta)$, $r > r_o$, where $R = |\mathbf{r} - \mathbf{r}_o| = [r^2 - r_o^2 - 2rr_o\cos\alpha]^{1/2}$ and α is the angle between $\mathbf{r}$ and $\mathbf{r}_o$.

2.41 Show that

$$\int T_0(x)\,dx = T_1(x)$$
$$\int T_1(x)\,dx = \frac{1}{4}T_2(x) + \frac{1}{4}$$
$$\int T_n(x)\,dx = \frac{1}{2}\left(\frac{T_{n+1}(x)}{n+1} - \frac{T_{n-1}(x)}{n-1}\right), \qquad n > 1$$

so that integration can be done directly in Chebyshev polynomials.

2.42 A function is defined by

$$f(x) = \begin{cases} 1, & -1 \le x \le 1 \\ 0, & \text{otherwise} \end{cases}$$

(a) Expand $f(x)$ in a series of Hermite functions,

(b) expand $f(x)$ in a series of Laguerre functions.

2.43 By expressing E_θ^i and E_ϕ^i in terms of the spherical wave functions, show that Eq. (2.235) is valid.

2.44 By defining

$$\rho_n(x) = \frac{d}{dx}\ln\left[xh_n^{(2)}(x)\right], \qquad \sigma_n(x) = \frac{d}{dx}\ln\left[xj_n(x)\right] ,$$

show that the scattering amplitude coefficients can be written as

$$a_n = \frac{j_n(\alpha)}{h_n^{(2)}(\alpha)}\left[\frac{\sigma_n(\alpha) - m\sigma_n(m\alpha)}{\rho_n(\alpha) - m\sigma_n(m\alpha)}\right]$$
$$b_n = \frac{j_n(\alpha)}{h_n^{(2)}(\alpha)}\left[\frac{\sigma_n(m\alpha) - m\sigma_n(\alpha)}{\sigma_n(m\alpha) - m\rho_n(\alpha)}\right]$$

2.45 For the problem in Fig. 2.14, plot $|E_z^t|/|E_x^i|$ for $-a < z < a$ along the axis of the dielectric sphere of radius $a = 9$ cm in the $x - z$ plane. Take $E_o = 1$, $\omega = 2\pi \times 5 \times 10^9$ rad/s, $\epsilon_1 = 4\epsilon_o$, $\mu_1 = \mu_o$, $\sigma_1 = 0$. You may modify the program in Fig. 2.16 or write your own.

2.46 In analytical treatment of the radio-frequency radiation effect on the human body, the human skull is frequently modeled as a lossy sphere. Of major concern is the calculation of the normalized heating potential

$$\Phi(r) = \frac{1}{2}\sigma\frac{|E^t(r)|^2}{|E_o|^2} \qquad (\Omega \cdot m)^{-1} ,$$

where E^t is the internal electric field strength and E_o is the peak incident field strength. If the human skull can be represented by a homogeneous sphere of radius $a = 10$ cm, plot $\Phi(r)$ against the radial distance $-10 \le r = z \le 10$ cm. Assume an incident field as in Fig. 2.14 with $f = 1$ GHz, $\mu_r = 1$, $\epsilon_r = 60$, $\sigma = 0.9$ mhos/m, $E_o = 1$.

2.47 Instead of the homogeneous spherical model assumed in the previous problem, consider the multilayered spherical model shown in Fig. 2.25 with each region labeled by an integer p, such that $p = 1$ represents the central core region and $p = 4$ represents air. At $f = 2.45$ GHz, plot the heating potential along the x axis, y axis, and z axis. Assume the data given below.

Region p	Tissue	Radius (mm)	ϵ_r	σ (mho/m)
1	muscle	18.5	46	2.5
2	fat	19	6.95	0.29
3	skin	20	43	2.5
4	air		1	0
$\mu_r = 1$				

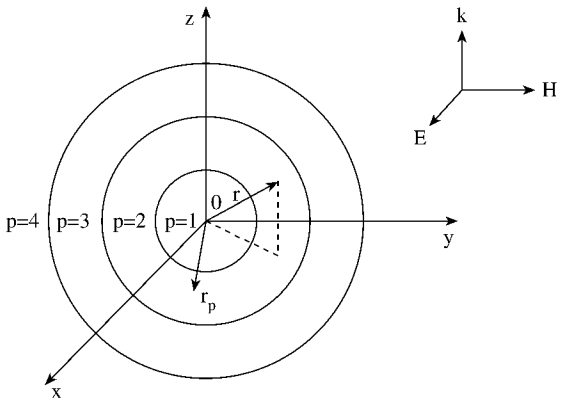

Figure 2.25
For problem 2.47, a multilayered spherical model of the human skull.

Note that for each region p, the resultant field consists of the transmitted and scattered fields and is in general given by

$$E_p(r,\theta,\phi) = E_o e^{j\omega t} \sum_{n=1}^{\infty} (-j)^n \frac{2n+1}{n(n+1)} \Big[a_{np} \mathbf{M}_{np}^{(4)}(k) + j b_{np} \mathbf{N}_{np}^{(4)}(k) + c_{np} \mathbf{M}_{np}^{(1)}(k_1) + j d_{np} \mathbf{N}_{np}^{(1)}(k1) \Big]$$

2.48 The absorption characteristic of biological bodies is determined in terms of the specific absorption rate (SAR) defined as the total power absorbed divided as the power incident on the geometrical cross section. For an incident power density of 1 mW/cm^2 in a spherical model of the human head,

$$\text{SAR} = 2\frac{Q_{\text{abs}}}{\pi a} \qquad \text{mW/cm}^3$$

where a is in centimeters. Using the above relation, plot SAR against frequency for $0.1 < f < 3$ GHz, $a = 10$ cm assuming frequency-dependent and dielectric properties of head as

$$\epsilon_r = 5\left(\frac{12 + (f/f_o)^2}{1 + (f/f_o)^2}\right)$$
$$\sigma = 6\left(\frac{1 + 62(f/f_o)^2}{1 + (f/f_o)^2}\right)$$

where f is in GHz and $f_o = 20$ GHz.

2.49 For the previous problem, repeat the calculations of SAR assuming a six-layered spherical model of the human skull (similar to that of Fig. 2.25) of outer radius

$a = 10$ cm. Plot P_a/P_i vs. frequency for $0.1 < f < 3$ GHz where

$$\frac{P_a}{P_i} = \frac{2}{\alpha^2} \sum (2n+1) \left[\text{Re}\,(a_n + b_n) - \left(|a_n|^2 + |b_n|^2 \right) \right] ,$$

$P_a =$ absorbed power, $P_i =$ incident power, $\alpha = 2\pi a/\lambda$, λ is the wavelength in the external medium. Use the dimensions and electrical properties shown below.

Layer p	Tissue	Radius (mm)	ϵ_r	σ_o(mho/m)
1	brain	9	$5\nabla(f)$	$6\Delta(f)$
2	CSF	12	$7\nabla(f)$	$8\Delta(f)$
3	dura	13	$4\nabla(f)$	$8\Delta(f)$
4	bone	17.3	5	62
5	fat	18.5	6.95	0.29
6	skin	20	43	2.5

where $\mu_r = 1$,

$$\nabla(f) = \frac{1 + 12(f/f_o)^2}{1 + (f/f_o)^2} ,$$

$$\Delta(f) = \frac{1 + 62(f/f_o)^2}{1 + (f/f_o)^2} ,$$

f is in GHz, and $f_o = 20$ GHz. Compare your result with that from the previous problem.

Chapter 3

Finite Difference Methods

"Those who know others are clever; those who know themselves have discernment; those who overcome others have force; those who overcome themselves are strong; those who know contentment are rich; those who persevere are people of purpose."
Paraphrase of Lao Tzu

3.1 Introduction

It is rare for real-life EM problems to fall neatly into a class that can be solved by the analytical methods presented in the preceding chapter. Classical approaches may fail if [1]:

- the PDE is not linear and cannot be linearized without seriously affecting the result
- the solution region is complex
- the boundary conditions are of mixed types
- the boundary conditions are time-dependent
- the medium is inhomogeneous or anisotropic

Whenever a problem with such complexity arises, numerical solutions must be employed. Of the numerical methods available for solving PDEs, those employing finite differences are more easily understood, more frequently used, and more universally applicable than any other.

The finite difference method (FDM) was first developed by A. Thom [2] in the 1920s under the title "the method of squares" to solve nonlinear hydrodynamic equations. Since then, the method has found applications in solving different field problems. The finite difference techniques are based upon approximations which permit replacing differential equations by finite difference equations. These finite difference approximations are algebraic in form; they relate the value of the dependent variable at a

point in the solution region to the values at some neighboring points. Thus a finite difference solution basically involves three steps:

(1) dividing the solution region into a grid of nodes

(2) approximating the given differential equation by finite difference equivalent that relates the dependent variable at a point in the solution region to its values at the neighboring points

(3) solving the difference equations subject to the prescribed boundary conditions and/or initial conditions

The course of action taken in three steps is dictated by the nature of the problem being solved, the solution region, and the boundary conditions. The most commonly used grid patterns for two-dimensional problems are shown in Fig. 3.1. A three-dimensional grid pattern will be considered later in the chapter.

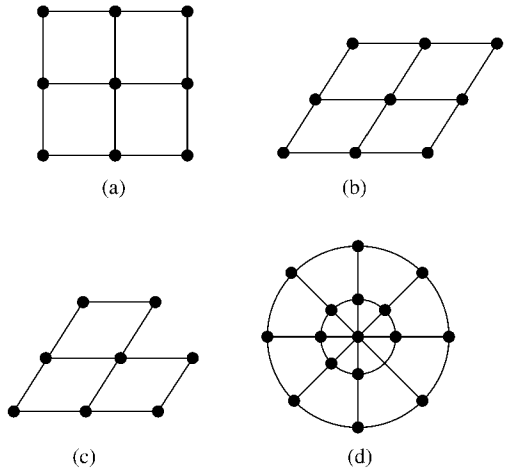

Figure 3.1
Common grid patterns: (a) rectangular grid, (b) skew grid, (c) triangular grid, (d) circular grid.

3.2 Finite Difference Schemes

Before finding the finite difference solutions to specific PDEs, we will look at how one constructs finite difference approximations from a given differential equation. This essentially involves estimating derivatives numerically.

Given a function $f(x)$ shown in Fig. 3.2, we can approximate its derivative, slope or the tangent at P by the slope of the arc PB, giving the *forward-difference* formula,

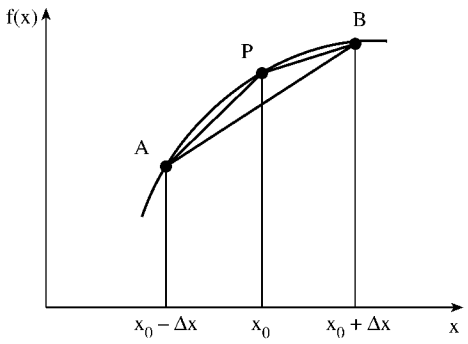

Figure 3.2
Estimates for the derivative of $f(x)$ at P using forward, backward, and central differences.

$$\boxed{f'(x_o) \simeq \frac{f(x_o + \Delta x) - f(x_o)}{\Delta x}} \tag{3.1}$$

or the slope of the arc AP, yielding the *backward-difference* formula,

$$\boxed{f'(x_o) \simeq \frac{f(x_o) - f(x_o - \Delta x)}{\Delta x}} \tag{3.2}$$

or the slope of the arc AB, resulting in the *central-difference* formula,

$$\boxed{f'(x_o) \simeq \frac{f(x_o + \Delta x) - f(x_o - \Delta x)}{2\Delta x}} \tag{3.3}$$

We can also estimate the second derivative of $f(x)$ at P as

$$\begin{aligned} f''(x_o) &\simeq \frac{f'(x_o + \Delta x/2) - f'(x_o - \Delta x/2)}{\Delta x} \\ &= \frac{1}{\Delta x}\left[\frac{f(x_o + \Delta x) - f(x_o)}{\Delta x} - \frac{f(x_o) - f(x_o - \Delta x)}{\Delta x}\right] \end{aligned}$$

or

$$f''(x_o) \simeq \frac{f(x_o + \Delta x) - 2f(x_o) + f(x_o - \Delta x)}{(\Delta x)^2} \tag{3.4}$$

Any approximation of a derivative in terms of values at a discrete set of points is called *finite difference* approximation.

The approach used above in obtaining finite difference approximations is rather intuitive. A more general approach is using Taylor's series. According to the well-known expansion,

$$f(x_o + \Delta x) = f(x_o) + \Delta x f'(x_o) + \frac{1}{2!}(\Delta x)^2 f''(x_o) + \frac{1}{3!}(\Delta x)^3 f'''(x_o) + \cdots \tag{3.5}$$

and

$$f(x_o - \Delta x) = f(x_o) - \Delta x f'(x_o) + \frac{1}{2!}(\Delta x)^2 f''(x_o) - \frac{1}{3!}(\Delta x)^3 f'''(x_o) + \cdots \tag{3.6}$$

Upon adding these expansions,

$$f(x_o + \Delta x) + f(x_o - \Delta x) = 2f(x_o) + (\Delta x)^2 f''(x_o) + O(\Delta x)^4 \tag{3.7}$$

where $O(\Delta x)^4$ is the error introduced by truncating the series. We say that this error is of the order $(\Delta x)^4$ or simply $O(\Delta x)^4$. Therefore, $O(\Delta x)^4$ represents terms that are not greater than $(\Delta x)^4$. Assuming that these terms are negligible,

$$f''(x_o) \simeq \frac{f(x_o + \Delta x) - 2f(x_o) + f(x_o - \Delta x)}{(\Delta x)^2}$$

which is Eq. (3.4). Subtracting Eq. (3.6) from Eq. (3.5) and neglecting terms of the order $(\Delta x)^3$ yields

$$f'(x_o) \simeq \frac{f(x_o + \Delta x) - f(x_o - \Delta x)}{2\Delta x}$$

which is Eq. (3.3). This shows that the leading errors in Eqs. (3.3) and (3.4) are of the order $(\Delta x)^2$. Similarly, the difference formula in Eqs. (3.1) and (3.2) have truncation errors of $O(\Delta x)$. Higher order finite difference approximations can be obtained by taking more terms in Taylor series expansion. If the infinite Taylor series were retained, an exact solution would be realized for the problem. However, for practical reasons, the infinite series is usually truncated after the second-order term. This imposes an error which exists in all finite difference solutions.

To apply the difference method to find the solution of a function $\Phi(x, t)$, we divide the solution region in the $x - t$ plane into equal rectangles or meshes of sides Δx and Δt as in Fig. 3.3. We let the coordinates (x, t) of a typical grid point or node be

$$\begin{aligned} x &= i\Delta x, \qquad i = 0, 1, 2, \ldots \\ t &= j\Delta t, \qquad j = 0, 1, 2, \ldots \end{aligned} \tag{3.8a}$$

and the value of Φ at P be

$$\Phi_P = \Phi(i\Delta x, j\Delta t) = \Phi(i, j) \tag{3.8b}$$

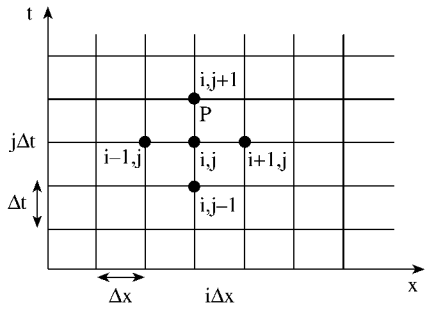

Figure 3.3
Finite difference mesh for two independent variables x and t.

With this notation, the central difference approximations of the derivatives of Φ at the (i, j)th node are

$$\Phi_x|_{i,j} \simeq \frac{\Phi(i+1, j) - \Phi(i-1, j)}{2\Delta x}, \tag{3.9a}$$

$$\Phi_t|_{i,j} \simeq \frac{\Phi(i, j+1) - \Phi(i, j-1)}{2\Delta t}, \tag{3.9b}$$

$$\Phi_{xx}|_{i,j} \simeq \frac{\Phi(i+1, j) - 2\Phi(i, j) + \Phi(i-1, j)}{(\Delta x)^2}, \tag{3.9c}$$

$$\Phi_{tt}|_{i,j} \simeq \frac{\Phi(i, j+1) - 2\Phi(i, j) + \Phi(i, j-1)}{(\Delta t)^2} \tag{3.9d}$$

Table 3.1 gives some useful finite difference approximations for Φ_x and Φ_{xx}.

3.3 Finite Differencing of Parabolic PDEs

Consider a simple example of a parabolic (or diffusion) partial differential equation with one spatial independent variable

$$k\frac{\partial \Phi}{\partial t} = \frac{\partial^2 \Phi}{\partial x^2} \tag{3.10}$$

where k is a constant. The equivalent finite difference approximation is

$$k\frac{\Phi(i, j+1) - \Phi(i, j)}{\Delta t} = \frac{\Phi(i+1, j) - 2\Phi(i, j) + \Phi(i-1, j)}{(\Delta x)^2} \tag{3.11}$$

where $x = i\Delta x, i = 0, 1, 2, \ldots, n, t = j\Delta t, j = 0, 1, 2, \ldots$. In Eq. (3.11), we have used the forward difference formula for the derivative with respect to t and

Table 3.1 Finite Difference Approximations for Φ_x and Φ_{xx}

Derivative	Finite Difference Approximation	Type	Error
Φ_x	$\frac{\Phi_{i+1}-\Phi_i}{\Delta x}$	FD	$O(\Delta x)$
	$\frac{\Phi_i-\Phi_{i-1}}{\Delta x}$	BD	$O(\Delta x)$
	$\frac{\Phi_{i+1}-\Phi_{i-1}}{\Delta x}$	CD	$O(\Delta x)^2$
	$\frac{-\Phi_{i+2}+4\Phi_{i+1}-3\Phi_i}{2\Delta x}$	FD	$O(\Delta x)^2$
	$\frac{3\Phi_i-4\Phi_{i-1}+\Phi_{i-2}}{2\Delta x}$	BD	$O(\Delta x)^2$
	$\frac{-\Phi_{i+2}+8\Phi_{i+1}-8\Phi_{i-1}+\Phi_{i-2}}{12\Delta x}$	CD	$O(\Delta x)^4$
Φ_{xx}	$\frac{\Phi_{i+2}-2\Phi_{i+1}+\Phi_i}{(\Delta x)^2}$	FD	$O(\Delta x)^2$
	$\frac{\Phi_i-2\Phi_{i-1}+\Phi_{i-2}}{(\Delta x)^2}$	BD	$O(\Delta x)^2$
	$\frac{\Phi_{i+1}-2\Phi_i+\Phi_{i-1}}{(\Delta x)^2}$	CD	$O(\Delta x)^2$
	$\frac{-\Phi_{i+2}+16\Phi_{i+1}-30\Phi_i+16\Phi_{i-1}-\Phi_{i-2}}{(\Delta x)^2}$	CD	$O(\Delta x)^4$

where FD = Forward Difference, BD = Backward Difference, and CD = Central Difference.

central difference formula for that with respect to x. If we let

$$r = \frac{\Delta t}{k(\Delta x)^2}\,, \tag{3.12}$$

Eq. (3.11) can be written as

$$\boxed{\Phi(i, j+1) = r\Phi(i+1, j) + (1-2r)\Phi(i, j) + r\Phi(i-1, j)} \tag{3.13}$$

This *explicit formula* can be used to compute $\Phi(x, t+\Delta t)$ explicitly in terms of $\Phi(x, t)$. Thus the values of Φ along the first time row (see Fig. 3.3), $t = \Delta t$, can be calculated in terms of the boundary and initial conditions, then the values of Φ along the second time row, $t = 2\Delta t$, are calculated in terms of the first time row, and so on.

A graphic way of describing the difference formula of Eq. (3.13) is through the *computational molecule* of Fig. 3.4(a), where the square is used to represent the grid point where Φ is presumed known and a circle where Φ is unknown.

In order to ensure a stable solution or reduce errors, care must be exercised in selecting the value of r in Eqs. (3.12) and (3.13). It will be shown in Section 3.6 that Eq. (3.13) is valid only if the coefficient $(1-2r)$ in Eq. (3.13) is nonnegative or $0 < r \leq 1/2$. If we choose $r = 1/2$, Eq. (3.13) becomes

$$\Phi(i, j+1) = \frac{1}{2}[\Phi(i+1, j) + \Phi(i-1, j)] \tag{3.14}$$

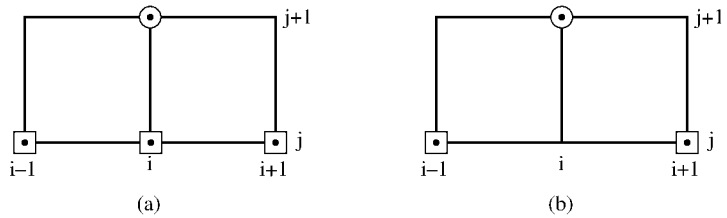

Figure 3.4
Computational molecule for parabolic PDE: (a) for $0 < r \leq 1/2$, (b) for $r = 1/2$.

so that the computational molecule becomes that shown in Fig. 3.4(b).

The fact that obtaining stable solutions depends on r or the size of the time step Δt renders the explicit formula of Eq. (3.13) inefficient. Although the formula is simple to implement, its computation is slow. An *implicit formula,* proposed by Crank and Nicholson in 1974, is valid for all finite values of r. We replace $\partial^2\Phi/\partial x^2$ in Eq. (3.10) by the average of the central difference formulas on the jth and $(j+1)$th time rows so that

$$k\frac{\Phi(i, j+1) - \Phi(i, j)}{\Delta t} = \frac{1}{2}\left[\frac{\Phi(i+1, j) - 2\Phi(i, j) + \Phi(i-1, j)}{(\Delta x)^2} + \frac{\Phi(i+1, j+1) - 2\Phi(i, j+1) + \Phi(i-1, j+1)}{(\Delta x)^2}\right]$$

This can be rewritten as

$$\begin{aligned} -r\Phi(i-1, j+1) + 2(1+r)\Phi(i, j+1) - r\Phi(i+1, j+1) \\ = r\Phi(i-1, j) + 2(1-r)\Phi(i, j) + r\Phi(i+1, j) \end{aligned} \tag{3.15}$$

where r is given by Eq. (3.12). The right side of Eq. (3.15) consists of three known values, while the left side has the three unknown values of Φ. This is illustrated in the computational molecule of Fig. 3.5(a). Thus if there are n free nodes along each time row, then for $j = 0$, applying Eq. (3.15) to nodes $i = 1, 2, \ldots, n$ results in n

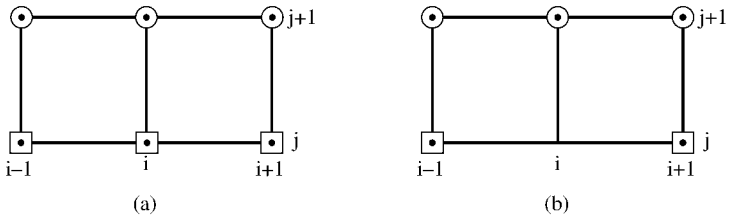

Figure 3.5
Computational molecule for Crank-Nicholson method: (a) for finite values of r, (b) for $r = 1$.

simultaneous equations with n unknown values of Φ and known initial and boundary values of Φ. Similarly, for $j = 1$, we obtain n simultaneous equations for n unknown values of Φ in terms of the known values $j = 0$, and so on. The combination of accuracy and unconditional stability allows the use of a much larger time step with Crank-Nicholson method than is possible with the explicit formula. Although the method is valid for all finite values of r, a convenient choice of $r = 1$ reduces Eq. (3.15) to

$$-\Phi(i-1, j+1) + 4\Phi(i, j+1) - \Phi(i+1, j+1) = \Phi(i-1, j) + \Phi(i+1, j) \tag{3.16}$$

with the computational molecule of Fig. 3.5(b).

More complex finite difference schemes can be developed by applying the same principles discussed above. Two of such schemes are the Leapfrog method and the Dufort-Frankel method [3, 4]. These and those discussed earlier are summarized in Table 3.2. Notice that the last two methods are two-step finite difference schemes in that finding Φ at time $j + 1$ requires knowing Φ at two previous time steps j and $j - 1$, whereas the first two methods are one-step schemes. For further treatment on the finite difference solution of parabolic PDEs, see Smith [5] and Ferziger [6].

Example 3.1

Solve the diffusion equation

$$\frac{\partial^2 \Phi}{\partial x^2} = \frac{\partial \Phi}{\partial t}, \qquad 0 \le x \le 1 \tag{3.17}$$

subject to the boundary conditions

$$\Phi(0, t) = 0 = \Phi(1, t) = 0, \qquad t > 0 \tag{3.18a}$$

and initial condition

$$\Phi(x, 0) = 100 \tag{3.18b}$$

Solution

This problem may be regarded as a mathematical model of the temperature distribution in a rod of length $L = 1$ m with its end in contacts with ice blocks (or held at 0°C) and the rod initially at 100°C. With that physical interpretation, our problem is finding the internal temperature Φ as a function of position and time. We will solve this problem using both explicit and implicit methods.

(a) Explicit Method

For easy hand calculations, let us choose $\Delta x = 0.1, r = 1/2$ so that

$$\Delta t = \frac{r(\Delta x)^2}{k} = 0.05$$

Table 3.2 Finite Difference Approximation to the Parabolic Equation:

$$\frac{\partial \Phi}{\partial t} = \frac{1}{k}\frac{\partial^2 \Phi}{\partial x^2}, \qquad k > 0$$

Method	Algorithm	Molecule
1. First order (Euler)	$\frac{\Phi_i^{j+1} - \Phi_i^j}{\Delta t} = \frac{\Phi_{i+1}^j - 2\Phi_i^j + \Phi_{i-1}^j}{k(\Delta x)^2}$ explicit, stable for $r = \Delta t / k(\Delta x)^2 \le 0.5$	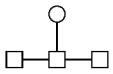
2. Crank-Nicholson	$\frac{\Phi_i^{j+1} - \Phi_i^j}{\Delta t} = \frac{\Phi_{i+1}^{j+1} - 2\Phi_i^{j+1} + \Phi_{i-1}^{j+1}}{2k(\Delta x)^2} + \frac{\Phi_{i+1}^j - 2\Phi_i^j + \Phi_{i-1}^j}{2k(\Delta x)^2}$ implicit, always stable	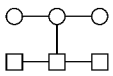
3. Leapfrog	$\frac{\Phi_i^{j+1} - \Phi_i^{j-1}}{2\Delta t} = \frac{\Phi_{i+1}^j - 2\Phi_i^j + \Phi_{i-1}^j}{k(\Delta x)^2}$ explicit, always unstable	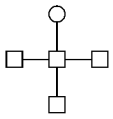
4. Dufort-Frankel	$\frac{\Phi_i^{j+1} - \Phi_i^{j-1}}{2\Delta t} = \frac{\Phi_{i+1}^j - \Phi_i^{j+1} - \Phi_i^{j-1} + \Phi_{i-1}^j}{k(\Delta x)^2}$ explicit, unconditionally stable	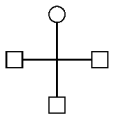

since $k = 1$. We need the solution for only $0 \le x \le 0.5$ due to the fact that the problem is symmetric with respect to $x = 0.5$. First we calculate the initial and boundary values using Eq. (3.18). These values of Φ at the fixed nodes are shown in Table 3.3 for $x = 0, x = 1$, and $t = 0$. Notice that the values of $\Phi(0, 0)$ and $\Phi(1, 0)$ are taken as the average of 0 and 100. We now calculate Φ at the free nodes using Eq. (3.14) or the molecule of Fig. 3.4(b). The result is shown in Table 3.3. The analytic solution to Eq. (3.17) subject to Eq. (3.18) is

$$\Phi(x, t) = \frac{400}{\pi}\sum_{k=0}^{\infty}\frac{1}{n}\sin n\pi x \exp\left(-n^2\pi^2 t\right), \qquad n = 2k + 1$$

Comparison of the explicit finite difference solution with the analytic solution at $x = 0.4$ is shown in Table 3.4. The table shows that the finite difference solution is

reasonably accurate. Greater accuracy can be achieved by choosing smaller values of Δx and Δt.

Table 3.3 Result for Example 3.1

x / t	0	0.1	0.2	0.3	0.4	0.5	0.6	...	1.0
0	50	100	100	100	100	100	100		50
0.005	0	75.0	100	100	100	100	100		0
0.01	0	50	87.5	100	100	100	100		0
0.015	0	43.75	75	93.75	100	100	100		0
0.02	0	37.5	68.75	87.5	96.87	100	96.87		0
0.025	0	34.37	62.5	82.81	93.75	96.87	93.75		0
0.03	0	31.25	58.59	78.21	89.84	93.75	89.84		0
⋮									
0.1	0	14.66	27.92	38.39	45.18	47.44	45.18		0

Table 3.4 Comparison of Explicit Finite Difference Solution with Analytic Solution; for Example 3.1

t	Finite difference solution at $x = 0.4$	Analytic solution at $x = 0.4$	Percentage error
0.005	100	99.99	0.01
0.01	100	99.53	0.47
0.015	100	97.85	2.2
0.02	96.87	95.18	1.8
0.025	93.75	91.91	2.0
0.03	89.84	88.32	1.7
0.035	85.94	84.61	1.6
0.04	82.03	80.88	1.4
⋮			
0.10	45.18	45.13	0.11

(b) Implicit Method

Let us choose $\Delta x = 0.2, r = 1$ so that $\Delta t = 0.04$. The values of Φ at the fixed nodes are calculated as in part (a) (see Table 3.3). For the free nodes, we apply Eq. (3.16) or the molecule of Fig. 3.5(b). If we denote $\Phi(i, j+1)$ by $\Phi_i (i = 1, 2, 3, 4)$, the values of Φ for the first time step (Fig. 3.6) can be obtained by solving the following simultaneous equations

$$
\begin{aligned}
-0 + 4\Phi_1 - \Phi_2 &= 50 + 100 \\
-\Phi_1 + 4\Phi_2 + \Phi_3 &= 100 + 100 \\
-\Phi_2 + 4\Phi_3 - \Phi_4 &= 100 + 100 \\
-\Phi_3 + 4\Phi_4 - 0 &= 100 + 50
\end{aligned}
$$

We obtain

$$\Phi_1 = 58.13, \qquad \Phi_2 = 82.54, \qquad \Phi_3 = 72, \qquad \Phi_4 = 55.5$$

at $t = 0.04$. Using these values of Φ, we apply Eq. (3.16) to obtain another set of simultaneous equations for $t = 0.08$ as

$$\begin{aligned} -0 + 4\Phi_1 - \Phi_2 &= 0 + 82.54 \\ -\Phi_1 + 4\Phi_2 - \Phi_3 &= 58.13 + 72 \\ -\Phi_2 + 4\Phi_3 - \Phi_4 &= 82.54 + 55.5 \\ -\Phi_3 + 4\Phi_4 - 0 &= 72 + 0 \end{aligned}$$

which results in

$$\Phi_1 = 34.44, \qquad \Phi_2 = 55.23, \qquad \Phi_3 = 56.33, \qquad \Phi_4 = 32.08$$

This procedure can be programmed and accuracy can be increased by choosing more points for each time step. ∎

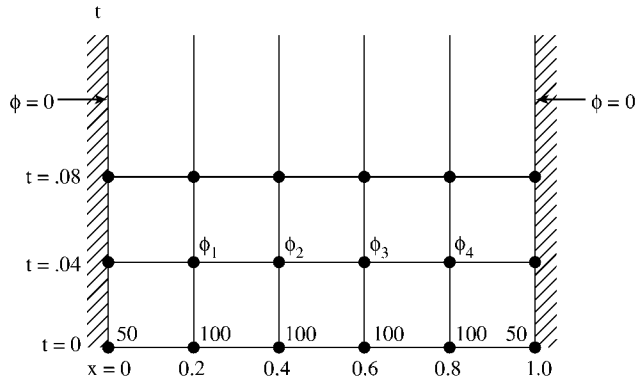

Figure 3.6
For Example 3.1, part (b).

3.4 Finite Differencing of Hyperbolic PDEs

The simplest hyperbolic partial differential equation is the wave equation of the form

$$u^2 \frac{\partial^2 \Phi}{\partial x^2} = \frac{\partial^2 \Phi}{\partial t^2} \tag{3.19}$$

where u is the speed of the wave. An equivalent finite difference formula is

$$u^2 \frac{\Phi(i+1, j) - 2\Phi(i, j) + \Phi(i-1, j)}{(\Delta x)^2} = \frac{\Phi(i, j+1) - 2\Phi(i, j) + \Phi(i, j-1)}{(\Delta t)^2}$$

where $x = i\Delta x, t = j\Delta t, i, j = 0, 1, 2, \ldots$. This equation can be written as

$$\boxed{\Phi(i, j+1) = 2(1-r)\Phi(i, j) + r[\Phi(i+1, j) + \Phi(i-1, j)] - \Phi(i, j-1)} \tag{3.20}$$

where $\Phi(i, j)$ is an approximation to $\Phi(x, t)$ and r is the "aspect ratio" given by

$$r = \left(\frac{u\Delta t}{\Delta x}\right)^2 \tag{3.21}$$

Equation (3.20) is an explicit formula for the wave equation. The corresponding computational molecule is shown in Fig. 3.7(a). For the solution algorithm in Eq. (3.20)

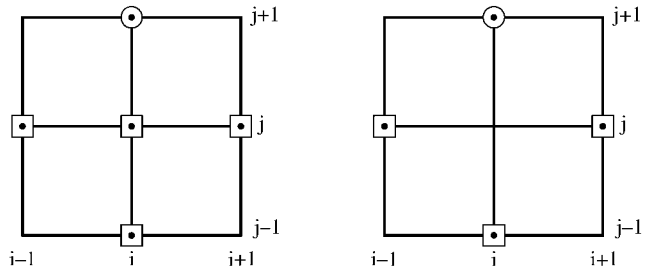

Figure 3.7
Computational molecule for wave equation: (a) for arbitrary $r \leq 1$, (b) for $r = 1$.

to be stable, the aspect ratio $r \leq 1$, as will be shown in Example 3.5. If we choose $r = 1$, Eq. (3.20) becomes

$$\Phi(i, j+1) = \Phi(i+1, j) + \Phi(i-1, j) - \Phi(i, j-1) \tag{3.22}$$

with the computational molecule in Fig. 3.7(b). Unlike the single-step schemes of Eqs. (3.13) and (3.15), the two-step schemes of Eqs. (3.20) and (3.22) require that the values of Φ at times j and $j-1$ be known to get Φ at time $j+1$. Thus, we must derive a separate algorithm to "start" the solution of Eq. (3.20) or (3.22); that is, we must compute $\Phi(i, 1)$ and $\Phi(i, 2)$. To do this, we utilize the prescribed initial condition. For example, suppose the initial condition on the PDE in Eq. (3.19) is

$$\left.\frac{\partial \Phi}{\partial t}\right|_{t=0} = 0$$

We use the backward-difference formula

$$\frac{\partial \Phi(x,0)}{\partial t} \simeq \frac{\Phi(i,1) - \Phi(i,-1)}{2\Delta t} = 0$$

or

$$\Phi(i,1) = \Phi(i,-1) \tag{3.23}$$

Substituting Eq. (3.23) into Eq. (3.20) and taking $j = 0$ (i.e., at $t = 0$), we get

$$\Phi(i,1) = 2(1-r)\Phi(i,0) + r[\Phi(i-1,0) + \Phi(i+1,0)] - \Phi(i,1)$$

or

$$\Phi(i,1) = (1-r)\Phi(i,0) + \frac{r}{2}[\Phi(i-1,0) + \Phi(i+1,0)] \tag{3.24}$$

Using the starting formula in Eq. (3.24) together with the prescribed boundary and initial conditions, the value of Φ at any grid point (i, j) can be obtained directly from Eq. (3.20).

There are implicit methods for solving hyperbolic PDEs just as we have implicit methods for parabolic PDEs. However, for hyperbolic PDEs, implicit methods result in an infinite number of simultaneous equations to be solved and therefore cannot be used without making some simplifying assumptions. Interested readers are referred to Smith [5] or Ferziger [6].

Example 3.2

Solve the wave equation

$$\Phi_{tt} = \Phi_{xx}, \qquad 0 < x < 1, \quad t \geq 0$$

subject to the boundary conditions

$$\Phi(0,t) = 0 = \Phi(1,t), \qquad t \geq 0$$

and the initial conditions

$$\Phi(x,0) = \sin \pi x, \qquad 0 < x < 1,$$
$$\Phi_t(x,0) = 0, \qquad 0 < x < 1 \quad \square$$

Solution

The analytical solution is easily obtained as

$$\Phi(x,t) = \sin \pi x \cos \pi t \tag{3.25}$$

Using the explicit finite difference scheme of Eq. (3.20) with $r = 1$, we obtain

$$\Phi(i, j+1) = \Phi(i-1, j) + \Phi(i+1, j) - \Phi(i, j-1), \quad j \geq 1 \tag{3.26}$$

For $j = 0$, substituting

$$\Phi_t = \frac{\Phi(i, 1) - \Phi(i, -1)}{2\Delta t} = 0$$

or

$$\Phi(i, 1) = \Phi(i, -1)$$

into Eq. (3.26) gives the starting formula

$$\Phi(i, 1) = \frac{1}{2}[\Phi(i - 1, 0) + \Phi(i + 1, 0)] \tag{3.27}$$

Since $u = 1$, and $r = 1$, $\Delta t = \Delta x$. Also, since the problem is symmetric with respect to $x = 0.5$, we solve for Φ using Eqs. (3.26) and (3.27) within $0 < x < 0.5, t \geq 0$. We can either calculate the values by hand or write a simple computer program. With the FORTRAN code in Fig. 3.8, the result shown in Table 3.5 is obtained for $\Delta t = \Delta x = 0.1$. The finite difference solution agrees with the exact solution in Eq. (3.25) to six decimal places. The accuracy of the FD solution can be increased by choosing a smaller spatial increment Δx and a smaller time increment Δt. ∎

Table 3.5 Solution of the Wave Equation in Example 3.2

x	0	0.1	0.2	0.3	0.4	0.5	0.6	...
t								
0.0	0	0.3090	0.5879	0.8990	0.9511	1.0	0.9511	
0.1	0	0.2939	0.5590	0.7694	0.9045	0.9511	0.9045	
0.2	0	0.2500	0.4755	0.6545	0.7694	0.8090	0.7694	
0.3	0	0.1816	0.3455	0.4755	0.5590	0.5878	0.5590	
0.4	0	0.0955	0.1816	0.2500	0.2939	0.3090	0.2939	
0.5	0	0	0	0	0	0	0	
0.6	0	-0.0955	-0.1816	-0.2500	-0.2939	-0.3090	-0.2939	
0.7	0	-0.1816	-0.3455	-0.4755	-0.5590	-0.5878	-0.5590	
⋮	⋮	⋮	⋮	⋮	⋮	⋮	⋮	

3.5 Finite Differencing of Elliptic PDEs

A typical elliptic PDE is Poisson's equation, which in two dimensions is given by

$$\nabla^2\Phi = \frac{\partial^2\Phi}{\partial x^2} + \frac{\partial^2\Phi}{\partial y^2} = g(x, y) \tag{3.28}$$

```
0001
0002    C ***************************************************
0003    C  FORTRAN CODE FOR EXAMPLE 3.2
0004    C  ON ONE-DIMENSIONAL WAVE EQUATION
0005    C  SOLVED USING AN EXPLICIT FINITE DIFFERENCE SCHEME
0006    C ***************************************************
0007
0008          DIMENSION PHI(0:50,0:200), PHIEX(0:50,0:200)
0009          DATA  PIE/3.141592654/
0010    C   SET SPATIAL AND TIME INCREMENTS
0011          DX = 0.1
0012          DT = 0.1
0013    C   INITIALIZE - THIS ALSO TAKES CARE OF BOUNDARY CONDITIONS
0014          DO 10 I = 0,10
0015          DO 10 J = 0,20
0016          PHI(I,J) = 0.0
0017    10    CONTINUE
0018    C   INSERT THE INITIAL CONDITIONS
0019          DO 20 I = 0,10
0020          X = DX*FLOAT(I)
0021          PHI(I,0) = SIN(PIE*X)
0022    20    CONTINUE
0023        DO 30 I=1,9
0024          PHI(I,1) = ( PHI(I-1,0) + PHI(I+1,0) )/2.0
0025    30    CONTINUE
0026    C     NOW APPLY THE EXPLICIT FD SCHEME
0027          DO 40 J = 1,10
0028          DO 40 I = 1,9
0029            PHI(I,J+1) = PHI(I-1,J) + PHI(I+1,J) - PHI(I,J-1)
0030    40    CONTINUE
0031    C   CALCULATE EXACT RESULT
0032          DO 50 J = 0,10
0033          T = DT*FLOAT(J)
0034          CT = COS(PIE*T)
0035          DO 50 I=0,10
0036          X = DX*FLOAT(I)
0037          PHIEX(I,J) = SIN(PIE*X)*CT
0038    50    CONTINUE
0039    C   OUTPUT THE FD APPROXIMATE AND EXACT RESULTS
0040          DO 70 J = 0,7
0041          DO 70 I = 0,7
0042          WRITE(6,60) J,I,PHI(I,J),PHIEX(I,J)
0043    60    FORMAT(3X,'J=',I3,3X,'I=',I3,3X,2(F14.10,3X),/)
0044    70    CONTINUE
0045        STOP
0046      END
```

Figure 3.8
FORTRAN code for Example 3.2.

We can use the central difference approximation for the partial derivatives of which the simplest forms are

$$\frac{\partial^2 \Phi}{\partial x^2} = \frac{\Phi(i+1, j) - 2\Phi(i, j) + \Phi(i-1, j)}{(\Delta x)^2} + O(\Delta x)^2 \tag{3.29a}$$

$$\frac{\partial^2 \Phi}{\partial y^2} = \frac{\Phi(i, j+1) - 2\Phi(i, j) + \Phi(i, j-1)}{(\Delta y)^2} + O(\Delta y)^2 \tag{3.29b}$$

where $x = i\Delta x$, $y = j\Delta y$, and $i, j = 0, 1, 2, \ldots$. If we assume that $\Delta x = \Delta y = h$, to simplify calculations, substituting Eq. (3.29) into Eq. (3.28) gives

$$\Big[\Phi(i+1, j) + \Phi(i-1, j) + \Phi(i, j+1) + \Phi(i, j-1)\Big] - 4\Phi(i, j) = h^2 g(i, j)$$

or

$$\boxed{\Phi(i, j) = \frac{1}{4}\Big[\Phi(i+1, j) + \Phi(i-1, j) + \Phi(i, j+1) + \Phi(i, j-1) - h^2 g(i, j)\Big]} \tag{3.30}$$

at every point (i, j) in the mesh for Poisson's equation. The spatial increment h is called the *mesh size*. A special case of Eq. (3.28) is when the source term vanishes, i.e., $g(x, y) = 0$. This leads to Laplace's equation. Thus for Laplace's equation, Eq. (3.30) becomes

$$\boxed{\Phi(i, j) = \frac{1}{4}[\Phi(i+1, j) + \Phi(i-1, j) + \Phi(i, j+1) + \Phi(i, j-1)]} \tag{3.31}$$

It is worth noting that Eq. (3.31) states that the value of Φ for each point is the average of those at the four surrounding points. The five-point computational molecule for the difference scheme in Eq. (3.31) is illustrated in Fig. 3.9(a) where values of the coefficients are shown. This is a convenient way of displaying finite difference algorithms

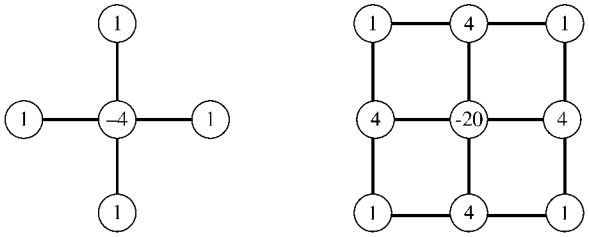

Figure 3.9
Computational molecules for Laplace's equation based on: (a) second order approximation, (b) fourth order approximation.

for elliptic PDEs. The molecule in Fig. 3.9(a) is the second order approximation of Laplace's equation. This is obviously not the only way to approximate Laplace's equation, but it is the most popular choice. An alternative fourth order difference is

$$\begin{aligned} -20\Phi(i, j) + 4[&\Phi(i+1, j) + \Phi(i-1, j) + \Phi(i, j+1) + \Phi(i, j-1)] \\ &+ \Phi(i+1, j-1) + \Phi(i-1, j-1) + \Phi(i-1, j+1) \\ &+ \Phi(i+1, j+1) = 0 \end{aligned} \tag{3.32}$$

The corresponding computational molecule is shown in Fig. 3.9(b).

The application of the finite difference method to elliptic PDEs often leads to a large system of algebraic equations, and their solution is a major problem in itself. Two commonly used methods of solving the system of equations are band matrix and iterative methods.

3.5.1 Band Matrix Method

From Eqs. (3.30) to (3.32), we notice that only nearest neighboring nodes affect the value of Φ at each node. Hence application of any of Eqs. (3.30) to (3.32) to all free nodes in the solution region results in a set of simultaneous equations of the form

$$[A][X] = [B] \tag{3.33}$$

where $[A]$ is a *sparse* matrix (it has many zero elements), $[X]$ is a column matrix consisting of the unknown values of Φ at the free nodes, and $[B]$ is a column matrix containing the known values of Φ at fixed nodes. Matrix $[A]$ is also banded in that its nonzero terms appear clustered near the main diagonal. Matrix $[X]$, containing the unknown elements, can be obtained from

$$[X] = [A]^{-1}[B] \tag{3.34}$$

or by solving Eq. (3.33) using the Gauss elimination discussed in Appendix D.1.

3.5.2 Iterative Methods

The iterative methods are generally used to solve a large system of simultaneous equations. An iterative method for solving equations is one in which a first approximation is used to calculate a second approximation, which in turn is used to calculate the third approximation, and so on. The three common iterative methods (Jacobi, Gauss-Seidel, and successive over-relaxation (SOR)) are discussed in Appendix D.2. We will apply only SOR here.

To apply the method of SOR to Eq. (3.30), for example, we first define the *residual* $R(i, j)$ at node (i, j) as the amount by which the value of $\Phi(i, j)$ does not satisfy Eq. (3.30), i.e.,

$$\begin{aligned} R(i, j) = {} & \Phi(i+1, j) + \Phi(i-1, j) + \Phi(i, j+1) \\ & + \Phi(i, j-1) - 4\Phi(i, j) - h^2 g(i, j) \end{aligned} \tag{3.35}$$

The value of the residual at kth iteration, denoted by $R^k(i, j)$, may be regarded as a correction which must be added to $\Phi(i, j)$ to make it nearer to the correct value. As convergence to the correct value is approached, $R^k(i, j)$ tends to zero. Hence to improve the rate of convergence, we multiply the residual by a number ω and add that to $\Phi(i, j)$ at the kth iteration to get $\Phi(i, j)$ at $(k+1)$th iteration. Thus

$$\Phi^{k+1}(i, j) = \Phi^k(i, j) + \frac{\omega}{4} R^k(i, j)$$

or

$$\Phi^{k+1}(i, j) = \Phi^k(i, j) + \frac{\omega}{4}\Big[\Phi^k(i+1, j) + \Phi^{k+1}(i-1, j) + \Phi^{k+1}(i, j-1) + \Phi^k(i, j+1) - 4\Phi^k(i, j) - h^2 g(i, j)\Big] \tag{3.36}$$

The parameter ω is called the *relaxation factor* while the technique is known as the method of *successive over-relaxation* (SOR). The value of ω lies between 1 and 2. (When $\omega = 1$, the method is simply called successive relaxation.) Its optimum value ω_{opt} must be found by trial-and-error. In order to start Eq. (3.36), an initial guess, $\Phi^0(i, j)$, is made at every free node. Typically, we may choose $\Phi^0(i, j) = 0$ or the average of Φ at the fixed nodes.

Example 3.3

Solve Laplace's equation

$$\nabla^2 V = 0, \qquad 0 \le x, y \le 1$$

with $V(x, 1) = 45x(1 - x)$, $V(x, 0) = 0 = V(0, y) = V(1, y)$. □

Solution

Let $h = 1/3$ so that the solution region is as in Fig. 3.10. Applying Eq. (3.31) to each

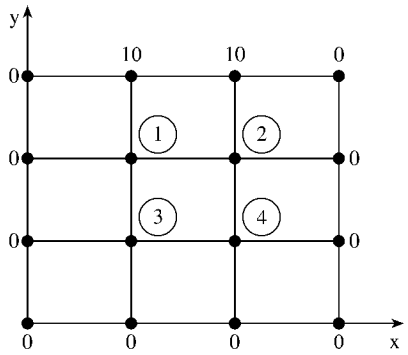

Figure 3.10
Finite difference grid for Example 3.3.

of the four points leads to

$$\begin{aligned} 4V_1 - V_2 - V_3 - 0 &= 10 \\ -V_1 + 4V_2 - 0 - V_4 &= 10 \\ -V_1 - 0 + 4V_3 - V_4 &= 0 \\ -0 - V_2 - V_3 + 4V_4 &= 0 \end{aligned}$$

This can be written as

$$\begin{bmatrix} 4 & -1 & -1 & 0 \\ -1 & 4 & 0 & -1 \\ -1 & 0 & 4 & -1 \\ 0 & -1 & -1 & 4 \end{bmatrix} \begin{bmatrix} V_1 \\ V_2 \\ V_3 \\ V_4 \end{bmatrix} = \begin{bmatrix} 10 \\ 10 \\ 0 \\ 0 \end{bmatrix}$$

or

$$[A][V] = [B]$$

where $[A]$ is the band matrix, $[V]$ is the column matrix containing the unknown potentials at the free nodes, and $[B]$ is the column matrix of potentials at the fixed nodes. Solving the equations either by matrix inversion or by Gauss elimination, we obtain

$$V_1 = 3.75, \qquad V_2 = 3.75, \qquad V_3 = 1.25, \qquad V_4 = 1.25 \quad \blacksquare$$

Example 3.4

Solve Poisson's equation

$$\nabla^2 V = -\frac{\rho_S}{\epsilon}, \qquad 0 \le x, y \le 1$$

and obtain the potential at the grid points shown in Fig. 3.11. Assume $\rho_S = x(y-1)$ nC/m^2 and $\epsilon_r = 1.0$. Use the method of successive over-relaxation. □

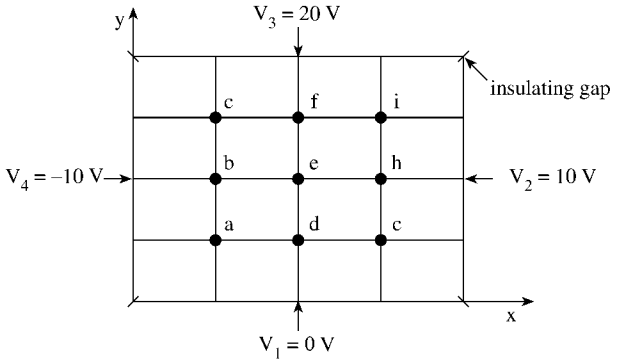

Figure 3.11
Solution region for the problem in Example 3.4.

Solution

This problem has an exact analytical solution and is deliberately chosen so that we can verify the numerical results with exact ones, and we can also see how a problem

with a complicated analytical solution is easily solved using finite difference method. For the exact solution, we use the superposition theorem and let

$$V = V_1 + V_2$$

where V_1 is the solution to Laplace's equation $\nabla^2 V_1 = 0$ with the inhomogeneous boundary conditions shown in Fig. 3.11 and V_2 is the solution to Poisson's equation $\nabla^2 V_2 = g = -\rho_S/\epsilon$ subject to homogeneous boundary conditions. From Example 2.1, it is evident that

$$V_1 = V_I + V_{II} + V_{III} + V_{IV}$$

where V_I to V_{IV} are defined by Eqs. (2.53) to (2.56). V_2 can be obtained by the series expansion method of Section 2.7. From example 2.12,

$$V_2 = \sum_{m=1}^{\infty}\sum_{n=1}^{\infty} A_{mn} \sin\frac{m\pi x}{a} \sin\frac{n\pi y}{b}$$

where

$$\begin{aligned} A_{mn} &= \int_0^a \int_0^b g(x, y) \sin\frac{m\pi x}{a} \sin\frac{n\pi y}{b}\, dx\, dy \\ &= \frac{\left[1.0 - \frac{1}{b}[1 - (-1)^n]\right]}{[(m\pi/a)^2 + (n\pi/b)^2]} \cdot \frac{(-1)^{m+n} 144ab}{mn\pi}, \end{aligned}$$

$a = b = 1$, and $g(x, y) = -x(y-1) \cdot 10^{-9}/\epsilon_o$.

For the finite difference solution, it can be shown that in a rectangular region, the optimum over-relaxation factor is given by the smaller root of the quadratic equation [10]

$$t^2\omega^2 - 16\omega + 16 = 0$$

where $t = \cos(\pi/N_x) + \cos(\pi/N_y)$ and N_x and N_y are the number of intervals along x and y axes, respectively. Hence

$$\omega = \frac{8 - \sqrt{64 - 16t^2}}{t^2}$$

We try three cases of $N_x = N_y = 4$, 12 and 20 so that $\Delta x = \Delta y = h = 1/4$, $1/12$, and $1/20$, respectively. Also we set

$$g(x, y) = -\frac{\rho_S}{\epsilon} = -\frac{x(y-1) \cdot 10^{-9}}{10^{-9}/36\pi} = -36\pi x(y-1)$$

Figure 3.12 presents the FORTRAN code for the solution of this problem. The potentials at the free nodes for the different cases of h are shown in Table 3.6. Notice that as the mesh size h reduces, the solution becomes more accurate, but it takes more iterations for the same tolerance. ∎

```
0001    C*******************************************************
0002    C   FINITE DIFFERENCE SOLUTION OF POISSON'S EQUATION
0003    C   Vxx + Vyy = G
0004    C   USING THE METHOD OF SUCCESSIVE OVER-RELAXATION
0005    C
0006    C   NX      :  NO. OF INTERVALS ALONG X-AXIS
0007    C   NY      :  NO. OF INTERVALS ALONG Y-AXIS
0008    C   A X B   :  DIMENSION OF THE SOLUTION REGION
0009    C   V(I,J)  :  POTENTIAL AT GRID POINT (X,Y) = H*(I,J)
0010    C              WHERE I = 0,1,...,NX, J = 0,1,....,NY
0011    C   H       :  MESH SIZE
0012    C *******************************************************
0013
0014            DIMENSION  V(0:20,0:20)
0015            DATA PIE/3.14159/
0016            DATA A,B/1.0,1.0/
0017            DATA V1,V2,V3,V4/0.0,10.0,20.0,-10.0/
0018
0019    C   SPECIFY BOUNDARY VALUES AND NECESSARY PARAMETERS
0020            NX= 4
0021            NY= 4
0022            H = A/FLOAT(NX)
0023    C   SET INITIAL GUESS EQUAL TO ZEROS OR TO AVERAGE OF
0024    C   FIXED VALUES
0025            DO 10 I=1,NX-1
0026            DO 10 J=1,NY-1
0027            V(I,J)=(V1 + V2 + V3 + V4)/4.0
0028    10      CONTINUE
0029    C   SET POTENTIALS AT FIXED NODES
0030            DO 20 I = 1, NX-1
0031            V(I,0)=V1
0032            V(I,NY)=V3
0033    20      CONTINUE
0034            DO 30 J=1,NY-1
0035            V(0,J)=V4
0036            V(NX,J)=V2
0037    30      CONTINUE
0038            V(0,0)=(V1 + V4)/2.0
0039            V(NX,0)=(V1 + V2)/2.0
0040            V(0,NY)=(V3 + V4)/2.0
0041            V(NX,NY)=(V2 + V3)/2.0
0042    C   FIND THE OPTIMUM OVER-RELAXATION FACTOR
0043            T = COS(PIE/NX) + COS(PIE/NY)
0044            W = ( 8.0 - SQRT(64.0 - 16.0*T*T))/(T*T)
0045            WRITE(6,40) W
0046    40      FORMAT(2X,'SOR FACTOR OMEGA=',F10.6)
0047            W4 = W/4.0
0048    C   ITERATION BEGINS
0049            NCOUNT = 0
0050    50      RMIN = 0.0
0051            DO 70 I =1,NX-1
0052            X = H*FLOAT(I)
0053            DO 70 J = 1,NY-1
0054            Y = H*FLOAT(J)
0055            G = -36.0*PIE*X*(Y - 1.0)
0056            R = W4*( V(I+1,J) + V(I-1,J) + V(I,J+1) + V(I,J-1)
0057           1      -4.0*V(I,J) - G*H*H  )
0058            RMIN = RMIN + ABS(R)
0059            V(I,J) =  V(I,J) + R
0060    70      CONTINUE
```

Figure 3.12
FORTRAN code for Example 3.4 ***(Continued).***

```
0061          RMIN = RMIN/FLOAT(NX*NY)
0062           IF(RMIN.GE.0.0001) THEN
0063    C   SOLUTION HAS CONVERGED
0064          NCOUNT = NCOUNT + 1
0065          IF(NCOUNT.LT.100) THEN
0066          GO TO 50
0067          ELSE
0068          WRITE(6,80)
0069    80  FORMAT(2X,'SOLUTION DOES NOT CONVERGE IN 100 ITERATIONS')
0070          GO TO 100
0071          ENDIF
0072        ENDIF
0073    C   SOLUTION HAS CONVERGED
0074        WRITE(6,90) NCOUNT
0075    90  FORMAT(2X,'SOLUTION CONVERGES IN',2X,I3,2X,'ITERATIONS',/)
0076    100  CONTINUE
0077    C   OUTPUT THE FINITE DIFFERENCE APPROX. RESULTS
0078        DO 120 I = 1,NX-1
0079        DO 120 J = 1,NY-1
0080        WRITE(6,110) I,J,V(I,J)
0081    110 FORMAT(2X,'I=',I3,2X,'J=',I3,2X,'V =',E12.6,/)
0082    120 CONTINUE
0083    C  ------------------------------------------------------------
0084    C   CALCULATE THE EXACT SOLUTION
0085    C
0086    C   POISSON'S EQUATION WITH HOMOGENEOUS BOUNDARY CONDITIONS
0087    C   SOLVED BY SERIES EXPANSION
0088    C
0089          DO 150 I =1,NX-1
0090          X = H*FLOAT(I)
0091          DO 150 J = 1,NY-1
0092          Y = H*FLOAT(J)
0093          SUM = 0.0
0094          DO 130 M = 1,10    ! TAKE ONLY 10 TERMS OF THE SERIES
0095          FM = FLOAT(M)
0096          DO 130 N = 1,10
0097          FN = FLOAT(N)
0098          FACTOR1 = (FM*PIE/A)**2  +  (FN*PIE/B)**2
0099          FACTOR2 = ( (-1.0)**(M+N) )*144.0*A*B/(PIE*FM*FN)
0100          FACTOR3 = 1.0 - (1.0 - (-1.0)**N)/B
0101          FACTOR = FACTOR2*FACTOR3/FACTOR1
0102          SUM = SUM + FACTOR*SIN(FM*PIE*X/A)*SIN(FN*PIE*Y/B)
0103    130     CONTINUE
0104          VH = SUM
0105    C
0106    C   LAPLACE'S EQUATION WITH INHOMOGENEOUS BOUNDARY CONDITIONS
0107    C   SOLVED USING THE METHOD OF SEPARATION OF VARIABLES
0108    C
0109          C1=4.0*V1/PIE
0110          C2=4.0*V2/PIE
0111          C3=4.0*V3/PIE
0112          C4=4.0*V4/PIE
0113          SUM=0.0
0114          DO 140 K =1,10  ! TAKE ONLY 10 TERMS OF THE SERIES
0115            N=2*K-1
0116            AN=FLOAT(N)
0117            A1=SIN(AN*PIE*X/B)
0118            A2=SINH(AN*PIE*(A-Y)/B)
0119            A3=AN*SINH(AN*PIE*A/B)
0120            TERM1=C1*A1*A2/A3
```

Figure 3.12

(Cont.)* FORTRAN code for Example 3.4 *(Continued).

```
0121              B1=SINH(AN*PIE*X/A)
0122              B2=SIN(AN*PIE*Y/A)
0123              B3=AN*SINH(AN*PIE*B/A)
0124              TERM2=C2*B1*B2/B3
0125              D1=SIN(AN*PIE*X/B)
0126              D2=SINH(AN*PIE*Y/B)
0127              D3=AN*SINH(AN*PIE*A/B)
0128              TERM3=C3*D1*D2/D3
0129              E1=SINH(AN*PIE*(B-X)/A)
0130              E2=SIN(AN*PIE*Y/A)
0131              E3=AN*SINH(AN*PIE*B/A)
0132              TERM4=C4*E1*E2/E3
0133              TERM = TERM1 + TERM2 + TERM3 + TERM4
0134              SUM=SUM + TERM
0135     140      CONTINUE
0136              VI = SUM
0137              V(I,J) = VH + VI
0138     150      CONTINUE
0139     C
0140     C   OUTPUT EXACT RESULTS
0141     C
0142              DO 160 I = 1,NX-1
0143              DO 160 J = 1,NY-1
0144              WRITE(6,110) I,J,V(I,J)
0145     160      CONTINUE
0146              STOP
0147              END
```

Figure 3.12
***(Cont.)* FORTRAN code for Example 3.4.**

Table 3.6 Successive Over-relaxation Solution of Example 3.4

Node	$h = 1/4$ $\omega_{opt} = 1.171$ 8 iterations	$h = 1/2$ $\omega_{opt} = 1.729$ 26 iterations	$h = 1/20$ $\omega_{opt} = 1.729$ 43 iterations	Exact Solution
a	−3.247	−3.409	−3.424	−3.429
b	−1.703	−1.982	−2.012	−2.029
c	4.305	4.279	4.277	4.277
d	−0.0393	−0.0961	−0.1087	−0.1182
e	3.012	2.928	2.921	2.913
f	9.368	9.556	9.578	9.593
g	3.044	2.921	2.909	2.902
h	6.111	6.072	6.069	6.065
i	11.04	11.12	11.23	11.13

3.6 Accuracy and Stability of FD Solutions

The question of accuracy and stability of numerical methods is extremely important if our solution is to be reliable and useful. Accuracy has to do with the closeness of the approximate solution to exact solutions (assuming they exist). Stability is the

requirement that the scheme does not increase the magnitude of the solution with increase in time.

There are three sources of errors that are nearly unavoidable in numerical solution of physical problems [8]:

- modeling errors,
- truncation (or discretization) errors, and
- roundoff errors.

Each of these error types will affect accuracy and therefore degrade the solution.

The modeling errors are due to several assumptions made in arriving at the mathematical model. For example, a nonlinear system may be represented by a linear PDE. Truncation errors arise from the fact that in numerical analysis, we can deal only with a finite number of terms from processes which are usually described by infinite series. For example, in deriving finite difference schemes, some higher-order terms in the Taylor series expansion were neglected, thereby introducing truncation error. Truncation errors may be reduced by using finer meshes, that is, by reducing the mesh size h and time increment Δt. Alternatively, truncation errors may be reduced by using a large number of terms in the series expansion of derivatives, that is, by using higher-order approximations. However, care must be exercised in applying higher-order approximations. Instability may result if we apply a difference equation of an order higher than the PDE being examined. These higher-order difference equations may introduce "spurious solutions."

Roundoff errors reflect the fact that computations can be done only with a finite precision on a computer. This unavoidable source of errors is due to the limited size of registers in the arithmetic unit of the computer. Roundoff errors can be minimized by the use of double-precision arithmetic. The only way to avoid roundoff errors completely it to code all operations using integer arithmetic. This is hardly possible in most practical situations.

Although it has been noted that reducing the mesh size h will increase accuracy, it is not possible to indefinitely reduce h. Decreasing the truncation error by using a finer mesh may result in increasing the roundoff error due to the increased number of arithmetic operations. A point is reached where the minimum total error occurs for any particular algorithm using any given word length [9]. This is illustrated in Fig. 3.13. The concern about accuracy leads us to question whether the finite difference solution can grow unbounded, a property termed the instability of the difference scheme. A numerical algorithm is said to be stable if a small error at any stage produces a smaller cumulative error. It is unstable otherwise. The consequence of instability (producing unbonded solution) is disastrous. To determine whether a finite difference scheme is stable, we define an error, ϵ^n, which occurs at time step n, assuming that there is one independent variable. We define the amplification of this error at time step $n+1$ as

$$\epsilon^{n+1} = g\epsilon^n \tag{3.37}$$

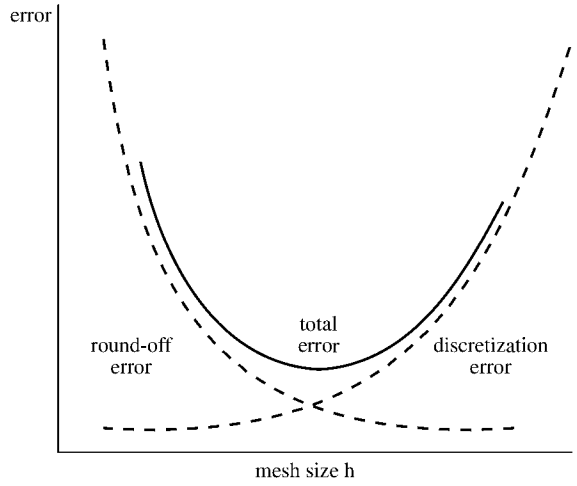

Figure 3.13
Error as a function of the mesh size.

where g is known as the *amplification factor.* In more complex situations, we have two or more independent variables, and Eq. (3.37) becomes

$$[\epsilon]^{n+1} = [G][\epsilon]^n \tag{3.38}$$

where $[G]$ is the amplification matrix. For the stability of the difference scheme, it is required that Eq. (3.37) satisfy

$$\left|\epsilon^{n+1}\right| \leq \left|\epsilon^n\right|$$

or

$$|g| \leq 1 \tag{3.39a}$$

For the case in Eq. (3.38),

$$\|G\| \leq 1 \tag{3.39b}$$

One useful and simple method of finding a stability criterion for a difference scheme is to construct a Fourier analysis of the difference equation and thereby derive the amplification factor. We illustrate this technique, known as *von Neumann's method* [4, 5, 7, 10], by considering the explicit scheme of Eq. (3.13):

$$\Phi_i^{n+1} = (1 - 2r)\Phi_i^n + r\left(\Phi_{i+1}^n + \Phi_{i-1}^n\right) \tag{3.40}$$

where $r = \Delta t/k(\Delta x)^2$. We have changed our usual notation so that we can use $j = \sqrt{-1}$ in the Fourier series. Let the solution be

$$\Phi_i^n = \sum A_n(t)e^{jkix}, \qquad 0 \leq x \leq 1 \tag{3.41a}$$

where k is the wave number. Since the differential equation (3.10) approximated by Eq. (3.13) is linear, we need consider only a Fourier mode, i.e.,

$$\Phi_i^n = A(t)e^{jkix} \tag{3.41b}$$

Substituting Eq. (3.41b) into Eq. (3.40) gives

$$A^{n+1}e^{jkix} = (1-2r)A^n e^{jkix} + r\left(e^{jkx} + e^{-jkx}\right)A^n e^{jkix}$$

or

$$A^{n+1} = A^n[1 - 2r + 2\cos kx] \tag{3.42}$$

Hence the amplification factor is

$$\begin{aligned} g &= \frac{A^{n+1}}{A^n} = 1 - 2r + 2\cos kx \\ &= 1 - 4r\sin^2\frac{kx}{2} \end{aligned} \tag{3.43}$$

In order to satisfy Eq. (3.39a),

$$\left|1 - 4r\sin^2\frac{kx}{2}\right| \leq 1$$

Since this condition must hold for every wave number k, we take the maximum value of the sine function so that

$$1 - 4r \geq -1 \qquad \text{and} \qquad r \geq 0$$

or

$$r \geq \frac{1}{2} \qquad \text{and} \qquad r \geq 0$$

Of course, $r = 0$ implies $\Delta t = 0$, which is impractical. Thus

$$0 < r \leq \frac{1}{2} \tag{3.44}$$

Example 3.5

For the finite difference scheme of Eq. (3.20), use the von Neumann approach to determine the stability condition. □

Solution

We assume a trial solution of the form

$$\Phi_i^n = A^n e^{jkix}$$

Substituting this into Eq. (3.20) results in

$$A^{n+1}e^{jkix} = 2(1-r)A^n e^{jkix} + r\left(e^{jkx} + e^{-jkx}\right)A^n e^{jkix} - A^{n-1}e^{jkix}$$

or

$$A^{n+1} = A^n\left[2(1-r) + 2r\cos kx\right] - A^{n-1} \tag{3.45}$$

In terms of $g = A^{n+1}/A^n$, Eq. (3.45) becomes

$$g^2 - 2pg + 1 = 0 \tag{3.46}$$

where $p = 1 - 2r\sin^2\frac{kx}{2}$. The quadratic equation (3.46) has solutions

$$g_1 = p + \left[p^2 - 1\right]^{1/2}, \qquad g_2 = p - \left[p^2 - 1\right]^{1/2}$$

For $|gj| \leq 1$, where $i = 1, 2$, p must lie between 1 and -1, i.e., $-1 \leq p \leq 1$ or

$$-1 \leq 1 - 2r\sin^2\frac{kx}{2} \leq 1$$

which implies that $r \leq 1$ or $u\Delta t \leq \Delta x$ for stability. This idea can be extended to show that the stability condition for two-dimensional wave equation is $u\Delta t/h < \dfrac{1}{\sqrt{2}}$, where $h = \Delta x = \Delta y$. ∎

3.7 Practical Applications I — Guided Structures

The finite difference method has been applied successfully to solve many EM-related problems. Besides those simple examples we have considered earlier in this chapter, the method has been applied to diverse problems [11] including:

- Transmission-line problems [12]–[21],
- Waveguides [21]–[26],
- Microwave circuit [27]–[30],
- EM penetration and scattering problems [31, 32],
- EM pulse (EMP) problems [33],
- EM exploration of minerals [34], and
- EM energy deposition in human bodies [35, 36].

It is practically impossible to cover all those applications within the limited scope of this text. In this section, we consider the relatively easier problems of transmission lines and waveguides while the problems of penetration and scattering of EM waves will be treated in the next section. Other applications utilize basically similar techniques.

3.7.1 Transmission Lines

The finite difference techniques are suited for computing the characteristic impedance, phase velocity, and attenuation of several transmission lines—polygonal lines, shielded strip lines, coupled strip lines, microstrip lines, coaxial lines, and rectangular lines [12]–[19]. The knowledge of the basic parameters of these lines is of paramount importance in the design of microwave circuits.

For concreteness, consider the microstrip line shown in Fig. 3.14(a). The geometry in Fig. 3.14(a) is deliberately selected to be able to illustrate how one accounts for discrete inhomogeneities (i.e., homogeneous media separated by interfaces) and lines of symmetry using a finite difference technique. The techniques presented are equally applicable to other lines. Assuming that the mode is TEM, having components of neither **E** nor **H** fields in the direction of propagation, the fields obey Laplace's equation over the line cross section. The TEM mode assumption provides good approximations if the line dimensions are much smaller than half a wavelength, which means that the operating frequency is far below cutoff frequency for all higher order modes [16]. Also owing to biaxial symmetry about the two axes only one quarter of the cross section need to be considered as shown in Fig. 3.14(b).

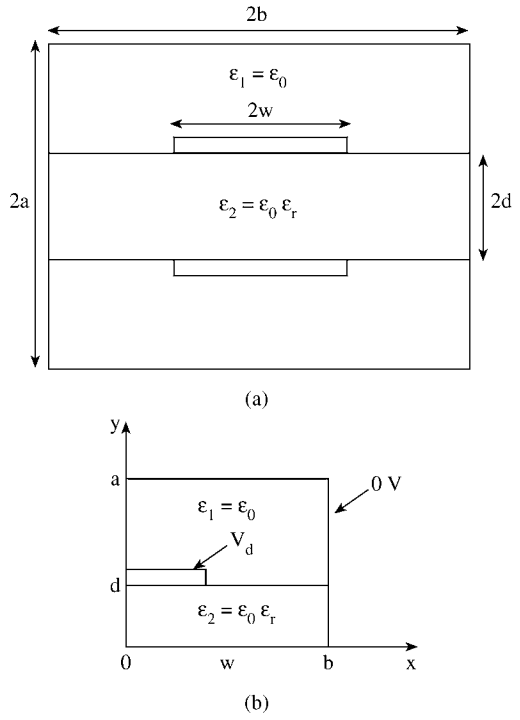

Figure 3.14

(a) Shielded double strip line with partial dielectric support; (b) problem in (a) simplified by making full use of symmetry.

The finite difference approximation of Laplace's equation, $\nabla^2 V = 0$, has been derived in Eq. (3.31), namely,

$$V(i, j) = \frac{1}{4}[V(i+1, j) + V(i-1, j) + V(i, j+1) + V(i, j-1)] \tag{3.47}$$

For the sake of conciseness, let us denote

$$\begin{aligned} V_o &= V(i, j) \\ V_1 &= V(i, j+1) \\ V_2 &= V(i-1, j) \\ V_3 &= V(i, j-1) \\ V_4 &= V(i+1, j) \end{aligned} \tag{3.48}$$

so that Eq. (3.47) becomes

$$\boxed{V_o = \frac{1}{4}[V_1 + V_2 + V_3 + V_4]} \tag{3.49}$$

with the computation molecule shown in Fig. 3.15. Equation (3.49) is the general formula to be applied to all free nodes in the free space and dielectric region of Fig. 3.14(b).

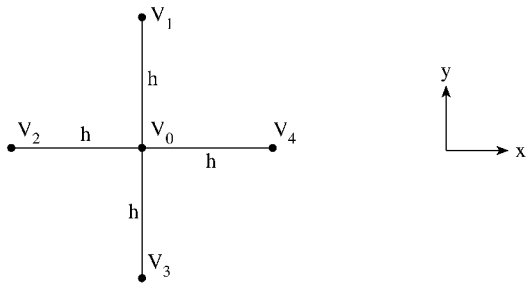

Figure 3.15
Computation molecule for Laplace's equation.

On the dielectric boundary, the boundary condition,

$$D_{1n} = D_{2n}\ , \tag{3.50}$$

must be imposed. We recall that this condition is based on Gauss's law for the electric field, i.e.,

$$\oint_\ell \mathbf{D} \cdot d\mathbf{l} = \oint_\ell \epsilon \mathbf{E} \cdot d\mathbf{l} = Q_{\text{enc}} = 0 \tag{3.51}$$

since no free charge is deliberately placed on the dielectric boundary. Substituting $\mathbf{E} = -\nabla V$ in Eq. (3.51) gives

$$0 = \oint_\ell \epsilon \nabla V \cdot d\mathbf{l} = \oint_\ell \epsilon \frac{\partial V}{\partial n}\, dl \tag{3.52}$$

where $\partial V/\partial n$ denotes the derivative of V normal to the contour ℓ. Applying Eq. (3.52) to the interface in Fig. 3.16 yields

$$\begin{aligned} 0 = \epsilon_1 \frac{(V_1 - V_0)}{h} h + \epsilon_1 \frac{(V_2 - V_0)}{h} \frac{h}{2} + \epsilon_2 \frac{(V_2 - V_0)}{h} \frac{h}{2} \\ + \epsilon_2 \frac{(V_3 - V_0)}{h} h + \epsilon_2 \frac{(V_4 - V_0)}{h} \frac{h}{2} + \epsilon_1 \frac{(V_4 - V_0)}{h} \frac{h}{2} \end{aligned}$$

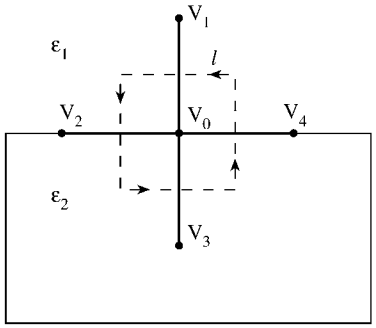

Figure 3.16
Interface between media of dielectric permittivities ϵ_1 and ϵ_2.

Rearranging the terms,

$$2(\epsilon_1 + \epsilon_2) V_0 = \epsilon_1 V_1 + \epsilon_2 V_3 + \frac{(\epsilon_1 + \epsilon_2)}{2} (V_2 + V_4)$$

or

$$\boxed{V_0 = \frac{\epsilon_1}{2(\epsilon_1 + \epsilon_2)} V_1 + \frac{\epsilon_2}{2(\epsilon_1 + \epsilon_2)} V_3 + \frac{1}{4} V_2 + \frac{1}{4} V_4} \tag{3.53}$$

This is the finite difference equivalent of the boundary condition in Eq. (3.50). Notice that the discrete inhomogeneity does not affect points 2 and 4 on the boundary but affects points 1 and 3 in proportion to their corresponding permittivities. Also note that when $\epsilon_1 = \epsilon_2$, Eq. (3.53) reduces to Eq. (3.49).

On the line of symmetry, we impose the condition

$$\frac{\partial V}{\partial n} = 0 \tag{3.54}$$

This implies that on the line of symmetry along the y-axis, ($x = 0$ or $i = 0$) $\dfrac{\partial V}{\partial x} = (V_4 - V_2)/h = 0$ or $V_2 = V_4$ so that Eq. (3.49) becomes

$$\boxed{V_o = \frac{1}{4}[V_1 + V_3 + 2V_4]} \tag{3.55a}$$

or

$$V(0, j) = \frac{1}{4}[V(0, j+1) + V(0, j-1) + 2V(1, j)] \tag{3.55b}$$

On the line of symmetry along the x-axis ($y = 0$ or $j = 0$), $\dfrac{\partial V}{\partial y} = (V_1 - V_3)/h = 0$ or $V_3 = V_1$ so that

$$\boxed{V_o = \frac{1}{4}[2V_1 + V_2 + V_4]} \tag{3.56a}$$

or

$$V(i, 0) = \frac{1}{4}[2V(i, 1) + V(i-1, 0) + V(i+1, 0)] \tag{3.56b}$$

The computation molecules for Eqs. (3.55) and (3.56) are displayed in Fig. 3.17.

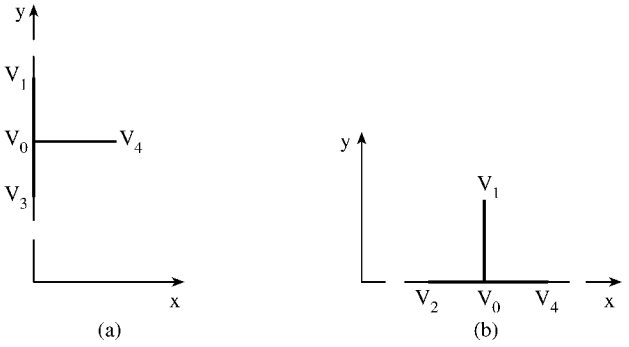

Figure 3.17
Computation molecule used for satisfying symmetry conditions: (a) $\partial V/\partial x = 0$, (b) $\partial V/\partial y = 0$.

By setting the potential at the fixed nodes equal to their prescribed values and applying Eqs. (3.49), (3.53), (3.55), and (3.56) to the free nodes according to the band matrix or iterative methods discussed in Section 3.5, the potential at the free nodes can be determined. Once this is accomplished, the quantities of interest can be calculated.

The characteristic impedance Z_o and phase velocity u of the line are defined as

$$Z_o = \sqrt{\frac{L}{C}} \tag{3.57a}$$

$$u = \frac{1}{\sqrt{LC}} \tag{3.57b}$$

where L and C are the inductance and capacitance per unit length, respectively. If the dielectric medium is nonmagnetic ($\mu = \mu_o$), the characteristic impedance Z_{oo} and phase velocity u_o with the dielectric removed (i.e., the line is air-filled) are given by

$$Z_{oo} = \sqrt{\frac{L}{C_o}} \tag{3.58a}$$

$$u_o = \frac{1}{\sqrt{LC_o}} \tag{3.58b}$$

where C_o is the capacitance per unit length without the dielectric. Combining Eqs. (3.57) and (3.58) yields

$$Z_o = \frac{1}{u_o\sqrt{CC_o}} = \frac{1}{uC} \tag{3.59a}$$

$$u = u_o\sqrt{\frac{C_o}{C}} = \frac{u_o}{\sqrt{\epsilon_{\text{eff}}}} \tag{3.59b}$$

$$\epsilon_{\text{eff}} = \frac{C}{C_o} \tag{3.59c}$$

where $u_o = c = 3 \times 10^8$ m/s, the speed of light in free space, and ϵ_{eff} is the effective dielectric constant. Thus to find Z_o and u for an inhomogeneous medium requires calculating the capacitance per unit length of the structure, with and without the dielectric substrate.

If V_d is the potential difference between the inner and the outer conductors,

$$C = \frac{4Q}{V_d}\,, \tag{3.60}$$

so that the problem is reduced to finding the charge per unit length Q. (The factor 4 is needed since we are working on only one quarter of the cross section.) To find Q, we apply Gauss's law to a closed path ℓ enclosing the inner conductor. We may select ℓ as the rectangular path between two adjacent rectangles as shown in Fig. 3.18.

$$\begin{aligned} Q &= \oint_\ell \mathbf{D}\cdot d\mathbf{l} = \oint_\ell \epsilon \frac{\partial V}{\partial n}\, d\ell \\ &= \epsilon\left(\frac{V_P - V_N}{\Delta x}\right)\Delta y + \epsilon\left(\frac{V_M - V_L}{\Delta x}\right)\Delta y + \epsilon\left(\frac{V_H - V_L}{\Delta y}\right)\Delta x \\ &\quad + \epsilon\left(\frac{V_G - V_K}{\Delta y}\right)\Delta x + \cdots \end{aligned} \tag{3.61}$$

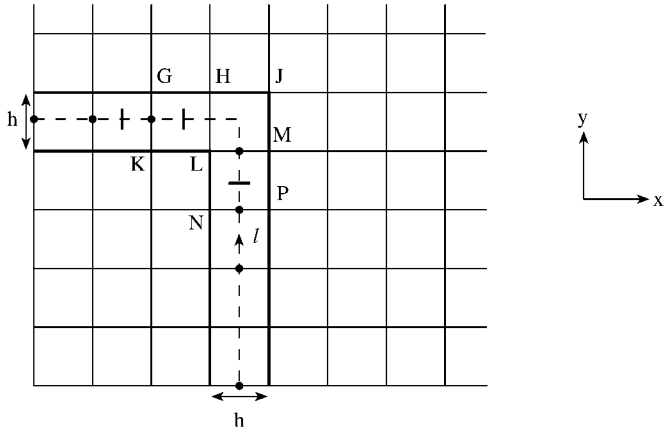

Figure 3.18
The rectangular path ℓ used in calculating charge enclosed.

Since $\Delta x = \Delta y = h$,

$$Q = (\epsilon V_P + \epsilon V_M + \epsilon V_H + \epsilon V_G + \cdots) - (\epsilon V_N + 2\epsilon V_L + \epsilon V_K + \cdots)$$

or

$$\begin{aligned} Q = \epsilon_o \Big[&\sum \epsilon_{ri} V_i \quad \text{for nodes } i \text{ on outer rectangle GHJMP} \\ &\text{with corners (such as J) not counted} \Big] \\ - \epsilon_o \Big[&\sum \epsilon_{ri} V_i \quad \text{for nodes } i \text{ on inner rectangle KLN} \\ &\text{with corners (such as L) counted twice} \Big] , \end{aligned} \tag{3.62}$$

where V_i and ϵ_{ri} are the potential and dielectric constant at the ith node. If i is on the dielectric interface, $\epsilon_{ri} = (\epsilon_{r1} + \epsilon_{r2})/2$. Also if i is on the line of symmetry, we use $V_i/2$ instead of V_i to avoid including V_i twice in Eq. (3.60), where factor 4 is applied. We also find

$$C_o = 4Q_o/V_d \tag{3.63}$$

where Q_o is obtained by removing the dielectric, finding V_i at the free nodes and then using Eq. (3.62) with $\epsilon_{r1} = 1$ at all nodes. Once Q and Q_o are calculated, we obtain C and C_o from Eqs. (3.60) and (3.63) and Z_o and u from Eq. (3.59).

An outline of the procedure is given below:

(1) Calculate V (with the dielectric space replaced by free space) using Eqs. (3.49), (3.53), (3.55), and (3.56).

(2) Determine Q using Eq. (3.62).

(3) Find $C_o = \dfrac{4Q}{V_d}$.

(4) Repeat steps (1) and (2) (with the dielectric space) and find $C = \dfrac{4Q}{V_d}$.

(5) Finally, calculate $Z_o = \dfrac{1}{c\sqrt{CC_o}}$, $c = 3 \times 10^8$ m/s

The attenuation of the line can be calculated by following similar procedure outlined in [14, 20, 21]. The procedure for handling boundaries at infinity and that for boundary singularities in finite difference analysis are discussed in [37, 38].

3.7.2 Waveguides

The solution of waveguide problems is well suited for finite difference schemes because the solution region is closed. This amounts to solving the Helmholtz or wave equation

$$\nabla^2\Phi + k^2\Phi = 0 \tag{3.64}$$

where $\Phi = E_z$ for TM modes or $\Phi = H_z$ for TE modes, while k is the wave number given by

$$k^2 = \omega^2\mu\epsilon - \beta^2 \tag{3.65}$$

The permittivity ϵ of the dielectric medium can be real for a lossless medium or complex for a lossy medium. We consider all fields to vary with time and axial distance as $\exp j(\omega t - \beta z)$. In the eigenvalue problem of Eq. (3.64), both k and Φ are to be determined. The cutoff wavelength is $\lambda_c = 2\pi/k_c$. For each value of the cutoff wave number k_c, there is a solution for the eigenfunction Φ_i, which represents the field configuration of a propagating mode.

To apply the finite difference method, we discretize the cross section of the waveguide by a suitable square mesh. Applying Eq. (3.29) to Eq. (3.64) gives

$$\boxed{\Phi(i+1, j) + \Phi(i-1, j) + \Phi(i, j+1) + \Phi(i, j-1) - (4 - h^2k^2)\Phi(i, j) = 0} \tag{3.66}$$

where $\Delta x = \Delta y = h$ is the mesh size. Equation (3.66) applies to all the free or interior nodes. At the boundary points, we apply Dirichlet condition ($\Phi = 0$) for the TM modes and Neumann condition ($\partial\Phi/\partial n = 0$) for the TE modes. This implies that at point A in Fig. 3.19, for example,

$$\Phi_A = 0 \tag{3.67}$$

for TM modes. At point A, $\partial\Phi/\partial n = 0$ implies that $\Phi_D = \Phi_E$ so that Eq. (3.64) becomes

$$\Phi_B + \Phi_C + 2\Phi_D - (4 - h^2k^2)\Phi_A = 0 \tag{3.68}$$

for TE modes. By applying Eq. (3.66) and either Eq. (3.67) or (3.68) to all mesh points in the waveguide cross section, we obtain m simultaneous equations involving the m unknowns $(\Phi_1, \Phi_2, \ldots, \Phi_m)$. These simultaneous equations may be conveniently

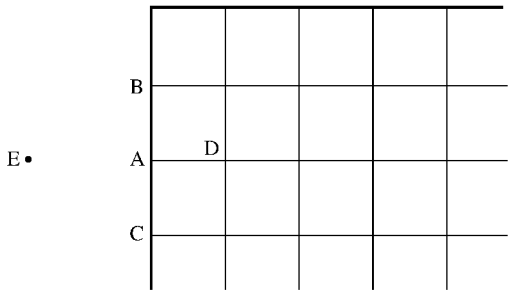

Figure 3.19
Finite difference mesh for a waveguide.

cast into the matrix equation

$$(A - \lambda I)\Phi = 0 \tag{3.69a}$$

or

$$A\Phi = \lambda\Phi \tag{3.69b}$$

where A is an $m \times m$ band matrix of known integer elements, I is an identity matrix, $\Phi = (\Phi_1, \Phi_2, \ldots, \Phi_m)$ is the eigenvector, and

$$\lambda = (kh)^2 = \left(\frac{2\pi h}{\lambda_c}\right)^2 \tag{3.70}$$

is the eigenvalue. There are several ways of determining λ and the corresponding Φ. We consider two of these options.

The first option is the *direct method.* Equation (3.69) can be satisfied only if the determinant of $(A - \lambda I)$ vanishes, i.e.,

$$|A - \lambda I| = 0 \tag{3.71}$$

This results in a polynomial in λ, which can be solved [39] for the various eigenvalues λ. For each λ, we obtain the corresponding Φ from Eq. (3.66). This method requires storing the relevant matrix elements and does not take advantage of the fact that matrix A is sparse. In favor of the method is the fact that a computer subroutine usually exists (see [40] or Appendix D.4) that solves the eingenvalue problem in Eq. (3.71) and that determines all the eigenvalues of the matrix. These eigenvalues give the dominant and higher modes of the waveguide, although accuracy deteriorates rapidly with mode number.

The second option is the *iterative method.* In this case, the matrix elements are usually generated rather than stored. We begin with $\Phi_1 = \Phi_2 = \cdots = \Phi_m = 1$ and a guessed value for k. The field Φ_{ij}^{k+1} at the (i, j)th node in the $(k+1)$th iteration is obtained from its known value in the kth iteration using

$$\Phi^{k+1}(i, j) = \Phi^k(i, j) + \frac{\omega R_{ij}}{(4 - h^2k^2)} \tag{3.72}$$

where ω is the acceleration factor, $1 < \omega < 2$, and R_{ij} is the residual at the (i, j)th node given by

$$\begin{aligned} R_{ij} = {} & \Phi(i, j+1) + \Phi(i, j-1) + \Phi(i+1, j) \\ & + \Phi(i-1, j) - \left(4 - h^2k^2\right) \Phi(i, j) \end{aligned} \tag{3.73}$$

After three or four scans of the complete mesh using Eq. (3.73), the value of $\lambda = h^2k^2$ should be updated using Raleigh formula

$$k^2 = \frac{-\int_S \Phi \nabla^2 \Phi \, dS}{\int_S \Phi^2 \, dS} \tag{3.74}$$

The finite difference equivalent of Eq. (3.74) is

$$k^2 = \frac{-\sum_{i=1} \sum_{j=1} \Phi(i,j)[\Phi(i+1,j)+\Phi(i-1,j)+\Phi(i,j+1)+\Phi(i,j-1)-4\Phi(i,j)]}{h^2 \sum_{i=1} \sum_{j=1} \Phi^2(i,j)} \tag{3.75}$$

where Φs are the latest field values after three or four scans of the mesh and the summation is carried out over all points in the mesh. The new value of k obtained from Eq. (3.75) is now used in applying Eq. (3.72) over the mesh for another three or four times to give more accurate field values, which are again substituted into Eq. (3.75) to update k. This process is continued until the difference between consecutive values of k is within a specified acceptable tolerance.

If the first option is to be applied, matrix A must first be found. To obtain matrix A is not easy. Assuming TM modes, one way of calculating A is to number the free nodes from left to right, bottom to top, starting from the left-hand corner as shown typically in Fig. 3.20. If there are n_x and n_y divisions along the x and y directions, the number of free nodes is

$$n_f = (n_x - 1)\left(n_y - 1\right) \tag{3.76}$$

Each free node must be assigned two sets of numbers, one to correspond to m in Φ_m and the other to correspond to (i, j) in $\Phi(i, j)$. An array $NL(i, j) = m$, $i = 1, 2, \ldots, n_x - 1$, $j = 1, 2, \ldots, n_y - 1$ is easily developed to relate the two numbering schemes. To determine the value of element A_{mn}, we search $NL(i, j)$ to find (i_m, j_m) and (i_n, j_n), which are the values of (i, j) corresponding to nodes m

and n, respectively. With these ideas, we obtain

$$A_{mn} = \begin{cases} 4, & m = n \\ -1, & i_m = i_n, \quad j_m = j_n + 1 \\ -1, & i_m = i_n, \quad j_m = j_n - 1 \\ -1, & i_m = i_n + 1, \quad j_m = j_n \\ -1, & i_m = i_n - 1, \quad j_m = j_n \\ 0, & \text{otherwise} \end{cases} \tag{3.77}$$

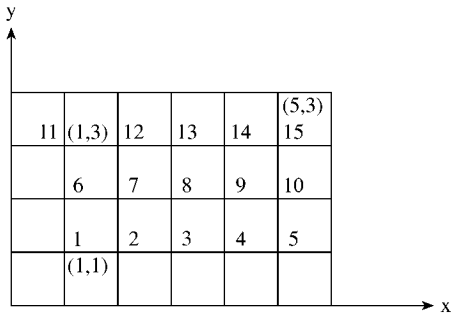

Figure 3.20
Relating node numbering schemes for $n_x = 6, n_y = 4$.

Example 3.6
Calculate Z_o for the microstrip transmission line in Fig. 3.14 with

$$a = b = 2.5 \text{ cm}, \quad d = 0.5 \text{ cm}, \quad \omega = 1 \text{ cm}$$
$$t = 0.001 \text{ cm}, \quad \epsilon_1 = \epsilon_o, \quad \epsilon_2 = 2.35\epsilon_o \quad \square$$

Solution
This problem is representative of the various types of problems that can be solved using the concepts developed in Section 3.7.1. The computer program in Fig. 3.21 was developed based on the five-step procedure outlined above. By specifying the step size h and the number of iterations, the program first sets the potential at all nodes equal to zero. The potential on the outer conductor is set equal to zero, while that on the inner conductor is set to 100 volts so that $V_d = 100$. The program finds C_o when the dielectric slab is removed and C when the slab is in place and finally determines Z_o. For a selected h, the number of iterations must be large enough and greater than the number of divisions along x or y direction. Table 3.7 shows some typical results. ∎

```
0001    C*********************************************************
0002    C USING THE FINITE DIFFERENCE METHOD
0003    C THIS PROGRAM CALCULATES THE CHARACTERISTIC IMPEDANCE
0004    C OF A MICROSTRIP LINE
0005    C*********************************************************
0006
0007      DIMENSION V(-1:200,-1:200), SV(2),Q(2)
0008      DATA A,B,D,W/2.5,2.5,0.5,1.0/ ! line data
0009      DATA ER,E0,U/2.35,8.81E-12,3.0E+8/
0010
0011           H = 0.025
0012           NT = 1000  ! NO. OF ITERATIONS
0013           NX = A/H
0014           NY = B/H
0015           ND = D/H
0016           NW = W/H
0017           VD = 100.0
0018    C
0019    C CALCULATE CHARGE WITH AND WITHOUT DIELECTRIC
0020    C
0021           ERR = 1.0
0022           DO 90 L=1,2
0023           E1 = E0
0024           E2 = E0*ERR
0025    C
0026    C  INITIALIZATION
0027    C
0028           DO 10 I=0,NX
0029           DO 10 J=0,NY
0030           V(I,J) = 0.0
0031    10     CONTINUE
0032    C
0033    C  SET POTENTIAL ON INNER CONDUCTOR (FIXED NODES) EQUAL
           TO VD
0034    C
0035            DO 20 I=0,NW
0036            V(I,ND) = VD
0037    20      CONTINUE
0038    C
0039    C  CALCULATE POTENTIAL AT FREE NODES
0040    C
0041            P1 = E1/(2.0*(E1 + E2))
0042            P2 = E2/(2.0*(E1 + E2))
0043            DO 50 K=1,NT
0044            DO 40 I=0,NX-1
0045            DO 40 J=0,NX-1
0046            IF( (J.EQ.ND).AND.(I.LE.NW) ) GO TO 40
0047            IF(J.EQ.ND) THEN
0048    C IMPOSE BOUNDARY CONDITION AT THE INTERFACE
0049            V(I,J) = 0.25*(V(I+1,J) + V(I-1,J)) +
0050         1           P1*V(I,J+1) + P2*V(I,J-1)
0051            GO TO 40
0052            ENDIF
0053            IF(I.EQ.0) THEN
0054    C IMPOSE SYMMETRY CONDITION ALONG Y-AXIS
0055            V(I,J) = (2.0*V(I+1,J) + V(I,J+1) + V(I,J-1) )/4.0
0056            GO TO 40
0057            ENDIF
0058            IF(J.EQ.0) THEN
0059    C IMPOSE SYMMETRY CONDITION ALONG X-AXIS
0060            V(I,J) = (V(I+1,J) + V(I-1,J) + 2.0*V(I,J+1) )/4.0
```

Figure 3.21

Computer program for Example 3.6 ***(Continued).***

```
0061            GO TO 40
0062            ENDIF
0063    30      V(I,J) =(V(I+1,J)+V(I-1,J)+V(I,J+1)+V(I,J-1))/4.0
0064    40      CONTINUE
0065    50      CONTINUE
0066    C
0067    C  NOW, CALCULATE THE TOTAL CHARGE ENCLOSED IN A
0068    C  RECTANGULAR PATH SURROUNDING THE INNER CONDUCTOR
0069    C
0070            IOUT = (NX + NW)/2
0071            JOUT = (NY + ND)/2
0072    C SUM POTENTIAL ON INNER AND OUTER LOOPS
0073            DO 80 K=1,2
0074            SUM = 0.0
0075            DO 60 I=1,IOUT-1
0076            SUM = SUM + E1*V(I,JOUT)
0077    60      CONTINUE
0078            SUM = SUM + E1*V(0,JOUT)/2.0 ! SYMMETRY POINT
0079            DO 70 J=1,JOUT-1
0080            IF(J.LT.ND) SUM = SUM + E2*V(IOUT,J)
0081            IF(J.EQ.ND) SUM = SUM + (E1+E2)*V(IOUT,J)/2.0
0082            IF(J.GT.ND) SUM = SUM + E1*V(IOUT,J)
0083    70      CONTINUE
0084            SUM = SUM + E2*V(IOUT,0)/2.0 ! SYMMETRY POINT
0085            IF(K.EQ.1) SV(1) = SUM
0086            IOUT = IOUT -1  ! FOR INNER LOOP
0087            JOUT = JOUT -1
0088    80      CONTINUE
0089            SUM = SUM + 2.0*E1*V(IOUT,JOUT) ! CORNER POINT
0090            SV(2) = SUM
0091            Q(L) = ABS( SV(1) - SV(2) )
0092            ERR = ER
0093    90      CONTINUE
0094    C
0095    C  FINALLY, CALCULATE Zo
0096    C
0097            C0 = 4.0*Q(1)/VD
0098            C1 = 4.0*Q(2)/VD
0099            Z0 = 1.0/( U*SQRT(C0*C1) )
0100            WRITE(6,*) H,NT,Z0
0101            PRINT *,H,NT,Z0
0102            STOP
0103            END
```

Figure 3.21
(Cont.) **Computer program for Example 3.6.**

3.8 Practical Applications II — Wave Scattering (FDTD)

The finite-difference time-domain (FDTD) formulation of EM field problems is a convenient tool for solving scattering problems. The FDTD method, first introduced by Yee [42] in 1966 and later developed by Taflove and others [31, 32, 35], [43]–[46], is a direct solution of Maxwell's time-dependent curl equations. The scheme treats the irradiation of the scatterer as an initial value problem. Our discussion on the FD-TD method will cover:

- Yee's finite difference algorithm,
- accuracy and stability,

Table 3.7 Characteristic Impedance of a Microstrip Line for Example 3.6

h	Number of iterations	Z_o
0.25	700	49.05
0.1	500	57.85
0.05	500	65.82
0.05	700	63.10
0.05	1000	61.53
Other method [41]: $Z_o = 62.50$		

- absorbing boundary conditions,
- initial fields, and
- programming aspects.

Some model examples with FORTRAN codes will be provided to illustrate the method.

3.8.1 Yee's Finite Difference Algorithm

In an isotropic medium, Maxwell's equations can be written as

$$\nabla \times \mathbf{E} = -\mu \frac{\partial \mathbf{H}}{\partial t} \tag{3.78a}$$

$$\nabla \times \mathbf{H} = \sigma \mathbf{E} + \epsilon \frac{\partial \mathbf{E}}{\partial t} \tag{3.78b}$$

The vector Eq. (3.78) represents a system of six scalar equations, which can be expressed in rectangular coordinate system as:

$$\frac{\partial H_x}{\partial t} = \frac{1}{\mu}\left(\frac{\partial E_y}{\partial z} - \frac{\partial E_z}{\partial y}\right), \tag{3.79a}$$

$$\frac{\partial H_y}{\partial t} = \frac{1}{\mu}\left(\frac{\partial E_z}{\partial x} - \frac{\partial E_x}{\partial z}\right), \tag{3.79b}$$

$$\frac{\partial H_z}{\partial t} = \frac{1}{\mu}\left(\frac{\partial E_x}{\partial y} - \frac{\partial E_y}{\partial x}\right), \tag{3.79c}$$

$$\frac{\partial E_x}{\partial t} = \frac{1}{\epsilon}\left(\frac{\partial H_z}{\partial y} - \frac{\partial H_y}{\partial z} - \sigma E_x\right), \tag{3.79d}$$

$$\frac{\partial E_y}{\partial t} = \frac{1}{\epsilon}\left(\frac{\partial H_x}{\partial z} - \frac{\partial H_z}{\partial x} - \sigma E_y\right), \tag{3.79e}$$

$$\frac{\partial E_z}{\partial t} = \frac{1}{\epsilon}\left(\frac{\partial H_y}{\partial x} - \frac{\partial H_x}{\partial y} - \sigma E_z\right) \tag{3.79f}$$

Following Yee's notation, we define a grid point in the solution region as

$$(i, j, k) \equiv (i\Delta x, j\Delta y, k\Delta z) \tag{3.80}$$

and any function of space and time as

$$F^n(i, j, k) \equiv F(i\delta, j\delta, k\delta, n\Delta t) \tag{3.81}$$

where $\delta = \Delta x = \Delta y = \Delta z$ is the space increment, Δt is the time increment, while i, j, k, and n are integers. Using central finite difference approximation for space and time derivatives that are second-order accurate,

$$\frac{\partial F^n(i, j, k)}{\partial x} = \frac{F^n(i + 1/2, j, k) - F^n(i - 1/2, j, k)}{\delta} + O\left(\delta^2\right) \tag{3.82}$$

$$\frac{\partial F^n(i, j, k)}{\partial t} = \frac{F^{n+1/2}(i, j, k) - F^{n-1/2}(i, j, k)}{\Delta t} + O\left(\Delta t^2\right) \tag{3.83}$$

In applying Eq. (3.82) to all the space derivatives in Eq. (3.79), Yee positions the components of **E** and **H** about a unit cell of the lattice as shown in Fig. 3.22. To

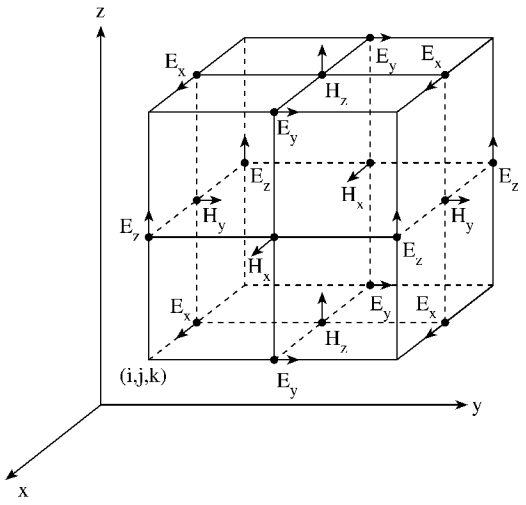

Figure 3.22
Positions of the field components in a unit cell of the Yee's lattice.

incorporate Eq. (3.83), the components of **E** and **H** are evaluated at alternate half-time steps. Thus we obtain the explicit finite difference approximation of Eq. (3.79) as:

$$
\begin{aligned}
H_x^{n+1/2}\ (i,\, j+1/2,\, k+1/2) &= H_x^{n-1/2}(i,\, j+1/2,\, k+1/2) \\
&+ \frac{\delta t}{\mu(i,\, j+1/2,\, k+1/2)\delta}\Big[E_y^n(i,\, j+1/2,\, k+1) \\
&- E_y^n(i,\, j+1/2,\, k) \\
&+ E_z^n(i,\, j,\, k+1/2) - E_z^n(i,\, j+1,\, k+1/2)\Big],
\end{aligned}
\tag{3.84a}
$$

$$
\begin{aligned}
H_y^{n+1/2}\ (i+1/2,\, j,\, k+1/2) &= H_y^{n-1/2}(i+1/2,\, j,\, k+1/2) \\
&+ \frac{\delta t}{\mu(i+1/2,\, j,\, k+1/2)\delta}\Big[E_z^n(i+1,\, j,\, k+1/2) \\
&- E_z^n(i,\, j,\, k+1/2) \\
&+ E_x^n(i+1/2,\, j,\, k) - E_x^n(i+1/2,\, j,\, k+1)\Big],
\end{aligned}
\tag{3.84b}
$$

$$
\begin{aligned}
H_z^{n+1/2}\ (i+1/2,\, j+1/2,\, k) &= H_z^{n-1/2}(i+1/2,\, j+1/2,\, k) \\
&+ \frac{\delta t}{\mu(i+1/2,\, j+1/2,\, k)\delta}\left[E_x^n(i+1/2,\, j+1,\, k)\right. \\
&- E_x^n(i+1/2,\, j,\, k) \\
&\left.+\ E_y^n(i,\, j+1/2,\, k) - E_y^n(i+1,\, j+1/2,\, k\right],
\end{aligned}
\tag{3.84c}
$$

$$
\begin{aligned}
E_x^{n+1}\ (i+1/2,\, j,\, k) &= \left(1 - \frac{\sigma(i+1/2,\, j,\, k)\delta t}{\epsilon(i+1/2,\, j,\, k)}\right) \cdot \\
&\quad E_x^n(i+1/2,\, j,\, k) \\
&+ \frac{\delta t}{\epsilon(i+1/2,\, j,\, k)\delta}\left[H_z^{n+1/2}(i+1/2,\, j+1/2,\, k)\right. \\
&- H_z^{n+1/2}(i+1/2,\, j-1/2,\, k) \\
&+ H_y^{n+1/2}(i+1/2,\, j,\, k-1/2) \\
&\left.-\ H_y^{n+1/2}(i+1/2,\, j,\, k+1/2)\right],
\end{aligned}
\tag{3.84d}
$$

$$
\begin{aligned}
E_y^{n+1}\ (i,\, j+1/2,\, k) = &\left(1-\frac{\sigma(i,\, j+1/2,\, k)\delta t}{\epsilon(i,\, j+1/2,\, k)}\right)\cdot \\
&E_y^n(i,\, j+1/2,\, k) \\
&+\frac{\delta t}{\epsilon(i,\, j+1/2,\, k)\delta}\Big[H_x^{n+1/2}(i,\, j+1/2,\, k+1/2) \\
&-H_x^{n+1/2}(i,\, j+1/2,\, k-1/2) \\
&+H_z^{n+1/2}(i-1/2,\, j+1/2,\, k) \\
&-\ H_z^{n+1/2}(i+1/2,\, j+1/2,\, k)\Big]\ ,
\end{aligned}
\tag{3.84e}
$$

$$
\begin{aligned}
E_z^{n+1}\ (i,\, j,\, k+1/2) = &\left(1-\frac{\sigma(i,\, j,\, k+1/2)\delta t}{\epsilon(i,\, j,\, k+1/2)}\right)\cdot \\
&E_z^n(i,\, j,\, k+1/2) \\
&+\frac{\delta t}{\epsilon(i,\, j,\, k+1/2)\delta}\Big[H_y^{n+1/2}(i+1/2,\, j,\, k+1/2) \\
&-H_y^{n+1/2}(i-1/2,\, j,\, k+1/2) \\
&+H_x^{n+1/2}(i,\, j-1/2,\, k+1/2) \\
&-\ H_x^{n+1/2}(i,\, j+1/2,\, k+1/2)\Big]
\end{aligned}
\tag{3.84f}
$$

Notice from Eqs. (3.84a)–(3.84f) and Fig. 3.22 that the components of **E** and **H** are interlaced within the unit cell and are evaluated at alternate half-time steps. All the field components are present in a quarter of a unit cell as shown typically in Fig. 3.23(a). Figure 3.23(b) illustrates typical relations between field components on a plane; this is particularly useful when incorporating boundary conditions. The figure can be inferred from Eq. (3.79d) or Eq. (3.84d). In translating the hyperbolic system of Eqs. (3.84a)–(3.84f) into a computer code, one must make sure that, within the same time loop, one type of field components is calculated first and the results obtained are used in calculating another type.

3.8.2 Accuracy and Stability

To ensure the accuracy of the computed results, the spatial increment δ must be small compared to the wavelength (usually $\leq \lambda/10$) or minimum dimension of the scatterer. This amounts to having 10 or more cells per wavelength. To ensure the stability of the finite difference scheme of Eqs. (3.84a)–(3.84f), the time increment Δt must satisfy the following stability condition [43, 47]:

$$
u_{\max}\Delta t \leq \left[\frac{1}{\Delta x^2}+\frac{1}{\Delta y^2}+\frac{1}{\Delta z^2}\right]^{-1/2} \tag{3.85}
$$

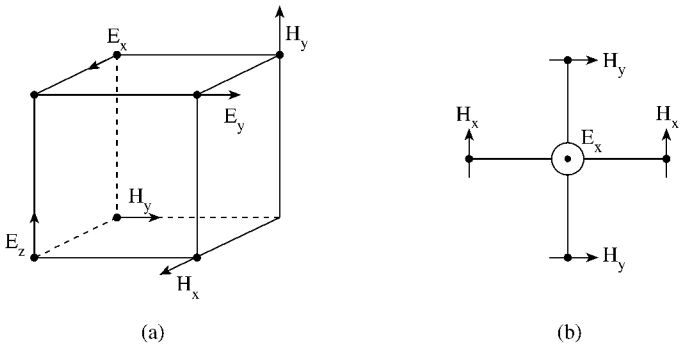

Figure 3.23
Typical relations between field components: (a) within a quarter of a unit cell, (b) in a plane.

where $u_{\max}$ is the maximum wave phase velocity within the model. Since we are using a cubic cell with $\Delta x = \Delta y = \Delta z = \delta$, Eq. (3.85) becomes

$$\boxed{\frac{u_{\max}\Delta t}{\delta} \leq \frac{1}{\sqrt{n}}} \tag{3.86}$$

where n is the number of space dimensions. For practical reasons, it is best to choose the ratio of the time increment to spatial increment as large as possible yet satisfying Eq. (3.86).

3.8.3 Lattice Truncation Conditions

A basic difficulty encountered in applying the FD-TD method to scattering problems is that the domain in which the field is to be computed is open or unbounded (see Fig. 1.3). Since no computer can store an unlimited amount of data, a finite difference scheme over the whole domain is impractical. We must limit the extent of our solution region. In other words, an artificial boundary must be enforced, as in Fig. 3.24, to create the numerical illusion of an infinite space. The solution region must be large enough to enclose the scatterer, and suitable boundary conditions on the artificial boundary must be used to simulate the extension of the solution region to infinity. Outer boundary conditions of this type have been called either *radiation conditions, absorbing boundary conditions,* or *lattice truncation conditions.* Although several types of boundary conditions have been proposed [48, 49], we will only consider those developed by Taflove et al. [43, 44].

The lattice truncation conditions developed by Taflove et al. allow excellent overall accuracy and numerical stability even when the lattice truncation planes are positioned no more than 5δ from the surface of the scatterer. The conditions relate in a simple way the values of the field components at the truncation planes to the field components at points one or more δ within the lattice (or solution region).

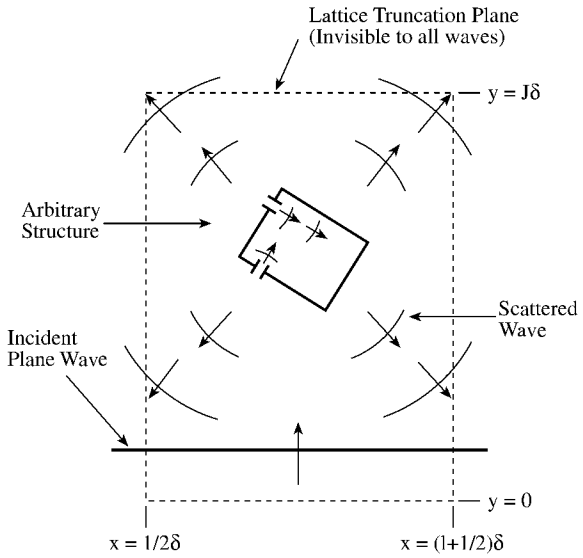

Figure 3.24
Solution region with lattice truncation.

For simplicity, we first consider one-dimensional wave propagation. Assume waves have only E_z and H_x components and propagate in the $\pm y$ directions. Also assume a time step of $\delta t = \delta y/c$, the maximum allowed by the stability condition of Eq. (3.86). If the lattice extends from $y = 0$ to $y = J\Delta y$, with E_z component at the end points, the truncation conditions are:

$$E_z^n(0) = E_z^{n-1}(1) \tag{3.87a}$$

$$E_z^n(J) = E_z^{n-1}(J-1) \tag{3.87b}$$

With these lattice conditions, all possible $\pm y$-directed waves are absorbed at $y = 0$ and $J\Delta y$ without reflection. Equation (3.87) assumes free-space propagation. If we wish to simulate the lattice truncation in a dielectric medium of refractive index m, Eq. (3.87) is modified to

$$E_z^n(0) = E_z^{n-m}(1) \tag{3.88a}$$

$$E_z^n(J) = E_z^{n-m}(J-1) \tag{3.88b}$$

For the three-dimensional case, we consider scattered waves having all six field components and propagating in all possible directions. Assume a time-step of $\delta t = \delta/2c$, a value which is about 13% lower than the maximum allowed ($\delta t = \delta/\sqrt{3}c$) by Eq. (3.86). If the lattice occupies $\frac{1}{2}\delta < x < (I_{\max} + \frac{1}{2})\delta$, $0 < y < J_{\max}\delta$, $0 < z < K_{\max}\delta$, the truncation conditions are [36, 44]:

(a) plane $i = 1/2$

$$H_y^n(1/2,\, j,\, k+1/2) = \frac{1}{3}\Big[H_y^{n-2}(3/2,\, j,\, k-1/2) + H_y^{n-2}(3/2,\, j,\, k+1/2) + H_y^{n-2}(3/2,\, j,\, k+3/2)\Big]\,, \tag{3.89a}$$

$$H_z^n(1/2,\, j+1/2,\, k) = \frac{1}{3}\Big[H_z^{n-2}(3/2,\, j+1/2,\, k-1) + H_z^{n-2}(3/2,\, j+1/2,\, k) + H_z^{n-2}(3/2,\, j+1/2,\, k+1)\Big]\,, \tag{3.89b}$$

(b) plane $i = I_{\max} + 1/2$

$$H_y^n(I_{\max}+1/2,\, j,\, k+1/2) = \frac{1}{3}\Big[H_y^{n-2}(I_{\max}-1/2,\, j,\, k-1/2) + H_y^{n-2}(I_{\max}-1/2,\, j,\, k+1/2) + H_y^{n-2}(I_{\max}-1/2,\, j,\, k+3/2)\Big]\,, \tag{3.89c}$$

$$H_z^n(I_{\max}+1/2,\, j+1/2,\, k) = \frac{1}{3}\Big[H_z^{n-2}(I_{\max}-1/2,\, j+1/2,\, k-1) + H_z^{n-2}(I_{\max}-1/2,\, j+1/2,\, k) + H_z^{n-2}(I_{\max}-1/2,\, j+1/2,\, k+1)\Big]\,, \tag{3.89d}$$

(c) plane $j = 0$,

$$E_x^n(i+1/2,\, 0,\, k) = E_x^{n-2}(i+1/2,\, 1,\, k)\,, \tag{3.89e}$$

$$E_z^n(i,\, 0,\, k+1/2) = E_z^{n-2}(i,\, 1,\, k+1/2)\,, \tag{3.89f}$$

(d) plane $j = J_{\max}$

$$E_x^n(i+1/2,\, J_{\max},\, k) = E_x^{n-2}(i+1/2,\, J_{\max}-1,\, k) \tag{3.89g}$$

$$E_z^n(i,\, J_{\max},\, k+1/2) = E_z^{n-2}(i,\, J_{\max}-1,\, k+1/2)\,, \tag{3.89h}$$

(e) plane $k = 0$,

$$E_x^n(i+1/2,\, j,\, 0) = \frac{1}{3}\Big[E_x^{n-2}(i-1/2,\, j,\, 1) + E_x^{n-2}(i+1/2,\, j,\, 1) + E_x^{n-2}(i+3/2,\, j,\, 1)\Big]\,, \tag{3.89i}$$

$$E_y^n(i,\, j+1/2,\, 0) = \frac{1}{3}\Big[E_y^{n-2}(i-1,\, j+1/2,\, 1) + E_y^{n-2}(i,\, j+1/2,\, 1) + E_y^{n-2}(i+1,\, j+1/2,\, 1)\Big]\,, \tag{3.89j}$$

(f) plane $k = K_{\max}$,

$$E_x^n(i+1/2, j, K_{\max}) = \frac{1}{3}\Big[E_x^{n-2}(i-1/2, j, K_{\max}-1) + E_x^{n-2}(i+1/2, j, K_{\max}-1) + E_x^{n-2}(i+3/2, j, K_{\max}-1)\Big], \tag{3.89k}$$

$$E_y^n(i, j+1/2, K_{\max}) = \frac{1}{3}\Big[E_y^{n-2}(i-1, j+1/2, K_{\max}-1) + E_y^{n-2}(i, j+1/2, K_{\max}-1) + E_y^{n-2}(i+1, j+1/2, K_{\max}-1)\Big] \tag{3.89l}$$

These boundary conditions minimize the reflection of any outgoing waves by simulating the propagation of the wave from the lattice plane adjacent to the lattice truncation plane in a number of time steps corresponding to the propagation delay. The averaging process is used to take into account all possible local angles of incidence of the outgoing wave at the lattice boundary and possible multiple incidences [43]. If the solution region is a dielectric medium of refractive index m rather than free space, we replace the superscript $n-2$ in Eqs. (3.89a)–(3.89l) by $n-m$.

3.8.4 Initial Fields

The initial field components are obtained by simulating either an incident plane wave pulse or single-frequency plane wave. The simulation should not take excessive storage nor cause spurious wave-reflections. A desirable plane wave source condition takes into account the scattered fields at the source plane. For the three-dimensional case, a typical wave source condition at plane $y = j_s$ (near $y = 0$) is

$$E_z^n(i, j_s, k+1/2) \leftarrow 1000\sin(2\pi f n\delta t) + E_z^n(i, j_s, k+1/2) \tag{3.90}$$

where f is the irradiation frequency. Equation (3.90) is a modification of the algorithm for all points on plane $y = j_s$; the value of the sinusoid is added to the value of E_z^n obtained from Eqs. (3.84a)–(3.84f).

At $t = 0$, the plane wave source of frequency f is assumed to be turned on. The propagation of waves from this source is simulated by time stepping, that is, repeatedly implementing Yee's finite difference algorithm on a lattice of points. The incident wave is tracked as it first propagates to the scatterer and then interacts with it via surface-current excitation, diffusion, penetration, and diffraction. Time stepping is continued until the sinusoidal steady state is achieved at each point. The field envelope, or maximum absolute value, during the final half-wave cycle of time stepping is taken as the magnitude of the phasor of the steady-state field [32, 43].

From experience, the number of time steps needed to reach the sinusoidal steady state can be greatly reduced by introducing a small isotropic conductivity σ_{ext} within the solution region exterior to the scatterer. This causes the fields to converge more rapidly to the expected steady state condition.

3.8.5 Programming Aspects

Since most EM scattering problems involve nonmagnetic media ($\mu_r = 1$), the quantity $\delta t/\mu(i, j, k)\delta$ can be assumed constant for all (i, j, k). The nine multiplications per unit cell per time required by Yee's algorithm of Eqs. (3.84a)–(3.84f) can be reduced to six multiplications, thereby reducing computer time. Following Taflove et al. [31, 35, 44], we define the following constants:

$$R = \delta t/2\epsilon_o \,, \tag{3.91a}$$

$$R_a = (c\delta t/\delta)^2 \,, \tag{3.91b}$$

$$R_b = \delta t/\mu_o \delta \,, \tag{3.91c}$$

$$C_a = \frac{1 - R\sigma(m)/\epsilon_r(m)}{1 + R\sigma(m)/\epsilon_r(m)} \,, \tag{3.91d}$$

$$C_b = \frac{R_a}{\epsilon_r(m) + R\sigma(m)} \tag{3.91e}$$

where $m = \text{MEDIA}(i, j, k)$ is an integer referring to the dielectric or conducting medium type at location (i, j, k). For example, for a solution region comprising of three different homogeneous media shown in Fig. 3.25, m is assumed to be 1 to 3.

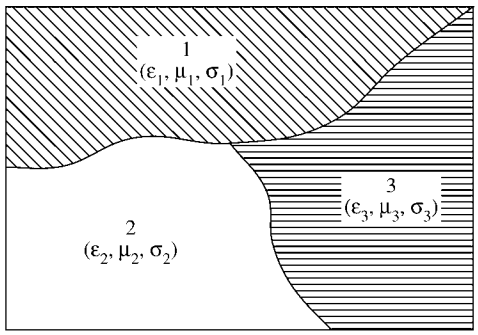

Figure 3.25
A typical inhomogeneous solution region with integer m assigned to each medium.

(This m should not be confused with the refractive index of the medium, mentioned earlier.) In addition to the constants in Eq. (3.91), we define proportional electric field

$$\widetilde{\mathbf{E}} = R_b \mathbf{E} \tag{3.92}$$

Thus Yee's algorithm is modified and simplified for easy programming as [50, 51]:

$$H_x^n(i,j,k) = H_x^{n-1}(i,j,k) + \widetilde{E}_y^{n-1}(i,j,k+1) - \widetilde{E}_y^{n-1}(i,j,k) - \widetilde{E}_z^{n-1}(i,j+1,k) + \widetilde{E}_z^{n-1}(i,j,k)\,, \tag{3.93a}$$

$$H_y^n(i,j,k) = H_y^{n-1}(i,j,k) + \widetilde{E}_z^{n-1}(i+1,j,k) - \widetilde{E}_z^{n-1}(i,j,k) - \widetilde{E}_x^{n-1}(i,j,k+1) + \widetilde{E}_x^{n-1}(i,j,k)\,, \tag{3.93b}$$

$$H_z^n(i,j,k) = H_z^{n-1}(i,j,k) + \widetilde{E}_x^{n-1}(i,j+1,k) - \widetilde{E}_x^{n-1}(i,j,k) - \widetilde{E}_y^{n-1}(i+1,j,k) + \widetilde{E}_y^{n-1}(i,j,k)\,, \tag{3.93c}$$

$$\widetilde{E}_x^n(i,j,k) = C_a(m)\widetilde{E}_x^{n-1}(i,j,k) + C_b(m)\Big[H_z^{n-1}(i,j,k) - H_z^{n-1}(i,j-1,k) - H_y^{n-1}(i,j,k) + H_y^{n-1}(i,j,k-1)\Big]\,, \tag{3.93d}$$

$$\widetilde{E}_y^n(i,j,k) = C_a(m)\widetilde{E}_y^{n-1}(i,j,k) + C_b(m)\Big[H_x^{n-1}(i,j,k) - H_x^{n-1}(i,j,k-1) - H_z^{n-1}(i,j,k) + H_z^{n-1}(i-1,j,k)\Big]\,, \tag{3.93e}$$

$$\widetilde{E}_z^n(i,j,k) = C_a(m)\widetilde{E}_z^{n-1}(i,j,k) + C_b(m)\Big[H_y^{n-1}(i,j,k) - H_y^{n-1}(i-1,j,k) - H_x^{n-1}(i,j,k) + H_x^{n-1}(i,j-1,k)\Big] \tag{3.93f}$$

The relationship between the original and modified algorithms is illustrated in Fig. 3.26 and shown in Table 3.8. Needless to say, the truncation conditions in Eqs. (3.89a)–(3.89l) must be modified accordingly. This modification eliminates the need for computer storage of separate ϵ and σ arrays; only a MEDIA array which specifies the type-integer of the dielectric or conducting medium at the location of each electric field component in the lattice need be stored. Also the programming problem of handling half integral values of i, j, k has been eliminated.

With the modified algorithm, we determine the scattered fields as follows. Let the solution region, completely enclosing the scatterer, be defined by $0 < i < I_{max}$, $0 < j < J_{\max}, 0 < k < K_{\max}$. At $t \leq 0$, the program is started by setting all field components at the grip points equal to zero:

$$\widetilde{E}_x^0(i,j,k) = \widetilde{E}_y^0(i,j,k) = \widetilde{E}_z^0(i,j,k) = 0 \tag{3.94a}$$

$$H_x^0(i,j,k) = H_y^0(i,j,k) = H_z^0(i,j,k) = 0 \tag{3.94b}$$

for $0 < i < I_{\max}, 0 < j < J_{\max}, 0 < k < K_{\max}$. If we know

$$H_x^{n-1}(i,j,k),\ E_z^{n-1}(i,j,k)\,,$$

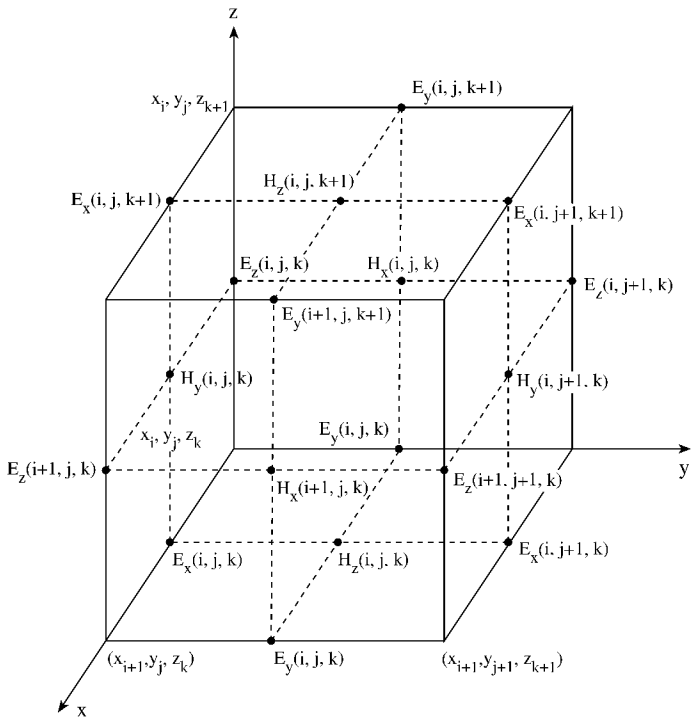

Figure 3.26
Modified node numbering.

and

$$E_y^{n-1}(i, j, k)$$

at all grid points in the solution region, we can determine new $H_x^n(i, j, k)$ everywhere from Eq. (3.93a). The same applies for finding other field components except that the lattice truncation conditions of Eqs. (3.89a)–(3.89l) must be applied when necessary. The plane wave source is activated at $t = \delta t$, the first time step, and left on during the entire run. The field components are advanced by Yee's finite difference formulas in Eqs. (3.93a)–(3.93f) and by the lattice truncation condition in Eqs. (3.89a)–(3.89l). The time stepping is continued for $t = N_{\max}\delta t$, where $N_{\max}$ is chosen large enough that the sinusoidal steady state is achieved. In obtaining the steady state solutions, the program must not be left for too long (i.e., $N_{\max}$ should not be too large), otherwise the imperfection of the boundary conditions causes the model to become unstable.

The FD-TD method has the following inherent advantages over other modeling techniques, such as the moment method and transmission-line modeling:

- It is conceptually simple.

Table 3.8 Relationship Between Original and Modified Field Components (lattice size = $I_{\max}\delta \times J_{\max}\delta \times K_{\max}\delta$)

Original	Modified	Limits on modified (i, j, k)
$H_x^{n+1/2}(x_i, y_{j+1/2}, z_{k+1/2})$	$H_x^n(i, j, k)$	$i = 0, \ldots, I_{\max}$ $j = 0, \ldots, J_{\max} - 1$ $k = 0, \ldots, K_{\max} - 1$
$H_y^{n+1/2}(x_{i+1/2}, y_j, z_{k+1/2})$	$H_y^n(i, j, k)$	$i = 0, \ldots, I_{\max} - 1$ $j = 0, \ldots, J_{\max}$ $k = 0, \ldots, K_{\max} - 1$
$H_z^{n+1/2}(x_{i+1/2}, y_{j+1/2}, z_k)$	$H_z^n(i, j, k)$	$i = 0, \ldots, I_{\max} - 1$ $j = 0, \ldots, J_{\max} - 1$ $k = 0, \ldots, K_{\max}$
$E_x^n(x_{i+1/2}, y_j, z_k)$	$E_x^n(i, j, k)$	$i = 0, \ldots, I_{\max} - 1$ $j = 0, \ldots, J_{\max}$ $k = 0, \ldots, K_{\max}$
$E_y^n(x_i, y_{j+1/2}, z_k)$	$E_y^n(i, j, k)$	$i = 0, \ldots, I_{\max}$ $j = 0, \ldots, J_{\max} - 1$ $k = 0, \ldots, K_{\max}$
$E_z^n(x_i, y_j, z_{k+1/2})$	$E_z^n(i, j, k)$	$i = 0, \ldots, I_{\max}$ $j = 0, \ldots, J_{\max}$ $k = 0, \ldots, K_{\max} - 1$

- The algorithm does not require the formulation of integral equations, and relatively complex scatterers can be treated without the inversion of large matrices.
- It is simple to implement for complicated, inhomogeneous conducting or dielectric structures because constitutive parameters (σ, μ, ϵ) can be assigned to each lattice point.
- Its computer memory requirement is not prohibitive for many complex structures of interest.
- The algorithm makes use of the memory in a simple sequential order.
- It is much easier to obtain frequency domain data from time domain results than the converse. Thus, it is more convenient to obtain frequency domain results via time domain when many frequencies are involved.

The method has the following disadvantages:

- Its implementation necessitates modeling object as well as its surroundings. Thus, the required program execution time may be excessive.
- Its accuracy is at least one order of magnitude worse than that of the method of moments, for example.

- Since the computational meshes are rectangular in shape, they do not conform to scatterers with curved surfaces, as is the case of the cylindrical or spherical boundary.

- As in all finite difference algorithms, the field quantities are only known at grid nodes.

Time-domain modeling in three dimensions involves a number of issues which are yet to be resolved even for frequency-domain modeling. Among these are whether it is best to reduce Maxwell's equations to a second-order equation for the electric (or magnetic) field or to work directly with the coupled first-order equation. The former approach is used in [35], for example, for solving the problem of EM exploration for minerals. The latter approach has been used with great success in computing EM scattering from objects as demonstrated in this section. In spite of these unresolved issues, the FD-TD algorithm has been applied to solve scattering and other problems including:

- aperture penetration [44, 52, 53],

- antenna/radiation problems [54]–[60],

- microwave circuits [63]–[68],

- eigenvalue problems [69],

- EM absorption in human tissues (bioectromagnetics) [35, 36],[70]–[74], and

- other areas [75]–[79].

The following two examples are taken from the work of Taflove et al. [32, 43, 44]. The problems whose exact solutions are known will be used to illustrate the applications and accuracy of FD-TD algorithm.

Example 3.7

Consider the scattering of $a + y$-directed plane wave of frequency 2.5 GHz by a uniform, circular, dielectric cylinder of radius 6 cm. We assume that the cylinder is infinite in the z direction and that the incident fields do not vary along z. Thus $\partial/\partial z = 0$ and the problem is reduced to the two-dimensional scattering of the incident wave with only E_z, H_x, and H_y components. Our objective is to compute one of the components, say E_z, at points within the cylinder. □

Solution

Assuming a lossless dielectric with

$$\epsilon_d = 4\epsilon_o, \qquad \mu_d = \mu_o, \qquad \sigma_d = 0\,, \tag{3.95}$$

the speed of the wave in the cylinder is

$$u_d = \frac{c}{\sqrt{\epsilon_r}} = 1.5 \times 10^8 \text{ m/s} \tag{3.96}$$

Hence $\lambda_d = u_d/f = 6$ cm. We may select $\delta = \Delta x = \Delta y = \Delta z = \lambda_d/20 = 0.3$ cm and $\delta t = \delta/2c = 5$ ps Thus we use the two-dimensional grid of Fig. 3.27 as the solution domain. Due to the symmetry of the scatterer, the domain can be reduced relative to Fig. 3.27 to the 25×49 subdomain of Fig. 3.28. Choosing the cylinder

Assumptions:

$$E_x = E_y = 0; \quad H_z = 0$$
$$\frac{\partial}{\partial z} = 0$$

Maxwell's Equations:

$$\frac{\partial H_x}{\partial t} = -\frac{1}{\mu}\frac{\partial E_z}{\partial y}$$
$$\frac{\partial H_y}{\partial t} = \frac{1}{\mu}\frac{\partial E_z}{\partial x}$$
$$\frac{\partial E_z}{\partial t} = \frac{1}{\varepsilon}\left(\frac{\partial H_y}{\partial x} - \frac{\partial H_x}{\partial y} - \sigma E_x\right)$$

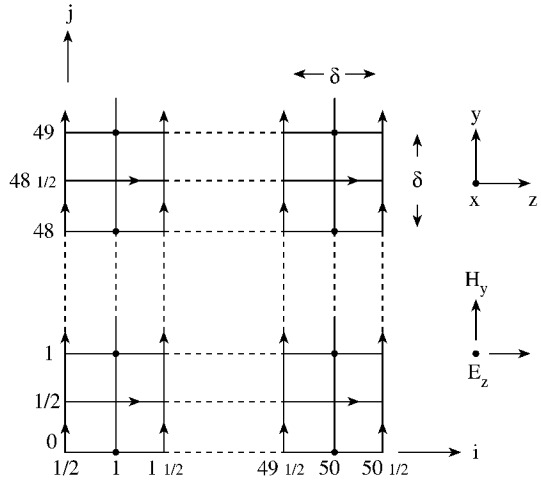

Figure 3.27
Two-dimensional lattice for Example 3.7.

axis as passing through point $(i, j) = (25.5, 24.5)$ allows the *symmetry condition* to be imposed at line $i = 26$, i.e.,

$$\widetilde{E}_z^n(26, j) = \widetilde{E}_z^n(25, j) \tag{3.97}$$

Soft grid truncation conditions are applied at $j = 0, 49$ and $i = 1/2$, i.e.,

$$\widetilde{E}_z^n(i, 0) = \frac{1}{3}\left[\widetilde{E}_z^{n-2}(i-1, 1) + \widetilde{E}_z^{n-2}(i, 1) + \widetilde{E}_z^{n-2}(i+1, 1)\right], \tag{3.98}$$

$$\widetilde{E}_z^n(i, 49) = \frac{1}{3}\left[\widetilde{E}_z^{n-2}(i-1, 48) + \widetilde{E}_z^{n-2}(i, 48) + \widetilde{E}_z^{n-2}(i+1, 48)\right], \tag{3.99}$$

$$H_y^n(0.5, 49) = \frac{1}{3}\left[H_y^{n-2}(1.5, j) + H_y^{n-2}(1.5, j-1) + H_y^{n-2}(1.5, j+1)\right] \tag{3.100}$$

where $n - 2$ is due to the fact that $\delta = 2c\delta t$ is selected. Notice that the actual values of (i, j, k) are used here, while the modified values for easy programming are used in the program; the relationship between the two types of values is in Table 3.8.

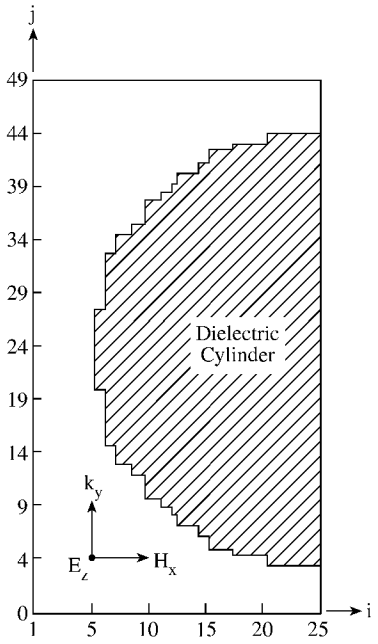

Figure 3.28
Finite difference model of cylindrical dielectric scatterer relative to the grid of Figure 3.27.

Grid points (i, j) internal to the cylinder, determined by

$$\left[(i - 25.5)^2 + (j - 24.5)^2\right]^{1/2} \leq 20\,, \tag{3.101}$$

are assigned the constitutive parameters ϵ_d, μ_o, and ϵ_d, while grid points external to the cylinder are assigned parameters of free space ($\epsilon = \epsilon_o$, $\mu = \mu_o$, $\sigma = 0$).

A FORTRAN program has been developed by Bemmel [80] based on the ideas expounded above. A similar but more general code is THREDE developed by Holland [50]. The program starts by setting all field components at grid points equal to zero. A plane wave source

$$\widetilde{E}_z^n(i, 2) \leftarrow 1000 \sin(2\pi f n \delta t) + \widetilde{E}_z^n(i, 2) \tag{3.102}$$

is used to generate the incident wave at $j = 2$ and $n = 1$, the first time step, and left on during the entire run. The program is time stepped to $t = N_{\max}\delta t$, where $N_{\max}$ is large enough that sinusoidal steady state is achieved. Since $f = 2.5$ GHz, the wave period $T = 1/f = 400$ ps $= 80\delta t$. Hence $N_{\max} = 500 = 6.25T/\delta t$ is sufficient to reach steady state. Thus the process is terminated after 500 timesteps. Typical results are portrayed in Fig. 3.29 for the envelope of $E_z^n(15, j)$ for $460 \leq n \leq 500$. Figure 3.29 also shows the exact solution using series expansion [81]. Bemmel's code has both

the numerical and exact solutions. By simply changing the constitutive parameters of the media and specifying the boundary of the scatterer (through a look-up table for complex objects), the program can be applied to almost any two-dimensional scattering or penetration problem. ∎

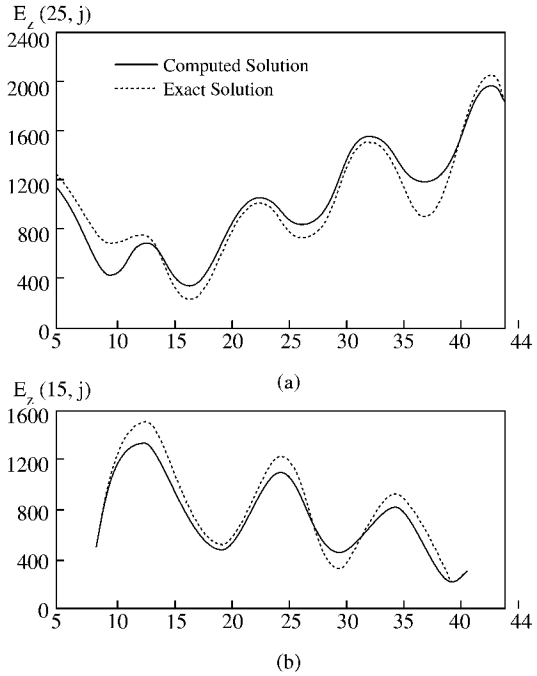

Figure 3.29
Computed internal E_z on line: (a) $i = 25$, (b) $i = 15$.

Example 3.8

Consider the penetration of $a + y$-directed plane wave of frequency 2.5 GHz by a uniform, dielectric sphere of radius 4.5 cm. The problem is similar to the previous example except that it is three-dimensional and more general. We assume that the incident wave has only E_z and H_x components. □

Solution

Like in the previous example, we assume that internal to the lossless dielectric sphere,

$$\epsilon_d = 4\epsilon_o, \qquad \mu_d = \mu_o, \qquad \sigma_d = 0 \tag{3.103}$$

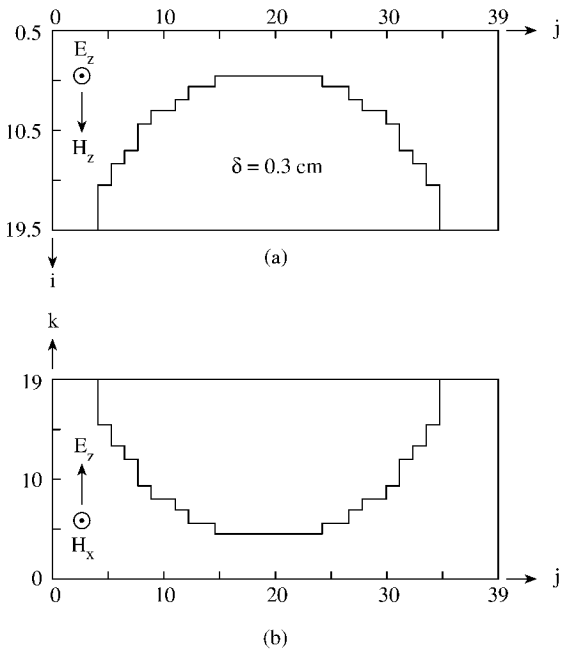

Figure 3.30
FD-TD model of dielectric sphere.

We select

$$\delta = \lambda_d/20 = 0.3 \text{ cm} \tag{3.104}$$

and

$$\delta t = \delta/2c = 5 \text{ ps} \tag{3.105}$$

This choice of the grid size implies that the radius of the sphere is $4.5/0.3 = 15$ units. The sphere model centered at grid point (19.5, 20, 19) in a $19 \times 39 \times 19$ lattice is portrayed in Fig. 3.30 at two lattice symmetry planes $k = 19$ and $i = 19.5$. Grid points (i, j, k) internal to the sphere are determined by

$$\left[(i - 19.5)^2 + (j - 20)^2 + (k - 19)^2\right]^{1/2} \leq 15 \tag{3.106}$$

Rather than assigning $\sigma = 0$ to points external to the sphere, a value $\sigma = 0.1$ mho/m is assumed to reduce spurious wave reflections. The FORTRAN code shown in Fig. 3.31, a modified version of Bemmel's [80], is used to generate field components E_y and E_z near the sphere irradiation axis. With the dimensions and constitutive parameters of the sphere specified as input data, the program is developed based on the following steps:

1. Compute the parameters of each medium using Eq. (3.91) where $m = 1, 2$.
2. Initialize field components.
3. Use the FD-TD algorithm in Eqs. (3.93a)–(3.93f) to generate field components. This is the heart of the program. It entails taking the following steps:
   (i) Calculate actual values of grid point (x, y, z) using the relationship in Table 3.8. This will be needed later to identify the constitutive parameters of the medium at that point using subroutine MEDIA.
   (ii) Apply soft lattice truncation conditions in Eqs. (3.89a)–(3.89l) at appropriate boundaries, i.e., at $x = \delta/2$, $y = 0$, $y_{\max}$, and $z = 0$. Notice that some of the conditions in Eqs. (3.89a)–(3.89l) are not necessary in this case because we restrict the solution to one-fourth of the sphere due to geometrical symmetry. At other boundaries ($x = x_{\max}$ and $z = z_{\max}$), the symmetry conditions are imposed. For example, at $k = 19$,

$$\widetilde{E}_x^n(i, j, 20) = \widetilde{E}_x^n(i, j, 18)$$

   (iii) Apply FD-TD algorithm in Eqs. (3.93a)–(3.93f).
   (iv) Activate the plane wave source, i.e.,

$$\widetilde{E}_z^n(i, j, k) \leftarrow \sin(2\pi f n \delta t) + \widetilde{E}_z^n(i, j_s, k)$$

   where $j_s = 3$ or any plane near $y = 0$.
   (v) Time step until steady state is reached.
4. Obtain the maximum absolute values (envelopes) of field components in the last half-wave and output the results.

Figure 3.32 illustrates the results of the program. The values of $|E_y|$ and $|E_z|$ near the sphere axis are plotted against j for observation period $460 \leq n \leq 500$. The computed results are compared with Mie's exact solution [82] covered in Section 2.8. The code for calculating the exact solution is also found in Bemmel's work [80]. ∎

3.9 Absorbing Boundary Conditions for FDTD

The finite difference time domain (FDTD) method is a robust, flexible (adaptable to complex geometries), efficient, versatile, easy-to-understand, easy-to-implement, and user-friendly technique to solve Maxwell's equations in the time domain. Although the method did not receive much attention it deserved when it was suggested, it is now becoming the most popular method of choice in computational EM. It is finding

```
0001    C*********************************************************
0002    C   APPLICATION OF THE FINITE DIFFERENCE METHOD
0003    C   This program involves the penetration of a
0004    C   lossless dielectric SPHERE by a plane wave.
0005    C   The program provides in the maximum absolute value of
0006    C   Ey and Ez during the final half-wave of time-stepping
0007    C   Assumption:
0008    C   +y-directed incident wave with components Ez and Hx.
0009    C   I,J,K,NN correspond to X,Y,Z, and Time.
0010    C   IMAX,JMAX,KMAX are the maximum values of x,y,z
0011    C   NNMAX is the total number of timesteps.
0012    C   NHW represents one half-wave cycle.
0013    C   MED is the number of different uniform media
            sections.
0014    C   JS is the j-position of the plane wave front.
0015    C
0016    C   THIS PROGRAM WAS DEVELOPED BY V. BEMMEL [80]
0017    C   AND LATER IMPROVED BY D. TERRY
0018    C*********************************************************
0019
0020        PARAMETER( IMAX=19, JMAX=39, KMAX=19)
0021        PARAMETER( NMAX=2, NNMAX=500, NHW=40, MED=2, JS=3 )
0022        PARAMETER( DELTA=3E-3, CL=3.0E8, F=2.5E9 )
0023        PARAMETER(  PIE=3.141592654)
0024
0025    C Define scatterer dimensions
0026          PARAMETER( OI=19.5, OJ=20.0, OK=19.0, RADIUS=15.0)
0027
0028          DIMENSION EX(0:IMAX+1, 0:JMAX+1, 0:KMAX+1, 0:NMAX),
0029         &    EY(0:IMAX+1, 0:JMAX+1, 0:KMAX+1, 0:NMAX),
0030         &    EZ(0:IMAX+1, 0:JMAX+1, 0:KMAX+1, 0:NMAX),
0031         &    HX(0:IMAX+1, 0:JMAX+1, 0:KMAX+1, 0:NMAX),
0032         &    HY(0:IMAX+1, 0:JMAX+1, 0:KMAX+1, 0:NMAX),
0033         &    HZ(0:IMAX+1, 0:JMAX+1, 0:KMAX+1, 0:NMAX),
0034         &    EY1(0:JMAX+1), EZ1(0:JMAX+1),
0035         &    ER(MED), SIG(MED), CA(MED), CB(MED)
0036
0037          DIMENSION IXMED(0:IMAX+1, 0:JMAX+1, 0:KMAX+1)
0038          DIMENSION IYMED(0:IMAX+1, 0:JMAX+1, 0:KMAX+1)
0039          DIMENSION IZMED(0:IMAX+1, 0:JMAX+1, 0:KMAX+1)
0040
0041          DIMENSION CBMRB( 2 )  ! STORE CB(M)/RB HERE
0042          DATA ER/1.0,4.0/   ! CONSTITUTIVE PARAMETERS
0043          DATA SIG/0.1,0.0/
0044    C
0045    C  Statement function to compute position w.r.t. center
           of sphere
0046    C
0047                position(RI,RJ,RK)=SQRT((RI-OI)**2+(RJ-OJ)
                                      **2+(RK-OK)**2)
0048          EO=(1E-9)/(36*PIE)
0049          UO=(1E-7)*4*PIE
0050          DT=DELTA/(2*CL)
0051          R=DT/EO
0052          RA=(DT**2)/(UO*EO*(DELTA**2))
0053          RB=DT/(UO*DELTA)
0054          TPIFDT = 2.0*PIE*F*DT
```

Figure 3.31

Computer program for FDTD three-dimensional scattering problem *(Continued).*

```
0055    C*********************************************************
0056    C  STEP # 1 - COMPUTE MEDIA PARAMETERS
0057    C*********************************************************
0058           DO 1 M=1,MED
0059           CA(M)=1.0-R*SIG(M)/ER(M)
0060           CB(M)=RA/ER(M)
0061           CBMRB(M) = CB(M)/RB
0062    1      CONTINUE
0063    C
0064    C  (i) CALCULATE THE REAL/ACTUAL GRID POINTS
0065    C
0066    C Initialize the media arrays.Index (M) determines which
0067    C medium each point is actually located in and is used to
0068    C index into arrays which determine the constitutive
0069    C parameters of the medium.There are separate M
          determining
0070    C arrays for EX, EY, and EZ.  These arrays correlate the
0071    C integer values of I,J,K to the actual position within
0072    C the lattice.Computing these values now and storing them
          in these
0073    C arrays as opposed to computing them each time they are
0074    C needed saves a large amount of computation time.
0075    C
0076           DO 3 I=0, IMAX+1
0077           DO 3 J=0, JMAX+1
0078           DO 3 K=0, KMAX+1
0079           IF(position(float(I)+0.5,float(J),float(K))
               .LE.RADIUS) then
0080           IXMED( I, J, K ) = 2
0081           else
0082           IXMED( I, J, K ) = 1
0083           endif
0084           IF(position(float(I),float(J)+0.5,float(K))
               .LE.RADIUS) then
0085           IYMED( I, J, K ) = 2
0086           else
0087           IYMED( I, J, K ) = 1
0088           endif
0089           IF(position(float(I),float(J),float(K)+0.5)
               .LE.RADIUS) then
0090           IZMED( I, J, K ) = 2
0091           else
0092           IZMED( I, J, K ) = 1
0093           endif
0094    3      CONTINUE

0095    C*********************************************
0096    C  STEP # 2 - INITIALIZE FIELD COMPONENTS
0097    C*********************************************
0098    C components for output
0099           DO 4 J=0,JMAX+1
0100           EY1(J)=0.
0101           EZ1(J)=0.
0102     4     CONTINUE
0103
0104           DO 5 I=0,IMAX+1
0105           DO 5 J=0,JMAX+1
0106           DO 5 K=0,KMAX+1
0107           DO 5 M = 0, MMAX
0108           EX(I,J,K,M)=0.
0109           EY(I,J,K,M)=0.
```

Figure 3.31

(Cont.) **Computer program for FDTD three-dimensional scattering problem** ***(Continued).***

```
0110          EZ(I,J,K,N)=0.
0111          HX(I,J,K,N)=0.
0112          HY(I,J,K,N)=0.
0113          HZ(I,J,K,N)=0.
0114       5  CONTINUE
0115          print *, 'initialization complete'

0116      C*************************************************************
0117      C STEP # 3 - USE FD/TD ALGORITHM TO GENERATE
0118      C FIELD COMPONENTS
0119      C*************************************************************
0120      C  SINCE ONLY FIELD COMPONENTS AT CURRENT TIME (t) AND
             PREVIOUS
0121      C  TWO TIME STEPS ( t-1 AND t-2) ARE REQUIRED FOR
             COMPUTATION,
0122      C  WE SAVE MEMORY SPACE BY USING THE FOLLOWING INDICES
0123      C       NCUR is index in for time t
0124      C       NPR1 is index in for t-1
0125      C       NPR2 is index in for t-2
0126      C
0127          NCUR = 2
0128          NPR1 = 1
0129          NPR2 = 0
0130          DO 15 NN = 1, NNMAX  ! TIME LOOP
0131          IF (MOD( NN,10).EQ.0) THEN
0132          print *,'NN=',NN  ! DISPLAY PROGRESS
0133          ENDIF
0134      C     Next time step - move indices up a notch.
0135          NPR2 = NPR1
0136          NPR1 = NCUR
0137          NCUR = MOD( NCUR+1, 3)
0138          DO 20 K=0,KMAX  ! Z LOOP
0139          DO 25 J=0,JMAX  ! Y LOOP
0140          DO 30 I=0,IMAX   ! X LOOP
0141      C
0142      C  (ii)-APPLY SOFT LATTICE TRUNCATION CONDITIONS
0143      C
0144      C---x=delta/2
0145              IF(I.EQ.0) THEN
0146                 IF ((K.NE.KMAX).AND.(K.NE.0)) THEN
0147           HY(0,J,K,NCUR) = (HY(1,J,K-1,NPR2)
0148          &         + HY(1,J,K,NPR2)+HY(1,J,K+1,NPR2))/3.
0149           HZ(0,J,K,NCUR)=(HZ(1,J,K-1,NPR2)
0150          &         + HZ(1,J,K,NPR2)+HZ(1,J,K+1,NPR2))/3.
0151            else
0152            IF (K.EQ.KMAX) THEN
0153            HY(0,J,KMAX,NCUR) = (HY(1,J,KMAX-1,NPR2)
0154          &        + HY(1,J,KMAX,NPR2))/2.
0155            HZ(0,J,K,NCUR)=( HZ(1,J,K-1,NPR2)
0156          &         + HZ(1,J,K,NPR2) )/2.
0157            ELSE
0158            HY(0,J,K,NCUR) = ( HY(1,J,K,NPR2)
0159          &         + HY(1,J,K+1,NPR2))/2.
0160            HZ(0,J,0,NPR2)=(HZ(1,J,0,NPR2)
0161          &         + HZ(1,J,1,NPR2))/2.
0162                ENDIF
0163                ENDIF
0164            ENDIF
0165      C---y=0
0166          IF(J.EQ.0) THEN
0167          EX(I,0,K,NCUR)=EX(I,1,K,NPR2)
0168          EZ(I,0,K,NCUR)=EZ(I,1,K,NPR2)
```

Figure 3.31

(Cont.) **Computer program for FDTD three-dimensional scattering problem *(Continued).***

```
0169                ELSE
0170    C---y=ymax
0171          IF(J.EQ.JMAX) THEN
0172          EX(I,JMAX,K,NCUR)=EX(I,JMAX-1,K,NPR2)
0173          EZ(I,JMAX,K,NCUR)=EZ(I,JMAX-1,K,NPR2)
0174          ENDIF
0175               ENDIF
0176    C---z=0
0177          IF(K.EQ.0) THEN
0178          IF ((I.NE.0).AND.(I.NE.IMAX)) THEN
0179          EX(I,J,0,NCUR) = (EX(I-1,J,1,NPR2)
0180         &              + EX(I,J,1,NPR2)+EX(I+1,J,1,NPR2))/3.
0181          EY(I,J,0,NCUR) = (EY(I-1,J,1,NPR2)
0182         &      + EY(I,J,1,NPR2)+EY(I+1,J,1,NPR2))/3.
0183          ELSE
0184          IF(I.EQ.0)  THEN
0185          EX(0,J,0,NCUR)=(EX(0,J,1,NPR2)+EX(1,J,1,NPR2))/2.
0186          EY(I,J,0,NCUR)=(EY(I,J,1,NPR2)+EY(I+1,J,1,NPR2))/2.
0187              ELSE
0188          EX(I,J,0,NCUR)=(EX(I-1,J,1,NPR2)+EX(I,J,1,NPR2))/2.
0189          EY(I,J,0,NCUR)=(EY(I-1,J,1,NPR2)+EY(I,J,1,NPR2))/2.
0190              ENDIF
0191             ENDIF
0192          ENDIF
0193    C
0194    C  (iii)  APPLY FD/TD ALGORITHM
0195    C
0196    C-----a. HX  generation:
0197          HX(I,J,K,NCUR)=HX(I,J,K,NPR1)+RB*(EY(I,J,K+1,NPR1)
0198         & - EY(I,J,K,NPR1)+EZ(I,J,K,NPR1)-EZ(I,J+1,K,NPR1))
0199    C-----b. HY  generation:
0200          HY(I,J,K,NCUR)=HY(I,J,K,NPR1)+RB*(EZ(I+1,J,K,NPR1)
0201         & - EZ(I,J,K,NPR1)+EX(I,J,K,NPR1)-EX(I,J,K+1,NPR1))
0202    C-----c. HZ  generation:
0203          HZ(I,J,K,NCUR)=HZ(I,J,K,NPR1)+RB*(EX(I,J+1,K,NPR1)
0204         & - EX(I,J,K,NPR1)+EY(I,J,K,NPR1)-EY(I+1,J,K,NPR1))
0205    C---k=kmax  ! SYMMETRY
0206          IF(K.EQ.KMAX) THEN
0207          HX(I,J,KMAX,NCUR)=HX(I,J,KMAX-1,NCUR)
0208          HY(I,J,KMAX,NCUR)=HY(I,J,KMAX-1,NCUR)
0209          ENDIF
0210    C-----d. EX  generation:
0211          IF((J.NE.0).AND.(J.NE.JMAX).AND.(K.NE.0)) THEN
0212          M = IXMED( I, J, K )
0213          EX(I,J,K,NCUR) = CA(M)*EX(I,J,K,NPR1) + CBMRB(M)*
0214         &  (HZ(I,J,K,NCUR)-HZ(I,J-1,K,NCUR)+HY(I,J,K-1,NCUR)
0215         &                  -HY(I,J,K,NCUR))
0216          ENDIF
0217    C-----e. EY  generation:
0218          IF(K.NE.0) THEN
0219          M = IYMED( I, J, K )
0220          EY(I,J,K,NCUR)=CA(M)*EY(I,J,K,NPR1) + CBMRB(M)*
0221         &  HX(I,J,K,NCUR)-HX(I,J,K-1,NCUR)+HZ(I-1,J,K,NCUR)
0222         &                 -HZ(I,J,K,NCUR))
0223          ENDIF
0224    C-----f. EZ  generation:
0225          IF ((J.NE.0).AND.(J.NE.JMAX)) THEN
0226          M = IZMED( I, J, K )
0227    C  sig(ext)=0 for Ez only from Taflove[14]
0228          IF(M.EQ.1) THEN
0229          CAM=1.0
0230          ELSE
```

Figure 3.31

(Cont.) **Computer program for FDTD three-dimensional scattering problem** ***(Continued).***

```
0231          CAM=CA(M)
0232          ENDIF
0233          EZ(I,J,K,NCUR)=CAM*EZ(I,J,K,NPR1)+CBMRB(M)*
0234         &  (HY(I,J,K,NCUR)-HY(I-1,J,K,NCUR)+HX(I,J-1,K,NCUR)
0235         &                  -HX(I,J,K,NCUR))
0236      C
0237      C   (iv)  APPLY THE PLANE-WAVE SOURCE
0238      C
0239          IF(J.EQ.JS) THEN
0240          EZ(I,JS,K,NCUR) = EZ(I,JS,K,NCUR)+SIN( TPIFDT*NN )
0241          ENDIF
0242          ENDIF
0243      C---i=imax+1/2  ! SYMMETRY
0244          IF(I.EQ.IMAX) THEN
0245          EY(IMAX+1,J,K,NCUR)=EY(IMAX,J,K,NCUR)
0246          EZ(IMAX+1,J,K,NCUR)=EZ(IMAX,J,K,NCUR)
0247          ENDIF
0248      c---k=kmax
0249          IF(K.EQ.KMAX) THEN
0250          EX(I,J,KMAX+1,NCUR)=EX(I,J,KMAX-1,NCUR)
0251          EY(I,J,KMAX+1,NCUR)=EY(I,J,KMAX-1,NCUR)
0252          ENDIF
0253       30   CONTINUE !  I LOOP

0254      C*********************************************************
0255      C  STEP # 4 - RETAIN THE MAXIMUM ABSOLUTE VALUES DURING
0256      C              THE LAST HALF-WAVE
0257      C*********************************************************
0258          IF ( (K.EQ.KMAX).AND.(NN.GT.(NNMAX-NHW)) ) THEN
0259          TEMP = ABS( EY(IMAX,J,KMAX-1,NCUR) )
0260          IF (TEMP .GT. EY1(J) ) THEN
0261          EY1(J) = TEMP
0262          ENDIF
0263          TEMP = ABS( EZ(IMAX,J,KMAX,NCUR) )
0264          IF (TEMP .GT. EZ1(J) ) THEN
0265          EZ1(J) = TEMP
0266          ENDIF
0267          ENDIF
0268       25   CONTINUE  ! J LOOP
0269       20   CONTINUE       ! K LOOP
0270       15   CONTINUE         ! NN (time) LOOP
0271      C*********************************************************
0272      C-----Output E as a function of j
0273          DO 130 J = 0, JMAX-1
0274          WRITE(6,135) J+1, float(J), EY1(J)
0275       130  CONTINUE
0276          DO 140 J = 0, JMAX-1
0277          WRITE(6,135) J+1, float(J), EZ1(J)
0278       140  CONTINUE
0279       135  FORMAT(I5,2F15.8)
0280          STOP
0281          END
```

Figure 3.31

(Cont.) **Computer program for FDTD three-dimensional scattering problem.**

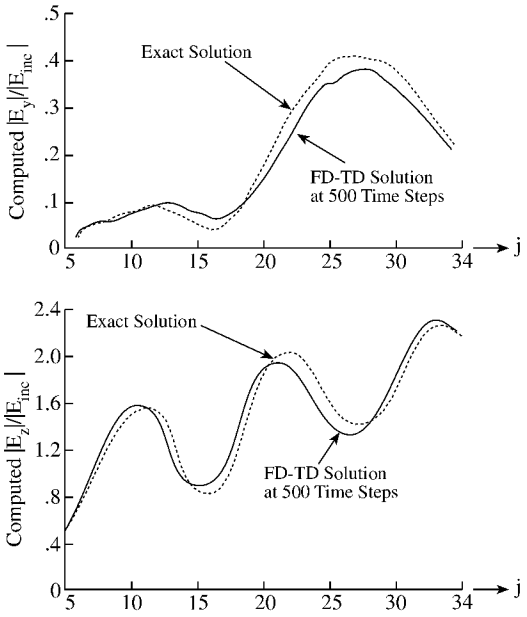

Figure 3.32
Computed $E_y(19.5, j, 18)$ and $E_z(19, j, 18.5)$ within the lossless dielectric sphere.

widespread use for solving open-region scattering, radiation, penetration/absorption, electromagnetic interference (EMI), electromagnetic compatibility (EMC), diffusion, transient, bioelectromagnetics, and microwave circuit modeling problems. However, the method exhibits some problems such as slow convergence for solving resonant structures, requirement of large memory for inhomogeneous waveguide structures due to the necessity of a full-wave analysis, inability to properly handle curved boundaries due to its orthogonal nature, low stability, and low accuracy unless fine mesh is used, to mention a few. These problems prohibit the application of the standard FDTD technique and have led to various forms of its modifications [83]–[93] and hybrid FDTD methods [94]–[96]. Although these new FDTD methods have enhanced the standard FDTD (increase accuracy and stability, etc.), some researchers still prefer the standard FDTD.

One of the major problems inherent in the standard FDTD, however, is that the requirement for artificial mesh truncation (boundary) condition. The artificial termination truncates the solution region electrically close to the radiating/scattering object but effectively simulates the solution to infinity. These artificial termination conditions are known as *absorbing boundary conditions* (ABCs) as they theoretically absorb incident and scattered fields. The accuracy of the ABC dictates the accuracy of the FDTD method. The need for accurate ABCs has resulted in various types of ABCs [97]–[107], which are fully discussed in [104]. Due to space limitation, we will

only consider Berenger's *perfectly matched layer* (PML) type of ABC [100]–[104] since PML has been the most widely accepted and is set to revolutionize the FDTD method.

In the perfectly matched layer (PML) truncation technique, an artificial layer of absorbing material is placed around the outer boundary of the computational domain. The goal is to ensure that a plane wave that is incident from FDTD free space to the PML region at an arbitrary angle is completely absorbed there without reflection. This is the same as saying that there is complete transmission of the incident plane wave at the interface between free space and the PML region (see Fig. 3.33). Thus the FDTD and the PML region are said to be *perfectly matched.*

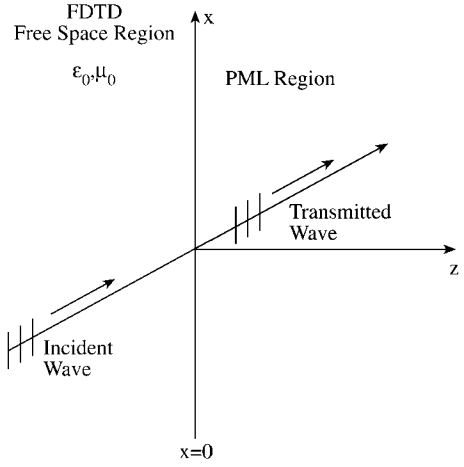

Figure 3.33
Reflectionless transmission of a plane wave at a PML/free-space interface.

To illustrate the PML technique, consider Maxwell's equation in two dimensions for transverse electric (TE) case with field components E_x, E_y and H_z and no variation with z. Expanding Eqs. (1.22c) and (1.22d) in Cartesian coordinates and setting $E_z = 0 = \dfrac{\partial}{\partial z}$, we obtain

$$\epsilon_o \frac{\partial E_x}{\partial t} + \sigma E_x = \frac{\partial H_z}{\partial y} \tag{3.107a}$$

$$\epsilon_o \frac{\partial E_y}{\partial t} + \sigma E_y = -\frac{\partial H_z}{\partial x} \tag{3.107b}$$

$$\mu_o \frac{\partial H_z}{\partial t} + \sigma^* H_z = \frac{\partial E_x}{\partial y} - \frac{\partial E_y}{\partial x} \tag{3.107c}$$

where the PML, as a lossy medium, is characterized by an electrical conductivity σ

and a magnetic conductivity σ^*. The conductivities are related as

$$\frac{\sigma}{\epsilon_0} = \frac{\sigma^*}{\mu_o} \tag{3.108}$$

This relationship ensures a required level of attenuation and forces the wave impedance of the PML to be equal to that the free space. Thus a reflectionless transmission of a plane wave propagation across the interface is permitted. For oblique incident angles, the conductivity of the PML must have a certain anisotropy characteristic to ensure reflectionless transmission. To achieve this, the H_z component must be split into two subcomponents, H_{zx} and H_{zy}, with the possibility of assigning losses to the individual split field components. This is the cornerstone of the PML technique. It leads to four components E_x, E_y, H_{zx}, and H_{zy} and four (rather than the usual three) coupled field equations.

$$\epsilon_o \frac{\partial E_x}{\partial t} + \sigma_y E_x = \frac{\partial (H_{zx} + H_{zy})}{\partial y} \tag{3.109a}$$

$$\epsilon_o \frac{\partial E_y}{\partial t} + \sigma_x E_y = -\frac{\partial (H_{zx} + H_{zy})}{\partial x} \tag{3.109b}$$

$$\mu_o \frac{\partial H_{zx}}{\partial t} + \sigma_x^* H_{zx} = -\frac{\partial E_y}{\partial x} \tag{3.109c}$$

$$\mu_o \frac{\partial H_{zy}}{\partial t} + \sigma_y^* H_{zy} = \frac{\partial E_x}{\partial y} \tag{3.109d}$$

These equations can be discretized to provide the FDTD time-stepping equations for the PML region. The standard Yee time-stepping cannot be used because of the rapid attenuation to outgoing waves afforded by a PML medium. We use the exponentially differenced equations to preclude any possibility of diffusion instability. In the usual FDTD notations, the resulting four time-stepping equations for the PML region are [101]:

$$\begin{aligned} E_x^{n+1}(i+1/2, j) &= e^{-\sigma_y(j)\delta t/\epsilon_0} E_x^n(i+1/2, j) \\ &+ \frac{(1 - e^{-\sigma_y(j)\delta t/\epsilon_0})}{\sigma_y(j)\delta} \Big[H_{zx}^{n+1/2}(i+1/2, j+1/2) + H_{zy}^{n+1/2}(i+1/2, j+1/2) \\ &- H_{zx}^{n+1/2}(i+1/2, j-1/2) - H_{zy}^{n+1/2}(i+1/2, j-1/2) \Big] \end{aligned} \tag{3.110a}$$

$$\begin{aligned} E_y^{n+1}(i, j+1/2) &= e^{-\sigma_x(i)\delta t/\epsilon_0} E_y^n(i, j+1/2, k) \\ &+ \frac{(1 - e^{-\sigma_x(i)\delta t/\epsilon_0})}{\sigma_x(i)\delta} \Big[H_{zx}^{n+1/2}(i-1/2, j+1/2) + H_{zy}^{n+1/2}(i-1/2, j+1/2) \\ &- H_{zx}^{n+1/2}(i+1/2, j+1/2) - H_{zy}^{n+1/2}(i+1/2, j+1/2) \Big] \end{aligned} \tag{3.110b}$$

$$H_{zx}^{n+1/2}(i+1/2, j+1/2) = e^{-\sigma_x^*(i+1/2)\delta t/\mu_0} H_{zx}^{n-1/2}(i+1/2, j+1/2) + \frac{(1-e^{-\sigma_x^*(i+1/2)\delta t/\mu_0})}{\sigma_x^*(i+1/2)\delta}\left[E_y^n(i, j+1/2) - E_y^n(i+1, j+1/2)\right] \quad (3.110c)$$

$$H_{zy}^{n+1/2}(i+1/2, j+1/2) = e^{-\sigma_y^*(i+1/2)\delta t/\mu_0} H_{zy}^{n-1/2}(i+1/2, j+1/2) + \frac{(1-e^{-\sigma_y^*(i+1/2)\delta t/\mu_0})}{\sigma_y^*(i+1/2)\delta}\left[E_x^n(i+1/2, j+1) - E_x^n(i+1/2, j)\right] \quad (3.110d)$$

These equations can be directly implemented in an FDTD simulation to model PML medium. All that is required to select the depth of the PML and its conductivity. In theory, the PML could δ deep and have near-infinite conductivity. It has been shown, however, that increasing the conductivity gradually with depth minimizes reflections; hence the "layering" of the medium and the dependence of σ on i and j.

The TM case can be obtained by duality, with E_z split so that $E_z = E_{zx} + E_{zy}$. In three dimensions, all six Cartesian field components are split so that the resulting PML modification of Maxwell's equations yields 12 equations [104].

3.10 Finite Differencing for Nonrectangular Systems

So far in this chapter, we have considered only rectangular solution regions within which a rectangular grid can be readily placed. Although we can always replace a nonrectangular solution region by an approximate rectangular one, our discussion in this chapter would be incomplete if we failed to apply the method to nonrectangular coordinates since it is sometimes preferable to use these coordinates. We will demonstrate the finite differencing technique in cylindrical coordinates (ρ, ϕ, z) and spherical coordinates (r, θ, ϕ) by solving Laplace's equation $\nabla^2 V = 0$. The idea is readily extended to other PDEs.

3.10.1 Cylindrical Coordinates

Laplace's equation in cylindrical coordinates can be written as

$$\nabla^2 V = \frac{\partial^2 V}{\partial \rho^2} + \frac{1}{\rho}\frac{\partial V}{\partial \rho} + \frac{1}{\rho^2}\frac{\partial^2 V}{\partial \phi^2} + \frac{\partial^2 V}{\partial z^2}. \quad (3.111)$$

Refer to the cylindrical system and finite difference molecule shown in Fig. 3.34. At point $O(\rho_o, \phi_o, z_o)$, the equivalent finite difference approximation is

$$\frac{V_1 - 2V_o + V_2}{(\Delta\rho)^2} + \frac{1}{\rho_o}\frac{V_1 - V_2}{2\Delta\rho} + \frac{V_3 - 2V_o + V_4}{(\rho_o \Delta\phi)^2} + \frac{V_5 - 2V_o + V_6}{(\Delta z)^2} = 0 \quad (3.112)$$

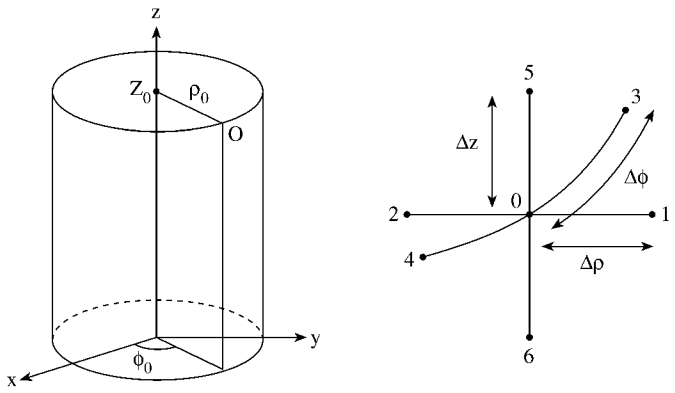

Figure 3.34
Typical node in cylindrical coordinate.

where $\Delta\rho$, $\Delta\phi$ and Δz are the step sizes along ρ, ϕ, and z, respectively, and

$$\begin{aligned} &V_o = V(\rho_o, \phi_o, z_o),\ \ V_1 = V(\rho_o + \Delta\rho, \phi_o, z_o),\ \ V_2 = V(\rho_o - \Delta\rho, \phi_o, z_o)\ , \\ &V_3 = V(\rho_o, \phi_o + \rho_o\Delta\phi, z_o),\ \ V_4 = V(\rho_o, \phi_o - \rho_o\Delta\phi, z_o)\ , \\ &V_5 = V(\rho_o, \phi_o, z_o + \Delta z),\ \ V_6 = V(\rho_o, \phi_o, z_o - \Delta z) \end{aligned} \tag{3.113}$$

We now consider a special case of Eq. (3.112) for an axisymmetric system [108]. In this case, there is no dependence on ϕ so that $V = V(\rho, z)$. If we assume square nets so that $\Delta\rho = \Delta z = h$, the solution region is discretized as in Fig. 3.35 and Eq. (3.112) becomes

$$\left(1 + \frac{h}{2\rho_o}\right) V_1 + \left(1 - \frac{h}{2\rho_o}\right) V_2 + V_5 + V_6 - 4V_o = 0 \tag{3.114}$$

If point O is at $(\rho_o, z_o) = (ih, jh)$, then

$$1 + \frac{h}{2\rho_o} = \frac{2i+1}{2i}, \quad 1 - \frac{h}{2\rho_o} = \frac{2i-1}{2i}$$

so that Eq. (3.114) becomes

$$\boxed{V(i,j) = \frac{1}{4}\left[V(i,j-1) + V(i,j+1) + \left(\frac{2i-1}{2i}\right)V(i-1,j) + \left(\frac{2i+1}{2i}\right)V(i+1,j)\right]} \tag{3.115}$$

Notice that in Eq. (3.114), it appears we have a singularity for $\rho_o = 0$. However, by symmetry, all odd order derivatives must be zero. Hence

$$\left.\frac{\partial V}{\partial \rho}\right|_{\rho=0} = 0 \tag{3.116}$$

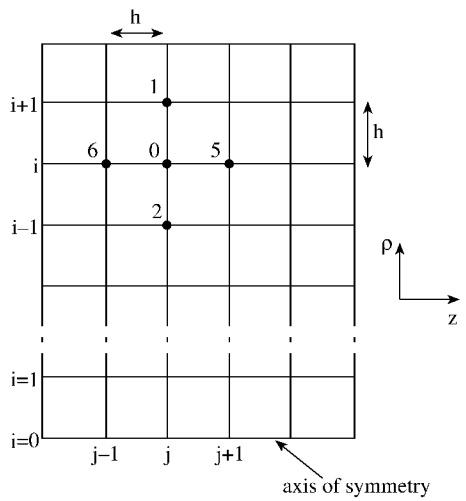

Figure 3.35
Finite difference grid for an axisymmetric system.

since

$$V(\Delta\rho, z_o) = V(-\Delta\rho, z_o) \tag{3.117}$$

Therefore by L'Hopital's rule,

$$\lim_{\rho_o \to 0} \frac{1}{\rho_o} \frac{\partial V}{\partial \rho}\bigg|_{\rho_o} = \frac{\partial^2 V}{\partial \rho^2}\bigg|_{\rho_o} \tag{3.118}$$

Thus, at $\rho = 0$, Laplace's equation becomes

$$2\frac{\partial^2 V}{\partial \rho^2} + \frac{\partial^2 V}{\partial z^2} = 0 \tag{3.119}$$

The finite difference equivalent to Eq. (3.119) is

$$V_o = \frac{1}{6}(4V_1 + V_5 + V_6)$$

or

$$\boxed{V(0, j) = \frac{1}{6}[V(0, j-1) + V(0, j+1) + 4V(1, j)]} \tag{3.120}$$

which is used at $\rho = 0$.

To solve Poisson's equation $\nabla^2 V = -\rho_v/\epsilon$ in cylindrical coordinates, we obtain the finite difference form by replacing zero on the right-hand side of Eq. (3.112) with $g = -\rho_v/\epsilon$. We obtain

$$\boxed{V(i, j) = \frac{1}{4}\left[V(i, j+1) + V(i, j-1) + \frac{2i-1}{2i}V(i-1, j) + \frac{2i+1}{2i}V(i+1, j) + gh^2\right]} \tag{3.121}$$

where h is the step size.

As in Section 3.7.1, the boundary condition $D_{1n} = D_{2n}$ must be imposed at the interface between two media. As an alternative to applying Gauss's law as in Section 3.7.1, we will apply Taylor series expansion [109]. Applying the series

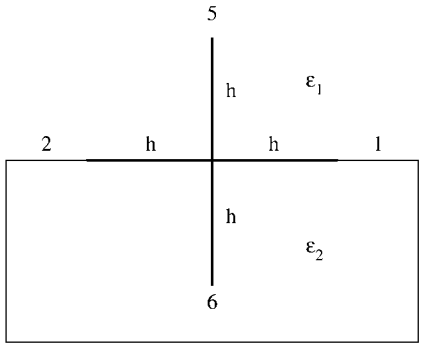

Figure 3.36
Interface between two dielectric media.

expansion to point 1, 2, 5 in medium 1 in Fig. 3.36, we obtain

$$\begin{aligned} V_1 &= V_o + \frac{\partial V_o^{(1)}}{\partial \rho} h + \frac{\partial^2 V_o^{(1)}}{\partial \rho^2} \frac{h^2}{2} + \cdots \\ V_2 &= V_o - \frac{\partial V_o^{(1)}}{\partial \rho} h + \frac{\partial^2 V_o^{(1)}}{\partial \rho^2} \frac{h^2}{2} - \cdots \\ V_5 &= V_o + \frac{\partial V_o^{(1)}}{\partial z} h + \frac{\partial^2 V_o^{(1)}}{\partial z^2} \frac{h^2}{2} + \cdots \end{aligned} \tag{3.122}$$

where superscript (1) denotes medium 1. Combining Eqs. (3.111) and (3.122) results in

$$h^2 \nabla^2 V = V_1 + V_2 + 2V_5 - 4V_o - 2h \frac{\partial V_o^{(1)}}{\partial z} + \frac{h(V_1 - V_2)}{2\rho_o} = 0$$

or

$$\frac{\partial V_o^{(1)}}{\partial z} = \frac{V_1 + V_2 + 2V_5 - 4V_o + \dfrac{h(V_1 - V_2)}{2\rho_o}}{2h} \tag{3.123}$$

Similarly, applying Taylor series to points 1, 2, and 6 in medium 2, we get

$$\begin{aligned} V_1 &= V_o + \frac{\partial V_o^{(1)}}{\partial \rho} h + \frac{\partial^2 V_o^{(1)}}{\partial \rho^2} \frac{h^2}{2} + \cdots \\ V_2 &= V_o - \frac{\partial V_o^{(1)}}{\partial \rho} h + \frac{\partial^2 V_o^{(1)}}{\partial \rho^2} \frac{h^2}{2} - \cdots \\ V_6 &= V_o - \frac{\partial V_o^{(1)}}{\partial z} h + \frac{\partial^2 V_o^{(1)}}{\partial z^2} \frac{h^2}{2} - \cdots \end{aligned} \tag{3.124}$$

Combining Eqs. (3.111) and (3.124) leads to

$$h^2\nabla^2 V = V_1 + V_2 + 2V_6 - 4V_o - 2h\frac{\partial V_o^{(2)}}{\partial z} + \frac{h(V_1 - V_2)}{2\rho_o} = 0$$

or

$$-\frac{\partial V_o^{(2)}}{\partial z} = \frac{V_1 + V_2 + 2V_6 - 4V_o + \dfrac{h(V_1 - V_2)}{2\rho_o}}{2h} \tag{3.125}$$

But $D_{1n} = D_{2n}$ or

$$\epsilon_1 \frac{\partial V_o^{(1)}}{\partial z} = \epsilon_2 \frac{\partial V_o^{(2)}}{\partial z} \tag{3.126}$$

Substituting Eqs. (3.123) and (3.125) into Eq. (3.126) and solving for V_o yields

$$V_o = \frac{1}{4}\left(1 + \frac{h}{2\rho_o}\right)V_1 + \frac{1}{4}\left(1 - \frac{h}{2\rho_o}\right)V_2 + \frac{\epsilon_1}{2(\epsilon_1 + \epsilon_2)}V_5 + \frac{\epsilon_2}{2(\epsilon_1 + \epsilon_2)}V_6 \tag{3.127}$$

Equation (3.127) is only applicable to interface points. Notice that Eq. (3.127) becomes Eq. (3.114) if $\epsilon_1 = \epsilon_2$.

Typical examples of finite difference approximations for boundary points, written for square nets in rectangular and cylindrical systems, are tabulated in Table 3.9. For more examples, see [12, 110]. The FDTD has also been applied in solving time-varying axisymmetric problems [93, 111].

3.10.2 Spherical Coordinates

In spherical coordinates, Laplace's equation can be written as

$$\nabla^2 V = \frac{\partial^2 V}{\partial r^2} + \frac{2}{r}\frac{\partial V}{\partial r} + \frac{1}{r^2}\frac{\partial^2 V}{\partial \theta^2} + \frac{\cot\theta}{r^2}\frac{\partial V}{\partial \theta} + \frac{1}{r^2 \sin^2\theta}\frac{\partial^2 V}{\partial \phi^2} = 0 \tag{3.128}$$

At a grid point $O(r_o, \theta_o, \phi_o)$ shown in Fig. 3.37, the finite difference approximation to Eq. (3.128) is

$$\frac{V_1 - 2V_o + V_2}{(\Delta r)^2} + \frac{2}{r_o}\left(\frac{V_1 - V_2}{2\Delta r}\right) + \frac{V_6 - 2V_o + V_5}{(r_o \Delta\theta)^2} + \frac{\cot\theta_o}{r_o^2}\left(\frac{V_5 - V_6}{2\Delta\theta}\right) + \frac{V_3 - 2V_o + V_4}{(r_o \Delta\phi \sin\theta_o)^2} = 0 \tag{3.129}$$

Note that θ increases from node 6 to 5 and hence we have $V_5 - V_6$ and not $V_6 - V_5$ in Eq. (3.129).

Example 3.9

Consider an earthed metal cylindrical tank partly filled with a charge liquid, such as hydrocarbons, as illustrated in Fig. 3.38 (a). Using the finite difference method,

Table 3.9 Finite Difference Approximations at Boundary Points.

Description	Figure	Cartesian Equation	Cylindrical Equation
1. Bottom edge	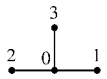	$4V_0 = V_1 + V_2 + 2V_3$	$4V_0 = V_1 + V_2 + 4V_3$
2. Top edge	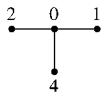	$4V_0 = V_1 + V_2 + 2V_4$	$4V_0 = V_1 + V_2 + 2V_3$
3. Left edge	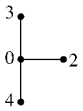	$4V_0 = 2V_1 + V_3 + V_4$	$8V_0 = 4V_1 + (\frac{2i+1}{i})V_3 + (\frac{2i-1}{i})V_4$
4. Right edge	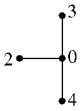	$4V_0 = 2V_1 + V_3 + V_4$	$8V_0 = 4V_2 + (\frac{2i+1}{i})V_3 + (\frac{2i-1}{i})V_4$
5. Bottom left corner point	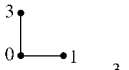	$2V_0 = V_1 + V_3$	$3V_0 = V_1 + 2V_3$
6. Bottom right corner point		$2V_0 = V_2 + V_3$	$3V_0 = V_2 + 2V_3$
7. Top left corner point	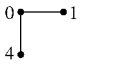	$2V_0 = V_1 + V_4$	$3V_0 = V_1 + 2V_4$
8. Top right corner point		$2V_0 = V_2 + V_4$	$3V_0 = V_2 + 2V_4$

determine the potential distribution in the entire domain. Plot the potential along $\rho = 0.5,\ 0 < z < 2$ m and on the surface of the liquid. Take

$$a = b = c = 1.0 \text{ m},$$
$$\epsilon_r = 2.0 \text{ (hydrocarbons)},$$
$$\rho_v = 10^{-5} \text{ C/m}^3 \quad \square$$

Solution The exact analytic solution to this problem was given in Section 2.7.2. ∎

It is apparent from Fig. 3.38 (a) and from the fact that ρ_v is uniform that $V = V(\rho, z)$ (i.e., the problem is two-dimensional) and the domain of the problem is symmetrical about the z-axis. Therefore, it is only necessary to investigate the solution region in Fig. 3.38 (b) and impose the condition that the z-axis is a flux line, i.e., $\partial V/\partial n = \partial V/\partial \rho = 0$.

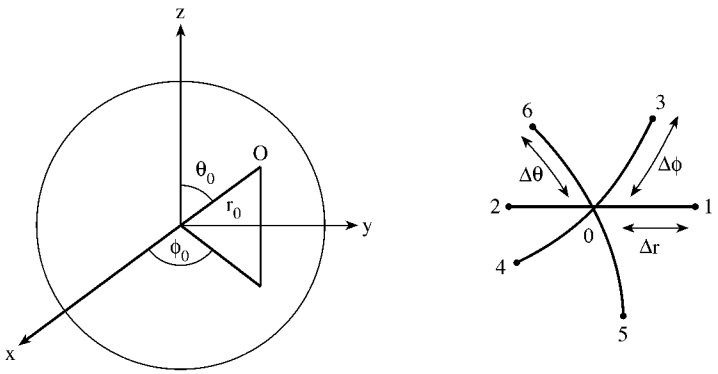

Figure 3.37
Typical node in spherical coordinates.

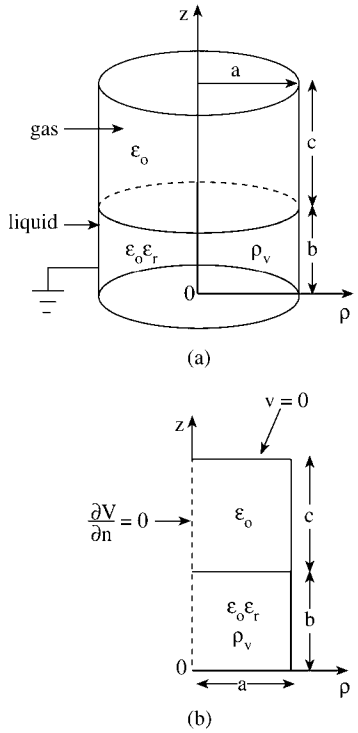

Figure 3.38
For Example 3.9: (a) earth cylindrical tank, (b) solution region.

The finite difference grid of Fig. 3.35 is used with $0 \leq i \leq I_{\max}$ and $0 \leq j \leq J_{\max}$. Choosing $\Delta\rho = \Delta z = h = 0.05$ m makes $I_{\max} = 20$ and $J_{\max} = 40$. Equation (3.115) is applied for gas space, and Eq. (3.123) for liquid space. Along the z-axis, i.e., $i = 0$, we impose the Neumann condition in Eq. (3.120). To account for the fact that the gas has dielectric constant ϵ_{r1} while the liquid has ϵ_{r2}, we impose the boundary condition in Eq. (3.127) on the liquid-gas interface.

Based on these ideas, the computer program shown in Fig. 3.39 was developed to determine the potential distribution in the entire domain. The values of the potential along $\rho = 0.5,\ 0 < z < 2$ and along the gas-liquid interface are plotted in Fig. 3.40. It is evident from the figure that the finite difference solution compares well with the exact solution in Section 2.7.2. It is the simplicity in concept and ease of programming finite difference schemes that make them very attractive for solving problems such as this.

3.11 Numerical Integration

Numerical integration (also called *numerical quadrature*) is used in science and engineering whenever a function cannot easily be integrated in closed form or when the function is described in the form of discrete data. Integration is a more stable and reliable process than differentiation. The term quadrature or integration rule will be used to indicate any formula that yields an integral approximation. Several integration rules have been developed over the years. The common ones include:

- Euler's rule,
- Trapezoidal rule,
- Simpson's rule,
- Newton-Cotes rules, and
- Gaussian (quadrature) rules.

The first three are simple and will be considered first to help build up background for other rules which are more general and accurate. A discussion on the subject of numerical integration with diverse FORTRAN codes can be found in Davis and Rabinowitz [112]. A program package called QUADPACK for automatic integration covering a wide variety of problems and various degrees of difficulty is presented in Piessens et al. [113]. Our discussion will be brief but sufficient for the purpose of this text.

```
0001    C ************************************************
0002    C  FORTRAN CODE FOR EXAMPLE 3.9
0003    C  AN AXISYMMETRIC PROBLEM OF AN EARTHED CYLINDER
0004    C  PARTIALLY FILLED WITH A CHARGED LIQUID
0005    C  SOLVED USING FINITE DIFFERENCE SCHEME
0006    C ************************************************
0007
0008          DIMENSION V(0:50,0:50)
0009          DATA  A,B,C/1.0,1.0,1.0/
0010          DATA  ER1,ER2,E0/1.0,2.0,8.854E-12/
0011
0012          H = 0.05
0013          NA = A/H ! same as Imax
0014          NB = B/H
0015          NC = C/H
0016          NBC = NB + NC  ! same as Jmax
0017          NMAX = 500   ! NO. OF ITERATIONS
0018          RHOV = 1.E-5
0019          G = -RHOV/(ER2*E0)
0020          GH2 = G*H*H
0021    C
0022    C  INITIALIZE - THIS ALSO TAKES CARE OF DIRICHLET
          CONDITIONS
0023    C
0024          DO 10 I = 0,NA
0025          DO 10 J = 0,NBC
0026          V(I,J) = 0.0
0027    10    CONTINUE
0028    C
0029    C  NOW,  APPLY FINITE DIFFERENCE SCHEME
0030    C
0031          DO 60 N = 1,NMAX
0032          DO 40 I=1,NA-1
0033          FM = FLOAT(2*I - 1)/FLOAT(2*I)
0034          FP = FLOAT(2*I + 1)/FLOAT(2*I)
0035    C    IN LIQUID
0036          DO 20 J = 1,NB-1
0037          V(I,J) = 0.25*( V(I,J-1) + V(I,J+1) + FM*V(I-1,J)
0038         &            + FP*V(I+1,J) - GH2 )
0039    20    CONTINUE
0040    C    IN GAS
0041          DO 30 J = NB+1,NBC-1
0042          V(I,J) = 0.25*( V(I,J-1) + V(I,J+1) + FM*V(I-1,J)
0043         &             + FP*V(I+1,J) )
0044    30    CONTINUE
0045    C  ALONG THE GAS-LIQUID INTERFACE
0046          V(I,NB)=V(I,NB+1)*ER1/(ER1+ER2)
                    +V(I,NB-1)*ER2/(ER1+ER2)+FM* V(I-1,NB)+FP*V(I+1,NB)
0047    40    CONTINUE
0048    C  IMPOSE NEUMANN CONDITION ALONG THE Z-AXIS
0049          DO 50 J = 1,NBC-1
0050          V(0,J) = ( 4.0*V(1,J) + V(0,J-1) + V(0,J+1) )
0051    50    CONTINUE
0052    60    CONTINUE
0053    C
0054    C  OUTPUT THE POTENTIAL ALONG RHO = 0.5, 0 < Z < 1.0
0055    C
0056          NR5=0.5/H
0057          DO 80 J = 0,NBC
0058          WRITE(6,90) J, V(NR5,J)/1000.0  ! IN kV
```

Figure 3.39
FORTRAN code for Example 3.9 ***(Continued).***

```
0059     80     CONTINUE
0060     90     FORMAT(2X,'J=',I3,3X,'V(0.5,J)=',E12.5,/)
0061     C
0062     C  OUTPUT THE POTENTIAL ON THE INTERFACE BETWEEN
            GAS-LIQUID
0063     C
0064           DO 100  I = 0,NA
0065           WRITE(6,110) I, V(I,NB)/1000.0 ! IN kV
0066     100   CONTINUE
0067     110   FORMAT(2X,'I=',I3,3X,'V(I,NB)=',E12.5,/)
0068           STOP
0069           END
```

Figure 3.39
(Cont.) **FORTRAN code for Example 3.9.**

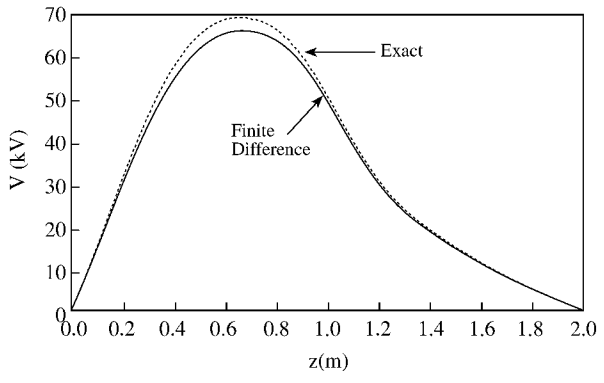

(a)

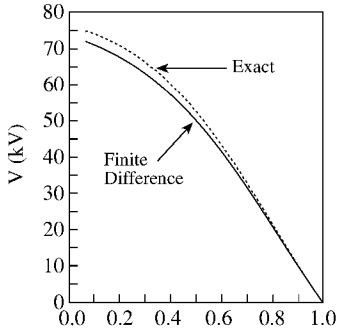

(b)

Figure 3.40
Potential distribution in the tank of Fig. 3.38: (a) along $\rho = 0.5$ m, $0 \leq z \leq 2$ m: (b) along the gas-liquid interface.

3.11.1 Euler's Rule

To apply the Euler or rectangular rule in evaluating the integral

$$I = \int_a^b f(x)\,dx\,, \tag{3.130}$$

where $f(x)$ is shown in Fig. 3.41, we seek an approximation for the area under the curve. We divide the curve into n equal intervals as shown. The subarea under the

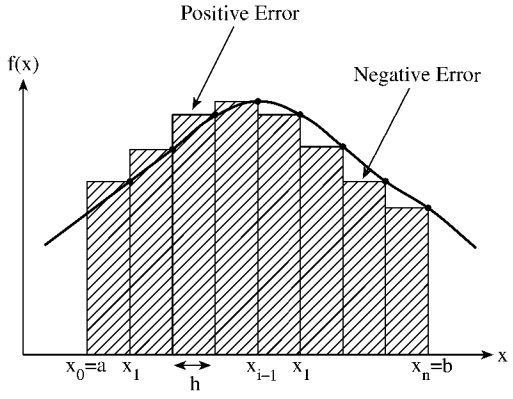

Figure 3.41
Integration using Euler's rule.

curve within $x_{i-1} < x < x_i$ is

$$A_i = \int_{x_{i-1}}^{x_i} f(x)\,dx \simeq hf_i \tag{3.131}$$

where $f_i = f(x_i)$. The total area under the curve is

$$\begin{aligned} I &= \int_a^b f(x)\,dx \simeq \sum_{i=1}^{n} A_i \\ &= h\,[f_1 + f_2 + \cdots + f_n] \end{aligned}$$

or

$$\boxed{I = h \sum_{i=1}^{n} f_i} \tag{3.132}$$

It is clear from Fig. 3.41 that this quadrature method gives an inaccurate result since each A_i is less or greater than the true area introducing negative or positive error, respectively.

3.11.2 Trapezoidal Rule

To evaluate the same integral in Eq. (3.130) using the trapezoidal rule, the subareas are chosen as shown in Fig. 3.42. For the interval $x_{i-1} < x < x_i$,

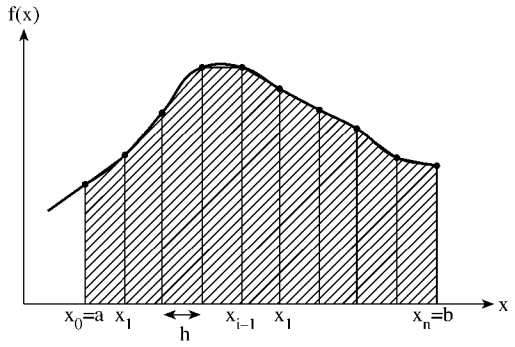

Figure 3.42
Integration using the trapezoidal rule.

$$A_i = \int_{x_{i-1}}^{x_i} f(x)\,dx \simeq \left(\frac{f_{i-1} + f_i}{2}\right) h \tag{3.133}$$

Hence

$$\begin{aligned} I &= \int_a^b f(x)\,dx \simeq \sum_{i=1}^{n} A_i \\ &= h\left[\frac{f_o + f_1}{2} + \frac{f_1 + f_2}{2} + \cdots + \frac{f_{n-2} + f_{n-1}}{2} + \frac{f_{n-1} + f_n}{2}\right] \\ &= \frac{h}{2}\left[f_o + 2f_1 + 2f_2 + \cdots + 2f_{n-1} + f_n\right] \end{aligned}$$

or

$$\boxed{I = h\sum_{i=1}^{n-1} f_i + \frac{h}{2}(f_o + f_n)} \tag{3.134}$$

3.11.3 Simpson's Rule

Simpson's rule gives a still more accurate result than the trapezoidal rule. While the trapezoidal rule approximates the curve by connecting successive points on the curve by straight lines, Simpson's rule connects successive groups of three points on the curve by a second-degree polynomial (i.e., a parabola). Thus

$$A_i = \int_{x_{i-1}}^{x_i} f(x)\,dx \simeq \frac{h}{3}(f_{i-1} + f_i + f_{i+1}) \tag{3.135}$$

Therefore

$$I = \int_a^b f(x)\,dx \simeq \sum_{i=1}^{n} A_i$$

$$\boxed{I = \frac{h}{3}\left[f_o + 4f_1 + 2f_2 + 4f_3 + \cdots + 2f_{n-2} + 4f_{n-1} + f_n\right]} \quad (3.136)$$

where n is even.

The computational molecules for Euler's, trapezoidal, and Simpson's rules are shown in Fig. 3.43. Now that we have considered simple quadrature rules to help build up background, we now consider more general, accurate methods.

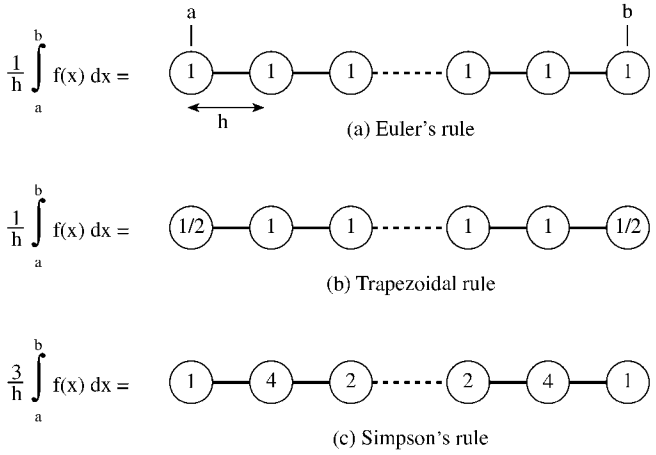

Figure 3.43
Computational molecules for integration.

3.11.4 Newton-Cotes Rules

To apply a Newton-Cotes rule to evaluate the integral in Eq. (3.130), we divide the interval $a < x < b$ into m equal intervals so that

$$h = \frac{b-a}{m} \quad (3.137)$$

where m is a multiple of n, and n is the number of intervals covered at a time or the order of the approximating polynomial. The subarea in the interval $x_{n(i-1)} < x < x_{ni}$ is

$$A_i = \int_{x_{n(i-1)}}^{x_{ni}} f(x)\,dx \simeq \frac{nh}{N}\sum_{k=0}^{n} C_k^n f\left(x_{n(i-1)+k}\right) \quad (3.138)$$

The coefficients C_k^n, $0 \le k \le n$, are called Newton-Cotes numbers and tabulated in Table 3.10. The numbers are obtained from

$$C_k^n = \frac{1}{n} \int_0^N L_k(s)\, ds \tag{3.139}$$

where

$$L_k(s) = \prod_{j=0,\, j \neq k}^{n} \frac{s-j}{k-j} \tag{3.140}$$

It is easily shown that the coefficients are symmetric, i.e.,

$$C_k^n = C_{n-k}^n \tag{3.141a}$$

and they sum up to unity, i.e.,

$$\sum_{k=0}^{n} C_k^n = 1 \tag{3.141b}$$

Table 3.10 Newton-Cotes Numbers.

n	N	NC_o^n	NC_1^n	NC_2^n	NC_3^n	NC_4^n	NC_5^n	NC_6^n	NC_7^n	NC_8^n
1	2	1	1							
2	6	1	4	1						
3	8	1	3	3	1					
4	90	7	32	12	32	7				
5	288	19	75	50	50	75	19			
6	840	41	216	27	272	27	216	41		
7	17280	751	3577	1323	2989	2989	1323	3577	751	
8	24350	989	5888	−928	10946	−4540	10946	−928	5888	989

For example, for $n = 2$,

$$C_0^2 = \frac{1}{2} \int_0^6 \frac{(s-1)(s-2)}{(-1)(-2)}\, ds = \frac{1}{6},$$

$$C_1^2 = \frac{1}{2} \int_0^6 \frac{s(s-2)}{1(-1)}\, ds = \frac{4}{6},$$

$$C_2^2 = \frac{1}{2} \int_0^6 \frac{s(s-1)}{2(1)}\, ds = \frac{1}{6}$$

Once the subareas are found using Eq. (3.138), then

$$\boxed{I = \int_a^b f(x)\, dx \simeq \sum_{i=1}^{m/n} A_i} \tag{3.142}$$

The most widely known Newton-Cotes formulas are:

$n = 1$ (2-point; trapezoidal rule)

$$A_i \simeq \frac{h}{2}(f_{i+1} + f_i) \ , \tag{3.143}$$

$n = 2$ (3-point; Simpson's 1/3 rule)

$$A_i \simeq \frac{h}{3}(f_{i-1} + 4f_i + f_{i+1}) \ , \tag{3.144}$$

$n = 3$ (4-point; Newton's rule)

$$A_i \simeq \frac{3h}{8}(f_i + 3f_{i+1} + 3f_{i+2} + f_{i+3}) \tag{3.145}$$

3.11.5 Gaussian Rules

The integration rules considered so far involve the use of equally spaced abscissa points. The idea of integration rules using unequally spaced abscissa points stems from Gauss. The Gaussian rules are more complicated but more accurate than the Newton-Cotes rules. A Gaussian rule has the general form

$$\boxed{\int_a^b f(x)\,dx \simeq \sum_{i=1}^{n} w_i f(x_i)} \tag{3.146}$$

where (a, b) is the interval for which a sequence of orthogonal polynomials $\{w_i(x)\}$ exists, x_i are the zeros of $w_i(x)$, and the weights w_i are such that Eq. (3.146) is of degree of precision $2n - 1$. Any of the orthogonal polynomials discussed in Chapter 2 can be used to give a particular Gaussian rule. Commonly used rules are Gauss-Legendre, Gauss-Chebyshev, etc., since the sample point x_i are the roots of the Legendre, Chebyshev, etc., of degree n. For the Legendre ($n = 1$ to 16) and Laguerre ($n = 1$ to 16) polynomials, the zeros x_i and weights w_i have been tabulated in [114].

Using Gauss-Legendre rule,

$$\int_a^b f(x)\,dx \simeq \frac{b-a}{2}\sum_{i=1}^{n} w_i f(u_i) \tag{3.147}$$

where $u_i = \dfrac{b-a}{2}x_i + \dfrac{b+a}{2}$ are the transformation of the roots x_i of Legendre polynomials from limits $(-1, 1)$ to finite limits (a, b). The values of the abscissas x_i and weights w_i for n up to 7 are presented in Table 3.11; for higher values of n, the interested reader is referred to [114, 115]. Note that $-1 < x_i < 1$ and $\sum_{i=1}^{n} w_i = 2$.

The Gauss-Chebyshev rule is similar to Gauss-Legendre rule. We use Eq. (3.147) except that the sample points x_i, the roots of Chebyshev polynomial $T_n(x)$, are

$$x_i = \cos\frac{(2i-1)}{2n}, \quad i = 1, 2, \ldots, n \tag{3.148}$$

Table 3.11 Abscissas (Roots of Legendre Polynomials) and Weights for Gauss-Legendre Integration

$\pm x_i$	w_i
$n = 2$	
0.57735 02691 89626	1.00000 00000 00000
$n = 3$	
0.00000 00000 00000	0.88888 88888 88889
0.77459 66692 41483	0.55555 55555 55556
$n = 4$	
0.33998 10435 84856	0.65214 51548 62546
0.86113 63115 94053	0.34785 48451 37454
$n = 5$	
0.00000 00000 00000	0.56888 88888 88889
0.53846 93101 05683	0.47862 86704 99366
0.90617 98459 38664	0.23692 68850 56189
$n = 6$	
0.23861 91860 83197	0.46791 39345 72691
0.66120 93864 66265	0.36076 15730 48139
0.93246 95142 03152	0.17132 44923 79170
$n = 7$	
0.00000 00000 00000	0.41795 91836 73469
0.40584 51513 77397	0.38183 00505 05119
0.74153 11855 99394	0.27970 53914 89277
0.94910 79123 42759	0.12948 49661 68870

and the weights are all equal [116], i.e.,

$$w_i = \frac{\pi}{n} \tag{3.149}$$

When either of the limits of integration a or b or both are $\pm\infty$, we use Gauss-Laguerre or Gauss-Hermite rule. For the Gauss-Laguerre rule,

$$\int_0^\infty f(x)\,dx \simeq \sum_{i=1}^{n} w_i f(x_i) \tag{3.150}$$

where the appropriate abscissas x_i, the roots of Laguerre polynomials, and weights w_i are listed for n up to 7 in Table 3.12. For the Gauss-Hermite rule,

$$\int_{-\infty}^\infty f(x)\,dx \simeq \sum_{i=1}^{n} w_i f(x_i) \tag{3.151}$$

where the abscissas x_i, the roots of the Hermite polynomials, and weights w_i are listed for n up to 7 in Table 3.13. An integral over (a, ∞) is taken care of by a change

of variable so that

$$\int_a^\infty f(x)\,dx = \int_0^\infty f(y+a)\,dy \tag{3.152}$$

Table 3.12 Abscissas (Roots of Laguerre Polynomials) and Weights for Gauss-Laguerre Integration.

$\pm x_i$	w_i
$n = 2$	
0.58578 64376 27	1.53332 603312
3.41421 35623 73	4.45095 733505
$n = 3$	
0.41577 45567 83	1.07769 285927
2.29428 03602 79	2.76214 296190
6.28994 50829 37	5.60109 462543
$n = 4$	
0.32254 76896 19	0.83273 912383
1.74576 11011 58	2.04810 243845
4.53662 02969 21	3.63114 630582
9.39507 09123 01	6.48714 508441
$n = 5$	
0.26356 03197 18	0.67909 404220
1.41340 30591 07	1.63848 787360
3.59642 57710 41	2.76944 324237
12.64080 08442 76	7.21918 635435
$n = 6$	
0.22284 66041 79	0.57353 550742
1.18893 21016 73	1.36925 259071
2.99273 63260 59	2.26068 459338
5.77514 35691 05	3.35052 458236
9.83746 74183 83	4.88682 680021
15.98287 39806 02	7.84901 594560
$n = 7$	
0.19304 36765 60	0.49647 759754
1.02666 48953 39	1.17764 306086
2.56787 67449 51	1.91824 978166
4.90035 30845 26	2.77184 863623
8.18215 34445 63	3.84124 912249
12.73418 02917 98	5.38067 820792
19.39572 78622 63	8.40543 248683

We apply Eq. (3.146) with $f(x)$ evaluated at points $x_i + a,\ i = 1, 2, \ldots, n$ and x_is are tabulated in Table 3.12.

Table 3.13 Abscissas (Roots of Hermite Polynomials) and Weights for Gauss-Hermite Integration.

$\pm x_i$	w_i
$n = 2$	
0.70710 67811 86548	1.46114 11826 611
$n = 3$	
0.00000 00000 00000	1.18163 59006 037
1.22474 48713 91589	1.32393 11752 136
$n = 4$	
0.52464 76232 75290	1.05996 44828 950
1.65068 01238 85785	1.24022 58176 958
$n = 5$	
0.00000 00000 00000	0.94530 87204 829
0.95857 24646 13819	0.98658 09967 514
2.02018 28704 56086	1.18148 86255 360
$n = 6$	
0.43607 74119 27617	0.87640 13344 362
1.33584 90740 13697	0.93558 05576 312
2.35060 49736 74492	1.13690 83326 745
$n = 7$	
0.00000 00000 00000	0.81026 46175 568
0.81628 78828 58965	0.82868 73032 836
1.67355 16287 67471	0.89718 46002 252
2.65196 13568 35233	1.10133 07296 103

A major drawback with Gaussian rules is that if one wishes to improve the accuracy, one must increase n which means that the values of w_i and x_i must be included in the program for each value of n. Another disadvantage is that the function $f(x)$ must be explicit since the sample points x_i are unassigned.

3.11.6 Multiple Integration

This is an extension of one-dimensional (1D) integration discussed so far. A double integral is evaluated by means of two successive applications of the rules presented above for single integral [117]. To evaluate the integral using the Newton-Cotes or Simpson's 1/3 rule ($n = 2$), for example,

$$I = \int_a^b \int_c^d f(x, y)\, dx\, dy \tag{3.153}$$

over a rectangular region $a < x < b$, $c < y < d$, we divide the region into $m \cdot l$ smaller rectangles with sides

$$h_x = \frac{b-a}{m} \tag{3.154a}$$

$$h_y = \frac{d-c}{l} \tag{3.154b}$$

where m and l are multiples of $n = 2$. The subarea

$$A_{ij} = \int_{y_{n(j-1)}}^{y_{n(j+1)}} dy \int_{x_{(i-1)}}^{x_{n(i+1)}} f(x, y)\, dy \tag{3.155}$$

is evaluated by integrating along x and then along y according to Eq. (3.140):

$$A_{ij} \simeq \frac{h_x}{3}\left(g_{j-1} + 4g_j + g_{j+1}\right) \tag{3.156}$$

where

$$g_j \simeq \frac{h_y}{3}\left(f_{i-1,j} + 4f_{i,j} + f_{i+1,j}\right) \tag{3.157}$$

Substitution of Eq. (3.157) into Eq. (3.156) yields

$$\begin{aligned} A_{ij} = \frac{h_x h_y}{9}\big[&\left(f_{i+1,j+1} + f_{i+1,j-1} + f_{i-1,j+1} + f_{i-1,j-1}\right) \\ &+ 4\left(f_{i,j+1} + f_{i,j-1} + f_{i+1,j} + f_{i-1,j}\right) + 16 f_{i,j}\big] \end{aligned} \tag{3.158}$$

The corresponding schematic or integration molecule is shown in Fig. 3.44. Summing the value of A_{ij} for all subareas yields

$$I = \sum_{i=1}^{m/n} \sum_{j=1}^{l/n} A_{ij} \tag{3.159}$$

The procedure applied in the 2D integral can be extended to a 3D integral. To evaluate

$$I = \int_a^b \int_c^d \int_e^f f(x, y, z)\, dx\, dy\, dz \tag{3.160}$$

using the $n = 2$ rule, the cuboid $a < x < b$, $c < y < d$, $e < z < f$ is divided into $m \cdot l \cdot p$ smaller cuboids of sides

$$\begin{aligned} h_x &= \frac{b-a}{m} \\ h_y &= \frac{d-c}{l} \\ h_z &= \frac{f-e}{p} \end{aligned} \tag{3.161}$$

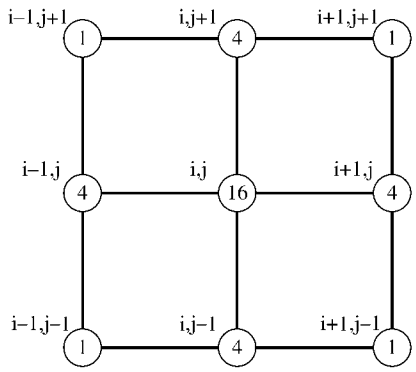

Figure 3.44
Double integration molecule for Simpson's 1/3 rule.

where m, l, and p are multiples of $n = 2$. The subvolume A_{ijk} is evaluated by integrating along x according to Eq. (3.144) to obtain

$$g_{j,k} = \frac{h_x}{3}\left(f_{i+1,j,k} + 4f_{i,j,k} + f_{i-1,j,k}\right) , \tag{3.162}$$

then along y

$$g_k = \frac{h_y}{3}\left(g_{j+1,k} + 4g_{j,k} + g_{j-1,k}\right) , \tag{3.163}$$

and finally along z to obtain

$$A_{ijk} = \frac{h_z}{3}\left(g_{k+1} + 4g_k + g_{k-1}\right) \tag{3.164}$$

Substituting Eqs. (3.162) and (3.163) into Eq. (3.164) results in [117]

$$\begin{aligned} A_{ijk} = \frac{h_x h_y h_z}{27}\big[&\left(f_{i-1,j-1,k+1} + 4f_{i-1,j,k+1} + f_{i-1,j+1,k+1}\right) \\ &+ \left(4f_{i,j-1,k+1} + 16f_{i,j,k+1} + 4f_{i,j+1,k+1}\right) \\ &+ \left(f_{i+1,j-1,k+1} + 4f_{i+1,j,k+1} + f_{i+1,j+1,k+1}\right) \\ &+ \left(4f_{i-1,j-1,k} + 16f_{i-1,j,k} + 4f_{i-1,j+1,k}\right) \\ &+ \left(16f_{i,j-1,k} + 64f_{i,j,k} + 16f_{i,j+1,k}\right) \\ &+ \left(4f_{i+1,j-1,k} + 16f_{i+1,j,k} + 4f_{i+1,j+1,k}\right) \\ &+ \left(f_{i-1,j-1,k-1} + 4f_{i-1,j,k-1} + f_{i-1,j+1,k-1}\right) \\ &+ \left(4f_{i,j-1,k-1} + 16f_{i,j,k-1} + 4f_{i,j+1,k-1}\right) \\ &+ \left(f_{i+1,j-1,k-1} + 4f_{i+1,j,k-1} + f_{i+1,j+1,k-1}\right)\big] \end{aligned} \tag{3.165}$$

The integration molecule is portrayed in Fig. 3.45. Observe that the molecule is symmetric with respect to all planes that cut the molecule in half.

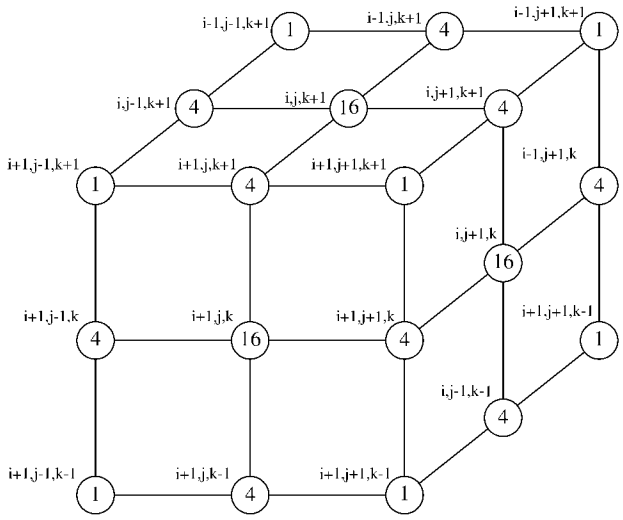

Figure 3.45
Triple integration molecule for Simpson's 1/3 rule.

Example 3.10

Write a program that uses the Newton-Cotes rule ($n = 6$) to evaluate Bessel function of order m, i.e.,

$$J_m(x) = \frac{1}{\pi} \int_0^{\pi} \cos(x \sin\theta - m\theta)\, d\theta$$

Run the program for $m = 0$ and $x = 0.1, 0.2, \ldots, 2.0$. □

Solution The computer program is shown in Fig. 3.46. The program is based on Eqs. (3.138) and (3.142). It evaluates the integral within a subinterval $\theta_{n(i-1)} < \theta < \theta_{ni}$. The summation over all the subintervals gives the required integral. The result for $m = 0$ and $0.1 < x < 2.0$ is shown in Table 3.14; the values agree up to six significant figures with those in standard tables [115, p. 390]. The program is intentionally made general so that n, the corresponding Newton-Cotes numbers, and the integrand can be changed easily. Although the integrand in Fig. 3.46 is real, the program can be modified for complex integrand by simply declaring complex the affected variables. ■

```
0001
0002    C   ********************************************************
0003    C   INTEGRATION BY NEWTON-COTES RULE (N=6)
0004    C
0005    C   A, B = ARE THE INTEGRATION LIMITS
0006    C   SUM  = THE RESULT OF THE INTEGRATION
0007    C   THE FUNCTION TO BE INTEGRATED MUST BE DEFINED IN
0008    C   A SUBPROGRAM FUNCTION FUN(ARGUMENTS)
0009    C
0010    C   SPECIFICALLY, THIS PROGRAM EVALUATES BESSEL FUNCTION
0011    C   JN(X), OF ORDER N AND ARGUMENT X
0012    C   ********************************************************
0013
0014          DATA  PIE/3.1415927/
0015
0016          A=0.0
0017          B=PIE
0018          N=4
0019          DO 20 I=1,20
0020          X=0.1*FLOAT(I)
0021          CALL INTEGRATION(A,B,N,X,SUM)
0022          WRITE(6,10) X,SUM
0023          PRINT *,X,SUM
0024    10    FORMAT(2X,'X = ',F6.3,2X,'JO = ',E20.12,/)
0025    20    CONTINUE
0026          STOP
0027          END

0001    C  ***********************************************************
0002    C      SUBROUTINE FOR INTEGRATION USING NEWTON-COTES RULE (N=6)
0003    C      A IS THE LOWER LIMIT OF INTEGRATION
0004    C      B IS THE UPPER LIMIT OF INTEGRATION
0005    C      H IS THE INTERVAL SIZE
0006    C  ***********************************************************
0007          SUBROUTINE INTEGRATION(AA,BB,NO,X,SUM)
0008          IMPLICIT REAL(A-H,O-Z)
0009          DIMENSION  C(0:6)
0010          DATA  NC /840/
0011          DATA  ( C(I),I=0,6 )/41.,216.,27.,272.,27.,216.,41./
0012
0013    C     START COMPUTATION
0014
0015          N=6
0016          M=240   ! M MUST BE A MULTIPLE OF N
0017          H=(BB-AA)/FLOAT(M)
0018          SUM=0.0
0019          NN=M/N
0020          T=AA
0021          DO 20 I=1,NN
0022          DO 10 J=0,N
0023          A=C(J)*FUN(T,NO,X)
0024          SUM=SUM + A
0025          T=T + H
0026    10    CONTINUE
0027          T=T - H
0028    20    CONTINUE
0029          SUM=SUM*H*FLOAT(N)/FLOAT(NC)
0030          RETURN
0031          END
```

Figure 3.46
Computer program for Example 3.10 ***(Continued).***

```
0001    C  ***********************************
0002    C     THE FUNCTION TO BE INTEGRATED
0003    C  ***********************************
0004          FUNCTION FUN(THETA,N,X)
0005          DATA  PIE/3.1415927/
0006
0007          FUN = COS( X*SIN(THETA) - FLOAT(N)*THETA )/PIE
0008          RETURN
0009          END
```

Figure 3.46
(Cont.) **Computer program for Example 3.10.**

Table 3.14 Result of the Program in Fig. 3.45 for $m = 0$.

x	$J_0(x)$
0.1	0.9975015
0.2	0.9900251
0.3	0.9776263
0.4	0.9603984
0.5	0.9384694
⋮	⋮
1.5	0.5118274
1.6	0.4554018
1.7	0.3979859
1.8	0.3399859
1.9	0.2818182
2.0	0.2238902

3.12 Concluding Remarks

Only a brief treatment of the finite difference analysis of PDEs is given here. There are many valuable references on the subject which answer many of the questions left unanswered here [3]–[8], [10, 104, 105]. The book by Smith [5] gives an excellent exposition with numerous examples. The problems of stability and convergence of finite difference solutions are further discussed in [118, 119], while the error estimates in [120].

As noted in Section 3.8, the finite difference method has some inherent advantages and disadvantages. It is conceptually simple and easy to program. The finite difference approximation to a given PDE is by no means unique; more accurate expressions can be obtained by employing more elaborate and complicated formulas. However, the relatively simple approximations may be employed to yield solutions

of any specified accuracy simply by reducing the mesh size provided that the criteria for stability and convergence are met.

A very important difficulty in finite differencing of PDEs, especially parabolic and hyperbolic types, is that if one value of Φ is not calculated and therefore set equal to zero by mistake, the solution may become unstable. For example, in finding the difference between $\Phi_i = 1000$ and $\Phi_{i+1} = 1002$, if Φ_{i+1} is set equal to zero by mistake, the difference of 1000 instead of 2 may cause instability. To guard against such error, care must be taken to ensure that Φ is calculated at every point, particularly at boundary points.

A serious limitation of the finite difference method is that interpolation of some kind must be used to determine solutions at points not on the grid. Suppose we want to find Φ at a point P which is not on the grid, as in Fig. 3.47. Assuming Φ is known at the four grid points surrounding P, at a distance x_o along the bottom edge of the rectangle in Fig. 3.47,

$$\Phi_b = \frac{x_o}{\Delta x}[\Phi(i+1, j) - \Phi(i, j)] + \Phi(i, j) \tag{3.166}$$

At a distance x_o along the top edge,

$$\Phi_t = \frac{x_o}{\Delta x}[\Phi(i+1, j+1) - \Phi(i, j+1)] + \Phi(i, j+1) \tag{3.167}$$

The value of Φ at P is estimated by combining Eqs. (3.166) and (3.167), i.e.,

$$\Phi_P = \frac{y_o}{\Delta y}(\Phi_t - \Phi_b) + \Phi_b \tag{3.168}$$

One obvious way to avoid interpolation is to use a finer grid if possible.

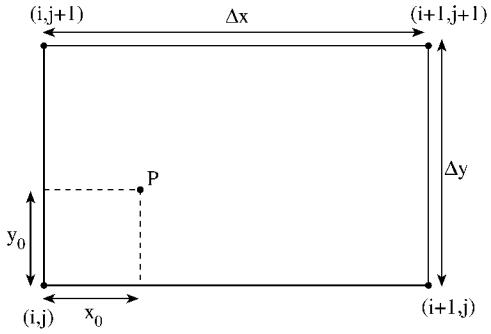

Figure 3.47
Evaluating Φ at a point P not on the grid.

References

[1] L.D. Kovach, *Boundary-value Problems.* Reading, MA: Addison-Wesley, 1984, pp. 355–379.

[2] A. Thom and C.J. Apelt, *Field Computations in Engineering and Physics.* London: D. Van Nostrand, 1961, p. v.

[3] R.D. Richtmyer and K.W. Morton, *Difference Methods for Initial-value Problems,* 2nd ed. New York: Interscience Publ., 1976, pp. 185–193.

[4] D. Potter, *Computational Physics.* London: John Wiley, 1973, pp. 40–79.

[5] G.D. Smith, *Numerical Solution of Partial Differential Equations: Finite Difference Methods,* 3rd ed., Oxford Univ. Press, New York, 1985.

[6] J.H. Ferziger, *Numerical Methods for Engineering Application.* New York: John Wiley, 1981.

[7] L. Lapidus and G.F. Pinder, *Numerical Solution of Partial Differential Equations in Science and Engineering.* New York: John Wiley, 1982, pp. 166–185.

[8] V. Vemuri and W.J. Karplus, *Digital Computer Treatment of Partial Differential Equations.* Englewood Cliffs, NJ: Prentice-Hall, 1981, pp. 88–92.

[9] A. Wexler, " Computation of electromagnetic fields," *IEEE Trans. Micro. Theo. Tech.,* vol. MTT-17, no. 8, Aug. 1969, pp. 416–439.

[10] G. de Vahl Davis, *Numerical Methods in Engineering and Science.* London: Allen & Unwin, 1986.

[11] Special issue of IEEE Transactions on Microwave Theory and Techniques, vol. MTT-17, no. 8, Aug. 1969 on "Computer-oriented microwave practices" covers various applications of finite difference methods to EM problems.

[12] H.E. Green, "The numerical solution of some important transmission-line problems," *IEEE Trans. Micro. Theo. Tech.,* vol. MTT-13, no. 5, Sept. 1965, pp. 676–692.

[13] M.N.O. Sadiku, "Finite difference solution of electrodynamic problems," *Int. Jour. Elect. Engr. Educ.,* vol. 28, April 1991, pp. 107–122.

[14] M.F. Iskander, "A new course on computational methods in electromagnetics," *IEEE Trans. Educ.,* vol. 31, no. 2, May 1988, pp. 101–115.

[15] W.S. Metcalf, "Characteristic impedance of rectangular transmission lines," *Proc. IEE,* vol. 112, no. 11, Nov. 1965, pp. 2033–2039.

[16] M.V. Schneider, "Computation of impedance and attenuation of TEM-lines by finite difference methods," *IEEE Micro. Theo. Tech.*, vol. MTT-13, no. 6, Nov. 1965, pp. 793–800.

[17] M. Sendaula, M. Sadiku, and R. Heiman, "Crosstalk computation in coupled transmission lines," *Proc. IEEE Southeastcon,* April 1991, pp. 790–795.

[18] A.R. Djordjevic, et al., "Time-domain response of multiconductor transmission lines," *Proc. IEEE,* vol. 75, no. 6, June 1987, pp. 743–764.

[19] R.R. Gupta, "Accurate impedance determination of coupled TEM conductors," *IEEE Trans. Micro. Theo. Tech.*, vol. MTT-17, no. 12, Aug. 1969, pp. 479–489.

[20] E. Yamashita, et al., "Characterization method and simple design formulas of MDS lines proposed for MMIC's," *IEEE Trans. Micro. Theo. Tech.*, vol. MTT-35, no. 12, Dec. 1987, pp. 1355–1362.

[21] J.R. Molberg and D.K. Reynolds, "Iterative solutions of the scalar Helmholtz equations in lossy regions," *IEEE Trans. Micro. Theo. Tech.*, vol. MTT-17, no. 8, Aug. 1969, pp. 460–477.

[22] J.B. Davies and C.A. Muilwyk, "Numerical solution of uniform hollow waveguides with boundaries of arbitrary shape," *Proc. IEEE,* vol. 113, no. 2, Feb. 1966, pp. 277–284.

[23] J.S. Hornsby and A. Gopinath, "Numerical analysis of a dielectric-loaded waveguide with a microstrip line—finite-difference methods," *IEEE Trans. Micro. Theo. Tech.*, vol. MTT-17, no. 9, Sept. 1969, pp. 684–690.

[24] M.J. Beubien and A. Wexler, "An accurate finite-difference method for higher-order waveguide modes," *IEEE Trans. Micro. Theo. Tech.*, vol. MTT-16, no. 12, Dec. 1968, pp. 1007–1017.

[25] C.A. Muilwyk and J.B. Davies, "The numerical solution of rectangular waveguide junctions and discontinuities of arbitrary cross section," *IEEE Trans. Micro. Theo. Tech.*, vol. MTT-15, no. 8, Aug. 1967, pp. 450–455.

[26] J.H. Collins and P. Daly, "Calculations for guided electromagnetic waves using finite-difference methods," *J. Electronics & Control,* vol. 14, 1963, pp. 361–380.

[27] T. Itoh (ed.), *Numerical Techniques for Microwaves and Millimeterwave Passive Structures*. New York: John Wiley, 1989.

[28] D.H. Sinnott, et al., "The finite difference solution of microwave circuit problems," *IEEE Trans. Micro. Theo. Tech.*, vol. MTT-17, no. 8, Aug. 1969, pp. 464–478.

[29] W.K. Gwarek, "Analysis of an arbitrarily-shaped planar circuit—a time-domain approach," *IEEE Trans. Micro. Theo. Tech.*, vol. MTT-33, no. 10, Oct. 1985, pp. 1067–1072.

[30] M. De Pourceq, "Field and power-density calculations in closed microwave systems by three-dimensional finite differences," *IEEE Proc.*, vol. 132, Pt. H, no. 6, Oct. 1985, pp. 360–368.

[31] A. Taflove and K.R. Umashankar, "Solution of complex electromagnetic penetration and scattering problems in unbounded regions," in A.J. Kalinowski (ed.), *Computational Methods for Infinite Domain Media-structure Interaction*. Washington, DC: ASME, vol. 46, 1981, pp. 83–113.

[32] A. Taflove, "Application of the finite-difference time-domain method to sinusoidal steady-state electromagnetic-penetration problems," *IEEE Trans. EM Comp.*, vol. EMC-22, no. 3, Aug. 1980, pp. 191–202.

[33] K.S. Kunz and K.M. Lee, "A three-dimensional finite-difference solution of the external response of an aircraft to a complex transient EM environment" (2 parts), *IEEE Trans. EM Comp.*, vol. EMC-20, no. 2, May 1978, pp. 328–341.

[34] M.L. Oristaglio and G.W. Hohman, "Diffusion of electromagnetic fields into a two-dimensional earth: a finite-difference approach," *Geophysics*, vol. 49, no. 7, July 1984, pp. 870–894.

[35] K. Umashankar and A. Taflove, "A novel method to analyze electromagnetic scattering of complex objects," *IEEE Trans. EM Comp.*, vol. EMC-24, no. 4, Nov. 1982, pp. 397–405.

[36] R.W.M. Lau and R.J. Sheppard, "The modelling of biological systems in three dimensions using the time domain finite-difference method" (2 parts), *Phys. Med. Biol.*, vol. 31, no. 11, 1986, pp. 1247–1266.

[37] F. Sandy and J. Sage, "Use of finite difference approximations to partial differential equations for problems having boundaries at infinity," *IEEE Trans. Micro. Theo. Tech.*, May 1971, pp. 484–486.

[38] K.B. Whiting, "A treatment for boundary singularities in finite difference solutions of Laplace's equation," *IEEE Trans. Micro. Theo. Tech.*, vol. MTT-16, no. 10, Oct. 1968, pp. 889–891.

[39] G.E. Forsythe and W.R. Wasow, *Finite Difference Methods for Partial Differential Equations*. New York: John Wiley, 1960.

[40] M.L. James et al., *Applied Numerical Methods for Digital Computation*, 3rd ed. New York: Harper & Row, 1985, pp. 203–274.

[41] Y. Naiheng and R.F. Harrington, "Characteristic impedance of transmission lines with arbitrary dielectrics under the TEM approximation," *IEEE Trans. Micro. Theo. Tech.*, vol. MTT-34, no. 4, April 1986, pp. 472–475.

[42] K.S. Yee, "Numerical solution of initial boundary-value problems involving Maxwell's equations in isotropic media," *IEEE Trans. Ant. Prop.*, vol. AP-14, May 1966, pp. 302–307.

[43] A. Taflove and M.E. Brodwin, "Numerical solution of steady-state electromagnetic scattering problems using the time-dependent Maxwell's equations," *IEEE Micro. Theo. Tech.*, vol. MTT-23, no. 8, Aug. 1975, pp. 623–630.

[44] A. Taflove and K. Umashankar, "A hybrid moment method/finite-difference time-domain approach to electromagnetic coupling and aperture penetration into complex geometries," *IEEE Trans. Ant. Prop.*, vol. AP-30, no. 4, July 1982, pp. 617–627. Also in B. J. Strait (ed.), *Applications of the Method of Moments to Electromagnetic Fields*. Orlando, FL: SCEE Press, Feb. 1980, pp. 361–426.

[45] M. Okoniewski, "Vector wave equation 2D-FDTD method for guided wave equation," *IEEE Micro. Guided Wave Lett.*, vol. 3, no. 9, Sept. 1993, pp. 307–309.

[46] A. Taflove and K.R. Umashankar, "The finite-difference time-domain method for numerical modeling of electromagnetic wave interactions," *Electromagnetics*, vol. 10, 1990, pp. 105–126.

[47] M.N.O. Sadiku, V. Bemmel, and S. Agbo, "Stability criteria for finite-difference time-domain algorithm," *Proc. IEEE Southeastcon*, April 1990, pp. 48–50.

[48] J.G. Blaschak and G.A. Kriegsmann, "A comparative study of absorbing boundary conditions," *J. Comp. Phys.*, vol. 77, 1988, pp. 109–139.

[49] G. Mux, "Absorbing boundary conditions for the finite-difference approximation of the time-domain electromagnetic-field equations," *IEEE Trans. EM Comp.*, vol. EMC-23, no. 4, Nov. 1981, pp. 377–382.

[50] R. Holland, "THREDE: A free-field EMP coupling and scattering code," *IEEE Trans. Nucl. Sci.*, vol. NS-24, no. 6, Dec. 1977, pp. 2416–2421.

[51] R.W. Ziolkowski et al., "Three-dimensional computer modeling of electromagnetic fields: a global lookback lattice truncation scheme," *J. Comp. Phy.*, vol. 50, 1983, pp. 360–408.

[52] E.R. Demarest, "A finite difference—time domain technique for modeling narrow apertures in conducting scatterers," *IEEE Trans. Ant. Prog.*, vol. AP-35, no. 7, July 1987, pp. 826–831.

[53] A. Taflove et al., "Detailed FD-TD analysis of electromagnetic fields penetrating narrow slots and lapped joints in thick conducting screens," *IEEE Trans. Ant. Prog.*, vol. 36, no. 2, Feb. 1988, pp. 24–257.

[54] H. Meskanen and O. Pekonen, "FDTD analysis of field distribution in an elevator car by using various antenna positions and orientations," *Elect. Lett.*, vol. 34, no. 6, March 1998, pp. 534–535.

[55] J.G. Maloney, G.S. Smith, and W.R. Scott, "Accurate computation of the radiation from simple antennas using the finite-difference time-domain method," *IEEE Trans. Ant. Prog.*, vol. 38, no. 7, July 1990, pp. 1059–1068.

[56] J.G. Maloney and Smith, "The efficient modeling of thin material sheets in the finite-difference time-domain (FDTD) method," *IEEE Trans. Ant. Prog.*, vol. 40, no. 3, March 1992, pp. 323–330.

[57] P.A. Tirkas and C.A. Balanis, "Finite-difference time-domain method for antenna radiation," *IEEE Trans. Ant. Prog.*, vol. 40, no. 4, March 1992, pp. 334–340.

[58] E. Thiele and A. Taflove, "FD-TD analysis of vivaldi flared horn antennas and arrays," *IEEE Trans. Ant. Prog.*, vol. 42, no. 5, May 1994, pp. 633–641.

[59] J.S. Colburn and Y. Rahmat-Samii, "Human proximity effects on circular polarized handset antennas in personal satellite communications," *IEEE Trans. Ant. Prog.*, vol. 46, no. 6, June 1998, pp. 813–820.

[60] K. Uehara and K. Kagoshima, "Rigorous analysis of microstrip phased array antennas using a new FDTD method," *Elect. Lett.*, vol. 30, no. 2, Jan. 1994, pp. 100–101.

[61] H. Klingbell, K. Beilenhoff, and H.L. Hartnagel, "FDTD full-wave analysis and modeling of dielectric and metallic losses of CPW short circuits," *IEEE Trans. Micro. Theo. Tech.*, vol. 44, no. 3, March 1996, pp. 485–487.

[62] C. Zhao and I. Awai, "Applications of the finite difference techniques to the compensated VIP 3 dB directional coupler," *IEEE Trans. Micro. Theo. Tech.*, vol. 44, no. 11, Nov. 1996, pp. 2045–2052.

[63] T. Shibata et al., "Analysis of microstrip circuits using three-dimensional full-wave electromagnetic field analysis in the time-domain." *IEEE Trans. Micro. Theo. Tech.*, vol. 36, no. 6, June 1988, pp. 1064–1070.

[64] W.K. Gwarek, "Analysis of arbitrarily shaped two-dimensional microwave circuits by finite-difference time-domain method," *IEEE Trans. Micro. Theo. Tech.*, vol. 36, no. 4, April 1988, pp. 738–744.

[65] X. Zhang, et al., "Calculation of the dispersive characteristics of microstrips by the time-domain finite-difference method," *IEEE Trans. Micro. Theo. Tech.*, vol. 36, no. 2, Feb. 1988, pp. 263–267.

[66] X. Zhang and K.K. Mei, "Time-domain finite-difference approach to the calculation of the frequency-dependent characteristics of microstrip discontinuities," *IEEE Trans. Micro. Theo. Tech.*, vol. 36, no. 12, Dec. 1988, pp. 1775–1787.

[67] R.W. Larson, "Special purpose computers for the time domain advance of Maxwell's equations," *IEEE Trans. Magnetics*, vol. 25, no. 4, July 1989, pp. 2913–2915.

[68] K.K. Mei, et al., "Conformal time domain finite difference method," *Radio Sci.*, vol. 19, no. 5, Sept./Oct. 1984, pp. 1145–1147.

[69] D.H. Choi and W.J.R. Hoefer, "The finite-difference time-domain method and its application to eigenvalue problems," *IEEE Trans. Micro. Theo. Tech.*, vol. MTT-36, no. 12, Dec. 1986, pp. 1464–1470.

[70] D.M. Sullivan, et al., "Use of the finite-difference time-domain method in calculating EM absorption in human tissues," *IEEE Trans. Biomed. Engr.*, vol. BME-34, no. 2, Feb. 1987, pp. 148–157.

[71] A.D. Tinniswood, C.M. Furse, and O.P. Gandhi, "Computations of SAR distributions for two anatomically based models of the human head using CAD files of commercial telephone and the parallelized FDTD code," *IEEE Trans. Ant. Prog.*, vol. 46, no. 6, June 1998, pp. 829–833.

[72] D. Dunn, C.M. Rappaport and A.J. Terzuoli, "FDTD verification of deep-set brain tumor hyperthermia using a spherical microwave source distribution," *IEEE Trans. Micro. Theo. Tech.*, vol. 44, no. 10, Oct. 1996, pp. 1769–1777.

[73] V. Hombach et al., "The dependence of EM energy absorption upon human head modeling at 900 MHz," *IEEE Trans. Micro. Theo. Tech.*, vol. 44, no. 10, Oct. 1996, pp. 1865–1873.

[74] O. Fujiwara and A. Kato, "Computation of SAR inside eyeball for 1.5-GHz microwave exposure using finite-difference time-domain technique," *IEICE Trans. Comm.*, vol. E77-B, no. 6, June 1994, pp. 732–737.

[75] A. Christ and H.L. Hartnagel, "Three-dimensional finite-difference method for the analysis of microwave-device embedding," *IEEE Trans. Micro. Theo. Tech.*, vol. MTT-35, no. 8, Aug. 1987, pp. 688–696.

[76] J.H. Whealton, "A 3D analysis of Maxwell's equations for cavities of arbitrary shape," *J. Comp. Phys.*, vol. 75, 1988, pp. 168–189.

[77] R. Luebbers et al., "A frequency-dependence finite-difference time-domain formulation for dispersive materials," *IEEE Trans. EMC*, vol. 32, no. 3, Aug. 1990, pp. 222–227.

[78] R. Holland, "Finite-difference time-domain (FDTD) analysis of magnetic diffusion," *IEEE Trans. EMC*, vol. 36, no. 1, Feb. 1994, pp. 32–39.

[79] A. Taflove and K.R. Umashankar, "Review of FD-TD numerical modeling of electromagnetic wave scattering and radar cross section." *Proc. IEEE*, vol. 77, no. 5, May 1989, pp. 682–699.

[80] V. Bemmel, "Time-domain finite-difference analysis of electromagnetic scattering and penetration problems," *M. Sc. Thesis*, Dept. of Electrical and Computer Engr., Florida Atlantic University, Boca Raton, Dec. 1987.

[81] D.S. Jones, *The Theory of Electromagnetism*. New York: MacMillan, 1964, pp. 450–452.

[82] J.A. Stratton, *Electromagnetic Theory.* New York: McGraw-Hill, 1941, pp. 563–573.

[83] G.A. Kriegsmann, A. Taflove, and K.R. Umashankar, "A new formulation of electromagnetic wave scattering using an on-surface radiation boundary condition approach," *IEEE Trans. Ant. Prop.,* vol. 35, no. 2, Feb. 1987, pp. 153–161.

[84] B. Zhiqiang et al., "A new finite-difference time-domain algorithm for solving Maxwell's equation," *IEEE Micro. Guided Wave Lett.,* vol. 1, no. 12, Dec. 1991, pp. 382–384.

[85] S.X.R. Vahldieck and H. Jin, "Full-wave analysis of guided wave structures using a novel 2-D FDTD," *IEEE Micro. Guided Wave Lett.,* vol. 2, no. 5, May 1992, pp. 165–167.

[86] R. Mittra and P.H. Harms, "A new finite-difference time-domain (FDTD) algorithm for efficient field computation in resonator narrow-band structures," *IEEE Micro. Guided Wave Lett.,* vol. 3, no. 9, Sept. 1993, pp. 336–318.

[87] J.B. Cole, "A high accuracy realization of the Yee algorithm using non-standard finite differences," *IEEE Trans. Micro. Theo. Tech.,* vol. 45, no. 6, June 1997, pp. 991–996.

[88] J.B. Cole, "A high accuracy FDTD algorithm to solve microwave propagation and scattering problems on a coarse grid," *IEEE Trans. Micro. Theo. Tech.,* vol. 43, no. 9, Sept. 1995, pp. 2053–2058.

[89] U. Oguz, L. Gurel, and O. Arkan, "An efficient and accurate technique for the incident-wave excitations in the FDTD method," *IEEE Trans. Micro. Theo. Tech.,* vol. 46, no. 6, June 1998, pp. 869–882.

[90] I.J. Craddock and C.J. Railton, "A new technique for the stable incorporation of static field solutions in the FDTD method for the analysis of thin wires and narrow strips," *IEEE Trans. Micro. Theo. Tech.,* vol. 46, no. 8, Aug. 1998, pp. 1091–1096.

[91] J.B. Cole et al., "Finite-difference time-domain simulations of wave propagation and scattering as a research and educational tool," *Computer in Physics,* vol. 9, no. 2, March/April 1995, pp. 235–239.

[92] P.H. Harms, J.F. Lee, and R. Mittra, "A study of the nonorthogonal FDTD method versus the conventional FDTD technique for computing resonant frequency of cylindrical cavities," *IEEE Trans. Micro. Theo. Tech.,* vol. 40, no. 4, April 1992, pp. 741–746.

[93] Y. Chen, R. Mittra, and P. Harms, "Finite-difference time-domain algorithm for solving Maxwell's equations in rotationally symmetric geometries," *IEEE Trans. Micro. Theo. Tech.,* vol. 44, no. 6, June 1996, pp. 832–839.

[94] C. Wang, B.Q. Gao, and C.P. Deng, "Q factor of a resonator by the finite difference time-domain method incorporating perturbation techniques," *Elect. Lett.*, vol. 29, no. 21, Oct. 1993, pp. 1866–1867.

[95] G. Cerri et al., "MoM-FDTD hybrid technique for analysing scattering problems," *Elect. Lett.*, vol. 34, no. 5, March 1998, pp. 438–440.

[96] A.R. Bretones, R. Mittra, and R.G. Martin, "A hybrid technique combining the method of moments in the time domain and FDTD," *IEEE Micro. Guided Wave Lett.*, vol. 8, no. 8, Aug. 1998, pp. 281–283.

[97] C.J. Railton, E.M. Daniel, and J.P. McGeehan, "Use of second order absorbing boundary conditions for the termination of planar waveguides in the FDTD method," *Elect. Lett.*, vol. 29, no. 10, May 1993, pp. 900–902.

[98] P.Y. Wang et al., "Higher order formulation of absorbing boundary conditions for finite-difference time-domain method," *Elect. Lett.*, vol. 29, no. 23, Nov. 1993, pp. 2018–2019.

[99] J.C. Olivier, "On the synthesis of exact free space absorbing boundary conditions for the finite-difference time-domain method," *IEEE Trans. Ant. Prog.*, vol. 40, no. 4, April 1992, pp. 456–460.

[100] D.S. Katz, E.T. Thiele, and A. Taflove, "Validation and extension to three dimensions of the Berenger PML absorbing boundary conditions for FD-TD meshes," *IEEE Micro. Guided Wave Lett.*, vol. 4, no. 6, Aug. 1994, pp. 268–270.

[101] J.P. Berenger, "A perfectly matched layer for the absorption of electromagnetic waves," *Jour. Comp. Phys.*, vol. 114, Aug. 1994, pp. 185–200.

[102] J.P. Berenger, "Perfectly matched layer for the FDTD solution of wave-structure interaction problems," *IEEE Trans. Ant. Prop.*, vol. 44, no. 1, Jan. 1996, pp. 110–117.

[103] D.T. Prescott and N.V. Shuley, "Reflection analysis of FDTD boundary conditions – Part I: Time-space absorbing boundaries," *IEEE Trans. Micro. Theo. Tech.*, vol. 45, no. 8, Aug. 1997, pp. 1162–1170. For Part II, see the same issue, pp. 1171–1178.

[104] A. Taflove, *Computational Electrodynamics: The Finite-Difference Time-Domain Method.* Boston, MA: Artech House, 1995, pp. 145–202.

[105] K.S. Kunz and R.J. Luebbers, *The Finite-Difference Time-Domain Method for Electromagnetic.* Boca Raton, FL: CRC Press, 1993, pp. 347–358.

[106] A. Taflove and K.R. Umashankar, "The finite-difference time-domain method for numerical modeling of electromagnetic wave interactions with arbitrary structures," in M.A. Morgan (ed.), *Finite Element and Difference Methods in Electromagnetic Scattering.* New York: Elsevier, 1990, pp. 287–373.

[107] K.K. Mei and J. Fang, "Superabsorption — a method to improve absorbing boundary conditions," *IEEE Trans. Ant. Prop.*, vol. 40, no. 9, Sept. 1992, pp. 1001–1010.

[108] M. DiStasio and W.C. McHarris, "Electrostatic problems? Relax!," *Am. J. Phys.*, vol. 47, no. 5, May 1979, pp. 440–444.

[109] M.N.O. Sadiku, "Finite difference solution of axisymmetric potential problems," *Int. J. Appl. Engr. Educ.*, vol. 6, no. 4, 1990, pp. 479–485.

[110] H.E. Green, "The numerical solution of transmission line problems," in L. Young (ed.), *Advances in Microwaves*, vol. 2. New York: Academic Press, 1967, pp. 327–393.

[111] C.D. Taylor, et al., "Electromagnetic pulse scattering in time varying inhomogeneous media," *IEEE Trans. Ant. Prog.*, vol. AP-17, no. 5, Sept. 1969, pp. 585–589.

[112] P.J. Davis and P. Rabinowitz, *Methods of Numerical Integration*. New York: Academic Press, 1975.

[113] R. Piessens, et al., *QUADPACK: A Subroutine Package for Automatic Integration*. Berlin: Springer-Verlag, 1980.

[114] *Tables of Functions and Zeros of Functions*. Washington, DC: National Bureau of Standards, Applied Mathematical Series, no. 37, 1954.

[115] M. Abramwitz and I.A. Stegun (eds.), *Handbook of Mathematical Functions*. Washington, DC: National Bureau of Standards, Applied Mathematical Series, no. 55, 1964.

[116] L.G. Kelly, *Handbook of Numerical Methods and Applications*. Reading, MA: Addison-Wesley, 1967, pp. 57–61.

[117] M.N.O. Sadiku and R. Jongakiem, "Newton-Cotes rules for triple integrals," *Proc. IEEE Southeastcon*, April 1990, pp. 471–475.

[118] B.P. Rynne, "Instabilities in time marching methods for scattering problems," *Electromagnetics*, vol. 6, no. 2, 1986, pp. 129–144.

[119] J.I. Steger and R.F. Warming, "On the convergence of certain finite-difference schemes by an inverse-matrix method," *J. Comp. Phys.*, vol. 17, 1975, pp. 103–121.

[120] D.W. Kelly, et al., "A posteriori error estimates in finite difference techniques," *J. Comp. Phys.*, vol. 74, 1988, pp. 214–232.

Problems

3.1 Show that the following finite difference approximations for Φ_x are valid:

(a) forward difference,

$$\frac{-\Phi_{i+2} + 4\Phi_{i+1} - 3\Phi_i}{2\Delta x}$$

(b) backward difference,

$$\frac{3\Phi_i - 4\Phi_{i-1} + \Phi_{i-2}}{2\Delta x}$$

(c) central difference

$$\frac{-\Phi_{i+2} + 8\Phi_{i+1} - 8\Phi_{i-1} + \Phi_{i-2}}{12\Delta x}$$

3.2 Solve the equation $\Phi_t = \Phi_{xx}$, $0 \le x \le 1$, subject to initial and boundary conditions

$$\Phi(x, 0) = \sin \pi x, \quad 0 \le x \le 1 ,$$
$$\Phi(0, t) = 0 = \Phi(1, t) \quad t > 0$$

Obtain the solution by hand calculation and use $\Delta x = 0.25$ and $r = 0.5$.

3.3 Derive the Crank-Nicholson implicit algorithm for the hyperbolic equation $\Phi_{xx} = a^2 \Phi_{yy}$, $a^2 =$ constant. Let $\Delta x = \Delta y = \Delta$.

3.4 Given a boundary-value problem defined by

$$\frac{d^2\Phi}{dx^2} = x + 1, \quad 0 < x < 1$$

subject to $\Phi(0) = 0$ and $\Phi(1) = 1$, use the finite difference method to find $\Phi(0.5)$. You may take $\Delta = 0.25$ and perform 5 iterations. Compare your result with the exact solution.

3.5 Prove that the fourth-order approximation of Laplace's equation $\Phi_{xx} + \Phi_{yy} = 0$ is

$$60\Phi(i, j) - 16\,[\Phi(i + 1, j) + \Phi(i - 1, j) + \Phi(i, j + 1) + \Phi(i, j - 1)]$$
$$+\Phi(i + 2, j) + \Phi(i - 2, j) + \Phi(i, j + 2) + \Phi(i, j - 2) = 0$$

Draw the computational molecule for the finite difference scheme.

3.6 (a) If $\Delta x \neq \Delta y$, show that for the computational molecule in Fig. 3.48 (a), Eq. (3.49) becomes

$$V_o = \frac{V_1}{2(1+\alpha)} + \frac{V_2}{2(1+\alpha)} + \frac{V_3}{2(1+1/\alpha)} + \frac{V_4}{2(1+1/\alpha)}$$

where $\alpha = (\Delta x/\Delta y)^2$.

(b) Show that for the molecule in Fig. 3.48 (b), Eq. (3.49) becomes

$$\begin{aligned} V_o = & \frac{V_1}{(1+\Delta x_1/\Delta x_2)(1+\Delta x_1 \Delta x_2/\Delta y_3 \Delta y_4)} \\ & + \frac{V_2}{(1+\Delta x_2/\Delta x_1)(1+\Delta x_1 \Delta x_2/\Delta y_3 \Delta y_4)} \\ & + \frac{V_3}{(1+\Delta y_3/\Delta y_4)(1+\Delta y_3 \Delta y_4/\Delta x_1 \Delta x_2)} \\ & + \frac{V_4}{(1+\Delta y_4/\Delta y_3)(1+\Delta y_3 \Delta y_4/\Delta x_1 \Delta x_2)} \end{aligned}$$

The molecule in Fig. 3.48 (b) is useful in treating irregular boundaries.

(c) For the nine-point molecule in Fig. 3.48 (c), show that

$$V_o = \frac{1}{8} \sum_{i=1}^{8} V_i$$

This is a more accurate difference equation than Eq. (3.49).

3.7 For a long hollow conductor with a uniform U-shape cross-section shown in Fig. 3.49, find the potential at points A, B, C, D, and E.

3.8 It is desired to solve

$$\frac{\partial^2 \Phi}{\partial x^2} + \frac{\partial^2 \Phi}{\partial y^2} + 50 = 0$$

in the square region $0 \leq x, y \leq 1$ subject to the boundary conditions $\Phi = 10$ at $x = 0, 1$, $\Phi_y = 40$ at $y = 0$, $\Phi_y = -20$ at $y = 1$.

(a) Set up a system of finite difference equations which will allow the solution to be found at $x = y = 0.25$ using $\Delta x = \Delta y = h = 0.25$. Perform three iterations.

(b) Develop a program to solve the same problem using $h = 0.05, 0.1$, and 0.2.

3.9 Modify the FORTRAN code of Fig. 3.12 to solve the following three-dimensional problem:

$$\nabla^2 V = -\rho_v/\epsilon, \qquad 0 \leq x, y, z \leq 1 \text{ meter},$$

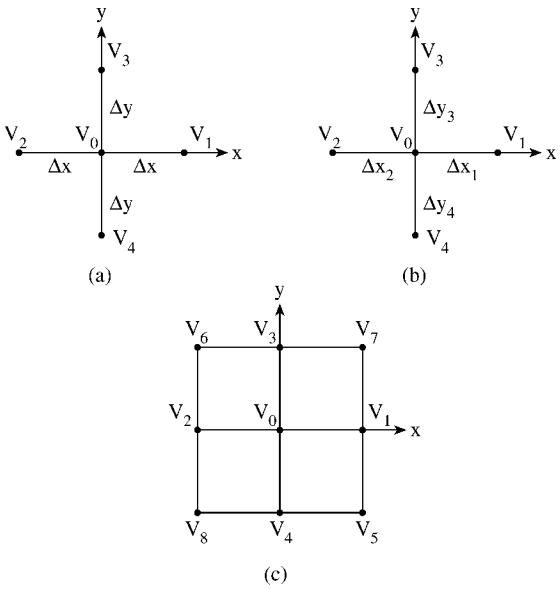

Figure 3.48
For Problem 3.6.

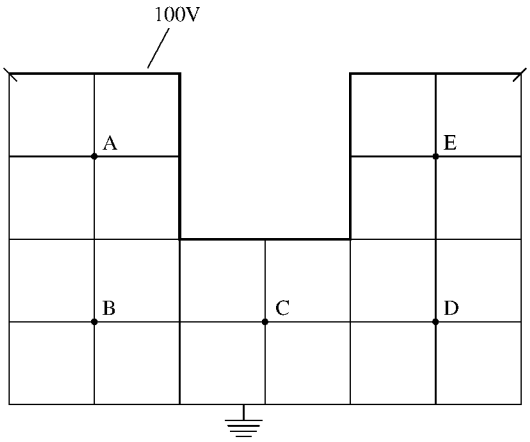

Figure 3.49
For Problem 3.7.

where $\rho_v = xyz^2 nC/m^2$ and $\epsilon = 2\epsilon_o$ subject to the boundary conditions

$$V(0, y, z) = 0 = V(1, y, z)$$
$$V(x, 0, z) = 0 = V(x, 1, z)$$
$$V(x, y, 0) = 0,\ V(x, y, 1) = V_o$$

Find the potential at the center of the cube and compare your result with the analytic solution. Take $V_o = 100$ volts.

3.10 Show that the leapfrog method applied to the parabolic equation (3.10) is unstable, whereas applying the DuFort-Frankel scheme yields an unconditionally stable solution.

3.11 The advective equation

$$\frac{\partial \Phi}{\partial t} + u\frac{\partial \Phi}{\partial x} = 0, \qquad u > 0$$

can be discretized as

$$\Phi_i^{n+1} = \Phi_i^n - r(\Phi_{i+1}^n - \Phi_{i-1}^n)\,,$$

where $r = u\Delta t/2\Delta x$. Show that the difference scheme is unstable. An alternative scheme is:

$$\Phi_{n+1} = \frac{1}{2}(\Phi_{i+1}^n + \Phi_{i-1}^n) - r(\Phi_{i+1}^n - \Phi_{i-1}^n)$$

Find the condition on r for which this scheme is stable.

3.12 The two-dimensional parabolic equation

$$\frac{\partial U}{\partial t} = \frac{\partial^2 U}{\partial x^2} + \frac{\partial^2 U}{\partial y^2}, \quad 0 \le x, y \le 1\,, \quad 1 > 0$$

is approximated by the finite difference methods:

(i) $U_{i,j}^{n+1} = [1 + r(\delta_x^2 + \delta_y^2)]U_{ij}^n$

(ii) $U_{i,j}^{n+1} = (1 + r\delta_x^2)(1 + r\delta_y^2)U_{ij}^n$ where $r = \Delta t/h^2$, $h = \Delta x = \Delta y$ and

$$\delta_x^2 U_{i,j}^n = U_{i-1,j}^n - 2U_{i,j}^n + U_{i+1,j}^n$$
$$\delta_y^2 U_{i,j}^n = U_{i,j-1}^n - 2U_{i,j}^n + U_{i,j+1}^n$$

Show that (i) is stable for $r \le 1/4$ and (ii) is stable for $r \le 1/2$

3.13 (a) The constitutive parameters of the earth allow the displacement currents to be negligibly small. In this type of medium, show that Maxwell's equations for two-dimensional TM mode, where

$$\mathbf{E}(x, y, t) = E_z \mathbf{a}_z$$

and

$$\mathbf{H}(x, y, t) = H_x \mathbf{a}_x + H_y \mathbf{a}_y \ ,$$

reduce to the diffusion equation

$$\frac{\partial^2 E}{\partial x^2} + \frac{\partial^2 E}{\partial y^2} - \mu\sigma \frac{\partial E}{\partial t} = \mu \frac{\partial J_s}{\partial t}$$

where $E = E_z$ and J_s is the source current density in the z direction.

(b) Taking $J_s = 0,\ \Delta x = \Delta y = \Delta$ and

$$\sum E_{i,j} = E^n_{i+1,j} + E^n_{i-1,j} + E^n_{i,j+1} + E^n_{i,j-1} \ ,$$

show that applying Euler, leapfrog, and DuFort-Frankel difference methods to the diffusion equation gives:

Euler:

$$E^{n+1}_{i,j} = (1 - 4r) E^n_{i,j} + r \sum E^n_{i,j} \ ,$$

Leapfrog:

$$E^{n+1}_{i,j} = E^{n-1}_{i,j} + 2r \left(\sum E^n_{i,j} - 4E^n_{i,j} \right) \ ,$$

DuFort-Frankel:

$$E^{n+1}_{i,j} = \frac{1 - 4r}{1 + 4r} E^{n-1}_{i,j} + \frac{2r}{1 + 4r} \sum E^n_{i,j}$$

where $r = \Delta t / (\sigma \mu \Delta^2)$.

(c) Analyze the stability of these finite difference schemes by substituting for $E^n_{i,j}$ a Fourier mode of the form

$$E^n_{i,j} = E(x = i\Delta, y = j\Delta, t = n\Delta t) = A_n \cos(k_x i \Delta) \cos(k_y j \Delta)$$

3.14 Yee's FD-TD algorithm for one-dimensional wave problems is given by

$$H_y^{n+1/2}(k + 1/2) = H_y^{n-1/2}(k + 1/2) + \frac{\delta t}{\mu \delta} \left[E_x^n(k) - E_x^n(k + 1) \right]$$

Determine the stability criterion for the scheme by letting

$$E_x^n(k) = A^n e^{j\beta k\delta}, \quad H_y^n(k) = \frac{A^n}{\eta} e^{j\beta k\delta} \ ,$$

where $\eta = (\mu/\epsilon)^{1/2}$ is the intrinsic impedance of the medium.

3.15 (a) The potential system in Fig. 3.50 (a) is symmetric about the y-axis. Set the initial values at free nodes equal to zero and calculate (by hand) the potential at nodes 1 to 5 for 5 or more iterations.

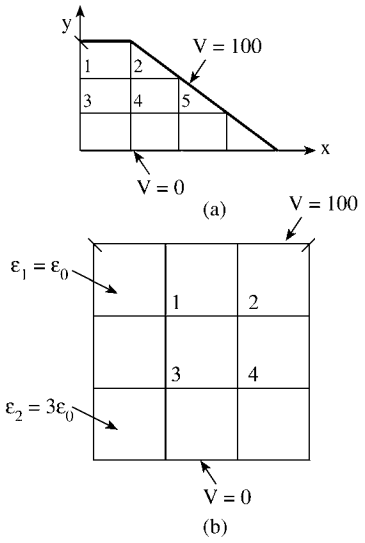

Figure 3.50
For Problem 3.15.

(b) Consider the square mesh in Fig. 3.50(b). By setting initial values at the free nodes equal to zero, find (by hand calculation) the potential at nodes 1 to 4 for 5 or more iterations.

3.16 The potential system shown in Fig. 3.51 is a quarter section of a transmission line. Using hand calculation, find the potential at nodes 1, 2, 3, 4, and 5 after 5 iterations.

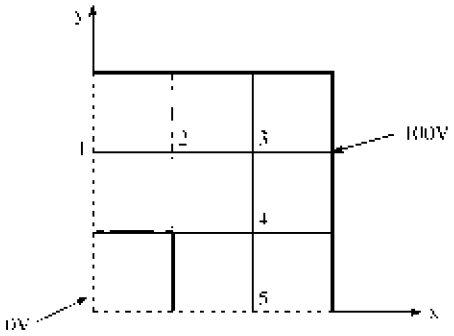

Figure 3.51
For Problem 3.16.

3.17 A transformer has its primary and secondary windings maintained at 100 and 0 V, respectively, as shown in Fig. 3.52. Assuming a square mesh of $h = 0.2$ cm,

determine the potential distribution between the windings. Find its value at (8 cm, 4 cm).

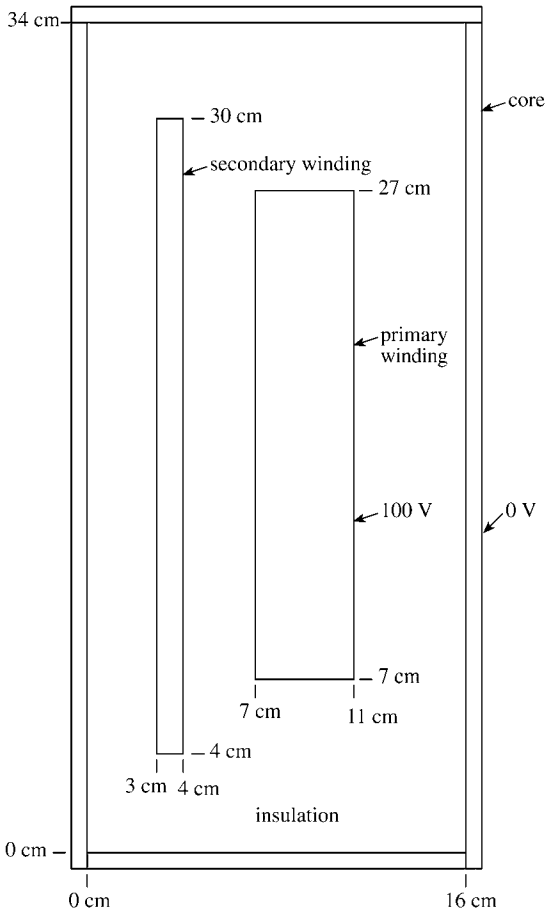

Figure 3.52
For Problem 3.17.

3.18 Modify the program in Fig. 3.21 or write your own program to calculate Z_o for the microstrip line shown in Fig. 3.53. Take $a = 2.02,\ b = 7.0,\ h = 1.0 = w,\ t = 0.01,\ \epsilon_1 = \epsilon_0,\ \epsilon_2 = 9.6\epsilon_o$.

3.19 Use the FDM to calculate the characteristic impedance of the high-frequency, air-filled rectangular transmission line shown in Fig. 3.54. Take advantage of the symmetry of the problem and consider cases for which:

(a) $B/A = 1.0,\ a/A = 1/3,\ b/B = 1/3,\ a = 1,$

(b) $B/A = 1/2,\ a/A = 1/3,\ b/B = 1/3,\ a = 1.$

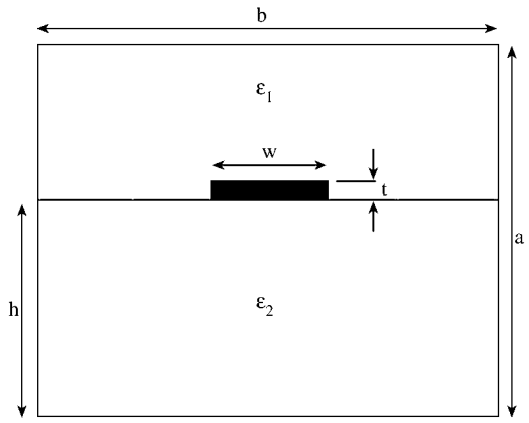

Figure 3.53
For Problem 3.18.

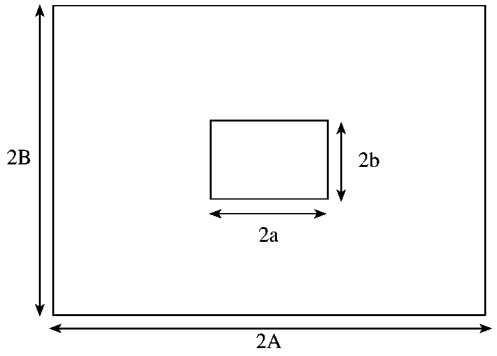

Figure 3.54
For Problem 3.19.

3.20 Figure 3.55 shows a shield microstrip line. Write a program to calculate the potential distribution within the cross-section of the line. Take $\epsilon_1 = \epsilon_o$, $\epsilon_2 = 3.5\epsilon_o$ and $h = 0.5$ mm. Find the potential at the middle of the conducting plates.

3.21 Use the FDM to determine the lowest (or dominant) cut-off wave-number k_c of the TM_{11} mode in waveguides with square $(a \times a)$ and rectangular $(a \times b,\ b = 2a)$ crosssections. Compare your results with the exact solution

$$k_c = \sqrt{(m\pi/a)^2 + (n\pi/a)^2}$$

where $m = n = 1$. Take $a = 1$.

3.22 Instead of the 5-point scheme of Eq. (3.115), use a more accurate 5-point

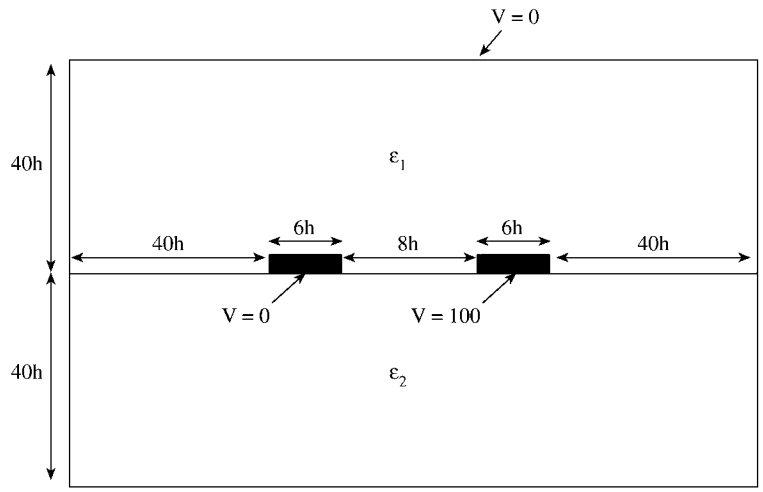

Figure 3.55
For Problem 3.20.

formula

$$2i(8i^2-5)V(i,j) = (4i^3+2i^2-4i+1)V(i+1,j) + (4i^3-2i^2-4i-1)V(i-1,j) \quad i(4i^2-1)V(i,j+1) + i(4i^2-1)V(i,j-1)$$

in Example 3.9 while other things remain the same.

3.23 For two-dimensional problems in which the field components do not vary with z coordinate ($\partial/\partial z = 0$), show that Yee's algorithm of Eqs. (3.84a)–(3.84f) becomes:

(a) for TE waves ($E_z = 0$)

$$H_z^{n+1/2}(i+1/2, j+1/2) = H_z^{n-1/2}(i+1/2, j+1/2) - \alpha\left[E_y^n(i+1, j+1/2) - E_y^n(i, j+1/2)\right] + \alpha\left[E_x^n(i+1/2, j+1) - E_x^n(i+1/2, j)\right],$$

$$E_x^{n+1}(i+1/2, j) = E_x^n(i+1/2, j) + \beta\left[H_z^{n+1/2}(i+1/2, j+1/2) - H_z^{n+1/2}(i+1/2, j-1/2)\right],$$

$$E_z^{n+1}(i, j+1/2) = \gamma E_y^n(i, j+1/2) - \beta\left[H_z^{n+1/2}(i+1/2, j+1/2) - H_z^{n+1/2}(i-1/2, j+1/2)\right];$$

(b) for TM waves ($H_z = 0$)

$$E_z^{n+1}(i, j) = \gamma E_z^n(i, j) + \beta \Big[H_y^{n+1/2}(i + 1/2, j) - H_y^{n+1/2}(i - 1/2, j) \Big] - \beta \Big[H_x^{n+1/2}(i, j + 1/2) - H_x^{n+1/2}(i, j - 1/2) \Big] ,$$

$$H_x^{n+1/2}(i, j + 1/2) = H_x^{n-1/2}(i, j + 1/2) - \alpha \big[E_z^n(i, j + 1) - E_z^n(i, j) \big] ,$$

$$H_y^{n+1/2}(i + 1/2, j) = H_y^{n-1/2}(i + 1/2, j) + \alpha \big[E_z^n(i + 1, j) - E_z^n(i, j) \big] ,$$

where

$$\alpha = \frac{\delta t}{\mu \delta} , \quad \beta = \frac{\delta t}{\epsilon \delta} , \quad \gamma = 1 - \frac{\sigma \delta t}{\epsilon} ,$$

and $\delta = \Delta x = \Delta y$.

3.24 Consider the diffraction/scattering of an incident TM wave by a perfectly conducting square of side $4a$. The conducting obstacle occupies $17 < i < 49, 33 < j < 65$, while artificial boundaries are placed at $i = 1, 81$, $j = 0.5, 97.5$ as shown in Fig. 3.56. Assume an incident wave with only E_z and H_y components given by

$$E_z = \begin{cases} \sin \pi\theta, & 0 < \theta < 1 \\ 0, & \text{otherwise} \end{cases}$$

$$H_y = \frac{1}{\eta_o} E_z$$

where $\eta_o = 120\pi\,\Omega$, $\theta = \frac{(x - 50a + ct)}{8a}$, $\Delta x = \Delta y = a/8$, $\Delta t = c\Delta x = a/16$. Write a program that applies the algorithm in Problem 3.23 (b). Assume "hard lattice truncation conditions" at the artificial boundaries shown in Fig. 3.56 and reproduce Yee's result [42] in his figure 3.

3.25 Repeat the previous problem but assume "soft lattice truncation conditions" of Eqs. (3.87) to (3.89a)–(3.89l) at the artificial boundaries.

3.26 In cylindrical coordinates with the vector magnetic potential $\mathbf{A} = A_z(\rho, \phi)\mathbf{a}_z$, Laplace's equation is

$$\nabla^2 A_z = -\mu J_z$$

Obtain the finite difference equivalent.

3.27 Consider the finite cylindrical conductor held at $V = 100$ volts and enclosed in a larger grounded cylinder as in Fig. 3.57. Such a deceptively simple

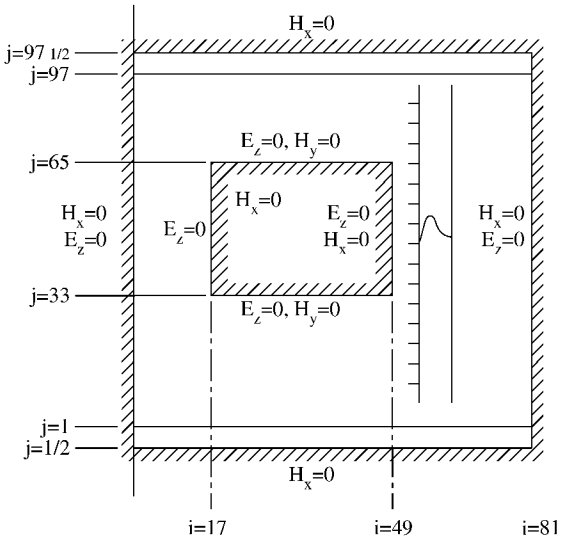

Figure 3.56
For Problem 3.24.

looking problem is beyond closed form solution, but by employing finite difference techniques, the problem can be solved without much effort. Using the finite difference method, write a program that determines the potential distribution in the axisymmetric solution region. Output the potential at $(\rho, z) = (2, 10)$, $(5, 10)$, $(8, 10)$, $(5, 2)$, and $(5, 18)$.

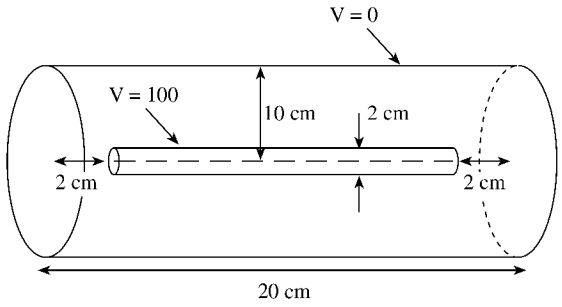

Figure 3.57
For Problem 3.27.

3.28 The problem in Fig. 3.58 is a prototype of an electrostatic particle focusing system which is employed in a recoil-mass time-of-flight spectrometer. Write a program to determine the potential distribution in the system. The problem is similar to the previous problem except that the outer conductor

abruptly expands radius by a factor of 2. Output the potential at $(\rho, z) = (5, 18)$, $(5, 10)$, $(5, 2)$, $(10, 2)$, and $(15, 2)$.

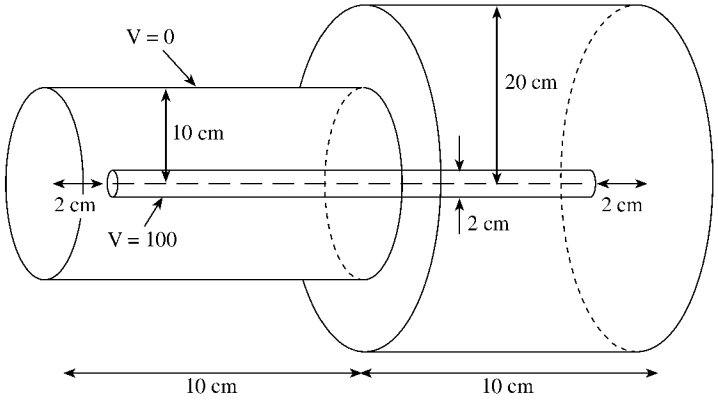

Figure 3.58
For Problem 3.28.

3.29 For axisymmetric problems (no variation with respect to ϕ), show that Yee's algorithm for TM waves can be written as

$$H_\phi^{n+1}(i, j) = H_\phi^n(i, j) + \alpha\left[E_z^{n+1/2}(i, j + 1/2) - E_z^{n+1/2}(i, j - 1/2)\right] - \alpha\left[E_\rho^{n+1/2}(i + 1/2, j) - E_\rho^{n+1/2}(i - 1/2, j)\right]$$

$$E_z^{n+3/2}(i, j + 1/2) = \gamma E_z^{n+1/2}(i, j + 1/2) + \beta\left[\frac{1}{j}H_\phi^{n+1}(i, j + 1/2) + H_\phi^{n+1}(i, j + 1) - H_\phi^{n+1}(i, j)\right],$$

$$E_\rho^{n+3/2}(i + 1/2, j) = \gamma E_\rho^{n+1/2}(i + 1/2, j) - \beta\left[H_\phi^{n+1}(i + 1, j) - H_\phi^{n+1}(i, j)\right],$$

where

$$\alpha = \frac{\delta t}{\mu\delta}, \quad \beta = \frac{\delta t}{\epsilon\delta}, \quad \gamma = 1 - \frac{\sigma\delta t}{\epsilon}, \quad \delta = \Delta\rho = \Delta z,$$

and $H_\phi(z, \rho, t) = H_\phi(z = i\Delta z, \rho = (j - 1/2)\Delta\rho, t = n\delta t) = H_\phi^n(i, j)$.

3.30 (a) Show that the finite difference discretization of Mur's ABC for two-dimensional problem

$$\frac{\partial E_z}{\partial x} - \frac{1}{c_o}\frac{\partial E_z}{\partial t} - \frac{c_o\mu_o}{2}\frac{\partial H_x}{\partial y} = 0$$

at the boundary $x = 0$ is

$$E_z^{n+1}(0, j) = E_z^n(i, j) + \frac{c_o\delta t - \delta}{c_o\delta t + \delta}\left[E_z^{n+1}(i, j) - E_z^n(0, j)\right]$$
$$- \frac{\mu_o c_o}{2(c_o\delta t + \delta)}\left[H_x^{n+1/2}(0, j + 1/2) - H_x^{n+1/2}(0, j - 1/2)\right.$$
$$\left. + H_x^{n+1/2}(1, j + 1/2) - H_x^{n+1/2}(1, j - 1/2)\right]$$

where c_o is the velocity of wave propagation.

(b) Discretize the first-order boundary condition

$$\frac{\partial E_z}{\partial x} - \frac{1}{c_o}\frac{\partial E_z}{\partial t} = 0$$

at $x = 0$.

3.31 For a three-dimensional problem, the PML modification of Maxwell's equations yields 12 equations because all the six Cartesian field components split. Obtain the 12 resulting equations.

3.32 (a) In a PML region, E_z is split into E_{zx} and E_{zy} for the TM case. Show that Maxwell's equation becomes

$$\epsilon_o\frac{\partial E_{zx}}{\partial t} + \sigma_x E_{zx} = \frac{\partial H_y}{\partial x}$$
$$\epsilon_o\frac{\partial E_{zy}}{\partial t} + \sigma_y E_{zy} = -\frac{\partial H_x}{\partial y}$$
$$\mu_o\frac{\partial H_x}{\partial t} + \sigma_y^* H_x = -\frac{\partial}{\partial y}(E_{zx} + E_{zy})$$
$$\mu_o\frac{\partial H_y}{\partial t} + \sigma_x^* H_y = \frac{\partial}{\partial x}(E_{zx} + E_{zy})$$

3.33 An FDTD equation for a PML region is given by

$$H_z^{n+1/2}(i + 1/2, k) = H_z^{n-1/2}(i + 1/2, k)$$
$$- \frac{\delta t}{\mu\delta}\left[E_{yx}^n(i + 1, k) + E_{yz}^n(i + 1, k) - E_{yx}(i, k) - E_{yz}^n(i, k)\right]$$

where δ, δt, n, i, and k have their usual FDTD meanings. By substituting the harmonic dependence $e^{j\omega t}e^{-jk_z z}$, show that the impedance of the PML region is

$$Z_z = \frac{E_y}{H_z} = \frac{\mu_o\delta}{\delta t}\frac{\sin(\omega\delta t/2)}{\sin(k_o\delta/2)}$$

3.34 The conventional 3-D FDTD lattice in cylindrical coordinates is shown in Fig. 3.59 (a) while its projection on the $\rho - z$ plane is in Fig. 3.59 (b). Show that by discretizing Maxwell's equation,

$$E_\rho^{n+1}(i,\, j) = \frac{(1 - \frac{\sigma\delta}{2\epsilon})}{(1 + \frac{\sigma\delta}{2\epsilon})} E_\rho^n(i,\, j) - \frac{\delta t}{\epsilon\delta} \frac{1}{(1 + \frac{\sigma\delta}{2\epsilon})} \cdot \left[H_\phi^{n+1/2}(i,\, j) - H_\phi^{n+1/2}(i,\, j-1) \right]$$

where $\delta = \Delta z = \Delta\rho$. Obtain the FDTD equations for H_ρ and H_ϕ.

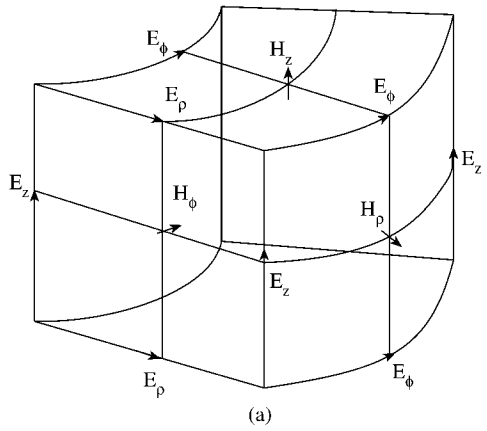

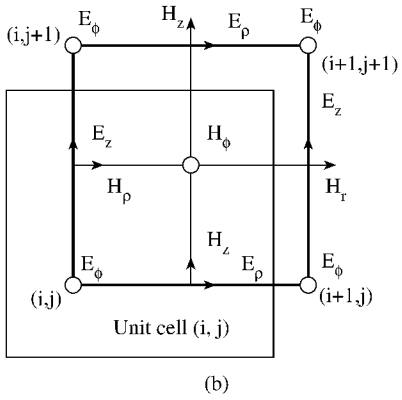

Figure 3.59

For Problem 3.34: (a) A conventional 3-D FDTD lattice in cylindrical coordinates, (b) projection of 3-D FDTD cell at $\rho - z$ plane.

3.35 Given the tabulated values of $y = \sin x$ for $x = 0.4$ to 0.52 radians in intervals of $\Delta x = 0.02$, find: (a) $\dfrac{dy}{dx}$ at $x = 0.44$, (b) $\int_{0.4}^{0.52} y\, dx$ using Simpson's rule.

x	$\sin x$
0.40	0.38942
0.42	0.40776
0.44	0.42594
0.46	0.44395
0.48	0.46178
0.50	0.47943
0.52	0.49688

3.36 (a) Use a pocket calculator to determine the approximate area under the curve $f(x) = 4 - x^2,\ 0 < x < 1$ by the trapezoidal rule with $h = 0.2$.

(b) Repeat part (a) using the Newton-Cotes rule with $n = 3$.

3.37 For a half-wave dipole, evaluating the integral

$$\int_0^{1/2} \frac{\cos^2(\frac{\pi}{2}\cos\theta)}{\sin\theta} d\theta$$

is usually required. Evaluate this integral numerically using any quadrature rule of your choice.

3.38 Compute

$$\int_0^1 e^{-x}\, dx$$

using the Newton-Cotes rule for cases $n = 2, 4$, and 6. Compare your results with exact values.

3.39 Evaluate

$$\int_0^{2\pi} x \cos 10x \sin 20x\, dx$$

(a) using the trapezoidal rule with $\Delta x = \pi/10$

(b) using Simpson's $\frac{1}{3}$-rule with $\Delta x = \pi/10$

(c) using Gaussian quadrature.

3.40 The criterion for accuracy of the numerical approximation of an integral

$$I = \int_a^b f(x)\, dx \simeq \sum_{i=0}^{\infty} a_i f(x_i)$$

is that the formula is exact for all polynomials of degree less than or equal to n. If $a = 0,\ b = 4$, and the values of $f(x)$ are available at points $x_o = 0,\ x_1 = 1,\ x_2 = 3,\ x_4 = 4$, find the values of the coefficients a_i for which the above requirement of accuracy is met.

3.41 The elliptic integral of the first type

$$F(k, \phi) = \int_0^{\phi} (1 - k^2 \sin^2 \theta)^{-1/2} d\theta$$

cannot be evaluated in a closed form. Write a program using Simpson's rule to determine $F(k, \phi)$ for $k = 0.5$ and $\phi = \pi/2$.

3.42 The following integral represents radiation from a circular aperture antenna with a constant current amplitude and phase distribution

$$I = \int_0^1 \int_o^{2\pi} e^{j\alpha\rho\cos\phi} \rho d\phi d\rho$$

Find I numerically for $\alpha = 5$ and compare your result with the exact result

$$I(\alpha) = \frac{2\pi J_1(\alpha)}{\alpha}$$

3.43 Evaluate the following double integral using the trapezoidal rule:

(a) $\displaystyle\int_0^{\pi/2} \int_0^{\pi/2} \sin(\sqrt{2xy})\, dx\, dy,$

(b) $\displaystyle\int_1^5 \int_1^5 \left[x^2 + y^2\right]^{-1/2} dx\, dy,$

(c) $\displaystyle\int_2^4 \left[\int_4^6 \ln(xy^2)\, dx\right] dy$

Chapter 4

Variational Methods

"You can do anything if you have enthusiasm. Enthusiasm is the yeast that makes your hopes rise to the stars. Enthusiasm is the spark in your eye, the swing in your gait, the grip of your hand, the irresistible surge of your will and your energy to execute your ideas. Enthusiasts are fighters; they have fortitude; they have staying qualities. Enthusiasm is at the bottom of all progress! With it, there is accomplishment. Without it, there are only alibis." Henry Ford

4.1 Introduction

In solving problems arising from mathematical physics and engineering, we find that it is often possible to replace the problem of integrating a differential equation by the equivalent problem of seeking a function that gives a minimum value of some integral. Problems of this type are called *variational problems*. The methods that allow us to reduce the problem of integrating a differential equation to the equivalent variational problem are usually called *variational methods* [1]. The variational methods form a common base for both the method of moments (MOM) and the finite element method (FEM). Therefore, it is appropriate that we study the variational methods before MOM and FEM. Besides, it is relatively easy to formulate the solution of certain differential and integral equations in variational terms. Also, variational methods give accurate results without making excessive demands on computer storage and time.

Variational methods can be classified into two groups: direct and indirect methods. The direct method is the classical Rayleigh-Ritz method, while the indirect methods are collectively referred to as the method of weighted residuals: collocation (or point-matching), subdomain, Galerkin, and least square methods. The variational solution of a given PDE using an indirect method usually involves two basic steps [2]:

- cast the PDE into variational form, and
- determine the approximate solution using one of the methods.

The literature on the theory and applications of variational methods to EM problems is quite extensive, and no attempt will be made to provide an exhaustive list of references. Numerous additional references may be found in those cited in this chapter. Owing to a lack of space, we only can hint at some of the topics usually covered in an introduction to this subject.

4.2 Operators in Linear Spaces

In this section, we will review some principles of operators in linear spaces and establish notation [2]–[5]. We define the *inner (dot* or *scalar) product* of functions u and v as

$$\boxed{\langle u, v\rangle = \int_{\Omega} uv^* \, d\Omega} \tag{4.1}$$

where * denotes the complex conjugate and the integration is performed over Ω, which may be one-, two-, or three-dimensional physical space depending on the problem. In a sense, the inner product $\langle u, v\rangle$ gives the component or projection of function u in the direction of v. If $\mathbf{u}$ and $\mathbf{v}$ are vector fields, we modify Eq. (4.1) slightly to include a dot between them, i.e.,

$$\langle \mathbf{u}, \mathbf{v}\rangle = \int_{\Omega} \mathbf{u} \cdot \mathbf{v}^* \, d\Omega \tag{4.2}$$

However, we shall consider u and v to be complex-valued scalar functions. For each pair of u and v belonging to the linear space, a number $\langle u, v\rangle$ is obtained that satisfies:

$$\boxed{\begin{aligned}
&(1) \quad \langle u, v\rangle = \langle v, u\rangle^* , && (4.3a)\\
&(2) \quad \langle \alpha u_1 + \beta u_2, v\rangle = \alpha\langle u_1, v\rangle + \beta\langle u_2, v\rangle , && (4.3b)\\
&(3) \quad \langle u, v\rangle > 0 \quad \text{if } u \neq 0 , && (4.3c)\\
&(4) \quad \langle u, v\rangle = 0 \quad \text{if } u = 0 && (4.3d)
\end{aligned}}$$

If $\langle u, v\rangle = 0$, u and v are said to be *orthogonal*. Notice that these properties mimic familiar properties of the dot product in three-dimensional space. Equation (4.3) is easily derived from Eq. (4.1). Note that from Eqs. (4.3a) and (4.3b),

$$\langle u, \alpha v\rangle = \alpha^*\langle v, u\rangle^* = \alpha^*\langle u, v\rangle$$

where α is a complex scalar.

Equation (4.1) is called an *unweighted* or *standard inner product.* A *weighted inner product* is given by

$$\langle u, v\rangle = \int_{\Omega} uv^* w \, d\Omega \tag{4.4}$$

where w is a suitable weight function.

We define the norm of the function u as

$$\|u\| = \sqrt{\langle u, u\rangle} \tag{4.5}$$

The norm is a measure of the "length" or "magnitude" of the function. (As far as a field is concerned, the norm is its rms value.) A vector is said to be *normal* if its norm is 1. Since the *Schwarz inequality*

$$|\langle u, v\rangle| \leq \|u\|\|v\| \tag{4.6}$$

holds for any inner product space, the angle θ between two nonzero vectors $\mathbf{u}$ and $\mathbf{v}$ can be obtained as

$$\theta = \cos^{-1} \frac{\langle \mathbf{u}, \mathbf{v}\rangle}{\|\mathbf{u}\|\|\mathbf{v}\|} \tag{4.7}$$

We now consider the operator equation

$$\boxed{L\Phi = g} \tag{4.8}$$

where L is any linear operator, Φ is the unknown function, and g is the source function. The space spanned by all functions resulting from the operator L is

$$\langle L\Phi, g\rangle = \langle \Phi, L^a g\rangle \tag{4.9}$$

The operator L is said to be:

(1) self-adjoint if $L = L^a$, i.e, $\langle L\Phi, g\rangle = \langle \Phi, Lg\rangle$,

(2) positive definite if $\langle L\Phi, \Phi\rangle > 0$ for any $\Phi \neq 0$ in the domain of L,

(3) negative definite if $\langle L\Phi, \Phi\rangle < 0$ for any $\Phi \neq 0$ in the domain of L.

The properties of the solution of Eq. (4.8) depend strongly on the properties of the operator L. If, for example, L is positive definite, we can easily show that the solution of Φ in Eq. (4.8) is unique, i.e., Eq. (4.8) cannot have more than one solution. To do this, suppose that Φ and Ψ are two solutions to Eq. (4.8) such that $L\Phi = g$ and $L\Psi = g$. Then, by virtue of linearity of L, $f = \Phi - \Psi$ is also a solution. Therefore, $Lf = 0$. Since L is positive definite, $f = 0$ implying that $\Phi = \Psi$ and confirming the uniqueness of the solution Φ.

Example 4.1

Find the inner product of $u(x) = 1 - x$ and $v(x) = 2x$ in the interval $(0, 1)$. □

Solution
In this case, both u and v are real functions. Hence

$$\langle u, v\rangle = \langle v, u\rangle = \int_0^1 (1-x)2x\,dx$$
$$= 2\left(\frac{x^2}{2} - \frac{x^3}{3}\right)\Big|_0^1 = 0.333 \quad \blacksquare$$

Example 4.2
Show that the operator

$$L = -\nabla^2 = -\frac{\partial^2}{\partial x^2} - \frac{\partial^2}{\partial y^2}$$

is self-adjoint. □

Solution

$$\langle Lu, v\rangle = -\int_S v\nabla^2 u\,dS$$

Taking u and v to be real functions (for convenience) and applying the Green's identity

$$\oint_\ell v\frac{\partial u}{\partial n}\,dl = \int_S \nabla u\cdot\nabla v\,dS + \int_S v\nabla^2 u\,dS$$

yields

$$\langle Lu, v\rangle = \int_S \nabla u\cdot\nabla v\,dS - \oint_\ell v\frac{\partial u}{\partial n}\,dl \tag{4.10}$$

where S is bounded by ℓ and $\mathbf{n}$ is the outward normal. Similarly

$$\langle u, Lv\rangle = \int_S \nabla u\cdot\nabla v\,dS - \oint_\ell u\frac{\partial v}{\partial n}\,dl \tag{4.11}$$

The line integrals in Eqs. (4.10) and (4.11) vanish under either the homogeneous Dirichlet or Neumann boundary conditions. Under the homogeneous mixed boundary conditions, they become equal. Thus, L is self-adjoint under any one of these boundary conditions. L is also positive definite. ■

4.3 Calculus of Variations

The calculus of variations, an extension of ordinary calculus, is a discipline that is concerned primarily with the theory of maxima and minima. Here we are concerned

with seeking the extremum (minima or maxima) of an integral expression involving a function of functions or *functionals*. Whereas a function produces a number as a result of giving values to one or more independent variables, a functional produces a number that depends on the entire form of one or more functions between prescribed limits. In a sense, a functional is a measure of the function. A simple example is the inner product $\langle u, v \rangle$.

In the calculus of variation, we are interested in the necessary condition for a functional to achieve a stationary value. This necessary condition on the functional is generally in the form of a differential equation with boundary conditions on the required function.

Consider the problem of finding a function $y(x)$ such that the function

$$I(y) = \int_a^b F(x, y, y')\, dx \,, \tag{4.12a}$$

subject to the boundary conditions

$$y(a) = A, \qquad y(b) = B \,, \tag{4.12b}$$

is rendered stationary. The integrand $F(x, y, y')$ is a given function of x, y, and $y' = dy/dx$. In Eq. (4.12a), $I(y)$ is called a *functional* or *variational* (or *stationary) principle*. The problem here is finding an extremizing function $y(x)$ for which the functional $I(y)$ has an extremum. Before attacking this problem, it is necessary that we introduce the operator δ, called the *variational symbol*.

The variation δy of a function $y(x)$ is an infinitesimal change in y for a fixed value of the independent variable x, i.e., for $\delta x = 0$. The variation δy of y vanishes at points where y is prescribed (since the prescribed value cannot be varied) and it is arbitrary elsewhere (see Fig. 4.1). Due to the change in y (i.e., $y \to y + \delta y$), there

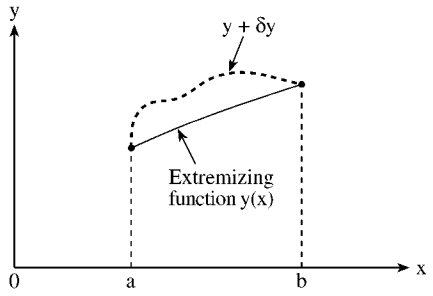

Figure 4.1
Variation of extremizing function with fixed ends.

is a corresponding change in F. The first variation of F at y is defined by

$$\delta F = \frac{\partial F}{\partial y}\delta y + \frac{\partial F}{\partial y'}\delta y' \tag{4.13}$$

This is analogous to the total differential of F,

$$dF = \frac{\partial F}{\partial x}\,dx + \frac{\partial F}{\partial y}\,dy + \frac{\partial F}{\partial y'}\,dy' \tag{4.14}$$

where $\delta x = 0$ since x does not change as y changes to $y + \delta y$. Thus, we note that the operator δ is similar to the differential operator. Therefore, if $F_1 = F_1(y)$ and $F_2 = F_2(y)$, then

$$(i) \qquad \delta\left(F_1 \pm F_2\right) = \delta F_1 \pm \delta F_2\,, \tag{4.15a}$$

$$(ii) \qquad \delta\left(F_1 F_2\right) = F_2 \delta F_1 + F_1 \delta F_2\,, \tag{4.15b}$$

$$(iii) \qquad \delta\left(\frac{F_1}{F_2}\right) = \frac{F_2 \delta F_1 - F_1 \delta F_2}{F_2^2}\,, \tag{4.15c}$$

$$(iv) \qquad \delta\left(F_1\right)^n = n\left(F_1\right)^{n-1} \delta F_1\,, \tag{4.15d}$$

$$(v) \qquad \frac{d}{dx}(\delta y) = \delta\left(\frac{dy}{dx}\right)\,, \tag{4.15e}$$

$$(vi) \qquad \delta \int_a^b y(x)\,dx = \int_a^b \delta y(x)\,dx \tag{4.15f}$$

A necessary condition for the function $I(y)$ in Eq. (4.12a) to have an extremum is that the variation vanishes, i.e.,

$$\boxed{\delta I = 0} \tag{4.16}$$

To apply this condition, we must be able to find the variation δI of I in Eq. (4.12a). To this end, let $h(x)$ be an increment in $y(x)$. For Eq. (4.12b) to be satisfied by $y(x) + h(x)$,

$$h(a) = h(b) = 0 \tag{4.17}$$

The corresponding increment in I in Eq. (4.12a) is

$$\begin{aligned}\Delta I &= I(y+h) - I(y) \\ &= \int_a^b \left[F\left(x, y+h, y'+h'\right) - F\left(x, y, y'\right)\right] dx\end{aligned}$$

On applying Taylor's expansion,

$$\begin{aligned}\Delta I &= \int_a^b \left[F_y\left(x, y, y'\right) h - F_{y'}\left(x, y, y'\right) h'\right] dx \\ &\quad + \text{higher order terms} \\ &= \delta I + O\left(h^2\right)\end{aligned}$$

where

$$\delta I = \int_a^b \left[F_y\left(x, y, y'\right) h - F_{y'}\left(x, y, y'\right) h'\right] dx$$

Integration by parts leads to

$$\delta I = \int_a^b \left[\frac{\partial F}{\partial y} - \frac{d}{dx}\left(\frac{\partial F}{\partial y'}\right) \right] h\, dx + \left. \frac{\partial F}{\partial y'} h \right|_{x=0}^{x=b}$$

The last term vanishes since $h(b) = h(a) = 0$ according to Eq. (4.17). In order that $\delta I = 0$, the integrand must vanish, i.e.,

$$\frac{\partial F}{\partial y} - \frac{d}{dx}\left(\frac{\partial F}{\partial y'}\right) = 0$$

or

$$\boxed{F_y - \frac{d}{dx} F_{y'} = 0} \tag{4.18}$$

This is called *Euler's* (or *Euler-Lagrange) equation.* Thus a necessary condition for $I(y)$ to have an extremum for a given function $y(x)$ is that $y(x)$ satisfies Euler's equation.

This idea can be extended to more general cases. In the case considered so far, we have one dependent variable y and one independent variable x, i.e., $y = y(x)$. If we have one dependent variable u and two independent variables x and y, i.e., $u = u(x, y)$, then

$$I(u) = \int_S F\left(x, y, u, u_x, u_y\right) dS \tag{4.19}$$

where $u_x = \partial u/\partial x$, $u_y = \partial u/\partial y$, and $dS = dxdy$. The functional in Eq. (4.19) is stationary when $\delta I = 0$, and it is easily shown that the corresponding Euler's equation is [6]

$$\boxed{\frac{\partial F}{\partial u} - \frac{\partial}{\partial x}\left(\frac{\partial F}{\partial u_x}\right) - \frac{\partial}{\partial y}\left(\frac{\partial F}{\partial u_y}\right) = 0} \tag{4.20}$$

Next we consider the case of two independent variables x and y and two dependent variables $u(x, y)$ and $v(x, y)$. The functional to be minimized is

$$I(u, v) = \int_S F\left(x, y, u, v, u_x, u_y, v_x, v_y\right) dS \tag{4.21}$$

The corresponding Euler's equation is

$$\boxed{\begin{aligned} &\frac{\partial F}{\partial u} - \frac{\partial}{\partial x}\left(\frac{\partial F}{\partial u_x}\right) - \frac{\partial}{\partial y}\left(\frac{\partial F}{\partial u_y}\right) = 0 \qquad (4.22a)\\ &\frac{\partial F}{\partial v} - \frac{\partial}{\partial x}\left(\frac{\partial F}{\partial v_x}\right) - \frac{\partial}{\partial y}\left(\frac{\partial F}{\partial v_y}\right) = 0 \qquad (4.22b) \end{aligned}}$$

Another case is when the functional depends on second- or higher-order derivatives. For example,

$$I(y) = \int_a^b F\left(x, y, y', y'', \ldots, y^{(n)}\right) dx \tag{4.23}$$

In this case, the corresponding Euler's equation is

$$\boxed{F_y - \frac{d}{dx}F_{y'} + \frac{d^2}{dx^2}F_{y''} - \frac{d^3}{dx^3}F_{y'''} + \cdots + (-1)^n \frac{d^n}{dx^n}F_{y^{(n)}} = 0} \tag{4.24}$$

Note that each of Euler's equations (4.18), (4.20), (4.22), and (4.24) is a differential equation.

Example 4.3

Given the functional

$$I(\Phi) = \int_S \left[\frac{1}{2}\left(\Phi_x^2 + \Phi_y^2\right) - f(x, y)\Phi\right] dxdy\,,$$

obtain the relevant Euler's equation. □

Solution

Let

$$F\left(x, y, \Phi, \Phi_x, \Phi_y\right) = \frac{1}{2}\left(\Phi_x^2 + \Phi_y^2\right) - f(x, y)\Phi$$

showing that we have two independent variables x and y and one dependent variable Φ. Hence, Euler's equation (4.20) becomes

$$-f(x, y) - \frac{\partial}{\partial x}\Phi_x - \frac{\partial}{\partial y}\Phi_y = 0$$

or

$$\Phi_{xx} + \Phi_{yy} = -f(x, y)\,,$$

i.e.,

$$\nabla^2\Phi = -f(x, y)$$

which is Poisson's equation. Thus, solving Poisson's equation is equivalent to finding Φ that extremizes the given functional $I(\Phi)$. ■

4.4 Construction of Functionals from PDEs

In the previous section, we noticed that Euler's equation produces the governing differential equation corresponding to a given functional or variational principle. Here we seek the inverse procedure of constructing a variational principle for a given differential equation. The procedure for finding the functional associated with the differential equation involves four basic steps [2, 7]:

- Multiply the operator equation $L\Phi = g$ (Euler's equation) with the variational $\delta\Phi$ of the dependent variable Φ and integrate over the domain of the problem.
- Use the divergence theorem or integration by parts to transfer the derivatives to variation $\delta\Phi$.
- Express the boundary integrals in terms of the specified boundary conditions.
- Bring the variational operator δ outside the integrals.

The procedure is best illustrated with an example. Suppose we are interested in finding the variational principle associated with the Poisson's equation

$$\nabla^2\Phi = -f(x, y) \tag{4.25}$$

which is the converse of what we did in Example 4.3. After taking step 1, we have

$$\begin{aligned}\delta I &= \iint \left[-\nabla^2\Phi - f\right]\delta\Phi\, dxdy = 0\\ &= -\iint \nabla^2\Phi\delta\Phi\, dxdy - \iint f\delta\Phi\, dxdy\end{aligned}$$

This can be evaluated by applying divergence theorem or integrating by parts. To integrate by parts, let $u = \delta\Phi, dv = \dfrac{\partial}{\partial x}\left(\dfrac{\partial\Phi}{\partial x}\right)dx$ so that $du = \dfrac{\partial}{\partial x}\delta\Phi\, dx, v = \dfrac{\partial\Phi}{\partial x}$ and

$$-\int\left[\int\frac{\partial}{\partial x}\left(\frac{\partial\Phi}{\partial x}\right)\delta\Phi\, dx\right]dy = -\int\left[\delta\Phi\frac{\partial\Phi}{\partial x} - \int\frac{\partial\Phi}{\partial x}\frac{\partial}{\partial x}\delta\Phi\, dx\right]dy$$

Thus

$$\begin{aligned}\delta I &= \iint\left[\frac{\partial\Phi}{\partial x}\frac{\partial}{\partial x}\delta\Phi + \frac{\partial\Phi}{\partial y}\frac{\partial}{\partial y}\delta\Phi - \delta f\Phi\right]dxdy\\ &\quad -\int\delta\Phi\frac{\partial\Phi}{\partial x}dy - \int\delta\Phi\frac{\partial\Phi}{\partial y}dx\\ \delta I &= \frac{\delta}{2}\iint\left[\left(\frac{\partial\Phi}{\partial x}\right)^2 + \left(\frac{\partial\Phi}{\partial y}\right)^2 - 2f\Phi\right]dxdy\\ &\quad -\delta\int\Phi\frac{\partial\Phi}{\partial x}dy - \delta\int\Phi\frac{\partial\Phi}{\partial y}dx\end{aligned} \tag{4.26}$$

The last two terms vanish if we assume either the homogeneous Dirichlet or Neumann conditions at the boundaries. Hence

$$\delta I = \delta\iint\frac{1}{2}\left[\Phi_x^2 + \Phi_y^2 - 2\Phi f\right]dxdy\,,$$

i.e.,

$$I(\Phi) = \frac{1}{2}\iint \left[\Phi_x^2 + \Phi_y^2 - 2\Phi f\right] dxdy \tag{4.27}$$

as expected.

Rather than following the four steps listed above to find the function $I(\Phi)$ corresponding to the operator equation (4.8), an alternative approach is provided by Mikhlin [1, pp. 74–78]. According to Mikhlin, if L in Eq. (4.8) is real, self-adjoint, and positive definite, the solution of Eq. (4.8) minimizes the functional

$$\boxed{I(\Phi) = \langle L\Phi, \Phi\rangle - 2\langle \Phi, g\rangle} \tag{4.28}$$

(See Prob. 4.6 for a proof.) Thus Eq. (4.27), for example, can be obtained from Eq. (4.25) by applying Eq. (4.28). This approach has been applied to derive variational solutions of integral equations [8].

Other systematic approaches for the derivation of variational principles for EM problems include Hamilton's principle or the principle of least action [9, 10], Lagrange multipliers [10]–[14], and a technique described as variational electromagnetics [15, 16]. The method of Lagrange undetermined multipliers is particularly useful for deriving a functional for a PDE whose arguments are constrained. Table 4.1 provides the variational principles for some differential equations commonly found in EM-related problems.

Table 4.1 Variational Principle Associated with Common PDEs in EM[1]

Name of equation	Partial Differential Equation (PDE)	Variational principle
Inhomogeneous wave equation	$\nabla^2\Phi + k^2\Phi = g$	$I(\Phi) = \frac{1}{2}\int_v \left[\lvert\nabla\Phi\rvert^2 - k^2\Phi^2 + 2g\Phi\right] dv$
Homogeneous wave equation	$\nabla^2\Phi + k^2\Phi = 0$	$I(\Phi) = \frac{1}{2}\int_v \left[\lvert\nabla\Phi\rvert^2 - k^2\Phi^2\right] dv$
	or	
	$\nabla^2\Phi - \frac{1}{u^2}\Phi_{tt} = 0$	$I(\Phi) = \frac{1}{2}\int^{t_o}\int_v \left[\lvert\nabla\Phi\rvert^2 - \frac{1}{u^2}\Phi_t^2\right] dv\,dt$
Diffusion equation	$\nabla^2\Phi - k\Phi_t = 0$	$I(\Phi) = \frac{1}{2}\int^{t_o}\int_v \left[\lvert\nabla\Phi\rvert^2 - k\Phi\Phi_t\right] dv\,dt$
Poisson's equation	$\nabla^2\Phi = g$	$I(\Phi) = \frac{1}{2}\int_v \left[\lvert\nabla\Phi\rvert^2 + 2g\Phi\right] dv$
Laplace's equation	$\nabla^2\Phi = 0$	$I(\Phi) = \frac{1}{2}\int_v \left[\lvert\nabla\Phi\rvert^2\right] dv$

[1] Note that $|\nabla\Phi|^2 = \nabla\Phi\cdot\nabla\Phi = \Phi_x^2 + \Phi_y^2 + \Phi_z^2$.

Example 4.4
Find the functional for the ordinary differential equation

$$y'' + y + x = 0, \qquad 0 < x < 1$$

subject to $y(0) = y(1) = 0$. □

Solution
Given that

$$\frac{d^2y}{dx^2} + y + x = 0, \qquad 0 < x < 1\,,$$

we obtain

$$\begin{aligned}\delta I &= \int_0^1 \left(\frac{d^2y}{dx^2} + y + x\right)\delta y\, dx = 0 \\ &= \int_0^1 \frac{d^2y}{dx^2}\delta y\, dx + \int_0^1 y\,\delta y\, dx + \int_0^1 x\,\delta y\, dx\end{aligned}$$

Integrating the first term by parts,

$$\delta I = \delta y\,\frac{dy}{dx}\bigg|_{x=0}^{x=1} - \int_0^1 \frac{dy}{dx}\frac{d}{dx}\delta y + \int_0^1 \frac{1}{2}\delta\left(y^2\right) dx + \delta\int_0^1 xy\, dx$$

Since y is fixed at $x = 0, 1$, $\delta y(1) = \delta y(0) = 0$. Hence

$$\begin{aligned}\delta I &= -\delta\int_0^1 \frac{1}{2}\left(\frac{dy}{dx}\right)^2 dx + \frac{1}{2}\delta\int_0^1 y^2\, dx + \delta\int_0^1 xy\, dx \\ &= \frac{\delta}{2}\int_0^1 \left[-y'^2 + y^2 + 2xy\right] dx\end{aligned}$$

or

$$I(y) = \frac{1}{2}\int_0^1 \left[-y'^2 + y^2 + 2xy\right] dx$$

Check: Taking $F(x, y, y') = y'^2 - y^2 - 2xy$, Euler's equation $F_y - \dfrac{d}{dx}F_{y'} = 0$ gives the differential equation

$$y'' + y + x = 0 \quad \blacksquare$$

4.5 Rayleigh-Ritz Method

The Rayleigh-Ritz method is the direct variational method for minimizing a given functional. It is direct in that it yields a solution to the variational problem without

recourse to the associated differential equation [17]. In other words, it is the direct application of variational principles discussed in the previous sections. The method was first presented by Rayleigh in 1877 and extended by Ritz in 1909. Without loss of generality, let the associated variational principle be

$$I(\Phi) = \int_S F\left(x, y, \Phi, \Phi_x, \Phi_y\right) dS \tag{4.29}$$

Our objective is to minimize this integral. In the Rayleigh-Ritz method, we select a linearly independent set of functions called *expansion functions* (or *basis functions)* u_n and construct an approximate solution to Eq. (4.29), satisfying some prescribed boundary conditions. The solution is in the form of a finite series

$$\widetilde{\Phi} \simeq \sum_{n=1}^{N} a_n u_n + u_o \tag{4.30}$$

where u_o meets the nonhomogeneous boundary conditions, and u_n satisfies homogeneous boundary conditions. a_n are expansion coefficients to be determined and $\widetilde{\Phi}$ is an approximate solution to Φ (the exact solution). We substitute Eq. (4.30) into Eq. (4.29) and convert the integral $I(\Phi)$ into a function of N coefficients $a_1, a_2, \ldots, a_N$, i.e.,

$$I(\Phi) = I\left(a_1, a_2, \ldots, a_N\right)$$

The minimum of this function is obtained when its partial derivatives with respect to each coefficient is zero:

$$\frac{\partial I}{\partial a_1} = 0, \quad \frac{\partial I}{\partial a_2} = 0, \ldots, \frac{\partial I}{\partial a_N} = 0$$

or

$$\boxed{\frac{\partial I}{\partial a_n} = 0, \quad n = 1, 2, \ldots, N} \tag{4.31}$$

Thus we obtain a set of N simultaneous equations. The system of linear algebraic equations obtained is solved to get a_n, which are finally substituted into the approximate solution of Eq. (4.30). In the approximate solution of Eq. (4.30), if $\widetilde{\Phi} \to \Phi$ as $N \to \infty$ in some sense, then the procedure is said to *converge* to the exact solution.

An alternative, perhaps easier, procedure to determine the expansion coefficients a_n is by solving a system of simultaneous equations obtained as follows [4, 18]. Substituting Eq. (4.30) (ignoring u_o since it can be lumped with the right-hand side of the equation) into Eq. (4.28) yields

$$\begin{aligned} I &= \left\langle \sum_{m=1}^{N} a_m L u_m, \sum_{n=1}^{N} a_n u_n \right\rangle - 2\left\langle \sum_{m=1}^{N} a_m u_m, g \right\rangle \\ &= \sum_{m=1}^{N}\sum_{n=1}^{N} \langle L u_m, u_n \rangle a_n a_m - 2\sum_{m=1}^{N} \langle u_m, g \rangle a_m \end{aligned}$$

Expanding this into powers of a_m results in

$$I = \langle Lu_m, u_m\rangle a_m^2 + \sum_{n/m}^{N} \langle Lu_m, u_n\rangle a_m a_n + \sum_{k/m}^{N} \langle Lu_k, u_m\rangle a_k a_m - 2\langle g, u_m\rangle a_m + \text{terms not containing } a_m \tag{4.32}$$

Assuming L is self-adjoint and replacing k with n in the second summation,

$$I = \langle Lu_m, u_m\rangle a_m^2 + 2\sum_{n/m}^{N} \langle Lu_m, u_n\rangle a_n a_m - 2\langle g, u_m\rangle a_m + \cdots \tag{4.33}$$

Since we are interested in selecting a_m such that I is minimized, Eq. (4.33) must satisfy Eq. (4.31). Thus differentiating Eq. (4.33) with respect to a_m and setting the result equal to zero leads to

$$\sum_{n=1}^{N} \langle Lu_m, u_n\rangle a_n = \langle g, u_m\rangle, \qquad m = 1, 2, \ldots, N \tag{4.34}$$

which can be put in matrix form as

$$\boxed{\begin{bmatrix} \langle Lu_1, u_1\rangle & \langle Lu_1, u_2\rangle & \cdots & \langle Lu_1, u_N\rangle \\ \vdots & & & \vdots \\ \langle Lu_N, u_1\rangle & \langle Lu_N, u_2\rangle & \cdots & \langle Lu_N, u_N\rangle \end{bmatrix} \begin{bmatrix} a_1 \\ \vdots \\ a_N \end{bmatrix} = \begin{bmatrix} \langle g, u_1\rangle \\ \vdots \\ \langle g, u_N\rangle \end{bmatrix}} \tag{4.35a}$$

or

$$[A][X] = [B] \tag{4.35b}$$

where $A_{mn} = \langle Lu_m, u_n\rangle$, $B_m = \langle g, u_m\rangle$, $X_n = a_n$. Solving for $[X]$ in Eq. (4.35) and substituting a_m in Eq. (4.30) gives the approximate solution $\widetilde{\Phi}$. Equation (4.35) is called the *Rayleigh-Ritz system.*

We are yet to know how the expansion functions are selected. They are selected to satisfy the prescribed boundary conditions of the problem. u_o is chosen to satisfy the inhomogeneous boundary conditions, while $u_n (n = 1, 2, \ldots, N)$ are selected to satisfy the homogeneous boundary conditions. If the prescribed boundary conditions are all homogeneous (Dirichlet conditions), $u_o = 0$. The next section will discuss more on the selection of the expansion functions.

The Rayleigh-Ritz method has two major limitations. First, the variational principle in Eq. (4.29) may not exist in some problems such as in nonself-adjoint equations (odd order derivatives). Second, it is difficult, if not impossible, to find the functions u_o satisfying the global boundary conditions for the domains with complicated geometries [19].

Example 4.5

Use the Rayleigh-Ritz method to solve the ordinary differential equation:

$$\Phi'' + 4\Phi - x^2 = 0, \qquad 0 < x < 1$$

subject to $\Phi(0) = 0 = \Phi(1)$. □

Solution

The exact solution is

$$\Phi(x) = \frac{\sin 2(1-x) - \sin 2x}{8 \sin 2} + \frac{x^2}{4} - \frac{1}{8}$$

The variational principle associated with $\Phi'' + 4\Phi - x^2 = 0$ is

$$I(\Phi) = \int_0^1 \left[(\Phi')^2 - 4\Phi^2 + 2x^2\Phi \right] dx \tag{4.36}$$

This is readily verified using Euler's equation. We let the approximate solution be

$$\widetilde{\Phi} = u_o + \sum_{n=1}^{N} a_n u_n \tag{4.37}$$

where $u_o = 0, u_n = x^n(1-x)$ since $\Phi(0) = 0 = \Phi(1)$ must be satisfied. (This choice of u_n is not unique. Other possible choices are $u_n = x(1-x^n)$ and $u_n = \sin n\pi x$. Note that each choice satisfies the prescribed boundary conditions.) Let us try different values of N, the number of expansion coefficients. We can find the expansion coefficients a_n in two ways: using the functional directly as in Eq. (4.31) or using the Rayleigh-Ritz system of Eq. (4.35).

Method 1

For $N = 1$, $\widetilde{\Phi} = a_1 u_1 = a_1 x(1-x)$. Substituting this into Eq. (4.36) gives

$$\begin{aligned} I(a_1) &= \int_0^1 \left[a_1^2(1-2x)^2 - 4a_1^2 \left(x - x^2 \right)^2 + 2a_1 x^3 (1-x) \right] dx \\ &= \frac{1}{5} a_1^2 + \frac{1}{10} a_1 \end{aligned}$$

$I(a_1)$ is minimum when

$$\frac{\partial I}{\partial a_1} = 0 \quad \rightarrow \quad \frac{2}{5} a_1 + \frac{1}{10} = 0 \quad \text{or} \quad a_1 = -\frac{1}{4}$$

Hence the quadratic approximate solution is

$$\widetilde{\Phi} = -\frac{1}{4} x(1-x) \tag{4.38}$$

For $N = 2$, $\widetilde{\Phi} = a_1 u_1 + a_2 u_2 = a_1 x(1-x) + a_2 x^2(1-x)$. Substituting $\widetilde{\Phi}$ into Eq. (4.36),

$$I(a_1, a_2) = \int_0^1 \left[\left[a_1(1-2x) + a_2\left(2x - 3x^2\right) \right]^2 - 4\left[a_1\left(x - x^2\right) + a_2\left(x^2 - x^3\right) \right]^2 + 2a_1 x^2\left(x - x^2\right) + 2a_2 x^2\left(x^2 - x^3\right) \right] dx$$

$$= \frac{1}{5}a_1^2 + \frac{2}{21}a_2^2 + \frac{1}{5}a_1 a_2 + \frac{1}{10}a_1 + \frac{1}{15}a_2$$

$$\frac{\partial I}{\partial a_1} = 0 \quad \rightarrow \quad \frac{2}{5}a_1 + \frac{1}{5}a_2 + \frac{1}{10} = 0$$

or

$$4a_1 + 2a_2 = -1 \tag{4.39a}$$

$$\frac{\partial I}{\partial a_2} = 0 \quad \rightarrow \quad \frac{4}{21}a_1 + \frac{1}{5}a_2 + \frac{1}{15} = 0$$

or

$$21a_1 + 20a_2 = -7 \tag{4.39b}$$

Solving Eq. (4.39) gives

$$a_1 = -\frac{6}{38}, \qquad a_2 = -\frac{7}{38}$$

and hence the cubic approximate solution is

$$\widetilde{\Phi} = -\frac{6}{38}x(1-x) - \frac{7}{38}x^2(1-x)$$

or

$$\widetilde{\Phi} = \frac{x}{38}\left(7x^2 - x - 6\right)$$

Method 2

We now determine a_m using Eq. (4.35). From the given differential equation,

$$L = \frac{d^2}{dx^2} + 4, \qquad g = x^2$$

Hence

$$A_{mn} = \langle Lu_m, u_n \rangle = \langle u_m, Lu_n \rangle$$

$$= \int_0^1 x^m(1-x)\left[\left(\frac{d^2}{dx^2} + 4 \right) x^n(1-x) \right] dx\,,$$

$$A_{mn} = \frac{n(n-1)}{m+n-1} - \frac{2n^2}{m+n} + \frac{n(n+1)+4}{m+n+1} - \frac{8}{m+n+2} + \frac{4}{m+n+3}\,,$$

$$B_n = \langle g, u_n \rangle = \int_0^1 x^2 n^n(1-x)\,dx = \frac{1}{n+3} - \frac{1}{n+4}$$

When $N = 1$, $A_{11} = -\frac{1}{5}$, $B_1 = \frac{1}{20}$, i.e.,

$$-\frac{1}{5}a_1 = \frac{1}{20} \quad \rightarrow \quad a_1 = -\frac{1}{4}$$

as before. When $N = 2$,

$$A_{11} = -\frac{1}{5},\ A_{12} = A_{21} = -\frac{1}{10},\ A_{22} = -\frac{2}{21},\ B_1 = \frac{1}{20},\ B_2 = \frac{1}{30}$$

Hence

$$\begin{bmatrix} -\frac{1}{5} & -\frac{1}{10} \\ -\frac{1}{10} & -\frac{2}{21} \end{bmatrix} \begin{bmatrix} a_1 \\ a_2 \end{bmatrix} = \begin{bmatrix} \frac{1}{20} \\ \frac{1}{30} \end{bmatrix}$$

which gives $a_1 = -\frac{6}{38}$, $a_2 = -\frac{7}{38}$ as obtained previously. When $N = 3$,

$$A_{13} = A_{31} = -\frac{13}{210},\ A_{23} = A_{32} = -\frac{28}{105},\ A_{33} = -\frac{22}{315},\ B_3 = \frac{1}{42},$$

i.e.,

$$\begin{bmatrix} -\frac{1}{5} & -\frac{1}{10} & -\frac{13}{210} \\ -\frac{1}{10} & -\frac{2}{21} & -\frac{28}{105} \\ -\frac{13}{210} & -\frac{28}{105} & -\frac{22}{315} \end{bmatrix} \begin{bmatrix} a_1 \\ a_2 \\ a_3 \end{bmatrix} = \begin{bmatrix} \frac{1}{20} \\ \frac{1}{30} \\ \frac{1}{42} \end{bmatrix}$$

from which we obtain

$$a_1 = -\frac{6}{38}, \qquad a_2 = -\frac{7}{38}, \qquad a_3 = 0$$

showing that we obtain the same solution as for the case $N = 2$. For different values of x, $0 < x < 1$, the Rayleigh-Ritz solution is compared with the exact solution in Table 4.2. ∎

Table 4.2 Comparison of Exact Solution with the Rayleigh-Ritz Solution of $\Phi'' + 4\Phi - x^2 = 0$, $\Phi(0) = 0 = \Phi(1)$

x	Exact solution	Rayleigh-Ritz $N = 1$	Solution $N = 2$
0.0	0.0	0.0	0.0
0.2	−0.0301	−0.0400	−0.0312
0.4	−0.0555	−0.0600	−0.0556
0.6	−0.0625	−0.0625	−0.0644
0.8	−0.0489	−0.0400	−0.0488
1.0	0.0	0.0	0.0

Example 4.6

Using the Rayleigh-Ritz method, solve Poisson's equation:

$$\nabla^2 V = -\rho_o, \qquad \rho_o = \text{constant}$$

in a square $-1 \leq x, y \leq 1$, subject to the homogeneous boundary conditions $V(x, \pm 1) = 0 = V(\pm 1, y)$. □

Solution

Due to the symmetry of the problem, we choose the basis functions as

$$u_{mn} = \left(1 - x^2\right)\left(1 - y^2\right)\left(x^{2m} y^{2n} + x^{2n} y^{2m}\right), \quad m, n = 0, 1, 2, \ldots$$

Hence

$$\widetilde{\Phi} = \left(1 - x^2\right)\left(1 - y^2\right)\left[a_1 + a_2\left(x^2 + y^2\right) + a_3 x^2 y^2 + a_4\left(x^4 + y^4\right) + \cdots\right]$$

Case 1: When $m = n = 0$, we obtain the first approximation ($N = 1$) as

$$\widetilde{\Phi} = a_1 u_1$$

where $u_1 = (1 - x^2)(1 - y^2)$.

$$\begin{aligned} A_{11} &= \langle L u_1, u_1 \rangle = \int_{-1}^{1}\int_{-1}^{1}\left(\frac{\partial^2 u_1}{\partial x^2} + \frac{\partial^2 u_1}{\partial y^2}\right) u_1 \, dxdy \\ &= -8\int_0^1\int_0^1 \left(2 - x^2 - y^2\right)\left(1 - x^2\right)\left(1 - y^2\right) dxdy \\ &= -\frac{256}{45}, \\ B_1 &= \langle g, u_1 \rangle = -\int_{-1}^{1}\int_{-1}^{1}\left(1 - x^2\right)\left(1 - y^2\right)\rho_o \, dxdy = -\frac{16\rho_o}{9} \end{aligned}$$

Hence

$$-\frac{256}{45}a_1 = -\frac{16}{9}\rho_o \quad \rightarrow \quad a_1 = \frac{5}{16}\rho_o$$

and

$$\widetilde{\Phi} = \frac{5}{16}\rho_o\left(1 - x^2\right)\left(1 - y^2\right)$$

Case 2: When $m = n = 1$, we obtain the second order approximation ($N = 2$) as

$$\widetilde{\Phi} = a_1 u_1 + a_2 u_2$$

where $u_1 = (1-x^2)(1-y^2)$, $u_2 = (1-x^2)(1-y^2)(x^2+y^2)$. A_{11} and B_1 are the same as in case 1.

$$A_{12} = A_{21} = \langle Lu_1, u_2 \rangle = -\frac{1024}{525},$$
$$A_{22} = \langle Lu_2, u_2 \rangle = -\frac{11264}{4725},$$
$$B_2 = \langle g, u_2 \rangle = -\frac{32}{45}\rho_o$$

Hence

$$\begin{bmatrix} -\frac{256}{45} & -\frac{1024}{525} \\ -\frac{1024}{525} & -\frac{11264}{4725} \end{bmatrix} \begin{bmatrix} a_1 \\ a_2 \end{bmatrix} = \begin{bmatrix} -\frac{16}{9}\rho_o \\ -\frac{32}{45}\rho_o \end{bmatrix}$$

Solving this yields

$$a_1 = \frac{1295}{4432}\rho_o = 0.2922\rho_o, \quad a_2 = \frac{525}{8864}\rho_o = 0.0592\rho_o$$

and

$$\widetilde{\Phi} = \left(1-x^2\right)\left(1-y^2\right)\left(0.2922 + 0.0592\left(x^2+y^2\right)\right)\rho_o \quad \blacksquare$$

4.6 Weighted Residual Method

As noted earlier, the Rayleigh-Ritz method is applicable when a suitable functional exists. In cases where such a functional cannot be found, we apply one of the techniques collectively referred to as the *method of weighted residuals*. The method is more general and has wider application than the Rayleigh-Ritz method because it is not limited to a class of variational problems.

Consider the operator equation

$$L\Phi = g \tag{4.40}$$

In the weighted residual method, the solution to Eq. (4.40) is approximated, in the same manner as in the Rayleigh-Ritz method, using the expansion functions, u_n, i.e.,

$$\widetilde{\Phi} = \sum_{n=1}^{N} a_n u_n \tag{4.41a}$$

where a_n are the expansion coefficients. We seek to make

$$L\widetilde{\Phi} \approx g \tag{4.41b}$$

Substitution of the approximate solution in the operator equation results in a *residual* R (an error in the equation), i.e.,

$$\boxed{R = L(\widetilde{\Phi} - \Phi) = L\widetilde{\Phi} - g} \tag{4.42}$$

In the weighted residual method, the weighting functions w_m (which, in general, are not the same as the expansion functions u_n) are chosen such that the integral of a weighted residual of the approximation is zero, i.e.,

$$\int w_m R \, dv = 0$$

or

$$\boxed{\langle w_m, R \rangle = 0} \tag{4.43}$$

If a set of *weighting functions* $\{w_m\}$ (also known as *testing functions*) are chosen and the inner product of Eq. (4.41) is taken for each w_m, we obtain

$$\sum_{n=1}^{N} a_n \langle w_m, Lu_n \rangle = \langle w_m, g \rangle, \qquad m = 1, 2, \ldots, N \tag{4.44}$$

The system of linear equations (4.42) can be cast into matrix form as

$$[A][X] = [B] \tag{4.45}$$

where $A_{mn} = \langle w_m, Lu_n \rangle$, $B_m = \langle w_m, g \rangle$, $X_n = a_n$. Solving for $[X]$ in Eq. (4.45) and substituting for a_n in Eq. (4.41a) gives the approximate solution to Eq. (4.40). However, there are different ways of choosing the weighting functions w_m leading to:

- collocation (or point-matching method),
- subdomain method,
- Galerkin method,
- least squares method.

4.6.1 Collocation Method

We select the Dirac delta function as the weighting function, i.e.,

$$w_m(\mathbf{r}) = \delta(\mathbf{r} - \mathbf{r}_m) = \begin{cases} 1, & \mathbf{r} = \mathbf{r}_m \\ 0, & \mathbf{r} \neq \mathbf{r}_m \end{cases} \tag{4.46}$$

Substituting Eq. (4.46) into Eq. (4.43) results in

$$R(\mathbf{r}) = 0 \tag{4.47}$$

Thus we select as many collocation (or matching) points in the interval as there are unknown coefficients a_n and make the residual zero at those points. This is equivalent to enforcing

$$\sum_{n=1}^{N} La_n u_n = g \tag{4.48}$$

at discrete points in the region of interest, generally where boundary conditions must be met. Although the point-matching method is the simplest specialization for computation, it is not possible to determine in advance for a particular operator equation what collocation points would be suitable. An accurate result is ensured only if judicious choice of the match points is taken. (This will be illustrated in Example 4.7.) It is important to note that the finite difference method is a particular case of collocation with locally defined expansion functions [20]. The validity and legitimacy of the point-matching technique are discussed in [21, 22].

4.6.2 Subdomain Method

We select weighting functions w_m, each of which exists only over subdomains of the domain of Φ. Typical examples of such functions for one-dimensional problems are illustrated in Fig. 4.2 and defined as follows.

(1) piecewise uniform (or pulse) function:

$$w_m(x) = \begin{cases} 1, & x_{m-1} < x < x_{m+1} \\ 0, & \text{otherwise} \end{cases} \tag{4.49a}$$

(2) piecewise linear (or triangular) function:

$$w_m(x) = \begin{cases} \dfrac{\Delta - |x - x_m|}{\Delta}, & x_{m-1} < x < x_{m+1} \\ 0, & \text{otherwise} \end{cases} \tag{4.49b}$$

(3) piecewise sinusoidal function:

$$w_m(x) = \begin{cases} \dfrac{\sin k(x - |x - x_m|)}{\Delta}, & x_{m-1} < x < x_{m+1} \\ 0, & \text{otherwise} \end{cases} \tag{4.49c}$$

Using the unit pulse function, for example, is equivalent to dividing the domain of Φ into as many subdomains as there are unknown terms and letting the average value of R over such subdomains vanish.

4.6.3 Galerkin Method

We select basis functions as the weighting function, i.e., $w_m = u_m$. When the operator is a linear differential operator of even order, the Galerkin method[1] reduces

[1]The Galerkin method was developed by the Russian engineer B.G. Galerkin in 1915.

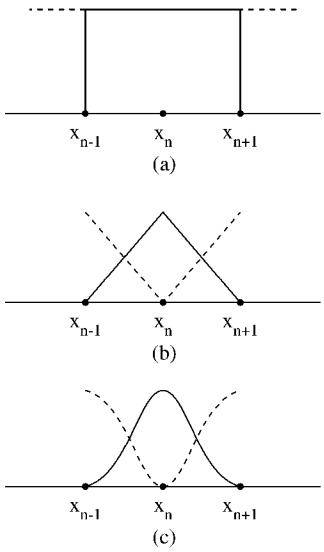

Figure 4.2
Typical subdomain weighting functions: (a) piecewise uniform function, (b) piecewise linear function, (c) piecewise sinusoidal function.

to the Rayleigh-Ritz method. This is due to the fact that the differentiation can be transferred to the weighting functions and the resulting coefficient matrix $[A]$ will be symmetric [7]. In order for the Galerkin method to be applicable, the operator must be of a certain type. Also, the expansion function u_n must span both the domain and the range of the operator.

4.6.4 Least Squares Method

This involves minimizing the integral of the square of the residual, i.e.,

$$\frac{\partial}{\partial a_m} \int R^2 \, dv = 0$$

or

$$\int \frac{\partial R}{\partial a_m} R \, dv = 0 \tag{4.50}$$

Comparing Eq. (4.50) with Eq. (4.43) shows that we must choose

$$w_m = \frac{\partial R}{\partial a_m} = L u_m \tag{4.51}$$

This may be viewed as requiring that

$$\frac{1}{2} \int R^2 \, dv$$

be minimum. In other words, the choice of w_m corresponds to minimizing the mean square residual. It should be noted that the least squares method involves higher order derivatives which will, in general, lead to a better convergence than the Rayleigh-Ritz method or Galerkin method, but it has the disadvantage of requiring higher order weighting functions [19].

The concept of convergence discussed in the previous section applies here as well. That is, if the approximate solution $\widetilde{\Phi}$ were to converge to the exact solution Φ as $N \to \infty$, the residual must approach zero as $N \to \infty$. Otherwise, the sequence of approximate solutions may not converge to any meaningful result.

The inner product involved in applying a weighted residual method can sometimes be evaluated analytically, but in most practical situations it is evaluated numerically. Due to a careless evaluation of the inner product, one may think that the least squares technique is being used when the resulting solution is identical to a point-matching solution. To avoid such erroneous results or conclusions, one must be certain that the overall number of points involved in the numerical integration is not smaller than the number of unknowns, N, involved in the weighted residual method [23].

The accuracy and efficiency of a weighted residual method is largely dependent on the selection of expansion functions. The solution may be exact or approximate depending on how we select the expansion and weighting functions [17]. The criteria for selecting expansion and weighting functions in a weighted residual method are provided in the work of Sarkar and others [24]–[27]. We summarize their results here. The expansion functions u_n are selected to satisfy the following requirements [27]:

(1) The expansion functions should be in the domain of the operator L in some sense, i.e., they should satisfy the differentiability criterion and they must satisfy the boundary conditions for the operator. It is not necessary for each expansion function to satisfy exactly the boundary conditions. What is required is that the total solution must satisfy the boundary conditions at least in some distributional sense. The same holds for the differentiability conditions.

(2) The expansion functions must be such that $L\,u_n$ form a complete set for the range of the operator. It really does not matter whether the expansion functions are complete in the domain of the operator. What is important is that u_n must be chosen in such a way that $L\,u_n$ is complete. This will be illustrated in Example 4.8.

From a mathematical point of view, the choice of expansion functions does not depend on the choice of weighting functions. It is required that the weighting functions w_n must take the difference $\Phi - \widetilde{\Phi}$ small. For the Galerkin method to be applicable, the expansion functions u_n must span both the domain and the range of the operator. For the least squares method, the weighting functions are already presented and defined by $L\,u_n$. It is necessary that $L\,u_n$ form a complete set. The least squares technique mathematically and numerically is one of the safest techniques to utilize when very little is known about the nature of the operator and the exact solution.

Example 4.7

Find an approximate solution to

$$\Phi'' + 4\Phi - x^2 = 0, \qquad 0 < x < 1,$$

with $\Phi(0) = 0$, $\Phi'(1) = 1$, using the method of weighted residuals. □

Solution

The exact solution is

$$\Phi(x) = \frac{\cos 2(x-1) + 2\sin 2x}{8\cos 2} - \frac{x^2}{4} - \frac{1}{8} \tag{4.52}$$

Let the approximate solution be

$$\widetilde{\Phi} = u_0 + \sum_{n=1}^{N} a_n u_n \tag{4.53}$$

The boundary conditions can be decomposed into two parts:

(1) homogeneous part $\rightarrow$ $\Phi(0) = 0$, $\Phi'(0) = 0$,

(2) inhomogeneous part $\rightarrow$ $\Phi'(1) = 1$.

We choose u_0 to satisfy the inhomogeneous boundary condition. A reasonable choice is

$$u_0 = x \tag{4.54a}$$

We choose $u_n (n = 1, 2, \ldots, N)$ to satisfy the homogeneous boundary condition. Suppose we select

$$u_n(x) = x^n \left(x - \frac{n+1}{n} \right) \tag{4.54b}$$

Thus, if we take $N = 2$, the approximate solution is

$$\begin{aligned} \widetilde{\Phi} &= u_0 + a_1 u_1 + a_2 u_2 \\ &= x + a_1 x(x-2) + a_2 x^2 (x - 3/2) \end{aligned} \tag{4.55}$$

where the expansion coefficients, a_1 and a_2, are to be determined. We find the residual R using Eq. (4.42), namely,

$$\begin{aligned} R &= L\widetilde{\Phi} - g \\ &= \left(\frac{d^2}{dx^2} + 4 \right) \widetilde{\Phi} - x^2 \\ &= a_1 \left(4x^2 - 8x + 2 \right) + a_2 \left(4x^3 - 6x^2 + 6x - 3 \right) - x^2 + 4x \end{aligned} \tag{4.56}$$

We now apply each of the four techniques discussed and compare the solutions.

Method 1: (collocation or point-matching method)
Since we have two unknowns a_1 and a_2, we select two match points, at $x = \frac{1}{3}$ and $x = \frac{2}{3}$, and set the residual equal to zero at those points, i.e.,

$$R\left(\frac{1}{3}\right) = 0 \quad \rightarrow \quad 6a_1 + 41a_2 = 33$$
$$R\left(\frac{2}{3}\right) = 0 \quad \rightarrow \quad 42a_1 + 13a_2 = 60$$

Solving these equations,

$$a_1 = \frac{677}{548}, \qquad a_2 = \frac{342}{548}$$

Substituting a_1 and a_2 into Eq. (4.55) gives

$$\widetilde{\Phi}(x) = -1.471x + 0.2993x^2 + 0.6241x^3 \tag{4.57}$$

To illustrate the dependence of the solution on the match points, suppose we select $x = \frac{1}{4}$ and $x = \frac{3}{4}$ as the match points. Then

$$R\left(\frac{1}{4}\right) = 0 \quad \rightarrow \quad -4a_1 + 29a_2 = 15$$
$$R\left(\frac{3}{4}\right) = 0 \quad \rightarrow \quad 28a_1 + 3a_2 = 39$$

Solving for a_1 and a_2, we obtain

$$a_1 = \frac{543}{412}, \qquad a_2 = \frac{288}{412}$$

with the approximate solution

$$\widetilde{\Phi}(x) = -1.636x + 0.2694x^2 + 0.699x^3 \tag{4.58}$$

We will refer to the solutions in Eqs. (4.57) and (4.58) as collocation 1 and collocation 2, respectively. It is evident from Table 4.3 that collocation 2 is more accurate than collocation 1.

Method 2: (subdomain method)
Divide the interval $0 < x < 1$ into two segments since we have two unknowns a_1 and a_2. We select pulse functions as weighting functions:

$$w_1 = 1, \qquad 0 < x < \frac{1}{2},$$
$$w_2 = 1, \qquad \frac{1}{2} < x < 1$$

so that

$$\int_0^{1/2} w_1 R\,dx = 0 \quad \rightarrow \quad -8a_1 + 45a_2 = 22$$
$$\int_{1/2}^{1} w_2 R\,dx = 0 \quad \rightarrow \quad 40a_1 + 3a_2 = 58$$

Solving the two equations gives

$$a_1 = \frac{53}{38}, \qquad a_2 = \frac{28}{38}$$

and hence Eq. (4.55) becomes

$$\widetilde{\Phi}(x) = -1.789x + 0.2895x^2 + 0.7368x^3 \tag{4.59}$$

Method 3: (Galerkin method)
In this case, we select $w_m = u_m$, i.e.,

$$w_1 = x(x-2), \qquad w_2 = x^2(x - 3/2)$$

We now apply Eq. (4.43), namely, $\int w_m R\,dx = 0$. We obtain

$$\int_0^1 \left(x^2 - 2x\right) R\,dx = 0 \quad \rightarrow \quad 24a_1 + 11a_2 = 41$$
$$\int_0^1 \left(x^3 - \frac{3}{2}x^2\right) R\,dx = 0 \quad \rightarrow \quad 77a_1 + 15a_2 = 119$$

Solving these leads to

$$a_1 = \frac{694}{487}, \qquad a_2 = \frac{301}{487}$$

Substituting a_1 and a_2 into Eq. (4.55) gives

$$\widetilde{\Phi}(x) = -1.85x + 0.4979x^2 + 0.6181x^3 \tag{4.60}$$

Method 4: (least squares method)
For this method, we select $w_m = \dfrac{\partial R}{\partial a_m}$, i.e.,

$$w_1 = 4x^2 - 8x + 2, \qquad w_2 = 4x^3 - 6x^2 + 6x - 3$$

Applying Eq. (4.43)

$$\int_0^1 w_1 R\,dx = 0 \quad \rightarrow \quad 7a_1 - 2a_2 = 8$$
$$\int_0^1 w_2 R\,dx = 0 \quad \rightarrow \quad -112a_1 + 438a_2 = 161$$

Thus

$$a_1 = \frac{3826}{2842}, \qquad a_2 = \frac{2023}{2842}$$

and Eq. (4.55) becomes

$$\tilde{\Phi}(x) = -1.6925x + 0.2785x^2 + 0.7118x^3 \tag{4.61}$$

Notice that the approximate solutions in Eqs. (4.57) to (4.61) all satisfy the boundary conditions $\Phi(0) = 0$ and $\Phi'(1) = 1$. The five approximate solutions are compared in Table 4.3. ∎

Table 4.3 Comparison of the Weighted Residual Solutions of the Problem in Example 4.7 with the Exact Solution in Eq. (4.52)

x	Exact solution	Collocation 1	Collocation 2	Subdomain	Galerkin	Least squares
0.0	0.0000	0.0000	0.0000	0.0000	0.0000	0.0000
0.1	−0.1736	−0.1435	−0.1602	−0.1753	−0.1794	−0.1657
0.2	−0.3402	−0.2772	−0.3108	−0.3403	−0.3451	−0.3217
0.3	−0.4928	−0.3975	−0.4477	−0.4907	−0.4935	−0.4635
0.4	−0.6248	−0.5006	−0.5666	−0.6221	−0.6208	−0.5869
0.5	−0.7303	−0.5827	−0.6633	−0.7300	−0.7233	−0.6877
0.6	−0.8042	−0.6400	−0.7336	−0.8100	−0.7972	−0.7615
0.7	−0.8424	−0.6690	−0.7734	−0.8577	−0.8390	−0.8041
0.8	−0.8422	−0.6657	−0.7785	−0.8687	−0.8449	−0.8113
0.9	−0.8019	−0.6264	−0.7446	−0.8385	−0.8111	−0.7788
1.0	−0.7216	−0.5476	−0.6676	−0.7627	−0.7340	−0.7022

Example 4.8

This example illustrates the fact that expansion functions u_n must be selected such that $L\,u_n$ form a complete set for the range of the operator L. Consider the differential equation

$$-\Phi'' = 2 + \sin x, \qquad 0 \le x \le 2\pi \tag{4.62}$$

subject to

$$\Phi(0) = \Phi(2\pi) = 0 \tag{4.63}$$

Suppose we carelessly select

$$u_n = \sin nx, \qquad n = 1, 2, \ldots \tag{4.64}$$

as the expansion functions, the approximate solution is

$$\tilde{\Phi} = \sum_{n=1}^{N} a_n \sin nx \tag{4.65}$$

If we apply the Galerkin method, we obtain

$$\widetilde{\Phi} = \sin x \tag{4.66}$$

Although u_n satisfy both the differentiability and boundary conditions, Eq. (4.66) does not satisfy Eq. (4.62). Hence Eq. (4.66) is an incorrect solution. The problem is that the set $\{\sin nx\}$ does not form a complete set. If we add constant and cosine terms to the expansion functions in Eq. (4.65), then

$$\widetilde{\Phi} = a_0 + \sum_{n=1}^{N} [a_n \sin nx + b_n \cos nx] \tag{4.67}$$

As $N \to \infty$, Eq. (4.67) is the classical Fourier series solution. Applying the Galerkin method leads to

$$\widetilde{\Phi} = \sin nx \tag{4.68}$$

which is again an incorrect solution. The problem is that even though u_n form a complete set, $L\,u_n$ do not. For example, nonzero constants cannot be approximated by $L\,u_n$. In order for $L\,u_n$ to form a complete set, $\widetilde{\Phi}$ must be of the form

$$\widetilde{\Phi} = \sum_{n=1}^{n} [a_n \sin nx + b_n \cos nx] + a_0 + cx + dx^2 \tag{4.69}$$

Notice that the expansion functions $\{1, x, x^2, \sin nx, \cos nx\}$ in the interval $[0, 2\pi]$ form a linearly dependent set. This is because any function such as x or x^2 can be represented in the interval $[0, 2\pi]$ by the set $\{\sin nx, \cos nx\}$. Applying the Galerkin method, Eq. (4.69) leads to

$$\widetilde{\Phi} = \sin x + x(2\pi - x) \tag{4.70}$$

which is the exact solution Φ. □

4.7 Eigenvalue Problems

As mentioned in Section 1.3.2, eigenvalue (nondeterministic) problems are described by equations of the type

$$L\Phi = \lambda M\Phi \tag{4.71}$$

where L and M are differential or integral, scalar or vector operators. The problem here is the determination of the eigenvalues λ and the corresponding eigenfunctions

Φ. It can be shown [11] that the variational principle for λ takes the form

$$\boxed{\lambda = \min \frac{\langle \Phi, L\Phi \rangle}{\langle \Phi, M\Phi \rangle} = \min \frac{\int \Phi L \Phi \, dv}{\int \Phi M \Phi \, dv}} \tag{4.72}$$

We may apply Eq. (4.72) to the Helmholtz equation for scalar waves, for example,

$$\nabla^2 \Phi + k^2 \Phi = 0 \tag{4.73}$$

Comparing Eq. (4.73) with Eq. (4.71), we obtain $L = -\nabla^2, M = 1$ (the identity operator), $\lambda = k^2$ so that

$$k^2 = \min \frac{\int \Phi \nabla^2 \Phi \, dv}{\int \Phi^2 \, dv} \tag{4.74}$$

Applying Green's identity (see Example 1.1),

$$\int_v \left(U \nabla^2 V + \nabla U \cdot \nabla V \right) dv = \oint U \frac{\partial V}{\partial n} \, dS \, ,$$

to Eq. (4.74) yields

$$\boxed{k^2 = \min \frac{\int_v |\nabla \Phi|^2 \, dv - \oint \Phi \frac{\partial \Phi}{\partial n} \, dS}{\int_v \Phi^2 \, dv}} \tag{4.75}$$

Consider the following special cases.

(a) For homogeneous boundary conditions of the Dirichlet type ($\Phi = 0$) or Neumann type $\left(\dfrac{\partial \Phi}{\partial n} = 0 \right)$. Equation (4.75) reduces to

$$k^2 = \min \frac{\int_v |\nabla \Phi|^2 \, dv}{\int_v \Phi^2 \, dv} \tag{4.76}$$

(b) For mixed boundary conditions $\left(\dfrac{\partial \Phi}{\partial n} + h\Phi = 0 \right)$, Eq. (4.75) becomes

$$k^2 = \min \frac{\int_v |\nabla \Phi|^2 \, dv + \oint h \Phi^2 \, dS}{\int_v \Phi^2 \, dv} \tag{4.77}$$

It is usually possible to solve Eq. (4.71) in a different way. We choose the basis functions $u_1, u_2, \ldots, u_N$ which satisfy the boundary conditions and assume the approximate solution

$$\tilde{\Phi} = a_1 u_1 + a_2 u_2 + \cdots + a_N u_N$$

or

$$\widetilde{\Phi} = \sum_{n=1}^{N} a_n u_n \tag{4.78}$$

Substituting this into Eq. (4.71) gives

$$\sum_{n=1}^{N} a_n L u_n = \lambda \sum_{n=1}^{N} a_n M u_n \tag{4.79}$$

Choosing the weighting functions w_m and taking the inner product of Eq. (4.79) with each w_m, we obtain

$$\sum_{n=1}^{N} \left[\langle w_m, L u_n \rangle - \lambda \langle w_m, M u_n \rangle \right] a_n = 0, \qquad m = 1, 2, \ldots, N \tag{4.80}$$

This can be cast into matrix form as

$$\sum_{n=1}^{N} (A_{mn} - \lambda B_{mn}) X_n = 0 \tag{4.81}$$

where $A_{mn} = \langle w_m, L u_n \rangle$, $B_{mn} = \langle w_m, M u_n \rangle$, $X_n = a_n$. Thus we have a set of homogeneous equations. In order for $\widetilde{\Phi}$ in Eq. (4.78) not to vanish, it is necessary that the expansion coefficients a_n not all be equal to zero. This implies that the determinant of simultaneous equations (4.81) vanish, i.e.,

$$\begin{vmatrix} A_{11} - \lambda B_{11} & A_{12} - \lambda B_{12} & \cdots & A_{1N} - \lambda B_{1N} \\ \vdots & & & \vdots \\ A_{N1} - \lambda B_{N1} & A_{N2} - \lambda B_{N2} & \cdots & A_{NN} - \lambda B_{NN} \end{vmatrix} = 0$$

or

$$|[A] - \lambda [B]| = 0 \tag{4.82}$$

Solving this gives N approximate eigenvalues $\lambda_1, \ldots, \lambda_N$. The various ways of choosing w_m leads to different weighted residual techniques as discussed in the previous section.

Examples of eigenvalue problems for which variational methods have been applied include [28]–[37]:

- the cutoff frequency of a waveguide,
- the propagation constant of a waveguide, and
- the resonant frequency of a resonator.

Example 4.9

Solve the eigenvalue problem

$$\Phi'' + \lambda\Phi = 0, \qquad 0 < x < 1$$

with boundary conditions $\Phi(0) = 0 = \Phi(1)$. □

Solution

The exact eigenvalues are

$$\lambda_n = (n\pi)^2, \qquad n = 1, 2, 3, \ldots \tag{4.83}$$

and the corresponding (normalized) eigenfunctions are

$$\Phi_n = \sqrt{2}\sin(n\pi x) \tag{4.84}$$

where Φ_n has been normalized to unity, i.e., $\langle \Phi_n, \Phi_n \rangle = 1$.

The approximate eigenvalues and eigenfunctions can be obtained by either using Eq. (4.72) or Eq. (4.82). Let the approximate solution be

$$\widetilde{\Phi}(x) = \sum_{k=0}^{N} a_k u_k, \qquad u_k = x\left(1 - x^k\right) \tag{4.85}$$

From the given problem, $L = -\dfrac{d^2}{dx^2}$, $M = 1$ (identity operator). Using the Galerkin method, $w_m = u_m$.

$$\begin{aligned} A_{mn} &= \langle u_m, Lu_n \rangle = \int_0^1 \left(x - x^{m+1}\right)\left[-\frac{d^2}{dx^2}\left(x - x^{n+1}\right)\right] dx \\ &= \frac{mn}{m+n+1}, \end{aligned} \tag{4.86}$$

$$\begin{aligned} B_{mn} &= \langle u_m, Mu_n \rangle = \int_0^1 \left(x - x^{m+1}\right)\left(x - x^{n+1}\right) dx \\ &= \frac{mn(m+n+6)}{3(m+3)(n+3)(m+n+3)} \end{aligned} \tag{4.87}$$

The eigenvalues are obtained from

$$|\,[A] - \lambda\,[B]\,| = 0 \tag{4.88}$$

For $N = 1$,

$$A_{11} = \frac{1}{3}, \qquad B_1 = \frac{1}{30},$$

giving

$$\frac{1}{3} - \lambda\frac{1}{30} = 0 \qquad \rightarrow \qquad \lambda = 10$$

The first approximate eigenvalue is $\lambda = 10$, a good approximation to the exact value of $\pi^2 = 9.8696$. The corresponding eigenfunction $\widetilde{\Phi} = a_1(x - x^2)$ can be normalized to unity so that

$$\widetilde{\Phi} = \sqrt{30}(x - x^2)$$

For $N = 2$, evaluating Eqs. (4.86) and (4.87), we obtain

$$\begin{bmatrix} \frac{1}{3} & \frac{1}{2} \\ \frac{1}{2} & \frac{4}{5} \end{bmatrix} \begin{bmatrix} a_1 \\ a_2 \end{bmatrix} = \lambda \begin{bmatrix} \frac{1}{30} & \frac{1}{20} \\ \frac{1}{20} & \frac{8}{105} \end{bmatrix} \begin{bmatrix} a_1 \\ a_2 \end{bmatrix}$$

or

$$\begin{vmatrix} 10 - \lambda & 0 \\ 0 & 42 - \lambda \end{vmatrix} = 0$$

giving eigenvalues $\lambda_1 = 10, \lambda_2 = 42$, compared with the exact values $\lambda_1 = \pi^2 = 9.8696, \lambda_2 = 4\pi^2 = 39.4784$, and the corresponding normalized eigenfunctions are

$$\widetilde{\Phi}_1 = \sqrt{30}\left(x - x^2\right)$$

$$\widetilde{\Phi}_2 = 2\sqrt{210}\left(x - x^2\right) - 2\sqrt{210}\left(x - x^3\right)$$

Continuing this way for higher N, the approximate eigenvalues shown in Table 4.4 are obtained. Unfortunately, the labor of computation increases as more u_k are included in $\widetilde{\Phi}$. Notice from Table 4.4 that the approximate eigenvalues are always greater than the exact values. This is always true for a self-adjoint, positive definite operator [17]. Figure 4.3 shows the comparison between the approximate and exact eigenfunctions. ∎

Table 4.4 Comparison Between Approximate and Exact Eigenvalues for Example 4.9

Exact	Approximate			
	$N = 1$	$N = 2$	$N = 3$	$N = 4$
9.870	10.0	10.0	9.8697	9.8697
39.478		42.0	39.497	39.478
88.826			102.133	102.133
157.914				200.583

Example 4.10

Calculate the cutoff frequency of the inhomogeneous rectangular waveguide shown in Fig. 4.4. Take $\epsilon = 4\epsilon_o$ and $s = a/3$. □

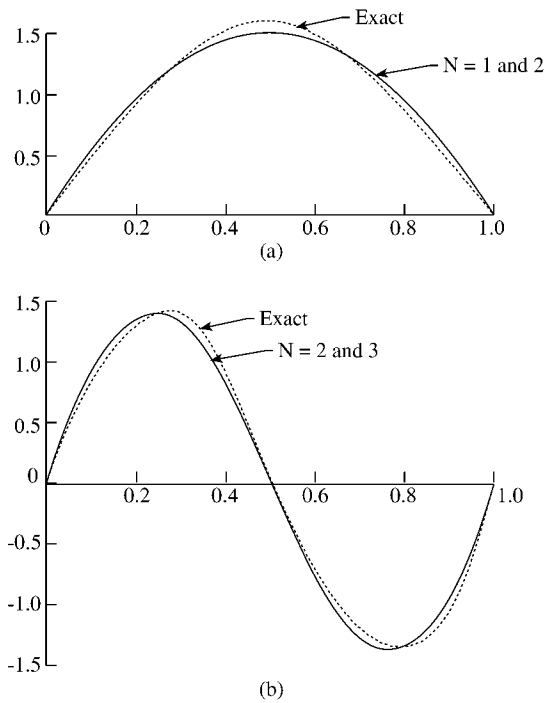

Figure 4.3
Comparison of approximate eigenfunctions with the exact solutions: (a) first eigenfunction, (b) second eigenfunction. (After Harrington [17]; with permission of Krieger Publishing Co.).

Solution

We will find the lowest mode having $\frac{\partial}{\partial y} \equiv 0$. It is this dominant mode that is of most practical value. Since the dielectric constant varies from one region to another, it is reasonable to choose Φ to be an electric field, i.e., $\Phi = E_y$. Also, since $k^2 = \frac{\omega^2}{u^2} = \omega^2 \mu \epsilon$, Eq. (4.74) becomes

$$\omega^2 \mu_o \epsilon_o \int_0^s E_y^2 \, dx + \omega^2 \mu_o \epsilon_o \epsilon_r \int_s^{a-s} E_y^2 \, dx + \omega^2 \mu_o \epsilon_o \int_{a-s}^{a} E_y^2 \, dx = -\int_0^a E_y \frac{d^2 E_y}{dx^2} \, dx \tag{4.89}$$

Notice that in this implementation of Eq. (4.74), there are no coefficients so that there is nothing to minimize. We simply take k^2 as a ratio. Equation (4.89) can be written

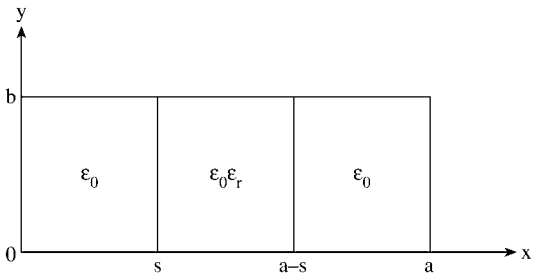

Figure 4.4
A symmetrically loaded rectangular waveguide.

as

$$\omega^2\mu_o\epsilon_o\int_0^a E_y^2\,dx+\omega^2\mu_o\epsilon_o(\epsilon_r-1)\int_s^{a-s}E_y^2\,dx=-\int_0^a E_y\frac{d^2E_y}{dx^2}\,dx \tag{4.90}$$

We now choose the trial function for E_y. It must be chosen to satisfy the boundary conditions, namely, $E_y = 0$ at $x = 0, a$. Since $E_y \sim \sin\dfrac{n\pi x}{a}$ for the empty waveguide, it makes sense to choose the trial function of the form

$$E_y=\sum_{n=1,3,5}^{\infty}c_n\sin\frac{n\pi x}{a} \tag{4.91}$$

We choose the odd values of n because the dielectric is symmetrically placed; otherwise we would have both odd and even terms.

Let us consider the trial function

$$E_y=\sin\frac{\pi x}{a} \tag{4.92}$$

Substituting Eq. (4.92) into Eq. (4.90) yields

$$\omega^2\mu_o\epsilon_o\int_0^a\sin^2\frac{\pi x}{a}\,dx+\omega^2\mu_o\epsilon_o(\epsilon_r-1)\int_s^{a-s}\sin^2\frac{\pi x}{a}\,dx$$
$$=\frac{\pi^2}{a^2}\int_0^a\sin^2\frac{\pi x}{a}\,dx \tag{4.93}$$

which leads to

$$\omega^2\mu_o\epsilon_o\left\{1+(\epsilon_r-1)\left[\left(1-\frac{2s}{a}\right)+\frac{1}{\pi}\sin\frac{2\pi s}{a}\right]\right\}=\frac{\pi^2}{a^2}$$

But $k_o^2=\omega^2\mu_o\epsilon_o=\dfrac{4\pi^2}{\lambda_c^2}$, where λ_c is the cutoff wavelength of the waveguide filled with vacuum. Hence

$$\frac{4\pi^2}{\lambda_c^2}=\frac{(\pi/a)^2}{1+(\epsilon_r-1)\left[(1-\frac{2s}{a})+\frac{1}{\pi}\sin\frac{2\pi s}{a}\right]}$$

Taking $\epsilon_r = 4$ and $s = a/3$ gives

$$\frac{4\pi^2}{\lambda_c^2} = \frac{(\pi/a)^2}{2 + \frac{3\sqrt{3}}{2\pi}}$$

or

$$\frac{a}{\lambda_c} = 0.2974$$

This is a considerable reduction in a/λ_c compared with the value of $a/\lambda_c = 0.5$ for the empty guide. The accuracy of the result may be improved by choosing more terms in Eq. (4.91). ∎

4.8 Practical Applications

The various techniques discussed in this chapter have been applied to solve a considerable number of EM problems. We select a simple example for illustration [38, 39]. This example illustrates the conventional use of the least squares method.

Consider a strip transmission line enclosed in a box containing a homogeneous medium as shown in Fig. 4.5. If a TEM mode of propagation is assumed, Laplace's

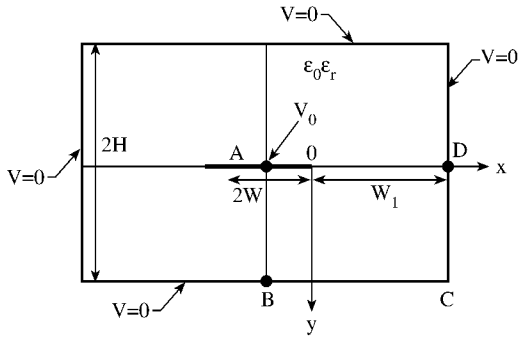

Figure 4.5
The strip line enclosed in a shielded box.

equation

$$\nabla^2 V = 0 \tag{4.94}$$

is obeyed. Due to symmetry, we will consider only one quarter section of the line as in Fig. 4.6 and adopt a boundary condition $\frac{\partial V}{\partial x} = 0$ at $x = -W$. We allow for the singularity at the edge of the strip. The variation of the potential in the vicinity of

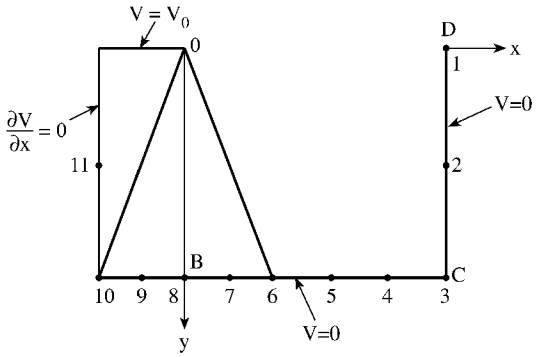

Figure 4.6
A quarter-section of the strip line.

such a singularity is approximated, in terms of trigonometric basis functions, as

$$V = V_o + \sum_{k=1,3,5}^{\infty} c_k \rho^{k/2} \cos \frac{k\phi}{2}, \tag{4.95}$$

where V_o is the potential on the trip conductor and the expansion coefficients c_k are to be determined. If we truncate the infinite series in Eq. (4.95) so that we have N unknown coefficients, we determine the coefficients by requiring that Eq. (4.95) be satisfied at $M(\geq N)$ points on the boundary. If $M = N$, we are applying the collocation method. If $M > N$, we obtain an overdetermined system of equations which can be solved by the method of least squares. Enforcing Eq. (4.95) at M boundary points, we obtain M simultaneous equations

$$\begin{bmatrix} V_1 \\ V_2 \\ \vdots \\ V_M \end{bmatrix} = \begin{bmatrix} A_{11} & A_{12} & \dots & A_{1N} \\ A_{21} & A_{22} & \dots & A_{2N} \\ \vdots & & & \vdots \\ A_{M1} & A_{M2} & \dots & A_{MN} \end{bmatrix} \begin{bmatrix} c_1 \\ c_2 \\ \vdots \\ c_M \end{bmatrix}$$

i.e.,

$$[V] = [A][X] \tag{4.96}$$

where $[X]$ is an $N \times 1$ matrix containing the unknown expansion coefficients, $[V]$ is an $M \times 1$ column matrix containing the boundary conditions, and $[A]$ is the $M \times N$ coefficient matrix. Due to redundancy, $[X]$ cannot be uniquely determined from Eq. (4.96) if $M > N$. To solve this redundant system of equations by the method of least squares, we define the residual matrix $[R]$ as

$$[R] = [A][X] - [V] \tag{4.97}$$

We seek for $[X]$, which minimizes $[R]^2$. Consider

$$[I] = [R]^t [R] = [[A][X] - [V]]^t [[A][X] - [V]]$$
$$\frac{\partial [I]}{\partial [X]} = 0 \quad \rightarrow \quad [A]^t [A][X] - [A]^t [V] = 0$$

or

$$[X] = \left[[A]^t [A]\right]^{-1} [A]^t [V] \tag{4.98}$$

where the superscript t denotes the transposition of the relevant matrix. Thus we have reduced the original redundant system of equations to a determinate set of N simultaneous equations in N unknown coefficients $c_1, c_2, \ldots, c_N$.

Once $[X] = [c_1, c_2, \ldots, c_N]$ is determined from Eq. (4.98), the approximate solution in Eq. (4.95) is completely determined. We can now determine the capacitance and consequently the characteristic impedance of the line for a given value of width-to-height ratio. The capacitance is determined from

$$C = \frac{Q}{V_o} = Q \tag{4.99}$$

If we let $V_o = 1$ V. The characteristic impedance is found from [40]

$$Z_o = \frac{\sqrt{\epsilon_r}}{cC} \tag{4.100}$$

where $c = 3 \times 10^8$ m/s, the speed of light in vacuum. The major problem here is finding Q in Eq. (4.99). If we divide the boundary BCD into segments,

$$Q = \int \rho_L \, dl = 4 \sum_{BCD} \rho_L \Delta l$$

where the charge density $\rho_L = \mathbf{D} \cdot \mathbf{a}_n = \epsilon \mathbf{E} \cdot \mathbf{a}_n$, $\mathbf{E} = -\nabla V$, and the factor 4 is due to the fact that we consider only one quarter section of the line. But

$$\nabla V = \frac{\partial V}{\partial \rho}\mathbf{a}_\rho + \frac{1}{\rho}\frac{\partial V}{\partial \phi}\mathbf{a}_\phi \,,$$
$$\mathbf{E} = -\sum_{k=\text{odd}} \frac{k}{2} c_k \rho^{k/2-1} \left(\cos\frac{k\phi}{2}\mathbf{a}_\rho - \sin\frac{k\phi}{2}\mathbf{a}_\phi\right)$$

Since $\mathbf{a}_x = \cos\phi\mathbf{a}_\rho - \sin\phi\mathbf{a}_\phi$ and $\mathbf{a}_y = \sin\phi\mathbf{a}_\rho + \cos\phi\mathbf{a}_\phi$,

$$\rho_L|_{CD} = \epsilon \mathbf{E} \cdot \mathbf{a}_x$$
$$= -\epsilon \sum_{k=\text{odd}} \frac{k}{2} c_k \rho^{k/2-1} \left(\cos\frac{k\phi}{2}\cos\phi + \sin\frac{k\phi}{2}\sin\phi\right) \tag{4.101a}$$

and

$$\rho_L|_{BC} = \epsilon \mathbf{E} \cdot \mathbf{a}_y$$
$$= -\epsilon \sum_{k=\text{odd}} \frac{k}{2} c_k \rho^{k/2-1} \left(\cos \frac{k\phi}{2} \sin\phi - \sin \frac{k\phi}{2} \cos\phi \right) \tag{4.101b}$$

Example 4.11

Using the collocation (or point matching) method, write a computer program to calculate the characteristics impedance of the line shown in Fig. 4.5. Take:

(a) $W = H = 1.0$ m, $W_1 = 5.0$ m, $\epsilon_r = 1$, $V_0 = 1$ V,

(b) $W = H = 0.5$ m, $W_1 = 5.0$ m, $\epsilon_r = 1$, $V_0 = 1$ V. □

Solution

The computer program is presented in Fig. 4.7. For the first run, we take the number of matching points $N = 11$; the points are selected as illustrated in Fig. 4.6. The selection of the points is based on our prior knowledge of the fact that the flux lines are concentrated on the side of the strip line numbered 6 to 10; hence more points are chosen on that side.

The first step is to determine the potential distribution within the strip line using Eq. (4.95). In order to determine the expansion coefficients c_k in Eq. (4.95), we let Eq. (4.95) be satisfied at the matching points. On points 1 to 10 in Fig. 4.6, $V = 0$ so that Eq. (4.95) can be written as

$$-V_o = \sum_{k=1,3,5}^{\infty} c_k \rho^{k/2} \cos \frac{k\phi}{2} \tag{4.102}$$

The infinite series is terminated at $k = 19$ so that 10 points are selected on the sides of the strip line. The 11th point is selected such that $\dfrac{\partial V}{\partial x} = 0$ is satisfied at the point. Hence at point 11,

$$0 = \frac{\partial V}{\partial x} = \cos\phi \frac{\partial V}{\partial \rho} - \frac{\sin\phi}{\rho} \frac{\partial V}{\partial \phi}$$

or

$$0 = \sum_{k=1,3,5} \frac{k}{2} c_k \rho^{k/2-1} \left(\cos \frac{k\phi}{2} \cos\phi + \sin \frac{k\phi}{2} \sin\phi \right) \tag{4.103}$$

With Eqs. (4.102) and (4.103), we set up a matrix equation of the form

$$[B] = [F][A] \tag{4.104}$$

```
0001    C  ******************************************************
0002    C  THIS PROGRAM CALCULATES THE CHARACTERISTIC IMPEDANCE
0003    C  Zo  OF A BOXED MICROSTRIP LINE USING COLLOCATION
0004    C  POINT-MATCHING METHOD
0005    C  ******************************************************
0006
0007          DIMENSION X(30), Y(30), R(30), PHI(30), F(30,30)
0008          DIMENSION A(30), B(30)
0009          DATA (X(I),I=1,11)/3*5.0,4.0,2.0,1.0,0.5,
                    0.0,-0.5,2*-1.0/
0010          DATA ( Y(J),J=1,11 )/0.0,0.5,8*1.0,0.5/
0011          DATA E0,PIE,VL/8.8541E-12,3.141592,3.0E+8/
0012
0013    C     INPUT DATA
0014           ER = 1.0
0015           EPS = E0*ER
0016           W = 1.0
0017           H = 1.0
0018           W1 = 5.0
0019           V0 = 1.0
0020           NMAX = 11
0021           NBC = 7     ! NO. OF POINTS ON BC OR X-AXIS
0022           NCD = NMAX - NBC  ! NO. OF POINTS ON DC OR Y-AXIS
0023           DX = (W + W1)/FLOAT(NBC)
0024           DY = H/FLOAT(NCD)
0025    C
0026    C      CALCULATE (R,PHI) FOR EACH POINT (X,Y)
0027    C
0028           DO 40 N = 1,NMAX
0029           R(N) = SQRT( X(N)**2 + Y(N)**2 )
0030           IF( X(N) ) 10,20,30
0031    10      PHI(N) = PIE - ATAN( Y(N)/ABS(X(N)) )
0032            GO TO 40
0033    20      PHI(N) = PIE/2.0
0034            GO TO 40
0035    30      PHI(N) = ATAN( Y(N)/X(N) )
0036    40      CONTINUE
0037    C
0038    C       CALCULATE MATRICES F(I,J) AND B(I)
0039    C
0040            DO 60 I = 1,NMAX
0041            B(I) = -V0
0042            M = 0
0043            DO 60 J = 1,NMAX
0044            M = 2*J - 1
0045            FM = FLOAT(M)/2.0
0046            IF(I.EQ.NMAX) GO TO 50
0047            F(I,J) = ( R(I)**(FM) )*COS(FM*PHI(I))
0048            GO TO 60
0049    50      CC = COS(PHI(I))*COS(PHI(I)*FM)
0050            SS = SIN(PHI(I))*SIN(PHI(I)*FM)
0051            F(I,J) = ( R(I)**(FM-1.) )*(CC + SS)*FM
0052            B(I) = 0.0
0053    60      CONTINUE
0054    C
0055    C       DETERMINE THE EXPANSION COEFFICIENTS A(I)
0056    C
0057            IDM = 30
0058            CALL INVERSE(F,NMAX,IDM)
0059            DO 80 I = 1, NMAX
```

Figure 4.7
Computer program for Example 4.11 ***(Continued)*****.**

```
0060            A(I) = 0.0
0061            DO 70 J=1,NMAX
0062            A(I) = A(I) + F(I,J)*B(J)
0063    70      CONTINUE
0064    80      CONTINUE
0065    C
0066    C       NOW, CALCULATE CHARGE ON THE X-SIDE, i.e. BC
0067    C
0068            RHO = 0.0
0069            YC = H
0070            XC = - W - DX/2.0
0071            DO 120 I=1,NBC
0072            XC = XC + DX
0073            RC = SQRT(XC**2 + YC**2 )
0074            IF(XC) 90,90,100
0075    90      PC = PIE - ATAN(YC/ABS(XC))
0076            GO TO 110
0077    100     PC = ATAN(YC/XC)
0078    110     CONTINUE
0079            DO 120 K=1,NMAX
0080            FK = FLOAT(2*K - 1)/2.0
0081            RRO = SIN(PC)*COS(FK*PC) - COS(PC)*SIN(FK*PC)
0082            RHO = RHO - A(K)*FK*(RC**(FK-1))*RRO*DX*EPS
0083    120     CONTINUE
0084    C
0085    C      NEXT, CALCULATE THE CHARGE ON THE Y-SIDE, i.e. DC
0086    C
0087            XC = W1
0088            YC = - DY/2.0
0089            DO 130 I=1,NCD
0090            YC = YC + DY
0091            RC = SQRT(XC**2 + YC**2)
0092            PC = ATAN(YC/XC)
0093            DO 130 K =1, NMAX
0094            FK = FLOAT(2*K - 1)/2.0
0095            RRO = COS(PC)*COS(FK*PC) + SIN(PC)*SIN(FK*PC)
0096            RHO = RHO - A(K)*FK*(RC**(FK-1))*RRO*DY*EPS
0097    130     CONTINUE
0098    C
0099    C       CALCULATE THE CHARACTERISTIC IMPEDANCE Zo
0100    C
0101            Q = 4.0*RHO
0102            C = ABS(Q)/V0
0103            ZO = SQRT(ER)/( C*VL )
0104            PRINT *,C,ZO
0105            WRITE(6,140) ZO
0106    140     FORMAT(2X,'Zo = ',3X,E12.6)
0107            STOP
0108            END
```

Figure 4.7
(Cont.) **Computer program for Example 4.11.**

where

$$B_k = \begin{cases} -V_o, & k \neq N \\ 0, & k = N \end{cases},$$

$$F_{ki} = \begin{cases} \rho_i^{k/2} \cos k\phi_i/2, & i = 1, \ldots, N-1, \\ & k = 1, \ldots, N \\ \dfrac{k}{2}\rho_i^{k/2-1} \left(\cos\left(k\phi_i/2\right)\cos\phi_i + \sin\left(k\phi_i/2\right)\sin\phi_i\right), & i = N,\ k = 1, \ldots, N \end{cases}$$

where (ρ_i, ϕ_i) are the cylindrical coordinates of the ith point. Matrix $[A]$ consists of the unknown expansion coefficients c_k. By matrix inversion using subroutine INVERSE in Appendix D, we obtain $[A]$ as

$$[A] = [F]^{-1}[B] \tag{4.105}$$

Once the expansion coefficients are determined, we now calculate the total charge on the sides of the strip line using Eq. (4.101) and

$$Q = 4 \sum_{BDC} \rho_L \Delta l$$

Finally, we obtain Z_o from Eqs. (4.99) and (4.100). Table 4.5 shows the results obtained using the program in Fig. 4.7 for different cases. In Table 4.5, $N = N_x + N_y$, where N_x and N_y are the number of matching points selected along the x and y axes, respectively. By comparing Fig. 4.5 with Fig. 2.13, one may be tempted to apply Eq. (2.223) to obtain the exact solution of part (a) as 61.1 Ω. But we must recall that Eq. (2.223) was derived based on the assumption that $w >> b$ in Fig. 2.12 or $W >> H$ in Fig. 4.5. The assumption is not valid in this case, the exact solution given in [39] is more appropriate. ∎

Table 4.5 Characteristic Impedance of the Strip Transmission Line of Fig. 4.5; for Example 4.11 with $W_1 = 5.0$

$W = H$	N	N_x	N_y	c_1	Calculated $Z_o(\Omega)$	Exact [39] $Z_o(\Omega)$
1.0	7	5	2	−1.1549	67.846	65.16
	11	8	3	−1.1266	65.16	
0.5	7	5	2	−1.1549	96.92	100.57
	11	8	3	−1.1266	99.60	

4.9 Concluding Remarks

This chapter has provided an elementary introduction to the basic idea of variational techniques. The variational methods provide simple but powerful solutions to physical problems provided we can find approximate basis functions. A prominent feature of the variational method lies in the ability to achieve high accuracy with few terms in the approximate solution. A major drawback is the difficulty encountered in selecting the basis functions. In spite of the drawback, the variational methods have been very useful and provide basis for both the method of moments and the finite element method to be discussed in the forthcoming chapters.

Needless to say, our discussion on variational techniques in this chapter has only been introductory. An exhaustive treatment of the subject can be found in [1, 6, 10, 11], [41]–[43]. Various applications of variational methods to EM-related problems include:

- waveguides and resonators [28]–[37]
- transmission lines [38, 39], [44]–[47]
- acoustic radiation [48]
- wave propagation [49]–[51]
- transient problems [52]
- scattering problems [53]–[59].

The problem of variational principles for EM waves in inhomogeneous media is discussed in [60].

References

[1] S.G. Mikhlin, *Variational Methods in Mathematical Physics.* New York: Macmillan, 1964, pp. xv, 4–78.

[2] J.N. Reddy, *An Introduction to the Finite Element Method.* New York: McGraw-Hill, 2nd ed., 1993, pp. 18–64.

[3] R.B. Guenther and J.W. Lee, *Partial Differential Equations of Mathematical Physics and Integral Equations.* Englewood Cliffs, NJ: Prentice-Hall, 1988, pp. 434–485.

[4] A. Wexler, "Computation of electromagnetic fields," *IEEE Trans. Micro. Theo. Tech.,* vol. MTT-17, no. 8, Aug. 1969, pp. 416–439.

[5] M.M. Ney, "Method of moments as applied to electromagnetic problems," *IEEE Trans. Micro. Theo. Tech.,* vol. MTT-33, no. 10, Oct. 1985, pp. 972–980.

[6] I.M. Gelfand and S.V. Fomin, *Calculus of Variations* (translated from Russian by R.A. Silverman). Englewood Cliffs, NJ: Prentice-Hall, 1963.

[7] J.N. Reddy and M.L. Rasmussen, *Advanced Engineering Analysis.* New York: John Wiley, 1982, pp. 377–386.

[8] B.H. McDonald, et al., "Variational solution of integral equations," *IEEE Trans. Micro. Theo. Tech.,* vol. MTT-22, no. 3, Mar. 1974, pp. 237–248. See also vol. MTT-23, no. 2, Feb. 1975, pp. 265–266 for correction to the paper.

[9] K. Morishita and N. Kumagai, "Unified approach to the derivation of variational expression for electromagnetic fields," *IEEE Trans. Micro. Theo. Tech.*, vol. MTT-25, no. 1, Jan. 1977, pp. 34–39.

[10] B.L. Moiseiwitch, *Variational Principles*. London: Interscience Pub., 1966.

[11] L. Cairo and T. Kahan, *Variational Technique in Electromagnetics*. New York: Gordon & Breach, 1965, pp. 48–65.

[12] K. Kalikstein, "Formulation of variational principles via Lagrange multipliers," *J. Math. Phys.*, vol. 22, no. 7, July 1981, pp. 1433–1437.

[13] K. Kalikstein and A. Sepulveda, "Variational principles and variational functions in electromagnetic scattering," *IEEE Trans. Ant. Prog.*, vol. AP-29, no. 5, Sept. 1981, pp. 811–815.

[14] P. Hammond, "Equilibrium and duality in electromagnetic field problems," *J. Frank. Inst.*, vol. 306, no. 1, July 1978, pp. 133–157.

[15] S.K. Jeng and C.H. Chen, "On variational electromagnetics," *IEEE Trans. Ant. Prog.*, vol. AP-32, no. 9, Sept. 1984, pp. 902–907.

[16] S.J. Chung and C.H. Chen, "Partial variational principle for electromagnetic field problems: theory and applications," *IEEE Trans. Micro. Theo. Tech.*, vol. 36, no. 3, Mar. 1988, pp. 473–479.

[17] R.F. Harrington, *Field Computation by Moment Methods*. Malabar, FL: R.E. Krieger, 1968, pp. 19, 126–131.

[18] S.G. Mikhlin and K.I. Smolitskiy, *Approximate Methods for Solution of Differential and Integral Equations*. New York: Elsevier, 1967, pp. 147–270.

[19] T.J. Chung, *Finite Element Analysis in Fluid Dynamics*. New York: McGraw-Hill, 1978, pp. 36–43.

[20] O.C. Zienkiewicz and R.L. Taylor, *The Finite Element Method*. London: MacGraw-Hill, 1989, vol. 1, 4th ed., pp. 206–259.

[21] L. Lewin, "On the restricted validity of point-matching techniques," *IEEE Trans. Micro. Theo. Tech.*, vol. MTT-18, no. 12, Dec. 1970, pp. 1041–1047.

[22] R.F. Muller, "On the legitimacy of an assumption underlying the point-matching method," *IEEE Trans. Micro. Theo. Tech.*, vol. MTT-18, June 1970, pp. 325–327.

[23] A.R. Djordjevic and T.K. Sarkar, "A theorem on the moment methods," *IEEE Trans. Ant. Prog.*, vol. AP-35, no. 3, Mar. 1987, pp. 353–355.

[24] T.K. Sarkar, "A study of the various methods for computing electromagnetic field utilizing thin wire integral equations," *Radio Sci.*, vol. 18, no. 1, Jan./Feb., pp. 29–38.

[25] T.K. Sarkar, "A note on the variational method (Rayleigh-Ritz), Galerkin's method, and the method of least squares," *Radio Sci.*, vol. 18, no. 6, Nov./Dec. 1983, pp. 1207–1224.

[26] T.K. Sarkar, "A note on the choice of weighting functions in the method of moments," *IEEE Trans. Ant. Prog.*, vol. AP-33, no. 4, April 1985, pp. 436–441.

[27] T.K. Sarkar, et al., "On the choice of expansion and weighting functions in the numerical solution of operator equations," *IEEE Trans. Ant. Prog.*, vol. AP-33, no. 9, Sept. 1985, pp. 988–996.

[28] A.D. Berk, "Variational principles for electromagnetic resonators and waveguides," *IRE Trans. Ant. Prog.*, vol. AP-4, April 1956, pp. 104–111.

[29] G.J. Gabriel and M.E. Brodwin, "The solution of guided waves in inhomogeneous anisotropic media by perturbation and variation methods," *IEEE Trans. Micro. Theo. Tech.*, vol. MTT-13, May 1965, pp. 364–370.

[30] W. English and F. Young, "An E vector variational formulation of the Maxwell equations for cylindrical waveguide problems," *IEEE Trans. Micro. Theo. Tech.*, vol. MTT-19, Jan. 1971, pp. 40–46.

[31] H.Y. Yee and N.F. Audeh, "Uniform waveguides with arbitrary cross-section considered by the point-matching method," *IEEE Trans. Micro. Theo. Tech.*, vol. MTT-13, Nov. 1965, pp. 847–851.

[32] J.A. Fuller and N.F. Audeh, "The point-matching solution of uniform nonsymmetric waveguides," *IEEE Trans. Micro. Theo. Tech.*, vol. MTT-17, no. 2, Feb. 1969.

[33] R.B. Wu and C.H. Chen, "On the variational reaction theory for dielectric waveguides," *IEEE Trans. Micro. Theo. Tech.*, no. 6, June 1985, pp. 477–483.

[34] T.E. Rozzi, "The variational treatment of thick interacting inductive irises," *IEEE Trans. Micro. Theo. Tech.*, vol. MTT-21, no. 2, Feb. 1973, pp. 82–88.

[35] A.D. McAulay, "Variational finite-element solution of dissipative waveguide and transportation application," *IEEE Trans. Micro. Theo. Tech.*, vol. MTT-25, no. 5, May 1977, pp. 382–392.

[36] L.V. Lindell, "A variational method for nonstandard eigenvalue problems in waveguides and resonator analysis," *IEEE Trans. Micro. Theo. Tech.*, vol. MTT-30, no. 8, Aug. 1982, pp. 1194–1204. See comment on this paper in vol. MTT-31, no. 9, Sept. 1983, pp. 786–789.

[37] K. Chang, "Variational solutions on two opposite narrow resonant strips in waveguide," *IEEE Trans. Micro. Theo. Tech.*, vol. MTT-35, no. 2, Feb. 1987, pp. 151–158.

[38] T.K. Seshadri, et al., "Application of 'corner function approach' to strip line problems," *Int. Jour. Electron.*, vol. 44, no. 5, May 1978, pp. 525–528.

[39] T.K. Seshadri, et al., "Least squares collocation as applied to the analysis of strip transmission lines," *Proc. IEEE,* vol. 67, no. 2, Feb. 1979, pp. 314–315.

[40] M.N.O. Sadiku, *Elements of Electromagnetics*. New York: Oxford Univ. Press, Chap. 11, 1994.

[41] P.M. Morse and H. Feshback, *Methods of Theoretical Physics*. New York: McGraw-Hill, 2 volumes, 1953.

[42] R.E. Collin, *Field Theory of Guided Waves*. New York: McGraw-Hill, 1960, pp. 148–164, 314–367.

[43] D.G. Bodner and D.T. Paris, "New variational principle in electromagnetics," *IEEE Trans. Ant. Prog.,* vol. AP-18, no. 2, March 1970, pp. 216–223.

[44] T.D. Tsiboukis, "Estimation of the characteristic impedance of a transmission line by variational methods," *IEEE Proc.,* vol. 132, Pt. H, no. 3, June 1985, pp. 171–175.

[45] E. Yamashita and R. Mittra, "Variational method for the analysis of microstrip lines," *IEEE Trans. Micro. Theo. Tech.,* vol. MTT-16, no. 4, Apr. 1968, pp. 251–256.

[46] E. Yamashita, "Variational method for the analysis of microstrip-like transmission lines," *IEEE Trans. Micro. Theo. Tech.,* vol. MTT-16, no. 8, Aug. 1968, pp. 529–535.

[47] F. Medina and M. Horno, "Capacitance and inductance matrices for multistrip structures in multilayered anisotropic dielectrics," *IEEE Trans. Micro. Theo. Tech.,* vol. MTT-35, no. 11, Nov. 1987, pp. 1002–1008.

[48] F.H. Fenlon, "Calculation of the acoustic radiation of field at the surface of a finite cylinder by the method of weighted residuals," *Proc. IEEE,* vol. 57, no. 3, March 1969, pp. 291–306.

[49] C.H. Chen and Y.W. Kiang, "A variational theory for wave propagation in a one-dimensional inhomogeneous medium," *IEEE Trans. Ant. Prog.,* vol. AP-28, no. 6, Nov. 1980, pp. 762–769.

[50] S.K. Jeng and C.H. Chen, "Variational finite element solution of electromagnetic wave propagation in a one-dimensional inhomogeneous anisotropic medium," *J. Appl. Phys.,* vol. 55, no. 3, Feb. 1984, pp. 630–636.

[51] J.A. Bennett, "On the application of variation techniques to the ray theory of radio propagation," *Radio Sci.,* vol. 4, no. 8, Aug. 1969, pp. 667–678.

[52] J.T. Kuo and D.H. Cho, "Transient time-domain electromagnetics," *Geophys.,* vol. 45, no. 2, Feb. 1980, pp. 271–291.

[53] R.D. Kodis, "An introduction to variational methods in electromagnetic scattering," *J. Soc. Industr. Appl. Math.,* vol. 2, no. 2, June 1954, pp. 89–112.

[54] D.S. Jones, "A critique of the variational method in scattering problems," *IRE Trans.*, vol. AP-4, no. 3, 1965, pp. 297–301.

[55] R.J. Wagner, "Variational principles for electromagnetic potential scattering," *Phys. Rev.*, vol. 131, no. 1, July 1963, pp. 423–434.

[56] J.A. Krill and R.A. Farrell, "Comparison between variational, perturbational, and exact solutions for scattering from a random rough-surface model," *J. Opt. Soc. Am.*, vol. 68, June 1978, pp. 768–774.

[57] R.B. Wu and C.H. Chen, "Variational reaction formulation of scattering problem for anisotropic dielectric cylinders," *IEEE Trans. Ant. Prog.*, vol. 34, no. 5, May 1986, pp. 640–645.

[58] J.A. Krill and R.H. Andreo, "Vector stochastic variational principles for electromagnetic wave scattering," *IEEE Trans. Ant. Prog.*, vol. AP-28, no. 6, Nov. 1980, pp. 770–776.

[59] R.W. Hart and R.A. Farrell, "A variational principle for scattering from rough surfaces," *IEEE Trans. Ant. Prog.*, vol. AP-25, no. 5, Sept. 1977, pp. 708–713.

[60] J.R. Willis, "Variational principles and operator equations for electromagnetic waves in inhomogeneous media," *Wave Motion*, vol. 6, no. 2, 1984, pp. 127–139.

Problems

4.1 Find $\langle u, v \rangle$ if:

(a) $u = x^2,\ v = 2 - x$ in the interval $-1 < x < 1$,

(b) $u = 1,\ v = x^2 - 2y^2$ in the rectangular region $0 < x < 1,\ 1 < y < 2$,

(c) $u = x + y,\ v = xz$ in the cylindrical region $x^2 + y^2 \leq 4,\ 0 < z < 5$.

4.2 Show that:

(a) $\langle h(x), f(x) \rangle = \langle h(x), f(-x) \rangle$,

(b) $\langle h(ax), f(x) \rangle = \left\langle h(x), \frac{1}{a} f\left(\frac{x}{a}\right) \right\rangle$,

(c) $\left\langle \frac{df}{dx}, h(x) \right\rangle = -\left\langle f(x), \frac{dh}{dx} \right\rangle$,

(d) $\left\langle \frac{d^n f}{dx^n}, h(x) \right\rangle = (-1)^n - \left\langle f(x), \frac{d^n h}{dx^n} \right\rangle$

Note from (d) that $L = \dfrac{d}{dx}, \dfrac{d^3}{dx^3}$, etc., are not self-adjoint, whereas $L = \dfrac{d^2}{dx^2}, \dfrac{d^4}{dx^4}$, etc., are.

4.3 Find the Euler partial differential equation for each of the following functionals:

(a) $\displaystyle\int_a^b \sqrt{1+y'}\,dx$

(b) $\displaystyle\int_a^b y\sqrt{1+y'^2}\,dx$

(c) $\displaystyle\int_a^b \cos(xy')\,dx$

4.4 Repeat Problem 4.3 for the following functionals:

(a) $\displaystyle\int_a^b (y'^2 - y^2)\,dx$

(b) $\displaystyle\int_a^b [5y^2 - (y'')^2 + 10x]\,dx$

(c) $\displaystyle\int_a^b (3uv - u^2 + u'^2 - v'^2)\,dx$

4.5 Determine the extremal $y(x)$ for each of the following variational problems:

(a) $\displaystyle\int_0^1 (2y'^2 + yy' + y' + y)\,dx,\ y(0) = 0,\ y(1) = 1$

(b) $\displaystyle\int (y'^2 - y^2)\,dx,\ y(0) = 1,\ y(\pi/2)$

4.6 If L is a positive definite, self-adjoint operator and $L\Phi = g$ has a solution Φ_o, show that the function

$$I = \langle L\Phi, \Phi\rangle - 2\langle \Phi, g\rangle\ ,$$

where Φ and g are real functions, is minimized by the solution Φ_o.

4.7 Show that a function that minimizes the functional

$$I(\Phi) = \frac{1}{2}\int_S \left[|\nabla\Phi|^2 - k^2\Phi^2 + 2g\Phi\right] dS$$

is the solution to the inhomogeneous Helmholtz equation

$$\nabla^2\Phi + k^2\Phi = g$$

4.8 Show that minimizing the energy functional

$$I = \frac{1}{2}\int_v |\nabla V|^2\, dv$$

is equivalent to solving Laplace's equation.

4.9 Using Euler's equation, obtain the differential equation corresponding to the electrostatic field functional

$$I = \int_v \left[\frac{1}{2}\epsilon E^2 - \rho_v V\right] dv$$

where $E = |\mathbf{E}|$ and ρ_v is the volume charge density.

4.10 Repeat Problem 4.9 for the energy function for steady state currents

$$I = \int_v \frac{1}{2}\mathbf{J}\cdot\mathbf{E}\, dv$$

where $\mathbf{J} = \sigma\mathbf{E}$.

4.11 Poisson's equation in an anisotropic medium is

$$\frac{\partial}{\partial x}\left(\epsilon_x \frac{\partial V}{\partial x}\right) + \frac{\partial}{\partial y}\left(\epsilon_y \frac{\partial V}{\partial y}\right) + \frac{\partial}{\partial z}\left(\epsilon_z \frac{\partial V}{\partial z}\right) = -\rho_v$$

in three dimensions. Derive the functional for the boundary value problem. Assume ϵ_x, ϵ_y, and ϵ_z are constants.

4.12 Show that the variational principle for the boundary value problem

$$\nabla^2\Phi = f(x, y, z)$$

subject to the mixed boundary condition

$$\frac{\partial\Phi}{\partial n} + g\Phi = h \quad \text{on} \quad S$$

is

$$I(\Phi) = \int_v \left[|\nabla\Phi|^2 - 2fg\right] dv + \oint \left[g\Phi^2 - 2h\Phi\right] dS$$

4.13 Obtain the variational principle for the differential equation

$$-\frac{d^2y}{dx^2} + y = \sin\pi x\,, \quad 0 < x < 1$$

subject to $y(0) = 0 = y(1)$.

4.14 Determine the variational principle for

$$\Phi'' = \Phi - 4xe^x\ , \quad 0 < x < 1$$

subject to $\Phi'(0) = \Phi(0) + 1$, $\Phi'(1) = \Phi(1) - e$.

4.15 For the boundary value problem

$$-\Phi'' = x\ ,\ 0 < x < 1$$
$$\Phi(0) = 0\ ,\ \Phi(1) = 2$$

determine the approximate solution using the Rayleigh-Ritz method with basis functions

$$u_k = x^k(x-1)\ , \qquad k = 0, 1, 2, \ldots, M$$

Try cases when $M = 1, 2$, and 3.

4.16 Rework Example 4.5 using

(a) $u_m = x(1 - x^m)$,

(b) $u_m = \sin m\pi x$, $m = 1, 2, 3, \ldots, M$. Try cases when $M = 1, 2$, and 3.

4.17 Solve the differential equation

$$-\Phi''(x) + 0.1\Phi(x) = 1, \quad 0 \le x \le 10$$

subject to the boundary conditions $\Phi'(0) = 0 = \Phi(0)$ using the trial function

$$\widetilde{\Phi}(x) = a_1 \cos\frac{\pi x}{20} + a_2 \cos\frac{3\pi x}{20} + a_3 \cos\frac{5\pi x}{20}$$

Determine the expansion coefficients using: (a) collocation method, (b) subdomain method, (c) Galerkin method, (d) least squares method.

4.18 For the boundary value problem

$$\Phi'' + \Phi + x = 0\ , \quad 0 < x < 1$$

with homogeneous boundary conditions $\Phi = 0$ at $x = 0$ and $x = 1$, determine the coefficients of the approximate solution function

$$\widetilde{\Phi}(x) = x(1-x)\,(a_1 + a_2 x)$$

using: (a) collocation method (choose $x = 1/4$, $x = 1/2$ as collocation points), (b) Galerkin method, (c) least squares method.

4.19 Given the boundary value problem

$$y'' + (1 + x^2)y + 1 = 0\ , \quad -1 < x < 1\ ,$$
$$y(-1) = 0 = y(1)\ ,$$

find the expansion coefficients of the approximate solution

$$\widetilde{y} = a_1(1 - x^2) + a_2 x^2(1 - x^2)$$

by using: (i) the various weighted residual methods, (ii) the Rayleigh-Ritz method.

4.20 Rework the previous problem using the approximate solution

$$\widetilde{y} = a_1(1 - x^2)(1 - 4x^2) + a_2 x^2(1 - x^2)$$

Use the Galerkin and the least squares methods to determine a_1 and a_2.

4.21 Consider the problem

$$\Phi'' + x\Phi' + \Phi = 2x\,, \quad 0 < x < 1$$

subject to $\Phi(0) = 1, \Phi(1) = 0$. Find the approximate solution using the Galerkin method. Use $u_k = x^k(1 - x)$, $k = 0, 1, \ldots, N$. Try $N = 3$.

4.22 Determine the first three eigenvalues of the equation

$$y'' + \lambda y = 0\,, \quad 0 < x < 1\,,$$

$y(0) = 0 = y(1)$ using collocation at $x = 1/4, 1/2, 3/4$.

4.23 Determine the fundamental eigenvalue of the problem

$$-\Phi''(x) + 0.1\Phi(x) = \lambda\Phi(x)\,, \quad 0 < x < 10$$

subject to $\Phi(0) = 0 = \Phi(10)$. Use the trial function

$$\widetilde{\Phi}(x) = x(x - 10)$$

4.24 Obtain the lowest eigenvalue of the problem

$$\nabla^2\Phi + \lambda\Phi = 0\,, \quad 0 < \rho < 1$$

with $\Phi = 0$ at $\rho = 1$.

4.25 Rework Example 4.10 using the trial function

$$E_y = \sin\frac{\pi x}{a} + c_1 \sin\frac{3\pi x}{a}$$

where c_1 is a coefficient to be chosen such that $\omega^2\epsilon_o\mu_o$ is minimized.

4.26 Consider the waveguide in Fig. 4.4 as homogeneous. To determine the cutoff frequency, we may use the polynomial trial function

$$H_z = Ax^3 + Bx^2 + Cx + D$$

By applying the conditions

$$H_z = 1 \quad \text{at } x = a\,, \qquad H_z = -1 \text{ at } x = a\,,$$
$$\frac{\partial H_z}{\partial x} = 0 \quad \text{at } x = 0, a\,,$$

determine A, B, C, and D. Using the trial function, calculate the cutoff frequency.

Chapter 5

Moment Methods

"He who will not reason is a bigot; he who cannot is a fool; he who dares not is a slave."
William Drummond

5.1 Introduction

In Section 1.3.2, it was mentioned that most EM problems can be stated in terms of an inhomogeneous equation

$$L\Phi = g \tag{5.1}$$

where L is an operator which may be differential, integral or integro-differential, g is the known excitation or source function, and Φ is the unknown function to be determined. So far, we have limited our discussion to cases for which L is differential. In this chapter, we will treat L as an integral or integro-differential operator.

The *method of moments* (MOM) is a general procedure for solving Eq. (5.1). The method owes its name to the process of taking moments by multiplying with appropriate weighing functions and integrating, as discussed in Section 4.6. The name "method of moments" has its origin in Russian literature [1, 2]. In western literature, the first use of the name is usually attributed to Harrington [3]. The origin and development of the moment method are fully documented by Harrington [4, 5].

The method of moments is essentially the method of weighted residuals discussed in Section 4.6. Therefore, the method is applicable for solving both differential and integral equations.

The use of MOM in EM has become popular since the work of Richmond in 1965 and Harrington [7] in 1967. The method has been successfully applied to a wide variety of EM problems of practical interest such as radiation due to thin-wire elements and arrays, scattering problems, analysis of microstrips and lossy structures, propagation over an inhomogeneous earth, and antenna beam pattern, to mention a few. An updated review of the method is found in a paper by Ney [8]. The literature on MOM is already so large as to prohibit a comprehensive bibliography. A partial bibliography is provided by Adams [9].

The procedure for applying MOM to solve Eq. (5.1) usually involves four steps:

(1) derivation of the appropriate integral equation (IE),

(2) conversion (discretization) of the IE into a matrix equation using basis (or expansions) functions and weighting (or testing) functions,

(3) evaluation of the matrix elements, and

(4) solving the matrix equation and obtaining the parameters of interest.

The basic tools for step (2) have already been mastered in Section 4.6; in this chapter we will apply them to IEs rather than PDEs. Just as we studied PDEs themselves in Section 1.3.2, we will first study IEs.

5.2 Integral Equations

An integral equation is any equation involving unknown function Φ under the integral sign. Simple examples of integral equations are Fourier, Laplace, and Hankel transforms.

5.2.1 Classification of Integral Equations

Linear integral equations that are most frequently studied fall into two categories named after Fredholm and Volterra. One class is the Fredholm equations of the first, second, and third kind, namely,

$$f(x) = \int_a^b K(x,t)\Phi(t)\,dt\,, \tag{5.2}$$

$$f(x) = \Phi(x) - \lambda \int_a^b K(x,t)\Phi(t)\,dt\,, \tag{5.3}$$

$$f(x) = a(x)\Phi(x) - \lambda \int_a^b K(x,t)\Phi(t)\,dt\,, \tag{5.4}$$

where λ is a scalar (or possibly complex) parameter. Functions $K(x,t)$ and $f(x)$ and the limits a and b are known, while $\Phi(x)$ is unknown. The function $K(x,t)$ is known as the *kernel* of the integral equation. The parameter λ is sometimes equal to unity.

The second class of integral equations are the Volterra equations of the first, second, and third kind, namely,

$$f(x) = \int_a^x K(x,t)\Phi(t)\,dt\,, \tag{5.5}$$

$$f(x) = \Phi(x) - \lambda \int_a^x K(x,t)\Phi(t)\,dt\,, \tag{5.6}$$

$$f(x) = a(x)\Phi(x) - \lambda \int_a^x K(x,t)\Phi(t)\,dt\,, \tag{5.7}$$

with a variable upper limit of integration. If $f(x) = 0$, the integral equations (5.2) to (5.7) become homogeneous. Note that Eqs. (5.2) to (5.7) are all linear equations in that Φ enters the equations in a linear manner. An integral equation is nonlinear if Φ appears in the power of $n > 1$ under the integral sign. For example, the integral equation

$$f(x) = \Phi(x) - \int_a^b K(x,t)\Phi^2(t)\,dt \tag{5.8}$$

is nonlinear. Also, if limit a or b or the kernel $K(x,t)$ becomes infinite, an integral equation is said to be singular. Finally, a kernel $K(x,t)$ is said to be symmetric if $K(x,t) = K(t,x)$.

5.2.2 Connection Between Differential and Integral Equations

The above classification of one-dimensional integral equations arises naturally from the theory of differential equations, thereby showing a close connection between the integral and differential formulation of a given problem. Most ordinary differential equations can be expressed as integral equations, but the reverse is not true. While boundary conditions are imposed externally in differential equations, they are incorporated within an integral equation.

For example, consider the first order ordinary differential equation

$$\frac{d\Phi}{dx} = F(x,\Phi), \quad a \le x \le b \tag{5.9}$$

subject to $\Phi(a) =$ constant. This can be written as the Volterra integral of the second kind. Integrating Eq. (5.9) gives

$$\Phi(x) = \int_a^x F(t,\Phi(t))\,dt + c_1$$

where $c_1 = \Phi(a)$. Hence Eq. (5.9) is the same as

$$\Phi(x) = \Phi(a) + \int_a^x F(t,\Phi)\,dt \tag{5.10}$$

Any solution of Eq. (5.10) satisfies both Eq. (5.9) and the boundary conditions. Thus an integral equation formulation includes both the differential equation and the boundary conditions.

Similarly, consider the second order ordinary differential equation

$$\frac{d^2\Phi}{dx^2} = F(x, \Phi), \quad a \leq x \leq b \tag{5.11}$$

Integrating once yields

$$\frac{d\Phi}{dx} = \int_a^x F(x, \Phi(t))\, dt + c_1 \tag{5.12}$$

where $c_1 = \Phi'(a)$. Integrating Eq. (5.12) by parts,

$$\Phi(x) = c_2 + c_1 x + \int_a^x (x - t) F(x, \Phi(t))\, dt$$

where $c_2 = \Phi(a) - \Phi'(a)a$. Hence

$$\Phi(x) = \Phi(a) + (x - a)\Phi'(a) + \int_a^x (x - t) F(x, \Phi)\, dt \tag{5.13}$$

Again, we notice that the integral equation (5.13) represents both the differential equation (5.11) and the boundary conditions. We have only considered one-dimensional integral equations. Integral equations involving unknown functions in two or more space dimensions will be discussed later.

Example 5.1

Solve the Volterra integral equation

$$\Phi(x) = 1 + \int_0^x \Phi(t)\, dt \quad \square$$

Solution

This can be solved directly or indirectly by finding the solution of the corresponding differential equation. To solve it directly, we differentiate both sides of the given integral equation. In general, given an integral

$$g(x) = \int_{\alpha(x)}^{\beta(x)} f(x, t)\, dt \tag{5.14}$$

with variable limits, we differentiate this using the Leibnitz rule, namely,

$$g'(x) = \int_{\alpha(x)}^{\beta(x)} \frac{\partial f(x, t)}{\partial x}\, dt + f(x, \beta)\beta' - f(x, \alpha)\alpha' \tag{5.15}$$

Differentiating the given integral equation, we obtain

$$\frac{d\Phi}{dx} = \Phi(x) \tag{5.16a}$$

or

$$\frac{d\Phi}{\Phi} = dx \tag{5.16b}$$

Integrating gives

$$\ln \Phi = x + \ln c_o$$

or

$$\Phi = c_o e^x$$

where $\ln c_o$ is the integration constant. From the given integral equation

$$\Phi(0) = 1 = c_o$$

Hence

$$\Phi(x) = e^x \tag{5.17}$$

is the required solution. This can be checked by substituting it into the given integral equation.

An indirect way of solving the integral equation is by comparing it with Eq. (5.10) and noting that

$$a = 0, \Phi(a) = \Phi(0) = 1$$

and that $F(x, \Phi) = \Phi(x)$. Hence the corresponding first order differential equation is

$$\frac{d\Phi}{dx} = \Phi, \quad \Phi(0) = 1$$

which is the same as Eq. (5.16), and the solution in Eq. (5.17) follows. ∎

Example 5.2

Find the integral equation corresponding to the differential equation

$$\Phi''' - 3\Phi'' - 6\Phi' + 8\Phi = 0$$

subject to $\Phi''(0) = \Phi'(0) = \Phi(0) = 1$. □

Solution

Let $\Phi''' = F(\Phi, \Phi, \phi, x) = 3\Phi'' + 6\Phi' - 8\Phi$. Integrating both sides,

$$\Phi'' = 3\Phi' + 6\Phi - 8\int_0^x \Phi(t)\,dt + c_1 \tag{5.18}$$

where c_1 is determined from the initial values, i.e.,

$$1 = 3 + 6 + c_1 \quad \rightarrow \quad c_1 = -8$$

Integrating both sides of Eq. (5.18) gives

$$\Phi' = 3\Phi + 6\int_o^x \Phi(t)\,dt - 8\int_0^x (x-t)\Phi(t)\,dt - 8x + c_2 \tag{5.19}$$

where

$$1 = 3 + c_2 \quad \rightarrow \quad c_2 = -2$$

Finally, we integrate both sides of Eq. (5.19) to get

$$\Phi = 3\int_o^x \Phi(t)\,dt + 6\int_o^x (x-t)\Phi(t)\,dt - 4\int_o^x (x-t)^2\Phi(t)\,dt - 4x^2 - 2x + c_3$$

where $1 = c_3$. Thus the integral equation equivalent to the given differential equation is

$$\Phi(x) = 1 - 2x - 4x^2 + \int_o^x \left[3 + 6(x-t) - 4(x-t)^2\right]\Phi(t)\,dt \qquad \blacksquare$$

5.3 Green's Functions

A more systematic means of obtaining an IE from a PDE is by constructing an auxiliary function known as the *Green's function*[1] for that problem [10]–[13]. The Green's function, also known as the *source function* or *influence function,* is the kernel function obtained from a linear boundary value problem and forms the essential link between the differential and integral formulations. Green's function also provides a method of dealing with the source term (g in $L\Phi = g$) in a PDE. In other words, it provides an alternative approach to the series expansion method of Section 2.7 for solving inhomogeneous boundary-value problems by reducing the inhomogeneous problem to a homogeneous one.

To obtain the field caused by a distributed source by the Green's function technique, we find the effects of each elementary portion of source and sum them up. If $G(\mathbf{r}, \mathbf{r}')$ is the field at the observation point (or field point) $\mathbf{r}$ caused by a unit point source at the source point $\mathbf{r}'$, then the field at $\mathbf{r}$ by a source distribution $g(\mathbf{r}')$ is the integral of $g(\mathbf{r}')G(\mathbf{r}, \mathbf{r}')$ over the range of $\mathbf{r}'$ occupied by the source. The function G is the Green's function. Thus, physically, the Green's function $G(\mathbf{r}, \mathbf{r}')$ represents the potential at $\mathbf{r}$ due to a unit point charge at $\mathbf{r}'$. For example, the solution to the Dirichlet problem

$$\begin{aligned} \nabla^2\Phi &= g \quad \text{in} \quad R \\ \Phi &= f \quad \text{on} \quad B \end{aligned} \tag{5.20}$$

[1] Named after George Green (1793–1841), an English mathematician.

is given by

$$\Phi = \int_R g\left(\mathbf{r}'\right) G\left(\mathbf{r}, \mathbf{r}'\right) dv' + \oint_B f \frac{\partial G}{\partial n} dS \tag{5.21}$$

where n denotes the outward normal to the boundary B of the solution region R. It is obvious from Eq. (5.21) that the solution Φ can be determined provided the Green's function G is known. So the real problem is not that of finding the solution but that of constructing the Green's function for the problem.

Consider the linear second order PDE

$$L\Phi = g \tag{5.22}$$

We define the Green's function corresponding to the differential operator L as a solution of the point source inhomogeneous equation

$$LG\left(\mathbf{r}, \mathbf{r}'\right) = \delta\left(\mathbf{r}, \mathbf{r}'\right) \tag{5.23}$$

where $\mathbf{r}$ and $\mathbf{r}'$ are the position vectors of the field point (x, y, z) and source point (x', y', z'), respectively, and $\delta(\mathbf{r}, \mathbf{r}')$ is the Dirac delta function, which vanishes for $\mathbf{r} \neq \mathbf{r}'$ and satisfies

$$\int \delta\left(\mathbf{r}, \mathbf{r}'\right) g\left(\mathbf{r}'\right) dv' = g(\mathbf{r}) \tag{5.24}$$

From Eq. (5.23), we notice that the Green function $G(\mathbf{r}, \mathbf{r}')$ can be interpreted as the solution to the given boundary value problem with the source term g replaced by the unit impulse function. Thus $G(\mathbf{r}, \mathbf{r}')$ physically represents the response of the linear system to a unit impulse applied at the point $\mathbf{r} = \mathbf{r}'$.

The Green's function has the following properties [13]:

(a) G satisfies the equation $LG = 0$ except at the source point $\mathbf{r}'$, i.e.,

$$LG\left(\mathbf{r}, \mathbf{r}'\right) = \delta\left(\mathbf{r}, \mathbf{r}'\right) \tag{5.23}$$

(b) G is symmetric in the sense that

$$G\left(\mathbf{r}, \mathbf{r}'\right) = G\left(\mathbf{r}', \mathbf{r}\right) \tag{5.25}$$

(c) G satisfies that prescribed boundary value f on B, i.e.,

$$G = f \text{ on } B \tag{5.26}$$

(d) The directional derivative $\partial G/\partial n$ has a discontinuity at $\mathbf{r}'$ which is specified by the equation

$$\lim_{\epsilon \to 0} \oint_S \frac{\partial G}{\partial n} dS = 1 \tag{5.27}$$

where n is the outward normal to the sphere of radius ϵ as shown in Fig. 5.1, i.e.,

$$\left|\mathbf{r} - \mathbf{r}'\right| = \epsilon^2$$

Property (b) expresses the *principle of reciprocity*; it implies that an exchange of source and observer does not affect G. The property is proved by Myint–U [13] by applying Green's second identity in conjunction with Eq. (5.23) while property (d) is proved by applying divergence theorem along with Eq. (5.23).

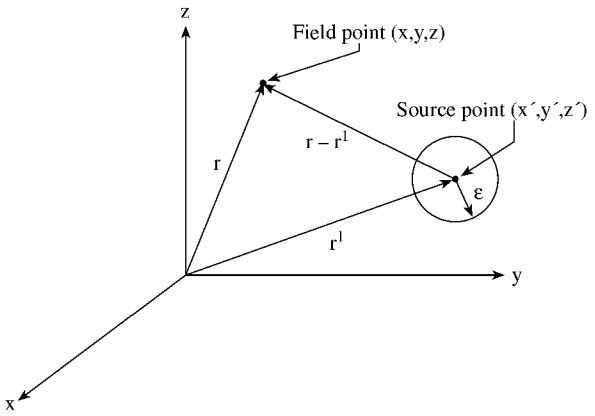

Figure 5.1
Illustration of the field point (x, y, z) and source point (x', y', z').

5.3.1 For Free Space

We now illustrate how to construct the free space Green's function G corresponding to a PDE. It is usually convenient to let G be the sum of a particular integral of the inhomogeneous equation $LG = g$ and the solution of the associated homogeneous equation $LG = 0$. In other words, we let

$$G\left(\mathbf{r}, \mathbf{r}'\right) = F\left(\mathbf{r}, \mathbf{r}'\right) + U\left(\mathbf{r}, \mathbf{r}'\right) \tag{5.28}$$

where F, known as the free-space Green's function or fundamental solution, satisfies

$$LF = \delta\left(\mathbf{r}, \mathbf{r}'\right) \text{ in } R \tag{5.29}$$

and U satisfies

$$LU = 0 \text{ in } R \tag{5.30}$$

so that by superposition $G = F + U$ satisfies Eq. (5.23). Also $G = f$ on the boundary B requires that

$$U = -F + f \text{ on } B \tag{5.31}$$

Notice that F need not satisfy the boundary condition.

We apply this to two specific examples. First, consider the two-dimensional problem for which

$$L = \frac{\partial^2}{\partial x^2} + \frac{\partial^2}{\partial y^2} = \nabla^2 \tag{5.32}$$

The corresponding Green's function $G(x, y; x', y')$ satisfies

$$\nabla^2 G\left(x, y; x', y'\right) = \delta\left(x - x'\right)\delta\left(y - y'\right) \tag{5.33}$$

Hence, F must satisfy

$$\nabla^2 F = \delta\left(x - x'\right)\delta\left(y - y'\right)$$

For $\rho = [(x - x')^2 + (y - y')^2]^{1/2} > 0$, i.e., for $x \neq x'$, $y \neq y'$,

$$\nabla^2 F = \frac{1}{\rho}\frac{\partial}{\partial \rho}\left(\rho \frac{\partial F}{\partial \rho}\right) = 0 \tag{5.34}$$

which is integrated twice to give

$$F = A \ln \rho + B \tag{5.35}$$

Applying the property in Eq. (5.27)

$$\lim_{\epsilon \to 0} \oint \frac{dF}{d\rho}\, dl = \lim_{\epsilon \to 0} \int_0^{2\pi} \frac{A}{\rho} \rho\, d\phi = 2\pi A = 1$$

or $A = \dfrac{1}{2\pi}$. Since B is arbitrary, we may choose $B = 0$. Thus

$$F = \frac{1}{2\pi} \ln \rho$$

and

$$G = F + U = \frac{1}{2\pi} \ln \rho + U \tag{5.36}$$

We choose U so that G satisfies prescribed boundary conditions.

For the three-dimensional problem,

$$L = \nabla^2 = \frac{\partial^2}{\partial x^2} + \frac{\partial^2}{\partial y^2} + \frac{\partial^2}{\partial z^2} \tag{5.37}$$

and the corresponding Green's function $G(x, y, z; x', y', z')$ satisfies

$$LG\left(x, y, z; x', y', z'\right) = \delta\left(x - x'\right)\delta\left(y - y'\right)\delta\left(z - z'\right) \tag{5.38}$$

Hence, F must satisfy

$$\begin{aligned} \nabla^2 F &= \delta\left(x - x'\right)\delta\left(y - y'\right)\delta\left(z - z'\right) \\ &= \delta\left(\mathbf{r} - \mathbf{r}'\right) \end{aligned}$$

For $\mathbf{r} \neq \mathbf{r}'$,

$$\nabla^2 F = \frac{1}{r^2}\frac{d}{dr}\left(r^2 \frac{dF}{dr}\right) = 0 \tag{5.39}$$

which is integrated twice to yield

$$F = -\frac{A}{r} + B \tag{5.40}$$

Applying Eq. (5.27),

$$1 = \lim_{\epsilon \to 0} \oint \frac{dF}{dr} dS = \lim_{\epsilon \to 0} \int_0^{2\pi} \int_0^{\pi} \frac{A}{r^2} r^2 \sin\phi \, d\theta \, d\phi = 4\pi A$$

or $A = \dfrac{1}{4\pi}$. Choosing $B = 0$ leads to

$$F = -\frac{1}{4\pi r}$$

and

$$G = F + U = -\frac{1}{4\pi r} + U \tag{5.41}$$

where U is chosen so that G satisfies prescribed boundary conditions.

Table 5.1 lists some Green functions that are commonly used in the solution of EM-related problems. It should be observed from Table 5.1 that the form of the three-dimensional Green's function for the steady-state wave equation tends to the Green's function for Laplace's equation as the wave number k approaches zero. It is also worthy of remark that each of the Green's functions in closed form as in Table 5.1 can be expressed in series form. For example, the Green's function

$$\begin{aligned} F &= -\frac{j}{4} H_0^{(1)} \left(k \left| \boldsymbol{\rho} - \boldsymbol{\rho}' \right| \right) \\ &= -\frac{j}{4} H_0^{(1)} \left(k \left[\rho^2 + \rho'^2 - 2\rho\rho' \cos\left(\phi - \phi'\right) \right]^{1/2} \right) \end{aligned} \tag{5.42}$$

can be written in series form as

$$F = \begin{cases} -\dfrac{j}{4} \displaystyle\sum_{n=-\infty}^{\infty} H_n^{(1)} \left(k\rho'\right) J_n(k\rho) e^{-jn(\phi - \phi')}, & \rho < \rho' \\ -\dfrac{j}{4} \displaystyle\sum_{n=-\infty}^{\infty} H_n^{(1)}(k\rho) J_n \left(k\rho'\right) e^{-jn(\phi - \phi')}, & \rho > \rho' \end{cases} \tag{5.43}$$

This is obtained from addition theorem for Hankel functions [14]. It should be noted that Green's functions are very difficult to construct in an explicit form except for the simplest shapes of domain.

With the aid of the Green's function, we can construct the integral equation corresponding to Poisson's equation in three dimensions

$$\nabla^2 V = -\frac{\rho_v}{\epsilon} \tag{5.44}$$

as

$$V = \int \frac{\rho_v}{\epsilon} G\left(\mathbf{r}, \mathbf{r}'\right) dv'$$

Table 5.1 Free-Space Green's Functions

Operator equation	Laplace's equation	Steady-state Helmholtz's (or wave) equation[1]	Modified steady-state Helmholtz's (or wave) equation
Solution Region	$\nabla^2 G = \delta(\mathbf{r}, \mathbf{r}')$	$\nabla^2 G + k^2 G = \delta(\mathbf{r}, \mathbf{r}')$	$\nabla^2 G - k^2 G = \delta(\mathbf{r}, \mathbf{r}')$
1- dimensional	no solution for $(-\infty, \infty)$	$-\frac{j}{2k}\exp(jk\lvert x - x'\rvert)$	$-\frac{1}{2k}\exp(-k\lvert x - x'\rvert)$
2-dimensional	$\frac{1}{2\pi}\ln\lvert\rho - \rho'\rvert$	$-\frac{j}{4}H_0^{(1)}(k\lvert\rho - \rho'\rvert)$	$-\frac{1}{2\pi}K_o(k\lvert\rho - \rho'\rvert)$
3-dimensional	$-\frac{1}{4\pi(\mathbf{r}-\mathbf{r}')}$	$-\frac{\exp(jk\lvert\mathbf{r}-\mathbf{r}'\rvert)}{4\pi\lvert\mathbf{r}-\mathbf{r}'\rvert}$	$-\frac{\exp(-k\lvert\mathbf{r}-\mathbf{r}'\rvert)}{4\pi\lvert\mathbf{r}-\mathbf{r}'\rvert}$

[1] The wave equation has the time factor $e^{j\omega t}$ so that $k = \omega\sqrt{\mu\epsilon}$.

or

$$V = \int \frac{\rho_v \, dv'}{4\pi\epsilon r} \tag{5.45}$$

Similarly, the integral equation corresponding to Helmholtz's equation in three dimensions

$$\nabla^2\Phi + k^2\Phi = g \tag{5.46}$$

as

$$\Phi = \int gG(\mathbf{r}, \mathbf{r}') \, dv'$$

or

$$\Phi = \int \frac{ge^{jkr} \, dv'}{4\pi r} \tag{5.47}$$

where an outgoing wave is assumed.

5.3.2 For Domain with Conducting Boundaries

The Green's functions derived so far are useful if the domain is free space. When the domain is bounded by one or more grounded planes, there are two ways to obtain Green's function:

(a) the method of images [12], [15]–[22] and

(b) the eigenfunction expansion [12, 16, 17], [22]–[30].

(a) Method of Images

The method of images is a powerful technique for obtaining the field due to one or more sources with conducting boundary planes. If a point charge q is at some distance h from a grounded conducting plane, the boundary condition imposed by the plane on the resulting potential field may be satisfied by replacing the plane with an "image charge" $-q$ located at a position which is the mirror location of q. Using this idea to obtain the Green's function is perhaps best illustrated with an example.

Consider the region between the ground planes at $y = 0$ and $y = h$ as shown in Fig. 5.2. The Green's function $G(x, y; x', y')$ is the potential at the point (x, y), which results when a unit line charge of 1 C/m is placed at the point (x', y'). If no ground planes were present, the potential at distance ρ from a unit line charge would be

$$V(\rho) = \frac{1}{4\pi\epsilon} \ln \rho^2 \tag{5.48}$$

In order to satisfy the boundary conditions on the ground planes, an infinite set of images is derived as shown in Fig. 5.2. The potential due to such a sequence of line charges (including the original) within the strip is the superposition of an infinite series of images:

$$\begin{aligned} G\left(x, y; x', y'\right) = \frac{1}{4\pi\epsilon} \Bigg(& \ln\left[\left(x - x'\right)^2 + \left(y + y'\right)^2\right] - \ln\left[\left(x - x'\right)^2 + \left(y + y'\right)^2\right] \\ & + \sum_{n=1}^{\infty} (-1)^n \Big\{ \ln\left[\left(x - x'\right)^2 + \left(y + y' - 2nh\right)^2\right] \\ & - \ln\left[\left(x - x'\right)^2 + \left(y - y' - 2nh\right)^2\right] \\ & + \ln\left[\left(x - x'\right)^2 + \left(y + y' - 2nh\right)^2\right] \\ & - \ln\left[\left(x - x'\right)^2 + \left(y - y' - 2nh\right)^2\right] \Big\} \Bigg) \\ = \frac{1}{4\pi\epsilon} & \sum_{n=-\infty}^{\infty} \ln\left[\frac{\left(x - x'\right)^2 + \left(y + y' - 2nh\right)^2}{(x - x')^2 + (y - y' - 2nh)^2}\right] \end{aligned} \tag{5.49}$$

This series converges slowly and is awkward for numerical computation. It can be summed to give [15]

$$G\left(x, y; x', y'\right) = \frac{1}{4\pi\epsilon} \ln\left[\frac{\sinh^2\left(\frac{\pi(x-x')}{2h}\right) + \sin^2\left(\frac{\pi(y+y')}{2h}\right)}{\sinh^2\left(\frac{\pi(x-x')}{2h}\right) + \sin^2\left(\frac{\pi(y-y')}{2h}\right)}\right] \tag{5.50}$$

This expression can be shown to satisfy the appropriate boundary conditions along the ground plane, i.e., $G(x, y; x', y') = 0$ at $y = 0$ or $y = h$. Note that G has exactly one singularity at $x = x',\ y = y'$ in the region $0 \le y \le h$.

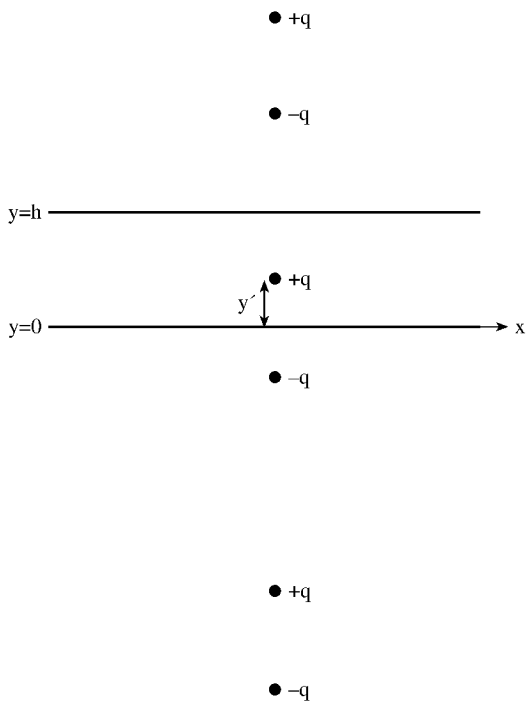

Figure 5.2
A single charge placed between two conducting planes produces the same potential as does the system of image charges when no conducting planes are present.

In order to evaluate an integral involving $G(x, y; x', y')$ in Eq. (5.50), it is convenient to take out the singular portion of the unit source function. We rewrite Eq. (5.50) as

$$G\left(x, y; x', y'\right) = -\frac{1}{4\pi\epsilon} \ln\left[\left(x - x'\right)^2 + \left(y + y'\right)^2\right] + g\left(x, y; x', y'\right) \qquad (5.51)$$

where

$$g\left(x, y; x', y'\right) =$$

$$\frac{1}{4\pi\epsilon} \ln\left[\frac{\left[\left(x - x'\right)^2 \left(y - y'\right)^2\right]\left[\sinh^2\left(\frac{\pi\left(x-x'\right)}{2h}\right) + \sin^2\left(\frac{\pi\left(y+y'\right)}{2h}\right)\right]}{\sinh^2\left(\frac{\pi\left(x-x'\right)}{2h}\right) + \sin^2\left(\frac{\pi\left(y-y'\right)}{2h}\right)}\right] \qquad (5.52)$$

Note that $g(x, y; x', y')$ is finite everywhere in $0 \leq y \leq h$. The integral involving g is evaluated numerically, while the one involving the singular logarithmic term is evaluated analytically with the aid of integral tables.

The method of images has been applied in derivating the Green's functions for multiconductor transmission lines [18]–[20] and planar microwave circuits [16, 17, 21]. The method is restricted to the shapes enclosed by boundaries that are straight conductors.

(b) Eigenfunction Expansion

This method is suitable for deriving the Green's function for differential equations whose homogeneous solution is known. The Green's function is represented in terms of a series of orthonormal functions that satisfy the boundary conditions associated with the differential equation. To illustrate the eigenfunction expansion procedure, suppose we are interested in the Green's function for the wave equation

$$\frac{\partial^2 \Psi}{\partial x^2} + \frac{\partial^2 \Psi}{\partial y^2} + k^2 \Psi = 0 \tag{5.53}$$

subject to

$$\frac{\partial \Psi}{\partial n} = 0 \quad \text{or} \quad \Psi = 0 \tag{5.54}$$

Let the eigenfunctions and eigenvalues of Eq. (5.53) that satisfy Eq. (5.54) be Ψ_j and k_j, respectively, i.e.,

$$\nabla^2 \Psi_j + k_j^2 \Psi_j = 0 \tag{5.55}$$

Assuming that Ψ_j form a complete set of orthonormal functions,

$$\int_S \Psi_j^* \Psi_i \, dxdy = \begin{cases} 1, & j = i \\ 0, & j \neq i \end{cases} \tag{5.56}$$

where the asterisk $(*)$ denotes complex conjugation. $G(x, y; x', y')$ can be expanded in terms of Ψ_j, i.e.,

$$G\left(x, y; x', y'\right) = \sum_{j=1}^{\infty} a_j \Psi_j(x, y) \tag{5.57}$$

Since the Green's function must satisfy

$$\left(\nabla^2 + k^2\right) G\left(x, y; x', y'\right) = \delta\left(x - x'\right) \, \delta\left(y - y'\right) \, , \tag{5.58}$$

substituting Eqs. (5.55) and (5.57) into Eq. (5.58), we obtain

$$\sum_{j=1}^{\infty} a_j \left(k^2 - k_j^2\right) \Psi_j = \delta\left(x - x'\right) \, \delta\left(y - y'\right) \tag{5.59}$$

Multiplying both sides by Ψ_i^* and integrating over the region S gives

$$\sum_{j=1}^{\infty} a_j \left(k^2 - k_j^2\right) \int_S \Psi_j \Psi_i^* \, dxdy = \Psi_i^* \left(x', y'\right) \tag{5.60}$$

Imposing the orthonormal property in Eq. (5.56) leads to

$$a_i \left(k^2 - k_i^2\right) = \Psi_i^* \left(x', y'\right)$$

or

$$a_i = \frac{\Psi_i^* \left(x', y'\right)}{\left(k^2 - k_i^2\right)} \tag{5.61}$$

Thus

$$G\left(x, y; x', y'\right) = \sum_{j=1}^{\infty} \frac{\Psi_j(x, y)\Psi_j^* \left(x', y'\right)}{\left(k^2 - k_j^2\right)} \tag{5.62}$$

The eigenfunction expansion approach has been applied to derive the Green's functions for plane conducting boundaries such as rectangular box and prism [22], planar microwave circuits [16, 17, 25], multilayered dielectric structures [23, 24], waveguides [28], and surfaces of revolution [27]. The approach is limited to separable coordinate systems since the requisite eigenfunctions can be determined for only these cases.

Example 5.3

Construct a Green's function for

$$\nabla^2 V = 0$$

subject to $V(a, \phi) = f(\phi)$ within a circular disk $\rho \leq a$. □

Solution

Since $g = 0$, the solution is obtained from Eq. (5.21) as

$$V = \oint_C f \frac{\partial G}{\partial n} \, dl \tag{5.63}$$

where the circle C is the boundary of the disk as shown in Fig. 5.3. Let

$$G = F + U \, ,$$

where F is already found to be

$$F = \frac{1}{2\pi} \ln \left|\rho - \rho'\right| \, ,$$

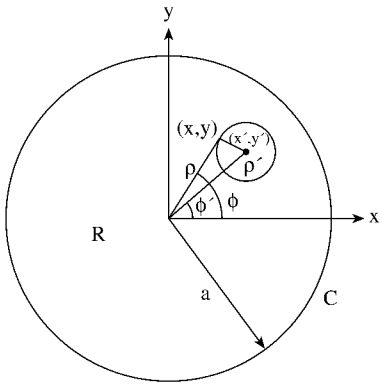

Figure 5.3
A disk of radius a.

i.e.,

$$F\left(\rho, \phi; \rho', \phi'\right) = \frac{1}{4\pi} \ln\left[\rho'^2 + \rho'^2 - 2\rho\rho' \cos\left(\phi - \phi'\right)\right] \tag{5.64}$$

The major problem is finding U. But

$$\nabla^2 U = 0 \quad \text{in } R \tag{5.65a}$$

with

$$U = -F \quad \text{on} \quad C$$

or

$$U\left(a, \phi; \rho', \phi'\right) = -\frac{1}{4\pi} \ln\left[a^2 + \rho'^2 - 2a\rho' \cos\left(\phi - \phi'\right)\right] \tag{5.65b}$$

Thus U can be found by solving the PDE in Eq. (5.65a) subject to the condition in Eq. (5.65b). Applying the separation of variables method,

$$U = \frac{A_0}{2} \sum_{n=1}^{\infty} \rho^n \left[A_n \cos n\phi + B_n \sin n\phi\right] \tag{5.66}$$

The term ρ^{-n} is not included since U must be bounded at $\rho = 0$. To impose the boundary condition in Eq. (5.65b) on the solution in Eq. (5.66), we first express Eq. (5.65b) in Fourier series using the identity

$$\sum_{n=1}^{\infty} \frac{z^n}{n} \cos n\theta = \int_0^z \frac{\cos\theta - \lambda}{1 + \lambda^2 - 2\lambda\cos\theta}\, d\lambda = -\frac{1}{2} \ln\left[1 + z^2 - 2z\cos\theta\right] \tag{5.67}$$

Hence Eq. (5.65b) becomes

$$U\left(a,\phi;\rho',\phi'\right) = -\frac{1}{4\pi}\ln a^2\left[1+\left(\rho'/a\right)^2-\frac{2\rho'}{a}\cos\left(\phi-\phi'\right)\right]$$
$$= -\frac{1}{2\pi}\ln a+\frac{1}{2\pi}\sum_{n=1}^{\infty}\left[\frac{\rho'}{a}\right]^n\frac{\cos n\left(\phi-\phi'\right)}{n}$$
$$= -\frac{1}{2\pi}\ln a+\frac{1}{2\pi}\sum_{n=1}^{\infty}\left[\frac{\rho'}{a}\right]^n\cdot$$
$$\frac{\left(\cos n\phi\cos n\phi'+\sin n\phi\sin n\phi'\right)}{n} \tag{5.68}$$

Comparing Eq. (5.66) with Eq. (5.68) at $\rho = a$, we obtain the coefficients A_n and B_n as

$$\frac{A_0}{2} = -\frac{1}{2\pi}\ln a$$
$$a^n A_n = \frac{1}{2\pi n}\left[\frac{\rho'}{a}\right]^n\cos n\phi'$$
$$a^n B_n = \frac{1}{2\pi n}\left[\frac{\rho'}{a}\right]^n\sin n\phi'$$

Thus Eq. (5.66) becomes

$$U\left(\rho,\phi;\rho',\phi'\right) = -\frac{1}{2\pi}\ln a+\frac{1}{2\pi}\sum_{n=1}^{\infty}\left[\frac{\rho'}{a}\right]^n\left[\frac{\rho}{a}\right]^n\frac{\cos n\left(\phi-\phi'\right)}{n}$$
$$= -\frac{1}{2\pi}\ln a-\frac{1}{4\pi}\ln\left[1+\left[\frac{\rho\rho'}{a^2}\right]^2-\frac{2\rho\rho'}{a^2}\cos\left(\phi-\phi'\right)\right] \tag{5.69}$$

From Eqs. (5.64) and Eq. (5.69), we obtain the Green's function as

$$G = \frac{1}{4\pi}\ln\left[\rho^2+\rho'^2-2\rho\rho'\cos\left(\phi-\phi'\right)\right]$$
$$-\frac{1}{4\pi}\ln\left[a^2+\frac{\rho'^2\rho^2}{a^2}-2\rho\rho'\cos\left(\phi-\phi'\right)\right] \tag{5.70}$$

An alternative means of constructing the Green's function is the method of images. Let us obtain Eq. (5.70) using the method of images. Let

$$G\left(P,P'\right) = \frac{1}{2\pi}\ln r+U$$

The problem reduces to finding the induced field U, which is harmonic within the disk and is equal to $-\frac{1}{2\pi}\ln r$ on C. Let P' be the singular point of Green's function

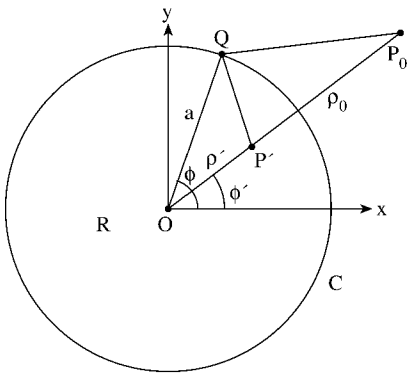

Figure 5.4
The image point P_o of P' with respect to circle C so that $OP'.OP_o = OQ = a^2$ and OQP' and OP_oQ are similar triangles.

and let P_o be the image of P' with respect to the circle C as shown in Fig. 5.4. The triangles OQP' and OQP_0 are similar because the angle at O is common and the sides adjacent to it are proportional. Thus

$$\frac{\rho'}{a} = \frac{a}{\rho_o} \quad \rightarrow \quad \rho'\rho_o = a^2 \tag{5.71}$$

That is, the product of OP' and OP_o is equal to the square of the radius OQ. At a point Q on C, it is evident from Fig. 5.4 that

$$r_{QP'} = \frac{\rho'}{a} r_{QP_o}$$

Therefore,

$$U = -\frac{1}{2\pi} \ln \frac{\rho' r_{PP_o}}{a} \tag{5.72}$$

and

$$G = \frac{1}{2\pi} \ln r_{PP'} - \frac{1}{2\pi} \ln \frac{\rho'}{a} r_{PP_o} \tag{5.73}$$

Since $r_{PP'}$ is the distance between $P(\rho, \phi)$ and $P'(\rho', \phi')$ while r_{PP_o} is the distance between $P(\rho, \phi)$ and $P_o(\rho'_o, \phi) = P_o(a^2/\rho', \phi)$,

$$r^2_{PP'} = \rho^2 + \rho'^2 - 2\rho\rho' \cos(\phi - \phi') \ ,$$
$$r^2_{PP_o} = \rho^2 + \frac{a^4}{\rho'^2} - 2\rho\frac{a^2}{\rho'} \cos(\phi - \phi')$$

Substituting these in Eq. (5.73), we obtain

$$G = \frac{1}{4\pi} \ln\left[\rho^2 + \rho'^2 - 2\rho\rho' \cos\left(\phi - \phi'\right)\right] - \frac{1}{4\pi} \ln\left[a^2 + \frac{\rho'^2\rho^2}{a^2} - 2\rho\rho' \cos\left(\phi - \phi'\right)\right] \tag{5.74}$$

which is the same as Eq. (5.70). From Eq. (5.70) or (5.74), the directional derivative $\partial G/\partial n = (\nabla G \cdot \mathbf{a}_n)$ on C is given by

$$\left.\frac{\partial G}{\partial \rho'}\right|_{\rho'=a} = \frac{2a - 2\rho\cos\left(\phi - \phi'\right)}{4\pi\left[a^2 + \rho^2 - 2a\rho\cos\left(\phi - \phi'\right)\right]} - \frac{\frac{2\rho^2}{a} - 2\rho\cos\left(\phi - \phi'\right)}{4\pi\left[a^2 + \rho^2 - 2a\rho\cos\left(\phi - \phi'\right)\right]},$$

$$= \frac{a^2 - \rho^2}{2\pi a\left[a^2 + \rho^2 - 2a\rho\cos\left(\phi - \phi'\right)\right]}$$

Hence the solution in Eq. (5.63) becomes (with $dl = ad\phi'$)

$$V(\rho, \phi) = \frac{1}{2\pi}\int_0^{2\pi} \frac{\left(a^2 - \rho^2\right) f\left(\phi'\right) d\phi'}{\left[a^2 + \rho^2 - 2a\rho\cos\left(\phi - \phi'\right)\right]} \tag{5.75}$$

which is known as *Poisson's integral formula.* ∎

Example 5.4

Obtain the solution for the Laplace operator on unbounded half-space, $z \leq 0$ with the condition $V(z = 0) = f$. □

Solution

Again the solution is

$$V = \oint_S f \frac{\partial G}{\partial n} dS$$

where S is the plane $z = 0$. We let

$$G = \frac{1}{4\pi\left|\mathbf{r} - \mathbf{r}'\right|} + U,$$

so that the major problem is reduced to finding U. Using the method of images, it is easy to see that the image point of $P'(x', y', z')$ is $P_o(x', y', -z')$ as shown in Fig. 5.5. Hence

$$U = -\frac{1}{4\pi\left|\mathbf{r} - \mathbf{r}_o\right|}$$

and

$$G = \frac{1}{4\pi\left|\mathbf{r} - \mathbf{r}'\right|} - \frac{1}{4\pi\left|\mathbf{r} - \mathbf{r}_o\right|},$$

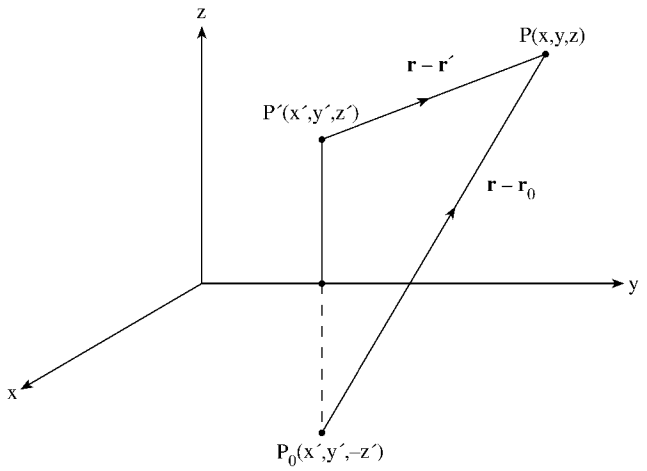

Figure 5.5
Half-space problem of Example 5.4.

where

$$|\mathbf{r}-\mathbf{r}'| = \left[(x-x')^2+(y-y')^2+(z-z')^2\right]^{1/2}$$
$$|\mathbf{r}-\mathbf{r}_o| = \left[(x-x')^2+(y-y')^2+(z+z')^2\right]^{1/2}$$

Notice that G reduces to zero at $z = 0$ and has the required singularity at $P'(x', y', z')$. The directional derivative $\partial G/\partial n$ on plane $z = 0$ is

$$\left.\frac{\partial G}{\partial z'}\right|_{z'=0} = \frac{1}{4\pi}\left[\frac{(z-z')}{|\mathbf{r}-\mathbf{r}'|^3}+\frac{(z+z')}{|\mathbf{r}-\mathbf{r}_o|^3}\right]\Bigg|_{z'=0}$$
$$= \frac{z}{2\pi\left[(x-x')^2+(y-y')^2+z^2\right]^{3/2}}$$

Hence

$$V(x,y,z) = \frac{1}{2\pi}\int_{-\infty}^{\infty}\int_{-\infty}^{\infty}\frac{zf(x',y')\,dx'dy'}{\left[(x-x')^2+(y-y')^2+z^2\right]^{3/2}} \quad \blacksquare$$

Example 5.5
Using Green's function, construct the solution for Poisson's equation

$$\frac{\partial^2 V}{\partial x^2}+\frac{\partial^2 V}{\partial y^2} = f(x,y)$$

subject to the boundary conditions

$$V(0, y) = V(a, y) = V(x, 0) = V(x, b) = 0 \qquad \square$$

Solution

According to Eq. (5.21), the solution is

$$V(x, y) = \int_0^b \int_0^a f\left(x', y'\right) G\left(x, y; x', y'\right) \, dx'dy' \tag{5.76}$$

so that our problem is essentially that of obtaining the Green's function $G(x, y; x', y')$. The Green's function satisfies

$$\frac{\partial^2 G}{\partial x^2} + \frac{\partial^2 G}{\partial y^2} = \delta\left(x - x'\right)\delta\left(y - y'\right) \tag{5.77}$$

To apply the series expansion method of finding G, we must first determine eigenfunctions $\Psi(x, y)$ of Laplace's equation, i.e.,

$$\nabla^2 \Psi = \lambda \Psi$$

where Ψ satisfies the boundary conditions. It is evident that the normalized eigenfunctions are

$$\Psi_{mn} = \frac{2}{\sqrt{ab}} \sin\frac{m\pi x}{a} \sin\frac{n\pi y}{b}$$

with the corresponding eigenvalues

$$\lambda_{mn} = -\left(\frac{m^2\pi^2}{a^2} + \frac{n^2\pi^2}{b^2}\right)$$

Thus,

$$G\left(x, y; x', y'\right) = \frac{2}{\sqrt{ab}} \sum_{m=1}^{\infty} \sum_{n=1}^{\infty} A_{mn}\left(x', y'\right) \sin\frac{m\pi x}{a} \sin\frac{n\pi y}{b} \tag{5.78}$$

The expansion coefficients, A_{mn} are determined by substituting Eq. (5.78) into Eq. (5.77), multiplying both sides by $\sin\dfrac{m\pi x}{a} \sin\dfrac{n\pi y}{b}$ and integrating over $0 < x < a$, $0 < y < b$. Using the orthonormality property of the eigenfunctions and the shifting property of the delta function results in

$$-\left(\frac{m^2\pi^2}{a^2} + \frac{n^2\pi^2}{b^2}\right) A_{mn} = \frac{2}{\sqrt{ab}} \sin\frac{m\pi x'}{a} \sin\frac{n\pi y'}{b}$$

Obtaining A_{mn} from this and substituting in Eq. (5.78) gives

$$G\left(x, y; x', y'\right) = -\frac{4}{ab} \sum_{m=1}^{\infty} \sum_{n=1}^{\infty} \frac{\sin\frac{m\pi x}{a} \sin\frac{m\pi x'}{a} \sin\frac{n\pi y}{b} \sin\frac{n\pi y'}{b}}{m^2\pi^2/a^2 + n^2\pi^2/b^2} \tag{5.79}$$

Another way of obtaining Green's function is by means of a single series rather than a double summation in Eq. (5.79). It can be shown that [28, 29]

$$G(x, y; x', y') = \begin{cases} -\frac{2}{\pi}\sum_{n=1}^{\infty} \frac{\sin\frac{n\pi x}{b}\sinh\frac{n\pi(a-x')}{b}\sin\frac{n\pi y}{b}\sinh\frac{n\pi y'}{b}}{n\sinh\frac{n\pi a}{b}}, & x < x' \\ -\frac{2}{\pi}\sum_{n=1}^{\infty} \frac{\sinh\frac{n\pi x'}{b}\sinh\frac{n\pi(a-x)}{b}\sin\frac{n\pi y}{b}\sinh\frac{n\pi y'}{b}}{n\sinh\frac{n\pi a}{b}}, & x > x' \end{cases} \tag{5.80}$$

By Fourier series expansion, it can be verified that the expressions in Eqs. (5.79) and (5.80) are identical. Besides the factor $\frac{1}{\epsilon}$, the Green's function in Eq. (5.79) or Eq. (5.80) gives the potential V due to a unit line source at (x', y') in the region $0 < x < a,\ 0 < y < b$ as shown in Fig. 5.6. ∎

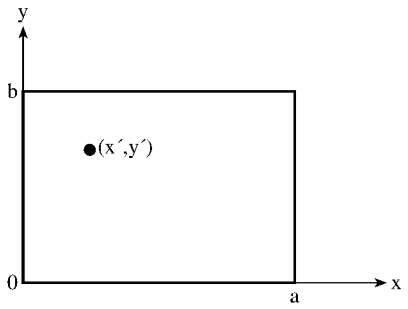

Figure 5.6
Line source in a rectangular region.

Example 5.6

An infinite line source I_z is located at (ρ', ϕ') in a wedge waveguide shown in Fig. 5.7. Derive the electric field due to the line. □

Solution

Assuming the time factor $e^{j\omega t}$, the z-component of **E** for the TE mode satisfies the wave equation

$$\nabla^2 E_z + k^2 E_z = j\omega\mu I_z \tag{5.81}$$

with

$$\frac{\partial E_z}{\partial n} = 0$$

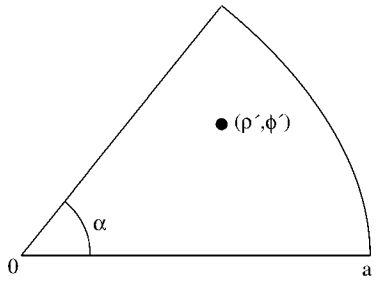

Figure 5.7
Line source in a waveguide.

where $k = \omega\sqrt{\mu\epsilon}$ and n is the outward unit normal at any point on the periphery of the cross section. The Green's function for this problem satisfies

$$\nabla^2 G + k^2 G = j\omega\mu\delta\left(\rho - \rho'\right) \tag{5.82}$$

with

$$\frac{\partial G}{\partial n} = 0$$

so that the solution to Eq. (5.81) is

$$E_z = j\omega\mu \int_S I_z\left(\rho', \phi'\right) G\left(\rho, \phi; \rho', \phi'\right) dS \tag{5.83}$$

To determine the Green's function $G(\rho, \phi; \rho', \phi')$, we find Ψ_i so that Eq. (5.62) can be applied. The boundary condition $\dfrac{\partial G}{\partial n} = 0$ implies that

$$\frac{1}{\rho}\frac{\partial G}{\partial \phi}\bigg|_{\phi=0} = 0 = \frac{1}{\rho}\frac{\partial G}{\partial \phi}\bigg|_{\phi=\alpha} = \frac{\partial G}{\partial \rho}\bigg|_{\rho=a} \tag{5.84}$$

The set of functions which satisfy the boundary conditions are

$$\Psi_{m\nu}(\rho, \phi) = J_\nu\left(k_{m\nu}\rho\right)\cos\nu\phi \tag{5.85}$$

where

$$\nu = n\pi/\alpha, \quad n = 0, 1, 2, \ldots, \tag{5.86a}$$

$k_{m\nu}$ are chosen to satisfy

$$\frac{\partial}{\partial \rho} J_\nu\left(k_{m\nu}\rho\right)\bigg|_{\rho=a} = 0\,, \tag{5.86b}$$

and the subscript m is used to denote the mth root of Eq. (5.86b); m can take the value zero for $n = 0$. The functions $\Psi_{m\nu}$ are orthogonal if and only if ν is an integer

which implies that ν is an integral multiple of α. Let $\alpha = \pi/\ell$, where ℓ is a positive integer, so that $\Phi_{m\nu}$ are mutually orthogonal. To obtain the Green's function using Eq. (5.62), these eigenfunctions must be normalized over the region, i.e.,

$$\int_0^a J_\nu^2\left(k_{m\nu}\rho\right) d\rho = \begin{cases} a^2/2, & m = \nu \\ \dfrac{1}{2}\left[a^2 - \left(\nu^2/k_{m\nu}^2\right)\right] J_\nu^2\left(k_{m\nu}a\right), & \text{otherwise} \end{cases} \tag{5.87a}$$

$$\int_0^\alpha \cos^2 \nu\phi \, d\phi = \begin{cases} \dfrac{\pi}{\ell}, & \nu = 0 \\ \dfrac{\pi}{2\ell}, & \text{otherwise} \end{cases} \tag{5.87b}$$

where $\nu = n\ell$. Using the normalized eigenfunctions, we obtain

$$G\left(\rho, \phi; \rho', \phi'\right) = \frac{j2\ell}{\omega\epsilon\pi a^2} - 4j\ell\omega\mu \sum_{n=1}^{\infty}\sum_{m=1}^{\infty} \frac{J_\nu\left(k_{m\nu}\rho\right) J_\nu\left(k_{m\nu}\rho'\right) \cos\nu\phi \cos\nu\phi'}{\epsilon_\nu\pi\left(a^2 - \frac{\nu^2}{k_{m\nu}^2}\right) J_\nu^2\left(k_{m\nu}a\right)\left(k^2 - k_{m\nu}^2\right)} \tag{5.88}$$

where

$$\epsilon_\nu = \begin{cases} 2, & \nu = 0 \\ 1, & \nu \neq 0 \end{cases} \tag{5.89}$$

We have employed the fact that $\omega\mu/k^2 = \dfrac{1}{\omega\epsilon}$ to obtain the first term on the right-hand side of Eq. (5.88). ∎

5.4 Applications I — Quasi-Static Problems

The method of moments has been applied to so many EM problems that covering all of them is practically impossible. We will only consider the relatively easy ones to illustrate the techniques involved. Once the basic approach has been mastered, it will be easy for the reader to extend the idea to attack more complicated problems.

We will apply MOM to a static problem in this section; more involved application will be considered in the sections to follow. We will consider the problem of determining the characteristic impedance Z_o of a strip transmission line [31].

Consider the strip transmission of Fig. 5.8(a). If the line is assumed to be infinitely long, the problem is reduced to a two-dimensional TEM problem of line sources in a plane as in Fig. 5.8(b). Let the potential difference of the strips be $V_d = 2V$ so that strip 1 is maintained at $+1V$ while strip 2 is at $-1V$. Our objective is to find the

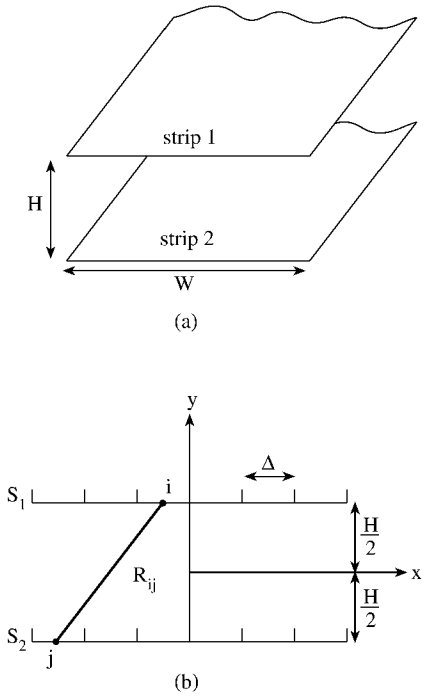

Figure 5.8
(a) The strip transmission line. (b) The two-dimensional view.

surface charge density $\rho(x, y)$ on the strips so that the total charge per unit length on one strip can be found as

$$Q_\ell = \int \rho \, dl \tag{5.90}$$

(Q_ℓ is charge per unit length as distinct from the total charge on the strip because we are treating a three-dimensional problem as a two-dimensional one.) Once Q is known, the capacitance per unit length C_ℓ can be found from

$$C_\ell = \frac{Q_\ell}{V_d} \tag{5.91}$$

Finally, the line characteristic impedance is obtained:

$$Z_o = \frac{(\mu\epsilon)^{1/2}}{C_\ell} = \frac{1}{uC_\ell} \tag{5.92}$$

where $u = 1/\sqrt{\mu\epsilon}$ is the speed of the wave in the (lossless) dielectric medium between the strips. Everything is straightforward once the charge density $\rho(x, y)$ in Eq. (5.90) is known. To find ρ using MOM, we divide each strip into n subareas of

equal width Δ so that subareas in strip 1 are numbered $1, 2, \ldots, n$, while those in strip 2 are numbered $n+1, n+2, n+3, \ldots, 2n$. The potential at an arbitrary field point is

$$V(x, y) = \frac{1}{2\pi\epsilon} \int \rho\left(x', y'\right) \ln \frac{R}{r_o} \, dx' dy' \tag{5.93}$$

where R is the distance between source and field points, i.e.,

$$R = \left[\left(x - x'\right)^2 + \left(y - y'\right)^2\right]^{1/2} \tag{5.94}$$

Since the integral in Eq. (5.93) may be regarded as rectangular subareas in a numerical sense, the potential at the center of a typical subarea S_i is

$$V_i = \frac{1}{2\pi\epsilon} \sum_{j=1}^{2n} \rho_j \int_{S_i} \ln \frac{R_{ij}}{r_o} \, dx'$$

or

$$V_i = \sum_{j=1}^{2n} A_{ij} \rho_j \tag{5.95}$$

where

$$A_{ij} = \frac{1}{2\pi\epsilon} \int_{S_i} \ln \frac{R_{ij}}{r_o} \, dx' \,, \tag{5.96}$$

R_{ij} is the distance between ith and jth subareas, and $A_{ij}\rho_j$ represents the potential at point i due to subarea j. In Eq. (5.95), we have assumed that the charge density ρ is constant within each subarea. For all the subareas S_i, $i = 1, 2, \ldots, 2n$ we have

$$\begin{aligned}
V_1 &= \sum_{j=1}^{2n} \rho_j A_{1j} = 1 \\
V_2 &= \sum_{j=1}^{2n} \rho_j A_{2j} = 1 \\
&\vdots \\
V_n &= \sum_{j=1}^{2n} \rho_j A_{nj} = 1 \\
V_{n+1} &= \sum_{j=1}^{2n} \rho_j A_{n+1,j} = -1 \\
&\vdots \\
V_{2n} &= \sum_{j=1}^{2n} \rho_j A_{2n,j} = -1
\end{aligned}$$

Thus we obtain a set of $2n$ simultaneous equations with $2n$ unknown charge densities ρ_i. In matrix form,

$$\begin{bmatrix} A_{11} & A_{12} & \cdots & A_{1,2n} \\ A_{21} & A_{22} & \cdots & A_{2,2n} \\ \vdots & & & \\ A_{2n,l} & A_{2n,2} & \cdots & A_{2n,2n} \end{bmatrix} \begin{bmatrix} \rho_1 \\ \rho_2 \\ \vdots \\ \rho_{2n} \end{bmatrix} = \begin{bmatrix} 1 \\ 1 \\ \vdots \\ -1 \\ -1 \end{bmatrix}$$

or simply

$$[A][\rho] = [B] \tag{5.97}$$

It can be shown that [32] the elements of matrix [A] expressed in Eq. (5.96) can be reduced to

$$A_{ij} = \begin{cases} \dfrac{\Delta}{2\pi\epsilon} \ln \dfrac{R_{ij}}{r_o}, & i \neq j \\ \dfrac{\Delta}{2\pi\epsilon} \left[\ln \dfrac{\Delta}{r_o} - 1.5 \right], & i = j \end{cases} \tag{5.98}$$

where r_o is a constant scale factor (commonly taken as unity). From Eq. (5.97), we obtain $[\rho]$ either by solving the simultaneous equation or by matrix inversion, i.e.,

$$[\rho] = [A]^{-1}[B] \tag{5.99}$$

Once $[\rho]$ is known, we determine C_ℓ from Eqs. (5.90) and (5.91) as

$$C_\ell = \sum_{j=1}^{n} \rho_j \Delta / V_d \tag{5.100}$$

where $V_d = 2V$. Obtaining Z_o follows from Eqs. (5.92) and (5.100).

Example 5.7

Write a program to find the characteristic impedance Z_o of a strip line with $H = 2\text{m}$, $W = 5\text{m}$, $\epsilon = \epsilon_o$, $\mu_o = \mu_o$, and $V_d = 2V$. □

Solution

The FORTRAN program is shown in Fig. 5.9. With the given data, the program calculates the elements of matrices [A] and [B] and determines $[\rho]$ by matrix inversion. With the computed charge densities the capacitance per unit length is calculated using Eq. (5.100) and the characteristic impedance from Eq. (5.92). Table 5.2 presents the computed values of Z_o for a different number of segments per strip, n. The results agree well with $Z_o = 50\ \Omega$ from Wheeler's curve [33]. ■

```
0001    C ****************************************************************
0002    C     USING MOMENTS METHOD,
0003    C     THIS PROGRAM DETERMINES THE CHARACTERISTIC IMPEDANCE
0004    C     OF A STRIP TRANSMISSION LINE
0005    C     WITH CROSS-SECTION  W X H
0006    C     THE STRIPS MAINTAINED AT 1 VOLT AND - 1 VOLT.
0007    C
0008    C     ONE STRIP IS LOCATED ON THE Y= H/2 PLANE WHILE THE OTHER
0009    C     IS LOCATED ON THE  Y= -H/2  PLANE.
0010    C
0011    C     ALL DIMENSIONS ARE IN S.I. UNITS
0012    C
0013    C     N IS THE NUMBER OF SUBSECTIONS INTO WHICH
              EACH STRIP IS DIVIDED
0014    C****************************************************************
0015
0016          DIMENSION  A(100,100), B(100), X(100), Y(100), RO(100)
0017          DATA  PIE/3.14159/
0018
0019    C     FIRST, SPECIFY THE PARAMETERS
0020
0021          CL=3.E+8  ! SPEED OF LIGHT IN FREE SPACE
0022          ER=1.0
0023          E0=8.8541E-12
0024          H=2.0
0025          W=5.0
0026          N=10
0027          NT=2N
0028          DELTA = W/FLOAT(N)
0029    C
0030    C     SECOND, CALCULATE THE MATCH POINTS
0031    C     AND THE COEFFICIENT MATRIX [A]
0032    C
0033          DO 10 K=1,N
0034          X(K) = DELTA*( FLOAT(K) -0.5 )  ! FOR LOWER STRIP
0035          Y(K) = -H/2.0
0036          X(K+N) = X(K)                   ! FOR UPPER STRIP
0037          Y(K+N) = H/2.0
0038    10    CONTINUE
0039
0040          FACTOR = DELTA/(2.0*PIE*E0)
0041
0042          DO 20 I=1,NT
0043          DO 20 J=1,NT
0044          IF(I-J)  12,11,12
0045
0046    11    A(I,J)= -( ALOG(DELTA) - 1.5)*FACTOR
0047          GO TO 13
0048    12    R=SQRT( (X(I) - X(J))**2 + (Y(I) - Y(J))**2 )
0049          A(I,J)= - ALOG(R)*FACTOR
0050    13    CONTINUE
0051    20    CONTINUE
0052    C
0053    C     NOW DETERMINE THE MATRIX OF CONSTANT VECTOR [B]
0054    C
0055          DO 30 K=1,N
0056          B(K)=1.0
0057    C      B(K+N)= -1.0
0058    30    CONTINUE
0059    C
```

Figure 5.9
FORTRAN program for Example 5.7 ***(Continued).***

```
0060    C     INVERT MATRIX  A(I,J) AND CALCULATE MATRIX RO(M)
0061    C     CONSISTING OF THE UNKNOWN ELEMENTS
0062    C     ALSO CALCULATE THE TOTAL CHARGE Q,
0063    C     THE CAPACITANCE C, AND THE CHARACTERISTIC IMPEDANCE Zo.
0064
0065          NIV=NT
0066          NMAX=100
0067          CALL INVERSE(A,NIV,NMAX) !  APPENDIX D
0068          DO 50 I=1,NT
0069          RO(I)=0.0
0070          DO 40 M=1,NT
0071          RO(I)=RO(I) + A(I,M)*B(M)
0072    40    CONTINUE
0073    50    CONTINUE
0074          SUM=0.0
0075          DO 60 I=1,N
0076          SUM= SUM + RO(I)
0077    60    CONTINUE
0078          Q=SUM*DELTA
0079          VD=2.0
0080          C=ABS(Q)/VD
0081          ZO = SQRT(ER)/CL*C
0082          PRINT *,ZO
0083          WRITE(6,70) ZO
0084    70    FORMAT(2X,'ZO=',E14.6,/)
0085          STOP
0086          END
```

Figure 5.9
(Cont.) **FORTRAN program for Example 5.7.**

Table 5.2 Characteristic Impedance of a Strip Transmission Line

n	Z_o(in Ω)
3	53.02
7	51.07
11	50.49
18	50.39
39	49.71
59	49.61

5.5 Applications II — Scattering Problems

The purpose of this section is to illustrate, with two examples, how the method of moments can be applied to solve electromagnetic scattering problems. The first example is on scattering of a plane wave by a perfectly conducting cylinder [3], while the second is on scattering of a plane wave by an arbitrary array of parallel wires [34].

5.5.1 Scattering by Conducting Cylinder

Consider an infinitely long, perfectly conducting cylinder located at a far distance from a radiating source. Assuming a time-harmonic field with time factor $e^{j\omega t}$, Maxwell's equations can be written in phasor form as

$$\nabla \cdot \mathbf{E}_s = 0 \tag{5.101a}$$

$$\nabla \cdot \mathbf{H}_s = 0 \tag{5.101b}$$

$$\nabla \times \mathbf{E}_s = -j\omega\mu\mathbf{H}_s \tag{5.101c}$$

$$\nabla \times \mathbf{H}_s = \mathbf{J}_s + j\omega\epsilon\mathbf{E}_s \tag{5.101d}$$

where the subscript s denotes phasor or complex quantities. Henceforth, we will drop subscript s for simplicity and use the same symbols for the frequency-domain quantities and time-domain quantities. It is assumed that the reader can differentiate between the two quantities. Taking the curl of Eq. (5.101c) and applying Eq. (5.101d), we obtain

$$\nabla \times \nabla \times \mathbf{E} = -j\omega\mu\nabla \times \mathbf{H} = -j\omega\mu(\mathbf{J} + j\omega\epsilon\mathbf{E}) \tag{5.102}$$

Introducing the vector identity

$$\nabla \times \nabla \times \mathbf{A} = \nabla(\nabla \cdot \mathbf{A}) - \nabla^2\mathbf{A}$$

into Eq. (5.102) gives

$$\nabla(\nabla \cdot \mathbf{E}) - \nabla^2\mathbf{E} = -j\omega\mu(\mathbf{J} + j\omega\epsilon\mathbf{E})$$

In view of Eq. (5.101a), $\nabla(\nabla \cdot \mathbf{E}) = 0$ so that

$$\nabla^2\mathbf{E} + k^2\mathbf{E} = j\omega\mu\mathbf{J} \tag{5.103}$$

where $k = \omega(\mu\epsilon)^{1/2} = 2\pi/\lambda$ is the wave number and λ is the wavelength. Equation (5.103) is the vector form of the Helmholtz wave equation. If we assume a TM wave ($H_z = 0$) with $\mathbf{E} = \mathbf{E}_z(x, y)\mathbf{a}_z$, the vector equation (5.103) becomes a scalar equation, namely,

$$\nabla^2 E_z + k^2 E_z = j\omega\mu J_z \tag{5.104}$$

where $\mathbf{J} = J_z\mathbf{a}_z$ is the source current density. The integral solution to Eq. (5.104) is

$$E_z(x, y) = E_z(\rho) = -\frac{k\eta_o}{4}\int_S J_z\left(\rho'\right) H_0^{(2)}\left(k\left|\rho - \rho'\right|\right) dS' \tag{5.105}$$

where $\rho = x\mathbf{a}_x + y\mathbf{a}_y$ is the field point, $\rho' = x'\mathbf{a}_x + y'\mathbf{a}_y$ is the source point, $\eta_o = (\mu_o/\epsilon_o)^{1/2} \simeq 377\,\Omega$ is the intrinsic impedance of free space, and $H_0^{(2)} =$ Hankel function of the second kind of zero order since an outward-traveling wave is assumed and there is no ϕ dependence. The integration in Eq. (5.105) is over the cross section of the cylinder shown in Fig. 5.10.

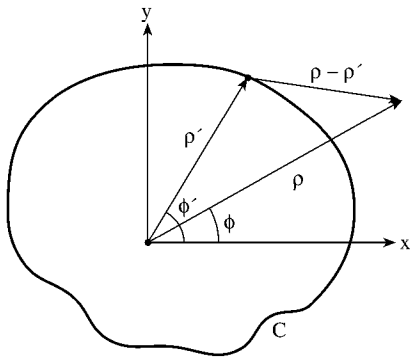

Figure 5.10
Cross section of the cylinder.

If field E_z^i is incident on a perfectly conducting cylinder, it induces surface current J_z on the conducting cylinder, which in turn produces a scattered field E_z^s. The scattered field E_z^s due to J_z is expressed by Eq. (5.105). On the boundary C, the tangential component of the total field must vanish. Thus

$$E_z^i + E_z^s = 0 \text{ on } C \tag{5.106}$$

Substitution of Eq. (5.105) into Eq. (5.106) yields

$$E_z^i(\rho) = \frac{k\eta_o}{4} \int_C J_z\left(\rho'\right) H_0^{(2)}\left(k\left|\rho - \rho'\right|\right) dl' \tag{5.107}$$

In the integral equation (5.107), the induced surface current density J_z is the only unknown. We determine J_z using the moment method.

We divide the boundary C into N segments and apply the point matching technique. On a segment ΔC_n, Eq. (5.107) becomes

$$E_z^i\left(\rho_n\right) = \frac{k\eta_o}{4} \sum_{m=1}^{N} J_z\left(\rho_m\right) H_0^{(2)}\left(k\left|\rho_n - \rho_m\right|\right) \Delta C_m \tag{5.108}$$

where the integration in Eq. (5.107) has been replaced by summation. On applying Eq. (5.108) to all segments, a system of simultaneous equations results. The system of equations can be cast in matrix form as

$$\begin{bmatrix} E_z^i\left(\rho_1\right) \\ E_z^i\left(\rho_2\right) \\ \vdots \\ E_z^i\left(\rho_N\right) \end{bmatrix} = \begin{bmatrix} A_{11} & A_{12} & \ldots & A_{1N} \\ A_{21} & A_{22} & \ldots & A_{2N} \\ \vdots & & \vdots & \\ A_{N1} & A_{N2} & \ldots & A_{NN} \end{bmatrix} \begin{bmatrix} J_z\left(\rho_1\right) \\ J_z\left(\rho_2\right) \\ \vdots \\ J_z\left(\rho_N\right) \end{bmatrix} \tag{5.109a}$$

or

$$[E] = [A][J] \tag{5.109b}$$

Hence

$$[J] = [A]^{-1}[E] \tag{5.110}$$

To determine the exact values of elements of matrix [A] may be difficult. Approximately [6],

$$A_{mn} \simeq \begin{cases} \dfrac{\eta_o k}{4} \Delta C_n H_0^{(2)} \left\{ k \left[(x_n - x_m)^2 + (y_n - y_m)^2 \right]^{(1/2)} \right\}, & m \neq n \\ \dfrac{\eta_o k}{4} \left[1 - j \dfrac{2}{\pi} \log_{10} \left(\dfrac{\gamma k \Delta C_n}{4e} \right) \right], & m = n \end{cases} \tag{5.111}$$

where (x_n, y_n) is the midpoint of ΔC_n, $e = 2.718\ldots$, and $\gamma = 1.781\ldots$. Thus for a given cross section and specified incident field E_z^i, the induced surface current density J_z can be found from Eq. (5.110). To be specific, assume the propagation vector $\mathbf{k}$ is directed as shown in Fig. 5.11 so that

$$E_z^i = E_o e^{j\mathbf{k}\cdot\mathbf{r}}$$

where $\mathbf{r} = x\mathbf{a}_x + y\mathbf{a}_y$, $\mathbf{k} = k(\cos\phi_i \mathbf{a}_x + \sin\phi_i \mathbf{a}_y)$, $k = 2\pi/\lambda$, and ϕ_i is the incidence angle. Taking $E_o = 1$ so that $|E_z^i| = 1$,

$$E_z^i = e^{jk(x\cos\phi_i + y\sin\phi_i)} \tag{5.112}$$

Given any C (dictated by the cross section of the cylinder), we can substitute Eqs. (5.111) and (5.112) into Eq. (5.109) and determine $[J]$ from Eq. (5.110). Once J_z, the induced current density, is known, we calculate the *scattering cross section* σ defined by

$$\begin{aligned} \sigma(\phi, \phi_i) &= 2\pi\rho \left| \frac{E_z^s(\phi)}{E_z^s(\phi_i)} \right|^2 \\ &= \frac{k\eta_o^2}{4} \left| \int_C J_z(x', y') e^{jk(x'\cos\phi + y'\sin\phi)} dl' \right|^2 \end{aligned} \tag{5.113}$$

where ϕ is the angle at the observation point, the point at which σ is evaluated. In matrix form,

$$\sigma(\phi_i, \phi) = \frac{k\eta^2}{4} \left| \left[V_n^s \right] [Z_{nm}]^{-1} \left[V_m^i \right] \right|^2 \tag{5.114}$$

where

$$V_m^i = \Delta C_m e^{jk(x_m\cos\phi_i + y_m\cos\phi_i)}, \tag{5.115a}$$

$$V_n^s = \Delta C_n e^{jk(x_n\cos\phi + y_n\cos\phi)}, \tag{5.115b}$$

and

$$Z_{mn} = \Delta C_m A_{mn} \tag{5.115c}$$

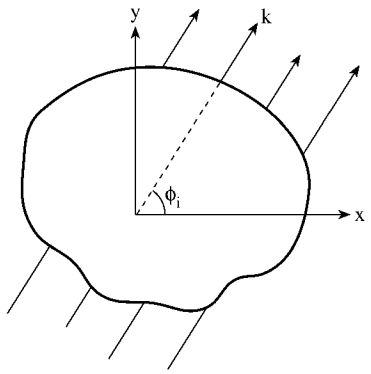

Figure 5.11
Typical propagation of vector k.

5.5.2 Scattering by an Arbitrary Array of Parallel Wires

This problem is of more general nature than the one just described. As a matter of fact, any infinitely long, perfectly conducting, thin metal can be modeled as an array of parallel wires. It will be shown that the scattering pattern due to an arbitrary array of line sources approaches that of a solid conducting cylinder of the same cross-sectional geometry if a sufficiently large number of wires are present and they are arrayed on a closed curve. Hence the problem of scattering by a conducting cylinder presented above can also be modeled with the techniques to be described here (see Problems 5.17 and 5.19).

Consider an arbitrary array of N parallel, infinitely long wires placed parallel to the z-axis [34]. Three of such wires are illustrated in Fig. 5.12. Let a harmonic TM wave be incident on the wires. Assuming a time factor $e^{j\omega t}$, the incident wave in phasor form is given by

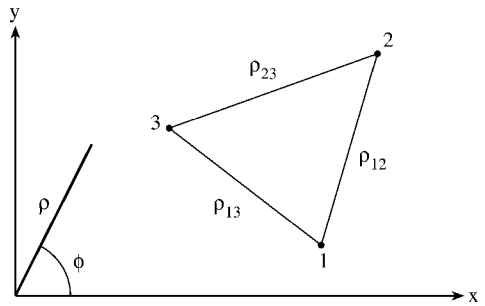

Figure 5.12
An array of three wires parallel to the z-axis.

$$E_z^i = E_i(x, y)e^{-jhz} \tag{5.116}$$

where

$$E_i(x, y) = E_o e^{-jk(x \sin\theta_i \cos\phi_i + y \sin\theta_i \sin\phi_i)} \tag{5.117a}$$

$$h = k\cos\theta_i \ , \tag{5.117b}$$

$$k = \frac{2\pi}{\lambda} = \omega(\mu\epsilon)^{1/2} \ , \tag{5.117c}$$

and θ_i and ϕ_i define the axis of propagation as illustrated in Fig. 5.13. The incident wave induces current on the surface of wire n. The induced current density has only z component.

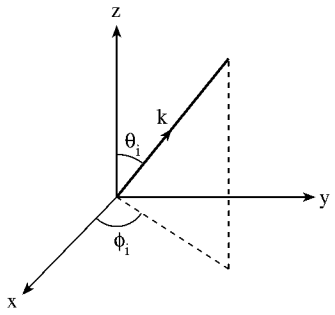

Figure 5.13
Propagation vector k.

It can be shown that the field due to a harmonic current I_n uniformly distributed on a circular cylinder of radius a_n has a z component given by

$$E_n = -I_n' H_0^{(2)}(g\rho_n)\, e^{-jhz}, \quad \rho_n > a_n \tag{5.118}$$

where

$$I_n' = \frac{\omega\mu g^2}{4k^2} I_n J_0(ga_n) \ , \tag{5.119}$$

$$g^2 + h^2 = k^2 \ , \tag{5.120}$$

J_0 is Bessel function of order zero, and H_0 is Hankel function of the second kind of order zero. By induction theorem, if I_n is regarded as the induced current, Eq. (5.118) may be considered as the scattered field, i.e.,

$$E_z^s = -\sum_{n=1}^{N} I_n' H_0^{(2)}(g\rho_n)\, e^{-jhz} \tag{5.121}$$

where the summation is taken over all the N wires. On the surface of each wire (assumed perfectly conducting),

$$E_z^i + E_z^s = 0$$

or

$$E_z^i = -E_z^s, \quad \rho = \rho_n \tag{5.122}$$

Substitution of Eqs. (5.116) and (5.121) into Eq. (5.122) leads to

$$\sum_{n=1}^{N} I_n' H_0^{(2)}(g\rho_{mn}) = E_i(x_m, y_m) \tag{5.123}$$

where

$$\rho_{mn} = \begin{cases} \sqrt{(x_m - x_n)^2 + (y_m - y_n)^2} & , m \neq n \\ a_m & , m = n \end{cases} \tag{5.124}$$

and a_m is the radius of the mth wire. In matrix form, Eq. (5.123) can be written as

$$[A][I] = [B]$$

or

$$[I] = [A]^{-1}[B] \tag{5.125}$$

where

$$I_n = I_n' , \tag{5.126a}$$

$$A_{mn} = H_0^{(2)}(g\rho_{mn}) , \tag{5.126b}$$

$$B_m = E_o e^{-jk(x_m \sin\theta_i \cos\phi_i + y_m \sin\theta_i \sin\phi_i)} \tag{5.126c}$$

Once I_n' is calculated from Eq. (5.125), the scattered field can be obtained as

$$E_z^s = -\sum_{n=1}^{N} I_n' H_0^{(2)}(g\rho_n) e^{-jhz} \tag{5.127}$$

Finally, we may calculate the "distant scattering pattern," defined as

$$E(\phi) = \sum_{n=1}^{N} I_n' e^{jg(x_n \cos\phi + y_n \sin\phi)} \tag{5.128}$$

The following example, taken from Richmond's work [34], will be used to illustrate the techniques discussed in the latter half of this section.

Example 5.8

Consider the two arrays shown in Fig. 5.14. For Fig. 5.14(a), take

$$\text{no. of wires, } N = 15$$
$$\text{wire radius, } ka = 0.05$$
$$\text{wire spacing, } ks = 1.0$$
$$\theta_o = 90^\circ,\ \phi_o = 40^\circ,\ 270^\circ < \phi < 90^\circ$$

and for Fig. 5.14(b), take

$$\begin{aligned} \text{no. of wires,} \quad & N = 30 \\ \text{wire radius,} \quad & ka = 0.05 \\ \text{cylinder radius,} \quad & R = 1.12\,\lambda \\ \theta_o = 90°, \quad & \phi_o = 0,\ 0 < \phi < 180° \end{aligned}$$

For the two arrays, calculate and plot the scattering pattern as a function of ϕ. □

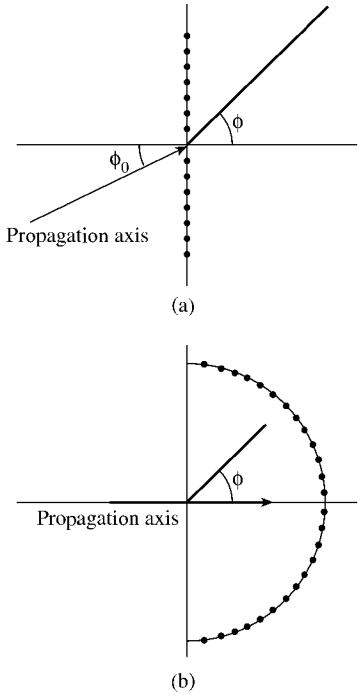

Figure 5.14
For Example 5.8: (a) A plane array of 15 parallel wires, (b) a semicircular array of 30 parallel wires.

Solution

The FORTRAN code for calculating the scattering pattern $E(\phi)$ based on Eq. (5.128) is shown in Fig. 5.15. The same program can be used for the two arrays in Fig. 5.14, except that the input data on N, ka, ks and the locations $(x_n, y_n), n = 1, 2, \ldots, N$ of the wires are different. The program essentially calculates I_n required

```
0001    C ======================================================
0002    C   THIS PROGRAM CALCULATES THE SCATTERING PATTERN OF AN
0003    C   ARRAY OF PARALLEL WIRES
0004    C   REFERENCE - RICHMOND'S WORK [8]
0005    C ======================================================
0006
0007        PARAMETER (IDM=50)
0008        DIMENSION X(IDM),Y(IDM),RHO(IDM,IDM),E(IDM)
0009        REAL LAMBDA,K
0010        COMPLEX J,H0,SUM,A(IDM,IDM),B(IDM),I(IDM)
0011        DATA  PIE,LAMBDA/3.14159,1.0/
0012
0013        J=(0.0,1.0)
0014    C
0015    C   SPECIFY NECESSARY DATA AND CALCULATE
            RELEVANT PARAMETERS
0016    C
0017        NN = 30
0018        THETA0 = PIE/2.0
0019        PHI0 = 0.0
0020        E0 = 1.0
0021        R = 1.125*LAMBDA
0022        K = 2.0*PIE/LAMBDA
0023        AA = 0.05/K
0024        S = 1.0/K
0025        H = K*COS(THETA0)
0026        G = SQRT( K**2 - H**2 )
0027    C
0028    C   DEFINE WIRE LOCATIONS AND CALCULATE RHO
0029    C
0030        DO 10 N=1,NN
0031        PHI = PIE*( FLOAT(N-1)/FLOAT(NN-1) ) - PIE/2.0
0032        X(N) = R*COS(PHI)
0033        Y(N) = R*SIN(PHI)
0034    10  CONTINUE
0035        DO 40 M=1,NN
0036        DO 40 N=1,NN
0037        IF(M-N) 20,30,20
0038    20  RHO(M,N) = SQRT( (X(M) - X(N))**2 + (Y(M) - Y(N))**2 )
0039        GO TO 40
0040    30  RHO(M,N) = AA
0041    40  CONTINUE
0042    C
0043    C CONSTRUCT MATRIX [A]
0044    C
0045        DO 50 M=1,NN
0046        DO 50 N=1,NN
0047        ARGU = G*RHO(M,N)
0048        CALL HANKEL(ARGU,H0)
0049        A(M,N) = H0
0050    50  CONTINUE
0051    C
0052    C CONSTRUCT MATRIX [B]
0053    C
0054        DO 60 M=1,NN
0055        ALPHA = X(M)*SIN(THETA0)*COS(PHI0)
0056       1       +  Y(M)*SIN(THETA0)*SIN(PHI0)
0057        B(M) = E0*CEXP( -J*K*ALPHA )
0058    60  CONTINUE
0059    C
```

Figure 5.15
Computer program for Example 5.8 ***(Continued).***

```
0060    C SOLVE FOR MATRIX [I] CONSISTING OF "MODIFIED CURRENT"OR
0061    C CURRENT COEFFICIENTS
0062    C
0063        CALL INVERSE(A,NN,IDM)
0064        DO 70 N=1,NN
0065        I(N) = (0.0,0.0)
0066        DO 70 M=1,NN
0067        I(N) = I(N) + A(N,M)*B(M)
0068    70  CONTINUE
0069    C
0070    C FINALLY, CALCULATE THE SCATTERING PATTERN E(PHI)
0071    C
0072        DPHI = 5.0
0073        DO 90 L=1,37
0074        PHI = DPHI*FLOAT(L-1)
0075        SUM = (0.0,0.0)
0076        DO 80 N=1,NN
0077        ALP = X(N)*COSD(PHI) + Y(N)*SIND(PHI)
0078        SUM = SUM + I(N)*CEXP( J*G*ALP )
0079    80  CONTINUE
0080        E(L) = CABS(SUM)
0081        WRITE(6,100) PHI,E(L)
0082    90  CONTINUE
0083    100 FORMAT(2X,'PHI=',F8.2,3X,'E(PHI)=',F12.6,/)
0084        CALL PLOT(E,37,0.0,DPHI,1)
0085        STOP
0086        END

0001    C*************************************************************
0002    C THIS PROGRAM EVALUATES HANKEL FUNCTION OF THE SECOND KIND
0003    C AND ORDER ZERO USING NEWTON-COTES RULE (N=5)
0004    C*************************************************************
0005    C
0006    C INITIALIZATION OF VARIABLES
0007    C
0008          SUBROUTINE HANKEL(X,H)
0009          DIMENSION O1(150),C(10),A1(10),A2(100),O2(150)
0010          DATA  ( C(I), I=1,6 )/19.0,75.0,50.0,50.0,75.0,19.0/
0011          COMPLEX H
0012          A=0.
0013          B=3.141592654
0014          M=30.
0015          H1=(B-A)/M
0016          H2=H1/2
0017          N=5
0018          NX=288
0019          E=.577216
0020    C
0021    C SET VALUES OF ANGLES
0022    C
0023          DO 5 I=1,M+1
0024          O1(I)=(I-1)*H1
0025          O2(I)=(I-1)*H2
0026     5    CONTINUE
0027    C
0028    C COMPUTE VALUES OF XJO &YO
0029    C
0030          L=M/N
0031          SUM1=0.
0032          SUM3=0.
0033          DO 500 I=1,L
0034          SUM2=0.
```

Figure 5.15
(Cont.) **Computer program for Example 5.8** ***(Continued).***

```
0035            SUM4=0.
0036      C
0037      C SET UP COMPUTATIONS OF AIS
0038      C
0039            DO 100 II=1,N+1
0040            J=(I-1)*N+II
0041            SUM2=SUM2+C(II)*COS(X*COS(O1(J)))
0042            IF(J.EQ.1)O2(J)=.00405
0043            SUM4=SUM4+C(II)*COS(X*COS(O2(J)))*(E+
0044           2 ALOG(2*X*(SIN(O2(J)))**2))
0045       100  CONTINUE
0046      C
0047      C COMPUTE THE SUM A1S
0048      C
0049            A1(I)=SUM2
0050            A2(I)=SUM4
0051            SUM1=SUM1+A1(I)
0052            SUM3=SUM3+A2(I)
0053       500  CONTINUE
0054      C
0055      C COMPUTE HO(X)=XJO(X)+I*YO(X)
0056      C
0057            XJO=(N*H1*SUM1)/(NX*B)
0058            YO=(N*H2*4*SUM3)/(NX*B**2)
0059            H=CMPLX( XJO,-YO )
0060            RETURN
0061            END
```

Figure 5.15
(Cont.) **Computer program for Example 5.8.**

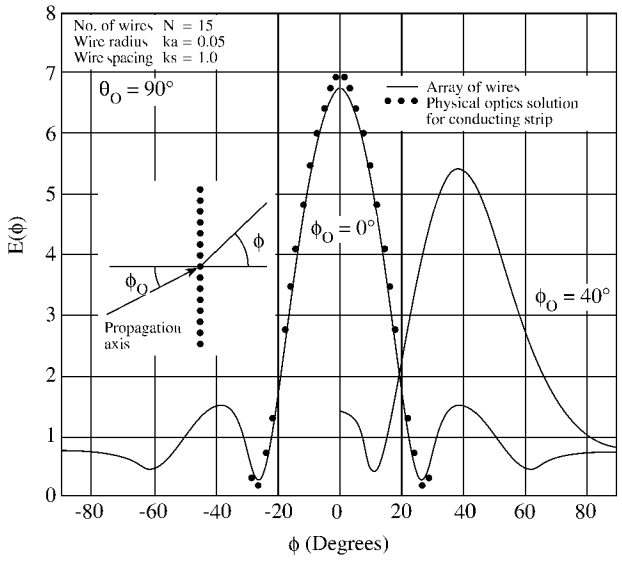

Figure 5.16
Scattering pattern for the plane array of Fig. 5.14(a).

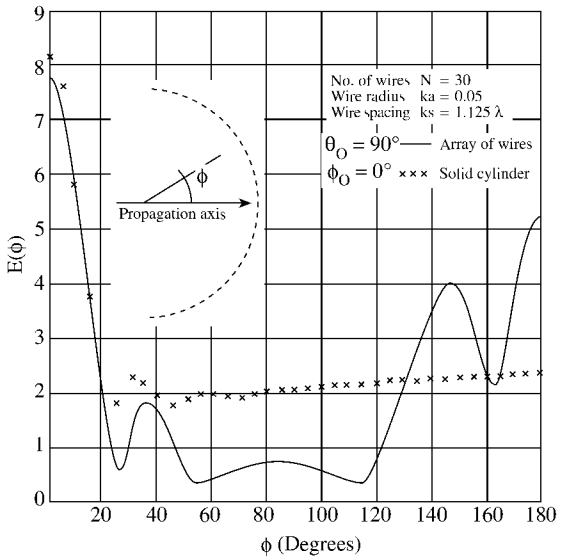

Figure 5.17
Scattering pattern for the semicircular array of Fig. 5.14(b).

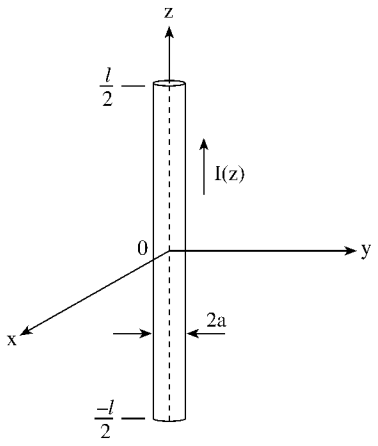

Figure 5.18
Cylindrical antenna of length l and radius a.

in Eq. (5.128) using Eqs. (5.125) and (5.126). The plots of $E(\phi)$ against ϕ are portrayed in Figs. 5.16 and 5.17 for the arrays in Fig. 5.14(a) and 5.14(b), respectively. ∎

5.6 Applications III — Radiation Problems

In this section, we consider the application of MOM to wires or cylindrical antennas. The distinction between scatterers considered in the previous section and antennas to be treated here is primarily that of the location of the source. An object acts as a scatterer if it is far from the source; it acts as an antenna if the source is on it [3].

Consider a perfectly conducting cylindrical antenna of radius a, extending from $z = -\ell/2$ to $z = \ell/2$ as shown in Fig. 5.18. Let the antenna be situated in a lossless homogeneous dielectric medium ($\sigma = 0$). Assuming a z-directed current on the cylinder ($\mathbf{J} = J_z a_z$), only axial electric field E_z is produced due to axial symmetry. The electric field can be expressed in terms of the retarded potentials of Eq. (1.38) as

$$E_z = -j\omega A_z - \frac{\partial V}{\partial z} \tag{5.129}$$

Applying the Lorentz condition of Eq. (1.41), namely,

$$\frac{\partial A_z}{\partial_z} = -j\omega\mu\epsilon V \ , \tag{5.130}$$

Eq. (5.129) becomes

$$E_z = -j\omega\left(1 + \frac{1}{k^2}\frac{\partial^2}{\partial z^2}\right) A_z \tag{5.131}$$

where $k = \omega(\mu\epsilon)^{1/2} = 2\pi/\lambda$, ω is the angular frequency of the suppressed harmonic time variation $e^{j\omega t}$. From Eq. (1.44)

$$A_z = \mu \int_{-\ell/2}^{\ell/2} I\left(z'\right) G\left(x, y, z; x', y', z'\right) dz' \tag{5.132}$$

where $G(x, y, z; x', y', z')$ is the free space Greens' function, i.e.,

$$G\left(x, y, z; x', y', z'\right) = \frac{e^{-jkR}}{4\pi R} \tag{5.133}$$

and R is the distance between observation point (x, y, z) and source point (x', y', z') or

$$R = \left[\left(x - x'\right)^2 + \left(y - y'\right)^2 + \left(z - z'\right)^2\right]^{1/2} \tag{5.134}$$

Combining Eqs. (5.131) and (5.132) gives

$$E_z = -j\omega\mu \left(1 + \frac{1}{k^2}\frac{d^2}{dz^2}\right) \int_{-\ell/2}^{\ell/2} I\left(z'\right) G\left(x, y, z; x', y', z'\right) dz' \tag{5.135}$$

This integro-differential equation is not convenient for numerical analysis because it requires evaluation of the second derivative with respect to z of the integral. We will now consider two types of modification of Eq. (5.135) leading to Hallen's (magnetic vector potential) and Pocklington's (electric field) integral equations. Either of these integral equations can be used to determine the current distribution on a cylindrical antenna or scatterer and subsequently calculate all other quantities of interest.

5.6.1 Hallen's Integral Equation

We can rewrite Eq. (5.135) in a compact form as

$$\left(\frac{d^2}{dz^2} + k^2\right) F(z) = k^2 S(z), \quad -\ell/2 < z < \ell/2 \tag{5.136}$$

where

$$F(z) = \int_{-\ell/2}^{\ell/2} I\left(z'\right) G\left(z, z'\right) dz' , \tag{5.137a}$$

$$S(z) = -\frac{E_z}{j\omega\mu} \tag{5.137b}$$

Equation (5.136) is a second-order linear ordinary differential equation. The general solution to the homogeneous equation

$$\left(\frac{d^2}{dz^2} + k^2\right) F(z) = 0 ,$$

which is consistent with the boundary condition that the current must be zero at the wire ends ($z = \pm\ell/2$), is

$$F_h(z) = c_1 \cos kz + c_2 \sin kz \tag{5.138}$$

where c_1 and c_2 are integration constants. The particular solution of Eq. (5.136) can be obtained, for example, by the Lagrange method of varying constants [35] as

$$F_p(z) = k \int_{-\ell/2}^{\ell/2} S\left(z'\right) \sin k\left|z - z'\right| dz' \tag{5.139}$$

Thus from Eqs. (5.137) to (5.139), the solution to Eq. (5.136) is

$$\int_{-\ell/2}^{\ell/2} I\left(z'\right) G\left(z, z'\right) dz' = c_1 \cos kz + c_2 \sin kz - \frac{j}{\eta} \int_{-\ell/2}^{\ell/2} E_z\left(z'\right) \sin k\left|z - z'\right| dz' \tag{5.140}$$

where $\eta = \sqrt{\mu/\epsilon}$ is the intrinsic impedance of the surrounding medium. Equation (5.140) is referred to as *Hallen's integral equation* [36] for a perfectly conducting cylindrical antenna or scatterer. The equation has been generalized by Mei [37] to perfectly conducting wires of arbitrary shape. Hallen's IE is computationally convenient since its kernel contains only ℓ/r terms. Its major advantage is the ease with which a converged solution may be obtained, while its major drawback lies in the additional work required in finding the integration constants c_1 and c_2 [35, 38].

5.6.2 Pocklington's Integral Equation

We can also rewrite Eq. (5.135) by introducing the operator in parentheses under the integral sign so that

$$\int_{-\ell/2}^{\ell/2} I\left(z'\right)\left(\frac{\partial^2}{\partial z^2}+k^2\right) G\left(z, z'\right) dz' = j\omega\epsilon E_z \tag{5.141}$$

This is known as *Pocklington's integral equation* [39]. Note that Pocklington's IE has E_z, which represents the field from the source on the right-hand side. Both Pocklington's and Hallen's IEs can be used to treat wire antennas. The third type of IE derivable from Eq. (5.135) is the Schelkunoff's IE, found in [35].

5.6.3 Expansion and Weighting Functions

Having derived suitable integral equations, we can now find solutions for a variety of wire antennas or scatterers. This usually entails reducing the integral equations to a set of simultaneous linear equations using the method of moments. The unknown current $I(z)$ along the wire is approximated by a finite set $u_n(z)$ of basis (or expansion) functions with unknown amplitudes as discussed in the last chapter. That is, we let

$$I(z) = \sum_{n=1}^{N} I_n u_n(z) , \tag{5.142}$$

where N is the number of basis functions needed to cover the wire and the expansion coefficients I_n are to be determined. The functions u_n are chosen to be linearly independent. The basis functions commonly used in solving antenna or scattering problems are of two types: entire domain functions and subdomain functions. The entire domain basis functions exist over the full domain $-\ell/2 < z < \ell/2$. Typical examples are [8, 40]:

(1) Fourier:

$$u_n(z) = \cos(n-1)v/2 , \tag{5.143a}$$

(2) Chebychev:

$$u_n(z) = T_{2n-2}(v) , \tag{5.143b}$$

(3) Mauclaurin:

$$u_n(z) = v^{2n-2}\,, \tag{5.143c}$$

(4) Legendre:

$$u_n(z) = P_{2n-2}(v)\,, \tag{5.143d}$$

(5) Hermite:

$$u_n(z) = H_{2n-2}(v)\,, \tag{5.143e}$$

where $v = 2z/\ell$ and $n = 1, 2, \ldots, N$. The subdomain basis functions exist only on one of the N nonoverlapping segments into which the domain is divided. Typical examples are [41, 42]:

(1) piecewise constant (pulse) function:

$$u_n(z) = \begin{cases} 1, & z_{n-1/2} < z < z_{n+1/2} \\ 0, & \text{otherwise,} \end{cases} \tag{5.144a}$$

(2) piecewise linear (triangular) function:

$$u_n(z) = \begin{cases} \dfrac{\Delta - |z - z_n|}{\Delta}, & z_{n-1} < z < z_{n+1} \\ 0, & \text{otherwise,} \end{cases} \tag{5.144b}$$

(3) piecewise sinusoidal function:

$$u_n(z) = \begin{cases} \dfrac{\sin k\,(z - |z - z_n|}{\sin k\Delta}, & z_{n-1} < z < z_{n+1} \\ 0, & \text{otherwise,} \end{cases} \tag{5.144c}$$

where $\Delta = \ell/N$, assuming equal subintervals although this is unnecessary. Figure 5.19 illustrates these subdomain functions. The entire domain basis functions are of limited applications since they require a prior knowledge of the nature of the function to be represented. The subdomain functions are the most commonly used, particularly in developing general-purpose user-oriented computer codes for treating wire problems. For this reason, we will focus on using subdomain functions as basis functions.

Substitution of the approximate representation of current $I(z)$ in Eq. (5.142) into Pocklington's IE of Eq. (5.141) gives

$$\int_{-\ell/2}^{\ell/2} \sum_{n=1}^{N} I_n u_n\left(z'\right) K\left(z_m, z'\right) dz' \simeq E_z\left(z_m\right) \tag{5.145}$$

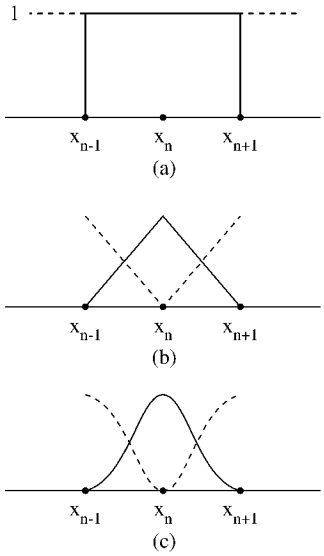

Figure 5.19

Typical subdomain weighting functions: (a) Piecewise uniform function, (b) piecewise linear function, (c) piecewise sinusoidal function.

where

$$K\left(z_m, z'\right) = \frac{1}{j\omega\epsilon}\left(\frac{\partial^2}{\partial z^2} + k^2\right) G\left(z_m, z'\right)$$

is the kernel $z = z_m$ on segment m is the point on the wire at which the IE is being enforced. Equation (5.145) may be written as

$$\sum_{n=1}^{N} I_n \int_{\Delta z_n} K\left(z_m, z'\right) u_n\left(z'\right) dz' \simeq E_z\left(z_m\right)$$

or

$$\sum_{n=1}^{N} I_n g_m = E_z\left(z_m\right) \tag{5.146}$$

where

$$g_m = \int_{\Delta z_n'} K\left(z_m, z'\right) u_n\left(z'\right) dz' \tag{5.147}$$

In order to solve for the unknown current amplitudes I_n $(n = 1, 2, \ldots, N)$, N equations need to be derived from Eq. (5.146). We achieve this by multiplying Eq. (5.146) by weighting (or testing) functions w_n $(n = 1, 2, \ldots, n)$ and integrating

over the wire length. In other words, we let Eq. (5.146) be satisfied in an average sense over the entire domain. This leads to forming the inner product between each of the weighting functions and g_m so that Eq. (5.146) is reduced to

$$\sum_{n=1}^{N} I_n \langle \omega_n, g_m \rangle = \langle \omega_n, E_z \rangle, \quad m = 1, 2, \ldots, N \tag{5.148}$$

Thus we have a set of N simultaneous equations which can be written in matrix form as

$$\begin{bmatrix} \langle \omega_1, g_1 \rangle & \ldots & \langle \omega_1, g_N \rangle \\ \langle \omega_2, g_1 \rangle & \ldots & \langle \omega_2, g_N \rangle \\ \vdots & & \vdots \\ \langle \omega_N, g_1 \rangle & \ldots & \langle \omega_N, g_N \rangle \end{bmatrix} \begin{bmatrix} I_1 \\ I_2 \\ \vdots \\ I_N \end{bmatrix} = \begin{bmatrix} \langle \omega_1, E_{z1} \rangle \\ \langle \omega_2, E_{z2} \rangle \\ \vdots \\ \langle \omega_N, E_{zN} \rangle \end{bmatrix}$$

or

$$[Z][I] = [V] \tag{5.149}$$

where $z_{mn} = \langle \omega_n, g_m \rangle$ and $V_m = \langle \omega_m, E_z \rangle$. The desired solution for the current is then obtained by solving the simultaneous equations (5.149) or by matrix inversion, i.e.,

$$[I] = [Z]^{-1}[V] \tag{5.150}$$

Because of the similarity of Eq. (5.149) to the network equations, the matrices $[Z]$, $[V]$, and $[I]$ are referred to as *generalized* impedance, voltage, and current matrices, respectively [6]. Once the current distribution $I(z')$ is determined from Eq. (5.149) or (5.150), parameters of practical interest such as input impedance and radiation patterns are readily obtained.

The weighting functions $\{w_n\}$ must be chosen so that each Eq. (5.148) is linearly independent and computation of the necessary numerical integration is minimized. Evaluation of the integrals in Eq. (5.149) is often the most time-consuming portion of scattering or radiation problems. Sometimes we select similar types of functions for both weighting and expansion. As discussed in the previous chapter, choosing $w_n = u_n$ leads to Galerkin's method, while choosing $w_n = \delta(z - z_n)$ results in point matching (or colocation) method. The point matching method is simpler than Galerkin's method and is sufficiently adequate for many EM problems. However, it tends to be a slower converging method. The general rules that should be followed in selecting the weighting functions are addressed in [43]. The following examples are taken from [41], [44]–[46].

Example 5.9

Solve the Hallen's integral equation

$$\int_{-\ell/2}^{\ell/2} I\left(z'\right) G\left(z, z'\right) dz' = -\frac{j}{\eta_o}(A \cos kz + B \sin k|z|)$$

where $k = 2\pi/\lambda$ is the phase constant and $\eta_o = 377\ \Omega$ is the intrinsic impedance of free space. Consider a straight wire dipole with length $L = 0.5\ \lambda$ and radius $a = 0.005\ \lambda$. □

Solution
The integral equation has the form

$$\int_{-\ell/2}^{\ell/2} I\left(z'\right) K\left(z, z'\right) dz' = D(z) \tag{5.151}$$

which is a Fredholm integral equation of the first kind. In Eq. (5.151),

$$K\left(z, z'\right) = G\left(z, z'\right) = \frac{e^{-jkR}}{4\pi R}\ , \tag{5.152a}$$

$$R = \sqrt{a^2 + (z - z')^2}\ , \tag{5.152b}$$

and

$$D(z) = -\frac{j}{\eta_o}[A\cos(kz) + B\sin(k|z|)] \tag{5.152c}$$

If the terminal voltage of the wire antenna is V_T, the constant $B = V_T/2$. The absolute value in $\sin k|z|$ expresses the assumption of antenna symmetry, i.e., $I(-z') = I(z')$. Thus

$$\int_{-\ell/2}^{\ell/2} I\left(z'\right) \frac{e^{-jkR}}{4\pi R}\, dz' = -\frac{j}{\eta_o}\left[A\cos kz + \frac{V_T}{2}\sin k|z|\right] \tag{5.153}$$

If we let

$$I(z) = \sum_{n=1}^{N} I_n u_n(z)\ , \tag{5.154}$$

Eq. (5.153) will contain N unknown variables I_n and the unknown constant A. To determine the $N + 1$ unknowns, we divide the wire into N segments. For the sake of simplicity, we choose segments of equal lengths $\Delta z = \ell/N$ and select $N + 1$ matching points such as:

$$z = -\ell/2, -\ell/2 + \Delta z, \ldots,\ 0, \ldots, \ell/2 - \Delta z, \ell/2$$

At each match point $z = z_m$,

$$\int_{-\ell/2}^{\ell/2} \sum_{n=1}^{N} I_n u_n\left(z'\right) K\left(z_m, z'\right)\, dz' = D\left(z_m\right) \tag{5.155}$$

Taking the inner products (moments) by multiplying either side with a weighting function $w_m(z)$ and integrating both sides,

$$\int_{-\ell/2}^{\ell/2} \int_{-\ell/2}^{\ell/2} \sum_{n=1}^{N} I_n u_n\left(z'\right) K\left(z_m, z'\right) dz' w_m(z) dz$$
$$= \int_{-\ell/2}^{\ell/2} D\left(z_m\right) w_m(z)\, dz \tag{5.156}$$

By reversing the order of the summation and integration,

$$\sum_{n=1}^{N} I_n \int_{-\ell/2}^{\ell/2} u_n\left(z'\right) \int_{-\ell/2}^{\ell/2} K\left(z_m, z'\right) w_m(z)\, dz dz'$$
$$= \int_{-\ell/2}^{\ell/2} D\left(z_m\right) w_m(z)\, dz \tag{5.157}$$

The integration on either side of Eq. (5.157) can be carried out numerically or analytically if possible. If we use the point matching method by selecting the weighting function as delta function, then

$$w_m(z) = \delta\left(z - z_m\right)$$

Since the integral of any function multiplied by $\delta(z - z_m)$ gives the value of the function at $z = z_m$, Eq. (5.157) becomes

$$\sum_{n=1}^{N} I_n \int_{-\ell/2}^{\ell/2} u_n\left(z'\right) K\left(z_m, z'\right) dz' = D\left(z_m\right)\ , \tag{5.158}$$

where $m = 1, 2, \ldots, N + 1$. Also, if we choose pulse function as the basis or expansion function,

$$u_n(z) = \begin{cases} 1, & z_n - \Delta z/2 < z < z_n + \Delta z/2 \\ 0, & \text{elsewhere,} \end{cases}$$

and Eq. (5.158) yields

$$\sum_{n=1}^{N} I_n \int_{z_n - \Delta z/2}^{z_n + \Delta z/2} K\left(z_m, z'\right) dz' = D\left(z_m\right) \tag{5.159}$$

Substitution of Eq. (5.152) into Eq. (5.159) gives

$$\sum_{n=1}^{N} I_n \int_{z_n - \Delta z/2}^{z_n + \Delta z/2} \frac{e^{jkR_m}}{4\pi R_m} dz' = -\frac{j}{\eta_o}\left[A \cos k z_m + \frac{V_T}{2} \sin k\left|z_m\right|\right] \tag{5.160}$$

where $m = 1, 2, \ldots, N+1$ and $R_m = [a^2 + (z_m - z')^2]^{1/2}$. Thus we have a set of $N+1$ simultaneous equations, which can be cast in matrix form as

$$\begin{bmatrix} F_{11} & F_{12} & \ldots & F_{1,N} & \dfrac{j}{\eta}\cos(kz_1) \\ F_{21} & F_{22} & \ldots & F_{2,N} & \dfrac{j}{\eta}\cos(kz_2) \\ \vdots & & & & \vdots \\ F_{N+1,1} & F_{N+1,2} & \ldots & F_{N+1,N} & \dfrac{j}{\eta}\cos(kz_{N+1}) \end{bmatrix} \begin{bmatrix} I_1 \\ I_2 \\ \vdots \\ A \end{bmatrix}$$

$$= \begin{bmatrix} -\dfrac{j}{2\eta}V_T \sin k|z_1| \\ -\dfrac{j}{2\eta}V_T \sin k|z_2| \\ \vdots \\ -\dfrac{j}{2\eta}V_T \sin k|z_{N+1}| \end{bmatrix} \tag{5.161a}$$

or

$$[F][X] = [Q] \tag{5.161b}$$

where

$$F_{mn} = \int_{z_n - \Delta z/2}^{z_n + \Delta z/2} \frac{e^{-jkR_m}}{4\pi R_m}\, dz' \tag{5.162}$$

The $N+1$ unknowns are determined by solving Eq. (5.161) in the usual manner. To evaluate F_{mn} analytically rather than numerically, let the integrand in Eq. (5.162) be separated into its real (RE) and imaginary (IM) parts,

$$\begin{aligned} \frac{e^{-jkR_m}}{R_m} &= \mathrm{RE} + j\,\mathrm{IM} \\ &= \frac{\cos kR_m}{R_m} - j\frac{\sin kR_m}{R_m} \end{aligned} \tag{5.163}$$

IM as a function of z' is a smooth curve so that

$$\begin{aligned} \int_{z_n - \Delta z/2}^{z_n + \Delta z/2} \mathrm{IM}(z')\, dz' &= -\int_{z_n - \Delta z/2}^{z_n + \Delta z/2} \frac{\sin k\left[a^2 + (z_m - z')^2\right]^{1/2}}{\left[a^2 + (z_m - z')^2\right]^{1/2}}\, dz' \\ &\simeq -\frac{\Delta z \sin k\left[a^2 + (z_m - z_n)^2\right]^{1/2}}{\left[a^2 + (z_m - z_n)^2\right]^{1/2}} \end{aligned} \tag{5.164}$$

The approximation is accurate as long as $\Delta z < 0.05\ \lambda$. On the other hand, RE changes rapidly as $z' \to z_m$ due to R_m. Hence

$$\begin{aligned}\int_{z_n-\Delta z/2}^{z_n+\Delta z/2} \mathrm{RE}\left(z'\right)\, dz' &= -\int_{z_n-\Delta z/2}^{z_n+\Delta z/2} \frac{\cos k\left[a^2+\left(z_m-z'\right)^2\right]^{1/2}}{\left[a^2+(z_m-z')^2\right]^{1/2}}\, dz' \\ &\simeq \cos k\left[a^2+(z_m-z_n)^2\right]^{1/2} \int_{z_n-\Delta z/2}^{z_n+\Delta z/2} \frac{dz'}{\left[a^2+(z_m-z')^2\right]^{1/2}} \\ &= \cos k\left[a^2+(z_m-z_n)^2\right]^{1/2} \\ &\quad \ln\left[\frac{z_m+\Delta z/2-z_n+\left[a^2+(z_m-z_n+\Delta z/2)^2\right]^{1/2}}{z_m-\Delta z/2-z_n+\left[a^2+(z_m-z_n-\Delta z/2)^2\right]^{1/2}}\right] \end{aligned} \tag{5.165}$$

Thus

$$\begin{aligned} F_{mn} \simeq{}& \frac{1}{4\pi}\cos k\left[a^2+(z_m-z_n)^2\right]^{1/2} \\ &\times \ln\left[\frac{z_m+\Delta z/2-z_n+\left[a^2+(z_m-z_n+\Delta z/2)^2\right]^{1/2}}{z_m-\Delta z/2-z_n+\left[a^2+(z_m-z_n-\Delta z/2)^2\right]^{1/2}}\right] \\ &- \frac{j\Delta z \sin k\left[a^2+(z_m-z_n)^2\right]^{1/2}}{4\pi\left[a^2+(z_m-z_n)^2\right]^{1/2}} \end{aligned} \tag{5.166}$$

A typical example of the current distribution obtained for $\ell = \lambda$, $a = 0.01\ \lambda$ is shown in Fig. 5.20, where the sinusoidal distribution commonly assumed for wire antennas is also shown for comparison. Notice the remarkable difference between the two near the dipole center. ∎

Example 5.10

Consider a perfectly conducting scatterer or antenna of cylindrical cross section shown in Fig. 5.21. Determine the axial current $I(z)$ on the structure by solving the electric field integral equation (EFIE)

$$\frac{j\eta}{4k\pi}\left(\frac{d^2}{dz^2}+k^2\right)\int_{-h}^{h} I\left(z'\right) G\left(z,z'\right) dz' = E_z^i(z) \tag{5.167}$$

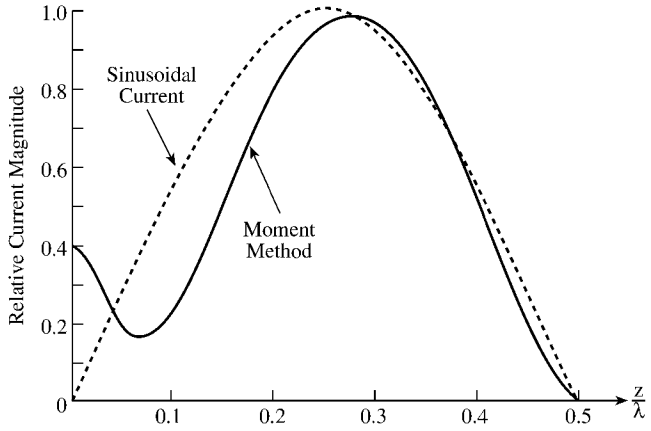

Figure 5.20
Current distribution of straight center-fed dipole.

where

$$G(z, z') = \frac{1}{2\pi} \int_0^{2\pi} \frac{e^{-jkR}}{R} d\phi' ,$$

$$R = \left[(z - z')^2 + 4a^2 \sin^2 \frac{\phi'}{2} \right]^{1/2} ,$$

$$\eta = \sqrt{\frac{\mu}{\epsilon}}, \quad \text{and} \quad k = \frac{2\pi}{\lambda} \quad \square$$

Solution
If the radius $a << \lambda$ (the wavelength) and $a << 2h$ (the length of the wire), the structure can be regarded as a "thin-wire" antenna or scatterer. As a scatterer, we may consider a plane wave excitation

$$E_z^i(z) = E_o \sin\theta e^{jkz\cos\theta} \tag{5.168a}$$

where θ is the angle of incidence. As an antenna, we may assume a delta-gap generator

$$E_z^i = V\delta(z - z_g) \tag{5.168b}$$

where V is the generator voltage and $z = z_g$ is the location of the generator.

In order to apply the method of moments to the given integral equation (5.167), we expand the currents in terms of pulse basis function as

$$I(z) = \sum_{n=1}^{N} I_n u_n(z) \tag{5.169}$$

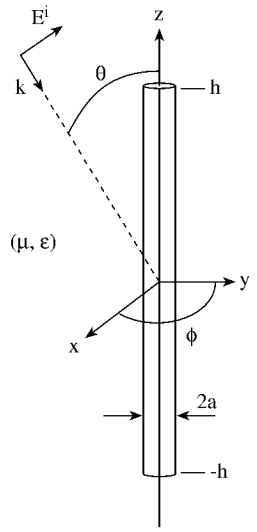

Figure 5.21
Cylindrical scatterer or antenna.

where

$$u_n(z) = \begin{cases} 1, & z_{n-1/2} < z < z_{n+1/2} \\ 0, & \text{elsewhere} \end{cases}$$

Substituting Eq. (5.169) into Eq. (5.167) and weighting the result with triangular functions

$$w_m(z) = \begin{cases} \dfrac{z - z_{m-1}}{\Delta}, & z_{m-1} < z < z_m \\ -\dfrac{z - z_{m+1}}{\Delta}, & z_{m-1} < z < z_{m+1} \\ 0, & \text{elsewhere,} \end{cases} \tag{5.170}$$

where $\Delta = 2h/N$, leads to

$$\sum_{n=1}^{N} Z_{mn} I_n = V_m, \quad m = 1, 2, \ldots, N \tag{5.171}$$

Figure 5.22 illustrates $u_n(z)$ and $w_m(z)$. Equation (5.171) can be cast in matrix form as

$$[Z][I] = [V] \tag{5.172}$$

where $[I]$ can be solved using any standard method. For the impedance matrix $[Z]$, the elements are given by

$$Z_{mn} = \frac{j\eta}{4\pi k}\frac{2}{\Delta}\left[\frac{1}{2}G_{m-1,n} - \left(1 - \frac{k^2\Delta^2}{2}\right)G_{m,n} + \frac{1}{2}G_{m+1,n}\right] \tag{5.173}$$

where

$$G_{m,n} = \int_{z_n-\Delta/2}^{z_n+\Delta/2} G\left(z_m, z'\right) dz' \tag{5.174}$$

To obtain Eq. (5.173), we have used the approximation

$$\int_{z_{m-1}}^{z_{m+1}} w_m(z) f(z)\, dz = \Delta f\ (z_m)$$

For the plane wave excitation, the elements of the forcing vector [V] are

$$V_m = \Delta E_0 e^{jkz_m \cos\theta} \tag{5.175a}$$

For delta-gap generator,

$$V_m = V\delta_{mg} \tag{5.175b}$$

where g is the index of the feed zone pulse.

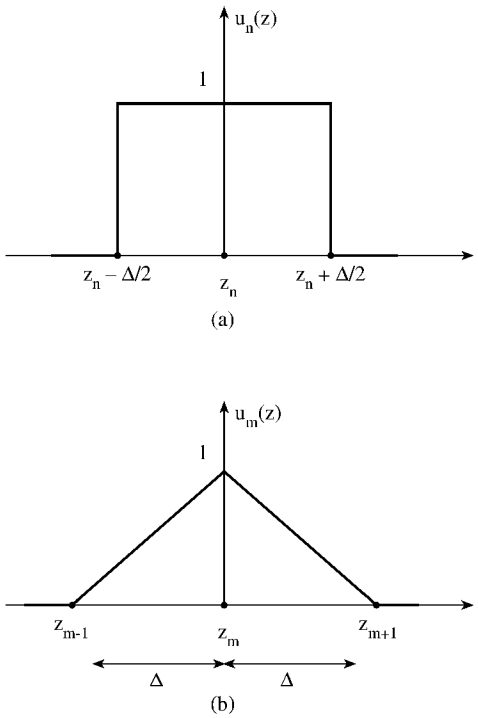

Figure 5.22
For Example 5.10: (a) Pulse basis function, (b) triangular weighting function.

Solving Eq. (5.172) requires that we incorporate a method to perform numerically the double integration in Eq. (5.174). The kernel $G(z, z')$ exhibits a logarithmic singularity as $|z - z'| \to 0$, and therefore care must be exercised. To circumvent the difficulty, we let

$$G(z, z') = \frac{1}{2\pi} \int_0^{2\pi} \frac{e^{-jkR}}{R} d\phi' = G_o(z, z') + G_1(z, z') \tag{5.176}$$

where

$$G_o(z, z') = \frac{1}{2\pi} \int_0^{2\pi} \frac{d\phi'}{R} \tag{5.177}$$

and

$$G_1(z, z') = \frac{1}{2\pi} \int_0^{2\pi} \frac{e^{-jkR} - 1}{R} d\phi' \tag{5.178}$$

We note that

$$G_o(z, z') \xrightarrow{\left(\frac{z-z'}{2a}\right) \to 0} -\frac{1}{\pi a} \ln \frac{|z - z'|}{8a}$$

and hence we replace $G_o(z, z')$ by

$$\left[G_o(z, z') + \frac{1}{\pi a} \ln \frac{|z - z'|}{8a} \right] - \frac{1}{\pi a} \ln \frac{|z - z'|}{8a} \tag{5.179}$$

The term $G_1(z, z')$ is nonsingular, while the singularity of $G_o(z, z')$ can be avoided by using Eq. (5.179). Thus the double integral involved in evaluating Z_{mn} is easily done numerically. It is interesting to note that Z_{mn} would remain the same if we had chosen the triangular basis function and pulse weighting function [46]. ∎

5.7 Applications IV — EM Absorption in the Human Body

The interest in hyperthermia (or electromagnetic heating of deep-seated tumors) and in the assessment of possible health hazards due to EM radiation have prompted the development of analytical and numerical techniques for evaluating EM power deposition in the interior of the human body or a biological system [47]. The overall need is to provide a scientific basis for the establishment of an EM radiation safety standard. Since human experimentation is not possible, irradiation experiments must be performed on animals. Theoretical models are required to interpret and confirm the experiment, develop an extrapolation process, and thereby develop a radiation safety standard for man [48].

The mathematical complexity of the problem has led researchers to investigate simple models of tissue structures such as plane slab, dielectric cylinder homogeneous and layered spheres, and prolate spheroid. A review of these earlier efforts is given in [49, 50]. Although spherical models are still being used to study the power deposition characteristics of the head of man and animals, realistic block model composed of cubical cells is being used to simulate the whole body.

The key issue in this bioelectromagnetic effort is how much EM energy is absorbed by a biological body and where is it deposited. This is usually quantified in terms of the specific absorption rate (SAR), which is the mass normalized rate of energy absorbed by the body. At a specific location, SAR may be defined by

$$\text{SAR} = \frac{\sigma}{\rho}|E|^2 \tag{5.180}$$

where σ = tissue conductivity, ρ = tissue mass density, E = RMS value of the internal field strength. Thus the localized SAR is directly related to the internal electric field and the major effort involves the determination of the electric field distribution within the biological body. The method of moments has been extensively utilized to calculate localized SARs in block model representation of humans and animals.

As mentioned in Section 5.1, an application of MOM to EM problems usually involves four steps:

- deriving the appropriate IE,
- transforming the IE into a matrix equation (discretization),
- evaluating the matrix elements, and
- solving the resulting set of simultaneous equations.

We will apply these steps for calculating the electric field induced in an arbitrary human body or a biological system illuminated by an incident EM wave.

5.7.1 Derivation of Integral Equations

In general, the induced electric field inside a biological body was found to be quite complicated even for the simple case of assuming the plane wave as the incident field. The complexity is due to the irregularity of the body geometry, and the fact that the body is finitely conducting. To handle the complexity, the so-called *tensor integral-equation* (TIE) was developed by Livesay and Chen [51]. Only the essential steps will be provided here; the interested reader is referred to [51]–[53].

Consider a biological body of an arbitrary shape, with constitutive parameters ϵ, μ, σ illuminated by an incident (or impressed) plane EM wave as shown in Fig. 5.23. The induced current in the body gives rise to a scattered field $\mathbf{E}^s$, which may be accounted for by replacing the body with an equivalent free-space current density $\mathbf{J}_{eq}$ given by

$$\mathbf{J}_{eq}(\mathbf{r}) = \big(\sigma(\mathbf{r}) + j\omega[\epsilon(\mathbf{r}) - \epsilon_o]\big)\mathbf{E}(\mathbf{r}) = \tau(\mathbf{r})\mathbf{E}(\mathbf{r}) \tag{5.181}$$

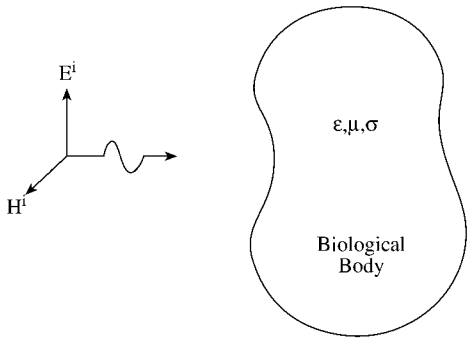

Figure 5.23
A biological body illuminated by a plane EM wave.

where a time factor $e^{j\omega t}$ is assumed. The first term in Eq. (5.181) is the conduction current density, while the second term is the polarization current density. With the equivalent current density $\mathbf{J}_{eq}$, we can obtain the scattered fields $\mathbf{E}^s$ and $\mathbf{H}^s$ by solving Maxwell's equations

$$\nabla \times \mathbf{E}^s = -\mathbf{J}_{eq} - j\omega \mathbf{H}^s \tag{5.182a}$$

$$\nabla \times \mathbf{H}^s = j\omega \mathbf{E}^s \tag{5.182b}$$

where $\mathbf{E}^s$, $\mathbf{H}^s$, and $\mathbf{J}_{eq}$ are all in phasor (complex) form. Elimination of $\mathbf{E}^s$ or $\mathbf{H}^s$ in Eq. (5.182) leads to

$$\nabla \times \nabla \times \mathbf{E}^s - k_o^2 \mathbf{E}^s = -j\omega\mu_o \mathbf{J}_{eq} \tag{5.183a}$$

$$\nabla \times \nabla \times \mathbf{H}^s - k_o^2 \mathbf{H}^s = \nabla \times \mathbf{J}_{eq} \tag{5.183b}$$

where $k_o^2 = \omega^2 \mu_o \epsilon_o$. The solutions to Eq. (5.183) are

$$\mathbf{E}^s = -j\omega \left[1 + \frac{1}{k_o^2} \nabla\nabla\cdot\right] \mathbf{A} \tag{5.184a}$$

$$\mathbf{H}^s = \frac{1}{\mu_o} \nabla \times \mathbf{A} \tag{5.184b}$$

where

$$\mathbf{A} = \mu_o \int_v G_o\left(\mathbf{r}, \mathbf{r}'\right) \mathbf{J}_{eq}\left(\mathbf{r}'\right) \, dv' \tag{5.185}$$

and

$$G_o\left(\mathbf{r}, \mathbf{r}'\right) = \frac{e^{-jk_o(\mathbf{r}-\mathbf{r}')}}{4\pi \left|\mathbf{r} - \mathbf{r}'\right|} \tag{5.186}$$

is the free-space scalar Green's function. By the operator $\nabla\nabla\cdot$, we mean that $\nabla\nabla\cdot\mathbf{A} = \nabla(\nabla \cdot \mathbf{A})$. It is evident from Eqs. (5.184) to (5.186) that $\mathbf{E}^s$ and $\mathbf{H}^s$ depend on $\mathbf{J}_{eq}$.

Suppose $\mathbf{J}_{eq}$ is an infinitesimal, elementary source at $\mathbf{r}'$ pointed in the x direction so that

$$\mathbf{J}_{eq} = \delta\left(\mathbf{r} - \mathbf{r}'\right)\mathbf{a}_x \ , \tag{5.187}$$

the corresponding vector potential is obtained from Eq. (5.185) as

$$\mathbf{A} = \mu_o G_o\left(\mathbf{r}, \mathbf{r}'\right)\mathbf{a}_x \tag{5.188}$$

If $\mathbf{G}_{ox}(\mathbf{r}, \mathbf{r}')$ is the electric field produced by the elementary source, then $\mathbf{G}_{ox}(\mathbf{r}, \mathbf{r}')$ must satisfy

$$\nabla \times \nabla \times \mathbf{G}_{ox}\left(\mathbf{r}, \mathbf{r}'\right) - k_o^2 \mathbf{G}_{ox}\left(\mathbf{r}, \mathbf{r}'\right) = -j\omega\mu_o \delta\left(\mathbf{r}, \mathbf{r}'\right) \tag{5.189}$$

with solution

$$\mathbf{G}_{ox}\left(\mathbf{r}, \mathbf{r}'\right) = -j\omega\mu_o\left(1 + \frac{1}{k^2}\nabla\nabla\cdot\right) G_o\left(\mathbf{r}, \mathbf{r}'\right) \tag{5.190}$$

$\mathbf{G}_{ox}(\mathbf{r}, \mathbf{r}')$ is referred to as a free-space vector Green's function with a source pointed in the x direction. We could also have $\mathbf{G}_{oy}(\mathbf{r}, \mathbf{r}')$ and $\mathbf{G}_{oz}(\mathbf{r}, \mathbf{r}')$ corresponding to infinitesimal, elementary sources pointed in the y and z direction, respectively. We now introduce a dyadic function[2] which can store the three vector Green functions $\mathbf{G}_{ox}(\mathbf{r}, \mathbf{r}')$, $\mathbf{G}_{oy}(\mathbf{r}, \mathbf{r}')$, and $\mathbf{G}_{oz}(\mathbf{r}, \mathbf{r}')$, i.e.,

$$\mathbf{G}_o\left(\mathbf{r}, \mathbf{r}'\right) = \mathbf{G}_{ox}\left(\mathbf{r}, \mathbf{r}'\right)\mathbf{a}_x + \mathbf{G}_{oy}\left(\mathbf{r}, \mathbf{r}'\right)\mathbf{a}_y + \mathbf{G}_{oz}\left(\mathbf{r}, \mathbf{r}'\right)\mathbf{a}_z \tag{5.191}$$

This is called free-space dyadic Green's function [53]. It is a solution to the dyadic differential equation

$$\nabla \times \nabla \times \mathbf{G}_o\left(\mathbf{r}, \mathbf{r}'\right) - k_o^2 \mathbf{G}_o\left(\mathbf{r}, \mathbf{r}'\right) = \widetilde{I}\delta\left(\mathbf{r} - \mathbf{r}'\right) \tag{5.192}$$

where $\widetilde{I}$ denotes the unit dyad (or idem factor) defined by

$$\widetilde{I} = \mathbf{a}_x\mathbf{a}_x + \mathbf{a}_y\mathbf{a}_y + \mathbf{a}_z\mathbf{a}_z \tag{5.193}$$

The physical meaning of $\mathbf{G}_o(\mathbf{r}, \mathbf{r}')$ is rather obvious. $\mathbf{G}_o(\mathbf{r}, \mathbf{r}')$ is the electric field at a field point $\mathbf{r}$ due to an infinitesimal source at $\mathbf{r}'$.

From Eqs. (5.183a) and (5.192), the solution of $\mathbf{E}$ is

$$\mathbf{E}^s(\mathbf{r}) = -j\omega\mu_o \int \mathbf{G}_o\left(\mathbf{r}, \mathbf{r}'\right) \cdot \mathbf{J}_{eq}\left(\mathbf{r}'\right)\, dv' \tag{5.194}$$

Since $\mathbf{G}_o(\mathbf{r}, \mathbf{r}')$ has a singularity of the order $|\mathbf{r} - \mathbf{r}'|^3$, the integral in Eq. (5.194) diverges if the field point $\mathbf{r}$ is inside the volume v of the body (or source region).

[2] A dyad is a group of two or a pair of quantities. A dyadic function, denoted by $\widetilde{D}$, is formed by two functions, i.e., $\widetilde{D} = \mathbf{AB}$. See Tai [53] or Balanis [28] for an exposition on dyadic functions.

This difficulty is overcome by excluding a small volume surrounding the field point first and then letting the small volume approach zero. The process entails defining the principal value (PV) and adding a correction term needed to yield the correct solution. Thus

$$\mathbf{E}^s(\mathbf{r}) = PV \int_v \mathbf{J}_{eq}(\mathbf{r}) \cdot \mathbf{G}\left(\mathbf{r}, \mathbf{r}'\right) \, dv' + \left[\mathbf{E}^s(\mathbf{r})\right]_{\text{correction}} \tag{5.195}$$

The correction term has been evaluated [51, 52] to be $-\mathbf{J}_{eq}/j3\omega\epsilon_o$ so that

$$\mathbf{E}^s(\mathbf{r}) = PV \int_v \mathbf{J}_{eq}(\mathbf{r}) \cdot \mathbf{G}\left(\mathbf{r}, \mathbf{r}'\right) \, dv' - \frac{\mathbf{J}_{eq}(\mathbf{r})}{j3\omega\epsilon_o} \tag{5.196}$$

The total electric field inside the body is the sum of the incident field $\mathbf{E}^i$ and scattered field $\mathbf{E}^s$, i.e.,

$$\mathbf{E}(\mathbf{r}) = \mathbf{E}^i(\mathbf{r}) + \mathbf{E}^s(\mathbf{r}) \tag{5.197}$$

Combining Eqs. (5.181), (5.196), and (5.197) gives the desired tensor integral equation for $\mathbf{E}(\mathbf{r})$:

$$\left[1 + \frac{\tau(\mathbf{r})}{3j\omega\epsilon_o}\right] \mathbf{E}(\mathbf{r}) - PV \int_v \tau\left(\mathbf{r}'\right) \mathbf{E}(\mathbf{r}) \cdot \mathbf{G}\left(\mathbf{r}, \mathbf{r}'\right) \, dv' = \mathbf{E}^i(\mathbf{r}) \tag{5.198}$$

In Eq. (5.198), $\tau(\mathbf{r}) = \sigma(\mathbf{r}) + j\omega[\epsilon(\mathbf{r}) - \epsilon_o]$ and the incident electric field $\mathbf{E}^i$ are known quantities; the total electric field $\mathbf{E}$ inside the body is unknown and is to be determined by MOM.

5.7.2 Transformation to Matrix Equation (Discretization)

The inner product $\mathbf{E}(\mathbf{r}) \cdot \mathbf{G}(\mathbf{r}, \mathbf{r}')$ in Eq. (5.198) may be represented as

$$\mathbf{E}(\mathbf{r}) \cdot \mathbf{G}\left(\mathbf{r}, \mathbf{r}'\right) = \begin{bmatrix} \mathbf{G}_{xx}\left(\mathbf{r}, \mathbf{r}'\right) & \mathbf{G}_{xy}\left(\mathbf{r}, \mathbf{r}'\right) & \mathbf{G}_{xz}\left(\mathbf{r}, \mathbf{r}'\right) \\ \mathbf{G}_{yx}\left(\mathbf{r}, \mathbf{r}'\right) & \mathbf{G}_{yy}\left(\mathbf{r}, \mathbf{r}'\right) & \mathbf{G}_{yz}\left(\mathbf{r}, \mathbf{r}'\right) \\ \mathbf{G}_{zx}\left(\mathbf{r}, \mathbf{r}'\right) & \mathbf{G}_{zy}\left(\mathbf{r}, \mathbf{r}'\right) & \mathbf{G}_{zz}\left(\mathbf{r}, \mathbf{r}'\right) \end{bmatrix} \begin{bmatrix} E_x\left(\mathbf{r}'\right) \\ E_y\left(\mathbf{r}'\right) \\ E_z\left(\mathbf{r}'\right) \end{bmatrix} \tag{5.199}$$

showing that $\mathbf{G}(\mathbf{r}, \mathbf{r}')$ is a symmetric dyad. If we let

$$x_1 = x, \quad x_2 = y, \quad x_3 = z \, ,$$

then $G_{x_p x_q}(\mathbf{r}, \mathbf{r}')$ can be written as

$$G_{x_p x_q}\left(\mathbf{r}, \mathbf{r}'\right) = -j\omega\mu_o \left[\delta_{pq} + \frac{1}{k_o^2} \frac{\partial^2}{\partial x_q \partial x_p}\right] G_o\left(\mathbf{r}, \mathbf{r}'\right), \quad p, q = 1, 2, 3 \tag{5.200}$$

We now apply MOM to transform Eq. (5.198) into a matrix equation. We partition the body into N subvolumes or cells, each denoted by v_m ($m = 1, 2, \ldots, N$), and

assume that $\mathbf{E}(\mathbf{r})$ and $\tau(\mathbf{r})$ are constant within each cell. If $\mathbf{r}_m$ is the center of the mth cell, requiring that each scalar component of Eq. (5.198) be satisfied at $\mathbf{r}_m$ this leads to

$$\left[1+\frac{\tau(\mathbf{r})}{3j\omega\epsilon_o}\right]E_{x_p}(\mathbf{r}_m)-\sum_{q=1}^{3}\left[\sum_{q=1}^{3}\tau(\mathbf{r}_n)\,PV\int_{v_m}G_{x_px_q}(\mathbf{r}_m,\mathbf{r}')\,dv'\right]E_{x_q}(\mathbf{r}_n)$$
$$=E^i_{x_p}(\mathbf{r}_m) \tag{5.201}$$

If we let $[G_{x_px_q}]$ be an $N\times N$ matrix with elements

$$G^{mn}_{x_px_q}=\tau(\mathbf{r}_n)\,PV\int_{v_n}G_{x_px_q}(\mathbf{r}_m,\mathbf{r}')\,dv'-\delta_{pq}\delta_{mn}\left[1+\frac{\tau(\mathbf{r})}{3j\omega\epsilon_o}\right], \tag{5.202}$$

where $m,n=1,2,\ldots,N,\ \ p,q=1,2,3$, and let $[E_{x_p}]$ and $[E^i_{x_p}]$ be column matrices with elements

$$E_{x_p}=\begin{bmatrix}E_{x_p}(\mathbf{r}_1)\\ \vdots\\ E_{x_p}(\mathbf{r}_N)\end{bmatrix},\quad E^i_{x_p}=\begin{bmatrix}E^i_{x_p}(\mathbf{r}_1)\\ \vdots\\ E^i_{x_p}(\mathbf{r}_N)\end{bmatrix}, \tag{5.203}$$

then from Eqs. (5.198) and (5.201), we obtain $3N$ simultaneous equations for E_x, E_y and E_z at the centers of N cells by the point matching technique. These simultaneous equations can be written in matrix form as

$$\left[\begin{array}{ccc}[G_{xx}]&[G_{xy}]&[G_{xz}]\\ \hline [G_{yx}]&[G_{yy}]&[G_{yz}]\\ \hline [G_{zx}]&[G_{zy}]&[G_{zz}]\end{array}\right]\left[\begin{array}{c}[E_x]\\ \hline [E_y]\\ \hline [E_z]\end{array}\right]=-\left[\begin{array}{c}[E^i_x]\\ \hline [E^i_y]\\ \hline [E^i_z]\end{array}\right] \tag{5.204a}$$

or simply

$$[G][E]=-[E^i] \tag{5.204b}$$

where $[G]$ is $3N\times 3N$ matrix and $[E]$ and $[E^i]$ are $3N$ column matrices.

5.7.3 Evaluation of Matrix Elements

Although the matrix $[E^i]$ in Eq. (5.204) is known, while the matrix $[E]$ is to be determined, the elements of the matrix [G], defined in Eq. (5.202), are yet to be calculated. For the off-diagonal elements of $[G_{x_px_q}]$, $\mathbf{r}_m$ is not in the nth cell ($\mathbf{r}_m$ is not in v_n) so that $G_{x_px_q}(\mathbf{r}_m,\mathbf{r}')$ is continuous in v_n and the principal value operation can be dropped. Equation (5.202) becomes

$$G^{mn}_{x_px_q}=\tau(\mathbf{r}_n)\int_{v_n}G_{x_px_q}(\mathbf{r}_m,\mathbf{r}')\,dv',\quad m\neq n \tag{5.205}$$

As a first approximation,

$$G_{x_p x_q}^{mn} = \tau\left(\mathbf{r}_n\right) G_{x_p x_q}\left(\mathbf{r}_m, \mathbf{r}'\right) \Delta v_n, \quad m \neq n \tag{5.206}$$

where Δv_n is the volume of cell v_n. Incorporating Eqs. (5.190) and (5.200) into Eq. (5.206) yields

$$G_{x_p x_q}^{mn} = \frac{-j\omega\mu k_o \Delta v_n \tau\left(\mathbf{r}_n\right) \exp(-j\alpha_{mn})}{4\pi\alpha_{mn}^3} \Big[\left(\alpha_{mn} - 1 - j\alpha_{mn}\right) \delta_{pq} + \cos\theta_{x_p}^{mn} \cos\theta_{x_q}^{mn} \left(3 - \alpha_{mn}^2 + 3j\alpha_{mn}\right)\Big], \quad m \neq n \tag{5.207}$$

where

$$\alpha_{mn} = k_o R_{mn}, \quad R_{mn} = \left|\mathbf{r}_m - \mathbf{r}_n\right| ,$$
$$\cos\theta_{x_p}^{mn} = \frac{x_p^m - x_p^n}{R_{mn}}, \quad \cos\theta_{x_q}^{mn} = \frac{x_q^m - x_q^n}{R_{mn}} ,$$
$$\mathbf{r}_m = \left(x_1^m, x_2^m, x_3^m\right), \quad \mathbf{r}_n = \left(x_1^n, x_2^n, x_3^n\right)$$

The approximation in Eq. (5.207) yields adequate results provided N is large. If greater accuracy is desired, the integral in Eq. (5.205) must be evaluated numerically.

For the diagonal terms ($m = n$), Eq. (5.202) becomes

$$G_{x_p x_q}^{nn} = \tau\left(\mathbf{r}_n\right) PV \int_{v_n} G_{x_p x_q}\left(\mathbf{r}_n, \mathbf{r}'\right) dv' - \delta_{pq}\left[1 + \frac{\tau(\mathbf{r})}{3j\omega\epsilon_o}\right] \tag{5.208}$$

To evaluate this integral, we approximate cell v_n by an equivolumic sphere of radius a_n centered at $\mathbf{r}_n$, i.e.,

$$\Delta v = \frac{4}{3}\pi a_n^3$$

or

$$a_n = \left(\frac{3\Delta v}{4\pi}\right)^{1/3} \tag{5.209}$$

After a lengthy calculation, we obtain [51]

$$G_{x_p x_q}^{nn} = \delta_{pq}\left[\frac{-2j\omega\mu_o\tau\left(r_n\right)}{3k_o^3}\left(\exp\left(-jk_o a_n\right)\left(1 + jk_o a_n\right) - 1\right) - \left(1 + \frac{\tau\left(r_n\right)}{3j\omega\epsilon_o}\right)\right], \quad m = n \tag{5.210}$$

In case the shape of cell v_n differs considerably from that of a sphere, the approximation in Eq. (5.210) may yield poor results. To have a greater accuracy, a small cube, cylinder, or sphere is created around $\mathbf{r}_n$ to evaluate the correction term, and the integration through the remainder of v_n is performed numerically.

5.7.4 Solution of the Matrix Equation

Once the elements of matrix $[G]$ are evaluated, we are ready to solve Eq. (5.204), namely,

$$[G][E] = -[E^i] \tag{5.204}$$

With the known incident electric field represented by $[E^i]$, the total induced electric field represented by $[E]$ can be obtained from Eq. (5.204) by inverting $[G]$ or by employing a Gauss–Jordan elimination method. If matrix inversion is used, the total induced electric field inside the biological body is obtained from

$$[E] = -[G]^{-1}[E^i] \tag{5.211}$$

Guru and Chen [55] have developed computer programs that yield accurate results on the induced electric field and the absorption power density in various biological bodies irradiated by various EM waves. The validity and accuracy of their numerical results were verified by experiments.

In the following examples, we illustrate the accuracy of the numerical procedure with one simple elementary shape and one advanced shape of biological bodies. The examples are taken from the works of Chen and others [52], [56]–[58].

Example 5.11

Determine the distribution of the energy absorption rate or EM heating induced by plane EM waves of 918 MHz in spherical models of animal brain having radius 3 cm. Assume the $\mathbf{E}^i$ field expressed as

$$\mathbf{E}^i = E_o e^{-jk_o z}\mathbf{a}_x = \mathbf{a}_x E_o\,(\cos k_o z - j \sin k_o z)\ \text{V/m} \tag{5.212}$$

where $k_o = 2\pi/\lambda = 2\pi f/c$, $E_o = \sqrt{2\eta_o P_i}$, P_i is the incident power in mW/cm^2 and $\eta_o = 377\ \Omega$ is the intrinsic impedance of free space. Take $P_i = 1$ mW/cm^2 ($E_o = 86.83$ V/m), $\epsilon_r = 35$, $\sigma = 0.7$ mhos/m. □

Solution

In order to apply MOM, we first approximate the spherical model by a "cubic sphere." Figure 5.24 portrays an example in which one eighth of a sphere is approximated by 40 or 73 cubic cells. The center of each cell, for the case of 40 cells, is determined from Fig. 5.25. $\mathbf{E}^i$ at the center of each cell can be calculated using Eq. (5.212). With the computed $\mathbf{E}^i$ and the elements of the matrix $[G_{x_p x_q}]$ calculated using Eqs. (5.207) and (5.210), the induced electric field $\mathbf{E}$ in each cell is computed from Eq. (5.211). Once $\mathbf{E}$ is obtained, the absorption rate of the EM energy is determined using

$$P = \frac{\sigma}{2}|\mathbf{E}|^2 \tag{5.213}$$

The average heating is obtained by averaging P in the brain. The curve showing relative heating as a function of location is obtained by normalizing the distribution of P with respect to the maximum value of P at a certain location in the brain.

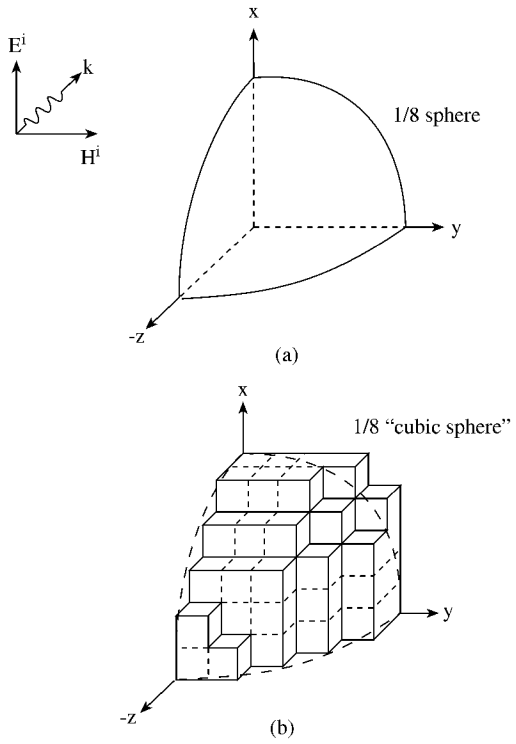

Figure 5.24

For Example 5.11: (a) One eighth of a sphere, (b) a "cubic sphere" constructed from 73 cubic cells.

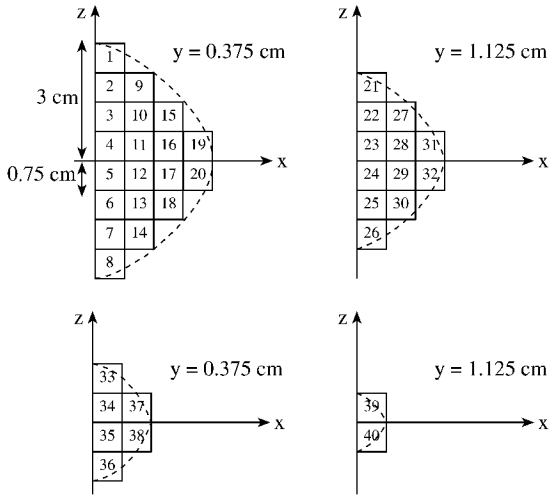

Figure 5.25

Geometry and dimensions of one half of the spherical model of the brain constructed from 40 cells. The cell numbering is used in the program of Fig. 5.26.

The computer program for the computation is shown in Fig. 5.26. It is a modified version of the one developed by Jongakiem [58]. The numerical results are shown in Fig. 5.27(a), where relative heating along the x-, y-, and z-axes in the brain is plotted. The three curves identified by X, Y, and Z correspond with the distributions of the relative heating along x-, y-, and z-axes, respectively. Observe the strong standing wave patterns with peak heating located somewhere near the center of the brain. The average and maximum heating are found to be 0.3202 and 0.885 in mW/cm^3. The exact solution obtained from Mie theory (see Section 2.8) is shown in Fig. 5.27(b). The average and maximum heating from exact solution are 0.295 and 0.814 mW/cm^3, respectively. A comparison of Figs. 5.27(a) and (b) confirms the accuracy of the numerical procedure. ∎

Example 5.12

Having validated the accuracy of the tensor-integral-equation (TIE) method, determine the induced electric field and specific absorption rate (SAR) of EM energy inside a model of typical human body irradiation (Fig. 5.28), by EM wave at 80 MHz with vertical polarization, i.e.,

$$\mathbf{E} = \mathbf{a}_x \quad \text{V/m}$$

at normal incidence. Assume the body at 80 MHz is that of a high-water content tissue with $\epsilon = 80\epsilon_o$, $\mu = \mu_o$, $\sigma = 0.84$ mhos/m. □

Solution

The body is partitioned into 108 cubic cells of various sizes ranging from 5 cm^3 to 12 cm^3. To ensure accurate results, the cell size is kept smaller than a quarter-wavelength (of the medium). With the coordinates of the center of each cell figured out from Fig. 5.28, the program in Fig. 5.26 can be used to find induced electric field components E_x, E_y, and E_z at the centers of the cells due to an incident electric field 1 V/m (maximum value) at normal incidence. The SAR is calculated from $(\sigma/2)(E_x^2 + E_y^2 + E_z^2)$. Figures 5.29 to 5.31 illustrate E_x, E_y, and E_z at the center of each cell. Observe that E_y and E_z are much smaller than E_x at this frequency due to the polarization of the incident wave.

As mentioned earlier, the model of the human body shown in Fig. 5.28 is due to Chen et al. [52]. An improved, more realistic model due to Gandhi et al. [59]–[61] is shown in Fig. 5.32. ∎

5.8 Concluding Remarks

The method of moments is a powerful numerical method capable of applying weighted residual techniques to reduce an integral equation to a matrix equation. The

```
0001    C*****************************************************************
0002    C  THIS PROGRAM DETERMINED EM POWER ABSORPTION
           OF BIOLOGICAL BODIES
0003    C  PROGRAMMER: JONG A KIEM RAYMOND
0004    C  PROGRAM LIMITATIONS:
0005    C
0006    C     BODIES ARE ASSUMED TO HAVE A PERMEABILITY EQUAL
              TO FREE SPACE
0007    C     MAX NUMBER OF CELLS = 150
0008    C     MAX NUMBER OF CELLS IS SUFFICIENTLY LARGE ELSE G-MATRIX
0009    C     NEED TO BE OBTAINED BY INTEGRATION METHODS
0010    C     THE SHAPE OF A CELL CAN BE APPROXIMATED BY A SPHERE
0011    C
0012    C     DIST = R(M,N) = DISTANCE BETWEEN CENTER OF CELL M AND N
0013    C     E(N) = CONCANTINATED MATRIX OF ALL FIELD INTENSITIES
0014    C     EI(N) = CONCANTINATED MATRIX OF ALL INPUT FIELD INTENSITIES
0015    C
0016    C    NOTE: IN THE CONCANTINATED MATRICES, THE ORDER IN WHICH
                   THE DATA IS
0017    C          STORED IS X,Y,Z I.E. ALL X FIRST, THEN ALL Y,
                   FINALLY ALL Z
0018    C          COORDINATES IN SEQUENTIAL ORDER
0019    C
0020    C            EPS(N) = EPSO*EPSR(N) = PERMITTIVITY OF CELL N
0021    C            EPSO = FREE SPACE PERMITTIVITY
0022    C            F = FREQUENCY
0023    C            G = COEFFICIENT MATRIX
0024    C            J = COMPLEX VALUE
0025    C            KO = FREE SPACE WAVE NUMBER
0026    C            MXCLL = MAXIMUM NUMBER OF CELLS
0027    C            MXCLL3 = MAXIMUM DIMENSION COEFFICIENT
                     MATRIX = 3*MXCLL
0028    C            PZ(I) = POWER ALONG THE Z DIRECTION
0029    C            NCELL = NUMBER OF CELLS
0030    C            SIGMA(N) = CONDUCTIVITY OF CELL N
0031    C            SAR = SPECIFIC ABSORPTION RATE
0032    C            TAU(N) = ARRAY STORING VALUES OF CELL N = E(N)/Jeq(N)
0033    C            UO = FREE SPACE PERMEABILITY
0034    C            V(N) = VOLUME OF CELL N
0035    C            W = RADIAN FREQUENCY
0036    C            X1 = ROW LOCATION IN G-MATRIX
0037    C            X2 = COLUMN LOCATION IN G-MATRIX
0038    C            X(1,N) = X COMPONENT OF CENTER OF CELL N
0039    C            X(2,N) = Y COMPONENT OF CENTER OF CELL N
0040    C            X(3,N) = Z COMPONENT OF CENTER OF CELL N
0041    C
0042    C ------ INPUT DATA MUST OBEY THE FOLLOWING FORMAT ----------- C
0043    C
0044    C    **** DATA ****                  ***** FORMAT *****
0045    C
0046    C    NCELL,F                         FORMAT(1X,I4,E10.4)
0047    C    V(N),X(1,N),X(2,N),X(3,N),
             SIGMA(N),EPS(N)                 FORMAT(1X,E10.5,4F10.5,E10.4)
0048    C    EI(I),EI(I+NCELL),EI(I+2*NCELL) FORMAT(1X,6E12.5)
0049
0050    C ------------ SUBROUTINES AND FUNCTIONS ---------------------- C
0051
0052    C            DELTA = DELTA FUNCTION
0053    C            MAGSQ(C) = MAGNITUDE SQUARED OF COMPLEX NUMBER
0054    C            R(M,N) = DISTANCE BETWEEN CENTERS OF VOLUME M
                     AND VOLUME N
0055    C
```

Figure 5.26
Computer program for Example 5.11 ***(Continued).***

```
0056
0057          IMPLICIT COMPLEX (C), INTEGER (K-N)
0058
0059          PARAMETER (MXCLL=600,MXCLL3=1800,MXCL31=1801)
0060          COMPLEX J,TAU,G,E,EI,G1
0061          REAL KO,COSANGLE,MAGSQ,PZ(10)
0062          INTEGER P,Q,X2,X1
0063
0064          DIMENSION G1(MXCLL3,MXCL31),X(3,MXCLL),SIGMA(MXCLL)
0065      C   DIMENSION EPS(MXCLL)
0066          DIMENSION V(MXCLL),E(MXCLL3),EI(MXCLL3),TAU(MXCLL)
0067
0068
0069      C ---------- STATEMENT FUNCTIONS ------------------------- C
0070
0071          R2(M,N) = (X(1,M)-X(1,N))**2+(X(2,M)-X(2,N))
                        **2+(X(3,M)-X(3,N))**2
0072          R(M,N) = SQRT(R2(M,N))
0073          COSANGLE(P,M,N,DIST)= ( X(P,M) - X(P,N) )/DIST
0074          MAGSQ(C) = (CABS(C))**2
0075
0076          J = (0.,1.)
0077          PI = 4.*ATAN(1.)
0078          EPSO = 1.E-9/(36.*PI)
0079          UO = 4.E-7*PI
0080
0081      C ------------- READ AND GENERATE DATA ----------------- C
0082
0083          READ(5,1) NCELL,F
0084          WRITE(6,1) NCELL,F
0085      1   FORMAT(1X,I4,E10.4)
0086
0087          W = 2.*PI*F
0088          KO = W*SQRT(UO*EPSO)
0089
0090          DO 10 M = 1,NCELL
0091             READ(5,15)  V(M),X(1,M),X(2,M),X(3,M),SIGMA(M),EPS
0092             WRITE(6,15) V(M),X(1,M),X(2,M),X(3,M),SIGMA(M),EPS
0093             TAU(M) = SIGMA(M) + J*W*( EPS - EPSO)
0094      10  CONTINUE
0095      15  FORMAT(1X,E10.5,4F10.5,E10.4)
0096
0097          DO 20 I=1,NCELL
0098              READ (5,25) EI(I),EI(I+NCELL),EI(I+2*NCELL)
0099              G1(I,3*NCELL+1) = -EI(I)
0100              G1(I+NCELL,3*NCELL+1)= -EI(I+NCELL)
0101              G1(I+2*NCELL,3*NCELL+1)= -EI(I+2*NCELL)
0102      20      WRITE(6,25) EI(I),EI(I+NCELL),EI(I+2*NCELL)
0103      25  FORMAT(1X,6E12.5)
0104
0105      C -------- GENERATION OF COEFFICIENT MATRIX  G -------------- C
0106
0107      C ------  M CONTROLS THE NUMBER OF VOLUMES
0108      C ------  P
0109      C ------  Q IS DUE TO DOTPRODUCT
0110      C ------  N IS ALSO DUE TO DOTPRODUCT
0111
0112          C = -J*W*UO*KO
0113          C1 = -2.*J*W*UO/(3.*KO**2)
0114          C2 = 3.*J*W*EPSO
0115
0116          DO 50 P = 1,3
0117             DO 50 Q = 1,3
```

Figure 5.26
(Cont.)* Computer program for Example 5.11 *(Continued).

```
0118            X1 = (P-1) * NCELL
0119          DO 50 M = 1,NCELL
0120            X1 = X1 + 1
0121            X2 = (Q-1) * NCELL
0122          DO 50 N = 1,NCELL
0123          X2= X2 + 1
0124          IF (M .EQ. N) THEN
0125            AN = ( 3.*V(N)/(4.*PI) )**(1./3.)
0126            C3 = J*KO*AN
0127            C4 = TAU(N)/C2
0128
0129          G1(X1,X2)=DELTA(P,Q)*( C1*TAU(N)*((1.+C3)
                                *EXP(-C3)-1.)-(1.+C4) )
0130
0131          ELSE
0132            DIST = R(M,N)
0133            IF ( DIST .EQ. 0. ) THEN
0134                PRINT *, 'CELLS HAVE SAME CENTER ',M,N
0135            END IF
0136            AMN = KO*DIST
0137            C3 = ( C*TAU(N)*V(N)*EXP(-J*AMN) )/(4.*PI*(AMN**3))
0138            G1(X1,X2) = C3*( (AMN**2 - 1. - J*AMN)*DELTA(P,Q)
0139         &  +COSANGLE(P,M,N,DIST)*COSANGLE(Q,M,N,DIST)
                                    *(3.-AMN**2+3.*J*AMN))
0140          END IF
0141
0142    50    CONTINUE
0143
0144          CALL GAUSSC(MXCLL3,MXCLL3,MXCL31,3*NCELL,3*NCELL+1,G1,E)
0145
0146          WRITE (6,105)
0147    105   FORMAT (1X,'OUTPUT DATA')
0148          WRITE (6,106)
0149    106   FORMAT(1X,'VOLUME  EX   EY  EZ SAR')
0150
0151          DO 110 I = 1,NCELL
0152           SAR = SQRT(MAGSQ(E(I))+MAGSQ(E(I+NCELL))
                                    +MAGSQ(E(I+2*NCELL)) )
0153           SAR = 0.5 * SIGMA(I) * SAR
0154    110   WRITE(6,115) I,E(I),E(I+NCELL),E(I+2*NCELL),SAR
0155    115   FORMAT(I4,7E10.4)
0156
0157          CLOSE (6)
0158          OPEN (6,FILE='PLHEAD.DAT',STATUS='NEW')
0159    C
0160    C NOTE: THERE ARE 8 CELLS ALONG THE Z-DIRECTION
0161    C       SEE FIG. 5.22 DR. SADIKU'S NOTES
0162    C
0163          PZMAX = -1.E-10
0164          DO 140 I=1,8
0165            PZ(I) = MAGSQ(E(I))+MAGSQ(E(I+NCELL))+MAGSQ(E(I+2*NCELL))
0166            PZ(I) = (SIGMA(I)/2.)*PZ(I)
0167    140     PZMAX = AMAX1(PZ(I),PZMAX)
0168
0169    145   FORMAT(1X,'MAXIMUM POWER FOR CELLS
                      ALONG THE Z-AXIS IS ',F10.5)
0170    146   FORMAT(1X,'NORMALIZED POWER ALONG THE Z-AXIS')
0171          WRITE(6,145) PZMAX
0172          WRITE(6,146)
0173          DO 150 I=1,8
0174            PZ(I) = PZ(I)/PZMAX
0175    150   WRITE(6,155) I,PZ(I)
0176    155   FORMAT(1X,I4,F10.6)
```

Figure 5.26

(Cont.) **Computer program for Example 5.11.** ***(Continued).***

```
0177    C
0178    C AVERAGE POWER CALCULATION
0179    C
0180          SPOW = 0.
0181          SVOL = 0.
0182          PMAX = -1.E-10
0183          DO 160 I=1,NCELL
0184             POWER = MAGSQ(E(I))+MAGSQ(E(I+NCELL))
                                 +MAGSQ(E(I+2*NCELL))
0185             POWER = (SIGMA(I)/2.)*POWER*VOL(I)
0186             PMAX = AMAX1(PMAX,POWER)
0187             IF ( ABS( PMAX - POWER ) .LT. 1.E-6) IVPMAX = I
0188             SVOL = SVOL + V(I)
0189    160      SPOW = POWER + SPOW
0190
0191          WRITE(6,165) SPOW
0192          WRITE(6,170) PMAX/V(IVPMAX)
0193    165   FORMAT(1X,'AVERAGE HEATING IN W/M**3 IS ',E12.6)
0194    170   FORMAT(1X,'MAX HEATING IN W/M**3 IS ',E12.6)
0195          CLOSE (6)
0196          STOP
0197          END
```

```
0001    C*************************************************
0002    C   SUBROUTINE FOR GAUSSIAN ELIMINATION
0003    C  THIS SUBROUTINE SOLVES COMPLEX SIMULTANEOUS EQUATIONS
0004    C  USING GAUSS ELIMIANATION WITH PARTIAL PIVOTING
0005    C  THE ORIGINAL PROGRAM WAS WRITTEN TO HANDLE REAL MATRICES
0006    C  AND CAN BE FOUND IN:
0007    C        APPLIED NUMERICAL METHODS FOR DIGITAL COMPUTATION
0008    C        WITH FORTRAN AND CSMP - SECOND EDITION
0009    C        BY M. L. JAMES, G. M. SMITH, AND J. C. WOLFORD
0010    C  A(I,J) = AUGMENTED MATRIX
0011    C  JJ = PIVOT PURPOSES
0012    C  BIG = VALUE THAT MAY BE USED AS PIVOT ELEMENT
0013    C  CMAX = MAXIMUM DIMENSION OF MATRIX CONTAINING RESULTS
0014    C  CMAX1 = MAXIMUM DIMENSION OF AUGMENTED MATRIX
0015    C  M = NUMBER OF COLUMNS IN AUGMENTED MATRIX = N+1
0016    C  N = NUMBER OF SIMULTANEOUS EQUATIONS
0017    C  RMAX = MAXIMUM ROW DIMENSION OF AUGMENTED MATRIX
0018    C  X(N) = RESULT
0019    C
0020
0021          SUBROUTINE GAUSSC(RMAX,CMAX,CMAX1,N,M,A,X)
0022
0023
0024          COMPLEX A,AB,X,TEMP,QUOT,SUM,BIG
0025          INTEGER RMAX,CMAX1,CMAX
0026          DIMENSION A(RMAX,CMAX1),X(CMAX)
0027
0028          L = N-1
0029          DO 12 K = 1,L
0030          JJ = K
0031          BIG = ABS( A(K,K) )
0032          KP1 = K + 1
0033    C
0034    C  SEARCH FOR THE LARGEST POSSIBLE PIVOT ELEMENT
0035    C
0036          DO 7 I = KP1,N
0037          AB = ABS( A(I,K) )
0038          IF ( ABS(BIG - AB) ) 6,7,7
0039    6     BIG = AB
0040          JJ = I
```

Figure 5.26

(Cont.)* Computer program for Example 5.11. *(Continued).

```
0041    7     CONTINUE
0042    C
0043    C DECISION ON NECESSITY OF ROW INTERCHANGE
0044    C
0045          IF (JJ-K) 8,10,8
0046    C
0047    C ROW INTERCHANGE
0048    C
0049    8     DO 9 J=K,M
0050          TEMP = A(JJ,J)
0051          A(JJ,J) = A(K,J)
0052    9     A(K,J) = TEMP
0053    C
0054    C CALCULATION OF ELEMENTS OF NEW MATRIX
0055    C
0056    10    DO 11 I = KP1,N
0057          QUOT = A(I,K)/A(K,K)
0058          DO 11 J=KP1,M
0059    11    A(I,J) = A(I,J) - QUOT*A(K,J)
0060          DO 12 I = KP1,N
0061    12    A(I,K) = (0.,0.)
0062    C
0063    C FIRST STEP IN BACKSUBSTITUTION
0064    C
0065          X(N) = A(N,M)/A(N,N)
0066    C
0067    C REMAINDER IN BACKSUBSTITUTION
0068    C
0069          DO 14 NN=1,L
0070          SUM = (0.,0.)
0071          I = N-NN
0072          IP1 = I + 1
0073          DO 13 J = IP1,N
0074    13    SUM = SUM + A(I,J)*X(J)
0075    14    X(I) = (A(I,M)-SUM)/A(I,I)
0076          RETURN
0077          END

0001    C**********************************
0002    C   SUBPROGRAM DELTA
0003          FUNCTION DELTA(M,N)
0004
0005          IF (M .EQ. N) THEN
0006                DELTA = 1.
0007          ELSE
0008                DELTA = 0.
0009          END IF
0010          RETURN
0011          END
```

Figure 5.26
***(Cont.)* Computer program for Example 5.11.**

solution of the matrix equation is usually carried out via inversion, elimination, or iterative techniques. Although MOM is commonly applied to open problems such as those involving radiation and scattering, it has been successfully applied to closed problems such as waveguides and cavities.

Needless to say, the issues on MOM covered in this chapter have been carefully selected. We have only attempted to cover the background and reference material upon which the reader can easily build. The interested reader is referred to the literature for more in-depth treatment of each subject. General concepts on MOM

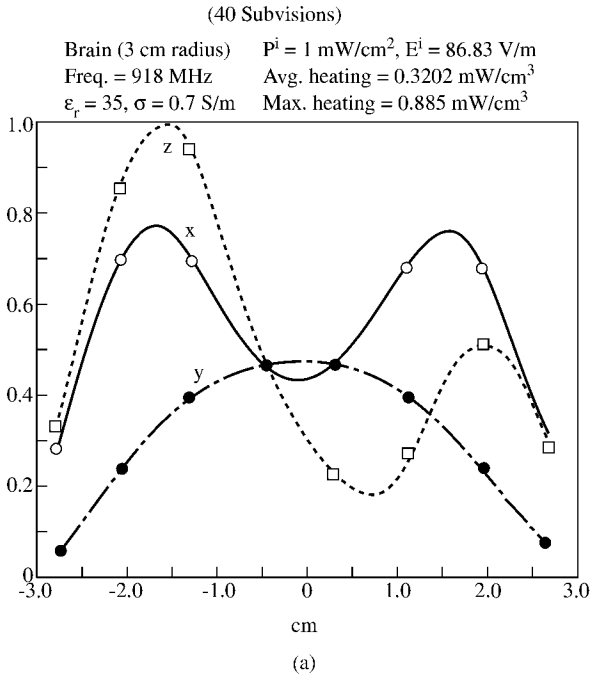

Figure 5.27
Distributions of heating along the x-, y-, and z-axis of a spherical model of an animal brain [57]: (a) MOM solution, (b) exact solution.

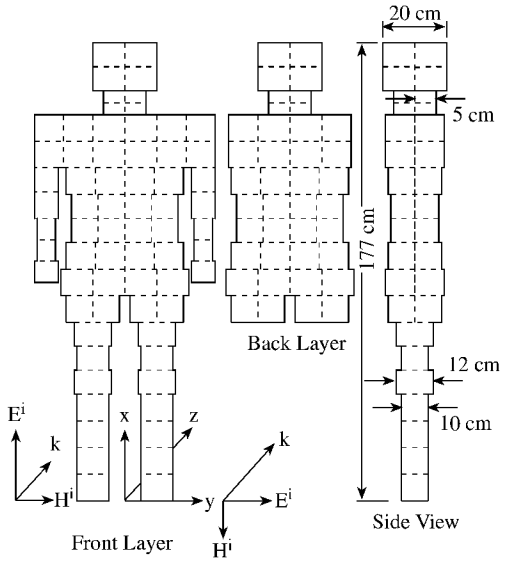

Figure 5.28
Geometry and dimensions of a model of typical human body of height 1.77 m [52].

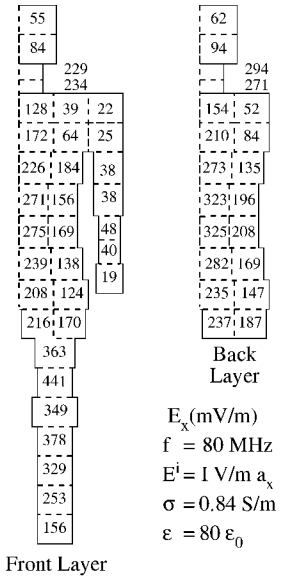

Figure 5.29
Induced E_x (in mV/m) at the center of each cell due to E_x^i of 1 V/m [52].

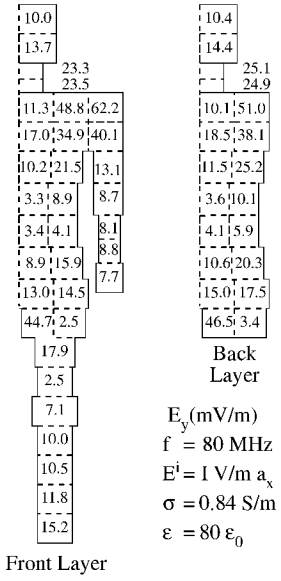

Figure 5.30
Induced E_y (in mV/m) at the center of each cell due to E_x^i of 1 V/m [52].

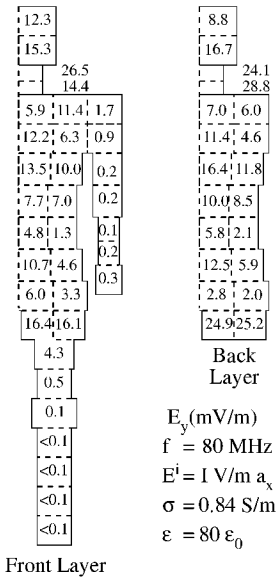

Figure 5.31
Induced E_z (in mV/m) at the center of each cell due to E_x^i of 1 V/m [52].

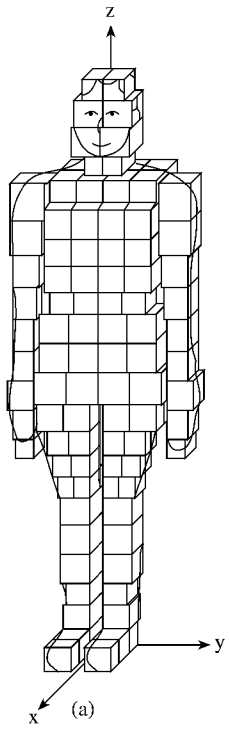

Figure 5.32
A more realistic block model of the human body [59]: (a) In three dimensions *(Continued)*.

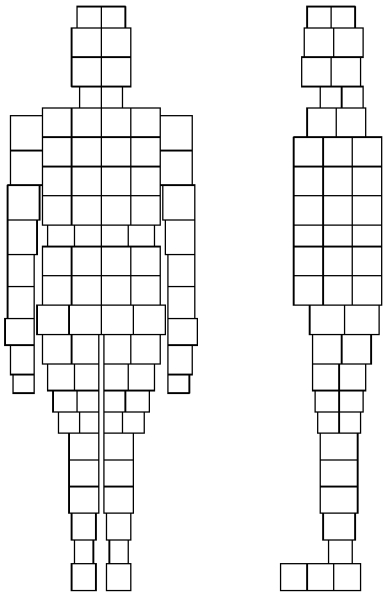

(b)

Figure 5.32
(Cont.) **A more realistic block model of the human body [59]: (b) Front and side views.**

are covered in [10] and [62]. Clear and elementary discussions on IEs and Green's functions may be found in [12], [28]–[30], [62]–[65]. For further study on the theory of the method of moments, one should see [6, 9, 10, 28, 40].

The number of problems that can be treated by MOM is endless, and the examples given in this chapter just scratch the surface. The following problems represent typical EM-related application areas:

- electrostatic problems [31], [66]–[69]
- wire antennas and scatterers [34, 37, 42, 44, 70, 78]
- scattering and radiation from bodies of revolution [79, 80]
- scattering and radiation from bodies of arbitrary shapes [38, 81, 82]
- transmission lines [18]–[20], [23, 24], [83]–[86]
- aperture problems [87]–[89]
- biomagnetic problems [47]–[52], [90]–[92].

A number of user-oriented computer programs have evolved over the years to solve electromagnetic integral equations by the method of moments. These codes

can handle radiation and scattering problems in both the frequency and time domains. Reviews of the codes may be found in [7, 38, 93]. The most popular of these codes is the Numerical Electromagnetic Code (NEC) developed at the Lawrence Livermore National Laboratory [7, 94]. NEC is a frequency domain antenna modeling FORTRAN code applying the MOM to IEs for wire and surface structures. Its most notable features are probably that it is user oriented, includes documentation, and is available; for these reasons, it is being used in public and private institutions. A compact version of NEC is the mini-numerical electromagnetic code (MININEC) [95], which is intended to be used in personal computers.

It is important that we recognize the fact that MOM is limited in application to radiation and scattering from bodies that are electrically large. The size of the scatterer or radiator must be of the order λ^3. This is because the cost of storing, inverting, and computing matrix elements becomes prohibitively large. At high frequencies, asymptotic techniques such as the geometrical theory of diffraction (GTD) are usually employed to derive approximate but accurate solutions [46, 96, 97].

References

[1] L.V. Kantorovich and V.I. Krylov, *Approximate Methods of Higher Analysis* (translated from Russian by C.D. Benster). New York: John Wiley, 1964.

[2] Y.U. Vorobev, *Method of Moments in Applied Mathematics* (translated from Russian by Seckler). New York: Gordon & Breach, 1965.

[3] R.F. Harrington, *Field Computation by Moment Methods*. Malabar, FL: Krieger, 1968.

[4] B.J. Strait, *Applications of the Method of Moments to Electromagnetics*. St. Cloud, FL: SCEEE Press, 1980.

[5] R.F. Harrington, "Origin and development of the method moments for field computation," in E.K. Miller et al., *Computational Electromagnetics*. New York: IEEE Press, 1992, pp. 43–47.

[6] J.H. Richmond, "Digital computer solutions of the rigorous equations for scattering problems," *Proc. IEEE*, vol. 53, Aug. 1965, pp. 796–804.

[7] R.F. Harrington, "Matrix methods for field problems," *Proc. IEEE*, vol. 55, no. 2, Feb. 1967, pp. 136–149.

[8] M.M. Ney, "Method of moments as applied to electromagnetics problems," *IEEE Trans. Micro. Theo. Tech.*, vol. MTT-33, no. 10, Oct. 1985, pp. 972–980.

[9] A.T. Adams, "An introduction to the method of moments," Syracuse Univ., *Report RADC* TR-73-217, vol. 1, Aug. 1974.

[10] M.D. Greenberg, *Application of Green Functions in Science and Engineering.* Englewood Cliffs, NJ: Prentice-Hall, 1971.

[11] A. Ishimaru, *Electromagnetic Wave Propagation, Radiation, and Scattering.* Englewood Cliffs, NJ: Prentice-Hall, 1991, pp. 121–148.

[12] P.M. Morse and H. Feshbach, *Methods of Theoretical Physics.* New York: McGraw-Hill, Part I, Chap. 7, 1953, pp. 791–895.

[13] T. Myint-U, *Partial Differential Equations of Mathematical Physics.* New York: North-Holland, 1980, 2nd ed., Chap. 10, pp. 282–305.

[14] R.F. Harrington, *Time-harmonic Electromagnetic Fields.* New York: McGraw-Hill, 1961, p. 232.

[15] I.V. Bewley, *Two-dimensional Fields in Electrical Engineering.* New York: Dover Publ., 1963, pp. 151–166.

[16] K.C. Gupta, et al., *Computer-aided Design of Microwave Circuits.* Dedham: Artech House, 1981, pp. 237–261.

[17] T. Itoh (ed.), *Numerical Techniques for Microwaves and Millimeterwave Passive Structures.* New York: John Wiley & Sons, 1989, pp. 221–250.

[18] D.W. Kammler, "Calculation of characteristic admittance and coupling coefficients for strip transmission lines," *IEEE Trans. Micro. Tech.,* vol. MTT-16, no. 11, Nov. 1968, pp. 925–937.

[19] Y.M. Hill, et al., "A general method for obtaining impedance and coupling characteristics of practical microstrip and triplate transmission line configurations," *IBM J. Res. Dev.,* vol. 13, May 1969, pp. 314–322.

[20] W.T. Weeks, "Calculation of coefficients of capacitance of multiconductor transmission lines in the presence of a dielectric interface," *IEEE Trans. Micro. Theo. Tech.,* vol. MTT-18, no. 1, Jan. 1970, pp. 35–43.

[21] R. Chadha and K.C. Gupta, "Green's functions for triangular segments in planar microwave circuits," *IEEE Trans. Micro. Theo. Tech.,* vol. MTT-28, no. 10, Oct. 1980, pp. 1139–1143.

[22] R. Terras and R. Swanson, "Image methods for constructing Green's functions and eigenfunctions for domains with plane boundaries," *J. Math. Phys.,* vol. 21, no. 8, Aug. 1980, pp. 2140–2153.

[23] E. Yamashita and K. Atsuki, "Stripline with rectangular outer conductor and three dielectric layers," *IEEE Trans. Micro. Theo. Tech.,* vol. MTT-18, no. 5, May 1970, pp. 238–244.

[24] R. Crampagne, et al., " A simple method for determining the Green's function for a large class of MIC lines having multilayered dielectric structures," *IEEE Trans. Micro. Theo. Tech.,* vol. MTT-26, no. 2, Feb. 1978, pp. 82–87.

[25] R. Chadha and K.C. Gupta, "Green's functions for circular sectors, annular rings, and annular sectors in planar microwave circuits," *IEEE Trans. Micro. Theo. Tech.*, vol. MTT-29, no. 1, Jan. 1981, pp. 68–71.

[26] P.H. Pathak, "On the eigenfunction expansion of electromagnetic dydadic Green's functions," *IEEE Trans. Ant. Prog.*, vol. AP-31, no. 6, Nov. 1983.

[27] R.F. Harrington and J.R. Mautz, "Green's functions for surfaces of revolution," *Radio Sci.*, vol. 7, no. 5, May 1972, pp. 603–611.

[28] C.A. Balanis, *Advanced Engineering Electromagnetics*. New York: John Wiley, 1989, pp. 670–742, 851–916.

[29] E. Butkov, *Mathematical Physics*. New York: Addison-Wesley, 1968, pp. 503–552.

[30] J.D. Jackson, *Classical Electrodynamics*, 2nd ed., New York: John Wiley, 1975, pp. 119–135.

[31] L.L. Tsai and C.E. Smith, "Moment Methods in electromagnetics undergraduates," *IEEE Trans. Educ.*, vol. E-21, no. 1, Feb. 1978, pp. 14–22.

[32] P.P. Silvester and R.L. Ferrari, *Finite Elements for Electrical Engineers*. Cambridge, UK: Cambridge University Press, 1983, pp. 103–105.

[33] H.A. Wheeler, "Transmission-line properties of parallel strips separated by a dielectric sheet," *IEEE Trans. Micro. Theo. Tech.*, vol. MTT-13, Mar. 1965, pp. 172–185.

[34] J.H. Richmond, "Scattering by an arbitrary array of parallel wires," *IEEE Trans. Micro. Theo. Tech.*, vol. MTT-13, no. 4, July 1965, pp. 408–412.

[35] B.D. Popovic, et al., *Analysis and Synthesis of Wire Antennas*. Chichester, UK: Research Studies Press, 1982, pp. 3–21.

[36] E. Hallen, "Theoretical investigations into the transmitting and receiving qualities of antennae," *Nova Acta Regiae Soc. Sci. Upsaliensis*, Ser. IV, no. 11, 1938, pp. 1–44.

[37] K.K. Mei, " On the integral equations of thin wire antennas," *IEEE Trans. Ant. Prog.*, vol. AP-13, 1965, pp. 374–378.

[38] J. Moore and P. Pizer (eds.), *Moment Methods in Electromagnetics: Techniques and Applications*. Letchworth, UK: Research Studies Press, 1984.

[39] H.C. Pocklington, " Electrical oscillations in wire," *Cambridge Phil. Soc. Proc.*, vol. 9, 1897, pp. 324–332.

[40] R. Mittra (ed.), *Computer Techniques for Electromagnetics*. Oxford: Pergamon Press, 1973, pp. 7–95.

[41] C.A. Balanis, *Antenna Theory: Analysis and Design*. New York: Harper & Row, 1982, pp. 283–321.

[42] C.M. Butler and D.R. Wilton, "Analysis of various numerical techniques applied to thin-wire scatterers," *IEEE Trans. Ant. Prog.*, vol. AP-23, no. 4, July 1975, pp. 524–540. Also in [46, pp. 46–52].

[43] T.K. Sarkar, "A note on the choice of weighting functions in the method of moments," *IEEE Trans. Ant. Prog.*, vol. AP-33, no. 4, April 1985, pp. 436–441.

[44] F.M. Landstorfer and R.F. Sacher, *Optimisation of Wire Antenna*. Letchworth, UK: Research Studies Press, 1985, pp. 18–33.

[45] K.A. Michalski and C.M. Butler, "An efficient technique for solving the wire integral equation with non-uniform sampling," *Conf. Proc. IEEE Southeastcon.*, April 1983, pp. 507–510.

[46] R.F. Harrington, et al. (eds.), *Lectures on Computational Methods in Electromagnetics*. St. Cloud, FL: SCEEE Press, 1981.

[47] R. Kastner and R. Mittra, "A new stacked two-dimensional spectral iterative technique (SIT) for analyzing microwave power deposition in biological media," *IEEE Trans. Micro. Theo. Tech.*, vol. MTT-31, no. 1, Nov. 1983, pp. 898–904.

[48] P.W. Barber, "Electromagnetic power deposition in prolate spheroidal models of man and animals at resonance," *IEEE Trans. Biomed. Engr.*, vol. BME-24, no. 6, Nov. 1977, pp. 513–521.

[49] J.M. Osepchuk (ed.), *Biological Effects of Electromagnetic Radiation*. New York: IEEE Press, 1983.

[50] R.J. Spiegel, "A review of numerical models for predicting the energy deposition and resultant thermal response of humans exposed to electromagnetic fields," *IEEE Trans. Micro. Theo. Tech.*, vol. MTT-32, no. 8, Aug. 1984, pp. 730–746.

[51] D.E. Livesay and K.M. Chen, "Electromagnetic fields induced inside arbitrary shaped biological bodies," *IEEE Trans. Micro. Theo. Tech.*, vol. MTT-22, no. 12, Dec. 1974, pp. 1273–1280.

[52] J.A. Kong (ed.), *Research Topics in Electromagnetic Theory*. New York: John Wiley, 1981, pp. 290–355.

[53] C.T. Tai, *Dyadic Green's Functions in Electromagnetic Theory*. Scranton, PA: Intex Educational Pub., 1971, pp. 46–54.

[54] J. Van Bladel, "Some remarks on Green's dyadic infinite space," *IRE Trans. Ant. Prog.*, vol. AP-9, Nov. 1961, pp. 563–566.

[55] B.S. Guru and K.M. Chen, "A computer program for calculating the induced EM field inside an irradiated body," Dept. of Electrical Engineering and System Science, Michigan State Univ., East Lansing, MI, 48824, 1976.

[56] K.M. Chen and B.S. Guru,"Internal EM field and absorbed power density in human torsos induced by 1-500 MHz EM waves," *IEEE Micro. Theo. Tech.*, vol. MTT-25, no. 9, Sept. 1977, pp. 746–756.

[57] R. Rukspollmuang and K.M. Chen, "Heating of spherical versus realistic models of human and infrahuman heads by electromagnetic waves," *Radio Sci.*, vol. 14, no. 6S, Nov.-Dec., 1979, pp. 51–62.

[58] R. Jongakiem, "Electromagnetic absorption in biological bodies," *M. S. Thesis*, Dept. of Electrical and Computer Engr., Florida Atlantic Univ., Boca Raton, Aug. 1988.

[59] O.P. Gandhi, "Electromagnetic absorption in an inhomogeneous model of man for realistic exposure conditions," *Bioelectromagnetics*, vol. 3, 1982, pp. 81–90.

[60] O.P. Gandhi, et al., "Part-body and multibody effects on absorption of radiofrequency electromagnetic energy by animals and by models of man," *Radio Sci.*, vol. 14, no. 6S, Nov.-Dec., 1979, pp. 15–21.

[61] M.J. Hagmann, O.P. Gandhi, and C.H. Durney, "Numerical calculation of electromagnetic energy deposition for a realistic model of man," *IEEE Trans. Micro. Theo. Tech.*, vol. MTT-27, no. 9, Sept. 1979, pp. 804–809.

[62] J.J. Wang, "Generalized moment methods in electromagnetics," *IEEE Proc.*, vol. 137, Pt. H, no. 2, April 1990, pp. 127–132.

[63] G. Goertzel and N. Tralli, *Some Mathematical Methods of Physics*. New York: McGraw-Hill, 1960.

[64] W.V. Lovitt, *Linear Integral Equations*. New York: Dover Publ., 1950.

[65] C.D. Green, *Integral Equation Methods*. New York: Barnes & Nobles, 1969.

[66] R.F. Harrington, et al., "Computation of Laplacian potentials by an equivalent source method," *Proc. IEEE*, vol. 116, no. 10, Oct. 1969, pp. 1715–1720.

[67] J.R. Mautz and R.F. Harrington, "Computation of rotationally symmetric Laplacian," *Proc. IEEE*, vol. 117, no. 4, April 1970, pp. 850–852.

[68] S.M. Rao, et al., "A simple numerical solution procedure for static problems involving arbitrary-shaped surfaces," *IEEE Trans. Ant. Prog.*, vol. AP-27, no. 5, Sept. 1979, pp. 604–608.

[69] K. Adamiak, "Application of integral equations for solving inverse problems in stationary electromagnetic fields," *Int. J. Num. Meth. Engr.*, vol. 21, 1985, pp. 1447–1485.

[70] A.W. Glisson, "An integral equation for electromagnetic scattering from homogeneous dielectric bodies," *IEEE Trans. Ant. Prog.*, vol. AP-33, no. 2, Sept. 1984, pp. 172–175.

[71] E. Max, "Integral equation for scattering by a dielectric," *IEEE Trans. Ant. Prog.*, vol. AP-32, no. 2, Feb. 1984, pp. 166–172.

[72] A.T. Adams, et al., "Near fields of wire antennas by matrix methods," *IEEE Trans. Ant. Prog.*, vol. AP-21, no. 5, Sept. 1973, pp. 602–610.

[73] R.F. Harrington and J.R. Mautz, "Electromagnetic behavior of circular wire loops with arbitrary excitation and loading," *Proc. IEEE*, vol. 115, Jan. 1969, pp. 68–77.

[74] S.A. Adekola and O.U. Okereke, "Analysis of a circular loop antenna using moment methods," *Int. J. Elect.*, vol. 66, no. 5, 1989, pp. 821–834.

[75] E.K. Miller, et al., "Computer evaluation of large low-frequency antennas," *IEEE Trans. Ant. Prog.*, vol. AP-21, no. 3, May 1973, pp. 386–389.

[76] K.S.H. Lee, et al., "Limitations of wire-grid modeling of a closed surface," *IEEE Trans. Elect. Comp.*, vol. EMC-18, no. 3, Aug. 1976, pp. 123–129.

[77] E.H. Newman and D.M. Pozar, "Considerations for efficient wire/surface modeling," *IEEE Trans. Ant. Prog.*, vol. AP-28, no. 1, Jan. 1980, pp. 121–125.

[78] J. Perini and D.J. Buchanan, "Assessment of MOM techniques for shipboard applications," *IEEE Trans. Elect. Comp.*, vol. EMC-24, no. 1, Feb. 1982, pp. 32–39.

[79] J.R. Mautz and R.F. Harrington, "Radiation and scattering from bodies of revolution," *Appl. Sci. Res.*, vol. 20, June 1969, pp. 405–435.

[80] A.W. Glisson and C.M. Butler, "Analysis of a wire antenna in the presence of a body of revolution," *IEEE Trans. Ant. Prog.*, vol. AP-28, Sept. 1980, pp. 604–609.

[81] J.H. Richmond, "A wire-grid model for scattering by conducting bodies," *IEEE Trans. Ant. Prog.*, vol. AP-14, Nov. 1966, pp. 782–786.

[82] S.M. Rao, et al., "Electromagnetic scattering by surfaces of arbitrary shape," *IEEE Trans. Ant. Prog.*, vol. AP-30, May 1966, pp. 409–418.

[83] A. Farrar and A.T. Adams, " Matrix methods for microstrip three-dimensional problems," *IEEE Trans. Micro. Theo. Tech.*, vol. MTT-20, no. 8, Aug. 1972, pp. 497–505.

[84] A. Farrar and A.T. Adams, "Computation of propagation constants for the fundamental and higher-order modes in microstrip," *IEEE Trans. Micro. Theo. Tech.*, vol. MTT-24, no. 7, July 1972, pp. 456–460.

[85] A. Farrar and A.T. Adams, "Characteristic impedance of microstrip by the method of moments," *IEEE Trans. Micro. Theo. Tech.*, vol. MTT-18, no. 1, Jan 1970, pp. 68, 69.

[86] A. Farrar and A.T. Adams, "Computation of lumped microstrip capacitance by matrix methods—rectangular sections and end effects," *IEEE Trans. Micro. Theo. Tech.*, vol. MTT-19, no. 5, May 1971, pp. 495, 496.

[87] R.F. Harrington and J.R. Mautz, "A generalized network formulation for aperture problems," *IEEE Trans. Ant. Prog.*, vol. AP-24, Nov. 1976, pp. 870–873.

[88] R.H. Harrington and D.T. Auckland, "Electromagnetic transmission through narrow slots in thick conducting screens," *IEEE Trans. Ant. Prog.*, vol. AP-28, Sept. 1980, pp. 616–622.

[89] C.M. Butler and K.R. Umashankar, "Electromagnetic excitation of a scatterer coupled to an aperture in a conducting screen," *Proc. IEEE*, vol. 127, Pt. H, June 1980, pp. 161–169.

[90] Special issue on electromagnetic wave interactions with biological systems, *IEEE Trans. Micro. Theo. Tech.*, vol. MTT-32, no. 8, Aug. 1984.

[91] Special issue on effects of electromagnetic radiation, *IEEE Engr. Med. Biol. Mag.*, March 1987.

[92] Helsinki symposium on biological effects of electromagnetic radiation, *Radio Sci.*, vol. 17, no. 5S, Sept.-Oct. 1982.

[93] R.M. Bevensee, "Computer codes for EMP interaction and coupling," *IEEE Trans. Ant. Prog.*, vol. AP-26, no. 1, Jan. 1978, pp. 156–165.

[94] G.J. Burke and A.J. Poggio, *Numerical Electromagnetic Code (NEC)—Method of Moments*. Lawrence Livermore National Lab., Jan. 1981.

[95] J.W. Rockway, et al., *The MININEC System: Microcomputer Analysis of Wire Antennas*. Norwood, MA: Artech House, 1988.

[96] R. Mittra (ed.), *Numerical and Asymptotic Techniques in Electromagnetics*. New York: Springer-Verlag, 1975.

[97] G.L. James, *Geometrical Theory of Diffraction for Electromagnetic Waves*, 3rd ed. London: Peregrinus, 1986.

Problems

5.1 Classify the following integral equations and show that they have the stated solutions:

(a) $\Phi(x)=\dfrac{5x}{b}+\dfrac{1}{2}\displaystyle\int_0^1 xt\Phi(t)\,dt$ [solution $\Phi(x)=x$],

(b) $\Phi(x)=\cos x-\sin x+2\displaystyle\int_0^x \sin(x-t)\Phi(t)\,dt$ [solution $\Phi(x)=e^{-x}$],

(c) $\Phi(x)=-\cosh x+\lambda\displaystyle\int_{-1}^1 \cosh(x+t)\Phi(t)\,dt$ [solution $\Phi(x)=\dfrac{\cosh x}{\frac{\lambda}{2}\sinh 2+\lambda-1}$]

5.2 Solve the following Volterra integral equations:

(a) $\Phi(x) = 5 + 2\int_0^x t\Phi(t)\,dt$,

(b) $\Phi(x) = x + \int_0^x (t - x)\Phi(t)\,dt$

5.3 Find the integral equation corresponding to each of the following differential equations:

(a) $y'' = -y,\ y(0) = 0,\ y'(1) = 1$,

(b) $y'' + y = \cos x,\ y(0) = 0,\ y'(0) = 1$

5.4 Construct the Green's function for the differential equation

$$G_{xx} + k^2 G = -\delta\left(x - x'\right), \quad 0 < x < a$$

subject to $G(0) = G(a) = 0$

5.5 Show that

$$G\left(x, z; x', z'\right) = \frac{j}{a}\sum_{n=1}^{\infty} \frac{\sin(n\pi x/a)\sin\left(n\pi x'/a\right)}{k_n} e^{jk_n(z-z')},$$

where $k_n^2 = k^2 - (n\pi/a)^2$ is the Green's function for Helmholtz's equation.

5.6 Derive the Green's function for

$$\nabla^2\Phi = f, \quad 0 < x, y < 1$$

subject to zero boundary conditions.

5.7 Find the Green's function satisfying

$$G_{xx} + G_{yy} + 2G_x = \delta\left(x - x'\right)\delta\left(y - y'\right), \quad 0 < x < a, 0 < y < b$$

and

$$G(0, y) = G(a, y) = G(x, 0) = G(x, b) = 0$$

5.8 (a) Verify by Fourier expansion that Eqs. (5.79) and (5.80) in Example 5.5 are equivalent.

(b) Show that another form of expressing Eq. (5.79) is

$$G\left(x, y; x', y'\right) = \begin{cases} -\dfrac{2}{\pi}\displaystyle\sum_{m=1}^{\infty} \sinh\frac{m\pi\left(b - y'\right)}{a} \sin\frac{m\pi y}{a}\frac{m\pi x}{a}\frac{m\pi x'}{a}, & y < y' \\ -\dfrac{2}{\pi}\displaystyle\sum_{m=1}^{\infty} \sinh\frac{m\pi y'}{a} \sin\frac{m\pi(b - y)}{a}\frac{m\pi x}{a}\frac{m\pi x'}{a}, & y > y' \end{cases}$$

5.9 The two-dimensional delta function expressed in cylindrical coordinates reads

$$\delta(\rho - \rho') = \frac{1}{\rho}\delta(\rho - \rho')\,\delta(\phi - \phi')$$

Obtain the Green's function for the potential problem

$$\nabla^2 G = \frac{1}{\rho}\delta(\rho - \rho')\,\delta(\phi - \phi')$$

with the region defined in Fig. 5.33. Assume homogeneous Dirichlet boundary conditions.

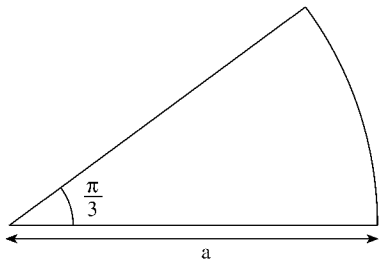

Figure 5.33
For Problem 5.9.

5.10 Consider the transmission line with cross section as shown in Fig. 5.34. In a TEM wave approximation, the potential distribution satisfies Poisson's equation

$$\nabla^2 V = -\frac{\rho_s}{\epsilon}$$

subject to the following continuity and boundary conditions:

$$\begin{aligned}
\frac{\partial}{\partial x}V(x, h_1 - 0) &= \frac{\partial}{\partial x}V(x, h_1 + 0) \\
\frac{\partial}{\partial x}V(x, h_1 + h_2 - 0) &= \frac{\partial}{\partial x}V(x, h_1 + h_2 + 0) \\
\epsilon_1\frac{\partial}{\partial y}V(x, h_1 - 0) &= \epsilon_2\frac{\partial}{\partial y}V(x, h_1 + 0) \\
\epsilon_2\frac{\partial}{\partial y}V(x, h_1 + h_2 - 0) &= \epsilon_3\frac{\partial}{\partial y}V(x, h_1 + h_2 + 0) - \rho_s(x, h_1 + h_2) \\
V(0, y) = V(a, y) &= V(x, 0) = V(x, b) = 0
\end{aligned}$$

Using series expansion method, evaluate the Green's function at $y = h_1 + h_2$, i.e., $G(x, y; x', h_1 + h_2)$.

5.11 Show that the free-space Green's function for $L = \nabla^2 + k^2$ in two-dimensional space is $-\frac{j}{4}H_0^{(1)}(k\rho)$.

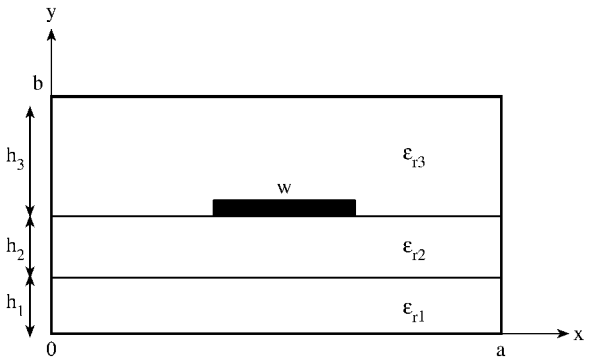

Figure 5.34
For Problem 5.10.

5.12 The spherical Green's function $h_0^{(2)}(|\mathbf{r}-\mathbf{r}'|)$ can be expanded in terms of spherical Bessel functions and Legendre polynomials. Show that

$$h_0^{(2)}\left(|\mathbf{r}-\mathbf{r}'|\right) =$$

$$\frac{j\exp\left(-j\,|\mathbf{r}-\mathbf{r}'|\right)}{(|\mathbf{r}-\mathbf{r}'|)} = \begin{cases} \displaystyle\sum_{n=0}^{\infty}(2n+1)h_n^2\left(\mathbf{r}'\right)j_n(r)P_n(\cos\alpha), & r<r' \\ \displaystyle\sum_{n=0}^{\infty}(2n+1)h_n^2(\mathbf{r})j_n\left(r'\right)P_n(\cos\alpha), & r>r' \end{cases}$$

where $\cos\alpha = \cos\theta\cos\theta' + \sin\theta\sin\theta'\cos(\phi-\phi')$. From this, derive the plane wave expansion

$$e^{-j\,\mathbf{k}\cdot\mathbf{r}} = \sum_{n=0}^{\infty}(-j)^n(2n+1)\,j_n(kr)P_n(\cos\alpha)$$

5.13 Given the kernel

$$K(x,y) = \begin{cases} (1-x)y, & 0\le y\le x\le 1 \\ (1-y)x, & 0\le x\le y\le 1 \end{cases}$$

Show that

$$K(x,y) = 2\sum_{n=1}^{\infty}\frac{\sin n\pi x\,\sin n\pi y}{n^2\pi^2}$$

and that

$$\frac{\pi^2}{4} = \sum_{n=1}^{\infty}\frac{1}{n^2}$$

5.14 Derive the closed form solution for Poisson's equation

$$\nabla^2 V = g$$

in the quarter-plane shown in Fig. 5.35 with

$$V = f(x),\ y = 0, \quad \frac{\partial V}{\partial x} = h(y),\ x = 0$$

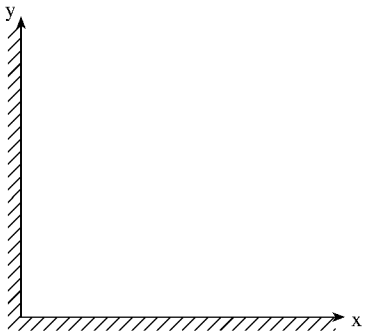

Figure 5.35
For Problem 5.14.

5.15 Consider the cross section of a microstrip transmission line shown in Fig. 5.36. Let $G_{ij}\rho_j$ be the potential at the field point i on the center conductor due to the charge on subsection j. (It is assumed that the charge is concentrated in the filament along the center of the subsection.) G_{ij} is the Green's function for this problem and is given by

$$G_{ij} = \frac{1}{4\pi\epsilon_r}\sum_{n=1}^{\infty}\left[k^{2(n-1)}\ln\frac{A_{ij}^2+(4n-2)^2}{A_{ij}^2+(4n-4)^2} + k^{2n-1}\ln\frac{A_{ij}^2+(4n-2)^2}{A_{ij}^2+(4n)^2}\right]$$

where

$$A_{ij} = \frac{\Delta}{H}|2(i-1)-2(j-1)-1|, \quad k = \frac{\epsilon_r - 1}{\epsilon_r + 1},$$

$\Delta = W/N$, and N is the number of equal subsections into which the center conductor is divided. By setting the potential equal to unity on the center conductor, one can find

$$C = \sum_{j=1}^{\infty}\rho_j \quad \text{(farads/m)}$$

and

$$Z_o = \frac{1}{c\sqrt{C_o C}}$$

where $c = 3 \times 10^8$ m/s and C_o is the capacitance per unit length for an air-filled transmission line (i.e., set $k = 1$ in G_{ij}). Find Z_o for $N = 30$ and:

(a) $\epsilon_r = 6.0, \quad W = 4$ cm, $\quad H = 4$ cm

(b) $\epsilon_r = 16.0, \quad W = 8$ cm, $\quad H = 4$ cm.

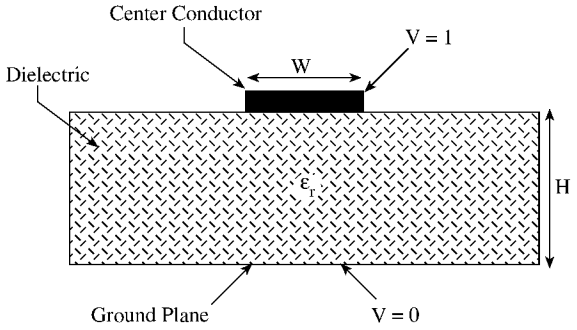

Figure 5.36
For Problem 5.15.

5.16 A rectangular section of microstrip transmission line of length L, width W, and height H above the ground plane is shown in Fig. 5.37. The section is subdivided into N subsections. A typical subsection ΔS_j, of sides Δx_j and Δy_j, is assumed to bear a uniform surface charge density ρ_j. The potential V_i at ΔS_i due to a uniform charge density ρ_j on $\Delta S_j (j = 1, 2, \ldots, N)$ is

$$V_i = \sum_{j=1}^{N} G_{ij} \rho_j$$

where

$$G_{ij} = \sum_{n=1}^{\infty} \frac{k^{n-1}(-1)^{n+1}}{2\pi\epsilon_o(\epsilon_r+1)}$$

$$\Bigg[(x_j - x_i) \ln \frac{(y_j - y_i) + \sqrt{(x_j - x_i)^2 + (y_j - y_i)^2 + (2n-2)^2 H^2}}{(y_j + \Delta y_j - y_i) + \sqrt{(x_j - x_i)^2 + (y_j + \Delta y_j - y_i)^2 + (2n-2)^2 H^2}}$$

$$+ (x_j + \Delta x_j - x_i) \ln \frac{(y_j + \Delta y_j - y_i) + \sqrt{(x_j + \Delta x_j - x_i)^2 + (y_j + \Delta y_j - y_i)^2 + (2n-2)^2 H^2}}{(y_j - y_i) + \sqrt{(x_j + \Delta x_j - x_i)^2 + (y_j - y_i)^2 + (2n-2)^2 H^2}}$$

$$+ (y_j - y_i) \ln \frac{(x_j - x_i) + \sqrt{(x_j - x_i)^2 + (y_j - y_i)^2 + (2n-2)^2 H^2}}{(x_j + \Delta x_j - x_i) + \sqrt{(x_j + \Delta x_j - x_i)^2 + (y_j - y_i)^2 + (2n-2)^2 H^2}}$$

$$+ (y_j + \Delta y_j - y_i) \ln \frac{(x_j + \Delta x_j - x_i) + \sqrt{(x_j + \Delta x_j - x_i)^2 + (y_j + \Delta y_j - y_i)^2 + (2n-2)^2 H^2}}{(x_j - x_i) + \sqrt{(x_j - x_i)^2 + (y_j + \Delta y_j - y_i)^2 + (2n-2)^2 H^2}}$$

$$- (2n-2) H \tan^{-1} \frac{(x_j - x_i)(y_j - y_i)}{(2n-2) H \sqrt{(x_j - x_i)^2 + (y_j - y_i)^2 + (2n-2)^2 H^2}}$$

$$- (2n-2) H \tan^{-1} \frac{(x_j + \Delta x_j - x_i)(y_j + \Delta y_j - y_i)}{(2n-2) H \sqrt{(x_j + \Delta x_j - x_i)^2 + (y_j + \Delta y_j - y_i)^2 + (2n-2)^2 H^2}}$$

$$+ (2n-2) H \tan^{-1} \frac{(x_j - x_i)(y_j + \Delta y_j - y_i)}{(2n-2) H \sqrt{(x_j - x_i)^2 + (y_j + \Delta y_j - y_i)^2 + (2n-2)^2 H^2}}$$

$$+ (2n-2) H \tan^{-1} \frac{(x_j + \Delta x_j - x_i)(y_j - y_i)}{(2n-2) H \sqrt{(x_j + \Delta x_j - x_i)^2 + (y_j - y_i)^2 + (2n-2)^2 H^2}} \Bigg]$$

and $k = \dfrac{\epsilon_r - 1}{\epsilon_r + 1}$. If the ground plane is assumed to be at zero potential while the conducting strip at 1 V potential, we can find

$$C = \sum_{j=1}^{N} \rho_j$$

Find C for:

(a) $\epsilon_r = 9.6, \quad W = L = H = 2$ cm,

(b) $\epsilon_r = 9.6, \quad W = H = 2$ cm , $\quad L = 1$ cm.

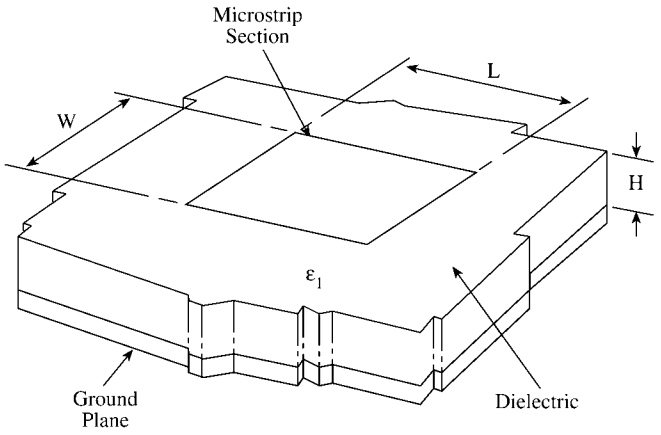

Figure 5.37
For Problem 5.16.

5.17 For a conducting elliptic cylinder with cross section in Fig. 5.38(a), write a program to determine the scattering cross section $\sigma(\phi_i, \phi)$ due to a plane TM wave. Consider $\phi = 0°, 10°, \cdots, 180°$ and cases $\phi_i = 0°, 30°$, and $90°$. Plot $\sigma(\phi_i, \phi)$ against ϕ for each ϕ_i. Take $\lambda = 1\text{m}, 2a = \lambda/2, 2b = \lambda, N = 18$.

Hint: Due to symmetry, consider only one half of the cross section as in Fig. 5.38(b). An ellipse is described by

$$\frac{x^2}{a^2} + \frac{y^2}{b^2} = 1$$

With $x = r\cos\phi,\ y = r\sin\phi$, it is readily shown that

$$r = \frac{a}{\sqrt{\cos^2\phi + v^2\sin^2\phi}}, \qquad v = a/b,\ dl = rd\phi.$$

5.18 Use the program in Fig. 5.17 (or develop your own program) to calculate the scattering pattern for each array of parallel wires shown in Fig. 5.39.

5.19 Repeat Problem 5.17 using the techniques of Section 5.5.2. That is, consider the cylinder in Fig. 5.38(a) as an array of parallel wires.

5.20 Consider the scattering problem of a dielectric cylinder with cross section shown in Fig. 5.40. It is illuminated by a TM wave. To obtain the field $[E]$ inside the dielectric cylinder, MOM formulation leads to the matrix equation

$$[A][E] = \left[E^i\right]$$

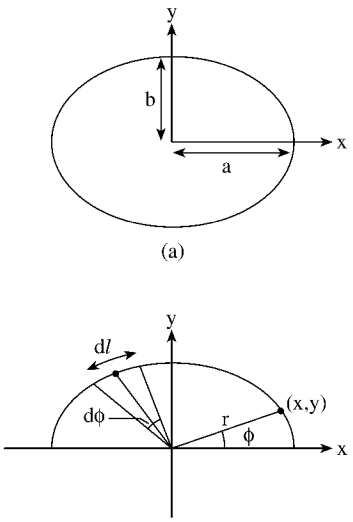

Figure 5.38
For Problem 5.17.

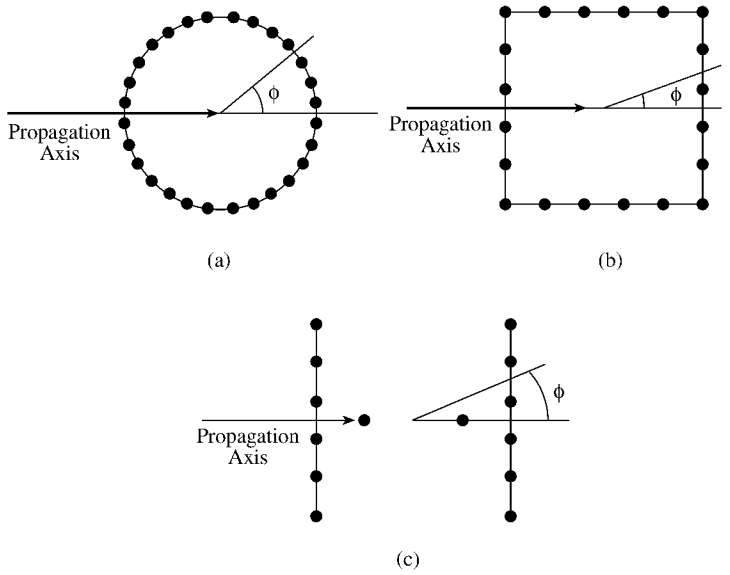

Figure 5.39
Arrays of parallel wires: (a) cylinder, (b) square, (c) I-beam, for Problem 5.18.

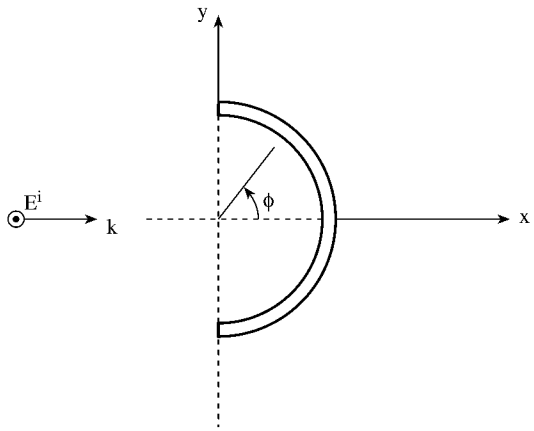

Figure 5.40
For Problem 5.20.

where

$$A_{mn} = \begin{cases} \epsilon_m + j\dfrac{\pi}{2}(\epsilon_m - 1)\, ka_n H_1^{(2)}(ka_m), & m = n \\ j\dfrac{\pi}{2}(\epsilon_m - 1)\, ka_n J_1(ka_n)\, H_0^{(2)}(k\rho_{mn}), & m \neq n \end{cases}$$

$$E_m^i = e^{jk(x_m \cos\phi_i + y_m \sin\phi_i)}$$

$$\rho_{mn} = \sqrt{(x_m - x_n)^2 + (y_m - y_n)^2},\ m, n = 1, 2, \ldots, N$$

N is the number of cells the cylinder is divided into, ϵ_m is the average dielectric constant of cell m, a_m is the radius of the equivalent circular cell which has the same cross section as cell m. Solve the above matrix equation and obtain E_n, $n = 1, 2, \ldots, N$. Use E_n to obtain the echo width of the dielectric cylinder, i.e.,

$$W(\phi) = \frac{\pi^2 k}{\left|E^i\right|^2}\left|\sum_{n=1}^{N}(\epsilon_n - 1)\, E_n a_n J_1(ka_n)\, e^{jk(x_n\cos\phi + y_n\sin\phi)}\right|^2$$

for $\phi = 0°, 5°, 10°, \ldots, 180°$. Plot $W(\phi)$ versus ϕ. For the dielectric cylinder, take $\mu = \mu_o$, $\epsilon = 4\epsilon_o$, inner radius is 0.25λ, outer radius is 0.4λ, and $\lambda = 1$m.

5.21 The integral equation

$$-\frac{1}{2\pi}\int_{-w}^{w} I\left(z'\right)\ln\left|z - z'\right| dz' = f(z), \quad -w < z < w$$

can be cast into matrix equation

$$[S][I] = [F]$$

using pulse basis function and delta expansion function (point matching).

(a) Show that

$$S_{mn} = \frac{\Delta}{2\pi}\left[1 - \ln\Delta - \frac{1}{2}\ln\left|(m-n)^2 - \frac{1}{4}\right| - (m-n)\ln\frac{|m-n+1/2|}{|m-n-1/2|}\right]$$
$$F_n = f(z_n)$$

where $z_n = -w + \Delta(n-1/2), n = 1, 2, \ldots, N, \Delta = 2w/N$. Note that $[S]$ is a Toepliz matrix having only N distinct elements.

(b) Determine the unknowns $\{I_m\}$ with $f(z) = 1, N = 10, 2w = 1$.

(c) Repeat part (b) with $f(z) = z,\ N = 10,\ 2w = 1$.

5.22 A two-term representation of the current distribution on a thin, center-fed half-wavelength dipole antenna is given by

$$I(z) = \sum_{n=1}^{2} B_n \sin\left(\frac{2\pi n}{\lambda}(\lambda/4 - |z|)\right)$$

Substituting this into Hallen's integral equation gives

$$\sum_{n=1}^{2} B_n \int_{-\lambda/4}^{\lambda/4} \sin\left[\frac{2\pi n}{\lambda}\left(\lambda/4 - |z'|\right)\right] G(z, z')\, dz' + \frac{jC_1}{\eta_o}\cos k_o z = -\frac{j}{\eta_o} V_T \sin k_o|z|$$

where $\eta_o = 120\,\pi$, $k_o = \dfrac{2\pi}{\lambda} = \dfrac{2\pi f}{c}$, and $G(z, z')$ is given by Eq. (5.152). Taking $V_T = 1$ volt, $\lambda = 1$ m, $a/\lambda = 7.022 \times 10^{-3}$, and match points at $z = 0, \lambda/8, \lambda/4$, determine the constants B_1, B_2, and C_1. Plot the real and imaginary parts of $I(z)$ against z.

5.23 Using Hallen's IE, determine the current distribution $I(z)$ on a straight dipole of length ℓ. Plot $|I| = |I_r + jI_i|$ against z. Assume excitation by a unit voltage, $N = 51$, $\Omega = 2\ln\dfrac{\ell}{a} = 12.5$, and consider cases: (a) $\ell = \lambda/2$, (b) $\ell = 1.5\lambda$.

5.24 (a) Show that Pocklington integral equation (5.141) can be written as

$$-E_z^i = \frac{\lambda\sqrt{\mu/\epsilon}}{8j\pi a^2}\int_{-\ell/2}^{\ell/2} \frac{I(z')\, e^{-jkR}}{R^5}\left[(1 + jkR)\left(2R^2 - 3a^2\right) + k^2a^2R^2\right] dz'$$

(b) By changing variables, $z' - z = a\tan\theta$, show that

$$-E_z^i = \frac{\lambda\sqrt{\mu/\epsilon}}{8j\pi^2 a^2}\int_{\theta_1}^{\theta_2} I(\theta')\, e^{-jka/\cos\theta'} \cdot\left[\left(jka + \cos\theta'\right)\left(2 - 2\cos^2\theta'\right) + k^2a^2\cos\theta'\right] d\theta'$$

$$\text{where } \theta_1 = -\tan^{-1}\frac{\ell/2+z}{a},\ \theta_2 = \tan^{-1}\frac{\ell/2-z}{a}.$$

5.25 Using the program in Fig. 5.26 (or your own self-developed program), calculate the electric field inside a thin conducting layer ($\mu = \mu_o$, $\epsilon = 70\epsilon_o$, $\sigma = 1$ mho/m) shown in Fig. 5.41. Assume plane wave with electric field perpendicular to the plane of the layer, i.e.,

$$\mathbf{E}^i = e^{-jk_o z}\mathbf{a}_x \quad \text{V/m}$$

where $k_o = 2\pi f/c$. Consider only one half of the layer. Calculate $|E_x|/|E^i|$ and neglect E_y and E_z at the center of the cells since they are very small compared with E_x. Take $a = 0.5$ cm, $b = 4$ cm, $c = 6$ cm.

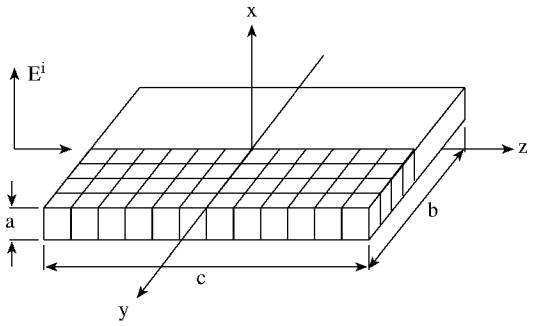

Figure 5.41
For Problem 5.25.

5.26 Consider an adult torso with a height 1.7 m and a shape shown in Fig. 5.42. If the torso is illuminated by a vertically polarized EM wave of 80 MHz with an incident electric field of 1 V/m, calculate the absorbed power density given by

$$\frac{\sigma}{2}\left(E_x^2 + E_y^2 + E_z^2\right)$$

at the center of each cell. Take $\mu = \mu_o$, $\epsilon = 80\epsilon_o$, $\sigma = 0.84$ mhos/m.

5.27 Suppose the dielectric cylinder in Problem 5.20 is a biological body modeled by a cylinder of cross-section 75×50 cm^2, shown in Fig. 5.43. A TM wave of frequency $f = 300$ MHz is normally incident on the body. Compute the fields inside the body using the MOM formulation of Problem 5.20. In this case, take ϵ_m as complex permittivity of cell m, i.e.,

$$\epsilon_m = \epsilon_{rm} - j\,(\sigma_m/\omega\epsilon_o)\,, \qquad m = 1, 2, \ldots, N = 150$$

To make the body inhomogeneous, take $\epsilon_{rm} = 8$ and $\sigma_m = 0.03$ for cells 65, 66, 75, 85, and 86; take $\epsilon_{rm} = 7$ and $\sigma_m = 0.04$ for cells 64, 67, 74, 77, 84, and 87; and take $\epsilon_{rm} = 5$ and $\sigma_m = 0.02$ for all the other cells. Compute E_n.

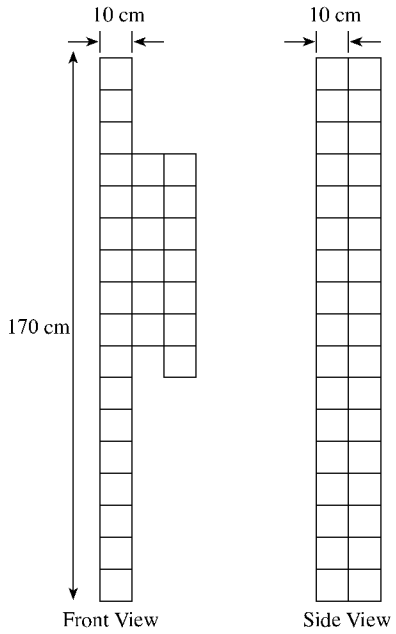

Figure 5.42
An adult torso: for Problem 5.26.

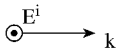

141									150
131									140
121									130
111									120
101									110
91									100
81			84	85	86	87			90
71			74	75	76	77			80
61			64	65	66	67			70
51									60
41									50
31									40
21									30
11									20
1	2	3	4	5	6	7	8	9	10

Figure 5.43
For Problem 5.27.

Chapter 6

Finite Element Method

"Who is wise? He that learns from everyone.
Who is powerful? He that governs his passion.
Who is rich? He that is content.
Who is that? Nobody." Benjamin Franklin

6.1 Introduction

The finite element method (FEM) has its origin in the field of structural analysis. Although the earlier mathematical treatment of the method was provided by Courant [1] in 1943, the method was not applied to electromagnetic (EM) problems until 1968. Since then the method has been employed in diverse areas such as waveguide problems, electric machines, semiconductor devices, microstrips, and absorption of EM radiation by biological bodies.

Although the finite difference method (FDM) and the method of moments (MOM) are conceptually simpler and easier to program than the finite element method (FEM), FEM is a more powerful and versatile numerical technique for handling problems involving complex geometries and inhomogeneous media. The systematic generality of the method makes it possible to construct general-purpose computer programs for solving a wide range of problems. Consequently, programs developed for a particular discipline have been applied successfully to solve problems in a different field with little or no modification [2].

The finite element analysis of any problem involves basically four steps [3]:

- discretizing the solution region into a finite number of *subregions* or *elements*,
- deriving governing equations for a typical element,
- assembling of all elements in the solution region, and
- solving the system of equations obtained.

Discretization of the continuum involves dividing up the solution region into subdomains, called *finite elements*. Figure 6.1 shows some typical elements for one-, two-, and three-dimensional problems. The problem of discretization will be fully treated in Sections 6.5 and 6.6. The other three steps will be described in detail in the subsequent sections.

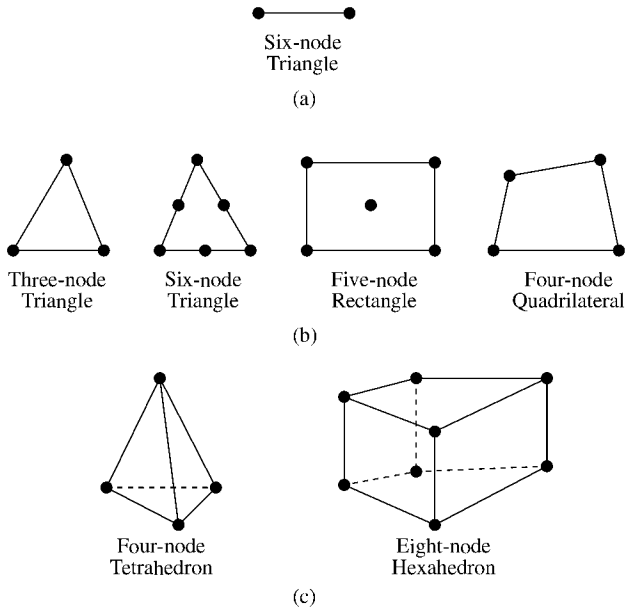

Figure 6.1
Typical finite elements: (a) One-dimensional, (b) two-dimensional, (c) three-dimensional.

6.2 Solution of Laplace's Equation

As an application of FEM to electrostatic problems, let us apply the four steps mentioned above to solve Laplace's equation, $\nabla^2 V = 0$. For the purpose of illustration, we will strictly follow the four steps mentioned above.

6.2.1 Finite Element Discretization

To find the potential distribution $V(x, y)$ for the two-dimensional solution region shown in Fig. 6.2(a), we divide the region into a number of finite elements as illustrated in Fig. 6.2(b). In Fig. 6.2(b), the solution region is subdivided into nine

nonoverlapping *finite elements*; elements 6, 8, and 9 are four-node quadrilaterals, while other elements are three-node triangles. In practical situations, however, it is preferred, for ease of computation, to have elements of the same type throughout the region. That is, in Fig. 6.2(b), we could have split each quadrilateral into two triangles so that we have 12 triangular elements altogether. The subdivision of the solution region into elements is usually done by hand, but in situations where a large number of elements is required, automatic schemes to be discussed in Sections 6.5 and 6.6 are used.

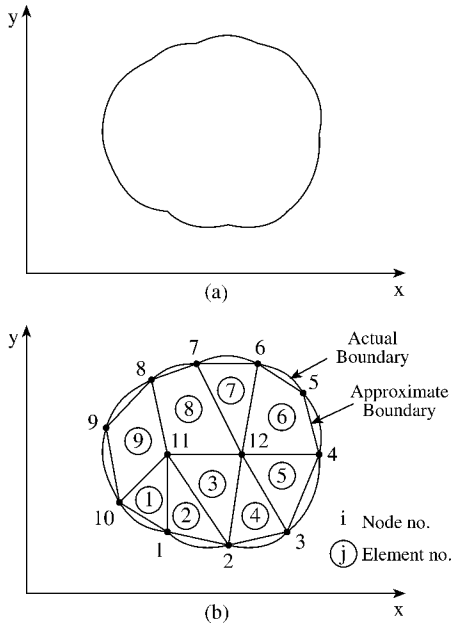

Figure 6.2
(a) The solution region; (b) its finite element discretization.

We seek an approximation for the potential V_e within an element e and then interrelate the potential distribution in various elements such that the potential is continuous across interelement boundaries. The approximate solution for the whole region is

$$V(x, y) \simeq \sum_{e=1}^{N} V_e(x, y), \tag{6.1}$$

where N is the number of triangular elements into which the solution region is divided. The most common form of approximation for V_e within an element is polynomial approximation, namely,

$$V_e(x, y) = a + bx + cy \tag{6.2}$$

for a triangular element and

$$V_e(x, y) = a + bx + cy + dxy \tag{6.3}$$

for a quadrilateral element. The constants a, b, c, and d are to be determined. The potential V_e in general is nonzero within element e but zero outside e. In view of the fact that quadrilateral elements do not conform to curved boundary as easily as triangular elements, we prefer to use triangular elements throughout our analysis in this chapter. Notice that our assumption of linear variation of potential within the triangular element as in Eq. (6.2) is the same as assuming that the electric field is uniform within the element, i.e.,

$$\mathbf{E}_e = -\nabla V_e = -\left(b\mathbf{a}_x + c\mathbf{a}_y\right) \tag{6.4}$$

6.2.2 Element Governing Equations

Consider a typical triangular element shown in Fig. 6.3. The potential V_{e1}, V_{e2}, and V_{e3} at nodes 1, 2, and 3, respectively, are obtained using Eq. (6.2), i.e.,

$$\begin{bmatrix} V_{e1} \\ V_{e2} \\ V_{e3} \end{bmatrix} = \begin{bmatrix} 1 & x_1 & y_1 \\ 1 & x_2 & y_2 \\ 1 & x_3 & y_3 \end{bmatrix} \begin{bmatrix} a \\ b \\ c \end{bmatrix} \tag{6.5}$$

The coefficients a, b and c are determined from Eq. (6.5) as

$$\begin{bmatrix} a \\ b \\ c \end{bmatrix} = \begin{bmatrix} 1 & x_1 & y_1 \\ 1 & x_2 & y_2 \\ 1 & x_3 & y_3 \end{bmatrix}^{-1} \begin{bmatrix} V_{e1} \\ V_{e2} \\ V_{e3} \end{bmatrix} \tag{6.6}$$

Substituting this into Eq. (6.2) gives

$$V_e = [1\ x\ y]\frac{1}{2A}\begin{bmatrix} (x_2y_3 - x_3y_2) & (x_3y_1 - x_1y_3) & (x_1y_2 - x_2y_1) \\ (y_2 - y_3) & (y_3 - y_1) & (y_1 - y_2) \\ (x_3 - x_2) & (x_1 - x_3) & (x_2 - x_1) \end{bmatrix} \begin{bmatrix} V_{e1} \\ V_{e2} \\ V_{e3} \end{bmatrix}$$

or

$$\boxed{V_e = \sum_{i=1}^{3} \alpha_i(x, y) V_{ei}} \tag{6.7}$$

where

$$\alpha_1 = \frac{1}{2A}\left[(x_2y_3 - x_3y_2) + (y_2 - y_3)\,x + (x_3 - x_2)\,y\right], \tag{6.8a}$$

$$\alpha_2 = \frac{1}{2A}\left[(x_3y_1 - x_1y_3) + (y_3 - y_1)\,x + (x_1 - x_3)\,y\right], \tag{6.8b}$$

$$\alpha_3 = \frac{1}{2A}\left[(x_1y_2 - x_2y_1) + (y_1 - y_2)\,x + (x_2 - x_1)\,y\right], \tag{6.8c}$$

and A is the area of the element e, i.e.,

$$2A = \begin{vmatrix} 1 & x_1 & y_1 \\ 1 & x_2 & y_2 \\ 1 & x_3 & y_3 \end{vmatrix}$$
$$= (x_1 y_2 - x_2 y_1) + (x_3 y_1 - x_1 y_3) + (x_2 y_3 - x_3 y_2)$$

or

$$A = \frac{1}{2}\left[(x_2 - x_1)(y_3 - y_1) - (x_3 - x_1)(y_2 - y_1)\right] \tag{6.9}$$

The value of A is positive if the nodes are numbered counterclockwise (starting from any node) as shown by the arrow in Fig. 6.3. Note that Eq. (6.7) gives the potential

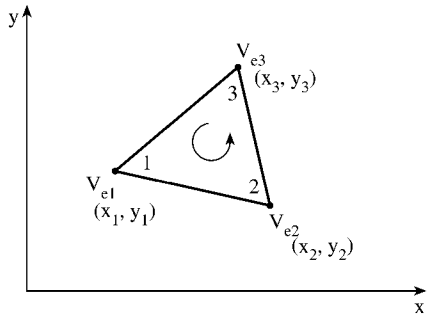

Figure 6.3
Typical triangular element; local node numbering 1-2-3 must proceed counterclockwise as indicated by the arrow.

at any point (x, y) within the element provided that the potentials at the vertices are known. This is unlike finite difference analysis, where the potential is known at the grid points only. Also note that α_i are linear interpolation functions. They are called the *element shape functions* and they have the following properties [4]:

$$\alpha_i = \begin{cases} 1, & i = j \\ 0, & i \neq j \end{cases} \tag{6.10a}$$

$$\sum_{i=1}^{3} \alpha_i(x, y) = 1 \tag{6.10b}$$

The shape functions α_1, α_2, and α_3 are illustrated in Fig. 6.4.

The functional corresponding to Laplace's equation, $\nabla^2 V = 0$, is given by

$$W_e = \frac{1}{2}\int \epsilon\, |\mathbf{E}_e|^2\, dS = \frac{1}{2}\int \epsilon\, |\nabla V_e|^2\, dS \tag{6.11}$$

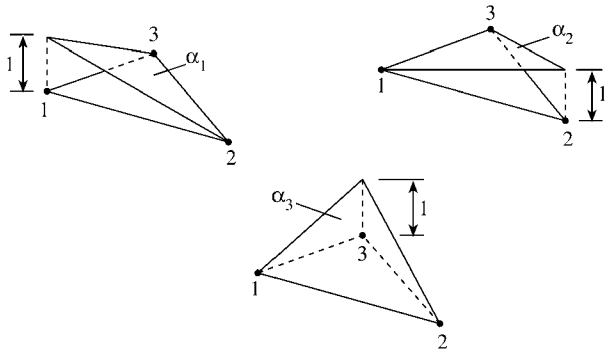

Figure 6.4
Shape functions α_1, α_2, and α_3 for a triangular element.

(Physically, the functional W_e is the energy per unit length associated with the element e.) From Eq. (6.7),

$$\nabla V_e = \sum_{i=1}^{3} V_{ei} \nabla \alpha_i \tag{6.12}$$

Substituting Eq. (6.12) into Eq. (6.11) gives

$$W_e = \frac{1}{2} \sum_{i=1}^{3} \sum_{j=1}^{3} \epsilon V_{ei} \left[\int \nabla \alpha_i \cdot \nabla \alpha_j \, dS \right] V_{ej} \tag{6.13}$$

If we define the term in brackets as

$$C_{ij}^{(e)} = \int \nabla \alpha_i \cdot \nabla \alpha_j \, dS \,, \tag{6.14}$$

we may write Eq. (6.13) in matrix form as

$$W_e = \frac{1}{2} \epsilon \left[V_e \right]^t \left[C^{(e)} \right] \left[V_e \right] \tag{6.15}$$

where the superscript t denotes the transpose of the matrix,

$$[V_e] = \begin{bmatrix} V_{e1} \\ V_{e2} \\ V_{e3} \end{bmatrix} \tag{6.16a}$$

and

$$\left[C^{(e)} \right] = \begin{bmatrix} C_{11}^{(e)} & C_{12}^{(e)} & C_{13}^{(e)} \\ C_{21}^{(e)} & C_{22}^{(e)} & C_{23}^{(e)} \\ C_{31}^{(e)} & C_{32}^{(e)} & C_{33}^{(e)} \end{bmatrix} \tag{6.16b}$$

The matrix $[C^{(e)}]$ is usually called the *element coefficient matrix* (or "stiffness matrix" in structural analysis). The element $C_{ij}^{(e)}$ of the coefficient matrix may be regarded as the coupling between nodes i and j; its value is obtained from Eqs. (6.8) and (6.14). For example,

$$\begin{aligned} C_{12}^{(e)} &= \int \nabla\alpha_1 \cdot \nabla\alpha_2 \, dS \\ &= \frac{1}{4A^2}\left[(y_2 - y_3)(y_3 - y_1) + (x_3 - x_2)(x_1 - x_3)\right] \int dS \\ &= \frac{1}{4A}\left[(y_2 - y_3)(y_3 - y_1) + (x_3 - x_2)(x_1 - x_3)\right] \end{aligned} \tag{6.17a}$$

Similarly,

$$C_{13}^{(e)} = \frac{1}{4A}\left[(y_2 - y_3)(y_1 - y_2) + (x_3 - x_2)(x_2 - x_1)\right] , \tag{6.17b}$$

$$C_{23}^{(e)} = \frac{1}{4A}\left[(y_3 - y_1)(y_1 - y_2) + (x_1 - x_3)(x_2 - x_1)\right] , \tag{6.17c}$$

$$C_{11}^{(e)} = \frac{1}{4A}\left[(y_2 - y_3)^2 + (x_3 - x_2)^2\right] , \tag{6.17d}$$

$$C_{22}^{(e)} = \frac{1}{4A}\left[(y_3 - y_1)^2 + (x_1 - x_3)^2\right] , \tag{6.17e}$$

$$C_{33}^{(e)} = \frac{1}{4A}\left[(y_1 - y_2)^2 + (x_2 - x_1)^2\right] \tag{6.17f}$$

Also

$$C_{21}^{(e)} = C_{12}^{(e)}, \quad C_{31}^{(e)} = C_{13}^{(e)}, \quad C_{32}^{(e)} = C_{23}^{(e)} \tag{6.18}$$

6.2.3 Assembling of All Elements

Having considered a typical element, the next step is to assemble all such elements in the solution region. The energy associated with the assemblage of elements is

$$W = \sum_{e=1}^{N} W_e = \frac{1}{2}\epsilon[V]^t[C][V] \tag{6.19}$$

where

$$[V] = \begin{bmatrix} V_1 \\ V_2 \\ V_3 \\ \vdots \\ V_n \end{bmatrix} , \tag{6.20}$$

n is the number of nodes, N is the number of elements, and $[C]$ is called the overall or *global coefficient matrix,* which is the assemblage of individual element coefficient matrices. Notice that to obtain Eq. (6.19), we have assumed that the whole solution region is homogeneous so that ϵ is constant. For an inhomogeneous solution region such as shown in Fig. 6.5, for example, the region is discretized such that each finite element is homogeneous. In this case, Eq. (6.11) still holds, but Eq. (6.19) does not apply since $\epsilon(=\epsilon_r\epsilon_o)$ or simply ϵ_r varies from element to element. To apply Eq. (6.19), we may replace ϵ by ϵ_o and multiply the integrand in Eq. (6.14) by ϵ_r.

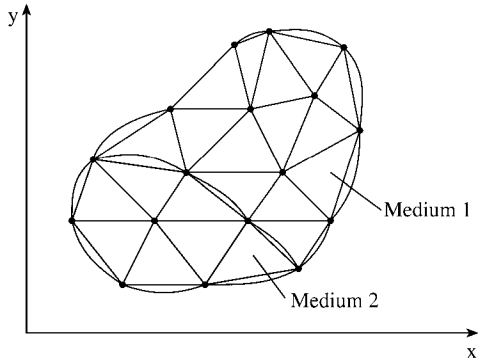

Figure 6.5
Discretization of an inhomogeneous solution region.

The process by which individual element coefficient matrices are assembled to obtain the global coefficient matrix is best illustrated with an example. Consider the finite element mesh consisting of three finite elements as shown in Fig. 6.6. Observe

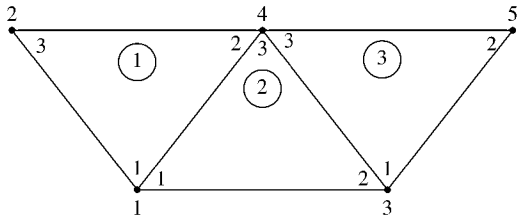

Figure 6.6
Assembly of three elements; i-j-k corresponds to local numbering (1-2-3) of the element in Fig. 6.3.

the numberings of the mesh. The numbering of nodes 1, 2, 3, 4, and 5 is called *global* numbering. The numbering i-j-k is called *local* numbering, and it corresponds with 1 - 2 - 3 of the element in Fig. 6.3. For example, for element 3 in Fig. 6.6, the global numbering 3 - 5 - 4 corresponds with local numbering 1 - 2 - 3 of the element in Fig. 6.3. (Note that the local numbering must be in counterclockwise sequence starting from any node of the element.) For element 3, we could choose 4 - 3 - 5

instead of 3 - 5 - 4 to correspond with 1 - 2 - 3 of the element in Fig. 6.3. Thus the numbering in Fig. 6.6 is not unique. But whichever numbering is used, the global coefficient matrix remains the same. Assuming the particular numbering in Fig. 6.6, the global coefficient matrix is expected to have the form

$$[C] = \begin{bmatrix} C_{11} & C_{12} & C_{13} & C_{14} & C_{15} \\ C_{21} & C_{22} & C_{23} & C_{24} & C_{25} \\ C_{31} & C_{32} & C_{33} & C_{34} & C_{35} \\ C_{41} & C_{42} & C_{43} & C_{44} & C_{45} \\ C_{51} & C_{52} & C_{53} & C_{54} & C_{55} \end{bmatrix} \tag{6.21}$$

which is a 5×5 matrix since five nodes ($n = 5$) are involved. Again, C_{ij} is the coupling between nodes i and j. We obtain C_{ij} by using the fact that the potential distribution must be continuous across interelement boundaries. The contribution to the i, j position in $[C]$ comes from all elements containing nodes i and j. For example, in Fig. 6.6, elements 1 and 2 have node 1 in common; hence

$$C_{11} = C_{11}^{(1)} + C_{11}^{(2)} \tag{6.22a}$$

Node 2 belongs to element 1 only; hence

$$C_{22} = C_{33}^{(1)} \tag{6.22b}$$

Node 4 belongs to elements 1, 2, and 3; consequently

$$C_{44} = C_{22}^{(1)} + C_{33}^{(2)} + C_{33}^{(3)} \tag{6.22c}$$

Nodes 1 and 4 belong simultaneously to elements 1 and 2; hence

$$C_{14} = C_{41} = C_{12}^{(1)} + C_{13}^{(2)} \tag{6.22d}$$

Since there is no coupling (or direct link) between nodes 2 and 3,

$$C_{23} = C_{32} = 0 \tag{6.22e}$$

Continuing in this manner, we obtain all the terms in the global coefficient matrix by inspection of Fig. 6.6 as

$$\begin{bmatrix} C_{11}^{(1)} + C_{11}^{(2)} & C_{13}^{(1)} & C_{12}^{(2)} & C_{12}^{(1)} + C_{13}^{(2)} & 0 \\ C_{31}^{(1)} & C_{33}^{(1)} & 0 & C_{32}^{(1)} & 0 \\ C_{21}^{(2)} & 0 & C_{22}^{(2)} + C_{11}^{(3)} & C_{23}^{(2)} + C_{13}^{(3)} & C_{12}^{(3)} \\ C_{21}^{(1)} + C_{31}^{(2)} & C_{23}^{(1)} & C_{32}^{(2)} + C_{31}^{(3)} & C_{22}^{(1)} + C_{33}^{(2)} + C_{33}^{(3)} & C_{32}^{(3)} \\ 0 & 0 & C_{21}^{(3)} & C_{23}^{(3)} & C_{22}^{(3)} \end{bmatrix} \tag{6.23}$$

Note that element coefficient matrices overlap at nodes shared by elements and that there are 27 terms (9 for each of the 3 elements) in the global coefficient matrix $[C]$. Also note the following properties of the matrix $[C]$:

(1) It is symmetric ($C_{ij} = C_{ji}$) just as the element coefficient matrix.

(2) Since $C_{ij} = 0$ if no coupling exists between nodes i and j, it is expected that for a large number of elements $[C]$ becomes sparse. Matrix $[C]$ is also banded if the nodes are carefully numbered. It can be shown using Eq. (6.17) that

$$\sum_{i=1}^{3} C_{ij}^{(e)} = 0 = \sum_{j=1}^{3} C_{ij}^{(e)}$$

(3) It is singular. Although this is not so obvious, it can be shown using the element coefficient matrix of Eq. (6.16b).

6.2.4 Solving the Resulting Equations

Using the concepts developed in Chapter 4, it can be shown that Laplace's equation is satisfied when the total energy in the solution region is minimum. Thus we require that the partial derivatives of W with respect to each nodal value of the potential be zero, i.e.,

$$\frac{\partial W}{\partial V_1} = \frac{\partial W}{\partial V_2} = \cdots = \frac{\partial W}{\partial V_n} = 0$$

or

$$\frac{\partial W}{\partial V_k} = 0, \qquad k = 1, 2, \ldots, n \tag{6.24}$$

For example, to get $\dfrac{\partial W}{\partial V_1} = 0$ for the finite element mesh of Fig. 6.6, we substitute Eq. (6.21) into Eq. (6.19) and take the partial derivative of W with respect to V_1. We obtain

$$\begin{aligned} 0 = \frac{\partial W}{\partial V_1} = {} & 2V_1C_{11} + V_2C_{12} + V_3C_{13} + V_4C_{14} + V_5C_{15} \\ & + V_2C_{21} + V_3C_{31} + V_4C_{41} + V_5C_{51} \end{aligned}$$

or

$$0 = V_1C_{11} + V_2C_{12} + V_3C_{13} + V_4C_{14} + V_5C_{15} \tag{6.25}$$

In general, $\dfrac{\partial W}{\partial V_k} = 0$ leads to

$$0 = \sum_{i=1}^{n} V_iC_{ik} \tag{6.26}$$

where n is the number of nodes in the mesh. By writing Eq. (6.26) for all nodes $k = 1, 2, \ldots, n$, we obtain a set of simultaneous equations from which the solution of $[V]^t = [V_1, V_2, \ldots, V_n]$ can be found. This can be done in two ways similar to those used in solving finite difference equations obtained from Laplace's equation in Section 3.5.

(1) Iteration Method: Suppose node 1 in Fig. 6.6, for example, is a free node. From Eq. (6.25),

$$V_1 = -\frac{1}{C_{11}} \sum_{i=2}^{5} V_i C_{1i} \tag{6.27}$$

Thus, in general, at node k in a mesh with n nodes

$$\boxed{V_k = -\frac{1}{C_{kk}} \sum_{i=1, i \neq k}^{n} V_i C_{ki}} \tag{6.28}$$

where node k is a free node. Since $C_{ki} = 0$ if node k is not directly connected to node i, only nodes that are directly linked to node k contribute to V_k in Eq. (6.28). Equation (6.28) can be applied iteratively to all the free nodes. The iteration process begins by setting the potentials of fixed nodes (where the potentials are prescribed or known) to their prescribed values and the potentials at the free nodes (where the potentials are unknown) equal to zero or to the average potential [5]

$$V_{\text{ave}} = \frac{1}{2}(V_{\min} + V_{\max}) \tag{6.29}$$

where $V_{\min}$ and $V_{\max}$ are the minimum and maximum values of V at the fixed nodes. With these initial values, the potentials at the free nodes are calculated using Eq. (6.28). At the end of the first iteration, when the new values have been calculated for all the free nodes, they become the old values for the second iteration. The procedure is repeated until the change between subsequent iterations is negligible enough.

(2) Band Matrix Method: If all free nodes are numbered first and the fixed nodes last, Eq. (6.19) can be written such that [4]

$$W = \frac{1}{2}\epsilon \begin{bmatrix} V_f & V_p \end{bmatrix} \begin{bmatrix} C_{ff} & C_{fp} \\ C_{pf} & C_{pp} \end{bmatrix} \begin{bmatrix} V_f \\ V_p \end{bmatrix} \tag{6.30}$$

where subscripts f and p, respectively, refer to nodes with free and fixed (or prescribed) potentials. Since V_p is constant (it consists of known, fixed values), we only differentiate with respect to V_f so that applying Eqs. (6.24) to (6.30) yields

$$\begin{bmatrix} C_{ff} & C_{fp} \end{bmatrix} \begin{bmatrix} V_f \\ V_p \end{bmatrix} = 0$$

or

$$\boxed{[C_{ff}][V_f] = -[C_{fp}][V_p]} \tag{6.31}$$

This equation can be written as

$$[A][V] = [B] \tag{6.32a}$$

or

$$[V] = [A]^{-1}[B] \tag{6.32b}$$

where $[V] = [V_f], [A] = [C_{ff}], [B] = -[C_{fp}][V_p]$. Since $[A]$ is, in general, nonsingular, the potential at the free nodes can be found using Eq. (6.32). We can solve for $[V]$ in Eq. (6.32a) using Gaussian elimination technique. We can also solve for $[V]$ in Eq. (6.32b) using matrix inversion if the size of the matrix to be inverted is not large.

It is sometimes necessary to impose Neumann condition ($\frac{\partial V}{\partial n} = 0$) as a boundary condition or at the line of symmetry when we take advantage of the symmetry of the problem. Suppose, for concreteness, that a solution region is symmetric along the y-axis as in Fig. 6.7. We impose condition ($\frac{\partial V}{\partial x} = 0$) along the y-axis by making

$$V_1 = V_2, \quad V_4 = V_5, \quad V_7 = V_8 \tag{6.33}$$

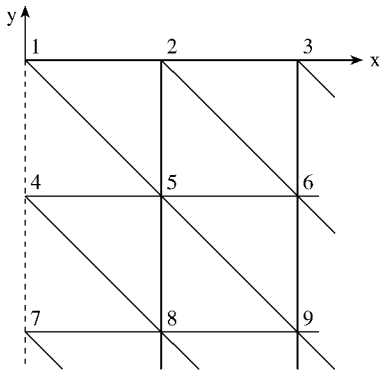

Figure 6.7
A solution region that is symmetric along the y-axis.

Notice that as from Eq. (6.11) onward, the solution has been restricted to a two-dimensional problem involving Laplace's equation, $\nabla^2 V = 0$. The basic concepts developed in this section will be extended to finite element analysis of problems involving Poisson's equation ($\nabla^2 V = -\rho_v/\epsilon$, $\nabla^2 \mathbf{A} = -\mu \mathbf{J}$) or wave equation ($\nabla^2 \Phi - \gamma^2 \Phi = 0$) in the next sections.

The following two examples were solved in [3] using the band matrix method; here they are solved using the iterative method.

Example 6.1

Consider the two-element mesh shown in Fig. 6.8(a). Using the finite element method, determine the potentials within the mesh. □

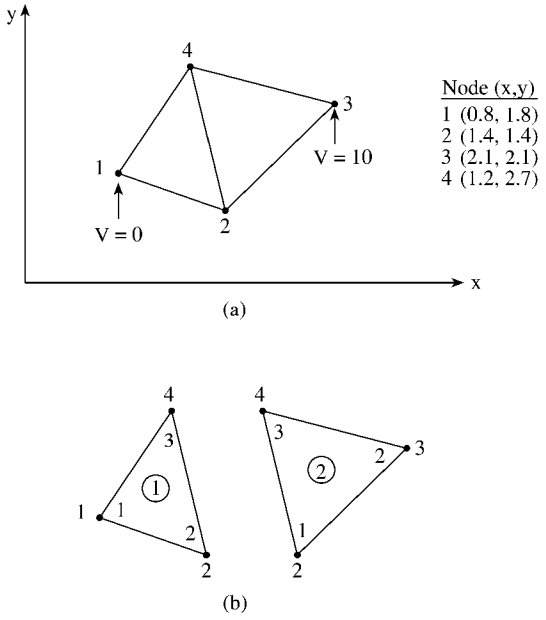

Figure 6.8

For Example 6.1: (a) Two-element mesh, (b) local and global numbering at the elements.

Solution

The element coefficient matrices can be calculated using Eqs. (6.17) and (6.18). However, our calculations will be easier if we define

$$P_1 = (y_2 - y_3)\,, \quad P_2 = (y_3 - y_1)\,, \quad P_3 = (y_1 - y_2)\,, \tag{6.34}$$
$$Q_1 = (x_3 - x_2)\,, \quad Q_2 = (x_1 - x_3)\,, \quad Q_3 = (x_2 - x_1)$$

With P_i and Q_i ($i = 1, 2, 3$ are the local node numbers), each term in the element coefficient matrix is found as

$$C_{ij}^{(e)} = \frac{1}{4A}\left(P_i P_j + Q_i Q_j\right) \tag{6.35}$$

where $A = \frac{1}{2}(P_2 Q_3 - P_3 Q_2)$. It is evident that Eq. (6.35) is more convenient to use than Eqs. (6.17) and (6.18). For element 1 consisting of nodes 1 - 2 - 4 corresponding to the local numbering 1 - 2 - 3 as in Fig. 6.8(b),

$$
\begin{aligned}
P_1 &= -1.3, \quad P_2 = 0.9, \quad P_3 = 0.4\,, \\
Q_1 &= -0.2, \quad Q_2 = -0.4, \quad Q_3 = 0.6\,, \\
A &= \frac{1}{2}(0.54 + 0.16) = 0.35
\end{aligned}
$$

Substituting all of these into Eq. (6.35) gives

$$
\left[C^{(1)}\right] = \begin{bmatrix} 1.2357 & -0.7786 & -0.4571 \\ -0.7786 & 0.6929 & 0.0857 \\ -0.4571 & 0.0857 & 0.3714 \end{bmatrix} \tag{6.36}
$$

Similarly, for element 2 consisting of nodes 2 - 3 - 4 corresponding to local numbering 1 - 2 - 3 as in Fig. 6.8(b),

$$
\begin{aligned}
P_1 &= -0.6, \quad P_2 = 1.3, \quad P_3 = -0.7\,, \\
Q_1 &= -0.9, \quad Q_2 = 0.2, \quad Q_3 = 0.7\,, \\
A &= \frac{1}{2}(0.91 + 0.14) = 0.525
\end{aligned}
$$

Hence

$$
\left[C^{(2)}\right] = \begin{bmatrix} 0.5571 & -0.4571 & -0.1 \\ -0.4571 & 0.8238 & -0.3667 \\ -0.1 & -0.3667 & 0.4667 \end{bmatrix} \tag{6.37}
$$

The terms of the global coefficient matrix are obtained as follows:

$$
\begin{aligned}
C_{22} &= C_{22}^{(1)} + C_{11}^{(2)} = 0.6929 + 0.5571 = 1.25 \\
C_{24} &= C_{23}^{(1)} + C_{13}^{(2)} = 0.0857 - 0.1 = -0.0143 \\
C_{44} &= C_{33}^{(1)} + C_{33}^{(2)} = 0.3714 + 0.4667 = 0.8381 \\
C_{21} &= C_{21}^{(1)} = -0.7786 \\
C_{23} &= C_{12}^{(2)} = -0.4571 \\
C_{41} &= C_{31}^{(1)} = -0.4571 \\
C_{43} &= C_{32}^{(2)} = -0.3667
\end{aligned}
$$

Note that we follow local numbering for the element coefficient matrix and global numbering for the global coefficient matrix. Thus

$$[C] = \begin{bmatrix} C_{11}^{(1)} & C_{12}^{(1)} & 0 & C_{13}^{(1)} \\ C_{21}^{(1)} & C_{22}^{(1)} + C_{11}^{(2)} & C_{12}^{(2)} & C_{23}^{(1)} + C_{12}^{(2)} \\ 0 & C_{21}^{(2)} & C_{22}^{(2)} & C_{23}^{(2)} \\ C_{31}^{(1)} & C_{32}^{(1)} + C_{31}^{(2)} & C_{32}^{(2)} & C_{33}^{(1)} + C_{33}^{(2)} \end{bmatrix}$$

$$= \begin{bmatrix} 1.2357 & -0.7786 & 0 & -0.4571 \\ -0.7786 & 1.25 & -0.4571 & -0.0143 \\ 0 & -0.4571 & 0.8238 & -0.3667 \\ -0.4571 & -0.0143 & -0.3667 & 0.8381 \end{bmatrix} \tag{6.38}$$

Note that $\sum_{i=1}^{4} C_{ij} = 0 = \sum_{j=1}^{4} C_{ij}$. This may be used to check if C is properly obtained. We now apply Eq. (6.28) to the free nodes 2 and 4, i.e.,

$$V_2 = -\frac{1}{C_{22}} (V_1 C_{12} + V_3 C_{32} + V_4 C_{42})$$

$$V_4 = -\frac{1}{C_{44}} (V_1 C_{14} + V_2 C_{24} + V_3 C_{34})$$

or

$$V_2 = -\frac{1}{1.25} (-4.571 - 0.0143 V_4) \tag{6.39a}$$

$$V_4 = -\frac{1}{0.8381} (-0.143 V_2 - 3.667) \tag{6.39b}$$

By initially setting $V_2 = 0 = V_4$, we apply Eqs. (6.39a), (6.39b) iteratively. The first iteration gives $V_2 = 3.6568$, $V_4 = 4.4378$ and at the second iteration $V_2 = 3.7075$, $V_4 = 4.4386$. Just after two iterations, we obtain the same results as those from the band matrix method [3]. Thus the iterative technique is faster and is usually preferred for a large number of nodes. Once the values of the potentials at the nodes are known, the potential at any point within the mesh can be determined using Eq. (6.7). ∎

Example 6.2

Write a FORTRAN program to solve Laplace's equation using the finite element method. Apply the program to the two-dimensional problem shown in Fig. 6.9(a). □

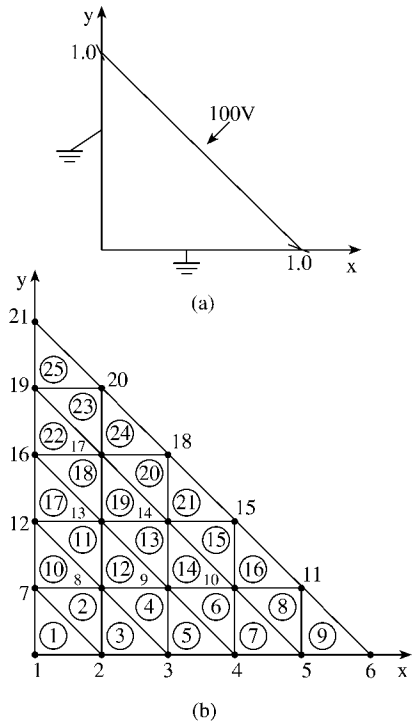

Figure 6.9

For Example 6.2: (a) Two-dimensional electrostatic problem, (b) solution region divided into 25 triangular elements.

Solution

The solution region is divided into 25 three-node triangular elements with total number of nodes being 21 as shown in Fig. 6.9(b). This is a necessary step in order to have input data defining the geometry of the problem. Based on the discussions in Section 6.2, a general FORTRAN program for solving problems involving Laplace's equation using three-node triangular elements is developed as shown in Fig. 6.10. The development of the program basically involves four steps indicated in the program and explained as follows.

Step 1: This involves inputting the necessary data defining the problem. This is the only step that depends on the geometry of the problem at hand. Through a data file, we input the number of elements, the number of nodes, the number of fixed nodes, the prescribed values of the potentials at the free nodes, the x and y coordinates of all nodes, and a list identifying the nodes belonging to each element in the order of the local numbering 1 - 2 - 3. For the problem in Fig. 6.9, the three sets of data for coordinates, element-node relationship, and prescribed potentials at fixed nodes are shown in Tables 6.1, 6.2, and 6.3, respectively.

```
0001    C       FINITE ELEMENT SOLUTION OF LAPLACE'S EQUATION FOR
0002    C       TWO-DIMENSIONAL PROBLEMS
0003    C       TRIANGULAR ELEMENTS ARE USED
0004    C
0005    C       THE UNKNOWN POTENTIALS ARE OBTAINED USING
0006    C       ITERATION METHOD
0007    C
0008    C       ND = NO. OF NODES
0009    C       NE = NO. OF ELEMENTS
0010    C       NP = NO. OF FIXED NODES (WHERE POTENTIAL IS PRESCRIBED)
0011    C       NDP(I) = NODE NO. OF PRESCRIBED POTENTIAL, I = 1,2,...NP
0012    C       VAL(I)) = VALUE OF PRESCRIBED POTENTIAL AT NODE NDP(I)
0013    C       NL(I,J) = LIST OF NODES FOR EACH ELEMENT I, WHERE
0014    c       LF(I) = LIST OF FREE NODES I = 1,2,...,NF=ND-NP
0015    C       J = 1, 2, 3  IS THE LOCAL NODE NUMBER
0016    C       CE(I,J) = ELEMENT COEFFICIENT MATRIX
0017    C       ER(I) = VALUE OF THE RELATIVE PERMITTIVITY FOR ELEMENT I
0018    C       C(I,J)  = GLOBAL COEFFICIENT MATRIX
0019    C       X(I), Y(I) = GLOBAL COORDINATES OF NODE I
0020    C       XL(J), YL(J) = LOCAL COORDINATES OF NODE J = 1,2,3
0021    C       V(I) = POTENTIAL AT NODE I
0022    C       MATRICES P(I) AND Q(I) ARE DEFINED IN EQ.(6.1.1)
0023
0024            DIMENSION  X(100), Y(100), C(100,100), CE(100,100)
0025            DIMENSION  NL(100,3), NDP(100), VAL(100),LF(100)
0026            DIMENSION  V(100),P(3),Q(3),XL(3),YL(3),ER(100)
0027
0028    C       ************************************************
0029    C       FIRST STEP - INPUT DATA DEFINING GEOMETRY AND
0030    C                    BOUNDARY CONDITIONS
0031    C       ************************************************
0032
0033            NI = 50  ! NO. OF ITERATIONS
0034            READ(5,*) NE,ND, NP
0035            READ(5,*)( I, ( NL(I,J), J=1,3),I=1,NE)
0036            READ(5,*) (I, X(I), Y(I), I=1,ND)
0037            READ(5,*) ( NDP(I), VAL(I), I=1,NP)
0038            PIE = 4.0*ATAN(1.0)
0039            E0 = 1.0E-9/(36.0*PIE)
0040            DO 10 I=1,NE
0041            ER(I) = 1.0
0042    10      CONTINUE
0043    C       ************************************************
0044    C       SECOND STEP - EVALUATE COEFFICIENT MATRIX FOR EACH
0045    C                     ELEMENT AND ASSEMBLE GLOBALLY
0046    C       ************************************************
0047            DO 20 M =1, ND
0048            DO 20 N=1,ND
0049            C(M,N) = 0.0
0050    20      CONTINUE
0051            DO 70 I = 1, NE
0052    C       FIND LOCAL COORDINATES XL(J), YL(J) FOR ELEMENT I
0053            DO 30 J=1,3
0054            K=NL(I,J)
0055            XL(J) = X(K)
0056            YL(J) = Y(K)
0057    30      CONTINUE
0058            P(1) = YL(2) - YL(3)
0059            P(2) = YL(3) - YL(1)
0060            P(3) = YL(1) - YL(2)
0061            Q(1) = XL(3) - XL(2)
0062            Q(2) = XL(1) - XL(3)
```

Figure 6.10

Computer program for Example 6.2 ***(Continued).***

```
0063          Q(3) = XL(2) - XL(1)
0064          AREA = 0.5*ABS( P(2)*Q(3) - Q(2)*P(3) )
0065    C     DETERMINE COEFFICIENT MATRIX FOR ELEMENT I
0066          DO 40 M=1,3
0067          DO 40 N=1,3
0068          CE(M,N) = ER(I)*( P(M)*P(N) + Q(M)*Q(N) )/(4.0*AREA)
0069    40    CONTINUE
0070    C     ASSEMBLE GLOBALLY - FIND C(I,J)
0071          DO 60 J=1,3
0072          IR = NL(I,J)
0073          DO 50 L=1,3
0074          IC = NL(I,L)
0075          C(IR,IC) = C(IR,IC) + CE(J,L)
0076    50    CONTINUE
0077    60    CONTINUE
0078    70    CONTINUE
0079    C     ************************************************
0080    C     THIRD STEP - SOLVE THE RESULTING SYSTEM
0081    C                  ITERATIVELY
0082    C     ************************************************
0083    C
0084    C     INITIALIZE AND DETERMINE LF(I) - LIST OF FREE NODES I
0085    C
0086          NF = 0
0087          DO 120 I=1,ND
0088          V(I) = 0.0
0089          DO 110 K=1,NP ! CHECK IF NODE I IS A PRESCRIBED NODE
0090          IF(I.EQ.NDP(K)) THEN
0091               V(I) = VAL(K)
0092          print *, i, v(i)
0093               GO TO 120
0094          ENDIF
0095    110   CONTINUE
0096          NF = NF + 1
0097          LF(NF) = I ! IF I IS NOT A PRESCRIBED NODE, IT IS FREE
0098    120   CONTINUE
0099          PRINT *,NF,ND-NP,'CHECK IF THESE ARE EQUAL'
0100    C
0101    C     NOW, APPLY ITERATIVE METHOD
0102    C
0103           DO 150  N = 1,NI
0104           DO 140 I = 1,NF
0105           SUM = 0.0
0106           K = LF(I)
0107           DO 130 J=1,ND
0108            IF(J.EQ.K) GO TO 130
0109           SUM = SUM + V(J)*C(J,K)
0110    130    CONTINUE
0111           V(K) = - SUM/C(K,K) ! APPLIES ONLY TO FREE NODES
0112    140    CONTINUE
0113    150    CONTINUE
0114    C     ************************************************
0115    C     FOURTH STEP - FINALLY OUTPUT THE RESULTS
0116    C     ************************************************
0117          WRITE(6,170) ND,NE,NP
0118          DO 160 I=1,ND
0119          WRITE(6,*)I, X(I),Y(I),V(I)
0120    160   CONTINUE
0121    170   FORMAT(2X,'NO. OF NODES = ',I3,2X,'NO. OF ELEMENTS =',
0122         1   I3,2X,'NO. OF FIXED NODES = ',I3,/)
0123          STOP
0124          END
```

Figure 6.10

(Cont.) **Computer program for Example 6.2.**

Table 6.1 Nodal Coordinates of the Finite Element Mesh in Fig. 6.9

Node	x	y	Node	x	y
1	0.0	0.0	12	0.0	0.4
2	0.2	0.0	13	0.2	0.4
3	0.4	0.0	14	0.4	0.4
4	0.6	0.0	15	0.6	0.4
5	0.8	0.0	16	0.0	0.6
6	1.0	0.0	17	0.2	0.6
7	0.0	0.2	18	0.4	0.6
8	0.2	0.2	19	0.0	0.8
9	0.4	0.2	20	0.2	0.8
10	0.6	0.2	21	0.0	1.0
11	0.8	0.2			

Table 6.2 Element-Node Identification

	Local	node	no.		Local	node	no.
Element	1	2	3	Element	1	2	3
1	1	2	7	14	9	10	14
2	2	8	7	15	10	15	14
3	2	3	8	16	10	11	15
4	3	9	8	17	12	13	16
5	3	4	9	18	13	17	16
6	4	10	9	19	13	14	17
7	4	5	10	20	14	18	17
8	5	11	10	21	14	15	18
9	5	6	11	22	16	17	19
10	7	8	12	23	17	20	19
11	8	13	12	24	17	18	20
12	8	9	13	25	19	20	21
13	9	14	13				

Step 2: This step entails finding the element coefficient matrix $[C^{(e)}]$ for each element and using the terms to form the global matrix $[C]$.

Step 3: At this stage, we first find the list of free nodes using the given list of prescribed nodes. We now apply Eq. (6.28) iteratively to all the free nodes. The solution converges at 50 iterations or less since only 6 nodes are involved in this case. The solution obtained is exactly the same as those obtained using the band matrix method [3].

Step 4: This involves outputting the result of the computation. The output data for the problem in Fig. 6.9 is presented in Table 6.4. The validity of the result in Table 6.4 is checked using the finite difference method. From the finite difference analysis, the

Table 6.3 Prescribed Potentials at Fixed Nodes

Node	Prescribed potential	Node	Prescribed potential
1	0.0	18	100.0
2	0.0	20	100.0
3	0.0	21	50.0
4	0.0	19	0.0
5	0.0	16	0.0
6	50.0	12	0.0
11	100.0	7	0.0
15	100.0		

Table 6.4 Output Data of the Program in Fig. 6.10. No. of Nodes = 21, No. of Elements = 25, No. of Fixed Nodes = 15

Node	X	Y	Potential
1	0.00	0.00	0.000
2	0.20	0.00	0.000
3	0.40	0.00	0.000
4	0.60	0.00	0.000
5	0.80	0.00	0.000
6	1.00	0.00	50.000
7	0.00	0.20	0.000
8	0.20	0.20	18.182
9	0.40	0.20	36.364
10	0.60	0.20	59.091
11	0.80	0.20	100.000
12	0.00	0.40	0.000
13	0.20	0.40	36.364
14	0.40	0.40	68.182
15	0.60	0.40	100.000
16	0.00	0.60	0.000
17	0.20	0.60	59.091
18	0.40	0.60	100.000
19	0.00	0.80	0.000
20	0.20	0.80	100.000
21	0.00	1.00	50.00

potentials at the free nodes are obtained as:

$$V_8 = 15.41, \quad V_9 = 26.74, \quad V_{10} = 56.69\,,$$
$$V_{13} = 34.88, \quad V_{14} = 65.41, \quad V_{17} = 58.72V$$

Although the result obtained using finite difference is considered more accurate in this problem, increased accuracy of finite element analysis can be obtained by dividing the solution region into a greater number of triangular elements, or using higher-order elements to be discussed in Section 6.8. As alluded to earlier, the finite element method has two major advantages over the finite difference method. Field quantities are obtained only at discrete positions in the solution region using FDM; they can be obtained at any point in the solution region in FEM. Also, it is easier to handle complex geometries using FEM than using FDM. ∎

6.3 Solution of Poisson's Equation

To solve the two-dimensional Poisson's equation,

$$\nabla^2 V = -\frac{\rho_s}{\epsilon} \tag{6.40}$$

using FEM, we take the same steps as in Section 6.2. Since the steps are essentially the same as in Section 6.2 except that we must include the source term, only the major differences will be highlighted here.

6.3.1 Deriving Element-governing Equations

After the solution region is divided into triangular elements, we approximate the potential distribution $V_e(x, y)$ and the source term ρ_{se} (for two-dimensional problems) over each triangular element by linear combinations of the local interpolation polynomial α_i, i.e.,

$$\boxed{V_e = \sum_{i=1}^{3} V_{ei}\alpha_i(x, y)} \tag{6.41}$$

$$\boxed{\rho_{se} = \sum_{i=1}^{3} \rho_{ei}\alpha_i(x, y)} \tag{6.42}$$

The coefficients V_{ei} and ρ_{ei}, respectively, represent the values of V and ρ_s at vertex i of element e as in Fig. 6.3. The values of ρ_{ei} are known since $\rho_s(x, y)$ is prescribed, while the values of V_{ei} are to be determined.

From Table 4.1, an energy functional whose associated Euler equation is Eq. (6.40) is

$$F(V_e) = \frac{1}{2}\int_S \left[\epsilon\,|\nabla V_e|^2 - 2\rho_{se}V_e\right] dS \tag{6.43}$$

$F(V_e)$ represents the total energy per length within element e. The first term under the integral sign, $\frac{1}{2}\mathbf{D}\cdot\mathbf{E} = \frac{1}{2}\epsilon|\nabla V_e|^2$, is the energy density in the electrostatic system, while the second term, $\rho_{se}V_e dS$, is the work done in moving the charge $\rho_{se}dS$ to its location at potential V_e. Substitution of Eqs. (6.41) and (6.42) into Eq. (6.43) yields

$$F(V_e) = \frac{1}{2}\sum_{i=1}^{3}\sum_{j=1}^{3}\epsilon V_{ei}\left[\int \nabla\alpha_i\cdot\nabla\alpha_j\,dS\right]V_{ej} - \sum_{i=1}^{3}\sum_{j=1}^{3}V_{ei}\left[\int \alpha_i\alpha_j\,dS\right]\rho_{ej}$$

This can be written in matrix form as

$$F(V_e) = \frac{1}{2}\epsilon\left[V_e\right]^t\left[C^{(e)}\right]\left[V_e\right] - \left[V_e\right]^t\left[T^{(e)}\right]\left[\rho_e\right] \tag{6.44}$$

where

$$C_{ij}^{(e)} = \int \nabla\alpha_i\cdot\nabla\alpha_j\,dS \tag{6.45}$$

which is already defined in Eq. (6.17) and

$$T_{ij}^{(e)} = \int \alpha_i\alpha_j\,dS \tag{6.46}$$

It will be shown in Section 6.8 that

$$\boxed{T_{ij}^{(e)} = \begin{cases} A/12, & i \neq j \\ A/6 & i = j \end{cases}} \tag{6.47}$$

where A is the area of the triangular element.

Equation (6.44) can be applied to every element in the solution region. We obtain the discretized functional for the whole solution region (with N elements and n nodes) as the sum of the functionals for the individual elements, i.e., from Eq. (6.44),

$$F(V) = \sum_{e=1}^{N} F(V_e) = \frac{1}{2}\epsilon[V]^t[C][V] - [V]^t[T][\rho] \tag{6.48}$$

where t denotes transposition. In Eq. (6.48), the column matrix $[V]$ consists of the values of V_{ei}, while the column matrix $[\rho]$ contains n values of the source function ρ_s at the nodes. The functional in Eq. (6.48) is now minimized by differentiating with respect to V_{ei} and setting the result equal to zero.

6.3.2 Solving the Resulting Equations

The resulting equations can be solved by either the iteration method or the band matrix method as discussed in Section 6.2.4.

Iteration Method: Consider a solution region in Fig. 6.6 having five nodes so that $n = 5$. From Eq. (6.48),

$$F = \frac{1}{2}\epsilon [V_1\ V_2\ \cdots\ V_5] \begin{bmatrix} C_{11} & C_{12} & \cdots & C_{15} \\ C_{21} & C_{22} & \cdots & C_{25} \\ \vdots & & & \vdots \\ C_{51} & C_{52} & \cdots & C_{55} \end{bmatrix} \begin{bmatrix} V_1 \\ V_2 \\ \vdots \\ V_5 \end{bmatrix}$$
$$- [V_1\ V_2\ \cdots\ V_5] \begin{bmatrix} T_{11} & T_{12} & \cdots & T_{15} \\ T_{21} & T_{22} & \cdots & T_{25} \\ \vdots & & & \vdots \\ T_{51} & T_{52} & \cdots & T_{55} \end{bmatrix} \begin{bmatrix} \rho_1 \\ \rho_2 \\ \vdots \\ \rho_5 \end{bmatrix} \tag{6.49}$$

We minimize the energy by applying

$$\frac{\partial F}{\partial V_k} = 0, \quad k = 1, 2, \ldots, n \tag{6.50}$$

From Eq. (6.49), we get $\dfrac{\partial F}{\partial V_1} = 0$, for example, as

$$\frac{\partial F}{\partial V_1} = \epsilon [V_1 C_{11} + V_2 C_{21} + \cdots + V_5 C_{51}] - [T_{11}\rho_1 + T_{21}\rho_2 + \cdots + T_{51}\rho_5] = 0$$

or

$$V_1 = -\frac{1}{C_{11}} \sum_{i=2}^{5} V_i C_{i1} + \frac{1}{\epsilon C_{11}} \sum_{i=1}^{5} T_{i1}\rho_i \tag{6.51}$$

Thus, in general, for a mesh with n nodes

$$\boxed{V_k = -\frac{1}{C_{kk}} \sum_{i=1, i\neq k}^{n} V_i C_{ki} + \frac{1}{\epsilon C_{kk}} \sum_{i=1}^{n} T_{ki}\rho_i} \tag{6.52}$$

where node k is assumed to be a free node.

By fixing the potential at the prescribed nodes and setting the potential at the free nodes initially equal to zero, we apply Eq. (6.52) iteratively to all free nodes until convergence is reached.

Band Matrix Method: If we choose to solve the problem using the band matrix method, we let the free nodes be numbered first and the prescribed nodes last. By

doing so, Eq. (6.48) can be written as

$$F(V) = \frac{1}{2}\epsilon \begin{bmatrix} V_f & V_p \end{bmatrix} \begin{bmatrix} C_{ff} & C_{fp} \\ C_{pf} & C_{pp} \end{bmatrix} \begin{bmatrix} V_f \\ V_p \end{bmatrix} - \begin{bmatrix} V_f & V_p \end{bmatrix} \begin{bmatrix} T_{ff} & T_{fp} \\ T_{pf} & T_{pp} \end{bmatrix} \begin{bmatrix} \rho_f \\ \rho_p \end{bmatrix} \tag{6.53}$$

Minimizing $F(V)$ with respect to V_f, i.e.,

$$\frac{\partial F}{\partial V_f} = 0$$

gives

$$0 = \epsilon \left(C_{ff} V_f + C_{pf} V_p \right) - \left(T_{ff} \rho_f + T_{fp} \rho_p \right)$$

or

$$\boxed{\left[C_{ff} \right] \left[V_f \right] = - \left[C_{fp} \right] \left[V_p \right] + \frac{1}{\epsilon} \left[T_{ff} \right] \left[\rho_f \right] + \frac{1}{\epsilon} \left[T_{fp} \right] \left[\rho_p \right]} \tag{6.54}$$

This can be written as

$$[A][V] = [B] \tag{6.55}$$

where $[A] = [C_{ff}]$, $[V] = [V_f]$ and $[B]$ is the right-hand side of Eq. (6.54). Equation (6.55) can be solved to determine $[V]$ either by matrix inversion or Gaussian elimination technique discussed in Appendix D. There is little point in giving examples on applying FEM to Poisson's problems, especially when it is noted that the difference between Eqs. (6.28) and (6.52) or Eqs. (6.54) and (6.31) is slight. See [19] for an example.

6.4 Solution of the Wave Equation

A typical wave equation is the inhomogeneous scalar Helmholtz's equation

$$\nabla^2 \Phi + k^2 \Phi = g \tag{6.56}$$

where Φ is the field quantity (for waveguide problem, $\Phi = H_z$ for TE mode or E_z for TM mode) to be determined, g is the source function, and $k = \omega\sqrt{\mu\epsilon}$ is the wave number of the medium. The following three distinct special cases of Eq. (6.56) should be noted:

(i) $k = 0 = g$: Laplace's equation;

(ii) $k = 0$: Poisson's equation; and

(iii) k is an unknown, $g = 0$: homogeneous, scalar Helmholtz's equation.

We know from Chapter 4 that the variational solution to the operator equation

$$L\Phi = g \tag{6.57}$$

is obtained by extremizing the functional

$$I(\Phi) =< L, \Phi > -2 < \Phi, g > \tag{6.58}$$

Hence the solution of Eq. (6.56) is equivalent to satisfying the boundary conditions and minimizing the functional

$$I(\Phi) = \frac{1}{2}\iint \left[|\nabla\Phi|^2 - k^2\Phi^2 + 2\Phi g\right] dS \tag{6.59}$$

If other than the natural boundary conditions (i.e., Dirichlet or homogeneous Neumann conditions) must be satisfied, appropriate terms must be added to the functional as discussed in Chapter 4.

We now express potential Φ and source function g in terms of the shape functions α_i over a triangular element as

$$\boxed{\Phi_e(x, y) = \sum_{i=1}^{3} \alpha_i \Phi_{ei}} \tag{6.60}$$

$$\boxed{g_e(x, y) = \sum_{i=1}^{3} \alpha_i g_{ei}} \tag{6.61}$$

where Φ_{ei} and g_{ei} are, respectively, the values of Φ and g at nodal point i of element e.

Substituting Eqs. (6.60) and (6.61) into Eq. (6.59) gives

$$\begin{aligned} I(\Phi_e) = {} & \frac{1}{2}\sum_{i=1}^{3}\sum_{j=1}^{3} \Phi_{ei}\Phi_{ej} \iint \nabla\alpha_i \cdot \nabla\alpha_j \, dS \\ & - \frac{k^2}{2}\sum_{i=1}^{3}\sum_{j=1}^{3} \Phi_{ei}\Phi_{ej} \iint \alpha_i\alpha_j \, dS \\ & + \sum_{i=1}^{3}\sum_{j=1}^{3} \Phi_{ei} g_{ej} \iint \alpha_i\alpha_j \, dS \\ = {} & \frac{1}{2}[\Phi_e]^t[C^{(e)}][\Phi_e] \\ & - \frac{k^2}{2}[\Phi_e]^t[T^{(e)}][\Phi_e] + [\Phi_e]^t[T^{(e)}][G_e] \end{aligned} \tag{6.62}$$

where $[\Phi_e] = [\Phi_{e1}, \Phi_{e2}, \Phi_{e3}]^t$, $[G_e] = [g_{e1}, g_{e2}, g_{e3}]^t$, and $[C^{(e)}]$ and $[T^{(e)}]$ are defined in Eqs. (6.17) and (6.47), respectively.

Equation (6.62), derived for a single element, can be applied for all N elements in the solution region. Thus,

$$I(\Phi) = \sum_{e=1}^{N} I(\Phi_e) \tag{6.63}$$

From Eqs. (6.62) and (6.63), $I(\Phi)$ can be expressed in matrix form as

$$I(\Phi) = \frac{1}{2}[\Phi]^t[C][\Phi] - \frac{k^2}{2}[\Phi]^t[T][\Phi] + [\Phi]^t[T][G] \tag{6.64}$$

where

$$[\Phi] = [\Phi_1, \Phi_2, \ldots, \Phi_N]^t \ , \tag{6.65a}$$

$$[G] = [g_1, g_2, \ldots, g_N]^t \ , \tag{6.65b}$$

$[C]$, and $[T]$ are global matrices consisting of local matrices $[C^{(e)}]$ and $[T^{(e)}]$, respectively.

Consider the special case in which the source function $g = 0$. Again, if free nodes are numbered first and the prescribed nodes last, we may write Eq. (6.64) as

$$\begin{aligned} I = \frac{1}{2}\begin{bmatrix}\Phi_f & \Phi_p\end{bmatrix}\begin{bmatrix}C_{ff} & C_{fp} \\ C_{pf} & C_{pp}\end{bmatrix}\begin{bmatrix}\Phi_f \\ \Phi_p\end{bmatrix} \\ - \frac{k^2}{2}\begin{bmatrix}\Phi_f & \Phi_p\end{bmatrix}\begin{bmatrix}T_{ff} & T_{fp} \\ T_{pf} & T_{pp}\end{bmatrix}\begin{bmatrix}\Phi_f \\ \Phi_p\end{bmatrix} \end{aligned} \tag{6.66}$$

Setting $\dfrac{\partial I}{\partial \Phi_f}$ equal to zero gives

$$\begin{bmatrix}C_{ff} & C_{fp}\end{bmatrix}\begin{bmatrix}\Phi_f \\ \Phi_p\end{bmatrix} - k^2\begin{bmatrix}T_{ff} & T_{fp}\end{bmatrix}\begin{bmatrix}\Phi_f \\ \Phi_p\end{bmatrix} = 0 \tag{6.67}$$

For TM modes, $\Phi_p = 0$ and hence

$$\left[C_{ff} - k^2 T_{ff}\right]\Phi_f = 0 \tag{6.68}$$

Premultiplying by T_{ff}^{-1} gives

$$\boxed{\left[T_{ff}^{-1}C_{ff} - k^2 I\right]\Phi_f = 0} \tag{6.69}$$

Letting

$$A = T_{ff}^{-1}C_{ff}, \quad k^2 = \lambda, \quad X = \Phi_f \tag{6.70a}$$

we obtain the standard eigenproblem

$$(A - \lambda I)X = 0 \tag{6.70b}$$

where I is a unit matrix. Any standard procedure [7] (or see Appendix D) may be used to obtain some or all of the eigenvalues $\lambda_1, \lambda_2, \ldots, \lambda_{n_f}$ and eigenvectors $X_1, X_2, \ldots, X_{n_f}$, where n_f is the number of free nodes. The eigenvalues are always real since C and T are symmetric.

Solution of the algebraic eigenvalue problems in Eq. (6.70) furnishes eigenvalues and eigenvectors, which form good approximations to the eigenvalues and eigenfunctions of the Helmholtz problem, i.e., the cuttoff wavelengths and field distribution patterns of the various modes possible in a given waveguide.

The solution of the problem presented in this section, as summarized in Eq. (6.69), can be viewed as the finite element solution of homogeneous waveguides. The idea can be extended to handle inhomogeneous waveguide problems [8]–[11]. However, in applying FEM to inhomogeneous problems, a serious difficulty is the appearance of spurious, nonphysical solutions. Several techniques have been proposed to overcome the difficulty [12]–[18].

Example 6.3

To apply the ideas presented in this section, we use the finite element analysis to determine the lowest (or dominant) cutoff wavenumber k_c of the TM_{11} mode in waveguides with square $(a \times a)$ and rectangular $(a \times b)$ cross sections for which the exact results are already known as

$$k_c = \sqrt{(m\pi/a)^2 + (n\pi/b)^2}$$

where $m = n = 1$.

It may be instructive to try with hand calculation the case of a square waveguide with 2 divisions in the x and y directions. In this case, there are 9 nodes, 8 triangular elements, and 1 free node ($n_f = 1$). Equation (6.68) becomes

$$C_{11} - k^2 T_{11} = 0$$

where C_{11} and T_{11} are obtained from Eqs. (6.34), (6.35), and (6.47) as

$$C_{11} = \frac{a^2}{2A}, \qquad T_{11} = A, \qquad A = \frac{a^2}{8}$$

Hence

$$k^2 = \frac{a^2}{2A^2} = \frac{32}{a^2}$$

or

$$ka = 5.656$$

which is about 27% off the exact solution. To improve the accuracy, we must use more elements.

The computer program in Fig. 6.11 applies the ideas in this section to find k_c. The main program calls subroutine GRID (to be discussed in Section 6.5) to generate the necessary input data from a given geometry. If n_x and n_y are the number of divisions in the x and y directions, the total number of elements $n_e = 2n_x n_y$. By simply specifying the values of a, b, n_x, and n_y, the program determines k_c using subroutines GRID, INVERSE, and POWER or EIGEN. Subroutine INVERSE available in Appendix D finds T_{ff}^{-1} required in Eq. (6.70a). Either subroutine POWER or EIGEN calculates the eigenvalues. EIGEN finds all the eigenvalues, while POWER only determines the lowest eigenvalue; both subroutines are available in Appendix D. The results for the square ($a = b$) and rectangular ($b = 2a$) waveguides are presented in Tables 6.5a and 6.5b, respectively. □

Table 6.5 (a) Lowest Wavenumber for a Square Waveguide ($b = a$)

n_x	n_e	$k_c a$	% error
2	8	5.656	27.3
3	18	5.030	13.2
5	50	4.657	4.82
7	98	4.553	2.47
10	200	4.497	1.22
Exact: $k_c a = 4.4429$, $n_y = n_x$			

Table 6.5 (b) Lowest Wavenumber for a Rectangular Waveguide ($b = 2a$)

n_x	n_e	$k_c a$	% error
2	16	4.092	16.5
4	64	3.659	4.17
6	144	3.578	1.87
8	256	3.549	1.04
Exact: $k_c a = 3.5124$, $n_y = 2n_x$			

```
0001    C*****************************************************
0002    C      FINITE ELEMENT SOLUTION OF THE WAVE EQUATION
0003    C      TRIANGULAR ELEMENTS ARE USED
0004    C
0005    C      ND = NO. OF NODES
0006    C      NE = NO. OF ELEMENTS
0007    C      NL(I,J) = LIST OF NODES FOR EACH ELEMENT I, WHERE
0008    C      CE(I,J) = ELEMENT COEFFICIENT MATRIX
0009    C      C(I,J)  = GLOBAL COEFFICIENT MATRIX
0010    C      X(I), Y(I) = GLOBAL COORDINATES OF NODE I
0011    C      XL(J), YL(J) = LOCAL COORDINATES OF NODE J = 1,2,3
0012    C      MATRICES P(I) AND Q(I) ARE DEFINED IN EQ.(9)
0013    C      LF(I) = LIST OF FREE NODES
0014    C      ALAM(I) = CONTAINS EIGENVALUES
0015
0016           DIMENSION  C(400,400), CE(400,400),LF(400)
0017           DIMENSION  V(400), P(3), Q(3), XL(3), YL(3)
0018           DIMENSION  T(400,400), A(400,400), ALAM(400)
0019           COMMON X(400),Y(400),DX(50),DY(50),NL(400,3),NDP(400)
0020
0021    C     ***************************************************
0022    C     FIRST STEP - INPUT DATA DEFINING GEOMETRY AND
0023    C                  BOUNDARY CONDITIONS (USE SUBROUTINE GRID)
0024    C     ***************************************************
0025           PRINT *, 'INPUT NX'
0026           READ(5,*)  NX
0027           NY = 2.0*NX
0028           AA = 1.0
0029           BB = 2.0
0030           DELTAX = AA/FLOAT(NX)
0031           DELTAY = BB/FLOAT(NY)
0032           DO 10 I=1,NX
0033           DX(I)=DELTAX
0034    10     CONTINUE
0035           DO 20 I=1,NY
0036           DY(I)=DELTAY
0037    20     CONTINUE
0038           CALL GRID(NX,NY,ND,NE,NP)
0039    C     ***************************************************
0040    C     SECOND STEP - EVALUATE COEFFICIENT MATRIX FOR EACH
0041    C                   ELEMENT AND ASSEMBLE GLOBALLY
0042    C     ***************************************************
0043          DO 30 M =1, ND
0044          DO 30 N=1,ND
0045          C(M,N) = 0.0
0046    30    CONTINUE
0047          DO 80 I = 1, NE
0048          DO 40 J=1,3
0049          K=NL(I,J)
0050          XL(J) = X(K)
0051          YL(J) = Y(K)
0052    40    CONTINUE
0053          P(1) = YL(2) - YL(3)
0054          P(2) = YL(3) - YL(1)
0055          P(3) = YL(1) - YL(2)
0056          Q(1) = XL(3) - XL(2)
0057          Q(2) = XL(1) - XL(3)
0058          Q(3) = XL(2) - XL(1)
0059          AREA = 0.5*ABS( P(2)*Q(3) - Q(2)*P(3) )
0060    C     DETERMINE COEFFICIENT MATRIX FOR ELEMENT I
0061          DO 50 M=1,3
```

Figure 6.11
Computer program for Example 6.3 ***(Continued).***

```
0062          DO 50 M=1,3
0063          CE(M,N) = ( P(M)*P(N) + Q(M)*Q(N) )/(4.0*AREA)
0064     50   CONTINUE
0065     C    ASSEMBLE GLOBALLY - FIND C(I,J) AND T(I,J)
0066          DO 70 J=1,3
0067          IR = NL(I,J)
0068          DO 60 L=1,3
0069          IC = NL(I,L)
0070          C(IR,IC) = C(IR,IC) + CE(J,L)
0071          IF(J.EQ.L) THEN
0072          T(IR,IC) = T(IR,IC) + AREA/6.0
0073          GO TO 60
0074          ELSE
0075             T(IR,IC) = T(IR,IC) + AREA/12.0
0076          ENDIF
0077     60   CONTINUE
0078     70   CONTINUE
0079     80   CONTINUE
0080          PRINT *, 'C AND T HAVE BEEN CALCULATED'
0081     C    ************************************************
0082     C    THIRD STEP - SOLVE THE RESULTING SYSTEM
0083     C    ************************************************
0084     C   DETERMINE LF(I) - LIST OF FREE NODES
0085          NF = 0
0086          DO 100 I=1,ND
0087          DO 90 K=1,NP ! CHECK IF NODE I IS PRESCRIBED
0088          IF(I.EQ.NDP(K)) GO TO 100
0089     90   CONTINUE
0090          NF = NF + 1
0091          LF(NF) = I   ! NODE I IS FREE
0092     100  CONTINUE
0093          PRINT *,NF,ND-NP,'  CHECK IF THESE ARE EQUAL'
0094     C
0095     C   FROM GLOBAL C AND T, FIND C_ff AND T_ff
0096     C
0097          DO 110 I=1,NF
0098          DO 110 J=1,NF
0099          C(I,J) = C(LF(I),LF(J))
0100          T(I,J) = T(LF(I),LF(J))
0101     110  CONTINUE
0102          NMAX = 400
0103          CALL INVERSE(T,NF,NMAX)
0104          DO 120 I = 1,NF
0105          DO 120 J = 1,NF
0106          DO 120 K=1,NF
0107          A(I,J) = A(I,J) + T(I,K)*C(K,J)
0108     120  CONTINUE
0109     C    CALL INVERSE(A,NF,NMAX)
0110     C    CALL POWER(A,ALAMBDA,X,NMAX,NF,IT)
0111          CALL  EIGEN(A,X,NMAX,NF,ALAM)
0112     C    ************************************************
0113     C    FOURTH STEP - OUTPUT THE RESULTS
0114     C    ************************************************
0115          WRITE(6,130) ND,NE,NP
0116     130  FORMAT(2X,'NO  OF NODES = ',I3,2X,'NO. OF ELEMENTS =',
0117        1    I3,2X,'NO. OF PRESCRIBED NODES',I3,/)
0118     C    AK = 1.0/SQRT(ALAMBDA)
0119     C    WRITE (6,*)NX,NY,AK,IT
```

Figure 6.11

(Cont.)* Computer program for Example 6.3 *(Continued).

```
0120        DO 140 I=1,NF
0121        ALAM(I) = SQRT( ALAM(I) )
0122        PRINT *,I,ALAM(I)
0123        WRITE(6,*) I,ALAM(I)
0124    140 CONTINUE
0125        STOP
0126        END
```

Figure 6.11
***(Cont.)* Computer program for Example 6.3.**

6.5 Automatic Mesh Generation I — Rectangular Domains

One of the major difficulties encountered in the finite element analysis of continuum problems is the tedious and time-consuming effort required in data preparation. Efficient finite element programs must have node and element generating schemes, referred to collectively as *mesh generators*. Automatic mesh generation minimizes the input data required to specify a problem. It not only reduces the time involved in data preparation, it eliminates human errors introduced when data preparation is performed manually. Combining the automatic mesh generation program with computer graphics is particularly valuable since the output can be monitored visually. Since some applications of the FEM to EM problems involve simple rectangular domains, we consider the generation of simple meshes [19] here; automatic mesh generator for arbitrary domains will be discussed in Section 6.6.

Consider a rectangular solution region of size $a \times b$ as in Fig. 6.12. Our goal is to divide the region into rectangular elements, each of which is later divided into two triangular elements. Suppose n_x and n_y are the number of divisions in x and y directions, the total number of elements and nodes are, respectively, given by

$$\begin{aligned} n_e &= 2\,n_x n_y \\ n_d &= (n_x + 1)\,(n_y + 1) \end{aligned} \tag{6.71}$$

Thus it is easy to figure out from Fig. 6.12 a systematic way of numbering the elements and nodes. To obtain the global coordinates (x, y) for each node, we need an array containing Δx_i, $i = 1, 2, \ldots, n_x$ and Δy_j, $j = 1, 2, \ldots, n_y$, which are, respectively, the distances between nodes in the x and y directions. If the order of node numbering is from left to right along horizontal rows and from bottom to top along the vertical rows, then the first node is the origin (0,0). The next node is obtained as $x \rightarrow x + \Delta x_1$ while $y = 0$ remains unchanged. The following node has $x \rightarrow x + \Delta x_2$, $y = 0$, and so on until Δx_i are exhausted. We start the second next horizontal row by starting with $x = 0$, $y \rightarrow y + \Delta y_1$ and increasing x until Δx_i are exhausted. We repeat the process until the last node $(n_x + 1)(n_y + 1)$ is reached, i.e., when Δx_i and Δy_i are exhausted simultaneously.

The procedure presented here allows for generating uniform and nonuniform meshes. A mesh is uniform if all Δx_i are equal and all Δy_i are equal; it is nonuniform otherwise. A nonuniform mesh is preferred if it is known in advance that the

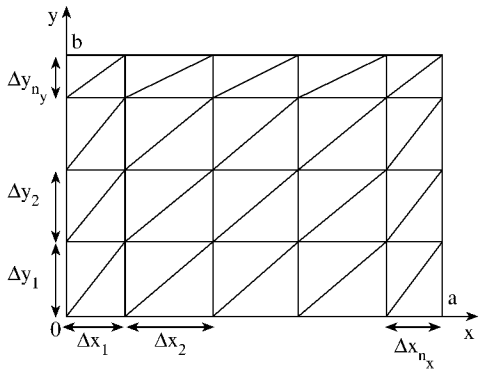

Figure 6.12
Discretization of a rectangular region into a nonuniform mesh.

parameter of interest varies rapidly in some parts of the solution domain. This allows a concentration of relatively small elements in the regions where the parameter changes rapidly, particularly since these regions are often of greatest interest in the solution. Without the preknowledge of the rapid change in the unknown parameter, a uniform mesh can be used. In that case, we set

$$\begin{aligned} \Delta x_1 &= \Delta x_2 = \cdots = h_x \\ \Delta y_1 &= \Delta y_2 = \cdots = h_y \end{aligned} \tag{6.72}$$

where $h_x = a/n_x$ and $h_y = b/n_y$.

In some cases, we also need a list of prescribed nodes. If we assume that all boundary points have prescribed potentials, the number n_p of prescribed node is given by

$$n_p = 2\left(n_x + n_y\right) \tag{6.73}$$

A simple way to obtain the list of boundary points is to enumerate points on the bottom, right, top, and left sides of the rectangular region in that order.

The ideas presented here are implemented in the subroutine GRID in Fig. 6.13. The subroutine can be used for generating a uniform or nonuniform mesh out of a given rectangular region. If a uniform mesh is desired, the required input parameters are a, b, n_x, and n_y. If, on the other hand, a nonuniform mesh is required, we need to supply $n_x, n_y, \Delta x_i, i = 1, 2, \ldots, n_x$, and $\Delta y_j, j = 1, 2, \ldots, n_y$. The output parameters are n_e, n_d, n_p, connectivity list, the global coordinates (x, y) of each node, and the list of prescribed nodes. It is needless to say that subroutine GRID is not useful for a nonrectangular solution region. See the program in Fig. 6.11 as an example on how to use subroutine GRID. A more general program for discretizing a solution region of any shape will be presented in the next section.

```
0001    C*************************************************************
0002    C       SUBROUTINE GRID
0003    C       THIS PROGRAM DIVIDES A RECTANGULAR DOMAIN INTO
0004    C       TRIANGULAR ELEMENTS (NX BY NY NONUNIFORM
0005    C       MESH IN GENERAL)
0006    C       NX & NY ARE THE NO S OF SUBDIVISION ALONG X & Y AXES
0007    C       NE = NO. OF ELEMENTS IN THE MESH
0008    C       ND = NO  OF NODES IN THE MESH
0009    C       NP = NO. OF BOUNDARY (PRESCRIBED) NODES
0010    C       X(I) & Y(I) ARE GLOBAL COORDINATES OF NODE I
0011    C       DX(I) & DY(I) ARE DISTANCES BETWEEN NODES ALONG X & Y AXES
0012    C       NL(I,J) IS THE LIST OF NODES FOR ELEMENT I, J=1,2,3  ARE
0013    C          LOCAL NUMBERS
0014    C       NDP(I) = LIST OF PRESCRIBED NODES I
0015    C
0016    C     REF:  J  N. REDDY, "AN INTRODUCTION TO THE FINITE ELEMENT
0017    C              METHOD",  NEW YORK: MCGRAW-HILL, 1984, P. 436.
0018
0019            SUBROUTINE GRID(NX,NY,ND,NE,NP)
0020            COMMON X(400),Y(400),DX(50),DY(50),NL(400,3),NDP(400)
0021
0022    C
0023    C   CALCULATE NE, ND, AND NP
0024    C
0025             NE=2*NX*NY
0026             NP = 2*(NX + NY)
0027             NX1=NX + 1
0028             NY1=NY + 1
0029             NXX1=2*NX
0030             NYY1=2*NY
0031             ND=NX1*NY1
0032    C
0033    C   DETERMINE NL(I,J) STARTING FROM LEFT BOTTOM CORNER
0034    C
0035            NL(1,1)=1
0036            NL(1,2)=NX1 + 2
0037            NL(1,3)=NX1 + 1
0038            NL(2,1)=1
0039            NL(2,2)=2
0040            NL(2,3)=NX1 + 2
0041            K=3
0042            DO 50 IY=1,NY
0043            L=IY*NXX1
0044            M=(IY - 1)*NXX1
0045            IF(NX.EQ.1) GO TO 30
0046            DO 20 N=K,L,2
0047            DO 10 I=1,3
0048            NL(N,I)=NL(N-2,I) + 1
0049    10      NL(N+1,I)=NL(N-1,I) + 1
0050    20      CONTINUE
0051    30      IF(NY.EQ.1) GO TO 50
0052            DO 40 I=1,3
0053            NL(L+1,I)=NL(M+1,I) + NX1
0054    40      NL(L+2,I)=NL(M+2,I) + NX1
0055    50      K=L + 3
0056    C
0057    C   DETERMINE X(I) AND Y(I)
0058    C
0059    60      L=0
```

Figure 6.13
Subroutine GRID ***(Continued).***

```
0060            YC=0.0
0061            DO 80 J=1,NY1
0062            XC=0.0
0063            DO 70 I=1,NX1
0064            L=L + 1
0065            X(L)=XC
0066            Y(L)=YC
0067    70      XC=XC + DX(I)
0068    80      YC=YC + DY(J)
0069    C
0070    C   DETERMINE NDP(I)
0071    C
0072             N = 0
0073             DO 90 K=1,NX1
0074             N = N + 1
0075             NDP(N) = N
0076    90       CONTINUE   ! BOTTOM SIDE
0077             DO 100 K=1,NY
0078             N = N+1
0079             NDP(N) = NDP(N-1) + NX1
0080    100      CONTINUE   ! RIGHT SIDE
0081             DO 110 K=1,NX
0082             N = N + 1
0083             NDP(N) = NDP(N-1) - 1
0084    110      CONTINUE   ! TOP SIDE
0085             DO 120 K=1,NY-1
0086             N = N + 1
0087             NDP(N) = NDP(N-1) - NX1
0088    120      CONTINUE   ! LEFT SIDE
0089             WRITE(6,*) NE,ND,NP
0090             DO 130 I=1,NE
0091             WRITE(6,*) I,( NL(I,J),J=1,3)
0092    130      CONTINUE
0093             DO 140 I=1,ND
0094             WRITE(6,*) I,X(I),Y(I)
0095    140      CONTINUE
0096             DO 150 I=1,NP
0097             WRITE(6,*)  NDP(I)
0098    150 CONTINUE
0099            RETURN
0100            END
```

Figure 6.13
(Cont.) **Subroutine GRID.**

6.6 Automatic Mesh Generation II — Arbitrary Domains

As the solution regions become more complex than the ones considered in Section 6.5, the task of developing mesh generators becomes more tedious. A number of mesh generation algorithms (e.g., [21]–[33]) of varying degrees of automation have been proposed for arbitrary solution domains. Reviews of various mesh generation techniques can be found in [34, 35].

The basic steps involved in a mesh generation are as follows [36]:

- subdivide solution region into few quadrilateral blocks,
- separately subdivide each block into elements,

- connect individual blocks.

Each step is explained as follows.

6.6.1 Definition of Blocks

The solution region is subdivided into quadrilateral blocks. Subdomains with different constitutive parameters (σ, μ, ϵ) must be represented by separate blocks. As input data, we specify block topologies and the coordinates at eight points describing each block. Each block is represented by an eight-node quadratic isoparametric element. With natural coordinate system (ζ, η), the x and y coordinates are represented as

$$x(\zeta, \eta) = \sum_{i=1}^{8} \alpha_i(\zeta, \eta)\, x_i \tag{6.74}$$

$$y(\zeta, \eta) = \sum_{i=1}^{8} \alpha_i(\zeta, \eta)\, y_i \tag{6.75}$$

where $\alpha_i(\zeta, \eta)$ is a shape function associated with node i, and (x_i, y_i) are the coordinates of node i defining the boundary of the quadrilateral block as shown in Fig. 6.14. The shape functions are expressed in terms of the quadratic or parabolic isoparametric elements shown in Fig. 6.15. They are given by:

$$\alpha_i = \frac{1}{4}(1 + \zeta\zeta_i)(1 + \eta\eta_i)(\zeta\zeta_i + \eta\eta_i + 1), \qquad i = 1, 3, 5, 7 \tag{6.76}$$

for corner nodes,

$$\alpha_i = \frac{1}{2}\zeta_i^2 (1 + \zeta\zeta_i)\left(1 - \eta^2\right) + \frac{1}{2}\eta_i^2 (1 + \eta\eta_i + 1)\left(1 - \zeta^2\right), \qquad i = 2, 4, 6, 8 \tag{6.77}$$

for midside nodes. Note the following properties of the shape functions:

(1) They satisfy the conditions

$$\sum_{i=1}^{n} \alpha_i(\zeta, \eta) = 1 \tag{6.78a}$$

$$\alpha_i\left(\zeta_j, \eta_j\right) = \begin{cases} 1, & i = j \\ 0, & i \neq j \end{cases} \tag{6.78b}$$

(2) They become quadratic along element edges ($\zeta = \pm 1$, $\eta = \pm 1$).

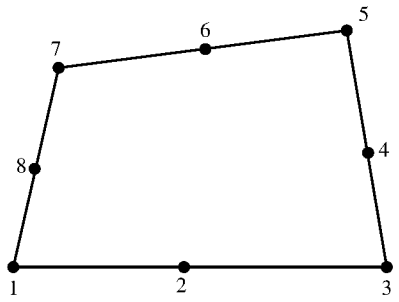

Figure 6.14
Typical quadrilateral block.

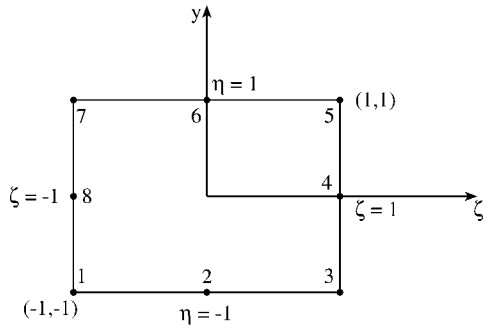

Figure 6.15
Eight-node Serendipity element.

6.6.2 Subdivision of Each Block

For each block, we specify *N DIV X* and *N DIV Y*, the number of element subdivisions to be made in the ζ and η directions, respectively. Also, we specify the weighting factors $(W_\zeta)_i$ and $(W_\eta)_i$ allowing for graded mesh within a block. In specifying *N DIV X*, *N DIV Y*, W_ζ, and W_η care must be taken to ensure that the subdivision along block interfaces (for adjacent blocks) are compatible. We initialize ζ and η to a value of -1 so that the natural coordinates are incremented according to

$$\zeta_i = \zeta_i + \frac{2\left(W_\zeta\right)_i}{W_\zeta^T \cdot F} \tag{6.79}$$

$$\eta_i = \eta_i + \frac{2\left(W_\eta\right)_i}{W_\eta^T \cdot F} \tag{6.80}$$

where

$$W_\zeta^T = \sum_{j=1}^{NDIVX} (W_\zeta)_j \tag{6.81a}$$

$$W_\eta^T = \sum_{j=1}^{NDIVX} (W_\eta)_j \tag{6.81b}$$

and

$$F = \begin{cases} 1, & \text{for linear elements} \\ 2, & \text{for quadratic elements} \end{cases}$$

Three element types are permitted: (a) linear four-node quadrilateral elements, (b) linear three-node triangular elements, (c) quadratic eight-node isoparametric elements.

6.6.3 Connection of Individual Blocks

After subdividing each block and numbering its nodal points separately, it is necessary to connect the blocks and have each node numbered uniquely. This is accomplished by comparing the coordinates of all nodal points and assigning the same number to all nodes having identical coordinates. That is, we compare the coordinates of node 1 with all other nodes, and then node 2 with other nodes, etc., until all repeated nodes are eliminated. The listing of the FORTRAN code for automatic mesh generation is shown in Fig. 6.16; it is essentially a modified version of the one in Hinton and Owen [36]. The following example taken from [36] illustrates the application of the code.

Example 6.4

Use the code in Fig. 6.16 to discretize the mesh in Fig. 6.17. □

Solution

The input data for the mesh generation is presented in Table 6.6. The subroutine INPUT reads the number of points (NPOIN) defining the mesh, the number of blocks (NELEM), the element type (NNODE), the number of coordinate dimensions (NDIME), the nodes defining each block, and the coordinates of each node in the mesh. The subroutine GENERATE reads the number of divisions and weighting factors along ζ and η directions for each block. It then subdivides the block into quadrilateral elements. At this point, the whole input data shown in Table 6.6 have been read. The subroutine TRIANGLE divides each four-node quadrilateral element across the shorter diagonal. The subroutine OUTPUT provides the coordinates of the nodes, element topologies, and material property numbers of the generated mesh. For the input data in Table 6.6, the generated mesh with 200 nodes and 330 elements is shown in Fig. 6.18. ■

```
0001    C*************************************************
0002    C THIS PROGRAM PERFORMS A MESH GENERATION OF AN
0003    C ARBITRARY SOLUTION DOMAIN USING A  SYSTEMATIC
0004    C APPROACH. A FEW POINTS ARE  GIVEN TO DETERMINE
0005    C THE  GENERAL  CONFIGURATION  OF  THE REGION.
0006    C THEN THE PROGRAM AUTOMATICALLY GENERATES
0007    C TRIANGULAR OR QUADRILATERAL ELEMENTS
0008    C     REFERENCE: HINTON AND OWEN [36]
0009    C*************************************************
0010          IMPLICIT INTEGER (I-N)
0011          IMPLICIT REAL (A-H,O-Z)
0012          COMMON /MESH1/COORD(1500,2),NL(750,8),MATNO(750),
0013         1 SHAPE(9),NP,NELEM,NTYPE,NDIME,MNODE
0014
0015    C THIS SUBROUTINE ACCEPTS DATA DEFINING THE SOLUTION REGION
0016          CALL INPUT
0017    C THIS SUBROUTINE UNDERTAKES THE MESH SUBDIVISION
0018          CALL GENERATE
0019    C THIS SUBROUTINE SUBDIVIDES INTO TRIANGULAR ELEMENTS
0020          IF(NTYPE.EQ.3)CALL TRIANGLE
0021    C THIS SUBROUTINE OUTPUTS THE GENERATED MESH
0022    C THE SUBROUTINE DOES NOT NEED TO BE CALLED IF A PLOTTING
0023    C SUBROUTINE USED IN DISPLAYING THE OUTPUT
0024          CALL OUTPUT
0025          STOP
0026          END

0001    C*************************************************
0002    C THIS SUBROUTINE ACCEPTS THE DATA WHICH DEFINES THE
0003    C SOLUTION REGION  OUTLINE AND THE MATERIAL ZONES
0004    C NP = NUMBER OF COORDINATE POINTS DEFINING THE
0005    C SOLUTION REGION
0006    C NELEM = NUMBER OF BLOCKS OR ZONES
0007    C NTYPE = THE TYPE OF ELEMENT INTO WHICH THE
0008    C STRUCTURE IS TO BE SUBDIVIDED
0009    C NDIME = THE NUMBER OF COORDINATE DIMENSIONS
0010    C          FOR A PLANE NDIME=2
0011    C NUMEL = BLOCK NUMBER
0012    C (  NL(NUMEL,INODE),INODE=1,NTYPE) )=THE
0013    C BLOCK TOPOLOGY DEFINITION
0014    C MATNO(NUMEL)THE MATERIAL IDENTIFICATION NUMBER:
0015    C INPUT SPECIFICATION FOR EACH BLOCK
0016    C JPOIN = POINT NUMBER
0017    C (COORD(JPOI,IDIME),IDIME=1,NDIME)=X&Y COORDINATES
0018
0019          SUBROUTINE INPUT
0020          COMMON/MESH1/COORD(1500,2),NL(750,8),
0021         1MATNO(750),SHAPE(9),NP,NELEM,NTYPE,NDIME,MNODE
0022          DATA LNODE/8/
0023    C
0024          READ(5,*) NP,NELEM,NTYPE,NDIME
0025          DO 10 IELEM=1,NELEM
0026          READ(5,*) NUMEL,( NL(NUMEL,I), I=1,LNODE ),
0027         1          MATNO(NUMEL)
0028    10    CONTINUE
0029          DO 20 IPOIN=1,NP
0030          READ(5,*)JPOIN, ( COORD(JPOIN,I), I=1,NDIME )
0031    20    CONTINUE
0032          RETURN
0033          END
```

Figure 6.16
FORTRAN code for automatic mesh generation *(Continued)*.

```
0001    C*******************************************************
0002    C THIS SUBROUTINE UNDERTAKES THE SUBDIVISION OF EACH
0003    C BLOCK AND ELIMINATES COMMON NODES ALONG BLOCK INTERFACES
0004    C KBLOC = BLOCK NUMBER
0005    C NDIVX/NDIVY = NUMBER OF ELEMENTS IN THE ZETA/ETA
0006    C DIRECTION INTO WHICH THE BLOCK IS TO BE SUBDIVIDED
0007    C WEITX(IDIVX) AND WEITHY = WEIGHTING FACTORS
0008    C
0009          SUBROUTINE GENERATE
0010          DIMENSION WEITX(40),WEITY(40),TCORD(81,2),
                 TNODS(50,8),
0011         1TMAT0(50),LREPN(350),LASOC(350),LFINN(350),LFASC(350)
0012          COMMON/MESH1/COORD(1500,2),NL(750,8),MATN0(750),
0013         1SHAPE(9),NP,NELEM,NTYPE,NDIME,MNODE
0014          DATA MREPN/350/,MPOIN/1500/,LNODE/8/
0015    C
0016    C INITIALIZATION SECTION
0017    C
0018          DO 10 IREPN=1,MREPN
0019    10    LREPN(IREPN)=0
0020          NPONT=NP
0021          NBLOC=NELEM
0022          NP=0
0023          NELEM=0
0024          MNODE=4
0025          IF(NTYPE.EQ.8)MNODE=8
0026          KNODE=MNODE/4
0027          FNODE=KNODE
0028          DO 20 IPONT=1,NPONT
0029          DO 20 IDIME=1,NDIME
0030    20    TCORD(IPONT,IDIME)=COORD(IPONT,IDIME)
0031          DO 30 IPOIN=1,MPOIN
0032          DO 30 IDIME=1,NDIME
0033    30    COORD(IPOIN,IDIME)=0.0
0034          DO 40 IBLOC=1,NBLOC
0035          TMAT0(IBLOC)=MATN0(IBLOC)
0036          DO 40 INODE=1,LNODE
0037    40    TNODS(IBLOC,INODE)=NL(IBLOC,INODE)
0038    C
0039    C READ AND WRITE BLOCK SUBDIVISION DATA
0040    C
0041          DO 170 IBLOC=1,NBLOC
0042          READ(5,*)KBLOC,NDIVX,NDIVY
0043          READ(5,*) ( WEITX(IDIVX), IDIVX=1,NDIVX )
0044          READ(5,*) ( WEITY(IDIVY), IDIVY=1,NDIVY )
0045    C
0046    C DIVIDE EACH BLOCK INTO ELEMENTS
0047    C
0048          TOTAL=0.0
0049          DO 50 IDIVX=1,NDIVX
0050          IF(WEITX(IDIVX).EQ.0.0)WEITX(IDIVX)=1.0
0051    50    TOTAL=TOTAL+WEITX(IDIVX)
0052          XNORM=2.0/TOTAL
0053          TOTAL=0.0
0054          DO 60 IDIVY=1,NDIVY
0055          IF(WEITY(IDIVY).EQ.0.0)WEITY(IDIVY)=1.0
0056    60    TOTAL=TOTAL+WEITY(IDIVY)
0057          YNORM=2.0/TOTAL
0058          NXTWO=NDIVX*KNODE+1
0059          NYTWO=NDIVY*KNODE+1
0060          IASEY=0
0061          ETASP=-1.0
```

Figure 6.16

(Cont.)* FORTRAN code for automatic mesh generation *(Continued).

```
0062          KWETY=0
0063          DO 160 IYTWO=1,NYTWO
0064          IASEY=IASEY+1
0065          IF(NTYPE.NE.8.AND.IASEY.EQ.3)IASEY=2
0066          IF(NTYPE.EQ.8.AND.IASEY.EQ.4)IASEY=2
0067          IASEX=0
0068          EXISP=-1.0
0069          KWETX=0
0070          DO 130 IXTWO=1,NXTWO
0071          IASEX=IASEX+1
0072          IF(NTYPE.NE.8.AND.IASEX.EQ.3)IASEX=2
0073          IF(NTYPE.EQ.8.AND.IASEX.EQ.4)IASEX=2
0074          NP=NP+1
0075          CALL SHAPEF(EXISP,ETASP)
0076          DO 70 INODE=1,LNODE
0077          JTEMP=TNODS(IBLOC,INODE)
0078          DO 70 IDIME=1,NDIME
0079     70   COORD(NP,IDIME)=COORD(NP,IDIME) +
0080         1           SHAPE(INODE)*TCORD(JTEMP,IDIME)
0081          GO TO (80,90) KNODE
0082     80   IF(IASEX.NE.2.OR.IASEY.NE.2)GO TO 100
0083          NELEM=NELEM+1
0084          JPOIN=NP-NXTWO
0085          NL(NELEM,1)=JPOIN-1
0086          NL(NELEM,2)=JPOIN
0087          NL(NELEM,3)=NP
0088          NL(NELEM,4)=NP-1
0089          MATNO(NELEM)=TMATO(IBLOC)
0090     90   IF(IASEX.NE.3.OR.IASEY.NE.3)GO TO 100
0091          NELEM=NELEM+1
0092          IPOIN=NP-IXTWO-NDIVX+(IXTWO-1)/2
0093          JPOIN=NP-NXTWO-NDIVX-1
0094          NL(NELEM,1)=JPOIN-2
0095          NL(NELEM,2)=JPOIN-1
0096          NL(NELEM,3)=JPOIN
0097          NL(NELEM,4)=IPOIN
0098          NL(NELEM,5)=NP
0099          NL(NELEM,6)=NP-1
0100          NL(NELEM,7)=NP-2
0101          NL(NELEM,8)=IPOIN-1
0102          MATNO(NELEM)=TMATO(IBLOC)
0103     100  CONTINUE
0104          GO TO (110,120),KNODE
0105     110  KWETX=KWETX+1
0106          GO TO 130
0107     120  IF(KONTX.LT.0) KWETX=KWETX + 1
0108          KONTX=KONTX*(-1)
0109     130  EXISP=EXISP+XNORM*WEITX(KWETX)/FNODE
0110          GO TO (140,150),KNODE
0111     140  KWETY=KWETY+1
0112          GO TO 160
0113     150  IF(KONTY.LT.0) KWETY=KWETY + 1
0114          KONTY=KONTY*(-1)
0115     160  ETASP=ETASP+YNORM*WEITY(KWETY)/FNODE
0116     170  CONTINUE
0117     C
0118     C ELIMINATE REPEATED NODES AT BLOCK INTERFACES
0119     C
0120          NREPN=0
0121          DO 210 IPOIN=1,NP
0122          IF(NREPN.EQ.0)GO TO 190
0123          DO 180 IREPN=1,NREPN
0124          IF(IPOIN.EQ.LREPN(IREPN))GO TO 210
```

Figure 6.16
(Cont.)* FORTRAN code for automatic mesh generation *(Continued).

```
0125    180   CONTINUE
0126    190   CONTINUE
0127          LPOIN=IPOIN+1
0128          DO 200 JPONT=LPOIN,NP
0129          TOTAL=ABS(COORD(IPOIN,1)-COORD(JPONT,1)) +
0130         1      ABS(COORD(IPOIN,2)-COORD(JPONT,2))
0131          IF(TOTAL.GT.0.00001)GO TO 200
0132          NREPN=NREPN+1
0133          LREPN(NREPN)=JPONT
0134          LASOC(NREPN)=IPOIN
0135    200   CONTINUE
0136    210   CONTINUE
0137          IF(NREPN.EQ.0)GO TO 360
0138          INDEX=0
0139          DO 240 IPOIN=1,NP
0140          DO 220 IREPN=1,NREPN
0141          IF(LREPN(IREPN).EQ.IPOIN)GO TO 230
0142    220   CONTINUE
0143          GO TO 240
0144    230   INDEX=INDEX+1
0145          LFINN(INDEX)=LREPN(IREPN)
0146          LFASC(INDEX)=LASOC(IREPN)
0147    240   CONTINUE
0148          DO 250 IREPN=1,NREPN
0149          LREPN(IREPN)=LFINN(IREPN)
0150    250   LASOC(IREPN)=LFASC(IREPN)
0151          DO 260 IREPN=1,NREPN
0152          DO 260 IELEM=1,NELEM
0153          DO 260 INODE=1,MNODE
0154          IF(NL(IELEM,INODE).EQ.LREPN(IREPN))
0155         1NL(IELEM,INODE)=LASOC(IREPN)
0156    260   CONTINUE
0157          DO 310 IPOIN=1,NP
0158          DO 270 IREPN=1,NREPN
0159          IF(IPOIN.EQ.LREPN(IREPN)) GO TO 310
0160    270   CONTINUE
0161          IF(IPOIN.LT.LREPN(1))GO TO 310
0162          IDIFF=IPOIN-NREPN
0163          IF(IPOIN.GT.LREPN(NREPN))GO TO 290
0164          DO 280 IREPN=1,NREPN
0165          KREPN=NREPN-IREPN+1
0166    280   IF(IPOIN.LT.LREPN(KREPN))IDIFF=IPOIN-KREPN+1
0167    290   DO 300 IDIME=1,NDIME
0168    300   COORD(IDIFF,IDIME)=COORD(IPOIN,IDIME)
0169    310   CONTINUE
0170          DO 350 IELEM=1,NELEM
0171          DO 350 INODE=1,MNODE
0172          NPOSI=NL(IELEM,INODE)
0173          DO 320 IREPN=1,NREPN
0174          IF(NPOSI.EQ.LREPN(IREPN))GO TO 350
0175    320   CONTINUE
0176          IF(NPOSI.LT.LREPN(1))GO TO 350
0177          IDIFF=NPOSI-NREPN
0178          IF(NPOSI.GT.LREPN(NREPN))GO TO 340
0179          DO 330 IREPN=1,NREPN
0180          KREPN=NREPN-IREPN+1
0181    330   IF(NPOSI.LT.LREPN(KREPN))IDIFF=NPOSI-KREPN+1
0182    340   NL(IELEM,INODE)=IDIFF
0183    350   CONTINUE
0184    360   CONTINUE
0185          NP=NP-NREPN
0186          RETURN
0187          END
```

Figure 6.16

(Cont.) **FORTRAN code for automatic mesh generation.** ***(Continued).***

```
0001    C************************************************
0002    C THIS SUBROUTINE EVALUATES THE SHAPE FUNCTIONS
0003    C
0004          SUBROUTINE SHAPEF(S,T)
0005          COMMON/MESH1/COORD(1500,2),ML(750,8),
0006         1MATNO(750),SHAPE(9),NP,NELEM,NTYPE,NDIME,MNODE
0007
0008          SHAPE(1)=0.25*(1.0-S)*(1.0-T)*(-S-T-1.0)
0009          SHAPE(2)=0.5*(1.0-S*S)*(1.0-T)
0010          SHAPE(3)=0.25*(1.0+S)*(1.0-T)*(S-T-1.0)
0011          SHAPE(4)=0.5*(1.0-T*T)*(1.0+S)
0012          SHAPE(5)=0.25*(1.0+S)*(1.0+T)*(S+T-1.0)
0013          SHAPE(6)=0.5*(1.0-S*S)*(1.0+T)
0014          SHAPE(7)=0.25*(1.0-S)*(1.0+T)*(-S+T-1.0)
0015          SHAPE(8)=0.5*(1.0-T*T)*(1.0-S)
0016          RETURN
0017          END

0001    C************************************************
0002    C THIS SUBROUTINE SUBDIVIDES EACH 4-NODED
0003    C QUADRILATERAL ELEMENT INTO TWO TRIANGULAR
0004    C ELEMENTS:THE SUBDIVISION IS DONE ACROSS THE
0005    C SHORTER DIAGONAL
0006    C
0007          SUBROUTINE TRIANGLE
0008          DIMENSION CORDE(4,2),LTEMP(4)
0009          COMMON/MESH1/ COORD(1500,2),ML(750,8),
0010         1MATNO(750),SHAPE(9),NP,NELEM,NTYPE,NDIME,MNODE
0011    C
0012          KOUNT=0
0013          DO 10 IELEM=1,NELEM
0014          NOTAL=NELEM+IELEM
0015          MATNO(NOTAL)=MATNO(IELEM)
0016          DO 10 INODE=1,MNODE
0017    10    ML(NOTAL,INODE)=ML(IELEM,INODE)
0018          DO 40 IELEM=1,NELEM
0019          NOTAL=NELEM+IELEM
0020          DO 20 INODE=1,MNODE
0021          INDEX=ML(NOTAL,INODE)
0022          LTEMP(INODE)=INDEX
0023          DO 20 IDIME=1,NDIME
0024    20    CORDE(INODE,IDIME)=COORD(INDEX,IDIME)
0025          DIAG1=SQRT((CORDE(1,1)-CORDE(3,1))**2 +
0026         1      (CORDE(1,2)-CORDE(3,2))**2)
0027          DIAG2=SQRT((CORDE(2,1)-CORDE(4,1))**2 +
0028         1      (CORDE(2,2)-CORDE(4,2))**2)
0029    C
0030    C DIVIDE ACROSS THE SHORTER DIAGONAL
0031    C
0032          DIFER=DIAG1-DIAG2
0033          IF(DIFER.GT.1.0E-9)GO TO 30
0034          KOUNT=KOUNT+1
0035          ML(KOUNT,1)=LTEMP(1)
0036          ML(KOUNT,2)=LTEMP(2)
0037          ML(KOUNT,3)=LTEMP(3)
0038          MATNO(KOUNT)=MATNO(NOTAL)
0039          KOUNT=KOUNT+1
0040          ML(KOUNT,1)=LTEMP(1)
0041          ML(KOUNT,2)=LTEMP(3)
0042          ML(KOUNT,3)=LTEMP(4)
0043          MATNO(KOUNT)=MATNO(NOTAL)
0044          GO TO 40
```

Figure 6.16

(Cont.) **FORTRAN code for automatic mesh generation.** ***(Continued).***

```
0045    30    KOUNT=KOUNT+1
0046          NL(KOUNT,1)=LTEMP(1)
0047          NL(KOUNT,2)=LTEMP(2)
0048          NL(KOUNT,3)=LTEMP(4)
0049          MATNO(KOUNT)=MATNO(NOTAL)
0050          KOUNT=KOUNT+1
0051          NL(KOUNT,1)=LTEMP(2)
0052          NL(KOUNT,2)=LTEMP(3)
0053          NL(KOUNT,3)=LTEMP(4)
0054          MATNO(KOUNT)=MATNO(NOTAL)
0055    40    CONTINUE
0056          NELEM=2*NELEM
0057          RETURN
0058          END

0001    C*************************************************
0002    C THIS SUBROUTINE OUTPUTS THE COORDINATES AND
0003    C ELEMENT TOPOLOGIES OF THE GENERATED MESH
0004    C
0005          SUBROUTINE OUTPUT
0006          COMMON/MESH1/ COORD(1500,2),NL(750,8),
0007         1 MATNO(750),SHAPE(9),NP,NELEM,NTYPE,NDIME,MNODE
0008    C
0009          WRITE(6,*)NP  ! TOTAL NO. OF POINTS
0010          WRITE(6,*)NELEM  ! TOTAL NO. OF ELEMENTS
0011          DO 10 IPOIN=1,NP
0012    10    WRITE(6,*)IPOIN,( COORD(IPOIN,I), I=1,NDIME )
0013          DO 20 IELEM=1,NELEM
0014    20    WRITE(6,*)IELEM,(NL(IELEM,I),I=1,NTYPE),MATNO(IELEM)
0015          RETURN
0016          END
```

Figure 6.16
(Cont.) **FORTRAN code for automatic mesh generation.**

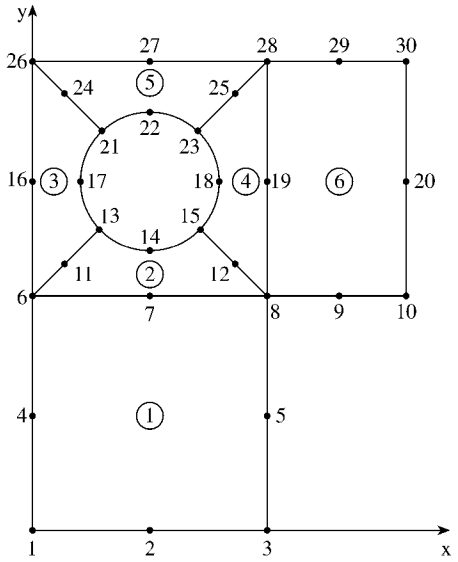

Figure 6.17
Solution region of Example 6.4.

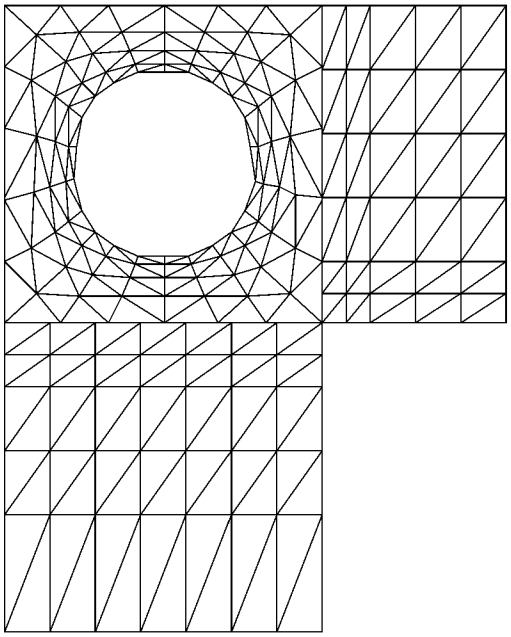

Figure 6.18
The generated mesh corresponding to input data in Table 6.6.

6.7 Bandwidth Reduction

Since most of the matrices involved in FEM are symmetric, sparse, and banded, we can minimize the storage requirements and the solution time by storing only the elements involved in half bandwidth instead of storing the whole matrix. To take the fullest advantage of the benefits from using a banded matrix solution technique, we must make sure that the matrix bandwidth is as narrow as possible.

If we let d be the maximum difference between the lowest and the highest node numbers of any single element in the mesh, we define the semi-bandwidth B (which includes the diagonal term) of the coefficient matrix $[C]$ as

$$B = (d + 1)f \tag{6.82}$$

where f is the number of degrees of freedom (or number of parameters) at each node. If, for example, we are interested in calculating the electric field intensity $\mathbf{E}$ for a three-dimensional problem, then we need E_x, E_y, and E_z at each node, and $f = 3$ in this case. Assuming that there is only one parameter per node,

$$B = d + 1 \tag{6.83}$$

Table 6.6 Input Data for Automatic Mesh Generation for the Solution Region in Fig. 6.17

```
30    6    3    2
1     1    2    3    5    8    7    6    4    1
2     6    7    8    12   15   14   13   11   1
3     6    11   13   17   21   24   26   16   1
4     8    19   28   25   23   18   15   12   1
5     21   22   23   25   28   27   26   24   1
6     8    9    10   20   30   29   28   19   2

1          0.0        0.0
2          2.5        0.0
3          5.0        0.0
4          0.0        2.5
5          5.0        2.5
6          0.0        5.0
7          2.5        5.0
8          5.0        5.0
9          6.5        5.0
10         8.0        5.0
11         0.7196     5.7196
12         4.2803     5.7196
13         1.4393     6.4393
14         2.5        6.0
15         3.5607     6.6493
16         0.0        7.5
17         1.0        7.5
18         4.0        7.5
19         5.0        7.5
20         8.0        7.5
21         1.4393     8.5607
22         2.5        9.0
23         3.5607     8.5607
24         0.7196     9.2805
25         4.2803     9.2805
26         0.0        10.0
27         2.5        10.0
28         2.5        10.0
29         6.5        10.0
30         8.0        10.0
1     7     5
1.0        1.0        1.0        1.0  1.0  1.0  1.0
2.0        1.0        1.0        0.5  0.5
2     7     4
1.0        1.0        1.0        1.0  1.0  1.0  1.0
1.0        0.75       0.5        0.25
3     4     6
1.0        0.75       0.5        0.25
1.0        1.0        1.0        1.0  1.0  1.0
4     6     4
1.0        1.0        2.0   2.0  2.0  2.0
1.0        0.75       0.5   0.25
5     6     4    1.0   1.0   1.0  1.0  1.0  1.0
0.25       0.5   0.75  1.0
6     5     6
1.0        1.0        2.0   2.0  2.0
1.0        1.0        2.0   2.0  2.0  2.0
```

The semi-bandwidth, which does not include the diagonal term, is obtained from Eq. (6.82) or (6.83) by subtracting one from the right-hand side, i.e., for $f = 1$,

$$B = d \tag{6.84}$$

Throughout our discussion in this section, we will stick to the definition of semi-bandwidth in Eq. (6.84). The total bandwidth may be obtained from Eq. (6.84) as $2B + 1$.

The bandwidth of the global coefficient matrix depends on the node numbering. Hence, to minimize the bandwidth, the node numbering should be selected to minimize d. Good node numbering is usually such that nodes with widely different numbers are widely separated. To minimize d, we must number nodes across the narrowest part of the region.

Consider, for the purpose of illustration, the mesh shown in Fig. 6.19. If the mesh is numbered originally as in Fig. 6.19, we obtain d_e for each element e as

$$d_1 = 2,\ d_2 = 3,\ d_3 = 4,\ d_4 = 5,\ d_5 = 6,\ d_6 = 7 \tag{6.85}$$

From this, we obtain

$$d = \text{ maximum } d_e = 7$$

or

$$B = 7 \tag{6.86}$$

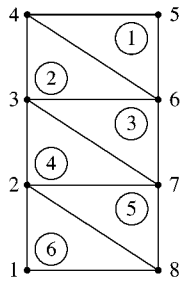

Figure 6.19
Original mesh with $B = 7$.

Alternatively, the semi-bandwidth may be determined from the coefficient matrix, which is obtained by mere inspection of Fig. 6.19 as

$$[C] = \begin{array}{c} \\ 1 \\ 2 \\ 3 \\ 4 \\ 5 \\ 6 \\ 7 \\ 8 \end{array} \begin{array}{c} \overset{\longleftarrow B=7 \longrightarrow}{\begin{array}{cccccccc} 1 & 2 & 3 & 4 & 5 & 6 & 7 & 8 \end{array}} \\ \begin{bmatrix} x & x & & & & & & x \\ x & x & x & & & & x & x \\ & x & x & x & & x & & \\ & & x & x & x & x & & \\ & & & x & x & x & & \\ & & x & x & x & x & x & \\ & x & & & & x & x & x \\ x & x & & & & & & x \end{bmatrix} \end{array} \tag{6.87}$$

where x indicates a possible nonzero term and blanks are zeros (i.e., $C_{ij} = 0$, indicating no coupling between nodes i and j). If the mesh is renumbered as in Fig. 6.20(a),

$$d_1 = 4 = d_2 = d_3 = d_4 = d_5 = d_6 \tag{6.88}$$

and hence

$$d = \text{ maximum } d_e = 4$$

or

$$B = 4 \tag{6.89}$$

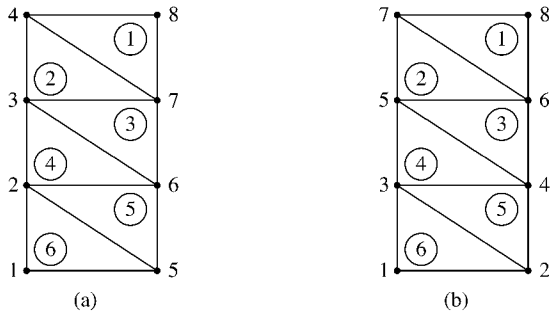

Figure 6.20
Renumbered nodes: (a) $B = 4$, (b) $B = 2$.

Finally, we may renumber the mesh as in Fig. 6.20(b). In this case

$$d_1 = 2 = d_2 = d_3 = d_4 = d_5 = d_6 \tag{6.90}$$

and

$$d = \text{ maximum } d_e = 2 \tag{6.91}$$

or

$$B = 2 \tag{6.92}$$

The value $B = 2$ may also be obtained from the coefficient matrix for the mesh in Fig. 6.20(b), namely,

$$[C] = \begin{array}{c} \\ \\ \\ 1 \\ 2 \\ 3 \\ 4 \\ 5 \\ 6 \\ 7 \\ 8 \end{array} \begin{array}{c} \overset{B=2}{\longleftrightarrow} \\ \mathbf{P}\quad\mathbf{Q} \\ 1\ 2\ 3\ 4\ 5\ 6\ 7\ 8 \\ \left[\begin{array}{cccccccc} x & x & x & & & & & \\ x & x & x & x & & & & \\ x & x & x & x & x & & & \\ & x & x & x & x & & & \\ & & x & x & x & x & x & \\ & & & x & x & x & x & x \\ & & & & x & x & x & x \\ & & & & & x & x & x \end{array}\right] \\ \\ \\ \\ \\ \\ \\ \\ \mathbf{R} \\ \\ \mathbf{S} \end{array} \tag{6.93}$$

From Eq. (6.93), one immediately notices that $[C]$ is symmetric and that terms are clustered in a band about the diagonal. Hence $[C]$ is sparse and banded so that only the data within the area **PQRS** of the matrix need to be stored—a total of 21 terms out of 64. This illustrates the savings in storage by a careful nodal numbering.

For a simple mesh, hand-labeling coupled with a careful inspection of the mesh (as we have done so far) can lead to a minimum bandwidth. However, for a large mesh, a hand-labeling technique becomes a tedious, time-consuming task, which in most cases may not be successful. It is particularly desirable that an automatic relabeling scheme is implemented within a mesh generation program. A number of algorithms have been proposed for bandwidth reduction by automatic mesh renumbering [37]–[40]. A simple, efficient algorithm is found in Collins [37].

6.8 Higher Order Elements

The finite elements we have used so far have been the linear type in that the shape function is of the order one. A higher order element is one in which the shape function or interpolation polynomial is of the order two or more.

The accuracy of a finite element solution can be improved by using finer mesh or using higher order elements or both. A discussion on mesh refinement versus higher order elements is given by Desai and Abel [2]; a motivation for using higher order elements is given by Csendes in [41]. In general, fewer higher order elements are needed to achieve the same degree of accuracy in the final results. The higher order elements are particularly useful when the gradient of the field variable is expected to vary rapidly. They have been applied with great success in solving EM-related problems [4], [41]–[46].

6.8.1 Pascal Triangle

Higher order triangular elements can be systematically developed with the aid of the so-called Pascal triangle given in Fig. 6.21. The family of finite elements generated in this manner with the distribution of nodes illustrated in Fig. 6.22. Note that in higher order elements, some secondary (side and/or interior) nodes are introduced in addition to the primary (corner) nodes so as to produce exactly the right number of nodes required to define the shape function of that order. The Pascal triangle contains terms of the basis functions of various degrees in variables x and y. An arbitrary function $\Phi_i(x, y)$ can be approximated in an element in terms of a complete nth order polynomial as

$$\Phi(x, y) = \sum_{i=1}^{m} \alpha_i \Phi_i \tag{6.94}$$

where

$$m = \frac{1}{2}(n + 1)(n + 2) \tag{6.95}$$

is the number of terms in complete polynomials (also the number of nodes in the triangle). For example, for second order ($n = 2$) or quadratic (six-node) triangular elements,

$$\Phi_e(x, y) = a_1 + a_2 x + a_3 y + a_4 xy + a_5 x^2 + a_6 y^2 \tag{6.96}$$

This equation has six coefficients, and hence the element must have six nodes. It is also complete through the second order terms. A systematic derivation of the interpolation function α for the higher order elements involves the use of the local coordinates.

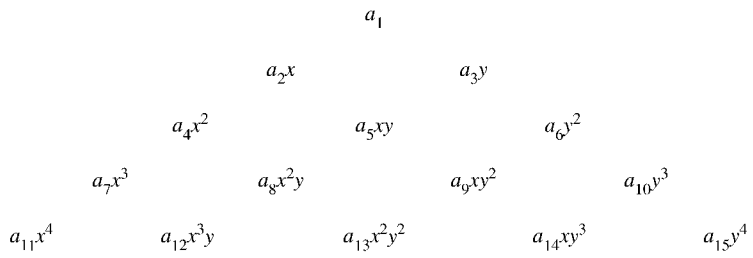

Figure 6.21

The Pascal Triangle. The first row is: (constant, $n = 0$), the second: (linear, $n = 1$), the third: (quadratic, $n = 2$), the fourth: (cubic, $n = 3$), the fifth: (quartic, $n = 4$).

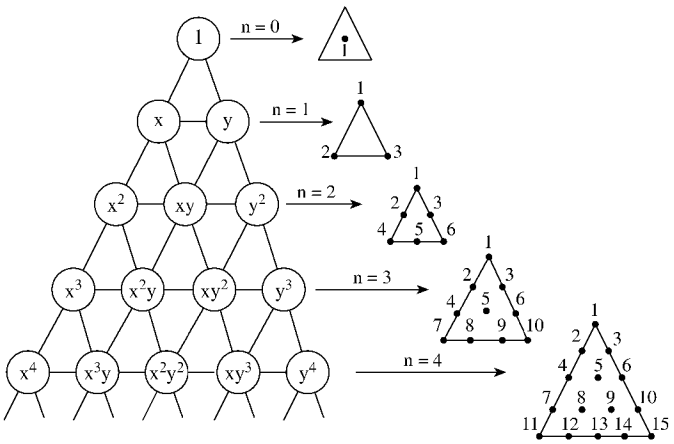

Figure 6.22
The Pascal triangle and the associated polynomial basis function for degree $n = 1$ to 4.

6.8.2 Local Coordinates

The triangular local coordinates (ξ_1, ξ_2, ξ_3) are related to Cartesian coordinates (x, y) as

$$x = \xi_1 x_1 + \xi_2 x_2 + \xi_3 x_3 \tag{6.97}$$

$$y = \xi_1 y_1 + \xi_2 y_2 + \xi_3 y_3 \tag{6.98}$$

The local coordinates are dimensionless with values ranging from 0 to 1. By definition, ξ_i at any point within the triangle is the ratio of the perpendicular distance from the point to the side opposite to vertex i to the length of the altitude drawn from vertex i. Thus, from Fig. 6.23 the value of ξ_1 at P, for example, is given by the ratio of the perpendicular distance d from the side opposite vertex 1 to the altitude h of that side, i.e.,

$$\xi_1 = \frac{d}{h} \tag{6.99}$$

Alternatively, from Fig. 6.23, ξ_i at P can be defined as

$$\xi_i = \frac{A_i}{A} \tag{6.100}$$

so that

$$\xi_1 + \xi_2 + \xi_3 = 1 \tag{6.101}$$

since $A_1 + A_2 + A_3 = A$. In view of Eq. (6.100), the local coordinates ξ_i are also called *area coordinates*. The variation of (ξ_1, ξ_2, ξ_3) inside an element is shown in

Fig. 6.24. Although the coordinates ξ_1, ξ_2, and ξ_3 are used to define a point P, only two are independent since they must satisfy Eq. (6.101). The inverted form of Eqs. (6.97) and (6.98) is

$$\xi_i = \frac{1}{2A}\left[c_i + b_i x + a_i y\right] \tag{6.102}$$

where

$$\begin{aligned} a_i &= x_k - x_j \ , \\ b_i &= y_j - y_k \ , \\ c_i &= x_j y_k - x_k y_j \\ A = &\quad \text{area of the triangle} \quad = \frac{1}{2}\left(b_1 a_2 - b_2 a_1\right) \ , \end{aligned} \tag{6.103}$$

and (i, j, k) is an even permutation of (1,2,3). (Notice that a_i and b_i are the same as Q_i and P_i in Eq. (6.34).) The differentiation and integration in local coordinates are carried out using [47]:

$$\frac{\partial f}{\partial \xi_1} = a_2 \frac{\partial f}{\partial x} - b_2 \frac{\partial f}{\partial y} \tag{6.104a}$$

$$\frac{\partial f}{\partial \xi_2} = -a_1 \frac{\partial f}{\partial x} + b_1 \frac{\partial f}{\partial y} \tag{6.104b}$$

$$\frac{\partial f}{\partial x} = \frac{1}{2A}\left(b_1 \frac{\partial f}{\partial \xi_1} + b_2 \frac{\partial f}{\partial \xi_2}\right) \tag{6.104c}$$

$$\frac{\partial f}{\partial y} = \frac{1}{2A}\left(a_1 \frac{\partial f}{\partial \xi_1} + a_2 \frac{\partial f}{\partial \xi_2}\right) \tag{6.104d}$$

$$\iint f \, dS = 2A \int_0^1 \left[\int_0^{1-\xi_2} f\left(\xi_1, \xi_2\right) \, d\xi_1 \right] d\xi_2 \tag{6.104e}$$

$$\iint \xi_1^i \xi_2^j \xi_3^k \, dS = \frac{i!\, j!\, k!}{(i + j + k + 2)!} 2A \tag{6.104f}$$

$$dS = 2A \, d\xi_1 \, d\xi_2 \tag{6.104g}$$

6.8.3 Shape Functions

We may now express the shape function for higher order elements in terms of local coordinates. Sometimes, it is convenient to label each point in the finite elements in Fig. 6.22 with three integers i, j, and k from which its local coordinates (ξ_1, ξ_2, ξ_3) can be found or vice versa. At each point P_{ijk}

$$\left(\xi_1, \xi_2, \xi_3\right) = \left(\frac{i}{n}, \frac{j}{n}, \frac{k}{n}\right) \tag{6.105}$$

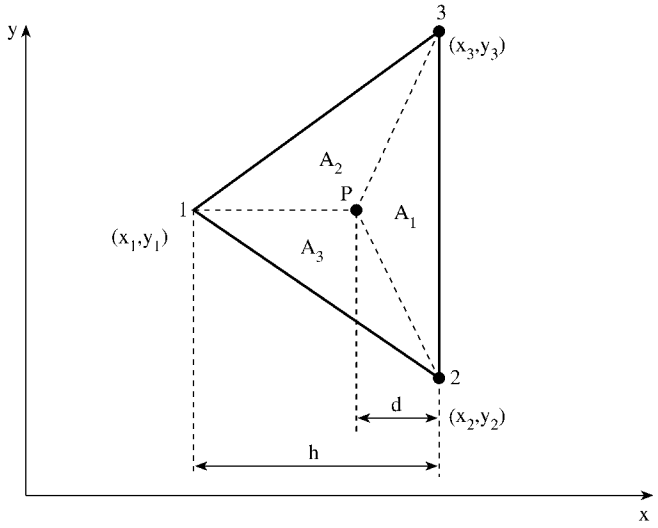

Figure 6.23
Definition of local coordinates.

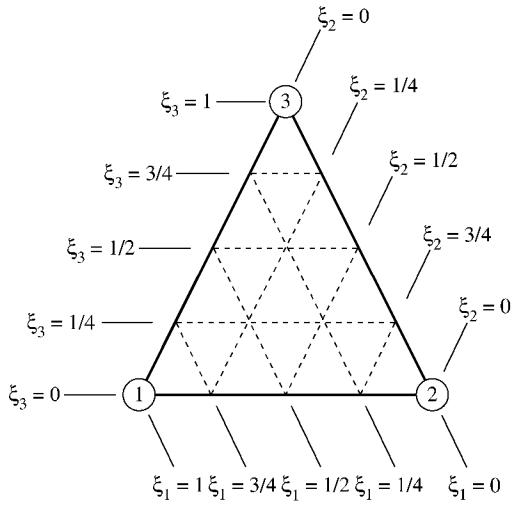

Figure 6.24
Variation of local coordinates.

Hence if a value of Φ, say Φ_{ijk}, is prescribed at each point P_{ijk}, Eq. (6.94) can be written as

$$\Phi(\xi_1, \xi_2, \xi_3) = \sum_{i=1}^{m} \sum_{j=1}^{m-i} \alpha_{ijk}(\xi_1, \xi_2, \xi_3)\, \Phi_{ijk} \tag{6.106}$$

where

$$\alpha_\ell = \alpha_{ijk} = p_i(\xi_1)\, p_j(\xi_2)\, p_k(\xi_3), \quad \ell = 1, 2, \ldots \tag{6.107}$$

$$p_r(\xi) = \begin{cases} \dfrac{1}{r!} \displaystyle\prod_{t=0}^{r-1} (n\xi - t), & r > 0 \\ 1, & r = 0 \end{cases} \tag{6.108}$$

and $r \in (i, j, k)$. $p_r(\xi)$ may also be written as

$$p_r(\xi) = \frac{(n\xi - r + 1)}{r} p_{r-1}(\xi), \quad r > 0 \tag{6.109}$$

where $p_0(\xi) = 1$.

The relationships between the subscripts $q \in \{1, 2, 3\}$ on ξ_q, $\ell \in \{1, 2, \ldots, m\}$ on α_ℓ, and $r \in (i, j, k)$ on p_r and P_{ijk} in Eqs. (6.107) to (6.109) are illustrated in Fig. 6.25 for n ranging from 1 to 4. Henceforth point P_{ijk} will be written as P_n for conciseness.

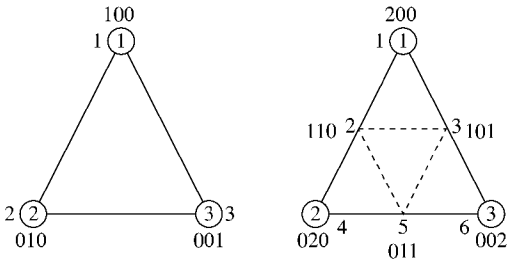

(a) n = 1 (b) n = 2

Figure 6.25
Distribution of nodes over triangles for $n = 1$ to 4. The triangles are in standard position *(Continued)*.

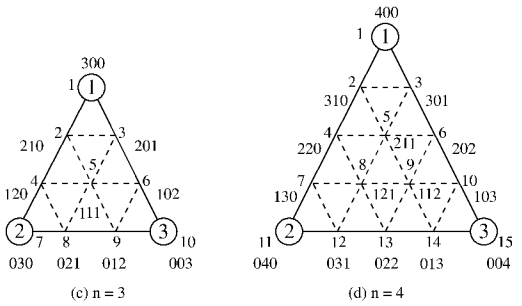

Figure 6.25
***(Cont.)* Distribution of nodes over triangles for $n = 1$ to 4. The triangles are in standard position.**

Notice from Eq. (6.108) or Eq. (6.109) that

$$\begin{aligned} p_0(\xi) &= 1 \\ p_1(\xi) &= n\xi \\ p_2(\xi) &= \frac{1}{2}(n\xi - 1)n\xi \\ p_3(\xi) &= \frac{1}{6}(n\xi - 2)(n\xi - 1)n\xi \\ p_4(\xi) &= \frac{1}{24}(n\xi - 3)(n\xi - 2)(n\xi - 1)n\xi, \quad \text{etc} \end{aligned} \tag{6.110}$$

Substituting Eq. (6.110) into Eq. (6.107) gives the shape functions α_ℓ for nodes $\ell = 1, 2, \ldots, m$, as shown in Table 6.7 for $n = 1$ to 4. Observe that each α_ℓ takes the value of 1 at node ℓ and value of 0 at all other nodes in the triangle. This is easily verified using Eq. (6.105) in conjunction with Fig. 6.25.

6.8.4 Fundamental Matrices

The fundamental matrices $[T]$ and $[Q]$ for triangular elements can be derived using the shape functions in Table 6.7. (For simplicity, the brackets [ ] denoting a matrix quantity will be dropped in the remaining part of this section.) In Eq. (6.46), the T matrix is defined as

$$T_{ij} = \iint \alpha_i \alpha_j \, dS \tag{6.46}$$

From Table 6.7, we substitute α_ℓ in Eq. (6.46) and apply Eqs. (6.104f) and (6.104g) to obtain elements of T. For example, for $n = 1$,

$$T_{ij} = 2A \int_0^1 \int_0^{1-\xi_2} \xi_i \xi_j \, d\xi_1 \, d\xi_2$$

Table 6.7 Polynomial Basis Function $\alpha_\ell(\xi_1, \xi_2, \xi_3, \xi_4)$ for First-, Second-, Third-, and Fourth-Order

$n=1$	$n=2$	$n=3$	$n=4$
$\alpha_1 = \xi_1$	$\alpha_1 = \xi_1(2\xi_1 - 1)$	$\alpha_1 = \frac{1}{2}\xi_1(3\xi_1 - 2)(3\xi_1 - 1)$	$\alpha_1 = \frac{1}{6}\xi_1(4\xi_1 - 3)(4\xi_1 - 2)(4\xi_1 - 1)$
$\alpha_2 = \xi_2$	$\alpha_2 = 4\xi_1\xi_2$	$\alpha_2 = \frac{9}{2}\xi_1(3\xi_1 - 1)\xi_2$	$\alpha_2 = \frac{8}{3}\xi_1(4\xi_1 - 2)(4\xi_1 - 1)\xi_2$
$\alpha_3 = \xi_3$	$\alpha_3 = 4\xi_1\xi_3$	$\alpha_3 = \frac{9}{2}\xi_1(3\xi_1 - 1)\xi_3$	$\alpha_3 = \frac{8}{3}\xi_1(4\xi_1 - 2)(4\xi_1 - 1)\xi_3$
	$\alpha_4 = \xi_2(2\xi_2 - 1)$	$\alpha_4 = \frac{9}{2}\xi_1(3\xi_2 - 1)\xi_2$	$\alpha_4 = 4\xi_1(4\xi_1 - 1)(4\xi_2 - 1)\xi_2$
	$\alpha_5 = 4\xi_2\xi_3$	$\alpha_5 = 27\xi_1\xi_2\xi_3$	$\alpha_5 = 32\xi_1(4\xi_1 - 1)\xi_2\xi_3$
	$\alpha_6 = \xi_3(2\xi_3 - 1)$	$\alpha_6 = \frac{9}{2}\xi_1(3\xi_3 - 1)\xi_3$	$\alpha_6 = 4\xi_1(4\xi_1 - 1)(4\xi_3 - 1)\xi_3$
		$\alpha_7 = \frac{1}{2}\xi_2(3\xi_2 - 2)(3\xi_2 - 1)$	$\alpha_7 = \frac{8}{3}\xi_1(4\xi_2 - 2)(4\xi_2 - 1)\xi_2$
		$\alpha_8 = \frac{9}{2}\xi_2(3\xi_2 - 1)\xi_3$	$\alpha_8 = 32\xi_1(4\xi_2 - 1)\xi_2\xi_3$
		$\alpha_9 = \frac{9}{2}\xi_2(3\xi_3 - 1)\xi_3$	$\alpha_9 = 32\xi_1\xi_2(4\xi_3 - 1)\xi_3$
		$\alpha_{10} = \frac{1}{2}\xi_3(3\xi_3 - 2)(3\xi_3 - 1)$	$\alpha_{10} = \frac{8}{3}\xi_1(4\xi_3 - 2)(4\xi_3 - 1)\xi_3$
			$\alpha_{11} = \frac{1}{6}\xi_2(4\xi_2 - 3)(4\xi_2 - 2)(4\xi_2 - 1)$
			$\alpha_{12} = \frac{8}{3}\xi_2(4\xi_2 - 2)(4\xi_2 - 1)\xi_3$
			$\alpha_{13} = 4\xi_2(4\xi_2 - 1)(4\xi_3 - 1)\xi_3$
			$\alpha_{14} = \frac{8}{3}\xi_2(4\xi_3 - 2)(4\xi_3 - 1)\xi_3$
			$\alpha_{15} = \frac{1}{6}\xi_3(4\xi_3 - 3)(4\xi_3 - 2)(4\xi_3 - 1)$

When $i \neq j$,

$$T_{ij} = \frac{2A(1!)(1!)(0!)}{4!} = \frac{A}{12}, \tag{6.111a}$$

when $i = j$,

$$T_{ij} = \frac{2A(2!)}{4!} = \frac{A}{6} \tag{6.111b}$$

Hence

$$T = \frac{A}{12}\begin{bmatrix} 2 & 1 & 1 \\ 1 & 2 & 1 \\ 1 & 1 & 2 \end{bmatrix} \tag{6.112}$$

By following the same procedure, higher order T matrices can be obtained. The T matrices for orders up to $n = 4$ are tabulated in Table 6.8 where the factor A, the area

of the element, has been suppressed. The actual matrix elements are obtained from Table 6.8 by multiplying the tabulated numbers by A and dividing by the indicated common denominator. The following properties of the T matrix are noteworthy:

(a) T is symmetric with positive elements;

(b) elements of T all add up to the area of the triangle, i.e., $\sum_{i}^{m}\sum_{j}^{m} T_{ij} = A$, since by definition $\sum_{\ell=1}^{m} \alpha_\ell = 1$ at any point within the element;

(c) elements for which the two triple subscripts form similar permutations are equal, i.e., $T_{ijk,prq} = T_{ikj,prq} = T_{kij,rpq} = T_{kji,rqp} = T_{jki,qrp} = T_{jik,qpr}$; this should be obvious from Eqs. (6.46) and (6.107).

These properties are not only useful in checking the matrix, they have proved useful in saving computer time and storage. It is interesting to know that the properties are independent of coordinate system [46].

Table 6.8 Table of T Matrix for $n = 1$ to 4 *(Continued)*

$n = 1$ Common denominator: 12

2	1	1
1	2	1
1	1	2

$n = 2$ Common denominator: 180

6	0	0	−1	−4	−1
0	32	16	0	16	−4
0	16	32	−4	16	0
−1	0	−4	6	0	−1
−4	16	16	0	32	0
−1	−4	0	−1	0	6

$n = 3$ Common denominator: 6720

76	18	18	0	36	0	11	27	27	11
18	540	270	−189	162	−135	0	−135	−54	27
18	270	540	−135	162	−189	27	−54	−135	0
0	−189	−135	540	162	−54	18	270	−135	27
36	162	162	162	1944	162	36	162	162	36
0	−135	−189	−54	162	540	27	−135	270	18
11	0	27	18	36	27	76	18	0	11
27	−135	−54	270	162	−135	18	540	−189	0
27	−54	−135	−135	162	270	0	−189	540	18
11	27	0	27	36	18	11	0	18	76

Table 6.8 *(Cont.)* Table of T Matrix for $n = 1$ to 4

$n = 4$	Common denominator: 56700												
290	160	160	−80	160	−80	0	−160	−160	0	−27	−112	−12	−112	−27
160	2560	1280	−1280	1280	−960	768	256	−256	512	0	512	64	256	−112
160	1280	2560	−960	1280	−1280	512	−256	256	768	−112	256	64	512	0
−80	−1280	−960	3168	384	48	−1280	384	−768	64	−80	−960	48	64	−12
160	1280	1280	384	10752	384	256	−1536	−1536	256	−160	−256	−768	−256	−160
−80	−960	−1280	48	384	3168	64	−768	384	−1280	−12	64	48	−960	−80
0	768	512	−1280	256	64	2560	1280	−256	256	160	1280	−960	512	−112
−160	256	−256	384	−1536	−768	1280	10752	−1536	−256	160	1280	384	256	−160
−160	−256	256	−768	−1536	384	−256	−1536	10752	1280	−160	256	384	1280	160
0	512	768	64	256	−1280	256	−256	1280	2560	−112	512	−960	1280	160
−27	0	−112	−80	−160	−12	160	160	−160	−112	290	160	−80	0	−27
−112	512	256	−960	−256	64	1280	1280	256	512	160	2560	−1280	768	0
−12	64	64	48	−768	48	−960	384	384	−960	−80	−1280	3168	−1280	−80
−112	256	512	64	−256	−960	512	256	1280	1280	0	768	−1280	2560	160
−27	−112	0	−12	−160	−80	−112	−160	160	160	−27	0	−80	160	290

In Eq. (6.14) or Eq. (6.45), elements of $[C]$ matrix are defined by

$$C_{ij} = \iint \left(\frac{\partial \alpha_i}{\partial x} \frac{\partial \alpha_j}{\partial x} + \frac{\partial \alpha_i}{\partial y} \frac{\partial \alpha_j}{\partial y} \right) dS \tag{6.113}$$

By applying Eqs. (6.104a) to (6.104d) to Eq. (6.113), it can be shown that [4, 43]

$$C_{ij} = \frac{1}{2A} \sum_{q=1}^{3} \cot \theta_q \iint \left(\frac{\partial \alpha_i}{\partial \xi_{q+1}} - \frac{\partial \alpha_i}{\partial \xi_{q-1}} \right) \left(\frac{\partial \alpha_j}{\partial \xi_{q+1}} - \frac{\partial \alpha_j}{\partial \xi_{q-1}} \right) dS$$

or

$$\boxed{C_{ij} = \sum_{q=1}^{3} Q_{ij}^{(q)} \cot \theta_q} \tag{6.114}$$

where θ_q is the included angle of vertex $q \in \{1, 2, 3\}$ of the triangle and

$$\boxed{Q_{ij}^{(q)} = \iint \left(\frac{\partial \alpha_i}{\partial \xi_{q+1}} - \frac{\partial \alpha_i}{\partial \xi_{q-1}} \right) \left(\frac{\partial \alpha_j}{\partial \xi_{q+1}} - \frac{\partial \alpha_j}{\partial \xi_{q-1}} \right) d\xi_1 \, d\xi_2} \tag{6.115}$$

We notice that matrix C depends on the triangle shape, whereas the matrices $Q^{(q)}$ do not. The $Q^{(1)}$ matrices for $n = 1$ to 4 are tabulated in Table 6.9. The following properties of Q matrices should be noted:

(a) they are symmetric;

(b) the row and column sums of any Q matrix are zero, i.e., $\sum_{i=1}^{m} Q_{ij}^{(q)} = 0 = \sum_{j=1}^{m} Q_{ij}^{(q)}$ so that the C matrix is singular.

$Q^{(2)}$ and $Q^{(3)}$ are easily obtained from $Q^{(1)}$ by row and column permutations so that the matrix C for any triangular element is constructed easily if $Q^{(1)}$ is known. One approach [48] involves using a rotation matrix R similar to that in Silvester and Ferrari [4], which is essentially a unit matrix with elements rearranged to correspond to one rotation of the triangle about its centroid in a counterclockwise direction. For example, for $n = 1$, the rotation matrix is basically derived from Fig. 6.26 as

$$\boxed{R = \begin{bmatrix} 0 & 0 & 1 \\ 1 & 0 & 0 \\ 0 & 1 & 0 \end{bmatrix}} \tag{6.116}$$

where $R_{ij} = 1$ node i is replaced by node j after one counterclockwise rotation, or $R_{ij} = 0$ otherwise. Table 6.10 presents the R matrices for $n = 1$ to 4. Note that each

Table 6.9 Table of Q Matrices for $n = 1$ to 4 *(Continued)*

$n = 1$ Common denominator: 2

$$\begin{pmatrix} 0 & 0 & 0 \\ 0 & 1 & -1 \\ 0 & -1 & 1 \end{pmatrix}$$

$n = 2$ Common denominator: 6

$$\begin{pmatrix} 0 & 0 & 0 & 0 & 0 & 0 \\ 0 & 8 & -8 & 0 & 0 & 0 \\ 0 & -8 & 8 & 0 & 0 & 0 \\ 0 & 0 & 0 & 3 & -4 & 1 \\ 0 & 0 & 0 & -4 & 8 & -4 \\ 0 & 0 & 0 & 1 & -4 & 3 \end{pmatrix}$$

$n = 3$ Common denominator: 80

$$\begin{pmatrix} 0 & 0 & 0 & 0 & 0 & 0 & 0 & 0 & 0 & 0 \\ 0 & 135 & -135 & -27 & 0 & 27 & 3 & 0 & 0 & -3 \\ 0 & -135 & 135 & 27 & 0 & -27 & -3 & 0 & 0 & 3 \\ 0 & -27 & 27 & 135 & -162 & 27 & 3 & 0 & 0 & -3 \\ 0 & 0 & 0 & -162 & 324 & -162 & 0 & 0 & 0 & 0 \\ 0 & 27 & -27 & 27 & -162 & 135 & -3 & 0 & 0 & 3 \\ 0 & 3 & -3 & 3 & 0 & -3 & 34 & -54 & 27 & -7 \\ 0 & 0 & 0 & 0 & 0 & 0 & -54 & 135 & -108 & 27 \\ 0 & 0 & 0 & 0 & 0 & 0 & 27 & -108 & 135 & -54 \\ 0 & -3 & 3 & -3 & 0 & 3 & -7 & 27 & -54 & 34 \end{pmatrix}$$

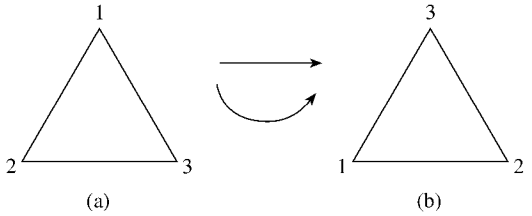

Figure 6.26
One counterclockwise rotation of the triangle in (a) gives the triangle in (b).

row or column of R has only one nonzero element since R is essentially a unit matrix with rearranged elements.

Once the R is known, we obtain

$$\boxed{Q^{(2)} = RQ^{(1)}R^t} \tag{6.117a}$$

$$\boxed{Q^{(3)} = RQ^{(2)}R^t} \tag{6.117b}$$

where R^t is the transpose of R.

Table 6.9 *(Cont.)* Table of Q Matrices for $n = 1$ to 4

$n = 4$	Common denominator: 1890													
0	0	0	0	0	0	0	0	0	0	0	0	0	0	0
0	3968	−3968	−1440	0	1440	640	0	0	−640	−80	0	0	0	80
0	−3968	3968	1440	0	−1440	−640	0	0	640	80	0	0	0	−80
0	−1440	1440	4632	−5376	744	−1248	768	768	−288	80	−128	96	−128	80
0	0	0	−5376	10752	−5376	1536	−1536	−1536	1536	−160	256	−192	256	−160
0	1440	−1440	744	−5376	4632	−288	768	768	−1248	80	−128	96	−128	80
0	640	−640	−1248	1536	−288	3456	−4608	1536	−384	240	−256	192	−256	80
0	0	0	768	−1536	768	−4608	10752	−7680	1536	−160	256	−192	256	−160
0	0	0	768	−1536	768	1536	−7680	10752	−4608	−160	256	−192	256	−160
0	−640	640	−288	1536	−1248	−384	1536	−4608	3456	80	−256	192	−256	240
0	−80	80	80	−160	80	240	−160	−160	80	705	−1232	884	−464	107
0	0	0	−128	256	−128	−256	256	256	−256	−1232	3456	−3680	1920	−464
0	0	0	96	−192	96	192	−192	−192	192	884	−3680	5592	−3680	884
0	0	0	−128	256	−128	−256	256	256	−256	−464	1920	−3680	3456	−1232
0	80	−80	80	−160	80	80	−160	−160	240	107	−464	884	−1232	705

Table 6.10 *R* Matrix for $n = 1$ to 4

$n = 1$

$$\begin{bmatrix} 0 & 0 & 1 \\ 1 & 0 & 0 \\ 0 & 1 & 0 \end{bmatrix}$$

$n = 2$

$$\begin{bmatrix} 0 & 0 & 0 & 0 & 0 & 1 \\ 0 & 0 & 1 & 0 & 0 & 0 \\ 0 & 0 & 0 & 0 & 1 & 0 \\ 1 & 0 & 0 & 0 & 0 & 0 \\ 0 & 1 & 0 & 0 & 0 & 0 \\ 0 & 0 & 0 & 1 & 0 & 0 \end{bmatrix}$$

$n = 3$

$$\begin{bmatrix} 0 & 0 & 0 & 0 & 0 & 0 & 0 & 0 & 0 & 1 \\ 0 & 0 & 0 & 0 & 0 & 1 & 0 & 0 & 0 & 0 \\ 0 & 0 & 0 & 0 & 0 & 0 & 0 & 0 & 1 & 0 \\ 0 & 0 & 1 & 0 & 0 & 0 & 0 & 0 & 0 & 0 \\ 0 & 0 & 0 & 0 & 1 & 0 & 0 & 0 & 0 & 0 \\ 0 & 0 & 0 & 0 & 0 & 0 & 0 & 1 & 0 & 0 \\ 1 & 0 & 0 & 0 & 0 & 0 & 0 & 0 & 0 & 0 \\ 0 & 1 & 0 & 0 & 0 & 0 & 0 & 0 & 0 & 0 \\ 0 & 0 & 0 & 1 & 0 & 0 & 0 & 0 & 0 & 0 \\ 0 & 0 & 0 & 0 & 0 & 0 & 1 & 0 & 0 & 0 \end{bmatrix}$$

$n = 4$

$$\begin{bmatrix} 0 & 0 & 0 & 0 & 0 & 0 & 0 & 0 & 0 & 0 & 0 & 0 & 0 & 0 & 1 \\ 0 & 0 & 0 & 0 & 0 & 0 & 0 & 0 & 0 & 1 & 0 & 0 & 0 & 0 & 0 \\ 0 & 0 & 0 & 0 & 0 & 0 & 0 & 0 & 0 & 0 & 0 & 0 & 0 & 1 & 0 \\ 0 & 0 & 0 & 0 & 0 & 1 & 0 & 0 & 0 & 0 & 0 & 0 & 0 & 0 & 0 \\ 0 & 0 & 0 & 0 & 0 & 0 & 0 & 0 & 1 & 0 & 0 & 0 & 0 & 0 & 0 \\ 0 & 0 & 0 & 0 & 0 & 0 & 0 & 0 & 0 & 0 & 0 & 0 & 1 & 0 & 0 \\ 0 & 0 & 1 & 0 & 0 & 0 & 0 & 0 & 0 & 0 & 0 & 0 & 0 & 0 & 0 \\ 0 & 0 & 0 & 0 & 1 & 0 & 0 & 0 & 0 & 0 & 0 & 0 & 0 & 0 & 0 \\ 0 & 0 & 0 & 0 & 0 & 0 & 0 & 1 & 0 & 0 & 0 & 0 & 0 & 0 & 0 \\ 0 & 0 & 0 & 0 & 0 & 0 & 0 & 0 & 0 & 0 & 0 & 1 & 0 & 0 & 0 \\ 1 & 0 & 0 & 0 & 0 & 0 & 0 & 0 & 0 & 0 & 0 & 0 & 0 & 0 & 0 \\ 0 & 1 & 0 & 0 & 0 & 0 & 0 & 0 & 0 & 0 & 0 & 0 & 0 & 0 & 0 \\ 0 & 0 & 0 & 1 & 0 & 0 & 0 & 0 & 0 & 0 & 0 & 0 & 0 & 0 & 0 \\ 0 & 0 & 0 & 0 & 0 & 0 & 1 & 0 & 0 & 0 & 0 & 0 & 0 & 0 & 0 \\ 0 & 0 & 0 & 0 & 0 & 0 & 0 & 0 & 0 & 0 & 1 & 0 & 0 & 0 & 0 \end{bmatrix}$$

Example 6.5

For $n = 2$, calculate $Q^{(1)}$ and obtain $Q^{(2)}$ from $Q^{(1)}$ using Eq. (6.117a). □

Solution

By definition,

$$Q_{ij}^{(1)} = \iint \left(\frac{\partial \alpha_i}{\partial \xi_2} - \frac{\partial \alpha_i}{\partial \xi_3}\right)\left(\frac{\partial \alpha_j}{\partial \xi_2} - \frac{\partial \alpha_j}{\partial \xi_3}\right) d\xi_1\, d\xi_2$$

For $n = 2$, $i, j = 1, 2, \ldots, 6$, and α_i are given in terms of the local coordinates in Table 6.7. Since $Q^{(1)}$ is symmetric, only some of the elements need be calculated. Substituting for α_ℓ from Table 6.7 and applying Eqs. (6.104e) and (6.104f), we obtain

$$\begin{aligned}
Q_{1j} &= 0, \quad j = 1 \text{ to } 6\,, \\
Q_{i1} &= 0, \quad i = 1 \text{ to } 6\,, \\
Q_{22} &= \frac{1}{2A}\iint (4\xi_1)^2\, d\xi_1\xi_2 = \frac{8}{6}\,, \\
Q_{23} &= \frac{1}{2A}\iint (4\xi_1)\,(-4\xi_1)\, d\xi_1\xi_2 = -\frac{8}{6}\,, \\
Q_{24} &= \frac{1}{2A}\iint (4\xi_1)\,(4\xi_1 - 1)\, d\xi_1\xi_2 = 0 = Q_{26}\,, \\
Q_{25} &= \frac{1}{2A}\iint (4\xi_1)\,(4\xi_3 - 4\xi_2)\, d\xi_1\xi_2 = 0\,, \\
Q_{33} &= \frac{1}{2A}\iint (-4\xi_1)^2\, d\xi_1\xi_2 = \frac{8}{6}\,, \\
Q_{34} &= \frac{1}{2A}\iint (-4\xi_1)\,(4\xi_2 - 1)\, d\xi_1\xi_2 = 0 = Q_{36}\,, \\
Q_{35} &= \frac{1}{2A}\iint (-4\xi_1)\,(4\xi_3 - 4\xi_2)\, d\xi_1\xi_2 = 0\,, \\
Q_{44} &= \frac{1}{2A}\iint (4\xi_2 - 1)^2\, d\xi_1\xi_2 = \frac{3}{6}\,, \\
Q_{45} &= \frac{1}{2A}\iint (4\xi_2 - 1)\,(4\xi_3 - 4\xi_2)\, d\xi_1\xi_2 = -\frac{4}{6}\,, \\
Q_{46} &= \frac{1}{2A}\iint (4\xi_2 - 1)\,(4\xi_3 - 1)\,(-1)\, d\xi_1\xi_2 = \frac{1}{6}\,, \\
Q_{55} &= \frac{1}{2A}\iint (4\xi_3 - 4\xi_2)^2\, d\xi_1\xi_2 = \frac{8}{6}\,, \\
Q_{56} &= \frac{1}{2A}\iint (4\xi_3 - 4\xi_2)\,(-1)\,(4\xi_3 - 1)\, d\xi_1\xi_2 = -\frac{4}{6}\,, \\
Q_{66} &= \frac{1}{2A}\iint (-1)\,(4\xi_3 - 1)^2\, d\xi_1\xi_2 = \frac{3}{6}
\end{aligned}$$

Hence

$$Q^{(1)} = \frac{1}{6}\begin{bmatrix} 0 & 0 & 0 & 0 & 0 & 0 \\ 0 & 8 & -8 & 0 & 0 & 0 \\ 0 & -8 & 8 & 0 & 0 & 0 \\ 0 & 0 & 0 & 3 & -4 & 1 \\ 0 & 0 & 0 & -4 & 8 & -4 \\ 0 & 0 & 0 & 1 & -4 & 3 \end{bmatrix}$$

We now obtain $Q^{(2)}$ from

$$\begin{aligned} Q^{(2)} &= RQ^{(1)}R^t \\ &= \frac{1}{6}R\begin{bmatrix} 0 & 0 & 0 & 0 & 0 & 0 \\ 0 & 8 & -8 & 0 & 0 & 0 \\ 0 & -8 & 8 & 0 & 0 & 0 \\ 0 & 0 & 0 & 3 & -4 & 1 \\ 0 & 0 & 0 & -4 & 8 & -4 \\ 0 & 0 & 0 & 1 & -4 & 3 \end{bmatrix}\begin{bmatrix} 0 & 0 & 0 & 1 & 0 & 0 \\ 0 & 0 & 0 & 0 & 1 & 0 \\ 0 & 1 & 0 & 0 & 0 & 0 \\ 0 & 0 & 0 & 0 & 0 & 1 \\ 0 & 0 & 1 & 0 & 0 & 0 \\ 1 & 0 & 0 & 0 & 0 & 0 \end{bmatrix} \\ &= \frac{1}{6}\begin{bmatrix} 0 & 0 & 0 & 0 & 0 & 1 \\ 0 & 0 & 1 & 0 & 0 & 0 \\ 0 & 0 & 0 & 0 & 1 & 0 \\ 1 & 0 & 0 & 0 & 0 & 0 \\ 0 & 1 & 0 & 0 & 0 & 0 \\ 0 & 0 & 0 & 1 & 0 & 0 \end{bmatrix}\begin{bmatrix} 0 & 0 & 0 & 0 & 0 & 0 \\ 0 & -8 & 0 & 0 & 8 & 0 \\ 0 & 8 & 0 & 0 & -8 & 0 \\ 1 & 0 & -4 & 0 & 0 & 3 \\ -4 & 0 & 8 & 0 & 0 & -4 \\ 3 & 0 & 4 & 0 & 0 & 1 \end{bmatrix} \\ Q^{(2)} &= \frac{1}{6}\begin{bmatrix} 3 & 0 & -4 & 0 & 0 & 1 \\ 0 & 8 & 0 & 0 & -8 & 0 \\ -4 & 0 & 8 & 0 & 0 & -4 \\ 0 & 0 & 0 & 0 & 0 & 0 \\ 0 & -8 & 0 & 0 & 8 & 0 \\ 1 & 0 & -4 & 0 & 0 & 3 \end{bmatrix} \quad \blacksquare \end{aligned}$$

6.9 Three-Dimensional Elements

The finite element techniques developed in the previous sections for two-dimensional elements can be extended to three-dimensional elements. One would expect three-dimensional problems to require a large total number of elements to achieve an accurate result and demand a large storage capacity and computational time. For the sake of completeness, we will discuss the finite element analysis of Helmholtz's equation in three dimensions, namely,

$$\nabla^2\Phi + k^2\Phi = g \tag{6.118}$$

We first divide the solution region into tetrahedral or hexahedral (rectangular prism) elements as in Fig. 6.27. Assuming a four-node tetrahedral element, the function Φ

is represented within the element by

$$\Phi_e = a + bx + cy + dz \tag{6.119}$$

The same applies to the function g. Since Eq. (6.119) must be satisfied at the four nodes of the tetrahedral elements,

$$\Phi_{ei} = a + bx_i + cy_i + dz_i, \qquad i = 1, \ldots, 4 \tag{6.120}$$

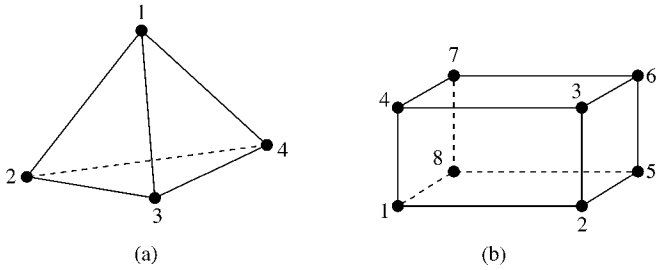

Figure 6.27
Three-dimensional elements: (a) Four-node or linear-order tetrahedral, (b) eight-node or linear-order hexahedral.

Thus we have four simultaneous equations (similar to Eq. (6.5)) from which the coefficients $a, b, c,$ and d can be determined. The determinant of the system of equations is

$$\det = \begin{vmatrix} 1 & x_1 & y_1 & z_1 \\ 1 & x_2 & y_2 & z_2 \\ 1 & x_3 & y_3 & z_3 \\ 1 & x_4 & y_4 & z_4 \end{vmatrix} = 6v\,, \tag{6.121}$$

where v is the volume of the tetrahedron. By finding $a, b, c,$ and d, we can write

$$\boxed{\Phi_e = \sum_{i=1}^{4} \alpha_i(x, y)\Phi_{ei}} \tag{6.122}$$

where

$$\alpha_1 = \frac{1}{6v} \begin{vmatrix} 1 & x & y & z \\ 1 & x_2 & y_2 & z_2 \\ 1 & x_3 & y_3 & z_3 \\ 1 & x_4 & y_4 & z_4 \end{vmatrix}\,, \tag{6.123a}$$

$$\alpha_2 = \frac{1}{6v} \begin{vmatrix} 1 & x_1 & y_1 & z_1 \\ 1 & x & y & z \\ 1 & x_3 & y_3 & z_3 \\ 1 & x_4 & y_4 & z_4 \end{vmatrix}\,, \tag{6.123b}$$

with α_3 and α_4 having similar expressions. For higher order approximation, the matrices for αs become large in size and we resort to local coordinates. Another motivation for using local coordinates is the existence of integration equations which simplify the evaluation of the fundamental matrices T and Q.

For the tetrahedral element, the local coordinates are ξ_1, ξ_2, ξ_3, and ξ_4, each perpendicular to a side. They are defined at a given point as the ratio of the distance from that point to the appropriate apex to the perpendicular distance from the side to the opposite apex. They can also be interpreted as volume ratios, i.e., at a point P

$$\xi_i = \frac{v_i}{v} \tag{6.124}$$

where v_i is the volume bound by P and face i. It is evident that

$$\sum_{i=1}^{4} \xi_i = 1 \tag{6.125a}$$

or

$$\xi_4 = 1 - \xi_1 - \xi_2 - \xi_3 \tag{6.125b}$$

The following properties are useful in evaluating integration involving local coordinates [47]:

$$dv = 6v\, d\xi_1\, d\xi_2\, d\xi_3\,, \tag{6.126a}$$

$$\iiint f dv = 6v \int_0^1 \left[\int_0^{1-\xi_3} \left(\int_0^{1-\xi_2-\xi_3} f\, d\xi_1 \right) d\xi_2 \right] d\xi_3\,, \tag{6.126b}$$

$$\iiint \xi_1^i \xi_2^j \xi_3^k \xi_4^\ell\, dv = \frac{i!j!k!\ell!}{(i+j+k+\ell+3)!} 6v \tag{6.126c}$$

In terms of the local coordinates, an arbitrary function $\Phi(x, y)$ can be approximated within an element in terms of a complete nth order polynomial as

$$\boxed{\Phi_e(x, y) = \sum_{i=1}^{m} \alpha_i(x, y)\Phi_{ei}} \tag{6.127}$$

where $m = \dfrac{1}{6}(n+1)(n+2)(n+3)$ is the number of nodes in the tetrahedron or the number of terms in the polynomial. The terms in a complete three-dimensional polynomial may be arrayed as shown in Fig. 6.28.

Each point in the tetrahedral element is represented by four integers i, j, k, and ℓ which can be used to determine the local coordinates $(\xi_1, \xi_2, \xi_3, \xi_4)$. That is at $P_{ijk\ell}$,

$$(\xi_1, \xi_2, \xi_3, \xi_4) = \left(\frac{i}{n}, \frac{j}{n}, \frac{k}{n}, \frac{\ell}{n} \right) \tag{6.128}$$

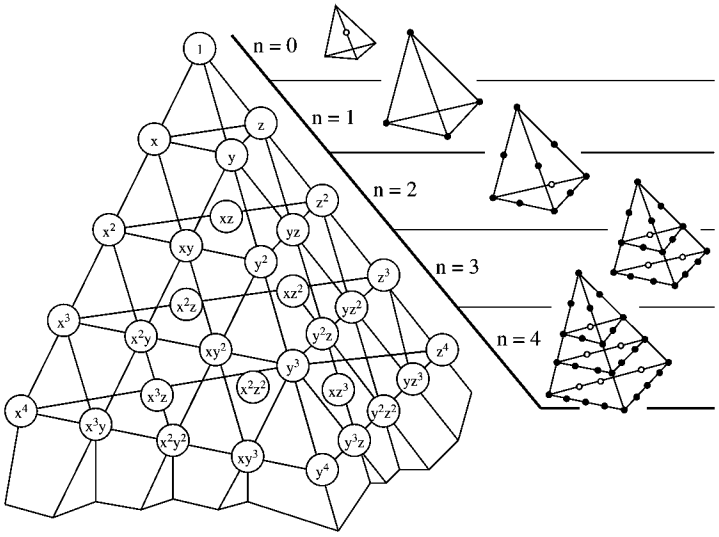

Figure 6.28
Pascal tetrahedron and associated array of terms.

Hence at each node,

$$\alpha_q = \alpha_{ijk\ell} = p_i\,(\xi_1)\,p_j\,(\xi_2)\,p_k\,(\xi_3)\,p_\ell\,(\xi_4)\ , \tag{6.129}$$

where $q = 1, 2, \ldots, m$ and p_r is defined in Eq. (6.108) or (6.109). The relationship between the node numbers q and $ijk\ell$ is illustrated in Fig. 6.29 for the second order tetrahedron ($n = 2$). The shape functions obtained by substituting Eq. (6.108) into Eq. (6.129) are presented in Table 6.11 for $n = 1$ to 3.

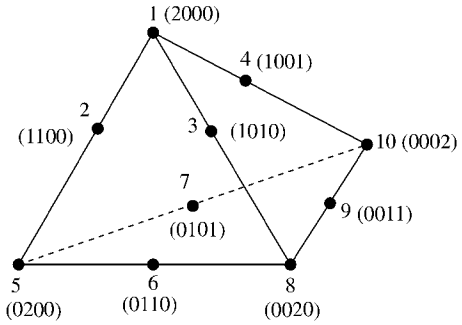

Figure 6.29
Numbering scheme for second-order tetrahedron.

The expressions derived from the variational principle for the two-dimensional problems in Sections 6.2 to 6.4 still hold except that the fundamental matrices $[T]$

Table 6.11 Shape Functions $\alpha_q(\xi_1, \xi_2, \xi_3, \xi_4)$ for $n = 1$ to 3

$n = 1$	$n = 2$	$n = 3$
$\alpha_1 = \xi_1$	$\alpha_1 = \xi_1(2\xi_2 - 1)$	$\alpha_1 = \frac{1}{2}\xi_1(3\xi_1 - 2)(3\xi_1 - 1)$
$\alpha_2 = \xi_2$	$\alpha_2 = 4\xi_1\xi_2$	$\alpha_2 = \frac{9}{2}\xi_1(3\xi_1 - 1)\xi_2$
$\alpha_3 = \xi_3$	$\alpha_3 = 4\xi_1\xi_3$	$\alpha_3 = \frac{9}{2}\xi_1(3\xi_1 - 1)\xi_3$
$\alpha_4 = \xi_4$	$\alpha_4 = 4\xi_1\xi_4$	$\alpha_4 = \frac{9}{2}\xi_1(3\xi_1 - 1)\xi_4$
	$\alpha_5 = \xi_2(2\xi_2 - 1)$	$\alpha_5 = \frac{9}{2}\xi_1(3\xi_3 - 1)\xi_2$
	$\alpha_6 = 4\xi_2\xi_3$	$\alpha_6 = 27\xi_1\xi_2\xi_3$
	$\alpha_7 = 4\xi_2\xi_4$	$\alpha_7 = 27\xi_1\xi_2\xi_4$
	$\alpha_8 = \xi_2(2\xi_3 - 1)$	$\alpha_8 = \frac{9}{2}\xi_1(3\xi_3 - 1)\xi_3$
	$\alpha_9 = 4\xi_3\xi_4$	$\alpha_9 = 27\xi_1\xi_3\xi_4$
	$\alpha_{10} = \xi_4(2\xi_4 - 1)$	$\alpha_{10} = \frac{9}{2}\xi_1(3\xi_4 - 1)\xi_4$
		$\alpha_{11} = \frac{1}{2}\xi_2(3\xi_2 - 1)(3\xi_2 - 2)$
		$\alpha_{12} = \frac{9}{2}\xi_2(3\xi_2 - 1)\xi_3$
		$\alpha_{13} = \frac{9}{2}\xi_2(3\xi_2 - 1)\xi_4$
		$\alpha_{14} = \frac{9}{2}\xi_2(3\xi_3 - 1)\xi_3$
		$\alpha_{15} = 27\xi_2\xi_3\xi_4$
		$\alpha_{16} = \frac{9}{2}\xi_2(3\xi_3 - 1)\xi_3$
		$\alpha_{17} = \frac{1}{2}\xi_3(3\xi_3 - 1)(3\xi_3 - 2)$
		$\alpha_{18} = \frac{9}{2}\xi_3(3\xi_3 - 1)\xi_4$
		$\alpha_{19} = \frac{9}{2}\xi_3(3\xi_4 - 1)\xi_4$
		$\alpha_{20} = \frac{1}{2}\xi_4(3\xi_4 - 1)(3\xi_4 - 2)$

and $[Q]$ now involve triple integration. For Helmholtz equation (6.56), for example, Eq. (6.68) applies, namely,

$$\left[C_{ff} - k^2 T_{ff}\right] \Phi_f = 0 \tag{6.130}$$

except that

$$\begin{aligned} C_{ij}^{(e)} &= \int_v \nabla\alpha_i \cdot \nabla\alpha_j \, dv \\ &= \int_v \left(\frac{\partial\alpha_i}{\partial x}\frac{\partial\alpha_j}{\partial x} + \frac{\partial\alpha_i}{\partial y}\frac{\partial\alpha_j}{\partial y} + \frac{\partial\alpha_i}{\partial z}\frac{\partial\alpha_j}{\partial z} \right) dv \,, \end{aligned} \tag{6.131}$$

$$T_{ij}^{(e)} = \int_v \alpha_i \alpha_j \, dv = v \iiint \alpha_i \alpha_j \, d\xi_1 \, d\xi_2 \, d\xi_3 \tag{6.132}$$

For further discussion on three-dimensional elements, one should consult Silvester and Ferrari [4]. Applications of three-dimensional elements to EM-related problems can be found in [49]–[53].

6.10 Finite Element Methods for Exterior Problems

Thus far in this chapter, the FEM has been presented for solving interior problems. To apply the FEM to exterior or unbounded problems such as open-type transmission lines (e.g., microstrip), scattering, and radiation problems poses certain difficulties. To overcome these difficulties, several approaches [54]–[82] have been proposed, all of which have strengths and weaknesses. We will consider three common approaches: the infinite element method, the boundary element method, and absorbing boundary condition.

6.10.1 Infinite Element Method

Consider the solution region shown in Fig. 6.30(a). We divide the entire domain into a near field (n.f.) region, which is bounded, and a far field (f.f.) region, which is unbounded. The n.f. region is divided into finite triangular elements as usual, while the f.f. region is divided into *infinite elements*. Each infinite elements shares two nodes with a finite element. Here we are mainly concerned with the infinite elements.

Consider the infinite element in Fig. 6.30(b) with nodes 1 and 2 and radial sides intersecting at point (x_o, y_o). We relate triangular polar coordinates (ρ, ξ) to the global Cartesian coordinates (x, y) as [62]

$$\begin{aligned} x &= x_o + \rho\left[(x_1 - x_o) + \xi\,(x_2 - x_1)\right] \\ y &= y_o + \rho\left[(y_1 - y_o) + \xi\,(y_2 - y_1)\right] \end{aligned} \tag{6.133}$$

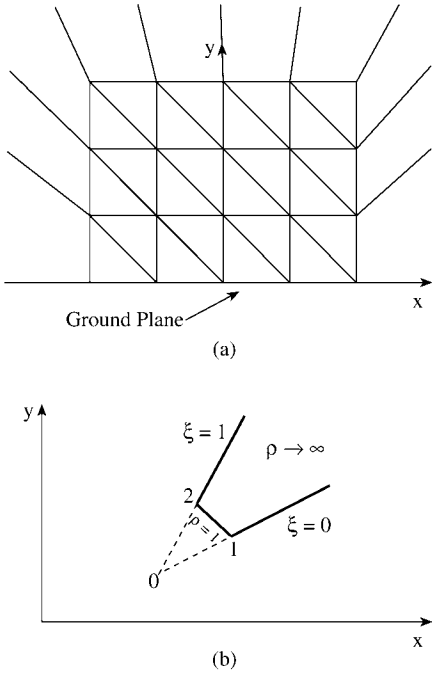

Figure 6.30
(a) Division of solution region into finite and infinite elements; (b) typical infinite element.

where $1 \leq \rho < \infty$, $0 \leq \xi \leq 1$. The potential distribution within the element is approximated by a linear variation as

$$V = \frac{1}{\rho}[V_1(1-\xi) + V_2\xi]$$

or

$$V = \sum_{i=1}^{2} \alpha_i V_i \tag{6.134}$$

where V_1 and V_2 are potentials at nodes 1 and 2 of the infinite elements, α_1 and α_2 are the interpolation or shape functions, i.e.,

$$\alpha_1 = \frac{1-\xi}{\rho}, \quad \alpha_2 = \frac{\xi}{\rho} \tag{6.135}$$

The infinite element is compatible with the ordinary first order finite element and satisfies the boundary condition at infinity. With the shape functions in Eq. (6.135), we can obtain the $[C^{(e)}]$ and $[T^{(e)}]$ matrices. We obtain solution for the exterior problem by using a standard finite element program with the $[C^{(e)}]$ and $[T^{(e)}]$ matrices of the infinite elements added to the $[C]$ and $[T]$ matrices of the n.f. region.

6.10.2 Boundary Element Method

A comparison between the finite element method (FEM) and the method of moments (MOM) is shown in Table 6.12. From the table, it is evident that the two methods have properties that complement each other. In view of this, hybrid methods have been proposed. These methods allow the use of both MOM and FEM with the aim of exploiting the strong points in each method.

Table 6.12 Comparison Between Method of Moments and Finite Element Method [83]

Method of Moments	Finite Element Method
Conceptually easy	Conceptually involved
Requires problem-dependent Green's functions	Avoids difficulties associated with singularity of Green's functions
Few equations; $O(n)$ for 2-D, $O(n^2)$ for 3-D	Many equations; $O(n^2)$ for 2-D, $O(n^3)$ for 3-D
Only boundary is discretized	Entire domain is discretized
Open boundary easy	Open boundary difficult
Fields by integration	Fields by differentiation
Good representation of far-field condition	Good representation of boundary conditions
Full matrices result	Sparse matrices result
Nonlinearity, inhomogeneity difficult	Nonlinearity, inhomogeneity easy

One of these hybrid methods is the so-called boundary element method (BEM). It is a finite element approach for handling exterior problems [68]–[80]. It basically involves obtaining the integral equation formulation of the boundary value problem [84], and solving this by a discretization procedure similar to that used in regular finite element analysis. Since the BEM is based on the boundary integral equivalent to the governing differential equation, only the surface of the problem domain needs to be modeled. Thus the dimension of the problem is reduced by one as in MOM. For 2-D problems, the boundary elements are taken to be straight line segments, whereas for 3-D problems, they are taken as triangular elements. Thus the shape or interpolation functions corresponding to subsectional bases in the MOM are used in the finite element analysis.

6.10.3 Absorbing Boundary Conditions

To apply the finite element approach to open region problems such as for scattering or radiation, an artificial boundary is introduced in order to bound the region and limit the number of unknowns to a manageable size. One would expect that as the boundary approaches infinity, the approximate solution tends to the exact one. But the closer the boundary to the radiating or scattering object, the less computer memory is required. To avoid the error caused by this truncation, an *absorbing boundary condition* (ABC)

is imposed on the artificial boundary S, as typically portrayed in Fig. 6.31. The ABC minimizes the nonphysical reflections from the boundary. Several ABCs have been proposed [85]–[91]. The major challenge of these ABCs is to bring the truncation boundary as close as possible to the object without sacrificing accuracy and to absorb the outgoing waves with little or no reflection. A popular approach is the PML-based ABC discussed in Section 3.8.3 for FD-TD. The finite element technique is used in enforcing the condition as a tool for mesh truncation [87].

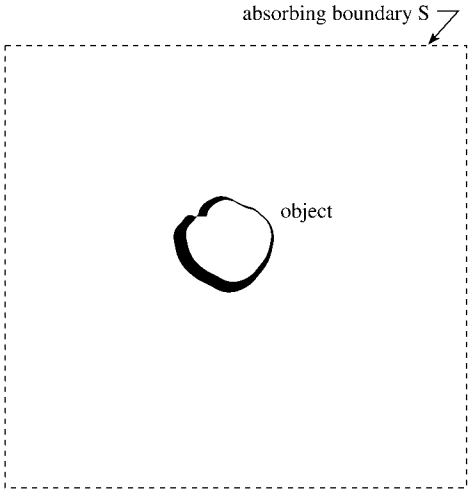

Figure 6.31
A radiating (or scattering) object surrounded by an absorbing boundary.

Another popular ABC derived Bayliss, Gunzburger, and Turkel (BGT) employs asymptotic analysis [91]. For example, for the solution of a three-dimensional problem, an expansion of the scalar Helmholtz equation is [90]:

$$\Phi(r,\theta,\phi) = \frac{e^{-jkr}}{kr} \sum_{i=0}^{\infty} \frac{F_i(\theta,\phi)}{(kr)^i} \tag{6.136}$$

The sequence of BGT operators is obtained by the recursion relation

$$\begin{aligned} B_1 &= \left(\frac{\partial}{\partial r} + jk + \frac{1}{r}\right) \\ B_m &= \left(\frac{\partial}{\partial r} + jk + \frac{2m-1}{r}\right) B_{m-1}\,, \quad m = 2, 3, \ldots \end{aligned} \tag{6.137}$$

Since Φ satisfies the higher-order radiation condition

$$B_m \Phi = O\left(1/r^{2m+1}\right) \tag{6.138}$$

imposing the mth-order boundary condition

$$B_m \Phi = 0 \quad \text{on } S \tag{6.139}$$

will compel the solution Φ to match the first $2m$ terms of the expansion in Eq. (6.136). Equation (6.139) along with other appropriate equations is solved for Φ using the finite element method.

6.11 Concluding Remarks

An introduction to the basic concepts and applications of the finite element method has been presented. It is by no means an exhaustive exposition of the subject. However, we have given the flavor of the way in which the ideas may be developed; the interested reader may build on this by consulting the references. Several introductory texts have been published on FEM. Although most of these texts are written for civil or mechanical engineers, the texts by Silvester and Ferrari [4], Chari and Silvester [41], Steele [92], Hoole [93], and Itoh [94] are for electrical engineers.

Due to its flexibility and versatility, the finite element method has become a powerful tool throughout engineering disciplines. It has been applied with great success to numerous EM-related problems. Such applications are:

- transmission line problems [95]–[97],
- optical and microwave waveguide problems [8]–[17], [92]–[103],
- electric machines [41], [104]–[106],
- scattering problems [71, 72, 75, 107, 108],
- human exposition to EM radiation [109]–[112], and
- others [113]–[116].

Applications of the FEM to time-dependent phenomena can be found in [108], [117]–[126].

For other issues on FEM not covered in this chapter, one is referred to introductory texts on FEM such as [2, 4, 36, 41, 47], [92]–[94], [126]–[133]. The issue of edge elements and absorbing boundary are covered in [126]. Estimating error in finite element solution is discussed in [52, 124, 125]. The reader may benefit from the numerous finite element codes that are commercially available. An extensive description of these systems and their capabilities can be found in [127, 134]. Although the codes were developed for one field of engineering or the other, they can be applied to problems in a different field with little or no modification.

References

[1] R. Courant, "Variational methods for the solution of problems of equilibrium and vibrations," *Bull. Am. Math. Soc.*, vol. 49, 1943, pp. 1–23.

[2] C.S. Desai and J.F. Abel, *Introduction to the Finite Element Method: A Numerical Approach for Engineering Analysis.* New York: Van Nostrand Reinhold, 1972.

[3] M.N.O. Sadiku, "A simple introduction to finite element analysis of electromagnetic problems," *IEEE Trans. Educ.*, vol. 32, no. 2, May 1989, pp. 85–93.

[4] P.P. Silvester and R.L. Ferrari, *Finite Elements for Electrical Engineers.* Cambridge: Cambridge University Press, 3rd ed., 1996.

[5] O.W. Andersen, "Laplacian electrostatic field calculations by finite elements with automatic grid generation," *IEEE Trans. Power App. Syst.*, vol. PAS-92, no. 5, Sept./Oct. 1973, pp. 1485–1492.

[6] S. Nakamura, *Computational Methods in Engineering and Science.* New York: John Wiley, 1977, pp. 446, 447.

[7] B.S. Garbow, *Matrix Eigensystem Routine—EISPACK Guide Extension.* Berlin: Springer-Verlag, 1977.

[8] S. Ahmed and P. Daly, "Finite-element methods for inhomogeneous waveguides," *Proc. IEEE*, vol. 116, no. 10, Oct. 1969, pp. 1661–1664.

[9] Z.J. Csendes and P. Silvester, "Numerical solution of dielectric loaded waveguides: I—Finite-element analysis," *IEEE Trans. Micro. Theo. Tech.*, vol. MTT-18, no. 12, Dec. 1970, pp. 1124–1131.

[10] Z.J. Csendes and P. Silvester, "Numerical solution of dielectric loaded waveguides: II—Modal approximation technique," *IEEE Trans. Micro. Theo. Tech.*, vol. MTT-19, no. 6, June 1971, pp. 504–509.

[11] M. Hano, "Finite-element analysis of dielectric-loaded waveguides," *IEEE Trans. Micro. Theo. Tech.*, vol. MTT-32, no. 10, Oct. 1984, pp. 1275–1279.

[12] A. Konrad, "Vector variational formulation of electromagnetic fields in anisotropic media," *IEEE Trans. Micro. Theo. Tech.*, vol. MTT-24, Sept. 1976, pp. 553–559.

[13] M. Koshiba, et al., "Improved finite-element formulation in terms of the magnetic field vector for dielectric waveguides," *IEEE Trans. Micro. Theo. Tech.*, vol. MTT-33, no. 3, March 1985, pp. 227–233.

[14] M. Koshiba, et al., "Finite-element formulation in terms of the electric-field vector for electromagnetic waveguide problems," *IEEE Trans. Micro. Theo. Tech.*, vol. MTT-33, no. 10, Oct. 1985, pp. 900–905.

[15] K. Hayata, et al., "Vectorial finite-element method without any spurious solutions for dielectric waveguiding problems using transverse magnetic-field component," *IEEE Trans. Micro. Theo. Tech.*, vol. MTT-34, no. 11, Nov. 1986.

[16] K. Hayata, et al., "Novel finite-element formulation without any spurious solutions for dielectric waveguides," *Elect. Lett.*, vol. 22, no. 6, March 1986, pp. 295, 296.

[17] S. Dervain, "Finite element analysis of inhomogeneous waveguides," Masters thesis, Department of Electrical and Computer Engineering, Florida Atlantic University, Boca Raton, April 1987.

[18] J.R. Winkler and J.B. Davies, "Elimination of spurious modes in finite element analysis," *J. Comp. Phys.*, vol. 56, no. 1, Oct. 1984, pp. 1–14.

[19] M.N.O. Sadiku, et al., "A further introduction to finite element analysis of electromagnetic problems," *IEEE Trans. Educ.*, vol. 34, no. 4, Nov. 1991, pp. 322–329.

[20] The IMSL Libraries: Problem-solving software systems for numerical FORTRAN programming, IMSL, Houston, TX, 1984.

[21] M. Kono, "A generalized automatic mesh generation scheme for finite element method," *Inter. J. Num. Method Engr.*, vol. 15, 1980, pp. 713–731.

[22] J.C. Cavendish, "Automatic triangulation of arbitrary planar domains for the finite element method," *Inter. J. Num. Meth. Engr.*, vol. 8, 1974, pp. 676–696.

[23] A.O. Moscardini, et al., "AGTHOM—Automatic generation of triangular and higher order meshes," *Inter. J. Num. Meth. Engr.*, vol. 19, 1983, pp. 1331–1353.

[24] C.O. Frederick, et al., "Two-dimensional automatic mesh generation for structured analysis," *Inter. J. Num. Meth. Engr.*, vol. 2, no. 1, 1970, pp. 133–144.

[25] E.A. Heighway, "A mesh generation for automatically subdividing irregular polygon into quadrilaterals," *IEEE Trans. Mag.*, vol. MAG-19, no. 6, Nov. 1983, pp. 2535–2538.

[26] C. Kleinstreuer and J.T. Holdeman, "A triangular finite element mesh generator for fluid dynamic systems of arbitrary geometry," *Inter. J. Num. Meth. Engr.*, vol. 15, 1980, pp. 1325–1334.

[27] A. Bykat, "Automatic generation of triangular grid I—subdivision of a general polygon into convex subregions. II—Triangulation of convex polygons," *Inter. J. Num. Meth. Engr.*, vol. 10, 1976, pp. 1329–1342.

[28] N.V. Phai, "Automatic mesh generator with tetrahedron elements," *Inter. J. Num. Meth. Engr.*, vol. 18, 1982, pp. 273–289.

[29] F.A. Akyuz, "Natural coordinates systems—an automatic input data generation scheme for a finite element method," *Nuclear Engr. Design,* vol. 11, 1970, pp. 195–207.

[30] P. Girdinio, et al., "New developments of grid optimization by the grid iteration method," in Z.J. Csendes (ed.), *Computational Electromagnetism.* New York: North-Holland, 1986, pp. 3–12.

[31] M. Yokoyama, "Automated computer simulation of two-dimensional elastrostatic problems by finite element method," *Inter. J. Num. Meth. Engr.,* vol. 21, 1985, pp. 2273–2287.

[32] G.F. Carey, "A mesh-refinement scheme for finite element computations," *Comp. Meth. Appl. Mech. Engr.,* vol. 7, 1976, pp. 93–105.

[33] K. Preiss, "Checking the topological consistency of a finite element mesh," *Inter. J. Meth. Engr.,* vol. 14, 1979, pp. 1805–1812.

[34] H. Kardestuncer (ed.), *Finite Element Handbook.* New York: McGraw-Hill, 1987, pp. 4.191–4.207.

[35] W.C. Thacker, "A brief review of techniques for generating irregular computational grids," *Inter. J. Num. Meth. Engr.,* vol. 15, 1980, pp. 1335–1341.

[36] E. Hinton and D.R.J. Owen, *An Introduction to Finite Element Computations.* Swansea, UK: Pineridge Press, 1979, pp. 247, 328–346.

[37] R.J. Collins, "Bandwidth reduction by automatic renumbering," *Inter. J. Num. Meth. Engr.,* vol. 6, 1973, pp. 345–356.

[38] E. Cuthill and J. McKee, "Reducing the bandwidth of sparse symmetric matrices," *ACM Nat. Conf.,* San Francisco, 1969, pp. 157–172.

[39] G.A. Akhras and G. Dhatt, "An automatic node relabelling scheme for minimizing a matrix or network bandwidth," *Inter. J. Num. Meth. Engr.,* vol. 10, 1976, pp. 787–797.

[40] F.A. Akyuz and S. Utku, "An automatic node-relabelling scheme for bandwidth minimization of stiffness matrices," *J. Amer. Inst. Aero. Astro.,* vol. 6, no. 4, 1968, pp. 728–730.

[41] M.V.K. Chari and P.P. Silvester (eds.), *Finite Elements for Electrical and Magnetic Field Problems.* Chichester: John Wiley, 1980, pp. 125–143.

[42] P. Silvester, "Construction of triangular finite element universal matrices," *Inter. J. Num. Meth. Engr.,* vol. 12, 1978, pp. 237–244.

[43] P. Silvester, "High-order polynomial triangular finite elements for potential problems," *Inter. J. Engr. Sci.,* vol. 7, 1969, pp. 849–861.

[44] G.O. Stone, "High-order finite elements for inhomogeneous acoustic guiding structures," *IEEE Trans. Micro. Theory Tech.,* vol. MTT-21, no. 8, Aug. 1973, pp. 538–542.

[45] A. Konrad, "High-order triangular finite elements for electromagnetic waves in anistropic media," *IEEE Trans. Micro. Theory Tech.*, vol. MTT-25, no. 5, May 1977, pp. 353–360.

[46] P. Daly, "Finite elements for field problems in cylindrical coordinates," *Inter. J. Num. Meth. Engr.*, vol. 6, 1973, pp. 169–178.

[47] C.A. Brebbia and J.J. Connor, *Fundamentals of Finite Element Technique.* London: Butterworth, 1973, pp. 114–118, 150–163, 191.

[48] M. Sadiku and L. Agba, "News rules for generating finite elements fundamental matrices," *Proc. IEEE Southeastcon,* 1989, pp. 797–801.

[49] R.L. Ferrari and G.L. Maile, "Three-dimensional finite element method for solving electromagnetic problems," *Elect. Lett.*, vol. 14, no. 15, 1978, pp. 467, 468.

[50] M. de Pourcq, "Field and power-density calculation by three-dimensional finite elements," *IEEE Proc.*, vol. 130, Pt. H, no. 6, Oct. 1983, pp. 377–384.

[51] M.V.K. Chari, et al., "Finite element computation of three-dimensional electrostatic and magnetostatic field problems," *IEEE Trans. Mag.*, vol. MAG-19, no. 16, Nov. 1983, pp. 2321–2324.

[52] O.A. Mohammed, et al., "Validity of finite element formulation and solution of three dimensional magnetostatic problems in electrical devices with applications to transformers and reactors," *IEEE Trans. Pow. App. Syst.*, vol. PAS-103, no. 7, July 1984, pp. 1846–1853.

[53] J.S. Savage and A.F. Peterson, "Higher-order vector finite elements for tetrahedral cells," *IEEE Trans. Micro. Theo. Tech.*, vol. 44, no. 6, June 1996, pp. 874–879.

[54] J.F. Lee and Z.J. Cendes, "Transfinite elements: a highly efficient procedure for modeling open field problems," *Jour. Appl. Phys.*, vol. 61, no. 8, April 1987, pp. 3913–3915.

[55] B.H. McDonald and A. Wexler, "Finite-element solution of unbounded field problems," *IEEE Trans. Micro. Theo. Tech.*, vol. MTT-20, no. 12, Dec. 1972, pp. 841–847.

[56] P.P. Silvester, et al., "Exterior finite elements for 2-dimensional field problems with open boundaries," *Proc. IEEE,* vol. 124, no. 12, Dec. 1977, pp. 1267–1270.

[57] S. Washisu, et al., "Extension of finite-element method to unbounded field problems," *Elect. Lett.*, vol. 15, no. 24, Nov. 1979, pp. 772–774.

[58] P. Silvester and M.S. Hsieh, "Finite-element solution of 2-dimensional exterior-field problems," *Proc. IEEE,* vol. 118, no. 12, Dec. 1971, pp. 1743–1747.

[59] Z.J. Csendes, "A note on the finite-element solution of exterior-field problems," *IEEE Trans. Micro. Theo. Tech.*, vol. MTT-24, no. 7, July 1976, pp. 468–473.

[60] T. Corzani, et al., "Numerical analysis of surface wave propagation using finite and infinite elements," *Alta Frequenza*, vol. 51, no. 3, June 1982, pp. 127–133.

[61] O.C. Zienkiewicz, et al., "Mapped infinite elements for exterior wave problems," *Inter. J. Num. Meth. Engr.*, vol. 21, 1985.

[62] F. Medina, "An axisymmetric infinite element," *Int. J. Num. Meth. Engr.*, vol. 17, 1981, pp. 1177–1185.

[63] S. Pissanetzky, "A simple infinite element," *Int. J. Comp. Math. Elect. Engr.*, (COMPEL), vol. 3, no. 2, 1984, pp. 107–114.

[64] Z. Pantic and R. Mittra, "Quasi-TEM analysis of microwave transmission lines by the finite-element method," *IEEE Trans. Micro. Theo. Tech.*, vol. MTT-34, no. 11, Nov. 1986, pp. 1096–1103.

[65] K. Hayata, et al., "Self-consistent finite/infinite element scheme for unbounded guided wave problems," *IEEE Trans. Micro. Theo. Tech.*, vol. MTT-36, no. 3, Mar. 1988, pp. 614–616.

[66] P. Petre and L. Zombory, "Infinite elements and base functions for rotationally symmetric electromagnetic waves," *IEEE Trans. Ant. Prog.*, vol. 36, no. 10, Oct. 1988, pp. 1490, 1491.

[67] Z.J. Csendes and J.F. Lee, "The transfinite element method for modeling MMIC devices," *IEEE Trans. Micro. Theo. Tech.* vol. 36, no. 12, Dec. 1988, pp. 1639–1649.

[68] K.H. Lee, et al., "A hybrid three-dimensional electromagnetic modeling scheme," *Geophys.*, vol. 46, no. 5, May 1981, pp. 796–805.

[69] S.J. Salon and J.M. Schneider, "A hybrid finite element-boundary integral formulation of Poisson's equation." *IEEE Trans. Mag.*, vol. MAG-17, no. 6, Nov. 1981, pp. 2574–2576.

[70] S.J. Salon and J. Peng, "Hybrid finite-element boundary-element solutions to axisymmetric scalar potential problems," in Z.J. Csendes (ed.), *Computational Electromagnetics*. New York: North-Holland/Elsevier, 1986, pp. 251–261.

[71] J.M. Lin and V.V. Liepa, "Application of hybrid finite element method for electromagnetic scattering from coated cylinders," *IEEE Trans. Ant. Prop.*, vol. 36, no. 1, Jan. 1988, pp. 50–54.

[72] J.M. Lin and V.V. Liepa, "A note on hybrid finite element method for solving scattering problems," *IEEE Trans. Ant. Prop.*, vol. 36, no. 10, Oct. 1988, pp. 1486–1490.

[73] M.H. Lean and A. Wexler, "Accurate field computation with boundary element method," *IEEE Trans. Mag.*, vol. MAG-18, no. 2, Mar. 1982, pp. 331-335.

[74] R.F. Harrington and T.K. Sarkar, "Boundary elements and the method of moments," in C.A. Brebbia, et al. (eds.), *Boundary Elements*. Southampton: CML Publ., 1983, pp. 31–40.

[75] M.A. Morgan, et al., "Finite element-boundary integral formulation for electromagnetic scattering," *Wave Motion,* vol. 6, no. 1, 1984, pp. 91–103.

[76] S. Kagami and I. Fukai, "Application of boundary-element method to electromagnetic field problems," *IEEE Trans. Micro. Theo. Tech.,* vol. 32, no. 4, Apr. 1984, pp. 455–461.

[77] Y. Tanaka, et al., "A boundary-element analysis of TEM cells in three dimensions," *IEEE Trans. Elect. Comp.,* vol. EMC-28, no. 4, Nov. 1986, pp. 179–184.

[78] N. Kishi and T. Okoshi, "Proposal for a boundary-integral method without using Green's function," *IEEE Trans. Micro. Theo. Tech.,* vol. MTT-35, no. 10, Oct. 1987, pp. 887–892.

[79] D.B. Ingham, et al., "Boundary integral equation analysis of transmission-line singularities," *IEEE Trans. Micro. Theo. Tech.,* vol. MTT-29, no. 11, Nov. 1981, pp. 1240–1243.

[80] S. Washiru, et al., "An analysis of unbounded field problems by finite element method," *Electr. Comm. Japan,* vol. 64-B, no. 1, 1981, pp. 60–66.

[81] T. Yamabuchi and Y. Kagawa, "Finite element approach to unbounded Poisson and Helmholtz problems using hybrid-type infinite element," *Electr. Comm. Japan,* Pt. I, vol. 68, no. 3, 1986, pp. 65–74.

[82] K.L. Wu and J. Litva, "Boundary element method for modelling MIC devices," *Elect. Lett.,* vol. 26, no. 8, April 1990, pp. 518–520.

[83] M.N.O. Sadiku and A.F. Peterson, "A comparison of numerical methods for computing electromagnetic fields," *Proc. of IEEE Southeastcon,* April 1990, pp. 42–47.

[84] P.K. Kythe, *An Introduction to Boundary Element Methods*. Boca Raton, FL: CRC Press, 1995, p. 2.

[85] J.M. Jin et al., "Fictitious absorber for truncating finite element meshes in scattering," *IEEE Proc. H,* vol. 139, Oct. 1992, pp. 472–476.

[86] R. Mittra and O. Ramahi, "Absorbing bounding conditions for direct solution of partial differential equations arising in electromagnetic scattering problems," in M.A. Morgan (ed.), *Finite Element and Finite Difference Methods in Electromagnetics*. New York: Elsevier, 1990, pp. 133–173.

[87] U. Pekel and R. Mittra, "Absorbing boundary conditions for finite element mesh truncation," in T. Itoh et al. (eds.), *Finite Element Software for Microwave Engineering*. New York: John Wiley & Sons, 1996, pp. 267–312.

[88] U. Pekel and R. Mittra, "A finite element method frequency domain application of the perfectly matched layer (PML) concept," *Micro. Opt. Technol. Lett.*, vol. 9, pp. 117–122.

[89] A. Boag and R. Mittra, "A numerical absorbing boundary condition for finite difference and finite element analysis of open periodic structures," *IEEE Trans. Micro. Theo. Tech.*, vol. 43, no. 1 Jan. 1995, pp. 150–154.

[90] P.P. Silvester and G. Pelosi (eds.), *Finite Elements for Wave Electromagnetics: Methods and Techniques*. New York: IEEE Press, 1994, pp. 351–490.

[91] A.M. Bayliss, M. Gunzburger, and E. Turkel, "Boundary conditions for the numerical solution of elliptic equation in exterior regions," *SIAM Jour. Appl. Math.*, vol. 42, 1982, pp. 430–451.

[92] C.W. Steele, *Numerical Computation of Electric and Magnetic Fields*. New York: Van Nostrand Reinhold, 1987.

[93] S.R. Hoole, *Computer-aided Analysis and Design of Electromagnetic Devices*. New York: Elsevier, 1989.

[94] T. Itoh (ed.), *Numerical Technique for Microwave and Millimeterwave Passive Structure*. New York: John Wiley, 1989.

[95] R.L. Khan and G.I. Costache, "Finite element method applied to modeling crosstalk problems on printed circuits boards," *IEEE Trans. Elect. Comp.*, vol. 31, no. 1, Feb. 1989, pp. 5–15.

[96] P. Daly, "Upper and lower bounds to the characteristic impedance of transmission lines using the finite method," *Inter. J. Comp. Math. Elect. Engr.*, (COMPEL), vol. 3, no. 2, 1984, pp. 65–78.

[97] A. Khebir, et al., "An absorbing boundary condition for quasi-TEM analysis of microwave transmission lines via the finite element method," *J. Elect. Waves Appl.*, vol. 4, no. 2, 1990, pp. 145–157.

[98] N. Mabaya, et al., "Finite element analysis of optical waveguides," *IEEE Trans. Micro. Theo. Tech.*, vol. MTT-29, no. 6, June 1981, pp. 600–605.

[99] M. Ikeuchi, et al., "Analysis of open-type dielectric waveguides by the finite-element iterative method," *IEEE Trans. Micro. Theo. Tech.*, vol. MTT-29, no. 3, Mar. 1981, pp. 234–239.

[100] C. Yeh, et al., "Single model optical waveguides," *Appl. Optics*, vol. 18, no. 10, May 1979, pp. 1490–1504.

[101] J. Katz, "Novel solution of 2-D waveguides using the finite element method," *Appl. Optics*, vol. 21, no. 15, Aug. 1982, pp. 2747–2750.

[102] B.A. Rahman and J.B. Davies, "Finite-element analysis of optical and microwave waveguide problems," *IEEE Trans. Micro. Theo. Tech.*, vol. MTT-32, no. 1, Jan. 1984, pp. 20–28.

[103] X.Q. Sheng and S. Xu, "An efficient high-order mixed-edge rectangular-element method for lossy anisotropic dielectric waveguide," *IEEE Micro. Theo. Tech.*, vol. 45, no. 7, July 1997, pp. 1009–1013.

[104] C.B. Rajanathan, et al., "Finite-element analysis of the Xi-core leviator," *IEEE Proc.*, vol. 131, Pt. A, no. 1, Jan. 1984, pp. 62–66.

[105] T.L. Ma and J.D. Lavers, "A finite-element package for the analysis of electromagnetic forces and power in an electric smelting furnace," *IEEE Trans. Indus. Appl.*, vol. IA-22, no. 4, July/Aug. 1986, pp. 578–585.

[106] C.O. Obiozor and M.N.O. Sadiku, "Finite element analysis of a solid rotor induction motor under stator winding effects," *Proc. IEEE Southeastcon*, 1991, pp. 449–453.

[107] J.L. Mason and W.J. Anderson, "Finite element solution for electromagnetic scattering from two-dimensional bodies," *Inter. J. Num. Meth. Engr.*, vol. 21, 1985, pp. 909–928.

[108] A.C. Cangellaris, et al., "Point-matching time domain finite element methods for electromagnetic radiation and scattering," *IEEE Trans. Ant. Prop.*, vol. AP35, 1987, pp. 1160–1173.

[109] A. Chiba, et al., "Application of finite element method to analysis of induced current densities inside human model exposed to 60 Hz electric field," *IEEE Trans. Power App. Sys.*, vol. PAS-103, no. 7, July 1984, pp. 1895–1902.

[110] Y. Yamashita and T. Takahashi, "Use of the finite element method to determine epicardial from body surface potentials under a realistic torso model," *IEEE Trans. Biomed. Engr.*, vol. BME-31, no. 9, Sept. 1984, pp. 611–621.

[111] M.A. Morgan, "Finite element calculation of microwave absorption by the cranial structure," *IEEE Trans. Biomed. Engr.*, vol. BME-28, no. 10, Oct. 1981, pp. 687–695.

[112] D.R. Lynch, et al., "Finite element solution of Maxwell's equation for hyperthermia treatment planning," *J. Comp. Phys.* vol. 58, 1985, pp. 246–269.

[113] J.R. Brauer, et al., "Dynamic electric fields computed by finite elements," *IEEE Trans. Ind. Appl.*, vol. 25, no. 6, Nov./Dec. 1989, pp. 1088–1092.

[114] C.H. Chen and C.D. Lien, "A finite element solution of the wave propagation problem for an inhomogeneous dielectric slab," *IEEE Trans. Ant. Prop.*, vol. AP-27, no. 6, Nov. 1979, pp. 877–880.

[115] T.L.W. Ma and J.D. Lavers, "A finite-element package for the analysis of electromagnetic forces and power in an electric smelting furnace," *IEEE Trans. Ind. Appl.*, vol. IA-22, no. 4, July/Aug., 1986, pp. 578–585.

[116] M.A. Kolbehdari and M.N.O. Sadiku, "Finite element analysis of an array of rods or rectangular bars between ground," *Jour. Franklin Inst.*, vol. 335B, no. 1, 1998, pp. 97–107.

[117] V. Shanka, "A time-domain, finite-volume treatment for Maxwell's equations," *Electromagnetics,* vol. 10, 1990, pp. 127–145.

[118] J.H. Argyris and D.W. Scharpf, "Finite elements in time and space," *Nucl. Engr. Space Des.,* vol. 10, no. 4, 1969, pp. 456–464.

[119] I. Fried,"Finite-element analysis of time-dependent phenomena," *AIAA J.,* vol. 7, no. 6, 1969, pp. 1170–1173.

[120] O.C. Zienkiewicz and C.J. Pareth, "Transient field problems: two-dimensional and three-dimensional analysis by isoparametric finite elements," *Inter. J. Num. Meth. Engr.,* vol. 2, 1970, pp. 61–71.

[121] J.H. Argyris and A.S.L. Chan, "Applications of finite elements in space and time," *Ingenieur-Archiv,* vol. 41, 1972, pp. 235–257.

[122] J.C. Bruch and G. Zyvoloski, "Transient two-dimensional heat conduction problems solved by the finite element method," *Inter. J. Num. Meth. Engr.,* vol. 8, 1974, pp. 481–494.

[123] B. Swartz and B. Wendroff, "The relative efficiency of finite difference and finite element methods I: hyperbolic problems and splines," *SIAM J. Numer. Anal.,* vol. 11, no. 5, Oct. 1974.

[124] J. Cushman, "Difference schemes or element schemes," *Int. J. Num. Meth. Engr.,* vol. 14, 1979, pp. 1643–1651.

[125] A.J. Baker and M.O. Soliman, "Utility of a finite element solution algorithm for initial-value problems," *J. Comp. Phys.,* vol. 32, 1979, pp. 289–324.

[126] J.N. Reddy, *An Introduction to the Finite Element Method.* New York: McGraw-Hill, 2nd ed., 1993, pp. 293–403.

[127] C.A. Brebbia (ed.), *Applied Numerical Modelling.* New York: John Wiley, 1978, pp. 571–586.

[128] C.A. Brebbia (ed.), *Finite Element Systems: A Handbook.* Berlin: Springer-Verlag, 1985.

[129] O.C. Zienkiewicz, *The Finite Element Method.* New York: McGraw-Hill, 1977.

[130] A.J. Davies, *The Finite Element Method: A First Approach.* Oxford: Clarendon, 1980.

[131] C. Martin and G.F. Carey, *Introduction to Finite Element Analysis: Theory and Application.* New York: McGraw-Hill, 1973.

[132] T.J. Chung, *Finite Element Analysis in Fluid Dynamics.* New York: McGraw-Hill, 1978.

[133] D.H. Norris and G de. Vries, *An Introduction to Finite Element Analysis.* New York: Academic Press, 1978.

[134] T. Itoh et al. (eds.), *Finite Element Software for Microwave Engineering*. New York: John Wiley & Sons, 1996.

[135] J.L. Volakis et al., *Finite Element Method for Electromagnetics*. New York: IEEE Press, 1998.

[136] G.R. Buchanan, *Finite Element Analysis* (Schaum's Outline). New York: McGraw-Hill, 2nd ed., 1995.

[137] J. Jin, *The Finite Element Method in Electromagnetics*. New York: John Wiley & Sons, 1993.

[138] R. Thatcher, "Assessing the error in a finite element solution," *IEEE Trans. Micro. Theo. Tech.*, vol. MTT-30, no. 6, June 1982, pp. 911–914.

[139] J. Penman and M. Grieve, "Self-adaptive finite-element techniques for the computation of inhomogeneous Poissonian fields," *IEEE Trans. Micro. Theo. Tech.*, vol. 24, no. 6, Nov./Dec. 1998, pp. 1042–1049.

Problems

6.1 For the triangular elements in Fig. 6.32, determine the element coefficient matrices.

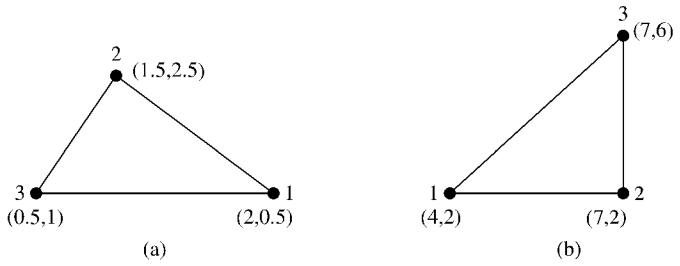

Figure 6.32
For Problem 6.1.

6.2 Find the coefficient matrix for the two-element mesh of Fig. 6.33. Given that $V_2 = 10$ and $V_4 = -10$, determine V_1 and V_3.

6.3 Determine the shape functions α_1, α_2, and α_3 for the element in Fig. 6.34.

6.4 Consider the mesh shown in Fig. 6.35. The shaded region is conducting and has no finite elements. Calculate the global elements $C_{3,10}$ and $C_{3,3}$.

6.5 With reference to the finite element in Fig. 6.36, calculate the energy per unit length associated with the element.

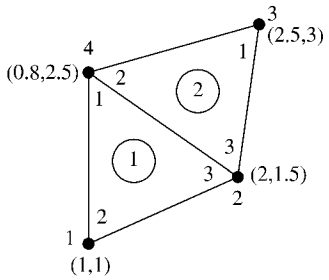

Figure 6.33
For Problem 6.2.

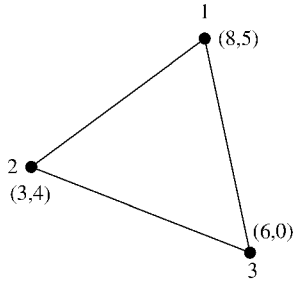

Figure 6.34
For Problem 6.3.

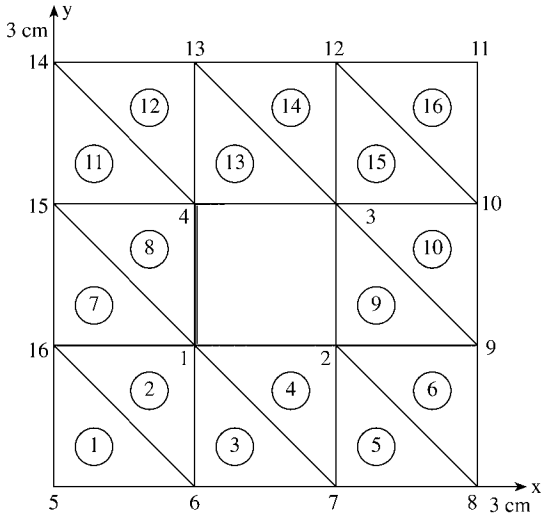

Figure 6.35
For Problem 6.4.

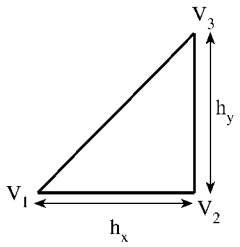

Figure 6.36
For Problem 6.5.

6.6 Consider the element whose sides are parallel to the x and y axis, as shown in Fig. 6.37. Verify that the potential distribution within the elements can be expressed as

$$V(x, y) = \alpha_1 V_1 + \alpha_2 V_2 + \alpha_3 V_3 + \alpha_4 V_4$$

where V_i are the nodal potentials and α_i are local interpolating functions defined as

$$\alpha_1 = \frac{(x - x_2)(y - y_4)}{(x_1 - x_2)(y_1 - y_4)}$$
$$\alpha_2 = \frac{(x - x_1)(y - y_3)}{(x_2 - x_1)(y_2 - y_3)}$$
$$\alpha_3 = \frac{(x - x_4)(y - y_2)}{(x_3 - x_4)(y_3 - y_2)}$$
$$\alpha_4 = \frac{(x - x_3)(y - y_1)}{(x_4 - x_3)(y_4 - y_1)}$$

6.7 The cross section of an infinitely long rectangular trough is shown in Fig. 6.38; develop a program using FEM to find the potential at the center of the cross section. Take $\epsilon_r = 4.5$.

6.8 Solve the problem in Example 3.3 using the finite element method.

6.9 Modify the program in Fig. 6.10 to calculate the electric field intensity **E** at any point in the solution region.

6.10 The program in Fig. 6.10 applies the iteration method to determine the potential at the free nodes. Modify the program and use the band matrix method to determine the potential. Test the program using the data in Example 6.2.

6.11 A grounded rectangular pipe with the cross section in Fig. 6.39 is half-filled with hydrocarbons ($\epsilon = 2.5\epsilon_o$, $\rho_o = 10^{-5}$ C/m^3). Use FEM to determine the potential along the liquid-air interface. Plot the potential versus x.

6.12 Solve the problem in Example 3.4 using the finite element method.

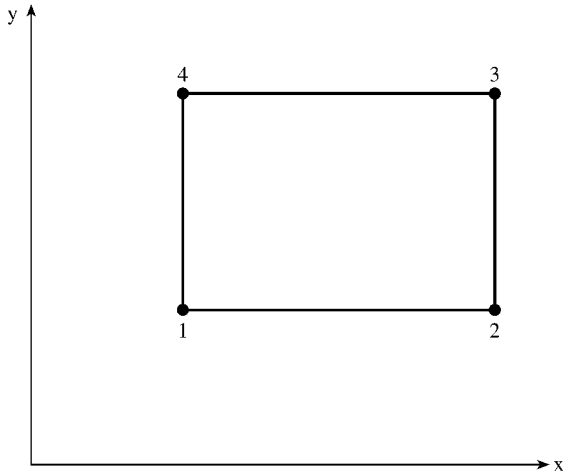

Figure 6.37
For Problem 6.6.

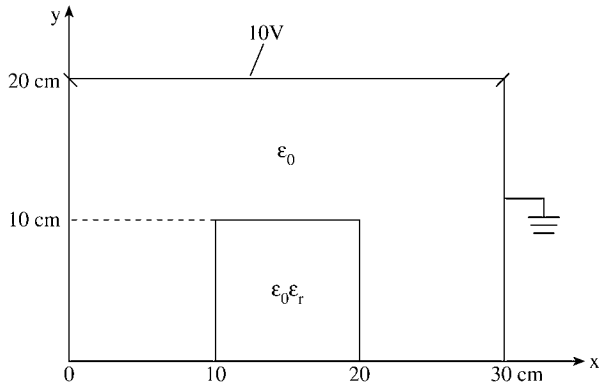

Figure 6.38
For Problem 6.7.

6.13 The cross section of an isosceles right-triangular waveguide is discretized as in Fig. 6.40. Determine the first 10 TM cutoff wavelengths of the guide.

6.14 Using FEM, determine the first 10 cutoff wavelengths of a rectangular waveguide of cross section 2 cm by 1 cm. Compare your results with exact solution. Assume the guide is air-filled.

6.15 Use the mesh generation program in Fig. 6.16 to subdivide the solution regions in Fig. 6.41. Subdivide into as many triangular elements as you choose.

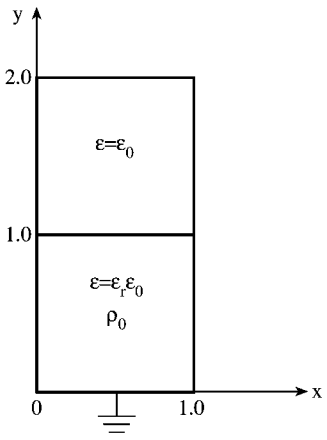

Figure 6.39
For Problem 6.11.

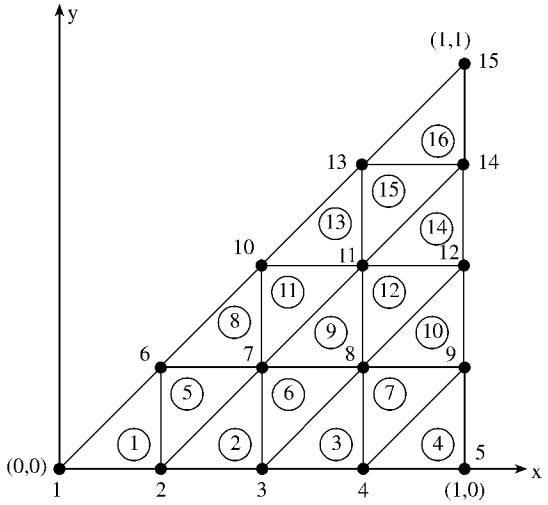

Figure 6.40
For Problem 6.13.

6.16 Determine the semi-bandwidth of the mesh shown in Fig. 6.42. Renumber the mesh so as to minimize the bandwidth.

6.17 Find the semi-bandwidth B of the mesh in Fig. 6.43. Renumber the mesh to minimize B and determine the new value of B.

6.18 Rework Problem 3.18 using the FEM.

Hint: After calculating V at all free nodes with ϵ lumped with C_{ij}, use Eq. (6.19)

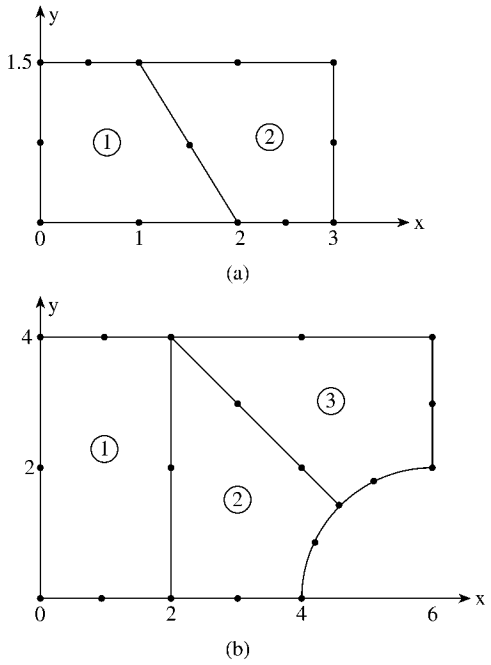

Figure 6.41
For Problem 6.15.

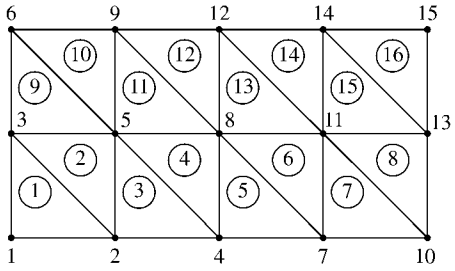

Figure 6.42
For Problem 6.16.

to calculate W, i.e.,

$$W = \frac{1}{2}[V]^t[C][V]$$

Then find the capacitance from

$$C = \frac{2W}{V_d^2}$$

where V_d is the potential difference between inner and outer conductors.

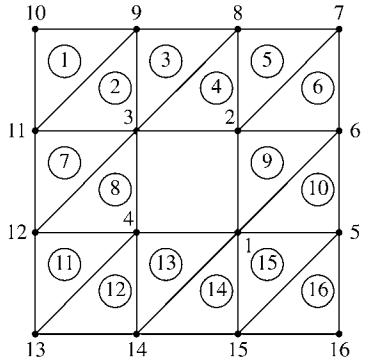

Figure 6.43
For Problem 6.17.

6.19 Verify the interpolation functions for the six-node quadratic triangular element.

6.20 Using the area coordinates (ξ_1, ξ_2, ξ_3) for the triangular element in Fig. 6.3, evaluate:

(a) $\int_S x\, dS$,
(b) $\int_S x\ dS$,
(c) $\int_S xy\, dS$

6.21 Evaluate the following integrals:

(a) $\int_S \alpha_2^3\, dS$,
(b) $\int_S \alpha_1\alpha_5\ dS$,
(c) $\int_S \alpha_1\alpha_2\alpha_3\, dS$

6.22 Evaluate the shape functions $\alpha_1, \ldots, \alpha_6$ for the second-order elements in Fig. 6.44.

6.23 Derive matrix T for $n = 2$.

6.24 By hand calculation, obtain $Q^{(2)}$ and $Q^{(3)}$ for $n = 1$ and $n = 2$.

6.25 The $D^{(q)}$ matrix is an auxilliary matrix used along with the T matrix to derive other fundamental matrices. An element of D is defined in [43] as the partial derivative of α_i with respect to ξ_q evaluated at node P_j, i.e.,

$$D_{ij}^{(q)} = \left.\frac{\partial \alpha_i}{\partial \xi_q}\right|_{P_i}, \qquad i, j = 1, 2, \ldots, m$$

where $q \in \{1, 2, 3\}$. For $n = 1$ and 2, derive $D^{(1)}$. From $D^{(1)}$, derive $D^{(2)}$ and $D^{(3)}$.

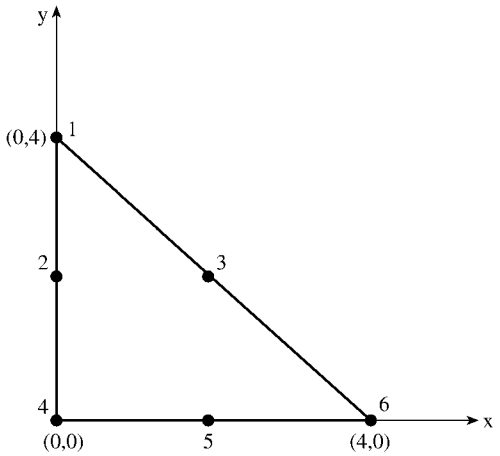

Figure 6.44
For Problem 6.22.

6.26 (a) The matrix $K^{(pq)}$ can be defined as

$$K_{ij}^{(pq)} = \iint \frac{\partial \alpha_i}{\partial \xi_p} \frac{\partial \alpha_j}{\partial \xi_q} \, dS$$

where $p, q = 1, 2, 3$. Using the $D^{(q)}$ matrix of the previous problem, show that

$$K^{(pq)} = D^{(p)} T D^{(q)^t}$$

where t denotes transposition.

(b) Show that the $Q^{(q)}$ matrix can be written as

$$Q^{(q)} = \left[D^{(q+1)} - D^{(q-1)} \right] T \left[D^{(q+1)} - D^{(q-1)} \right]^t$$

Use this formula to derive $Q^{(1)}$ for $n = 1$ and 2.

6.27 Verify the interpolation function for the 10-node tetrahedral element.

6.28 Using the volume coordinates for a tetrahedron, evaluate

$$\int z^2 \, dv$$

Assume that the origin is located at the centroid of the tetrahedron.

6.29 Obtain the T matrix for the first-order tetrahedral element.

6.30 For the tetrahedral cell, obtain the matrix M whose elements are defined by

$$M_{ij} = \frac{1}{v} \int_v \xi_i \xi_j \, dv$$

6.31 For the two-dimensional problem, the BGI sequence of operators are defined by the recurrence relation

$$B_m = \left(\frac{\partial}{\partial \rho} + jk + \frac{4m-3}{2\rho} \right) B_{m-1}$$

where $B_o = 1$. Obtain B_1 and B_2.

Chapter 7

Transmission-line-matrix Method

"Those who are quite satisfied sit still and do nothing; those who are not quite satisfied are the sole benefactors of the world." Walter S. Landor

7.1 Introduction

The link between field theory and circuit theory has been exploited in developing numerical techniques to solve certain types of partial differential equations arising in field problems with the aid of equivalent electrical networks [1]. There are three ranges in the frequency spectrum for which numerical techniques for field problems in general have been developed. In terms of the wavelength λ and the approximate dimension ℓ of the apparatus, these ranges are [2]:

$$\lambda >> \ell$$
$$\lambda \approx \ell$$
$$\lambda << \ell$$

In the first range, the special analysis techniques are known as *circuit theory;* in the second, as *microwave theory;* and in the third, as *geometric optics* (frequency independent). Hence the fundamental laws of circuit theory can be obtained from Maxwell's equations by applying an approximation valid when $\lambda >> \ell$. However, it should be noted that circuit theory was not developed by approximating Maxwell's equations, but rather was developed independently from experimentally obtained laws. The connection between circuit theory and Maxwell equations (summarizing field theory) is important; it adds to the comprehension of the fundamentals of electromagnetics. According to Silvester and Ferrari, circuits are mathematical abstractions of physically real fields; nevertheless, electrical engineers at times feel they understand circuit theory more clearly than fields [3].

The idea of replacing a complicated electrical system by a simple equivalent circuit goes back to Kirchhoff and Helmholtz. As a result of Park's [4], Kron's [5, 6] and Schwinger's [7, 8] works, the power and flexibility of equivalent circuits become more

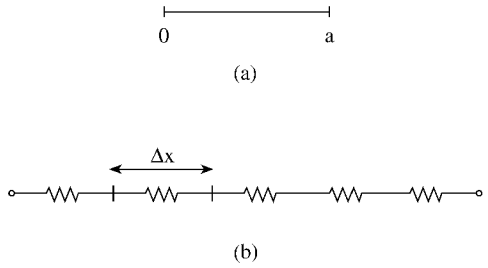

Figure 7.1
(a) One-dimensional conducting system, (b) discretized equivalent.

obvious to engineers. The recent applications of this idea to scattering problems, originally due to Johns [9], has made the method more popular and attractive.

Transmission-line modeling (TLM), otherwise known as the *transmission-line-matrix method,* is a numerical technique for solving field problems using circuit equivalent. It is based on the equivalence between Maxwell's equations and the equations for voltages and currents on a mesh of continuous two-wire transmission lines. The main feature of this method is the simplicity of formulation and programming for a wide range of applications [10, 11]. As compared with the lumped network model, the transmission-line model is more general and performs better at high frequencies where the transmission and reflection properties of geometrical discontinuities cannot be regarded as lumped [7].

Like other numerical techniques, the TLM method is a discretization process. Unlike other methods such as finite difference and finite element methods, which are mathematical discretization approaches, the TLM is a physical discretization approach. In the TLM, the discretization of a field involves replacing a continuous system by a network or array of lumped elements. For example, consider the one-dimensional system (a conducting wire) with no energy storage as in Fig. 7.1(a). The wire can be replaced by a number of lumped resistors providing a discretized equivalent in Fig. 7.1(b). The discretization of the two-dimensional, distributed field is show in Fig. 7.2. More general systems containing energy-reservoir elements as well as dissipative elements will be considered later.

The TLM method involves dividing the solution region into a rectangular mesh of transmission lines. Junctions are formed where the lines cross forming impedance discontinuities. A comparison between the transmission-line equations and Maxwell's equations allows equivalences to be drawn between voltages and currents on the lines and electromagnetic fields in the solution region. Thus, the TLM method involves two basic steps [12]:

- Replacing the field problem by the equivalent network and deriving analogy between the field and network quantities.

- Solving the equivalent network by iterative methods.

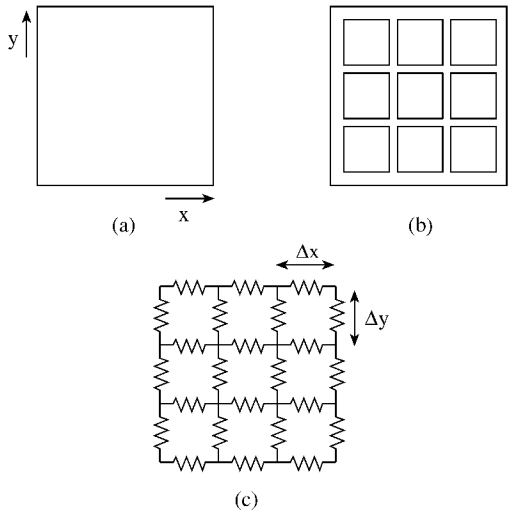

Figure 7.2
(a) Two-dimensional conductive sheet, (b) partially discretized equivalent, (c) fully discretized equivalent.

Before we apply the method, it seems fit to briefly review the basic concepts of transmission lines and then show how the TLM method can be applied to a wide range of EM-related problems.

7.2 Transmission-line Equations

Consider an elemental portion of length $\Delta\ell$ of a two-conductor transmission line. We intend to find an equivalent circuit for this line and derive the line equations. An equivalent circuit of a portion of the line is shown in Fig. 7.3, where the line parameters, R, L, G, and C are resistance per unit length, inductance per unit length, conductance per unit length, and capacitance per unit length of the line, respectively. The model in Fig. 7.3 may represent any two-conductor line. The model is called the T-type equivalent circuit; other types of equivalent circuits are possible, but we end up with the same set of equations. In the model of Fig. 7.3, we assume without loss of generality that wave propagates in the $+z$ direction, from the generator to the load.

By applying Kirchhoff's voltage law to the left loop of the circuit in Fig 7.3, we obtain

$$V(z,t) = R\frac{\Delta\ell}{2}I(z,t) + L\frac{\Delta\ell}{2}\frac{\partial I}{\partial t}(z,t) + V(z+\Delta\ell/2,t)$$

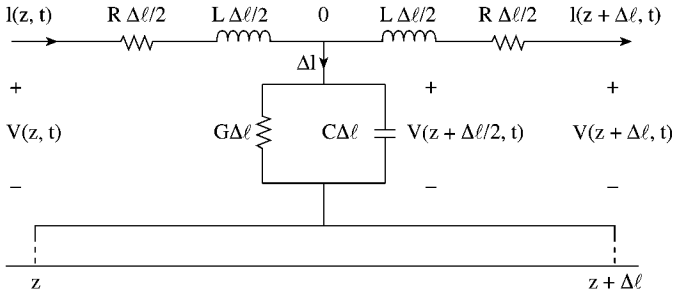

Figure 7.3

T-type equivalent circuit model of a differential length of a two conductor transmission line.

or

$$-\frac{V(z+\Delta\ell/2,t)-V(z,t)}{\Delta\ell/2}=RI(z,t)+L\frac{\partial I}{\partial t}(z,t) \tag{7.1}$$

Taking the limit of Eq. (7.1) as $\Delta\ell \rightarrow 0$ leads to

$$-\frac{\partial V(z,t)}{\partial z}=R\,I(z,t)+L\frac{\partial I}{\partial t}(z,t) \tag{7.2}$$

Similarly, applying Kirchhoff's current law to the main node of the circuit in Fig. 7.3 gives

$$\begin{aligned} I(z,t) &= I(z+\Delta\ell,t)+\Delta I \\ &= I(z+\Delta\ell,t)+G\Delta\ell V(z+\Delta\ell/2,t)+C\Delta\ell\frac{\partial V}{\partial t}(z+\Delta\ell/2,t) \end{aligned}$$

or

$$-\frac{I(z+\Delta\ell,t)-I(z,t)}{\Delta\ell}=GV(z+\Delta\ell/2,t)+C\frac{\partial V}{\partial t}(z+\Delta\ell/2,t) \tag{7.3}$$

As $\Delta\ell \rightarrow 0$, Eq. (7.3) becomes

$$-\frac{\partial I}{\partial z}(z,t)=GV(z,t)+C\frac{\partial V}{\partial t}(z,t) \tag{7.4}$$

Differentiating Eq. (7.2) with respect to z and Eq. (7.4) with respect to t, the two equations become

$$-\frac{\partial^2 V}{\partial z^2}=R\frac{\partial I}{\partial z}+L\frac{\partial^2 I}{\partial z\partial t} \tag{7.2a}$$

and

$$-\frac{\partial^2 I}{\partial t\partial z}=G\frac{\partial V}{\partial t}+C\frac{\partial^2 V}{\partial t^2} \tag{7.4a}$$

Substituting Eqs. (7.4) and (7.4a) into Eq. (7.2a) gives

$$\frac{\partial^2 V}{\partial z^2} = LC\frac{\partial^2 V}{\partial t^2} + (RC + GL)\frac{\partial V}{\partial t} + RGV \tag{7.5}$$

Similarly, we obtain the equation for current I as

$$\frac{\partial^2 I}{\partial z^2} = LC\frac{\partial^2 I}{\partial t^2} + (RC + GL)\frac{\partial I}{\partial t} + RGI \tag{7.6}$$

Equations (7.5) and (7.6) have the same mathematical form, which in general may be written as

$$\frac{\partial^2 \Phi}{\partial z^2} = LC\frac{\partial^2 \Phi}{\partial t^2} + (RC + GL)\frac{\partial \Phi}{\partial t} + RG\Phi \tag{7.7}$$

where $\Phi(z, t)$ has replaced either $V(z, t)$ or $I(z, t)$.

Ignoring certain transmission-line parameters in Eq. (7.7) leads to the following special cases [13]:

(a) $L = C = 0$ yields

$$\frac{\partial^2 \Phi}{\partial z^2} = k_1 \Phi \tag{7.8}$$

where $k_1 = RG$. Equation (7.8) is the one-dimensional elliptic partial differential equation called Poisson's equation.

(b) $R = C = 0$ or $G = L = 0$ yields

$$\frac{\partial^2 \Phi}{\partial z^2} = k_2\frac{\partial \Phi}{\partial t} \tag{7.9}$$

where $k_2 = GL$ or RC. Equation (7.9) is the one-dimensional parabolic partial differential equation called the diffusion equation.

(c) $R = G = 0$ (lossless line) yields

$$\frac{\partial^2 \Phi}{\partial z^2} = k_3\frac{\partial^2 \Phi}{\partial t^2} \tag{7.10}$$

where $k_3 = LC$. This is the one-dimensional hyperbolic partial differential equation called the Helmholtz equation, or simply the wave equation. Thus, under certain conditions, the one-dimensional transmission line can be used to model problems involving an elliptic, parabolic, or hyperbolic partial differential equation (PDE). The transmission line of Fig. 7.3 reduces to those in Fig. 7.4 for these three special cases.

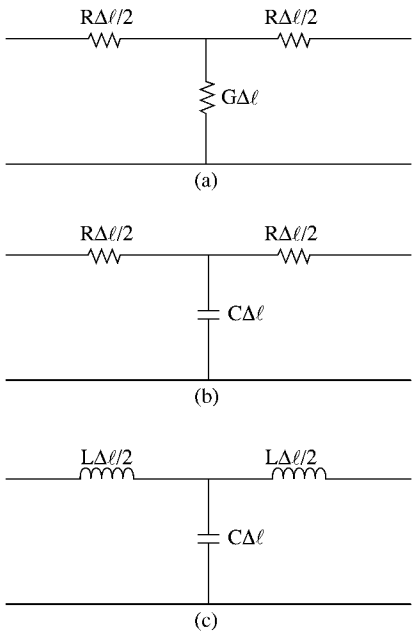

Figure 7.4
Transmission-line equivalent models for: (a) elliptic PDE, Poisson's equation, (b) parabolic PDE, diffusion equation, (c) hyperbolic PDE, wave equation.

Apart from the equivalent models, other transmission-line parameters are of interest. A detailed explanation of these parameters can be found in standard field theory texts, e.g., [14]. We briefly present these important parameters. For the lossless line in Fig. 7.4(c), the characteristic resistance

$$R_o = \sqrt{\frac{L}{C}}\,, \tag{7.11a}$$

the wave velocity

$$u = \frac{1}{\sqrt{LC}}\,, \tag{7.11b}$$

and the reflection coefficient at the load

$$\Gamma = \frac{R_L - R_o}{R_L + R_o}\,, \tag{7.11c}$$

where R_L is the load resistance.

The generality of the TLM method has been demonstrated in this section. In the following sections, the method is applied specifically to diffusion [15, 16] and wave propagation problems [10]–[13], [17, 18].

7.3 Solution of Diffusion Equation

We now apply the TLM method to the diffusion problem arising from current density distribution within a wire [15]. If the wire has a circular cross section with radius a and is infinitely long, then the problem becomes one-dimensional. We will assume sinusoidal source or harmonic fields (with time factor $e^{j\omega t}$).

The analytical solution of the problem has been treated in Example 2.3. For the TLM solution, consider the equivalent network of the cylindrical problem in Fig. 7.5, where $\Delta\ell$ is the distance between nodes or the mesh size. Applying Kirchhoff's laws to the network in Fig. 7.5 gives

$$\frac{\partial I_\rho}{\partial \rho} = -j\omega C V_\phi \tag{7.12a}$$

$$\frac{\partial V_\phi}{\partial \rho} = -R I_\rho \tag{7.12b}$$

where R and C are the resistance and capacitance per unit length.

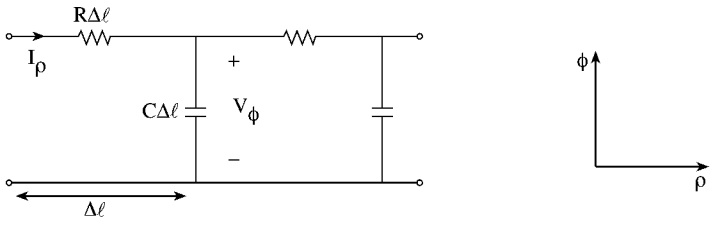

Figure 7.5
RC equivalent network.

Within the conductor, Maxwell's curl equations ($\sigma >> \omega\epsilon$) are

$$\nabla \times \mathbf{E} = -j\omega\mu\mathbf{H} \tag{7.13a}$$

$$\nabla \times \mathbf{H} = \sigma\mathbf{E} \tag{7.13b}$$

where $\mathbf{E}$ and $\mathbf{H}$ are assumed to be in phasor forms. In cylindrical coordinates, Eq. (7.13) becomes

$$-\frac{\partial E_z}{\partial \rho} = -j\omega\mu H_\phi$$

$$\frac{1}{\rho}\frac{\partial}{\partial \rho}(\rho H_\phi) = \sigma E_z$$

These equations can be written as

$$\frac{\partial E_z}{\partial \rho} = j\omega(\mu/\rho)\left(\rho H_\phi\right) \tag{7.14a}$$

$$\frac{\partial}{\partial \rho}\left(\rho H_\phi\right) = (\sigma\rho)E_z \tag{7.14b}$$

Comparing Eq. (7.12) with Eq. (7.14) leads to the following analogy between the network and field quantities:

$$\boxed{\begin{aligned} I_\rho &\equiv -E_z \\ V_\phi &\equiv \rho H_\phi \\ C &\equiv \mu/\rho \\ R &\equiv \sigma\rho \end{aligned}} \qquad \begin{aligned} &(7.15a)\\ &(7.15b)\\ &(7.15c)\\ &(7.15d) \end{aligned}$$

Therefore, solving the impedance network is equivalent to solving Maxwell's equations.

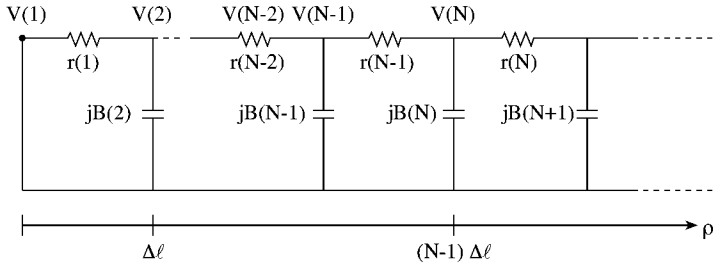

Figure 7.6
The overall equivalent network.

We can solve the overall impedance network in Fig. 7.6 by an iterative method. Since the network in Fig. 7.6 is in the form of a ladder, we apply the *ladder* method. By applying Kirchhoff's current law, the Nth nodal voltage ($N > 2$) is related to $(N-1)$th and $(N-2)$th voltages according to

$$\begin{aligned} V(N) = {} & \frac{r(N-1)}{r(N-2)}[V(N-1) - V(N-2)] \\ & + jB(N-1)r(N-1)V(N-1) + V(N-1) \end{aligned} \tag{7.16}$$

where the resistance r and susceptance B are given by

$$r(N) = R\Delta\ell = \sigma(N-0.5)(\Delta\ell)^2\,, \tag{7.17a}$$

$$B(N) = \omega C\Delta\ell = \frac{\omega\mu\Delta\ell}{(N-1)\Delta\ell} = \frac{\omega\mu}{N-1} \tag{7.17b}$$

We note that $V(1) = 0$ because the magnetic field at the center of the conductor ($\rho = 0$) is zero. Also $V(2) = I(1) \cdot r(1)$, where $I(1)$ can be arbitrarily chosen, say $I(1) = 1$. Once $V(1)$ and $V(2)$ are known, we can use Eq. (7.16) to scan all nodes in Fig. 7.6 once from left to right to determine all nodal voltages ($\equiv \rho H_\phi$) and currents ($\equiv E_z = J_z/\sigma$).

Example 7.1

Develop a computer program to determine the relative (or normalized) current density $J_z(\rho)/J_z(a)$ in a round copper wire operated at 1 GHz. Plot the relative current density against the radical position ρ/a for cases $a/\delta = 1, 2$, and 4. Take $\Delta\ell/\delta = 0.1$, $\mu = \mu_0, \sigma = 5.8 \times 10^7$ mhos/m. □

Solution

The computer program is presented in Fig. 7.7. It calculates the voltage at each node using Eqs. (7.16) and (7.17). The current on each $r(N)$ is found from Fig. 7.6 as

$$I(N-1) = \frac{V(N) - V(N-1)}{r(N-1)}$$

Since $J = \sigma E$, we obtain $J_z(\rho)/J_z(a)$ as the ratio of $I(N)$ and $I(NMAX)$, where $I(NMAX)$ is the current at $\rho = a$.

To verify the accuracy of the TLM solution, we also calculate the exact $J_z(\rho)/J_z(a)$ using Eq. (2.120). (For further details, see Example 2.3.) Table 7.1 shows a comparison between TLM results and exact results for the case $a/\delta = 4.0$. It is noticed that the percentage error is maximum (about 8%) at the center of the wire and diminishes to zero as we approach the surface of the wire. Figure 7.8 portrays the plot of the relative current density versus the radial position for cases $a/\delta = 1, 2$, and 4. ■

Table 7.1 Comparison of Relative Current Density Obtained from TLM and Exact Solutions ($a/\delta = 4.0$)

Radial position (ρ/a)	TLM result	Exact result
0.1	0.11581	0.10768
0.2	0.11765	0.11023
0.3	0.12644	0.12077
0.4	0.14953	0.14612
0.5	0.19301	0.19138
0.6	0.26150	0.26082
0.7	0.36147	0.36115
0.8	0.50423	0.50403
0.9	0.70796	0.70786
1.0	1.0	1.0

```
C=====================================================================
C USING THE TLM METHOD, THIS PROGRAM CALCULATES THE RELATIVE
C CURRENT DENSITY JR IN A ROUND COPPER WIRE
C THE EXACT SOLUTION JRE IS ALSO INCLUDED
C=====================================================================

      REAL MIU, JR(50), JRE(50)
      COMPLEX J, V(50), I(50)
      DIMENSION BERO(50), BEIO(50)
C
C FUNCTIONS FOR RESISTANCE AND SUSCEPTANCE
C
      R(N) = SIGMA*( FLOAT(N) - 0.5 )*(H**2)
      B(N) = OMEGA*MIU/FLOAT(N-1)
C
C SPECIFY INPUT DATA
C
      F = 1.0E+9
      SIGMA = 5.8E+7
      PIE = 4.0*ATAN(1.0)
      MIU = 4.0*PIE*1.0E-7
      OMEGA = 2.0*PIE*F
      DELTA = SQRT( 2.0/( SIGMA*MIU*OMEGA ) )
      H = 0.1*DELTA
      A = 4.0*DELTA
      NMAX = A/H
      J = (0.0,1)
C
C INITIALIZE AND CALCULATE RELATIVE CURRENT DENSITY JR
C USING TLM
C
      I(1) = (0.1, 0.0)
      V(1) = (0.0,0.0)
      V(2) = I(1)*R(1)
      DO 10  N = 3,NMAX + 1
      V(N) = ( R(N-1)/R(N-2) )*( V(N-1) - V(N-2) )
         1         + J*B(N-1)*R(N-1)*V(N-1)  +  V(N-1)
10    CONTINUE
      I(NMAX) = ( V(NMAX+1) - V(NMAX) )/R(NMAX)
      DO 20 N = 2,NMAX + 1
      I(N-1) = ( V(N) - V(N-1) )/R(N-1)
      JR(N-1) = CABS( I(N-1)/I(NMAX) )
20    CONTINUE
C
C CALCULATE THE CURRENT DENSITY JRE
C FROM THE EXACT SOLUTION
C
      DO 40 NRO = 1,NMAX
      BERO(NRO) = 0.0
      BEIO(NRO) = 0.0
      X = ( FLOAT(NRO)/FLOAT(NMAX) )*A*SQRT(2.0)/DELTA
      DO 30 K=0,20
      CALL FACTORIAL(K,FA)
      FB = ( (X/2.0)**(2*K) )/(FA**2)
      BERO(NRO) = BERO(NRO) + FB*COS(K*PIE/2.0)
      BEIO(NRO) = BEIO(NRO) + FB*SIN(K*PIE/2.0)
30    CONTINUE
      JRE(NRO) = SQRT( BERO(NRO)**2 + BEIO(NRO)**2 )
40    CONTINUE
      WRITE(6,50)
```

Figure 7.7

Computer program for Example 7.1 ***(Continued).***

```
0061    50      FORMAT(3X,'RADIAL POSITION',4X,'TLM J',12X,'EXACT J',/)
0062            DO 70 N=2,NMAX
0063            RHO = FLOAT(N)/FLOAT(NMAX)
0064            JRE(N) = JRE(N)/JRE(NMAX)     ! RELATIVE CURRENT DENSITY
0065            WRITE(6,60) RHO, JR(N), JRE(N)
0066    60     FORMAT(6X,F5.2,8X,F9.5,8X,F9.5,/)
0067    70     CONTINUE
0068            STOP
0069            END

0001    C ***************************************************
0002    C SUBROUTINE FOR CALCULATE K!
0003    C
0004     SUBROUTINE FACTORIAL(K,F)
0005
0006          F = 1.0
0007          IF(K.GE.2) THEN
0008          DO 10 J = 2,K
0009          F = F*FLOAT(J)
0010    10    CONTINUE
0011          ENDIF
0012          RETURN
0013          END
```

Figure 7.7
***(Cont.)* Computer program for Example 7.1.**

7.4 Solution of Wave Equations

In order to show how Maxwell's equations may be represented by the transmission-line equations, the differential length of the lossless transmission line between two nodes of the mesh is represented by lumped inductors and capacitors as shown in Fig. 7.9 for two-dimensional wave propagation problems [17, 18]. At the nodes, pairs of transmission lines form impedance discontinuity. The complete network of transmission-line-matrix is made up of a large number of such building blocks as depicted in Fig. 7.10. Notice that in Fig. 7.10 single lines are used to represent a transmission-line pair. Also, a uniform internodal distance of $\Delta\ell$ is assumed throughout the matrix (i.e., $\Delta\ell = \Delta x = \Delta z$). We shall first derive equivalences between network and field quantities.

7.4.1 Equivalence Between Network and Field Parameters

We refer to Fig. 7.9 and apply Kirchhoff's current law at node O to obtain

$$I_x(x - \Delta\ell/2) - I_x(x + \Delta\ell/2) + I_z(z - \Delta\ell/2) - I_z(z + \Delta\ell/2) = 2C\Delta\ell\frac{\partial V_y}{\partial t}$$

Dividing through by $\Delta\ell$ gives

$$\frac{I_x(x - \Delta\ell/2) - I_x(x + \Delta\ell/2)}{\Delta\ell} + \frac{I_z(z - \Delta\ell/2) - I_z(z + \Delta\ell/2)}{\Delta\ell} = 2C\frac{\partial V_y}{\partial t}$$

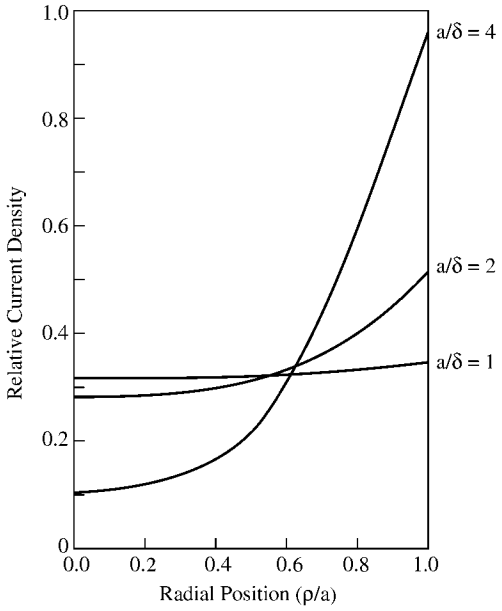

Figure 7.8
Relative current density versus radial position.

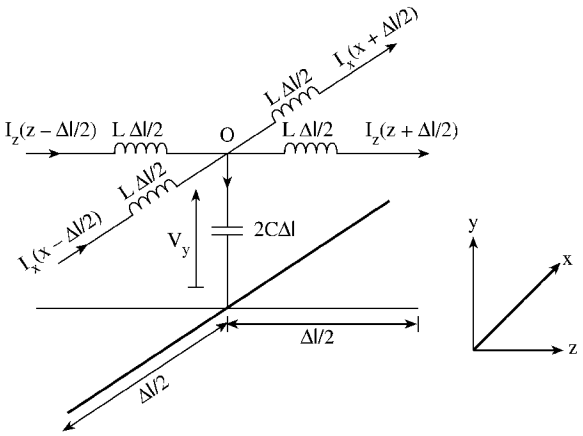

Figure 7.9
Equivalent network of a two-dimensional TLM shunt node.

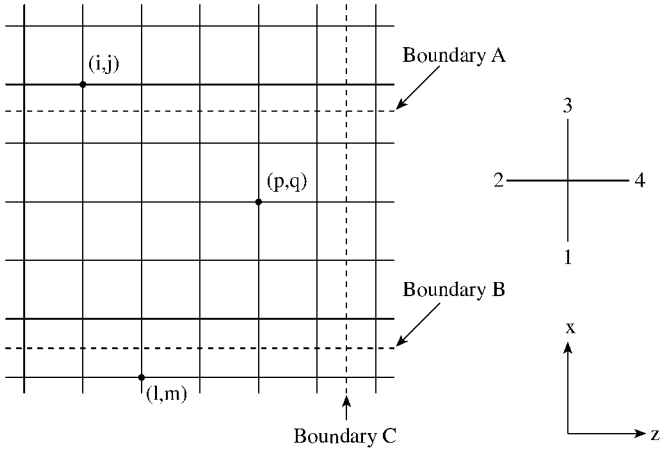

Figure 7.10
Transmission-line matrix and boundaries.

Taking the limit as $\Delta\ell \rightarrow 0$ results in

$$-\frac{\partial I_z}{\partial z} - \frac{\partial I_x}{\partial x} = 2C\frac{\partial V_y}{\partial t} \tag{7.18a}$$

Applying Kirchhoff's voltage law around the loop in the $x - y$ plane gives

$$V_y(x - \Delta\ell/2) - L\Delta\ell/2\frac{\partial I_x(x - \Delta\ell/2)}{\partial t}$$
$$-L\Delta\ell/2\frac{\partial I_x(x + \Delta\ell/2)}{\partial t} - V_y(x + \Delta\ell/2) = 0$$

Upon rearranging and dividing by $\Delta\ell$, we have

$$\frac{V_y(x - \Delta\ell/2) - V_y(x + \Delta\ell/2)}{\Delta\ell} = \frac{L}{2}\frac{\partial I_x(x - \Delta\ell/2)}{\partial t} + \frac{L}{2}\frac{\partial I_x(x + \Delta\ell/2)}{\partial t}$$

Again, taking the limit as $\Delta\ell \rightarrow 0$ gives

$$\frac{\partial V_y}{\partial x} = -L\frac{\partial I_x}{\partial t} \tag{7.18b}$$

Taking similar steps on the loop in the $y - z$ plane yields

$$\frac{\partial V_y}{\partial z} = -L\frac{\partial I_z}{\partial t} \tag{7.18c}$$

These equations will now be combined to form a wave equation. Differentiating Eq. (7.18a) with respect to t, Eq. (7.18b) with respect to x, and Eq. (7.18c) with

respect to z, we have

$$-\frac{\partial^2 I_z}{\partial z \partial t} - \frac{\partial^2 I_x}{\partial x \partial t} = 2C\frac{\partial^2 V_y}{\partial t^2} \tag{7.19a}$$

$$\frac{\partial^2 V_y}{\partial x^2} = -L\frac{\partial^2 I_x}{\partial t \partial x} \tag{7.19b}$$

$$\frac{\partial^2 V_y}{\partial z^2} = -L\frac{\partial^2 I_z}{\partial t \partial z} \tag{7.19c}$$

Substituting Eqs. (7.19b) and (7.19c) into Eq. (7.19a) leads to

$$\frac{\partial^2 V_y}{\partial x^2} + \frac{\partial^2 V_y}{\partial z^2} = 2LC\frac{\partial^2 V_y}{\partial t^2} \tag{7.20}$$

Equation (7.20) is the Helmholtz wave equation in two-dimensional space.

In order to show the field theory equivalence of Eqs. (7.19) and (7.20), consider Maxwell's equations

$$\nabla \times \mathbf{E} = -\mu\frac{\partial \mathbf{H}}{\partial t} \tag{7.21a}$$

and

$$\nabla \times \mathbf{H} = \epsilon\frac{\partial \mathbf{E}}{\partial t} \tag{7.21b}$$

Expansion of Eq. (7.21) in the rectangular coordinate system yields

$$\frac{\partial E_z}{\partial y} - \frac{\partial E_y}{\partial z} = -\mu\frac{\partial H_x}{\partial t}\,, \tag{7.22a}$$

$$\frac{\partial E_x}{\partial z} - \frac{\partial E_z}{\partial x} = -\mu\frac{\partial H_y}{\partial t}\,, \tag{7.22b}$$

$$\frac{\partial E_y}{\partial x} - \frac{\partial E_x}{\partial y} = -\mu\frac{\partial H_z}{\partial t}\,, \tag{7.22c}$$

$$\frac{\partial H_z}{\partial y} - \frac{\partial H_y}{\partial z} = \epsilon\frac{\partial E_x}{\partial t}\,, \tag{7.22d}$$

$$\frac{\partial H_x}{\partial z} - \frac{\partial H_z}{\partial x} = \epsilon\frac{\partial E_y}{\partial t}\,, \tag{7.22e}$$

$$\frac{\partial H_y}{\partial x} - \frac{\partial H_x}{\partial y} = \epsilon\frac{\partial E_z}{\partial t} \tag{7.22f}$$

Consider the situation for which $E_x = E_z = H_y = 0, \dfrac{\partial}{\partial y} = 0$. It is noticed at once that this mode is a transverse electric (TE) mode with respect to the z-axis but a transverse magnetic (TM) mode with respect to the y-axis. Thus by the principle of duality, the network in Fig. 7.9 can be used for E_y, H_x, H_z fields as well as for

E_x, E_z, H_y fields. A network capable of reproducing TE waves is also capable of reproducing TM waves. For TE waves, Eq. (7.22) reduces to

$$\frac{\partial H_x}{\partial z} - \frac{\partial H_z}{\partial x} = \epsilon \frac{\partial E_y}{\partial t} , \tag{7.23a}$$

$$\frac{\partial E_y}{\partial x} = -\mu \frac{\partial H_z}{\partial t} , \tag{7.23b}$$

$$\frac{\partial E_y}{\partial z} = \mu \frac{\partial H_x}{\partial t} \tag{7.23c}$$

Taking similar steps on Eqs. (7.23a)–(7.23c) as were taken for Eqs. (7.18a)–(7.18c) results in another Helmholtz equation

$$\frac{\partial^2 E_y}{\partial x^2} + \frac{\partial^2 E_y}{\partial z^2} = \mu\epsilon \frac{\partial^2 E_y}{\partial t^2} \tag{7.24}$$

Comparing Eqs. (7.23) and (7.24) with Eqs. 7.18 and (7.20) yields the following equivalence between the parameters

$$\boxed{\begin{aligned} E_y &\equiv V_y \\ H_x &\equiv -I_z \\ H_z &\equiv I_x \\ \mu &\equiv L \\ \epsilon &\equiv 2C \end{aligned}} \tag{7.25}$$

Thus in the equivalent circuit:

- the voltage at shunt node is E_y,
- the current in the z direction is $-H_x$,
- the current in the x direction is H_z,
- the inductance per unit length represents the permeability of the medium,
- twice the capacitance per unit length represents the permittivity of the medium.

7.4.2 Dispersion Relation of Propagation Velocity

For the basic transmission line in the TLM which has $\mu_r = \epsilon_r = 1$, the inductance and capacitance per unit length are related by [8]

$$\frac{1}{\sqrt{(LC)}} = \frac{1}{\sqrt{(\mu_0 \epsilon_0)}} = c \tag{7.26}$$

where $c = 3 \times 10^8$ m/s is the speed of light in vacuum. Notice from Eq. (7.26) that for the equivalence made in Eq. (7.25), if voltage and current waves on each transmission line component propagate at the speed of light c, the complete network

of intersecting transmission lines represents a medium of relative permittivity twice that of free space. This implies that as long as the equivalent circuit in Fig. 7.9 is valid, the propagation velocity in the TLM mesh is $1/\sqrt{2}$ of the velocity of light. The manner in which wave propagates on the mesh is now derived.

If the ratio of the length of the transmission-line element to the free-space wavelength of the wave is $\theta/2\pi = \Delta\ell/\lambda$ (θ is called the *electrical length* of the line), the voltage and current at node i are related to those at node $i+1$ by the transfer-matrix equation (see Prob. 7.2) given as [19]

$$\begin{bmatrix} V_i \\ I_i \end{bmatrix} = \begin{bmatrix} (\cos\theta/2) & (j\sin\theta/2) \\ (j\sin\theta/2) & (\cos\theta/2) \end{bmatrix} \begin{bmatrix} 1 & 0 \\ (2j\tan\theta/2) & 1 \end{bmatrix} \begin{bmatrix} (\cos\theta/2) & (j\sin\theta/2) \\ (j\sin\theta/2) & (\cos\theta/2) \end{bmatrix} \begin{bmatrix} V_{i+1} \\ I_{i+1} \end{bmatrix} \tag{7.27}$$

If the waves on the periodic structure have a propagation constant $\gamma_n = \alpha_n + j\beta_n$, then

$$\begin{bmatrix} V_i \\ I_i \end{bmatrix} = \begin{bmatrix} e^{\gamma_n \Delta\ell} & 0 \\ 0 & e^{\gamma_n \Delta\ell} \end{bmatrix} \begin{bmatrix} V_{i+1} \\ I_{i+1} \end{bmatrix} \tag{7.28}$$

Solution of Eqs. (7.27) and (7.28) gives

$$\cosh(\gamma_n \Delta\ell) = \cos(\theta) - \tan(\theta/2)\sin(\theta) \tag{7.29}$$

This equation describes the range of frequencies over which propagation can take place (passbands), i.e.,

$$|\cos(\theta) - \tan(\theta/2)\sin(\theta)| < 1\,, \tag{7.30a}$$

and the range of frequencies over which propagation cannot occur (stop-bands), i.e.,

$$|\cos(\theta) - \tan(\theta/2)\sin(\theta)| > 1 \tag{7.30b}$$

For the lowest frequency propagation region,

$$\gamma_n = j\beta_n \tag{7.31a}$$

and

$$\theta = \frac{2\pi\Delta\ell}{\lambda} = \frac{\omega}{c}\Delta\ell \tag{7.31b}$$

Introducing Eq. (7.31) in Eq. (7.29), we obtain

$$\cos(\beta_n \Delta\ell) = \cos\left(\frac{\omega\Delta\ell}{c}\right) - \tan\left(\frac{\omega\Delta\ell}{2c}\right)\sin\left(\frac{\omega\Delta\ell}{c}\right) \tag{7.32}$$

Applying trigonometric identities

$$\sin(2A) = 2\sin(A)\cos(A)$$

and

$$\cos(2A) = 1 - 2\sin^2(A)$$

to Eq. (7.32) results in

$$\sin\left(\frac{\beta_n \Delta\ell}{2}\right) = \sqrt{2}\sin\left(\frac{\omega\Delta\ell}{2c}\right) \tag{7.33}$$

which is a transcendental equation. If we let r be the ratio of the velocity u_n of the waves on the network to the free-space wave velocity c, then

$$r = u_n/c = \frac{\omega}{\beta_n c} = \frac{2\pi}{\lambda\beta_n} \tag{7.34a}$$

or

$$\beta_n = \frac{2\pi}{\lambda r} \tag{7.34b}$$

Substituting Eqs. (7.34) into Eq. (7.33), the transcendental equation becomes

$$\sin\left(\frac{\pi}{r}\cdot\frac{\Delta\ell}{\lambda}\right) = \sqrt{2}\sin\left(\frac{\pi\Delta\ell}{\lambda}\right) \tag{7.35}$$

By selecting different values of $\Delta\ell/\lambda$, the corresponding values of $r = u_n/c$ can be obtained numerically as in Fig. 7.11 for two-dimensional problems. From Fig. 7.11, we conclude that the TLM can only represent Maxwell's equations over the range of frequencies from zero to the first network cutoff frequency, which occurs at $\omega\Delta\ell/c = \pi/2$ or $\Delta\ell/\lambda = 1/4$. Over this range, the velocity of the waves behaves according to the characteristic of Fig. 7.11. For frequencies much smaller than the network cutoff frequency, the propagation velocity approximates to $1/\sqrt{2}$ of the free-space velocity.

Following the same procedure, the dispersion relation for three-dimensional problems can be derived as

$$\sin\left(\frac{\pi}{r}\cdot\frac{\Delta\ell}{\lambda}\right) = 2\sin\left(\pi\frac{\Delta\ell}{\lambda}\right) \tag{7.36}$$

Thus for low frequencies ($\Delta\ell/\lambda < 0.1$), the network propagation velocity in three-dimensional space may be considered constant and equal to $c/2$.

7.4.3 Scattering Matrix

If ${}_kV_n^i$ and ${}_kV_n^r$ are the voltage impulses incident upon and reflected from terminal n of a node at time $t = k\Delta\ell/c$, we derive the relationship between the two quantities as follows. Let us assume that a voltage impulse function of unit magnitude is launched

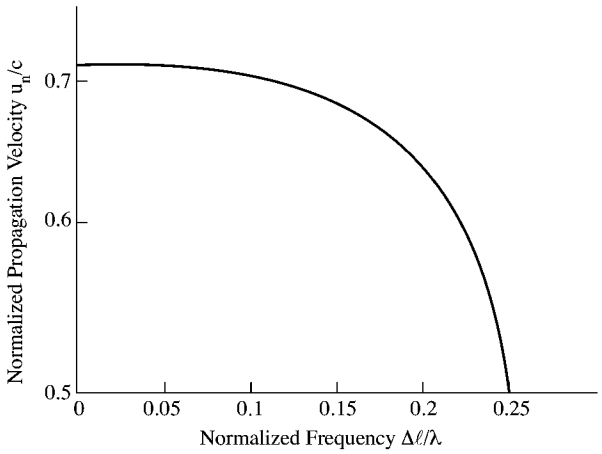

Figure 7.11
Dispersion of the velocity of waves in a two-dimensional TLM network.

into terminal 1 of a node, as shown in Fig. 7.12(a), and that the characteristic resistance of the line is normalized. A unit-magnitude delta function of voltage and current will then travel towards the junction with unit energy ($S_i = 1$). Since line 1 has three other lines joined to it, its effective terminal resistance is 1/3. With the knowledge of its reflection coefficient, both the reflected and transmitted voltage impulses can be calculated. The reflection coefficient is

$$\Gamma = \frac{R_L - R_o}{R_L + R_o} = \frac{1/3 - 1}{1/3 + 1} = -\frac{1}{2} \tag{7.37}$$

so that the reflected and transmitted energies are

$$S_r = S_i \Gamma^2 = \frac{1}{4} \tag{7.38a}$$

$$S_t = S_i \left(1 - \Gamma^2\right) = \frac{3}{4} \tag{7.38b}$$

where subscripts i, r, and t indicate incident, reflected, and transmitted quantities, respectively. Thus a voltage impulse of $-1/2$ is reflected back in terminal 1, while a voltage impulse of $1/2 = [\frac{3}{4} \div 3]^{1/2}$ will be launched into each of the other three terminals as shown in Fig. 7.12(b).

The more general case of four impulses being incident on four branches of a node can be obtained by applying the superposition principle to the previous case of a single pulse. Hence, if at time $t = k\Delta\ell/c$, voltage impulses ${}_kV_1^i$, ${}_kV_2^i$, ${}_kV_3^i$, and ${}_kV_4^i$ are incident on lines 1 to 4, respectively, at any node as in Fig. 7.12(c), the combined voltage reflected along line 1 at time $t = (k+1)\Delta\ell/c$ will be [9, 10]

$${}_{k+1}V_1^r = \frac{1}{2}\left\langle {}_kV_2^i + {}_kV_3^i + {}_kV_4^i - {}_kV_1^i \right\rangle \tag{7.39}$$

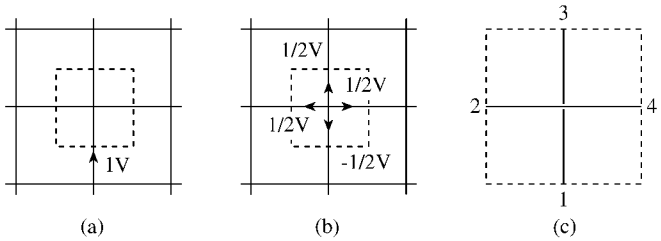

Figure 7.12
The impulse response of a node in a matrix.

In general, the total voltage impulse reflected along line n at time $t = (k+1)\Delta\ell/c$ will be

$$ {}_{k+1}V_n^r = \frac{1}{2}\left[\sum_{m=1}^{4} {}_kV_m^i\right] - {}_kV_n^i, \qquad n = 1, 2, 3, 4 \tag{7.40} $$

This idea is conveniently described by a *scattering matrix* equation relating the reflected voltages at time $(k+1)\Delta\ell/c$ to the incident voltages at the previous time step $k\Delta\ell/c$:

$$ \boxed{ {}_{k+1}\begin{bmatrix} V_1 \\ V_2 \\ V_3 \\ V_4 \end{bmatrix}^r = \frac{1}{2}\begin{bmatrix} -1 & 1 & 1 & 1 \\ 1 & -1 & 1 & 1 \\ 1 & 1 & -1 & 1 \\ 1 & 1 & 1 & -1 \end{bmatrix} {}_k\begin{bmatrix} V_1 \\ V_2 \\ V_3 \\ V_4 \end{bmatrix}^i } \tag{7.41} $$

Also an impulse emerging from a node at position (z, x) in the mesh (reflected impulse) becomes automatically an incident impulse at the neighboring node. Hence

$$ \boxed{ \begin{aligned} {}_{k+1}V_1^i(z, x+\Delta\ell) &= {}_{k+1}V_3^r(z, x) \\ {}_{k+1}V_2^i(z+\Delta\ell, x) &= {}_{k+1}V_4^r(z, x) \\ {}_{k+1}V_3^i(z, x-\Delta\ell) &= {}_{k+1}V_1^r(z, x) \\ {}_{k+1}V_4^i(z-\Delta\ell, x) &= {}_{k+1}V_2^r(z, x) \end{aligned} } \tag{7.42} $$

Thus by applying Eqs. (7.41) and (7.42), the magnitudes, positions, and directions of all impulses at time $(k+1)\Delta\ell/c$ can be obtained at each node in the network provided that their corresponding values at time $k\Delta\ell/c$ are known. The impulse response may, therefore, be found by initially fixing the magnitude, position, and direction of travel of impulse voltages at time $t = 0$, and then calculating the state of the network at successive time intervals. The scattering process forms the basic algorithm of the TLM method [10, 17].

The propagating of pulses in the TLM model is illustrated in Fig. 7.13, where the first two iterations following an initial excitation pulse in a two-dimensional shunt-

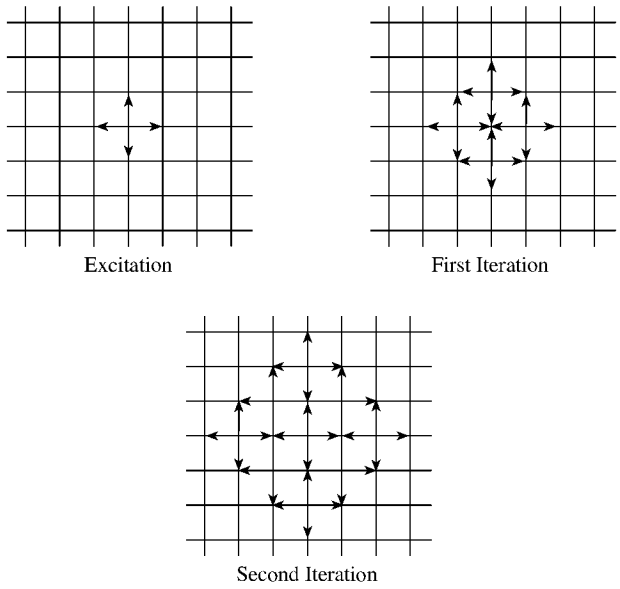

Figure 7.13
Scattering in a two-dimensional TLM network excited by a Dirac impulse.

connected TLM are shown. We have assumed free-space propagation for the sake of simplicity.

7.4.4 Boundary Representation

Boundaries are usually placed halfway between two nodes in order to ensure synchronism. In practice, this is achieved by making the mesh size $\Delta\ell$ an integer fraction of the structure's dimensions.

Any resistive load at boundary C (see Fig. 7.10) may be simulated by introducing a reflection coefficient Γ

$$ {}_{k+1}V_4^i(p,q) = {}_kV_2^r(p+1,q) = \Gamma\left[{}_kV_4^r(p,q)\right] \tag{7.43} $$

where

$$ \Gamma = \frac{R_s - 1}{R_s + 1} \tag{7.44} $$

and R_s is the surface resistance of the boundary normalized by the line characteristic impedance. If, for example, a perfectly conducting wall ($R_s = 0$) is to be simulated along boundary C, Eq. (7.44) gives $\Gamma = -1$, which represents a short circuit, and

$$ {}_{k+1}V_4^i(p,q) = -{}_kV_4^r(p,q) \tag{7.45} $$

is used in the simulation. For waves striking the boundary at arbitrary angles of incidence, a method for modeling free-space boundaries is discussed in [20].

7.4.5 Computation of Fields and Frequency Response

We continue with the TE mode of Eq. (7.23) as our example and calculate E_y, H_x, and H_z. E_y at any point corresponds to the node voltage at the point, H_z corresponds to the net current entering the node in the x direction (see Eq. (7.25)), while H_x is the net current in the negative z direction. For any point ($z = m, x = n$) on the grid of Fig. 7.10, we have for each kth transient time

$$ {}_kE_y(m,n) = \frac{1}{2}\left[{}_kV_1^i(m,n) + {}_kV_2^i(m,n) + {}_kV_3^i(m,n) + {}_kV_4^i(m,n)\right] \quad (7.46) $$

$$ -{}_kH_x(m,n) = {}_kV_2^i(m,n) - {}_kV_4^i(m,n)\,, \quad (7.47) $$

and

$$ {}_kH_z(m,n) = {}_kV_3^i(m,n) - {}_kV_1^i(m,n) \quad (7.48) $$

Thus, a series of discrete delta-function of magnitudes E_y, H_x, and H_z corresponding to time intervals of $\Delta\ell/c$ are obtained by the iteration of Eqs. (7.41) and (7.42). (Notice that reflections at the boundaries A and B in Fig. 7.10 will cancel out, thus $H_z = 0$.) Any point in the mesh can serve as an output or observation point. Equations (7.46) to (7.48) provide the output-impulse functions for the point representing the response of the system to an impulsive excitation. These output functions may be used to obtain the output waveform. For example, the output waveform corresponding to a pulse input may be obtained by convolving the output-impulse function with the shape of the input pulse.

Sometimes we are interested in the response to a sinusoidal excitation. This is obtained by taking the Fourier transform of the impulse response. Since the response is a series of delta functions, the Fourier transform integral becomes a summation, and the real and imaginary parts of the output spectrum are given by [9, 10]

$$ \boxed{\mathrm{Re}\,[F(\Delta\ell/\lambda)] = \sum_{k=1}^{N} {}_kI \cos\left(\frac{2\pi k\Delta\ell}{\lambda}\right)} \quad (7.49a) $$

$$ \boxed{\mathrm{Im}\,[F(\Delta\ell/\lambda)] = \sum_{k=1}^{N} {}_kI \sin\left(\frac{2\pi k\Delta\ell}{\lambda}\right)} \quad (7.49b) $$

where $F(\Delta\ell/\lambda)$ is the frequency response, ${}_kI$ is the value of the output impulse response at time $t = k\Delta\ell/c$, and N is the total number of time intervals for which the calculation is made. Henceforth, N will be referred to as the number of iterations.

7.4.6 Output Response and Accuracy of Results

The output impulse function, in terms of voltage or current, may be taken from any point in the TLM mesh. It consists of a train of impulses of varying magnitude in the time domain separated by a time interval $\Delta\ell/c$. Thus, the frequency response obtained

by taking the Fourier transform of the output response consists of series of delta functions in the frequency domain corresponding to the discrete modal frequencies for which a solution exists. For practical reasons, the output response has to be truncated, and this results in a spreading of the solution delta function $\sin x/x$ type of curves.

To investigate the accuracy of the result, let the output response be truncated after N iterations. Let $V_{out}(t)$ be the output impulse function taken within $0 < t < N\Delta\ell/c$. We may regard $V_{out}(t)$ as an impulse function $V_\infty(t)$, taken within $0 < t < \infty$, multiplied by a unit pulse function $V_p(t)$ of width $N\Delta\ell/c$, i.e.,

$$V_{out}(t) = V_\infty(t) \times V_p(t) \tag{7.50}$$

where

$$V_p = \begin{cases} 1, & 0 \le t \le N\Delta\ell/c \\ 0, & \text{elsewhere} \end{cases} \tag{7.51}$$

Let $S_{out}(f)$, $S_\infty(f)$, and $S_p(f)$ be the Fourier transform of $V_{out}(t)$, $V_\infty(t)$, and $V_p(t)$, respectively. The Fourier transform of Eq. (7.50) is the convolution of $S_\infty(f)$ and $S_p(f)$. Hence

$$S_{out}(f) = \int_{-\infty}^{\infty} S_\infty(\alpha) S_p(f-\alpha)\, d\alpha \tag{7.52}$$

where

$$S_p(f) = \frac{N\Delta\ell}{c} \frac{\sin \dfrac{\pi N\Delta\ell f}{c}}{\dfrac{\pi N\Delta\ell f}{c}} e^{-(\pi N\Delta\ell f)/c} \tag{7.53}$$

which is of the form $\sin x/x$. Equations (7.52) and (7.53) show that $S_p(f)$ is placed in each of the positions of the exact response $S_\infty(f)$. Since the greater the number of iterations N the sharper the maximum peak of the curve, the accuracy of the result depends on N. Thus the solution of a wave equation by TLM method involves the following four steps [21]:

1. Space discretization: The solution region is divided into a number of blocks to fit the geometrical and frequency requirements. Each block is replaced by a network of transmission lines interconnected to form a "node." Transmission lines from adjacent nodes are connected to form a mesh describing the entire solution region.

2. Excitation: This involves imposing the initial conditions and source terms.

3. Scattering: With the use of the scattering matrix, pulses propagate along transmission lines toward each node. At each new time step, a multiple of propagation time δt, scattered pulses from each node become incident on adjacent nodes. The scattering and connection processes may be repeated to simulate propagation for any desired length of time.

4. Output: At any time step, voltages and currents on transmission lines are available. These represent the electric and magnetic fields corresponding to the particular problem and excitation. The quantities available at each time step are the solution in the time domain — there is no need for an iterative solution procedure. If desired, frequency-domain information may be obtained by using Fourier transform techniques.

The following examples are taken from Johns's work [9, 18].

Example 7.2

The FORTRAN program in Fig. 7.14 is for the numerical calculations of one-dimensional TEM wave problems. It should be mentioned that the computer program in this example and the following ones are modified versions of those in Agba [22]. The calculations were carried out on a 25 by 11 rectangular matrix. TEM field-continuation boundaries were fixed along $x = 2$ and $x = 10$, producing boundaries, in effect, along the lines $x = 1.5$ and $x = 10.5$. The initial impulse excitation was on all points along the line $z = 4$, and the field along this line was set to zero at all subsequent time intervals. In this way, interference from boundaries to the left of the excitation line was avoided. Calculations in the z direction were terminated at $z = 24$, so that no reflections were received from points at $z = 25$ in the matrix, and the boundary C in Fig. 7.10, situated at $z = 24.5$, was therefore matched to free space. The output-impulse response for E_y and H_x was taken at the point $z = 14, x = 6$, which is 10.5 mesh points away from the boundary C, for 100, 150, and 200 iterations.

Since the velocity of waves on the matrix is less than that in free space by a factor u_n/c (see Fig. 7.11), the effective intrinsic impedance presented by the network matrix is less by the same factor. The magnitude of the wave impedance on the matrix, normalized to the intrinsic impedance of free space, is given by $Z = |E_y|/|H_x|$ and is tabulated in Table 7.2, together with Arg(Z), for the various numbers of iterations made. A comparison is made with the exact impedance values [14]. □

Table 7.2 Normalized Impedance of a TEM Wave with Free-Space Discontinuity

	TLM results						Exact results	
$\Delta\ell/\lambda$	$\|Z\|$	Arg(Z)	$\|Z\|$	Arg(Z)	$\|Z\|$	Arg(Z)	$\|Z\|$	Arg(Z)
Number of iterations	100		150		200			
0.002	0.9789	−0.1368	0.9730	−0.1396	0.9781	−0.1253	0.9747	−0.1282
0.004	0.9028	−0.2432	0.8980	−0.2322	0.9072	−0.2400	0.9077	−0.2356
0.006	0.8114	−0.3068	0.8229	−0.2979	0.8170	−0.3046	0.8185	−0.3081
0.008	0.7238	−0.3307	0.7328	−0.3457	0.7287	−0.3404	0.7256	−0.3390
0.010	0.6455	−0.3201	0.6367	−0.3350	0.6396	−0.3281	0.6414	−0.3263
0.012	0.5783	−0.2730	0.5694	−0.2619	0.5742	−0.2680	0.5731	−0.2707
0.014	0.5272	−0.1850	0.5313	−0.1712	0.5266	−0.1797	0.5255	−0.1765
0.016	0.4993	−0.0609	0.5043	−0.0657	0.5009	−0.0538	0.5018	−0.0545
0.018	0.5002	−0.0790	0.4987	−0.0748	0.5057	−0.0785	0.5057	0.0768

```
0001    C ********************************************************
0002    C THIS PROGRAM APPLIES THE TLM METHOD TO SOLVE
0003    C ONE-DIMENSIONAL WAVE PROBLEMS. THE SPECIFIC EXAMPLE
0004    C SOLVED HERE IS DESCRIBED AS FOLLOWS:-
0005    C
0006    C THE TEM WAVES ON A 25 X 11 MATRIX
0007    C THE BOUNDARIES ARE AT X = 2 AND X = 10.
0008    C INITIAL IMPULSE EXCITATION IS ALONG Z = 4 AT t = 0
0009    C AND SUBSEQUENTLY THIS LINE IS SET TO ZERO. THE GRID
0010    C IS TERMINATED AT Z = 25. OUTPUT IS TAKEN AT Z = 14,
0011    C X = 6 FOR Ey AND Hx FOR 100,150,200 ITERATIONS
0012    C VI(IT,I,J,K) -- ARRAY FOR INCIDENT VOLTAGE
0013    C VR(IT,I,J,K) -- ARRAY FOR REFLECTED VOLTAGE
0014    C IT = 1        -- FOR PREVIOUS PULSE VALUE
0015    C    = 2       -- FOR CURRENT PULSE VALUE
0016    C I,J       -- CORRESPOND TO NODE LOCATION (Z,X)
0017    C K = 1 ..4     -- FOR TERMINALS, SEE FIG. 6C
0018    C NX            -- INDEX OF NODES IN X-DIRECTION
0019    C NZ       -- INDEX OF NODES IN Z-DIRECTION
0020    C NX/NZ B,E     -- INDEX OF BEGINNING,END NODE
0021    C NX/NZ O       -- INDEX OF OUTPUT NODE
0022    C       GAMMA         -- REFLECTION COEFFICIENT AT
0023    C                        THE BOUNDARY C
0024    C       DELTA         -- MESH SIZE DIVIDED BY LAMDA
0025    C       ITRATE        -- NO. OF ITERATIONS
0026    C*************************************************************
0027
0028            IMPLICIT  INTEGER*2(I-N),REAL*8(A,D-H,O-Y),
0029         1            COMPLEX*8(C,Z)
0030            DIMENSION VI(2,25,11,4),VR(2,25,11,4),
0031         1            OUT(20,10),EFI(20),EFR(20),
0032         2    HFI(20),HFR(20)
0033
0034           DATA NXB,NXE,NZB,NZE,NT,ITRATE/2,10,4,24,4,200/
0035           DATA NXO,NZO,PIE,GAMMA,DELTA/6,14,3.1415927,0,.002/
0036
0037    C STEP #1 ********************************************
0038    C INSERT INITIAL PULSE EXCITATION ALONG LINE Z = 4
0039    C
0040           DO 10 J = NXB, NXE
0041    10   VI(1,NZB+1,J,2) = 1.0
0042    C
0043    C STEP #2 ********************************************
0044    C USING EQS. (7.40) TO (7.42), CALCULATE THE
0045    C REFLECTED VOLTAGE AND SUBMIT IT DIRECTLY
0046    C TO THE NEIGHBORING NODE.
0047    C
0048            DO 90 ITIME = 1, ITRATE
0049                 IT = 2
0050            DO 50 I  = NZB+1, NZE
0051            DO 50 J  = NXB, NXE
0052              SUM = 0.0
0053            DO 20 K = 1, NT
0054    20        SUM = SUM + VI(IT-1,I,J,K)
0055            DO 30 K = 1, NT
0056            VR(IT,I,J,K) = 0.5*SUM - VI(IT-1,I,J,K)
0057    30    CONTINUE
0058    40    CONTINUE
0059               VI(IT,I,J-1,3) = VR(IT,I,J,1)
0060               VI(IT,I-1,J,4) = VR(IT,I,J,2)
```

Figure 7.14
Computer program for Example 7.2 *(Continued)*.

```
0061              VI(IT,I,J+1,1) = VR(IT,I,J,3)
0062              VI(IT,I+1,J,2) = VR(IT,I,J,4)
0063     C
0064     C STEP #3 *********************************************
0065     C USING EQS. (7.43) AND (7.44), INSERT BOUNDARY CONDITIONS
0066     C
0067              IF(J .EQ. NXE)VI(IT,I,NXE,3)=VR(IT,I,NXE,1)
0068              IF(J .EQ  NXB)VI(IT,I,NXB,1)=VR(IT,I,NXB,3)
0069              IF(I .EQ  NZE)VI(IT,NZE,J,4)=GAMMA*VR(IT,NZE,J,4)
0070
0071     50       CONTINUE
0072     C
0073     C STEP #4 *********************************************
0074     C USING EQS. (7.46) - (7.49), CALCULATE IMPULSE RESPONSE
0075     C OF Ey and Hx AT Z=NZO,X=NXO
0076     C
0077              EI = 0.0
0078              DO 60 K = 1, NT
0079     60       EI = EI + VI(IT,NZO,NXO,K) * 0.5
0080              HI = VI(IT,NZO,NXO,2) - VI(IT,NZO,NXO,4)
0081     C
0082     C SUM THE FREQUENCY RESPONSE (imaginary and real
0083     C parts) FOR DIFFERENT VALUES OF MESH-SIZE DIVIDED
0084     C BY WAVELENGTH
0085     C
0086               DEL = DELTA
0087               II = 1
0088             DO 70 K = 1, 20
0089              T = DFLOAT(ITIME)
0090              EFI(K) = EFI(K) + EI * SIN(2 * PIE * T * DEL)
0091              EFR(K) = EFR(K) + EI * COS(2 * PIE * T * DEL)
0092              HFI(K) = HFI(K) + HI * SIN(2 * PIE * T * DEL)
0093              HFR(K) = HFR(K) + HI * COS(2 * PIE * T * DEL)
0094              OUT(K,II) = DEL
0095     70       DEL = DEL + 0.002
0096     C
0097     C SAVE THE CURRENT PULSE MAGNITUDE FOR NEXT ITERATION
0098     C
0099           DO 80 I = NZB, NZE
0100           DO 80 J = NXB, NXE
0101           DO 80 K = 1, NT
0102           VI(IT-1,I,J,K) = VI(IT,I,J,K)
0103           VR(IT-1,I,J,K) = VR(IT,I,J,K)
0104     80    CONTINUE
0105           IT = ITIME
0106              IF((IT .EQ  100) .OR.( IT .EQ. 150)
0107          1                    .OR.(IT .EQ. 200))THEN
0108               PRINT*, IT
0109               IF(IT .EQ. 100) II = 2
0110               IF(IT .EQ  150) II = 3
0111               IF(IT .EQ. 200) II = 4
0112     C
0113     C STEP #5 *********************************************
0114     C CALCULATE MAGNITUDE & ARGUMENT OF IMPEDANCE
0115     C
0116               DO K = 1, 20
0117               CEF = CMPLX(EFR(K),EFI(K))
0118               CHF = CMPLX(HFR(K),HFI(K))
0119               OUT(K,II) = CABS(CEF)/CABS(CHF) ! MAGNITUDE
```

Figure 7.14

***(Cont.)* Computer program for Example 7.2 *(Continued)*.**

```
0120
0121              ZARG = CEF/CHF
0122              XZ   = REAL( ZARG )
0123              YZ   = AIMAG( ZARG )
0124              XYZ  = YZ / XZ
0125              OUT(K,II+4) = -ATAN( XYZ ) ! ARGUMENT
0126
0127              END DO
0128              END IF
0129     90       CONTINUE
0130     C
0131     C STEP #6 ******************************************
0132     C CALCULATE EXACT VALUE OF IMPEDANCE [ REF. 13]
0133     C
0134              DEL = DELTA
0135              DO 100 K = 1, 20
0136              R2 = 1.0/TRANSC(DEL)
0137              PRINT*,R2
0138              R3 = TAN(21.0*R2*PIE*DEL)
0139              CNUM = CMPLX(R2, R3)
0140              RIG = R2 * R3
0141              RR = 1.0
0142              CDEM = CMPLX(RR, RIG)
0143              OUT(K,5) = CABS(CNUM)/(CABS(CDEM)*R2)
0144              ZARG = CNUM/CDEM
0145              XZ   = REAL( ZARG )
0146              YZ   = AIMAG( ZARG )
0147              XYZ  = YZ / XZ
0148              OUT(K,9) = ATAN( XYZ )
0149              DEL = DEL + .002
0150     100      CONTINUE
0151              DO 110 K = 1, 20
0152     110      WRITE(6,120) (OUT(K,J),J = 1, 10)
0153     120      FORMAT(2X,10F10.4)
0154              STOP
0155              END

0001     C ***************************************
0002     C THIS SUBPROGRAM USE EQ. (7.35) TO CALCULATE
0003     C RATIO Vn/c, GIVEN (DELTA/LAMDA).
0004     C
0005              FUNCTION TRANSC(DELTA)
0006              REAL LAMDA,LAMDAC
0007              PIE = 3.14159265
0008              TETA = PIE * DELTA
0009              TET  = SQRT(2.0) * SIN(TETA)
0010              TRANSC = TETA/ASIN(TET)
0011              RETURN
0012              END
```

Figure 7.14
***(Cont.)* Computer program for Example 7.2.**

Example 7.3

The second example is on a rectangular waveguide with a simple load. The FORTRAN program used for the numerical analysis is basically similar to that of one-dimensional simulation. A 25×11 matrix was used for the numerical analysis of the waveguide. Short-circuit boundaries were placed at $x = 2$ and $x = 10$, the width between the waveguide walls thus being 9 mesh points. The system was excited at all points along the line $z = 2$, and the impulse function of the output was taken from the point $(x = 6, z = 12)$. The C boundary at $z = 24$ represented an

abrupt change to the intrinsic impedance of free space. The minor changes in the program of Fig. 7.14 are shown in Fig. 7.15. The cutoff frequency for the waveguide occurs [19] at $\Delta\ell/\lambda_n = 1/18$, λ_n is the network-matrix wavelength, which corresponds to $\Delta\ell/\lambda = \sqrt{2}/18$ since

$$\frac{\lambda_n}{\lambda} = \frac{u_n}{c} = \frac{\sqrt{\mu_o \epsilon_o}}{\sqrt{\mu_n \epsilon_n}} = \frac{\sqrt{LC}}{\sqrt{2LC}} = \frac{1}{\sqrt{2}}$$

A comparison between the results for the normalized guide impedance using this method is made with exact results in Table 7.3. □

Table 7.3 Normalized Impedance of a Rectangular Waveguide with Simple Load

	TLM results		Exact results	
$\Delta\ell/\lambda$	$\|Z\|$	Arg(Z)	$\|Z\|$	Arg(Z)
0.020	1.9391	0.8936	1.9325	0.9131
0.021	2.0594	0.6175	2.0964	0.6415
0.022	1.9697	0.3553	2.0250	0.3603
0.023	1.7556	0.1530	1.7800	0.1438
0.024	1.5173	0.0189	1.5132	0.0163
0.025	1.3036	−0.0518	1.2989	−0.0388
0.026	1.1370	−0.0648	1.1471	−0.0457
0.027	1.0297	−0.0350	1.0482	−0.0249
0.028	0.9776	0.0088	0.9900	0.0075
0.029	0.9620	0.0416	0.9622	0.0396
0.030	0.9623	0.0554	0.9556	0.0632

7.5 Inhomogeneous and Lossy Media in TLM

In our discussion on the transmission-line-matrix (TLM) method in the last section, it was assumed that the medium in which wave propagates was homogeneous and lossless. In this section, we consider media that are inhomogeneous or lossy or both. This necessitates that we modify the equivalent network of Fig. 7.9 and the corresponding transmission line matrix of Fig. 7.10. Also, we need to draw the corresponding equivalence between the network and Maxwell's equations and derive the scattering matrix. We will finally consider how lossy boundaries are represented.

```
:
:
:
0034          DATA NXB,NXE,NZB,NZE,NT,ITRATE/2,10,2,24,4,200/
0035          DATA NXO,NZO,PIE,GAMMA,DELTA/6,12,3.1415927,0,.02/
:
:
:
0064     C STEP #3 ******************************************
0065     C USING EQS. (7.43) AND (7.44), INSERT BOUNDARY CONDITIONS
0066     C
0067               IF(J .EQ. NXE)VI(IT,I,NXE,3)= - VR(IT,I,NXE,1)
0068               IF(J .EQ. NXB)VI(IT,I,NXB,1)=VR(IT,I,NXB,1)
0069               IF(I .EQ. NZE)VI(IT,NZE,J,4)=GAMMA*VR(IT,NZE,J,4)
:
:
:
0095     70         DEL = DEL + 0.001
:
:
:
```

Figure 7.15
Modification in the program in Fig. 7.14 for simulating waveguide problem in Example 7.3.

7.5.1 General Two-Dimensional Shunt Node

To account for the inhomogeneity of a medium (where ϵ is not constant), we introduce additional capacitance at nodes to represent an increase in permittivity [17], [23]–[25]. We achieve this by introducing an additional length of line or stub to the node as shown in Fig. 7.16 (a). The stub of length $\Delta\ell/2$ is open circuited at the end and is of variable characteristic admittance Y_o relative to the unity characteristic admittance assumed for the main transmission line. At low frequencies, the effect of the stub is to add to each node an additional lumped shunt capacitance $CY_o\Delta\ell/2$, where C is the shunt capacitance per unit length of the main lines that are of unity characteristic admittance. Thus at each node, the total shunt capacitance becomes

$$C' = 2C\Delta\ell + CY_o\Delta\ell/2$$

or

$$C' = 2C\Delta\ell\,(1 + Y_o/4) \tag{7.54}$$

To account for the loss in the medium, we introduce a power-absorbing line at each node, lumped into a single resistor, and this is simulated by an infinite or matched line of characteristic admittance G_o normalized to the characteristic impedance of the main lines as illustrated in Fig. 7.16 (b).

Due to these additional lines, the equivalent network now becomes that shown in Fig. 7.17. (Compare Fig. 7.17 with Fig. 7.9). Applying Kirchhoff's current law to

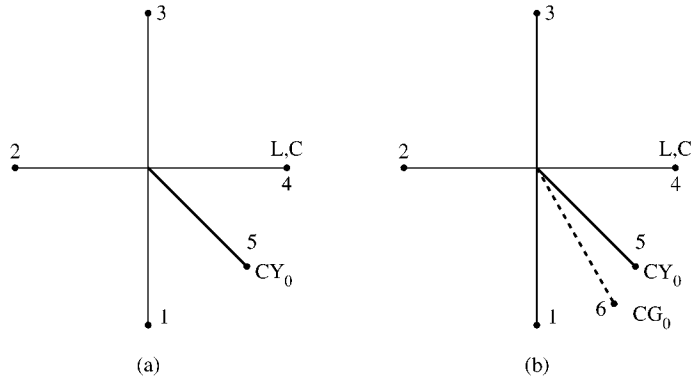

Figure 7.16
A two-dimensional node with: (a) Permittivity stub, (b) permittivity and loss stub.

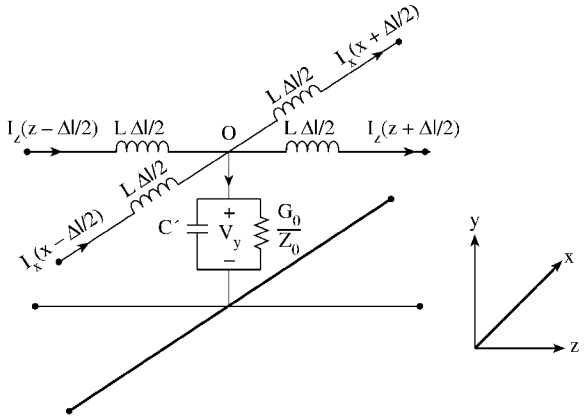

Figure 7.17
General two-dimensional shunt node.

shunt node O in the x-z plane in Fig. 7.17 and taking limits as $\Delta\ell \rightarrow 0$ results in

$$-\frac{\partial I_z}{\partial z} - \frac{\partial I_x}{\partial x} = \frac{G_o V_y}{Z_o \Delta\ell} + 2C\,(1 + Y_o/4)\,\frac{\partial V_y}{\partial t} \tag{7.55}$$

Expanding Maxwell's equations $\nabla \times \mathbf{E} = -\mu \dfrac{\partial \mathbf{H}}{\partial t}$ and $\nabla \times \mathbf{H} = \sigma \mathbf{E} + \epsilon \dfrac{\partial \mathbf{E}}{\partial t}$ for $\partial/\partial y \equiv 0$ leads to

$$\frac{\partial H_x}{\partial z} - \frac{\partial H_z}{\partial x} = \sigma E_y + \epsilon_o \epsilon_r \frac{\partial E_y}{\partial t} \tag{7.56}$$

This may be considered as denoting TE_{m0} modes with field components H_z, H_x, and E_y. From Eqs. (7.55) and (7.56), the following equivalence between the TLM

equations and Maxwell's equations can be drawn:

$$\boxed{\begin{aligned} E_y &\equiv V_y \\ H_x &\equiv -I_z \\ H_z &\equiv I_x \\ \epsilon_o &\equiv 2C \\ \epsilon_r &\equiv \tfrac{4+Y_o}{4} \\ \sigma &\equiv \tfrac{G_o}{Z_o \Delta\ell} \end{aligned}} \tag{7.57}$$

where $Z_o = \sqrt{L/C}$. From Eq. (7.57), the normalized characteristic admittance G_o of the loss stub is related to the conductivity of the medium by

$$G_o = \sigma \Delta\ell Z_o \tag{7.58}$$

Thus losses on the matrix can be varied by altering the value of G_o. Also from Eq. (7.57), the variable characteristic admittance Y_o of the permittivity stub is related to the relative permittivity of the medium as

$$Y_o = 4\,(\epsilon_r - 1) \tag{7.59}$$

7.5.2 Scattering Matrix

We now derive the impulse response of the network comprising of the interconnection of many generalized nodes such as that in Fig. 7.17. As in the previous section, if ${}_kV_n(z, x)$ is unit voltage impulse reflected from the node at (z, x) into the nth coordinate direction ($n = 1, 2, \ldots, 5$) at time $k\Delta\ell/c$, then at node (z, x),

$$\boxed{{}_{k+1}\begin{bmatrix} V_1(z,x) \\ V_2(z,x) \\ V_3(z,x) \\ V_4(z,x) \\ V_5(z,x) \end{bmatrix}^r = [S]\,{}_k\begin{bmatrix} V_3(z, x-\Delta\ell) \\ V_4(z-\Delta\ell, x) \\ V_1(z, x+\Delta\ell) \\ V_2(z+\Delta\ell, x) \\ V_5(z, x+\Delta\ell) \end{bmatrix}^i} \tag{7.60}$$

where $[S]$ is the scattering matrix given by

$$\boxed{[S] = \frac{2}{Y}\begin{bmatrix} 1 & 1 & 1 & 1 & Y_o \\ 1 & 1 & 1 & 1 & Y_o \\ 1 & 1 & 1 & 1 & Y_o \\ 1 & 1 & 1 & 1 & Y_o \\ 1 & 1 & 1 & 1 & Y_o \end{bmatrix} - [I]} \tag{7.61}$$

$[I]$ is a unit matrix and $Y = 4 + Y_o + G_o$. The coordinate directions 1, 2, 3, and 4 correspond to $-x$, $-z$, $+x$, and $+z$, respectively (as in the last section), and 5 refers to the permittivity stub. Notice that the voltage V_6 (see Fig. 7.16) scattered into the

loss stub is dropped across G_o and not returned to the matrix. We apply Eq. (7.60) just as Eq. (7.41).

As in the last section, the output impulse function at a particular node in the mesh can be obtained by recording the amplitude and the time of the stream of pulses as they pass through the node. By taking the Fourier transform of the output impulse function using Eq. (7.49), the required information can be extracted.

The dispersion relation can be derived in the same manner as in the last section. If $\gamma_n = \alpha_n + j\beta_n$ is the network propagation constant and $\gamma = \alpha + j\beta$ is the propagation constant of the medium, the two propagation constants are related as

$$\frac{\beta}{\beta_n} = \frac{\theta/2}{\sin^{-1}\left[\sqrt{2(1+Y_o/4)}\sin\theta/2\right]} \tag{7.62a}$$

$$\frac{\alpha}{\alpha_n} = \frac{\sqrt{1-2(1+Y_o/4)\sin^2\theta/2}}{\sqrt{2(1+Y_o/4)}\cos\theta/2} \tag{7.62b}$$

where $\theta = 2\pi\Delta\ell/\lambda$ and

$$\alpha = \frac{G_o}{8\Delta\ell(1+Y_o/4)} \tag{7.63}$$

In arriving at Eq. (7.62), we have assumed that $\alpha_n\Delta\ell << 1$. For low frequencies, the attenuation constant α_n and phase constant β_n of the network are fairly constant so that Eq. (7.62) reduces to

$$\gamma_n = \sqrt{2(1+Y_o/4)}\gamma \tag{7.64}$$

From this, the network velocity $u_n(= \omega/\beta_n = \beta c/\beta_n)$ of waves on the matrix is readily obtained as

$$u_n^2 = \frac{c^2}{2(1+Y_o/4)} \tag{7.65}$$

where c is the free-space velocity of waves.

7.5.3 Representation of Lossy Boundaries

The above analysis has incorporated conductivity σ of the medium in the TLM formulation. To account for a lossy boundary [25]–[27], we define the reflection coefficient

$$\Gamma = \frac{Z_s - Z_o}{Z_s + Z_o} \tag{7.66}$$

where $Z_o = \sqrt{\mu_o/\epsilon_o}$ is the characteristic impedance of the main lines and Z_s is the surface impedance of the lossy boundary given by

$$Z_s = \sqrt{\frac{\mu\omega}{2\sigma_c}}(1+j) \tag{7.67}$$

where μ and σ_c are the permeability and conductivity of the boundary. It is evident from Eqs. (7.66) and (7.67) that the reflection coefficient Γ is in general complex. However, complex Γ implies that the shape of the pulse functions is altered on reflection at the conducting boundary, and this cannot be accounted for in the TLM method [22]. Therefore, assuming that Z_s is small compared with Z_o and that the imaginary part of Γ is negligible,

$$\Gamma \simeq -1 + \sqrt{\frac{2\epsilon_o \omega}{\sigma_c}} \tag{7.68}$$

where $\mu = \mu_o$ is assumed. We notice that Γ is slightly less than -1. Also, we notice that Γ depends on the frequency ω and hence calculations involving lossy boundaries are only accurate for the specific frequency; calculations must be repeated for a different value of $\Delta\ell/\lambda$. The following example is taken from Akhtarzad and Johns [24].

Example 7.4

Consider the lossy homogeneous filled waveguide shown in Fig. 7.18. The guide is 6 cm wide and 13 cm long. It is filled with a dielectric of relative permittivity $\epsilon_r = 4.9$ and conductivity $\sigma = 0.05$ mhos/m and terminated in an open circuit discontinuity. Calculate the normalized wave impedance. □

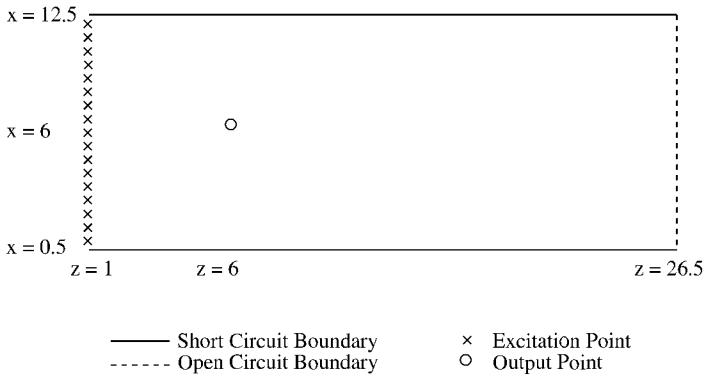

Figure 7.18
A lossy homogeneously filled waveguide.

Solution

The computer program for this problem is in Fig. 7.19. It is an extension of the program in Fig. 7.14 with the incorporation of new concepts developed in this section. Enough comments are added to make it self-explanatory. The program is suitable for a two-dimensional TE_{m0} mode.

The waveguide geometry shown in Fig. 7.18 is simulated on a matrix of 12×26 nodes. The matrix is excited at all points along line $z = 1$ with impulses corresponding to E_y. The impulse function of the output at point $(z, x) = (6, 6)$ is taken after 700 iterations. Table 7.4 presents both the TLM and theoretical values of the normalized wave impedance and shows a good agreement between the two. ∎

Table 7.4 Impedance of a Homogeneously Filled Waveguide with Losses

	TLM results		Exact results	
$\Delta\ell/\lambda$	$\|Z\|$	Arg(Z)	$\|Z\|$	Arg(Z)
0.003	0.0725	1.5591	0.0729	1.5575
0.006	0.1511	1.5446	0.1518	1.5420
0.009	0.2446	1.5243	0.2453	1.5205
0.012	0.3706	1.4890	0.3712	1.4840
0.015	0.5803	1.4032	0.5792	1.3977
0.018	1.0000	1.0056	0.9979	1.0065
0.021	1.1735	0.5156	1.1676	0.5121
0.024	0.5032	−0.1901	0.5093	−0.2141
0.027	0.6766	0.6917	0.6609	0.6853
0.030	0.8921	−0.3869	0.8921	−0.4185

7.6 Three-Dimensional TLM Mesh

The TLM mesh considered in Sections 7.4 and 7.5 is two-dimensional. The choice of shunt-connected nodes to represent the two-dimensional wave propagation was quite arbitrary; the TLM mesh could have equally been made up of series-connected nodes. To represent a three-dimensional space, however, we must apply a hybrid TLM mesh consisting of three shunt and three series nodes to simultaneously describe all the six field components. First of all, we need to understand what a series-connected node is.

7.6.1 Series Nodes

Figure 7.20 portrays a lossless series-connected node that is equipped with a short-circuited stub called the permeability stub. The corresponding network representation is illustrated in Fig. 7.21. The input impedance of the short-circuited stub is

$$Z_{in} = jZ_o\sqrt{\frac{L}{C}}\tan\left(\frac{\omega\Delta\ell}{2c}\right) \simeq j\omega L Z_o \Delta\ell/2 \tag{7.69}$$

```
0001    C=====================================================
0002    C THIS PROGRAM SOLVES A TYPICAL TWO-DIMENSIONAL
0003    C WAVE PROPAGATION PROBLEM AS STATED BELOW:
0004    C A WAVE GUIDE 6cm X 13cm LONG IS FILLED WITH A
0005    C DIELECTRIC OF RELATIVE PERMITTIVITY EQUAL TO 4.9
0006    C AND CONDUCTIVITY 0.05 MHO/M. THIS GEOMETRY IS
0007    C BEING SIMULATED ON A MATRIX OF 12 X 26 NODES.
0008    C THE MATRIX WAS EXCITED AT ALL POINTS ALONG THE
0009    C LINE Z = 1 WITH IMPULSES CORRESPONDING TO Ey.
0010    C THE IMPULSE FUNCTION OF THE OUTPUT WAS TAKEN FROM
0011    C THE POINT (Z = 6, X = 6) AFTER 750 ITERATIONS.
0012    C THE BOUNDARIES WERE SHORT CIRCUITED AT X = 0.5
0013    C AND X = 12.5 AND TERMINATED AT Z = 26.5 IN AN
0014    C OPEN CIRCUIT DISCONTINUITY.
0015    C VI -- ARRAY FOR INCIDENT VOLTAGE
0016    C VR -- ARRAY FOR REFLECTED VOLTAGE
0017    C NX -- INDEX OF NODES IN X-DIRECTION
0018    C NZ -- INDEX OF NODES IN Z-DIRECTION
0019    C RO -- REFLECTION COEFFIENT
0020    C DELTA  -- MESH SIZE (SPACING)
0021    C DELTA   -- MESH SIZE DIVIDED BY LAMBDA
0022
0023            IMPLICIT REAL*8(A,D-H,O-Y),COMPLEX*8(C,Z)
0024            DIMENSION VI(0:1,27,13,5),VR(0:1,27,13,5)
0025         1  ,EFI(50),EFR(50),HFI(50),HFR(50),OUT(10,5)
0026
0027           DATA NXB,NXE,NZB,NZE,NT,ITRATE/1,12,1,26,5,750/
0028           DATA NXI,NZI,NXO,NZO,RoS,RoC/0,1,6,6,-1.0,1.0/
0029           DATA Eo,Er,SIGMA,DELTA,PI/8.854E-12,4.9,0.05,
0030        1                    0.005,3.1415927/
0031
0032           Yo = 4.0 * (Er/2.0 - 1)
0033           Ur = 1.0
0034           Uo = 4.0 * PI * 1.0E-07
0035           Go = SIGMA * DELTA * SQRT( Uo/Eo )
0036            Y = 4.0 + Yo + Go
0037    C
0038    C SINCE REFLECTION COEFFICIENT, RO, DEPENDS ON
0039    C FREQUENCY, THE ITERATIONS MUST BE REPEATED FOR
0040    C EACH VALUE OF THE MESH-SIZE DIVIDED BY WAVELENGTH.
0041    C
0042            DELTA = 0.0
0043            DO 90 L = 1, 10
0044            DELTA = DELTA + 0.003
0045    C
0046    C INITIALIZE ALL NODES (BOTH FREE AND FIXED)
0047    C
0048            DO 10 I = NZB, NZE
0049            DO 10 J = NXB, NXE
0050            DO 10 K = 1, NT
0051            VI(O,I,J,K) = 0.0
0052    10      VR(O,I,J,K) = 0.0
0053    C
0054    C START THE ITERATION
0055    C
0056            DO 90 ITime = 0, ITRATE
0057            IT = 1
0058            DO 60 I  = NZB, NZE
0059            DO 50 J  = NXB, NXE
0060            SUM = 0.0
```

Figure 7.19
Computer program for Example 7.4 ***(Continued).***

```
0061
0062            DO 30 K = 1, 4
0063    30      SUM = SUM + VI(IT-1,I,J,K)
0064            SUM = (SUM + Yo*VI(IT-1,I,J,5)) * 2.0/Y
0065    C
0066    C  INSERT THE INITIAL CONDITION AT I = 1
0067    C
0068            IF(ITIME .EQ. 0 .AND. I .EQ. NZI) SUM = 1.0
0069
0070            DO 40 K = 1, NT
0071    40         VR(IT,I,J,K) = SUM - VI(IT-1,I,J,K)
0072
0073            IF(J .NE. NXB) VI(IT,I,J-1,3) = VR(IT,I,J,1)
0074            IF(I .NE. NZB+1)VI(IT,I-1,J,4)= VR(IT,I,J,2)
0075            IF(J .NE. NXE) VI(IT,I,J+1,1) = VR(IT,I,J,3)
0076            IF(I .NE. NZE) VI(IT,I+1,J,2) = VR(IT,I,J,4)
0077               VI(IT,I,J,5)   = VR(IT,I,J,5)
0078    C
0079    C INSERT THE BOUNDARY CONDITIONS
0080    C FOR THE SHORT CIRCUIT AT X = 0.5
0081    C
0082            IF(J .EQ. NXB) VI(IT,I,1,1) =RoS*VR(IT,I,1,1)
0083    C
0084    C FOR THE SHORT CIRCUIT AT X = 12.5
0085    C
0086            IF(J .EQ. NXE) VI(IT,I,J,3) =RoS*VR(IT,I,J,3)
0087    C
0088    C FOR THE OPEN CIRCUIT DISCONTINUITY AT Z = 26.5
0089    C
0090            IF(I .EQ. NZE) VI(IT,I,J,4) =RoC*VR(IT,I,J,4)
0091
0092    50      CONTINUE
0093    60      CONTINUE
0094    C
0095    C IN ORDER TO CONSERVE SPACE, THE ARRAYS
0096    C HAVE TO BE UPDATED
0097    C
0098            DO 70 I = 1, NZE
0099            DO 70 J = 1, NXE
0100            DO 70 K = 1, NT
0101            VI(IT-1,I,J,K) = VI(IT,I,J,K)
0102    70      VR(IT-1,I,J,K) = VR(IT,I,J,K)
0103    C
0104    C CALCULATE IMPULSE RESPONSE  AT Z=NZO, X=NXO
0105    C
0106            EI = 0.0
0107            DO 80 K = 1, 4
0108    80      EI = EI + VI(IT,NZO,NXO,K)
0109            EI = (EI + Yo * VI(IT,NZO,NXO,5)) * 2.0/Y
0110            HI = -(VI(IT,NZO,NXO,2)-VI(IT,NZO,NXO,4))
0111    C
0112    C SUM THE FREQUENCY RESPONSE (imaginary and
0113    C real parts) FOR DIFFERENT VALUES OF
0114    C MESH-SIZE DIVIDED BY WAVELENGTH
0115    C
0116            T = DFLOAT(ITIME)
0117            EFI(L)=EFI(L)+EI*DSIN(2.0 * PI * T * DELTA)
0118            EFR(L)=EFR(L)+EI*DCOS(2.0 * PI * T * DELTA)
0119            HFI(L)=HFI(L)+HI*DSIN(2.0 * PI * T * DELTA)
0120            HFR(L)=HFR(L)+HI*DCOS(2.0 * PI * T * DELTA)
```

Figure 7.19

(Cont.)* Computer program for Example 7.4 *(Continued).

```
0121            OUT(L,1) = DELTA
0122            IF( ITIME .EQ. ITRATE ) THEN
0123            CEF = CMPLX(EFR(L),EFI(L))
0124            CHF = CMPLX( HFR(L), HFI(L))
0125            OUT(L,2) = CABS(CEF)/CABS(CHF)
0126      C
0127      C CALCULATE ARGUMENT Z
0128      C
0129            ZARG = CEF/CHF
0130            XZ   = REAL( ZARG )
0131            YZ   = AIMAG( ZARG )
0132            XYZ  = YZ / XZ
0133            OUT(L,3) = -ATAN( XYZ )
0134            print*,out(l,1),out(l,2),out(l,3)
0135            END IF
0136      90    CONTINUE
0137            DO 100 K = 1, L-1
0138      100   WRITE(6,110) (OUT(K,J),J = 1, 3)
0139      110   FORMAT(2X,10F10.4)
0140            STOP
0141            END
```

Figure 7.19
***(Cont.)* Computer program for Example 7.4.**

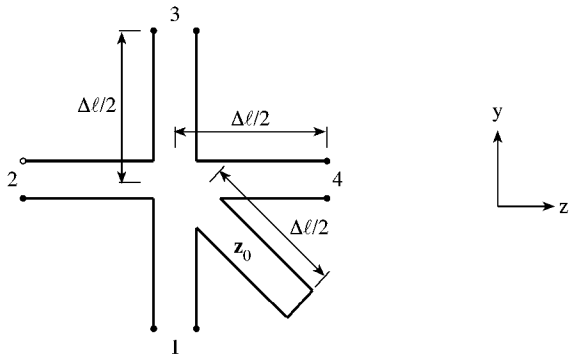

Figure 7.20
A lossless series connected node with permeability stub.

where Eq. (7.26) has been applied. This represents an impedance with inductance

$$L' = L\frac{\Delta\ell}{2}Z_o \tag{7.70}$$

Hence the total inductance on the side in which the stub is inserted is $L\Delta\ell(1+Z_o)/2$ as in Fig. 7.21. We now apply Kirchhoff's voltage law around the series node of Fig. 7.21 and obtain

$$V_z + L\frac{\Delta\ell}{2}(1+Z_o)\frac{\partial I_x}{\partial t} + V_y + \frac{\partial V_y}{\partial z}\Delta\ell - \left(V_z + \frac{\partial V_z}{\partial y}\Delta\ell\right) + 3L\frac{\Delta\ell}{2}\frac{\partial I_x}{\partial t} - V_y = 0$$

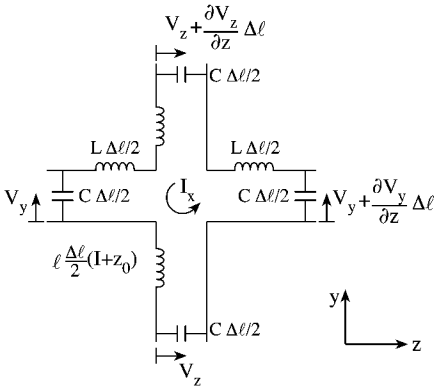

Figure 7.21
Network representation of a series node.

Dividing through by $\Delta\ell$ and rearranging terms leads to

$$\frac{\partial V_z}{\partial y} - \frac{\partial V_y}{\partial z} = 2L\,(1 + Z_o/4)\,\frac{\partial I_x}{\partial t} \tag{7.71}$$

Note that the series node is oriented in the y-z plane. Equations for series nodes in the x-y and x-z planes can be obtained in a similar manner as

$$\frac{\partial V_y}{\partial x} - \frac{\partial V_x}{\partial y} = 2L\,(1 + Z_o/4)\,\frac{\partial I_z}{\partial t} \tag{7.72}$$

and

$$\frac{\partial V_x}{\partial z} - \frac{\partial V_z}{\partial x} = 2L\,(1 + Z_o/4)\,\frac{\partial I_y}{\partial t}\,, \tag{7.73}$$

respectively.

Comparing Eqs. (7.71) to (7.73) with Maxwell's equations in Eq. (7.22), the following equivalences can be identified:

$$\boxed{\begin{aligned} E_x &\equiv V_x \\ E_z &\equiv V_z \\ \mu_o &\equiv 2L \\ \mu_r &\equiv \frac{4 + Z_o}{4} \end{aligned}} \tag{7.74}$$

A series-connected two-dimensional TLM mesh is shown in Fig. 7.22 (a). while the equivalent one-dimensional mesh is in Fig. 7.22 (b). A voltage impulse incident on a series node is scattered in accordance with Eq. (7.60), where the scattering matrix

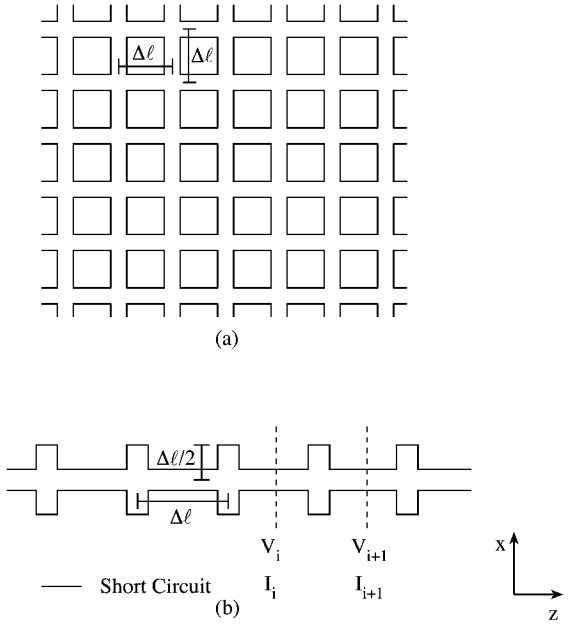

Figure 7.22
(a) A two-dimensional series-connected TLM mesh. (b) A one-dimensional series-connected TLM mesh.

is now

$$[S] = \frac{2}{Z}\begin{bmatrix} -1 & 1 & 1 & -1 & -1 \\ 1 & -1 & -1 & 1 & 1 \\ 1 & -1 & -1 & 1 & 1 \\ -1 & 1 & 1 & -1 & -1 \\ -Z_o & Z_o & Z_o & -Z_o & -Z_o \end{bmatrix} + [I] \tag{7.75}$$

$Z = 4 + Z_o$, and $[I]$ is the unit matrix. The velocity characteristic for the two-dimensional series matrix is the same as for the shunt node [24]. For low frequencies ($\Delta\ell/\lambda < 0.1$) the velocity of the waves on the matrix is approximately $1/\sqrt{2}$ of the free-space velocity. This is due to the fact that the stubs have twice the inductance per unit length, while the capacitance per unit length remains unchanged. This is the dual of the two-dimensional shunt case in which the capacitance was doubled and the inductance was unchanged.

7.6.2 Three-Dimensional Node

A three-dimensional TLM node [27] consists of three shunt nodes in conjunction with three series nodes. The voltages at the three shunt nodes represent the three components of the **E** field, while the currents of the series nodes represent the three

components of the **H** field. In the x-z plane, for example, the voltage-current equations for the shunt node are

$$\frac{\partial I_x}{\partial z} - \frac{\partial I_z}{\partial x} = 2C\frac{\partial V_y}{\partial t} \tag{7.76a}$$

$$\frac{\partial V_y}{\partial x} = -L\frac{\partial I_x}{\partial t} \tag{7.76b}$$

$$\frac{\partial V_y}{\partial z} = -L\frac{\partial I_z}{\partial t} \tag{7.76c}$$

and for the series node in the x-z plane, the equations are

$$\frac{\partial V_x}{\partial z} - \frac{\partial V_z}{\partial x} = 2L\frac{\partial I_y}{\partial t} \tag{7.77a}$$

$$\frac{\partial I_y}{\partial x} = -C\frac{\partial V_z}{\partial t} \tag{7.77b}$$

$$\frac{\partial I_y}{\partial z} = -C\frac{\partial V_x}{\partial t} \tag{7.77c}$$

Maxwell's equations $\nabla \times \mathbf{E} = \dfrac{\partial \mathbf{B}}{\partial t}$ and $\nabla \times \mathbf{H} = \epsilon\dfrac{\partial \mathbf{E}}{\partial t}$ for $\dfrac{\partial}{\partial y} \equiv 0$ give

$$\frac{\partial H_x}{\partial z} - \frac{\partial H_z}{\partial x} = \epsilon\frac{\partial E_y}{\partial t} \tag{7.78a}$$

$$\frac{\partial E_y}{\partial x} = \mu\frac{\partial H_x}{\partial t} \tag{7.78b}$$

$$\frac{\partial E_y}{\partial z} = -\mu\frac{\partial H_z}{\partial t} \tag{7.78c}$$

and

$$\frac{\partial E_x}{\partial z} - \frac{\partial E_z}{\partial x} = -\mu\frac{\partial H_y}{\partial t} \tag{7.79a}$$

$$\frac{\partial H_y}{\partial x} = -\epsilon\frac{\partial E_x}{\partial t} \tag{7.79b}$$

$$\frac{\partial H_y}{\partial z} = -\epsilon\frac{\partial E_z}{\partial t} \tag{7.79c}$$

A similar analysis for shunt and series nodes in the x-y and y-z planes will yield the voltage-current equations and the corresponding Maxwell's equations. The three sets of two-dimensional shunt and series nodes oriented in the x-y, y-z, and z-x planes form a three-dimensional model. The two-dimensional nodes must be connected in such a way as to correctly describe Maxwell's equations at each three-dimensional node. Each of the shunt and series nodes has a spacing of $\Delta\ell/2$ so that like nodes are spaced $\Delta\ell$ apart.

Figure 7.23 illustrates a three-dimensional node representing a cubical volume of space $\Delta\ell/2$ long in each direction. A close examination shows that if the voltage

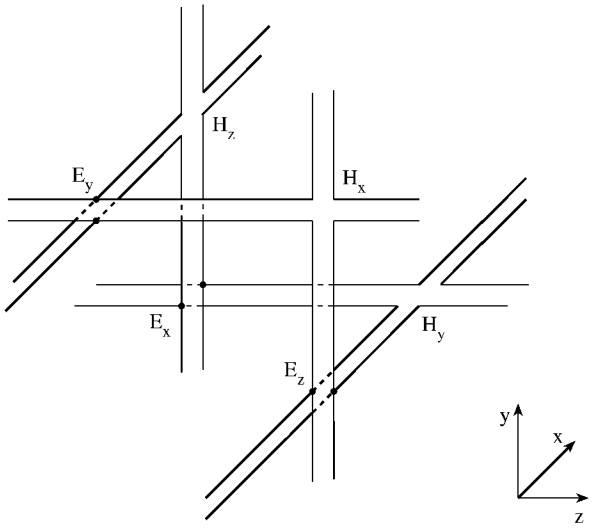

Figure 7.23
A three-dimensional node consisting of three shunt nodes and three series nodes.

between lines represents the **E** field and the current in the lines represents the **H** field, then the following Maxwell's equations are satisfied:

$$\frac{\partial H_x}{\partial z} - \frac{\partial H_z}{\partial x} = \epsilon \frac{\partial E_y}{\partial t} \tag{7.80a}$$

$$\frac{\partial E_z}{\partial y} - \frac{\partial E_y}{\partial z} = -\mu \frac{\partial H_x}{\partial t} \tag{7.80b}$$

$$\frac{\partial E_y}{\partial x} - \frac{\partial E_x}{\partial y} = -\mu \frac{\partial H_z}{\partial t} \tag{7.80c}$$

$$\frac{\partial E_x}{\partial z} - \frac{\partial E_z}{\partial x} = -\mu \frac{\partial H_y}{\partial t} \tag{7.80d}$$

$$\frac{\partial H_z}{\partial y} - \frac{\partial H_y}{\partial z} = \epsilon \frac{\partial E_x}{\partial t} \tag{7.80e}$$

$$\frac{\partial H_y}{\partial x} - \frac{\partial H_x}{\partial y} = \epsilon \frac{\partial E_z}{\partial t} \tag{7.80f}$$

In the upper half of the node in Fig. 7.23, we have a shunt node in the x-z plane (representing Eq. (7.80a)) connected to a series node in the y-z plane (representing Eq. (7.80b)) and a series node in the x-y plane (representing Eq. (7.80c)). In the lower half of the node, a series node in the x-z plane (representing Eq. (7.80d)) is connected to a shunt node in the y-z plane (representing Eq. (7.80e)) and a shunt node

in the x-y plane (representing Eq. (7.80f)). Thus Maxwell's equations are completely satisfied at the three-dimensional node. A three-dimensional TLM mesh is obtained by stacking similar nodes in x, y, and z directions (see Fig. 7.25, for example).

The wave characteristics of the three-dimensional mesh are similar to those of the two-dimensional mesh with the difference that low-frequency velocity is now $c/2$ instead of $c/\sqrt{2}$.

Figure 7.24 illustrates a schematic diagram of a three-dimensional node using single lines to represent pairs of transmission lines. It is more general than the representation in Fig. 7.23 in that it includes the permittivity, permeability, and loss stubs. Note that the dotted lines making up the corners of the cube are guidelines and do not represent transmission lines or stubs. It can be shown that for the general node the following equivalences apply [28]:

$$
\begin{aligned}
E_x &\equiv \text{ the common voltage at shunt node } E_x \\
E_y &\equiv \text{ the common voltage at shunt node } E_y \\
E_z &\equiv \text{ the common voltage at shunt node } E_z \\
H_x &\equiv \text{ the common current at series node } H_x \\
H_y &\equiv \text{ the common current at series node } H_y \\
H_z &\equiv \text{ the common current at series node } H_z \\
\epsilon_o &\equiv C \text{ (the capacitance per unit length of lines)} \\
\epsilon_r &\equiv 2\,(1 + Y_o/4) \\
\mu_o &\equiv L \text{ (the inductance per unit length of lines)} \\
\mu_r &\equiv 2\,(1 + Z_o/4) \\
\sigma &\equiv \frac{G_o}{\Delta\ell\frac{L}{C}}
\end{aligned}
\tag{7.81}
$$

where Y_o, Z_o, and G_o remain as defined in Sections 7.4 and 7.5. Interconnection of many of such three-dimensional nodes forms a TLM mesh representing any inhomogeneous media. The TLM method for three-dimensional problems is therefore concerned with applying Eq. (7.60) in conjunction with Eqs. (7.61) and (7.75) and obtaining the impulse response. Any of the field components may be excited initially by specifying initial impulses at the appropriate nodes. Also, the response at any node may be monitored by recording the pulses that pass through the node.

7.6.3 Boundary Conditions

Boundary conditions are simulated by short-circuiting shunt nodes (electric wall) or open-circuiting series nodes (magnetic wall) situated on a boundary. The tangential components of **E** must vanish in the plane of an electric wall, while the tangential components of **H** must be zero in the plane of a magnetic wall. For example, to set E_x and E_y equal to zero in a particular plane, all shunt nodes E_x and E_y lying in that plane are shorted. Similarly, to set H_y and H_z equal to zero in some plane, the series nodes H_y and H_z in that plane are simply open-circuited.

The continuity of the tangential components of **E** and **H** fields across a dielectric/dielectric boundary is automatically satisfied in the TLM mesh. For example,

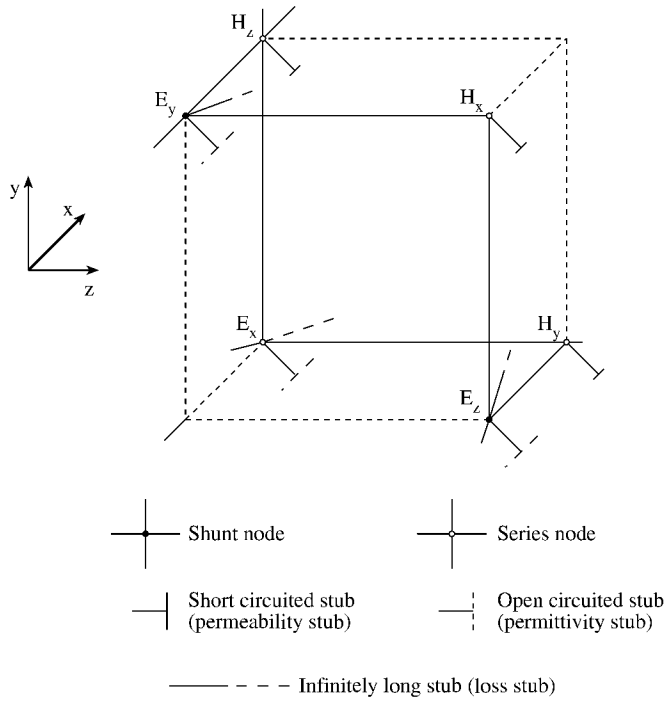

Figure 7.24
A general three-dimensional node.

for a dielectric/dielectric boundary in the x-z plane such as shown in Fig. 7.25, the following equations valid for a transmission-line element joining the nodes on either side of the boundaries are applicable:

$$\begin{aligned} E_{z1} &= E_{z2} + \frac{\partial E_{z2}}{\partial y}\Delta\ell \\ E_{x1} &= E_{x2} + \frac{\partial E_{x2}}{\partial y}\Delta\ell \\ H_{x1} &= H_{x2} + \frac{\partial H_{x2}}{\partial y}\Delta\ell \\ H_{z1} &= H_{z2} + \frac{\partial H_{z2}}{\partial y}\Delta\ell \end{aligned} \tag{7.82}$$

Finally, wall losses are included by introducing imperfect reflection coefficients as discussed in Section 7.5. The three-dimensional TLM mesh will be applied in solving the three-dimensional problems of resonant cavities in the following examples, taken from Akhtarzad and Johns [27].

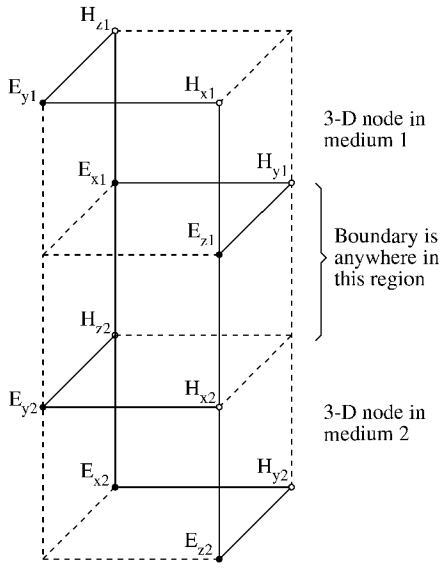

Figure 7.25
A dielectric/dielectric boundary in TLM mesh.

Example 7.5

Determine the resonant frequency of an $a \times b \times d$ empty rectangular cavity using the TLM method. Take $a = 12\Delta\ell$, $b = 8\Delta\ell$, and $d = 6\Delta\ell$. □

Solution

The exact solution [13, 14] for TE_{mnp} or TM_{mnp} mode is

$$f_r = \frac{c}{2}\sqrt{(m/a)^2 + (n/b)^2 + (p/d)^2}$$

from which we readily obtain

$$k_c = \frac{w_r}{c} = \frac{2\pi f_r}{c} = \pi\sqrt{(m/a)^2 + (n/b)^2 + (p/d)^2}$$

The TLM program, the modified version of the program in [22], is shown in Fig. 7.26. The program initializes all field components by setting them equal to zero at all nodes in the $12\Delta\ell \times 8\Delta\ell \times 8\Delta\ell$ TLM mesh and exciting one field component. With subroutine COMPUTE, it applies Eq. (7.60) in conjunction with Eq. (7.61) and (7.75) to calculate the reflected **E** and **H** field components at all nodes. It applies the boundary conditions and calculates the impulse response at a particular node in the mesh.

The results of the computation along with the exact analytical values for the first few modes in the cavity are shown in Table 7.5. ■

```
C*********************************************************
C  THIS PROGRAM ANLYZES THREE-DIMENSIONAL WAVE PROBLEMS
C  USING THE TLM METHOD
C  THE SPECIFIC EXAMPLE SOLVED HERE IS THE DETERMINATION
C  OF THE TM DOMINANT MODE OF RECTANGULAR LOSSLESS CAVITY
C  OF DIMENSION 12 X 8 X 6
C        E     ...  E - field
C        H     ...  H - field
C        X     ...  X - component
C        Y     ...  Y - component
C        Z     ...  Z - component
C        I     ...  incident impulse
C        R      ..  reflected impulse
C        NX     ..  number of nodes in X-direction
C        NY    ...  number of nodes in Y-direction
C        NZ    ...  number of nodes in Z-direction
C  SHUNT and SERIES   ...  scattering matrix
C   DELTA = DELTA/LAMDA  (FREE SPACE)

          IMPLICIT  REAL*8(A,B,D-H,O-Z),COMPLEX*8(C),
     1       INTEGER*2(I-N)
          DIMENSION EXR(2,7,9,13,5), EXI(2,7,9,13,5),
     1             EYR(2,7,9,13,5), EYI(2,7,9,13,5),
     2             EZR(2,7,9,13,5), EZI(2,7,9,13,5),
     3             HXR(2,7,9,13,5), HXI(2,7,9,13,5),
     4             HYR(2,7,9,13,5), HYI(2,7,9,13,5),
     5             HZR(2,7,9,13,5), HZI(2,7,9,13,5),
     6             EX(2,1000),EY(2,1000),EZ(2,1000),
     7             HX(2,1000),HY(2,1000),HZ(2,1000),
     8             OUT(12,1000),SHUNT(5,5),SERIES(5,5)

          COMMON / PART1 /NT,NXB,NXE,NYB,NYE,NZB,NZE,IT
          SQMAG(CM) = ( CABS(CM) ) ** 2
          DATA ITRATE,NXB,NXE,NYB,NYE,NZB,NZE,NT,DELTA
     1         /1000, 1,  12, 1,  8,  1,  6,  4, 1.0/
          DATA NXI,NYI,NZI,NXO,NYO,NZO,RoH,NUMPT,DEL
     1        /11, 7,  0,  2,  2, 2,-1.0,1000,0.0001/
          DATA PI,         Eo,       Er, Ur,SIGMA,DELTA
     1       /3.1415927,8.854E-12,1.0,1.0,0.0,0.01 /
          DATA SERIES /-1.0,1.0,1.0,-1.0,-1.0,
     1                  1.0,-1.0,-1.0,1.0,1.0,
     2                  1.0,-1.0,-1.0,1.0,1.0,
     3                 -1.0,1.0,1.0,-1.0,-1.0,
     4                 -1.0,1.0,1.0,-1.0,-1.0/
          DATA SHUNT / 1.0,1.0,1.0,1.0,1.0,
     1                 1.0,1.0,1.0,1.0,1.0,
     2                 1.0,1.0,1.0,1.0,1.0,
     3                 1.0,1.0,1.0,1.0,1.0,
     4                 1.0,1.0,1.0,1.0,1.0/

          Uo =  4.0 * PI * 1.0E-07
          Yo = 4.0 * (Er - 1.0)
          Zo = 4.0 * (Ur - 1.0)
          Go = SIGMA * DELTA * SQRT(Uo/Eo)
          Y = 4.0 + Yo + Go
          Z = 4.0 + Zo
          DO 5 I = 1,5
          SHUNT(I,5)  = SHUNT(I,5) * Yo
          SERIES(5,I) =  SERIES(5,I) * Zo
5         CONTINUE
C
```

Figure 7.26
Computer program for Example 7.5 ***(Continued).***

```
0062    C  INITIALIZE ALL THE NODES
0063    C
0064              DO 10 IT = 1,2
0065              DO 10 K = NZB, NZE
0066              DO 10 J = NYB, NYE
0067              DO 10 I = NXB, NXE
0068              DO 10 L = 1, NT
0069                 EXI(IT,K,J,I,L) = 0.0
0070                 EYI(IT,K,J,I,L) = 0.0
0071                 EZI(IT,K,J,I,L) = 0.0
0072                 HXI(IT,K,J,I,L) = 0.0
0073                 HYI(IT,K,J,I,L) = 0.0
0074                 HZI(IT,K,J,I,L) = 0.0
0075                 EXR(IT,K,J,I,L) = 0.0
0076                 EYR(IT,K,J,I,L) = 0.0
0077                 EZR(IT,K,J,I,L) = 0.0
0078                 HXR(IT,K,J,I,L) = 0.0
0079                 HYR(IT,K,J,I,L) = 0.0
0080    10           HZR(IT,K,J,I,L) = 0.0
0081    C
0082    C INSERT THE INITIAL EXCITATION
0083    C
0084              DO 15 K = NZB, NZE
0085              DO 15 L = 1, 4
0086                EZR(2,K,NYI,NXI,L) = 1.0
0087    15        CONTINUE
0088                 IT = 2
0089    C
0090    C START ITERATION
0091    C
0092              DO 60 ITime = 1, ITRATE
0093                 IF(ITIME .EQ. 1) GOTO 25
0094    C
0095    C COMPUTE THE REFLECTED E-FIELD AT ALL NODES
0096    C
0097              ISIGN = -1
0098              CALL COMPUTE(EXR,EYR,EZR,SHUNT
0099         1                      ,Y,EXI,EYI,EZI,ISIGN)
0100    C
0101    C RE-INITIALIZE MATRIX AND FORCE TANGENTIAL
0102    C E-FIELD TO ZERO AT BOUNDARY
0103    C
0104              DO 20 K = NZB, NZE
0105              DO 20 J = NYB, NYE
0106              DO 20 I = NXB, NXE
0107              DO 20 L = 1, NT
0108                 HXI(IT-1,K,J,I,L) = 0.0
0109                 HYI(IT-1,K,J,I,L) = 0.0
0110                 HZI(IT-1,K,J,I,L) = 0.0
0111               IF(I .EQ. NXB) THEN
0112                 EYR(IT,K,J,I,L) = 0.0
0113                 EZR(IT,K,J,I,L) = 0.0
0114                 HXR(IT,K,J,I,L) = 0.0
0115               END IF
0116               IF(J .EQ. NYB)THEN
0117                 EXR(IT,K,J,I,L) = 0.0
0118                 EZR(IT,K,J,I,L) = 0.0
0119                 HYR(IT,K,J,I,L) = 0.0
0120               END IF
0121               IF(K .EQ. NZB)THEN
0122                 EXR(IT,K,J,I,L) = 0.0
0123                 EYR(IT,K,J,I,L) = 0.0
0124                 HZR(IT,K,J,I,L) = 0.0
```

Figure 7.26
(Cont.)* Computer program for Example 7.5 *(Continued).

```
0125              END IF
0126     20       CONTINUE
0127     25       CONTINUE
0128              DO 30 K = NZB, NZE
0129              DO 30 J = NYB, NYE
0130              DO 30 I = NXB, NXE
0131            IF(J .NE. NYB)HZI(IT-1,K,J-1,I,4)=EXR(IT,K,J,I,1)
0132            IF(K .NE. NZB)HYI(IT-1,K-1,J,I,4)=EXR(IT,K,J,I,2)
0133                          HZI(IT-1,K,J,I,2)  =EXR(IT,K,J,I,3)
0134                          HYI(IT-1,K,J,I,2)  =EXR(IT,K,J,I,4)
0135            IF(I .NE. NXB)HZI(IT-1,K,J,I-1,3)=EYR(IT,K,J,I,1)
0136            IF(K .NE. NZB)HXI(IT-1,K-1,J,I,4)=EYR(IT,K,J,I,2)
0137                          HZI(IT-1,K,J,I,1)  =EYR(IT,K,J,I,3)
0138                          HXI(IT-1,K,J,I,2)  =EYR(IT,K,J,I,4)
0139            IF(I .NE. NXB)HYI(IT-1,K,J,I-1,3)=EZR(IT,K,J,I,1)
0140            IF(J .NE. NYB)HXI(IT-1,K,J-1,I,3)=EZR(IT,K,J,I,2)
0141                          HYI(IT-1,K,J,I,1)  =EZR(IT,K,J,I,3)
0142                          HXI(IT-1,K,J,I,1)  =EZR(IT,K,J,I,4)
0143     30       CONTINUE
0144     C
0145     C INSERT THE BOUNDARY CONDITIONS AT ALL BOUNDARIES
0146     C
0147              DO 35 K = NZB, NZE
0148              DO 35 J = NYB, NYE
0149              DO 35 I = NXB, NXE
0150                 IF(I .EQ. NXB)THEN
0151                   HYI(IT-1,K,J,I,1) = RoH * HYR(IT,K,J,I,1)
0152                   HZI(IT-1,K,J,I,1) = RoH * HZR(IT,K,J,I,1)
0153                 END IF
0154                 IF(I .EQ. NXE)THEN
0155                   HZI(IT-1,K,J,I,3) = RoH * HZR(IT,K,J,I,3)
0156                   HYI(IT-1,K,J,I,3) = RoH * HYR(IT,K,J,I,3)
0157                 END IF
0158                 IF(J .EQ. NYB)THEN
0159                   HXI(IT-1,K,J,I,1) = RoH * HXR(IT,K,J,I,1)
0160                   HZI(IT-1,K,J,I,2) = RoH * HZR(IT,K,J,I,2)
0161                 END IF
0162                 IF(J .EQ. NYE)THEN
0163                   HXI(IT-1,K,J,I,3) = RoH * HXR(IT,K,J,I,3)
0164                   HZI(IT-1,K,J,I,4) = RoH * HZR(IT,K,J,I,4)
0165                 END IF
0166                 IF(K .EQ. NZB)THEN
0167                   HXI(IT-1,K,J,I,2) = RoH * HXR(IT,K,J,I,2)
0168                   HYI(IT-1,K,J,I,2) = RoH * HYR(IT,K,J,I,2)
0169                 END IF
0170                 IF(K .EQ. NZE)THEN
0171                   HXI(IT-1,K,J,I,4) = RoH * HXR(IT,K,J,I,4)
0172                   HYI(IT-1,K,J,I,4) = RoH * HYR(IT,K,J,I,4)
0173                 END IF
0174     35       CONTINUE
0175     C
0176     C  COMPUTE THE H-FIELDS AT ALL THE NODES
0177     C
0178              ISIGN = 1
0179            CALL COMPUTE(HXR,HYR,HZR,SERIES,
0180          1                     Z,HXI,HYI,HZI,ISIGN)
0181     C
0182     C  RE-INITIALIZE ALL THE NODES
0183     C
0184              DO 40 K = NZB, NZE
0185              DO 40 J = NYB, NYE
0186              DO 40 I = NXB, NXE
0187              DO 40 L = 1, NT
```

Figure 7.26

(Cont.)* Computer program for Example 7.5 *(Continued).

```
0188                EXI(IT-1,K,J,I,L) = 0.0
0189                EYI(IT-1,K,J,I,L) = 0.0
0190                EZI(IT-1,K,J,I,L) = 0.0
0191     40       CONTINUE
0192              DO 45 K = NZB, NZE
0193              DO 45 J = NYB, NYE
0194              DO 45 I = NXB, NXE
0195                         EZI(IT-1,K,J,I,4)  =HXR(IT,K,J,I,1)
0196                         EYI(IT-1,K,J,I,4)  =HXR(IT,K,J,I,2)
0197              IF(J .NE. NYE)EZI(IT-1,K,J+1,I,2)=HXR(IT,K,J,I,3)
0198              IF(K .NE. NZE)EYI(IT-1,K+1,J,I,2)=HXR(IT,K,J,I,4)
0199                         EZI(IT-1,K,J,I,3)  =HYR(IT,K,J,I,1)
0200                         EXI(IT-1,K,J,I,4)  =HYR(IT,K,J,I,2)
0201              IF(I .NE. NXE)EZI(IT-1,K,J,I+1,1)=HYR(IT,K,J,I,3)
0202              IF(K .NE. NZE)EXI(IT-1,K+1,J,I,2)=HYR(IT,K,J,I,4)
0203                         EYI(IT-1,K,J,I,3)  =HZR(IT,K,J,I,1)
0204                         EXI(IT-1,K,J,I,3)  =HZR(IT,K,J,I,2)
0205              IF(I .NE. NXE)EYI(IT-1,K,J,I+1,1)=HZR(IT,K,J,I,3)
0206              IF(J .NE. NYE)EXI(IT-1,K,J+1,I,1)=HZR(IT,K,J,I,4)
0207     45       CONTINUE
0208     C
0209     C  CALCULATE THE IMPULSE RESPONSE AT NXO,NYO,NZO
0210     C
0211              EXT = 0.0
0212              EYT = 0.0
0213              EZT = 0.0
0214              HXT = 0.0
0215              HYT = 0.0
0216              HZT = 0.0
0217              DO 50 L = 1, NT
0218                 EXT = EXT + EXI(IT-1,NZO,NYO,NXO,L) * (2.0/Y)
0219                 EYT = EYT + EYI(IT-1,NZO,NYO,NXO,L) * (2.0/Y)
0220                 EZT = EZT + EZI(IT-1,NZO,NYO,NXO,L) * (2.0/Y)
0221                 HXT = HXT + HXI(IT-1,NZO,NYO,NXO,L) * (2.0/Y)
0222                 HYT = HYT + HYI(IT-1,NZO,NYO,NXO,L) * (2.0/Y)
0223     50          HZT = HZT + HZI(IT-1,NZO,NYO,NXO,L) * (2.0/Y)
0224     C
0225     C  SUM THE FREQUENCY RESPONSE(imaginary and real
0226     C  parts) FOR DIFFERENT VALUES OF MESH-SIZE DIVIDED
0227     C  BY WAVELENGTH BUT FIRST CONVOLVE IMPULSE RESPONSE
0228     C  WITH HANNING PROFILE
0229     C
0230            DINCR = DELTA
0231            DO 55 L = 1, NUMPT
0232               T = DFLOAT(ITIME)
0233               AMT = DFLOAT(ITRATE)
0234               EXTH = EXT * (1.0 + DCOS(PI * T/AMT)) * 0.5
0235               EYTH = EYT * (1.0 + DCOS(PI * T/AMT)) * 0.5
0236               EZTH = EZT * (1.0 + DCOS(PI * T/AMT)) * 0.5
0237               HXTH = HXT * (1.0 + DCOS(PI * T/AMT)) * 0.5
0238               HYTH = HYT * (1.0 + DCOS(PI * T/AMT)) * 0.5
0239               HZTH = HZT * (1.0 + DCOS(PI * T/AMT)) * 0.5
0240           EX(1,L) = EX(1,L) + EXTH * DCOS(2.0*PI*T*DINCR)
0241           EX(2,L) = EX(2,L) + EXTH * DSIN(2.0*PI*T*DINCR)
0242           EY(1,L) = EY(1,L) + EYTH * DCOS(2.0*PI*T*DINCR)
0243           EY(2,L) = EY(2,L) + EYTH * DSIN(2.0*PI*T*DINCR)
0244           EZ(1,L) = EZ(1,L) + EZTH * DCOS(2.0*PI*T*DINCR)
0245           EZ(2,L) = EZ(2,L) + EZTH * DSIN(2.0*PI*T*DINCR)
0246           HX(1,L) = HX(1,L) + HXTH * DCOS(2.0*PI*T*DINCR)
0247           HX(2,L) = HX(2,L) + HXTH * DSIN(2.0*PI*T*DINCR)
0248           HY(1,L) = HY(1,L) + HYTH * DCOS(2.0*PI*T*DINCR)
0249           HY(2,L) = HY(2,L) + HYTH * DSIN(2.0*PI*T*DINCR)
```

Figure 7.26

(Cont.)* Computer program for Example 7.5 *(Continued).

```
0250          HZ(1,L) = HZ(1,L) + HZTH * DCOS(2.0*PI*T*DINCR)
0251          HZ(2,L) = HZ(2,L) + HZTH * DSIN(2.0*PI*T*DINCR)
0252              OUT(1,L) = DINCR
0253    55        DINCR = DINCR + DEL
0254    60      CONTINUE
0255              DO L = 1, NUMPT
0256                 CEX = CMPLX(EX(1,L),EX(2,L))
0257                 CEY = CMPLX(EY(1,L),EY(2,L))
0258                 CEZ = CMPLX(EZ(1,L),EZ(2,L))
0259                 CHX = CMPLX(HX(1,L),HX(2,L))
0260                 CHY = CMPLX(HY(1,L),HY(2,L))
0261                 CHZ = CMPLX(HZ(1,L),HZ(2,L))
0262                 OUT(2,L) = CABS(CEX)
0263                 OUT(3,L) = CABS(CEY)
0264                 OUT(4,L) = CABS(CEZ)
0265                 OUT(5,L) = CABS(CHX)
0266                 OUT(6,L) = CABS(CHY)
0267                 OUT(7,L) = CABS(CHZ)
0268          OUT(8,L)=SQRT(SQMAG(CEX)+SQMAG(CEY)+SQMAG(CEZ))
0269          OUT(9,L)=SQRT(SQMAG(CHX)+SQMAG(CHY)+SQMAG(CHZ))
0270              END DO
0271    C
0272    C  PICK THE MODES
0273    C
0274              DO 65 L = 2, 9
0275              DO 65 K = 1, NUMPT
0276                 IF(K .NE. 1 .AND. K .NE. NUMPT) THEN
0277                    IF(OUT(L,K) .GT. OUT(L,K-1) .AND.
0278         1            OUT(L,K) .GT. OUT(L,K+1)) THEN
0279                      WRITE(6,80) L,K,(OUT(J,K),J=1,9)
0280                    END IF
0281                 END IF
0282    65         CONTINUE
0283    C
0284    C  WRITE OUT DATA FOR PLOTTING
0285    C
0286              DO 70 L = 2, 9
0287              DO 70 K = 1, NUMPT
0288              WRITE(6,75) K, OUT(1,K), OUT(L,K)
0289    70        CONTINUE
0290    75        FORMAT(I5,4F15.8)
0291    80        FORMAT(2I5,10F8.4)
0292              STOP
0293              END

0001    C************************************************
0002    C  THIS SUBROUTINE COMPUTES THE REFLECTED PULSES
0003    C
0004              SUBROUTINE COMPUTE(AXR,AYR,AZR,SCATTER,
0005         1                                 W,AXI,AYI,AZI,ISIGN)
0006              IMPLICIT REAL*8(A-H,O-Z), INTEGER*2(I-N)
0007              DIMENSION AXR(2,NZE,NYE,NXE,NT),
0008         1     AYR(2,NZE,NYE,NXE,NT),SCATTER(5,5),
0009         2     AZR(2,NZE,NYE,NXE,NT),AXI(2,NZE,NYE,NXE,NT),
0010         3      AYI(2,NZE,NYE,NXE,NT),AZI(2,NZE,NYE,NXE,NT)
0011
0012              COMMON / PART1 /NT,NXB,NXE,NYB,NYE,NZB,NZE,IT
0013
0014              DO 20 K = NZB, NZE
0015              DO 20 J = NYB, NYE
0016              DO 20 I = NXB, NXE
0017    C   INSERT FEW LINES HERE FOR INHOMOGENEOUS CAVITY
0018                DO 15 L = 1, NT
```

Figure 7.26

(Cont.)* Computer program for Example 7.5 *(Continued).

```
0019                AXRS = 0.0
0020                AYRS = 0.0
0021                AZRS = 0.0
0022                DO 10 M = 1, MT
0023          AXRS = AXRS+2./W*SCATTER(L,M)*AXI(IT-1,K,J,I,M)
0024          AYRS = AYRS+2./W*SCATTER(L,M)*AYI(IT-1,K,J,I,M)
0025          AZRS = AZRS+2./W*SCATTER(L,M)*AZI(IT-1,K,J,I,M)
0026     10         CONTINUE
0027          AXR(IT,K,J,I,L)=AXRS+ISIGN*AXI(IT-1,K,J,I,L)
0028          AYR(IT,K,J,I,L)=AYRS+ISIGN*AYI(IT-1,K,J,I,L)
0029          AZR(IT,K,J,I,L)=AZRS+ISIGN*AZI(IT-1,K,J,I,L)
0030     15         CONTINUE
0031     20       CONTINUE
0032              RETURN
0033              END
```

Figure 7.26
(Cont.) **Computer program for Example 7.5.**

Table 7.5 Resonant Wavenumber ($k_c a$) of an Empty Rectangular Cavity, where $k_c a = 4\pi a/c$ and λ is the Free-space Wavelength

Modes	Exact results	TLM results	Error %
TM_{110}	5.6636	5.6400	0.42
TE_{101}	7.0249	6.9819	0.61
TM_{210}, TE_{011}	7.8540	7.8112	0.54

Example 7.6

Modify the TLM program in Fig. 7.26 to calculate the resonant wavenumber $k_c a$ of the inhomogeneous cavities in Fig. 7.27. Take $\epsilon_r = 16, a = \Delta\ell, b = 3a/10, d = 4a/10, s = 7a/12$. □

Solution

The main program in Fig. 7.26 is applicable to this example. Only the subroutine COMPUTE requires slight modification to take care of the inhomogeneity of the cavity. The modifications in the subprogram for the cavities in Fig. 7.27 (a) and (b) are shown in Fig. 7.28 (a) and (b), respectively. For each modification, the few lines in Fig. 7.28 are inserted in between lines 15 and 17 in subroutine COMPUTE of Fig. 7.26. The results are shown in Table 7.6 for TE_{101} mode. ▮

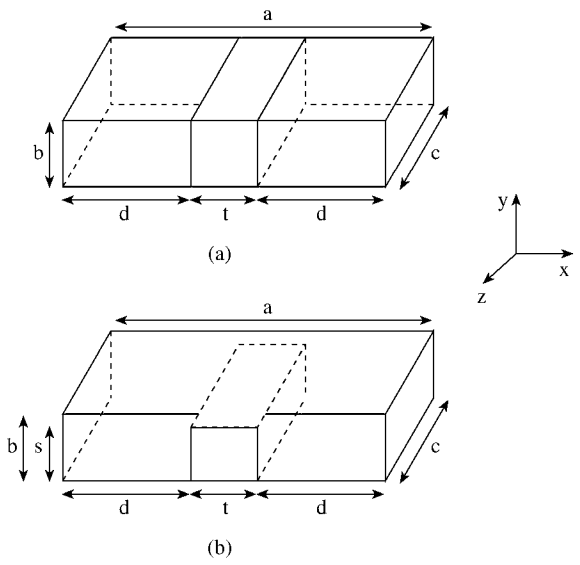

Figure 7.27
Rectangular cavity loaded with dielectric slab.

```
      :
      :
      :

0001     C************************************************
0002     C  THIS SUBROUTINE COMPUTES THE REFLECTED PULSES
0003     C
0004              SUBROUTINE COMPUTE(AXR,AYR,AZR,SCATTER,
0005          1                              WW,AXI,AYI,AZI,ISIGN)

      :
      :
      :

0017     C   INSERT FEW LINES HERE FOR INHOMOGENEOUS CAVITY
0018         IF ((I.GE.9).AND.(I.LE.13)
0019          1                .AND.(ISIGN.EQ.-1)) THEN
0020           NT = 5
0021            W = WW
0022                       ELSE
0023           NT = 4
0024            W = 4.0
0025            END IF

      :
      :
      :
```

Figure 7.28
(a) Modification in subroutine COMPUTE for the inhomogeneous cavity of Fig. 7.27 (a) ***(Continued).***

```
0001    C*************************************************
0002    C  THIS SUBROUTINE COMPUTES THE REFLECTED PULSES
0003    C
0004              SUBROUTINE COMPUTE(AXR,AYR,AZR,SCATTER,
0005           1                             WW,AXI,AYI,AZI,ISIGN)

:
:
:

0017    C   INSERT FEW LINES HERE FOR INHOMOGENEOUS CAVITY
0018        IF (J.GT.4) GO TO 5
0019        IF ((I.GE.9).AND.(I.LE.13)
0020         1                  .AND.(ISIGN.EQ.-1)) THEN
0021          NT = 5
0022           W = WW
0023                 GO TO 6
0024        END IF
0025    5   CONTINUE
0026          NT = 4
0027           W = 4.0
0028    6   CONTINUE
0029                DO 15 L = 1, NT

:
:
```

Figure 7.28
***(Cont.)* (b) Modification in subroutine COMPUTE for the inhomogeneous cavity of Fig. 7.27 (b).**

Table 7.6 Resonant Wavenumber ($k_c a$) for TE_{101} Mode of Inhomogeneous Rectangular Cavities, where $k_c a = 4\pi a/c$, and λ is the Free-space Wavelength

Modes	Exact results	TLM results	Error %
Fig. 7.27 (a)	2.589	2.5761	0.26
Fig. 7.27 (b)	(none)	3.5387	

7.7 Error Sources and Correction

As in all approximate solutions such as the TLM technique, it is important that the error in the final result be minimal. In the TLM method, four principal sources of error can be identified [10, 28, 29]:

- truncation error,
- coarseness error,

- velocity error,
- misalignment error.

Each of these sources of error and ways of minimizing it will be discussed.

7.7.1 Truncation Error

The truncation error is due to the need to truncate the impulse response in time. As a result of the finite duration of the impulse response, its Fourier transform is not a line spectrum but rather a superposition of $\sin x/x$ functions, which may interfere with each other and cause a slight shift in their maxima. The maximum truncation error is given by

$$e_T = \frac{\Delta S}{\Delta \ell / \lambda c} = \frac{3\lambda_c}{SN^2\pi^2\Delta\ell} \tag{7.83}$$

where λ_c is the cutoff wavelength to be calculated, ΔS is the absolute error in $\Delta\ell/\lambda_c$, S is the frequency separation (expressed in terms of $\Delta\ell/\lambda_c$, λ_c being the free-space wavelength) between two neighboring peaks as shown in Fig. 7.29, and N is the number of iterations. Equation (7.83) indicates that e_T decreases with increasing N and increasing S. It is therefore desirable to make N large and suppress all unwanted modes close to the desired mode by carefully selecting the input and output points in the TLM mesh. An alternative way of reducing the truncation error is to use a Hanning window in the Fourier transform. For further details on this, one should consult [10, 31].

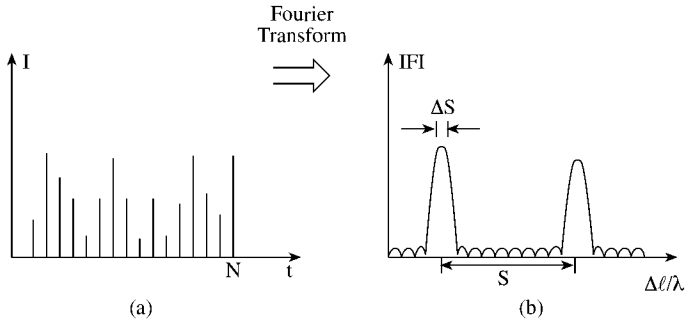

Figure 7.29
Source of truncation error: (a) Truncated output impulse, (b) resulting truncation error in the frequency domain.

7.7.2 Coarseness Error

This occurs when the TLM mesh is too coarse to resolve highly nonuniform fields as can be found at corners and edges. An obvious solution is to use a finer mesh

($\Delta\ell \rightarrow 0$), but this would lead to large memory requirements and there are limits to this refinement. A better approach is to use variable mesh size so that a higher resolution can be obtained in the nonuniform field region [71]. This approach requires more complicated programming.

7.7.3 Velocity Error

This stems from the assumption that propagation velocity in the TLM mesh is the same in all directions and equal to $u_n = u/\sqrt{2}$, where u is the propagation velocity in the medium filling the structure. The assumption is only valid if the wavelength λ_n in the TLM mesh is large compared with the mesh size $\Delta\ell(\Delta\ell/\lambda_n < 0.1)$. Thus the cutoff frequency f_{cn} in the TLM mesh is related to the cutoff frequency f_c of the real structure according to $f_c = f_{cn}\sqrt{2}$. If $\Delta\ell$ is comparable with λ_n, the velocity of propagation depends on the direction and the assumption of constant velocity results in a velocity error in f_c. Fortunately, a measure to reduce the coarseness error takes care of the velocity error as well.

7.7.4 Misalignment Error

This error occurs in dielectric interfaces in three-dimensional inhomogeneous structures such as microstrip or fin line. It is due to the manner in which boundaries are simulated in a three-dimensional TLM mesh; dielectric interfaces appear halfway between nodes, while electric and magnetic boundaries appear across such nodes. If the resulting error is not acceptable, one must make two computations, one with recessed and one with protruding dielectric, and take the average of the results.

7.8 Absorbing Boundary Conditions

Just like FDTD and FEM, the TLM method requires absorbing boundary conditions (ABCs) at the limit of the solution region. Several ABCs have proposed for TLM simulations [32]–[37]. It has been recognized that the perfectly matched-layer (PML) technique, discussed for FDTD in Section 3.9, has excellent absorbing performances that are significantly superior to other techniques. So only PML will be discussed here.

Consider the PML region and the governing Maxwell's equations. Each field component is split into two. For example, $E_x = E_{xy} + E_{xz}$. In 3-D, Maxwell's

equations become twelve [38]:

$$\mu_o \frac{H_{xy}}{\partial t} + \sigma_y^* H_{xy} = -\frac{\partial (E_{zx} + E_{zy})}{\partial y} \tag{7.84a}$$

$$\mu_o \frac{H_{xz}}{\partial t} + \sigma_z^* H_{xz} = \frac{\partial (E_{yx} + E_{yz})}{\partial z} \tag{7.84b}$$

$$\mu_o \frac{H_{yz}}{\partial t} + \sigma_z^* H_{yz} = -\frac{\partial (E_{xy} + E_{xz})}{\partial z} \tag{7.84c}$$

$$\mu_o \frac{H_{yx}}{\partial t} + \sigma_x^* H_{yx} = \frac{\partial (E_{zx} + E_{zy})}{\partial x} \tag{7.84d}$$

$$\mu_o \frac{H_{zx}}{\partial t} + \sigma_x^* H_{zx} = -\frac{\partial (E_{yx} + E_{yz})}{\partial x} \tag{7.84e}$$

$$\mu_o \frac{H_{zy}}{\partial t} + \sigma_y^* H_{zy} = \frac{\partial (E_{xy} + E_{xz})}{\partial y} \tag{7.84f}$$

$$\epsilon_o \frac{E_{xy}}{\partial t} + \sigma_y E_{xy} = \frac{\partial (H_{zx} + H_{zy})}{\partial y} \tag{7.84g}$$

$$\epsilon_o \frac{E_{xz}}{\partial t} + \sigma_z E_{xz} = -\frac{\partial (H_{yx} + H_{yz})}{\partial z} \tag{7.84h}$$

$$\epsilon_o \frac{E_{yz}}{\partial t} + \sigma_z E_{yz} = \frac{\partial (H_{xy} + H_{xz})}{\partial z} \tag{7.84i}$$

$$\epsilon_o \frac{E_{yx}}{\partial t} + \sigma_x E_{yx} = -\frac{\partial (H_{zx} + H_{zy})}{\partial x} \tag{7.84j}$$

$$\epsilon_o \frac{E_{zx}}{\partial t} + \sigma_x E_{zx} = \frac{\partial (H_{yx} + H_{yz})}{\partial x} \tag{7.84k}$$

$$\epsilon_o \frac{E_{zy}}{\partial t} + \sigma_y E_{zy} = -\frac{\partial (H_{xy} + H_{xz})}{\partial y} \tag{7.84l}$$

in which (σ_i, σ_i^*) where $i \in \{x, y, z\}$ are, respectively, the electric and magnetic conductivities of the PML region and they satisfy

$$\frac{\sigma_i}{\epsilon_o} = \frac{\sigma_i^*}{\mu_o} \tag{7.85}$$

Using the usual Yees's notation, the field samples are expressed as

$$\begin{aligned}
E_x^n(i, j, k) &= E_x[(i + 1/2)\delta, j\delta, k\delta, (n + 1/2)\delta t] \\
E_y^n(i, j, k) &= E_y[i\delta, (j + 1/2)\delta, k\delta, (n + 1/2)\delta t] \\
E_z^n(i, j, k) &= E_z[i\delta, j\delta, (k + 1/2)\delta, (n + 1/2)\delta t] \\
H_x^n(i, j, k) &= H_x[i\delta, (j + 1/2)\delta, (k + 1/2)\delta, n\delta t] \\
H_y^n(i, j, k) &= H_y[(i + 1/2)\delta, j\delta, (k + 1/2)\delta, n\delta t] \\
H_z^n(i, j, k) &= H_z[(i + 1/2)\delta, (j + 1/2)\delta, k\delta, n\delta t]
\end{aligned} \tag{7.86}$$

where $\delta = \Delta x = \Delta y = \Delta z = \Delta \ell$. Without loss of generality, we set $\delta t = \delta/2c$. Since we want to interface the FDTD algorithm with the TLM, we express the fields

in terms of voltages. For a cubic cell,

$$V^n_{ers}(i,j,k) = \delta E^n_{rs}(i,j,k) \quad \text{with } r \in \{x,y\}, \quad s \in \{x,z\} \tag{7.87a}$$

$$V^n_{ms}(i,j,k) = \sqrt{\frac{\mu_o}{\epsilon_o}}\delta H^n_s(i,j,k) \quad \text{with } s \in \{y,z\} \tag{7.87b}$$

where the subscripts e and m denote electric and magnetic, respectively. By applying the central-difference scheme to Eq. (7.84), we obtain after some algebraic manipulations

$$V^n_{exy}(i,j,k) = \left(\frac{4-G_{ey}}{4+G_{ey}}\right) V^{n-1}_{exy}(i,j,k) + \left(\frac{2}{4+G_{ey}}\right)\left(V^n_{mz}(i,j,k) - V^n_{mz}(i,j-1,k)\right) \tag{7.88a}$$

$$V^n_{exz}(i,j,k) = \left(\frac{4-G_{ez}}{4+G_{ez}}\right) V^{n-1}_{exz}(i,j,k) - \left(\frac{2}{4+G_{ez}}\right)\left(V^n_{my}(i,j,k) - V^n_{my}(i,j,k-1)\right) \tag{7.88b}$$

$$V^n_{ex}(i,j,k) = V^n_{exy}(i,j,k) + V^n_{exz}(i,j,k) \tag{7.88c}$$

where $G_{es} = \delta\sigma_s(i,j,k)\sqrt{\mu_o\epsilon_o}$ with $s \in \{y,z\}$. Applying this TLM FDTD-PML algorithm has been found to yield excellent performance with reflection level below -55 dB [37].

7.9 Concluding Remarks

This chapter has described the transmission-line-matrix (TLM) method which is a modeling process rather than a numerical method for solving differential or equations. The flexibility, versatility, and generality of the time-domain method have been demonstrated. Our discussion in this chapter has been introductory, and one is advised to consult [10], [39]–[41] for a more in-depth treatment. A generalized treatment of TLM in the curvilinear coordinate system is presented in [42], while a theoretical basics of TLM is derived in [43]. Further developments in TLM can be found in [44]–[50].

Although the application of the TLM method in this chapter has been limited to diffusion and wave propagation problems, the method has a wide range of applications. The technique has been applied to other problems such as:

- cutoff frequencies in fin lines [29, 30],
- transient analysis of striplines [51, 52],

- linear and nonlinear lumped networks [53]–[58],
- microstrip lines and resonators [17, 59, 60],
- diffusion problems [61]–[63],
- electromagnetic compatibility problems [21], [64]–[67],
- antenna problems [43, 53, 68, 69],
- induced currents in biological bodies exposed to EM fields [70],
- cylindrical and spherical waves [53, 71, 72], and
- others [73]–[78].

A major advantage of the TLM method, as compared with other numerical techniques, is the ease with which even the most complicated structures can be analyzed. The great flexibility and versatility of the method reside in the fact that the TLM mesh incorporates the properties of EM fields and their interaction with the boundaries and material media. Hence, the EM problem need not be formulated for every new structure. Thus a general-purpose program such as in [79] can be developed such that only the parameters of the structure need be entered for computation. Another advantage of using the TLM method is that certain stability properties can be deduced by inspection of the circuit. There are no problems with convergence, stability or spurious solutions. The method is limited only by the amount of memory storage required, which depends on the complexity of the TLM mesh. Also, being an explicit numerical solutions, the TLM method is suitable for nonlinear or inhomogeneous problems since any variation of material properties may be updated at each time step.

Perhaps the best way to conclude this chapter is to compare the TLM method with the finite difference method, especially FDTD [80]–[86]. While TLM is a physical model based on Huygens' principle using interconnected transmission lines, the FDTD is an approximate mathematical model directly based on Maxwell's equations. In the two-dimensional TLM, the magnetic and electric field components are located at the same position with respect to space and time, whereas in the corresponding two-dimensional FDTD cell, the magnetic field components are shifted by half an interval in space and time with respect to the electric field components. Due to this displacement between electric and magnetic field components in Yee's FDTD, Chen et al. [83] derived a new FDTD and demonstrated that the new FDTD formulation is exactly equivalent to the symmetric condensed node model used in the TLM method. This implies that the TLM algorithm can be formulated in FDTD form and vice versa. However, both algorithms retain their unique advantages. For example, the FDTD model has a simpler algorithm where constitutive parameters are directly introduced, while the TLM has certain advantages in the modeling of boundaries and the partitioning of the solution region. Furthermore, the FDTD requires less than one-half of the CPU time spent by the equivalent TLM program under identical conditions. While the TLM scheme requires 22 real memory stores per node, the FDTD method requires only seven real memory stores per 3-D node in an isotropic dielectric medium [81].

Although both are time-domain schemes, the quantities available at each time step are the solution in TLM model and there is no need for an iterative procedure. The dispersion relations for TLM and FDTD are identical for 2-D but are different for 3-D problems. The comparison is summarized in Table 7.7. According to Johns, the two methods complement each other rather than compete with each other [80].

Table 7.7 A Comparison of TLM and FDTD Methods

FDTD	TLM
A mathematical model based on Maxwell's equations	A physical model based on Huygen's principle
E and H are shifted with respect to space and time	E and H are calculated at the same time and position
Requires less memory and one-half the CPU time	Needs more memory and more CPU time
Provides solution at each time step	Requires some iterative procedure

References

[1] G. Kron, "Numerical solution of ordinary and partial differential equations by means of equivalent circuits," *J. Appl. Phys.*, Vol. 16, Mar. 1945, pp. 172–186.

[2] C.H. Durney and C.C. Johnson, *Introduction to Modern Electromagnetics*. New York: McGraw-Hill, 1969, pp. 286–287.

[3] P.P. Silvester and F.L. Ferrari, *Finite Elements for Electrical Engineers*. Cambridge: Cambridge University Press, 1983, p. 24.

[4] R.H. Park, "Definition of an ideal synchronous machine and formulators for armature flux linkages," *Gen. Elect. Rev.*, vol. 31, 1928, pp. 332–334.

[5] G. Kron, "Equivalent circuit of the field equations of Maxwell," *Proc. IRE*, May 1944, pp. 289–299.

[6] G. Kron, *Equivalent Circuits os Electrical Machinery*. New York: John Wiley, 1951.

[7] N. Marcovitz and J. Schwinger, "On the reproduction of the electric and magnetic fields produced by currents and discontinuity in wave guides, I," *J. Appl. Phys.*, vol. 22, no. 6, June 1951. pp. 806–819.

[8] J. Schwinger and D.S. Saxon, *Discontinuities in Waveguides*. New York: Gordon and Breach, 1968.

[9] P.B. Johns and R.L. Beurle, "Numerical solution of 2-dimensional scattering problems using a transmission line matrix," *Proc. IEEE,* vol. 118, no. 9, Sept. 1971, pp. 1203–1208.

[10] W.J.R. Hoefer, "The transmission-line matrix method—theory and applications," *IEEE Trans. Microwave Theory Tech.*, vol. MTT-33, no. 10, Oct. 1985, pp. 882–893.

[11] C. Christopoulos, *The Transmission-Line Modeling Method (TLM).* New York: IEEE Press, 1995.

[12] M.N.O. Sadiku and L.C. Agba, "A simple introduction to the transmission-line modeling," *IEEE Trans. Cir. Sys.*, vol. CAS-37, no. 8, Aug. 1990, pp. 991–999.

[13] B.J. Ley, *Computer Aided Analysis and Design for Electrical Engineers.* New York: Holt, Rinehart and Winston, 1970, pp. 815–817.

[14] M.N.O. Sadiku, *Elements of Electromagnetics.* New York: Oxford Univ. Press, 2nd ed., 1992, pp. 518–592.

[15] C.C. Wong, "Solution of the network analog of one-dimensional field equations using the ladder method," *IEEE Trans. Educ.*, vol. E-28, no. 3, Aug. 1985, pp. 176–179.

[16] C.C. Wong and W.S. Wong, "Multigrid TLM for diffusion problems," *Int. J. Num. Model.*, vol. 2, no. 2, 1989, pp. 103–111.

[17] G.E. Marike and G. Yek, "Dynamic three-dimensional T.L.M. analysis of microstrip lines on anisotropic substrate," *IEEE Trans. Micro. Theo. Tech.*, vol. MTT-33, no. 9, Sept. 1985, pp. 789–799.

[18] P.B. Johns, "Applications of the transmission-line matrix method to homogeneous waveguides of arbitrary cross-section," *Proc. IEEE,* vol. 119, no. 8, Aug. 1972, pp. 1086–1091.

[19] R.A. Waldron, *Theory of Guided Electromagnetic Waves.* London: Van Nostrand Reinhold Co., 1969, pp. 157–172.

[20] N.R.S. Simons and E. Bridges, "Method for modeling free space boundaries in TLM situations," *Elect. Lett.*, vol. 26, no. 7, March 1990, pp. 453–455.

[21] C. Christopoulos and J.L. Herring, "The application of the transmission-line modeling (TLM) to electromagnetic compatibility problems," *IEEE Trans. Elect. Magn. Comp.*, vol. 35, no. 2, May 1993, pp. 185–191.

[22] L.C. Agba, "Transmission-line-matrix modeling of inhomogeneous rectangular waveguides and cavities," M.S. thesis, Department of Electrical and Computer Engr., Florida Atlantic University, Boca Raton, Aug. 1987.

[23] P.B. Johns, "The solution of inhomogeneous waveguide problems using a transmission line matrix," *IEEE Trans. Micro. Theo. Tech.*, vol. MTT-22, no. 3, Mar. 1974, pp. 209–215.

[24] S. Akhtarzad and P.B. Johns, "Generalized elements for t.l.m. method of numerical analysis," *Proc. IEEE*, vol. 122, no. 12, Dec. 1975, pp. 1349–1352.

[25] S. Akhtarzad and P.B. Johns, "Numerical solution of lossy waveguides: T.L.M. computer programs," *Elec. Lett.*, vol. 10, no. 15, July 25, 1974, pp. 309–311.

[26] S. Akhtarzad and P.B. Johns, "Transmission line matrix solution of waveguides with wall losses," *Elec. Lett.*, vol. 9, no. 15, July 1973, pp. 335–336.

[27] S. Akhtarzad and P.B. Johns, "Solution of Maxwell's equations in three space dimensional and time by the T.L.M. method of numerical analysis," *Proc. IEEE*, vol. 122, no. 12, Dec. 1975, pp. 1344–1348.

[28] S. Akhtarzad and P.B. Johns, "Three-dimensional transmission-line Matrix computer analysis of microstrip resonators," *IEEE Trans. Micro. Theo. Tech.*, vol. MTT-23, no. 12, Dec. 1975, pp. 990–997.

[29] Y.C. Shih and W.J.R. Hoefer, "The accuracy of TLM analysis of finned rectangular waveguides," *IEEE Trans. Micro. Theo. Tech.*, vol. MTT-28, no. 7, July 1980, pp. 743–746.

[30] Y.C. Shih and W.J.R. Hoefer, "Dominant and second-order mode cutoff frequencies in fin lines calculated with a two-dimensional TLM program," *IEEE Trans. Micro. Theo. Tech.*, vol. MTT-28, no. 12, Dec. 1980, pp. 1443–1448.

[31] N. Yoshida, et al., "Transient analysis of two-dimensional Maxwell's equations by Bergeron's method," *Trans. IECE* (Japan), vol. J62B, June 1979, pp. 511–518.

[32] J.A. Morente and J.A. Porti, and M. Khalladi, "Absorbing boundary conditions for the TLM method," *IEEE Trans. Micro. Theo. Tech.*, vol. 40, no. 11, Nov. 1992, pp. 2095–2099.

[33] S.C. Pomeroy, G. Zhang, and C. Wykes, "Variable coefficient absorbing boundary condition for TLM," *Elect. Lett.*, vol. 29, no. 13, June 1993, pp. 1198–1200.

[34] C. Eswarappa and W.J.R. Hoefer, "One-way equation absorbing boundary conditions for 3-D TLM analysis of planar and quasi-planar structures," *IEEE Trans. Micro. Theo. Tech.*, vol. 42, no. 9, Sept. 1994, pp. 1669–1677.

[35] N. Kukutsu and R. Konno, "Super absorption boundary conditions for guided waves in the 3-D TLM simulation," *IEEE Micro. Guided Wave Lett.*, vol. 5, Sept. 1995, pp. 299–301.

[36] N. Pena and M.M. Ney, "A new TLM node for Berenger's perfectly matched layer (PML)," *IEEE Micro. Guided Wave Lett.*, vol. 6, Nov. 1996, pp. 410–412.

[37] N. Pena and M.M. Ney, "Absorbing-boundary conditions using perfectly matched-layer (PML) technique for three-dimensional TLM simulations," *IEEE Trans. Micro. Theo. Tech.*, vol. 45, no. 10, Oct. 1997, pp. 1749–1755.

[38] A. Taflove, *Computational Electrodynamics*. Boston, MA: Artech House, 1995, pp. 189–190.

[39] P.B. Johns. "Numerical modeling by the TLM method," in A. Wexler (ed.), *Large Engineering Systems*. Oxford: Pergamon, 1977.

[40] T. Itoh (ed.), *Numerical Techniques for Microwave and Millimeterwave Passive Structure*. New York: John Wiley, 1989, pp. 496–591.

[41] P.B. Johns, "Simulation of electromagnetic wave interactions by transmission-line modeling (TLM)," *Wave Motion*, vol. 10, no. 6, 1988, pp. 597–610.

[42] A.K. Bhattacharyya and R. Garg, "Generalized transmission line model for microstrip patches," *IEEE Proc.*, vol. 132, Pt. H, no. 2, April 1985, pp. 93–98.

[43] M. Krumpholz and P. Russer, "A field theoretical derivation of TLM," *IEEE Trans. Micro. Theo. Tech.*, vol. 42, no. 9, Sept. 1994, pp. 1660–1668.

[44] P. Naylor and C. Christopoulos, "A comparison between the time-domain and the frequency-domain diakopic methods of solving field problems by transmission-line modeling," *Int. Jour. Num. Model.*, vol. 2, no. 1, 1989, pp. 17–30.

[45] P. Saguet, "The 3-D transmission-line matrix method theory and comparison of the processes," *Int. Jour. Num. Model.*, vol. 2, 1989, pp. 191–201.

[46] W.J.R. Hoefer, "The discrete time domain Green's function or Johns matrix — a new powerful concept in transmission line modeling (TLM)," *Int. Jour. Num. Model.*, vol. 2, no. 4, 1989, pp. 215–225.

[47] L.R.A.X. de Menezes and W.J.R. Hoefer, "Modeling of general constitutive relationship in SCN TLM," *IEEE Trans. Micro. Theo. Tech.*, vol. 44, no. 6, June 1996, pp. 854–861.

[48] V. Trenkic, C. Christopoulos, and T.M. Benson, "Simple and elegant formulation of scattering in TLM nodes," *Elec. Lett.*, vol. 29, no. 18, Sept. 1993, pp. 1651–1652.

[49] J.L. Herring and C. Christopoulos, "Solving electromagnetic field problems using a multiple grid transmission-line modeling method," *IEEE Trans. Ant. Prop.*, vol. 42, no. 12, Dec. 1994, pp. 1655–1658.

[50] J.A. Porti, J.A. Morente, and M.C. Carrion, "Simple derivation of scattering matrix for TLM nodes," *Elect. Lett.*, vol. 34, no. 18, Sept. 1998, pp. 1763–1764.

[51] N. Yoshida, I. Fukai, and J. Fukuoka, "Transient analysis of three-dimensional electromagnetic fields by nodal equations," *Trans. Inst. Electron. Comm. Engr. Japan*, vol. J63B, Sept. 1980, pp. 876–883.

[52] N. Yoshida and I. Fukai, "Transient analysis of a stripline having corner in three-dimensional space," *IEEE Trans. Micro. Theo. Tech.*, vol. MTT-32, no. 5, May 1984, pp. 491–498.

[53] W.R. Zimmerman, "Network analog of Maxwell's field equations in one and two dimensions," *IEEE Trans. Educ.*, vol. E-25, no. 1, Feb. 1982, pp. 4–9.

[54] P.B. Johns and M. O'Brien, "Use of the transmission-line modeling (t.l.m.) method to solve non-linear lumped networks," *Radio Electron. Engr.*, vol. 50, no. 1/2, Jan./Feb., 1980, pp. 59–70.

[55] J.W. Bandler, et al., "Transmission-line modeling and sensitivity evaluation for lumped network simulation and design in the time domain," *J. Franklin Inst.*, vol. 304, no. 1, 1971, pp. 15–23.

[56] C.R. Brewitt-Taylor and P.B. Johns, "On the construction and numerical solution of transmission line and lumped network models of Maxwell's equations," *Inter. J. Numer. Meth. Engr.*, vol. 15, 1980, pp. 13–30.

[57] P. Saguet and W.J.R. Hoefer, "The modeling of multiaxial discontinuities in quasi-planar structures with the modified TLM method," *Int. J. Num. Model.*, vol. 1, 1988, pp. 7–17.

[58] E.M. El-Sayed and M.N. Morsy, "Analysis of microwave ovens loaded with lossy process materials using the transmission-line matrix method," *Int. J. Num. Meth. Engr.*, vol. 20, 1984, pp. 2213–2220.

[59] N.G. Alexopoulos, "Integrated-circuit structures on anisotropic substrates," *IEEE Trans. Micro. Theo. Tech.*, vol. MTT-33, no. 10, Oct. 1985, pp. 847–881.

[60] S. Akhatarzad and P.B. Johns, "TLMRES-the TLM computer program for the analysis of microstrip resonators," *IEEE Trans. Micro. Theo. Tech.*, vol. 35, no. 1, Jan. 1987, pp. 60–61.

[61] P.B. Johns, "A simple explicit and unconditionally stable numerical routine for the solution of the diffusion equation," *Int. Jour. Numer. Methods Engr.*, vol. 11, 1977, pp. 1307–1328.

[62] P.B. Johns and G. Butler, "The consistency and accuracy of the TLM method for diffusion and its relationship to existing methods," *Int. Jour. Numer. Methods Engr.*, vol. 19, 1983, pp. 1549–1554.

[63] P.W. Webb, "Simulation of thermal diffusion in transistors using transmission line matrix modeling," *Electron. Comm. Engr. Jour.*, vol. 4, no. 6, Dec. 1992, pp. 362–366.

[64] P. Naylor, C. Christopoulos, and P.B. Johns, "Coupling between electromagnetic field and wires using transmission-line modeling," *IEEE Proc.*, Pt. A, vol. 134, no. 8, 1987, pp. 679–686.

[65] P. Naylor and C. Christopoulos, "A new wire node for modeling thin wires in electromagnetic field problems solved by transmission line modeling," *IEEE Trans. Micro. Theo. Tech.*, vol. 38, no. 3, March 1990, pp. 328–330.

[66] J.A. Porti et al., "Comparison of the thin-wire models for TLM method," *Elect. Lett.*, vol. 28, no. 20, Sept. 1992, pp. 1910–1911.

[67] A.P. Duffy et al., "New methods for accurate modeling of wires using TLM," *Elect. Lett.*, vol. 29, no. 2, Jan. 1993, pp. 224–226.

[68] I. Palocz and N. Marcovitz, "A network-oriented approach in the teaching of electromagnetics," *IEEE Trans. Educ.*, vol. E-28, no. 3, Aug. 1985, pp. 150–154.

[69] H. Pues and A. Van de Capelle, "Accurate transmission-line model for the rectangular microstrip antenna," *IEEE Proc.*, vol. 131, Pt. H, no. 6, Dec. 1984, pp. 334–340.

[70] J.F. Deford and O.P. Gandhi, "An impedance method to calculate currents induced in biological bodies exposed to quasi-static electromagnetic fields," *IEEE Trans. Elect. Comp.*, vol. EMC-27, no. 3, Aug. 1985, pp. 168–173.

[71] D.A. Al-Mukhtar and T.E. Sitch, "Transmission-line matrix method with irregularly graded space," *IEEE Proc.*, vol. 128, Pt. H, no. 6, Dec. 1981, pp. 299–305.

[72] H.L. Thal, Exact circuit analysis of spherical waves," *IEEE Trans. Ant. Prog.*, vol. AP-26, no. 2, Mar. 1978, pp. 282–287.

[73] C.V. Jones and D.L. Prior, "Unification of fields and circuit theories of electrical machines," *Proc. IEEE*, vol. 119, no. 7, July 1972, pp. 871–876.

[74] P. Hammond and G.J. Rogers, "Use of equivalent circuits in electrical-machine studies," *Proc. IEEE*, vol. 121, no. 6, June 1974, pp. 500–507.

[75] E.M. Freeman, "Equivalent circuits from electromagnetic theory: low-frequency induction devices," *Proc. IEEE*, vol. 121, no. 10, Oct. 1974, pp. 1117–1121.

[76] W.J. Karplus and W.W. Soroka, *Analog Methods: Computation and Simulation*. New York: McGraw-Hill, 1959.

[77] G.L. Ragan (ed.), *Microwave Transmission Circuits*. New York: McGraw-Hill, 1948, pp. 544–547.

[78] R.H. MacNeal, *Electric Circuit Analogies for Elastic Structures*, vol. 2. New York: John Wiley & Sons, 1962.

[79] S. Akhtarzad, "Analysis of lossy microwave structures and microstrip resonators by the TLM method," Ph.D. thesis, University of Nottingham, England, July 1975.

[80] P.B. Johns, "On the relationship between TLM and finite-difference methods for Maxwell's equations," *IEEE Trans. Micro. Theo. Tech.*, vol. MTT-35, no. 1, Jan. 1987, pp. 60, 61.

[81] D.H. Choi and W.J.R. Hoefer, "The finite-difference time-domain method and its application to eingenvalue problems," *IEEE Trans. Micro. Theo. Tech.*, vol. 34, no. 12, Dec. 1986, pp. 1464–1472.

[82] D.H. Choi, "A comparison of the dispersion characteristics associated with the TLM and FD-TD methods," *Int. Jour. Num. Model.*, vol. 2, 1989, pp. 203–214.

[83] Z. Chen, M. Ney, and W.J.R. Hoefer, "A new finite-difference time-domain formulation and its equivalence with the TLM symmetrical condensed node," *IEEE Trans. Micro. Theo. Tech.*, vol. 39, no. 12, Dec. 1992, pp. 2160–2169.

[84] M. Krumpholz and P. Russer, "Two-dimensional FDTD and TLM," *Int. Jour. Num. Model.*, vol. 7, no. 2, 1994, pp. 141–143.

[85] M. Krumpholz and P. Russer, "On the dispersion of TLM and FDTD," *IEEE Trans. Micro. Theo. Tech.*, vol. 42, no. 7, July 1994, pp. 1275–1279.

[86] M. Krumpholz, C. Huber, and P. Russer, "A field theoretical comparison of FDTD and TLM," *IEEE Trans. Micro. Theo. Tech.*, vol. 43, no. 8, Aug. 1995, pp. 1935–1950.

Problems

7.1 Verify Eq. (7.16).

7.2 For the two-port network in Fig. 7.30 (a), the relation between the input and output variables can be written in matrix form as

$$\begin{bmatrix} V_1 \\ I_1 \end{bmatrix} = \begin{bmatrix} A & B \\ C & D \end{bmatrix} \begin{bmatrix} V_2 \\ -I_2 \end{bmatrix}$$

For the lossy line in Fig. 7.30 (b), show that the ABCD matrix (also called the cascaded matrix) is

$$\begin{bmatrix} \cosh \gamma \ell & Z_o \sinh \gamma \ell \\ \frac{1}{Z_0} \sinh \gamma \ell & \cosh \gamma \ell \end{bmatrix}$$

7.3 The circuit in Fig. 7.31 is used to model diffusion processes and presents a Δz section of a lossy transmission line. Show that

$$\frac{\partial^2 V}{\partial z^2} = -Ri + RC\frac{\partial V}{\partial t} - L\frac{\partial i}{\partial t} + LC\frac{\partial^2 V}{\partial t^2}$$

where $i = I_m/\Delta z$, the current density.

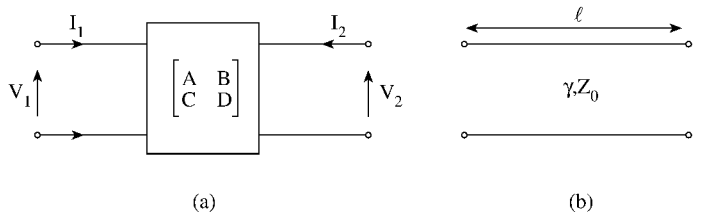

Figure 7.30
For Problem 7.2.

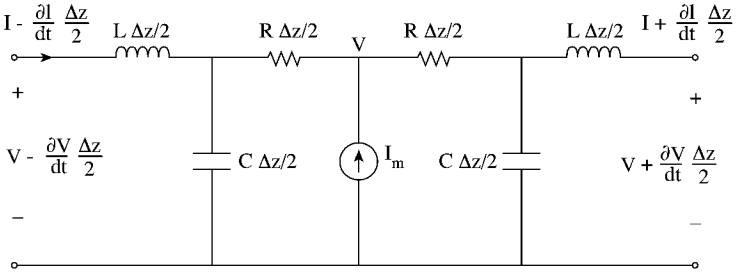

Figure 7.31
For Problem 7.3.

7.4 Consider an EM wave propagation in a lossless medium in TEM mode ($E_y = 0 = E_z = H_z = H_x$) along the z direction. Using one-dimensional TLM mesh, derive the equivalencies between network and field quantities.

7.5 Modify the program in Fig. 7.14 to calculate the cutoff frequency (expressed in terms of $\Delta\ell/\lambda$) in a square section waveguide of size $10\Delta\ell$. Perform the calculation for the TM_{11} mode by using open-circuit symmetry boundaries to suppress even-order modes and by taking the excitation and output points as in Fig. 7.32 to suppress the TM_{13}, TM_{33}, and TM_{15} modes. Use $N = 500$.

7.6 Repeat Prob. 7.5 of higher-order modes but take excitation and output points as in Fig. 7.33.

7.7 For the waveguide with a free space discontinuity considered in Example 7.2, plot the variation of the magnitude of the normalized impedance of the guide with $\Delta\ell/\lambda$. The plot should be for frequencies above and below the cutoff frequency, i.e., including both evanescent and propagating modes.

7.8 Rework Example 7.5, but take the output point at $(x = 6, z = 13)$.

7.9 Verify Eq. (7.62).

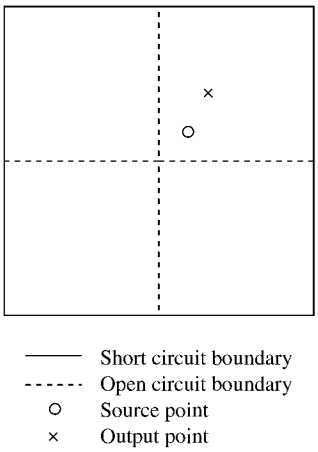

Figure 7.32
Square cross section waveguide of Problem 7.4.

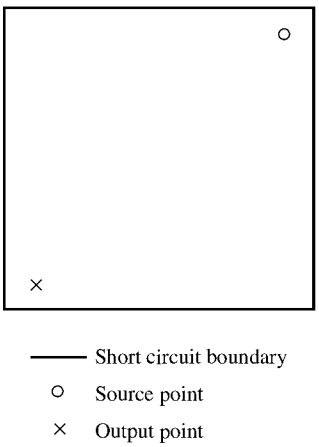

Figure 7.33
Square cross section waveguide of Problem 7.6.

7.10 For transverse waves on a stub-loaded transmission-line matrix, the dispersion relation is given by

$$\sin^2\left(\frac{\beta_n \Delta\ell}{2}\right) = 2\,(1 + Y_o/4)\sin^2\left(\frac{\omega\Delta\ell}{2c}\right)$$

Plot the velocity characteristic similar to that in Fig. 7.11 for $Y_o = 0, 1, 2, 10, 20, 100$.

7.11 Verify Eq. (7.68).

7.12 The transmission equation for one cell in a stub-loaded three-dimensional TLM network is

$$\begin{bmatrix} V_i \\ I_i \end{bmatrix} = T \cdot \begin{bmatrix} 1 & j(2+z_o)\tan\theta/2 \\ 0 & 1 \end{bmatrix} \cdot T \cdot T \cdot \begin{bmatrix} 1 & 0 \\ g_o + j(2+y_o)\tan\theta/2 & 1 \end{bmatrix} \cdot T \cdot \begin{bmatrix} V_{i+1} \\ I_{i+1} \end{bmatrix}$$

where

$$T = \begin{bmatrix} \cos\theta/4 & j\sin\theta/4 \\ j\sin\theta/4 & \cos\theta/4 \end{bmatrix}$$

$\theta = 2\pi\Delta\ell/\lambda$, $y_o = 4(\epsilon_r - 1)$, $z_o = 4(\mu_r - 1)$, and $g_o = \sigma\Delta\ell\sqrt{L/C}$. Assuming small losses $\alpha_n\Delta\ell << 1$, show that the transmission equation can be reduced to

$$\begin{bmatrix} V_i \\ I_i \end{bmatrix} = \begin{bmatrix} e^{\gamma_n\Delta\ell} & 0 \\ 0 & e^{\gamma_n\Delta\ell} \end{bmatrix} \begin{bmatrix} V_{i+1} \\ I_{i+1} \end{bmatrix}$$

where $\gamma_n = \alpha_n + j\beta_n$ is the propagation constant and

$$\cos(\beta_n\Delta\ell) = 1 - 8(1 + y_o/4)(1 + z_o/4)\sin^2\theta/2$$

$$\alpha_n\Delta\ell\sin(\beta_n\Delta\ell) = \frac{g_o}{2}(4 + z_o)\sin\theta/2\cos\theta/2$$

7.13 In the y-z plane of a symmetric condensed node of the TLM mesh, the normalized characteristic impedance of the inductive stub is

$$Z_x = \frac{2\mu_r}{u_o\Delta t} \cdot \frac{\Delta y\Delta z}{\Delta x} - 4$$

Assuming that $\Delta x = \Delta y = \Delta z = 0.1$ m, determine the stubs required to model a medium with $\epsilon_r = 4$, $\mu_r = 1$, $u_o = c$, and the value of Δt for stability.

7.14 Consider the 61×8 rectangular matrix with boundaries at $x = 0.5$ and $x = 8.5$ as in Fig. 7.34. By making one of the boundaries, say $x = 8.5$, an open circuit, a waveguide of twice the width can be simulated. For the TE_{m0} family of modes, excite the system at all points on line $z = 1$ with impulses corresponding to E_y and take the impulse function of the output at point $x = 7$, $z = 6$. Calculate the normalized wave impedance $Z = E_y/H_x$ for frequencies above cutoff, i.e., $\Delta\ell/\lambda = 0.023, 0.025, 0.027, \ldots, 0.041$. Take $\sigma = 0$, $\epsilon_r = 2$, $\mu_r = 1$.

7.15 Repeat Prob. 7.14 for a lossy waveguide with $\sigma = 278$ mhos/m, $\epsilon_r = 1$, $\mu_r = 1$.

7.16 Using the TLM method, determine the cutoff frequency (expressed in terms of $\Delta\ell/\lambda$) of the lowest order TE and TM modes for the square waveguide with cross section shown in Fig. 7.35. Take $\epsilon_r = 2.45$.

7.17 For the dielectric ridge waveguide of Fig. 7.36, use the TLM method to calculated the cutoff wavenumber k_c of the dominant mode. Express the result in terms of $k_c a (= \omega a/c)$ and try $\epsilon_r = 2$ and $\epsilon_r = 8$. Take $a = 10\Delta\ell$.

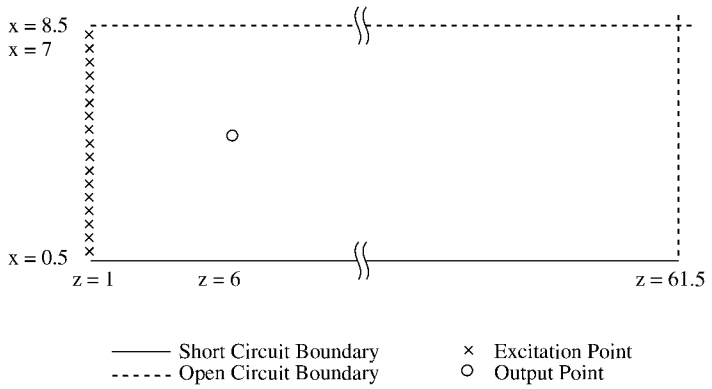

Figure 7.34
The 61×8 TLM mesh of Problem 7.14.

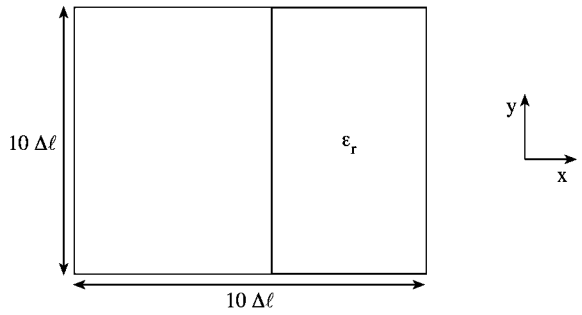

Figure 7.35
For Problem 7.16.

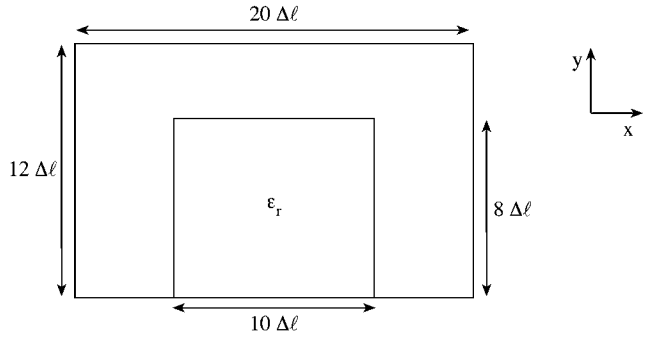

Figure 7.36
For Problem 7.17.

7.18 Rework Example 7.6 for the inhomogeneous cavity of Fig. 7.37. Take $\epsilon_r = 16$, $a = 12\Delta\ell$, $b = 3a/10$, $d = 4a/10$, $s = 7a/12$, $u = 3d/8$.

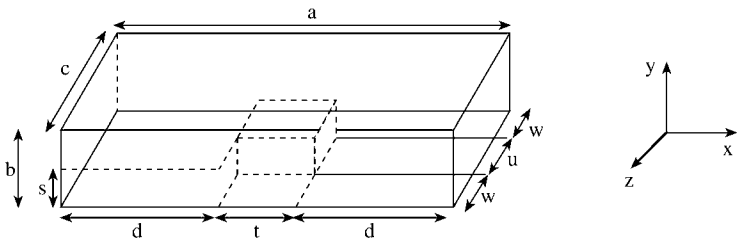

Figure 7.37
The inhomogeneous cavity of Problem 7.18.

7.19 Consider a single microstrip line whose cross section is shown in Fig. 7.38. Dispersion analysis of the line by the TLM method involves resonating a section

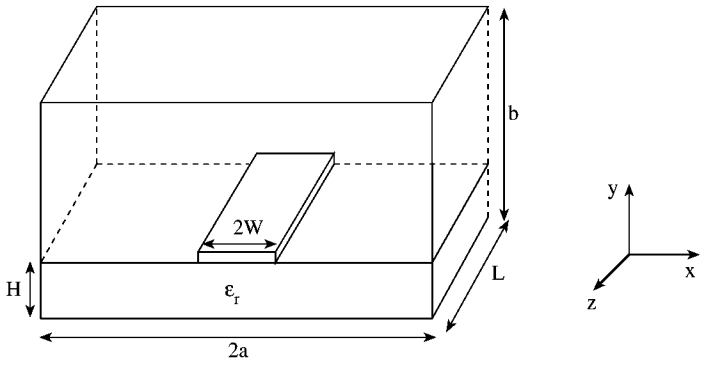

Figure 7.38
The microstrip line of Problem 7.19.

of the transmission line by placing shorting planes along the axis of propagation (the z-axis in this case). Write a TLM computer program and specify the input data as:

$$
\begin{aligned}
&E_x = 0 = E_z \text{ along } y = 0,\ y = b,\\
&E_x = 0 = E_z \text{ along } x = 2a,\\
&E_x = 0 = E_z \text{ for } y = H,\ -W \le x \le W,\\
&H_y = 0 = H_z \text{ along } x = 0
\end{aligned}
$$

Plot the dispersion curves depicting the phase constant β as a function of frequency f for cases when the line is air-filled and dielectric-filled. The distance $L(= \pi/\beta)$ between the shorting planes is the variable. Assume the dielectric

substrate and the walls of the enclosure are lossless. Take $\epsilon_r = 4.0$, $a = 2$ mm, $H = 1.0$ mm, $W = 1.0$ mm, $b = 2$ mm, $\Delta\ell = a/8$.

7.20 For the cubical cavity of Fig. 7.39, use the TLM technique to calculate the time taken for the total power in the lossy dielectric cavity to decay to $1/e$ of its original value. Consider cases when the cavity is completely filled with dielectric material and half-filled. Take $\epsilon_r = 2.45$, $\sigma = 0.884$ mhos/m, $\mu_r = 1$, $\Delta\ell = 0.3$ cm, $2a = 7\Delta\ell$.

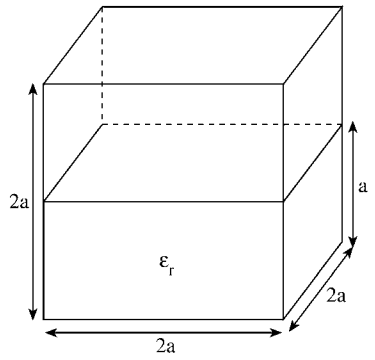

Figure 7.39
The lossy cavity of Problem 7.20.

Chapter 8

Monte Carlo Methods

"Chance favors the prepared mind." Anonymous

8.1 Introduction

Unlike the deterministic numerical methods covered in the foregoing chapters, Monte Carlo methods are nondeterministic (probabilistic or stochastic) numerical methods employed in solving mathematical and physical problems. The Monte Carlo method (MCM), also known as the *method of statistical trials,* is the marriage of two major branches of theoretical physics: the probabilistic theory of random process dealing with Brownian motion or random-walk experiments and potential theory, which studies the equilibrium states of a homogeneous medium [1]. It is a method of approximately solving problems using sequences of random numbers. It is a means of treating mathematical problems by finding a probabilistic analog and then obtaining approximate answers to this analog by some experimental sampling procedure. The solution of a problem by this method is closer in spirit to physical experiments than to classical numerical techniques.

It is generally accepted that the development of Monte Carlo techniques as we presently use them dates from about 1944, although there are a number of undeveloped instances on much earlier occasions. Credit for the development of MCM goes to a group of scientists, particularly von Neumann and Ulam, at Los Alamos during the early work on nuclear weapons. The groundwork of the Los Alamos group stimulated a vast outpouring of literature on the subject and encouraged the use of MCM for a variety of problems [2]–[4]. The name "Monte Carlo" comes from the city in Monaco, famous for its gambling casinos.

Monte Carlo methods are applied in two ways: simulation and sampling. Simulation refers to methods of providing mathematical imitation of real random phenomena. A typical example is the simulation of a neutron's motion into a reactor wall, its zigzag path being imitated by a random walk. Sampling refers to methods of deducing properties of a large set of elements by studying only a small, random

subset. For example, the average value of $f(x)$ over $a < x < b$ can be estimated from its average over a finite number of points selected randomly in the interval. This amounts to a Monte Carlo method of numerical integration. MCMs have been applied successfully for solving differential and integral equations, for finding eigenvalues, for inverting matrices, and particularly for evaluating multiple integrals.

The simulation of any process or system in which there are inherently random components requires a method of generating or obtaining numbers that are random. Examples of such simulation occur in random collisions of neutrons, in statistics, in queueing models, in games of strategy, and in other competitive enterprises. Monte Carlo calculations require having available sequences of numbers which appear to be drawn at random from particular probability distributions.

8.2 Generation of Random Numbers and Variables

Various techniques for generating random numbers are discussed fully in [5]–[10]. The almost universally used method of generating random numbers is to select a function $g(x)$ that maps integers into random numbers. Select x_0 somehow, and generate the next random number as $x_{k+1} = g(x_k)$. The commonest function $g(x)$ takes the form

$$g(x) = (ax + c) \bmod m \tag{8.1}$$

where

$$\begin{aligned} x_0 &= \text{starting value or a seed } (x_0 > 0) , \\ a &= \text{multiplier } (a \geq 0) , \\ c &= \text{increment } (c \geq 0) , \\ m &= \text{the modulus} \end{aligned}$$

The modulus m is usually 2^t for t-digit binary integers. For a 31-bit computer machine, for example, m may be 2^{31-1}. Here x_0, a, and c are integers in the same range as $m > a, m > c, m > x_0$. The desired sequence of random numbers $\{x_n\}$ is obtained from

$$\boxed{x_{n+1} = (ax_n + c) \bmod m} \tag{8.2}$$

This is called a *linear congruential sequence.* For example, if $x_0 = a = c = 7$ and $m = 10$, the sequence is

$$7, 6, 9, 0, 7, 6, 9, 0, \ldots \tag{8.3}$$

It is evident that congruential sequences always get into a loop; i.e., there is ultimately a cycle of numbers that is repeated endlessly. The sequence in Eq. (8.3) has a period

of length 4. A useful sequence will of course have a relatively long period. The terms *multiplicative congruential method* and *mixed congruential method* are used by many authors to denote linear congruential methods with $c = 0$ and $c \neq 0$, respectively. Rules for selecting x_0, a, c, and m can be found in [6, 10].

Here we are interested in generating random numbers from the uniform distribution in the interval (0,1). These numbers will be designated by the letter U and are obtained from Eq. (8.2) as

$$U = \frac{x_{n+1}}{m} \tag{8.4}$$

Thus U can only assume values from the set $\{0, 1/m, 2/m, \ldots, (m-1)/m\}$. (For random numbers in the interval (0,1), a quick test of the randomness is that the mean is 0.5. Other tests can be found in [3, 6].) For generating random numbers X uniformly distributed in the interval (a, b), we use

$$\boxed{X = a + (b - a)\, U} \tag{8.5}$$

Random numbers produced by a computer code (using Eqs. (8.2) and (8.4)) are not truly random; in fact, given the seed of the sequence, all numbers U of the sequence are completely predictable. Some authors emphasize this point by calling such computer-generated sequences *pseudorandom numbers*. However, with a good choice of a, c, and m, the sequences of U appear to be sufficiently random in that they pass a series of statistical tests of randomness. They have the advantage over truly random numbers of being generated in a fast way and of being reproducible, when desired, especially for program debugging.

It is usually necessary in a Monte Carlo procedure to generate random variable X from a given probability distribution $F(x)$. This can be accomplished using several techniques [6], [13]–[15] including the *direct method* and *rejection method*.

The direct method, otherwise known as inversion or transform method, entails inverting the cumulative probability function $F(x) = \text{Prob}(X \leq x)$ associated with the random variable X. The fact that $0 \leq F(x) \leq 1$ intuitively suggests that by generating random number U uniformly distributed over (0,1), we can produce a random sample X from the distribution of $F(x)$ by inversion. Thus to generate random X with probability distribution $F(x)$, we set $U = F(x)$ and obtain

$$X = F^{-1}(U) \tag{8.6}$$

where X has the distribution function $F(x)$. For example, if X is a random variable that is exponentially distributed with mean μ, then

$$F(x) = 1 - e^{-x/\mu}, \quad 0 < x < \infty \tag{8.7}$$

Solving for X in $U = F(X)$ gives

$$X = -\mu \ln (1 - U) \tag{8.8}$$

Since $(1 - U)$ is itself a random number in the interval (0,1), we simply write

$$X = -\mu \ln U \tag{8.9}$$

Sometimes the inverse $F^{-1}(x)$ required in Eq. (8.6) does not exist or is difficult to obtain. This situation can be handled using the rejection method. Let $f(x) = \dfrac{dF(x)}{dx}$ be the probability density function of the random variable X. Let $f(x) = 0$ for $a > x > b$, and $f(x)$ is bounded by M (i.e., $f(x) \leq M$) as shown in Fig. 8.1. We generate two random numbers (U_1, U_2) in the interval (0,1). Then

$$X_1 = a + (b - a)U_1 \text{ and } f_1 = U_2 M \tag{8.10}$$

are two random numbers with uniform distributions in (a, b) and $(0, M)$, respectively. If

$$f_1 \leq f(X_1) \tag{8.11}$$

then X_1 is accepted as choice of X, otherwise X_1 is rejected and a new pair (U_1, U_2) is tried again. Thus in the rejection technique all points falling above $f(x)$ are rejected, while those points falling on or below $f(x)$ are utilized to generate X_1 through $X_1 = a + (b - a)U_1$.

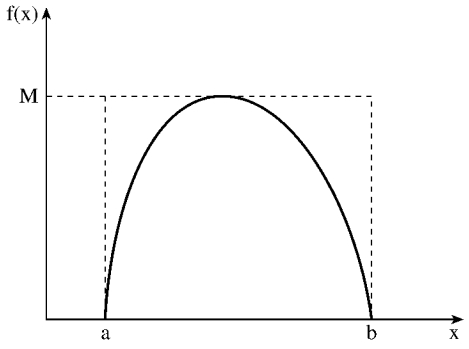

Figure 8.1
The rejection method of generating a random variable with probability density function $f(x)$.

Example 8.1

Develop a subroutine for generating random number U uniformly distributed between 0 and 1. Using this subroutine, generate random variable Θ with probability distribution given by

$$T(\theta) = \frac{1}{2}(1 - \cos\theta), \quad 0 < \theta < \pi \qquad \square$$

Solution

The subroutine for generating U is shown in Fig. 8.2. In this subroutine, $m = 2^{21} - 1 = 2147483647$, $c = 0$, and $a = 7^5 = 16807$. By supplying a seed (e.g., 1234), the subroutine provides one random number U per call in the main program. The seed is selected as any integer between 1 and m.

```
0001    ********************************************************
0002    C  PROGRAM FOR GENERATING RANDOM VARIABLES WITH A GIVEN
0003    C  PROBABILITY DISTRIBUTION
0004    C********************************************************
0005
0006          DOUBLE PRECISION ISEED
0007
0008          ISEED = 1234.D0
0009          DO 10 I=1,100
0010          CALL RANDOM (ISEED,R)
0011          THETA = ACOSD(1.0 - 2.0*R)
0012          WRITE(6,*) I,THETA
0013    10    CONTINUE
0014          STOP
0015          END

0001    C++++++++++++++++++++++++++++++++++++++++++++++++
0002    C  SUBROUTINE FOR GENERATING RANDOM NUMBERS IN
0003    C  THE INTERVAL (0,1)
0004    C++++++++++++++++++++++++++++++++++++++++++++++++
0005
0006          SUBROUTINE RANDOM (ISEED,R)
0007          DOUBLE PRECISION  ISEED, DEL, A
0008          DATA DEL,A/2147483647.D0, 16807.D0/
0009
0010          ISEED = DMOD( A*ISEED, DEL )
0011          R = ISEED/DEL
0012          RETURN
0013          END
```

Figure 8.2
Random number generator; for Example 8.1.

The subroutine in Fig. 8.2 is meant to illustrate the concepts explained in this section. Most computers have routines for generating random numbers.

To generate the random variable Θ, set

$$U = T(\Theta) = \frac{1}{2}(1 - \cos\Theta) ,$$

then

$$\Theta = T^{-1}(U) = \cos^{-1}(1 - 2U)$$

Using this, a sequence of random numbers Θ with the given distribution is generated in the main program of Fig. 8.2. ∎

8.3 Evaluation of Error

Monte Carlo procedures give solutions which are averages over a number of tests. For this reason, the solutions contain fluctuations about a mean value, and it is impossible to ascribe a 100% confidence in the results. To evaluate the statistical uncertainty in Monte Carlo calculations, we must resort to various statistical techniques associated with random variables. We briefly introduce the concepts of expected value and variance, and utilize the central limit theorem to arrive at an error estimate [13, 16].

Suppose that X is a random variable. The *expected value* or *mean value* $\bar{x}$ of X is defined as

$$\bar{x} = \int_{-\infty}^{\infty} x f(x)\, dx \tag{8.12}$$

where $f(x)$ is the probability density distribution of X. If we draw random and independent samples, $x_1, x_2, \ldots, x_N$ from $f(x)$, our estimate of x would take the form of the mean of N samples, namely,

$$\hat{x} = \frac{1}{N} \sum_{n=1}^{N} x_n \tag{8.13}$$

While $\bar{x}$ is the true mean value of X, $\hat{x}$ is the unbiased estimator of $\bar{x}$, an unbiased estimator being one with the correct expectation value. Although the expected value of $\hat{x}$ is equal to $\bar{x}$, $\hat{x}$ $/\!\!=\!\!x$. Therefore, we need a measure of the spread in the values of $\hat{x}$ about $\bar{x}$.

To estimate the spread of values of X, and eventually of $\hat{x}$ about $\bar{x}$, we introduce the *variance* of X defined as the expected value of the square of the deviation of X from $\bar{x}$, i.e.,

$$\mathrm{Var}(x) = \sigma^2 = \overline{(x - \bar{x})^2} = \int_{-\infty}^{\infty} (x - \bar{x})^2 f(x)\, dx \tag{8.14}$$

But $(x - \bar{x})^2 = x^2 - 2x\bar{x} + \bar{x}^2$. Hence

$$\sigma^2(x) = \int_{-\infty}^{\infty} x^2 f(x)\, dx - 2\bar{x} \int_{-\infty}^{\infty} x f(x)\, dx + \bar{x}^2 \int_{-\infty}^{\infty} f(x)\, dx \tag{8.15}$$

or

$$\sigma^2(x) = \overline{x^2} - \bar{x}^2 \tag{8.16}$$

The square root of the variance is called the *standard deviation,* i.e.,

$$\sigma(x) = \left(\overline{x^2} - \bar{x}^2\right)^{1/2} \tag{8.17}$$

The standard deviation provides a measure of the spread of x about the mean value $\bar{x}$; it yields the order of magnitude of the error. The relationship between the variance of $\hat{x}$ and the variance of x is

$$\sigma\left(\hat{x}\right) = \frac{\sigma(x)}{\sqrt{N}} \tag{8.18}$$

This shows that if we use $\hat{x}$ constructed from N values of x_n according to Eq. (8.13) to estimate $\bar{x}$, then the spread in our results of $\hat{x}$ about $\bar{x}$ is proportional to $\sigma(x)$ and falls off as the number of N of samples increases.

In order to estimate the spread in $\hat{x}$, we define the *sample variance*

$$S^2 = \frac{1}{N-1}\sum_{n=1}^{N}\left(x_n - \hat{x}\right)^2 \tag{8.19}$$

Again, it can be shown that the expected value of S^2 is equal to $\sigma^2(x)$. Therefore the sample variance is an unbiased estimator of $\sigma^2(x)$. Multiplying out the square term in Eq. (8.19), it is readily shown that the *sample standard deviation* is

$$S = \left(\frac{N}{N-1}\right)^{1/2}\left[\frac{1}{N}\sum_{n=1}^{N}x_n^2 - \hat{x}^2\right]^{1/2} \tag{8.20}$$

For large N, the factor $N/(N-1)$ is set equal to one.

As a way of arriving at the *central limit theorem*, a fundamental result in probability theory, consider the binomial function

$$B(M) = \frac{N!}{M!(N-M)!}p^M q^{N-M} \tag{8.21}$$

which is the probability of M successes in N independent trials. In Eq. (8.21), p is the probability of success in a trial, and $q = 1 - p$. If M and $N - M$ are large, we may use *Stirling's formula*

$$n! \sim n^n e^{-n}\sqrt{2\pi n} \tag{8.22}$$

so that Eq. (8.21) is approximated [17] as the normal distribution:

$$B(M) \simeq f\left(\hat{x}\right) = \frac{1}{\sigma\left(\hat{x}\right)\sqrt{2\pi}}\exp\left[-\frac{\left(\hat{x}-\bar{x}\right)^2}{2\sigma^2\left(\hat{x}\right)}\right] \tag{8.23}$$

where $\bar{x} = N_p$ and $\sigma(\hat{x}) = \sqrt{Npq}$. Thus as $N \to \infty$, the central limit theorem states that the probability density function which describes the distribution of $\hat{x}$ that results from N Monte Carlo calculations is the normal distribution $f(\hat{x})$ in Eq. (8.23). In other words, the sum of a large number of random variables tends to be normally distributed. Inserting Eq. (8.18) into Eq. (8.23) gives

$$f\left(\hat{x}\right) = \sqrt{\frac{N}{2\pi}}\frac{1}{\sigma(x)}\exp\left[-\frac{N\left(\hat{x}-\bar{x}\right)^2}{2\sigma^2(x)}\right] \tag{8.24}$$

The normal (or Gaussian) distribution is very useful in various problems in engineering, physics, and statistics. The remarkable versatility of the Gaussian model stems from the central limit theorem. For this reason, the Gaussian model often applies to situations in which the quantity of interest results from the summation of many irregular and fluctuating components. In Example 8.2, we present an algorithm based on central limit theorem for generating Gaussian random variables.

Since the number of samples N is finite, absolute certainty in Monte Carlo calculations is unattainable. We try to estimate some limit or interval around $\bar{x}$ such that we can predict with some confidence that $\hat{x}$ falls within that limit. Suppose we want the probability that $\hat{x}$ lies between $\bar{x} - \delta$ and $\bar{x} + \delta$. By definition,

$$\text{Prob}\left\{\bar{x} - \delta < \hat{x} < \bar{x} + \delta\right\} = \int_{\bar{x}-\delta}^{\bar{x}+\delta} f\left(\hat{x}\right) d\hat{x} \tag{8.25}$$

By letting $\lambda = \dfrac{(\hat{x} - \bar{x})}{\sqrt{2/N}\sigma(x)}$,

$$\begin{aligned}\text{Prob}\left\{\bar{x} - \delta < \hat{x} < \bar{x} + \delta\right\} &= \frac{2}{\sqrt{\pi}} \int_0^{(\sqrt{N/2})(\delta/\sigma)} e^{-\lambda^2} d\lambda \\ &= \text{erf}\left(\sqrt{N/2}\frac{\delta}{\sigma(x)}\right)\end{aligned} \tag{8.26a}$$

or

$$\text{Prob}\left\{\bar{x} - z_{\alpha/2}\frac{\sigma}{\sqrt{N}} \leq \hat{x} \leq \bar{x} + z_{\alpha/2}\frac{\sigma}{\sqrt{N}}\right\} = 1 - \alpha \tag{8.26b}$$

where $\text{erf}(x)$ is the error function and $z_{\alpha/2}$ is the upper $\alpha/2 \times 100$ percentile of the standard normal deviation. Equation (8.26) may be interpreted as follows: if the Monte Carlo procedure of taking random and independent observations and constructing the associated random interval $\bar{x} \pm \delta$ is repeated for large N, approximately $\text{erf}\left(\sqrt{\dfrac{N}{2}}\dfrac{\delta}{\sigma(x)}\right) \times 100$ percent of these random intervals will contain $\hat{x}$. The random interval $\hat{x} \pm \delta$ is called a *confidence interval* and $\text{erf}\left(\sqrt{\dfrac{N}{2}}\dfrac{\delta}{\sigma(x)}\right)$ is the *confidence level.* Most Monte Carlo calculations use error $\delta = \sigma(x)/\sqrt{N}$, which implies that $\hat{x}$ is within one standard deviation of $\bar{x}$, the true mean. From Eq. (8.26), it means that the probability that the sample mean $\hat{x}$ lies within the interval $\hat{x} \pm \sigma(x)/\sqrt{N}$ is 0.6826 or 68.3%. If higher confidence levels are desired, two or three standard deviations may be used. For example,

$$\text{Prob}\left(\bar{x} - M\frac{\sigma(x)}{\sqrt{N}} < \hat{x} < \bar{x} + M\frac{\sigma(x)}{\sqrt{N}}\right) = \begin{cases} 0.6826, & M = 1 \\ 0.954, & M = 2 \\ 0.997, & M = 3 \end{cases} \tag{8.27}$$

where M is the number of standard deviations.

In Eqs. (8.26) and (8.27), it is assumed that the population standard deviation σ is known. Since this is rarely the case, σ must be estimated by the sample standard deviation S calculated from Eq. (8.20) so that the normal distribution is replaced by the student's t-distribution. It is well known that the t-distribution approaches the normal distribution as N becomes large, say $N > 30$. Equation (8.26) is equivalent to

$$\text{Prob}\left\{\bar{x} - \frac{St_{\alpha/2;N-1}}{\sqrt{N}} \leq \hat{x} \leq \bar{x} + \frac{St_{\alpha/2;N-1}}{\sqrt{N}}\right\} = 1 - \alpha \tag{8.28}$$

where $t_{\alpha/2;N-1}$ is the upper $100 \times \alpha/2$ percentage point of the student's t-distribution with $(N-1)$ degrees of freedom; and its values are listed in any standard statistics text. Thus the upper and lower limits of a confidence interval are given by

$$\text{upper limit} = \bar{x} + \frac{St_{\alpha/2;N-1}}{\sqrt{N}} \tag{8.29}$$

$$\text{lower limit} = \bar{x} - \frac{St_{\alpha/2;N-1}}{\sqrt{N}} \tag{8.30}$$

For further discussion on error estimates in Monte Carlo computations, consult [18, 19].

Example 8.2

A random variable X with Gaussian (or normal) distribution is generated using the central limit theorem. According to the central limit theorem, the sum of a large number of independent random variables about a mean value approaches a Gaussian distribution regardless of the distribution of the individual variables. In other words, for any random numbers, Y_i, $i = 1, 2, \ldots, N$ with mean $\overline{Y}$ and variance $\text{Var}(Y)$,

$$Z = \frac{\sum_{i=1}^{N} Y_i - N\overline{Y}}{\sqrt{N}\,\text{Var}(Y)} \tag{8.31}$$

converges asymptotically with N to a normal distribution with zero mean and a standard deviation of unity. If Y_i are uniformly distributed variables (i.e., $Y_i = U_i$), then $\overline{Y} = 1/2$, $\text{Var}(Y) = 1/\sqrt{12}$, and

$$Z = \frac{\sum_{i=1}^{N} U_i - N/2}{\sqrt{N/12}} \tag{8.32}$$

and the variable

$$X = \sigma Z + \mu \tag{8.33}$$

approximates the normal variable with mean μ and variance σ^2. A value of N as low as 3 provides a close approximation to the familiar bell-shaped Gaussian distribution. To ease computation, it is a common practice to set $N = 12$ since this choice eliminates the square root term in Eq. (8.32). However, this value of N truncates the distribution at $\pm 6\sigma$ limits and is unable to generate values beyond 3σ. For simulations in which the tail of the distribution is important, other schemes for generating Gaussian distribution must be used [20]–[22].

Thus, to generate a Gaussian variable X with mean μ and standard deviation σ, we follow these steps:

(1) Generate 12 uniformly distributed random numbers $U_1, U_2, \ldots, U_{12}$.

(2) Obtain $Z = \sum_{i=1}^{12} U_i - 6$.

(3) Set $X = \sigma Z + \mu$. □

8.4 Numerical Integration

For one-dimensional integration, several quadrature formulas, such as presented in Section 3.10, exist. The numbers of such formulas are relatively few for multidimensional integration. It is for such multidimensional integrals that a Monte Carlo technique becomes valuable for at least two reasons. The quadrature formulas become very complex for multiple integrals, while the MCM remains almost unchanged. The convergence of Monte Carlo integration is independent of dimensionality, which is not true for quadrature formulas. The statistical method of integration has been found to be an efficient way to evaluate two- or three-dimensional integrals in antenna problems, particularly those involving very large structures [23]. Two types of Monte Carlo integration procedures, the crude MCM and the MCM with antithetic variates, will be discussed. For other types, such as hit-or-miss and control variates, see [24]–[26]. Application of MCM to improper integrals will be covered briefly.

8.4.1 Crude Monte Carlo Integration

Suppose we wish to evaluate the integral

$$I = \int_R f \tag{8.34}$$

where R is an n-dimensional space. Let $\mathbf{X} = (X^1, X^2, \ldots, X^n)$ be a random variable that is uniformly distributed in R. Then $f(\mathbf{X})$ is a random variable whose mean value

is given by [27, 28]

$$\overline{f(\mathbf{X})} = \frac{1}{|R|}\int_R f = \frac{I}{|R|} \tag{8.35}$$

and the variance by

$$\mathrm{Var}(f(\mathbf{X})) = \frac{1}{|R|}\int_R f^2 - \left(\frac{1}{|R|}\int_R f\right)^2 \tag{8.36}$$

where

$$|R| = \int_R d\mathbf{X} \tag{8.37}$$

If we take N independent samples of $\mathbf{X}$, i.e., $\mathbf{X}_1, \mathbf{X}_2, \ldots \mathbf{X}_N$, all having the same distribution as $\mathbf{X}$ and form the average

$$\frac{f(\mathbf{X}_1) + f(\mathbf{X}_2) + \cdots + f(\mathbf{X}_N)}{N} = \frac{1}{N}\sum_{i=1}^{N} f(\mathbf{X}_i) \tag{8.38}$$

we might expect this average to be close to the mean of $f(\mathbf{X})$. Thus, from Eqs. (8.35) and (8.38),

$$\boxed{I = \frac{|R|}{N}\sum_{i=1}^{N} f(\mathbf{X}_i)} \tag{8.39}$$

This Monte Carlo formula applies to any integration over a finite region R. For the purpose of illustration, we now apply Eq. (8.39) to one- and two-dimensional integrals.

For a one-dimensional integral, suppose

$$I = \int_a^b f(x)\,dx \tag{8.40}$$

Applying Eq. (8.39) yields

$$\boxed{I = \frac{b-a}{N}\sum_{i=1}^{N} f(X_i)} \tag{8.41}$$

where X_i is a random number in the interval (a, b), i.e.,

$$X_i = a + (b-a)\,U, \quad 0 < U < 1 \tag{8.42}$$

For a two-dimensional integral

$$I = \int_a^b \int_c^d f\left(X^1, X^2\right) dX^1\, dX^2\,, \tag{8.43}$$

the corresponding Monte Carlo formula is

$$\boxed{I = \frac{(b-a)(d-c)}{N} \sum_{i=1}^{N} f\left(X_i^1, X_i^2\right)} \tag{8.44}$$

where

$$\begin{aligned} X_i^1 &= a + (b-a)\, U^1, \quad 0 < U^1 < 1 \\ X_i^2 &= c + (d-c)\, U^2, \quad 0 < U^2 < 1 \end{aligned} \tag{8.45}$$

The convergence behavior of the unbiased estimator I in Eq. (8.39) is slow since the variance of the estimator is of the order $1/N$. Accuracy and convergence is increased by reducing the variance of the estimator using an improved method, the method of antithetic variates.

8.4.2 Monte Carlo Integration with Antithetic Variates

The term *antithetic variates* [29, 30] is used to describe any set of estimators which mutually compensate each other's variations. For convenience, we assume that the integral is over the interval (0,1). Suppose we want an estimator for the single integral

$$I = \int_0^1 g(U)\, dU \tag{8.46}$$

We expect the quantity $\frac{1}{2}[g(U) + g(1-U)]$ to have smaller variance than $g(U)$. If $g(U)$ is too small, then $g(1-U)$ will have a good chance of being too large and conversely. Therefore, we define the estimator

$$I = \frac{1}{N} \sum_{i=1}^{N} \frac{1}{2} \left[g\left(U_i\right) + g\left(1 - U_i\right)\right] \tag{8.47}$$

where U_i are random numbers between 0 and 1. The variance of the estimator is of the order $\frac{1}{N^4}$, a tremendous improvement over Eq. (8.39). For two-dimensional integral,

$$I = \int_0^1 \int_0^1 g\left(U^1, U^2\right) dU^1\, dU^2\,, \tag{8.48}$$

and the corresponding estimator is

$$\begin{aligned} I = \frac{1}{N} \sum_{i=1}^{N} \frac{1}{4} \Big[& g\left(U_i^1, U_i^2\right) + g\left(U_i^1, 1 - U_i^2\right) \\ & + g\left(1 - U_i^1, U_i^2\right) + g\left(1 - U_i^1, 1 - U_i^2\right) \Big] \end{aligned} \tag{8.49}$$

Following similar lines, the idea can be extended to higher order integrals. For intervals other than (0,1), transformations such as in Eqs. (8.41) to (8.45) should be applied. For example,

$$\int_a^b f(x)\,dx = (b-a)\int_0^1 g(U)\,dU$$
$$\simeq \frac{b-a}{N}\sum_{i=1}^{N}\frac{1}{2}\left[g(U_i) + g(1-U_i)\right] \tag{8.50}$$

where $g(U) = f(X)$ and $X = a+(b-a)U$. It is observed from Eqs. (8.47) and (8.49) that as the number of dimensions increases, the minimum number of antithetic variates per dimension required to obtain an increase in efficiency over crude Monte Carlo also increases. Thus the crude Monte Carlo method becomes preferable in many dimensions.

8.4.3 Improper Integrals

The integral

$$I = \int_0^\infty g(x)\,dx \tag{8.51}$$

may be evaluated using Monte Carlo simulations [31]. For a random variable X having probability density function $f(x)$, where $f(x)$ integrates to 1 on interval $(0, \infty)$,

$$\int_0^\infty \frac{g(x)}{f(x)}\,dx = \int_0^\infty g(x)\,dx \tag{8.52}$$

Hence, to compute I in Eq. (8.51), we generate N independent random variables distributed according to a probability density function $f(x)$ integrating to 1 on the interval $(0, \infty)$. The sample mean

$$\overline{g(x)} = \frac{1}{N}\sum_{i=1}^{N}\frac{g(x_i)}{f(x_i)} \tag{8.53}$$

gives an estimate for I.

Example 8.3

Evaluate the integral

$$I = \int_0^1\int_0^{2\pi} e^{j\alpha\rho\cos\phi}\rho\,d\rho\,d\phi$$

using the Monte Carlo method. □

Solution

This integral represents radiation from a circular aperture-antenna with a constant amplitude and phase distribution. It is selected because it forms at least part of every radiation integral. The solution is available in the closed form, which can be used to assess the accuracy of the Monte Carlo results. In closed form,

$$I(\alpha) = \frac{2\pi J_1(\alpha)}{\alpha}$$

where $J_1(\alpha)$ is Bessel function of the first order.

A simple program for evaluating the integral employing Eqs. (8.44) and (8.45), where $a = 0, b = 1, c = 0$, and $d = 2\pi$, is shown in Fig. 8.3. The program calls the routine RANDU in Vax 11/780 to generate random numbers U^1 and U^2. For different values of N, both the crude and antithetic variate Monte Carlo methods are used in evaluating the radiation integral, and the results are compared with the exact value in Table 8.1 for $\alpha = 5$. In applying Eq. (8.49), the following correspondences are used:

$$U^1 \equiv X^1, U^2 \equiv X^2, 1 - U^1 \equiv b - X^1 = (b-a)\left(1 - U^1\right),$$
$$1 - U^2 \equiv d - X^2 = (d-c)\left(1 - U^2\right) \quad \blacksquare$$

Table 8.1 Results of Example 8.3 on Monte Carlo Integration of Radiation Integral

N	Crude MCM	Antihetic variates MCM
500	$-0.2892 - j0.0742$	$-0.2887 - j0.0585$
1000	$-0.5737 + j0.0808$	$-0.4982 - j0.0080$
2000	$-0.4922 - j0.0040$	$-0.4682 - j0.0082$
4000	$-0.3999 - j0.0345$	$-0.4216 - j0.0323$
6000	$-0.3608 - j0.0270$	$-0.3787 - j0.0440$
8000	$-0.4327 - j0.0378$	$-0.4139 - j0.0241$
10,000	$-0.4229 - j0.0237$	$-0.4121 - j0.0240$
Exact: $-0.4116 + j0$		

8.5 Solution of Potential Problems

The connection between potential theory and Brownian motion (or random walk) was first shown in 1944 by Kakutani [32]. Since then the resulting so-called probabilistic potential theory has been applied to problems in many disciplines such as heat conduction [33]–[38], electrostatics [39]–[46], and electrical power engineering [47, 48]. An underlying concept of the probabilistic or Monte Carlo solution of

```
0001    C*********************************************
0002    C  INTEGRATION USING CRUDE MONTE CARLO
0003    C  AND ANTITHETIC METHODS
0004    C
0005    C ONLY FEW LINES NEED BE CHANGED TO USE THIS
0006    C PROGRAM FOR ANY MULTI-DIMENSIONAL INTEGRATION
0007    C*********************************************
0008
0009          DATA  IS1,IS2,IS3,IS4/1234,5678,9012,3456/
0010          DATA  A,B,C/0.0,1.0,0.0/
0011                        ! LIMITS OF INTEGRATION
0012          COMPLEX F,SUM1, SUM2, J, AREA1, AREA2
0013
0014    C
0015    C   SPECIFY THE INTEGRAND
0016    C
0017          F(RHO,PHI) = RHO*CEXP(J*ALPHA*RHO*COS(PHI))
0018
0019          J = (0.0,1.0)
0020          ALPHA = 5.0
0021          PIE = 3.1415927
0022          D = 2.0*PIE
0023          DO 30 NRUN = 500,10000,500  ! NO. OF RUNS
0024          SUM1 = (0.0,0.0)
0025          SUM2 = (0.0,0.0)
0026          DO 10 I=1,NRUN
0027          CALL RANDU(IS1,IS2,U1)
0028          CALL RANDU(IS3,IS4,U2)
0029          X1 = A + (B - A)*U1
0030          X2 = C + (D - C)*U2
0031          X3 = (B - A)*(1.0 - U1)
0032          X4 = (D - C)*(1.0 - U2)
0033          SUM1 = SUM1 + F(X1,X2)
0034          SUM2 = SUM2 + F(X1,X2) + F(X1,X4) + F(X3,X2)
0035         1            + F(X3,X4)
0036    10    CONTINUE
0037          AREA1 = (B-A)*(D-C)*SUM1/FLOAT(NRUN)
0038          AREA2 = (B-A)*(D-C)*SUM2/(4.0*FLOAT(NRUN))
0039          PRINT *,NRUN, AREA1, AREA2
0040          WRITE(6,*) NRUN, AREA1,AREA2
0041          WRITE(6,20) NRUN,AREA1,AREA2
0042    20    FORMAT(2X,'NRUN =',I5,3X,'AREA1 = ',F12.6,3X,F12.6,'AREA2 = ',
0043         1           F12.6,3X,F12.6,/)
0044    30    CONTINUE
0045          STOP
0046          END
```

Figure 8.3

Program for Monte Carlo evaluation of two-dimensional integral; for Example 8.3.

differential equations is the random walk. Different types of random walk lead to different Monte Carlo methods. The most popular types are the *fixed-random walk* and *floating random walk.* Other types that are less popular include the *Exodus method, shrinking boundary method, inscribed figure method,* and the *surface density method.*

8.5.1 Fixed Random Walk

Suppose, for concreteness, that the MCM with fixed random walk is to be applied to solve Laplace's equation

$$\nabla^2 V = 0 \quad \text{in region } R \tag{8.54a}$$

subject to Dirichlet boundary condition

$$V = V_p \text{ on boundary } B \tag{8.54b}$$

We begin by dividing R into mesh and replacing ∇^2 by its finite difference equivalent. The finite difference representation of Eq. (8.54a) in two-dimensional R is given by Eq. (3.26), namely,

$$\boxed{\begin{aligned} V(x, y) = p_{x+} V(x + \Delta, y) + p_{x-} V(x - \Delta, y) \\ + p_{y+} V(x, y + \Delta) + p_{y-} V(x, y - \Delta) \end{aligned}} \tag{8.55a}$$

where

$$\boxed{p_{x+} = p_{x-} = p_{y+} = p_{y-} = \frac{1}{4}} \tag{8.55b}$$

In Eq. (8.55), a square grid of mesh size Δ, such as in Fig. 8.4, is assumed. The equation may be given a probabilistic interpretation. If a random walking particle is instantaneously at the point (x, y), it has probabilities p_{x+}, p_{x-}, p_{y+}, and p_{y-} of moving from (x, y) to $(x+\Delta, y)$, $(x-\Delta, y)$, $(x, y+\Delta)$, and $(x, y-\Delta)$, respectively. A means of determining which way the particle should move is to generate a random number U, $0 < U < 1$ and instruct the particle to walk as follows:

$$\boxed{\begin{array}{ll} (x, y) \to (x + \Delta, y) & \text{if } 0 < U < 0.25 \\ (x, y) \to (x - \Delta, y) & \text{if } 0.25 < U < 0.5 \\ (x, y) \to (x, y + \Delta) & \text{if } 0.5 < U < 0.75 \\ (x, y) \to (x, y - \Delta) & \text{if } 0.75 < U < 1 \end{array}} \tag{8.56}$$

If a rectangular grid rather than a square grid is employed, then $p_{x+} = p_{x-}$ and $p_{y+} = p_{y-}$, but $p_x \neq p_y$. Also for a three-dimensional problem in which cubical cells are used, $p_{x+} = p_{x-} = p_{y+} = p_{y-} = p_{z+} = p_{z-} = \frac{1}{6}$. In both cases, the interval $0 < U < 1$ is subdivided according to the probabilities.

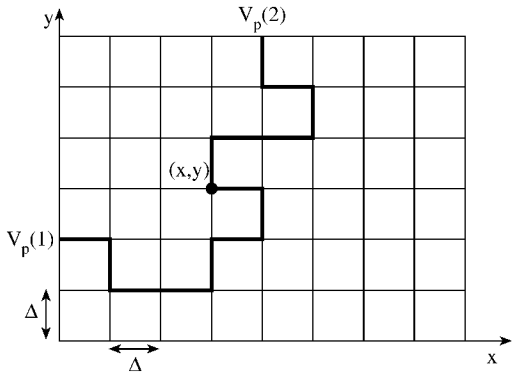

Figure 8.4
Configuration for fixed random walks.

To calculate the potential at (x, y), a random-walking particle is instructed to start at that point. The particle proceeds to wander from node to node in the grid until it reaches the boundary. When it does, the walk is terminated and the prescribed potential V_p at that boundary point is recorded. Let the value of V_p at the end of the first walk be denoted by $V_p(1)$, as illustrated in Fig. 8.4. Then a second particle is released from (x, y) and allowed to wander until it reaches a boundary point, where the walk is terminated and the corresponding value of V_p is recorded as $V_p(2)$. This procedure is repeated for the third, fourth, ..., and Nth particle released from (x, y), and the corresponding prescribed potential $V_p(3)$, $V_p(4)$, ..., $V_p(N)$ are noted. According to Kakutani [32], the expected value of $V_p(1)$, $V_P(2)$, ..., $V_p(N)$ is the solution of the Dirichlet problem at (x, y), i.e.,

$$\boxed{V(x, y) = \frac{1}{N} \sum_{i=1}^{N} V_p(i)} \tag{8.57}$$

where N, the total number of walks, is large. The rate of convergence varies as $\sqrt{N}$ so that many random walks are required to ensure accurate results.

If it is desired to solve Poisson's equation

$$\nabla^2 V = -g(x, y) \quad \text{in } R \tag{8.58a}$$

subject to

$$V = V_p \quad \text{on } B\,, \tag{8.58b}$$

then the finite difference representation is in Eq. (8.25), namely,

$$\begin{aligned} V(x, y) = {} & p_{x+} V(x + \Delta, y) + p_{x-} V(x - \Delta, y) \\ & + p_{y+} V(x, y + \Delta) + p_{y-} V(x, y - \Delta) + \frac{\Delta^2 g}{4} \end{aligned} \tag{8.59}$$

where the probabilities remain as stated in Eq. (8.55b). The probabilistic interpretation of Eq. (8.59) is similar to that for Eq. (8.55). However, the term $\Delta^2 g/4$ in Eq. (8.59) must be recorded at each step of the random walk. If m_i steps are required for the ith random walk originating at (x, y) to reach the boundary, then one records

$$V_p(i) + \frac{\Delta^2}{4} \sum_{j=1}^{m_i - 1} g\left(x_j, y_j\right) \tag{8.60}$$

Thus the Monte Carlo result for $V(x, y)$ is

$$\boxed{V(x, y) = \frac{1}{N} \sum_{i=1}^{N} V_p(i) + \frac{\Delta^2}{4N} \sum_{i=1}^{N} \left[\sum_{j=1}^{m_i - 1} g\left(x_j, y_j\right) \right]} \tag{8.61}$$

An interesting analogy to the MCM just described is the walking drunk problem [15, 35]. We regard the random-walking particle as a "drunk," the squares of the mesh as the "blocks in a city," the nodes as "crossroads," the boundary B as the "city limits," and the terminus on B as the "policeman." Though the drunk is trying to walk home, he is so intoxicated that he wanders randomly throughout the city. The job of the policeman is to seize the drunk in his first appearance at the city limits and ask him to pay a fine V_p. What is the expected fine the drunk will receive? The answer to this problem is in Eq. (8.57).

On the dielectric boundary, the boundary condition $D_{1n} = D_{2n}$ is imposed. Consider the interface along y = constant plane as shown in Fig. 8.5. According to Eq. 3.46, the finite difference equivalent of the boundary condition at the interface is

$$V_o = p_{x+} V_1 + p_{x-} V_2 + p_{y+} V_3 + p_{y-} V_4 \tag{8.62a}$$

where

$$p_{x+} = p_{x-} = \frac{1}{4}, \qquad p_{y+} = \frac{\epsilon_1}{2\left(\epsilon_1 + \epsilon_2\right)}, \qquad p_{y-} = \frac{\epsilon_2}{2\left(\epsilon_1 + \epsilon_2\right)} \tag{8.62b}$$

An interface along x = constant plane can be treated in a similar manner.

On a line of symmetry, the condition $\dfrac{\partial V}{\partial n} = 0$ must be imposed. If the line of symmetry is along the y-axis as in Fig. 8.6(a), according to Eq. 3.48.

$$V_o = p_{x+} V_1 + p_{y+} V_3 + p_{y-} V_4 \tag{8.63a}$$

where

$$p_{x+} = \frac{1}{2} \quad p_{y+} = p_{y-} = \frac{1}{4} \tag{8.63b}$$

The line of symmetry along the x-axis, shown in Fig. 8.6(b), is treated similarly following Eq. 3.49.

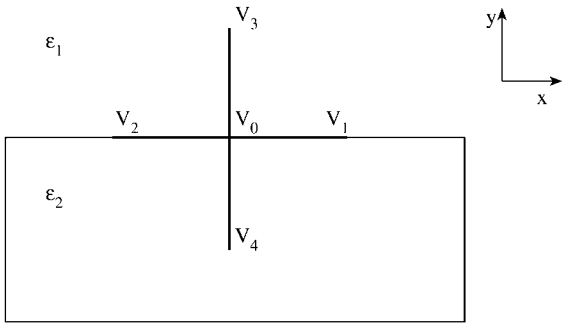

Figure 8.5
Interface between media of dielectric permittivities ϵ_1 and ϵ_2.

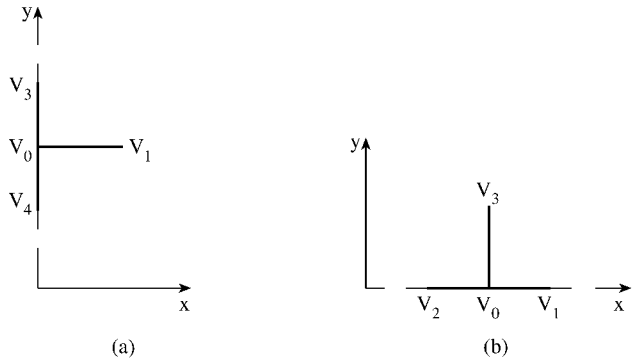

Figure 8.6
Satisfying symmetry conditions: (a) $\partial V/\partial x = 0$, (b) $\partial V/\partial y = 0$.

For an axisymmetric solution region such as shown in Fig. 8.7, $V = V(\rho, z)$. The finite difference equivalent of Eq. (8.54a) for $\rho \neq 0$ is obtained in Section 3.10 as

$$V(\rho, z) = p_{\rho+}V(\rho + \Delta, z) + p_{\rho-}V(\rho - \Delta, z) + p_{z+}V(\rho, z + \Delta) + p_{z-}V(\rho, z - \Delta) \tag{8.64}$$

where $\Delta\rho = \Delta z = \Delta$ and the random walk probabilities are given by

$$\begin{aligned} p_{z+} &= p_{z-} = \frac{1}{4} \\ p_{\rho+} &= \frac{1}{4} + \frac{\Delta}{8\rho} \\ p_{\rho-} &= \frac{1}{4} - \frac{\Delta}{8\rho} \end{aligned} \tag{8.65}$$

For $\rho = 0$, the finite difference equivalent of Eq. (8.54a) is Eq. 3.120, namely

$$V(0, z) = p_{\rho+}V(\Delta, z) + p_{z+}V(0, z + \Delta) + p_{z-}V(0, z - \Delta) \tag{8.66}$$

so that

$$p_{\rho+} = \frac{4}{6}, \quad p_{\rho-} = 0, \quad p_{z+} = \frac{1}{6} = p_{z-} \tag{8.67}$$

The random-walking particle is instructed to begin walk at (ρ_o, z_o). It wanders through the mesh according to the probabilities in Eqs. (8.65) and (8.67) until it reaches the boundary where it is absorbed and the prescribed potential $V_p(1)$ is recorded. By sending out N particles from (ρ_o, z_o) and recording the potential at the end of each walk, we obtain the potential at (ρ_o, z_o) as [49]

$$V(\rho_o, z_o) = \frac{1}{N}\sum_{i=1}^{N} V_p(i) \tag{8.68}$$

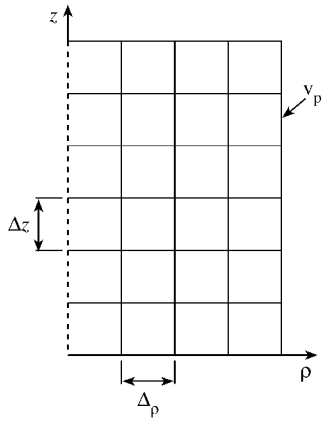

Figure 8.7
Typical axisymmetric solution region.

This MCM is called *fixed random walk* type since the step size Δ is fixed and the steps of the walks are constrained to lie parallel to the coordinate axes. Unlike in the finite difference method (FDM), where the potential at all mesh points are determined simultaneously, MCM is able to solve for the potential at one point at a time. One disadvantage of this MCM is that it is slow if potential at many points is required and is therefore recommended for solving problems for which only a few potentials are required. It shares a common difficulty with FDM in connection with irregularly shaped bodies having Neumann boundary conditions. This drawback is fully removed by employing MCM with floating random walk.

8.5.2 Floating Random Walk

The mathematical basis of the floating random walk method is the mean value theorem of potential theory. If S is a sphere of radius r, centered at (x, y, z), which lies wholly within region R, then

$$V(x, y, z) = \frac{1}{4\pi a^2} \int_S V\left(r'\right) dS' \tag{8.69}$$

That is, the potential at the center of any sphere within R is equal to the average value of the potential taken over its surface. When the potential varies in two dimensions, $V(x, y)$ is given by

$$V(x, y) = \frac{1}{2\pi\rho} \oint_L V\left(\rho'\right) dl' \tag{8.70}$$

where the integration is around a circle of radius ρ centered at (x, y). It can be shown that Eqs. (8.69) and (8.70) follow from Laplace's equation. Also, Eqs. (8.69) and (8.70) can be written as

$$V(x, y, z) = \int_0^1 \int_0^1 V(a, \theta, \phi)\, dF\, dT \tag{8.71}$$

$$V(x, y) = \int_0^1 V(a, \phi)\, dF \tag{8.72}$$

where

$$F = \frac{\phi}{2\pi}, \quad T = \frac{1}{2}(1 - \cos\theta) \tag{8.73}$$

and θ and ϕ are regular spherical coordinate variables. The functions F and T may be interpreted as the probability distributions corresponding to ϕ and θ. While $dF/d\phi =$ constant, $dT/d\theta = \frac{1}{2}\sin\theta$; i.e., all angles ϕ are equally probable, but the same is not true for θ.

The floating random walk MCM depends on the application of Eqs. (8.69) and (8.70) in a statistical sense. For a two-dimensional problem, suppose that a random-walking particle is at some point (x_j, y_j) after j steps in the ith walk. The next $(j + 1)$th step is taken as follows. First, a circle is constructed with center at (x_j, y_j) and radius ρ_j, which is equal to the shortest distance between (x_j, y_j) and the boundary. The ϕ coordinate is generated as a random variable uniformly distributed over $(0, 2\pi)$, i.e., $\phi = 2\pi U$, where $0 < U < 1$. Thus the location of the random-walking particle after the $(j + 1)$th step is illustrated in Fig. 8.8 and given as

$$\boxed{\begin{aligned} x_{j+1} &= x_j + \rho_j \cos\phi_j \\ y_{j+1} &= y_j + \rho_j \sin\phi_j \end{aligned}} \qquad \begin{aligned} &(8.74a) \\ &(8.74b) \end{aligned}$$

The next random walk is executed by constructing a circle centered at (x_{j+1}, y_{j+1}) and of radius ρ_{j+1}, which is the shortest distance between (x_{j+1}, y_{j+1}) and the

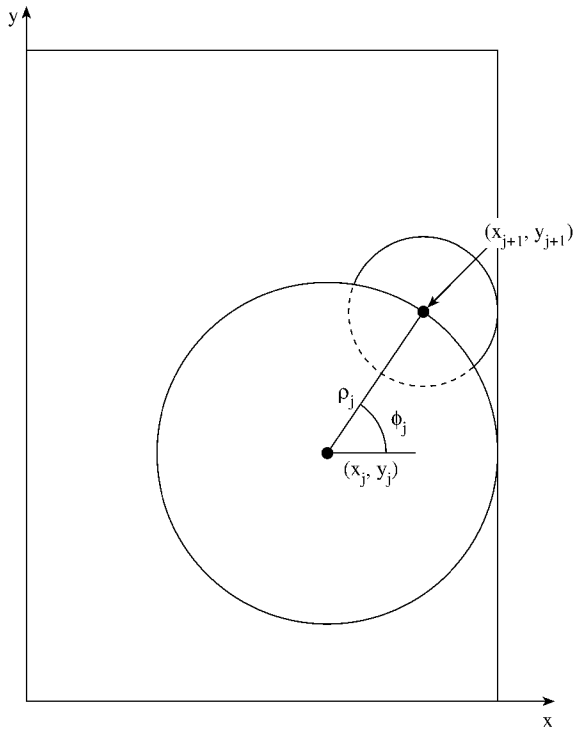

Figure 8.8
Configuration for floating random walks.

boundary. This procedure is repeated several times, and the walk is terminated when the walk approaches some prescribed small distance τ of the boundary. The potential $V_p(i)$ at the end of this ith walk is recorded as in fixed random walk MCM and the potential at (x, y) is eventually determined after N walks using Eq. (8.57).

The floating random walk MCM can be applied to a three-dimensional Laplace problem by proceeding along lines similar to those outlined above. A random-walking particle at (x_j, y_j, z_j) will step to a new location on the surface of a sphere whose radius r_j is equal to the shortest distance between point (x_j, y_j, z_j) and the boundary. The ϕ coordinate is selected as a random number U between 0 and 1, multiplied by 2π. The coordinate θ is determined by selecting another random number U between 0 and 1, and solving for $\theta = \cos^{-1}(1 - 2U)$ as in Example 8.1. Thus the location of the particle after its $(j + 1)$th step in the ith walk is

$$x_{j+1} = x_j + r_j \cos\phi_j \sin\theta_j \tag{8.75a}$$

$$y_{j+1} = y_j + r_j \sin\phi_j \sin\theta_j \tag{8.75b}$$

$$z_{j+1} = z_j + r_j \cos\theta_j \tag{8.75c}$$

Finally, we apply Eq. (8.57).

Solving Poisson's equation (8.58) for a two-dimensional problem requires only a slight modification. For a three-dimensional problem, $V(a, \theta, \phi)$ in Eq. (8.71) is replaced by $[V(a, \theta, \phi) + r^2 g/6]$. This requires that the term $gr_j^2/6$ at every jth step of the ith random walk be recorded.

An approach for handling a discretely inhomogeneous medium is presented in [39, 43, 44, 50].

It is evident that in the floating random walk MCM, neither the step sizes nor the directions of the walk are fixed in advance. The quantities may be regarded as "floating" and hence the designation *floating random walk.* A floating random walk bypasses many intermediate steps of a fixed random walk in favor of a long jump. Fewer steps are needed to reach the boundary, and so computation is much more rapid than in fixed random walk.

8.5.3 Exodus Method

The *Exodus method,* first suggested in [51] and developed for electromagnetics in [52, 53], does not employ random numbers and is generally faster and more accurate than the fixed random walk. It basically consists of dispatching numerous walkers (say 10^6) simultaneously in directions controlled by the random walk probabilities of going from one node to its neighbors. As these walkers arrive at new nodes, they are dispatched according to the probabilities until a set number (say 99.999%) have reached the boundaries. The advantage of the Exodus method is its independence of the random number generator.

To implement the Exodus method, we first divide the solution region R into mesh, such as in Fig. 8.4. Suppose p_k is the probability that a random walk starting from point (x, y) ends at node k on the boundary with prescribed potential $V_p(k)$. For M boundary nodes (excluding the corner points since a random walk never terminates at those points), the potential at the starting point (x, y) of the random walks is

$$\boxed{V(x, y) = \sum_{k=1}^{M} p_k V_p(k)} \tag{8.76}$$

If m is the number of different boundary potentials ($m = 4$ in Fig. 8.4), Eq. (8.76) can be simplified to

$$V(x, y) = \sum_{k=1}^{m} p_k V_p(k) \tag{8.77}$$

where p_k in this case is the probability that a random walk terminates on boundary k. Since $V_p(k)$ is specified, our problem is reduced to finding p_k. We find p_k using the Exodus method in a manner similar to the iterative process applied in Section 3.5.

Let $P(i, j)$ be the number of particles at point (i, j) in R. We begin by setting $P(i, j) = 0$ at all points (both fixed and free) except at point (x, y), where $P(i, j)$ assumes a large number N (say, $N = 10^6$ or more). By a scanning process, we dispatch

the particles at each free node to its neighboring nodes according to the probabilities p_{x+}, p_{x-}, p_{y+}, and p_{y-} as illustrated in Fig. 8.9. Note that in Fig. 8.9(b), new $P(i, j) = 0$ at that node, while old $P(i, j)$ is shared among the neighboring nodes. When all the free nodes in R are scanned as illustrated in Fig. 8.9, we record the number of particles that have reached the boundary (i.e., the fixed nodes). We keep scanning the mesh until a set number of particles (say 99.99% of N) have reached the boundary, where the particles are absorbed. If N_k is the number of particles that reached side k, we calculate

$$p_k = \frac{N_k}{N} \tag{8.78}$$

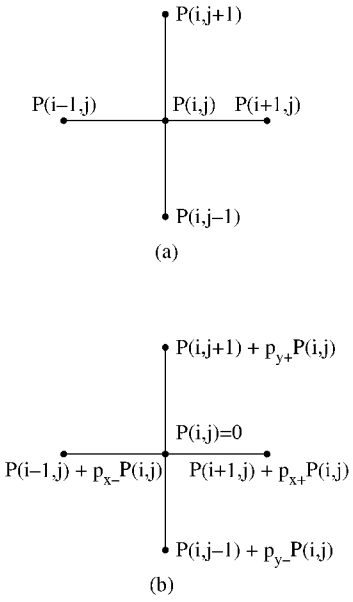

Figure 8.9
(a) Before the particles at (i, j) are dispatched, (b) after the particles at (i, j) are dispatched.

Hence Eq. (8.77) can be written as

$$V(x, y) = \frac{\sum_{k=1}^{M} N_k V_p(k)}{N} \tag{8.79}$$

Thus the problem is reduced to just finding N_k using the Exodus method, given N and $V_p(k)$. We notice that if $N \to \infty, \Delta \to 0$, and all the particles were allowed to reach the boundary points, the values of p_k and consequently $V(x, y)$ would be

exact. It is easier to approach this exact solution using the Exodus method than any other MCMs or any other numerical techniques such as difference and finite element methods.

We now apply the Exodus method to Poisson's equation. To compute the solution of the problem defined in Eq. (8.58), for example, at a specific point (x_o, y_o), we need the *transition probability* p_k and the *transient probability* q_ℓ. The transition probability p_k is already defined as the probability that a random walk starting at the point of interest (x_o, y_o) in R ends at a boundary point (x_k, y_k), where potential $V_p(k)$ is prescribed, i.e.,

$$p_k = \text{Prob}\,(x_o, y_o \rightarrow x_k, y_k) \tag{8.80}$$

The transient probability q_k is the probability that a random walk starting at point (x_o, y_o) passes through point (x_ℓ, y_ℓ) on the way to the boundary, i.e.,

$$p_\ell = \text{Prob}\left(x_o, y_o \xrightarrow{x_\ell, y_\ell} \text{boundary } B\right) \tag{8.81}$$

If there are m boundary (or fixed) nodes (excluding the corner points since a random walk never terminates at those points) and M_f free nodes in the mesh, the potential at the starting point (x_o, y_o) of the random walks is

$$V\,(x_o, y_o) = \sum_{k=1}^{m} p_k V_p(k) + \sum_{\ell=1}^{M_f} q_\ell G_\ell\,, \tag{8.82}$$

where

$$G_\ell = \Delta^2 g\,(x_\ell, y_\ell)\,/4$$

If M_b is the number of different boundary potentials, the first term in Eq. (8.82) can be simplified so that

$$V\,(x_o, y_o) = \sum_{k=1}^{M_b} p_k V_p(k) + \sum_{\ell=1}^{M_f} q_\ell G_\ell\,, \tag{8.83}$$

where p_k in this case is the probability that a random walk terminates on boundary k. Since $V_p(k)$ is specified and the source term G_ℓ is known, our problem is reduced to finding the probabilities p_k and q_ℓ. We notice from Eq. (8.83) that the value of $V(x_o, y_o)$ would be "exact" if the transition probabilities p_k and the transient probabilities q_ℓ were known exactly. These probabilities can be obtained in one of two ways: either analytically or numerically. The analytical approach involves using an expansion technique described in [54]. But this approach is limited to homogeneous rectangular solution regions. For inhomogeneous or non-rectangular regions, we must resort to some numerical simulation. The Exodus method offers a numerical means of finding p_k and q_ℓ. The fixed random walk can also be used to compute the transient and transition probabilities.

To apply the Exodus method, let $P(i, j)$ be the number of particles at point (i, j) in R, while $Q(i, j)$ is the number of particles passing through the same point. We begin

the application of the Exodus method by setting $P(i, j) = 0 = Q(i, j)$ at all nodes (both fixed and free) except at free node $(x_o y_o)$ where both $P(i, j)$ and $Q(i, j)$ are set equal to a large number N_p (say, $N_p = 10^6$ or more). In other words, we inject a large number of particles at (x_o, y_o) to start with. By scanning the mesh iteratively as is usually done in finite difference analysis, we dispatch the particles at each free node to its neighboring nodes according to the random walk probabilities p_{x+}, p_{x-}, p_{y+}, and p_{y-} as illustrated in Fig. 8.9. Note that in Fig. 8.9(b), new $P(i, j) = 0$ at that node, while old $P(i, j)$ is shared among the neighboring nodes. As shown in Fig. 8.10, the value of $Q(i, j)$ does not change at that node, while Q at the neighboring nodes is increased by the old $P(i, j)$ that is shared by those nodes. While $P(i, j)$ keeps records of the number of particles at point (i, j) during each iteration, $Q(i, j)$ tallies the number of particles passing through that point.

At the end of each iteration (i.e., scanning of the free nodes in R as illustrated in Figs. 8.9 and 8.10), we record the number of particles that have reached the boundary (i.e., the fixed nodes) where the particles are absorbed. We keep scanning the mesh in a manner similar to the iterative process applied in finite difference solution until a set number of particles (say 99.99% of N_p) have reached the boundary. If N_k is the number of particles that reached boundary k, we calculate

$$p_k = \frac{N_k}{N_p} \tag{8.84}$$

Also, at each free node, we calculate

$$q_\ell = \frac{Q_\ell}{N_p}\,, \tag{8.85}$$

where $Q_\ell = Q(i, j)$ is now the total number of particles that have passed through that node on their way to the boundary. Hence (8.83) can be written as

$$\boxed{V(x_o, y_o) = \frac{\sum_{k=1}^{M_b} N_k V_p(k)}{N_p} + \frac{\sum_{\ell=1}^{M_f} Q_\ell G_\ell}{N_p}} \tag{8.86}$$

Thus the problem is reduced to just finding N_k and Q_ℓ using the Exodus method, given N_p, $V_p(k)$, and G_ℓ. If $N_p \to \infty$, $\Delta \to 0$, and all the particles were allowed to reach the boundary points, the values of p_k and q_ℓ and consequently $V(x_o, y_o)$ would be exact. It is interesting to note that the accuracy of the Exodus method does not really depend on the number of particle N_p. The accuracy depends on the step size Δ and the number of iteration or the tolerance, the number of particles (say 0.001% of N_p), which are yet to reach the boundary before the iteration is terminated. However, a large value of N_p reduces the truncation error in the computation.

Example 8.4

Give a probabilistic interpretation using the finite difference form of the energy

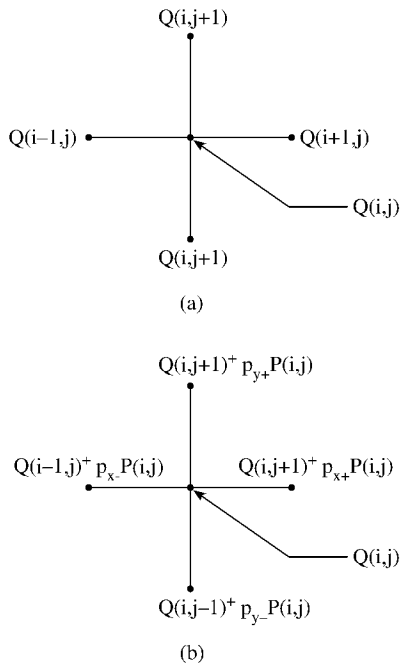

Figure 8.10
Number of particles passing through node (i, j) and its neighboring nodes: (a) before the particles at the node are dispatched, (b) after the particles at the node are dispatched.

equation

$$u\frac{\partial T}{\partial x} + v\frac{\partial T}{\partial y} = \alpha\left(\frac{\partial^2 T}{\partial x^2} + \frac{\partial^2 T}{\partial y^2}\right)$$

Assume a square grid of size Δ. □

Solution

Applying a backward difference to the left-hand side and a central difference to the right-hand side, we obtain

$$\begin{aligned} u\frac{T(x, y) - T(x - \Delta, y)}{\Delta} + v\frac{T(x, y) - T(x, y - \Delta)}{\Delta} \\ = \alpha\frac{T(x + \Delta, y) - 2T(x, y) + T(x - \Delta, y)}{\Delta^2} \\ + \alpha\frac{T(x, y + \Delta) - 2T(x, y) + T(x, y - \Delta)}{\Delta^2} \end{aligned} \tag{8.87}$$

Rearranging terms leads to

$$T(x, y) = p_{x+}T(x + \Delta, y) + p_{x-}T(x - \Delta, y) + p_{y+}T(x, y + \Delta) + p_{y-}T(x, y - \Delta) \tag{8.88}$$

where

$$p_{x+} = p_{y+} = \frac{1}{\frac{u\Delta}{\alpha} + \frac{v\Delta}{\alpha} + 4} \tag{8.89a}$$

$$p_{x-} = \frac{\left(1 + \frac{\Delta u}{\alpha}\right)}{\frac{u\Delta}{\alpha} + \frac{v\Delta}{\alpha} + 4} \tag{8.89b}$$

$$p_{y-} = \frac{\left(1 + \frac{\Delta v}{\alpha}\right)}{\frac{u\Delta}{\alpha} + \frac{v\Delta}{\alpha} + 4} \tag{8.89c}$$

Equation (8.88) is given probabilistic interpretation as follows: a walker at point (x, y) has probabilities p_{x+}, p_{x-}, p_{y+}, and p_{y-} of moving to point $(x + \Delta, y)$, $(x - \Delta, y)$, $(x, y + \Delta)$, and $(x, y - \Delta)$, respectively. With this interpretation, Eq. (8.88) can be used to solve the differential equation with fixed random MCM. ∎

Example 8.5

Consider a conducting trough of infinite length with square cross section shown in Fig. 8.11. The trough wall at $y = 1$ is connected to 100 V, while the other walls are grounded as shown. We intend to find the potential within the trough using the fixed random walk MCM. □

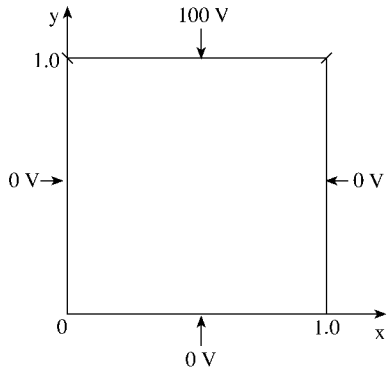

Figure 8.11
For Example 8.5.

Solution

The problem is solving Laplace's equation subject to

$$V(0, y) = V(1, y) = V(x, 0) = 0, V(x, 1) = 100 \tag{8.90}$$

The exact solution obtained by the method of separation of variables is given in Eq (2.31), namely,

$$V(x, y) = \frac{400}{\pi} \sum_{n=0}^{\infty} \frac{\sin k\pi x \sinh k\pi y}{k \sinh k\pi}, \quad k = 2n + 1 \tag{8.91}$$

Applying the fixed random MCM, the flowchart in Fig. 8.12 was developed. Based on the flowchart, the program of Fig. 8.13 was developed. A built-in standard subroutine RANDU in VAX 750 (also in VAX 780) was used to generate random numbers U uniformly distributed between 0 and 1. The step size Δ was selected as 0.05. The results of the potential computation are listed in Table 8.2 for three different locations. The average number of random steps $\overline{m}$ taken to reach the boundary is also shown. It is observed from Table 8.2 that it takes a large number of random steps for small step size and that the error in MCM results can be less than 1%.

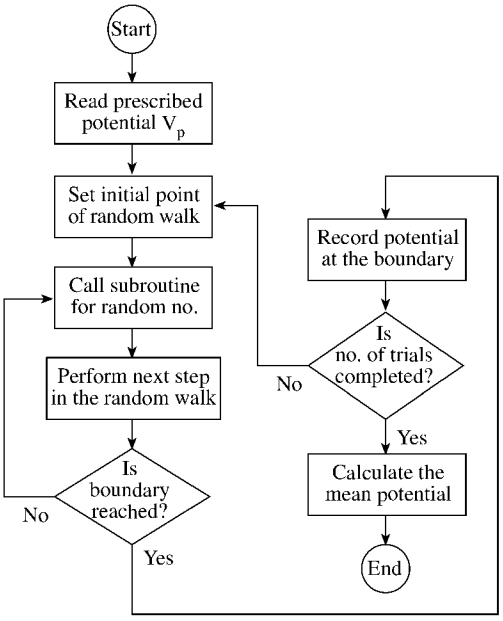

Figure 8.12
Flowchart for random walk of Example 8.5.

Rather than using Eq. (8.57), an alternative approach of determining $V(x, y)$ is to calculate the probability of a random walk terminating at a grid point located on the

```
0001    C*************************************************
0002    C  MONTE CARLO SOLUTION OF POTENTIAL PROBLEM
0003    C  INVOLVING LAPLACE'S EQUATION
0004    C*************************************************
0005    C
0006    C   SPECIFY INPUT PARAMETERS
0007    C
0008           DATA  V1,V2,V3,V4/0.0,0.0,100.0,0.0/
0009           DATA  IS1,IS2/1234,5678/
0010           DATA  P1,P2,P3/0.25,0.5,0.75/
0011           DATA A,B/1.0,1.0/
0012
0013           NRUN = 1000  ! NO. OF RUNS
0014           DELTA = 0.05   ! STEP SIZE
0015    C
0016    C  INITIALIZE VARIABLES
0017    C
0018           XO = 0.25
0019           YO = 0.75
0020           IO = XO/DELTA
0021           JO = YO/DELTA
0022           IMAX = A/DELTA
0023           JMAX = B/DELTA
0024           SUM = 0.0
0025           NS = 0  ! NO. OF WALKS BEFORE REACHING BOUNDARY
0026           M1 = 0  ! NO. OF WALKS TERMINATING AT V1
0027           M2 = 0
0028           M3 = 0
0029           M4 = 0  ! NO. OF WALKS TERMINATING AT V4
0030    C
0031    C   START RUNNING MONTE CARLO SIMULATION
0032    C
0033           DO 70 K=1,NRUN
0034           I=IO
0035           J=JO
0036    10     CALL RANDU(IS1,IS2,R)
0037           NS = NS + 1
0038           IF( R.GE.0.0.AND. R.LT.P1)  I = I + 1
0039           IF( R.GE.P1. AND. R.LT.P2)  J = J + 1
0040           IF( R.GE.P2. AND. R.LT.P3)  I = I - 1
0041           IF( R.GE.P3)                J = J - 1
0042    C
0043    C   CHECK IF (I,J) IS ON THE BOUNDARY
0044    C
0045            IF( I.EQ.0) THEN
0046           SUM = SUM + V4
0047           M4 = M4 +1
0048           GO TO 60
0049           ELSE
0050           ENDIF
0051           IF( IMAX - I) 20,20,30
0052    20      SUM = SUM +  V2
0053           M2 = M2 +1
0054            GO TO 60
0055    30     IF( J.EQ.0) THEN
0056           SUM = SUM + V1
0057           M1 = M1 + 1
0058           GO TO 60
0059           ELSE
0060           ENDIF
```

Figure 8.13
Program for Example 8.5 ***(Continued).***

```
0061            IF( JMAX - J) 40,40,50
0062    40      SUM = SUM + V3
0063            M3 = M3 + 1
0064            GO TO 60
0065    50      GO TO 10
0066    60      IF( MOD(K,250).NE.0.0 ) GO TO 70
0067            V = SUM/FLOAT(K)
0068            STEPS = FLOAT(NS)/FLOAT(K)  ! AVERAGE NO. OF WALKS
0069            PRINT *,X0,Y0,K,V,STEPS
0070    70      CONTINUE
0071           PRINT *, V
0072           WRITE(6,80) NRUN,V,M1,M2,M3,M4
0073    80     FORMAT(2X,'NRUN=',I6,3X,'V=',F12.6,3X,'Ms =',4I6,/)
0074           STOP
0075           END
```

Figure 8.13
(Cont.) **Program for Example 8.5.**

boundary. The information is easily extracted from the program used for obtaining the results in Table 8.2. To illustrate the validity of this approach, the potential at (0.25, 0.75) was calculated. For $N = 1000$ random walks, the number of walks terminating at $x = 0$, $x = 1$, $y = 0$ and $y = 1$ are 461, 62, 66, and 411, respectively. Hence, according to Eq. (8.79)

$$V(x, y) = \frac{461}{1000}(0) + \frac{62}{1000}(0) + \frac{66}{1000}(0) + \frac{411}{1000}(100) = 41.1 \tag{8.92}$$

The statistical error in the simulation can be found. In this case, the potential on the boundary takes values 0 or $V_o = 100$ so that $V(x, y)$ has a binomial distribution with mean $V(x, y)$ and variance

$$\sigma^2 = \frac{V(x, y)\,[V_o - V(x, y)]}{N} \tag{8.93}$$

At point (0.5, 0.5), for example, $N = 1000$ gives $\sigma = 1.384$ so that at 68% confidence interval, the error is $\delta = \sigma/\sqrt{N} = 0.04375$. ∎

Example 8.6

Use the floating random walk MCM to determine the potential at points (1.5, 0.5), (1.0, 1.5), and (1.5, 2.0) in the two-dimensional potential system in Fig. 8.14. □

Solution

To apply the floating random walk, we use the flowchart in Fig. 8.12 except that we apply Eq. (8.74) instead of Eq. (8.56) at every step in the random walk. A program based on the modified flowchart was developed. The shortest distance ρ from (x, y) to the boundary was found by dividing the solution region in Fig. 8.14 into three

Table 8.2 Results of Example 8.5

x	y	N	$\overline{m}$	Monte Carlo solution	Exact solution
0.25	0.75	250	66.20	42.80	43.20
		500	69.65	41.80	
		750	73.19	41.60	
		1000	73.95	41.10	
		1250	73.67	42.48	
		1500	73.39	42.48	
		1750	74.08	42.67	
		2000	74.54	43.35	
0.5	0.5	250	118.62	21.60	25.00
		500	120.00	23.60	
		750	120.27	25.89	
		1000	120.92	25.80	
		1250	120.92	25.92	
		1500	120.78	25.27	
		1750	121.50	25.26	
		2000	121.74	25.10	
0.75	0.25	250	64.82	7.60	6.797
		500	68.52	6.60	
		750	68.56	6.93	
		1000	70.17	7.50	
		1250	72.12	8.00	
		1500	71.78	7.60	
		1750	72.40	7.43	
		2000	72.40	7.30	

rectangles and checking

$$\text{if } \{(x, y) : 1 < x < 2, 0 < y < 1\}, \rho = \text{minimum}\{x - 1, 2 - x, y\}$$
$$\text{if } \{(x, y) : 0 < x < 1, 1 < y < 2.5\}, \rho = \text{minimum}\{x, y - 1, 2.5 - y\}$$
$$\text{if } \{(x, y) : 1 < x < 2, 1 < y < 2.5\},$$
$$\rho = \text{minimum}\left\{2 - x, 2.5 - y, \sqrt{(x-1)^2 + (y-1)^2}\right\}$$

A prescribed tolerance $\tau = 0.05$ was selected so that if the distance between a new point in the random walk and the boundary is less than τ, it is assumed that the boundary is reached and the potential at the closest boundary point is recorded.

Table 8.3 presents the Monte Carlo result with the average number of random steps $\overline{m}$. It should be observed that it takes fewer walks to reach the boundary in floating random walk than in fixed random walk. Since no analytic solution exists, we compare Monte Carlo results with those obtained using finite difference with $\Delta = 0.05$ and 500 iterations. As evident in Table 8.3, the Monte Carlo results agree well with the finite difference results even with 1000 walks. Also, by dividing the solution region

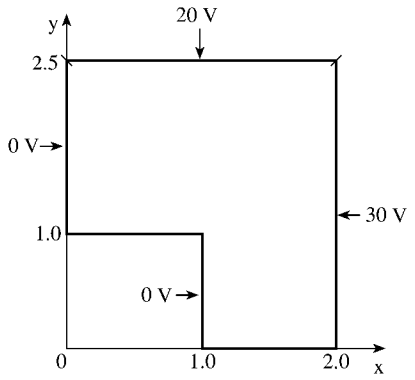

Figure 8.14
For Example 8.6.

into 32 elements, the finite element results [58] at points (1.5, 0.5), (1.0, 1.5), and (1.5, 2.0) are 11.265, 9.788, and 21.05 V, respectively.

Unlike the program in Fig. 8.13, where the error estimates are not provided for the sake of simplicity, the program in Fig. 8.15 incorporates evaluation of error estimates in the Monte Carlo calculations. Using Eq. (8.29), the error is calculated as

$$\delta = \frac{St_{\alpha/2;n-1}}{\sqrt{n}}$$

In the program in Fig. 8.15, the number of trials n (the same of N in Section 8.3), with different seed values, is taken as 5 so that $t_{\alpha/2;n-1} = 2.776$. The sample variance S is calculated using Eq. (8.19). The values of δ are also listed in Table 8.3. Notice that unlike in Table 8.2, where $\overline{m}$ and V are the mean values after N walks, $\overline{m}$ and V in Table 8.3 are the mean values of n trials, each of which involves N walks, i.e., the "mean of the mean" values. Hence the results in Table 8.3 should be regarded as more accurate than those in Table 8.2. ∎

Example 8.7

Apply the Exodus method to solve the potential problem shown in Fig. 8.16. The potentials at $x = 0$, $x = a$, and $y = 0$ sides are zero while the potential at $y = b$ sides is V_o. Typically, let

$$V_o = 100, \quad \epsilon_1 = \epsilon_o, \quad \epsilon_2 = 2.25\epsilon_o, \quad a = 3.0,\ b = 2.0,\ c = 1.0 \qquad \square$$

Solution

The analytic solution to this problem using series expansion technique discussed in Section 2.7 is:

```
0001    ************************************************
0002    C  MONTE CARLO (FLOATING RANDOM WALK) SOLUTION OF
0003    C  POTENTIAL PROBLEM  INVOLVING LAPLACE'S EQUATION
0004    C  ERROR ESTIMATES ARE ALSO EVALUATED
0005    C************************************************
0006
0007          DATA   PIE/3.1415/
0008          DIMENSION  T(10),V(10),STEPS(10)
0009          DATA ( T(I), I=2,10 )/12.706, 4.303, 3.182, 2.776,
0010         1              2.571,   2.447, 2.365, 2.306, 2.262/
0011                ! T(I) ARE THE  T-DISTRIBUTION PARAMETERS
0012
0013    C
0014    C  INITIALIZE VARIABLES
0015    C
0016          NTRIALS = 5 ! NO. OF TRIALS
0017          XO = 1.5  !  STARTING POINT, WHERE POTENTIAL IS
0018          YO = 0.5  !                        REQUIRED
0019          TOL = 0.005  ! TOLERANCE
0020    C
0021    C   START RUNNING MONTE CARLO SIMULATION
0022    C
0023          DO 120 NRUN=250,2000,250  ! NO. OF RUNS
0024          DO 80 J=1,NTRIALS
0025          IS1 = 1000*FLOAT(J)
0026          IS2 = 2000*FLOAT(J)
0027          SUM = 0.0
0028          M = 0 ! NO. OF STEPS TAKEN TO REACH BOUNDARY
0029          DO 60 I=1,NRUN
0030          X = XO
0031          Y = YO
0032    10    CALL RANDU(IS1,IS2,RN)
0033          PHI = 2.0*PIE*RN
0034    C     FIND THE SHORTEST DISTANCE
0035          RC = SQRT( (X-1.0)**2  +  (Y-1.0)**2 )
0036          IF(Y.GT.1.0)  GO TO 20
0037          R = X - 1.0
0038          IF( R.GT.(2.0-X) ) R = 2.0 - X
0039          IF(R.GT.Y) R = Y
0040          GO TO 40
0041    20    IF(X.GT.1.0) GO TO 30
0042          R = X
0043          IF( R.GT.(Y-1.0) ) R = Y - 1.0
0044          IF( R.GT.(2.5-Y) ) R = 2.5 - Y
0045          GO TO 40
0046    30    R = 2.0 - X
0047          IF(R.GT.RC) R = RC
0048          IF( R.GT.(2.5-Y) ) R = 2.5 - Y
0049    40    X = X + R*COS(PHI)
0050          Y = Y + R*SIN(PHI)
0051          M = M + 1
0052    C
0053    C   CHECK IF (X,Y) IS ON THE BOUNDARY
0054    C
0055          IF( (X.LT.(1.0+TOL)).AND.(Y.LT.(1.0+TOL)) ) GO TO !
0056                          ! FOR THE CORNER POINT
0057          IF( X.GE.(2.0-TOL) ) THEN
0058           SUM = SUM + 30.0
0059           GO TO 50
```

Figure 8.15

Applying floating random walk to solve the problem in Fig. 8.14; for Example 8.6 ***(Continued).***

```
0060            ELSE
0061           ENDIF
0062           IF( Y.GE.(2.5-TOL) ) THEN
0063            SUM = SUM + 20.0
0064            GO TO 50
0065           ELSE
0066           ENDIF
0067           IF(Y.GT.1.0. AND. X.LT.TOL) GO TO 50
0068           IF(Y.LT.1.0.AND.X.LT.(1.0-TOL)) GO TO 50
0069           IF(Y.LE.TOL.AND.X.GE.1.0) GO TO 50
0070           IF(Y.LE.(1.0+TOL) AND.X.LT.1.0) GO TO 50
0071           GO TO 10
0072    50     CONTINUE
0073    60     CONTINUE
0074            V(J) = SUM/FLOAT(NRUN)
0075            STEPS(J) = FLOAT(M)/FLOAT(NRUN)  ! AVERAGE NO. OF WALKS
0076             PRINT *,XO,YO,V(J),STEPS(J)
0077             WRITE(6,*) XO,YO,V(J),STEPS(J)
0078            WRITE(6,70) XO,YO,NRUN,V(J),STEPS(J)
0079    70     FORMAT(2X,'X = ',F5.2,3X,'Y=',F5.2,3X,
0080         1         'NRUN=',I6,3X,'V=',F12.6,3X,'STEPS=',F10.3,/)
0081    80     CONTINUE
0082    C
0083    C   FIND THE MEAN VALUE OF V AND MEAN NO. OF STEP
0084    C
0085           SUM = 0.0
0086           SUM1 = 0.0
0087           DO 90 I=1,NTRIALS
0088           SUM = SUM + V(I)
0089           SUM1 = SUM1 + STEPS(I)
0090    90     CONTINUE
0091           VMEAN = SUM/FLOAT(NTRIALS)
0092           STEPM = SUM1/FLOAT(NTRIALS)
0093    C
0094    C  CALCULATE ERROR
0095    C
0096           SUM = 0.0
0097           DO 100 I=1,NTRIALS
0098           SUM = SUM + ( V(I) - VMEAN )**2
0099    100    CONTINUE
0100           STD = SQRT( SUM/FLOAT(NTRIALS-1) )
0101           ERROR = STD*T(NTRIALS)/SQRT( FLOAT(NTRIALS) )
0102           PRINT *,NTRIALS,VMEAN,STEPM,ERROR
0103           WRITE(6,110) NTRIALS,VMEAN,STEPM,ERROR
0104    110    FORMAT(2X,'NO. OF TRIALS',I6,3X,'MEAN V =',F12.6,3X,
0105         1         'MEAN M = ',F12.6,3X,'ERROR=',F12.6,//)
0106    120    CONTINUE
0107           STOP
0108           END
```

Figure 8.15

(Cont.) **Applying floating random walk to solve the problem in Fig. 8.13; for Example 8.6.**

Table 8.3 Results of Example 8.6

x	y	N	$\overline{m}$	Monte Carlo solution ($V \pm \delta$)	Finite Difference solution (V)
1.5	0.5	250	6.738	11.52 ± 0.8973	11.44
		500	6.668	11.80 ± 0.9378	
		750	6.535	11.83 ± 0.4092	
		1000	6.476	11.82 ± 0.6205	
		1250	6.483	11.85 ± 0.6683	
		1500	6.465	11.72 ± 0.7973	
		1750	6.468	11.70 ± 0.6894	
		2000	6.460	11.55 ± 0.5956	
1.0	1.5	250	8.902	10.74 ± 0.8365	10.44
		500	8.984	10.82 ± 0.3709	
		750	8.937	10.75 ± 0.5032	
		1000	8.928	10.90 ± 0.7231	
		1250	8.836	10.84 ± 0.7255	
		1500	8.791	10.93 ± 0.5983	
		1750	8.788	10.87 ± 0.4803	
		2000	8.811	10.84 ± 0.3646	
1.5	2.0	250	7.242	21.66 ± 0.7509	21.07
		500	7.293	21.57 ± 0.5162	
		750	7.278	21.53 ± 0.3505	
		1000	7.316	21.53 ± 0.2601	
		1250	7.322	21.53 ± 0.3298	
		1500	7.348	21.51 ± 0.3083	
		1750	7.372	21.55 ± 0.2592	
		2000	7.371	21.45 ± 0.2521	

$$V = \begin{cases} \displaystyle\sum_{k=1}^{\infty} \sin \beta x \left[a_n \sinh \beta y + b_n \cosh \beta y \right], & 0 \le y \le c \\ \displaystyle\sum_{k=1}^{\infty} c_n \sin \beta x \sinh \beta y, & c \le y \le b \end{cases} \tag{24}$$

where

$$\begin{aligned} \beta &= \frac{n\pi}{a}, \quad n = 2k - 1 \\ a_n &= 4V_o \left[\epsilon_1 \tanh \beta c - \epsilon_2 \coth \beta c \right] / d_n \,, \\ b_n &= 4V_o \left(\epsilon_2 - \epsilon_1 \right) / d_n \,, \\ c_n &= 4V_o \left[\epsilon_1 \tanh \beta c - \epsilon_2 \coth \beta c + (\epsilon_2 - \epsilon_1) \coth \beta c \right] / d_n \,, \\ d_n &= n\pi \sinh \beta b \left[\epsilon_1 \tanh \beta c - \epsilon_2 \coth \beta c + (\epsilon_2 - \epsilon_1) \coth \beta b \right] \end{aligned} \tag{25}$$

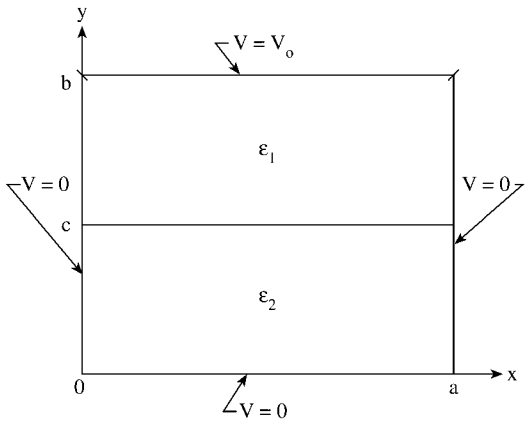

Figure 8.16
Potential system for Example 8.7.

The potentials were calculated at five typical points using the Exodus method, the fixed random walk Monte Carlo method, and the analytic solution. The number of particles, N, was taken as 10^7 for the Exodus method and the step size $\Delta = 0.05$ was used. For the fixed random walk method, $\Delta = 0.05$ and 2000 walks were used. It was noted that 2000 walks were sufficient for the random walk solutions to converge. The results are displayed in Table 8.4. In the table, δ is the error estimate, which is obtained by repeating each calculation five times and using statistical formulas provided in [13]. It should be noted from the table that the results of the Exodus method agree to four significant places with the exact solution. Thus the Exodus method is more accurate than the random walk technique. It should also be noted that the Exodus method does not require the use of a random number routine and also the need of calculating the error estimate. The Exodus method, therefore, takes less computation time than the random walk method. ∎

Table 8.4 Results of Example 8.7

x	y	Exodus Method V	Fixed Random Walk ($V \pm \delta$)	Finite Difference V	Exact Solution V
0.5	1.0	13.41	13.40 ± 1.113	13.16	13.41
1.0	1.0	21.13	20.85 ± 1.612	20.74	21.13
1.5	1.0	23.43	23.58 ± 1.2129	22.99	23.43
1.5	0.5	10.52	10.13 ± 0.8789	10.21	10.52
1.5	1.5	59.36	58.89 ± 2.1382	59.06	59.34

8.6 Regional Monte Carlo Methods

A major limitation inherent with the standard Monte Carlo methods discussed above is that they only permit single point calculations. In view of this limitation, several techniques have been proposed for using Monte Carlo for whole field computation. The popular ones are the *shrinking boundary method* [37] and *inscribed figure method* [38].

The shrinking boundary method is similar to the regular fixed random walk except that once the potential at an interior point is calculated, that point is treated as a boundary or absorbing point. This way, the random walking particles will have more points to terminate their walks and the walking time is reduced.

The inscribed figure method is based on the concept of subregion calculation. It involves dividing the solution region into standard shapes or inscribing standard shapes into the region. (By standard shapes is meant circles, squares, triangles, rectangles, etc. for which Green's function can be obtained analytically or numerically.) Then, a Monte Carlo method is used in computing potential along the dividing lines between the shapes and the regions that have nonstandard shapes. Standard analytical methods are used to compute the potential in the subregions.

Both the shrinking boundary method and the inscribed figure method do not make Monte Carlo methods efficient for whole field calculation. They still require point-by-point calculations and a number large of tests as standard Monte Carlo techniques. Therefore, they offer no significant advantage over the standard Monte Carlo methods. Using Markov chains for whole field calculations has been found to be more efficient than the shrinking boundary method and the inscribed figure method. The technique basically calculates the transition probabilities using absorbing Markov chains [55, 56].

A Markov chain is a sequence of random variables $X^{(0)}, X^{(1)}, \ldots$, where the probability distribution for $X^{(n)}$ is determined entirely by the probability distribution of $X^{(n-1)}$. A Markov process is a type of random process that is characterized by the memoryless property [57]–[60]. It is a process evolving in time that remembers only the most recent past and whose conditional distributions are time invariant. Markov chains are mathematical models of this kind of process. The Markov chain of interest to us are *discrete-state, discrete-time* Markov chains. In our case, the Markov chain is the random walk and the states are the grid nodes. The transition probability P_{ij} is the probability that a random-walking particle at node i moves to node j. It is expressed by the Markov property

$$\begin{aligned} P_{ij} &= P\left(x_{n+1} = j | x_o, x_1, \ldots, x_n\right) \\ &= P\left(x_{n+1} = j | x_n\right) \qquad j \in \mathbf{X},\ n = 0, 1, 2, \ldots \end{aligned} \tag{8.94}$$

The Markov chain is characterized by its transition probability matrix **P**, defined by

$$\mathbf{P} = \begin{bmatrix} P_{00} & P_{01} & P_{02} & \cdots \\ P_{10} & P_{11} & P_{12} & \cdots \\ P_{20} & P_{21} & P_{22} & \cdots \\ \vdots & \vdots & \vdots & \cdots \end{bmatrix} \tag{8.95}$$

P is a stochastic matrix, meaning that the sum of the elements in each row is unity, i.e.,

$$\sum_{j \in \mathbf{X}} P_{ij} = 1 \qquad i \in \mathbf{X} \tag{8.96}$$

We may also use the state transition diagram as a way of representing the evolution of a Markov chain. An example is shown in Fig. 8.17 for a three-state Markov chain.

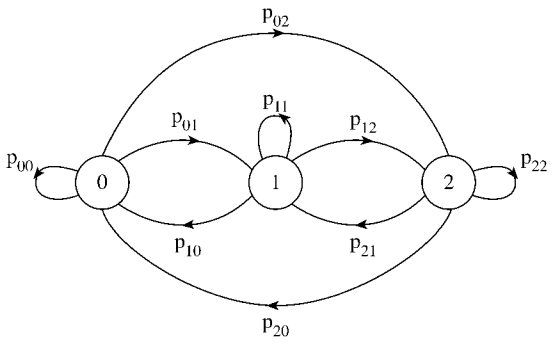

Figure 8.17
State Transition diagram for a three-state Markov Chain.

If we assume that there are n_f free (or nonabsorbing) nodes and n_p fixed (prescribed or absorbing) nodes, the size of the transition matrix **P** is n, where

$$n = n_f + n_p \tag{8.97}$$

If the absorbing nodes are numbered first and the nonabsorbing states are numbered last, the $n \times n$ transition matrix becomes

$$\mathbf{P} = \begin{bmatrix} \mathbf{I} & 0 \\ \mathbf{R} & \mathbf{Q} \end{bmatrix} \tag{8.98}$$

where the $n_f \times n_p$ matrix **R** represents the probabilities of moving from nonabsorbing nodes to absorbing ones; the $n_f \times n_f$ matrix **Q** represents the probabilities of moving from one nonabsorbing node to another; **I** is the identity matrix representing transitions between the absorbing nodes ($P_{ii} = 1$ and $P_{ij} = 0$); and 0 is the null matrix showing that there are no transitions from absorbing to nonabsorbing nodes.

For the solution of Laplace's equation, we obtain the elements of $\mathbf{Q}$ from Eq. (8.55b) as

$$Q_{ij} = \begin{cases} \dfrac{1}{4}, & \text{if } i \text{ is directly connected to } j, \\ 0, & \text{if } i = j \text{ or } i \text{ is not directly connected to } j \end{cases} \tag{8.99}$$

The same applies to R_{ij} except that j is an absorbing node.

For any absorbing Markov chain, $\mathbf{I} - \mathbf{Q}$ has an inverse. This is usually referred as the fundamental matrix

$$\mathbf{N} = (\mathbf{I} - \mathbf{Q})^{-1} \tag{8.100}$$

where N_{ij} is the average number of times the random-walking particle starting from node i passes through node j before being absorbed. The absorption probability matrix $\mathbf{B}$ is

$$\mathbf{B} = \mathbf{NR} \tag{8.101}$$

where B_{ij} is the probability that a random-walking particle originating from a non-absorbing node i will end up at the absorbing node j. $\mathbf{B}$ is an $n_f \times n_p$ matrix and is stochastic like the transition probability matrix, i.e.,

$$\sum_{j=1}^{n_p} B_{ij} = 1, \qquad i = 1, 2, \ldots, n_f \tag{8.102}$$

If $\mathbf{V}_f$ and $\mathbf{V}_p$ contain potentials at the free and fixed nodes, respectively, then

$$\boxed{\mathbf{V}_f = \mathbf{B}\mathbf{V}_p} \tag{8.103}$$

In terms of the prescribed potentials $V_1, V_2, \ldots, V_{n_p}$, Eq. (8.103) becomes

$$V_i = \sum_{j=1}^{n_p} B_{ij} V_j, \qquad i = 1, 2, \ldots, n_f \tag{8.104}$$

where V_i the potential at any free node i. Unlike Eq. (8.57), Eq. (8.103) or (8.104) provides the solution at all the free nodes at once.

An alternative way to obtain the solution in Eq. (8.103) is to exploit a property of the transition probability matrix $\mathbf{P}$. When $\mathbf{P}$ is multiplied by itself repeatedly for a large number of times, we obtain

$$\lim_{n\to\infty} \mathbf{P}^n = \begin{bmatrix} \mathbf{I} & 0 \\ \mathbf{B} & 0 \end{bmatrix} \tag{8.105}$$

Thus

$$\begin{bmatrix} \mathbf{V}_p \\ \mathbf{V}_f \end{bmatrix} = \mathbf{P}^n \begin{bmatrix} \mathbf{V}_p \\ \mathbf{V}_f \end{bmatrix} = \begin{bmatrix} \mathbf{I} & 0 \\ \mathbf{B} & 0 \end{bmatrix} \begin{bmatrix} \mathbf{V}_p \\ \mathbf{V}_f \end{bmatrix} \tag{8.106}$$

Either Eq. (8.103) or (8.106) can be used to find $\mathbf{V}_f$ but it is evident that Eq. (8.103) will be more efficient and accurate. From Eq. (8.103) or (8.104), it should be noticed that if $\mathbf{N}$ is calculated accurately, the solution is "exact."

There are several other procedures for whole field computation [37, 38], [61]–[64]. One technique involves using Green's function in the floating random walk [42].

The random walk MCMs and the Markov chain MCM applied to elliptic PDEs in this chapter can be applied to parabolic PDEs as well [65, 66].

The following two examples will corroborate Markov chain Monte Carlo method. The first example requires no computer programming and can be done by hand, while the second one needs computer programming.

Example 8.8

Rework Example 8.5 using Markov chain. The problem is shown in Fig. 8.11. We wish to determine the potential at points $(a/3, a/3)$, $(a/3, 2a/3)$, $(2a/3, a/3)$, and $(2a/3, 2a/3)$. Although we may assume that $a = 1$, that is not necessary. □

Solution

In this case, there are four free nodes ($n_f = 4$) and eight fixed nodes ($n_p = 8$) as shown in Fig. 8.18. The transition probability matrix is obtained by inspection as

$$\mathbf{P} = \begin{array}{c} \\ 1 \\ 2 \\ 3 \\ 4 \\ 5 \\ 6 \\ 7 \\ 8 \\ 9 \\ 10 \\ 11 \\ 12 \end{array} \begin{array}{c} \begin{array}{cccccccccccc} 1 & 2 & 3 & 4 & 5 & 6 & 7 & 8 & 9 & 10 & 11 & 12 \end{array} \\ \left[\begin{array}{cccccccccccc} 1 & & & & & & & & & & & \\ & 1 & & & & & & & & & & \\ & & 1 & & & & & & & & & \\ & & & 1 & & & & & & & & \\ & & & & 1 & & & & & & & \\ & & & & & 1 & & & & & & \\ & & & & & & 1 & & & & & \\ & & & & & & & 1 & & & & \\ & & & & & & & & 1 & & & \\ \frac{1}{4} & & & & & & & & \frac{1}{4} & 0 & \frac{1}{4} & \frac{1}{4} & 0 \\ 0 & \frac{1}{4} & \frac{1}{4} & & & & & & & \frac{1}{4} & 0 & 0 & \frac{1}{4} \\ 0 & 0 & 0 & & & & \frac{1}{4} & \frac{1}{4} & & \frac{1}{4} & & & \frac{1}{4} \\ 0 & & & \frac{1}{4} & \frac{1}{4} & & 0 & 0 & 0 & 0 & \frac{1}{4} & \frac{1}{4} & 0 \end{array}\right] \end{array}$$

Other entries in $\mathbf{P}$ shown vacant are zeros.

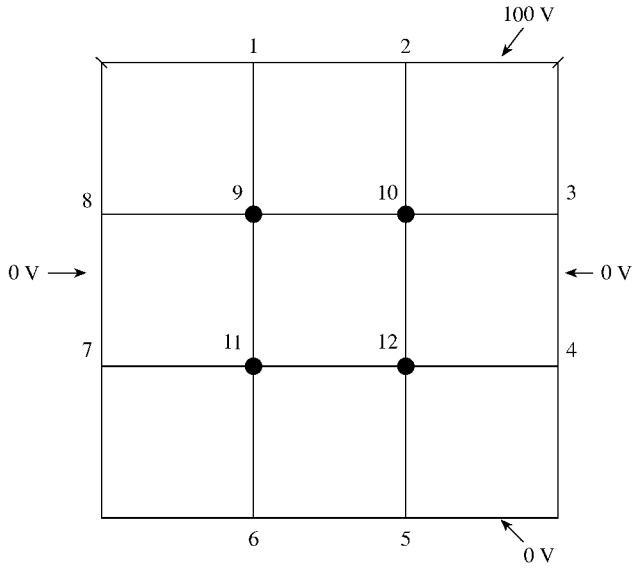

Figure 8.18
For Example 8.8.

From **P**, we obtain

$$\mathbf{R} = \begin{array}{c} \\ 9 \\ 10 \\ 11 \\ 12 \end{array} \begin{array}{c} \begin{array}{cccccccc} 1 & 2 & 3 & 4 & 5 & 6 & 7 & 8 \end{array} \\ \begin{bmatrix} \frac{1}{4} & 0 & 0 & 0 & 0 & 0 & 0 & \frac{1}{4} \\ 0 & \frac{1}{4} & \frac{1}{4} & 0 & 0 & 0 & 0 & 0 \\ 0 & 0 & 0 & 0 & 0 & \frac{1}{4} & \frac{1}{4} & 0 \\ 0 & 0 & 0 & \frac{1}{4} & \frac{1}{4} & 0 & 0 & 0 \end{bmatrix} \end{array}$$

$$\mathbf{Q} = \begin{array}{c} \\ 9 \\ 10 \\ 11 \\ 12 \end{array} \begin{array}{c} \begin{array}{cccc} 9 & 10 & 11 & 12 \end{array} \\ \begin{bmatrix} 0 & \frac{1}{4} & \frac{1}{4} & 0 \\ \frac{1}{4} & 0 & 0 & \frac{1}{4} \\ \frac{1}{4} & 0 & 0 & \frac{1}{4} \\ 0 & \frac{1}{4} & \frac{1}{4} & 0 \end{bmatrix} \end{array}$$

The fundamental matrix **N** is obtained as

$$\mathbf{N} = (\mathbf{I} - \mathbf{Q})^{-1} = \begin{bmatrix} 1 & -\frac{1}{4} & -\frac{1}{4} & 0 \\ -\frac{1}{4} & 1 & 0 & -\frac{1}{4} \\ -\frac{1}{4} & 0 & 1 & -\frac{1}{4} \\ 0 & -\frac{1}{4} & -\frac{1}{4} & 1 \end{bmatrix}^{-1}$$

or

$$\mathbf{N} = \frac{1}{6}\begin{bmatrix} 7 & 2 & 2 & 1 \\ 2 & 7 & 1 & 2 \\ 2 & 1 & 7 & 2 \\ 1 & 2 & 2 & 7 \end{bmatrix}$$

The absorption probability matrix **B** is obtained as

$$\mathbf{B} = \mathbf{NR} = \begin{array}{c} \\ 9 \\ 10 \\ 11 \\ 12 \end{array} \begin{array}{c} \begin{array}{cccccccc} 1 & 2 & 3 & 4 & 5 & 6 & 7 & 8 \end{array} \\ \begin{bmatrix} \frac{7}{24} & \frac{1}{12} & \frac{1}{12} & \frac{1}{24} & \frac{1}{24} & \frac{1}{12} & \frac{1}{12} & \frac{7}{24} \\ \frac{1}{12} & \frac{7}{24} & \frac{7}{24} & \frac{1}{12} & \frac{1}{12} & \frac{1}{24} & \frac{1}{24} & \frac{1}{12} \\ \frac{1}{12} & \frac{1}{24} & \frac{1}{24} & \frac{1}{12} & \frac{1}{12} & \frac{7}{24} & \frac{7}{24} & \frac{1}{12} \\ \frac{1}{24} & \frac{1}{12} & \frac{1}{12} & \frac{7}{24} & \frac{7}{24} & \frac{1}{12} & \frac{1}{12} & \frac{1}{24} \end{bmatrix} \end{array}$$

Notice that Eq. (8.102) is satisfied. We now use Eq. (8.104) to obtain the potentials at he free nodes. For example,

$$V_9 = \frac{7}{24}V_1 + \frac{1}{12}V_2 + \frac{1}{12}V_3 + \frac{1}{24}V_4 + \frac{1}{24}V_5 + \frac{1}{12}V_6 + \frac{1}{12}V_7 + \frac{7}{24}V_8$$

Since $V_1 = V_2 = 100$ while $V_3 = V_4 = \cdots = V_8 = 0$,

$$V_9 = \left(\frac{7}{24} + \frac{1}{12}\right)100 = 37.5$$

By symmetry, $V_{10} = V_9 = 37.5$. Similarly,

$$V_{11} = V_{12} = \left(\frac{1}{24} + \frac{1}{12}\right)100 = 12.5$$

Table 8.5 compares these results with the finite difference solution (with 10 iterations) and the exact solution using Eq. (2.31b) or (8.91). It is evident that the Markov chain solution compares well. ∎

Table 8.5 Results of Example 8.8

Node	Finite Difference Solution	Markov Chain Solution	Exact Solution
9	37.499	37.5	38.074
10	37.499	37.5	38.074
11	12.499	12.5	11.926
12	12.499	12.5	11.926

Example 8.9

Consider the potential problem shown in Fig. 8.19. Let

$$V_o = 100, \quad \epsilon_1 = \epsilon_o, \quad \epsilon_2 = 3\epsilon_o$$
$$a = b = 0.5, \quad h = w = 1.0 \quad \square$$

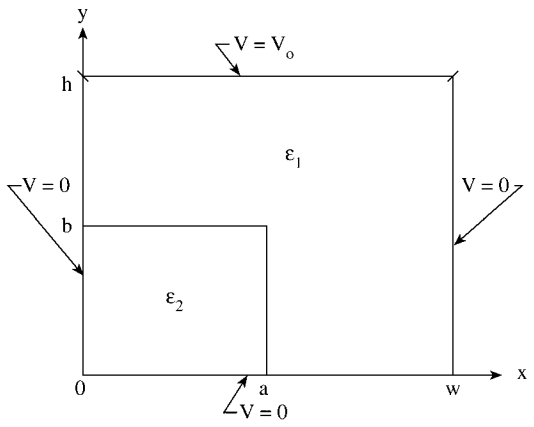

Figure 8.19
Potential system for Example 8.9.

Solution

The Markov chain solution was implemented using MATLAB. The approach involved writing code that generated the transition probability matrices using the random walk probabilities, computing the appropriate inverse, and manipulating the solution matrix. The use of MATLAB significantly reduced the programming complexity by the way the software internally handles matrices. The Q–matrix was selected as a timing index since the absorbing Markov chain algorithm involves inverting it. In this example, the Q–matrix is 361×361 and the running time was 90 and 34 seconds on 486DX2 and Pentium, respectively. $\Delta = 0.05$ was assumed. At the corner point $(x, y) = (a, b)$, the random walk probabilities are

$$p_{x+} = p_{y+} = \frac{\epsilon_1}{3\epsilon_1 + \epsilon_2}, \quad p_{x-} = p_{y-} = \frac{\epsilon_1 + \epsilon_2}{2\,(3\epsilon_1 + \epsilon_2)}$$

The plot of the potential distribution is portrayed in Fig. 8.20. Since the problem has no exact solution, the results at five typical points are compared with those from the Exodus method and finite difference in Table 8.6. It should be observed that the Markov chain approach provides a solution that is close to that by the Exodus method. ∎

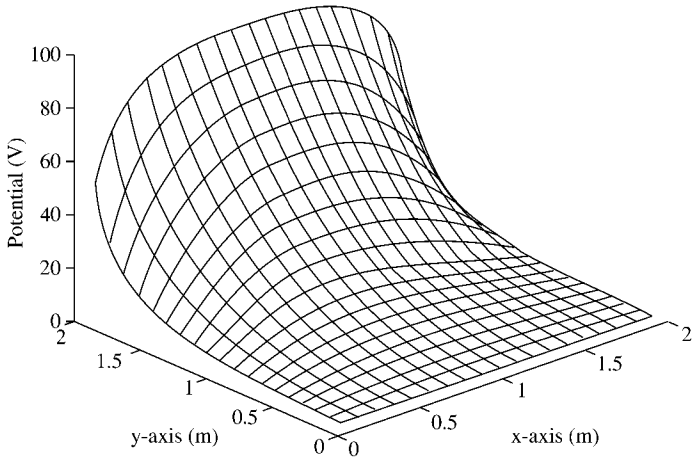

Figure 8.20
Potential distribution obtained by Markov chains; for Example 8.9.

Table 8.6 Results of Example 8.9

Node		Markov Chain	Exodus Method	Finite Difference
x	y			
0.25	0.5	10.2688	10.269	10.166
0.5	0.5	16.6667	16.667	16.576
0.75	0.5	15.9311	15.931	15.887
0.5	0.75	51.0987	51.931	50.928
0.5	0.25	6.2163	6.2163	6.1772

8.7 Concluding Remarks

The Monte Carlo technique is essentially a means of estimating expected values and hence is a form of numerical quadrature. Although the technique can be applied to simple processes and estimating multidimensional integrals, the power of the technique rests in the fact that [66]:

- it is often more efficient than other quadrature formulas for estimating multidimensional integrals,
- it is adaptable in the sense that variance reduction techniques can be tailored to the specific problem, and
- it can be applied to highly complex problems for which the definite integral formulation is not obvious and standard analytic techniques are ineffective.

For rigorous mathematical justification for the methods employed in Monte Carlo simulations, one is urged to read [32, 67]. As is typical with current MCMs, other numerical methods of solutions appear to be preferable when they may be used. Monte Carlo techniques often yield numerical answers of limited accuracy and are therefore employed as a last resort. However, there are problems for which the solution is not feasible using other methods. Problems that are probabilistic and continuous in nature (e.g., neutron absorption, charge transport in semiconductors, and scattering of waves by random media) are ideally suited to these methods and represent the most logical and efficient use of the stochastic methods. Since the recent appearance of vector machines, the importance of the Monte Carlo methods is growing.

It should be emphasized that in any Monte Carlo simulation, it is important to indicate the degree of confidence of the estimates or insert error bars in graphs illustrating Monte Carlo estimates. Without such information, Monte Carlo results are of questionable significance.

Applications of MCMs to other branches of science and engineering are summarized in [14, 15, 25, 68]. EM-related problems, besides those covered in this chapter, to which Monte Carlo procedures have been applied include:

- diffusion problems [62, 64, 70]
- strip transmission lines [40]
- random periodic arrays [71]
- waveguide structures [72]–[77]
- scattering of waves by random media [78]–[84]
- noise in magnetic recording [85, 86]
- induced currents in biological bodies [87].

We conclude this chapter by referring to two new Monte Carlo methods. One new MCM, known as the equilateral triangular mesh fixed random walk, has been proposed to handle Neumann problems [88]. Another new MCM, known as Neuro-Monte Carlo solution, is an attempt at whole field computation [89]. It combines an artificial neural network and a Monte Carlo method as a training data source. For further exposition on Monte Carlo techniques, one should consult [25, 26, 61, 90, 91].

References

[1] R. Hersch and R.J. Griego, "Brownian motion and potential theory," *Sci. Amer.*, Mar. 1969, pp. 67–74.

[2] T.F. Irvine and J.P. Hartnett (eds.), *Advances in Heat Transfer.* New York: Academic Press, 1968.

[3] H.A. Meyer (ed.), *Symposium on Monte Carlo Methods.* New York: John Wiley, 1956.

[4] D.D. McCracken, "The Monte Carlo method," *Sci. Amer.*, vol. 192, May 1955, pp. 90–96.

[5] T.E. Hull and A.R. Dobell, "Random number generators," *SIAM Review*, vol. 4, no. 3, July 1982, pp. 230–254.

[6] D.E. Knuth, *The Art of Computer Programming*, vol. 2. Reading, MA: Addison-Wesley, 1969, pp. 9, 10, 78, 155.

[7] J. Banks and J. Carson, *Discrete Event System Simulation.* Englewood Cliffs, NJ: Prentice-Hall, 1984, pp. 257–288.

[8] P.A.W. Lewis, et al., " A pseudo-random number generator for the system/360," *IBM System Jour.*, vol. 8, no. 2, 1969, pp. 136–146.

[9] S.S. Kuo, *Computer Applications of Numerical Methods.* Reading, MA: Addison-Wesley, 1972, pp. 327–345.

[10] A.M. Law and W.D. Kelton, *Simulation Modeling and Analysis.* New York: McGraw-Hill, 1982, pp. 219–228.

[11] D.E. Raeside, "An introduction to Monte Carlo methods," *Amer. Jour. Phys.*, vol. 42, Jan. 1974, pp. 20–26.

[12] C. Jacoboni and L. Reggiani, "The Monte Carlo method for the solution of charge transport in semiconductors with applications to covalent materials," *Rev. Mod. Phys.*, vol. 55, no. 3, July 1983, pp. 645–705.

[13] H. Kobayashi, *Modeling and Analysis: An Introduction to System Performance Evaluation Methodology.* Reading, MA: Addison-Wesley, 1978, pp. 221–247.

[14] I.M. Sobol, *The Monte Carlo Method.* Chicago: University of Chicago Press, 1974, pp. 24–30.

[15] Y.A. Shreider, *Method of Statistical Testing (Monte Carlo Method)*, Amsterdam: Elsevier, 1964, pp. 39–83. Another translation of the same Russian text: Y.A. Shreider, *The Monte Carlo Method (The Method of Statistical Trials).* Oxford: Pergamon, 1966.

[16] E.E. Lewis and W.F. Miller, *Computational Methods of Neutron Transport.* New York: John Wiley, 1984, pp. 296–360.

[17] I.S. Sokolinkoff and R.M. Redheffer, *Mathematics of Physics and Modern Engineering.* New York: McGraw-Hill, 1958, pp. 644–649.

[18] M.H. Merel and F.J. Mullin, "Analytic Monte Carlo error analysis," *J. Spacecraft*, vol. 5, no. 11, Nov. 1968, pp. 1304–1308.

[19] A.J. Chorin, "Hermite expansions in Monte-Carlo computation," *J. Comp. Phys.*, vol. 8, 1971, pp. 472–482.

[20] R.Y. Rubinstein, *Simulation and the Monte Carlo Method.* New York: John Wiley, 1981, pp. 20–90.

[21] W.J. Graybeal and U.W. Pooch, *Simulation: Principles and Methods.* Cambridge, MA: Winthrop Pub., 1980, pp. 77–97.

[22] B.J.T. Morgan, *Elements of Simulation.* London: Chapman & Hall, 1984, pp. 77–81.

[23] C.W. Alexion, et al., "Evaluation of radiation fields using statistical methods of integration," *IEEE Trans. Ant. Prog.*, vol. AP-26, no. 2, Mar. 1979, pp. 288–293.

[24] R.C. Millikan, "The magic of the Monte Carlo method," *BYTE*, vol. 8, Feb. 1988, pp. 371–373.

[25] M.H. Kalos and P.A. Whitlook, *Monte Carlo Methods.* New York: John Wiley, 1986, vol. 1, pp. 89–116.

[26] J.M. Hammersley and D.C. Handscomb, *Monte Carlo Methods.* London: Methuen, 1964.

[27] S. Haber, "A modified Monte-Carlo quadrature II," *Math. Comp.*, vol. 21, July 1967, pp. 388–397.

[28] S. Haber, "Numerical evaluation of multiple integrals," *SIAM Rev.*, vol. 12, no. 4, Oct. 1970, pp. 481–527.

[29] J.M. Hammersley and K.W. Morton, "A new Monte Carlo technique: antithetic variates," *Proc. Camb. Phil. Soc.*, vol. 52, 1955, pp. 449–475.

[30] J.H. Halton and D.C. Handscom, "A method for increasing the efficiency of Monte Carlo integration," *J. ACM*, vol. 4, 1957, pp. 329–340.

[31] S.J. Yakowitz, *Computational Probability and Simulation.* Reading, MA: Addison-Wesley, 1977, pp. 192, 193.

[32] S. Kakutani, "Two-dimensional Brownian motion harmonic functions," *Proc. Imp. Acad.*, (Tokyo), vol. 20, 1944, pp. 706–714.

[33] A. Haji-Sheikh and E.M. Sparrow, "The floating random walk and its application to Monte Carlo solutions of heat equations," *J. SIAM Appl. Math.*, vol. 14, no 2, Mar. 1966, pp. 370–389.

[34] A. Haji-Sheikh and E.M. Sparrow, "The solution of heat conduction problems by probability methods," *J. Heat Transfer*, Trans. ASME, Series C, vol. 89, no. 2, May 1967, pp. 121–131.

[35] G.E. Zinsmeiter, "Monte Carlo methods as an aid in teaching heat conduction," *Bull. Mech. Engr. Educ.*, vol. 7, 1968, pp. 77–86.

[36] R. Chandler, et al., "The solution of steady state convection problems by the fixed random walk method," *J. Heat Transfer,* Trans. ASME, Series C, vol. 90, Aug. 1968, pp. 361–363.

[37] G.E. Zinsmeiter and S.S. Pan, "A method for improving the efficiency of Monte Carlo calculation of heat conduction problems," *J. Heat Transfer,* Trans. ASME, Series C, vol. 96, 1974, pp. 246–248.

[38] G.E. Zinsmeiter and S.S. Pan, "A modification of the Monte Carlo method," *Inter. J. Num. Meth. Engr.,* vol. 10, 1976, pp. 1057–1064.

[39] G.M. Royer, "A Monte Carlo procedure for potential theory of problems," *IEEE Trans. Micro. Theo. Tech.,* vol. MTT-19, no. 10, Oct. 1971, pp. 813–818.

[40] R.M. Bevensee, "Probabilistic potential theory applied to electrical engineering problems," *Proc. IEEE,* vol. 61, no. 4, April 1973, pp. 423–437.

[41] R.L. Gibbs and J.D. Beason, "Solutions to boundary value problems of the potential type by random walk method," *Am. J. Phys.,* vol. 43, no. 9, Sept. 1975, pp. 782–785.

[42] J.H. Pickles, "Monte Carlo field calculations," *Proc. IEEE,* vol. 124, no. 12, Dec. 1977, pp. 1271–1276.

[43] F. Sanchez-Quesada, et al., "Monte-Carlo method for discrete inhomogeneous problems," *Proc. IEEE,* no. 125, no. 12, Dec. 1978, pp. 1400–1402.

[44] R. Schlott, "A Monte Carlo method for the Dirichlet problem of dielectric wedges," *IEEE Trans. Micro. Theo. Tech.,* vol. 36, no. 4, April 1988, pp. 724–730.

[45] M.N.O. Sadiku, "Monte Carlo methods in an introductory electromagnetic class," *IEEE Trans. Educ.,* vol. 33, no. 1, Feb. 1990, pp. 73–80.

[46] M.D.R. Beasley, et al., "Comparative study of three methods for computing electric fields," *Proc. IEEE,* vol. 126, no. 1, Jan. 1979, pp. 126–134.

[47] J.R. Currie, et al., "Monte Carlo determination of the frequency of lightning strokes and shielding failures on transmission lines," *IEEE Trans. Power Appl. Syst.,* vol. PAS-90, 1971, pp. 2305–2310.

[48] R.S. Velazquez, et al., "Probabilistic calculations of lightning protection for tall buildings," *IEEE Trans. Indust. Appl.,* vol. IA-18, no. 3, May/June 1982, pp. 252–259.

[49] M.N.O. Sadiku, "Monte Carlo Solution of Axisymmetric Potential Problems," *IEEE Trans. on Industry Applications,* vol. 29, no. 6, 1993, Nov./Dec. pp. 1042–1046.

[50] J.N. Jere and Y.L.L. Coz, "An Improved Floating-random-walk Algorithm for Solving Multi-dielectric Dirichlet Problem," *IEEE Trans. Micro. Theo. & Tech.,* vol. 41, no. 2, Feb. 1993, pp. 252–329.

[51] A.F. Emery and W.W. Carson, "A modification to the Monte Carlo method—the Exodus method," *J. Heat Transfer,* Trans. ASME, Series C, vol. 90, 1968, pp. 328–332.

[52] M.N.O. Sadiku and D. Hunt, "Solution of Dirichlet Problems by the Exodus Method," *IEEE Trans. Microwave Theory and Techniques,* vol. 40, no. 1, Jan. 1992, pp. 89–95.

[53] M.N.O. Sadiku, S.O. Ajose, and Zhibao Fu, "Appling the Exodus Method to Solve Poisson's Equation," *IEEE Trans. Microwave Theory and Techniques,* vol. 42, no. 4, April 1994, pp. 661–666.

[54] W.H. McCrea and F.J.W. Whipple, "Random paths in two and three dimensions," *Proc. Roy. Soc. Edinb.,* vol. 60, 1940, pp. 281–298.

[55] Fusco, V.F. and Linden, P.A., "A Markov Chain Approach for Static Field Analysis," *Microwave and Optical Technology Letters,* vol. 1, no. 6, Aug. 1988, pp. 216–220.

[56] M.N.O. Sadiku and R. Garcia, "Whole field computation using Monte Carlo Method," *Inter. Jour. Num. Model.,* vol. 10, 1997, pp. 303–312.

[57] M.E. Woodward, *Communication and Computer Networks.* Los Alamitos, CA: IEEE Computer Society Press, 1994, pp. 53–57.

[58] J.G. Kemeny and J.L. Snell, *Finite Markov Chains.* New York: Spring-Verlag, 1976, pp. 43–68.

[59] M. Iosifescu, *Finite Markov Processes and Their Applications.* New York: John Wiley & Sons, 1980, pp. 45, 99–106.

[60] G.J. Anders, *Probability Concepts in Electric Power Systems.* New York: John Wiley & Sons, 1990, pp. 160–170.

[61] T.J. Hoffman and N.E. Banks, "Monte Carlo surface density solution to the Dirichlet heat transfer problem," *Nucl. Sci. Engr.,* vol. 59, 1976, pp. 205–214.

[62] T.J. Hoffman and N.E. Banks, "Monte Carlo solution to the Dirichlet problem with the double-layer potential density," *Trans. Amer. Nucl. Sci.,* vol. 18, 1974, pp. 136, 137. See also vol. 19, 1974, p. 164; vol. 24, 1976, p. 181.

[63] T.E. Booth, "Exact Monte Carlo solution of elliptic partial differential equations," *J. Comp. Phys.,* vol. 39, 1981, pp. 396–404.

[64] T.E. Booth, "Regional Monte Carlo solution of elliptic partial differential equations," *J. Comp. Phys.,* vol. 47, 1982, pp. 281–290.

[65] A.F. Ghoniem, "Grid-free simulation of diffusion using random walk methods," *J. Comp. Phys.,* vol. 61, 1985, pp. 1–37.

[66] E.S. Troubetzkoy and N.E. Banks, "Solution of the heat diffusion equation by Monte Carlo," *Trans. Amer. Nucl. Soc.,* vol. 19, 1974, pp. 163, 164.

[67] A.W. Knapp, "Connection between Brownian motion and potential theory," *J. Math. Analy. Appl.*, vol. 12, 1965, pp. 328–349.

[68] J.H. Halton, "A retrospective and prospective survey of the Monte Carlo method," *SIAM Rev.*, vol. 12, no. 1, Jan. 1970, pp. 1–61.

[69] A.T. Bharucha-Reid (ed.), *Probabilistic Methods in Applied Mathematics*. New York: Academic Press, vol. 1, 1968; vol. 2, 1970; vol. 3, 1973.

[70] G.W. King, "Monte Carlo method for solving diffusion problems," *Ind. Engr. Chem.*, vol. 43, no. 11, Nov. 1951, pp. 2475–2478.

[71] Y.T. Lo, "Random periodic arrays," *Rad. Sci.*, vol. 3, no. 5, May 1968, pp. 425–436.

[72] T. Troudet and R.J. Hawkins, "Monte Carlo simulation of the propagation of single-mode dielectric waveguide structures," *Appl. Opt.*, vol. 27, no. 24, Feb. 1988, pp. 765–773.

[73] T.R. Rowbotham and P.B. Johns, "Waveguide analysis by random walks," *Elect. Lett.*, vol. 8, no. 10, May 1972, pp. 251–253.

[74] P.B. Johns and T.R. Rowbothan, "Solution of resistive meshes by deterministic and Monte Carlo transmission-line modelling," *IEEE Proc.*, vol. 128, Part A, no. 6, Sept. 1981, pp. 453–462.

[75] R.G. Olsen, "The application of Monte Carlo techniques to the study of impairments in the waveguide transmission system," *B. S. T. J.*, vol. 50, no. 4, April 1971, pp. 1293–1310.

[76] H.E. Rowe and D.T. Young, "Transmission distortion in multimode random waveguides," *IEEE Trans. Micro. Theo. Tech.*, vol. MMT-20, no. 6, June 1972, pp. 349–365.

[77] C. Huang et al., "Stationary phase Monte Carlo path integral analysis of electromagnetic wave propagation in graded-index waveguides," *IEEE Trans. Micro. Theo. Tech.*, vol. 42, no. 9, Sept. 1994, pp. 1709–1714.

[78] H.T. Chou and J.T. Johnson, "A novel acceleration algorithm for the computation of scattering from a rough surfaces with the forward-backward method," *Radio Science*, vol. 33, no. 5, Sept./Oct. 1998, pp. 1277–1287.

[79] M. Nieto-Vesperinas and J.M. Soto-Crespo, "Monte Carlo simulations for scattering of electromagnetic waves from perfectly conductive random rough surfaces," *Opt. Lett.*, vol. 12, no. 12, Dec. 1987, pp. 979–981.

[80] G.P. Bein, "Monte Carlo computer technique for one-dimensional random media," *IEEE Trans. Ant. Prop.*, vol. AP-21, no. 1, Jan. 1973, pp. 83–88.

[81] N. Garcia and E. Stoll, "Monte Carlo calculation for electromagnetic-wave scattering from random rough surfaces," *Phy. Rev. Lett.*, vol. 52, no. 20, May 1984, pp. 1798–1801.

[82] J. Nakayama, "Anomalous scattering from a slightly random surface," *Rad. Sci.*, vol. 17, no. 3, May-June 1982, pp. 558–564.

[83] A. Ishimaru, *Wave Propagation and Scattering in Random Media*. New York: Academic Press, vol. 2, 1978.

[84] A.K. Fung And M.F. Chen, "Numerical simulation of scattering from simple and composite random surfaces," *J. Opt. Soc. Am.*, vol. 2, no. 12, Dec. 1985, pp. 2274–2284.

[85] R.A. Arratia and H.N. Bertram, "Monte Carlo simulation of particulate noise in magnetic recording," *IEEE Trans. Mag.*, vol. MAG-20, no. 2, Mar. 1984, pp. 412–420.

[86] P.K. Davis, "Monte Carlo analysis of recording codes," *IEEE Trans. Mag.*, vol. MAG-20, no. 5, Sept. 1984, p. 887.

[87] J.H. Pickles, "Monte-Carlo calculation of electrically induced human-body currents," *IEEE Proc.*, vol. 134, Pt. A, no. 9, Nov. 1987, pp. 705–711.

[88] K. Gu and M.N.O. Sadiku, "A triangular mesh random walk for Dirichlet problems," *Jour. Franklin Inst.*, vol. 332B, no. 5, 1995, pp. 569–578.

[89] R.C. Garcia and M.N.O. Sadiku, "Neuro-Monte Carlo solution of electrostatic problems," *Jour. Franklin Inst.*, vol. 335B, no. 1, 1998, pp. 53–69.

[90] M.N. Barber and B.W. Ninham, *Random and Restricted Walks*. New York: Gordon and Breach, 1970.

[91] K.K. Sabelfeld, *Monte Carlo Methods in Boundary Value Problems*. New York: Springer-Verlag, 1991.

Problems

8.1 Write a program to generate 1000 pseudorandom numbers U uniformly distributed between 0 and 1. Calculate their mean and compare the calculated mean with the expected mean (0.5) as a test of randomness.

8.2 Generate 10,000 random numbers uniformly distributed between 0 and 1. Find the percentage of numbers between 0 and 0.1, between 0.1 and 0.2, etc., and compare your results with the expected distribution of 10% in each interval.

8.3 (a) Using the linear congruential scheme, generate 10 pseudorandom numbers with $a = 1573$, $c = 19$, $m = 10^3$, and seed value $X_0 = 89$.

(b) Repeat the generation with $c = 0$.

8.4 For $a = 13, m = 2^6 = 64$, and $X_0 = 1, 2, 3$, and 4, find the period of the random number generator using the multiplicative congruential method.

8.5 Develop a subroutine that uses the inverse transformation method to generate a random number from a distribution with the probability density function

$$f(x) = \begin{cases} 0.25, & 0 \le x \le 1 \\ 0.75, & 1 \le x \le 1 \end{cases}$$

8.6 It is not easy to apply the inverse transform method to generate normal distribution. However, by making use of the approximation

$$e^{-x^2/2} \simeq \frac{2e^{-kx}}{\left(1 + e^{-kx}\right)^2}, \quad x > 0$$

where $k = \sqrt{\frac{8}{\pi}}$, the inverse transform method can be applied. Develop a subroutine to generate normal deviates using inverse transform method.

8.7 Using the rejection method, generate a random variable from $f(x) = 5x^2$, $0 \le x \le 1$.

8.8 Use the rejection method to generate Gaussian (or normal) deviates in the truncated region $-a \le X \le a$.

8.9 Use sample mean Monte Carlo integration to evaluate:

(a) $\int_0^1 4\sqrt{1 - x^2}\, dx$,

(b) $\int_0^1 \sin x\, dx$,

(c) $\int_0^1 e^x\, dx$,

(d) $\int_0^1 \frac{1}{\sqrt{x}}\, dx$

8.10 Evaluate the following four-dimensional integrals:

(a) $\int_0^1 \int_0^1 \int_0^1 \int_0^1 \exp(x^1 x^2 x^3 x^4 - 1)\, dx^1\, dx^2\, dx^3\, dx^4$,

(b) $\int_0^1 \int_0^1 \int_0^1 \int_0^1 \sin(x^1 + x^2 + x^3 + x^4)\, dx^1\, dx^2\, dx^3\, dx^4$

8.11 The radiation from a rectangular aperture with constant amplitude and phase distribution may be represented by the integral

$$I(\alpha, \beta) = \int_{-1/2}^{1/2} \int_{-1/2}^{1/2} e^{j(\alpha x + \beta y)}\, dx\, dy$$

Evaluate this integral using a Monte Carlo procedure and compare your result for $\alpha = \beta = \pi$ with the exact solution

$$I(\alpha, \beta) = \frac{\sin(\alpha/2)\, \sin(\beta/2)}{\alpha\beta/4}$$

8.12 Consider the differential equation

$$\frac{\partial^2 W}{\partial x^2} + \frac{\partial^2 W}{\partial y^2} + \frac{k}{y}\frac{\partial W}{\partial y} = 0$$

where k = constant. By finding its finite difference form, give a probabilistic interpretation to the equation.

8.13 Given the one-dimensional differential equation

$$y'' = 0, \qquad 0 \le x \le 1$$

subject to $y(0) = 0$, $y(1) = 10$, use an MCM to find $y(0.25)$ assuming $\Delta x = 0.25$ and the following 20 random numbers:

0.1306, 0.0422, 0.6597, 0.7905, 0.7695, 0.5106, 0.2961, 0.1428, 0.3666, 0.6543, 0.9975, 0.4866, 0.8239, 0.8722, 0.1330, 0.2296, 0.3582, 0.5872, 0.1134, 0.1403.

8.14 Consider N equal resistors connected in series as in Fig. 8.21. By making $V(0) = 0$ and $V(N) = 10$ volts, find $V(k)$ using the fixed random walk for the following cases: (a) $N = 5$, $k = 2$, (b) $N = 10$, $k = 7$, (c) $N = 20$, $k = 11$.

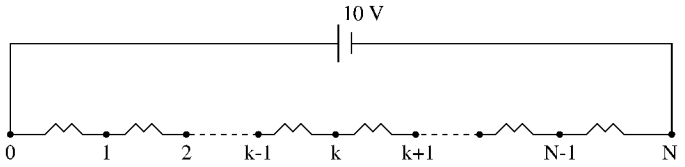

Figure 8.21
For Problem 8.14.

8.15 Use a Monte Carlo method to solve Laplace's equation in the triangular region $x \ge 0$, $y \ge 0$, $x + y \le 1$ with the boundary condition $V(x, y) = x + y + 0.5$. Determine V at (0.4, 0.2), (0.35, 0.2), (0.4, 0.15), (0.45, 0.2), and (0.4, 0.25).

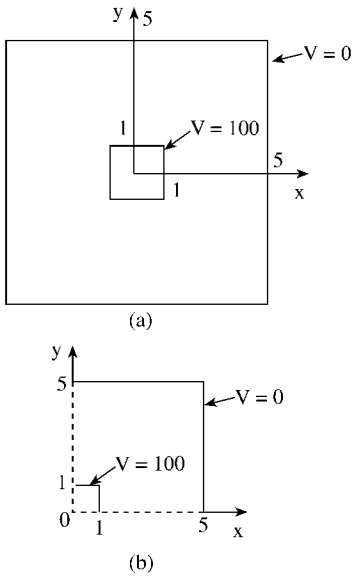

Figure 8.22
For Problem 8.16.

8.16 Use a Monte Carlo procedure to determine the potential at points (2,2), (3,3), and (4,4) in the problem shown in Fig. 8.22(a). By virtue of double symmetry, it is sufficient to consider a quarter of the solution region as shown in Fig. 8.22(b).

8.17 In the solution region of Fig. 8.23, $\rho_s = x(y-1)\,n\text{C}/m^2$. Find the potential at the center of the region using a Monte Carlo method.

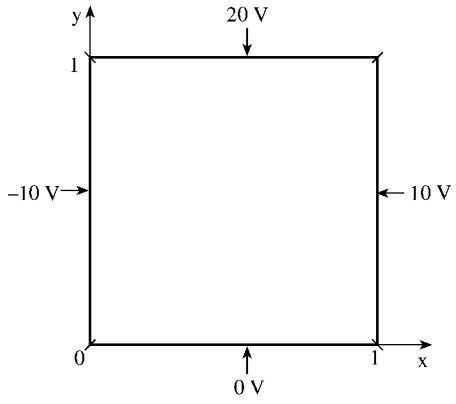

Figure 8.23
For Problem 8.17.

8.18 Consider the potential system shown in Fig. 8.24. Determine the potential at the center of the solution region. Take $\epsilon_r = 2.25$.

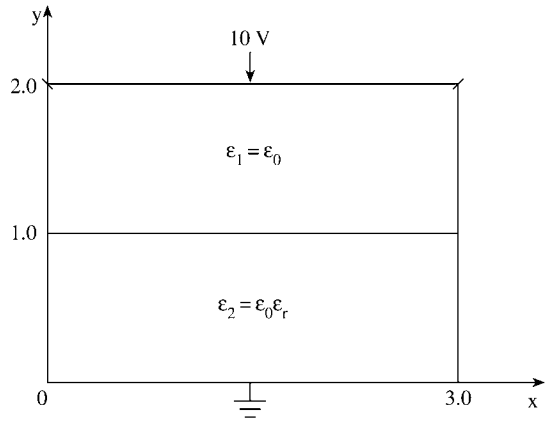

Figure 8.24
For Problem 8.18.

8.19 Apply an MCM to solve Laplace's equation in the three-dimensional region

$$|x| \leq 1, \quad |y| \leq 0.5, \quad |z| \leq 0.5$$

subject to the boundary condition

$$V(x, y, z) = x + y + z + 0.5$$

Find the solution at (0.5, 0.1, 0.1).

8.20 Consider the interface separating two homogeneous media in Fig. 8.25. By applying Gauss's law

$$\oint_S \epsilon \frac{\partial V}{\partial n} dS = 0$$

show that

$$V(\rho, z) = p_{\rho+} V(\rho + \Delta, z) + p_{\rho-} V(\rho - \Delta, z) + p_{z+} V(\rho, z + \Delta) + p_{z-} V(\rho, z - \Delta)$$

where

$$p_{z+} = \frac{\epsilon_1}{2(\epsilon_1 + \epsilon_2)}, \qquad p_{z-} = \frac{\epsilon_2}{2(\epsilon_1 + \epsilon_2)}$$
$$p_{\rho+} = p_{\rho-} = \frac{1}{4}$$

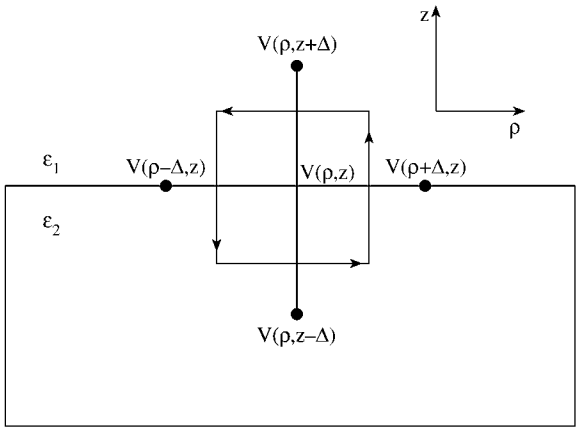

Figure 8.25
For Problem 8.20.

8.21 Consider the finite cylindrical conductor held at $V = 100$ enclosed in a larger grounded cylinder. The axial symmetric problem is portrayed in Fig. 8.26 for your convenience. Using a Monte Carlo technique, write a program to determine the potential at points (ρ, z) = (2,10), (5,10), (8,10), (5,2), and (5,18).

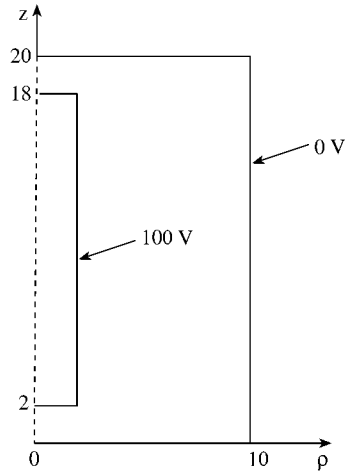

Figure 8.26
For Problem 8.21.

8.22 Figure 8.27 shows a prototype of an electrostatic particle focusing system employed in a recoil-mass time-of-flight spectometer. It is essentially a finite cylindrical conductor that abruptly expands radius by a factor of 2. Write a

program based on an MCM to calculate the potential at points $(\rho, z) = (5,18)$, (5,10), (5,2), (10,2), and (15,2).

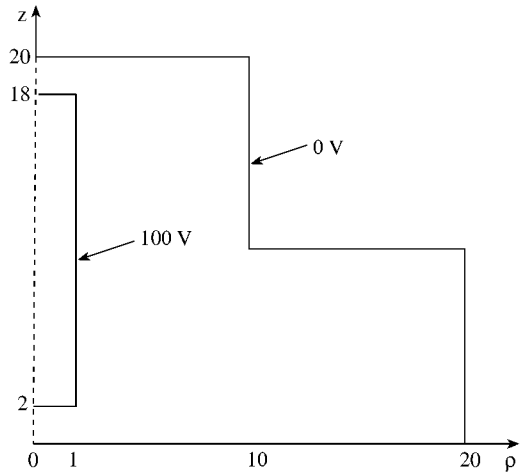

Figure 8.27
For Problem 8.22.

8.23 Consider the square region shown in Fig. 8.28. The transition probability $p(Q, S_i)$ is defined as the probability that a randomly walking particle leaving point Q will arrive at side S_i of the square boundary. Using the Exodus method, write a program to determine:

(a) $p(Q_1, S_i), \quad i = 1, 2, 3, 4,$
(b) $p(Q_2, S_i), \quad i = 1, 2, 3, 4.$

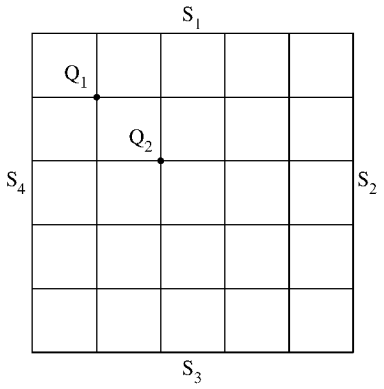

Figure 8.28
For Problem 8.23.

8.24 Given the one-dimensional differential equation

$$\frac{d^2\Phi}{dx^2} = 0, \quad 0 \leq x \leq 1$$

subject to $\Phi(0) = 0, \Phi(1) = 10$, use the Exodus method to find $\Phi(0.25)$ by injecting 256 particles at $x = 0.25$. You can solve this problem by hand calculation.

8.25 Use the Exodus method to find the potential at node 4 in Fig. 8.29. Inject 256 particles at node 4 and scan nodes in the order 1, 2, 3, 4. You can solve this problem by hand calculation.

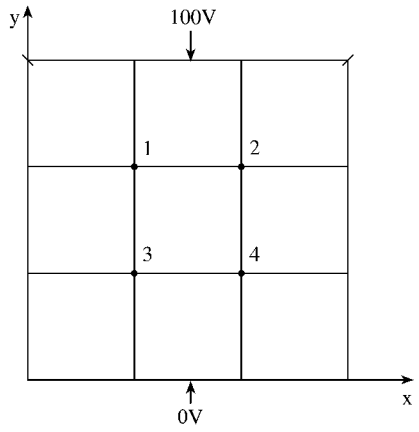

Figure 8.29
For Problem 8.25

8.26 Using the Exodus method, write a program to calculate $V(0.25, 0.75)$ in Example 8.5.

8.27 Write a program to calculate $V(1.0, 1.5)$ in Example 8.6 using the Exodus method.

8.28 Write a program that will apply the Exodus method to determine the potential at point (0.2, 0.4) in the system shown in Fig. 8.30.

8.29 Use Markov chain MCM to determine the potential at node 5 in Fig. 8.31.

8.30 Rework Problem 8.18 using Markov chain.

8.31 Rework Problem 8.22 using Markov chain.

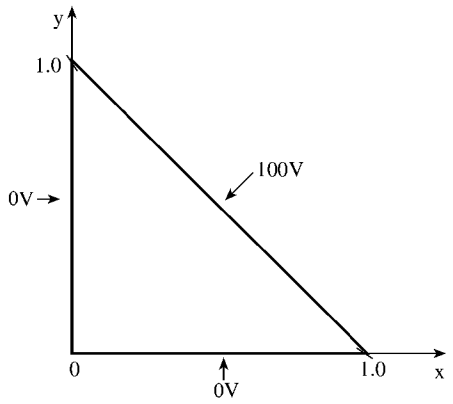

Figure 8.30
For Problem 8.28.

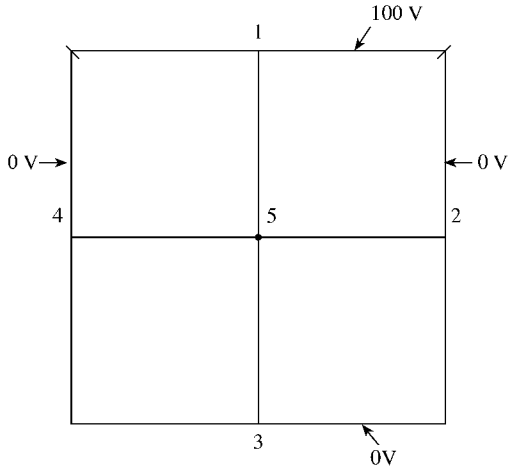

Figure 8.31
For Problem 8.29.

Chapter 9

Method of Lines

"Prejudice is the child of ignorance." William Hazlitt

9.1 Introduction

The method of lines (MOL) is a well-established numerical technique (or rather a semianalytical method) for the analysis of transmission lines, waveguide structures, and scattering problems. The method was originally developed by mathematicians and used for boundary value problems in physics and mathematics (e.g., [1]–[5]). A review of these earlier uses (1930–1965) of MOL is found in Liskovets [6]. The method was introduced into the EM community around 1980 and further developed by Pregla et al. [7]–[14] and other researchers. Although the formulation of this modern application is different from the earlier approach, the basic principles are the same.

The method of lines is regarded as a special finite difference method but more effective with respect to accuracy and computational time than the regular finite difference method. It basically involves discretizing a given differential equation in one or two dimensions while using analytical solution in the remaining direction. MOL has the merits of both the finite difference method and analytical method; it does not yield spurious modes nor does it have the problem of "relative convergence."

Besides, the method of lines has the following properties that justify its use:

(a) Computational efficiency: the semianalytical character of the formulation leads to a simple and compact algorithm, which yields accurate results with less computational effort than other techniques.

(b) Numerical stability: by separating discretization of space and time, it is easy to establish stability and convergence for a wide range of problems.

(c) Reduced programming effort: by making use of the state-of-the-art well documented and reliable ordinary differential equations (ODE) solvers, programming effort can be substantially reduced.

(d) Reduced computational time: since only a small amount of discretization lines are necessary in the computation, there is no need to solve a large system of equations; hence computing time is small.

To apply MOL usually involves the following five basic steps:

- partitioning the solution region into layers
- discretization of the differential equation in one coordinate direction
- transformation to obtain decouple ordinary differential equations
- inverse transformation and introduction of the boundary conditions
- solution of the equations

We begin to apply these steps to the problem of solving Laplace's equation. Since MOL involves many matrix manipulations, it is expedient that all computer codes in chapters are written in Matlab.

9.2 Solution of Laplace's Equation

Although the method of lines is commonly used in the EM community for solving hyperbolic (wave equation), it can be used to solve parabolic and elliptic equations [1], [15]–[18]. In this section, we consider the application of MOL to solve Laplace's equation (elliptic problem) involving two-dimensional rectangular and cylindrical regions.

9.2.1 Rectangular Coordinates

Laplace's equation in Cartesian system is

$$\frac{\partial^2 V}{\partial x^2} + \frac{\partial^2 V}{\partial y^2} = 0 \tag{9.1}$$

Consider a two-dimensional solution shown in Fig. 9.1. The first step is discretization of the x-variable. The region is divided into strips by N dividing straight lines (hence the name *method of lines*) parallel to the y-axis. Since we are discretizing along x, we replace the second derivative with respect to x with its finite difference equivalent. We apply the three-point central difference scheme,

$$\frac{\partial^2 V_i}{\partial x^2} = \frac{V_{i+1} - 2V_i + V_{i-1}}{h^2} \tag{9.2}$$

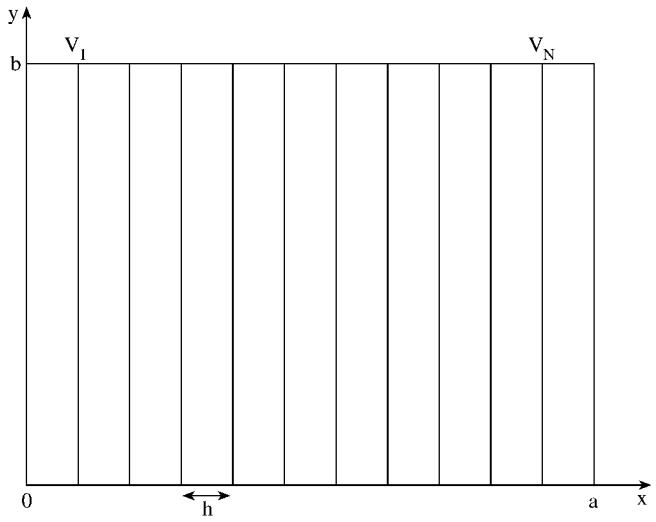

Figure 9.1
Illustration of discretization in the x-direction.

where h is the spacing between discretized lines, i.e.,

$$h = \Delta x = \frac{a}{N+1} \tag{9.3}$$

Replacing the derivative with respect to x by its finite difference equivalent, Eq. (9.1) becomes

$$\frac{\partial^2 V_i}{\partial y^2} + \frac{1}{h^2}\left[V_{i+1}(y) - 2V_i(y) + V_{i-1}(y)\right] = 0 \tag{9.4}$$

Thus the potential V in Eq. (9.1) can be replaced by a vector of size N, namely

$$[V] = [V_1, V_2, \ldots, V_N]^t \tag{9.5a}$$

where t denotes the transpose,

$$V_i(y) = V(x_i, y), \quad i = 1.2, \ldots, N \tag{9.5b}$$

and $x_i = i\,\Delta x$. Substituting Eqs. (9.4) and (9.5) into Eq. (9.1) yields

$$\frac{\partial^2 [V(y)]}{\partial y^2} - \frac{1}{h^2}[P][V(y)] = [0] \tag{9.6}$$

where [0] is a zero column vector and $[P]$ is an $N \times N$ tridiagonal matrix representing the discretized form of the second derivative with respect to x.

$$[P] = \begin{bmatrix} p_\ell & -1 & 0 & \dots & 0 \\ -1 & 2 & -1 & \dots & 0 \\ & \ddots & \ddots & \ddots & \\ 0 & \dots & -1 & 2 & -1 \\ 0 & \dots & 0 & -1 & p_r \end{bmatrix} \tag{9.7}$$

All the elements of matrix $[P]$ are zeros except the tridiagonal terms; the elements of the first and the last row of $[P]$ depend on the boundary conditions at $x = 0$ and $x = a$. $p_\ell = 2$ for Dirichlet boundary condition and $p_\ell = 1$ for Neumann boundary condition. The same is true of p_r.

The next step is to analytically solve the resulting equations along the y coordinate. To solve Eq. (9.6) analytically, we need to obtain a system of uncoupled ordinary differential equations from the coupled equations (9.6). To achieve this, we define the transformed potential $[\overline{V}]$ by letting

$$[V] = [T][\overline{V}] \tag{9.8}$$

and requiring that

$$[T]^t[P][T] = [\lambda^2] \tag{9.9}$$

where $[\lambda^2]$ is a diagonal matrix and $[T]^t$ is the transpose of $[T]$. $[\lambda^2]$ and $[T]$ are eigenvalue and eigenvector matrices belonging to $[P]$. The transformation matrix $[T]$ and the eigenvalue matrix $[\lambda^2]$ depend on the boundary conditions and are given in Table 9.1 for various combinations of boundaries. It should be noted that the

Table 9.1 Elements of Transformation Matrix $[T]$ and Eigenvalues

Left boundary	Right boundary	T_{ij}	λ_i
Dirichlet	Dirichlet	$\sqrt{\frac{2}{N+1}} \sin \frac{ij\pi}{N+1}$, $[T_{DD}]$	$2 \sin \frac{i\pi}{2(N+1)}$
Dirichlet	Neumann	$\sqrt{\frac{2}{N+0.5}} \sin \frac{i(j-0.5)\pi}{N+0.5}$, $[T_{DN}]$	$2 \sin \frac{(i-0.5)\pi}{2N+1}$
Neumann	Dirichlet	$\sqrt{\frac{2}{N+0.5}} \cos \frac{(i-0.5)(j-0.5)\pi}{N+0.5}$, $[T_{ND}]$	$2 \sin \frac{(i-0.5)\pi}{2N+1}$
Neumann	Neumann	$\sqrt{\frac{2}{N}} \cos \frac{(i-0.5)(j-1)\pi}{N}$, $j > 1$, $[T_{NN}]$	$2 \sin \frac{(i-1)\pi}{2N}$
		$\frac{1}{\sqrt{N}}$, $j = 1$	

Note: where $i, j = 1, 2, \dots, N$ and subscripts D and N are for Dirichlet and Neumann conditions, respectively.

eigenvector matrix $[T]$ has the following properties:

$$[T]^{-1} = [T]^t$$
$$[T][T]^t = [T]^t[T] = [I] \tag{9.10}$$

where $[I]$ is an identity matrix. Substituting Eq. (9.8) into Eq. (9.6) gives

$$\frac{\partial^2[T][\overline{V}]}{\partial y^2} - \frac{1}{h^2}[P][T][\overline{V}] = [0]$$

Multiplying through by $[T]^{-1} = [T]^t$ yields

$$\left(\frac{\partial^2}{\partial y^2} - \frac{1}{h^2}[\lambda^2]\right)[\overline{V}] = [0] \tag{9.11}$$

This is an ordinary differential equation with solution

$$\overline{V_i} = A_i \cosh \alpha_i y + B_i \sinh \alpha_i y \tag{9.12}$$

where $\alpha_i = \lambda_i / h$.

Thus, Laplace's equation is solved numerically using a finite difference scheme in the x-direction and analytically in the y-direction. However, we have only demonstrated three out of the five basic steps for applying MOL. There remain two more steps to complete the solution: imposing the boundary conditions and solving the resulting equations. Imposing the boundary conditions is problem dependent and will be illustrated in Example 9.1. The resulting equations can be solved using the existing packages for solving ODE or developing our own codes in Fortran, Matlab, C, or any programming language. We will take the latter approach in Example 9.1.

Example 9.1

For the rectangular region in Fig. 9.1, let

$$V(0, y) = V(a, y) = V(x, 0) = 0\,, \quad V(x, b) = 100$$

and $a = b = 1$. Find the potential at (0.25, 0.75), (0.5, 0.5), (0.75, 0.25). □

Solution

In this case, we have Dirichlet boundaries at $x = 0$ and $x = 1$, which are already indirectly taken care of in the solution in Eq. (9.12). Hence, from **Table 9.1**,

$$\lambda_i = 2 \sin \frac{i\pi}{2(N+1)} \tag{9.13}$$

and

$$T_{ij} = \sqrt{\frac{2}{N+1}} \sin \frac{ij\pi}{N+1} \tag{9.14}$$

Let $N = 15$ so that $h = \Delta x = 1/16$ and $x = 0.25, 0.5, 0.75$ will correspond to $i = 4, 8, 12$, respectively.

By combining Eqs. (9.8) and (9.12), we obtain the required solution. To get constants A_i and B_i, we apply boundary conditions at $y = 0$ and $y = b$ to V and perform inverse transformation. Imposing $V(x, y = 0) = 0$ to the combination of Eqs. (9.8) and (9.12), we obtain

$$\begin{bmatrix} V_1 \\ V_2 \\ \vdots \\ V_N \end{bmatrix} = [0] = \begin{bmatrix} T_{11} & T_{12} & \dots & T_{1N} \\ T_{21} & T_{22} & \dots & T_{2N} \\ \vdots & & \dots & \vdots \\ T_{N1} & T_{N2} & \dots & T_{NN} \end{bmatrix} \begin{bmatrix} A_1 \\ A_2 \\ \vdots \\ A_N \end{bmatrix}$$

which implies that

$$[A] = 0 \quad \text{or} \quad A_i = 0 \tag{9.15}$$

Imposing $V(x, y = b) = 100$ yields

$$\begin{bmatrix} 100 \\ 100 \\ \vdots \\ 100 \end{bmatrix} = [T] \begin{bmatrix} B_1 \sinh \alpha_1 b \\ B_2 \sinh \alpha_2 b \\ \vdots \\ B_N \sinh \alpha_N b \end{bmatrix}$$

If we let

$$[C] = \begin{bmatrix} B_1 \sinh \alpha_1 b \\ B_2 \sinh \alpha_2 b \\ \vdots \\ B_N \sinh \alpha_N b \end{bmatrix} = [T]^{-1} \begin{bmatrix} 100 \\ 100 \\ \vdots \\ 100 \end{bmatrix}$$

then

$$B_i = C_i / \sinh \alpha_i b \tag{9.16}$$

With A_i and B_i found in Eqs. (9.15) and (9.16), the potential $V(x, y)$ is determined as

$$V_i(y) = \sum_{j=1}^{N} T_{ij} B_j \sinh(\alpha_j y) \tag{9.17}$$

By applying Eqs. (9.13) to (9.17), the Matlab code in Fig. 9.2 was developed to obtain

$$V(0.25, 0.75) = 43.1\,, \quad V(0.5, 0.5) = 24.96\,, \quad V(0.75, 0.25) = 6.798$$

The result compares well with the exact solution:

$$V(0.25, 0.75) = 43.2\,, \quad V(0.5, 0.5) = 25.0\,, \quad V(0.75, 0.25) = 6.797$$

```
AA = 1;
BB = 1;
N = 15;
% DETERMINE VECTOR ALPHA
H = AA/(N+1);
LAM = 2*sin ((1:N)*pi*0.5/(N+1) );
ALPHA = LAM/H;
% CALCULATE THE TRANSFORMATION MATRIX AND COEFFICIENT B
K = sqrt (2/(N+1));
T = zeros(N,N);
for  I=1:N
  for J=1:N
    T(I,J) = K*sin (I*J*pi/(N+1));
  end
end
V = 100*ones(N,1);
C = inv(T)*V;
A = ALPHA';
B = C./sinh(BB*A);
% CALCULATE V AT THE GIVEN POINTS
V1 = 0;  V2 = 0;  V3 = 0;
for K=1:N
V1 = V1 + T(4,K)*B(K)*sinh(ALPHA(K)*0.75);
V2 = V2 + T(8,K)*B(K)*sinh(ALPHA(K)*0.5);
V3 = V3 + T(12,K)*B(K)*sinh(ALPHA(K)*0.25);
end
diary
V1, V2, V3
diary off
```

Figure 9.2
Matlab code for Example 9.1.

Notice that it is not necessary to invert the transformation matrix $[T]$ in view of Eq. (9.10). ∎

Example 9.2

For Dirichlet–Neumann conditions, derive the transformation matrix $[T_{DN}]$ and the corresponding eigenvalues $[\lambda^2]$. □

Solution

Let λ_k^2 be the elements of eigenvalue matrix $[\lambda^2]$ and $[t_k]$ be the column vectors of the transformation matrix $[T_{DN}]$ corresponding to matrix $[P]$. Then, by definition,

$$\Big([P] - \lambda_k^2[I]\Big)[t_k] = [0] \tag{9.18}$$

Substituting $[P]$ for Dirichlet–Neumann condition in Eq. (9.7) into Eq. (9.18) gives

a second-order difference equation

$$-t_{i-1}^{(k)} + \left(2 - \lambda_k^2\right) t_i^{(k)} - t_{i+1}^{(k)} = 0 \tag{9.19}$$

except the first and last equations in (9.18). If we let

$$t_i^{(k)} = A_k e^{ji\phi_k} + B_k e^{-ji\phi_k} \tag{9.20}$$

and substitute this into Eq. (9.19), we obtain

$$0 = \left(A_k e^{ji\phi_k} + B_k e^{-ji\phi_k}\right)\left(-2\cos\phi_k + 2 - \lambda_k^2\right)$$

from which we obtain the characteristic equation

$$\lambda_k^2 = 2\left(1 - \cos\phi_k\right) = 4\sin^2\frac{\phi_k}{2} \tag{9.21}$$

or

$$\lambda_k = 2\sin\frac{\phi_k}{2} \tag{9.22}$$

This is valid for all types of boundary combinations but ϕ_k will depend on the boundary conditions. To determine ϕ_k, A_k, and B_k, we use the first and the last equations in Eq. (9.18). For DN conditions,

$$t_0^{(k)} = 0 \tag{9.23a}$$

$$-t_N^{(k)} + t_{N+1}^{(k)} = 0 \tag{9.23b}$$

Substituting this into Eq. (9.20), we obtain

$$\begin{bmatrix} 1 & 1 \\ e^{jN\phi_k}\left(e^{j\phi_k} - 1\right) & e^{-jN\phi_k}\left(e^{-j\phi_k} - 1\right) \end{bmatrix} \begin{bmatrix} A_k \\ B_k \end{bmatrix} = \begin{bmatrix} 0 \end{bmatrix} \tag{9.24}$$

For nontrivial solutions,

$$\phi_k = \frac{k - 0.5}{N + 0.5}\pi\ , \quad k = 1, 2, \ldots, N \tag{9.25}$$

Also from Eqs. (9.23a) and (9.20), $A_k = -B_k$ so that

$$t_i^{(k)} = A_k \sin\left(i\phi_k\right) \tag{9.26}$$

Thus, for Dirichlet–Neumann conditions, we obtain

$$\lambda_k = 2\sin\left(0.5\pi\frac{k - 0.5}{N + 0.5}\right) \tag{9.27a}$$

$$T_{ij} = \sqrt{\frac{2}{N + 0.5}}\sin\left(0.5\pi\frac{i(k - 0.5)}{N + 0.5}\right) \tag{9.27b}$$

9.2.2 Cylindrical Coordinates

Although MOL is not applicable to problems with complex geometry, the method can be used to analyze homogeneous and inhomogeneous cylindrical problems. The principal steps in applying MOL in cylindrical coordinates are the same as in Cartesian coordinates.

Here, we illustrate with the use of MOL to solve Laplace's equation in cylindrical coordinates [18]. We apply discretization procedure in the angular direction. The resulting coupled ordinary differential equations are decoupled by matrix transformation and solved analytically.

Assume that we are interested in finding the potential distribution in a cylindrical transmission line with a uniform but arbitrary cross section. We assume that the inner conductor is grounded while the outer conductor is maintained at constant potential V_o, as shown in Fig. 9.3. In cylindrical coordinates (ρ, ϕ), Laplace's equation can be

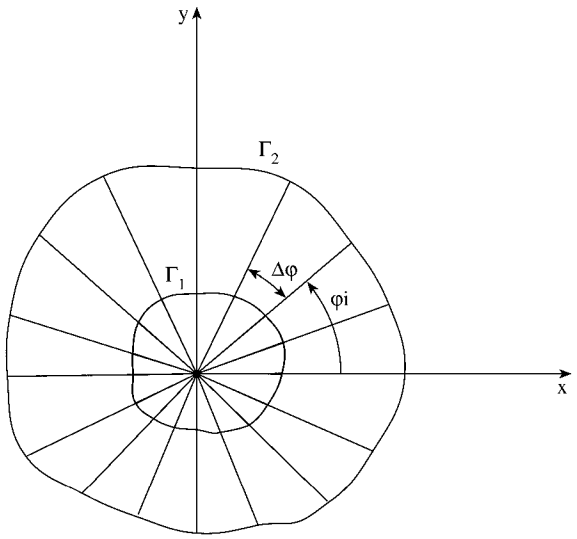

Figure 9.3
Discretization along φ-direction.

expressed as

$$\rho^2 \frac{\partial^2 V}{\partial \rho^2} + \rho^2 \frac{\partial V}{\partial \rho} + \frac{\partial^2 V}{\partial \phi^2} = 0 \tag{9.28}$$

subject to

$$V(\rho) = 0\,, \quad \rho \in \Gamma_1 \tag{9.29a}$$
$$V(\rho) = V_o\,, \quad \rho \in \Gamma_2 \tag{9.29b}$$

We discretize in the ϕ-direction by using N radial lines, as shown in Fig. 9.3, such that

$$V_i(\rho) = V(\rho, \phi_i) , \quad i = 1.2, \ldots, N \tag{9.30}$$

where

$$\phi_i = ih = \frac{2\pi i}{N} , \; h = \Delta\phi = \frac{2\pi}{N} \tag{9.31}$$

and h is the angular spacing between the lines. We have subdivided the solution region into N subregions with boundaries at Γ_1 and Γ_2. In each subregion, $V(\rho, \phi)$ is approximated by $V_i = V(\rho, \phi_i)$, with ϕ_i being constant.

Applying the three-point central finite difference scheme yields

$$\frac{\partial^2[V]}{\partial\phi^2} = -\frac{[P]}{h^2}[V] \tag{9.32}$$

where

$$[V] = [V_1, V_2, \ldots, V_N]^t \tag{9.33}$$

and

$$[P] = \begin{bmatrix} 2 & -1 & 0 & 0 & \ldots & 0 & 0 & -1 \\ -1 & 2 & -1 & 0 & \ldots & 0 & 0 & 0 \\ 0 & -1 & 2 & -1 & \ldots & 0 & 0 & 0 \\ \vdots & \vdots & \vdots & \vdots & \ldots & \vdots & \vdots & \vdots \\ 0 & 0 & 0 & 0 & \ldots & -1 & 2 & -1 \\ -1 & 0 & 0 & 0 & \ldots & 0 & -1 & 2 \end{bmatrix} \tag{9.34}$$

Notice that $[P]$ contains an element -1 in the lower left and upper right corners due to its angular periodicity. Also, notice that $[P]$ is a quasi-three-band symmetric matrix which is independent of the arbitrariness of the cross section as a result of the discretization over a finite interval $[0, 2\pi]$.

Introducing Eq. (9.32) into Eq. (9.28) leads to the following set of coupled differential equations

$$\rho^2\frac{\partial^2[V]}{\partial\rho^2} + \rho\frac{\partial[V]}{\partial\rho} - \frac{[P]}{h^2}[V] = 0 \tag{9.35}$$

To decouple Eq. (9.35), we must diagonalize $[P]$ by an orthogonal matrix $[T]$ such that

$$\left[\lambda^2\right] = \left[T\right]^t\left[P\right]\left[T\right] \tag{9.36}$$

with

$$[T]^t = [T] = [T]^{-1} \tag{9.37}$$

where $[\lambda^2]$ is a diagonal matrix of the eigenvalues λ_n^2 of $[P]$. The diagonalization is achieved using [19]

$$T_{ij} = \frac{\cos\alpha_{ij} + \sin\alpha_{ij}}{\sqrt{N}}\,, \quad \lambda_n^2 = 2(1 - \cos\alpha_n) \tag{9.38}$$

where

$$\alpha_{ij} = h \cdot i \cdot j\,, \quad \alpha_n = h \cdot n\,, \quad i, j, n = 1, 2, \ldots, N \tag{9.39}$$

If we introduce the transformed potential U that satisfies

$$[U] = [T][V] \tag{9.40}$$

Equation (9.35) becomes

$$\rho^2 \frac{\partial^2[U]}{\partial\rho^2} + \rho\frac{\partial[U]}{\partial\rho} - \Big[\mu^2\Big]\Big[U\Big] = 0 \tag{9.41}$$

where

$$\Big[U\Big] = \Big[U_1, U_2, \ldots, U_N\Big]^t \tag{9.42}$$

is a vector containing the transformed potential function and

$$\mu_n = \frac{\lambda_n}{h} = \frac{2}{h}\sin(\alpha_n/2) \tag{9.43}$$

Equation (9.41) is the Euler-type and has the analytical solution (see Section 2.4.1)

$$U_n = \begin{cases} A_n + B_n \ln\rho\,, & \mu_n = 0 \\ A_n\rho^{\mu_n} + B_n\rho^{-\mu_n}\,, & \mu_n \neq 0 \end{cases} \tag{9.44}$$

This is applied to each subregion. By taking the inverse transform using Eq. (9.40), we obtain the potential $V_i(\rho)$ as

$$V_i(\rho) = \sum_{j=1}^{N} T_{ij}U_j \tag{9.45}$$

where T_{ij} are the elements of matrix $[T]$.

We now impose the boundary conditions in Eq. (9.29), which can be rewritten as

$$V(\rho = r_i) = 0\,, \quad r_i \in \Gamma_1 \tag{9.46a}$$

$$V(\rho = R_i) = V_o\,, \quad R_i \in \Gamma_2 \tag{9.46b}$$

Applying these to Eqs. (9.44) and (9.45),

$$T_{ij}\left[A_j + B_j \ln r_i\right]\Big|_{\mu_j=0} + \sum_{j=1}^{N} T_{ij}\left[A_j r_i^{\mu_j} + B_j r_i^{-\mu_j}\right]\Big|_{\mu_j\neq 0} = 0\,,$$
$$i = 1, 2, \ldots, N \tag{9.47a}$$

$$T_{ij}\left[A_j + B_j \ln R_i\right]\Big|_{\mu_j=0} + \sum_{j=1}^{N} T_{ij}\left[A_j R_i^{\mu_j} + B_j R_i^{-\mu_j}\right]\Big|_{\mu_j\neq 0} = V_o\,,$$
$$i = 1, 2, \ldots, N \tag{9.47b}$$

Equation (9.47) is solved to determine the unknown coefficients A_i and B_i. The potential distribution is finally obtained from Eqs. (9.44) and (9.45).

Example 9.3

Consider a coaxial cable with inner radius a and outer radius b. Let $b = 2a = 2$ cm and $V_o = 100$ V. This simple example is selected to be able to compare MOL solution with the exact solution □

Solution

From Eq. (9.43), it is evident that $\mu_n = 0$ only when $n = N$. Hence, we may write U as

$$U_n = \begin{cases} A_n \rho^{\mu_n} + B_n \rho^{-\mu_n}\,, & n = 1, 2, \ldots, N-1 \\ A_n + B_n \ln \rho\,, & n = N \end{cases} \tag{9.48}$$

Equation (9.47) can be written as

$$\sum_{j=1}^{N-1} T_{ij}\left[A_j a_i^{\mu_j} + B_j a_i^{-\mu_j}\right] + T_{iN}\left[A_N + B_N \ln a\right] = 0\,,$$
$$i = 1, 2, \ldots, N \tag{9.49a}$$

for $\rho = a$, and

$$\sum_{j=1}^{N-1} T_{ij}\left[A_j b_i^{\mu_j} + B_j b_i^{-\mu_j}\right] + T_{iN}\left[A_N + B_N \ln b\right] = V_o\,,$$
$$i = 1, 2, \ldots, N \tag{9.49b}$$

for $\rho = b$. These $2N$ equations will enable us to find the $2N$ unknown coefficients

A_i and B_i. They can be cast into a matrix form as

$$\begin{bmatrix} T_{11}A_1a^{\mu_1} & \dots & T_{1N}A_N & T_{11}B_1a^{-\mu_1} & \dots & B_N \ln a \\ \vdots & & & & & \vdots \\ T_{N1}A_1a^{\mu_1} & \dots & T_{NN}A_N & T_{N1}B_1a^{-\mu_1} & \dots & B_N \ln a \\ T_{11}A_1b^{\mu_1} & \dots & T_{1N}A_N & T_{11}B_1b^{-\mu_1} & \dots & B_N \ln b \\ \vdots & & & & & \vdots \\ T_{N1}A_1b^{\mu_1} & \dots & T_{NN}A_N & T_{N1}B_1b^{-\mu_1} & \dots & B_N \ln b \end{bmatrix} \begin{bmatrix} A_1 \\ A_2 \\ \vdots \\ A_N \\ B_1 \\ B_2 \\ \vdots \\ B_N \end{bmatrix} = \begin{bmatrix} 0 \\ 0 \\ \vdots \\ 0 \\ 100 \\ 100 \\ \vdots \\ 100 \end{bmatrix} \tag{9.50}$$

This can be written as

$$[D][C] = [F] \tag{9.51}$$

from which we obtain

$$[C] = [D]^{-1}[F] \tag{9.52}$$

where C_j corresponds to A_j when $j = 1, 2, \dots, N$ and C_j corresponds to B_j when $j = N + 1, \dots, 2N$.

Once A_j and B_j are known, we substitute them into Eq. (9.48) to find U_j. We finally apply Eq. (9.45) to find V. The exact analytical solution of the problem is

$$V(\rho) = V_o \frac{\ln \frac{\rho}{a}}{\ln \frac{b}{a}} \tag{9.53}$$

For $a < \rho < b$, we obtain V for both exact and MOL solutions using the Matlab codes in Fig. 9.4. The results of the two solutions are shown in Fig. 9.5. The two solutions agree perfectly. ∎

9.3 Solution of Wave Equation

The method of lines is particularly suitable for modeling a wide range of transmission lines and planar waveguide structures with multiple layers [8, 11, 19]–[29]. This involves discretizing the Helmholtz wave equation in one direction while the other direction is treated analytically. Here we consider the general problem of two-layer structures covered on the top and bottom with perfectly conducting planes. The conducting strips are assumed to be thin. We will illustrate with two-layer planar and cylindrical microstrip structures.

```
EXAMPLE 9.3 SOLVED USING METHOD OF LINES

% OUR OBJECTIVE IS TO DETERMINE THE POTENTIAL
% DISTRIBUTION IN A COAXIAL CABLE OF INNER RADIUS a
% AND OUTER RADIUS b ASSUMING A POTENTIAL DIFFERENCE OF Vo

a= 0.01; b = 0.02; Vo = 100;
N = 15;
h = 2*pi/N;
K = 1/sqrt (N);
% COMPUTE THE TRANSFORMATION MATRIX T AND MIU
T = zeros(N,N);
miu = zeros(N,1);
for  I=1:N
 miu(I) = 2*sin (I*h*0.5 )/h;
  for J=1:N
     alpha = I*J*h;
     T(I,J) = K*( cos(alpha) + sin(alpha) );
  end
end
% CALCULATE THE MATRIX D IN EQ. (9.50)
D = zeros(2*N,2*N);
for i=1:2*N
   for j=1:2*N
%Do the upper part of the matrix
       if (i <= N & j < N)
          D(i,j) = T(i,j)*a^miu(j);
       end
       if (i <= N & j == N)
           D(i,j) = T(i,j);
       end
       if (i <= N & j > N & j < 2*N)
          D(i,j) = T(i,j-N)*a^(-miu(j-N));
       end
       if (i <= N & j == 2*N)
         D(i,j) = T(i,j-N)*log(a);
       end
%Now do the lower part of the matrix
       if (i > N & i <= 2*N & j < N)
          D(i,j) = T(i-N,j)*b^miu(j);
       end
       if (i > N & i <= 2*N & j == N)
            D(i,j) = T(i-N,j);
       end
       if (i > N & i <= 2*N & j > N & j < 2*N)
           D(i,j) = T(i-N,j-N)*b^(-miu(j-N));
       end
       if (i > N & i <= 2*N & j == 2*N)
          D(i,j) = T(i-N,j-N)*log(b);
       end
   end
end
```

Figure 9.4
Matlab code for Example 9.3 ***(Continued.)***

```
% DETERMINE THE BOUNDARY POTENTIAL MATRIX
% AND THE COEFFICIENT MATRIX
F = zeros(2*N,1);
for i=1:2*N
   if i > N
      F(i) = Vo;
   end
end
C = inv(D)*F;
% WITH THE COEFFICIENTS DETERMINED,
% NOW FIND TRANSFORMED POTENTIAL U
% AND FINALLY DETERMINE THE POTENTIAL V USING EQ. (9.45)
% WE MAY SELECT ANY VALUE OF phi, say, phi = 0^o, i.e. i=1
rho = 0.01:0.001:0.02;
M = 10; % no. of divisions along rho
Vmol = zeros(M+1,1);
for k=1:M+1
   Vmol(k) = 0.0;
   for j=1:N
    if (j <N)
   U(j) = C(j)*(rho(k))^miu(j) + C(j+N)*(rho(k))^(-miu(j));
    end
   if (j == N)
      U(j) = C(j) + C(j+N)*log(rho(k));
   end
      Vmol(k) = Vmol(k) + T(10,j)*U(j);
%        Vmol(k) = Vmol(k) + T(1,j)*U(j);
   end
end
% ALSO, CALCULATE THE EXACT VALUE OF V
Vex = Vo* (log(rho/a))/log(b/a);
diary
Vmol, Vex'
diary off
hold off
plot (rho,Vmol);
title( 'Fig. 9.5  Comparison of exact and method of lines solutions.')
xlabel('rho'), ylabel('V')
hold on
plot (rho,Vex);
hold off
```

Figure 9.4
***(Cont.)* Matlab code for Example 9.3.**

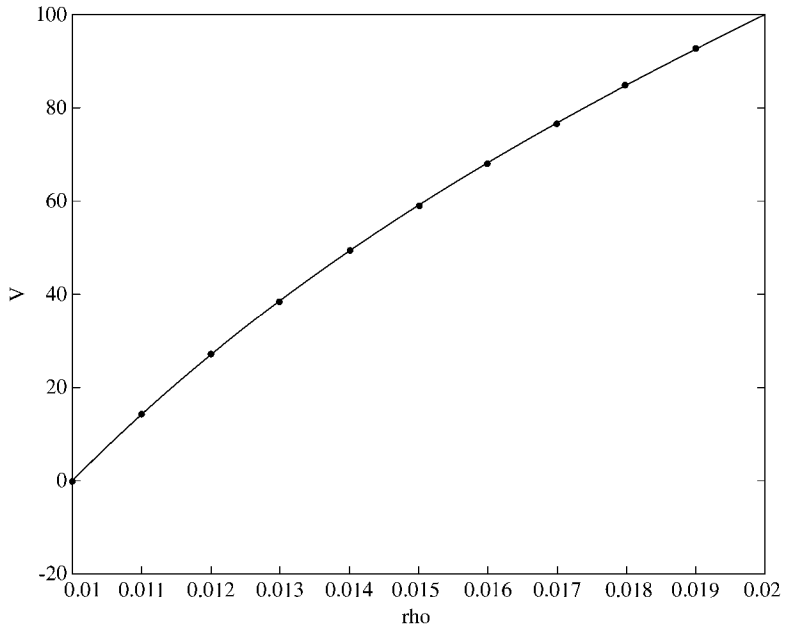

Figure 9.5
Comparison of exact and method of lines solutions.

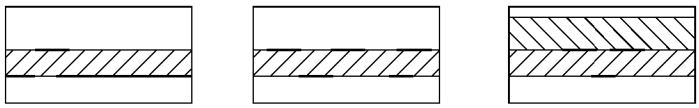

Figure 9.6
Typical planar structures.

9.3.1 Planar Microstrip Structures

Typical planar structures are shown in Fig. 9.6. The two independent field components E_z and H_z in each separate layer must satisfy the Helmholtz equation. Assuming the time factor $e^{j(\omega t-\beta z)}$ and that wave propagates along z,

$$\frac{\partial^2\psi}{\partial x}+\frac{\partial^2\psi}{\partial y}+\left(k^2-\beta^2\right)\psi=0 \tag{9.54}$$

where ψ represents either E_z or H_z and

$$k^2=\epsilon_r k_o^2\,,\quad k_o=\omega\sqrt{\mu_o\epsilon_o}=2\pi/\lambda_o \tag{9.55}$$

Applying the method of lines, we discretize the fields along the x direction by laying a family of straight lines parallel to the y axis and evaluating on the e-lines for E_z and h-lines for H_z, as shown in Fig. 9.7. The lines are evenly spaced although this is not

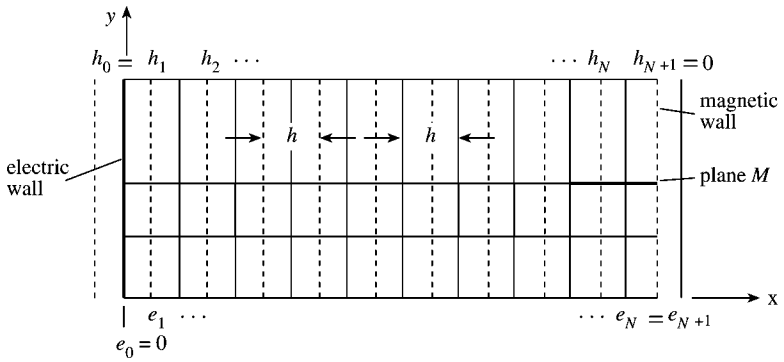

Figure 9.7
Cross section of planar microstrip structure with discretization lines; —— lines for E_z and - - - - for H_z.

necessary. If h is the spacing between adjacent lines, it is expedient to shift the e-lines and the h-lines by $h/2$ in order to guarantee a simple fitting of the literal boundary conditions. The potential in Eq. (9.54) can now be replaced by a set $[\psi_1, \psi_2, \ldots, \psi_N]$ at lines

$$x_i = x_0 + ih\,, \quad i = 1, 2, \ldots, N \tag{9.56}$$

and $\partial\psi_i/\partial x$ can be replaced by their finite difference equivalents. Thus, Eq. (9.54) becomes

$$\frac{\partial^2\psi_i}{\partial y^2} + \frac{1}{h^2}\left[\psi_{i+1}(y) - 2\psi_i(y) + \psi_{i-1}(y)\right] + k_c^2\psi_i(y) = 0\,. \qquad i = 1, 2, \ldots, N \tag{9.57}$$

where

$$k_c^2 = k^2 - \beta^2 \tag{9.58}$$

This is a system of N coupled ordinary differential equations. We cannot solve them in their present form because the equations are coupled due to the tridiagonal nature of $[P]$. We can decouple the equations by several suitable mathematical transformations and then analytically solve along the y direction.

If we let

$$[\psi] = [\psi_1, \psi_2, \ldots, \psi_N]^t \tag{9.59}$$

where t denotes the transpose and

$$[P] = \begin{bmatrix} p_\ell & -1 & & & \\ -1 & 2 & -1 & & \\ & \ddots & \ddots & \ddots & \\ & & -1 & 2 & -1 \\ & & & -1 & p_r \end{bmatrix} \tag{9.60}$$

which is the same as Eq. (9.7) where p_ℓ and p_r are defined. Introducing the column vector $[\psi]$ and the matrix $[P]$ into Eq. (9.57) leads to

$$h^2 \frac{\partial^2 [\psi]}{\partial y^2} - \left([P] - h^2 k_c^2 [I] \right) [\psi] = [0] \tag{9.61}$$

where $[I]$ is the identity matrix and $[0]$ is a zero column vector. Since $[P]$ is a real symmetric matrix, we can find an orthogonal matrix $[T]$ such that

$$[T]^t [P][T] = [\lambda^2] \tag{9.62}$$

where the elements λ_i^2 of the diagonal matrix $[\lambda^2]$ are the eigenvalues of $[P]$. With the orthogonal matrix $[T]$, we now introduce a transformed vector $[U]$ such that

$$[T]^t [\psi] = [U] \tag{9.63}$$

We can rewrite Eq. (9.61) in terms of $[U]$ and obtain

$$h^2 \frac{\partial^2 U_i}{\partial y^2} - \left(\lambda_i^2 - h^2 k_c^2 \right) U_i = 0 \,, \quad i = 1, 2, \ldots, N \tag{9.64}$$

Since Eq. (9.64) is uncoupled, it can be solved analytically for each homogeneous region. The solution is similar in form to the telegraph equation. It may be expressed as a relation between U_i and its normal derivative in a homogeneous dielectric layer from $y = y_1$ to $y = y_2$, i.e.,

$$\begin{bmatrix} U_i(y_1) \\ h \frac{\partial U_i(y_1)}{dy} \end{bmatrix} = \begin{bmatrix} \cosh \alpha_i (y_1 - y_2) & \frac{1}{k_i} \sinh \alpha_i (y_1 - y_2) \\ k_i \sinh \alpha_i (y_1 - y_2) & \cosh \alpha_i (y_1 - y_2) \end{bmatrix} \begin{bmatrix} U_i(y_2) \\ h \frac{\partial U_i(y_2)}{dy} \end{bmatrix} \tag{9.65}$$

where

$$\begin{aligned} k_i &= \left(\lambda_i^2 - h^2 k_c^2 \right)^{1/2} \\ \alpha_i &= \frac{k_i}{h} \,, \quad i = 1, 2, \ldots, N \end{aligned} \tag{9.66}$$

Equation (9.65) can be applied repeatedly to find the transformed potential $[U]$ from one homogeneous layer $y_1 < y < y_2$ to another. Keep in mind that each iteration will require that we recalculate the transformation matrix $[T]$ and its eigenvalues λ_i,

which are given in Table 9.1. The field components E_z and H_z are derivable from the scalar potentials $\psi^{(e)}$ and $\psi^{(h)}$ as

$$E_z = \frac{k_c}{j\omega\epsilon}\psi^{(e)} \tag{9.67a}$$

$$H_z = \frac{k_c}{j\omega\mu}\psi^{(h)} \tag{9.67b}$$

To be concrete, consider the shielded microstrip line shown in Fig. 9.8. Because of

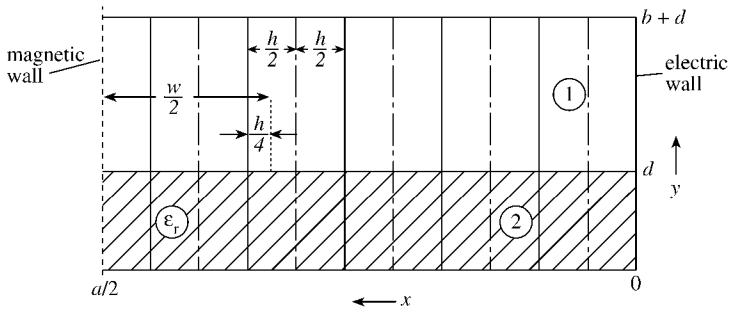

Figure 9.8
Half cross section of a shielded microstrip line.

the symmetry, only half of the solution region needs to be considered. At the interface $y = d$, the continuity conditions with Eq. (9.67) require that

$$\frac{\beta}{\omega\epsilon_o}\frac{\partial}{\partial x}\left(\psi_I^{(e)} - \frac{1}{\epsilon_r}\psi_{II}^{(e)}\right) = \frac{\partial\psi_{II}^{(h)}}{\partial y} - \frac{\partial\psi_I^{(h)}}{\partial y} \tag{9.68}$$

$$\left(k_o^2 - \beta^2\right)\psi_I^{(e)} = \frac{1}{\epsilon_r}\left(\epsilon_r k_o^2 - \beta^2\right)\psi_{II}^{(e)} \tag{9.69}$$

$$\frac{\partial\psi_I^{(h)}}{\partial y} - \frac{\partial\psi_{II}^{(h)}}{\partial y} = \frac{\beta}{\omega\mu}\frac{\partial}{\partial x}\left(\psi_I^{(h)} - \psi_{II}^{(h)}\right) - J_z \tag{9.70}$$

$$\left(k_o^2 - \beta^2\right)\psi_I^{(h)} = \left(\epsilon_r k_o^2 - \beta^2\right)\psi_{II}^{(h)} - j\omega\mu J_x \tag{9.71}$$

where the superscripts I and II refer to dielectric regions 1 and 2 and J_x and J_z are the current densities at the interface $y = d$.

We replace the partial derivative operator $\partial/\partial x$ with the difference operator $[D]$, where

$$[D] = \begin{bmatrix} 1 & -1 & 0 & \dots & 0 \\ 0 & 1 & -1 & \dots & 0 \\ \vdots & \ddots & \ddots & \ddots & \vdots \\ 0 & 0 & \dots & 1 & -1 \end{bmatrix} \tag{9.72}$$

so that

$$\begin{aligned}\frac{\partial \psi^{(e)}}{\partial x} &\rightarrow \frac{1}{h}[D][\psi^{(e)}] \\ \frac{\partial \psi^{(h)}}{\partial x} &\rightarrow -\frac{1}{h}[D]^t[\psi^{(h)}]\end{aligned} \tag{9.73}$$

We replace the normal derivatives of $\partial\psi/\partial n$ at the interface $y = d$ with following matrix operators.

$$\begin{aligned}\frac{\partial \psi_k^{(e)}}{\partial n} &\rightarrow \frac{1}{h}\left[G_k^{(e)}\right]\left[\psi_k^{(e)}\right], \qquad k = I, II \\ \frac{\partial \psi_k^{(h)}}{\partial n} &\rightarrow \frac{1}{h}\left[G_k^{(h)}\right]\left[\psi_k^{(h)}\right], \qquad k = I, II\end{aligned} \tag{9.74}$$

We can transform this into the diagonal form

$$\begin{aligned}h\frac{\partial\left[U_k^{(e)}\right]}{\partial n} &= \left[\gamma_k^{(e)}\right]\left[U_k^{(e)}\right], \qquad k = I, II \\ h\frac{\partial\left[U_k^{(h)}\right]}{\partial n} &= \left[\gamma_k^{(h)}\right]\left[U_k^{(h)}\right], \qquad k = I, II\end{aligned} \tag{9.75}$$

With the aid of Eq. (9.65) and the boundary conditions at $y = 0$ and $y = b + d$, the diagonal matrices $[\gamma_k]$ are determined analytically as

$$\begin{aligned}\left[\gamma_I^{(e)}\right] &= \text{diag}\left[\chi_i \coth\left(\chi_i b/h\right)\right] \\ \left[\gamma_I^{(h)}\right] &= \text{diag}\left[\chi_i \tanh\left(\chi_i b/h\right)\right] \\ \left[\gamma_{II}^{(e)}\right] &= \text{diag}\left[\eta_i \coth\left(\eta_i d/h\right)\right] \\ \left[\gamma_{II}^{(h)}\right] &= \text{diag}\left[\eta_i \tanh\left(\eta_i d/h\right)\right]\end{aligned} \tag{9.76}$$

where

$$\chi_i = \left[4\sin^2\left(\frac{i-0.5}{2N+1}\pi\right) - h^2\left(k_o^2 - \beta^2\right)\right]^{1/2} \tag{9.77}$$

and

$$\eta_i = \left[4\sin^2\left(\frac{i-0.5}{2N+1}\pi\right) - h^2\left(\epsilon_r k_o^2 - \beta^2\right)\right]^{1/2} \tag{9.78}$$

We can discretize Eqs. (9.68) to (9.71) and eliminate $\psi_{II}^{(e)}$ and $\psi_{II}^{(h)}$ using $[T^{(e)}]$ and $[T^{(h)}]$ matrices. Equations (9.68) and (9.70) become

$$\frac{\beta}{\omega\epsilon_o}(1-\tau)\left[\delta\right]\left[U_I^{(e)}\right] = \left(\left[\gamma_I^{(h)}\right] + \tau\left[\gamma_{II}^{(h)}\right]\right)\left[U_I^{(h)}\right] \tag{9.79}$$

$$\left(\left[\gamma_I^{(e)}\right] + \epsilon_r\tau\left[\gamma_{II}^{(e)}\right]\right)\left[U_I^{(e)}\right] = \frac{\beta}{\omega\mu}(1-\tau)\left[\delta\right]^t\left[U_I^{(h)}\right] - \left[T^{(e)}\right]^t\left[J_z\right] \tag{9.80}$$

where

$$\tau = \frac{1 - \epsilon_{\text{eff}}}{\epsilon_r - \epsilon_{\text{eff}}} \tag{9.81}$$

$$\epsilon_{\text{eff}} = \frac{\beta^2}{k_o^2} \tag{9.82}$$

$$\left[\delta\right] = \left[T^{(h)}\right]^t \left[D\right] \left[T^{(e)}\right] \tag{9.83}$$

and $[T^{(e)}] = [T_{ND}]$ and $[T^{(h)}] = [T_{DN}]$ as given in Table 9.1. Notice that $[\delta]$ is a diagonal matrix and is analytically determined as

$$\delta_i = \text{diag}\left[2\sin\left(\frac{i - 0.5}{2N + 1}\pi\right)\right] \tag{9.84}$$

Since J_x is negligibly small compared with J_z, we solve Eqs. (9.79) and (9.80) to obtain

$$\left[U_I^{(e)}\right] = \left[\rho\right] \left[T^{(e)}\right]^t \left[J_z\right] \tag{9.85}$$

where

$$\left[\rho\right] = \left[\left[\gamma_I^{(e)}\right] + \epsilon_r \tau \left[\gamma_{II}^{(e)}\right] - \epsilon_{\text{eff}}(1 - \tau)^2 \left[\delta\right]^t \left(\left[\gamma_I^{(h)}\right] + \tau \left[\gamma_{II}^{(h)}\right]\right)^{-1} \left[\delta\right]\right]^{-1} \tag{9.86}$$

which is a diagonal matrix. Using Eq. (9.63), we now take the inverse transform of Eq. (9.85) to obtain

$$\left[\psi_I^{(e)}\right] = \left[T^{(e)}\right] \left[\rho\right] \left[T^{(e)}\right]^t \left[J_z\right] \tag{9.87}$$

We finally impose the boundary condition on the strip, namely

$$\left[\psi_I^{(e)}\right] = \left[0\right] \qquad \text{on the strip} \tag{9.88}$$

which leads to a reduced matrix equation

$$\left[J_z\right] = \begin{cases} \left[J_z\right]_{\text{red}} & \text{on the strip} \\ 0 & \text{elsewhere} \end{cases} \tag{9.89}$$

and the corresponding characteristic equation

$$\left(\left[T^{(e)}\right] \left[\rho\right] \left[T^{(e)}\right]^t\right)_{\text{red}} \left[J_z\right]_{\text{red}} = \left[0\right] \tag{9.90}$$

It is known from mathematics that a homogeneous linear matrix equation shows nontrivial solutions only when the determinant of the matrix is equal to zero. Thus the propagation constant is determined by solving the determinant equation

$$\boxed{\det\left(\left[T^{(e)}\right]\left[\rho(\beta,\omega)\right]\left[T^{(e)}f\right]^{t}\right)_{\text{red}} = \left[0\right]} \tag{9.91}$$

The effective dielectric constant ϵ_{eff} is obtained from Eq. (9.82). Notice that only the number of points on the strip determines the size of the matrix and that Eq. (9.91) applies to a microstrip with more than one strip. We solve Eq. (9.91) using a root-finding algorithm [28] in Fortran, Maple, or Matlab. Although a microstrip example is considered here, the formulation is generally valid for any two-layer structures.

Once we solve Eq. (9.91) to determine the effective dielectric constant, the current distribution on the strip, the potential functions ψ_e and ψ_h, the electric field E_z, and magnetic field H_z can be computed. Finally, the characteristic impedance is obtained from

$$Z_o = \frac{2P}{I^2} \tag{9.92}$$

where P is the average power transport along the line

$$P = \frac{1}{2}\int (\mathbf{E} \times \mathbf{H}^*) \cdot dx\, dy\, \mathbf{a}_z \tag{9.93}$$

and I is the total current flowing on the strip

$$I = \int J_z\, dx\, dy \tag{9.94}$$

Since the above analysis applies to multiple strips, the characteristic impedance to the mth strip is

$$Z_{om} = \frac{2P_m}{I_m^2} \tag{9.95}$$

Example 9.4

Consider the shielded microstrip line shown in Fig. 9.8. Using the method of lines, find the effective dielectric constant of the line when $\epsilon_r = 9$, $w/d = 2$, $a/d = 7$, $b/d = 3$ and $d = 1$ mm. □

Solution

The number of lines along the x-axis is selected as $N = 18$ and the number of lines crossing the strip is $M = 6$. These numbers are for only one potential, say $[\psi_e]$. Since only one half of the structure is considered due to symmetry, only three points on the strip are necessary. Hence, the size of the matrix associated with Eq. (9.91) is 3×3.

Figure 9.9 shows the three Matlab codes for solving Eq. (9.91). The main program varies the values of d from 0.01 to 0.15, assuming that $\lambda_o = 1$, the wavelength in free space, since β or ϵ_{eff} are frequency-dependent. (Alternatively, we could keep d fixed and vary frequency, from say 1 to 50 GHz.) The program plots ϵ_{eff} with d/λ_o as shown in Fig. 9.10.

(a)

```
% EXAMPLE 9.4 SOLVED USING METHOD OF LINES
% THIS M-FILES REQUIRES TWO OTHER M-FILES
% "FUN.M" AND "ROOT.M" TO WORK
% FUN.M DETERMINES THE DETERMINANT OF MATRIX [F]
% ROOT.M FINDS THE ROOT(S) OF THE det(F)
global d

Nmax = 50; tol = 1E-5;
eeff1 = 5; eeff2 = 10;% initial/guessed values
for i=1:15
   d = 0.01*i;
   x(i) = d;
   [eeff] = root('fun', eeff1, eeff2, tol, Nmax)
   y(i) = eeff;
%diary a:test.out
end
diary
  plot(x,y)
diary off
```

Figure 9.9
For Example 9.4: (a) Main Matlab code, *(Continued).*

The M-file fun.m does the actual computation of the matrices involved using Eq. (9.76) to (9.91). It eventually finds the determinant of matrix $[F]$, where

$$[F] = \left([T_e][\rho(\beta, \omega)][T_e]^t\right)_{\text{red}} \tag{9.96}$$

The third M-file root.m is a root-finding algorithm based on the secant method [28] and is used to determine the value of ϵ_{eff} that will satisfy

$$\det[F] = 0 \tag{9.97}$$

9.3.2 Cylindrical Microstrip Structures

The method of lines can be used to analyze homogeneous and inhomogeneous cylindrical transmission structures [19, 29]–[36] and circular and elliptic waveguides [37]. The principal steps involved in applying MOL in cylindrical coordinates are the same as in Cartesian coordinates. Here, we illustrate with the use of MOL to analyze the dispersion characteristics of the cylindrical microstrip transmission line using full-wave analysis.

We introduce the scalar potentials $\Phi^{(e)}$ and $\Phi^{(h)}$ to represent the electric and magnetic field components. In cylindrical coordinates (ρ, ϕ), the two scalar functions

(b)

```
function determinant = fun(eeff)
%  THIS FUNCTION IS NEEDED FOR EXAMPLE 9.4
%  IT DETERMINES THE DETERMINANT OF MATRIX  [F]
%  FOR A GIVEN EFFECTIVE DIELECTRIC CONSTANT EEFF
global d

N = 9;
%d = 0.001;
a = 7*d;  b = 3*d; w = 2*d;
er = 9; h = a/N; M = w/h;
lambdao = 1; %assumed
ko = 2*pi/lambdao;
% First calculate the transformation matrices
% Te (= T_ND) and Th (=T_DN)
cons=sqrt(2/(N+0.5));
for i=1:N
    for j=1:N
        alj = (j - 0.5)*pi/(N + 0.5);
        if (j==1)
            te(i,j) = 1/sqrt(N);
        else
            te(i,j) = cons*cos( (i-0.5)*alj);
        end
    end
end
% Calculate matrices: chi, eta, delta, and gamma
beta = ko*sqrt(eeff);
tau = (1 - eeff)/(er - eeff);
chi = zeros(N,1);
eta = zeros(N,1);
%gammae1 = zeros(N,N)
for i=1:N
x = ((i -0.5)*pi)/(2*N + 1)
chi(i) = sqrt( 4*sin(x)*sin(x) -h^2*(ko^2 - beta^2) );
eta(i) = sqrt( 4*sin(x)*sin(x) -h^2*(er*ko^2 - beta^2) );
 end
 for i=1:N
    for j=1:N
        if(i==j)
            del(i,i) = 2*sin (((i - 0.5)*pi)/(2*N + 1));
            gammae1(i,i) = chi(i)*coth(b*chi(i)/h);
            gammah1(i,i) = chi(i)*tanh(b*chi(i)/h);
            gammae2(i,i) = eta(i)*coth(d*eta(i)/h);
            gammah2(i,i) = eta(i)*tanh(d*eta(i)/h);
        else
            del(i,j) = 0;
            gammae1(i,j) = 0; gammae2(i,j) = 0;
            gammah1(i,j) = 0; gammah2(i,j) = 0;
        end
    end
end
```

Figure 9.9

For Example 9.4: (b) fun M-file for calculating F and its determinant, *(Continued).*

```
% calculate rho matrix
rho = inv(gammae1 + er*tau*gammae2 - eeff*(1 - tau)^2*del'*(inv(gammah1 +
tau*gammah2))*del);
F = [te(1:3,1:3)*rho(1:3,1:3)*te(1:3,1:3)'];
determinant = det(F);
% Next, solve for the root det(X) = 0 using 'root.m'
```

Figure 9.9
For Example 9.4: *(Cont.)* (b) fun M-file for calculating F and its determinant, *(Continued).*

(c)

```
function [x2] = root(F, x0, x1, tol, Nmax)
% THIS FUNCTION FINDS THE ROOTS OF fun(x) USING
% THE SECANT METHOD
% fun(x) - EXTERNAL FUNCTION THAT COMPUTES THE VALUES OF f(x)
% x0, x1 - LIMITS OF THE INITIAL RANGE
% x2     - ROOT RETURNED TO THE CALLING ROUTINE
% tol    - TOLERANCE VALUE USED IN DETERMINING CONVERGENCE
% Nmax   - MAXIMUM NO. OF ITERATIONS
%
% AUTHORS: M. V. ZEIGLER AND E. CHAMPION [37a]

%F0 = eval( [F, '(x0)']);
F0 = fun(x0);
dx = x1 - x0;
for I=1:Nmax
    F1 = fun(x1);
   %F1 = eval( [F, '(x1)']);
   dx = F1*dx/(F1 - F0);
   x2 = x1 - dx;
% CHECK IF TOLERANCE HAS BEEN MET
   if (abs(dx) <= tol)
   fprintf('root at x = %5.g\n', x2);
   fprintf('root found after this no. of iterations %5.g\n',I);
   break
   end
   dx = x2 - x1;
   x0 = x1;
   x1 = x2;
   F0 = F1;
end
```

Figure 9.9
For Example 9.4: *(Cont.)* (c) root M-file for finding the roots of fun $(x) = 0$.

can be expressed as

$$\Psi^{(e,h)} = \Phi^{(e,h)}(\rho, \phi)e^{-j\beta z} \tag{9.98}$$

where β is the phase constant and the time harmonic dependence has been suppressed. Substituting Eq. (9.98) into the Helmholtz equation for the scalar potential functions

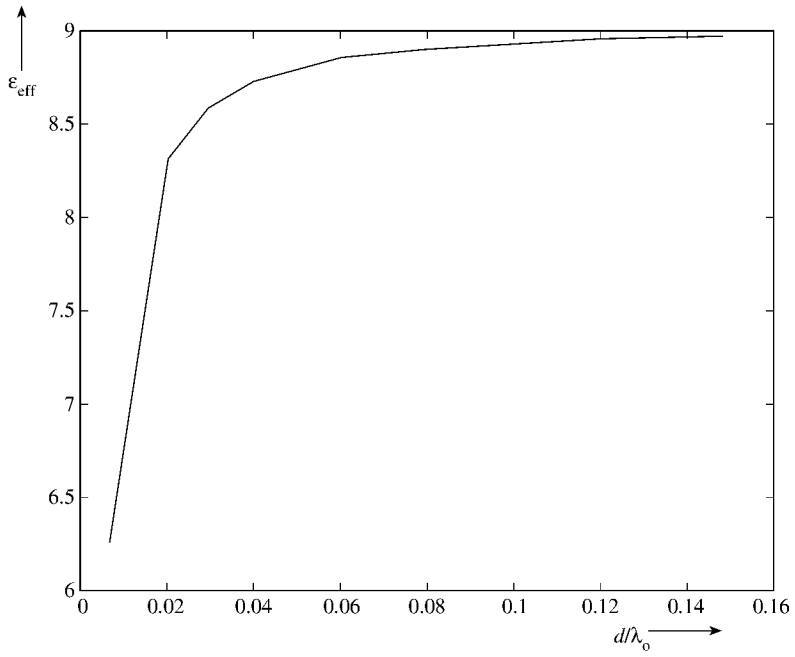

Figure 9.10
For Example 9.4: Effective dielectric constant of the microstrip line.

yields

$$\rho^2 \frac{\partial^2 \Phi}{\partial \rho^2} + \rho \frac{\partial \Phi}{\partial \rho} + \frac{\partial^2 \Phi}{\partial \phi^2} + \rho^2 \left(k^2 - \beta^2\right) \Phi = 0 \tag{9.99}$$

where $k^2 = \omega^2 \mu \epsilon$. Discretizing in the ϕ-direction by using N radial lines, as shown in Fig. 9.11, such that

$$\phi_i = \phi_o + (i-1)h = \frac{2\pi i}{N}, \qquad i = 1, 2, \ldots, N \tag{9.100}$$

where $h = \Delta\phi = 2\pi/N$ is the angular spacing between the lines. The discretization lines for the electric potential function $\Phi^{(e)}$ are shifted from the magnetic potential function $\Phi^{(h)}$ by $h/2$. Applying the central finite difference scheme yields

$$\frac{\partial^2 [\Phi]}{\partial \phi^2} = \frac{[P]}{h^2} [\Phi] \tag{9.101}$$

where

$$[\Phi] = [\Phi_1, \Phi_2, \ldots, \Phi_N]^t \tag{9.102}$$

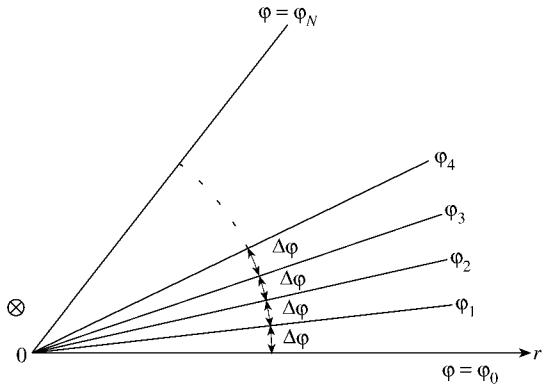

Figure 9.11
Discretization in the ϕ-direction.

and $[P]$ is given in Eq. (9.34). Introducing Eq. (9.101) into Eq. (9.99) leads to N coupled differential equations:

$$\rho^2 \frac{\partial^2[\Phi]}{\partial \rho^2} + \rho \frac{\partial[\Phi]}{\partial \rho} + \rho^2 k_c^2 [\Phi] - \frac{[P]}{h^2}[\Phi] = 0 \tag{9.103}$$

where $k_c^2 = k^2 - \beta^2$ and $[P]$ is the same as in Eq. (9.34) if ϕ goes from 0 to 2π otherwise $[P]$ is as in Eq. (9.7). Here we will assume $[P]$ in Eq. (9.7). To decouple Eq. (9.103), we must diagonalize $[P]$ by an orthogonal matrix $[T]$ given in Eq. (9.38) and introduce the transformed potential U that satisfies

$$[U] = [T][\Phi] \tag{9.104}$$

Thus Eq. (9.103) becomes

$$\rho^2 \frac{\partial^2[U]}{\partial \rho^2} + \rho \frac{\partial[U]}{\partial \rho} + \left[k_c^2 \rho^2 - \mu_i^2\right][U] = 0 \tag{9.105}$$

where

$$[U] = [U_1, U_2, \ldots, U_N]^t \tag{9.106}$$

is a vector containing the transformed potential function and

$$\mu_i = \frac{\lambda_i}{h} \tag{9.107}$$

We notice that Eq. (9.105) is essentially a Bessel equation and can be solved for every homogeneous region to produce Bessel function of order μ_n. The solution is

$$U_i(\rho) = A_i J_{\mu i}(k_c \rho) + B_i Y_{\mu i}(k_c \rho)\,, \quad i = 1, 2, \ldots, N \tag{9.108}$$

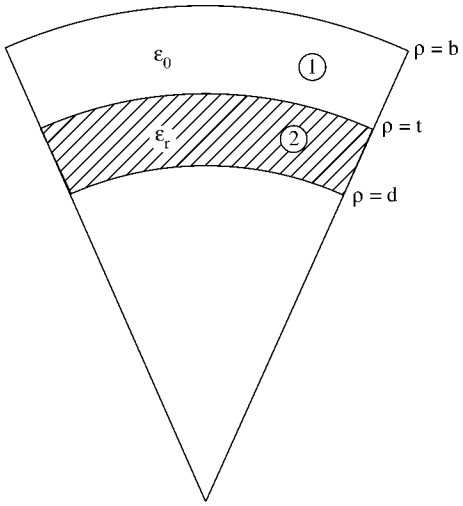

Figure 9.12
The cross section of a shielded cylindrical microstrip line.

where J and Y are Bessel functions of the first and second kind, respectively.

To be concrete, consider the cross section of a shield cylindrical microstrip line shown in Fig. 9.12. Due to the symmetry of the structure, we need only consider half the cross section as in Fig. 9.13. We have regions I and II and we apply Eq. (9.108) to each region. On the boundaries $\rho = d$ and $\rho = b$ (electric walls), we have the boundaries conditions

$$\begin{aligned} U_{Ii}^{(e)}(\rho = d) &= 0 \\ U_{IIi}^{(e)}(\rho = b) &= 0 \end{aligned} \tag{9.109}$$

Enforcing Eq. (9.109) on Eq. (9.108), we obtain

$$\begin{aligned} 0 &= A_i J_{\mu_i}(k_c d) + B_i Y_{\mu_i}(k_c d) \ , \\ 0 &= C_i J_{\mu_i}\left(k_c' b\right) + D_i Y_{\mu_i}\left(k_c' b\right) \end{aligned} \tag{9.110}$$

where $k_c = \sqrt{k_o^2 - \beta^2}$ and $k_c' = \sqrt{\epsilon_r k_o^2 - \beta^2}$, $k_o = 2\pi/\lambda_o$, and λ_o is the wavelength in free space. From Eq. (9.110),

$$\begin{aligned} \frac{B_i}{A_i} &= -\frac{J_{\mu_i}(k_c d)}{Y_{\mu_i}(k_c d)} \\ \frac{D_i}{C_i} &= -\frac{J_{\mu_i}(k_c' b)}{Y_{\mu_i}(k_c' b)} \end{aligned} \tag{9.111}$$

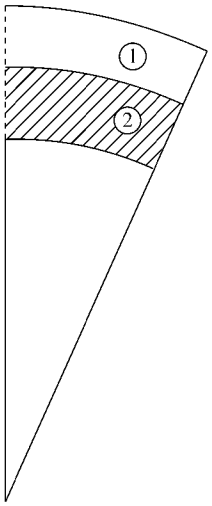

Figure 9.13
Half the cross section of the microstrip in Fig. 9.12 (— electric wall; - - - magnetic wall).

For $\Phi^{(h)}$, the boundary conditions are

$$\left.\frac{\partial U_{Ii}^{(h)}}{\partial \rho}\right|_{\rho=d} = 0$$
$$\left.\frac{\partial U_{IIi}^{(h)}}{\partial \rho}\right|_{\rho=b} = 0 \tag{9.112}$$

Enforcing this on Eq. (9.108) yields

$$0 = E_i J'_{\mu_i}(k_c d) + F_i Y'_{\mu_i}(k_c d) \ ,$$
$$0 = G_i J'_{\mu_i}(k'_c \rho) + H_i Y'_{\mu_i}\left(k'_c b\right) \ , \tag{9.113}$$

which leads to

$$\frac{F_i}{E_i} = -\frac{J'_{\mu_i}(k_c d)}{Y'_{\mu_i}(k_c d)}$$
$$\frac{H_i}{G_i} = -\frac{J'_{\mu_i}(k'_c b)}{Y'_{\mu_i}(k'_c b)} \tag{9.114}$$

At the interface $\rho = t$, both $\Phi^{(e)}$ and $\Phi^{(h)}$ are related by the continuity conditions of

the tangential components of the electric and magnetic fields. Since

$$\Phi^{(e)} = \frac{j\omega\epsilon_o\epsilon_r}{k_o^2\epsilon_r - \beta^2} E_z$$
$$\Phi^{(h)} = \frac{j\omega\mu_r}{k_o^2\epsilon_r - \beta^2} H_z \tag{9.115}$$

the continuity conditions are

$$\frac{1}{t}\frac{\beta}{\omega\epsilon_o}\frac{\partial}{\partial\phi}\left(\Phi_I^{(e)} - \frac{1}{\epsilon_r}\Phi_{II}^{(e)}\right) = \frac{\partial\Phi_{II}^{(h)}}{\partial\rho} - \frac{\partial\psi_I^{(h)}}{\partial\rho} \tag{9.116}$$

$$\left(k_o^2 - \beta^2\right)\psi_I^{(e)} = \frac{1}{\epsilon_r}\left(\epsilon_r k_o^2 - \beta^2\right)\psi_{II}^{(e)} \tag{9.117}$$

$$\frac{\partial\Phi_I^{(h)}}{\partial\rho} - \frac{\partial\Phi_{II}^{(h)}}{\partial\rho} = \frac{\beta}{\omega\mu_o t}\frac{\partial}{\partial\phi}\left(\Phi_I^{(h)} - \Phi_{II}^{(h)}\right) - J_z \tag{9.118}$$

$$\left(k_o^2 - \beta^2\right)\psi_I^{(h)} = \left(\epsilon_r k_o^2 - \beta^2\right)\psi_{II}^{(h)} - j\omega\mu J_\phi \tag{9.119}$$

As we did in Section 9.3.1, we replace the derivative operator $\partial/\partial\phi$ with the difference operator $[D]$ and transform the resulting equations into the diagonal matrices. We obtain the elements of the diagonal matrices as [30]

$$\gamma_{Ii}^{(e)} = S_o h\left[\frac{J'_{\mu_i}(S_o) + (B_i/A_i)Y'_{\mu_i}(S_o)}{J_{\mu_i}(S_o) + (B_i/A_i)Y_{\mu_i}(S_o)}\right] \tag{9.120a}$$

$$\gamma_{IIi}^{(e)} = -S'_o h\left[\frac{J'_{\mu_i}(S'_o) + (D_i/C_i)Y'_{\mu_i}(S'_o)}{J_{\mu_i}(S'_o) + (D_i/C_i)Y_{\mu_i}(S'_o)}\right] \tag{9.120b}$$

$$\gamma_{Ii}^{(h)} = S_o h\left[\frac{J'_{\mu_i}(S_o) + (F_i/E_i)Y'_{\mu_i}(S_o)}{J_{\mu_i}(S_o) + (F_i/E_i)Y_{\mu_i}(S_o)}\right] \tag{9.120c}$$

$$\gamma_{IIi}^{(h)} = -S'_o h\left[\frac{J'_{\mu_i}(S'_o) + (H_i/G_i)Y'_{\mu_i}(S'_o)}{J_{\mu_i}(S'_o) + (H_i/G_i)Y_{\mu_i}(S'_o)}\right] \tag{9.120d}$$

where $h = \Delta\phi$ and

$$S_o = t\sqrt{k_o^2 - \beta^2}\,, \quad S'_o = t\sqrt{k_o^2\epsilon - \beta^2} \tag{9.121}$$

By ignoring J_ϕ and reducing J_z to what we have in Eq. (9.89), we finally obtain the characteristic equation

$$\left(\left[T^{(e)}\right]\left[\rho\right]\left[T^{(e)}\right]^t\right)_{\text{red}}\left[J_z\right]_{\text{red}} = [0] \tag{9.122}$$

where

$$\left[\rho\right] = \left[\left[\gamma_I^{(e)}\right] + \epsilon_r \tau \left[\gamma_{II}^{(e)}\right] - \epsilon_{\text{eff}}(1-\tau)^2 \left[\delta\right]^t \left(\left[\gamma_I^{(h)}\right] + \tau \left[\gamma_{II}^{(h)}\right]\right)^{-1} \left[\delta\right]\right]^{-1} \quad (9.123)$$

$$\tau = \frac{1-\epsilon_{\text{eff}}}{\epsilon_r - \epsilon_{\text{eff}}}, \quad \epsilon_{\text{eff}} = \frac{\beta^2}{k_o^2}, \quad \left[\delta\right] = \left[T^{(h)}\right]^t \left[D\right] \left[T^{(e)}\right] \quad (9.124)$$

With a root-finding algorithm, Eq. (9.122) can be solved to obtain β or ϵ_{eff}. Notice that Eq. (9.122) is of the same form as Eq. (9.90) and only the number of points on the strip determines the size of the matrix. However, the expressions for $[\gamma_I^{(e)}]$, $[\gamma_{II}^{(e)}]$, $[\gamma_I^{(h)}]$ and $[\gamma_{II}^{(h)}]$ are given in Eq. (9.120).

9.4 Time-Domain Solution

The frequency-domain version of the method of lines covered in Section 9.3 can be extended to the time-domain [38]–[43]. In fact, MOL can also be used to solve parabolic equations [1, 44, 45]. However, in this section, we will use MOL to solve hyperbolic Maxwell's equations in the time-domain. Essentially, the MOL proceeds by leaving the derivatives along one selected axis untouched (usually in time), while all other partial derivatives (usually in space) are discretized using well-known techniques such as finite difference and finite element. The partial differential equation is reduced to a system of ordinary differential equations that can be solved numerically using standard methods.

Consider an empty rectangular waveguide which is infinite in the z-direction [38] and with cross-section $0 < x < a$, $0 < y < b$. We assume that the waveguide is excited by a uniform electric field E_z. The problem becomes a two-dimensional one. It corresponds to calculating the cutoff frequencies of various modes in the frequency-domain. Such information can be obtained from the time-domain data.

Due to the excitation, only E_z, H_x, and H_y exist and $\partial/\partial z = 0$. Maxwell's equations become

$$\begin{aligned} -\mu \frac{\partial H_x}{\partial t} &= \frac{\partial E_z}{\partial y} \\ \mu \frac{\partial H_y}{\partial t} &= \frac{\partial E_z}{\partial x} \\ \epsilon \frac{\partial E_z}{\partial t} &= \frac{\partial H_y}{\partial x} - \frac{\partial H_x}{\partial y} \end{aligned} \quad (9.125)$$

which can be manipulated to yield the wave equation

$$\frac{\partial^2 E_z}{\partial^2 x} + \frac{\partial^2 E_z}{\partial^2 y} - \mu\epsilon \frac{\partial^2 E_z}{\partial^2 t} = 0 \quad (9.126)$$

Discretizing in the x-direction only leads to

$$-\mu\frac{\partial[H_x]}{\partial t} = \frac{\partial[E_z]}{\partial y} \tag{9.127a}$$

$$\mu\frac{\partial[H_y]}{\partial t} = \frac{[D_x^{(e)}][E_z]}{\Delta x} \tag{9.127b}$$

$$\epsilon\frac{\partial[E_z]}{\partial t} = \frac{[\Delta_x^{(h)}][H_y]}{\Delta x} - \frac{\partial[H_x]}{\partial y} \tag{9.127c}$$

$$\frac{[D_{xx}^{(e)}][E_z]}{(\Delta x)^2} + \frac{\partial^2[E_z]}{\partial^2 y} - \mu\epsilon\frac{\partial^2[E_z]}{\partial^2 t} = 0 \tag{9.127d}$$

where $[E_z]$, $[H_x]$, and $[H_y]$ are column vectors representing the fields along each line and are functions of y and t. As given in Section 9.3.1, matrices $[D_x^{(e)}]$, $[D_x^{(h)}]$, and $[D_{xx}^{(e)}]$ represent difference operators in which the boundary conditions at the side walls are incorporated.

Due to the fact that $[D_{xx}^{(e)}]$ is a real symmetric matrix, there exists a real orthogonal matrix $[T_x^{(e)}]$ that transforms $[D_{xx}^{(e)}]$ into a diagonal matrix $[\lambda^2]$. We can transform $[E_z]$ into a transform

$$\left[\overline{E}_z\right] = \left[T_x^{(e)}\right]\left[E_z\right] \tag{9.128}$$

(and similarly $[H_x]$ and $[H_y]$) so that Eq. (9.127d) becomes

$$\frac{[\lambda^2][E_z]}{(\Delta x)^2} + \frac{\partial^2[\overline{E}_z]}{\partial^2 y} - \mu\epsilon\frac{\partial^2[\overline{E}_z]}{\partial^2 t} = 0 \tag{9.129}$$

This is a set of uncoupled partial differential equations. The solution for the ith line is

$$\overline{E}_{zi}(y,t) = \sum_n (A_{ni}\cos\omega_{ni}t + B_{ni}\sin\omega_{ni}t)\sin\alpha_n y \tag{9.130}$$

where

$$\omega_{ni} = \frac{u}{\sqrt{(n\pi/b)^2 - \lambda_i^2/(\Delta x)^2}}$$
$$\alpha_n = n\pi/b \tag{9.131}$$

and $u = 1/\sqrt{\mu\epsilon}$ is the wave velocity. Given the initial conditions for $\overline{E}_z$ and its time derivative, we can find A_{ni} and B_{ni}. The solution at any point at any time can be extracted from Eqs. (9.130) and (9.127a), (9.127b), and (9.127c) and the subsequent inverse transforms such as

$$\left[E_z(y,t)\right] = \left[T_x^{(e)}\right]\left[\overline{E}_z\right] \tag{9.132}$$

This completes the solution process.

9.5 Concluding Remarks

The method of lines (MOL) is a differential-difference approach of solving elliptic, parabolic, and hyperbolic PDEs. It involves a judicious combination of analysis and computation. Given a partial differential equation, all but one of the independent variables are discretized to obtain a system of ordinary differential equations.

MOL requires that the structures be at least piecewise uniform in one dimension. Also, the eigenmatrices and eigenvalues depend on the boundaries of the solution region. These requirements have limited the applications of the method. Although not applicable to problems with complex geometries, the method of lines has been efficient for the analysis of compatible planar structures. Applications of the method include but are not limited to the following EM-related problems:

- waveguides including optical types [46]–[65],
- planar and cylindrical microstrip transmission lines [19]–[27, 66, 67],
- scattering from discontinuities in planar structures [39, 40, 68],
- antennas [32],
- electro-optic modulator structures [17, 69, 70], and
- other areas [71]–[75]

Originally, MOL was developed for problems with closed solution domain. Recently, absorbing boundary conditions appropriate for MOL have been introduced [51, 76]–[78]. With these conditions, it is now possible to simulate and model unbounded electromagnetic structures. The equivalence between the method of lines and variational method is given in [79].

References

[1] A. Zafarullah, "Application of the method of lines to parabolic partial differential equation with error estimates," *Jour. ACM,* vol. 17, no. 2, Apr. 1970, pp. 294–302.

[2] M.B. Carver and H.W. Hinds, "The method of lines and the advection equation," *Simulation,* vol. 31, no. 2, 1978, pp. 59–69.

[3] W.E. Schiesser, *The Numerical Method of Lines.* San Diego: Academic Press, 1991.

[4] G.H. Meyer, "The method of lines for Poisson's equation with nonlinear or free boundary conditions," *Numer. Math.*, vol. 29, 1978, pp. 329–344.

[5] V.N. Sushch, "Difference Poisson equation on a curvilinear mesh," *Diff. Equations*, vol. 12, no. 5, 1996, pp. 693–697.

[6] O.A. Liskovets, "The method of lines (review)," *Differential Equations*, vol. 1, no. 12, 1965, pp. 1308–1323.

[7] R. Pregla and W. Pascher, "The method of lines," in T. Itoh (ed.), *Numerical Techniques for Microwave and Millimeter-wave passive structures*. New York: John Wiley, 1989, pp. 381–446.

[8] R. Pregla, "Analysis of planar microwave structures on magnetized ferrite substrate," *Arch. Elek. Ubertragung.*, vol. 40, 1986, pp. 270–273.

[9] R. Pregla, "About the nature of the method of lines," *Arch. Elek. Ubertragung.*, vol. 41, no. 6, 1987, pp. 368–370.

[10] R. Pregla, "Higher order approximation for the difference operators in the method of lines," *IEEE Micro. Guided Wave Lett.*, vol. 5, no. 2, Feb. 1995, pp. 53–55.

[11] U. Schulz and R. Pregla, "A new technique for the analysis of the dispersion characteristics of planar waveguides," *Arch. Elek. Ubertragung.*, vol. 34, Apr. 1980, pp. 169–173. Also in R. Sorrentino (ed.), *Numerical Methods for Passive Microwave and Millimeter Wave Structure*, New York: IEEE Press, 1989, pp. 233–237.

[12] U. Schulz and R. Pregla, "A new technique for the analysis of the dispersion characteristics of planar waveguides and its application to microstrips with tuning septums," *Radio Sci.*, vol. 16, Nov./Dec. 1981, pp. 1173–1178.

[13] R. Pregla and W. Pascher, "Diagonalization of difference operators and system matrices in the method of lines," *IEEE Micro. Guided Wave Lett.*, vol. 2, no. 2, Feb. 1992, pp. 52–54.

[14] A. Dreher and T. Rother, "New aspects of the method of lines," *IEEE Micro. Guided Wave Lett.*, vol. 5, no. 11, Nov. 1995, pp. 408–410.

[15] D.J. Jones et al., "On the numerical solution of elliptic partial differential equations by the method of lines," *Jour. Comp. Phys.*, vol. 9, 1972, pp. 496–527.

[16] B.H. Edwards, "The numerical solution of elliptic differential equation by the method of lines," *Revista Colombiana de Matematicas*, vol. 19, 1985, pp. 297–312.

[17] A.G. Keen et al., "Quasi-static analysis of electrooptic modulators by the method of lines," *J. Lightwave Tech.*, vol. 8, no. 1, Jan. 1990, pp. 42–50.

[18] J.G. Ma and Z. Chen, "Application of the method of lines to the Laplace equation," *Micro. Opt. Tech. Lett.*, vol. 14, no. 6, 1997, pp. 330–333.

[19] S. Xiao et al., " Analysis of cylindrical transmission lines with the method of lines," *IEEE Trans. Micro. Theo. Tech.*, vol. 44, no. 7, July 1996, pp. 993–999.

[20] H. Diestel, "Analysis of planar multiconductor transmission-line system with the method of lines," *AEU*, vol. 41, 1987, pp. 169–175.

[21] Z. Chen and B. Gao, "Full-wave analysis of multiconductor coupled lines in MICs by the method of lines," *IEEE Proc.*, Pt. H, vol. 136, no. 5, Oct. 1989, pp. 399–404.

[22] W. Pascher and R. Pregla, "Full wave analysis of complex planar microwave structures," *Radio Sci.*, vol. 22, no. 6, Nov. 1987, pp. 999–1002.

[23] M.A. Thorburn et al., "Application of the method of lines to planar transmission lines in waveguides with composite cross-section geometries," *IEEE Proc.*, Pt. H, vol. 139, no. 6, Dec. 1992, pp. 542–544.

[24] R. Pregla, "Analysis of a microstrip bend discontinuity by the method of lines," *Frequenza*, vol. 145, 1991, pp. 213–216.

[25] Y.J. He and S.F. Li, "Analysis of arbitrary cross-section microstrip using the method of lines," *IEEE Trans. Micro. Theo. Tech.*, vol. 42, no. 1, Jan. 1994, pp. 162–164.

[26] M. Thorburn et al., "Computation of frequency-dependent propagation characteristics of microstriplike propagation structures with discontinuous layers," *IEEE Trans. Micro. Theo. Tech.*, vol. 38, no. 2, Feb. 1990, pp. 148–153.

[27] P. Meyer and P.W. van der Walt, "Closed-form expression for implementing the method of lines for two-layer boxed planar structures," *Elect. Lett.*, vol. 30, no. 18, Sept. 1994, pp. 1497–1498.

[28] E.R. Champion, *Numerical methods for Engineering Applications*. New York: Marcel Dekker, 1993, pp. 196–215.

[29] L. Urshev and A. Stoeva, "Application of equivalent transmission line concept to the method of lines," *Micro. Opt. Tech. Lett.*, vol. 3, no. 10, Oct. 1990, pp. 341–343.

[30] Y. Xu, "Application of method of lines to solve problems in the cylindrical coordinates," *Micro. Opt. Tech. Lett.*, vol. 1, no. 5, May 1988, pp. 173–175.

[31] K. Gu and Y. Wang, "Analysis of dispersion characteristics of cylindrical microstrip line with method of lines," *Elect. Lett.*, vol. 26, no. 11, May 1990, pp. 748–749.

[32] R. Pregla, "New approach for the analysis of cylindrical antennas by the method of lines," *Elect. Lett.*, vol. 30, no. 8, April 1994, pp. 614–615.

[33] R. Pregla, "General formulas for the method of lines in cylindrical coordinates," *IEEE Trans. Micro. Theo. Tech.*, vol. 43, no. 7, July 1995, pp. 1617–1620.

[34] R. Pregla, "The method of lines for the analysis of dielectric waveguide bends," *J. Lightwave Tech.*, vol. 14, no. 4, 1996, pp. 634–639.

[35] D. Kremer and R. Pregla, "The method of lines for the hybrid analysis of multilayered cylindrical resonator structures," *IEEE Trans. Micro. Theo. Tech.*, vol. 45, no. 12, Dec. 1997, pp. 2152–2155.

[36] M. Thorburn et al., " Application of the method of lines to cylindrical inhomogeneous propagation structures," *Elect. Lett.*, vol. 26, no. 3, Feb. 1990, pp. 170–171.

[37] K. Wu and R. Vahldieck, "The method of lines applied to planar transmission lines in circular and elliptical waveguides," *IEEE Trans. Micro. Theo. Tech.*, vol. 37, no. 12, Dec. 1989, pp. 1958–1963.

[38] S. Nam et al., "Time-domain method of lines," *Elect. Lett.*, vol. 24, no. 2, Jan. 1988, pp. 128–129.

[39] S. Nam et al., "Time-domain method of lines applied to planar waveguide structures," *IEEE Trans. Micro. Theo. Tech.*, vol. 37, 1989, pp. 897–901.

[40] S. Nam et al., "Characterization of uniform microstrip line and its discontinuities using the time-domain method of lines," *IEEE Trans. Micro. Theo. Tech.*, vol. 37, 1989, pp. 2051–2057.

[41] H. Zhao et al., "Numerical solution of the power density distribution generated in a multimode cavity by using the method of lines technique to solve directly for the electric field," *IEEE Trans. Micro. Theo. Tech.*, vol. 44, no. 12, Dec. 1996, pp. 2185–2194.

[42] W. Fu and A. Metaxas, "Numerical prediction of three-dimensional power density distribution in a multi-mode cavity," *Jour. Micro. Power Electromag. Energy*, vol. 29, no. 2, 1994, pp. 67–75.

[43] W.B. Fu and A.C. Metaxas, "Numerical solution of Maxwell's equations in three dimensions using the method of lines with applications to microwave heating in a multimode cavity," *Int. Jour. Appl. Engr. Mech.*, vol. 6, 1995, pp. 165–186.

[44] J. Lawson and M. Berzins, "Towards an automatic algorithm for the numerical solution of parabolic partial differential equations using the method of lines," in J. R. Cash and I. Gladwell (eds.), *Computational Ordinary Differential Equations*. Oxford: Clarendon Press, 1992, pp. 309–322.

[45] B. Zubik-Kowal, "The method of lines for parabolic differential-functional equations," *IMA Jour. Num. Analy.*, vol. 17, 1997, pp. 103–123.

[46] W. Pascher and R. Pregla, "Analysis of rectangular waveguide junctions by the method of lines," *IEEE Trans. Micro. Theo. Tech.*, vol. 43, no. 12, Dec. 1993, pp. 2649–2653.

[47] S.J. Chung and T.R. Chrang, "Full-wave analysis of discontinuities in conductor-backed coplanar waveguides using the method of lines," *IEEE Trans. Micro. Theo. Tech.*, vol. 41, no. 9, 1993, pp. 1601–1605.

[48] A. Papachristoforos, "Method of lines for analysis of planar conductors with finite thickness," *IEEE Proc. Micro. Ant. Prog.*, vol. 141, no. 3, June 1994, pp. 223–228.

[49] R. Pregla and W. Yang, "Method of lines for analysis of multilayered dielectric waveguides with Bragg grating," *Elect. Lett.*, vol. 29, no. 22, Oct. 1993, pp. 1962–1963.

[50] R.R. Kumar et al., "Modes of a shielded conductor-backed coplanar waveguide," *Elect. Lett.*, vol. 30, no. 2, Jan. 1994, pp. 146–147.

[51] A. Dreher and R. Pregla, "Full-wave analysis of radiating planar resonators with the method of lines," *IEEE Trans. Micro. Theo. Tech.*, vol. 41, no. 8, Aug. 1993, pp. 1363–1368.

[52] U. Rogge and R. Pregla, "Method of lines for the analysis of strip-load optical waveguide," *J. Opt. Soc. Amer. B*, vol. 8, no. 2, pp. 463–489.

[53] F.J. Schmuckle and R. Pregla, "The method of lines for the analysis of lossy planar waveguides," *IEEE Trans. Micro. Theo. Tech.*, vol. 38, no. 10, Oct. 1990, pp. 1473–1479.

[54] F.J. Schmuckle and R. Pregla, "The method of lines for the analysis of planar waveguides with finite metallization thickness," *IEEE Trans. Micro. Theo. Tech.*, vol. 39, no. 1, Jan. 1991, pp. 107–111.

[55] R.S. Burton and T.E. Schlesinger, "Least squares technique for improving three-dimensional dielectric waveguide analysis by the method of lines," *Elect. Lett.*, vol. 30, no. 13, June 1994, pp. 1071–1072.

[56] R. Pregla and E. Ahlers, "Method of lines for analysis of arbitrarily curved waveguide bends," *Elect. Lett.*, vol. 30, no. 18, Sept. 1994, pp. 1478–1479.

[57] R. Pregla and E. Ahlers, "Method of lines for analysis of discontinuities in optical waveguides," *Elect. Lett.*, vol. 29, no. 21, Oct. 1993, pp. 1845–1846.

[58] J.J. Gerdes, "Bidirectional eigenmode propagation analysis of optical waveguides based on method of lines," *Elect. Lett.*, vol. 30, no. 7, March 1994, pp. 550–551.

[59] S.J. Al-Bader and H.A. Jamid, "Method of lines applied to nonlinear guided waves," *Elect. Lett.*, vol. 31, no. 17, Aug. 1995, pp. 1455–1457.

[60] W.D. Yang and R. Pregla, "Method of lines for analysis of waveguide structures with multidiscontinuities," *Elect. Lett.*, vol. 31, no. 11, May 1995, pp. 892–893.

[61] J. Gerdes et al., "Three-dimensional vectorial eigenmode algorithm for non-paraxal propagation in reflecting optical waveguide structures," *Elect. Lett.*, vol. 31, no. 1, Jan. 1995, pp. 65–66.

[62] W. Pascher and R. Pregla, "Vectorial analysis of bends in optical strip waveguides by the method of lines," *Radio Sci.*, vol. 28, no. 6, Nov./Dec. 1993, pp. 1229–1233.

[63] S.B. Worm, "Full-wave analysis of discontinuities in planar waveguides by the method of lines using a source approach," *IEEE Trans. Micro. Theo. Tech.*, vol. 38, no. 10, Oct. 1990, pp. 1510–1514.

[64] S.J. Al-Bader and H.A. Jamid, "Mode scattering by a nonlinear step-discontinuity in dielectric optical waveguide," *IEEE Trans. Micro. Theo. Tech.*, vol. 44, no. 2, Feb. 1996, pp. 218–224.

[65] S.J. Chung and L.K. Wu, "Analysis of the effects of a resistively coated upper dielectric layer on the propagation characteristics of hybrid modes in a waveguide-shielded microstrip using the method of lines," *IEEE Trans. Micro. Theo. Tech.*, vol. 41, no. 8, Aug. 1993, pp. 1393–1399.

[66] M.J. Webster et al., "Accurate determination of frequency dependent three element equivalent circuit for symmetric step microstrip discontinuity," *IEEE Proc.*, vol. 137, Pt. H, no. 1, Feb. 1990, pp. 51–54.

[67] Y. Chen and B. Beker, "Study of microstrip step discontinuities on bianisotropic substrates using the method of lines and transverse resonance technique," *IEEE Trans. Micro. Theo. Tech.*, vol. 42, no. 10, Oct. 1994, pp. 1945–1950.

[68] P. Meyer, "Solving microstrip discontinuities with a combined mode-matching and method-of-lines procedure," *Micro. Opt. Tech. Lett.*, vol. 8, no. 1, Jan. 1995, pp. 4–8.

[69] J. Gerdes et al., "Full wave analysis of traveling-wave electrodes with finite thickness for electro-optic modulators by the method of lines," *Jour. Lightwave Tech.*, vol. 9, no. 4, Aug. 1991, pp. 461–467.

[70] S.J. Chung, "A 3-dimensional analysis of electrooptic modulators by the method of lines," *IEEE Trans. Mag.*, vol. 29, no. 2, March 1993, pp. 1976–1980.

[71] A. Kormatz and R. Pregla, "Analysis of electromagnetic boundary-value problems in inhomogeneous media with the method of lines," *IEEE Trans. Micro. Theo. Tech.*, vol. 44, no. 12, Dec. 1996, pp. 2296–2299.

[72] B.M. Sherrill and N.G. Alexopoulos, "The method of lines applied to a finline/strip configuration on an anisotropic subtrate," *IEEE Trans. Micro. Theo. Tech.*, vol. 35, no. 6, June 1987, pp. 568–574.

[73] L. Vietzorreck and R. Pregla, "Hybrid analysis of three-dimensional MMIC elements by the method of lines," *IEEE Trans. Micro. Theo. Tech.*, vol. 44, no. 12, Dec. 1996, pp. 2580–2586.

[74] K. Suwan and A. Anderson, "Method of lines applied to Hyperbolic fluid transient equations," *Int. Jour. Num. Methods Engr.*, vol. 33, 1992, pp. 1501–1511.

[75] A.G. Bratsos, "The solution of the Boussinesq equation using the method of lines," *Comp. Methods Appl. Mech. Engr.*, vol. 157, 1998, pp. 33–44.

[76] A. Dreher and R. Pregla, "Analysis of planar waveguides with the method of lines and absorbing boundary conditions," *IEEE Micro. Guided Wave Lett.*, vol. 1, no. 6, June 1991, pp. 138–140.

[77] R. Pregla, and L. Vietzorreck, "Combination of the source method with absorbing boundary conditions in the method of lines," *IEEE Micro. Guided Wave Lett.*, vol. 5, no. 7, July 1995, pp. 227–229.

[78] K. Wu and X. Jiang, "The use of absorbing boundary conditions in the method of lines," *IEEE Micro. Guided Wave Lett.*, vol. 6, no. 5, May 1996, pp. 212–214.

[79] W. Hong and W.X. Zhang, "On the equivalence between the method of lines and the variational method," *AEU*, vol. 45, no. 1, 1991, pp. 198–201.

Problems

9.1 In Eq. (9.7), show that $p_\ell = 2$ for Dirichlet condition and $p_\ell = 1$ for Neumann condition.

9.2 If the first-order finite difference scheme can be written as

$$h\frac{\partial[V]}{\partial x} \simeq -[D_x]^t\,[V]$$

where the equidistance difference matrix $[D_x]$ is an $(N-1)\times N$ matrix given by

$$[D_x] = \begin{bmatrix} 1 & -1 & & \\ & \ddots & \ddots & \\ & & 1 & -1 \end{bmatrix}$$

show that the central finite difference scheme for second-order partial differential operator yields

$$h^2\frac{\partial^2[V]}{\partial x^2} \simeq [D_{xx}]\,[V]$$

where $[D_{xx}] = -[D_x]^t[D_x] = -[D_x][D_x]^t$. Assume Neumann conditions at both side walls and obtain D_{xx}.

9.3 Obtain the transformation matrix $[T]$ and its corresponding eigenvalue matrix $[\lambda^2]$ for Neumann-Dirichlet boundary conditions. Assume that $t_0^{(k)} - t_1^{(k)} = 0$ and $t_{N+1}^{(k)} = 0$ on the boundaries.

9.4 Using MOL, solve Laplace's equation

$$\nabla^2 \Phi = 0$$

in a rectangular domain $0 \leq x \leq 1$, $-1 \leq y \leq 1$ with the following Dirichlet boundary conditions:

$$\Phi(0, y) = \Phi(1, y) = 0$$
$$\Phi(x, 1) = \Phi(x, -1) = \sin \pi x$$

Obtain Φ at $(0, 0.5)$, $(0.5, 0.25)$, $(0.5, 0.5)$, $(0.5, 0.75)$. Compare your solution with the exact solution

$$\Phi(x, y) = \frac{\cosh(\pi y) \sin(\pi x)}{\cosh(\pi b)}$$

9.5 Obtain the solution of Prob. 2.4(a) using MOL.

9.6 Consider the coaxial cable of elliptical cylindrical cross section shown in Fig. 9.14. Take $A = 2$ cm, $B = 2$ cm, $a = 1$ cm, and $b = 2$ cm. For

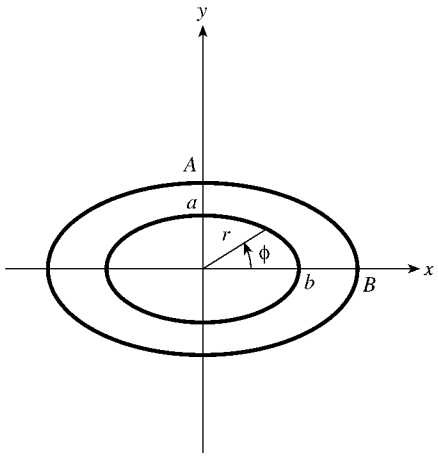

Figure 9.14
For Prob. 9.6.

the inner ellipse, for example,

$$r = \frac{a}{\sqrt{\sin^2 \phi + v^2 \cos^2 \phi}}, \qquad v = \frac{a}{b}$$

By modifying the MOL codes used in Example 9.3, plot the potential for $\phi = 0$, $a < \rho < b$.

9.7 Solve Prob. 2.8 using MOL and compare your result with the exact solution

$$V(\rho, z) = \frac{4V_o}{\pi} \sum_{n=\text{odd}} \frac{I_0(n\pi\rho/L)}{nI_0(n\pi a/L)} \sin\left(\frac{n\pi z}{L}\right)$$

Take $L = 2a = 1$ m and $V_o = 10$ V.

9.8 Rework Example 9.4 for a pair of coupled microstrips shown in Fig. 9.15. Let $\epsilon_r = 10.2$, $w = 1.5$, $s/d = 1.5$, $a/d = 20$, $h/d = 19$, and $d = 1$ cm. Plot the effective dielectric constant versus d/λ_o.

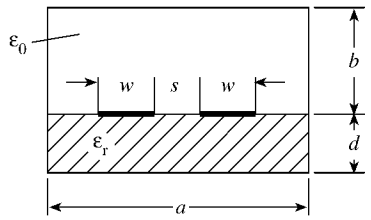

Figure 9.15
For Prob. 9.8.

9.9 Given the difference operator

$$[P] = \begin{bmatrix} 2 & -s^{*2} & \cdots & & -s^2 \\ -s^2 & 2 & -s^{*2} & \cdots & \\ & \ddots & \ddots & \ddots & \\ & & & & -s^{*2} \\ -s^{*2} & \cdots & & -s^2 & 2 \end{bmatrix}$$

which is Hermitian, i.e., $[P] = [P^*]$. Show that $[P]$ has the following eigenvalues

$$\lambda_k^2 = 4\sin^2\frac{\phi_k \beta h}{2}, \quad \phi_k = \frac{2\pi k}{N}, \quad k = 1, 2, \ldots, N$$

and the eigenvector matrices

$$T_{ik}^{(e)} = \frac{1}{\sqrt{N}} e^{ji\phi_k}, \quad T_{ik}^{(h)} = \frac{1}{\sqrt{N}} e^{j(i+0.5)\phi_k}$$

where $s = e^{j\beta h/2}$, s^* is the complex conjugate of s, β is the propagation constant, and h is the step size.

9.10 Show that for

$$[P] = \begin{bmatrix} 2 & -1/s & \dots & & -s \\ -s & 2 & -1/s & \dots & \\ & \ddots & \ddots & \ddots & \\ & & & & -1/s \\ -1/s & \dots & & -s & 2 \end{bmatrix}$$

the eigenvalue matrices remain the same as in the previous problem.

Appendix A

Vector Relations

A.1 Vector Identities

If **A** and **B** are vector fields while U and V are scalar fields, then

$$\nabla V(U+V) = \nabla U + \nabla V$$
$$\nabla(UV) = U\nabla V + V\nabla U$$
$$\nabla\left(\frac{U}{V}\right) = \frac{\nabla(\nabla U) - U(\nabla V)}{V^2}$$
$$\nabla V^n = nV^{n-1}\nabla V \qquad (n = \text{integer})$$
$$\nabla(\mathbf{A}\cdot\mathbf{B}) = (A\cdot\nabla)\mathbf{B} + (\mathbf{B}\cdot\nabla)\mathbf{A} + \mathbf{A}\times(\nabla\times\mathbf{B}) + \mathbf{B}\times(\nabla\times\mathbf{A})$$
$$\nabla\cdot(\mathbf{A}+\mathbf{B}) = \nabla\cdot\mathbf{A} + \nabla\cdot\mathbf{B}$$
$$\nabla\cdot(\mathbf{A}\times\mathbf{B}) = \mathbf{B}\cdot(\nabla\times\mathbf{A}) - \mathbf{A}\cdot(\nabla\times\mathbf{B})$$
$$\nabla\cdot(\nabla\mathbf{A}) = V\nabla\cdot\mathbf{A} + \mathbf{A}\cdot\nabla V$$
$$\nabla\cdot(\nabla V) = \nabla^2 V$$
$$\nabla\cdot(\nabla\times\mathbf{A}) = 0$$
$$\nabla\times(\mathbf{A}+\mathbf{B}) = \nabla\times\mathbf{A} + \nabla\times\mathbf{B}$$
$$\nabla\times(\mathbf{A}\times\mathbf{B}) = \mathbf{A}(\nabla\cdot\mathbf{B}) - \mathbf{B}(\nabla\cdot\mathbf{A}) + (\mathbf{B}\cdot\nabla)\mathbf{A} - (\mathbf{A}\cdot\nabla)\mathbf{B}$$
$$\nabla\times(V\mathbf{A}) = \nabla V\times\mathbf{A} + V(\nabla\times\mathbf{A})$$
$$\nabla\times(\nabla V) = 0$$
$$\nabla\times(\nabla\times\mathbf{A}) = \nabla(\nabla\cdot\mathbf{A}) - \nabla^2\mathbf{A}$$

A.2 Vector Theorems

If v is the volume bounded by the closed surface S, and $\mathbf{a}_n$ is a unit normal to S, then

$$\oint_S \mathbf{A} \cdot d\mathbf{S} = \int_v \nabla \cdot \mathbf{A}\, dv \quad \text{(Divergence theorem)}$$

$$\oint_S V\, d\mathbf{S} = \int_v \nabla V\, dv \quad \text{(Gradient theorem)}$$

$$\oint_S \mathbf{A} \times d\mathbf{S} = -\int_v \nabla \times \mathbf{A}\, dv$$

$$\oint_S \left[(\mathbf{A} \cdot d\mathbf{S})\mathbf{A} - \frac{1}{2} A^2\, d\mathbf{S} \right] = \int_v [(\nabla \times \mathbf{A}) \times \mathbf{A} + \mathbf{A}\nabla \cdot \mathbf{A}]\, dv$$

$$\oint_S U \nabla V \cdot d\mathbf{S} = \int_v \left[U\nabla^2 V + \nabla U \cdot \nabla V \right] dv \quad \text{(Green 1st identity)}$$

$$\oint_S [U\nabla V - V\nabla U] \cdot d\mathbf{S} = \int_v \left[U\nabla^2 V - V\nabla^2 U \right] dv \quad \text{(Green 2nd identity)}$$

where $d\mathbf{S} = dS\, \mathbf{a}_n$.

If S is the area bounded by the closed path L and the positive directions of elements $d\mathbf{S}$ and $d\mathbf{l}$ are related by the right-hand rule, then

$$\oint_L \mathbf{A} \cdot d\mathbf{l} = \int_S \nabla \times \mathbf{A} \cdot d\mathbf{S} \quad \text{(Stokes' theorem)}$$

$$\oint_L V\, d\mathbf{l} = -\int_S \nabla V \times d\mathbf{S}$$

A.3 Orthogonal Coordinates

Rectangular Coordinates (x, y, z)

$$\nabla V = \frac{\partial V}{\partial x}\mathbf{a}_x + \frac{\partial V}{\partial y}\mathbf{a}_y + \frac{\partial V}{\partial z}\mathbf{a}_z$$

$$\nabla \cdot \mathbf{A} = \frac{\partial A_x}{\partial x} + \frac{\partial A_y}{\partial y} + \frac{\partial A_z}{\partial z}$$

$$\nabla \times \mathbf{A} = \left[\frac{\partial A_z}{\partial y} - \frac{\partial A_y}{\partial z} \right] \mathbf{a}_x + \left[\frac{\partial A_x}{\partial z} - \frac{\partial A_z}{\partial x} \right] \mathbf{a}_y + \left[\frac{\partial A_y}{\partial x} - \frac{\partial A_x}{\partial y} \right] \mathbf{a}_z$$

$$\nabla^2 V = \frac{\partial^2 V}{\partial x^2} + \frac{\partial^2 V}{\partial y^2} + \frac{\partial^2 V}{\partial z^2}$$

$$\nabla^2 \mathbf{A} = \nabla^2 A_x \mathbf{a}_x + \nabla^2 A_y \mathbf{a}_y + \nabla^2 A_z \mathbf{a}_z$$

Cylindrical Coordinates (ρ, ϕ, z)

$$\nabla V = \frac{\partial V}{\partial \rho}\mathbf{a}_\rho + \frac{1}{\rho}\frac{\partial V}{\partial \phi}\mathbf{a}_\phi + \frac{\partial V}{\partial z}\mathbf{a}_z$$

$$\nabla \cdot \mathbf{A} = \frac{1}{\rho}\frac{\partial}{\partial \rho}(\rho A_\rho) + \frac{1}{\rho}\frac{\partial}{\partial \phi}A_\phi + \frac{\partial}{\partial z}A_z$$

$$\nabla \times \mathbf{A} = \left[\frac{1}{\rho}\frac{\partial}{\partial \phi}A_z - \frac{\partial}{\partial z}A_\phi\right]\mathbf{a}_\rho + \left[\frac{\partial}{\partial z}A_\rho - \frac{\partial}{\partial \rho}A_z\right]\mathbf{a}_\phi + \frac{1}{\rho}\left[\frac{\partial}{\partial \rho}(\rho A_\phi) - \frac{\partial}{\partial \phi}A_\rho\right]\mathbf{a}_z$$

$$\nabla^2 V = \frac{1}{\rho}\frac{\partial}{\partial \rho}\left(\rho\frac{\partial V}{\partial \rho}\right) + \frac{1}{\rho^2}\frac{\partial^2 V}{\partial \phi^2} + \frac{\partial^2 V}{\partial z^2}$$

$$\nabla^2 \mathbf{A} = \left[\nabla^2 A_\rho - \frac{2}{\rho^2}\frac{\partial}{\partial \phi}A_\phi - \frac{A_\rho}{\rho^2}\right]\mathbf{a}_\rho + \left[\nabla^2 A_\phi + \frac{2}{\rho^2}\frac{\partial}{\partial \phi}A_\rho - \frac{A_\phi}{\rho^2}\right]\mathbf{a}_\phi + \nabla^2 A_z \mathbf{a}_z$$

Spherical Coordinates (r, θ, ϕ)

$$\nabla V = \frac{\partial V}{\partial r}\mathbf{a}_r + \frac{1}{r}\frac{\partial V}{\partial \theta}\mathbf{a}_\theta + \frac{1}{r\sin\theta}\frac{\partial V}{\partial \phi}\mathbf{a}_\phi$$

$$\nabla \cdot \mathbf{A} = \frac{1}{r^2}\frac{\partial}{\partial r}(r^2 A_r) + \frac{1}{r\sin\theta}\frac{\partial}{\partial \theta}(\sin\theta A_\theta) + \frac{1}{r\sin\theta}\frac{\partial A_\phi}{\partial \phi}$$

$$\nabla \times \mathbf{A} = \frac{1}{r\sin\theta}\left[\frac{\partial}{\partial \theta}(\sin\theta A_\phi) - \frac{\partial}{\partial \phi}A_\theta\right]\mathbf{a}_r + \frac{1}{r}\left[\frac{1}{\sin\theta}\frac{\partial}{\partial \phi}A_r - \frac{\partial}{\partial r}(r A_\phi)\right]\mathbf{a}_\theta + \frac{1}{r}\left[\frac{\partial}{\partial r}(r A_\theta) - \frac{\partial}{\partial \theta}A_r\right]\mathbf{a}_\phi$$

$$\nabla^2 V = \frac{1}{r^2}\frac{\partial}{\partial r}\left(r^2\frac{\partial V}{\partial r}\right) + \frac{1}{r^2\sin\theta}\frac{\partial}{\partial \theta}\left(\sin\theta\frac{\partial V}{\partial \theta}\right) + \frac{1}{r^2\sin^2\theta}\frac{\partial^2 V}{\partial \phi^2}$$

$$\nabla^2 \mathbf{A} = \left[\nabla^2 A_r - \frac{2}{r^2\sin\theta}\frac{\partial}{\partial \theta}(\sin\theta A_\theta) - \frac{2}{r^2\sin\theta}\frac{\partial}{\partial \phi}A_\phi - \frac{2}{r^2}A_r\right]\mathbf{a}_r + \left[\nabla^2 A_\theta + \frac{2}{r^2}\frac{\partial}{\partial \theta}A_r - \frac{2\cos\theta}{r^2\sin^2\theta}\frac{\partial}{\partial \phi}A_\phi - \frac{1}{r^2\sin^2\theta}A_\theta\right]\mathbf{a}_\theta + \left[\nabla^2 A_\phi + \frac{2\cos\theta}{r^2\sin^2\theta}\frac{\partial}{\partial \phi}A_\theta + \frac{2}{r^2\sin\theta}\frac{\partial}{\partial \phi}A_r - \frac{1}{r^2\sin^2\theta}A_\phi\right]\mathbf{a}_\phi$$

Appendix B

Solving Electromagnetic Problems Using C++ [1]

B.1 Introduction

The C++ programming language was developed by Bjarne Stroustrup in 1980, at Bell Labs (Murray Hill, New Jersey). It was considered to be an improvement on the C language by adding support for object-oriented programming. This appendix is meant to be a brief review of C++ as well as an introduction to using C++ to solve electromagnetic problems. Examples are offered to illustrate the points previously discussed. Style notes are also included to offer insight into what good programming practices are.

Most of the main features of the language are covered but the reader is encouraged to consider the references at the end of this appendix to obtain supplemental information on the more advanced topics of object-oriented programming. The reader is encouraged to pay close attention to the examples. The programs may contain subtle implementations of other concepts in addition to the main concept being covered at the time. (All the programs were developed using Microsoft Visual C++ 5.0.)

B.2 A Brief Description of C++

A. What Every New Programmer to a Language Should See First

Consider the obligatory "hello" program:

[1] Written by Raymond C. Garcia, Georgia Institute of Technology, Atlanta, GA 30332-0320.

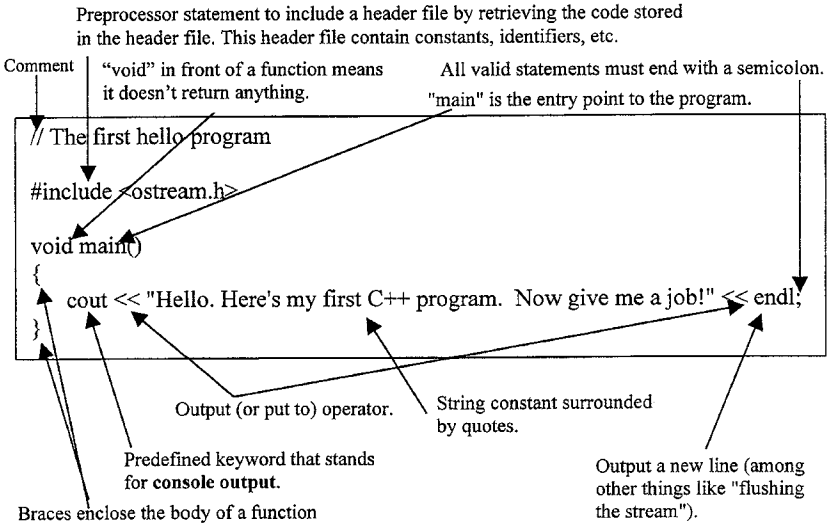

The "hello" program simply prints a statement along with a carriage return.

One of the most notable statements in every C++ program is the "#include" statement. It is here where preprocessed code is included and incorporated with a program code. Table B.1 contains information on what header file to include based on what function is needed [1, 2].

B. Types and Declarations

The C++ language supports the commom intrinsic types as well as user defined types:

- Boolean – the keywords *true* and *false* are supported. All logical expressions evaluate to the type *bool.*
- Integer – the keyword *int* is used to represent integer values. Commom "unmodified" integers range from $-32,768$ to $32,767$.
- Floating-point – the keywords *float* and *double* are used to represent floating-point types. The commom "unmodified" ranges are 3.4e−38 to 3.4e+38 for floats and 1.7e−308 to 1.7e+308 for doubles.
- Character – the keyword ***char*** is used to represent character data. Most compilers implement a char as an 8-bit value which can hold 256 different values.

All of the types mentioned above except for *bool* can be modified by the following keywords:

- signed
- unsigned

Table B.1 Inherited C Include Files

Header File	Comments
assert.h	Used for debugging.
ctype.h	Allows you to check the case and type of char (i.e., is it upper/lower case or a digit, etc.).
errno.h	Several macros are defined to report error conditions.
float.h	Macros and constants used for serious numerical, floating-point programming.
iso646.h	Provides readable alternatives to certain operators or punctuators (i.e., "and" instead of &&).
limits.h	Goes hand-in-hand with float.h; offers the range limits for all data types.
locale.h	Formatting of numeric data; mostly informative.
math.h	Contains mathematical functions (sin, cos, etc.).
setjmp.h	Contains a macro, function, and type for bypassing normal function calls (similar to goto); be careful.
signal.h	Supports the handling of "signals" (conditions occurring at run-time).
stdarg.h	Macros contained here allow you to walk through a variable argument list.
stddef.h	As the name suggests, this headers contains "standard definitions."
stdio.h	Contains functions that perform input and output (fopen, fclose, fprintf, etc.).
stdlib.h	Contains general utility functions.
string.h	Contains functions which facilitate the manupulation of array character data.
time.h	Provides time structures
wchar.h	Allows its user to perform input and output operations on wide streams or manipulate wide strings.
wctype.h	Similar to ctype.h except it acts on wide chars.

- long
- short

Table B.3 lists some of the basic types along with the commom bit widths and ranges [3].

<STYLE NOTE>: It is good programming practice to use the appropriate data type and modifier whenever possible. For example, do not use a long double when a float is really needed. This habit will prove more valuable for large programs where memory is a concern. This is especially useful when precision is of interest.

C. Input and Output with cin and cout

One of the major enhancements to C is the stream libraries which provide functionality for console/terminal and file input and output. This functionality is accessed through the keywords ***cin*** and ***cout***.

Table B.2 C++ Header Files [2]

C++ Headers	
Header File	**Comments**
bits	Provides a template and related function for manipulating a fixed-size sequences of bits.
bitstring	Similar to bits but functions operate on varying-length sequences of bits.
complex	Support functionality for representing and manipulating complex numbers.
defines	Defines a constant and several types that are used by many other headers.
dynarray	Defines a template which generically controls a sequence.
exception	Supports the handling of exceptions.
fstream	Provides stream buffers to assist the reading and writing of files.
iomanip	Provides template classes that provide extractors and inserters for information used in the class "ios."
ios	Provides function signatures for controlling how to interpret input and output from a sequence of characters.
iostream	Include to perform input and output from a C++ program.
istream	Controls input from a stream buffer. "cin" is its most popular object.
new	Manages the allocation and storage of a program.
ostream	Controls output to a stream buffer.
ptrdynarray	Defines a template that supports a varying-size sequence of pointers to a generic object.
sstream	Used to define several template classes that support iostreams operations on sequences stored in an allocated array object.
streambuf	Defines macros and data types that control input from and output to char sequences.
string	Assists in the manipulation of varying-length sequences of chars.
strstream	Designed to assist in reading and writing char sequences stored in memory.
wstring	Similar to string but applies to wide characters.

Example B.1:

```
#include <iostream.h> // used for C++ cin and cout functions

void main()
{
    float x_coord, y_coord;
    float multiplier = 4.657483F; // The 'F' specifies the type of constant (float) to avoid defaults
    double voltage;

    // C++ usage
    cout << "Enter the x and y coordinates separated with a space :";
    cin >> x_coord>> y_coord;
    voltage = multiplier*x_coord*y_coord;
    cout << "The voltage at the point ("
        << x_coord << ","<<y_coord<<") is "<<voltage<< " volts. \n";
}
```

Table B.3 Modified and Unmodified Types Commonly Implemented

Data Type	Modifier	Width (# of Bits)	Range
char		8	−128 to 127
	signed	"	0 to 255
	unsigned	"	−128 to 127
int		16	−32, 768 to 32, 767
	unsigned	"	0 to 65, 535
	unsigned short	"	"
	signed	"	−32, 768 to 32, 767
	short	"	"
	signed short	"	"
	long	32	−2, 147, 483, 648 to 2, 147, 483, 647
	signed long	"	"
	unsigned long	"	0 to 4, 294, 967, 295
float		"	3.4e−38 to 3.4e+38
double		64	1.7e−308 to 1.7e+308
	long	80	3.4e−4932 to 1.1e+4932

Output:

```
Enter the x and y coordinates separated with a space :4.4 5.5
The voltage at the point (4.4,5.5) is 112.711 volts.
```

D. Pointers

Pointers appear to be one of the most confused concepts in C++. When used incorrectly, programs became unstable. A pointer is an item that holds the address of a defined variable. There are pointers to pointers and the like. When a pointer holds the address to the first element in an array, incrementing it will move it to the next address in the array. This may seem obvious but the main point is that different data types are different sizes in the machine they reside in. An int pointer will increment 2 bytes and a float pointer will increment 4 bytes if integers are represented with 2 bytes and floats are represented by 4 bytes. This is a machine dependent concept.

Some of the more popular uses of pointers are linked lists, dynamic memory allocation, and argument modification. Since structures and functions have not been discussed yet, the two examples of pointer usage given here are simple pointer assignment and dynamic memory allocation.

Example B.2:

```
#include <iostream.h>
void main(){ // simple pointer assignment
    int *intptr;
    int intvar=10, array_size;
    int *int_array_ptr;
```

```
    intptr = &intvar; // set pointer equal to the intvar's address
    cout << "Contents of intptr: "<<*intptr<<endl; // here, the "*" is called a dereference operator

    cout<<"Enter the size of the array: ";
    cin>>array_size;
    if (array_size > 0){
        int_array_ptr = new int[array_size];  // dynamic memory allocation
        for (int x=0;x<array_size;x++)
            int_array_ptr[x]=array_size - x;
        for (int y=0;y<array_size;y++)
            cout<<" Element " << y << "= ("<< int_array_ptr[y]<<")";
        cout << endl;
    }
}
```

Output:

```
Contents of intptr: 10
Enter the size of the array: 5
Element 0= (5) Element 1= (4) Element 2= (3) Element 3= (2) Element 4= (1)
```

E. Arrays

Unspecified arrays take the following form:

```
array_item_type array_name[no_of_elements];
```

The statement above tells the compiler to reserve enough space to hold no_elements of array_item_type. These are valid array declarations:

```
int my_ints[10]; // simple one-dimensional array of ints
char buffer[80]; // simple one-dimensional array of chars
char screen[24][80]; // a two-dimensional array of chars
```

Arrays can also be declared where the size need not be indicated explicitly. For instance, the statement:

```
int my_ints[] = {1, 2, 3, 4, 5, 6, 7, 8, 9, 10};
```

implicitly tells the compiler that my_ints is an array of ten integers. To specify a particular element of the my_ints array you type the following:

```
my_ints[2].
```

Here, my_ints[2] refers to the item '3' not '2' as most people who deal with non zero-based arrays would expect.

Multi-dimensional arrays are initialized as shown in the following example:

Example B.3:

```
#include <iostream.h>

void main()
{
    int nums[2][3]={1,2,3,4,5,6};  // initialized 2-d array


    // print out the contents; element-by-element
    cout << "nums[0][0] = "<<nums[0][0] << endl;
    cout << "nums[0][1] = "<<nums[0][1] << endl;
    cout << "nums[0][2] = "<<nums[0][2] << endl;
    cout << "nums[1][0] = "<<nums[1][0] << endl;
    cout << "nums[1][1] = "<<nums[1][1] << endl;
    cout << "nums[1][2] = "<<nums[1][2] << endl;

}
```

Output:

```
nums[0][0] = 1
nums[0][1] = 2
nums[0][2] = 3
nums[1][0] = 4
nums[1][1] = 5
nums[1][2] = 6
```

<**STYLE NOTE**>: This is more of a warning than a style issue. One of the virtues of C++ is the fact that it is fast and compact. In order for the language to be fast, a feature such as array bounds checking is not included. This places more responsability on the programmer to be careful when assigning and referencing arrays. The consequences can be devastating.

F. Control Constructs

Relational operators, logical operators and control constructs go hand in hand. That is why they have been deferred until this section. Arithmetic operators are also an important part of control constructs. Table B.4 contains arithmetic, relational, and logical operators [4, 5].

The following control constructs are important.

Table B.4 Arithmetic, Relational, and Logical Operators

Operator	Type	Meaning	Comments
−−	Arithmetic	decrement	when placed in front a variable it is the decremented value that is used; when placed after a variable, the decrementing occurs after it is used
++	"	increment	prefix and postfix rules are the same as with the decrement operator
*	"	multiplication	
/	"	division	remainder of integer division is truncated (e.g., $3/4 = 0$).
%	"	modulus	used for integer division
−	"	subtraction and unary minus	
+	"	addition	
>	relational	greater than	
>=	"	greater than or equal to	
<	"	less than	
<=	"	less than or equal to	
==	"	equal to	
!=	"	not equal to	
&&	Logical	AND	
||	"	OR	
!	"	NOT	

The ***if*** *statement:*

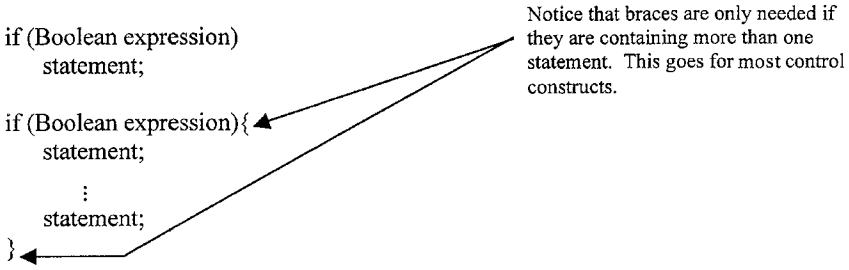

Nested ***if****s:*

```
if (Boolean expression)
    if (Boolean expression)
        statement;
```

A ladder of ***if-else-if*** *statements:*

```
if (Boolean expression)
      statement;
else if (Boolean expression)
      statement;
else if (Boolean expression)
      statement;
else
      statement;
```

The ***for*** *loop:*

```
for (initialization; expression; increment)
      statement;

for (initialization; expression; increment)
{
      statement;
            ⋮
      statement;
}
```

where "initialization" initializes the variable(s) that control the loop as a counter, "expression" sets the condition on which the loop repeats, and "increment" defines how the control variable(s) are changed.

The ***switch*** *statement*

```
switch(expression){
      case CONSTANT:
            statement;
                ⋮
            statement;
            break;
```

```
        case CONSTANT:
            statement;
                ⋮
            statement;
            break;
        default:
            statement;
                ⋮
            statement;
}
```

The expression being switched must evaluate to a character or integer value.

*The **while** loop*

```
while (Boolean expression)
{
    statement;
        ⋮
    statement;
}
```

*The **do-while** loop*

```
do {
        statement;
            ⋮
        statement;
  } while (Boolean expression);
```

Example B.4:

```
#include <iostream.h>

void main()
{
    int choice = 0;  // variable used to store the selection
```

```
        // This sets up the menu
        cout << "Enter the Monte Carlo Method to Run:\n"
             << endl
             << "     (1) Floating Random Walk\n"
             << "     (2) Fixed Random Walk\n"
             << "     (3) Fixed-Radius Floating Random Walk\n"
             << "   Choose: ";

        cin >> choice; // get the user's choice

        // switch-case statements
        switch (choice){
        case 1:
            cout << "\nRunning the Floating Random Walk...\n";
            break;
        case 2:
            cout << "\nRunning the Fixed Random Walk...\n";
            break;
        case 3:
            cout << "\nRunning the Fixed-Radius Floating Random Walk...\n";
            break;
        default:
            cout << "Invalid choice\n";

        }
    }
```

Output:

```
Enter the Monte Carlo Method to Run:

    (1) Floating Random Walk
    (2) Fixed Random Walk
    (3) Fixed-Radius Floating Random Walk
  Choose: 2

Running the Fixed Random Walk...
```

*The effect of using the **continue** and **break** keywords*

- A ***continue*** statement skips the statements following it without exiting the loop.

- A ***break*** statement will exit from the inner-most loop or the current ***switch*** statement it is in.

G. Structures and Unions

Structures form the building blocks for writing programs that deal with data. Whether dealing with simple things like a recipe in a cook book to defining boundary-value problems to perform Monte Carlo simulations, data structures are all around us.

Syntax:

```
struct struct_tag{
        type member1;
        type member2;
        type member3;
} variable declarations;

union union_tag{
        type member1;
        type member2;
                :
        type memberN;
} variable declarations;
```

Members of unions and structures are accessed using "dot" notation. For example, to access *member1* of the union *myunion,* the following syntax is used:

```
myunion.member1.
```

If a pointer to a union was defined, an arrow would replace the period. For example,

```
myunion->member1.
```

Example B.5:

```
// Structure example
//
// Allow the user to enter a series of points


#include <iostream.h>

struct p{
    float x;
    float y;
};
```

```
void main()
{
    int num=0,i=0, c=1;

    p *points, *index;

    while (num <= 0){
        cout << "Enter the number of points to consider: ";
        cin >> num;
    }

    points = new p[num]; // allocate enough memory for the points
    index = points;

    for (i=0;i<num;i++){

        cout << "\nEnter the x value of point number "<<i+1<<": ";
        cin >> index->x;

        cout << "Enter the y value of point number "<<i+1<<": ";
        cin >> index->y;

        index++;
    }

    index = points; // reset the index

    cout << "\n\nThis is what you've entered: \n\n";

    do{
        cout << "Point number " << c++ << " is (" << index->x<<","<<index->y<<")"<< endl;
        index++;
    } while (i-- > 1);

    delete [] points;  // free up the memory
}
```

Output:

```
Enter the number of points to consider: 3

Enter the x value of point number 1: 1.1
Enter the y value of point number 1: 1

Enter the x value of point number 2: 22.2
Enter the y value of point number 2: 2

Enter the x value of point number 3: 3
Enter the y value of point number 3: 3.33
        This is what you've entered:

        Point number 1 is (1.1,1)
        Point number 2 is (22.2,2)
        Point number 3 is (3,3.33)
```

A union allows several variables to share the same memory location. For example, if 4 bytes are used to represent a float and 1 byte is used to represent a char, the union of the two would occupy 4 bytes. This allows a union to be considered many things. The main point is that this example of a union can be used to hold either the float or the char. Table B.5 should help to illustrate this point

Table B.5 Byte Storage within a Union

The float uses all four bytes			
1st Byte	2nd Byte	3rd Byte	4th Byte
1 byte for the char	1 byte of float	1 byte of float	1 byte for the char

H. Functions

The role of functions is important to program development in C++. All executable statements exist within functions. Offering effective ways to implement numerical techniques in C++ is impossible to do without describing how to use functions.

Part of defining a function is through the use of a prototype. A function prototype is a program statement which indicates to the compiler the type and number of arguments that a function requires. Type checking is improved with the use of prototyping by allowing the compiler to accurately check for type mismatches.

A function prototype takes the following form:

```
return_type function_name(argument_type argument_name, argument_type argument_name, etc.);
```

For example, to tell the compiler that you have a function called "add_them" that takes two integer arguments which will be called val1 and val2, and returns an integer value, you would type the following:

```
int add_them(int val1, int val2);
```

<STYLE NOTE>: C++ allows a programmer to prototype without specifying all arguments of the function with the use of ellipsis (...). It is considered good style to have the prototype appear exactly as the function's declaration.

Here is the code for an example that uses a function that adds two numbers together.

Example B.6:

```
#include <ostream.h>

int add_them(int val1, int val2);

void main()
{
    int x = 1, y=2;
    int z;
    z = add_them(x,y);
    cout << "The sum is " << z ;
}

int add_them(int val1, int val2)
{
    int sum;
    sum = val1 + val2;
    return (sum);
}
```

Output:

```
The sum is 3
```

Call-By-Value

The process in which the compiler creates a copy of the variable's value that is being passed in the function call is called *call-by-value*. This is the default calling convention for C++. In the example above, copies of x and y were used by the sum function. The major point here is that call-by-value cannot allow a function to modify the arguments used in the function call.

Call-By-Reference

When call-by-reference is used, the address of the argument is used as opposed to a copy of it. Call-by-reference is more efficient and faster than call-by-value. Less program memory is needed and the return statement is not necessarily needed to modify the variable. In C++, pointers as well as the reference type is used to implement call-by-reference.

As the following example illustrates, call-by-reference is used to modify a variable. Pay particular attention to the need of the dereference operator (*) in the function 'will_change_with_ptr' but other than the address operator (&), the code in the function 'will_change_with_ref' does not require the added consideration when working with pointers.

<**STYLE NOTE**>: It is advantageous to use reference types when implementing call-by-reference. It becomes unnecessary to pay attention as to whether the argument being used is a pointer or not. A major source of bugs exists in a code that inappropriately uses a variable that should be de-referenced first.

Example B.7:

```
#include <ostream.h>
// function prototypes
void will_not_change(int a);
void will_change_with_ptr(int *a);
void will_change_with_ref(int &a);
void main(){
    int x = 1;
    cout << "x originally is " << x << ".\n";
    will_not_change(x);  // call-by-value
    cout << "x after will_not_change is " << x << ".\n";
    will_change_with_ptr(&x);  // call-by-reference
    cout << "x after will_change_with_ptr is " << x << ".\n";
    will_change_with_ref(x);  // call-by-reference
    cout << "x after will_change_with_ref is " << x << ".\n";}
void will_not_change(int a){
    a+=1; // increment it by 1}
void will_change_with_ptr(int *a){
    *a+=1; // increment it by 1}
void will_change_with_ref(int &a){
    a+=1; // increment it by 1}
```

Output:

```
x originally is 1.
x after will_not_change is 1.
x after will_change_with_ptr is 2.
x after will_change_with_ref is 3.
```

Array Arguments

A common necessity in programming is the need to pass arrays to functions. The following code example shows two ways to use arrays as arguments. The first function has a pointer to the first array element. The second example uses an unsized array.

Example B.8:

```
#include <ostream.h>
// define the structure that is used in the prototypes
struct point{
    float x;
    float y;};
// function prototypes
void print_points_using_ptr(point *p);
void print_points_using_unsized_array(point p[]);

void main(){
    // initialize the array of points
    point bunch_of_points[5]={{1,1},{2,2},{3,3},{4,4},{5,5}};
    // print them using address of the first element
    print_points_using_ptr(bunch_of_points);
    cout << endl; // blank line in between lists of points

    // print them using an unsized array
    print_points_using_unsized_array(bunch_of_points);}
void print_points_using_ptr(point *p){
    for (int j=0;j<5;j++)
        cout << "point[" << j << "]: (" << p[j].x << "," << p[j].y << ")\n";}
void print_points_using_unsized_array(point p[]){
    for (int j=0;j<5;j++)
        cout << "point[" << j << "]: (" << p[j].x << "," << p[j].y << ")\n";}
```

Output:

```
point[0]: (1,1)
point[1]: (2,2)
point[2]: (3,3)
point[3]: (4,4)
point[4]: (5,5)

point[0]: (1,1)
point[1]: (2,2)
point[2]: (3,3)
point[3]: (4,4)
point[4]: (5,5)
```

Three more things are left to conclude our discussion about functions:

First, the keyword ***inline*** instructs the compiler to directly place the function code at the point in which it is invoked as opposed to making a function call. This is most useful for time-saving situations with short functions that are called many times. The compiler may ignore this directive in cases where the function has loops, switch, or goto statements.

Syntax:

```
inline type function_name(argument list){
    code statements
}
```

Second, the scope resolution operator "::" is used when there are two variables with the same name at different scopes. Here is some example code that illustrates its use:

Example B.9:

```
#include <ostream.h>

// file scope variable
int x=4;

// function prototypes
int times2(int c);
int times4(int c);

void main(){
    int z=1;
    int y;

    y = times2(z); // call function that uses local variable

    cout << "y is " << y << endl;
    cout << endl;

    y = times4(z); // call function that uses global variable
    cout << "y is " << y << endl;
}
  int times2(int c){
      int x=2;  // local variable
      return (c*x);
  }

  int times4(int c){
      return(c*(::x));  // could have used 'return(c*::x)'
  }
```

Output:

```
y is 2

y is 4
```

Third, passing arguments on the command line. This is an important feature that allows programmers to call their program and pass arguments to it. The following example shows how this is done by calling the function "main" with a month string followed by a year.

Example B.10:

```
#include <iostream.h>
void main(int argc, char *argv[]){
    if (argc <3)
        cout << "You must enter the month and year!" << endl;
    else
        cout << "The month is: "<<argv[1]<< endl;
        cout << "The year is: "<< argv[2] <<endl;
}
```

Output:

```
Enter: exd12 "September" "1999"

The month is: September
The year is: 1999
```

B.3 Object-Orientation

In order to discuss object orientation, we must first define what an object is. For most readers familiar with imperative language programming, an object is looked upon as a variable. But in the object-oriented world, an object is something that not only represents a value but also its behavior. For example, we can have an object called list. This list would not only contain the items within it but it would also represent the "behavior" of maintaining itself. In particular, this list object can contain methods that would add and delete items.

Another example of an object is a random walk. This random walk can have data that indicates its current position as well as how many steps it is currently taken. This random walk object can also have methods that perform the steps as well as functionality used to determine when a border is reached.

Why Object-Oriented Programming?

Object-oriented programming emerged out of the need to compensate for the problems associated with *procedural* languages. Procedural languages, as defined in [6] are designed such that "...programs are organized around control structures such as iteration and procedure invocation." What this means is that procedural language

programs are simply a list of instructions that have the following principles [7]:

- single entry, single exit
- clearly defined inputs and outputs
- top-down hierarchical decomposition
- modular design for easy modification and reuse
- only sequence, selection, case, and iteration constructs.

For most small programs, procedural languages are suitable but as programs become larger and more complex, procedural programs become more difficult to change, debug, and adapt. Take a look at Fig. B.1 which describes the procedural paradigm [8].

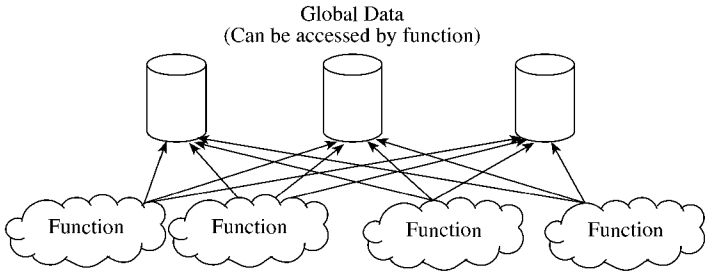

Figure B.1
Procedural programming paradigm.

As Fig. B.1 indicates, a procedural program is based on functions operating on data. The larger the program, the more functions there are that operate on the data. The problem here is that it becomes quite easy to have a function that corrupts the data shared by other functions. This can happen in several ways. A new programmer on a programming team for a large project may not be fully aware of the impact of a new function written, thereby inadvertently causing undesirable results. Another way of corrupting the data would be for a data structure to change without completely updating the rest of the program. For large programs, this is a daunting task. Every function that accessed the data structure needs to be modified to reflect the new changes.

Continuing our discussion on the limitations of procedural programming, take notice of Fig. B.2 which describes the object-oriented programming paradigm. The first point to make is that programs are organized in objects expressed as classes. Each class is composed of data and member functions that operate on the data. Given this object-centric approach to programming, both cases which would be problematic in a procedural language are inherently addressed in C++. For instance, any additional functions or data structure changes will benefit from the organized objects; the impact of the additional function is foreseen based on deciding which class it is a member of; and updates of objects due to data structure changes are tractable since it is known which members have access to it.

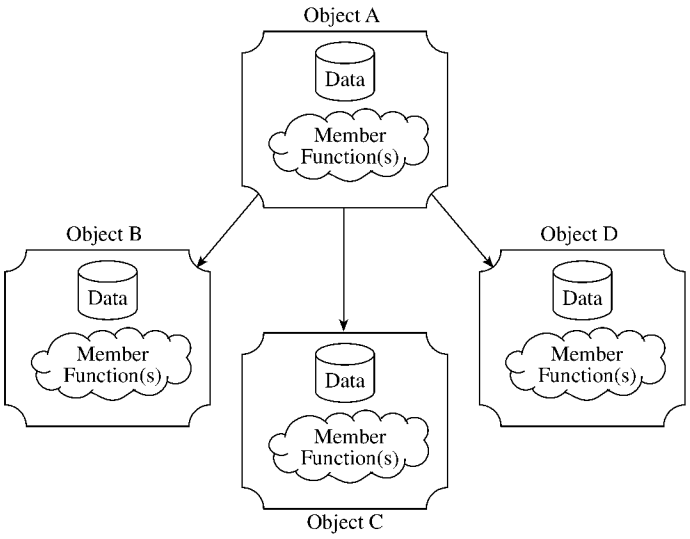

Figure B.2
Object-Oriented programming paradigm.

A. Inheritance

Inheritance is the process of having one object "inherit" data, functionality, etc. from another object. Taking another look at Fig. B.2, objects B, C, and D inherit from object A. Object A is known as the *base class* and objects B, C, and D are called *derived classes.*

Taking our random walk object described earlier, suppose we call this our "parent" object. Examples of "child" objects are floating random walk and fixed random walk. This parent-child relationship is such that both the floating random walk and fixed random walk objects inherit the mechanisms that represent their current location and amount of steps. Another inherited feature is the boundary checking functionality. Figure B.3 should help to drive this point home.

B. Polymorphism

Polymorphism is best described using functions. Recall our random walk object. In particular, the method used to perform steps. What if this method was aptly called "step." Now, since there are various types of walks (floating, fixed, etc.) with each differing by how they get to the border. The step method would need to act differently based on the type of object it was. For example, if it were a floating random walk object, it would have to take a step by picking a random point on a circle with radius set to the shortest distance to the border; but if it were a fixed random walk object, it would randomly choose one of four directions to step (simply north, south, east, or west). It is how the step method acts based on the object that invoked it that exemplifies

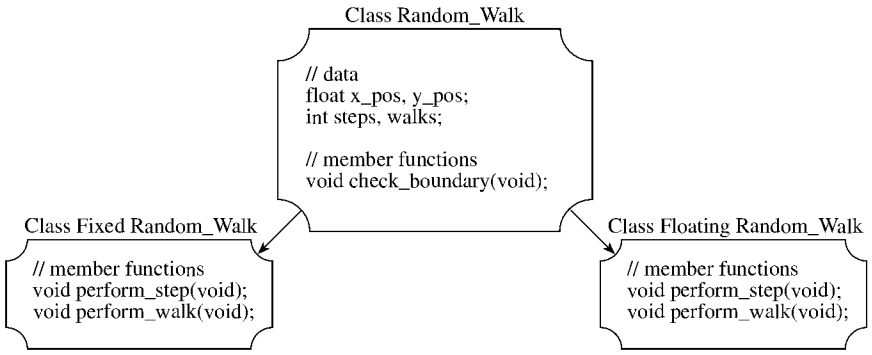

Figure B.3
Example illustrating inheritance.

polymorphism. The process of how the compiler knows which step member function to run is called *dynamic binding*.

C. Data Abstraction

Data abstraction is the concept of having data and methods that act on that data exist within one conceptual unit (namely a class). This concept of having data and "datacentric" methods existing within a single syntactic entity has at least two advantages:

- program modification is localized to this single class
- code changes pertaining to the encapsulated pieces can be changed in one area without being visible to the rest of the program and without affecting its behavior.

The simplest example to give about data abstraction is the common ***float*** data type. Here, the C++ language allows you to declare a float variable but it does not allow you to modify its floating-point representation. The language also allows you to add floating-point numbers but there is no way for you to write a program to change *how* the addition is performed.

D. Encapsulation

Encapsulation (also called data hiding) is the act of hiding object information details with various levels of access. Using our ***float*** example again, the floating-point representation as well as the mathematical operation details are *encapsulated*.

Using the class example in Fig. B.3. The encapsulation language feature allows an object to have members that are exclusive to just itself, derived objects, or the "public." Using the random walk example, the floating random walk object uses a

data member "walk" from the class Random_Walk (see Fig. B.3) that specifies the amount of times it has reached a border. Since the class Floating_Random_Walk inherits from the class Random_Walk, it now has an int variable named "walk" that it can use in its function "perform_walk." The data member "walk" is inherited. If the variable "walk" was made ***private***, derived classes would not be able to access it.

E. Overloading

Operator overloading is the process of changing the meaning of an operator. For instance, the add operator "+" naturally adds two numbers. This operator can be "overloaded" to work (or operate) on any type of object. Suppose we want to add two matrix objects. There is no built in functionality for adding two matrices. What needs to be done is to overload the "+" operator such that an element-by-element addition is performed. A more detailed look here requires looking at the matrix object as having a "+" method that operates on similar matrix objects such that the following expression:

matrixA + matrixB

calls the '+' method of matrixA with matrixB as a parameter.

B.4 C++ Object-Oriented Language Features

The C++ language has built-in features which support object-oriented programming. Namely classes, operator overloading, virtual functions, templates, and exception handling. What follows is a brief description of each language feature along with supporting examples.

A. Classes

The use of classes is a major language feature that supports object-oriented programming. For a solid concise look at classes the reader is referred to [5]. A class can be looked at as a more powerful ***struct***. This is what a class declaration looks like:

class class_name{
private:
    private data and methods
public:
    public data and methods
protected:
    protected data and methods
} object names;

where,

private- indicates that these data items are to be accessible to the object itself; no children or any other part of the program. ***Private*** is the ***default*** access if none are indicated.

public- the data items are accessible to all derived classes.

protected- it is an otherwise private member that can be used only by itself and other objects that inherit them.

Example B.11: This example illustrates the relationship between public and private members of a class.

```
#include<iostream.h>
#include<math.h>

class myclass{
    double num; // all unspecified sections are assumed by the compiler to be private
public:
    void set_num(double);     // sets the value of num
    void print_num(void);   // prints the value of num
    void get_tan(void);    // computes num = tan(num)
    void times2(void);     // computes num = 2*num
};

// now it's time to define the functions
void myclass::set_num(double val){
    num = val;
}
void myclass::print_num(void){
    cout << "The number is: " << num << endl;
}
void myclass::get_tan(void){
    num = tan(num);
}
void myclass::times2(void){
    num = 2*num;
        }
        void main(){
            myclass C;              // instantiate a myclass object named C
            C.set_num(3.1415);  // num = 3.1415
            C.print_num();
            C.get_tan();            // num = -92.65E-6
            C.print_num();
            C.times2();             // num = -185.3E-6
            C.print_num();
        }
```

Output:

```
The number is: 3.1415
The number is: -9.26536e-005
The number is: -0.000185307
```

Notice that in this example all member functions have access to the variable "num."

Constructors and Destructors

Within every class, member functions called a *constructor* and *destructor* exist. A constructor is used to initialize class variables or allocate memory storage. A destructor is used to return memory allocated. Constructors can accept arguments and can be overloaded while destructors cannot. The constructor takes on the same name as the class in which it exists while the destructor has the class name preceded with a "~" character. The compiler automatically creates a constructor and destructor whenever they are not defined.

Example B.12:

```
#include<iostream.h>
#include<math.h>

class myclass{
     double num; // all unspecified sections are assumed by the compiler to be private
public:
     myclass(double val) { cout << "Constructor Executed.\n"; num=val;};
     ~myclass(){cout << "Destructor Executed.\n";};
     void print_num(void);  // prints the value of num
     void get_tan(void);    // computes num = tan(num)
     void times2(void);     // computes num = 2*num
};
void myclass::print_num(void){
     cout << "The number is: " << num << endl;
}
void myclass::get_tan(void){
     num = tan(num);
}
void myclass::times2(void){
     num = 2*num;
}
void main(){
     myclass C(3.1415);  // instantiate a myclass object named C setting num to 3.1415
     C.print_num();
     C.get_tan();          // num = -92.65E-6
     C.print_num();
     C.times2();           // num = -185.3E-6
     C.print_num();
}
```

Output:

```
Constructor Executed.
The number is: 3.1415
The number is: -9.26536e-005
The number is: -0.000185307
Destructor Executed.
```

As illustrated in the example, the constructor and destructor are executed automatically every time the class is instantiated. This example also illustrates how a constructor is overloaded and takes a parameter to initialize the variable "num."

B. Operator Overloading

As described earlier, operator overloading takes place when a standard operator is redefined to mean something else. The syntax for overloading an operator is:

type ***operator*** overloaded_operator(parameter list)

Operator overloading can only occur from within the object that the method exists.

Member functions can also be overloaded. It is possible to have several member functions with the same name behaving differently. The one condition is that they must differ at least in the arguments they each take.

The following example is a class which converts from polar form to rectangular form and the reverse.

Example B.13:

```
#include <ostream.h>
#include <math.h>
// Create a Cartesian and polar structure
struct cartesian{ double x_pos,y_pos;}; struct polar{ double angle, magnitude;};
class myclass{
      polar pval; cartesian cval;
public:
      // constructor is overloaded
      myclass(cartesian cart){cval.x_pos=cart.x_pos;cval.y_pos=cart.y_pos;      pval.magnitude=0;pval.angle=0;};
      myclass(polar pol){pval.angle=pol.angle;pval.magnitude=pol.magnitude;  cval.x_pos=0;cval.y_pos=0;};
      // convert is overloaded; one takes polar the other takes cartesian
      void convert(polar);       void convert(cartesian);  void print_vals(void);};
void myclass::convert(polar pol){
      cval.x_pos=pol.magnitude*cos(pol.angle);   cval.y_pos=pol.magnitude*sin(pol.angle);}
void myclass::convert(cartesian cart){
      pval.angle = atan(cart.y_pos/cart.x_pos);      pval.magnitude = sqrt(pow(cart.y_pos,2)+pow(cart.x_pos,2));}
void myclass::print_vals(void){
      cout << "  x_pos: " << cval.x_pos << "  y_pos: "<< cval.y_pos << endl;
      cout << "  magnitude: " << pval.magnitude << "  angle: "<< pval.angle << endl;}
void main(){
      polar p;   p.magnitude = 10;  p.angle = 45;
      myclass X(p);
      cout << "Before Polar Conversion:\n";
      X.print_vals();X.convert(p); // convert the polar point to cartesian
      cout << "\nAfter Polar Conversion:\n";
      X.print_vals();
      cartesian c; // C++ is case sensitive so c is different from C
      c.x_pos = 15.5;      c.y_pos = 22.5;
      myclass Y(c);
      cout << "\nBefore Cartesian Conversion:\n";
      Y.print_vals();Y.convert(c); // convert the cartesian point to polar
      cout << "\nAfter Cartesian Conversion:\n";
      Y.print_vals();
}
```

Output:

```
Before Polar Conversion:
  x_pos: 0  y_pos: 0
  magnitude: 10  angle: 45

After Polar Conversion:
  x_pos: 5.25332  y_pos: 8.50904
  magnitude: 10  angle: 45

Before Cartesian Conversion:
  x_pos: 15.5  y_pos: 22.5
  magnitude: 0  angle: 0

After Cartesian Conversion:
  x_pos: 15.5  y_pos: 22.5
  magnitude: 27.5222  angle: 0.967566
```

C. Templates

For action that is the same for different data types, two options exist for implementing this case scenario. One option is to write a different class or function for each data type. Another option is to use templates to create generic functions and classes.

The following example illustrates this point. Suppose we want to swap two numbers. There has to be a different function for each type of number (an int, float,

double, etc.). What template functions allow us to do is create one function that acts independently of the data type it works on.

Example B.14:

```
// the use of a template function to
// swap values of any type
#include <ostream.h>

template <class type1>                  // no line can exist between the template keyword
void swapper(type1 &x, type1 &y) {      // and the function
    type1 z;                            // the '&' is used to reference the variable; meaning to
    z = x;                              // modify the variable itself not a copy of it.
    x = y;
    y = z;
}
void main(){
    int a = 1, b = 2;
    float i = 3.14F, d = 4.22F;
    cout << "Before swapping: \n";
    cout << "a = 1,   b = 2\n";
    cout << "i = 3.15, d = 4.22\n\n";
    swapper(a,b);
    swapper(i,d);
    cout << "After swapping: \n";
    cout << "a = " << a << " b = " << b << endl;
    cout << "i = " << i << " d = " << d << endl;
}
```

Output:

```
Before swapping:
a = 1,   b = 2
i = 3.15, d = 4.22

After swapping:
a = 2 b = 1
i = 4.22 d = 3.14
```

D. Exception Handling

Exception handling is a language feature that allows a programmer to have specific functionality executed given a particular error occurs. In the object-oriented world this is known as is *throwing* and *catching* exceptions.

Syntax:

```
try {
    // put code here that you want to trap erros
}
```

```
catch (type argument) {
    // code the execute in the event an exception is thrown.
}
more catch functions can follow...
```

Here is a simple example illustrating the use of exception handling. What it does is "throw" an exception immediately after it is found that a matrix element is negative.

Example B.15:

```
#include <iostream.h>
void main(){

    int int_matrix[5][5]={1,2,3,4,5,2,4,-6,8,10};
    int x,y;

    try{  // try block
        for (x=0;x<5;x++){
            for (y=0;y<5;y++){
                if (int_matrix[x][y] < 0)
                    throw (int_matrix[x][y]);    // exception thrown

                    // any code below this line (in this try block)
                    // will not execute if an exception has been
                    // thrown.
                cout << " Element["<<x<<"]"<<"["<<y<<"] = "<<int_matrix[x][y]<<endl;
            }
        }
    }

    catch(int ex_type){
        cout << "\nException Caught.  The type is: " << ex_type<<endl;
    }
}
```

Output:

```
Element[0][0] = 1
Element[0][1] = 2
Element[0][2] = 3
Element[0][3] = 4
Element[0][4] = 5
Element[1][0] = 2
Element[1][1] = 4

Exception Caught.  The type is: -6
```

E. Files and Streams

We all know what a file is, but what is a *stream?* In C++, a *stream* is a logical interface from which all I/O is operated through. The relationship between a file and a stream is one where a stream is associated and disassociated with a file through the "open" and "close" operations.

The following example creates a file with records where each record contains the following information:

- Coordinate value (x,y).
- Angle made with the x-axis (degrees).
- sine of the first-quadrant angle.

The file is then read back and the info is echoed out. Several concepts are illustrated in this example. Namely, the following:

- How to open a file for writing.
- How to open a file for reading.
- How to overload the extraction operator (<<).
- How to overload the insertion operator (>>).

Example B.16:

```
#include <iostream.h>
#include <fstream.h>
#include <math.h>
#include <stdlib.h>

#define PI 3.14159265

class point{
      double angle_rad;      // angle in radians
public:
      point(){};
      point(double xval,double yval){x=xval;y=yval;angle=0;sine_val=0;cosine_val=0;};
```

```
        double x,y;             // point ordinate values
        double angle;           // the angle formed with the x-axis
        double sine_val;        // the sin of the angle
        double cosine_val;      // the cosine of the angle
        void get_angle();       // get the angle from the point
        void get_cos();         // get the cos of the angle
        void get_sin();         // get the sin of the angle
};

void point::get_angle(void){
        angle_rad = atan(y/x);
        angle = atan(y/x)*180/PI;
}

void point::get_cos(){
        cosine_val = cos(angle_rad);
}

void point::get_sin(){
        sine_val = sin(angle_rad);
}

// overload the insertion operator
ostream &operator<<(ostream &ostr, point pt)
{
        ostr << pt.x <<" ";
        ostr << pt.y << " ";
        ostr << pt.angle << " ";
        ostr << pt.sine_val << " ";
        ostr << pt.cosine_val<< " ";
        return ostr;
}
// overload the extraction operator
istream &operator>>(istream &istr, point &pt)
{
        double val;
        istr >> pt.x;
        istr >> pt.y;
        istr >> pt.angle;
        istr >> pt.sine_val;
        istr >> pt.cosine_val;
        return istr;
}
void main()
{

    point p1(1,1), p2(2,2), p3(3,3);
    point p4, p5, p6;
    p1.get_angle(); p1.get_sin();
    p2.get_angle(); p2.get_sin();
    p3.get_angle(); p3.get_sin();

    ofstream out("example.out");
    if (!out)
    {
        cout << "Error with creating output file 'example.out.'\n";
        exit(0);
    }
```

```
    out << p1;
    out << p2;
    out << p3;
    out.close();

    ifstream in("example.out");
    if (!in)
    {
        cout << "Error with opening file 'example.out.'\n";
        exit(0);
    }

    in >> p4;
    in >> p5;
    in >> p6;
    in.close();

    cout << "Point: (" << p4.x << "," << p4.y << ")" << endl;
    cout << "Angle: " << p4.angle << endl;
    cout << "Sin(angle): " << p4.sine_val << endl;
    cout << "Point: (" << p5.x << "," << p5.y << ")" << endl;
    cout << "Angle: " << p5.angle << endl;
    cout << "Sin(angle): " << p5.sine_val << endl;
    cout << "Point: (" << p6.x << "," << p6.y << ")" << endl;
    cout << "Angle: " << p6.angle << endl;
    cout << "Sin(angle): " << p6.sine_val << endl;

}
```

Output:

```
Point: (1,1)
Angle: 45
Sin(angle): 0.707107
Point: (2,2)
Angle: 45
Sin(angle): 0.707107
Point: (3,3)
Angle: 45
Sin(angle): 0.707107
```

B.5 A Final Note

The C++ programming language is powerful. What comes with this power is the required complexity to tap into it. For a more comprehensive view of C++ with annotations and commentaries, [9] is the clear choice. Since becoming a solid C++ programmer requires practice and guidance, I recommend [10]–[12] for gaining good insight in solid design. As your skill increases, at some time you may come across obscure, subtle issues with C++. In these instances, you will find [13] a valued addition to your library. Furthermore, for a more advanced discussion on templates,

[14] is a good place to start. Finally, any confusion with object-orientation in general should be cleared with the help of [15, 16].

References

[1] Plauger, P.J., *The Standard C Library.* Englewood Cliffs, NJ: Prentice-Hall, 1992.

[2] Plauger, P.J., *The Draft Standard C++ Library.* Upper Saddle River, NJ: Prentice-Hall, 1995.

[3] Schildt, H., *C++ from the Ground Up.* Berkeley, CA: Osborne McGraw-Hill, 1994, p. 41.

[4] Stroustrup, B., *The C++ Programming Language.* 3rd ed., Reading, Massachusetts: Addison-Wesley Publishing Company, 1997, pp. 119–121.

[5] Pappas, C.H., Murray, W.H., *Borland C++ Handbook.* Berkeley, CA: Osborne McGraw-Hill, 1991, pp. 160–171.

[6] Finkel, R.A., *Advanced Programming Language Design.* Menlo Park, CA: Addison-Wesley Publishing Company, 1996, p. 267.

[7] Cezzar, Ruknet, *A Guide to Programming Languages: Overview Comparison,* Norwood, MA: Artech House, Inc., 1995, p. 263.

[8] Lafore, R., *Object-Oriented Programming in Microsoft C++.* CA: Waite Group Press, 1993, pp. 5–6.

[9] Ellis, M.A., Stroustrup, B., *The Annotated C++ Reference Manual.* Reading, MA: Addison-Wesley Publishing Company, 1990.

[10] Meyers, *Effective C++: 50 Specific Ways to Improve Your Programs and Designs.* MA: Addison-Wesley Publishing Company, Inc., 1992.

[11] Meyers, *More Effective C++: 35 new Ways to Improve Your Programs and Designs.* Massachusetts: Addison-Wesley Publishing Company, Inc., 1996.

[12] Eckel, B., "C++ Programming Style Guides," Unix Review, March 1995, pp. 43–54.

[13] Eckel, B., *C++ Inside & Out.* Berkeley, CA: Osborne McGraw-Hill, 1993.

[14] Glass, G., Schuchert, Brett, *The STL <Primer>.* New Jersey: Prentice-Hall, 1996.

[15] Khoshafian, S., Abnous, R., *Object Orientation: Concepts, Languages, Databases, User Interfaces*. New York: John Wiley & Sons, Inc., 1990, pp. 6–10.

[16] Meyer, Bertrand, *Object-Oriented Software Construction*, 2nd ed., Upper Saddle River, NJ: Prentice-Hall, 1997.

Appendix C

Numerical Techniques in C++[1]

What follows are four programs that exemplify some of the concepts covered in the previous appendix on C++. Each program applies a different numerical technique to solving particular kinds of problems in electromagnetics. The methods are namely:

1) Finite Difference

2) Finite Element

3) Transmission-line-matrix

4) Monte Carlo Fixed-Random walk

Listings 1 to 4, respectively, correspond to the FORTRAN programs in Figure 3.31 on FDTD, Figure 6.10 on the finite element method, Figure 7.14 on TLM, and Figure 8.13 on the Monte Carlo method.

[1]Written by Raymond C. Garcia, Georgia Institute of Technology, Atlanta, GA 30332-0320.

Listing 1: Finite Difference Program:

```
#include <iostream.h>
#include <fstream.h>
#include <math.h>


#define IMAX 19
#define JMAX 39
#define KMAX 19
#define ITER 100
#define NMAX 2
#define NHW 40
#define MED 2
#define JS 3
const double DELTA = 3E-3;
const double CL = 3.0E8;
const double F = 2.5E9;
const double PIE = 3.141592654;

// scatter dimensions
#define OI 19.5
#define OJ 20
#define OK 19
#define RADIUS 15

class matrix{
   int a,b,c,d;
   int amax,bmax,cmax,dmax;
   float *data;
   int checkMinus(int index);
   void getSize(void){cout << amax <<"x"<<
   bmax <<"x"<< cmax <<"x"<< dmax << endl;}
public:
   // constructors
   matrix();
   matrix(int s);
   matrix(int d1,int d2);
   matrix(int d1,int d2,int d3);
   matrix(int d1,int d2,int d3, int d4);

   void dumpit();

   // overload the parens
   float &operator()(int a);
   float &operator()(int a,int b);
   float &operator()(int a,int b,int c);
   float &operator()(int a,int b,int c, int d);
};


matrix::matrix(){
   cout << "void constructor\n";
}
```

```
matrix::matrix(int s){
    data = new float[s];
    amax=s,bmax=0,cmax=0,dmax=0;
    for (a=0;a<amax;a++)
        data[a]=0;
}

matrix::matrix(int d1,int d2){
    data = new float[d1*d2];
    amax=d1; bmax=d2,cmax=0,dmax=0;

    for(a=0;a<d1;a++)
        for(b=0;b<d2;b++)
            data[a*d2 + b]=0;
}

matrix::matrix(int d1,int d2,int d3){
    data = new float[d1*d2*d3];
    amax=d1; bmax=d2; cmax=d3,dmax=0;

    for(a=0;a<d1;a++)
        for(b=0;b<d2;b++)
            for(c=0;c<d3;c++)
                data[a*d2*d3 + b*d3 + c]=0;
}

matrix::matrix(int d1,int d2,int d3, int d4){
    data = new float[d1*d2*d3*d4];
    amax=d1; bmax=d2; cmax=d3; dmax=d4;

    for(a=0;a<d1;a++)
        for(b=0;b<d2;b++)
            for(c=0;c<d3;c++)
                for(d=0;d<d4;d++)
                    data[a*d2*d3*d4 + b*d3*d4 + c*d4 + d]=0;
}


void matrix::dumpit(){

    if (bmax==0){
        for (a=0;a<amax;a++)
            cout <<   data[a] << endl;
    }
    else if (cmax==0){
        for(a=0;a<amax;a++){
            for(b=0;b<bmax;b++)
                cout <<   data[a*bmax + b]<<" ";
            cout << endl;
        }
```

```
}
else if (dmax==0){
    for(a=0;a<amax;a++){
        for(b=0;b<bmax;b++){
            for(c=0;c<cmax;c++)
                cout << data[a*bmax*cmax + b*cmax + c]<<" ";
            cout << endl;
        }
        cout << endl;
    }
}
else{
        for(a=0;a<amax;a++){
            for(b=0;b<bmax;b++){
                for(c=0;c<cmax;c++){
                    for(d=0;d<dmax;d++)
                        cout << data[a*bmax*cmax*dmax
                        + b*cmax*dmax + c*dmax + d]<<" ";
                    cout << endl;
                }
                cout << endl;
            }
            cout << endl;
        }
    }
}

int matrix::checkMinus(int index){
    if (index < 0){
        //getSize();
        return 0;
    }
    else
        return index;
}

float & matrix::operator()(int a)
{a = checkMinus(a);return data[a];}
float & matrix::operator()(int a,int b)
{a = checkMinus(a); b=checkMinus(b);return data[a*bmax + b];}
float & matrix::operator()(int a,int b,int c){
    a=checkMinus(a);
    b=checkMinus(b);
    c=checkMinus(c);
    return data[a*bmax*cmax + b*cmax + c];
}
float & matrix::operator()(int a,int b,int c, int d){
    a=checkMinus(a);
    b=checkMinus(b);
    c=checkMinus(c);
    d=checkMinus(d);
    return data[a*bmax*cmax*dmax + b*cmax*dmax + c*dmax + d];
}
```

```
class pdesc{
   int a,b,c,d;
   double e0;  // permitivity
   double u0;  // permeability
   double dt;
   double r;
   double ra;
   double rb;
   double tpifdt;

   matrix ex, ey, ez;
   matrix hx, hy, hz;
   matrix ey1, ez1;
   matrix er, sig;
   matrix ca, cb;
   matrix ixmed, iymed, izmed;
   matrix cbmrb;


   // methods
   double position(double ri,double rj,double rk){
       return( sqrt(pow((ri-OI),2) + pow((rj-OJ),2)
       + pow((rk-OK),2) ) );
   };

public:

   // constructor
   pdesc():ex(IMAX+1,JMAX+1,KMAX+1,NMAX+1),
          ey(IMAX+1,JMAX+1,KMAX+1,NMAX+1),
          ez(IMAX+1,JMAX+1,KMAX+1,NMAX+1),
          hx(IMAX+1,JMAX+1,KMAX+1,NMAX+1),
          hy(IMAX+1,JMAX+1,KMAX+1,NMAX+1),
          hz(IMAX+1,JMAX+1,KMAX+1,NMAX+1),
          ey1(JMAX+1),
          ez1(JMAX+1),
          er(MED),
          sig(MED),
          ca(MED),
          cb(MED),
          ixmed(IMAX+1,JMAX+1,KMAX+1),
          iymed(IMAX+1,JMAX+1,KMAX+1),
          izmed(IMAX+1,JMAX+1,KMAX+1),
          cbmrb(2)
```

```
    {
        e0=(1e-9)/(36*PIE);  // permitivity
        u0=(1e-7)*4*PIE;
        dt=DELTA/(2*CL);
        r=dt/e0;
        ra=pow(dt,2)/(u0*e0*pow(DELTA,2));
        rb=dt/(u0*DELTA);
        tpifdt = 2*PIE*F*dt;

        er(0)=1.0;er(1)=4.0;
        sig(0)=0.1;sig(1)=0;
    }

    void compute_media_parms(); // step #1
    void gen_field_components(); // step #2
    void create_output(char*);
};

void pdesc::create_output(char* fname)
{
    int j;
    ofstream out(fname);
    if (!out)
        cout << "There is a problem with opening a file.\n";

    cout << "ey1\n";
    out << "ey1\n";

    for (j=0;j<=JMAX;j++){
        out << ey1(j);
        cout << ey1(j);
    }

    cout << "\nez1\n";
    out << "\nez1\n";


    for (j=0;j<=JMAX;j++){
        out << ez1(j);
        cout << ez1(j);
     }
     cout << endl;

 }
 void pdesc::gen_field_components()
 {
     // since only field components at current time (t)
     // and previous two time steps (t-1 and t-2) are
     // required for computation,

     // we save memory space by using the following indices
     // ncur is index in for time t
     // npr1 is index in for t-1
     // npr2 is index in for t-2
```

```
int ncur = 2, npr1 = 1,npr2 = 0;
int i,j,k,nn;  // loop indices
double m,cam,temp;

for (nn =1; nn<=ITER; nn++){
   if ((nn % 10) == 0)
      cout << "Iteration Count: " << nn << endl; // status

   npr2 = npr1;
   npr1 = ncur;
   ncur = (ncur+1) % 3;

   for (k=0; k<=KMAX;k++)
      for (j=0; j<=JMAX;j++){
         for (i=0;i<=IMAX;i++){
            if (i == 0){ // x=delta/2
               if ((k != KMAX) && (k != 0)){
                  hy(0,j,k,ncur) = (hy(1,j,k-1,npr2) +
                                    hy(1,j,k,npr2) +
                                    hy(1,j,k+1,npr2))/3;
                  hz(0,j,k,ncur) = (hz(1,j,k-1,npr2) +
                                    hz(1,j,k,npr2) +
                                    hz(1,j,k+1,npr2))/3;
               }
               else if (k == KMAX){
                     hy(0,j,KMAX,ncur) =
                     (hy(1,j,KMAX-1,npr2) +
                     hy(1,j,KMAX,npr2))/2;
                     hz(0,j,k,ncur) = (hz(1,j,k-1,npr2) +
                                       hz(1,j,k,npr2))/2;
               }
               else {
                  hy(0,j,k,ncur) = (hy(1,j,k,npr2) +
                                    hy(1,j,k+1,npr2))/2;
                  hz(0,j,0,npr2) = (hz(1,j,0,npr2) +
                                    hz(1,j,1,npr2))/2;
               }
            }
            if (j==0){ // y = 0
               ex(i,0,k,ncur) = ex(i,1,k,npr2);
               ez(i,0,k,ncur) = ez(i,1,k,npr2);
            }
            else if (j == JMAX){ // y = ymax
               ex(i,JMAX,k,ncur) = ex(i,JMAX-1,k,npr2);
               ez(i,JMAX,k,ncur) = ez(i,JMAX-1,k,npr2);
            }
            if (k == 0){ // z=0
               if ((i != 0) && (i != IMAX)){
```

```
                        ex(i,j,0,ncur) = (ex(i-1,j,1,npr2) +
                                          ex(i,j,1,npr2) +
                                          ex(i+1,j,1,npr2))/3;
                        ey(i,j,0,ncur) = (ey(i-1,j,1,npr2) +
                                          ey(i,j,1,npr2) +
                                          ey(i+1,j,1,npr2))/3;
                    }
                    else if (i == 0){
                        ex(0,j,0,ncur) = (ex(0,j,1,npr2) +
                                          ex(1,j,1,npr2))/2;
                        ey(i,j,0,ncur) = (ey(i,j,1,npr2) +
                                          ey(i+1,j,1,npr2))/2;
                    }
                    else{
                        ex(i,j,0,ncur) = (ex(i-1,j,1,npr2) +
                                          ex(i,j,1,npr2))/2;
                        ey(i,j,0,ncur) = (ey(i-1,j,1,npr2) +
                                          ey(i,j,1,npr2))/2;
                    }
                }
//
//      (iii) apply FD/TD algorithm
//
                // hx generation
                hx(i,j,k,ncur) = hx(i,j,k,npr1) +
                                 rb*(ey(i,j,k+1,npr1) -
                                 ey(i,j,k,npr1) +
                                 ez(i,j,k,npr1) -
                                 ez(i,j+1,k,npr1));
                // hy generation
                hy(i,j,k,ncur) = hy(i,j,k,npr1) +
                                 rb*(ez(i+1,j,k,npr1) -
                                 ez(i,j,k,npr1) +
                                 ex(i,j,k,npr1) -
                                 ex(i,j,k+1,npr1));
                // hz generation
                hz(i,j,k,ncur) = hz(i,j,k,npr1) +
                                 rb*(ex(i,j+1,k,npr1) -
                                 ex(i,j,k,npr1) +
                                 ey(i,j,k,npr1) -
                                 ey(i+1,j,k,npr1));
                // k = kmax  : symmetry
                if (k == KMAX){
                    hx(i,j,KMAX,ncur) = hx(i,j,KMAX-1,ncur);
                    hy(i,j,KMAX,ncur) = hy(i,j,KMAX-1,ncur);
```

```
}
// ex generation
if ((j != 0) && (j != JMAX) && (k != 0)){
   m = ixmed(i,j,k);
   ex(i,j,k,ncur) = ca(m)*ex(i,j,k,npr1) +
                    cbmrb(m)*(hz(i,j,k,ncur) -
                              hz(i,j-1,k,ncur) +
                             hy(i,j,k-1,ncur) -
                             hy(i,j,k,ncur));
}
// ey generation
if (k != 0){
   m = iymed(i,j,k);
   ey(i,j,k,ncur) = ca(m)*ey(i,j,k,npr1) +
                    cbmrb(m)*(hx(i,j,k,ncur) -
                              hx(i,j,k-1,ncur) +
                             hz(i-1,j,k,ncur) -
                             hz(i,j,k,ncur));
}
// ez generation
if ((j != 0) && (j != JMAX)){
   m = izmed(i,j,k);
   // sig(ext) = for Ez only from Taflove[14]
   if (m == 1)
      cam = 1;
   else
      cam = ca(m);

   ez(i,j,k,ncur) = cam*ez(i,j,k,npr1) +
                    cbmrb(m)*(hy(i,j,k,ncur) -
                             hy(i-1,j,k,ncur) +
                             hx(i,j-1,k,ncur) -
                             hx(i,j,k,ncur));

   // (iv) apply the plane-wave source
   if (j == JS)
      ez(i,JS,k,ncur) = ez(i,JS,k,ncur) +
      sin(tpifdt*nn);
}
if (j == IMAX){ // i = imax +1/2 : symmetry
   ey(IMAX+1,j,k,ncur) = ey(IMAX,j,k,ncur);
   ez(IMAX+1,j,k,ncur) = ez(IMAX,j,k,ncur);
```

```
                    }
                    if (k == KMAX){ // k = kmax
                        ex(i,j,KMAX+1,ncur) = ex(i,j,KMAX-1,ncur);
                        ey(i,j,KMAX+1,ncur) = ey(i,j,KMAX-1,ncur);
                    }
                    }
                //-------------------------------------------------
                // Step 4 - retain the maximum absolute values
                //          during the last half-wave
                //-------------------------------------------------
                if ((k== KMAX) && (nn > (ITER-NHW))){
                    temp = abs(ey(IMAX,j,KMAX-1,ncur));
                    if (temp > ey1(j))
                        ey1(j) = temp;
                    temp = abs(ez(IMAX,j,KMAX,ncur));
                    if (temp > ez1(j))
                        ez1(j) = temp;
                }
            }
        }

}
void pdesc::compute_media_parms()
{
    int m,i,j,k;

    for (m=0;m<MED;m++){
        ca(m)=1-r*sig(m)/er(m);
        cb(m)=ra/er(m);
        cbmrb(m) = cb(m)/rb;
    }

  //  (i) Calculate the real/actual grid points
  // Initialize the media arrays.  Index (m) determines
  // which medium each point is actually located in and
  // is used to index into arrays which determine the
  // constitutive parameters of the medium.  There are
  // separate M determining arrays as opposed to computing
  // them each time they are needed saves a large amount
  // of computation time.

    for (i=0;i<=IMAX;i++)
        for (j=0;j<=JMAX;j++)
            for (k=0;k<=KMAX;k++){
                if (position(i+.5,j,k) <= RADIUS)
                    ixmed(i,j,k) = 1;
                else
                    ixmed(i,j,k) = 0;
```

```
            if (position(i,j+.5,k) <= RADIUS)
               iymed(i,j,k) = 1;
            else
               iymed(i,j,k) = 0;

            if (position(i,j,k+.5) <= RADIUS)
               izmed(i,j,k) = 1;
            else
               izmed(i,j,k) = 0;
         }
}

void main()
{

   pdesc prob1;


   prob1.compute_media_parms(); // step #1
   prob1.gen_field_components(); // step #2
   prob1.create_output("fd1.out");
}
```

Listing 2: Finite Element Program:

```
// Finite Element solution of Laplace's Equation for
// two-dimensional Problems
// Triangular elements are used.
//
// The Unknown potentials are obtained using
// the iteration method.

/*************************************************************/
/***********         Variable Descriptions        ***********/
/*************************************************************/
/** ND = # of nodes                                          **/
/** NE = # of Elements                                       **/
/** NP = # of Fixed nodes ( where potential is Prescribed  **/
/** NDP(I) = Node # of prescribed potential, I = 1,2,...NP **/
/** VAL(I) = Value of prescribed potential at node NDP(I)  **/
/** NL(I,J) = List of nodes for each element I, where      **/
/** LF(I) = List of free nodes I = 1,2,...,NF = ND - NP    **/
/** J = 1, 2, 3, is the local node number                    **/
/** CE(I,J) = Element Coefficient Matrix                     **/
/** ER(I) = Value of the relative permittivity for           **/
/**         element I                                        **/
/** C(I,J) = Global Coefficient Matrix                       **/
/** X(I), Y(I) = Global Coordinates of Node I                **/
/** XL(J), YL(J) = Local Coordinates of Node J = 1,2,3     **/
/** V(I) = Potential at node I                               **/
/** Matrices P(I) and Q(I) are Defined earlier in the text **/
/*************************************************************/

/*******************************************************/
/****************** Please Note ********************/
/*******************************************************/
/**                                                   **/
/** This program assumes the input data is in a file **/
/** called "fem.in" in the following format:          **/
/**                                                   **/
/**           NE        ND        NP            **/
/**      NL(I,1)   NL(I,2)   NL(I,3)            **/
/**                    ...                 **/
/**                    ...                          **/
/**                    ...                          **/
/**      NL(I+a,1) NL(I+a,2) NL(I+a,3)          **/
/**      X(I)    Y(I)                           **/
/**            ...                            **/
/**            ...                                  **/
/**            ...                                  **/
/**      X(I+b)    Y(I+b)                       **/
/**       NDP(I)  VAL(I)                             **/
/**            ...                                  **/
/**            ...                                  **/
/**            ...                                  **/
/**       NDP(I+c)  VAL(I+c)                        **/
/**                                                   **/
```

```
/** The output is in a file called "fem.out"         **/
/*****************************************************/


#include <stdio.h>
#include <stdlib.h>
#include <iostream.h>
#include <fstream.h>
#include <math.h>

class CNodeCoordRecord{
public: double x,y;
   CNodeCoordRecord(){x=0.0;y=0.0;};

   friend istream &operator<<(istream &istr,
   CNodeCoordRecord obj); // used to read in values
};

istream &operator>>(istream &istr, CNodeCoordRecord &obj)
{
   istr >> obj.x;
   istr >> obj.y;

   return istr;
}


class CElementRecord{
public:   int FirstLocalNodeNumber,SecondLocalNodeNumber,
       ThirdLocalNodeNumber;
       CElementRecord(){FirstLocalNodeNumber=0;
                    SecondLocalNodeNumber=0;
                    ThirdLocalNodeNumber=0;};
   friend istream &operator<<(istream &istr,
   CElementRecord obj);  // used to read in values
};

istream &operator>>(istream &istr, CElementRecord &obj)
{
   istr >> obj.FirstLocalNodeNumber;
   istr >> obj.SecondLocalNodeNumber;
   istr >> obj.ThirdLocalNodeNumber;

   return istr;
}
```

```
class CPotentialRecord{
public:   int NodeNumber;
public:   double PrescribedPotential;
       CPotentialRecord(){NodeNumber = 0;
       PrescribedPotential=0.0;};

   friend istream &operator<<(istream &istr,
   CPotentialRecord obj);  // used to read in values
};

istream &operator>>(istream &istr, CPotentialRecord &obj)
{
   istr >> obj.NodeNumber;
   istr >> obj.PrescribedPotential;

   return istr;
}

void main()
{
   double x[100], y[100],c[100][100], ce[100][100];
   double ndp[100], val[100];
   double v[100], p[3], q[3], xl[3], yl[3], er[100];
   int nl[100][3], lf[100];


   /*************************************************/
   /** Get Geometry and boundary conditions from the **/
   /** command line.                                **/
   /*************************************************/

   intni = 50,ne,nd,np; // # of iterations
   ofstream out("fem.out");
   if (!out)
   {
      cout << "Error with creating output file 'fem.out.'\n";
      exit(0);
   }
   ifstream in("fem.in");
   if (!in)
   {
      cout << "Error with opening file.
      Make sure the file 'fem.in' exists\n";
      exit(0);
   }

   in >> ne; // get the number of elements
   in >> nd; // get the number of nodes
   in >> np; // get the number prescribed nodes
```

```
CElementRecord ElRec;
    // instantiate a CElementRecord object
CNodeCoordRecord NodeRec;
    // instantiate a CNodeCoordRecord object
CPotentialRecord PotRec;
    // instantiate a CPotentialRecord object
// populate nl
int i;
for (i = 0;i<ne;i++){
    in >> ElRec;
    nl[i][0] = ElRec.FirstLocalNodeNumber-1;
    nl[i][1] = ElRec.SecondLocalNodeNumber-1;
    nl[i][2] = ElRec.ThirdLocalNodeNumber-1;
}

// populate x and y
for (i = 0;i<nd;i++){
    in >> NodeRec;
    x[i] = NodeRec.x;
    y[i] = NodeRec.y;
}

// populate ndp and val
for (i = 0;i<np;i++){
    in >> PotRec;
    ndp[i] = PotRec.NodeNumber-1;
    val[i] = PotRec.PrescribedPotential;
}

in.close();
/*************************************************/

/*************************************************/
/** Evaluate Coefficient Matrix for each element **/
/** and assemble globally.                       **/
/*************************************************/
int m,n;
for (m =0;m<nd;m++)
    for (n=0;n<nd;n++)
        c[m][n] = 0.0;
int j,l,k;
double area;
for (i = 0;i<ne;i++)
{
    for(j=0;j<3;j++)
    {
        k = nl[i][j];
        xl[j] = x[k];
        yl[j] = y[k];
    }
```

```
    p[0] = yl[1] - yl[2];
    p[1] = yl[2] - yl[0];
    p[2] = yl[0] - yl[1];
    q[0] = xl[2] - xl[1];
    q[1] = xl[0] - xl[2];
    q[2] = xl[1] - xl[0];
    area = 0.5*fabs(p[1]*q[2] - q[1]*p[2]);

    // determine the coefficient matrix for element i
    for (m = 0;m<3;m++)
        for (n=0;n<3;n++)
            ce[m][n] = (p[m]*p[n] + q[m]*q[n])/(4.0*area);
    // assemble globally - find c[i][j]
    int ir,ic;
    for (j=0;j<3;j++)
    {
        ir = nl[i][j];
        for(l=0;l<3;l++)
        {
            ic = nl[i][l];
            c[ir][ic] += ce[j][l];
        }
    }

}

/*****************************************/
/** Solve the resulting system Iteratively **/
/*****************************************/

// initialize and determine lf[i] - list of
// free nodes i

int nf = 0;
int PrescribedNodeFlag = 0;
for (i=0;i<nd;i++)
{
    v[i] = 0.0;
    for(k=0;k<np;k++)
    {
        if (i == ndp[k])
        {
            v[i] = val[k];
            out << i << " " << v[i] << endl;
            PrescribedNodeFlag =1;
            break;
```

```
            }
        }
        if (!PrescribedNodeFlag)
        {
            lf[nf++] = i; // if i is not a prescribed node,
            it is free
        }
        else
            PrescribedNodeFlag = 0;
    }

    out << nf << " " << nd - np << " Check if these are equal.\n";

    // apply the iterative method
    double sum;
    for (n = 0; n< ni; n++)
    {
        for( i = 0;i<nf;i++)
        {
            sum = 0.0;
            k = lf[i];
            for (j = 0;j<nd;j++)
            {
                if (j!=k)
                    sum+= (v[j]*c[j][k]);
            }
            v[k] = -sum/c[k][k]; // applies only to free nodes
        }
    }

    /************************/
    /** Output the results **/
    /************************/
    out << "        # of Nodes: " << nd << endl;
    out << "    # of Elements: " << ne << endl;
    out << " # of Fixed Nodes: " << np << endl;

    for (i=0;i<nd;i++)
        out << "I: " << i << "\tx[" << i << "]\t"<< x[i]
            << "\t\ty[" << i << "]\t" << y[i]
            << "\t\tv[" << i << "]\t" << v[i] << endl;
}
```

Listing 3: Transmission-line-matrix:

```
/*********************************************************/
/** This Program applies the tlm method to solve         **/
/** One-dimensional wave problems.  The Specific Example **/
/** is described as follows:                             **/
/**                                                      **/
/** The TEM waves on a 25 x 11 matrix                    **/
/** The boundaries are at x = 2 and x = 10.              **/
/** Initial impulse excitation is along z = 4 at t = 0   **/
/** and subsequently this line is set to zero.  The grid **/
/** is terminated at z = 25.  Output is taken at z = 14, **/
/** x = 6 for Ey and Hx for 100, 150, 200 iterations     **/
/**                                                      **/
/** vi(it, i j k) -- array for incident voltage          **/
/** vr(it,i,j,k)  -- array for reflected voltage         **/
/** it = 1        -- for previous pulse value            **/
/** it = 2        -- for current pulse value             **/
/** i,j           -- correspond to node location (z,x)   **/
/** k = 1 ..4     -- for terminals,                      **/
/** nx            -- index of nodes in x-direction       **/
/** nz            -- index of nodes in z-direction       **/
/** nx/nz b,e     -- index of beginning, end nod         **/
/** nx/nz 0       -- index of output node                **/
/** Gamma         -- reflection of coefficient at the    **/
/**                      boundary c                      **/
/** Delta         -- Mesh Size Divided by lambda         **/
/** itrate        -- # of iterations                     **/
/*********************************************************/

/*******************************************************/
/****************** Please Note ************************/
/*******************************************************/
/** The output is in a file called "tlm.out"         **/
/*******************************************************/

#include <stdlib.h>
#include <iostream.h>
#include <fstream.h>
#include <math.h>

double transc(double delta)
{
   double lambda,lambdac;
   double pie = 3.14159265;
   double teta = pie*delta;
   double tet = sqrt(2.0)*sin(teta);
   return(teta/asin(tet));
}

// This is a support class to handle complex numbers
```

```
class CComplex
{
public: double Real, Imag;
    CComplex(){Real = 0;Imag = 0;};
     // constructor takes imag and real parts

    double mag();
    double ang();
};

double CComplex::mag()
{
    double result;

    result = sqrt(pow(Real,2) + pow(Imag,2));
    return(result);
}

double CComplex::ang()
{
    double result,pie = 3.1415927;

    result = atan(Imag/Real);

    if (Imag < 0 && Real > 0 && result
        >= pie/2 && result <= pie) // 4th quadrant
        result -= pie;
    if (Imag < 0 && Real < 0 && result
        >= 0 && result <= pie/2)   // 3rd quadrant
        result += pie;
    if (Imag > 0 && Real < 0 && result
        >= 3*pie/2 && result <= 2*pie)   // 2nd quadrant
        result -= pie;

    return (result);
}

void main()
{
    double vi[2][25][11][4], vr[2][25][11][4];
    double out[20][10], efi[20], efr[20], hfi[20],
    hfr[20]; int nxb=2,nxe=10,nzb=4,nze=24,nt=4,
    itrate=200, nxo=6,nzo=14, ii;
    double pie = 3.1415927,gamma=0,delta =.002;
    double ei = 0.0,hi,del;

    for (int row = 0;row<20;row++)
        for (int col =0;col<10;col++)
            out[row][col] = 0;
```

```
ofstream outf("tlm.out");
if (!outf)
{
   cout << "Error with creating output file 'tlm.out.'\n";
   exit(0);
}

/********************* Step 1 ***********************/
/** Insert initial pulse excitation along line z=4 **/
/****************************************************/
int j;
for (j=nxb-1;j<nxe;j++)
   vi[0][nzb][j][1] = 1.0;

/********************* Step 2 ***********************/
/** Calculate the reflected voltage and submit it  **/
/** directly to the neighboring node.              **/
/****************************************************/
int itime,i,k,it;
double sum;
for (itime = 0;itime < itrate; itime++){
   it = 1;
   for (i=nzb;i<nze;i++){
      for(j=nxb-1;j<nxe;j++){
         sum = 0.0;
         for (k=0;k<nt;k++)
            sum += vi[it-1][i][j][k];
         for (k=0;k<nt;k++)
            vr[it][i][j][k] = 0.5*sum - vi[it-1][i][j][k];
         vi[it][i][j-1][2] = vr[it][i][j][0];
         vi[it][i-1][j][3] = vr[it][i][j][1];
         vi[it][i+1][j][0] = vr[it][i][j][2];
         vi[it][i+1][j][1] = vr[it][i][j][3];

/********************* Step 3 ***********************/
/**          Insert boundary conditions            **/
/****************************************************/
         if (j == nxe-1)
            vi[it][i][nxe-1][2] = vr[it][i][nxe-1][0];
         if (j == nxb-1)
            vi[it][i][nxb-1][0] = vr[it][i][nxb-1][2];
         if (j == nze-1)
            vi[it][nze-1][j][3] = gamma*vr[it][nze-1][j][3];
      }
   }
```

```
/********************* Step 4 ***********************/
/** Calculate impulse response of Ey and Hx at     **/
/** z = nzo, x = nxo                               **/
/**************************************************/
   for (k=0;k<nt;k++)
      ei += vi[it][nzo-1][nxo-1][k]*0.5;
   hi = vi[it][nzo-1][nxo-1][1] - vi[it][nzo-1][nxo-1][3];

   // sum the frequency response (imaginary and real
   // parts) for different values of mesh-size divided
   // by wavelength

   double del = delta;
   ii = 0;
   double t=itime;
   for (k = 0;k<20;k++){
      efi[k] = efi[k] + ei*sin(2*pie*t*del);
      efr[k] = efr[k] + ei*cos(2*pie*t*del);
      hfi[k] = hfi[k] + hi*sin(2*pie*t*del);
      hfi[k] = hfr[k] + hi*cos(2*pie*t*del);
      out[k][ii] = del;
      del += 0.002;
   }

   // save the current pulse magnitude for nex iteration

   for (i=nzb-1;i<nze;i++)
      for(j=nxb-1;j<nxe;j++)
         for(k=0;k<nt;k++)
            vi[it-1][i][j][k];
   it = itime;

   if ((it == 100) || (it == 150) || (it == 200)){
      if (it == 100 ){
         ii = 1;
         outf << "@ " << it << " Iterations\n";
      }
      else if (it == 150){
         ii = 2;
         outf << "@ " << it << " Iterations\n";
      }
      else if (it == 200){
         ii = 3;
         outf << "@ " << it << " Iterations\n";
      }

/********************* Step 5 ***********************/
/** Calculate Magnitude and argument of impedance  **/
/**************************************************/
      CComplex cef,chf;
      for (k = 0;k<20;k++){
         cef.Real = efr[k]; cef.Imag = efi[k];
         chf.Real = hfr[k]; chf.Imag = hfi[k];
         out[k][ii] = cef.mag()/chf.mag();
```

```
            out[k][ii+4] = (cef.ang() - chf.ang());
        }
    }
}

/******************** Step 6 **********************/
/**       alculate exact value of impedance       **/
/**************************************************/

del = delta;
double r2,rig,rr,r3;
CComplex cnum,cdem;
for (k = 0;k<20;k++){
    r2 = 1/transc(del);
    outf << r2 << endl;
    r3 = tan(21.0*r2*pie*del);
    cnum.Real = r2; cnum.Imag = r3;
    rig = r2*r3;
    rr = 1;
    cdem.Real = rr; cdem.Imag = rig;
    out[k][4] = cnum.mag()/(cdem.mag()*r2);
    out[k][8] = cnum.ang() - cdem.ang();
    del += .002;
}

for (k = 0;k<20;k++){
    for (j = 0;j<10;j++)
        outf << "out[" << k <<"][" << j << "]:\t" << out[k][j] << "\t";
    outf << endl;
}

}
// end of main
```

Listing 4: Fixed-Random Walk Monte Carlo Method:

```
#include <stdio.h>
#include <stdlib.h>
#include <time.h>
#include <iostream.h>
#include <fstream.h>


void main()
{
   // create an ouput file
   ofstream out("monte.out");
   if (!out)
   {
      cout << "Error with creating output file
      'monte.out.'\n"; exit(0);
   }

   /*********************************************/
   /**********     Input Parameters     ***********/
   /*********************************************/
   double v1 = 0, v2 = 0, v3 = 100, v4 = 0,v;
   double p1 = 0.25, p2 = 0.5, p3=0.75;

   int nrun = 10000;
   double delta = 0.05;

   // initializing
   double xo = 0.75, yo = 0.25, io = xo/delta, jo = yo/delta;
   double imax = 1/delta, jmax = 1/delta, sum = 0.0;
   int ms =0, m1 = 0, m2 = 0, m3 = 0, m4 = 0;
   // number of walks at each boundary
   double r;

      /* Seed the random-number generator */
      srand( (unsigned)time( NULL ) );


   /*********************************************/
   /***********  Begin Simulation ***************/
   /*********************************************/
   double k,i,j;
   int inside = true,ns;
   for (k=1;k<=nrun;k++){
      i = io;
      j = jo;
      while (inside){
         r = rand();
```

```
            r = (double)r/RAND_MAX;
            ns++;
            if (r >= 0 && r < p1)
                i++;
            else if( r >= p1 && r < p2)
                j++;
            else if (r >= p2 && r < p3)
                i--;
            else if(r >= p3)
                j--;
            // is the next step at the boundary?
            if (i == 0){
                sum += v4;
                m4++;
                inside = false;
            }
            else if (i > imax){
                sum += v2;
                m2++;
                inside = false;
            }
            else if (j == 0){
                sum += v1;
                m1++;
                inside = false;
            }
            else if (j > jmax){
                sum += v3;
                m3++;
                inside = false;
            }
        }

        inside = true;

    }
    v = (double)sum/nrun;
    out << "-----------------------------------------" << endl;
    out << "-----------------------------------------" << endl;
    out << "Point: " << xo << ", " << yo << "  Voltage:
    " << v << endl;
    out << "-----------------------------------------" << endl;
    out << "Walk Distribution  (out of " << nrun << " total)
    " << endl;
    out << "-----------------------------------------" << endl;
    out << "       1st Border: " << m1 << endl;
    out << "       2nd Border: " << m2 << endl;
    out << "       3rd Border: " << m3 << endl;
    out << "       4th Border: " << m4 << endl;
    out << "-----------------------------------------" << endl;
    out << "-----------------------------------------" << endl;
}
```

Appendix D

Solution of Simultaneous Equations

Application of some numerical methods to EM problems often results in a set of simultaneous equations

$$\begin{bmatrix} a_{11} & a_{12} & \dots & a_{1n} \\ a_{21} & a_{22} & \dots & a_{2n} \\ \vdots & & & \vdots \\ a_{n1} & a_{n2} & \dots & a_{nn} \end{bmatrix} \begin{bmatrix} x_1 \\ x_2 \\ \vdots \\ x_n \end{bmatrix} = \begin{bmatrix} b_1 \\ b_2 \\ \vdots \\ b_n \end{bmatrix} \tag{D.1a}$$

or

$$[A][X] = [B] \tag{D.1b}$$

where $[A]$ is the coefficient matrix, $[X]$ is the column matrix of the unknowns to be determined, and $[B]$ is the column matrix of constants. Familiarity with the various techniques for solving Eq. (D.1) is therefore vital. In this appendix, we provide a brief coverage of direct and iterative procedures for solving Eq. (D.1); direct methods are more versatile for linear problems, while iterative methods are suitable for nonlinear problems. We also consider various techniques for solving eigenvalue systems $[A][X] = \lambda[X]$.

D.1 Elimination Methods

Elimination methods constitute the simplest direct approach to the solution of a set of simultaneous equations. They usually involve successive elimination of the unknowns by combining equations. Such methods include Gauss's method, Gauss-Jordan, Cholesky's or Crout's method, and the square-root method. Only Gauss's and Cholesky's methods will be discussed. The reader should consult [1]–[4] for the treatment of other methods.

D.1.1 Gauss's Method

This simple method involves eliminating one unknown at a time and proceeding with the remaining equations. This leads to a set of simultaneous equations in triangular form from which each unknown is determined by back-substitution. To describe this method, consider Eq. (D.1b), i.e.,

$$a_{11}x_1 + a_{12}x_2 + \cdots + a_{1n}x_n = b_1 \tag{D.2a}$$
$$a_{21}x_1 + a_{22}x_2 + \cdots + a_{2n}x_n = b_2 \tag{D.2b}$$
$$\vdots$$
$$a_{n1}x_1 + a_{n2}x_2 + \cdots + a_{nn}x_n = b_n \tag{D.2c}$$

We divide Eq. (D.2a) by a_{11} to give

$$x_1 + a'_{12}x_2 + \cdots + a'_{1n}x_n = b'_1 \tag{D.3}$$

where the primes denote that the coefficients are new. We multiply Eq. (D.3) by $-a_{i1}$ for $i = 2, 3, \ldots, n$ and add Eq. (D.3) to the ith equation in (D.2) to eliminate x_1 from other equations so that Eq. (D.2) becomes

$$x_1 + a'_{12}x_2 + \cdots + a'_{1n}x_n = b'_1 \tag{D.4a}$$
$$a'_{22}x_2 + \cdots + a'_{2n}x_n = b'_2 \tag{D.4b}$$
$$\vdots$$
$$a'_{n2}x_2 + \cdots + a'_{nn}x_n = b'_n \tag{D.4c}$$

Equation (D.2a) used to eliminate x_1 from other equations is called the *pivot equation* and a_{11} is called the *pivot coefficient.* We now use Eq. (D.4b) as the pivot equation and we take similar steps to eliminate x_2 from all equations following the pivot equation. Continuing this reduction procedure eventually leads to an equivalent triangular set of equations:

$$\begin{aligned} x_1 + u_{12}x_2 + u_{13}x_3 + \cdots + u_{1n}x_n &= c_1 \\ x_2 + u_{23}x_2 + \cdots + u_{2n}x_n &= c_2 \\ x_3 + \cdots + u_{3n}x_n &= c_3 \\ &\vdots \\ x_n &= c_n \end{aligned} \tag{D.5}$$

This completes the first phase known as *forward elimination* in the Gauss algorithm, and the system in Eq. (D.5) is said to be in *upper triangular* form. The second phase known as *back substitution* involves solving for the unknowns in Eq. (D.5) by starting

at the bottom. That is,

$$\begin{aligned} x_n &= c_n \\ x_{n-1} &= c_{n-1} - u_{n-1,n}x_n \\ &\vdots \\ x_1 &= c_1 - u_{12}x_2 - \cdots - u_{1n}x_n \end{aligned} \tag{D.6}$$

In summary, this algorithm can be stated as:

Forward elimination

$$\begin{aligned} a'_{kj} &= a_{kj}/a_{kk}, \quad b'_k = b_k/a_{kk}, \quad j = k, k+1, \ldots, n \\ a'_{ij} &= a_{ij} - a_{ik}a'_{kj}, \quad i = k+1, \ldots, n \\ b'_i &= b_i - a_{ik}b'_k, \quad i = k+1, \ldots, n \end{aligned} \tag{D.7a}$$

Backward substitution

$$\begin{aligned} x_n &= b_n, \qquad \text{for the last row} \\ x_i &= b_i - \sum_{j=i+1}^{n} a_{ij}x_j, \quad i = n-1, \ldots, 1 \end{aligned} \tag{D.7b}$$

Based on the idea outlined above, a general FORTRAN subroutine for solving a set of simultaneous equations by Gaussian elimination is shown in Fig. D.1.

D.1.2 Cholesky's Method

This method, also known as Crout's method or the method of matrix decomposition, involves determining a lower triangular matrix that will reduce the original system in Eq. (D.1) to a unit upper triangular matrix. If the original system

$$[A][X] = [B] \tag{D.1a}$$

or

$$\begin{bmatrix} a_{11} & a_{12} & \ldots & a_{1n} \\ a_{21} & a_{22} & \ldots & a_{2n} \\ \vdots & & & \vdots \\ a_{n1} & a_{n2} & \ldots & a_{nn} \end{bmatrix} \begin{bmatrix} x_1 \\ x_2 \\ \vdots \\ x_n \end{bmatrix} = \begin{bmatrix} b_1 \\ b_2 \\ \vdots \\ b_n \end{bmatrix} \tag{D.1b}$$

can be redefined in the upper unit triangular matrix $[T]$ such that

$$[T][X] = [C] \tag{D.8a}$$

```
0001    C*********************************************************
0002    C  THIS SUBROUTINE EMPLOYS GAUSSIAN ELIMINATION METHOD
0003    C  TO SOLVE A SET OF SIMULTANEOUS EQUATIONS [A][X] = [B]
0004    C  IDM = DIMENSION OF [A] IN THE CALLING PROGRAM
0005    C  N   = ACTUAL SIZE OF [A] IN THE CALLING PROGRAM
0006    C*********************************************************
0007
0008            SUBROUTINE GAUSS(A,B,X,N,IDM)
0009            DIMENSION A(IDM,IDM), B(IDM), X(IDM)
0010    C
0011    C  FORWARD ELIMINATION
0012    C
0013          DO 40 K=1,N-1
0014          DO 30 I=K+1,N
0015          FACTOR = A(I,K)/A(K,K)
0016    C
0017    C  CALCULATE ELEMENTS OF THE NEW MATRIX
0018    C
0019          DO 20 J=K+1,N
0020          A(I,J) =A(I,J) - FACTOR*A(K,J)
0021    20   CONTINUE
0022          A(I,K) = FACTOR
0023          B(I) = B(I) - FACTOR*B(K)
0024    30   CONTINUE
0025    40   CONTINUE
0026    C
0027    C  BACK SUBSTITUTION PROCESS BEGINS
0028    C
0029          X(N) = B(N)/A(N,N) !1ST STEP
0030          DO 60 I=N-1,1,-1
0031          SUM = 0.0
0032          DO 50 J=I+1,N
0033          SUM = SUM + A(I,J)*X(J)
0034    50   CONTINUE
0035          X(I) = ( B(I) - SUM )/A(I,I)
0036    60   CONTINUE
0037          RETURN
0038          END
```

Figure D.1
Gauss elimination method of solving $[A][X] = [B]$.

or

$$\begin{bmatrix} 1 & T_{12} & \dots & T_{1n} \\ 0 & 1 & \dots & T_{2n} \\ \vdots & & & \vdots \\ 0 & 0 & \dots & 1 \end{bmatrix} \begin{bmatrix} x_1 \\ x_2 \\ \vdots \\ x_n \end{bmatrix} = \begin{bmatrix} c_1 \\ c_2 \\ \vdots \\ c_n \end{bmatrix} \tag{D.8b}$$

the unknown x_i can be obtained by back substitution. Let $[A]$ be a product of an upper unit triangular matrix $[T]$ and a lower triangular matrix $[L]$, i.e.,

$$[L][T] = [A] \tag{D.9}$$

Since

$$[L][TX - C] = 0 = [AX - B], \tag{D.10}$$

it follows that

$$[L][C] = [B] \tag{D.11}$$

For computational reasons, it is convenient to work with the augmented form of the matrices. The augmented matrix is obtained by adding the column vector of constants to the square coefficient matrix. Equations (D.8) and (D.11) may be combined to give

$$\begin{bmatrix} a_{11} & a_{12} & \dots & a_{1n} \vdots b_1 \\ a_{21} & a_{22} & \dots & a_{2n} \vdots b_2 \\ \vdots & & & \vdots \\ a_{n1} & a_{n2} & \dots & a_{nn} \vdots b_n \end{bmatrix} =$$

$$\begin{bmatrix} L_{11} & 0 & \dots & 0 \\ L_{21} & L_{22} & \dots & 0 \\ \vdots & & & \\ L_{n1} & L_{n2} & \dots & L_{nn} \end{bmatrix} \begin{bmatrix} 1 & T_{12} & \dots & T_{1n} \vdots c_1 \\ 0 & 1 & \dots & T_{2n} \vdots c_2 \\ \vdots & & & \\ 0 & 0 & \dots & 1 \vdots c_n \end{bmatrix} \tag{D.12a}$$

or

$$[A \vdots B] = [L][T \vdots C] \tag{D.12b}$$

The elements of $[L]$, $[T]$, and $[C]$ can be defined in terms of $[A]$ and $[B]$ as follows [1, 2, 5]:

$$\begin{aligned} L_{ij} &= a_{ij} - \sum_{k=1}^{j-1} L_{ik} T_{kj}, \quad i \geq j,\ i = 1, 2, \dots, n \\ L_{ij} &= a_{i1}, \quad j = 1 \\ T_{ij} &= \frac{1}{L_{ii}} \left(a_{ij} - \sum_{k=1}^{i-1} L_{ik} T_{kj} \right), \quad i < j,\ j = 2, 3, \dots, n \\ T_{ij} &= a_{ij}/a_{11}, \quad i = 1 \\ c_i &= \frac{1}{L_{ii}} \left(b_i - \sum_{k=1}^{i-1} L_{ik} c_k \right), \quad i = 2, 3, \dots, n \\ c_1 &= b_1/L_{11} \end{aligned} \tag{D.13}$$

The unknown x_i are obtained by back substitution as follows:

$$\begin{aligned} x_n &= c_n \\ x_i &= c_i - \sum_{j=i+1}^{n} T_{ij} x_j, \quad i = 1, 2, \dots, n-1 \end{aligned} \tag{D.14}$$

Cholesky's method can easily be applied in calculating the determinant of $[A]$. Since

$$\det\left[A\right] = \det\left[L\right]\det\left[T\right] \tag{D.15}$$

and $\det[T] = 1$ due to the fact that $T_{ii} = 1$, it follows that

$$\det\left[A\right] = \det\left[L\right] = L_{11}L_{22}\ldots L_{nn}$$

or

$$\det\left[A\right] = \prod_{i=1}^{n} L_{ii} \tag{D.16}$$

Figure D.2 shows a subroutine based on Cholesky's method of solving a set of simultaneous equations.

D.2 Iterative Methods

The direct or elimination method for solving a system of simultaneous equations can be used for $n = 25$ to 60. This number can be greater if the system is well conditioned or the matrix is sparse. For very large systems, say $n = 100$ or even 1000, elimination methods become time-consuming and prove inadequate due to roundoff error. For these types of problems, indirect or iterative methods provide an alternative.

D.2.1 Jacobi's Method

This is the simplest iterative method. If the system in Eq. (D.1) is rearranged so that the ith equation is explicit in x_i, we obtain

$$x_1 = \frac{1}{a_{11}}\left[b_1 - a_{12}x_2 - a_{13}x_3 - \cdots - a_{1n}x_n\right] \tag{D.16a}$$

$$x_2 = \frac{1}{a_{22}}\left[b_2 - a_{21}x_1 - a_{23}x_3 - \cdots - a_{2n}x_n\right] \tag{D.16b}$$

$$\vdots$$

$$x_n = \frac{1}{a_{nn}}\left[b_n - a_{n1}x_1 - a_{n2}x_2 - \cdots - a_{n,n-1}x_{n-1}\right] \tag{D.16c}$$

assuming that the diagonal elements are all nonzero. We start the solution process by using guesses for the x's, say $x_1 = x_2 = \cdots = x_n = 0$. The first equation can be solved for x_1, the second for x_2, and so on. If we denote the estimates after the

```
0001    C*******************************************************
0002    C    THIS SUBROUTINE APPLIES CHOLESKY ELIMINATION METHOD
0003    C    TO SOLVE THE SYSTEM [AA][X] = [B]
0004    C        [A]  = AUGMENTED MATRIX = [AA : B]
0005    C        MAX  = MAXIMUM ROW DIMENSION OF [AA] AND [X] MATRIX
0006    C        MAX1 = MAXIMUM COLUMN DIMENSION OF [AA] = MAX + 1
0007    C        N    = ACTUAL ROW SIZE OF [AA]
0008    C        M    = ACTUAL COLUMN SIZE OF [AA] = N+1
0009    C        [X]  = STORES THE RESULTS
0010    C
0011    C REF: [2, PP. 184, 185]
0012    C*******************************************************
0013          SUBROUTINE CHOLESKY(A,MAX,MAX1,N,M,X)
0014    C
0015    C  NOTE:  THIS PROGRAM CAN BE USED TO SOLVE COMPLEX EQUATIONS
0016    C         BY REPLACING EVERY SUM = 0.0 WITH SUM = (0.0,0.0)
0017    C         USING THE NEXT LINE INSTEAD OF THE ONE FOLLOWING IT
0018    C     COMPLEX A,X,SUM
0019          REAL  A,X,SUM
0020          DIMENSION A(MAX,MAX1), X(MAX)
0021
0022    C
0023    C  CALCULATE THE FIRST ROW OF THE [T] MATRIX
0024    C
0025          DO 10 J = 2, M
0026             A(1,J)=A(1,J)/A(1,1)  !CALCULATES T(1,J)
0027    10     CONTINUE
0028    C
0029    C CALCULATE OTHER ELEMENTS OF [T] AND [L] MATRICES
0030    C
0031          DO 60 I=2,N
0032             DO 30 II=I,N
0033             SUM = 0.0
0034             DO 20 K=1,I-1
0035               SUM = SUM + A(II,K)*A(K,I)
0036    20       CONTINUE
0037               A(II,I) = A(II,I) - SUM  !CALCULATES [L]
0038    30  CONTINUE
0039                DO 50 J = I+1,M
0040                   SUM = 0.0
0041                   DO 40 K=1,I-1
0042                      SUM= SUM + A(I,K)*A(K,J)
0043    40  CONTINUE
0044                A(I,J) = ( A(I,J)-SUM )/A(I,I) !CALCULATES [T]
0045    50  CONTINUE
0046    60  CONTINUE
0047    C
0048    C SOLVE FOR [X] BY BACK SUBSTITUTION
0049    C
0050          X(N) = A(N,M)
0051          DO 80 NN = 1,N-1
0052             SUM = 0.0
0053             I= N - NN
0054             DO 70 J = I+1,N
0055               SUM = SUM + A(I,J)*X(J)
0056    70  CONTINUE
0057          X(I) = A(I,M) - SUM
0058    80    CONTINUE
0059          RETURN
0060          END
```

Figure D.2
Cholesky's elimination method of solving $[A][X] = [B]$.

kth iteration as $x_1^k, x_2^k, \ldots, x_n^k$, the estimates after $(k+1)$th iteration can be obtained from Eq. (D.16) as

$$x_i^{k+1} = \frac{1}{a_{ii}} \left[b_i - \sum_{j=1, j \neq i}^{n} a_{ij} x_j^k \right], \qquad i = 1, 2, \ldots, n \tag{D.17}$$

The iteration process is continued until values of x_i at two successive iterations are within an allowable prescribed deviation.

Convergence is measured in terms of the change in x_i from the kth iteration to the next. If we compute

$$d_i = \left| \frac{x_i^{k+1} - x_i^k}{x_i^{k+1}} \right| \cdot 100\% \tag{D.18}$$

for each x_i, convergence can be checked using the criterion

$$d_i < \epsilon_s \tag{D.19}$$

where ϵ_s is a specified small quantity. A better test would be to compute

$$d = \frac{\sum_{i=1}^{n} \left| x_i^{k+1} - x_i^k \right|}{\sum_{i=1}^{n} \left| x_i^{k+1} \right|} \cdot 100\% \tag{D.20}$$

and require that $d < \epsilon_s$.

D.2.2 Gauss-Seidel Method

This is the most commonly used iterative method. In Jacobi's method the entire set of x_i from the kth iteration is used in calculating the new set during the $(k+1)$th iteration, whereas the most recently calculated value of each variable is used at each step in the Gauss-Seidel method. This makes the Gauss-Seidel method converge more rapidly than (about twice as) Jacobi's method and is always used in preference to it. Instead of Eq. (D.17), we use

$$x_i^{k+1} = \frac{1}{a_{ii}} \left[b_i - \sum_{j=1}^{i-1} a_{ij} x_j^{k+1} - \sum_{j=i+1}^{n} a_{ij} x_j^k \right], \qquad i = 1, 2, \ldots, n \tag{D.21}$$

A computer program based on this method is displayed in Fig. D.3.

D.2.3 Relaxation Method

This is a slight modification of the Gauss-Seidel method and is designed to enhance convergence. If x_i^k is added to the right-hand side of Eq. (D.21) and $(a_{ii} x_i^k)/a_{ii}$ is

```
0001    C*********************************************************
0002    C  THIS SUBROUTINE EMPLOYS GAUSS-SEIDEL ITERATIVE METHOD
0003    C  TO SOLVE A SET OF SIMULTANEOUS EQUATIONS [A][X] = [B]
0004    C  IDM = DIMENSION OF [A] IN THE CALLING PROGRAM
0005    C    N = ACTUAL SIZE OF [A] IN THE CALLING PROGRAM
0006    C*********************************************************
0007
0008            SUBROUTINE GSEIDEL(A,B,X,N,IDM)
0009            DIMENSION A(IDM,IDM), B(IDM), X(IDM)
0010    C
0011    C  INITIALIZATION
0012    C
0013          DO 10 I=1,N
0014          X(I) = 0.0
0015    10    CONTINUE
0016          K = 0 !NO. OF ITERATIONS
0017          TOL = 1.0E-30  !TOLERANCE FOR ZERO
0018    20    RES = 0.0
0019          DO 40 I=1,N
0020          SUM = 0.0
0021          DO 30 J=1,N
0022          IF(J.EQ.I) GO TO 30
0023          SUM = SUM + A(I,J)*X(J)
0024    30    CONTINUE
0025          XNEW = ( B(I) - SUM )/A(I,I)
0026    C
0027    C  FIND THE LARGEST RESIDUE
0028    C
0029          DIFF = ABS( X(I) - XNEW )
0030          IF( DIFF.GT.RES ) RES = DIFF
0031    C
0032    C  REPLACE OLD VALUE WITH NEWLY COMPUTED VALUE
0033    C
0034          X(I) = XNEW
0035    40    CONTINUE
0036    C
0037    C  TEST FOR CONVERGENCE
0038    C
0039          K = K + 1
0040          PRINT *,K
0041          IF( RES.GE.TOL ) GO TO 20
0042           RETURN
0043           END
```

Figure D.3
Gauss-Seidel iterative method of solving $[A][X] = [B]$.

subtracted from it, we obtain

$$x_i^{k+1} = x_i^k + \frac{1}{a_{ii}} \left[b_i - \sum_{j=1}^{i-1} a_{ij} x_j^{k+1} - \sum_{j=i}^{n} a_{ij} x_j^k \right], \qquad i = 1, 2, \ldots, n \quad \text{(D.22)}$$

The second term on the right-hand side can be regarded as a correction term. The correction term tends to zero as convergence is approached. If this term is multiplied by ω, Eq. (D.22) becomes

$$x_i^{k+1} = x_i^k + \frac{\omega}{a_{ii}} \left[b_i - \sum_{j=1}^{i-1} a_{ij} x_j^{k+1} - \sum_{j=i}^{n} a_{ij} x_j^k \right], \qquad i = 1, 2, \ldots, n \quad \text{(D.23)}$$

The *relaxation factor* ω is selected such that $1 < \omega < 2$. The choice of a proper value of ω is problem dependent and is often determined by trial and error. The added weight of ω is intended to improve the estimate by pushing it closer to the exact value.

D.2.4 Gradient Methods

The iterative methods considered above may be broadly classified as *stationary* while the ones to be presented now are *gradient* (or nonstationary) methods. The two common gradient methods are the *steepest method* and *conjugate gradients method* [6]–[8]. A major advantage gradient methods have over stationary methods is that convergence is faster; hence gradient methods are particularly useful when the number of simultaneous equations is very large.

A set of n simultaneous equations may be solved by finding the position of the minimum of an error function defined over an n-dimensional space. In each step of a gradient method, a trial set of values for the variables is used to generate a new set corresponding to a lower value of the error function. If $\overline{X}$ is the trial vector, the vector residual is

$$R = B - A\overline{X} \tag{D.24}$$

where A is real, symmetric, and positive definite. If we define the error function as

$$e = R^t A^{-1} R\,, \tag{D.25}$$

then

$$e = \overline{X}^t A\overline{X} - 2B^t\overline{X} + B^t A^{-1} B \tag{D.26}$$

showing that e is quadratic in $\overline{X}$.

Starting from an arbitrary point X_o, we locate a sequence of points

$$X_{k+1} = X_k + \alpha_k D_k \tag{D.27}$$

which are successively closer to X, where X minimizes e in Eq. (D.26). The parameter α_k is proportional to the distance between X_i and X_{i+1} along the direction vector D_k. Substituting Eq. (D.27) into Eq. (D.26) and setting $\partial e/\partial\alpha_k$ equal to zero gives

$$\alpha_k = \frac{D_k^t R_k}{D_k^t A D_k} \tag{D.28}$$

Both the methods of steepest descent and conjugate gradients use Eq. (D.28) but differ in the choice of D_k.

In the method of descent, D_k is taken as the direction of maximum gradient of e at X_k. This direction is proportional to X_k so that the iterative algorithm has the form:

(i) select an arbitrary X_0

(ii) compute $R_0 = B - AX_0$

(iii) determine successively

$$\begin{aligned} U_k &= AR_k \\ \alpha_k &= \frac{R_k^t R_k}{R_k^t U_k} \\ X_{k+1} &= X_k + \alpha_k R_k \\ R_{k+1} &= R_k - \alpha_k U_k \end{aligned} \tag{D.29}$$

(iv) repeat step (iii) until residual vector $(R^T R)$ becomes sufficiently small.

In the method of conjugate gradients, D_k are selected as n vectors P_k which are mutually conjugate. The vectors P_k are conjugate or orthogonal to A, i.e.,

$$\begin{aligned} P_k^t A P_k &= 0, \qquad i \neq j \\ &\neq 0, \qquad i = j \end{aligned} \tag{D.30}$$

Thus the conjugate gradients algorithm is as follows:

(i) select an arbitrary X_0

(ii) set $P_0 = R_0 = B - AX_0$

(iii) determine successively

$$\begin{aligned} U_k &= AR_k \\ \alpha_k &= \frac{P_k^t R_k}{P_k^t U_k} \\ X_{k+1} &= X_k + \alpha_k R_k \\ R_{k+1} &= R_k - \alpha_k U_k \\ \beta_k &= -\frac{R_{k+1}^t U_k}{P_k^t U_k} \\ P_{k+1} &= R_k + \beta_k P_k \end{aligned} \tag{D.31}$$

(iv) repeat step (iii) until $k = n - 1$ or the residual vector $(R^T R)$ becomes sufficiently small.

This algorithm is guaranteed to yield the true solution in no more than n iterations—a condition known as *quadratic convergence*. Because of this, the conjugate gradients method has the advantage of an iterative scheme in that the roundoff error is limited only to the final step of the solution and also the advantage of a direct method in that it converges to the exact solution in a finite number of steps.

The subroutine in Fig. D.4 applies the conjugate gradients method to solve a given set of simultaneous equations. Typical areas where the conjugate gradient methods have been applied in EM can be found in [9]–[12].

```
0001    C*********************************************************
0002    C  THIS SUBROUTINE APPLIES THE CONJUGATE GRADIENTS METHOD
0003    C  TO SOLVE A SET OF SIMULTANEOUS EQUATIONS [A][X] = [B]
0004    C  IDM = DIMENSION OF [A] IN THE CALLING PROGRAM
0005    C    N = ACTUAL SIZE OF [A] IN THE CALLING PROGRAM
0006    C*********************************************************
0007
0008             SUBROUTINE CONJUGATE(A,B,N,IDM,X)
0009
0010            DIMENSION A(IDM,IDM), B(IDM), X(IDM)
0011            DIMENSION  U(100), R(100), P(100) !change 100
0012                                              !if N.GT.100
0013    C
0014    C   INITIALIZATION
0015    C
0016           K=0 !K=NO. OF ITERATIONS
0017           TOL = 1.0E-30 !TOLERANCE FOR ZERO
0018           DO 10 I=1,N
0019           X(I) = 0.0
0020           P(I) = B(I)
0021           R(I) = B(I)
0022    10     CONTINUE
0023    C
0024    C   ITERATION BEGINS HERE
0025    C
0026    20     K = K + 1
0027           DO 30 I=1,N
0028           U(I) = 0.0
0029           DO 30 J=1,N
0030           U(I) = U(I) + A(I,J)*P(J)
0031    30     CONTINUE
0032           SUM1 = 0.0
0033           SUM2 = 0.0
0034           DO 40 I=1,N
0035           SUM1 = SUM1 + P(I)*R(I)
0036           SUM2 = SUM2 + P(I)*U(I)
0037    40     CONTINUE
0038           ALPHA = SUM1/SUM2
0039           DO 50 I=1,N
0040           X(I) = X(I) + ALPHA*P(I)
0041    C      PRINT *,K,I,X(I)
0042           R(I) = R(I) - ALPHA*U(I)
0043    50     CONTINUE
0044    C
0045    C  CALCULATE RESIDUALS AND DIRECTION VECTORS
0046    C
0047           SUM3 = 0.0
0048           SUM4 = 0.0
0049           DO 60 I=1,N
0050           SUM3 = SUM3 + R(I)*R(I)
0051           SUM4 = SUM4 + R(I)*U(I)
0052    60     CONTINUE
0053    C
0054    C  CHECK IF RESIDUALS ARE ALREADY SMALL
0055    C  IF SO ALGORITHM HAS CONVERGED
0056    C
0057           IF( (K.EQ.N).OR.(SUM3.LT.TOL) ) GO TO 80
0058           BETA = - SUM4/SUM2
0059           DO 70 I=1,N
0060           P(I) = R(I) + BETA*P(I)
0061    70     CONTINUE
0062            GO TO 20
0063    80      RETURN
0064            END
```

Figure D.4

This subroutine applies the conjugate gradients method to solve $[A][X] = [B]$ *(Continued).*

D.3 Matrix Inversion

If $[A]$ is a square matrix, there is another matrix $[A]^{-1}$, called the *inverse* of $[A]$, such that

$$[A][A]^{-1} = [A]^{-1}[A] = [I] \tag{D.32}$$

where I is the *identity* or *unit matrix.* Matrix inversion can be used to solve a set of simultaneous equations in Eq. (D.1) as

$$[X] = [A]^{-1}[B] \tag{D.33}$$

The solution of a system of simultaneous equations by matrix inversion and multiplication is most valuable when several systems are to be solved, all of which have the same coefficient matrix but different column matrices of constants. This situation requires calculating the inverse matrix only once and using it as a premultiplier of each of the column matrices of constants [2, 13].

The inversion of matrices is closely related to the solution of sets of simultaneous equations. The inverse of $[A]$ can be determined from Eq. (D.32). If we let $[C] = [A]^{-1}$, then

$$[A][C] = [I] \tag{D.34a}$$

or

$$\begin{bmatrix} a_{11} & a_{12} & \dots & a_{1n} \\ a_{21} & a_{22} & \dots & a_{2n} \\ \vdots & & & \\ a_{n1} & a_{n2} & \dots & a_{nn} \end{bmatrix} \begin{bmatrix} c_{11} & c_{12} & \dots & c_{1n} \\ c_{21} & c_{22} & \dots & c_{2n} \\ \vdots & & & \\ c_{n1} & c_{n2} & \dots & c_{nn} \end{bmatrix} = \begin{bmatrix} 1 & 0 & \dots & 0 \\ 0 & 1 & \dots & 0 \\ \vdots & & & \\ 0 & 0 & \dots & 1 \end{bmatrix} \tag{D.34b}$$

This may be regarded as n sets of n simultaneous equations with identical coefficient matrix. The ith set of n simultaneous equations, for example, is

$$\begin{bmatrix} a_{11} & a_{12} & \dots & a_{1n} \\ a_{21} & a_{22} & \dots & a_{2n} \\ \vdots & & & \\ a_{ni} & a_{ni} & \dots & a_{ni} \\ \vdots & & & \\ a_{n1} & a_{n2} & \dots & a_{nn} \end{bmatrix} \begin{bmatrix} c_{1i} \\ c_{2i} \\ \vdots \\ c_{ii} \\ \vdots \\ c_{ni} \end{bmatrix} = \begin{bmatrix} 0 \\ 0 \\ \vdots \\ 1 \\ \vdots \\ 0 \end{bmatrix} \tag{D.35}$$

Thus, the inversion of $[A]$ may be accomplished by solving n sets of equations like Eq. (D.35). A common approach for matrix inversion is applying elimination method, with or without pivotal compensation. This implies that any elimination technique

(Gauss, Gauss-Jordan, or Cholesky's method) can be modified to calculate an inverse matrix. Here we apply the Gauss-Jordan elimination method.

To apply the Gauss-Jordan method, we first augment the coefficient matrix by the identity matrix to obtain

$$[A \vdots I] = \begin{bmatrix} a_{11} & a_{12} & \dots & a_{1n} & \vdots & 1 & 0 & \dots & 0 \\ a_{21} & a_{22} & \dots & a_{2n} & \vdots & 0 & 1 & \dots & 0 \\ \vdots & & & & \vdots & \vdots & & & \\ a_{n1} & a_{n2} & \dots & a_{nn} & \vdots & 0 & 0 & \dots & 1 \end{bmatrix} \tag{D.36}$$

The goal is to transform this augmented matrix to another augmented matrix of the form

$$[I \vdots C] = \begin{bmatrix} 1 & 0 & \dots & 0 & \vdots & c_{11} & c_{12} & \dots & c_{1n} \\ 0 & 1 & \dots & 0 & \vdots & c_{21} & c_{22} & \dots & c_{2n} \\ \vdots & & & & \vdots & \vdots & & & \\ 0 & 0 & \dots & 1 & \vdots & c_{n1} & c_{n2} & \dots & c_{nn} \end{bmatrix} \tag{D.37}$$

where $[C]$ is the inverse of $[A]$. The transformation is achieved using the Gauss-Jordan method, which involves applying the following equations in the order listed [2]:

$$\begin{aligned} a'_{kj} &= a_{kj}/a_{kk}, \qquad j = 1, 2, \dots, n, \quad j \neq k \\ a'_{kk} &= 1/a_{kk}, \\ a'_{ij} &= a_{ij} - a_{ik}a'_{kj}, \qquad i = 1, 2, \dots, n, \quad i \neq k \\ &\qquad\qquad j = 1, 2, \dots, n, \quad j \neq k \\ a'_{ik} &= -a_{ik}a'_{kk}, \qquad i = 1, 2, \dots, n, \quad i \neq k \end{aligned} \tag{D.38}$$

We apply Eq. (D.38) for $k = 1, 2, \dots, n$. A computer program applying Eq. (D.38) is presented in Fig. D.5. An iterative method of correcting the elements of the inverse matrix is available in [14].

D.4 Eigenvalue Problems

The nature of these problems is discussed in Section 1.3. Here we are concerned with the so-called standard eigenproblems

$$[A - \lambda I][X] = 0 \tag{D.39}$$

```
0001    C*******************************************************
0002    C     SUBROUTINE FOR MATRIX INVERSION USING GAUSS-JORDAN
0003    C     ELIMINATION METHOD
0004    C     A IS THE MATRIX TO BE INVERTED; IT IS DESTROYED
0005    C     IN THE COMPUTATION AND REPLACED BY THE INVERSE
0006    C     N   = THE ORDER OF A
0007    C     IDM = THE DIMENSION OF A
0008    C
0009    C     REF: [2, p. 197 ]
0010    C*******************************************************
0011          SUBROUTINE INVERSE(A,N,IDM)
0012          DIMENSION A(IDM,IDM)
0013    C
0014    C CALCULATE  ELEMENTS OF REDUCED MATRIX
0015    C
0016           DO  60 K=1,N
0017    C
0018    C CALCULATE NEW ELEMENTS OF PIVOT ROW
0019    C
0020           DO 40 J=1,N
0021           IF(J.EQ.K) GO TO 40
0022           A(K,J) = A(K,J)/A(K,K)
0023    40     CONTINUE
0024    C
0025    C  CALCULATE ELEMENT REPLACING PIVOT ELEMENT
0026    C
0027           A(K,K) = 1.0/A(K,K)
0028    C
0029    C  CALCULATE NEW ELEMENTS NOT IN PIVOT ROW OR PIVOT COLUMN
0030    C
0031           DO 50 I=1,N
0032           IF(I.EQ.K) GO TO 50
0033           DO 50 J=1,N
0034           IF(J.EQ.K) GO TO 50
0035           A(I,J) = A(I,J) - A(I,K)*A(K,J)
0036    50     CONTINUE
0037    C
0038    C  CALCULATE REPLACEMENT ELEMENTS FOR PIVOT
0039    C  COLUMN-EXCEPT PIVOT ELEMENT
0040    C
0041           DO 60 I=1,N
0042           IF(I.EQ.K) GO TO 60
0043           A(I,K) = - A(I,K)*A(K,K)
0044    60     CONTINUE
0045           RETURN
0046           END
```

Figure D.5
Matrix inversion using Gauss-Jordan elimination method.

or the generalized eigenproblem

$$[A - \lambda B][X] = 0 \tag{D.40}$$

To show that Eqs. (D.39) and (D.40) are solved in the same way, we premultiply Eq. (D.40) by B^{-1} to obtain

$$[B^{-1}A - \lambda I][X] = 0 \tag{D.41}$$

Assuming $C = B^{-1}A$ gives

$$[C - \lambda I][X] = 0 \tag{D.42}$$

showing that Eq. (D.39) is a special case of Eq. (D.40) in which $B = I$. Thus, the procedure for solving Eq. (D.39) applies to Eq. (D.40) or (D.42).

The eigenvalue problems of Eqs. (D.39) and (D.40) are solved by either direct or indirect methods. In direct methods, such as Jacobi's method, the relevant matrix elements are stored in the computer, and an explicit procedure is used to obtain some or all of the eigenvalues $\lambda_1, \lambda_2, \ldots, \lambda_n$ and eigenvalues $X_1, X_2, \ldots, X_n$. Indirect methods are basically iterative, and the matrix elements are usually generated rather than stored.

D.4.1 Iteration (or Power) Method

The most commonly used iterative method is the *power method.* The method is suitable in situations where either the greatest or the least eigenvalue is required. Suppose that one of the eigenvalues of A, say λ_1, satisfies the condition

$$|\lambda_1| > |\lambda_i|, \qquad i \neq 1, \tag{D.43}$$

then $|\lambda_1|$ is said to be the *dominant* eigenvalue of A. In many applications, the dominant eigenvalue is the most important and is probably the only eigenvalue we are interested in. The iteration method is specifically used for finding the dominant eigenvalues.

The iterative procedure is essentially based on the condition that should a trial vector $[X]_i$ be assumed, an approximate eigenvalue and a new trial eigenvector $[X]_{i+1}$ can be determined from Eq. (D.39) or Eq. (D.40). To find the largest eigenvalue $|\lambda_1|$, we rewrite Eq. (D.39) as

$$[A][X] = \lambda[X] \tag{D.44}$$

and follow these steps [2]:

(1) Assume a trial vector $[X]_0 = (x_1, x_2, \ldots, x_n)$, e.g., $[X]_0 = (1, 1, \ldots, 1)$. Substituting $[X]_0$ to the left-hand side of Eq. (D.44) gives the first approximation to the corresponding eigenvector, i.e.,

$$\lambda[X]_1 = (\lambda x_1, \lambda x_2, \ldots, \lambda x_n)$$

(2) Normalize the new vector $\lambda[X]$ by dividing it by the magnitude of its first component or by dividing the vector $[X]$ by the magnitude of the first component.

(3) Substitute the normalized vector into the left-hand side of Eq. (D.44) and obtain a new approximate eigenvector.

(4) Repeat steps (2) and (3) until the components of the new and previous eigenvectors differ by some prescribed tolerance. The normalizing factor will be the *largest eigenvalue* λ_1 while $[X]$ is the associated eigenvector.

To find the smallest eigenvalue, we first premultiply Eq. (D.44) by the inverse of $[A]$ to obtain

$$[X] = \lambda[A]^{-1}[X]$$

or

$$[A]^{-1}[X] = \frac{1}{\lambda}[X] \tag{D.45}$$

Thus the iteration formula becomes

$$[A]^{-1}[X]_i = \frac{1}{\lambda}[X]_{i+1} \tag{D.46}$$

In this form, the iteration converges to the largest value $1/\lambda$, which corresponds to the smallest eigenvalue λ of $[A]$.

Once the largest eigenvalue is found, the method can be used to obtain the next largest eigenvalue by transforming $[A]$ to another matrix possessing only the remaining eigenvalues [2]. This so-called *matrix deflation* procedure assumes that $[A]$ is symmetric. The matrix deflation is continued until all the eigenvalues have been extracted. Error propagation from one stage of the deflation to the next leads to inaccurate results, specially for large eigenproblems. Jacobi's method, to be discussed in the next section, is recommended for large eigenproblems.

The subroutine in Fig. D.6 is useful for finding the largest eigenvalues of a matrix.

D.4.2 Jacobi's Method

Jacobi's method is perhaps the most reliable method for solving eigenvalue problems. Its major advantage is that it finds all eigenvalues and eigenvectors simultaneously with excellent accuracy.

The method transforms a symmetric matrix $[A]$ into a diagonal matrix having the same eigenvalues as $[A]$. This is achieved by eliminating one pair of off-diagonal elements of $[A]$ at a time. Given

$$[A][X] = \lambda[X]\,, \tag{D.47}$$

let $\lambda_1, \lambda_2, \ldots, \lambda_n$ be the eigenvalues and $[V_1], [V_2], \ldots, [V_n]$ the corresponding eigenvectors. Then,

$$\begin{aligned} [A][V_1] &= \lambda_1[V_1] \\ [A][V_2] &= \lambda_2[V_2] \\ &\vdots \\ [A][V_n] &= \lambda_1[V_n] \end{aligned} \tag{D.48}$$

or simply

$$[A][V] = [V][\lambda] \tag{D.49}$$

```
0001    C*****************************************************
0002    C     THIS SUBROUTINE FINDS THE LARGEST EIGENVALUE AND
0003    C     THE ASSOCIATED EIGENVECTOR OF
0004    C     A MATRIX EQUATION [A][X] = LAMBDA*[X]
0005    C     IDM   = THE DIMENSION OF MATRIX [A]
0006    C     N     = THE ACTUAL SIZE OF MATRIX [A]
0007    C     IT    = THE NO. OF ITERATIONS USED
0008    C     REF: [2, p. 238,239]
0009    C*****************************************************
0010          SUBROUTINE POWER(A,LAMBDA,X,IDM,N,IT)
0011          REAL LAMBDA
0012          PARAMETER (ISIZE=100) !INCREASE ISIZE IF IDM > 100
0013          DIMENSION  A(IDM,IDM),X(IDM)
0014          DIMENSION  D(ISIZE), Z(ISIZE)
0015
0016          EPSI = 1.0E-30  !TOLERANCE FOR ZERO
0017    C
0018    C  INITIALIZATION
0019    C
0020          DO 20 I=1,N
0021          X(I) = 1.0
0022    20    CONTINUE
0023    C
0024    C  CALCULATE [A][X] AND CALL IT [D]
0025    C
0026          IT = 0
0027    30    DO 40 I=1,N
0028          D(I) = 0.0
0029          DO 40 J=1,N
0030          D(I) = D(I) + A(I,J)*X(J)
0031    40    CONTINUE
0032          IT = IT + 1
0033    C
0034    C  NORMALIZE VECTOR [D] AND CALL IT [Z]
0035    C
0036          DO 50 I=1,N
0037          Z(I) = D(I)/D(1)
0038    50    CONTINUE
0039    C
0040    C  CHECK IF RESULT IS SUFFICIENTLY ACCURATE
0041    C
0042          DO 60 I=1,N
0043          DIFF = X(I) - Z(I)
0044          IF( ABS(DIFF) - ESPI*ABS(Z(I)) ) 60, 60, 70
0045    60    CONTINUE
0046          GO TO 90
0047    C
0048    C   SUFFICIENT ACCURACY HAS NOT BEEN ATTAINED
0049    C   LET  [X] = [Z] AND REPEAT THE PROCESS
0050    C
0051    70    DO 80 I=1,N
0052          X(I) = Z(I)
0053    80    CONTINUE
0054          IF(IT.GE.100) GO TO 110
0055          GO TO 30
```

Figure D.6

Subroutine for finding the largest eigenvalue of equation $[A][X] = \mathbf{LAMBDA}[X]$ *(Continued).*

```
0056    C
0057    C  SUFFICIENT ACCURACY HAS BEEN ATTAINED
0058    C
0059    90      DO 100 I=1,N
0060            X(I) = Z(I)
0061    100     CONTINUE
0062    C
0063    C      OR MAXIMUM NUMBER OF ITERATIONS HAS BEEN REACHED
0064    C
0065    110     LAMBDA = D(1)
0066            RETURN
0067            END
```

Figure D.6

(Cont.) **Subroutine for finding the largest eigenvalue of equation** $[A][X] =$ **LAMBDA**$[X]$.

where

$$[V] = [[V_1], [V_2], \ldots, [V_n]] \tag{D.50a}$$

$$[\lambda] = \begin{bmatrix} \lambda_1 & 0 & \ldots & 0 \\ 0 & \lambda_2 & \ldots & 0 \\ \vdots & \vdots & & \vdots \\ 0 & 0 & \ldots & \lambda_n \end{bmatrix} \tag{D.50b}$$

From the theory of matrices, if $[A]$ is symmetric, $[V]$ is orthogonal, i.e.,

$$[V]^t = [V]^{-1} \tag{D.51}$$

hence, premultiplying Eq. (D.49) by $[V]^t$ leads to

$$[V]^t[A][V] = [\lambda] \tag{D.52}$$

signifying that the eigenvalues of $[V]^t[A][V]$, which is known as the orthogonal transformation of $[A]$, are the same as those of $[A]$. Thus the problem of finding the eigenvalues is reduced to finding the $[V]$ matrix.

The $[V]$ matrix is constructed iteratively by using unitary matrix (or plane rotation matrix) $[R]$. If we let

$$\begin{aligned} [A_1] &= [A] \\ [A_2] &= [R_1]^t[A_1][R_1] \\ [A_3] &= [R_2]^t[A_2][R_2] = [R_2]^t[R_1]^t[A][R_1][R_2] \\ &\vdots \\ [A_k] &= [R_{k-1}]^t \ldots [R_1]^t[A][R_1] \ldots [R_{k-1}] , \end{aligned} \tag{D.53}$$

then as $k \to \infty$

$$\begin{aligned} [A_k] &\to [\lambda] \\ [R_1][R_2] \ldots [R_{k-1}] &\to [V] \end{aligned} \tag{D.54}$$

The unitary transformation matrix $[R]$ eliminates the pair of equal elements a_{pq} and a_{qp}. It is given by [1, 2, 7]

$$[R_k] = \begin{array}{c} \\ \\ \\ \\ \\ \end{array} \begin{array}{c} \begin{array}{ccccc} & & p & & q \end{array} \\ \begin{bmatrix} 1 & & & & \\ & 1 & & & \\ & & \cos\theta & -\sin\theta & \\ & & & 1 & \\ & & \sin\theta & \cos\theta & \\ & & & & 1 \end{bmatrix} \end{array} \begin{array}{c} \\ \\ p \\ \\ q \\ \\ \end{array} \tag{D.55a}$$

i.e.,

$$\begin{aligned} R_{qq} &= R_{pp} = \cos\theta \\ -R_{pq} &= R_{qp} = \sin\theta \\ R_{ii} &= 1, \quad i \neq p, q \\ R_{ij} &= 0, \quad \text{elsewhere} \end{aligned} \tag{D.55b}$$

The choice of θ in the transformation matrix must be such that new elements $a'_{pq} = a'_{qp} = 0$, i.e.,

$$a'_{pq} = \left(-a_{pp} + a_{qq}\right)\cos\theta\sin\theta + a_{pq}\left(\cos^2\theta - \sin^2\theta\right) = 0 \tag{D.56}$$

Hence

$$\tan 2\theta = \frac{2a_{pq}}{a_{pp} - a_{qq}}, \qquad -45^\circ < \theta < 45^\circ \tag{D.57}$$

An alternative manipulation of Eq. (D.56) gives

$$\cos\theta = \left[\frac{\sqrt{(a_{pp} - a_{qq})^2 + 4a_{pq}^2} + (a_{pp} - a_{qq})}{2\sqrt{(a_{pp} - a_{qq})^2 + 4a_{pq}^2}}\right]^{1/2} \tag{D.58a}$$

$$\sin\theta = \frac{a_{pq}}{\sqrt{(a_{pp} - a_{qq})^2 + 4a_{pq}^2}\cos\theta} \tag{D.58b}$$

Notice that Eq. (D.53) requires an infinite number of transformations because the elimination of elements a_{pq} and a_{qp} in one step will in general undo the elimination of previously treated elements in the same row or column. However, the transformation converges rapidly and ceases when all the off-diagonal elements become negligible in magnitude.

The program in Fig. D.7 determines all the eigenvalues and eigenvectors of symmetric matrices employing Jacobi's method.

```
0001    C*************************************************
0002    C    USING JACOBI METHOD,
0003    C    THIS SUBROUTINE FINDS ALL THE EIGENVALUES AND
0004    C    THE ASSOCIATED EIGENVECTORS OF
0005    C    A MATRIX EQUATION [A][X] = LAMBDA*[X]
0006    C    A     = SYMMETRIC MATRIX
0007    C    LAMBDA(J) = EIGENVALUES, ORDERED FROM ALGEBRAICALLY
0008    C                LARGEST TO SMALLEST
0009    C    RT(I,J)   = MATRIX THAT WILL EVENTUALLY CONTAIN THE
0010    C                EIGENVECTORS (J) ASSOCIATED WITH LAMBDA (J)
0011    C    IDM   = THE DIMENSION OF MATRIX [A]
0012    C    N     = THE ACTUAL SIZE OF MATRIX [A]
0013    C    IT    = THE NO. OF ITERATIONS USED
0014    C    REF: [2, p. 268-271]
0015    C*************************************************
0016          SUBROUTINE EIGEN(A,RT,IDM,N,LAMBDA)
0017          DIMENSION  A(IDM,IDM),RT(IDM,IDM)
0018          REAL LAMBDA(IDM)
0019    C
0020    C   GENERATE AN N X N IDENTITY MATRIX RT WHICH WILL
0021    C   EVENTUALLY CONTAIN THE EIGENVECTORS
0022    C
0023          DO 20 I=1,N
0024          DO 10 J=1,N
0025          RT(I,J) = 0.0
0026    10    CONTINUE
0027          RT(I,I) = 1.0
0028    20    CONTINUE
0029          NSWEEP = 0
0030    30    NRSKIP = 0
0031    C
0032    C   BEGIN A SWEEP WHICH WILL TRANSFORM EACH OFF-DIAGONAL
0033    C   ELEMENT IN TURN TO ZERO
0034    C
0035          NMIN1 = N-1
0036          DO 130 I=1,NMIN1
0037          IP1 = I + 1
0038          DO 120 J=IP1.N
0039          AV = 0.5*( A(I,J) + A(J,I) )
0040          DIFF = A(I,I) - A(J,J)
0041          RAD = SQRT( DIFF*DIFF + 4.0*AV*AV )
0042    C
0043    C   CHECK IF RAD IS ZERO.  IF SO, NO NEED OF
0044    C   ROTATION
0045    C
0046          IF(RAD.EQ.0.0) GO TO 80
0047    C
0048    C  CHECK IF DIFF IS NEGATIVE.  IF SO, INTERCHANGE
0049    C  A(I,I) AND A(J,J) AND PERFORM ROTATION
0050    C
0051          IF(DIFF.LT.0.0) GO TO 60
0052          IF( ABS(A(I,I)).EQ.ABS(A(I,I))+100.*ABS(AV) ) GO TO 40
0053          GO TO 40
0054    40    IF( ABS(A(J,J)).EQ.ABS(A(J,J))+100.*ABS(AV) ) GO TO 80
0055    50    COSINE = SQRT( (RAD + DIFF)/(2.0*RAD) )
0056          SINE = AV/(RAD*COSINE)
0057          GO TO 70
0058    C
0059    C  FOR THE DIAGONAL ELEMENTS, PERFORM ROTATION
0060    C
0061    60    SINE = SQRT( (RAD-DIFF)/(2.0*RAD) )
0062          IF(AV.LT.0.0) SINE = -SINE
0063          COSINE = AV/(RAD*SINE)
```

Figure D.7

Subroutine for finding all the eigenvalues and eigenvectors of equation $[A][X] =$ LAMBDA$[x]$ ***(Continued.)***

```
0064    C
0065    C  CHECK IF SIN(THETA) IS NEGLIGIBLE
0066    C  IF SO, SKIP ROTATION
0067    C
0068    70      IF(1.0.LT.1.0 + ABS(SINE)) GO TO 90
0069    80      NRSKIP = NRSKIP + 1
0070            GO TO 120
0071    C
0072    C  FERFORM ROTATION
0073    C  PREMULTIPLY BY THE ROTATION MATRIX
0074    C
0075    90      DO 100 K=1,N
0076            Q = A(I,K)
0077            A(I,K) = COSINE*Q + SINE*A(J,K)
0078            A(J,K) = - SINE*Q + COSINE*A(J,K)
0079    100     CONTINUE
0080    C
0081    C  POSTMULTIPLY BY THE TRANSFORM OF THE ROTATION MATRIX
0082    C
0083            DO 110 K=1,N
0084            Q = A(K,I)
0085            A(K,I) = COSINE*Q + SINE*A(K,J)
0086            A(K,J) = - SINE*Q + COSINE*A(K,J)
0087    C
0088    C   POSTMULTIPLY THE CURRENT PRODUCT OF ALL THE RT MATRICES
0089    C   UP TO THIS POINT BY THE CURRENT RT MATRIX
0090    C
0091            Q = RT(K,I)
0092            RT(K,I) = COSINE*Q + SINE*RT(K,J)
0093            RT(K,J) = - SINE*Q + COSINE*RT(K,J)
0094    110     CONTINUE
0095    120     CONTINUE
0096    130     CONTINUE
0097    C
0098    C  KEEP A TALLY OF THE NUMBER OF SWEEPS
0099    C
0100            NSWEEP = NSWEEP + 1
0101            IF(NSWEEP.GT.50) GO TO 140
0102    C       WRITE(6,*)NRSKIP,NSWEEP
0103    C
0104    C  CHECKIF THE NUMBER OF ROTATIONS SKIPPED IS LESS/
0105    C  EQUAL TO THE NO. OF ELEMENTS ABOVE THE MAIN DIAGONAL
0106    C  IF EQUAL, CONVERGENCE HAS OCCURRED
0107    C
0108            IF(NRSKIP.LT.N*(N-1)/2) GO TO 30
0109    140     CONTINUE
0110    C       WRITE(6,*) NSWEEP
0111            DO 150 J=1,N
0112            LAMBDA(J) = A(J,J)
0113    150     CONTINUE
0114            RETURN
0115            END
```

Figure D.7

(Cont.) **Subroutine for finding all the eigenvalues and eigenvectors of equation** $[A][X] =$ **LAMBDA**$[x]$.

References

[1] A.W. Al-Khafaji and J.R. Tooley, *Numerical Methods in Engineering Practice.* New York: Rinehart and Winston, 1986, pp. 84–159, 203–270.

[2] M.L. James et al., *Applied Numerical Methods for Digital Computation.* 3rd ed., New York: Harper & Row, 1985, pp. 146–298.

[3] S.A. Hovanessian and L.A. Pipes, *Digital Computer Methods in Engineering.* New York: McGraw-Hill, 1969, pp. 1–48.

[4] W. Cheney and D. Kincaid, *Numerical Mathematics and Computing,* 2nd ed., Monterey, CA: Brooks/Cole, 1985, pp. 201–257.

[5] R.L. Ketter and S.P. Prawel, *Modern Methods of Engineering Computation.* New York: MacGraw-Hill, 1969, pp. 66–117.

[6] A. Ralston and H.S. Wilf (eds.), *Mathematical Methods for Digital Computers.* New York: John Wiley, 1960, pp. 62–72.

[7] A. Jennings, *Matrix Computation for Engineers and Scientists.* New York: John Wiley, 1977, pp. 182–222, 250–254.

[8] J.C. Nash, *Compact Numerical Methods for Computers: Linear Algebra and Function Minimization.* New York: John Wiley, 1979, pp. 195–199.

[9] T.K. Sarkar, et al., "A limited survey of various conjugate gradient methods for solving complex matrix equations arising in electromagnetic wave interaction," Wave Motion, vol. 10, no. 6, 1988, pp. 527–546.

[10] A.F. Peterson and R. Mittra, "Method of conjugate gradients for the numerical solution of large-body electromagnetic scattering problems," *J. Opt. Soc. Am.,* Pt. A, vol. 2, no. 6, June 1985, pp. 971–977.

[11] T.K. Sarkar, "Application of the Fast Fourier transform and the conjugate gradient method for efficient solution of electromagnetic scattering from both electrically large and small conducting bodies," *Electromagnetics,* vol. 5, 1985, pp. 99–122.

[12] D.T. Borup and O.P. Gandhi, "Calculation of high-resolution SAR distributions in biological bodies using the FFT algorithm and conjugate gradient method," *IEEE Trans. Micro. Theo. Tech.,* vol. MTT-33, no. 5, May 1985, pp. 417–419.

[13] R.W. Southworth and S.L. Deleeuw, *Digital Computation and Numerical Methods.* New York: MacGraw-Hill, 1965, pp. 247–251.

[14] S. Hovanessian, *Computational Mathematics in Engineering.* Lexington, MA: Lexington Books, 1976, p. 25.

Appendix E

Answers to Odd-Numbered Problems

Chapter 1

1.1 Proof.

1.3 Proof.

1.5 They satisfy Maxwell's equations.

1.7 $\mathbf{E}_s = \dfrac{1}{j\omega\epsilon_o}\dfrac{H_o}{\sqrt{\rho}}\left(\dfrac{1}{\rho^2} - j\beta\right)e^{-j\beta\rho}\mathbf{a}_z.$

1.9 $\mathbf{H}_s = -j\dfrac{20}{\omega\mu_o}\left[k_y \sin(k_x x)\sin(k_y y)\mathbf{a}_x + k_x \cos(k_x x)\cos(k_y y)\mathbf{a}_y\right].$

1.11 (a) $\cos(\omega t - 2z)\mathbf{a}_x - \sin(\omega t - 2z)\mathbf{a}_y$

(b) $-10\sin x \sin \omega t\mathbf{a}_x - 5\cos(\omega t - 2z + 45°)\mathbf{a}_z$

(c) $2\cos 2x \cos(\omega t - 3x - 90°) + e^{3x}\cos(\omega t - 4x).$

1.13 Proof.

1.15 (a) elliptic, (b) elliptic, (c) hyperbolic, (d) parabolic.

Chapter 2

2.1 If a and d are functions of x only; c and e are functions of y only; $b = 0$; and f is the sum of a function x only and a function of y only.

2.3 (a) $V = \displaystyle\sum_{n=1}^{\infty} A_n \sin\left(\frac{n\pi a}{a}\right)\sinh\left[\frac{n\pi}{a}(y-a)\right]$, where

$$A_n = \frac{2}{n \sinh\left(-\dfrac{n\pi b}{a}\right)} \int_0^a \frac{V_o x}{a} \sin\frac{n\pi x}{a}\, dx$$

(b) $V = V_o \dfrac{\cos\dfrac{\pi x}{a} \cosh\dfrac{\pi y}{a}}{\cosh\dfrac{\pi b}{a}}.$

2.5 (a) $\Phi(\rho, \phi) = \dfrac{\sin\phi}{\rho}$

(b) $\Phi(\rho, z) = \dfrac{4}{\pi} \displaystyle\sum_{n=1,3,5}^{\infty} \frac{I_0(n\pi\rho/L)}{I_0(n\pi a/L)} \frac{\sin(n\pi z/L)}{n}$

(c) $\Phi(\rho, \phi, t) = 2 \displaystyle\sum_{n=1}^{\infty} \frac{J_2(\rho x_n/a)}{x_n J_3(x_n)} \cos 2\phi \exp\left[-x_n^2 kt/a^2\right],$
where $J_2(x_n) = 0.$

2.7 $V(\rho, z) = \displaystyle\sum_{n=1}^{\infty} A_n \sin\left(\frac{n\pi z}{L}\right) I_0\left(\frac{n\pi\rho}{L}\right), 0.2639 V_o.$

2.9 $V(\rho, \phi) = \dfrac{4V_o}{\pi} \displaystyle\sum_{n=1,3,5}^{\infty} \frac{1}{n} \frac{\left[\left(\frac{\rho}{a}\right)^{3n} - \left(\frac{\rho}{a}\right)^{-3n}\right]}{\left[\left(\frac{b}{a}\right)^{3n} - \left(\frac{b}{a}\right)^{-3n}\right]} \sin 3n\phi.$

2.11 Proof.

2.13 Proof.

2.15 $\dfrac{a}{(\rho^2 + a^2)^{3/2}}, \dfrac{a^2 - \rho^2}{(\rho^2 + a^2)^{5/2}}.$

2.17 (a) 0, (b) $\dfrac{2}{9}$, (c) $\dfrac{1}{24}$.

2.19 (a) $\dfrac{1}{2} + \displaystyle\sum_{n=1}^{\infty} \frac{(2n+1)}{2n(n+1)} P_n^1(0)(r/a)^n P_n(\cos\theta)$

(b) $-\dfrac{7}{5}\dfrac{a^3}{r^2} P_1(\cos\theta) - \dfrac{3}{10}\dfrac{a^5}{r^4} P_3(\cos\theta).$

2.21 For $r < a$, $0 \le \theta \le \pi/2$,

$$V = \frac{a\rho}{2\epsilon}\left[-z + \sum_{n=0}^{\infty} \frac{(-1)^n (2n)!}{(n!2^n)^2} (r/a)^{2n} P_{2n}(\cos\theta)\right]$$

For $r > a$, $V = \dfrac{a\rho}{2\epsilon}\left[\displaystyle\sum_{n=0}^{\infty} \frac{(-1)^{n+1}(2n+2)!}{[(n+1)!2^{n+1}]^2} (r/a)^{2n+1} P_{2n}(\cos\theta)\right].$

2.23 Proof.

2.25 $V(r,\theta) = 2(r/a)^2 P_2(\cos\theta) + \dfrac{3r}{a} P_1(\cos\theta) + 2P_0(\cos\theta).$

2.27 For $r < a$, $V(r,\theta) = -\dfrac{3E_o}{\epsilon_r + 2}\cos\theta$

For $r > a$, $V(r,\theta) = -E_o r\cos\theta + E_o \dfrac{a^3(\epsilon_r - 1)}{r^2(\epsilon_r + 2)}\cos\theta.$

2.29 $\dfrac{1}{3}\cos 2\phi P_2^2(\cos\theta).$

2.31 (a) $\dfrac{32}{\pi^3}\displaystyle\sum_{m=1}^{\infty}\sum_{n=1}^{\infty}\sum_{p=1}^{\infty}\frac{m[1-(-1)^m e^{\pi}]}{(m^2+1)(2n-1)(2p-1)}$
$\cdot\dfrac{\sin mx\sin(2n-l)y\sin(2p-l)z}{[m^2+(2n-1)^2+(2p-1)^2]}$

(b) $-\dfrac{128}{\pi^3}\displaystyle\sum_{m=1}^{\infty}\sum_{n=1}^{\infty}\sum_{p=1}^{\infty}\frac{1}{(2m-3)(3m^2-1)(2n-1)(2p-1)}$
$\cdot\dfrac{\sin(2m-1)x\sin(2n-l)y\sin(2p-l)z}{[(2m-1)^2+(2n-1)^2+(2p-1)^2]}.$

2.33 $V(x,y) = \displaystyle\sum_{m=1}^{\infty}\sum_{n=1}^{\infty}\frac{2\rho_o\cos m\pi(\cos n\pi - 1)}{\pi^2 mn\epsilon[(m\pi/a)^2+(n\pi/b)^2]}\sin(m\pi x/a)\sin(n\pi y/b).$

2.35
$$V = \begin{cases} \displaystyle\sum_{k=1}^{\infty}\sin\beta x[a_n\sinh\beta y + b_n\cosh\beta y], & 0 \le y \le c \\ \displaystyle\sum_{k=1}^{\infty} c_n\sin\beta x\sinh\beta y, & c \le y \le b \end{cases}$$
where $\beta = \dfrac{n\pi}{a}$, $n = 2k-1$.

2.37 $P_1^0 = 0.5$, $P_2^0 = -1.250$, $P_2^1 = 1.29904$, $P_3^2 = 2.25$, $P_3^0 = -0.4375$, $P_3^1 = 0.32476$, $P_3^2 = 5.625$, $P_3^3 = 9.74279$, etc.

2.39 Derivation/Proof.

2.41 Proof.

2.43 Proof.

2.47 See Fig. E.1.

2.49 See Fig. E.2.

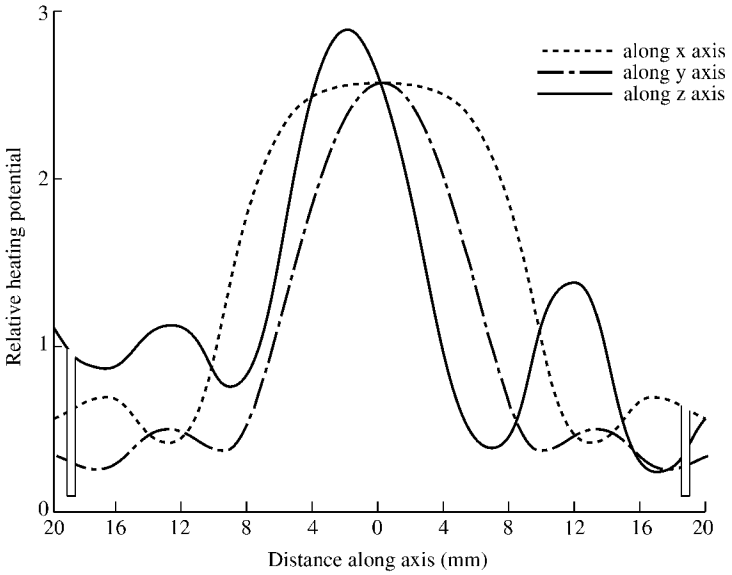

Figure E.1
For Problem 2.47.

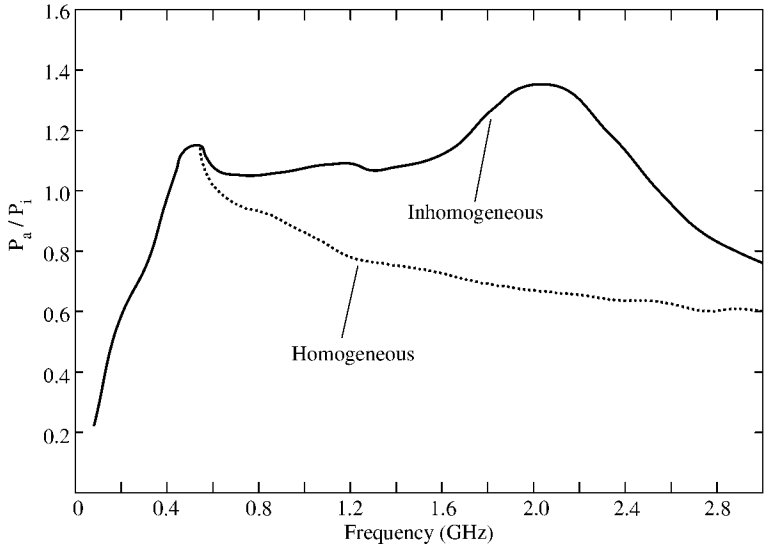

Figure E.2
For Problem 2.49.

Chapter 3

3.1 Proof.

3.3 $(1-a^2)[\Phi(i+1,\,j+1)+\Phi(i-1,\,j-1)]-2[\Phi(i,\,j+1)+\Phi(i,\,j-1)$ $-a^2\Phi(i+1,\,j)-a^2\Phi(i-1,\,j)]+\Phi(i-1,\,j+1)+\Phi(i-1,\,j-1)-\Phi(i+$ $1,\,j-1)-\Phi(i-1,\,j-1)=0.$

3.5 Proof.

3.7 $V_A = 61.46 = V_E$, $V_B = 21.95 = V_D$, $V_C = 45.99V$.

3.9 $16.67V$.

3.11 $r \leq 1/2$.

3.13 (a) Proof, (b) Proof, (c) Euler: $r \leq 1/4$ for stability, Leapfrog: unstable, Dufort-Frankel: unconditionally stable.

3.15 (a) After 5 iterations, $V_1 = 73.79$, $V_2 = 79.54$, $V_3 = 40.63$, $V_4 = 45.31$, $V_5 = 61.33$

(b) After 5 iterations, $V_1 = 19.93$, $V_2 = 19.96$, $V_3 = 6.634$, $V_4 = 6.649$.

3.19 (a) 60.51 Ω, (b) 50.44 Ω.

3.21 $k_c = 4.443$ (exact), $k_c = 3.5124$ (exact).

3.23 Proof.

3.25 See Fig. E.3.

3.27 68.85, 23.32, 6.4, 10.23, 10.34.

3.29 Proof.

3.31

$$\mu_o \frac{\partial H_{xy}}{\partial t} + \sigma_y^* H_{xy} = -\frac{\partial}{\partial y}\left(E_{zx} + E_{zy}\right)$$
$$\mu_o \frac{\partial H_{xz}}{\partial t} + \sigma_y^* H_{xz} = \frac{\partial}{\partial z}\left(E_{yx} + E_{yz}\right)$$
$$\vdots$$
$$\epsilon_o \frac{\partial}{\partial t} E_{zx} + \sigma_x E_{zx} = \frac{\partial}{\partial x}\left(H_{yx} + E_{yz}\right)$$
$$\epsilon_o \frac{\partial}{\partial t} E_{zy} + \sigma_y E_{zy} = -\frac{\partial}{\partial y}\left(H_{xy} + E_{xz}\right).$$

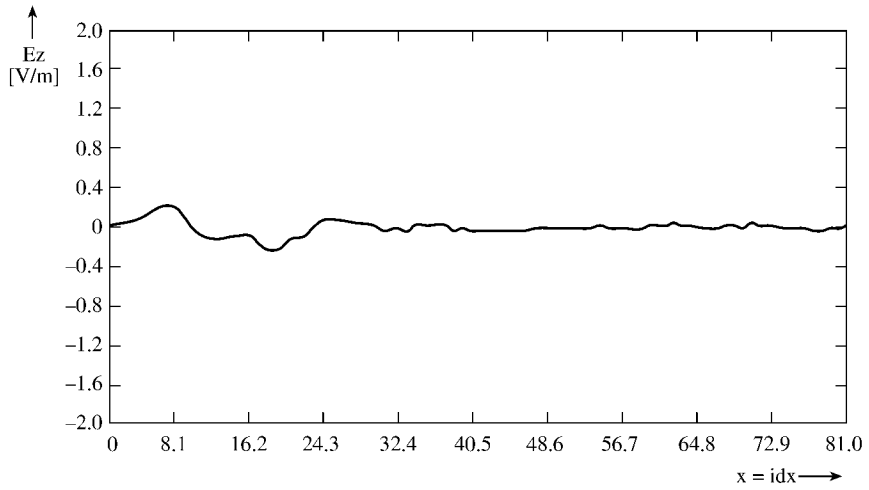

Figure E.3
For Problem 3.25.

3.33 Proof.

3.35 (a) 0.9047, (b) 0.05324.

3.37 1.218.

3.43 (a) 1.724, (b) 3.963, (c) 15.02.

Chapter 4

4.1 (a) 1.3333, (b) −4.667, (c) 157.08.

4.3 (a) $y'' = 0$, (b) $1 + y'^2 - yy'' = 0$,
(c) $xy' \cos(xy') + \sin(xy') = 0$, (d) $y'' + y = 0$,
(e) $2y^{iv} - 10y = 0$, (f) $3u + 2v'' = 0$.

4.5 Proof.

4.7 Proof.

4.9 $\rho_v = \nabla \cdot \mathbf{D}$.

4.11 $$I = \frac{1}{2}\int_v \left[\epsilon_x \left(\frac{\partial V}{\partial x}\right)^2 + \epsilon_y \left(\frac{\partial V}{\partial y}\right)^2 + \epsilon_z \left(\frac{\partial V}{\partial z}\right)^2 - 2\rho_v V\right] dv.$$

4.13 $\frac{1}{2}\int \left[(y')^2 + y^2 - 2y\sin \pi x\right] dx$

4.15 For exact, $\Phi = 2.1667x - 0.1667x^3$,

for $N = 1$, $\widetilde{\Phi} = 2.25x - 0.25x^2$

for $N = 2, 3$, $\widetilde{\Phi}$ is the same as the exact solution.

4.17 (a) $a_1 = 10.33, a_2 = -1.46, a_3 = 0.48$

(b) $a_1 = 10.44, a_2 = -1.61, a_3 = 0.67$

(c) $a_1 = 10.21, a_2 = -1.32, a_3 = 0.35$

(d) $a_1 = 10.21, a_2 = -1.32, a_3 = 0.35$

4.19 See table below.

Method	a_1	a_2
Collocation	0.9292	−0.05115
Subdomain	0.9237	−0.05991
Galerkin	0.9334	−0.05433
Least squares	0.9327	−0.06813
Rayleigh–Ritz	0.09334	−0.05433

4.21 $\widetilde{\Phi} = (1 - x)(1 - 0.2090x - 0.789x^2 + 0.2090x^3)$.

4.23 $\widetilde{\lambda} = 0.2, \lambda_o = 0.1969$ (exact).

4.25 $a/\lambda_c = 0.2948$.

Chapter 5

5.1 (a) Nonsingular, Fredholm IE of the 2nd kind,

(b) nonsingular, Volterra IE of the 2nd kind,

(c) nonsingular, Fredholm IE of the 2nd kind.

5.3 (a) $y = x - \int_0^x (x - t)y\, dt$

(b) $y = 1 + x - \cos x - \int_0^x (x - t)y(t)\, dt$

5.5 Proof.

5.7

$$G(x, y; x', y') = -\frac{4}{ab} e^{x'-x} \sum_{m=1}^{\infty} \sum_{n=1}^{\infty} \left[\frac{\sin \dfrac{m\pi x}{a} \sin \dfrac{m\pi y}{b} \sin \dfrac{m\pi x'}{a} \sin \dfrac{m\pi y'}{b}}{1 + (m\pi/a)^2 + (n\pi/b)^2} \right]$$

5.11 Proof.

5.13 Proof.

5.15 (a) 62.71 Ω, (b) 26.75 Ω.

5.21 (a) Proof, (b) See Fig. E.4(a), (c) See Fig. E.4(b).

5.23 (a) See Fig. E.5(a), (b) See Fig. E.5(b).

5.25 The distribution of normalized field, $|\mathbf{E}_x|/|\mathbf{E}^i|$, is shown in Fig. E.6.

5.27 See table below.

Cell	E_n
64	0.1342
65	0.3966
66	0.4292
67	0.1749
74	0.0965
75	0.3925
76	0.4173
77	0.1393
84	0.1342
85	0.3966
86	0.4293
87	0.1749

Chapter 6

6.1 (a)
$$\begin{bmatrix} 0.5909 & -0.1364 & -0.4545 \\ -0.1364 & 0.4545 & -0.3182 \\ -0.4545 & -0.3182 & 0.7727 \end{bmatrix}$$

(b)
$$\begin{bmatrix} 0.6667 & -0.6667 & 0 \\ -0.6667 & 1.042 & -0.375 \\ 0 & -0.375 & 0.375 \end{bmatrix}$$

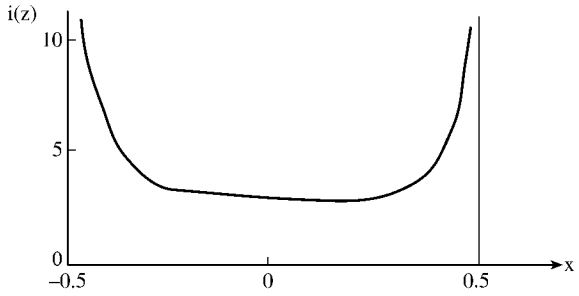

(a)

Figure E.4
(a) For Problem 5.21.

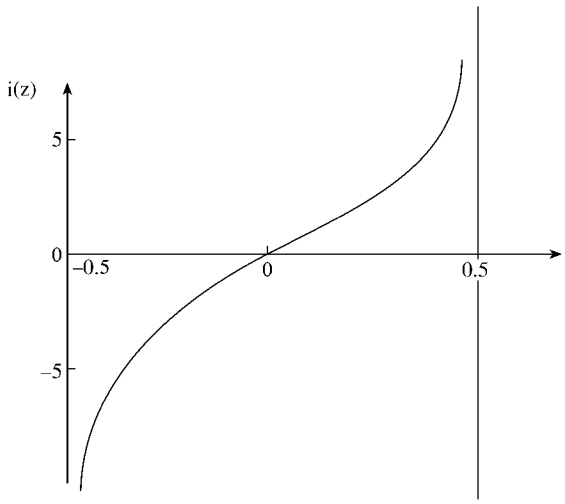

(b)

Figure E.4
(b) For Problem 5.21.

6.3 $\alpha_1 = \frac{1}{23}[4x + 3y - 24], \alpha_2 = \frac{1}{23}[-5x + 2y + 30], \alpha_3 = \frac{1}{23}[x - 5y + 17].$

6.5 $$\frac{1}{2}\epsilon \begin{bmatrix} V_1 & V_2 & V_3 \end{bmatrix} \begin{bmatrix} \frac{h_y V_1}{2h_x} - \frac{h_y V_2}{2h_x} \\ -\frac{h_y V_1}{2h_x} + \frac{V_2(h_x^2 + h_y^2)}{2h_x h_y} - \frac{V_3 h_x}{2h_y} \\ -\frac{h_x V_2}{2h_y} + \frac{h_x V_3}{2h_y} \end{bmatrix}$$

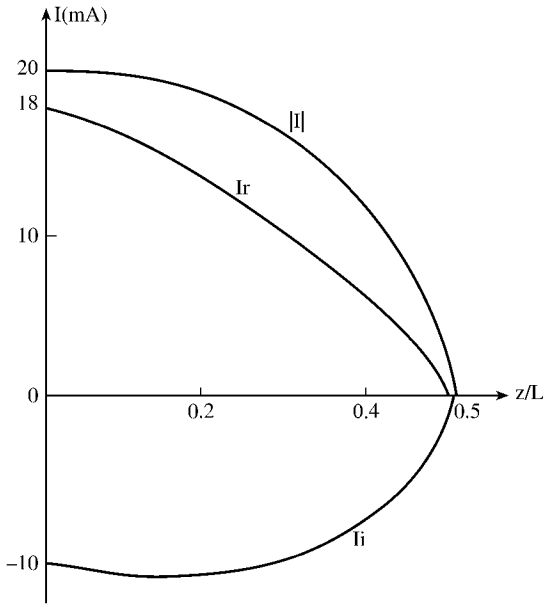

(a)

Figure E.5
(a) For Problem 5.23.

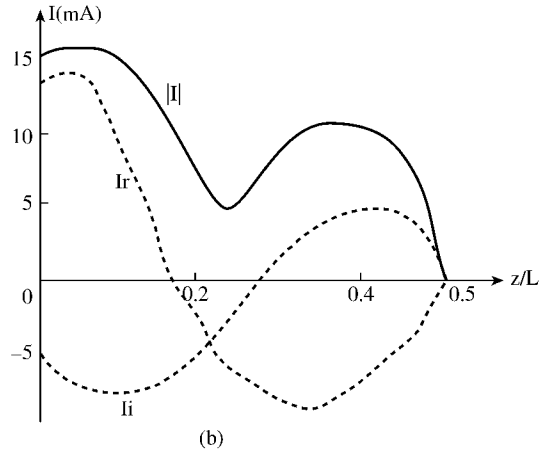

(b)

Figure E.5
(b) For Problem 5.23.

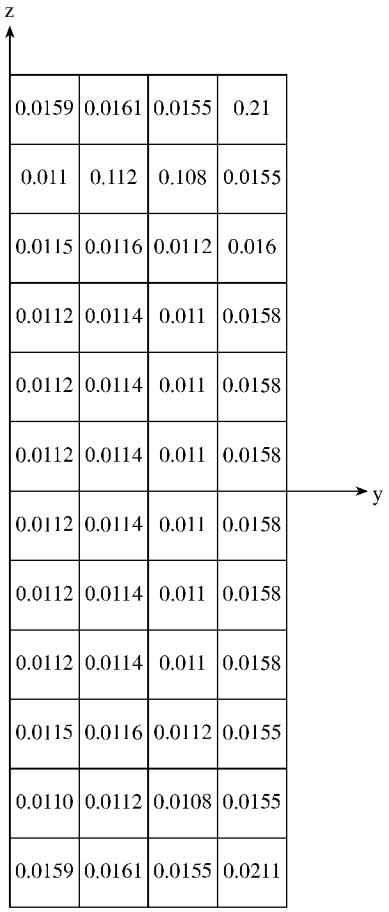

Figure E.6
For Problem 5.25.

6.9 Calculate **E** using

$$\mathbf{E} = -\frac{1}{2A}\sum_{i=1}^{3} P_i V_{ei}\mathbf{a}_x - \frac{1}{2A}\sum_{i=1}^{3} Q_i V_{ei}\mathbf{a}_y$$

6.11 See Fig. E.7.

6.13 $\lambda_{c,mn} = \dfrac{a}{2}\sqrt{(m+n)^2 + n^2}$, $a = 1$.

6.17 $B = 14$. See the mesh in Fig. E.8, $B = 4$.

6.19 Proof.

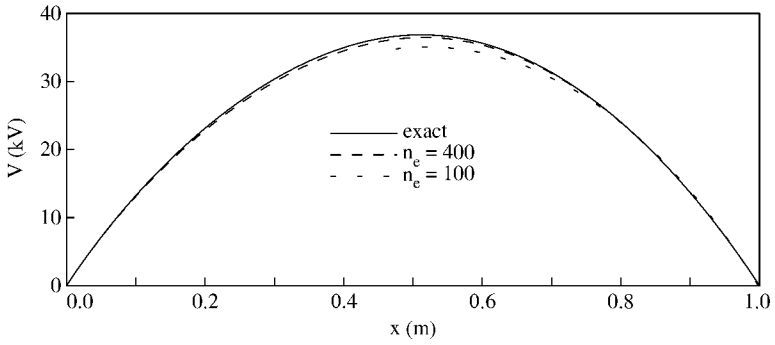

Figure E.7
For Problem 6.11.

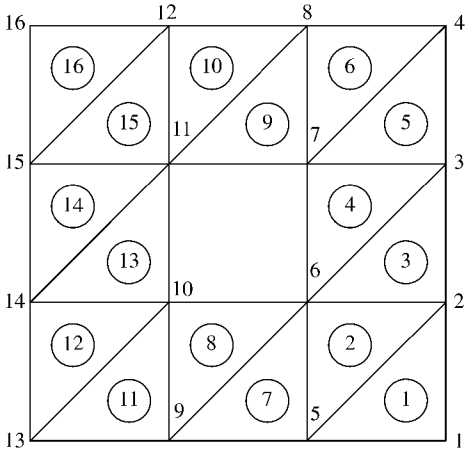

Figure E.8
For Problem 6.17.

6.21 (a) $\frac{32A}{180}$, (b) $-\frac{A}{45}$, (c) 0.

6.23
$$\frac{A}{180}\begin{bmatrix} 6 & 0 & 0 & -1 & 4 & -1 \\ 0 & 32 & 16 & 0 & 16 & -4 \\ 0 & 16 & 32 & -4 & 16 & 0 \\ -1 & 0 & -4 & 6 & 0 & -1 \\ -4 & 16 & 16 & 0 & 32 & 0 \\ -1 & -4 & 0 & -10 & 6 & \end{bmatrix}$$

6.25
$$D^{(1)} = \begin{bmatrix} 1 & 1 & 1 \\ 0 & 0 & 0 \\ 0 & 0 & 0 \end{bmatrix}, \qquad D^{(2)} = \begin{bmatrix} 0 & 0 & 1 \\ 1 & 1 & 1 \\ 0 & 0 & 0 \end{bmatrix}, \qquad D^{(3)} = \begin{bmatrix} 0 & 0 & 0 \\ 0 & 0 & 0 \\ 1 & 1 & 1 \end{bmatrix}$$

$$D^{(1)} = \begin{bmatrix} 3 & 1 & 1 & -1 & -1 & -1 \\ 0 & 2 & 0 & 4 & 2 & 0 \\ 0 & 0 & 2 & 0 & 2 & 4 \\ 0 & 0 & 0 & 0 & 0 & 0 \\ 0 & 0 & 0 & 0 & 0 & 0 \\ 0 & 0 & 0 & 0 & 0 & 0 \end{bmatrix}$$

$$D^{(2)} = \begin{bmatrix} 0 & 0 & 0 & 0 & 0 & 0 \\ 4 & 2 & 0 & 0 & 0 & 0 \\ 0 & 0 & 0 & 0 & 0 & 0 \\ -1 & 1 & -1 & 3 & 1 & -1 \\ 0 & 0 & 2 & 0 & 2 & 4 \\ 0 & 0 & 0 & 0 & 0 & 0 \end{bmatrix}$$

$$D^{(3)} = \begin{bmatrix} 0 & 0 & 0 & 0 & 0 & 0 \\ 0 & 0 & 0 & 0 & 0 & 0 \\ 4 & 2 & 2 & 0 & 0 & 0 \\ 0 & 0 & 0 & 0 & 0 & 0 \\ 0 & 2 & 0 & 4 & 2 & 0 \\ -1 & -1 & 1 & -1 & 1 & 3 \end{bmatrix}$$

6.27 Proof.

6.29 $\dfrac{v}{20}\begin{bmatrix} 2 & 1 & 1 & 1 \\ 1 & 2 & 1 & 1 \\ 1 & 1 & 2 & 1 \\ 1 & 1 & 1 & 2 \end{bmatrix}$

6.31 $B_1 = \dfrac{\partial}{\partial\rho} + jk + \dfrac{1}{2\rho}$

$$B_2 = \frac{\partial}{\partial\rho} + jk + \frac{1}{2\rho} - \frac{1}{8\rho(1+jk\rho)} - \frac{1}{2\rho(1+jk\rho)}\frac{\partial^2}{\partial\phi^2}.$$

Chapter 7

7.1 Proof.

7.3 Proof.

7.5 $\Delta\ell/\lambda = 0.0501$.

7.7 See Fig. E.9.

7.9 Proof.

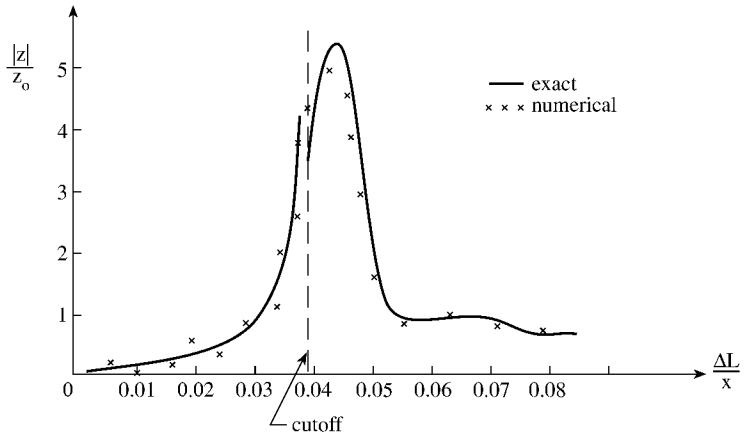

Figure E.9
For Problem 7.7.

7.11 Proof.

7.13 $\frac{1}{6}$ ns.

7.15 See Table below.

$\Delta\ell/\lambda$	$\lvert Z\rvert$ TLM	Exact	Arg(Z) TLM	Exact
0.023	4.1981	6.1272	−0.2806	−0.0106
0.025	2.382	2.4898	1.2546	1.0610
0.027	0.3281	0.3252	−0.7952	−0.8554
0.029	5.2724	5.1637	0.8459	0.8678
0.031	0.2963	0.3039	−1.1340	−1.1610
0.033	1.8117	1.8038	1.3408	1.3385
0.035	0.8505	0.8529	−1.3820	−1.4025
0.037	0.4912	0.4838	1.3914	1.3932
0.039	5.3772	5.4883	−1.1022	−1.1155
0.041	0.2115	0.2179	−1.2795	−1.3174

7.17 For $\epsilon_r = 2$, $k_c a = 1.303$; for $\epsilon_r = 8$, $k_c a = 0.968$.

7.19 See Fig. E.10.

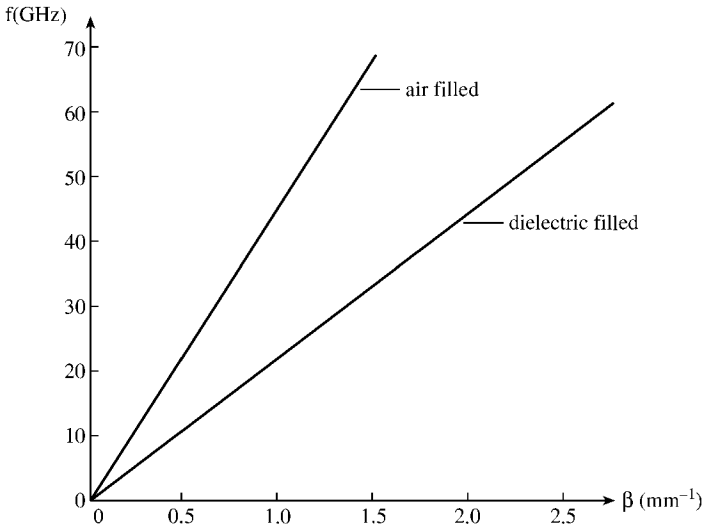

Figure E.10
For Problem 7.19.

Chapter 8

8.3 (a) 16, 187, 170, 429, 836, 47, 950, 369, 456, 307

(b) 997, 281, 13, 449, 277, 721, 133, 209, 757, 761.

8.7 $M = 5, a = 0, b = 1$. Generate the random variable as follows:

(1) Generate two uniformly distributed random variables U_1 and U_2 from (0, 1).

(2) Check if $U_2 \leq f_X(U_2)/M = U_2$.

(3) If the inequality holds, accept U_2.

(4) Otherwise, reject U_1 and U_2 and repeat (1) to (3).

8.9 (a) 3.14159 (exact), (b) 0.4597 (exact), (c) 1.71828 (exact), (d) 2.0.

8.11 0.4053 (exact).

8.13 2.5 (exact).

8.15 $V(0.4, 0.2) = 1.1$, $V(0.35, 0.2) = 1.005$, $V(0.4, 0.15) = 1.05$, $V(0.45, 0.2) = 1.15$, $V(0.4, 0.25) = 1.15$.

8.17 $2.991V$.

8.19 1.2 V.

8.21 $V(2, 10) = 65.85$, $V(5, 10) = 23.32$, $V(8, 10) = 6.4$, $V(5, 2) = 10.23$, $V(5, 18) = 10.34$.

8.23 (a) 0.33, 0.17, 0.17, 0.33,

(b) 0.455, 0.045, 0.045, 0.455.

8.25 12.11 V.

8.27 10.44 V.

8.29 25.0 V.

8.31 See Table below.

Node (ρ, z)	Markov chain	Exodus method	Finite difference
(5, 18)	11.39	11.44	11.47
(5, 10)	27.47	27.82	27.87
(5, 2)	12.31	12.18	12.13
(10, 2)	2.448	2.352	2.342
(15, 2)	0.4684	0.3842	0.3965

Chapter 9

9.1 Proof.

9.3 $$T_{ij} = \sqrt{\frac{2}{N + 1/2}} \cos \frac{(i - 0.5)(j - 0.5)\pi}{N + 0.5}$$

$$\lambda_k = 2 \sin \left(\frac{k - 0.5}{N + 0.5} \right) \pi$$

9.9 Proof.